



Saturated Zone In-Situ Testing

**NOTICE OF OPEN CHANGE DOCUMENTS - THIS DOCUMENT IS IMPACTED BY
THE LISTED CHANGE DOCUMENTS AND CANNOT BE USED WITHOUT THEM.**

-
- 1) ACN-001, DATED 09/05/2007**
 - 2) ACN-002, DATED 10/17/2007**



Prepared for:
U.S. Department of Energy
Office of Civilian Radioactive Waste Management
Office of Repository Development
1551 Hillshire Drive
Las Vegas, Nevada 89134-6321

Prepared by:
Sandia National Laboratories
OCRWM Lead Laboratory for Repository Systems
1180 Town Center Drive
Las Vegas, Nevada 89144

Under Contract Number
DE-AC04-94AL85000

DISCLAIMER

This report was prepared as an account of work sponsored by an agency of the United States Government. Neither the United States Government nor any agency thereof, nor any of their employees, nor any of their contractors, subcontractors or their employees, makes any warranty, express or implied, or assumes any legal liability or responsibility for the accuracy, completeness, or any third party's use or the results of such use of any information, apparatus, product, or process disclosed, or represents that its use would not infringe privately owned rights. Reference herein to any specific commercial product, process, or service by trade name, trademark, manufacturer, or otherwise, does not necessarily constitute or imply its endorsement, recommendation, or favoring by the United States Government or any agency thereof or its contractors or subcontractors. The views and opinions of authors expressed herein do not necessarily state or reflect those of the United States Government or any agency thereof.

QA: QA

Saturated Zone In-Situ Testing

ANL-NBS-HS-000039 REV 02

June 2007



Scientific Analysis/Calculation Signature Page/Change History

Complete only applicable items.

2. Document Title <i>Saturated Zone In-Situ Testing</i>			
3. D) (Including Revision No. and Addendum No.) ANL-NBS-HS-000039 REV 02			
	Printed Name	Signature	Date
4. Originator	P.W. Reimus <i>For</i>	<i>Kenneth Relfilat</i>	<i>6/6/2007</i>
5. Checker	R. Roback	<i>[Signature]</i>	<i>6/6/2007</i>
6. QCS/Lead Lab QA Reviewer	S. Kassabian-Darnell	<i>Soucie K. Darnell</i>	<i>06/06/2007</i>
7. Responsible Manager/Lead	B. Arnold <i>For Paul R. Dixon</i>	<i>Paul R. Dixon</i>	<i>6-6-07</i>
8. Responsible Manager	S. Kuzio	<i>[Signature]</i>	<i>6-6-07</i>
9. Remarks This scientific analysis report represents a joint effort by the Los Alamos National Laboratory, the U.S. Geological Survey, and the Sandia National Laboratories. In addition to the organizations mentioned above, the field-testing efforts described in this report were supported by Yucca Mountain Project M&O contractors (TRW and BSC), the Nye County Nuclear Waste Repository Project Office, and the U. S. Department of Energy.			
Change History			
10. Revision No. and Addendum No.	11. Description of Change		
REV 00	Initial issue.		
REV 01	Made changes to report in response to recommendations from Regulatory Integration Team/ Natural Systems Team. Entire scientific analysis documentation was revised. Changes were too extensive to use step 5.6e)I) per AP-SIII.9Q, REV 1 ICN 7.		
REV 02	This revision resolves CR 9081 by listing in Section 8.3 the applicable DTNs identified in the CR as included in the previous version Table 4-1 and reference list, but inadvertently omitted from Section 8.3. This revision also presents new testing results and analyses for the saturated alluvium at Nye County Site 22. Finally, this revision ensures the report complies with YMP Lead Lab procedures, SCI-PRO-005, <i>Scientific Analyses and Calculations</i> , and SCI-PRO-001, <i>Qualification of Unqualified Data</i> .		

INTENTIONALLY LEFT BLANK

CONTENTS

	Page
ACRONYMS AND ABBREVIATIONS	xxxi
1. PURPOSE	1-1
2. QUALITY ASSURANCE	2-1
3. USE OF SOFTWARE	3-1
3.1 SOFTWARE TRACKED BY CONFIGURATION MANAGEMENT	3-1
3.2 EXEMPT SOFTWARE	3-3
4. INPUTS	4-1
4.1 DIRECT INPUTS	4-1
4.2 CRITERIA	4-6
4.2.1 Acceptance Criteria from Section 2.2.1.3.8.3, <i>Flow Paths in the Saturated Zone</i>	4-7
4.2.2 Acceptance Criteria from Section 2.2.1.3.9.3, <i>Radionuclide Transport in the Saturated Zone</i>	4-9
4.3 CODES, STANDARDS, AND REGULATIONS	4-11
5. ASSUMPTIONS	5-1
6. SCIENTIFIC ANALYSIS DISCUSSION	6-1
6.1 INTRODUCTION	6-1
6.1.1 Hydrogeologic Settings	6-2
6.1.1.1 C-Wells	6-2
6.1.1.2 Alluvial Testing Complex and Nye County Site 22	6-11
6.1.2 Features, Events, and Processes Supported by This Scientific Analysis	6-17
6.2 HYDROLOGIC PROPERTIES OF FRACTURED TUFFS (C-WELLS COMPLEX)	6-20
6.2.1 Introduction	6-20
6.2.2 Summary of C-Wells Hydraulic Testing to Determine Hydrologic Properties	6-20
6.2.3 Hydraulic Test Interpretation Methods	6-21
6.2.4 Hydraulic Test Interpretations: Conceptual Flow Model Implications	6-24
6.2.5 Hydraulic Test Interpretations: Hydrologic Parameter Estimates at the C-Wells	6-25
6.2.6 Hydraulic Test Interpretations: Horizontal Anisotropy in Hydraulic Conductivity	6-26
6.2.7 Limitations and Uncertainties	6-31
6.3 TRANSPORT PROPERTIES OF FRACTURED TUFFS (C-WELLS COMPLEX)	6-32
6.3.1 Introduction	6-32
6.3.2 Summary of C-wells Tracer Testing, Including Objectives and Strategies	6-32
6.3.3 Tracer Test Interpretation Methods	6-36

CONTENTS (Continued)

	Page
6.3.4	Tracer Test Interpretations: Conceptual Transport Model Implications..... 6-37
6.3.5	Tracer Test Interpretations: Transport Parameter Estimates at the C-Wells 6-40
6.3.6	Laboratory Testing to Support C-wells Field Tracer Tests 6-41
6.3.7	Limitations and Uncertainties 6-43
6.4	HYDROLOGIC PROPERTIES OF THE ALLUVIUM (ATC AND NYE COUNTY SITE 22) 6-47
6.4.1	Introduction..... 6-47
6.4.2	Summary of Hydraulic Testing to Determine Hydrologic Properties 6-48
6.4.3	Hydraulic Test Interpretation Methods 6-48
6.4.4	Hydraulic Test Interpretations: Conceptual Flow Model Implications 6-51
6.4.5	Hydraulic Test Interpretations: Hydrologic Parameter Estimates 6-52
6.4.6	Limitations and Uncertainties 6-56
6.5	TRANSPORT PROPERTIES OF ALLUVIUM (ATC AND NYE COUNTY SITE 22)..... 6-57
6.5.1	Introduction..... 6-57
6.5.2	Summary of ATC and Site 22 Tracer Testing, Including Objectives and Strategies..... 6-57
6.5.3	Single-Well Tracer Test Results 6-62
6.5.4	Site 22 Cross-Hole Tracer Test Results 6-67
6.5.5	Tracer Test Interpretations: Estimates of Ambient Flow Velocity in Alluvium 6-71
6.5.5	Tracer Test Interpretations: Conceptual Transport Model Implications..... 6-73
6.5.6	Laboratory Testing to Support Field Tracer Tests 6-78
6.5.7	Limitations and Uncertainties 6-79
7.	CONCLUSIONS..... 7-1
7.1	SUMMARY OF SCIENTIFIC ANALYSIS 7-1
7.2	APPLICABLE ACCEPTANCE CRITERIA..... 7-3
7.2.1	Acceptance Criteria from Section 2.2.1.3.8.3, <i>Flow Paths in the Saturated Zone</i> 7-3
7.2.2	Acceptance Criteria from Section 2.2.1.3.9.3, <i>Radionuclide Transport in the Saturated Zone</i> 7-6
7.3	OUTPUTS..... 7-9
7.4	UNCERTAINTIES 7-12
8.	INPUTS AND REFERENCES..... 8-1
8.1	DOCUMENTS CITED..... 8-1
8.2	CODES, STANDARDS, REGULATIONS, AND PROCEDURES..... 8-17
8.3	SOURCE DATA, LISTED BY DATA TRACKING NUMBER 8-18
8.4	OUTPUT DATA, LISTED BY DATA TRACKING NUMBER 8-26
8.5	SOFTWARE CODES 8-28

CONTENTS (Continued)

	Page
APPENDIX A –QUALIFICATION OF EXTERNAL SOURCES	A-1
APPENDIX B –WELLS	B-1
APPENDIX C –DETAILS OF HYDRAULIC TESTING AND TEST INTERPRETATIONS AT THE C-WELLS COMPLEX.....	C-1
APPENDIX D –DETAILS OF TRACER TESTING AND TRACER TEST INTERPRETATIONS AT THE C-WELLS COMPLEX.....	D-1
APPENDIX E –LABORATORY TESTING CONDUCTED TO SUPPORT INTERPRETATIONS OF TRACER TESTS AT THE C-WELLS COMPLEX	E-1
APPENDIX F –DETAILS OF HYDRAULIC TESTING AND TEST INTERPRETATIONS AT THE ALLUVIAL TESTING COMPLEX (ATC).....	F-1
APPENDIX G –DETAILS OF TRACER TESTING AND TRACER TEST INTERPRETATIONS IN SATURATED ALLUVIUM SOUTH OF YUCCA MOUNTAIN.....	G-1
APPENDIX H –LABORATORY TESTING CONDUCTED TO SUPPORT PLANNED TRACER TESTING AT THE ALLUVIAL TESTING COMPLEX (ATC).....	H-1
APPENDIX I –TWO EXAMPLES OF STEPS INVOLVED IN PROCESSING INPUT DATA TO ARRIVE AT OUTPUT DATA	I-1
APPENDIX J –QUALIFICATION OF MINERALOGY DATA FOR SAMPLE FROM UE25C#2, 2406 FT BELOW LAND SURFACE (DTN: LA9909PR831231.004)	J-1
APPENDIX K –QUALIFICATION OF NC-EWDP-19IM2 WELL COMPLETION DATA (DTN: MO0306NYE05260.166).....	K-1
APPENDIX L –QUALIFICATION OF C-WELLS FLOW DISTRIBUTION DATA (DTN: GS031008312313.016)	L-1
APPENDIX M –QUALIFICATION OF UE25 ONC-1 DRAWDOWN DATA FROM APRIL 24, 1996 TO NOVEMBER 12, 1997 (DTN: MO0212SPANYESJ.149).....	M-1
APPENDIX N –QUALIFICATION OF NYE COUNTY CROSS-HOLE HYDRAULIC TESTING DATA AT NC-EWDP SITE 22, MARCH 2002, AND AUGUST TO SEPTEMBER 2003; AND CORROBORATIVE DATA FOR PUMP FLOW RATES MEASURED DURING TRACER TESTS AT NC-EWDP SITE 22	N-1
APPENDIX O –SURVEY OF SULFIDE MINERAL DISTRIBUTION AT YUCCA MOUNTAIN.....	O-1

CONTENTS (Continued)

	Page
APPENDIX P – DERIVATION OF EQUATIONS (59) AND (63) FROM APPENDIX F: LAPLACE DOMAIN SOLUTIONS FOR DRAWDOWNS IN TWO- AND THREE-AQUIFER SYSTEMS.....	P-1
APPENDIX Q – USGS ANALYSIS OF CROSS-HOLE HYDRAULIC TESTS CONDUCTED BETWEEN AUGUST AND SEPTEMBER 2003 AT THE NYE COUNTY NC-EWDP-22 COMPLEX	Q-1

FIGURES

	Page
1-1. Relationships and Flow of Key Information among Reports Pertaining to Flow and Transport in the SZ Source	1-4
6.1-1. Location and Surface Layout of the C-Wells Complex.....	6-3
6.1-2. Stratigraphy, Lithology, Matrix Porosity, Fracture Density, and Inflow from Open-Hole Flow Surveys at the C-Wells.....	6-7
6.1-3. Generalized Geologic Map Showing the Location of the C-Wells Complex and Nearby Boreholes.....	6-8
6.1-4. Potentiometric Surface of the Miocene Tuffaceous Rocks in the Vicinity of the C-Wells Complex, May 1995	6-10
6.1-5. Hydrogeologic Intervals in the C-Wells Identified During Hydraulic and Tracer Testing from 1995 to 1997.....	6-11
6.1-6. Map Showing Location of Alluvial Testing Complex (ATC) and Site 22 (22S) (Squares) in Relation to the Repository Footprint and the southwestern corner of the Nevada Test Site	6-14
6.1-7. Surface Layout of the Alluvial Testing Complex.....	6-15
6.1-8. Surface Layout of Nye County Site 22.....	6-15
6.1-9. Schematic Diagram of ATC Well Completions and Lithology.....	6-16
6.2-1. Example of a Match of an Analytical Flow Model to Drawdown Data in an Aquifer Pump Test.....	6-23
6.2-2. Anisotropy Ratio of 3.3 at 15° East of North Projected onto a North–South Anisotropy Ratio (0°) Resulting in a Projected Anisotropy Ratio of 2.5	6-30
6.2-3. Probability Density Function (a) and Corresponding Cumulative Distribution Function (b) for the North–South/East–West Anisotropy Ratio Used in FEHM Input Files	6-30
6.3-1. Hypothetical Cross-Hole Responses of Tracers with Different Physical and Chemical Characteristics in Single- and Dual-Porosity Media	6-35
6.3-2. Solute Tracer Breakthrough Curves in the Multiple-Tracer Test in the Lower Bullfrog Tuff and RELAP/MULTRAN Fits to the Breakthrough Curves	6-38
6.3-3. Solute Tracer Breakthrough Curves in the Multiple-Tracer Test in the Prow Pass Tuff and RELAP/MULTRAN Fits to the Breakthrough Curves.....	6-39
6.3-4. RELAP Fits to Iodide Data from Prow Pass Tracer Test in which 2,4,5-TFBA was also Injected	6-45
6.3-5. RELAP Fits to the Iodide and 2,4,5-TFBA Data from the Prow Pass Tracer Test	6-47
6.4-1. Fit to the Theis (1935 [DIRS 150327]) Confined-Aquifer Solution of the Drawdown in NC-EWDP-19IM2 Resulting from Pumping NC-EWDP-19D at 109 gpm	6-50
6.4-2. Schematic Depiction of the Hydraulic Parameters Estimated at NC-EWDP Site 22 in Relation to the Well Completions and Stratigraphy	6-55
6.5-1. Normalized Concentrations of Tracers in Production Water from NC-EWDP-19D as a Function of Gallons Pumped after a Rest Period of Approximately 30 Days.....	6-63
6.5-2. Normalized Concentrations of Fluorinated Benzoates as a Function of Gallons Pumped in Each of the Three Single-Well Tracer Tests in NC-EWDP-19D.....	6-64

FIGURES (Continued)

	Page
6.5-3. Normalized Concentrations of Tracers in Production Water from NC-EWDP-22S as a Function of Time after a Rest Period of Approximately 30 Days	6-65
6.5-4. Normalized Concentrations of Iodide as a Function of Pumping Time in the Two Single-Well Tracer Tests in NC-EWDP-22S	6-66
6.5-5. Normalized Breakthrough Curves of 2,4,5 TFBA, Bromide, Lithium (all from 22PA), and 2,6 DFBA (from 22PC) in the First Cross-hole Tracer Test at Site 22	6-68
6.5-6. Mass-based Normalized Breakthrough Curves of 2,4,5 TFBA and CML Microspheres in the First Cross-hole Tracer Test at Site 22.....	6-69
6.5-7. Mass-based and Concentration-based Normalized Breakthrough Curves of Iodide and Perrhenate in the Second Cross-hole Tracer Test at Site 22	6-70
6.5-8. MULTRAN Model Matches to the 22S Single-well Tracer Test Breakthrough Curves	6-74
6.5-9. Composite Three-pathway RELAP Fits to the First 1,000 Hours of the 2,4,5 TFBA (Concentration-based Normalizations) and Bromide (Mass-based Normalization) Breakthrough Curves at Site 22.....	6-75
6.5-10. Two-pathway RELAP Fits to the Iodide and Perrhenate (Mass-based Normalizations) Breakthrough Curves in the Second Cross-hole Tracer Test at Site 22	6-76
C-1. Result of Filtering Out Earth Tides on UE-25 c#2 Lower Bullfrog Interval Pressure Heads, June 23 to 29, 1995.....	C-9
C-2. Difference of the Atmospheric Pressure from Its Mean Plotted Against the Opposite of the Difference of Concurrent Pressure Head from Its Mean.....	C-10
C-3. Filtered Pressure-head Change in UE-25 c#2 Lower Bullfrog Interval as a Function of Filtered Atmospheric-Pressure Change at the C-Wells Complex, June 23 to 29, 1995	C-11
C-4. Flow Surveys in UE-25 c#3 During Hydraulic Testing in June 1995	C-14
C-5. UE-25 c#3 Discharge and Drawdown, June 12, 1995 (approximately 0 minutes), to June 16, 1995 (approximately 5,800 minutes).....	C-18
C-6. UE-25 c#1 Drawdown in June 1995	C-19
C-7. UE-25 c#2 Drawdown in June 1995	C-19
C-8. UE-25 c#3 Discharge and Drawdown, February 8, 1996 (approximately 0 minutes), to February 13, 1996 (approximately 7,000 minutes).....	C-21
C-9. UE-25 c#1 Drawdown, February 8, 1996 (approximately 0 minutes), to February 13, 1996 (approximately 7,000 minutes)	C-22
C-10. UE-25 c#2 Drawdown, February 8, 1996 (approximately 0 minutes), to February 13, 1996 (approximately 7,000 minutes)	C-22
C-11. UE-25 c#3 Discharge and Drawdown, May 8, 1996 (approximately 0 minutes), to November 12, 1997 (approximately 800,000 minutes)	C-24
C-12. UE-25 c#1 Drawdown, May 8, 1996 (approximately 0 minutes), to March 26, 1997 (approximately 470,000 minutes)	C-26
C-13. UE-25 c#2 Drawdown, May 8, 1996 (approximately 0 minutes), to March 26, 1997 (approximately 470,000 minutes)	C-27

FIGURES (Continued)

	Page
C-14. Disturbance of Drawdown in Lower Bullfrog Interval of UE-25 c#1 and UE-25 c#2 by Tracer Tests in (a) 1996 and (b) 1997.....	C-28
C-15. UE-25 c#1 Lower Bullfrog Recovery, November 12, 1997 (approximately 0 minutes), to December 31, 1997 (approximately 70,000 minutes).....	C-30
C-16. Drawdown in UE-25 ONC-1, May 8, 1996 (approximately 0 minutes), to November 12, 1997 (approximately 800,000 minutes)	C-31
C-17. Drawdown in UE-25 WT#3, May 8, 1996 (approximately 0 minutes), to March 26, 1997 (approximately 480,000 minutes)	C-32
C-18. Drawdown in USW H-4 and UE-25 WT#14, May 8, 1996 (approximately 0 minutes), to December 3, 1996 (approximately 300,000 minutes).....	C-34
C-19. UE-25 c#3 Prow Pass Drawdown, June 2, 1998 (approximately 0 minutes), to June 11, 1998 (approximately 12,800 minutes).....	C-36
C-20. UE-25 c#1 Prow Pass Drawdown, June 2, 1998 (approximately 0 minutes), to June 11, 1998 (approximately 12,800 minutes).....	C-37
C-21. Drawdown in the Prow Pass Interval of c#1 in Response to Pumping c#2, Starting June 2, 1998, Exhibiting Delayed Yield, Characteristic of a Fissure-Block Aquifer	C-37
C-22. Drawdown in the Prow Pass Interval of c#3 in Response to Pumping c#2, Starting June 2, 1998, Exhibiting Delayed Yield, Characteristic of a Fissure-Block Aquifer	C-38
C-23. UE-25 c#2 Prow Pass Drawdown, June 11, 1998 (approximately 0 minutes), to September 1, 1998 (approximately 120,000 minutes)	C-41
C-24. UE-25 c#3 Prow Pass Drawdown, June 11, 1998 (approximately 0 minutes), to September 1, 1998 (approximately 120,000 minutes)	C-42
C-25. UE-25 c#1 Prow Pass Drawdown, June 11, 1998 (approximately 0 minutes), to September 1, 1998 (approximately 120,000 minutes)	C-42
C-26. UE-25 ONC-1 Prow Pass Drawdown, June 11, 1998 (approximately 0 minutes), to September 1, 1998 (approximately 120,000 minutes).....	C-43
C-27. Analysis of Drawdown in the Calico Hills Interval of UE-25 c#2, May 8, 1996 (approximately 0 minutes), to March 26, 1997 (approximately 470,000 minutes)	C-48
C-28. Analysis of Drawdown in the Prow Pass Interval of UE-25 c#1, June 12 to 16, 1995.....	C-49
C-29. Analysis of Drawdown in UE-25 c#2 Upper Bullfrog Interval, June 12 to 16, 1995.....	C-50
C-30. Analysis of Drawdown in UE-25 c#1 Lower Bullfrog Interval, May 8, 1996, to March 26, 1997	C-51
C-31. Analysis of Drawdown in UE-25 c#1 Lower Bullfrog Interval, May 8, 1996, to March 26, 1997	C-52
C-32. Analysis of Drawdown in UE-25 ONC-1, May 8, 1996, to November 12, 1997.....	C-55
C-33. Analysis of Drawdown in USW H-4, May 8, 1996, to June 27, 1996	C-56
C-34. Analysis of Drawdown in UE-25 WT#14, May 8, 1996, to June 27, 1996.....	C-57
C-35. Analysis of Drawdown in UE-25 WT#3, May 8, 1996, to March 26, 1997.....	C-58
C-36. Inferred Distribution of Hydraulic Conductivity of Miocene Tuffaceous Rocks in the Vicinity of the C-Wells.....	C-60

FIGURES (Continued)

	Page
C-37. Analysis of Drawdown in Observation Wells as a Function of Time Divided by the Square of the Distance from Pumping Well, UE-25 c#3	C-61
C-38. Distribution of Drawdown in Observation Wells at Two Times after Pumping Started in UE-25 c#3 on May 8, 1996	C-62
C-39. Analyses of Drawdown in Observation Wells as a Function of Distance from the Pumping Well at Various Times after Pumping Started in UE-25 c#3	C-63
C-40. Water-Level Changes in UE-25 p#1, September 3 to November 2, 1996.....	C-65
C-41. Straight-Line Fits to the Filtered and Derivative-Analyzed Data at the Four Monitoring Wells	C-71
C-42. Optimal Papadopoulos-PEST Ellipse Fit to the Square Root of the Ratio of Directional Transmissivity to Storativity for USW H-4, UE-25 WT#3, UE-25 WT#14, and UE-25 ONC-1 for the 1,000 m ² /day Transmissivity Fit for All Wells.....	C-75
C-43. Optimal Modified-Papadopoulos Ellipse Fit to the Square Root of the Ratio of Directional Transmissivity to Storativity for USW H-4, UE-25 WT#3, UE-25 WT#14, and UE-25 ONC-1 Using PEST for Variable (700 to 2,600 m ² /day, Not in Order of Listed Wells) Transmissivities for the Four Wells	C-76
C-44. Optimal Modified-Papadopoulos Ellipse Fit to the Square Root of the Ratio of Directional Transmissivity to Storativity for USW H-4, UE-25 WT#3, UE-25 WT#14, and UE-25 ONC-1, using PEST, for Variable (700–1,230 m ² /day) Transmissivities Obtained from Filtered Water Levels for the Four Wells.....	C-77
C-45. Anisotropy Ratio of 3.3 at 15° East of North Projected onto a North-South Anisotropy Ratio (0°) Resulting in a Projected Anisotropy Ratio of 2.5.....	C-80
C-46. Probability Density Function (a) and Corresponding Cumulative Distribution Function (b) for the North-South/East-West Anisotropy Ratio Used in FEHM Input Files	C-80
C-47. Weighted Root-Mean-Square Error (RMSE) between Measured Heads and FEHM Modeled Heads Subject to a Range of Anisotropy Ratios between 0.01 and 100.....	C-82
D-1. Type-Curve Match for Iodide Injection into UE-25 c#2	D-3
D-2. Dominant Bullfrog Tuff Fracture Sets in Each of the C-Wells	D-4
D-3. Preliminary Moench Analytical Solution Fit for Iodide Injection in UE-25 c#2	D-8
D-4. Breakthrough Curve for February 13, 1996, Iodide Tracer Test	D-9
D-5. Type Curve Fit for 2,6 DFBA Injection in UE-25 c#2.....	D-11
D-6. Fit 1 Preliminary Moench Analytical Solution for 2,6 DFBA Injection in UE-25 c#2.....	D-12
D-7. Fit 2 Preliminary Moench Analytical Solution for 2,6 DFBA Injection in UE-25 c#2.....	D-13
D-8. Breakthrough Curve for January 10, 1997, DFBA Tracer Test.....	D-14
D-9. Breakthrough Curve for Pyridone Injection in UE-25 c#1	D-15
D-10. Breakthrough Curve for Iodide Injection in UE-25 c#1	D-17

FIGURES (Continued)

	Page
D-11. Breakthrough Curves for 2,4,5 TFBA and Iodide Tracer Test from UE-25 c#3 to UE-25 c#2	D-19
D-12. Breakthrough Curve for June 17, 1998, 2,4,5 TFBA and Iodide Tracer Test Matched by the Single-Porosity, Purely Convergent Moench Solution	D-20
D-13. Breakthrough Curve for June 17, 1998, 2,4,5 TFBA and Iodide Tracer Test Matched by the Single-Porosity, Partial-Recirculation Solution Derived from Moench	D-22
D-14. Streamlines for (a) Partial-Recirculation Flow Field and (b) Purely Convergent Flow Field	D-23
D-15. Breakthrough Curve for June 17, 1998, 2,4,5 TFBA and Iodide Tracer Test Matched with a Lower Storage Porosity and a Higher Diffusion Coefficient.....	D-26
D-16. Breakthrough Curve for June 17, 1998, 2,4,5 TFBA and Iodide Tracer Test Matched with a Higher Storage Porosity and a Higher Diffusion Coefficient	D-27
D-17. Breakthrough Curve for 2,3,4,5 TeFBA Tracer Test in Prow Pass from UE-25 c#1 to UE-25 c#2	D-28
D-18. Hypothetical Cross-Hole Responses of Tracers with Different Physical and Chemical Characteristics in Single- and Dual-Porosity Media	D-35
D-19. Normalized Tracer Concentrations Versus Time in the Bullfrog Tuff Tracer Test Conducted from October 1996 to September 1997	D-40
D-20. Normalized Concentrations of PFBA and 360-nm-Diameter Carboxylate-Modified Polystyrene Latex Microspheres in the Bullfrog Tuff Tracer Test.....	D-41
D-21. Comparison of Normalized PFBA Responses in the Bullfrog Tuff Resulting from Tracer Injections in May 1996 and October 1996	D-41
D-22. Normalized Tracer Concentrations versus Time in the Prow Pass Tracer Test Conducted from September 1998 to January 1999.....	D-43
D-23. Normalized Concentrations of PFBA and Carboxylate-Modified Polystyrene Latex Microspheres in the Prow Pass Tracer Test.....	D-44
D-24. Tracer Concentrations Mixing Loop 40 Days after Tracer Injection in UE-25 c#3 in the Prow Pass Tracer Test.....	D-45
D-25. System Geometry Assumed in the RELAP and MULTRAN Codes.....	D-46
D-26. RELAP and MULTRAN Fits to the Tracer Response Curves in the Bullfrog Tuff Tracer Test	D-54
D-27. RELAP/MULTRAN Fits to the Tracer Response Curves in the Prow Pass Tuff Tracer Test	D-56
D-28. MULTRAN Fits to Cation Responses in the Prow Pass Tracer Test	D-58
D-29. RELAP Fits to CML Microsphere Response in Bullfrog Tuff Tracer Test	D-59
D-30. RELAP Fits to the CML Microsphere Responses in the Prow Pass Tracer Test	D-61
D-31. RELAP Fits to the Iodide and 2,4,5-TFBA Responses in the Prow Pass Tuff Tracer Test Assuming an Injection Zone Time Constant of 0.0023 hr^{-1}	D-73
D-32. RELAP Fits to the Iodide and 2,4,5-TFBA Responses in the Prow Pass Tuff Tracer Test Assuming an Injection Borehole Time Constant of 0.11 hr^{-1}	D-74

FIGURES (Continued)

	Page
D-33. Tracer Responses as a Function of Injection Borehole Time Constant in a Hypothetical Flow System with a Mean Residence Time of 1 hr in the Aquifer, a Peclet Number of 100, and No Matrix Diffusion	D-75
D-34. Mean Residence Time (τ), Peclet Number, and MTC ($\times 1,000$) as a Function of Borehole Time Constant from RELAP Fits to the Iodide and 2,4,5-TFBA Data of Figure D-32	D-76
D-35. RELAP Fits to Iodide Data from Prow Pass Tracer Test	D-77
D-36. RELAP Fits to the Iodide and 2,4,5-TFBA Data from the Prow Pass Tracer Test	D-80
D-37. Correlation Between Best-Fitting Peclet Numbers and Mean Residence Times for the Multiple-Tracer Tests at the C-Wells.....	D-81
D-38. Correlation Between Best-Fitting Mass Fractions and Mean Residence Times for the Multiple-Tracer Tests at the C-Wells.....	D-81
E-1. C-Wells Hydrogeology Showing Sampling Locations of All Cores Used in the Laboratory Experiments Described in Sections E1, E2, and E3.....	E-4
E-2. Lithium Sorption Data and Fitted Langmuir Isotherm for the Central Bullfrog Tuff	E-8
E-3. Lithium Sorption Data and Fitted Langmuir Isotherm for the Lower Bullfrog Tuff (c#1, 795 m Below Land Surface)	E-9
E-4. Lithium Sorption Data and Fitted Langmuir Isotherm for the Upper Prow Pass Tuff (c#2, 533 m Below Land Surface)	E-10
E-5. Lithium Sorption Data and Fitted Langmuir Isotherm for the Central Prow Pass Tuff (c#2, 553 m Below Land Surface)	E-11
E-6. Lithium Sorption Data and Fitted Langmuir Isotherm for the Lower Prow Pass Tuff (c#1, 573 m Below Land Surface)	E-12
E-7. Lithium Sorption Data and Fitted Langmuir Isotherm for the Bedded Prow Pass Tuff (c#1, 643 m Below Land Surface)	E-13
E-8. Lithium Sorption Data and Fitted Langmuir Isotherm for the Upper Tram Tuff (c#2, 839 m Below Land Surface)	E-14
E-9. Fitted Langmuir Isotherms for the Seven C-Wells Tuffs	E-15
E-10. Cation-exchange Capacity Results for the Seven Different C-Wells Tuff Intervals	E-17
E-11. Diffusion Cell Experimental Apparatus.....	E-21
E-12. Diffusion Cell Data (Tracer Concentrations in Outlet Reservoir Normalized to Starting Concentrations in Inlet Reservoir, C_0) and DIFFCELL Fits for Bromide and PFBA in the Central Bullfrog Tuff	E-24
E-13. Diffusion Cell Data (Tracer Concentrations in Outlet Reservoir Normalized to Starting Concentrations in Inlet Reservoir, C_0) and DIFFCELL Fits for Bromide and PFBA in the Lower Bullfrog Tuff.....	E-25
E-14. Diffusion Cell Data (Tracer Concentrations in Outlet Reservoir Normalized to Starting Concentrations in Inlet Reservoir, C_0) and DIFFCELL Fits for Bromide and PFBA in the Upper Prow Pass Tuff.....	E-26
E-15. Diffusion Cell Data (Tracer Concentrations in Outlet Reservoir Normalized to Starting Concentrations in Inlet Reservoir, C_0) and DIFFCELL Fits for Bromide and PFBA in the Central Prow Pass Tuff	E-27

FIGURES (Continued)

	Page
E-16. First Diffusion Cell Data (Tracer Concentrations in Outlet Reservoir Normalized to Starting Concentrations in Inlet Reservoir, C_0) and DIFFCELL Fits for Bromide and PFBA in the Lower Prow Pass Tuff.....	E-28
E-17. Second Diffusion Cell Data (Tracer Concentrations in Outlet Reservoir Normalized to Starting Concentrations in Inlet Reservoir, C_0) and DIFFCELL Fits for Bromide and PFBA in the Lower Prow Pass Tuff.....	E-29
E-18. Bromide Diffusion Coefficients Versus Tuff Porosity for All C-Wells Diffusion Cell Experiments.....	E-30
E-19. Bromide Diffusion Coefficients Versus Tuff Permeability for All C-Wells Diffusion Cell Experiments	E-30
E-20. Bromide and Lithium Breakthrough Curves in Column 1 at a Flow Rate of 2.2 mL/hr and Corresponding RELAP and RETRAN Fits to Data.....	E-33
E-21. Bromide and Lithium Breakthrough Curves in Column 1 at a Flow Rate of 1.6 mL/hr and Corresponding RELAP Fits to Data.....	E-34
E-22. Bromide and Lithium Breakthrough Curves in Column 1 at a Flow Rate of 9.7 mL/hr and Corresponding RELAP Fits to Data.....	E-35
E-23. Bromide and Lithium Breakthrough Curves in Column 2 at a Flow Rate of 2.2 mL/hr and Corresponding RELAP Fits to Data.....	E-36
E-24. Bromide and Lithium Breakthrough Curves in Column 2 at a Flow Rate of 1.6 mL/hr and Corresponding RELAP Fits to Data.....	E-37
E-25. MULTRAN Fits to Complete Bromide and Lithium Breakthrough Curves from High-Concentration Experiment Conducted at 9.7 mL/hr in Column 1 (Figure E-22).....	E-39
E-26. MULTRAN Fits to Complete Bromide and Lithium Breakthrough Curves from High-Concentration Experiment Conducted at 2.2 mL/hr in Column 1 (Figure E-20).....	E-40
E-27. MULTRAN Fits to Complete Bromide and Lithium Breakthrough Curves from Low-Concentration Experiment Conducted at 2.2 mL/hr in Column 2 (Figure E-23).....	E-41
E-28. RELAP Fits to Complete Bromide and Lithium Breakthrough Curves from Experiment Conducted at 9.7 mL/hr in Column 1 (Figure E-25 Shows the MULTRAN Fits)	E-41
E-29. Schematic Illustration of a Fractured Rock Core Experimental System	E-42
E-30. Schematic Illustration of MULTRAN Simulation Domain.....	E-49
E-31. Experimental and Simulation Results from the Three Iodide-Only Transport Tests in Core 1.....	E-52
E-32. Experimental and Simulation Results from the Three Iodide-Only Transport Tests in Core 2.....	E-53
E-33. Experimental Data and MULTRAN Simulation Results for Multiple Tracer Tests 1 and 3 in the Upper Prow Pass Tuff Core (Core 1).....	E-55
E-34. Experimental Data and MULTRAN Simulation Results for Multiple Tracer Tests 1 and 2 in the Central Prow Pass Tuff Core (Core 2).....	E-56

FIGURES (Continued)

	Page
E-35. Experimental Data and MULTRAN Simulation Results for Multiple Tracer Tests 1 and 2 in the Lower Prow Pass Tuff Core (Core 3)	E-57
E-36. Experimental Data and MULTRAN Simulations Results for Multiple Tracer Tests 1 and 2 in the Lower Bullfrog Tuff Core (Core 4).	E-59
E-37. Comparison of Li ⁺ Isotherms Calculated from Best-Fitting MULTRAN Parameters (Designated by XXX_Y, where Y is the Fractured Core Test Number) and Obtained in Batch Sorption Experiments for the Four Different C-Wells Tuffs Used in the Fracture Experiments.....	E-61
E-38. Comparison of the Fits of the MULTRAN Multicomponent Ion-Exchange Model and the Single-Component RELAP Code to the Lithium Transport Data in the First Multiple-Tracer Test in Core 4.....	E-63
E-39. Longitudinal Dispersivity as a Function of Test Scale in Several Tracer Tests Conducted in the Vicinity of Yucca Mountain.....	E-64
E-40. Plot of Longitudinal Dispersivity Versus Length Scale Showing the Range of C-Wells Values Derived from Interpretations of the Prow Pass and Bullfrog Multiple Tracer Tests in Which Lithium Ion Was Used as a Sorbing Tracer	E-65
E-41. Matrix Diffusion Mass Transfer Coefficient as a Function of Experimental Time Scale in All C-Wells Laboratory and Field Multiple Tracer Tests.....	E-67
F-1. Drawdown and Recovery Data Associated with the Pump Test of the Four Combined Alluvium Intervals in NC-EWDP-19D, July 2000	F-3
F-2. Drawdown as a Function of Elapsed Time for the Combined Interval Hydraulic Test in NC-EWDP-19D Overlaid with the Neuman Unconfined Aquifer Type Curve Solution	F-4
F-3. Drawdown as a Function of Time for the Hydraulic Test in Screen #1 of NC-EWDP-19D, October 24 to October 27, 2000	F-5
F-4. Drawdown versus Elapsed Time for the Hydraulic Test in Screen #1 of NC-EWDP-19D Overlaid with the Neuman Unconfined Aquifer Type Curves.....	F-6
F-5. Drawdown as a Function of Time for the Hydraulic Test in Screen #2, NC-EWDP-19D, October 31 to November 6, 2000	F-7
F-6. Drawdown as a Function of Time during the Hydraulic Test in Screen #2, NC-EWDP-19D, Overlaid with the Neuman Unconfined Aquifer Type Curves.....	F-8
F-7. Drawdown as a Function of Elapsed Time for the Hydraulic Test in Screen #3 of NC-EWDP-19D, September 9 to September 16, 2000.....	F-9
F-8. Drawdown as a Function of Time during the Hydraulic Test in Screen #3, NC-EWDP-19D, Overlaid with the Neuman Unconfined Aquifer Type Curves.....	F-10
F-9. Drawdown as a Function of Time for the Hydraulic Test in NC-EWDP-19D, Screen #4, August 24 to August 31, 2000	F-11
F-10. Drawdown as a Function of Time during the Hydraulic Test in Screen #4, NC-EWDP-19D, Overlaid with the Neuman Unconfined Aquifer Type Curves.....	F-12
F-11. Transmissivity of Screens #1, #3, and #4 of NC-EWDP-19D as a Function of Screen Thickness	F-13

FIGURES (Continued)

	Page
F-12. Transmissivity of Screens #1, #3, and #4 of NC-EWDP-19D as a Function of Distance from Water Table to Bottom of Screen Divided by Distance from Water Table to Bottom of Screen #4	F-14
F-13. Transmissivity of Screens #1, #2, #3, and #4 of NC-EWDP-19D as a Function of Distance from Water Table to Bottom of Screen Divided by Distance from Water Table to Bottom of Screen #4	F-14
F-14. Step-Drawdown Test in the Open Alluvium of NC-EWDP-19D, July 6, 2000	F-17
F-15. Drawdown versus Elapsed Time Since Pumping Started for the Confirmatory Hydraulic Test in Which the Combined Screens #5, #6, and #7 Interval in NC-EWDP-19D was Pumped.....	F-20
F-16. Drawdown as a Function of Elapsed Time for the Confirmatory Hydraulic Test in Which the Screen #5 Interval in NC-EWDP-19D was Pumped.....	F-21
F-17. Drawdown as a Function of Elapsed Time in Screen #4 during Pumping and Recovery in the Confirmatory Hydraulic Test in that Screen, January 8 to 10, 2002.....	F-22
F-18. Recovery versus Elapsed Time for the Screens #5, #6, and #7 Interval during the Confirmatory Hydraulic Test in Screen #4 of NC-EWDP-19D, January 8 to 10, 2002.....	F-23
F-19. Drawdown in the Screens #5, #6, and #7 Interval during the August 24 to 31, 2000, Pumping Test in Screen #4	F-24
F-20. Comparing Drawdown in the Screens #5, #6, and #7 Interval While It Was Pumped During the December 18, 2001, Test with the Drawdown in the Same Interval during the August 24 to 31, 2000, Pumping Test in Screen #4.....	F-25
F-21. Comparing Drawdown in the Screens #5, #6, and #7 Interval While It Was Pumped During the December 18, 2001 Test with the Recovery in the Same Interval after Cessation of Pumping in Screen #4 during the January 8, 2002 Test.....	F-27
F-22. Drawdown in the Open-Alluvium Section of Observation Well NC-EWDP-19IM2 While Pumping NC-EWDP-19D at the Nominal Rate of 109 gpm	F-30
F-23. Fit to the Theis Confined-Aquifer Solution of the Drawdown in NC-EWDP-19IM2 Resulting from Pumping NC-EWDP-19D at 109 gpm.....	F-31
F-24. Relation of Low-Frequency Hydraulic-Pressure Change in NC-EWDP-19D to Low-Frequency Atmospheric-Pressure Change at the NC-EWDP-19D Location: Data and Regression Line.....	F-33
F-25. Total Porosities as a Function of Depth below Land Surface at NC-EWDP-19D, Obtained from the Borehole Gravity Meter (BHGGM) Survey Conducted in September 2000	F-36
F-26. Background Pressures Prior to Zone 4 Pumping	F-42
F-27. Correlation between the Pressures in Different Zones	F-44
F-28. Site 22 Schematic in the Vertical Cross Section.....	F-48
F-29. Zone 1 Pumping Test, Leaky Aquifer Solution	F-61
F-30. Zone 1 Pumping Test, Two-Aquifer Solution	F-63
F-31. Zone 1 Pumping Test, Three-Aquifer Solution	F-65
F-32. Zone 2 Pumping Test, Leaky Aquifer Solution.....	F-67

FIGURES (Continued)

	Page
F-33. Application of the Inflection Point Method to Zone 2 Pumping Test	F-68
F-34. Zone 2 Pumping Test, Three-Aquifer Solution	F-70
F-35. Ambient Fluctuations during the Zone 3 and Zone 4 Pumping Tests	F-72
F-36. Zone 3 Pumping Test, Leaky Aquifer Solution	F-73
F-37. Zone 3 Pumping Test, Three-Aquifer Solution	F-75
F-38. Zone 4 Pumping Test, Leaky Aquifer Solution	F-77
F-39. Zone 4 Pumping Test, Two-Aquifer Solution	F-79
F-40. Combined Zone Pumping Test, Three-Aquifer Solution	F-81
F-41. Pumping Test from Zone 1, Unconfined Aquifer Conceptual Model	F-85
F-42. Pumping Test from Zone 1, Unconfined Aquifer Conceptual Model	F-85
F-43. Pumping Test from Zone 2, Unconfined Aquifer Conceptual Model	F-86
F-44. Pumping Test from Zone 1, Unconfined Aquifer Conceptual Model	F-87
F-45. Hydraulic Conductivities Obtained for Multiple-Aquifer and Multiple-Layer Conceptual Models Based on the Estimated Parameter Ranges	F-90
F-46. Geochemistry Depth Profiles of Major Cations and Anions (upper) and Minor Cations (lower) in Boreholes 19D and 19IM1	F-97
F-47. Geochemistry Profiles of Major Cations, Major Anions, and Minor Cations in Samples from Sonic Borehole 19PB	F-98
F-48. Geochemistry Depth Profiles of Major Cations and Anions (upper) and Minor Cations (lower) in Boreholes 22S, 22PA, and 22PB	F-99
F-49. Geochemistry Profiles of Major Cations, Major Anions, and Minor Cations in Samples from Sonic Borehole 22PC	F-100
F-50. Log-saturated Hydraulic Conductivity as a Function of Depth below Land Surface in NC-EWDP-19PB	F-103
G-1. Schematic Illustration of Alternative Conceptual Transport Models for the Valley- Fill Deposits South of Yucca Mountain	G-3
G-2. Normalized Concentration Response of Any Nonsorbing Tracer in a Single-Well Test in a Porous Medium with No Diffusive Mass Transfer and/or No Stagnant Water (the Conceptual Model of Figure G-1a)	G-7
G-3. Normalized Concentration Responses of a Halide and a FBA in Single-Well Tests for the Conceptual Transport Model of Figure G-1b Using a Fixed Grain Diameter	G-9
G-4. Measured and Fitted Grain Size Distributions from NC-EWDP-19P	G-11
G-5. Normalized Concentration Responses of a Halide and an FBA in Single-Well Tests for the Conceptual Transport Model of Figure G-1b Using a Grain Size Distribution	G-12
G-6. Normalized Concentration Responses of a Halide and an FBA in Single-Well Tests for the Conceptual Transport Model of Figure G-1c	G-13
G-7. Comparison of FBA Responses for the Layered Conceptual Model (Figure G-1c) and the Grain-Diffusion Model (Figure G-1b) with a Lognormal Distribution of Grain Sizes	G-14

FIGURES (Continued)

	Page
G-8. Molar Responses of Injected Tracers (K^+ , Halide, FBA) and Naturally Occurring Cations (Na^+ and Ca^{++}) in the 2-Day-Rest-Period Test Assuming the Model of Figure G-1b.....	G-16
G-9. Relative Responses in a Single-Porosity Medium to a Pulse Function Input for Different Peclet Numbers	G-18
G-10. Ratios of First Arrival Time to Mean Arrival Time and Peak Arrival Time to Mean Arrival Time for Different Peclet Numbers.....	G-19
G-11. Prolate Spheroidal Coordinate System Used for Unbounded Three-Dimensional Flow and Transport Calculations Using the 2WELLS_3D Code.....	G-20
G-12. Ratio of Mean Arrival Time in Unbounded Three-Dimensional Flow to Mean Arrival Time in Two-Dimensional Flow as a Function of Distance between Wells Divided by Interval Thickness	G-22
G-13. Tracer Streamlines in a Weak Dipole Flow Pattern.....	G-22
G-14. Predicted Nonsorbing Tracer Responses in a Two-Dimensional Homogeneous Isotropic Medium as a Function of the Recirculated Fraction of Produced Water	G-23
G-15. Tracer Arrival Times as a Function of Fraction Recirculation in a Two-Dimensional Homogeneous Isotropic Medium	G-23
G-16. Predicted Cross-Hole Responses for a Halide, FBA, and Lithium Ion in a Single-Porosity System and a Layered System with Weak Lithium Sorption.....	G-26
G-17. Predicted Cross-Hole Responses for a Halide, FBA, and Lithium Ion in a Single-Porosity System and a Layered System with Strong Lithium Sorption.....	G-26
G-18. Normalized Concentrations of Tracers in Production Water from NC-EWDP-19D as a Function of Gallons Pumped after a Rest Period of Approximately 0.5 Hours	G-30
G-19. Normalized Concentrations of Tracers in Production Water from NC-EWDP-19D as a Function of Gallons Pumped after a Rest Period of Approximately 2 Days.....	G-31
G-20. Normalized Concentrations of Tracers in Production Water from NC-EWDP-19D as a Function of Gallons Pumped after a Rest Period of Approximately 30 Days.....	G-31
G-21. Normalized Concentrations of Tracers in Production Water from NC-EWDP-22S as a Function of Time after a Rest Period of Approximately 3 Days	G-32
G-22. Normalized Concentrations of Tracers in Production Water from NC-EWDP-22S as a Function of Time after a Rest Period of Approximately 30 Days	G-32
G-23. Normalized Concentrations of Fluorinated Benzoates as a Function of Gallons Pumped in Each of the Three Single-Well Tracer Tests in NC-EWDP-19D	G-33
G-24. Normalized Concentrations of Iodide as a Function of Pumping Time in the Two Single-Well Tracer Tests in NC-EWDP-22S	G-34
G-25. Depiction of How Tracer and Chase Water Might Be Distributed after Injection into a Heterogeneous Porous Medium.....	G-37
G-26. Depiction of Assumed Tracer Mass Distribution Immediately after Injection.....	G-38
G-27. Tracer Ring (Red-Hatched Area) and Chase Ring (Green-Hatched Area) around the Injection Well NC-EWDP-19D	G-46
G-28. Concentration Distribution of Tracer Plume Resulting from a 30-Day Drift of the Tracer Ring Shown in Figure G-27	G-47

FIGURES (Continued)

	Page
G-29. Fitting the Injection-Pumpback Tracer Tests in Screen #1 of NC-EWDP-19D Using the Linked-Analytical Solutions Method	G-49
G-30. Depiction of a Tracer Injection Scenario That Could Result in Underestimation of Groundwater Velocity.....	G-54
G-31. Comparison of the Theoretical Breakthrough Curve from the Linked-Analytical-Solutions Method to the Actual Breakthrough Curve from the Injection-Pumpback Tracer Test in Screen #4 of NC-EWDP-19D.....	G-55
G-32. MULTRAN Model Matches to the 22S Single-well Tracer Test Breakthrough Curves using the Diffusion-into-Blocks Conceptual Model.....	G-59
G-33. MULTRAN Model Matches to the 22S Single-well Tracer Test Breakthrough Curves Using the Diffusion-into-Layers Conceptual Model.....	G-63
G-34. Normalized Breakthrough Curves of 2,4,5 TFBA, Bromide, Lithium (all from 22PA), and 2,6 DFBA (from 22PC) in the First Cross-Hole Tracer Test at Site 22	G-68
G-35. Mass-Based and Concentration-Based Normalized Breakthrough Curves of Bromide in the First Cross-Hole Tracer Test at Site 22.....	G-69
G-36. Mass-Based and Concentration-Based Normalized Breakthrough Curves of 2,4,5 TFBA in the First Cross-Hole Tracer Test at Site 22	G-70
G-37. Mass-Based Normalized Breakthrough Curves of 2,4,5 TFBA and CML microspheres in the First Cross-Hole Tracer Test at Site 22	G-71
G-38. Mass-Based and Concentration-Based Normalized Breakthrough Curves of Iodide and Perrhenate in the Second Cross-Hole Tracer Test at Site 22	G-72
G-39. Depth Profiles of Tracer C/Co (based on specific conductance) as a Function of Time in 22PA after Tracer Injection.....	G-74
G-40. Tracer C/Co (based on specific conductance) as a Function of Time at 82.9 m below the Water Table in 22PA after Tracer Injection (Station 16 in Figure G-39)....	G-75
G-41. Derivative of Bromide Concentration with Respect to Time as a Function of Time since Injection in the First Cross-Hole Tracer Test at Site 22	G-77
G-42. Fit of a Single-Pathway Model (solid lines) to the First 1,000 Hours of the 2,4,5 TFBA (blue diamonds, mass-based normalization) and Bromide (red squares, concentration-based normalization) Breakthrough Curves at Site 22	G-78
G-43. Composite Three-pathway RELAP Fits to the First 1,000 Hours of the 2,4,5 TFBA (blue diamonds, mass-based normalization), 2,6 DFBA (magenta triangles, mass-based normalization) and Bromide (red squares, concentration-based normalization) Breakthrough Curves at Site 22	G-79
G-44. Composite Three-Pathway RELAP Fits to the First 1,000 Hours of the 2,4,5 TFBA (blue diamonds, concentration-based normalization) and Bromide (red squares, mass-based normalization) Breakthrough Curves at Site 22	G-80
G-45. RELAP Fits (solid lines) to the Peaks of the 2,4,5 TFBA (blue diamonds) and Bromide (red squares) Breakthrough Curves	G-82
G-46. Three-Pathway RELAP Fit to Lithium (mass-based normalization) Breakthrough Curve (diamonds) Using Flow Pathways Deduced from RELAP Fits to TFBA and Bromide Breakthrough Curves with Minimum Possible Differences (Figure G-43)...	G-84

FIGURES (Continued)

	Page
G-47. Three-Pathway RELAP Fit to the Lithium (mass-based normalization) Breakthrough Curve (diamonds) Using Flow Pathways Deduced from RELAP Fits to TFBA and Bromide Breakthrough Curves with Maximum Possible Differences (Figure G-44).....	G-84
G-48. MULTRAN Fit to Lithium (mass-based normalization) Breakthrough Curve (diamonds) Assuming Two Single-porosity Flow Pathways Deduced from RELAP Fits to TFBA and Bromide Breakthrough Curves (not shown)	G-85
G-49. Multi-Pathway RELAP Fit to Microsphere Breakthrough Curve Using Flow Pathways Deduced from RELAP Fits to TFBA and Bromide Breakthrough Curves with Minimum Possible Differences (Figure G-43).....	G-86
G-50. Two-Pathway RELAP Fits to Iodide (blue diamonds) and Perrhenate (magenta squares) (mass-based normalizations for both tracers) Breakthrough Curves in Second Cross-Hole Tracer Test at Site 22	G-87
G-51. Single-Pathway RELAP Fits to Iodide (blue diamonds) and Perrhenate (magenta squares) (both mass-based normalizations) Breakthrough Curves in Second Cross-Hole Tracer Test at Site 22	G-88
G-52. Normalized Concentrations of Nonsorbing Tracers used in the First Cross-Hole Tracer Test at Site 22 Minus Their Normalized Concentrations Prior to Pump Stoppage as a Function of Time Since Pumping Resumed	G-91
G-53. Schematic Illustration of One Possible Scenario for Tracer Drift at Site 22 Qualitatively Consistent with Observed Tracer Responses upon Resumption of Pumping after 159 Days of No Pumping	G-92
G-54. Graphical Depiction of the Analysis of Tracer Plume Migration during the 159-day Flow Interruption between Two Cross-Hole Tracer Tests at Site 22.....	G-94
G-55. Batch Sorption Data and Freundlich Isotherm Fits to the Data for Lithium Sorption onto Alluvium from Two Different Intervals of 22PC Within the Zone Tested in the Field.....	G-102
H-1. Particle Size Distributions of Material in NC-EWDP-19D and NC-EWDP-19P.....	H-2
H-2. Best Fits of the Three-Component Cation-Exchange Model to the Lithium Sorption Isotherm (left) and the (Na ⁺ + K ⁺) and Ca ⁺⁺ Concentration Data (right) for Alluvium Material from NC-EWDP-19D at 123 to 125 m (405 to 410 ft)	H-9
H-3. Best Fits of the Three-Component Cation-Exchange Model to the Lithium Sorption Isotherm (Left) and the (Na ⁺ + K ⁺) and Ca ⁺⁺ Concentration Data (Right) for Alluvium Material from NC-EWDP-19D at 128 to 130 m (420 to 425 ft)	H-9
H-4. Column Data and MULTRAN Fits for Experiments with a LiBr Injection Concentration of 0.0275 M.....	H-13
H-5. Column Data and MULTRAN Fits for Experiments with a LiBr Injection Concentration of 0.006 M.....	H-14
H-6. Column Data and MULTRAN Fits for Experiments with a LiBr Injection Concentration of 0.0013 M.....	H-15
K-1. NC-EWDP-19IM2 Well Completion Diagram	K-4

FIGURES (Continued)

	Page
K-2. NC-EWDP-22S Well Completion Diagram	K-5
K-3. NC-EWDP-22PA Well Completion Diagram	K-6
K-4. NC-EWDP-22PB Well Completion Diagram	K-7
K-5. NC-EWDP-22PC Well Completion Diagram	K-8
K-6. NC-EWDP-19D Well Completion Diagram	K-9
M-1. Pressure Readings from Transducers 8 and 9 in ONC-1 from April 24, 1996, to May 29, 1996	M-4
M-2. Differences in Pressure Readings from Transducers 8 and 9 in ONC-1 from April 24, 1996, to May 29, 1996	M-4
M-3. Differences in Pressure Readings from Transducers 8 and 9 in ONC-1, February 3 to 26, 1997, and October 28 to December 4, 1997	M-5
M-4. Uncorrected/Unfiltered ONC-1 Drawdown Curves from Pumping of UE25c#3 between May 8, 1996, and November 12, 1997, Based on Pressure Data from Transducers 8 and 9	M-6
N-1. Absolute Pressures Measured by Four Transducers (SNs 2295, 2554, 2292, and 2693)	N-6
N-2. Pressures Measured in the Second Interval from the Surface of 22S by Transducer SN 2323	N-8
N-3. Pressures Measured in the 22PA Deep Piezometer at the Start of Pumping of Zone 2 of 22S.....	N-9
N-4. Pressures Measured in the 22PB Shallow Piezometer at the Start of Pumping of Zone 2 of 22S.....	N-10
N-5. Pressures Measured in the 22PA Shallow Piezometer at the Start of Pumping of Zone 2 of 22S.....	N-11
Q-1.1. Drawdown in Screen #1 at NC-EWDP-22PA	Q-6
Q-1.2. Drawdown in Screen #1 at NC-EWDP-22PA	Q-7
Q-1.3. Drawdown in Screen #1 at NC-EWDP-22PA	Q-8
Q-1.4. Derivative of the 7.0×10^{-1} Type Curve of Hantush (1956 [DIRS 165169]) to which the Drawdown Data in Screen #1 at NC-EWDP-22PA	Q-9
Q-1.5. Derivative of the 7.0×10^{-1} Type Curve of Hantush (1956 [DIRS 165169]) to which the Drawdown Data in Screen #1 at NC-EWDP-22PA	Q-10
Q-1.6. Drawdown Data and Associated Derivatives in Screen #1 at NC-EWDP-22PA.....	Q-11
Q-1.7. Derivative of Drawdown Data in Screen #1 at NC-EWDP-22PA in Response to Pumping Screen #1 in NC-EWDP-22S	Q-12
Q-2.1. Drawdown in Screen #2 at NC-EWDP-22PA	Q-13
Q-2.2. Drawdown in Screen #2 at NC-EWDP-22PA	Q-14
Q-2.3. Drawdown in Screen #2 at NC-EWDP-22PA	Q-15
Q-2.4. Derivative of the 5.0×10^{-1} Type Curve of Hantush (1956 [DIRS 165169]) to which the Drawdown Data for Screen #2 are Fitted.....	Q-16

FIGURES (Continued)

	Page
Q-2.5. Derivative of the 5.0×10^{-1} Type Curve of Hantush (1956 [DIRS 165169]) to which the Drawdown Data for Screen #2 are Fitted.....	Q-17
Q-2.6. Drawdown Data and Associated Derivatives in Screen #2 at NC-EWDP-22PA.....	Q-18
Q-2.7. Derivative of Drawdown Data in Screen #2 at NC-EWDP-22PA	Q-19
Q-3.1. Drawdown in Screen #3 at NC-EWDP-22PB.	Q-20
Q-3.2. Drawdown in Screen #3 at NC-EWDP-22PB.	Q-21
Q-3.3. Drawdown in Screen #3 at NC-EWDP-22PB	Q-22
Q-3.4. Derivative of the 7.5×10^{-2} Type Curve of Hantush (1956 [DIRS 165169]) to which the Drawdown Data for Screen #3 are Fitted.....	Q-23
Q-3.5. Derivative of the 7.5×10^{-2} Type Curve of Hantush (1956 [DIRS 165169]) to which the Drawdown Data for Screen #3 are Fitted.....	Q-24
Q-3.6. Drawdown Data and Associated Derivatives in Screen #3 at NC-EWDP-22PB	Q-25
Q-3.7. Drawdown Data and Associated Derivatives in Screen #3 at NC-EWDP-22PB	Q-26
Q-4.1. Drawdown in Screen #4 at NC-EWDP-22PB	Q-27
Q-4.2. Drawdown in Screen #4 at NC-EWDP-22PB	Q-28
Q-4.3. Drawdown in Screen #4 at NC-EWDP-22PB	Q-29
Q-4.4. Derivative of the 7.5×10^{-2} Type Curve of Hantush (1956 [DIRS 165169]) to which these Data are Fitted.....	Q-30
Q-4.5. Derivative of the 7.5×10^{-2} Type Curve of Hantush (1956 [DIRS 165169]) to which these Data are Fitted.....	Q-31
Q-4.6. Drawdown Data and Associated Derivatives in Screen #4 at NC-EWDP-22PB	Q-32
Q-4.7. Drawdown Data and Associated Derivatives in Screen #4 at NC-EWDP-22PB	Q-33

INTENTIONALLY LEFT BLANK

TABLES

	Page
3-1. Software Used in Support of This Scientific Analysis	3-1
3-2. Exempt Software Used in Support of This Scientific Analysis.....	3-4
4-1. Input Data.....	4-1
5-1. Assumptions.....	5-1
6.1-1. Approximate Interborehole Distances at the Midpoints of Hydrogeologic Intervals as Monitored During Hydraulic Tests at the C-Wells Complex, August 1995 to April 1996	6-4
6.1-2. Stratigraphy of Miocene Tuffaceous Rocks in the C-Wells Area	6-5
6.1-3. Features, Events, and Processes Included in TSPA-LA and Relevant to This Report.....	6-18
6.2-1. Highlights of Testing at the C-Wells Complex to Determine Hydrologic Properties (See Appendix C for Complete Description of Tests).....	6-21
6.2-2. Ranges of Hydrologic Parameters Derived from C-Wells Cross-Hole Hydraulic Testing.....	6-26
6.2-3. Transmissivities and Storativities of Distant Wells for the Long-Term Pumping Test.....	6-28
6.2-4. Calculated and Reported Anisotropies and Principal Directions.....	6-28
6.3-1. Tracer Testing at the C-Wells Complex to Determine Transport Properties.....	6-33
6.3-2. Ratios of Observed Tracer Arrival Times and Distances Squared, as well as Apparent Flow Anisotropy Ratios, for C-Wells Nonsorbing Tracer Tests	6-40
6.3-3. Transport Parameter Estimates Deduced from the Lower Bullfrog and Prow Pass Multiple-Tracer Tests.....	6-41
6.3-4. Lithium Partition Coefficients Derived from Field Tracer Tests and Laboratory Measurements	6-43
6.3-5. Transport Parameters Obtained from RELAP Fits to Iodide Data Shown in Figure 6.3-4.....	6-46
6.3-6. Transport Parameter Ranges from Multiple-Tracer Tests at the C-Wells	6-46
6.4-1. Highlights of Testing at the ATC and Site 22 to Determine Alluvium Hydrologic Properties (See Appendix F for Complete Description of Tests)	6-49
6.4-2. Highlights of Testing at Nye County Site 22 to Determine Alluvium Hydrologic Properties (see Appendix F for Complete Description of Tests).....	6-49
6.4-3. Summary of the Hydraulic Parameter Estimates for Nye County Site 22.....	6-54
6.5-1. Summary of Tracers and Test Conditions in the Three Single-Well Tracer Tests in NC-EWDP-19D	6-59
6.5-2. Summary of Tracers and Test Conditions in the Two Single-Well Tracer Tests in NC-EWDP-22S.....	6-59
6.5-3. Tracer Characteristics, Injection Masses, Injection Concentrations, and Fractional Recoveries in the Two Cross-Hole Tracer Tests at Site 22	6-61

TABLES (Continued)

	Page
6.5-4. Times and Pumped Volumes Associated with Each of the Single-Well Tracer Test Arrival Times Used in the Different Methods of Estimating Groundwater Velocities	6-72
6.5-5. Specific Discharges and Groundwater Velocities Estimated from the Different Ambient Flow Velocity Analysis Methods as a Function of Assumed Flow Porosity at 19D	6-72
6.5-6. Specific Discharges and Seepage Velocities at 22S Estimated from Different Drift Analysis Methods as a Function of Assumed Flow Porosity	6-73
6.5-7. CML Microsphere Filtration Parameters	6-77
6.5-8. Transport Parameter Estimates Deduced from Tracer Tests in Saturated Alluvium.....	6-78
7-1. Output Data.....	7-10
B-1. Wells Discussed in This Report and Their Abbreviations.....	B-1
C-1. Location of Packers Emplaced in the C-Wells Complex for Hydraulic Tests, 1995 to 1997	C-4
C-2. Operative Transducers in the C-Wells, 1995 to 1997.....	C-5
C-3. Barometric Efficiency Values Determined for Borehole Intervals Monitored at the C-Wells Complex Through May 13, 1996	C-11
C-4. Interval Discharges 5,800 Minutes after Pumping Started in Hydraulic Tests in UE-25 c#3, June 1995 to November 1997.....	C-15
C-5. Barometric Efficiency in the C-Wells and UE-25 ONC-1	C-35
C-6. Hydrologic Properties of the Prow Pass Interval in the C-Wells and Input Parameters Used in Obtaining Them	C-39
C-7. Results of Hydraulic Tests in Borehole UE-25 c#3, June 1995 to November 1997	C-45
C-8. Hydrologic Properties Computed from Observation Well Responses to Pumping in UE-25-c#3, May 1995 to November 1997	C-54
C-9. Hydrologic Properties Determined from Drawdown in Observation Wells as a Function of Distance from the Pumping Well UE-25 c#3, May 1996 to November 1997.....	C-63
C-10. Transmissivities and Storativities Calculated by the Cooper-Jacob Method Using the Filtered and Derivative-Analyzed Data	C-72
C-11. Transmissivities and Storativities of Distant Wells for the Long-Term Pumping Test.....	C-72
C-12. Calculated and Reported Anisotropies and Principal Directions.....	C-78
D-1. Ratios of Observed Tracer Arrival Times and Distances Squared, as well as Apparent Flow Anisotropy Ratios, for C-Wells Nonsorbing Tracer Tests	D-29
D-2. Summary of Results and Transport Properties for the Bullfrog and Tram Tuffs from Nonsorbing Tracer Tests	D-30
D-3. Summary of Results and Transport Properties in a Partly Recirculating Tracer Test from Borehole c#3 to c#2 and from Borehole c#1 to c#2, Prow Pass Tuff.....	D-32

TABLES (Continued)

	Page
D-4. Tracer Characteristics, Injection Masses, and Injection Concentrations in the Two Multiple-Tracer Tests.....	D-35
D-5. Average Production and Recirculation Rates During the Bullfrog and Prow Pass Tracer Tests and Summary of Flow Interruptions During the Prow Pass Test	D-38
D-6. RELAP Model Parameters Providing the Best Fits to the Bullfrog Tracer Test Data	D-55
D-7. RELAP Parameters Providing the Best Fits to the First 1200 Hours of Prow Pass Tracer Test Data.....	D-57
D-8. Microsphere Filtration and Detachment Parameters Associated with the Fits Shown in Figure D-29.....	D-59
D-9. Filtration and Detachment Rate Constants for the CML Microspheres in the Prow Pass Tuff Tracer Test	D-61
D-10. Transport Parameter Estimates Deduced from the Bullfrog and Prow Pass Multiple-Tracer Tests.....	D-62
D-12. Transport Parameters Estimates from RELAP Fits of Figures D-31, D-32, and from the Fits to the PFBA and Bromide Responses in the Prow Pass Tuff.....	D-75
D-13. Transport Parameters Obtained from RELAP Fits to Iodide Data Shown in Figure D-35.....	D-78
D-14. Transport Parameter Ranges from Multiple-Tracer Tests at the C-wells	D-78
E-1. Comparison of Major Ion Chemistry of J-13 and c#3	E-2
E-2. Summary of C-Wells Experimental Batch Lithium Sorption Test Matrix	E-3
E-3. X-Ray Diffraction Results for Tuffs from Prow Pass, Bullfrog, and Tram Units	E-5
E-4. Lithium Sorption Isotherm Parameters Associated with the Different C-wells Tuffs	E-16
E-5. Cation-exchange Capacity Measurements for C-wells Tuffs	E-18
E-6. Measured Porosities, Permeabilities, and Matrix Diffusion Coefficients of Bromide and PFBA in C-wells Tuffs.....	E-29
E-7. Results of RELAP Fits to Rising Limbs of Lithium and Bromide Breakthrough Curves in Crushed Tuff Columns	E-32
E-8. Experimental Conditions for the Iodide Fracture Transport Tests, Upper Prow Pass Tuff Core (Core 1)	E-43
E-9. Experimental Conditions for the Multiple-Tracer Fracture Transport Tests, Upper Prow Pass Tuff Core (Core 1).....	E-44
E-10. Experimental Conditions for the Iodide Fracture Transport Tests, Central Prow Pass Tuff Core (Core 2)	E-45
E-11. Experimental Conditions for the Multiple-Tracer Fracture Transport Tests, Central Prow Pass Tuff Core (Core 2).....	E-45
E-12. Experimental Conditions for the Multiple-Tracer Fracture Transport Tests, Lower Prow Pass Tuff Core (Core 3).....	E-46
E-13. Experimental Conditions for the Multiple-Tracer Fracture Transport Tests, Lower Bullfrog Tuff Core (Core 4).....	E-47

TABLES (Continued)

	Page
E-14. Simulation Results for the Three Iodide Tracer Tests in Upper Prow Pass Tuff Core (Core 1)	E-54
E-15. Simulation Results for the Three Iodide Tracer Tests in Central Prow Pass Tuff Core (Core 2)	E-54
E-16. Best-Fit Model Parameters for the Multiple-Tracer Tests Conducted in Cores 1 and 2.....	E-58
E-17. Best-Fit Transport Parameters for the Multiple-Tracer Tests Conducted in Cores 3 and 4.....	E-62
E-18. Comparison of Matrix Diffusion Coefficients Calculated from Fractured-Core Tracer Tests and from Diffusion-Cell Experiments.....	E-67
F-1. Zones and Screen Depths in Site 22 Wells	F-39
F-2. Summary of the Pumping Test Duration and Rates.....	F-40
F-3. Results of the Correlation and Linear Regression Analysis Using Background Pressures in the Different Aquifer Zones.....	F-43
F-4. Summary of the Parameter Estimates for Nye County Site 22.....	F-82
G-1. Flow System Parameters Used in the Single-Well Simulations	G-6
G-2. Nonflow-System Input Parameters for the Single-Well Simulations	G-6
G-3. Single-Well Tracer Test Response Characteristics Consistent with the Conceptual Models of Figure G-1.....	G-15
G-4. Combinations of Flow-System Parameters and Production Flow Rate that Result in a Mean Nonsorbing Tracer Residence Time of 150 Hours in a Cross-Hole Tracer Test	G-27
G-5. Summary of Tracers and Test Conditions in the Three Single-Well Tracer Tests in NC-EWDP-19D	G-28
G-6. Summary of Tracers and Test Conditions in the Two Single-Well Tracer Tests in NC-EWDP-22S.....	G-29
G-7. Times and Pumped Volumes Associated with Each of the Single-Well Tracer Test Arrival Times Used in the Different Methods of Estimating Groundwater Velocities	G-36
G-8. Specific Discharges and Seepage Velocities at 19D Estimated from the Different Drift Analysis Methods as a Function of Assumed Flow Porosity.....	G-51
G-9. Specific Discharges and Seepage Velocities at 22S Estimated from Different Drift Analysis Methods as a Function of Assumed Flow Porosity	G-51
G-10. Specific Discharge and Seepage Velocity Estimates at 22S Using Different Natural Gradient Estimates and Assuming a Hydraulic Conductivity of 12 m/day from Cross-Hole Hydraulic Testing at Site 22	G-51
G-11. MULTRAN Model Parameters Associated with the Matches to the 22S Single-well Tracer Test Breakthrough Curves Shown in Figure G-32 (diffusion-into-blocks model).....	G-60

TABLES (Continued)

	Page
G-12. MULTRAN Model Parameters Associated with the Matches to the 22S Single-well Tracer Test Breakthrough Curves Shown in Figure G-33 (diffusion-into-layers model).....	G-64
G-13. Tracer Characteristics, Injection Masses, Injection Concentrations, and Fractional Recoveries in the Two Cross-Hole Tracer Tests at Site 22	G-66
G-14. RELAP Model Parameters Yielding Fits to the Solute Responses for the Three Pathways in the First Cross-hole Tracer Test at Site 22 for the Case with the Minimum Possible Differences between the TFBA and Bromide Breakthrough Curves and for the Single Pathway Interpreted for DFBA (Figure G-43).....	G-80
G-15. RELAP Model Parameters Yielding Fits to the TFBA, Bromide, and Lithium Responses in the First Cross-Hole Tracer Test at Site 22 for the Case with the Maximum Possible Differences between the TFBA and Bromide Breakthrough Curves (Figure G-44).....	G-81
G-16. RELAP Model Parameters Yielding the Single-pathway Fits to the TFBA and Bromide Responses in the First Cross-hole Tracer Test at Site 22 when the Bromide Breakthrough Curve is Adjusted so that the Recoveries of TFBA and Bromide are Approximately the Same (Figure G-45)	G-83
G-17. CML Microsphere Filtration Parameters for Multi-pathway Fits to Microsphere Response Using Nonreactive Transport Parameters Deduced from Fits to TFBA and Bromide Breakthrough Curves Assuming Minimum and Maximum Possible Amounts of Matrix Diffusion	G-86
G-18. RELAP Model Parameters Yielding Fits to Iodide and Perrhenate Responses in Second Cross-hole Tracer Test at Site 22 (Figure G-50).....	G-88
G-19. RELAP Model Parameters Associated with Single-pathway Fits to the Iodide and Perrhenate Responses in the Second Cross-hole Tracer Test at Site 22	G-89
G-20. Transport Parameter Estimates Deduced from Tracer Tests in Saturated Alluvium....	G-95
G-21. Calculated Lithium Partition Coefficients (K_d Values) for Various Assumed Porosities Using Retardation Factors Derived from Field Tracer Tests.....	G-101
G-22. Lithium Partition Coefficients (K_d Values) for Alluvium from NC-EWDP-22PC over a Wide Range of Lithium Concentrations Using Freundlich Isotherm Parameters obtained from Fitting Batch Sorption Data.....	G-102
H-1. Mineralogy of Alluvium Samples Used in the Cation-Exchange-Capacity and Lithium Batch-Sorption Experiments Determined by Quantitative X-ray Diffraction.....	H-3
H-2. Surface Areas and Lithium and Cesium Cation-Exchange-Capacities (CEC) of Alluvium Samples Used in the Lithium Batch-Sorption Experiments.....	H-5
H-3. Cation Exchange Coefficients (CEC) and Freundlich Isotherm Parameters Resulting in Best Fits to the Li^+ , Na^+ , and Ca^{++} Data from the Lithium Batch-Sorption Experiments for Alluvium Material	H-8
H-4. Major Ion Chemistry of NC-EWDP-19D Water Used in the Experiments.....	H-11
H-5. MULTRAN Model Parameters Associated with the Fits to the Column Transport Data	H-16

TABLES (Continued)

	Page
J-1. Mineral Weight Percentages and Reported Errors (in Weight Percent Units) from Quantitative XRD Analyses of UE25c#2-2406 and UE25c#1-2346.....	J-2
N-1. Serial Numbers, Tests, and Borehole Intervals for Key Pressure Transducers Used in Site 22 Hydraulic and Tracer Tests.....	N-2
O-1. Summary of Borehole Samples Examined for Sulfide Occurrence.....	O-2
O-2. Observed Sulfide Occurrences.....	O-3
O-3. Summary of Sulfide Occurrences and Lithostratigraphy in Cuttings from Boreholes USW H-3, H-4, and H-5	O-5
O-4. Summary of Legacy and New Petrographic Observations of Sulfides.....	O-6
Q-1. Summary of Hydraulic Parameters Obtained from Analyzing the Hydraulic Tests at NC-EWDP-22	Q-5
R-1. Predicted May 1996 Flow Rate Based on the February and May 1996 Drawdowns after 5,800 Minutes of Pumping and the February 1996 Flow Rate Using Equation R-1.....	R-3
R-2. Predicted June 1995 Flow Rate Based on the February and May 1996 Drawdowns after 5,800 Minutes of Pumping and on the February and May 1996 Flow Rates	R-5

ACRONYMS AND ABBREVIATIONS

ATC	Alluvial Testing Complex
BLS (bls)	below land surface
CDF	cumulative distribution function
DFBA	difluorobenzoic acid or difluorobenzoate
DTN	data tracking number
EPM	equivalent porous medium
FBA	fluorinated benzoic acid or fluorinated benzoate
FEHM	finite-element heat and mass
FEP	feature, event, and process
LA	license application
MTC	mass transfer coefficient (for matrix diffusion)
NTS	Nevada Test Site
PDF	probability distribution function
PFBA	pentafluorobenzoic acid or pentafluorobenzoate
SMR	software management report
SZ	saturated zone
TDMS	Technical Data Management System
TFBA	trifluorobenzoic acid
TSPA	total system performance assessment
USGS	U.S. Geological Survey
YMP	Yucca Mountain Project
YMRP	<i>Yucca Mountain Review Plan, Final Report</i>

INTENTIONALLY LEFT BLANK

1. PURPOSE

The purpose of this scientific analysis is to document the results and interpretations of field experiments that test and validate conceptual flow and radionuclide transport models in the saturated zone (SZ) near Yucca Mountain, Nevada. The test interpretations provide estimates of flow and transport parameters used in the development of parameter distributions for total system performance assessment (TSPA) calculations. These parameter distributions are documented in *Site-Scale Saturated Zone Transport* (SNL 2007 [DIRS 177392]), *Saturated Zone Colloid Transport* (BSC 2004 [DIRS 170006]), and *Saturated Zone Flow and Transport Model Abstraction* (SNL 2007 [DIRS 177390]).

Although this TWP was prepared before transition to the Lead Laboratory, it was considered appropriate for developing this report, because it was prepared in compliance with LP-2.29Q-BSC, *Planning for Science Activities* (a BSC procedure (predecessor)), which corresponds to SCI-PRO-002, *Planning for Science Activities* (the Lead Laboratory procedure). Specifically, this scientific analysis contributes the following to the assessment of the capability of the SZ to serve as part of a natural barrier for waste isolation for the Yucca Mountain repository system:

- The bases for selection of conceptual flow and transport models in the saturated volcanics and the saturated alluvium located near Yucca Mountain.
- Results and interpretations of hydraulic and tracer tests conducted in saturated fractured volcanics at the C-wells complex near Yucca Mountain. The test interpretations include estimates of hydraulic conductivities, anisotropy in hydraulic conductivity, storativities, total porosities, effective porosities, longitudinal dispersivities, matrix diffusion mass transfer coefficients, matrix diffusion coefficients, fracture apertures, and colloid transport parameters.
- Results and interpretations of hydraulic and tracer tests conducted in saturated alluvium at the Alluvial Testing Complex (ATC) located at the southwestern corner of the Nevada Test Site (NTS) and at Nye County Site 22, located just east of Fortymile Wash about 4.5 km northeast of the ATC (and about 13 km from the repository). The test interpretations include estimates of hydraulic conductivities, storativities, total porosities, effective porosities, longitudinal dispersivities, matrix diffusion mass transfer coefficients, and colloid transport parameters.
- Comparisons of sorption parameter estimates for a reactive solute tracer (lithium ion) derived from the C-wells field tracer tests and laboratory tests using C-wells core samples.
- Sorption parameter estimates for lithium ion derived from laboratory tests using alluvium samples from ATC well NC-EWDP-19D and from well NC-EWDP-22PC. For the latter well, these estimates allow a comparison of laboratory- and field-derived sorption parameters to be made for saturated alluvium (cross-hole tests were never conducted at the ATC, so a similar comparison is not possible for that location).

The comparisons between laboratory- and field-derived sorption parameter estimates for lithium ion are used to assess whether sorption parameters determined in the laboratory can be used reliably to predict field-scale transport. Favorable comparisons of lithium-ion sorption will lend credibility to the Yucca Mountain Project (YMP) use of laboratory-derived radionuclide sorption parameters when modeling field-scale radionuclide transport. The use of laboratory data for radionuclides is necessary because radionuclides cannot be tested in the field.

Additionally, Appendix O of this scientific analysis provides a survey of sulfide mineral distribution in the saturated zone at Yucca Mountain. This information supports the concept that reducing geochemical conditions may exist in at least portions of the saturated zone near Yucca Mountain. As discussed in *Impacts of Solubility and Other Geochemical Processes on Radionuclide Retardation in the Natural System - Rev 01* (BSC 2006 [DIRS 178672]), such reducing geochemical conditions would result in significantly greater sorption as well as lower solubility of some radionuclides than is predicted in Yucca Mountain performance assessments (which assume oxidizing geochemical conditions everywhere in the saturated zone). Potentially affected radionuclides include ⁹⁹Tc, isotopes of neptunium, and isotopes of uranium and plutonium.

Saturated-zone geochemistry measurements, including Eh and pH, and water-level measurements are not addressed in this scientific analysis, because they can be used directly as inputs (without intermediate analyses) in downstream reports. Geochemistry measurements are used extensively in Appendices A and B of *Saturated Zone Site-Scale Flow Model* (SNL 2007 [DIRS 177391]) to delineate flow pathways. Eh and pH measurements are factored into the development of radionuclide K_d distributions in Appendix A of *Site-Scale Saturated Zone Transport* (SNL 2007 [DIRS 177392]) and in *Radionuclide Transport Models Under Ambient Conditions* (SNL 2007 [DIRS 177396]); and water-level measurements are used as calibration targets in *Saturated Zone Site-Scale Flow Model* (SNL 2007 [DIRS 177391]).

None of the information in Rev. 01 of this analysis report was modified for Rev. 02 (the current revision). Rather, Rev. 02 contains additions to the report to include the results and interpretations of hydraulic and tracer tests conducted in the saturated alluvium at Nye County Site 22 since Rev. 01 was issued and also the survey of sulfide mineral distribution in the SZ at Yucca Mountain mentioned above. The additions to include the results and interpretations of testing at Site 22 appear primarily in Sections 6.4 and 6.5, and in Appendices F and G. Also, Appendix N provides a qualification of the hydraulic testing data at Site 22.

The work activities in Rev. 02 of this scientific analysis are governed by the work direction and planning document *Technical Work Plan for Saturated Zone Flow and Transport Modeling* (BSC 2006 [DIRS 177375], Sections 1.2.3, 2.1.3, and 2.2.3). There are only very minor deviations from this TWP in this report, and they have no technical impact on this or other SZ analysis and model reports:

- There is no discussion of new (since 2004) Eh, pH, and redox couple data in this report. These data were not included in Rev. 01 of the report, and none of the new data generated since 2004 change the conceptual understanding of the distribution of reducing geochemical conditions in the saturated zone near Yucca Mountain (most of the new measurements were near discharge locations of the flow system or were

believed to be far removed from potential flow pathways from the repository footprint). Also, Eh, pH, and redox couple data relevant to potential radionuclide transport from Yucca Mountain are discussed in considerable detail in *Impacts of Solubility and Other Geochemical Processes on Radionuclide Retardation in the Natural System - Rev 01* (BSC 2006 [DIRS 178672]).

- Comparisons of alluvium hydraulic parameter estimates and specific discharge estimates to estimates obtained from the calibrated SZ site-scale flow model are discussed in *Saturated Zone Site-Scale Flow Model* (SNL 2007 [DIRS 177391]) rather than in this analysis report.
- More software items are listed in Table 3-1 and used in this analysis than are listed in Table 6 of the TWP.

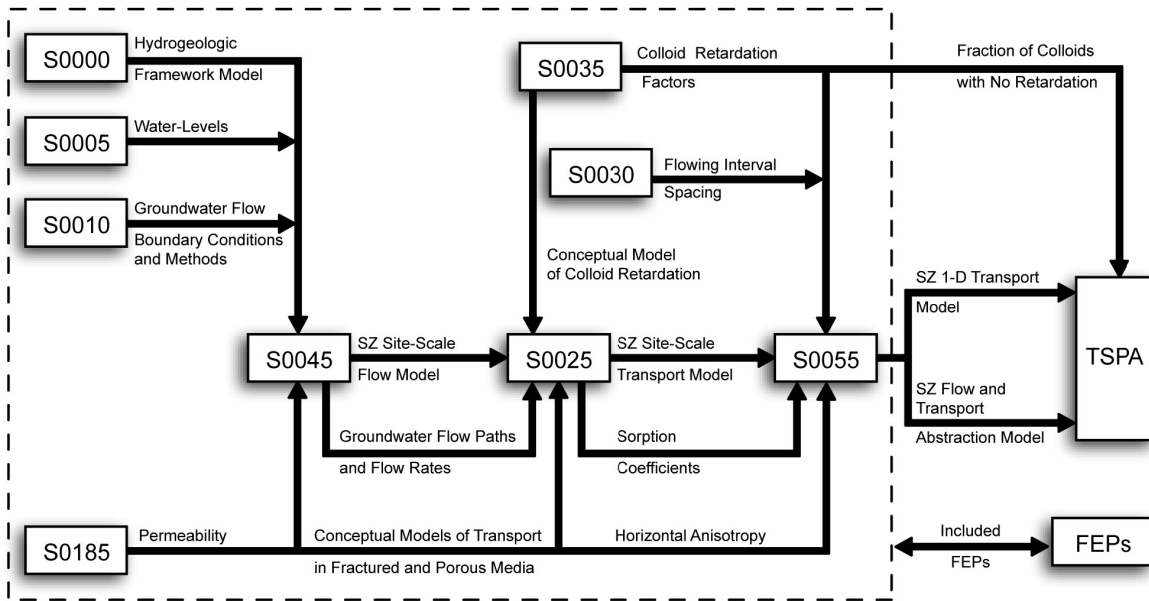
The data and analyses documented in this report are used as scientific supporting information in other Yucca Mountain Project reports including:

- *Saturated Zone Site-Scale Flow Model*
- *Site-Scale Saturated Zone Transport*
- *Saturated Zone Colloid Transport*
- *Saturated Zone Flow and Transport Model Abstraction*.

Figure 1-1 shows the relationship of this report to other analysis and model reports that pertain to flow and transport in the SZ. Figure 1-1 also shows the flow of key information among the SZ reports. It should be noted that Figure 1-1 does not contain a complete representation of the data and parameter inputs and outputs of all SZ reports, nor does it show inputs external to this suite of SZ reports. In addition to the SZ analysis and model reports in Figure 1-1, this analysis report provides input (longitudinal dispersivity estimates from C-wells tracer tests) to *Radionuclide Transport Models Under Ambient Conditions* (SNL 2007 [DIRS 177396]) and *Particle Tracking Model and Abstraction of Transport Processes* (SNL 2007 [DIRS 177397]).

The bases for the conceptual models and the estimates of flow and transport parameters presented in this scientific analysis are derived from tests conducted at only one location in the saturated fractured volcanics (C-wells complex) and two locations in the saturated alluvium (ATC and Nye County Site 22). Consequently, several other sources of information are used to develop broader uncertainty distributions for flow and transport parameters in the TSPA for license application (LA) analyses. The development and bases of these distributions are documented in *SZ Flow and Transport Model Abstraction* (SNL 2007 [DIRS 177390]), where it is shown that the overall parameter distributions used in the TSPA-LA analyses include considerations of literature data, expert elicitation input, and peer review input. The only uncertainty distribution presented in this report is one for the north-south/east-west anisotropy ratio of horizontal hydraulic conductivity in the fractured volcanics (Section 6.2.6).

The SZ FEPs included in the TSPA-LA and supported by the results of this report are listed in Table 6.1-3.



Legend	
S0000 - Hydrogeologic Framework Model	MDL-NBS-HS-000024
S0005 - Water-Level Data Analysis	ANL-NBS-HS-000034
S0010 - Recharge and Lateral Groundwater Flow Boundary Conditions	ANL-NBS-MD-000010
S0025 - Site-Scale Saturated Zone Transport	MDL-NBS-HS-000010
S0030 - Probability Distribution for Flowing Interval Spacing	ANL-NBS-MD-000003
S0035 - Saturated Zone Colloid Transport	ANL-NBS-HS-000031
S0045 - Site-Scale Saturated Zone Flow Model	MDL-NBS-HS-000011
S0055 - Saturated Zone Flow and Transport Model Abstraction	MDL-NBS-HS-000021
FEPs - Features, Events, and Processes in SZ Flow and Transport	DTN: MO0508SEPFEPPLA.002
S0185 - Saturated Zone In-Situ Testing	ANL-NBS-HS-000039

00438DC_001d.ai

NOTE: For illustrative purposes only. This figure is a simplified representation of the flow of information among SZ reports. See the DIRS of each report for a complete listing of data and parameter inputs. This figure does not show inputs external to this suite of SZ reports.

Figure 1-1. Relationships and Flow of Key Information among Reports Pertaining to Flow and Transport in the SZ Source

2. QUALITY ASSURANCE

Development of this report and supporting analyses are subject to *Quality Assurance Requirements Document* (QARD) (DOE 2006 [DIRS 177092]). Approved quality assurance procedures as indicated in *Technical Work Plan For: Natural System - Saturated Zone Analysis And Model Report Integration* (BSC 2006 [DIRS 177375]) have been used to conduct and document the activities described in this report. This report was prepared in accordance with SCI-PRO-005, *Scientific Analyses and Calculations*. Also, SCI-PRO-001, *Qualification of Unqualified Data*, was implemented to qualify unqualified data for specific use in this report. The technical work plan (BSC 2006 [DIRS 177375]) also identifies the methods used to control the electronic management of data. These methods were used to document the activities described in the technical work plan (TWP) and IM-PRO-002, *Control of the Electronic Management of Information*.

Although this TWP was prepared before transition to the Lead Laboratory, it was considered appropriate for developing this report, because it was prepared in compliance with LP-2.29Q-BSC, *Planning for Science Activities* (a BSC procedure (predecessor)), which corresponds to SCI-PRO-002, *Planning for Science Activities* (the Lead Laboratory procedure).

Planning and preparation of this report was initiated under the BSC QA Program. Therefore, forms and associated documentation/records prepared prior to October 2nd, 2006, the date this work transitioned to the Lead Laboratory, were completed in accordance with BSC procedures. Forms and associated documentation completed on or after October 2nd, 2006 were prepared in accordance with Lead Laboratory procedures.

This scientific analysis provides information on the saturated zone (SZ), which is part of a natural barrier classified in *Q-List* (BSC 2004 [DIRS 168361], Table A-1) as Safety Category because it is important to waste isolation. The results of this report are important to the demonstration of compliance with the postclosure performance objectives (10 CFR 63.114 [DIRS 176544]). The report contributes to the analysis and modeling data used to support performance assessment.

INTENTIONALLY LEFT BLANK

3. USE OF SOFTWARE

3.1 SOFTWARE TRACKED BY CONFIGURATION MANAGEMENT

The computer codes used directly in this scientific analysis are summarized in Table 3-1. The qualification status of the software is indicated in the electronic Document Input Reference System database and in the Software Configuration Management System Baseline Report. All software was obtained from Software Configuration Management and is appropriate for the application. Qualified codes were used only within the range of validation as required by IM-PRO-003, *Software Management*, the procedure governing software use when the outputs of this report were generated.

Table 3-1. Software Used in Support of This Scientific Analysis

Software Name and Version (V)	Software Tracking Number (STN)/DIRS Number	Description	Computer, Platform, and Operating System
2WELLS_2D V 1.0	10665-1.0-00 [DIRS 159067]	This software is used in the analysis of longitudinal dispersivity in the Prow Pass Tuff C-wells field tracer test. It is used to obtain predicted tracer responses in homogeneous, isotropic, confined (two-dimensional) aquifers under partial recirculation conditions. It has been used both to correct dispersion-coefficient estimates for dispersion caused by a dipole-flow pattern and for pretest predictions of ATC cross-hole tracer tests.	LANL, PC, Windows 2000/NT 4.0*/98
2WELLS_3D V 1.0	10667-1.0-00 [DIRS 159036]	This software is used to obtain predicted tracer responses in homogeneous, isotropic, confined three-dimensional aquifers under partial recirculation conditions. It has been used both to correct dispersion-coefficient estimates for dispersion caused by a dipole-flow pattern and for pretest predictions of ATC cross-hole tracer tests.	LANL, PC, Windows 2000/NT 4.0*/98
DIFFCELL V 2.0	10557-2.0-00 [DIRS 159063]	This software is used in the analysis of laboratory diffusion cell experiments. It provides a numerical solution to an equation describing one-dimensional diffusive transport through a rock wafer with time-dependent concentration boundary conditions.	LANL, PC, Windows 2000/NT 4.0*
EQUILFIT V 1.0	10668-1.0-00 [DIRS 159064]	This software is used to obtain cation-exchange coefficients, given experimental data on cation sorption (both for sorbing and displaced cations) and given independent cation-exchange-capacity measurements.	LANL, PC, Windows 2000/NT 4.0*/98
Filter.vi V 1	10970-1-00 [DIRS 162668]	This software uses the standard Butterworth filter with standard coefficients. It is for filtering higher-frequency diurnal pressure changes due to barometric pressure changes and tidal effects.	USGS, PC, Windows 2000/NT 4.0*/98
Injection_Pumpback.vi V 1	10675-1-00 [DIRS 162749]	This software is used for tracer test analysis for single-well testing. Analysis considers tracer injection, drift, and pumpback.	USGS, PC, Windows 2000/NT 4.0*/98

Table 3-1. Software Used in Support of This Scientific Analysis (Continued)

Software Name and Version (V)	Software Tracking Number (STN)/DIRS Number	Description	Computer, Platform, and Operating System
rcv2amos.exe and MOENCH.vi, Function(1), V 1.0	10583-1.0-00 [DIRS 162750]	The software routine rcv2amos.exe is used to analyze cross-hole tracer tests. In conjunction with the use of rcv2amos.exe, the routine MOENCH.vi was developed to serve as a user interface and to display the results.	USGS, PC, Windows 2000*/NT 4.0/98
MOENCH.vi Function(2) V 1.0	10582-1.0-00 [DIRS 162752]	This software is used for the analysis of cross-hole tracer tests.	USGS, PC, Windows 2000*/NT 4.0/98
MULTRAN V 1.0	10666-1.0-00 [DIRS 159068]	This is a two-dimensional numerical model that uses an implicit-in-time, alternating-direction, finite-difference method to solve the equations describing multicomponent transport of sorbing and nonsorbing solutes in a dual-porosity medium. This software is used for analysis of laboratory crushed-rock and alluvium column experiments. It is also used for the analysis of the first peak in the Bullfrog Tuff C-wells field tracer test and for prediction and analysis of ATC tracer experiments.	LANL, PC, Windows 2000/NT 4.0*
Neuman.vi V 1.0	10972-1.0-00 [DIRS 162754]	This software displays the standard and accepted type curve for unconfined aquifers and allows the fitting of the input data curves over the type curve. The .vi extension displays the appropriate resulting hydrologic parameters associated with the data curve matching (transmissivity and storativity).	USGS, PC, Windows 2000/NT 4.0*/98
PEST V 5.5	10289-5.5-00 [DIRS 161564]	This software assists in data interpretation, model calibration, and predictive analysis. PEST adjusts model parameters and/or excitations until the fit between model output and field or laboratory observations is optimized in the weighted least-squares sense.	USGS, PC, Windows 2000*
RECIRC.vi V 1.0	10673-1.0-00 [DIRS 164432]	This program is used for recirculating and partial-recirculation cross-hole tracer test analysis.	USGS, PC, Windows 98/NT 4.0*/2000
RELAP V. 2.0	10551-2.0-00 [DIRS 159065]	This software models tracer transport by convoluting a Laplace-domain transfer function for transport through dual-porosity media with transfer functions that describe tracer injection, mixing in the injection and production wellbores (or flow manifolds in laboratory experiments), and recirculation of the product fluid (in field experiments only). It also performs curve fits to field or laboratory tracer test data to obtain the best-fitting transport parameter values.	LANL, PC, Windows 2000/NT*
RETRAN V 2.0	10552-2.0-00 [DIRS 159066]	This software models reactive transport in dual-porosity media with a general, nonlinear sorption isotherm and with time-varying flow rates.	LANL, PC, Windows 2000/NT 4.0*
Streltsova-Adams.vi V 1	10971-1-00 [DIRS 162756]	This software displays the standard and accepted Streltsova-Adams type curve for fractured aquifers and allows the fitting of the input data curves over this type curve. The .vi extension displays the appropriate resulting hydrologic parameters associated with the data curve matching (transmissivity and storativity).	USGS, PC, Windows 2000/98/NT 4.0*

Table 3-1. Software Used in Support of This Scientific Analysis (Continued)

Software Name and Version (V)	Software Tracking Number (STN)/DIRS Number	Description	Computer, Platform, and Operating System
Theis.vi V 1.0	10974-1.0-00 [DIRS 162758]	This software displays the standard and accepted Theis type curve and allows the fitting of the input data curves over this type curve. The .vi extension displays the appropriate resulting hydrologic parameters associated with the data curve matching (transmissivity and storativity).	USGS, PC, Windows 2000/NT 4.0*/98

NOTE: Asterisks (*) indicate the operating system platform used for software applications described in this analysis report.

ATC=Alluvial Testing Complex; DIRS=Document Input Reference System; LANL=Los Alamos National Laboratory; USGS= U.S. Geological Survey.

All computer codes listed in Table 3-1 were selected for use in this scientific analysis because they were developed expressly for the purpose of conducting the various analyses to which they were applied. The range of use and the limitations on output of each code are specified in the Software Management Report (SMR) for each code. The codes were always used within their specified range of use, and their limitations on output, in addition to being identified in the SMRs, are discussed in appropriate places in this report (especially in sections that address “limitations and uncertainties”).

The software, finite element heat and mass transfer code (FEHM) (V. 2.20, STN: 10086-2.20-00 [DIRS 161725], PC Windows 2000), was used to conduct a sensitivity study to illustrate that the potentiometric head distributions calculated by the site-scale SZ flow model are quite insensitive to the horizontal hydraulic conductivity anisotropy ratio in the fractured volcanics. This sensitivity study (Appendix C, Section C6.4) was not used to generate any inputs or outputs for this report, so FEHM is not listed in Table 3-1.

3.2 EXEMPT SOFTWARE

Commercial, off-the-shelf software used in support of this scientific analysis is listed in Table 3-2. This software is exempt from the requirements of IM-PRO-003 and SCI-PRO-005.

Table 3-2. Exempt Software Used in Support of This Scientific Analysis

Software Name and Version (V)	Description	Computer and Platform Identification
Microsoft Excel, 97 SR-1	The commercial software, Microsoft Excel, 97 SR-1, was used for statistical analysis of data and plotting graphs. Only built-in standard functions in this software were used. No software routines or macros were used with the software to prepare this report. The output was visually checked for correctness, and the results of all calculations were hand-checked.	PC, Windows 2000/NT
MathCad [®] , Version 13.1	The commercial off-the-shelf (COTS) software, MathCad [®] , Version 13.1, was used for interpretations of hydraulic tests conducted at Nye County Site 22. Only built-in standard functions in this software were used. The equations solved using the software are provided in detail in Appendix F, Section F.6. The output was visually checked for correctness, and the equations solved by MathCad were independently derived to verify correctness of these equations.	PC, Windows 2000/NT

Calculations and spreadsheets used in this analysis can be found in the Technical Data Management System (TDMS) within data packages that have been assigned data tracking numbers (DTNs). Alternatively, some calculations and spreadsheets can be found in scientific notebooks. The DTN numbers or notebooks (including page numbers), or both, are identified in appropriate places throughout Section 6 and various appendices of this report to allow the independent reviewer to reproduce or verify results by visual inspection or hand calculation. Calculations and spreadsheets are not included as appendices to this report because of their voluminous nature.

4. INPUTS

4.1 DIRECT INPUTS

The data used in interpretation of the hydraulic tests discussed in Section 6.2 and Appendix C have been submitted as data packages (Table 4-1) to the TDMS. Data packages submitted to the U.S. Department of Energy are available for inspection at the Office of Repository Development, Records Processing Center in Las Vegas, Nevada. The data and other technical information providing input for the development of parameters documented in this scientific analysis are identified in Table 4-1. The listed data and the technical information are appropriate sources for the analyses documented in this report. A brief description of the data, the DTN used as input, or the source of the data are listed in Table 4-1. The table is divided according to the sections in this analysis in which the data are used. The qualification status of data input is indicated in the TDMS and in the Document Input Reference System database.

Table 4-1. Input Data

Data Description	Data Tracking Number (DTN) or Source
Direct Inputs Section 6.1	
Well completion information for NC-EWDP-19D	MO0112DQRWLNYE.018 [DIRS 157187]
Well completion information for NC-EWDP-19IM2, NC-EWDP-22S, NC-EWDP-22PA, NC-EWDP-22PB, and NC-EWDP-22PC	LA0705PR150304.007 [DIRS 181202] (Qualified for intended use in Appendix K)
Results of C-wells flow surveys	GS931008312313.016 [DIRS 148173] (Qualified for intended use in Appendix L)
C-Wells Packer Locations	MO0703U25CHPTL.000 [DIRS 180070]
Stratigraphy at Nye County NC-EWDP Site 22	GS030108314211.001 [DIRS 163483]
Direct Inputs Section 6.2	
Pumping Test Data Collected at the C-Well Complex, 5/7/96 - 12/31/96	GS970308312314.001 [DIRS 159240]
Pumping Test Data Collected at the C-Well Complex, 1/8/97 - 6/15/97	GS970708312314.005 [DIRS 159241]
Pumping Test Data Collected at the C-Well Complex, 1/8/97 - 3/31/97	GS981008312314.002 [DIRS 147068]
June 1995 C-Wells Pressure Data	LA0705PR150304.002 [DIRS 181198]
June 1995 C-Wells Flow Rate Data	LA0705PR150304.003 [DIRS 181201] (Qualified for intended use in Appendix R)
Water-level altitude data from four wells in the continuous network, May through December 1996	GS970308312314.002 [DIRS 161273]
Transducer, barometric pressure, and discharge data collected from 4/18/98 through 11/24/98 in support of the ongoing hydraulic tracer tests being conducted at the UE-25 C-wells complex, Nevada	GS990408312315.002 [DIRS 140115]
UE-25 ONC-1 transducer pressures, March 1996 to December, 1997	MO0212SPANYESJ.149 [DIRS 161274] (Qualified for intended use in Appendix M)
Direct Inputs Section 6.3	
Concentrations of 2,6 –DFBA and pyridone from tracer test conducted at the C-wells complex, 1/8/97 – 7/11/97	GS010508312315.001 [DIRS 155860]
Tracer recovery data from testing in the Prow Pass interval	GS990208312315.001 [DIRS 159238]

Table 4-1. Input Data (Continued)

Data Description	Data Tracking Number (DTN) or Source
Direct Inputs Section 6.3 (Continued)	
Prow Pass reactive-tracer-test field data	LAPR831231AQ99.001 [DIRS 140134]
Bullfrog reactive tracer test data	LA0007PR831231.001 [DIRS 156043]
Bromide and PFBA sorption data onto C-wells tufts	LA0302PR831231.001 [DIRS 162605]
2,3,4,5 TeFBA Response in Prow Pass from UE-25 c#1 to UE-25 c#2, 1998	MO0308SPATRCRC.000 [DIRS 164821]
Results of C-wells flow surveys	GS931008312313.016 [DIRS 148173] (Qualified for intended use in Appendix L)
Normalized Tracer Concentrations and Recoveries in C-Wells Tracer Tests	LA0410PR831231.001 [DIRS 171899]
Direct Inputs Section 6.4	
Flow rates, pressures, and temperatures for hydraulic and tracer testing at the NC-EWDP-19D, NC-EWDP-19IM1, and NC-EWDP-19IM2 Alluvial Testing Complex from December 18, 2001 to March 22, 2002	GS020908312316.002 [DIRS 162679]
Direct Inputs Section 6.5	
2,6 DFBA and I concentrations in single-well tracer test with 2-day rest period in NC-EWDP-19D	UN0102SPA008KS.003 [DIRS 162614]
2,4 DFBA and Cl concentrations in single-well tracer test with 0.5-hr rest period in NC-EWDP-19D	UN0109SPA008IF.006 [DIRS 162442]
PFBA concentrations in single-well tracer test with 30-day rest period in NC-EWDP-19D	UN0109SPA008KS.007 [DIRS 162615]
Bromide concentrations in single-well tracer test with 30-day rest period in NC-EWDP-19D	UN0109SPA008KS.008 [DIRS 162616]
NC-EWDP-19D, ATC single-hole hydraulic testing associated with the July 7, 2000 to April 26, 2001 tracer study	GS020708312316.001 [DIRS 162678]
Tracer injection masses in single-well tracer test with 2-day rest period in NC-EWDP-19D	Stetzenbach 2001 [DIRS 180730]
Tracer injection masses in single-well tracer test with 0.5-hr rest period in NC-EWDP-19D	Farnham 2001 [DIRS 180732]
Tracer injection masses in single-well tracer test with 30-day rest period in NC-EWDP-19D	Farnham 2001 [DIRS 180733]
Normalized breakthrough curves of tracers from first single-well tracer test in NC-EWDP-22S, conducted in December 2004	LA0612PR831231.001 [DIRS 178733]
Normalized breakthrough curves of tracers from second single-well tracer test in NC-EWDP-22S, conducted in December 2004 and January 2005	LA0612PR831231.002 [DIRS 178735]*
Normalized breakthrough curves of tracers from first cross-hole tracer test at NC-EWDP Site 22, conducted between January and October 2005	LA0612PR831231.003 [DIRS 178736] *
Normalized breakthrough curves of tracers from second cross-hole tracer test at NC-EWDP Site 22, conducted between August and October 2005	LA0612PR831231.004 [DIRS 178738]*
Raw data and normalized breakthrough curves of microspheres in first cross-hole tracer test at NC-EWDP Site 22, conducted between January and March 2005	LA0612PR831231.005 [DIRS 178739]

Table 4-1. Input Data (Continued)

Data Description	Data Tracking Number (DTN) or Source
Direct Inputs Appendix C	
Pumping Test Data Collected at the C-Well Complex, 5/7/96 - 12/31/96	GS970308312314.001 [DIRS 159240]
Pumping Test Data Collected at the C-Well Complex, 1/8/97 - 6/15/97	GS970708312314.005 [DIRS 159241]
Pumping Test Data Collected at the C-Well Complex, 1/8/97 - 3/31/97	GS981008312314.002 [DIRS 147068]
June 1995 C-Wells Pressure Data	LA0705PR150304.002 [DIRS 181198]
June 1995 C-Wells Flow Rate Data	LA0705PR150304.003 [DIRS 181201] (Qualified for intended use in Appendix R)
Revised Pumping Test Data Collected At The C-Hole Complex, September 28, 1995 (Pre-Test Data) and January through April, 1996	GS031108312314.005 [DIRS 179648]
Transducer, Barometer and Flowmeter Data Collected from April 2, 1997 to December 31, 1997 in Support of Hydraulic and Tracer Tests at the C-Hole Complex, Yucca Mountain, Nevada	GS010608312314.001 [DIRS 179647]
C-Wells Packer Locations	MO0703U25CHPTL.000 [DIRS 180070]
Flow Meter Survey Data from Borehole UE-25 C#3 for Use on the Yucca Mountain Project	MO0012FLOW25C3.001 [DIRS 154765]
Water-level altitude data from four wells in the continuous network, May through December 1996	GS970308312314.002 [DIRS 161273]
Water-level altitude data from four wells in the continuous network, December 1996 through March 1997	GS970708312314.006 [DIRS 144468]
Pump test data collected at the C-wells complex 5/7/96 – 12/31/96	GS981008312314.003 [DIRS 144464]
Transducer, barometric pressure, and discharge data collected from 4/18/98 through 11/24/98 in support of the ongoing hydraulic tracer tests being conducted at the UE-25 C-wells complex, Nevada	GS990408312315.002 [DIRS 140115]
Water-Level Altitude Data from the Continuous Network, 1995	GS960708312312.009 [DIRS 180534]
UE-25 ONC-1 transducer pressures, March 1996 to December, 1997	MO0212SPANYESJ.149 [DIRS 161274] (Qualified for intended use in Appendix M)
Direct Inputs Appendix D	
Results of C-wells flow surveys	GS931008312313.016 [DIRS 148173] (Qualified for intended use in Appendix L)
Concentrations of 2,6 –DFBA and pyridone from tracer test conducted at the C-wells complex, 1/8/97 – 7/11/97	GS010508312315.001 [DIRS 155860]
2,3,4,5 TeFBA Response in Prow Pass from UE-25 c#1 to UE-25 c#2, 1998	MO0308SPATRCRC.000 [DIRS 164821]
Data obtained from the analysis of the iodide tracer test water samples collected during the 2/13/96 convergent tracer test conducted at the C-wells complex	GS960808312315.001 [DIRS 159235]
Tracer recovery data from testing in the Prow Pass interval	GS990208312315.001 [DIRS 159238]
Transducer, barometric pressure, and discharge data collected from 4/18/98 through 11/24/98 in support of the ongoing hydraulic tracer tests being conducted at the UE-25 C-wells complex, Nevada	GS990408312315.002 [DIRS 140115]
Prow Pass reactive-tracer-test field data	LAPR831231AQ99.001 [DIRS 140134]
Bullfrog reactive tracer test data	LA0007PR831231.001 [DIRS 156043]

Table 4-1. Input Data (Continued)

Data Description	Data Tracking Number (DTN) or Source
Direct Inputs Appendix D (Continued)	
Injection and production flow rates for Prow Pass test	GS010799992315.001 [DIRS 157067]
Bromide and lithium matrix diffusion coefficients	Newman 1973 [DIRS 148719] (Qualified as external source in Appendix A)
Fluorinated benzoic acid diffusion coefficients	Bowman 1984 [DIRS 156645] (Qualified as external source in Appendix A)
Pump test data collected at the C-wells complex 1/8/97 - 3/31/97	GS981008312314.002 [DIRS 147068]
Pumping test data collected at the C-wells complex, 5/7/96 - 12/31/96	GS981008312314.003 [DIRS 144464]
Pumping Test Data Collected at the C-Well Complex, 5/7/96 to 12/31/96	GS970308312314.001 [DIRS 159240]
Pumping Test Data Collected at the C-Well Complex, 1/8/97 to 6/15/97	GS970708312314.005 [DIRS 159241]
Bullfrog Test Recirculation Flow Rate Data	MO0110BFROGREC.001 [DIRS 157066]
Tabulations of Data used in Tracer Test Interpretations	LA0401PR831231.001 [DIRS 171859]
Normalized Tracer Concentrations and Recoveries in C-Wells Tracer Tests	LA0410PR831231.001 [DIRS 171899]
Iodide diffusion coefficients	Skagius and Neretnieks 1986 [DIRS 156862] (Qualified as external source in Appendix A)
Direct Inputs Appendix E	
Mineral abundance data of C-well tuffs from UE-25 c#1 and c#2	MO0012MINLCHOL.000 [DIRS 153370]
Sorbing element concentration data of J-13 and C-3 well water from UE-25 c#1 and c#2	MO0012SORBCHOL.000 [DIRS 153375]
Cation exchange capacity data of C-well tuff from UE-25 c #1 and UE-25 c #2	MO0012CATECHOL.000 [DIRS 153371]
Cation exchange capacity measurements on C-wells tuffs involving displacement of lithium and other cations by cesium	LA0302PR831341.001 [DIRS 162604]
PFBA and bromide tracer diffusion in tuff from UE-25 c#1	MO0012DIFFCHOL.000 [DIRS 159243]
Porosity data for UE-25 c#1, c#2, and c#3	MO0012POROCHOL.000 [DIRS 153376]
Permeability data for UE-25 c#1, c#2, and c#3	MO0012PERMCHOL.000 [DIRS 153368]
Bromide and PFBA sorption data onto C-wells tuffs	LA0302PR831231.001 [DIRS 162605]
Mineralogy data for Central Bullfrog Tuff from UE-25 c#2, 2406 ft (non-Q)	LA9909PR831231.004 [DIRS 129623] (Qualified for intended use in Appendix J)
Bromide and lithium tracer movement in crushed tuff columns for UE-25 c#2 tuff	LA0301PR831231.001 [DIRS 162603]
Iodide concentrations in C-wells fractured core experiments	LA0212PR831231.001 [DIRS 162607]
Lithium, bromide, and PFBA concentrations in C-wells fractured core experiments	LA0212PR831231.003 [DIRS 162609]
Sodium and calcium concentrations in fractured core experiments in all C-wells cores except for core UE-25 c#2, 1,745 ft	LA0212PR831231.002 [DIRS 162608]
Sodium and calcium concentrations in fractured core experiments in core UE-25 c#2, 1,745 ft	LA0212PR831231.005 [DIRS 166215]
Results of C-wells flow surveys	GS931008312313.016 [DIRS 148173] (Qualified for intended use in Appendix L)
Water viscosity, water density, gravitational acceleration	Weast and Astle 1981 [DIRS 100833]

Table 4-1. Input Data (Continued)

Data Description	Data Tracking Number (DTN) or Source
Direct Inputs Appendix F	
Water Density, Water Viscosity, and Gravitational Acceleration	Weast and Astle 1981 [DIRS 100833] (Established Fact)
Unit Weight and Compressibility of Water	Lohman 1972 [DIRS 150250] (Established Fact)
Nominal Water Density	Fetter 2001 [DIRS 156668] (Established Fact)
NC-EWDP-19D, ATC single-hole hydraulic testing associated with the July 7, 2000 to April 26, 2001 tracer study	GS020708312316.001 [DIRS 162678]
Flow rates, pressures, and temperatures for hydraulic and tracer testing at the NC-EWDP-19D, NC-EWDP-19IM1, and NC-EWDP-19IM2 Alluvial Testing Complex from December 18, 2001 to March 22, 2002	GS020908312316.002 [DIRS 162679]
Background pressures and temperatures during barometric monitoring at the NC-EWDP-19D, NC-EWDP-19IM1, and NC-EWDP-19IM2 Alluvial Testing Complex from May 1, 2002 through July 3, 2002	GS020908312316.003 [DIRS 162680]
Grain size analysis of alluvium samples from wells 19D and 19P of the Alluvial Test Complex	LA0201JS831421.001 [DIRS 162613]
Geophysical log data from Borehole NC-EWDP-19D	MO0105GPLOG19D.000 [DIRS 163480]
Well completion information for NC-EWDP-22S, NC-EWDP-22PA, and NC-EWDP-22PB	LA0705PR150304.007 [DIRS 181202] (Qualified for intended use in Appendix K)
Nye County hydraulic test data from combined interval pump test at Nye County Site 22 in March 2002	LA0705PR150304.008 [DIRS 181203] (Qualified for intended use in Appendix N)
Nye County hydraulic test data from zone #1 pump test at Nye County Site 22 in August 2003	LA0705PR150304.009 [DIRS 181204] (Qualified for intended use in Appendix N)
Nye County hydraulic test data from zone #2 pump test at Nye County Site 22 in August 2003	LA0705PR150304.010 [DIRS 181205] (Qualified for intended use in Appendix N)
Nye County hydraulic test data from zone #3 pump test at Nye County Site 22 in September 2003	LA0705PR150304.011 [DIRS 181207] (Qualified for intended use in Appendix N)
Nye County hydraulic test data from zone #4 pump test at Nye County Site 22 in September 2003	LA0705PR150304.012 [DIRS 181208] (Qualified for intended use in Appendix N)
Flow rates used in Nye County Site 22 Hydraulic Test Interpretations	Downing 2003 [DIRS 178771]. (Qualified for intended use in Appendix N)
Direct Inputs Appendix G	
2,6 DFBA and I concentrations in single-well tracer test with 2-day rest period in NC-EWDP-19D	UN0102SPA008KS.003 [DIRS 162614]
2,4 DFBA and Cl concentrations in single-well tracer test with 0.5-hr rest period in NC-EWDP-19D	UN0109SPA008IF.006 [DIRS 162442]
PFBA concentrations in single-well tracer test with 30-day rest period in NC-EWDP-19D	UN0109SPA008KS.007 [DIRS 162615]
Bromide concentrations in single-well tracer test with 30-day rest period in NC-EWDP-19D	UN0109SPA008KS.008 [DIRS 162616]
2,4 DFBA concentrations in single-well tracer test in interval #4 of NC-EWDP-19D	MO0205UCC008IF.001 [DIRS 162617]
Tracer injection masses in single-well tracer test with 2-day rest period in NC-EWDP-19D	Stetzenbach 2001 [DIRS 180730]
Tracer injection masses in single-well tracer test with 0.5-hr rest period in NC-EWDP-19D	Farnham 2001 [DIRS 180732]

Table 4-1. Input Data (Continued)

Data Description	Data Tracking Number (DTN) or Source
Direct Inputs Appendix G (Continued)	
Tracer injection masses in single-well tracer test with 30-day rest period in NC-EWDP-19D	Farnham 2001 [DIRS 180733]
Microsphere concentrations in single-well tracer tests in NC-EWDP-19D	LA0207PR831352.001 [DIRS 162431]
NC-EWDP-19D, ATC single-hole hydraulic testing associated with the July 7, 2000 to April 26, 2001 tracer study	GS020708312316.001 [DIRS 162678]
Drawdown data for NC-EWDP boreholes	GS020908312316.002 [DIRS 162679]
Normalized breakthrough curves of tracers from first single-well tracer test in NC-EWDP-22S, conducted in December 2004	LA0612PR831231.001 [DIRS 178733]*
Normalized breakthrough curves of tracers from second single-well tracer test in NC-EWDP-22S, conducted in December 2004 and January 2005	LA0612PR831231.002 [DIRS 178735]*
Normalized breakthrough curves of tracers from first cross-hole tracer test at NC-EWDP Site 22, conducted between January and October 2005	LA0612PR831231.003 [DIRS178736]*
Normalized breakthrough curves of tracers from second cross-hole tracer test at NC-EWDP Site 22, conducted between August and October 2005	LA0612PR831231.004 [DIRS 178738]*
Raw data and normalized breakthrough curves of microspheres in first cross-hole tracer test at NC-EWDP Site 22, conducted between January and March 2005	LA0612PR831231.005 [DIRS 178739]*
Measurements of downhole specific conductance (converted to normalized tracer concentrations) at NC-EWDP Site 22 during and after tracer injections in Dec. 2004 and Jan. 2005	LA0612PR831231.006 [DIRS 178745]

NOTE: *Flow rates used in the testing associated with data in this DTN are qualified for intended use in Appendix N.

ATC = Alluvial Testing Complex; BET = Brunauer-Emmet-Teller; DFBA = difluorobenzoic acid; PFBA = pentafluorobenzoic acid; Q=qualified.

4.2 CRITERIA

The work described in this report has been determined to be subject to 10 CFR 63.114 [DIRS 176544], Requirements for Performance Assessment. The applicable federal regulations and technical requirements related to the work activities associated with this report are generally implemented through the appropriate implementing procedures identified in Section 4 of the TWP (BSC 2006 [DIRS 177375]). In particular, the requirements identified in 10 CFR 63.114 (a), (b), (c) and (g) [DIRS 176544] are implemented through SCI-PRO-006. There are no U.S. Department of Energy orders applicable to the scope of work identified in this report.

In accordance with Section 3.3 of the technical work plan (BSC 2006 [DIRS 177375]), the level of accuracy, precision, and representativeness of results are discussed in appropriate places in Section 6 and in Appendices C through H.

This report is subject to regulatory review per the provisions and criteria of *Yucca Mountain Review Plan, Final Report (YMRP)* (NRC 2003 [DIRS 163274]). Listed below are U.S. Nuclear Regulatory Commission acceptance criteria from Sections 2.2.1.3.8.3 (Flow Paths in the Saturated Zone) and 2.2.1.3.9.3 (Radionuclide Transport in the Saturated Zone) of the YMRP

(NRC 2003 [DIRS 163274]), based on the requirements of 10 CFR 63.114 [DIRS 176544]. In cases where subsidiary criteria are listed in the YMRP for a given criterion, only the subsidiary criteria addressed by this scientific analysis are listed below.

4.2.1 Acceptance Criteria from Section 2.2.1.3.8.3, *Flow Paths in the Saturated Zone*

Acceptance Criterion 1: *System Description and Model Integration Are Adequate.*

- **Subcriterion (2)**—The description of the aspects of hydrology, geology, geochemistry, design features, physical phenomena, and couplings, which may affect flow paths in the saturated zone, is adequate. Conditions and assumptions in the abstraction of flow paths in the saturated zone are readily identified, and consistent with the body of data presented in the description.
- **Subcriterion (3)**—The abstraction of flow paths in the saturated zone uses assumptions, technical bases, data, and models that are appropriate and consistent with other related DOE abstractions. For example, the assumptions used for flow paths in the saturated zone are consistent with the total system performance assessment abstraction of representative volume (Section 2.2.1.3.12 of the YMRP). The descriptions and technical bases provide transparent and traceable support for the abstraction of flow paths in the saturated zone.
- **Subcriterion (10)**—Guidance in NUREG–1297 and NUREG–1298 (Altman et al. 1988 [DIRS 103597]; [DIRS 103750]), or other acceptable approaches for peer review and data qualification is followed.

Acceptance Criterion 2: *Data Are Sufficient for Model Justification.*

- **Subcriterion (1)**—Geological, hydrological, and geochemical values used in the license application to evaluate flow paths in the saturated zone are adequately justified. Adequate descriptions of how the data were used, interpreted, and appropriately synthesized into the parameters are provided.
- **Subcriterion (2)**—Sufficient data have been collected on the natural system to establish initial and boundary conditions for the abstraction of flow paths in the saturated zone.
- **Subcriterion (3)**—Data on the geology, hydrology, and geochemistry of the saturated zone used in the total system performance assessment abstraction are based on appropriate techniques. These techniques may include laboratory experiments, site-specific field measurements, natural analog research, and process-level modeling studies. As appropriate, sensitivity or uncertainty analyses, used to support the DOE total system performance assessment abstraction, are adequate to determine the possible need for additional data.

- **Subcriterion (4)**—Sufficient information is provided to substantiate that the proposed mathematical groundwater modeling approach and proposed model(s) are calibrated and applicable to site conditions.

Acceptance Criterion 3: *Data Uncertainty Is Characterized and Propagated Through the Model Abstraction.*

- **Subcriterion (1)**—Models use parameter values, assumed ranges, probability distributions, and bounding assumptions that are technically defensible, reasonably account for uncertainties and variabilities, and do not result in an under-representation of the risk estimate.
- **Subcriterion (3)**—Uncertainty is adequately represented in parameter development for conceptual models, process-level models, and alternative conceptual models, considered in developing the abstraction of flow paths in the saturated zone. This may be done through either sensitivity analyses or use of conservative limits. For example, sensitivity analyses and/or similar analyses are sufficient to identify saturated zone flow parameters that are expected to significantly affect the abstraction model outcome.

Acceptance Criterion 4: *Model Uncertainty Is Characterized and Propagated Through the Model Abstraction.*

- **Subcriterion (1)**—Alternative modeling approaches of features, events, and processes are considered and are consistent with available data and current scientific understanding, and the results and limitations are appropriately considered in the abstraction.
- **Subcriterion (2)**—Conceptual model uncertainties are adequately defined and documented, and effects on conclusions regarding performance are properly assessed. For example, uncertainty in data interpretations is considered by either analyzing reasonable conceptual flow models that are supported by site data or demonstrating through sensitivity studies that the uncertainties have little impact on repository performance.
- **Subcriterion (3)**—Consideration of conceptual model uncertainty is consistent with available site characterization data, laboratory experiments, field measurements, natural analog information and process-level modeling studies; the treatment of conceptual model uncertainty does not result in an under-representation of the risk estimate.
- **Subcriterion (4)**—Appropriate alternative modeling approaches are consistent with available data and current scientific knowledge, and appropriately consider their results and limitations, using tests and analyses that are sensitive to the processes modeled.

Acceptance Criterion 5: *Model Abstraction Output Is Supported by Objective Comparisons.*

- **Subcriterion (4)**—Sensitivity analyses or bounding analyses are provided to support the abstraction of flow paths in the saturated zone, that cover ranges consistent with site data, field or laboratory experiments and tests, and natural analog research.

4.2.2 Acceptance Criteria from Section 2.2.1.3.9.3, *Radionuclide Transport in the Saturated Zone*

Acceptance Criterion 1: *System Description and Model Integration Are Adequate.*

- **Subcriterion (1)**—Total system performance assessment adequately incorporates important design features, physical phenomena, and couplings, and uses consistent and appropriate assumptions throughout the radionuclide transport in the saturated zone abstraction process.
- **Subcriterion (2)**—The description of the aspects of hydrology, geology, geochemistry, design features, physical phenomena, and couplings, that may affect radionuclide transport in the saturated zone, is adequate. For example, the description includes changes in transport properties in the saturated zone, from water-rock interaction. Conditions and assumptions in the abstraction of radionuclide transport in the saturated zone are readily identified, and consistent with the body of data presented in the description.
- **Subcriterion (3)**—The abstraction of radionuclide transport in the saturated zone uses assumptions, technical bases, data, and models that are appropriate and consistent with other related DOE abstractions. For example, assumptions used for radionuclide transport in the saturated zone are consistent with the total system performance assessment abstractions of radionuclide release rates and solubility limits, and flow paths in the saturated zone (Sections 2.2.1.3.4 and 2.2.1.3.8 of the YMRP, respectively). The descriptions and technical bases provide transparent and traceable support for the abstraction of radionuclide transport in the saturated zone.
- **Subcriterion (5)**—Sufficient data and technical bases for the inclusion of features, events, and processes related to radionuclide transport in the saturated zone in the total system performance assessment abstraction are provided.
- **Subcriterion (6)**—Guidance in NUREG–1297 and NUREG–1298 (Altman et al. 1988 [DIRS 103597; DIRS 103750]), or other acceptable approaches for peer review and data qualification is followed.

Acceptance Criterion 2: *Data Are Sufficient for Model Justification.*

- **Subcriterion (1)**—Geological, hydrological, and geochemical values used in the license application are adequately justified (e.g., flow path lengths, sorption coefficients, retardation factors, colloid concentrations, etc.). Adequate descriptions of how the data were used, interpreted, and appropriately synthesized into the parameters are provided.

- **Subcriterion (2)**—Sufficient data have been collected on the characteristics of the natural system to establish initial and boundary conditions for the total system performance assessment abstraction of radionuclide transport in the saturated zone.
- **Subcriterion (3)**—Data on the geology, hydrology, and geochemistry of the saturated zone, including the influence of structural features, fracture distributions, fracture properties, and stratigraphy, used in the total system performance assessment abstraction, are based on appropriate techniques. These techniques may include laboratory experiments, site-specific field measurements, natural analog research, and process-level modeling studies. As appropriate, sensitivity or uncertainty analyses used to support the DOE total system performance assessment abstraction are adequate to determine the possible need for additional data.

Acceptance Criterion 3: *Data Uncertainty Is Characterized and Propagated Through the Model Abstraction.*

- **Subcriterion (1)**—Models use parameter values, assumed ranges, probability distributions, and bounding assumptions that are technically defensible, reasonably account for uncertainties and variabilities, and do not result in an under-representation of the risk estimate.
- **Subcriterion (2)**—For those radionuclides where the total system performance assessment abstraction indicates that transport in fractures and matrix in the saturated zone is important to waste isolation: (i) estimated flow and transport parameters are appropriate and valid, based on techniques that may include laboratory experiments, field measurements, natural analog research, and process-level modeling studies conducted under conditions relevant to the saturated zone at Yucca Mountain; and (ii) models are demonstrated to adequately predict field transport test results. For example, if a sorption coefficient approach is used, the assumptions implicit in that approach are validated.
- **Subcriterion (4)**—Parameter values for processes, such as matrix diffusion, dispersion, and ground-water mixing, are based on reasonable assumptions about climate, aquifer properties, and ground-water volumetric fluxes (Section 2.2.1.3.8 of the YMRP).
- **Subcriterion (5)**—Uncertainty is adequately represented in parameter development for conceptual models, process-level models, and alternative conceptual models considered in developing the abstraction of radionuclide transport in the saturated zone. This may be done either through sensitivity analyses or use of conservative limits.

Acceptance Criterion 4: *Model Uncertainty Is Characterized and Propagated Through the Model Abstraction.*

- **Subcriterion (1)**—Alternative modeling approaches of features, events, and processes are considered and are consistent with available data and current scientific understanding, and the results and limitations are appropriately considered in the abstraction.

- **Subcriterion (2)**—Conceptual model uncertainties are adequately defined and documented, and effects on conclusions regarding performance are properly assessed.
- **Subcriterion (3)**—Consideration of conceptual model uncertainty is consistent with available site characterization data, laboratory experiments, field measurements, natural analog information and process-level modeling studies; and the treatment of conceptual model uncertainty does not result in an under-representation of the risk estimate.
- **Subcriterion (4)**—Appropriate alternative modeling approaches are consistent with available data and current scientific knowledge, and appropriately consider their results and limitations using tests and analyses that are sensitive to the processes modeled. For example, for radionuclide transport through fractures, the DOE adequately considers alternative modeling approaches to develop its understanding of fracture distributions and ranges of fracture flow and transport properties in the SZ.

4.3 CODES, STANDARDS, AND REGULATIONS

No codes, standards, or regulations other than those identified in Section 4.2 were used in this analysis.

INTENTIONALLY LEFT BLANK

5. ASSUMPTIONS

A list of the assumptions used in this scientific analysis is provided in Table 5-1. Subsections are identified where assumptions are used. The rationale for each assumption is also provided.

Table 5-1. Assumptions

Number	Assumption	Rationale	Location in Report
1	For the purposes of inferring radionuclide matrix diffusion coefficients from field and laboratory tracer tests, bromide and PFBA effectively bound the sizes (and hence diffusion coefficients) of radionuclide solute species expected in the SZ beneath Yucca Mountain.	Bromide is a simple halide, while PFBA is a large aromatic organic molecule. The latter should be similar in size or larger than radionuclide complexes with carbonate or other potential inorganic complexants. This assumption does not apply to colloidal radionuclides (including complexes to large natural organic matter).	Sections 6.3.5 (Table 6.3-3) and D4
2	For the purposes of calculating K_d values from retardation factors and for estimating total porosity from alluvium bulk density measurements made by borehole gravimetry, the density of crushed tuff and alluvium grains is 2.65 g/cm^3 .	In cases where extreme accuracy is not needed, as applies here, 2.65 g/cm^3 is a good assumption for the grain density of most mineral soils (Freeze and Cherry 1979 [DIRS 101173], p. 337). This value is in good agreement with the average grain density calculated for 4 columns packed with alluvium from NC-EWDP-19D and NC-EWDP-19IM1, which was 2.67 g/cm^3 (DTN: LA0511PR831361.001 [DIRS 175878]), so the assumption of 2.65 g/cm^3 is well justified for the alluvium at the NC-EWDP-19D location.	Sections 6.3.6, F4, E3, G3, and H1

PFBA=pentafluorobenzoic acid or pentafluorobenzoate; SZ=saturated zone.

INTENTIONALLY LEFT BLANK

6. SCIENTIFIC ANALYSIS DISCUSSION

6.1 INTRODUCTION

The saturated zone near Yucca Mountain, along potential flow paths from the repository to the accessible environment, can be divided into two types of flow systems: (1) fractured tuffs that underlie the repository and that extend for several kilometers to the south of Yucca Mountain (in the general direction of flow), and (2) valley-fill or alluvium deposits that the water table transitions into before the current approximately 18-km performance compliance boundary (10 CFR 63.114 [DIRS 176544], (a), (b), (c), and (g)). Radionuclides released from the repository would first have to travel through the saturated fractured tuffs and then through the saturated alluvium to reach the compliance boundary.

To support the characterization of the saturated fractured tuffs, several hydraulic and tracer tests were conducted at a three-well complex (UE-25 c#1, UE-25 c#2, and UE-25 c#3, hereafter referred to as c#1, c#2, and c#3, respectively) known as the C-wells. This complex is located approximately 2 km southeast of the repository footprint. Hydraulic tests conducted at the C-wells are summarized in Section 6.2, and tracer tests conducted at the C-wells are summarized in Section 6.3. These sections present both the conceptual understanding and the hydrologic and transport parameter estimates derived from hydraulic and tracer testing, respectively. Details of the results and interpretations of the hydraulic and tracer tests are provided in Appendices C and D, respectively. Laboratory testing conducted to support the interpretations of the C-wells tracer tests is discussed in detail in Appendix E.

To support the characterization of the saturated alluvium, both hydraulic and tracer testing were conducted at the Alluvial Testing Complex (ATC), centered around well NC-EWDP-19D (hereafter referred to as 19D), which is located just outside the southwest corner of the NTS, essentially right at the compliance boundary. Hydraulic and tracer tests were also conducted in saturated alluvium at Nye County Site 22, centered around NC-EWDP-22S and located approximately 4.5 km north–northeast of the ATC just east of Fortymile Wash. Hydraulic tests conducted at both the ATC and Site 22 are summarized in Section 6.4, and tracer tests conducted at the two locations are summarized in Section 6.5. Appendices F and G provide detailed discussions of the results and interpretations of hydraulic and tracer testing, respectively, conducted at both the ATC and Site 22. Appendix H provides a detailed discussion of laboratory testing conducted to support the planning and interpretation of cross-hole tracer tests that were going to be conducted at the ATC, but were not because of a revocation of environmental permits by the State of Nevada. Only minimal laboratory testing was conducted in support of the tracer tests at Site 22; this testing is summarized in Section G.5.4.3 of Appendix G. The NRC has indicated that the alluvium may provide a significant natural barrier to the transport of radionuclides (NRC 2004 [DIRS 170243], Sections 4.3.8 and 4.3.9).

The interpretive methods and corresponding software used to discriminate between conceptual models and to estimate flow and transport parameters in this report are primarily analytical or semi-analytical in nature. Numerical methods embodied in sophisticated three-dimensional computer codes were not used because detailed information on the spatial distribution of flow and transport properties in the subsurface, including boundary conditions, was not available for the in-situ tests. Such information is considered necessary to justify the use of sophisticated

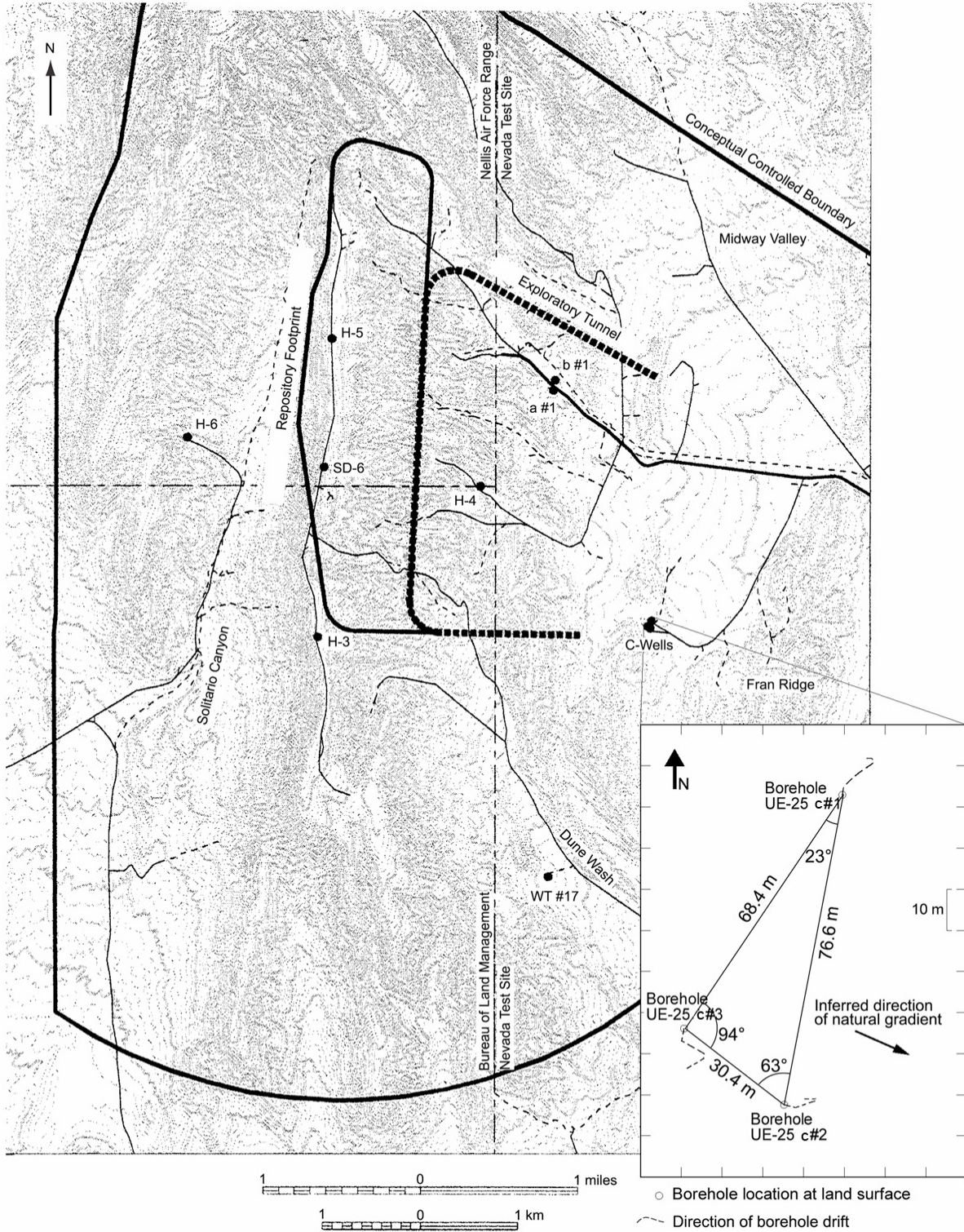
numerical models for conceptual model discrimination and parameter estimation. On the other hand, the analytical or semi-analytical methods and software employed for model discrimination and parameter estimation implicitly honor the lack of detailed subsurface information in the in-situ tests.

6.1.1 Hydrogeologic Settings

6.1.1.1 C-Wells

Figure 6.1-1 shows the location and surface layout of the C-wells. This location was chosen for drilling and testing because it was believed to be immediately down-gradient of the repository horizon and was thus thought to be highly representative of fractured volcanic tuffs that radionuclides would encounter should they reach the saturated zone. The wells were drilled on a two-tiered drill pad in a channel of an ephemeral stream that cuts through Bow Ridge, a spur of Yucca Mountain. The lower tier of the pad, in which Borehole c#1 was drilled, is at an altitude of 1,130.5 m above mean sea level. The upper tier, in which Boreholes c#2 and c#3 were drilled, is at an altitude of 1,132.3 m. The C-wells are 30.4 to 76.6 m apart at the land surface, but they deviate substantially at depth (Geldon 1993 [DIRS 101045], p. 6, Figure 2; p. 8, Figure 4) (Figure 6.1-1 and Table 6.1-1).

The C-wells were drilled to a depth of 914 m below land surface in Miocene tuffaceous rocks, mainly of the Paintbrush Group, the Calico Hills Formation, and the Crater Flat Group (Table 6.1-2), which are overlain by 0 to 24 m of Quaternary alluvium. The geology below the water table at the C-wells is depicted in Figure 6.1-2, along with fracture densities and estimated average matrix porosities in each unit. The tuffaceous rocks are estimated to be 1,000- to 1,600-m thick in the vicinity of the C-wells complex, where they consist of nonwelded to densely welded ash-flow tuff with intervals of ash-fall tuff and volcanoclastic rocks (Geldon 1993 [DIRS 101045]; Geldon et al. 1998 [DIRS 129721]). The tuffaceous rocks have pervasive tectonic and cooling fractures that strike predominantly north–northeast to north–northwest and dip westward at angles of 50° to 87° (Geldon 1996 [DIRS 100396], pp. 7 to 9). Several thousand meters of Paleozoic limestone and dolomite likely underlie the tuffaceous rocks about 460 m below the bottom of the C-wells or approximately 1,370 m below land surface [based on extrapolations from relations in Borehole UE-25 p#1, presented in *Geology of Drill Hole UE25p#1: A Test Hole Into Pre-Tertiary Rocks Near Yucca Mountain, Southern Nevada* (Carr et al. 1986 [DIRS 102046]). (Hereafter, in this report, UE-25 p#1 is referred to as p#1; see Table B-1 for a list of abbreviations.)



Source: Based on Geldon 1993 [DIRS 101045], p 6, Figure 2.

Figure 6.1-1. Location and Surface Layout of the C-Wells Complex

Table 6.1-1. Approximate Interborehole Distances at the Midpoints of Hydrogeologic Intervals as Monitored During Hydraulic Tests at the C-Wells Complex, August 1995 to April 1996

	Borehole Data (m)			Interborehole Distances (m)	
	c#1	c#2	c#3	c#1 to c#3	c#2 to c#3
Calico Hills					
Top depth	418	416	417	78.6	29.0
Bottom depth	547	531	540		
Midpoint depth	483	474	478		
North coordinate	230,771	230,691	230,703		
East coordinate	173,646	173,633	173,607		
Distance north/south from c#3	68.3	12.2	—		
Distance east/west from c#3	39.3	26.2	—		
Prow Pass					
Top depth	549	533	542	81.1	28.6
Bottom depth	605	606	610		
Midpoint depth	577	569	576		
North coordinate	230,772	230,691	230,702		
East coordinate	173,648	173,634	173,607		
Distance north/south from c#3	70.4	11.0	—		
Distance east/west from c#3	40.2	26.5	—		
Upper Bullfrog					
Top depth	607	607	612	83.2	28.6
Bottom depth	698	696	695		
Midpoint depth	653	652	653		
North coordinate	230,773	230,691	230,701		
East coordinate	173,648	173,634	173,607		
Distance north/south from c#3	72.2	9.75	—		
Distance east/west from c#3	41.4	26.8	—		
Lower Bullfrog					
Top depth (m)	700	698	697	85.6	29.3
Bottom depth (m)	797	792	813		
Midpoint depth (m)	749	745	755		
North coordinate (m)	230,774	230,692	230,700		
East coordinate (m)	173,649	173,633	173,606		
Distance north/south from c#3 (m)	73.8	8.84	—		
Distance east/west from c#3 (m)	43.3	27.7	—		
Upper Tram					
Top depth	799	794	814	86.9	29.6
Bottom depth	870	870	878		
Midpoint depth	834	832	846		
North coordinate	230,774	230,691	230,700		
East coordinate	173,648	173,632	173,604		
Distance north/south from c#3	74.7	8.53	—		
Distance east/west from c#3	44.2	28.3	—		

Table 6.1-1. Approximate Interborehole Distances at the Midpoints of Hydrogeologic Intervals as Monitored During Hydraulic Tests at the C-Wells Complex, August 1995 to April 1996 (Continued)

	Borehole Data (m)			Interborehole Distances (m)	
	c#1	c#2	c#3	c#1 to c#3	c#2 to c#3
Lower Tram					
Top depth	872	871	879	87.2	29.9
Bottom depth	898	903	900		
Midpoint depth	885	887	890		
North coordinate	230,774	230,691	230,700		
East coordinate	173,648	173,632	173,603		
Distance north/south from c#3	74.7	8.23	—		
Distance east/west from c#3	44.8	28.6	—		

Source: Geldon et al. 2002 ([DIRS 161163], p. 6, Table 1).

NOTE: North and south are referenced to Nevada State Z one 2 coordinates. Depths in c#3 and interborehole distances changed slightly in April 1996 when instrumentation in c#3 was reconfigured.

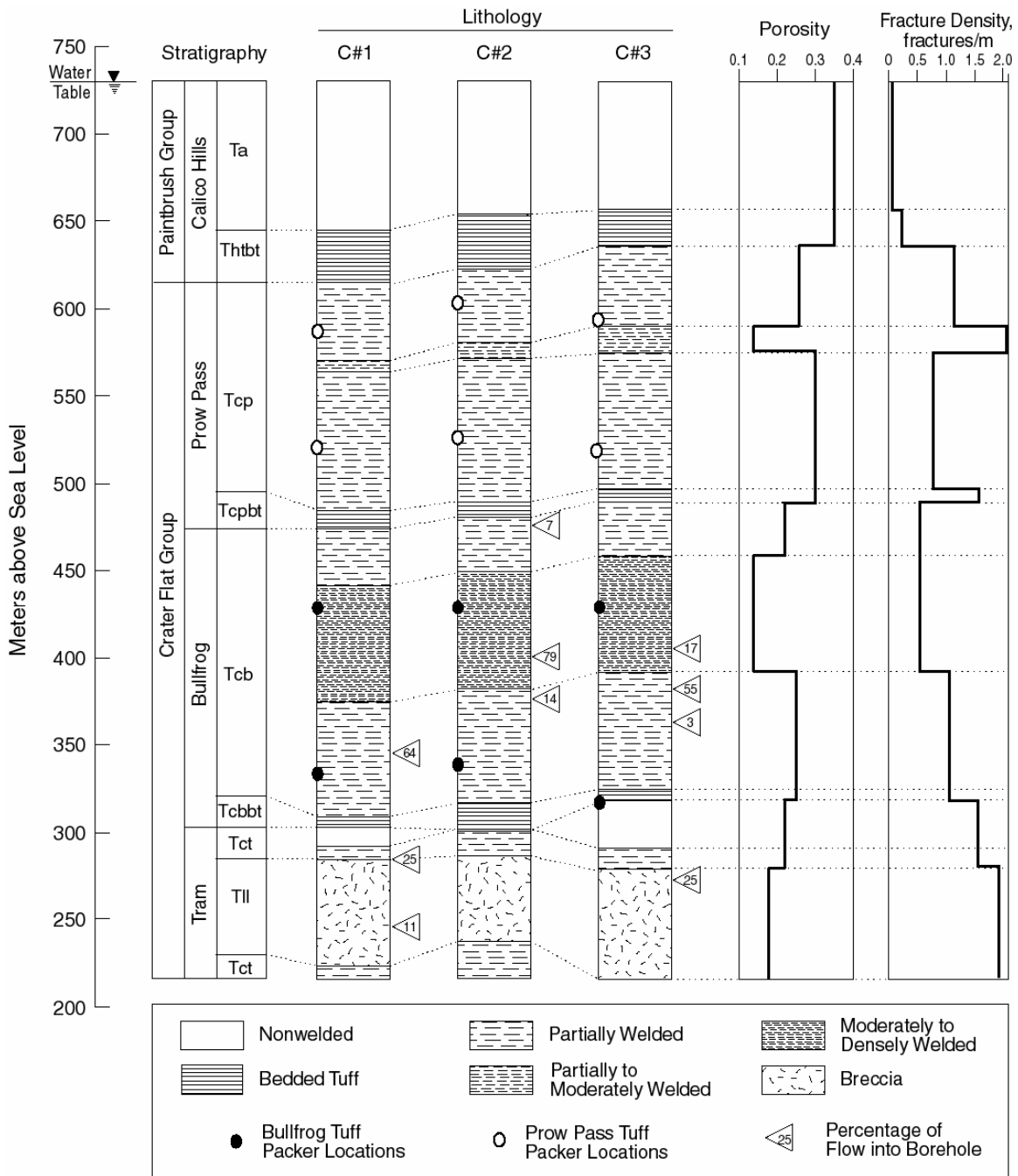
Table 6.1-2. Stratigraphy of Miocene Tuffaceous Rocks in the C-Wells Area

Geologic Unit	Depth Below Land Surface (m)				
	USW H-4	c#1	c#2	c#3	UE-25 p#1
Timber Mountain Group					
Rainier Mesa Tuff	not present	not present	not present	not present	39 to 55
Paintbrush Group					
Tiva Canyon Tuff	0 to 65	0 to 96	21 to 88	24 to 88	55 to 81
Topopah Spring Tuff	65 to 400	96 to 406	88 to 401	88 to 396	81 to 381
Calico Hills Formation	400 to 496	406 to 516	401 to 510	396 to 496	381 to 436
Crater Flat Group					
Prow Pass Tuff	496 to 693	516 to 656	510 to 652	496 to 644	436 to 558
Bullfrog Tuff	693 to 812	656 to 828	652 to 829	644 to 814	558 to 691
Tram Tuff	812 to 1,164	828 to 914+	829 to 914+	814 to 914+	691 to 873
Lithic Ridge Tuff	1,164 to 1,219+	not reached	not reached	not reached	873 to 1,068

Source: Geldon et al. 2002 ([DIRS 161163], p. 7, Table 2).

In the vicinity of the C-wells complex, northerly and northwesterly trending high-angle faults, such as the Paintbrush Canyon, Midway Valley, and Bow Ridge faults, have brecciated, offset, and tilted the tuffaceous rocks (Day et al. 1998 [DIRS 101557]; Dickerson and Drake 1998 [DIRS 102781]). Figure 6.1-3 shows major faults and structural features in the vicinity of Yucca Mountain. The dip of the tuffaceous rocks increases from 5° to 10° eastward at the crest of Yucca Mountain to about 20° eastward at the C-wells complex (Frizzell and Shulters 1990 [DIRS 105454], Map I-2046). At the C-wells complex, the north-striking Midway Valley fault or Paintbrush Canyon fault dropped Miocene tuffaceous rocks down to the west. Those rocks later were dropped to the northeast by a northwest-striking fault that cuts through Bow Ridge (Figure 6.1-3).

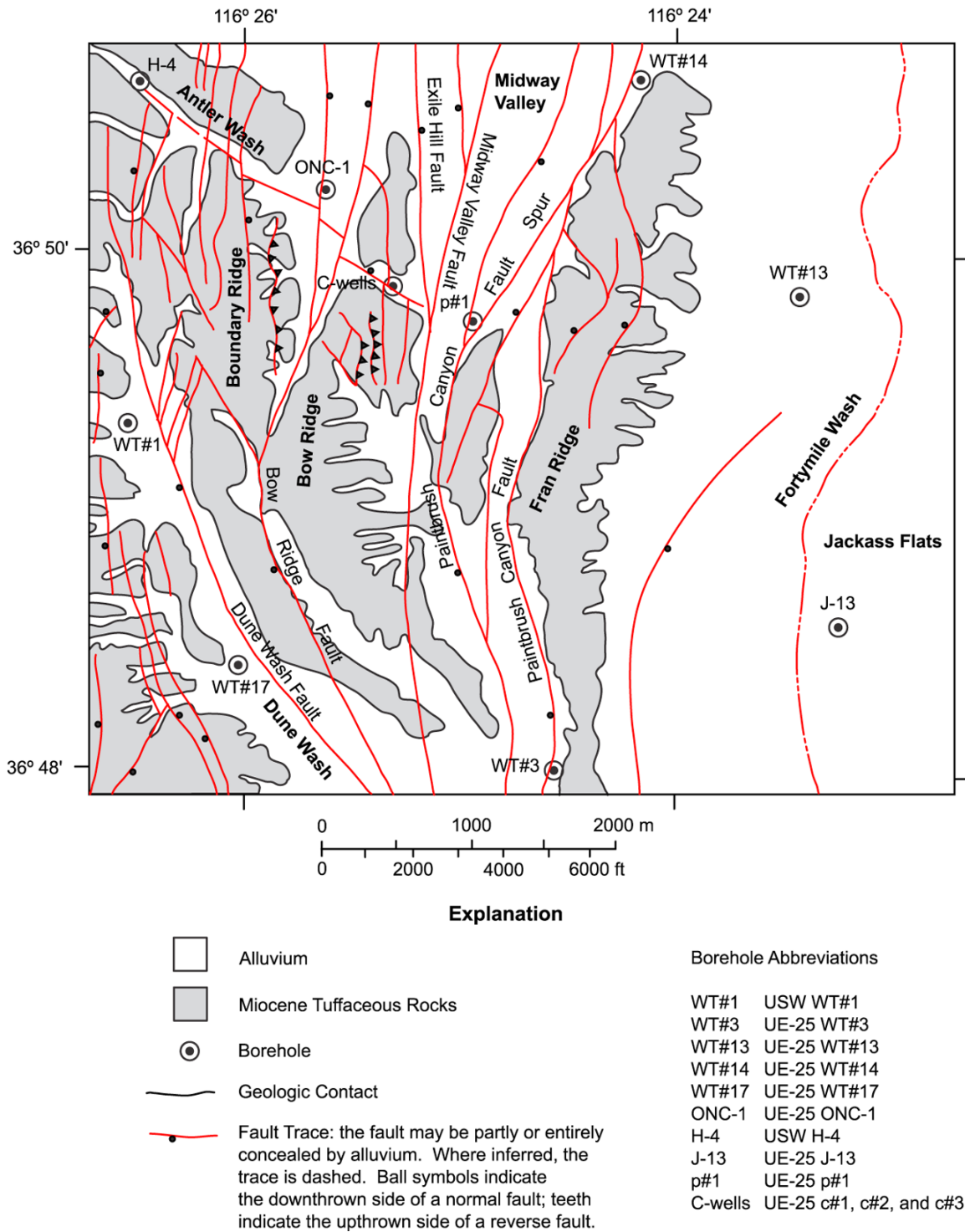
Hydrogeologic data and numerical modeling indicate that groundwater recharge in the Yucca Mountain area discharges mostly to Carson Slough, Ash Meadows, Alkali Flat, the lower Amargosa River Valley, and Death Valley (D'Agnese et al. 1997 [DIRS 100131]). Locally, groundwater flows mainly through Tertiary volcanic rocks and Quaternary and Tertiary alluvium and lacustrine deposits. Controlled largely by faults and related fractures, groundwater flows from basin to basin, mainly through deeper Paleozoic carbonate rocks (Faunt 1997 [DIRS 100146]). Cohen et al. (1996 [DIRS 156651]) demonstrated by two-dimensional numerical modeling that water in Miocene rocks at the C-wells complex could be derived from the Paleozoic carbonate rocks by upward flow along the Paintbrush Canyon, Midway Valley, or Bow Ridge faults. Geldon et al. (1998 [DIRS 129721], pp. 23 to 25, Figure 2; p. 31) concluded that a northwest-trending zone of discontinuous faults between Bow Ridge and Antler Wash also transmits groundwater.



Sources: Geldon 1993 [DIRS 101045], pp. 35 to 37, 68 to 70 (geologic information); Umari 2002 [DIRS 162858], Binder 10, Section L-11, pp. 70 to 71, Section L-9, pp. 57 to 58 (packer locations for Prow Pass Tuff in c#2 and c#3); DTNs: MO0703U25CHPTL.000 [DIRS 180070] (packer locations for Bullfrog Tuff and for Prow Pass Tuff in c#1) and GS931008312313.016 [DIRS 148173] (flow survey information; qualified for use in this report in Appendix L).

NOTE: Packer locations indicate intervals in which tracer tests described in this report were conducted. Fracture densities shown are from Borehole UE-25 c#1.

Figure 6.1-2. Stratigraphy, Lithology, Matrix Porosity, Fracture Density, and Inflow from Open-Hole Flow Surveys at the C-Wells



Source: Day et al. 1998 [DIRS 100027] (basis for geology).

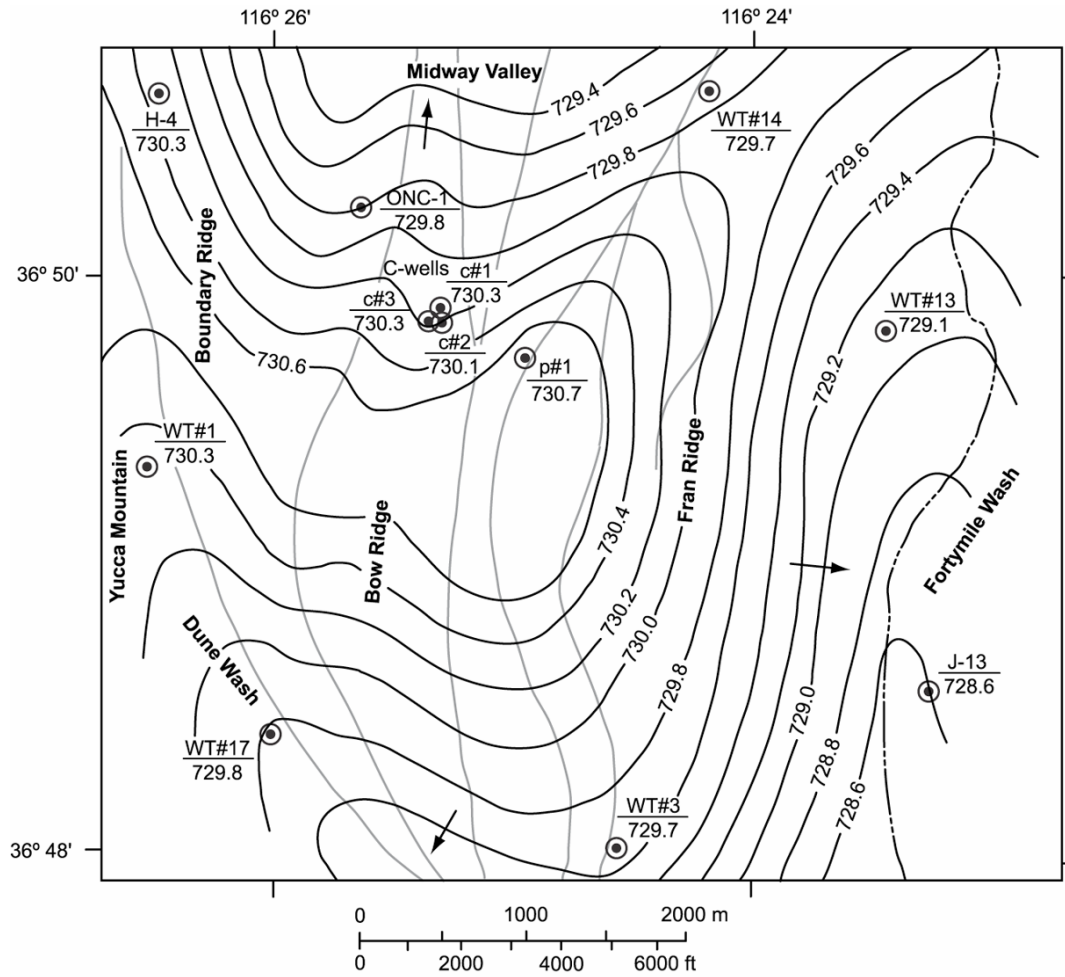
NOTE: Faults concealed beneath Quaternary cover are inferred and approximately located.

Figure 6.1-3. Generalized Geologic Map Showing the Location of the C-Wells Complex and Nearby Boreholes

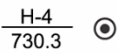
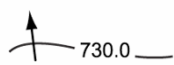

The water table in the Miocene tuffaceous rocks at Yucca Mountain in the vicinity of the C-wells complex ranges from about 335- to 520-m below land surface (O'Brien et al. 1995 [DIRS 101279], p. 3, Table 1; pp. 35 to 69) and from 400 to 402 m in the C-wells. These depths all correspond to a water-table elevation of approximately 730 m above mean sea level in the vicinity of the C-wells. Water in the tuffaceous rocks generally flows southeasterly (Ervin et al. 1994 [DIRS 100633]; Tucci and Burkhardt 1995 [DIRS 101060]), but flow patterns are disrupted by faults acting as conduits or barriers to flow. Water-level data are sparse in the vicinity of the C-wells complex, but the Paintbrush Canyon, Bow Ridge, and other faults apparently created a groundwater divide centered on Bow Ridge and Boundary Ridge that directs flow southward to Dune Wash, northward to Midway Valley, and eastward to Fortymile Wash (Figure 6.1-4). Flow from the west into the area of the C-wells is inhibited by the north-striking Solitario Canyon fault (Figure 6.1-3; Tucci and Burkhardt 1995 [DIRS 101060]).

The Miocene tuffs near the C-wells complex behave as a single fissure-block aquifer, in which the volume and direction of groundwater flow are controlled mainly by proximity to faults, fracture zones, and partings (Geldon et al. 1998 [DIRS 129721], p. 4). In a fissure-block aquifer, the permeability of the matrix is essentially negligible compared to the permeability of the fractures; and, hence, the aquifer behaves as a “dual-porosity” system in which the matrix acts as a reservoir for stagnant groundwater and flow occurs almost exclusively in fractures. Fractures in transmissive intervals have no preferred orientation, and fracture density appears unrelated to the extent of welding and permeability. Matrix permeability of the Calico Hills Formation and the Crater Flat Group within 5 km of the C-wells complex reaches 20 m Darcy (Geldon 1996 [DIRS 100396], Figure 5). On the basis of barometric efficiency and specific storage, the average effective porosity of the Calico Hills Formation near the water table in the C-wells was determined to be 36% (Geldon et al. 1997 [DIRS 156827], p. 11). The Crater Flat Group is less porous than the Calico Hills Formation. The average porosity of those geologic units in the C-wells is 21% [computed from porosity values reported by Geldon (1993 [DIRS 101045], pp. 60 to 62)]. Despite the influence of fractures, rock within about 3 km of the C-wells complex responds to hydraulic tests in a manner that is consistent with the response of a porous medium. In this report, such a rock mass is referred to as an “equivalent porous medium,” where the word “equivalent” indicates that the medium is not a true porous medium, but that, at the scale of observation, volume-averaged properties normally assigned to porous media can describe the hydraulic behavior of the rock mass.

Borehole flow surveys in combination with geophysical logs and aquifer tests show that flow within the tuffs at the C-wells complex comes primarily from discrete intervals (Figure 6.1-2). The total thickness of transmissive intervals identified in individual boreholes ranges from 165 to 274 m (Geldon 1996 [DIRS 100396], pp. 13 to 20). Hydraulic tests conducted in 1984 indicated that those intervals have layered heterogeneity (Geldon 1996 [DIRS 100396], pp. 9 to 69). Figure 6.1-5 is a depiction of the hydrogeologic intervals identified in the C-wells during hydraulic and tracer testing from 1995 to 1997 (Geldon 1996 [DIRS 100396], pp. 9 to 69).



Explanation

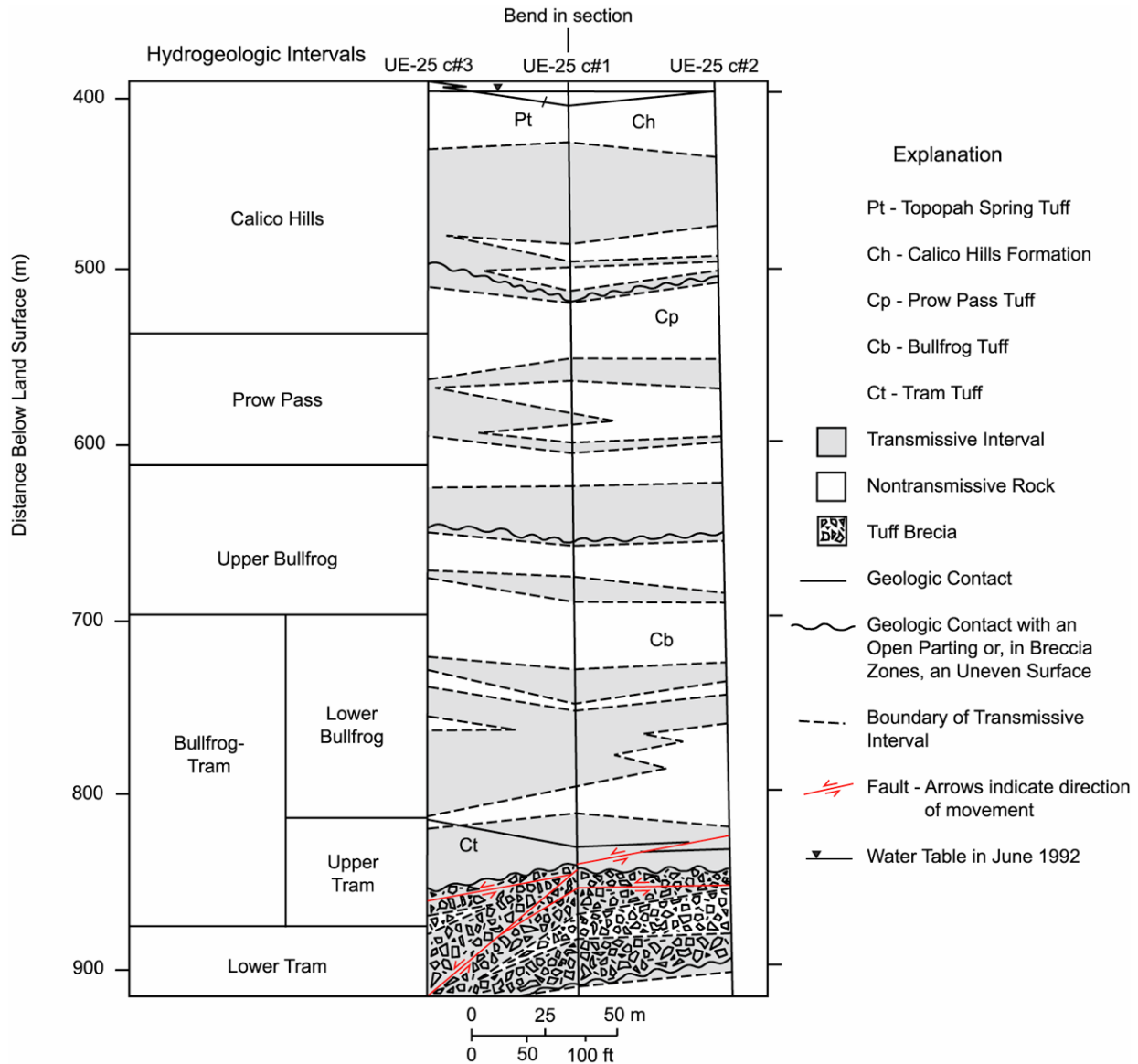
- 
Borehole. The circle indicates the position of the borehole; the numbers show the borehole number (above the line) and the water level altitude, in meters above NGVD of 1929 (below the line).
- 
Potentiometric Surface. The contours give the altitude above NGVD of 1929 at which water would have stood in tightly cased wells completed in the Miocene tuffaceous rocks in May 1995. The water-level altitude in UE-25 p#1 is estimated from the measured hydraulic head of Paleozoic carbonate rocks and the vertical head gradient between the Paleozoic carbonate rocks and Miocene tuffaceous rocks in the borehole. The arrows on the contour lines indicate the inferred direction of natural gradient. The contour interval is 0.2 m.
- 
Fault Trace.

For Illustration Purposes Only (qualitative interpretation)

Sources: Geldon et al. 2002, [DIRS 161163], p. 8, Figure 3 (Results of Hydraulic Tests in Miocene Tuffaceous Rocks at the C-Hole Complex, 1995-1997, Yucca Mountain, Nye County, Nevada); Nye County Nuclear Waste Repository Project Office 1995 [DIRS 156859], ONC-1 Drilling log.

NOTE: See Figure 6.1-3 for names of faults and complete borehole designations.

Figure 6.1-4. Potentiometric Surface of the Miocene Tuffaceous Rocks in the Vicinity of the C-Wells Complex, May 1995



Source: Geldon et al. 2002 [DIRS 161163], p. 9, Figure 4.

NOTE: For illustration purposes only (qualitative interpretation).

Figure 6.1-5. Hydrogeologic Intervals in the C-Wells Identified During Hydraulic and Tracer Testing from 1995 to 1997

6.1.1.2 Alluvial Testing Complex and Nye County Site 22

The SZ flow system to the south of Yucca Mountain transitions from a fractured tuff aquifer to a valley-fill (alluvium) aquifer before reaching the 18-km performance compliance boundary at approximately the southern boundary of the NTS. The exact location of this transition is uncertain and depends to a large extent on the direction of the flow pathways from the repository footprint to the compliance boundary, but available information suggests that radionuclides will transport through 2 to 10 km of saturated alluvium before reaching the boundary (SNL 2007 [DIRS 177391], Sections 6.3 and 6.4). Characterization of the valley-fill system was conducted

between 2000 and 2002 just outside the southwest corner of the NTS at the ATC, which is the site of the Nye County Early Warning Drilling Program (NC-EWDP) wells NC-EWDP-19D, -19P, -19IM1, and -19IM2 (these wells will be referred to as 19D, 19P, 19IM1, and 19IM2; Table B-1). Additional characterization of the valley-fill system was conducted between 2002 and 2005 at Nye County Site 22, located about 4.5 km north-northeast of the ATC, and consisting of wells NC-EWDP-22S, -22PA, -22PB, and -22PC. The locations of the ATC and Site 22 are shown in Figure 6.1-6. The surface layout of the wells at the ATC is shown in Figure 6.1-7, and the surface layout at Site 22 is shown in Figure 6.1-8.

Well 19D was drilled using a mud/rotary technique in March and April 2000 to a total depth of 443.8 m (1,456 ft) below land surface, with the water table being encountered at approximately 106 m (348 ft) below land surface (DTN: MO0101NVE03734.073 [DIRS 155267]). The well was completed using 18-cm (7.0-in.) outer dimension and 15.8-cm (6.24-in.) inner dimension steel pipe to allow pumps, packers, pressure transducers, and tracer injection equipment to be lowered into the hole (DTN: MO0112DQRWLNVE.018 [DIRS 157187]). This completion also allows for installation of a Westbay monitoring/sampling system that Nye County will use for long-term monitoring.

A piezometer well, 19P, was drilled just prior to drilling 19D at a location 25 m northeast of 19D at land surface. 19P was drilled using an air/hammer technique in March 2000 to a total depth of 142 m below land surface, with the water table being encountered at 112 m (368 ft) below land surface (DTN: MO0101NVE03734.073 [DIRS 155267]). This well was completed with a 7.3-cm (2-7/8-in.) outer diameter pipe casing and was screened from 109 to 139.5 m (358 to 458 ft) below land surface. The screened interval was developed by air injection. The well was intended to serve as a piezometer or monitoring well during pumping of 19D.

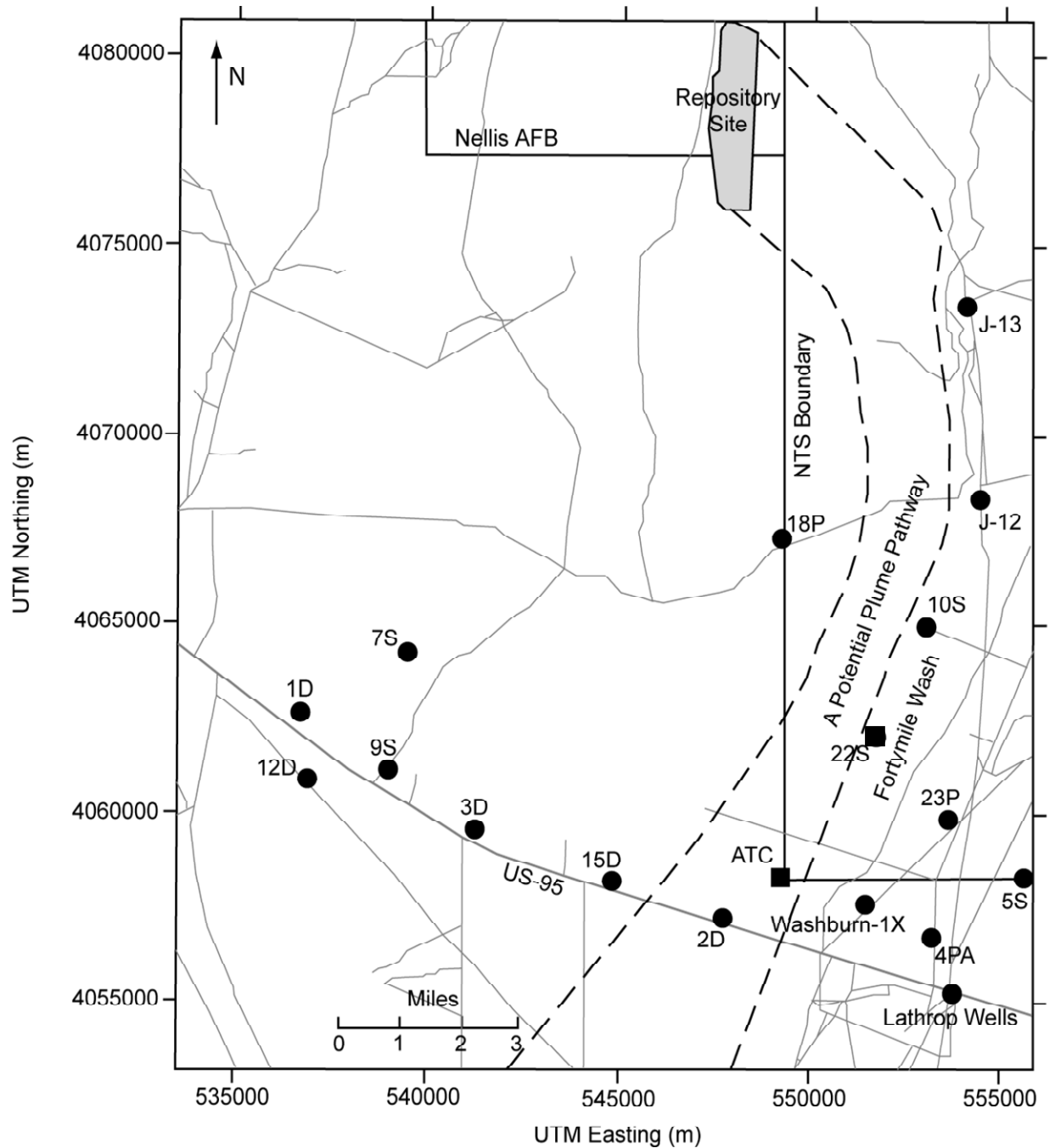
Wells 19IM1 and 19IM2 were drilled and completed in August and September, respectively, of 2001. 19IM1 was completed to a depth of 308.6 m (1,012.5 ft) below land surface, and 19IM2 was completed to 294.3 m (965.6 ft) below land surface. Figure 6.1-9 shows the completions of 19D, 19P, 19IM1, and 19IM2 along with the site lithology, as determined from onsite geological logging during drilling.

Well 19PB was added to the ATC complex after the hydraulic and tracer testing described in this report was completed. This piezometer was drilled to the depth of the second screened interval in 19D using a sonic coring method that preserved fine-scale layering in the alluvium. The borehole was intended for potential use as an injection well in a natural-gradient tracer test at the ATC. However, further testing at the ATC never occurred, so 19PB is not discussed further in this report, and it is not mentioned in the discussions of ATC hydraulic and tracer testing because it did not exist when the testing took place.

As Figure 6.1-9 shows, 19D was screened over seven different depth intervals, with the bottom three intervals completed below the valley-fill deposits (DTN: MO0112DQRWLNVE.018 [DIRS 157187]). A volcanic tuff was encountered at about 250 m (820 ft) below land surface, and a claystone/siltstone was encountered at approximately 378 m (approximately 1,260 ft) below land surface (DTN: GS011008314211.001 [DIRS 158690]). Although these intervals are potentially significant, they were not the primary focus of the ATC investigations. Thus, 19IM1 and 19IM2 were drilled and completed only to the depth of the highest screened interval in the

volcanic tuff in 19D. It was desirable to have one interval completed below the valley-fill deposits in each well so that hydraulic communication between the valley fill and the underlying tuff could be investigated. The wells were developed by air injection just below each of the screened intervals and also by pumping for 48 hours (hr) under open-hole conditions. In the case of 19D, the well was pumped in an open-hole configuration (no packers or plugs) at approximately 610 liters per minute (L/min) (approximately 160 gallons per minute) (gpm) with a total drawdown of 4.6 m to 6.1 m (15 ft to 20 ft).

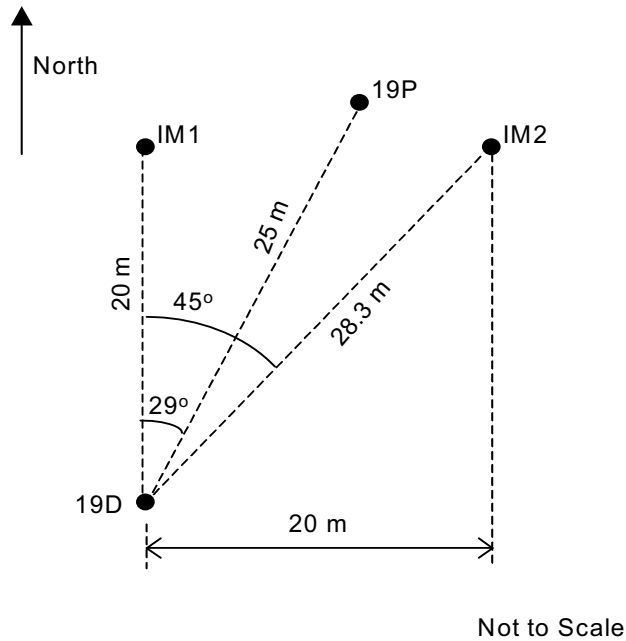
NC-EWDP-22S was drilled to a total depth of 364.7 m (1,196.5 ft) below land surface in July and August of 2001. It was completed with a 6" inside-diameter steel casing to make it suitable for pumping at high rates and for installation of a Westbay monitoring system. The bottom of this well is completed in what is classified as a nonwelded volcanic tuff breccia. The 22S completion includes four screened intervals at different depths in the alluvium (screens set at 159.0 m to 177.2 m (521.5 ft to 581.3 ft), 201.5 m to 231.8 m (661.2 ft to 760.6 ft), 268.3 m to 298.7 m (880.2 ft to 980.0 ft), and 347.5 m to 359.7 m (1,140.0 ft to 1,180.0 ft) below land surface (DTN: MO0306NYE05264.170 [DIRS 179376]), with the bottom screen in the volcanic breccia (Figure 6.1-10). The water table in 22S is 144.2 m (473 ft) below land surface (DTN: MO0306NYE05264.170 [DIRS 179376]) (see Figure 6.1-10). Well NC-EWDP-22PA, and -22PB were drilled in January and February 2002, respectively. These wells were installed as nested piezometers with two 2-in-diameter polyvinylchloride (PVC) tubes in each well screened at different depths. The two screens in 22PA correspond to the same depths as the two upper screens in 22S (DTN: MO0306NYE05265.171 [DIRS 179377]), and the two screens in 22PB correspond to the same depths as the two lower screens in 22S (DTN: MO0306NYE05266.172 [DIRS 179378]). NC-EWDP-22PC was drilled as a sonic core hole in October and November 2004. It was completed with 2" nested piezometers screened at the same depths as the upper two screens in 22S (DTN: MO0505NYE06464.314 [DIRS 179599]).



Source: DTN: MO0401COV03168.000 [DIRS 168534] is used as reference only.

NOTE: For illustration purposes only. Black circles indicate locations of other wells.

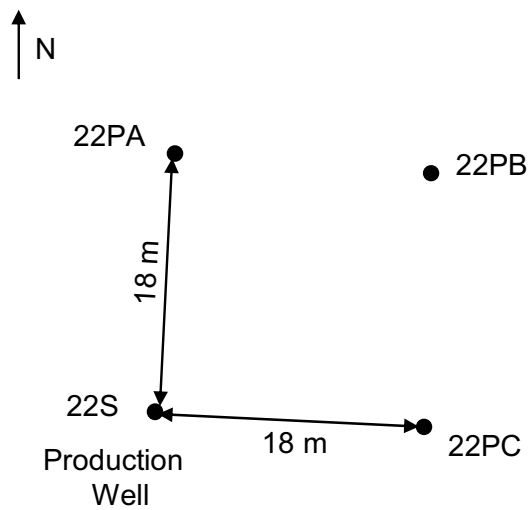
Figure 6.1-6. Map Showing Location of Alluvial Testing Complex (ATC) and Site 22 (22S) (Squares) in Relation to the Repository Footprint and the Southwestern Corner of the Nevada Test Site



Source: Based on BSC 2002 [DIRS 171585], p. 34, Figure 2.

NOTE: For illustration purposes only. Full well names are preceded by "NC-EWDP-."

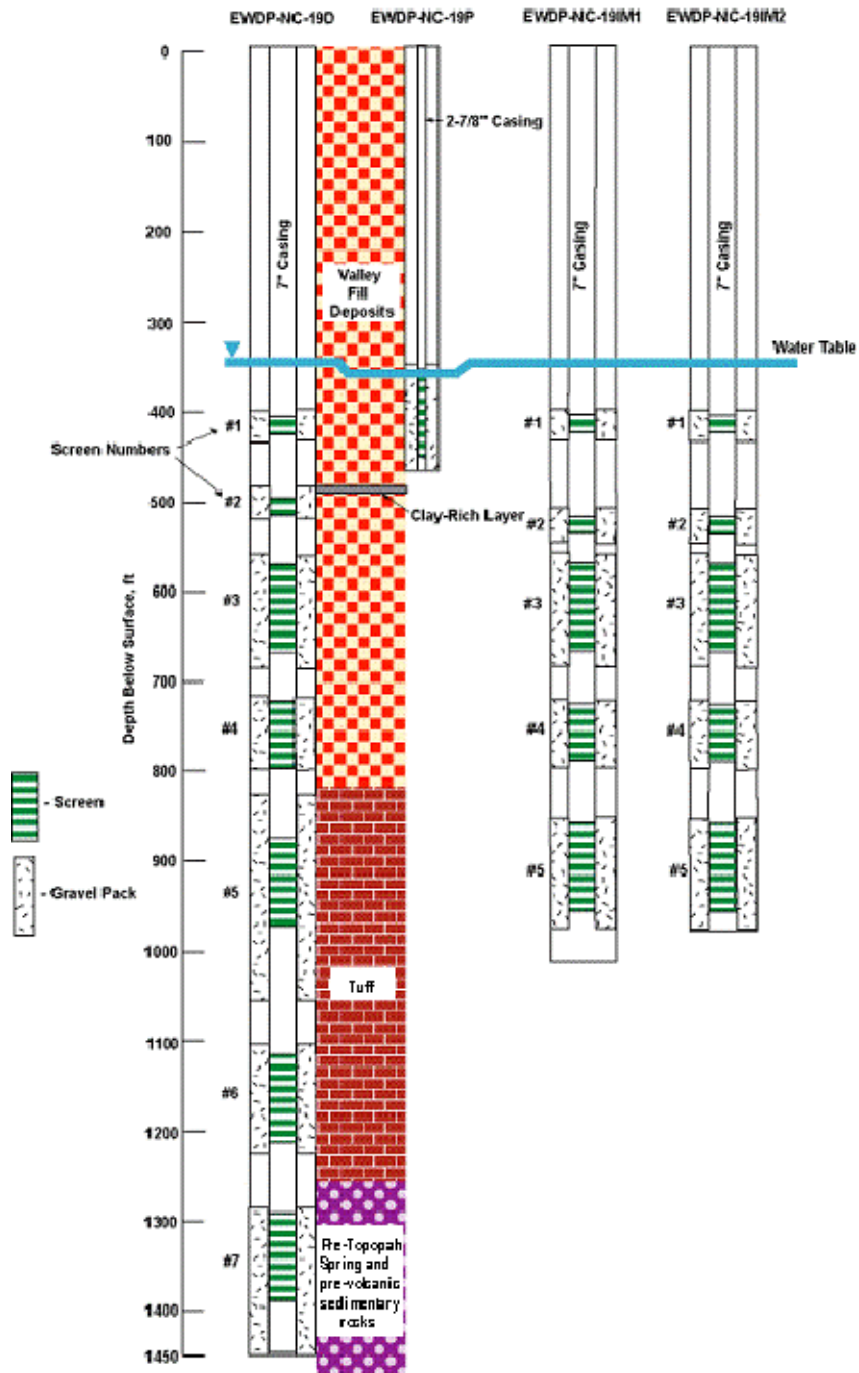
Figure 6.1-7. Surface Layout of the Alluvial Testing Complex



Sources: DTNs: MO0203GSC02034.000 [DIRS 168375] (22S location), MO0206GSC02074.000 [DIRS 168378] (22PA and 22PB locations), MO0503GSC05025.000 [DIRS 175275] (22PC location).

NOTE: For illustration purposes only. Full well names are preceded by "NC-EWDP-."

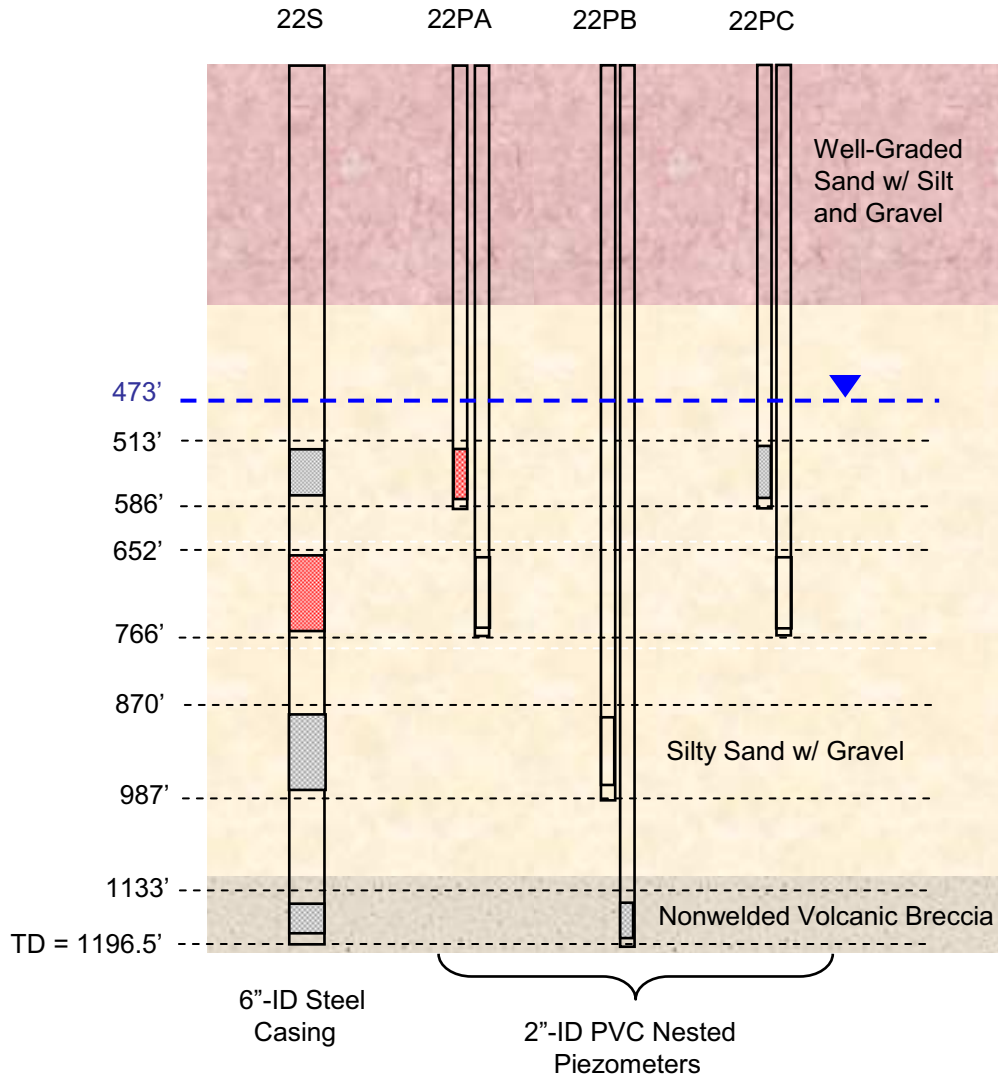
Figure 6.1-8. Surface Layout of Nye County Site 22.



Sources: DTNs: MO0112DQRWLNYE.018 [DIRS 157 187] (19D completion); MO0112DQRWLNYE.014 [DIRS 157184] (19P completion; for illustration only); GS011008314211.001 [DIRS 158690] (19D lithologic log); MO0306NYE05259.165 [DIRS 165876] (19IM1 well completion; for illustration only); LA0705PR150304.007 – qualified for use in this report in Appendix K [DIRS 181202] (19IM2 well completion).

NOTE: The water table is higher in NC-EWDP-19D than in -19P because hydraulic head increases with depth. The white spaces between gravel packs below the water table are “grout and bentonite seals.” The Nye County Nuclear Waste Repository Project Office reports all depths in feet.

Figure 6.1-9.Schematic Diagram of ATC Well Completions and Lithology



Sources: DTNs: GS030108314211.001 (Stratigraphy) [DIRS 163483], LA0705PR150304.007 (Well Completions) [DIRS 181202].

Figure 6.1-10. Schematic Diagram of NC-EWDP-22S, -22PA, -22PB, and -22PC Completions and Lithology. Red rectangles within wells indicate screens into which tracers were injected during single-well and cross-hole testing. The depths correspond to the tops and bottoms of sand packs (see text for tops and bottoms of screens)

6.1.2 Features, Events, and Processes Supported by This Scientific Analysis

As stipulated in the TWP (BSC 2006 [DIRS 177375]), this model report addresses the SZ FEPs pertaining to saturated zone in-situ testing included in TSPA-LA (Table 6.1-3). Table 6.1-3 provides a list of FEPs relevant to this model analysis in accordance with their assignment in the LA FEP list (DTN: MO0508SEPFELA.002 [DIRS 175064]). Specific reference to the various sections within this document where issues related to each FEP are addressed is provided in the table

Table 6.1-3. Features, Events, and Processes Included in TSPA-LA and Relevant to This Report

FEP No.	FEP Name	Sections Where Disposition Is Supported	FEP Topic Addressed in Other SZ Analysis or Model Reports
1.2.02.01.0A	Fractures	Flow in fractures is addressed throughout Section 6.2 and Appendix C. Transport in fractures is addressed throughout Section 6.3 and Appendix D. Also, discussion of lab transport studies in fractures is provided in Appendix E (Section E3.2).	Upstream Feeds ^a -N/A. Expanded Discussion ^b – BSC 2004 [DIRS 170014]. Corroborating ^c – SNL 2007 [DIRS 174109]; SNL 2007 [DIRS 177392]; SNL 2007 [DIRS 177391]; SNL 2007 [DIRS 177390]
1.2.02.02.0A	Faults	The influence of faults (or the potential influence of faults) on flow in the saturated volcanics is discussed in Sections 6.1.1.1, 6.2.3, 6.2.4, 6.2.7, C5, and C6.2.	Upstream Feeds ^a -N/A. Expanded Discussion ^b – SNL 2007 [DIRS 174109]. Corroborating ^c – SNL 2007 [DIRS 177392]; SNL 2007 [DIRS 177390]
2.2.03.01.0A	Stratigraphy	Hydrologic settings (including stratigraphy) for the hydraulic and tracer tests in the fractured volcanics and in the alluvium are discussed in Sections 6.1.1.1 and 6.1.1.2, respectively.	Upstream Feeds ^a - N/A. Expanded Discussion ^b – SNL 2007 [DIRS 174109]; SNL 2007 [DIRS 177391]. Corroborating ^c – SNL 2007 [DIRS 177390]; BSC 2004 [DIRS 170014]
2.2.03.02.0A	Rock properties of host rock and other units	Rock properties as they relate to flow and transport are addressed in many places throughout Sections 6.1.1, 6.2 through 6.5, and in Appendices C through H.	Upstream Feeds ^a -N/A. Expanded Discussion ^b – SNL 2007 [DIRS 174109]; SNL 2007 [DIRS 177391]. Corroborating ^c – SNL 2007 [DIRS 177391]; SNL 2007 [DIRS 177390]
2.2.07.12.0A	Saturated groundwater flow in the geosphere	Saturated groundwater flow in the fractured volcanics is addressed in Section 6.2 and Appendix C. Saturated groundwater flow in the alluvium is addressed in Section 6.4 and Appendix F.	Upstream Feeds ^a -N/A. Expanded Discussion ^b – SNL 2007 [DIRS 177391]. Corroborating ^c – SNL 2007 [DIRS 177391]; BSC 2004 [DIRS 170015]; BSC 2004 [DIRS 170014]; SNL 2007 [DIRS 177390]
2.2.07.13.0A	Water-conducting features in the SZ	Geologic features affecting flow in the fractured volcanics are addressed in Section 6.1.1.1, Section 6.2, and Appendix C. Geologic features affecting flow in the alluvium are addressed in Section 6.1.1.2, Section 6.4 and Appendix F.	Upstream Feeds ^a -N/A. Expanded Discussion ^b – SNL 2007 [DIRS 177391]; SNL 2007 [DIRS 177390]. Corroborating ^c – BSC 2004 [DIRS 170014]

Table 6.1-3. Features, Events, and Processes Included in TSPA-LA and Relevant to This Model Report (Continued)

FEP No.	FEP Name	Sections Where Disposition Is Supported	FEP Topic Addressed in Other SZ Analysis or Model Reports
2.2.07.15.0A	Advection and dispersion in the SZ	Advection and dispersion effects on transport in the fractured volcanics are discussed throughout Section 6.3 and Appendix D, and they are discussed for the alluvium throughout Section 6.5 and Appendix G. Scale dependence of dispersion in the fractured volcanics is addressed in Section E4.1.	Upstream Feeds ^a -N/A Expanded Discussion ^b – SNL 2007 [DIRS 177392]; SNL 2007 [DIRS 177390]. Corroborating ^c – SNL 2007 [DIRS 177391]; BSC 2004 [DIRS 170015]
2.2.07.17.0A	Diffusion in the SZ	Molecular diffusion processes in the volcanics are addressed in Section 6.3 and in several places in Appendices D and E. In Section 6.5 and Appendix G, molecular diffusion is discussed for the alluvium, but it was concluded that it did not have a major effect on transport in the alluvium.	Upstream Feeds ^a -N/A Expanded Discussion ^b – SNL 2007 [DIRS 177390]; SNL 2007 [DIRS 177392]. Corroborating ^c – BSC 2004 [DIRS 170014]; BSC 2004 [DIRS 170006]
2.2.08.08.0A	Matrix diffusion in the SZ	The effects of matrix diffusion on transport in the volcanics are discussed in Section 6.3.2 and in Sections D4. and E4.2. Observations and parameterizations of matrix diffusion in the volcanics are addressed in several places in Section 6.3 and Appendices D and E. Matrix diffusion in the alluvium is discussed in Sections 6.5.2, 6.5.4 and in Appendix G, but it was concluded that matrix diffusion did not have a significant effect on transport in the alluvium.	Upstream Feeds ^a -N/A Expanded Discussion ^b – SNL 2007 [DIRS 177390]; SNL 2007 [DIRS 177392]. Corroborating ^c – BSC 2004 [DIRS 170014]; BSC 2004 [DIRS 170006]
2.2.08.09.0A	Sorption in the SZ	Sorption in the SZ is addressed in Sections 6.3.4, 6.3.5, 6.3.6, and 6.5.6. It is also addressed in detail in the following appendix sections: D4, E1, E3, H1, and H2. The material in Sections 6.3 and D4 address field-scale observations of sorption, and the material in the other sections addresses laboratory observations of sorption of sorbing tracer used in the field tracer tests.	Upstream Feeds ^a -N/A Expanded Discussion ^b – SNL 2007 [DIRS 177392]; SNL 2007 [DIRS 177390]. Corroborating ^c – None (This analysis is corroborating to the two reports above that contain expanded discussions).

Table 6.1-3. Features, Events, and Processes Included in TSPA-LA and Relevant to This Model Report (Continued)

FEP No.	FEP Name	Sections Where Disposition Is Supported	FEP Topic Addressed in Other SZ Analysis or Model Reports
2.2.08.10.0A	Colloidal transport in the SZ	Colloid transport in the volcanics is addressed in Section D4. Colloid detachment rates in the alluvium are addressed in Section G4.6. Colloid-facilitated transport of radionuclides is not directly addressed in this report.	Upstream Feeds ^a -N/A Expanded Discussion ^b – BSC 2004 [DIRS 170006]; SNL 2007 [DIRS 177390]. Corroborating ^c – SNL 2007 [DIRS 177392]
2.2.12.00.0B	Undetected features in the SZ	Undetected features are indirectly addressed in the discussion of anisotropy in horizontal hydraulic conductivity in the fractured volcanics in Sections 6.2.6, C6.2, and C6.3. Flow anisotropy may be the result of undetected features such as fracture sets or faults.	Upstream Feeds ^a -N/A Expanded Discussion ^b – SNL 2007 [DIRS 177391]. Corroborating ^c – BSC 2004 [DIRS 170014]; SNL 2007 [DIRS 177390]

^a Upstream Feeds – Aspects of the SZ FEP screening position adopted in this report are a result of SZ analyses performed in a directly upstream SZ model or analyses.

^b Expanded Discussion – The FEP topic is addressed in more detail in an SZ analysis or model report.

^c Corroborating – Corroborative aspect(s) of the FEP topic is (are) discussed in an SZ analysis or model report.

FEP=feature, event, and process; SZ=saturated zone.

6.2 HYDROLOGIC PROPERTIES OF FRACTURED TUFFS (C-WELLS COMPLEX)

6.2.1 Introduction

This section of the report (1) summarizes the hydraulic tests conducted at the C-wells complex and the interpretive analyses performed on the test data; (2) discusses the implications of the test interpretations, including implications for conceptual understanding of groundwater flow in the fractured volcanics, hydrologic parameter estimates, and horizontal flow anisotropy in the fractured volcanics; and (3) discusses the uncertainties and limitations associated with the hydrologic properties determined from the test analyses.

6.2.2 Summary of C-Wells Hydraulic Testing to Determine Hydrologic Properties

Table 6.2-1 summarizes the hydraulic testing conducted at the C-wells complex over a fifteen-year period. Aquifer storativities and transmissivities were estimated primarily from water-level drawdowns measured in observation wells as a function of pumping time of a production well (i.e., drawdown curves) in the last five tests listed Table 6.2-1. The other tests listed in Table 6.2-1 provided valuable information on flowing intervals within each well; some of this information was used to convert aquifer transmissivity estimates to hydraulic conductivity estimates for flowing intervals. Details of hydraulic testing at the C-wells, especially the tests listed in the last four rows of Table 6.2-1, are provided in Appendix C.

In the last four tests of Table 6.2-1, the C-wells were equipped with packers that could be inflated to isolate selected intervals and allow observations of drawdown above, below, and in the pumped interval (or in isolated intervals in the observation well when the production well was pumped as an open hole). The test intervals were given names corresponding to the major lithologies located between each pair of packers, above the top packer, and below the bottom packer (although malfunctioning pressure/temperature transducers prevented data collection in some of the intervals during some time periods). In order of increasing depth, these intervals are referred to as the Calico Hills, Prow Pass, Upper Bullfrog, Lower Bullfrog, Upper Tram, and Lower Tram intervals (Table 6.1-1). Water-level drawdowns in the isolated intervals provided valuable insights into aquifer characteristics at the scale of the C-wells complex. Distant observation wells, which provided information on large-scale aquifer properties, were typically open holes. Drawdowns in production wells were not analyzed to estimate hydrologic parameters, as they proved to be unreliable indicators of aquifer transmissivity because of well losses.

6.2.3 Hydraulic Test Interpretation Methods

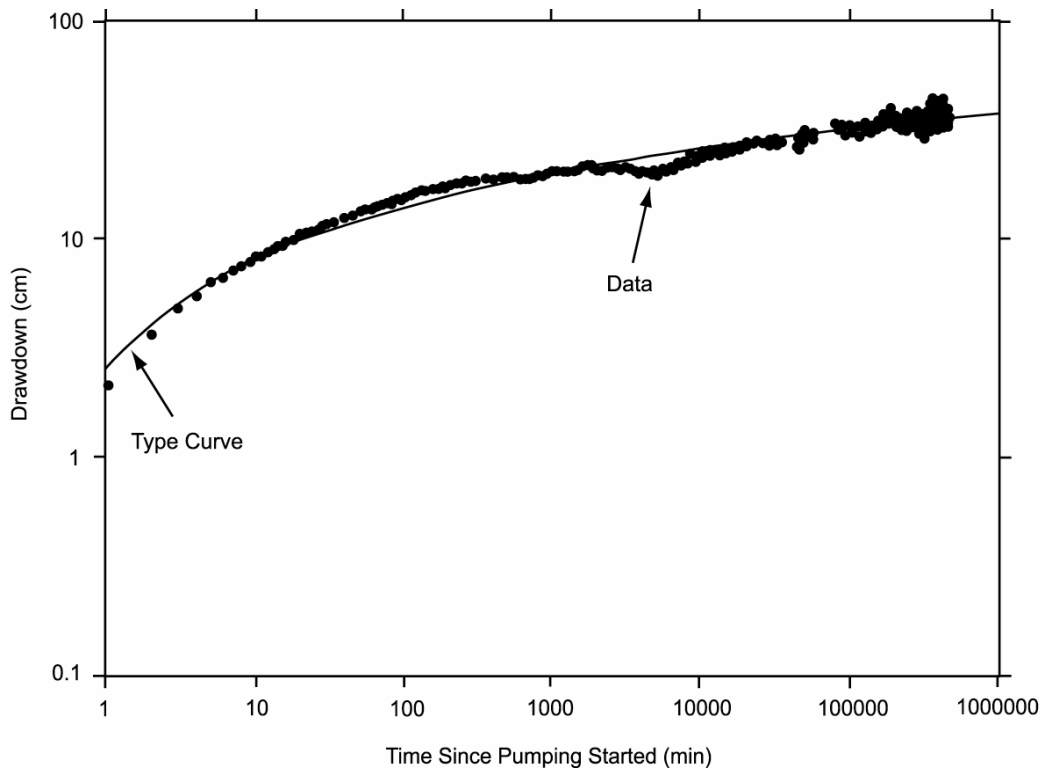
Storativity and transmissivity estimates were obtained from observation well drawdown data by adjusting these two hydrologic parameters in various analytical solutions of the groundwater flow equation until a match to the data was achieved. An example of a curve match is shown in Figure 6.2-1. The data were corrected for barometric pressure fluctuations and earth tide fluctuations prior to being analyzed. The analytical solutions employed included the unconfined aquifer solution from “Analysis of Pumping Test Data from Anisotropic Unconfined Aquifers Considering Delayed Gravity Response” (Neuman 1975 [DIRS 150321]); the confined-aquifer, single-porosity solution from “The Relation Between the Lowering of the Piezometric Surface and the Rate and Duration of Discharge of a Well Using Ground-Water Storage” (Theis 1935 [DIRS 150327]); the confined-aquifer, dual-porosity solution from “Well Hydraulics in Heterogeneous Aquifer Formations” (Streltsova-Adams 1978 [DIRS 150754]); and the leaky-confined aquifer solution from “Analysis of Data from Pumping Tests in Leaking Aquifers” (Hantush 1956 [DIRS 165169]). With the exception of the Neuman (1975 [DIRS 150321]) unconfined-aquifer solution, which assumes both vertical and horizontal flow, these analytical solutions all assume radial flow to the pumping well in a homogenous, isotropic aquifer of constant thickness.

Table 6.2-1. Highlights of Testing at the C-Wells Complex to Determine Hydrologic Properties (See Appendix C for Complete Description of Tests)

Dates	Testing Summary	References
1983-1984	Geophysical logs; open-hole flow and temperature surveys during pumping (with pump well drawdown monitored); tracejector surveys using radioactive iodide; falling-head and pressure-injection tests in c#1 (1983); constant-flux injection test in c#2 and 3 pump tests in c#2 and c#3 (1984)	Geldon 1993 [DIRS 101045] Geldon 1996 [DIRS 100396]
1991	Heat-pulse flowmeter surveys (nonpumping)	Geldon 1996 [DIRS 100396]
1992	Television logs	Geldon 1993 [DIRS 101045]
1993	Seismic tomogram between c#2 and c#3	Communication from E. Majer, LBNL (Geldon et al. 2002 [DIRS 161163], p. 2)

Table 6.2-1. Highlights of Testing at the C-Wells Complex to Determine Hydrologic Properties (See Appendix C for Complete Description of Tests) (Continued)

Dates	Testing Summary	References
1993	Barometric efficiency from simultaneous monitoring of water levels and atmospheric pressure	Geldon et al. 1997 [DIRS 156827], p. 11
June 1995	Spinner and oxygen-activation surveys in c#3	Geldon et al. 1998 [DIRS 129721]
May 22-June 12, 1995	Open hole pumping of c#3 while monitoring c#1, c#2, ONC-1, and USW H-4 (all open holes)	Geldon et al. 1998 [DIRS 129721]
June 12-22, 1995	Open hole pumping of c#3 while monitoring 6 intervals (with 5 inflated packers) in c#1 and c#2	Geldon et al. 2002 [DIRS 161163]
Feb. 8-13, 1996	Pumping of combined lower Bullfrog-Tram interval in c#3 while monitoring combined lower Bullfrog-upper Tram interval (and above and below this interval) in c#1 and c#2	Geldon et al. 2002 [DIRS 161163]
May 8 1996 to Nov. 12, 1997	Pumping of lower Bullfrog interval in c#3 while monitoring 6 intervals (with 5 inflated packers) in c#1 and c#2. Also, monitoring of ONC-1, USW H-4, UE25 WT#14, UE25 WT#3, and UE25 p#1	Geldon et al. 2002 [DIRS 161163]
June 2-Sept. 22, 1998	Pumping of Prow Pass interval in c#2 while monitoring the Prow Pass interval (and above and below this interval) in c#1 and c#3	Appendix C, Section C3.2



Source DTNs: GS970308312314.001 [DIRS 1592 40], GS970708312314.005 [DIRS 159241],
GS981008312314.002 [DIRS 147068], GS981008312314.003 [DIRS 144464].

Output DTN: GS031008312314.004.

NOTE: This figure also appears as Figure C-30 in Appendix C, where the details of the analysis are discussed. .
This plot shows the match of the Streltsova-Adams fissure-block aquifer solution to the drawdown in
UE-25 c#1, Lower Bullfrog Interval, May 8, 1996, to March 26, 1997

Figure 6.2-1. Example of a Match of an Analytical Flow Model to Drawdown Data in an Aquifer Pump Test

The analytical solutions used for each of the test intervals at the C-wells were selected based on both the knowledge of interval flow characteristics gained from previous logging and testing and on the characteristic shapes of the interval drawdown curves. The Neuman (1975 [DIRS 150321]) unconfined-aquifer solution was applied to the Calico Hills interval because the upper boundary for this interval is the water table (therefore, it is unconfined by definition). This solution was also applied to the hydraulic test conducted from May to June 1995, in which all three C-wells were open holes. This test provided a composite estimate of vertical hydraulic conductivity at the C-wells location. The Theis (1935 [DIRS 150327]) and Streltsova-Adams (1978 [DIRS 150754]) confined aquifer solutions were applied to the Prow Pass, Upper Bullfrog, and Lower Bullfrog intervals because these intervals responded as though they were confined by overlying aquitards. The Streltsova-Adams (1978 [DIRS 150754]) solution was used when there was a slight but noticeable increase in the slope of the drawdown curve at late times, indicative of water release from secondary porosity in the aquifer (assumed to be the matrix in fractured media). Finally, the Hantush (1956 [DIRS 165169]) leaky-confined aquifer solution was used for the Tram intervals, which are intersected by known faults present at the bottom of the C-wells that appear to provide a source of recharge or “leakage.” In each case, the analytical

solutions yielded satisfactory matches to the observation well drawdown curves. Details of the test interpretations are provided in Appendix C.

Methods used to estimate anisotropy in horizontal hydraulic conductivity over large scales in the fractured volcanics are discussed in more detail in Section 6.2.6. These methods rely on an initial well-by-well analysis of drawdown data in distant observation wells during the May 1996 to November 1997 test of the lower Bullfrog interval using simple analytical methods to estimate storativity and transmissivity in the general direction of each observation well that responded to pumping. Then, either the method of Hantush (1966 [DIRS 161160]) or the method of Papadopoulos (1967 [DIRS 150265]) was used to determine anisotropy in horizontal hydraulic conductivity from the individual well analyses.

6.2.4 Hydraulic Test Interpretations: Conceptual Flow Model Implications

The fact that the analytical solutions yielded satisfactory matches to the hydraulic test drawdown data suggests that, at least at scales of approximately 30 m or more, the fractured volcanic rocks in the vicinity of the C-wells behave as an “equivalent porous medium” (implicitly assumed in the analytical solutions), as noted in Section 6.1.1.1. The term “equivalent porous medium” is used to indicate that the flow intervals respond to pumping as if they were porous media, even though flow actually occurs within discrete fracture networks. Based on this consistent observation, flow and transport through the saturated fractured volcanic rocks was modeled using a continuum modeling approach (i.e., as an equivalent porous medium) in the SZ site-scale flow model (SNL 2007 [DIRS 177391]).

Another important aspect of conceptual flow modeling supported by C-wells hydraulic testing is that flow in the fractured volcanics is not confined to stratigraphic or lithologic boundaries. Although drawdown responses were often consistent with that of a confined aquifer (and analyzed as such), intervals in observation wells above and below the pumped intervals typically had significant responses to pumping (in some cases exhibiting even greater drawdown than in the interval that was pumped). These observations suggest that fracture networks conducting flow extend beyond stratigraphic and lithologic contacts. Also, the interpretation of the open-hole aquifer test conducted in May-June 1995 indicated that there is a significant composite vertical hydraulic conductivity at the C-wells, although it is anywhere from 2.5 to 12 times less than the composite horizontal hydraulic conductivity. Collectively, these results support the approach taken in the SZ site-scale flow model (SNL 2007 [DIRS 177391]) of allowing flow to occur across stratigraphic contacts, and assuming an overall vertical hydraulic conductivity (or permeability) smaller than the horizontal hydraulic conductivity.

Finally, the C-wells hydraulic testing results suggest that structures such as faults may play an important role in determining hydrologic characteristics both locally and over large distance scales. The most transmissive interval at the C-wells is the Lower Bullfrog Tuff, which is located adjacent to the fault zone that intersects the C-wells. The second most transmissive interval is the Upper Tram, in which the fault zone occurs. Transmissivities become progressively smaller in intervals further away from the fault zone (Table 6.2-2). Also, the responses of distant wells, especially ONC-1 and USW H-4, to pumping the C-wells suggest a correlation between hydraulic responses and structures inferred from surface topography. These structural influences are not explicitly accounted for in the SZ site-scale flow model (SNL 2007 [DIRS 177391]), but they are indirectly accounted for by specifying a horizontal anisotropy in

hydraulic conductivity in the fractured volcanics consistent with the responses in distant wells to pumping of the C-wells.

6.2.5 Hydraulic Test Interpretations: Hydrologic Parameter Estimates at the C-Wells

The storativity, transmissivity, and hydraulic conductivity estimates obtained from analyzing the C-wells responses in the hydraulic tests listed in the last five rows of Table 6.2-1 are provided in Table 6.2-2. Details of the test interpretations are provided in Appendix C. Ranges are provided for the parameters because the values represent the results from either multiple observation wells and/or multiple tests. When only one value is presented, it means that the parameters estimated from all wells and tests were identical. Table 6.2-2 does not include any hydrologic parameter estimates obtained from analyzing responses in distant observation wells (i.e., outside the C-wells complex). These responses are discussed in more detail in the next section on large-scale horizontal anisotropy of hydraulic conductivity.

The parameter values in Table 6.2-2 are not used directly in the SZ site-scale flow model (SNL 2007 [DIRS 177391]). Instead, the hydraulic conductivities (or permeabilities) of different stratigraphic or lithologic “layers” in the SZ site-scale flow model are adjusted to “calibrate” the model to water level measurements throughout the model domain and to flux targets at the boundaries of the domain. The results of this calibration (as well as some alternative calibrations), are discussed in the SZ site-scale flow model report (SNL 2007 [DIRS 177391], Sections 6.6, 6.7, 6.8, and 7). Interestingly, they suggest that the Bullfrog unit is one of the more permeable “layers” in the model (SNL 2007 [DIRS 177391], Table 6-19), a result that is qualitatively consistent with the hydraulic testing result that the Lower Bullfrog interval has the largest transmissivity and hydraulic conductivity at the C-wells complex.

Table 6.2-2. Ranges of Hydrologic Parameters Derived from C-Wells Cross-Hole Hydraulic Testing

Flow Interval	Storativity	Transmissivity (m ² /day)	Hydraulic Conductivity (m/day) ^a
Calico Hills ^(b)	0.0002 to 0.0006	4 to 10	0.08 to 0.2
Prow Pass	0.0002 to 0.003	30 to 60	0.8 to 3
Upper Bullfrog ^(b)	0.00002 to 0.0009	40 to 100	0.8 to 4
Lower Bullfrog	0.0002 to 0.003	1,300 to 1,900	30 to 60
Lower Bullfrog – Upper Tram	0.0003 to 0.002	2,500	20 to 50
Upper Tram ^(b)	0.0001 to 0.001	800 to 900	20 to 40
Composite ^(c)	0.001 to 0.003	1,800 to 2,100	Horizontal: 3.6 to 4.2 Vertical: 0.3 to 1.7

Output DTN: GS031008312314.004, (from Source DTNs: LA0705PR150304.002 [DIRS 181198], LA0705PR150304.003 [DIRS 181201], GS970308312314.001 [DIRS 159240], GS970708312314.005 [DIRS 159241], GS981008312314.002 [DIRS 147068], GS981008312314.003 [DIRS 144464], and GS990408312315.002 [DIRS 140115]).

^a Values obtained by estimating a transmissive thickness within each interval from various lines of evidence [Conductivity = Transmissivity/(Transmissive Thickness)].

^b Values obtained by estimating an “equivalent radial volumetric flow rate” for these intervals, which were never isolated for pumping (see Appendix C for details).

^c Composite values obtained from open-hole aquifer test conducted May 22 to June 12, 1995 (hence, the transmissivities for each interval do not add up to the composite). This test was interpreted using an unconfined aquifer solution to provide estimates of composite vertical hydraulic conductivity. The horizontal hydraulic conductivities were calculated assuming that the *entire* thickness of the saturated zone tested (approximately 500 m) was the transmissive thickness.

6.2.6 Hydraulic Test Interpretations: Horizontal Anisotropy in Hydraulic Conductivity

The hydraulic responses at the C-wells indicated very little flow anisotropy at the local scale (Table C-7). This apparent lack of anisotropy was qualitatively confirmed by C-wells tracer responses in both the lower Bullfrog and the Prow Pass intervals (Section 6.3.4, Table 6.3-2). However, hydraulic responses in more distant wells (to pumping the C-wells) indicated significant flow anisotropy at larger scales in the fractured volcanic tuffs. The long-term pumping test from May 8, 1996, through November 12, 1997 (in which the Lower Bullfrog interval in c#3 was pumped at about 570 L/min) was the only hydraulic test conducted at the C-wells that yielded data suitable for estimating the hydrologic properties of the fractured volcanics on a scale beyond the immediate vicinity of the C-wells. Changes in local groundwater elevations due to pumping at the C-wells complex were monitored at four distant wells (H-4, ONC-1, WT#3, and WT#14 exhibited sufficient drawdown for hydrologic parameter estimation), allowing a horizontal anisotropy ratio and principal direction to be estimated over an approximately 21-km² area in the fractured volcanics. The C-wells responses were not considered in analyses of anisotropy.

Four different sets of storativity and transmissivity estimates were obtained for each of the four wells that responded to pumping the Lower Bullfrog interval of the C-wells (Table 6.2-3). The first set was taken from the analysis of Winterle and LeFemina (1999 [DIRS 129796], Section 4.5), who processed the long-term pumping data using AQTESOLV, with the Theis (1935 [DIRS 150327]) confined-aquifer solution being used to obtain transmissivity and storativity estimates. The second set of estimates was obtained by applying the Cooper-Jacob

(1946 [DIRS 150245]) method to filtered and derivative-analyzed drawdown data. The third and fourth sets of estimates was obtained by applying the methods discussed in Section 6.2.3, with the Streltsova-Adams (1978 [DIRS 150754]) confined fissure-block solution being used for the ONC-1 analysis and the Theis (1935 [DIRS 150327]) confined aquifer solution being used for the other three wells. The differences between these two sets of estimates are attributable to different methods of filtering the drawdown data prior to the analyses. Details of these methods of estimating storativities and transmissivities are provided in Appendix C.

After storativity and transmissivity were estimated for each well, the horizontal anisotropy was estimated from these parameters using either the Hantush (1966 [DIRS 161160]) method, the Papadopulos (1967 [DIRS 150265]) method, or three different applications of the Papadopulos (1967 [DIRS 150265]) method combined with the PEST parameter-estimation program, Version 5.5 (STN: 10289-5.5-00 [DIRS 161564]). The method of Hantush (1966 [DIRS 161160]) was applied to the storativities and transmissivities obtained by the Cooper-Jacob (1946 [DIRS 150245]) method, although the H-4 results were excluded from this analysis because their inclusion yielded a negative anisotropy ratio. Winterle and LeFemina (1999 [DIRS 129796], Section 4.5) used the Papadopulos (1967 [DIRS 150265]) method to estimate anisotropy, and they also excluded the H-4 results to obtain a meaningful anisotropy ratio. Ferrill et al. (1999 [DIRS 118941]) conducted a separate analysis using the individual well parameter estimates of Winterle and LeFemina (1999 [DIRS 129796]) and the Papadopulos (1967 [DIRS 150265]) method, but with a slight modification of the WT#14 transmissivity (from 1,330 to 1,370 m²/day) due to a difference in technique for correcting barometric pressures. H-4 results were also excluded from their analyses. The Papadopulos (1967 [DIRS 150265])-PEST method was applied to two sets of transmissivity/storativity values obtained from the same analysis methods (Theis 1935 [DIRS 150327] for WT#3, WT#14, and H-4, Streltsova-Adams 1978 [DIRS 150754] for ONC-1) but with different methods of filtering the raw drawdown data (see Geldon et al. (2002 [DIRS 161163], pp. 15 to 16), and Appendix C, Section C6.2.1 for the two filtering methods). Finally, a third Papadopulos-PEST analysis was conducted assuming a transmissivity of 1,000 m²/day for each well. H-4 results were included in all the Papadopulos-PEST analyses. Details of the anisotropy analyses are presented in Appendix C. The results are summarized in Table 6.2-4.

Table 6.2-3. Transmissivities and Storativities of Distant Wells for the Long-Term Pumping Test

Well	Winterle and La Femina (1999) ^a		Cooper-Jacob Analysis ^b		Using Methods of Section 6.2.3 ^c	
	T (m ² /day)	S (-)	T (m ² /day)	S (-)	T (m ² /day)	S (-)
UE-25 ONC1	1,340	0.008	1,465	0.009	1,000 / 1,230	0.001 / 0.0012
UE-25 WT#3	1,230	0.005	1,566	0.003	2,600 / 861	0.002 / 0.0045
UE-25 WT#14	1,330/1,370 ^(d)	0.002	1,043	0.002	1,300 / 743	0.002 / 0.0029
USW H-4	670	0.002	598	0.002	700 / 700	0.002 / 0.0024

Sources: DTNs: GS970308312314.002 [DIRS 161273]; MO0212SPANYESJ.149 [DIRS 161274] (qualified for use in this report in Appendix M). (Filtered data taken from Output DTNs: GS030208312314.001 and GS030208312314.002).

Output DTNs: GS031008312314.004, SN0409T0502203.002.

^a The Theis 1935 [DIRS 150327] method was used by Winterle and La Femina 1999 [DIRS 129796], pp. 4 to 25, to obtain these estimates.

^b The Cooper-Jacob 1946 [DIRS 150245] method was used to obtain these estimates (see Appendix C for details).

^c Two sets of transmissivity and storativity estimates were obtained as a result of using different methods to filter the raw drawdown data (see text).

^d Ferrill et al. 1999 [DIRS 118941] used the second transmissivity value (see text).

Because the SZ site-scale flow model (SNL 2007 [DIRS 177391]) can only implement anisotropy oriented in a north-south or east-west direction, the principal anisotropy directions listed in Table 6.2-4 must be projected onto the north-south, east-west orientation of the model grid. For example, the analytical result for anisotropy using the Cooper-Jacob (1946 [DIRS 150245]), a ratio of 3.3 at 15° east of north, is converted to an anisotropy ratio of 2.5 with a north-south (0°) orientation (Figure 6.2-2). This anisotropy ratio was calculated by dividing the maximum y value on the anisotropy ellipse oriented 15° east of north (horizontal blue line at top in Figure 6.2-2) by its maximum x value (vertical green line at right). Similarly, the projected north-south anisotropy ratio for an anisotropy ratio of 5 oriented 33° east of north is 1.5.

Table 6.2-4. Calculated and Reported Anisotropies and Principal Directions

Data Set Used / Method	T_{\max} (m ² /day)	T_{\min} (m ² /day)	Anisotropy Ratio ^b	Azimuth ^b
Cooper-Jacob Data / Hantush ^a	2,457	752	3.3	15°E
Winterle and La Femina (1999) ^a / Papadopulos ^a	2,900	580	5	33°E
Ferrill et al. (1999) ^a / Papadopulos ^a	5,400	315	17	30°E
$T = 700 - 2,600$ m ² /day / Papadopulos-PEST ^a	3,272	599	5.5	1°E
$T = 700 - 1,230$ m ² /day / Papadopulos-PEST ^a	3,047	271	11.3	35°W
$T = 1,000$ m ² /day / Papadopulos-PEST ^a	1,863	537	3.5	79°W

Sources: DTNs: GS970308312314.002 [DIRS 161273]; MO0212SPANYESJ.149 [DIRS 161274] (qualified for use in this report in Appendix M). (Filtered data taken from Output DTNs: GS030208312314.001, and GS030208312314.002).

Output DTNs: GS031008312314.004 (Table 6.2-12), SN0409T0502203.002.

^a For a description of the methods used, refer to Hantush 1966 [DIRS 161160], Papadopulos 1967 [DIRS 150265], Ferrill et al. 1999 [DIRS 118941], and Winterle and La Femina 1999 [DIRS 129796].

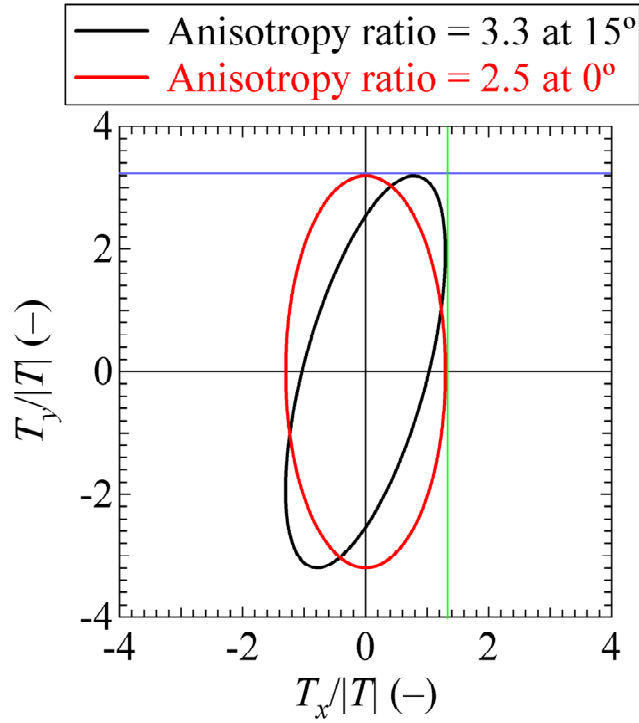
^b The last two columns list reported values.

Based on consultations between Sandia National Laboratories staff, Los Alamos National Laboratory staff, U.S. Geological Survey staff, and the YMP Parameters Team, as well as results from the analytical anisotropy analyses, curve (a) of Figure 6.2-3 is considered to be the best estimate of the probability density function (PDF) for the anisotropy ratio in the saturated zone near the C-wells complex (Eddebarh 2004 [DIRS 171918]). Curve (b) of Figure 6.2-3 is the corresponding cumulative distribution function (CDF).

There are three noteworthy points based on three distinct regions of the anisotropy ratio distribution (Output DTN: SN0302T0502203.001).

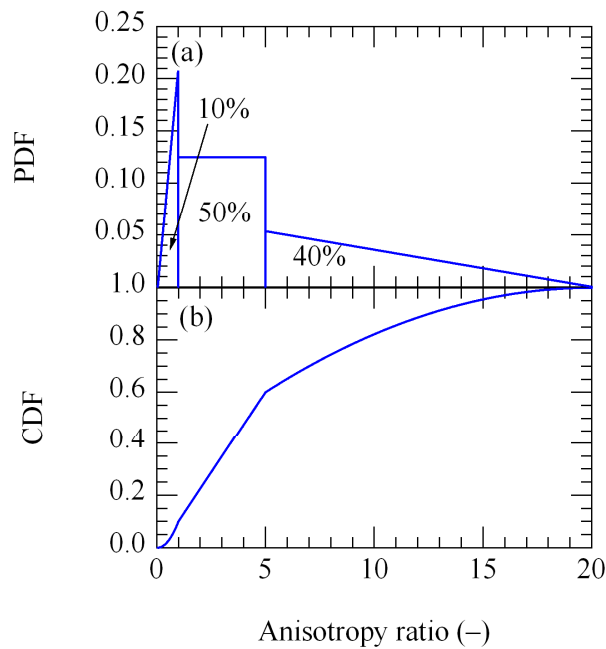
- *Anisotropy ratio between 5 and 20.* The maximum anisotropy ratio of 20:1 is physically based. Although features such as high transmissivity zones and fractures may yield very large anisotropy ratios locally, globally, their effects are attenuated. That is, over the area of the saturated-zone model, $45 \text{ km}^2 \times 30 \text{ km}^2$, an anisotropy ratio of 20 is the expected upper bound. Additionally, the highest calculated anisotropy ratio reported is 17:1 (Ferrill et al. 1999 [DIRS 118941], p. 7). The 5.5 anisotropy ratio calculated by the second approach of the modified Papadopulos-PEST method lies in this range near its highest probability point. Therefore, between 5 and 20, a triangularly distributed anisotropy ratio is constructed that decreases to zero probability at 20. Given that 3 of the 6 estimates of anisotropy ratio in Table 6.2-4 fall between 5 and 20, and one of these three estimates is just barely greater than 5 (5.5), a 40% probability is assigned to this portion of the PDF.
- *Anisotropy ratio between 0.05 and 1.* Discussions among Sandia National Laboratories and U.S. Geological Survey staff established that, although it is likely the saturated zone is anisotropic with principal direction approximately northeast, it is possible the media could be isotropic, as well as a small probability that the principal direction could be significantly different from northeast. Correspondingly, anisotropies less than one are possible, and the minimum anisotropy ratio is set equal to the inverse of the maximum, 1:20, with a triangularly distributed 10% probability decreasing to zero at a ratio of 0.05. The 3.5 anisotropy ratio calculated by the first approach of the modified Papadopulos-PEST method, when adjusted according to Figure 6.2-2, falls in this range.
- *Anisotropy ratio between 1 and 5.* A uniformly distributed 50% probability is assigned to the range of anisotropy ratios between 1 and 5. This interval comprises the most likely values of anisotropy ratios with no specific value more likely than another.

Figure 6.2-3, curves (a) and (b), are the best estimates for the PDF and the CDF, respectively, of north-south anisotropy ratios in the saturated zone modeled with FEHM in *Saturated Zone Site-Scale Flow Model* (SNL 2007 [DIRS 177391], Section 6.4.3).



Output DTN: GS031008312314.004.

Figure 6.2-2. Anisotropy Ratio of 3.3 at 15° East of North Projected onto a North–South Anisotropy Ratio (0°) Resulting in a Projected Anisotropy Ratio of 2.5



Output DTN: SN0302T0502203.001.

Figure 6.2-3. Probability Density Function (a) and Corresponding Cumulative Distribution Function (b) for the North–South/East–West Anisotropy Ratio Used in FEHM Input Files

6.2.7 Limitations and Uncertainties

Analytic solutions provide first-order estimates of hydrologic parameters consistent with both the current knowledge of the nature and extent of subsurface heterogeneities in the fractured volcanics at the scale of the C-wells complex and the manner in which hydrologic parameter estimates are used in the SZ site-scale flow model. The analytical methods assume simplified flow geometries in an equivalent porous medium, and they also assume that the test interval has one average transmissivity and storativity value between the pumping well and the observation well. Similarly, the SZ flow model assumes that single average intrinsic hydrologic property values (e.g., permeability, porosity) apply to individual stratigraphic intervals over large spatial areas in the SZ flow system, so the use of simple analytical methods to estimate parameters is consistent with simplifications that are, by necessity, made in the SZ site-scale flow model. Furthermore, with the exception of anisotropy of horizontal transmissivity, the hydrologic parameters derived from C-wells testing are not used as direct inputs in the SZ site-scale flow model, but rather they are used primarily for qualitative/corroborative consistency checks with the hydrologic parameters derived from calibrations of the SZ site-scale flow model.

All the analytical methods used in this study, except for the Neuman (1975 [DIRS 150321]) method, assume radial flow to the pumping well, and, therefore, ignore vertical flow (application of the Neuman fully penetrating-well solution, as was done in this analysis, to cases where pumping was in one interval and the analyzed drawdown response was in another also ignores vertical flow). The drawdown in intervals other than the one being pumped that was detected during hydraulic tests in February 1996 and May 1996 to November 1997 indicates that flow during those tests was actually three-dimensional. To obtain hydrologic parameter estimates in nonpumped intervals, it was necessary to assume an equivalent radial volumetric flow rate in these intervals. These estimates of equivalent radial flow were quite uncertain, and they could have resulted in significant errors in hydrologic parameter estimates in nonpumped intervals. However, parameter estimates based on an assumed radial flow in nonpumped intervals were generally in good agreement with estimates obtained from open-hole pumping of c#3 in May-June 1995, and also from later pumping of the intervals when they were isolated (e.g., estimates for the Prow Pass interval when the Lower Bullfrog was pumped in 1996-1997 were in good agreement with estimates obtained when the Prow Pass interval was pumped directly in 1998). Thus, the approach taken seems to have yielded reasonable hydrologic parameter estimates in the cases in which it could be verified with a more direct measurement.

Uncertainties in estimates of storativity, transmissivity, and hydraulic conductivity were not quantitatively analyzed because these parameter estimates were not used directly in the SZ site-scale flow model (SNL 2007 [DIRS 177391], Sections 6.6, 6.7 and 7); they were used only qualitatively/corroboratively in the flow model. Based on the ranges of transmissivity estimates obtained for a given hydrogeologic interval by different methods using either the drawdown or recovery data from the C-wells hydraulic tests (Table 6.2-2) or the drawdown data from distant wells that responded to pumping c#3 in 1996-97 (Table 6.2-3), the transmissivity estimates determined in this analysis can be considered accurate to within about factor of 1.5 for high-transmissivity intervals (lower Bullfrog and upper Tram Tuffs) and within a factor of 2.5 for low-transmissivity intervals (Calico Hills, Prow Pass, and upper Bullfrog Tuffs). The factor of 2.5 also applies to the assemblage of volcanic tuffs between the C-wells and distant wells. Storativity estimates for all intervals can be considered accurate to within an order of magnitude

or so. However, relative values of transmissivity estimates (that is, the ratios of transmissivities of different flow intervals) are considered more accurate because errors and biases should be reasonably consistent for estimates obtained by the same analyst using similar assumptions and methods (as is the case here). Estimates of hydraulic conductivity are more uncertain than transmissivity estimates because hydraulic conductivity is calculated by dividing the transmissivity by either the known thickness of transmissive intervals within a test interval, the entire thickness of the test interval, or an assumed thickness of transmissive rock between the observation and pumping wells. In many cases, the transmissive thickness was unknown, so it was only possible to obtain bounding estimates of the hydraulic conductivity. Even when hydraulic conductivity could be estimated, it was done with limited confidence. For example, it is impossible to know whether the hydraulic conductivity of the Lower Bullfrog interval in c#1 really is about half that in c#2 or whether these calculated hydraulic conductivity values result from dividing approximately the same transmissivity in each borehole by an assumed transmissive thickness twice as large in c#1 as in c#2.

Given the intended use of the hydrologic parameters derived from this scientific analysis in the SZ site-scale flow model (SNL 2007 [DIRS 177391]) (for qualitative/corroborative consistency checks), the uncertainties associated with the parameter estimates and the resulting assessment of their accuracy (discussed above) are considered acceptable. Because anisotropy in horizontal transmissivity in the fractured volcanics is a direct input in the SZ site-scale flow model, additional effort was expended to estimate its uncertainty and to present this uncertainty as probability distributions for both the direction and the magnitude of the anisotropy (Section 6.2.6). The implications of C-wells hydraulic test results for conceptual flow models are based primarily on qualitative observations (e.g., large-scale equivalent porous medium behavior, vertical flow communication between intervals with some vertical anisotropy, and the influence of structures, particularly faults), so these important implications are not significantly influenced by uncertainties in parameter estimates.

6.3 TRANSPORT PROPERTIES OF FRACTURED TUFFS (C-WELLS COMPLEX)

6.3.1 Introduction

This section (1) summarizes the tracer tests conducted at the C-wells complex and the interpretive analyses performed on the test data; (2) discusses the implications of the test interpretations, including transport parameter estimates and implications for conceptual transport modeling in the fractured volcanics; and (3) discusses the limitations and uncertainties associated with the transport properties determined from the test analyses.

6.3.2 Summary of C-Wells Tracer Testing, Including Objectives and Strategies

Table 6.3-1 summarizes the tracer testing conducted at the C-wells complex over a four-year period from 1996 to 1999. Details of each test are provided in Appendix D. Estimates of transport parameters were obtained from the tests by fitting the tracer breakthrough curves (normalized tracer concentrations vs. time) using semi-analytical dual-porosity transport models (Section 6.3.3). The term “dual-porosity” refers to a system in which flow occurs predominantly within a “primary” porosity (e.g., fractures in the volcanic tuffs) but there is a significant “secondary” porosity that contains stagnant or near-stagnant water into which solutes can diffuse from the primary porosity (e.g., the matrix in the volcanic tuffs). In contrast, a “single-porosity”

system is a system that contains only primary porosity; that is, flow occurs through all of the system porosity, and there is little or no stagnant water.

A key objective of tracer testing was to determine if a dual-porosity conceptualization is valid in the saturated volcanic tuffs or if the tuffs behave as a single-porosity system (with no secondary porosity into which solutes can diffuse). Distinguishing between these two types of conceptual models has important radionuclide transport implications because solutes moving through fractures in a dual-porosity system will spend a significant amount of time in the stagnant matrix water, thus resulting in a significant increase in their transport time through the system relative to the transport time they would experience in only the primary fracture porosity. Furthermore, sorbing radionuclides will come in contact with much more surface area for sorption in the matrix pores of a dual-porosity system than they would in a fracture-only system. Tracer tests were conducted in both a high transmissivity interval (the lower Bullfrog) and a low transmissivity interval (the Prow Pass) at the C-wells to determine if transport behavior and transport parameter estimates differ in intervals of significantly different hydrologic characteristics.

All tracer tests were conducted by injecting one or more tracers (dissolved or suspended in groundwater) into an isolated interval in one of the C-wells while the corresponding interval in another of the C-wells was pumped. These types of tests are called cross-hole tracer tests. The water produced from the pumped well was sampled at regular intervals and analyzed for the tracers to develop a tracer breakthrough curve. The test intervals in both the injection and production wells were isolated using inflatable packers in the same way that intervals were isolated for hydraulic testing (Section 6.2). In each tracer test, a steady flow field was established prior to tracer injection, and this flow field was maintained for an extended period of time after injection. Tracer tests were typically conducted immediately after hydraulic tests were completed in a given test interval, although hydraulic data continued to be collected throughout each tracer test.

Table 6.3-1. Tracer Testing at the C-Wells Complex to Determine Transport Properties

Dates	Testing Summary	Interpretative Method	References
Feb-April 1996	Injection of iodide into combined lower Bullfrog-upper Tram interval in c#2 while pumping the same interval in c#3 at approximately 450 L/min. No recirculation was employed.	Moench	Fahy 1997 [DIRS 137456]; Appendix D1
May-October 1996	Injection of pentafluorobenzoate (PFBA) into lower Bullfrog interval in c#2 while pumping the same interval in c#3 at approximately 575 L/min. Approximately 3.5% of the production water was recirculated into the injection well for 23 days after injection.	Qualitative only	Appendix D1
June-October 1996	Injection of iodide into lower Bullfrog interval in c#1 while pumping the same interval in c#3 at approximately 575 L/min. Approximately 2.6% of the production water was recirculated into the injection well for 16 days after injection.	Qualitative only	Appendix D1

Table 6.3-1. Tracer Testing at the C-Wells Complex to Determine Transport Properties (Continued)

Dates	Testing Summary	Interpretative Method	References
October 1996 - Sept. 1997	Simultaneous injection of PFBA, bromide, lithium, and polystyrene microspheres into lower Bullfrog interval in c#2 while pumping the same interval in c#3 at approximately 575 L/min. Approximately 3.3% of the production water was recirculated into the injection well for 40 days after injection	RELAP/ MULTRAN	Appendix D4
January-Nov. 1997	Injection of pyridone into lower Bullfrog interval in c#1 while pumping the same interval in c#3 at approximately 575 L/min. No recirculation was employed.	Moench	Appendix D1
January-Nov. 1997	Injection of 2,6 difluorobenzoate (DFBA) into lower Bullfrog interval in c#2 while pumping the same interval in c#3 at approximately 575 L/min. No recirculation was employed.	Moench	Appendix D1
June 1998 - January 1999	Injection of 2,4,5 trifluorobenzoate (TFBA) and iodide into Prow Pass interval in c#3 while pumping the same interval in c#2 at approximately 19 L/min. Approximately 30% of the production water was recirculated into the injection well for the duration of the test.	Moench with adjustments to account for recirculation. Also, RELAP	Appendix D2
July 1998 - January 1999	Injection of 2,3,4,5 tetrafluorobenzoate (TeFBA) into Prow Pass interval in c#1 while pumping the same interval in c#2 at approximately 19 L/min. No recirculation was employed (although recirculation into c#3 continued).	Qualitative only	Appendix D2
Sept. 1998 - January 1999	Injection of PFBA, bromide, lithium, and polystyrene microspheres into Prow Pass interval in c#3 while pumping the same interval in c#2 at approximately 19 L/min. Approximately 30% of the production water was recirculated into the injection well for the duration of the test.	RELAP/ MULTRAN	Appendix D4

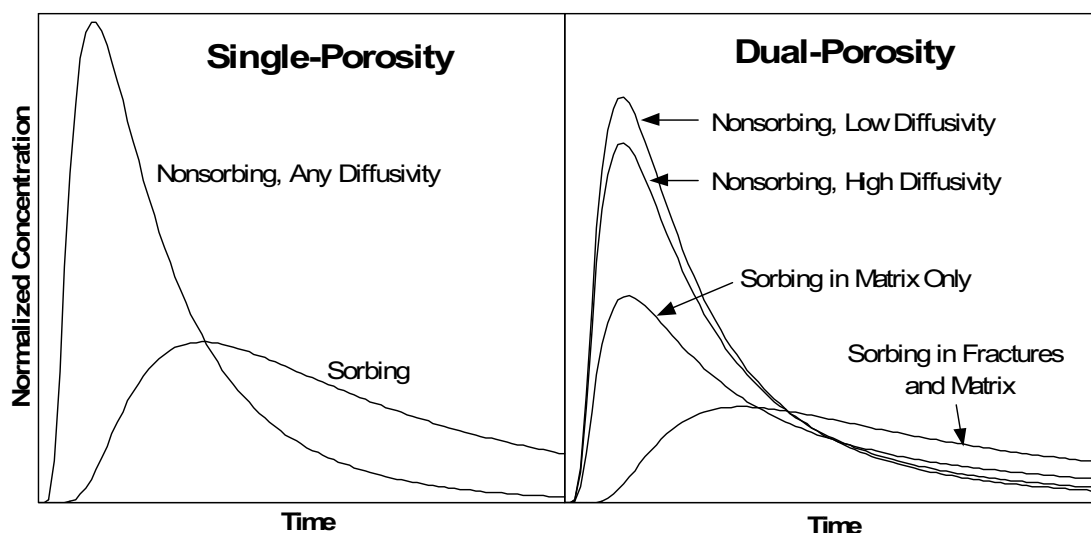
The tracer tests were conducted either in a radial-convergent flow configuration or in a partial recirculation flow configuration. In the latter case, a fraction of the water pumped from the production well was reinjected into the injection well for an extended period of time after tracer injection. For radial-convergent flow tests, there was no injection of water after tracer injection other than a small amount used to evacuate the injection tubing.

The best insights into conceptual transport characteristics of the fractured tuffs and the best-constrained transport parameter estimates were obtained from tracer tests in which two or three different solute tracers having different physical and/or chemical properties were simultaneously injected. By dissolving the tracers in the same solution and simultaneously introducing them, it was ensured that they all experienced the same flow field and, hence, initially followed identical flow pathways through the system.

The rationale for using multiple solute tracers in cross-hole tracer tests is illustrated in Figure 6.3-1 (Section 6.3.3). The left plot of this figure shows hypothetical solute tracer responses (log normalized concentration versus log time) for a cross-hole tracer test with a short injection pulse in a single-porosity system. Note that there is no distinction between nonsorbing

tracers with different diffusion coefficients in this plot because there is no secondary porosity for the tracers to diffuse into and, hence, no separation of their responses. The sorbing tracer response is delayed in time and lower in concentration than the nonsorbing tracers. In contrast, the right plot of Figure 6.3-1 shows hypothetical solute tracer responses for a test in a dual-porosity system. In this case, there is a separation between nonsorbing tracers with different diffusion coefficients, with the higher diffusivity tracer exhibiting a lower peak concentration and a longer tail than the lower diffusivity tracer. This separation occurs because the higher-diffusivity tracer diffuses more readily into the matrix than the lower-diffusivity tracer, resulting in a lower recovery at early times but a longer tail due to subsequent diffusion back out of the matrix after the tracer pulse has passed.

Figure 6.3-1 also shows two possible responses for a sorbing tracer: (1) one with sorption occurring in the matrix, and (2) one with sorption occurring in the fractures and the matrix (if the fractures have sorptive mineral coatings or are filled with sorptive granular material). Note that in the matrix-only case, the sorbing tracer response is attenuated in peak concentration but not significantly in time relative to the nonsorbing tracers, whereas in the latter case both a concentration and a time attenuation are apparent. The minimal time attenuation of the sorbing tracer relative to the nonsorbing tracers in the matrix-only sorption case is primarily a result of the relatively short duration of a typical cross-hole tracer test relative to characteristic times of diffusion into the matrix; as transport times increase, the time and concentration attenuation of a sorbing tracer relative to nonsorbing tracers should increase.



NOTE: For illustration purposes only. The figure illustrates how multiple tracers can be used to distinguish between single- and dual-porosity systems (Reimus 2003 [DIRS 165129], Attachment A, pp. A-198 to A-208). As cross-hole travel times increase, the “nonsorbing, high diffusivity” and “sorbing, matrix only” peaks on the right-hand plot will begin to arrive later than the “nonsorbing, low diffusivity” peak. The curves were generated using the RELAP V 2.0 code (STN: 10551-2.0-00 [DIRS 159065]) with arbitrary input parameters intended to qualitatively illustrate the differences between tracer responses in single- and dual-porosity media. The inputs and outputs of the simulations were not submitted to the TDMS and do not have a DTN.

Figure 6.3-1. Hypothetical Cross-Hole Responses of Tracers with Different Physical and Chemical Characteristics in Single- and Dual-Porosity Media

6.3.3 Tracer Test Interpretation Methods

To obtain estimates of solute transport parameters in the tracer tests, semi-analytical dual-porosity transport models with appropriate initial and boundary conditions were used to fit the normalized solute tracer responses (tracer concentrations in the production water divided by tracer injection masses as a function of time since injection). Two different interpretive approaches were used for the test interpretations. The first was based on the work of Moench (1989 [DIRS 101146]; 1995 [DIRS 148784]), implemented using the MOENCH.vi Function(1) code in conjunction with the *rcv2amos.exe* routine (STN: 10582-1.0-00 [DIRS 162750]) and the MOENCH.vi, Function(2), V 1.0 code (STN: 10583-1.0 [DIRS 162752]). These combined codes solve the dual-porosity advection-dispersion equation(s) in a steady-state radial-convergent flow field with initial and boundary conditions that correspond to a finite-pulse injection and well-mixed injection and production intervals. The second modeling approach employed the RELAP (REactive transport LAPlace transform inversion computer code) V 2.0 (STN: 10551-2.0-00 [DIRS 159065]) and MULTRAN V 1.0 (STN: 10666-1.0-00 [DIRS 159068]) codes. RELAP essentially combines a dual-porosity transport solution derived by Maloszewski and Zuber (1984 [DIRS 156840], Appendix; 1985 [DIRS 148312]) (modified to account for linear solute sorption) with functions that describe a finite-pulse injection, ideally mixed injection and production intervals, and recirculation. MULTRAN is a code that embodies a numerical model that duplicates what RELAP does analytically, but it also accounts for multicomponent transport processes and local charge balance to more accurately describe reactive tracer transport. The third column of Table 6.3-1 indicates which modeling approach was used for each tracer test.

For both modeling approaches, it was assumed that tracer transport in fractures can be described by the one-dimensional advection-dispersion equation with one-dimensional diffusion occurring into the surrounding matrix perpendicular to the flow direction in fractures. The geometry of the matrix is assumed to be planar in the RELAP/MULTRAN codes, and it is spherical in MOENCH.vi and its sister codes. Both assumptions are reasonable given the unknown and probably highly-variable geometry of the matrix blocks. Each model can be used to simulate single-porosity transport behavior by simply specifying a matrix with zero porosity. Details of the two modeling approaches are provided in Appendix D.

The Moench model was typically applied to tracer tests in which only a single nonsorbing (also called “nonreactive” or “conservative”) tracer was injected. The only exception was a test in the Prow Pass interval in which two nonsorbing tracers with different diffusion coefficients were injected. The interpretation of single-tracer tests was inherently less well-constrained than the interpretation of tests involving multiple tracers. Multiple-tracer tests involving both nonsorbing and reactive tracers were interpreted using the RELAP/MULTRAN codes. The test involving two nonsorbing tracers in the Prow Pass interval was interpreted using both modeling approaches to highlight some of the differences between the approaches and to assess the uncertainty in transport parameter estimates resulting from these differences. This topic is discussed in greater detail in Appendix D5.2.

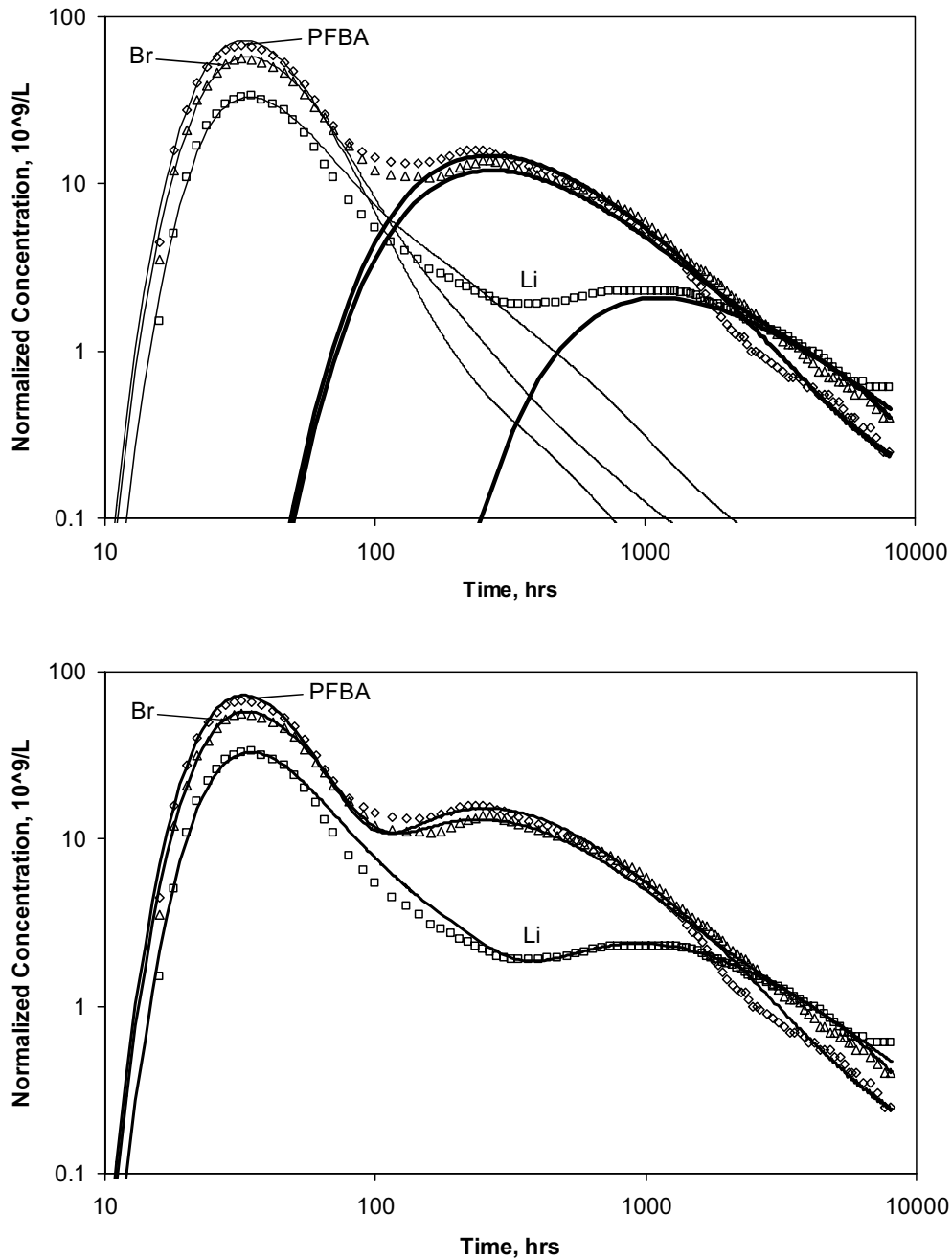
The process of obtaining transport parameter estimates from the tracer breakthrough curves in multiple-tracer tests was as follows:

- First, the breakthrough curves of the two nonsorbing solute tracers with different diffusion coefficients (pentafluorobenzoic acid or pentafluorobenzoate [PFBA] and bromide) were simultaneously fitted to obtain estimates of physical transport parameters for the flow system (e.g., mean residence time, longitudinal dispersivity, and matrix diffusion parameters).
- The transport parameters determined for the nonsorbing tracers were assumed to apply to the reactive tracer, lithium (with adjustments to account for differences in diffusion coefficient), and the lithium response was fitted by adjusting only the matrix and fracture retardation factors to obtain estimates of these parameters.
- Colloid transport parameters were estimated by assuming that the transport parameters obtained for the nonsorbing tracers also applied to the polystyrene microsphere tracers, except that the microspheres did not diffuse into the matrix. Attachment and detachment rate constants were then estimated by adjusting filtration rate constants and retardation factors to fit to the microsphere breakthrough curves (the filtration rate constant was then divided by the retardation factor minus one to obtain an estimate of the product of the detachment rate constant and the fracture aperture).

6.3.4 Tracer Test Interpretations: Conceptual Transport Model Implications

The solute tracer breakthrough curves and model fits for the multiple tracer tests involving the reactive tracer lithium in the lower Bullfrog interval and the Prow Pass interval at the C-wells are shown in Figures 6.3-2 and 6.3-3, respectively. The double-peaked tracer responses in the lower Bullfrog test (Figure 6.3-2) are attributed to a small fraction of the injected tracer mass entering relatively fast flow pathways in the upper portion of the injection interval, resulting in the early peaks, while the majority of the mass traveled through slower pathways in the lower portion of the injection interval, resulting in the later peaks. A detailed discussion of this explanation and of the interpretation of this test are provided in Appendix D.

Even without quantitative parameter estimation, it is clear that the tracer responses in both the lower Bullfrog and the Prow Pass tests are consistent with a dual-porosity conceptual transport model for the fractured volcanic tuffs illustrated in Figure 6.3-1. It is not possible to account for the differences in the bromide and PFBA responses or the relatively small time attenuation but significant concentration attenuation of the lithium responses relative to the nonsorbing tracers (in the Prow Pass test and the first peak of the Bullfrog test) without invoking diffusion between flowing fractures and stagnant matrix water. Some diffusion into stagnant water within fractures (e.g., dead-end fractures or along rough fracture walls) cannot be ruled out. However, if the stagnant water were primarily in fractures, the surface area for sorption would be limited, and it is unlikely that there would be as much concentration attenuation of lithium relative to the nonsorbing solutes as observed in the tracer tests. The large surface-area-to-volume ratio necessary to result in the large observed concentration attenuation of lithium is plausible only if a significant fraction of the stagnant water is in matrix pores. Thus, the tracer tests indicate that a dual-porosity conceptual transport model is applicable in the fractured volcanic tuffs in both high-transmissivity (lower Bullfrog) and low-transmissivity (Prow Pass) intervals.

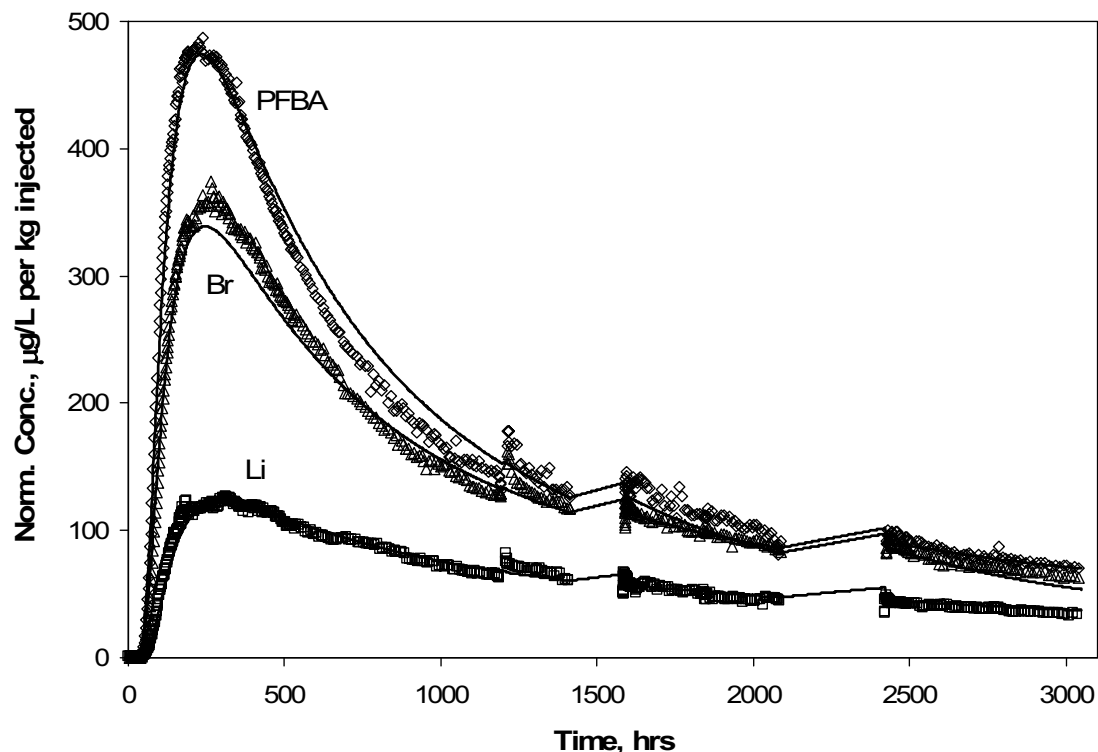


Sources: DTNs: LA0007PR831231.001 [DIRS 156043] (raw data), LA0410PR831231.001 [DIRS 171899] (normalized concentrations).

Output DTN: LA0303PR831231.003 (model).

NOTE: The upper plot shows individual fits to first and second tracer peaks (MULTRAN V 1.0 (STN: 10666-1.0-00 [DIRS 159068]) and RELAP V 2.0 (STN: 10551-2.0-00 [DIRS 159065], respectively), and the lower plot shows composite fits. For clarity, the data points shown are a subset of the actual data.

Figure 6.3-2. Solute Tracer Breakthrough Curves in the Multiple-Tracer Test in the Lower Bullfrog Tuff and RELAP/MULTRAN Fits to the Breakthrough Curves



Sources: DTNs: LAPR831231AQ99.001 [DIRS 140134] (raw data), LA0410PR831231.001 [DIRS 171899] (normalized concentrations).

Output DTN: LA0303PR831231.003 (model).

Figure 6.3-3. Solute Tracer Breakthrough Curves in the Multiple-Tracer Test in the Prow Pass Tuff and RELAP/MULTRAN Fits to the Breakthrough Curves

Flow anisotropy at the scale of the C-wells was examined by comparing tracer responses resulting from injections into well c#1 and into either well c#2 or c#3 (while pumping the other well). Table 6.3-2 lists the ratios of peak arrival times or first arrival times for nonsorbing tracers between c#1 and the production well (either c#2 or c#3) and between c#2 and c#3 for all tests in which a comparison was possible. For a homogeneous, isotropic medium, the arrival times under radial flow conditions are expected to vary as r_L^2 , the distance squared between injection and production well (Guimerà and Carrera 2000 [DIRS 156830], Equation 6). The ratios of r_L^2 values corresponding to each case are also listed in Table 6.3-2. If the ratio of arrival times is less than the ratio of distances squared, then the direction from c#1 to the production well is a preferred flow orientation; on the other hand, if the ratio of arrival times is greater than the ratio of distances squared, then the direction from c#2 to c#3 is a preferred flow orientation. Furthermore, the ratio of arrival times divided by the ratio of distances squared can be taken as a measure of the flow anisotropy ratio for the two different directions relative to the production well (note that these two directions are not strictly orthogonal).

Table 6.3-2. Ratios of Observed Tracer Arrival Times and Distances Squared, as well as Apparent Flow Anisotropy Ratios, for C-Wells Nonsorbing Tracer Tests

Tests (Injection Well)	Time _{c#1} / Time _{c#2-c#3} ^a	r _L ² _{c#1} / r _L ² _{c#2-c#3} ^a	Anisotropy Ratio ^a
Bullfrog: PFBA (c#2) and iodide (c#1) ^b	6	8.5	1.42
Bullfrog: 2,6-DFBA (c#2) and pyridone (c#1) ^c	11	8.5	0.77
Prow Pass: iodide and 2,4,5-TFBA (c#3) and 2,3,4,5-TeFBA (c#1) ^d	10	8.3	0.83

Sources: DTNs: GS010508312315.001 [DIRS 155860]; GS990208312315.001 [DIRS 159238]; LA0007PR831231.001 [DIRS 156043] (data); Borehole separation distances taken from Table 6.1-1.

Output DTN: LA0303PR831231.005.

NOTE: Because the borehole separation distances are unqualified data, the anisotropy ratios are provided for information purposes only. The uncertainties in the anisotropy ratios are quite large because vertical tracer transport distances, which were not accounted for in the calculations, could have been comparable to or even greater than the horizontal travel distances between the boreholes.

NOTE: c#1, c#2, and c#3 are abbreviations for Boreholes UE-25 c#1, UE-25 c#2, and UE-25 c#3. r_L^2 is the distance squared between injection and production wells.

^a Time_{c#1} and r_L^2 _{c#1} are the time and distance, respectively, between c#1 and the production well (either c#2 or c#3, depending on the test), and Time_{c#2-c#3} and r_L^2 _{c#2-c#3} are the time and distance, respectively between c#2 and c#3. Columns 2 and 3 give the ratios of these times and distances. Ratio is for c#1 to production well direction divided by c#2 to c#3 direction. For the anisotropy ratio, a value greater than 1.0 indicates that the c#1 to production well direction is the preferred flow orientation.

^b Both tests conducted with 2.5% to 3.5% recirculation into injection well. Peak tracer arrivals compared.

^c Both tests conducted with no recirculation. First tracer arrivals compared.

^d c#3-to-c#2 test conducted with 30% recirculation; c#1-to-c#2 test conducted with no recirculation. Peak tracer arrivals compared.

DFBA= difluorobenzoic acid; PFBA= pentafluorobenzoic acid; TeFBA= tetrafluorobenzoate; TFBA= trifluorobenzoic acid.

The ratios of tracer arrival times and r_L^2 values are in reasonably good agreement in all three cases, with apparent flow anisotropy ratios (c#1 to production well direction divided by c#2-c#3 direction) varying from 0.77 to 1.42. These relatively small ratios suggest that flow anisotropy at the scale of the C-wells may be relatively small despite the apparent orientation of the fracture network in the general direction of c#1 to c#2 (Geldon 1993 [DIRS 101045], pp. 43 to 51). The apparent flow anisotropy ratios deduced from the tracer arrival times should be carefully distinguished from the flow anisotropy ratios discussed in Section 6.2.6, which were based on drawdown observations over much larger scales.

6.3.5 Tracer Test Interpretations: Transport Parameter Estimates at the C-Wells

Estimates of transport parameters that can be used directly in solute transport models were derived from the best-fitting model parameters associated with the model fits shown in Figures 6.3-2 and 6.3-3, as well as from other model fits discussed in Appendix D. The parameter estimates associated with the fits of Figures 6.3-2 and 6.3-3 are presented in Table 6.3-3 as ranges of values consistent with the tracer test interpretation(s). Additional discussion of these ranges and how they were derived is provided in Appendix D. Transport parameter estimates obtained from other tracer tests were generally consistent with the ranges presented in Table 6.3-3 when differences in assumptions regarding tracer residence times in injection intervals were accounted for (Appendix D5.2).

Table 6.3-3. Transport Parameter Estimates Deduced from the Lower Bullfrog and Prow Pass Multiple-Tracer Tests

Parameter	Prow Pass		Bullfrog	
	Lower Bound	Upper Bound	Lower Bound	Upper Bound
Effective flow porosity (Appendix D, Section D4.8.5, Eq. D-6,)	0.003	0.006	0.003 ^a	0.031 ^a
Longitudinal dispersivity, m^b	13.0	61.5	3.2	62.5
MTC, $\frac{\phi}{b} \sqrt{D_m}$, for radionuclides ($s^{-1/2}$) ^c	0.00054	0.00095	0.00027	0.0015
Fracture aperture (cm)	0.18	1.05	0.081	1.31
Fracture spacing (cm)	6.4	∞	4.4	∞
Ratio of stagnant to flowing water volumes	3.1	∞	2.1	∞
Colloid filtration rate constant ($1/hr^d$)	0.043	0.2	0.04	0.175
Colloid detachment rate constant ($1/cm-hr^d$)	0.00015	0.00025	0.0002	1.08

Output DTNs: LA0303PR831231.003, LA0303PR831231.005.

NOTE: These values above are provided as ranges of values; see Appendix D for explanations.

^a These estimates assume that 75% of the production flow was associated with flow pathways that resulted in the first tracer peak and 25% was associated with the second tracer peak (based on flow survey information (DTN: GS931008312313.016 [DIRS 148173] – qualified for use in Appendix L).

^b Lower bounds assume Peclet numbers for radial flow and 30-m travel distance; upper bounds assume Peclet numbers for linear flow and interval thicknesses as travel distances (see Table 6.1-1 for actual borehole separations and interval thicknesses).

^c MTC is the matrix diffusion mass transfer coefficient. It is assumed that bromide and pentafluorobenzoate effectively bound molecular sizes and diffusion coefficients of radionuclide solution species.

^d Based on interpretations of polystyrene microsphere breakthrough curves; see Appendix D for details.

6.3.6 Laboratory Testing to Support C-Wells Field Tracer Tests

An additional objective of tracer testing at the C-wells complex was to assess the applicability of laboratory-derived tracer transport parameters to field-scale transport predictions. This objective is important because radionuclides cannot be tested in the field, so favorable comparisons of laboratory- and field-scale transport of nonradioactive tracers can lend credibility to the practice of using laboratory-derived radionuclide transport parameters in field-scale predictive simulations. Much of this laboratory testing focused on the sorption characteristics and reactive transport behavior of lithium ion. Comparison of lithium sorption behavior at laboratory and field scales was considered especially important because the TSPA relies heavily on radionuclide sorption parameters determined from laboratory experiments to predict field-scale reactive transport behavior in the saturated zone.

The laboratory experiments also provided information useful in constraining the interpretations of the field tracer tests (e.g., direct estimates of matrix diffusion coefficients), and they provided valuable insights into the scaling behavior of transport processes and parameters in the saturated volcanic tuffs. Laboratory testing conducted in support of C-wells tracer testing included:

- Batch sorption tests to determine lithium sorption parameters associated with various C-wells lithologies (Section E1)

- Batch sorption tests to verify that bromide and PFBA do not sorb to C-wells tuffs – DTN: LA0302PR831231.001 [DIRS 162605]
- Diffusion cell experiments to determine matrix diffusion coefficients of PFBA and bromide in various C-wells lithologies (Section E2)
- Matrix porosity and permeability measurements for various C-wells lithologies (Section E2)
- Lithium bromide tracer tests in columns packed with crushed Bullfrog tuff to determine lithium transport characteristics under flowing conditions (Appendix E3.1)
- Multiple-tracer experiments at different flow rates in fractured C-wells cores to determine tracer transport characteristics/parameters in fractured tuffs at much smaller time and length scales than in the field (also to determine if lithium transport behavior in laboratory scale fractures is consistent with batch sorption measurements onto same rock types) (Section E3.2).

Details of the conduct and results of all laboratory tests are provided in Appendix E. Because of its importance for TSPA, a comparison of laboratory- and field-derived partition coefficients (K_d values) for lithium is provided in Table 6.3-4. It is apparent that the lithium K_d values deduced from the field tracer tests (assuming any given lithologic unit) are consistently larger than the corresponding K_d values measured at the lowest lithium concentrations in the laboratory. A likely explanation for this result is that the lithium in the field tests came into contact mineral surfaces that were not present or were under-represented in the small-scale laboratory tests. These results suggest that the use of laboratory-derived K_d values to predict sorbing species transport in the saturated fractured tuffs near the C-wells location would tend to under predict the amount of sorption experienced by the species in the field.

Table 6.3-4. Lithium Partition Coefficients Derived from Field Tracer Tests and Laboratory Measurements

Parameter	Field K_d (mL/g)	Laboratory K_d^a (mL/g)
Prow Pass matrix K_d assuming Central Prow Pass Tuff	0.66	0.13 (0.26 at infinite dilution)
Prow Pass matrix K_d assuming Lower Prow Pass Tuff	1.68	0.084 (0.44 at infinite dilution)
Bullfrog matrix K_d in Pathway 1 assuming Central Bullfrog Tuff ^b	0.58 to 4.1 (nonlinear) ^c	0.19 (0.44 at infinite dilution)
Bullfrog matrix K_d in Pathway 1 assuming Lower Bullfrog Tuff ^b	0.58 to 4.1 (nonlinear) ^c	0.32 (1.64 at infinite dilution)
Bullfrog matrix K_d in Pathway 2 assuming Central Bullfrog Tuff ^b	0.74	0.19 (0.44 at infinite dilution)
Bullfrog matrix K_d in Pathway 2 assuming Lower Bullfrog Tuff ^b	3.04	0.32 (1.64 at infinite dilution)

Output DTN: LA0303PR831231.005.

NOTE: These lithium partition coefficients (K_d values) were derived from field tracer tests assuming transport in different lithologies within the test intervals.

^a Values at “infinite dilution” obtained from Langmuir isotherm fits to the data (asymptotic slope at very low concentrations (i.e., $K_L S_{max}$ – see Section 6.3.7.2 for definitions). Other values obtained from a simple linear fit to the entire range of data.

^b “Pathway 1” refers to pathways that resulted in the first tracer peak in the Bullfrog reactive tracer test, and “Pathway 2” refers to pathways that resulted in the second peak in this test. K_d values were calculated from the smallest matrix retardation factors obtained from alternative interpretations of the test.

^c The first number corresponds to a K_d value calculated at approximately 600 mg/L Li^+ using the three-component cation exchange model parameters yielding the best fit to the first lithium peak (see Section E3.1.3 for description of three-component model); the second number corresponds to a K_d value calculated at 0.5 mg/L Li^+ concentration using the same model parameters. In obtaining the field parameters, a matrix porosity of 0.10 was assumed in the MULTRAN V 1.0 (STN: 10666-1.0-00 [DIRS 159068]) simulations (approximately equal to that of the Central Bullfrog Tuff). The K_d values for pathway 1 would increase if a greater matrix porosity was assumed, and they would decrease if a smaller matrix porosity was assumed.

The scaling of longitudinal dispersivities and matrix diffusion mass transfer coefficients (MTC) values is also important for TSPA, as abstractions of these parameters for use in field-scale predictive modeling should account for apparent trends observed in laboratory and field tracer tests. The apparent scaling of these two parameters is discussed in detail at the end of Appendix E.

6.3.7 Limitations and Uncertainties

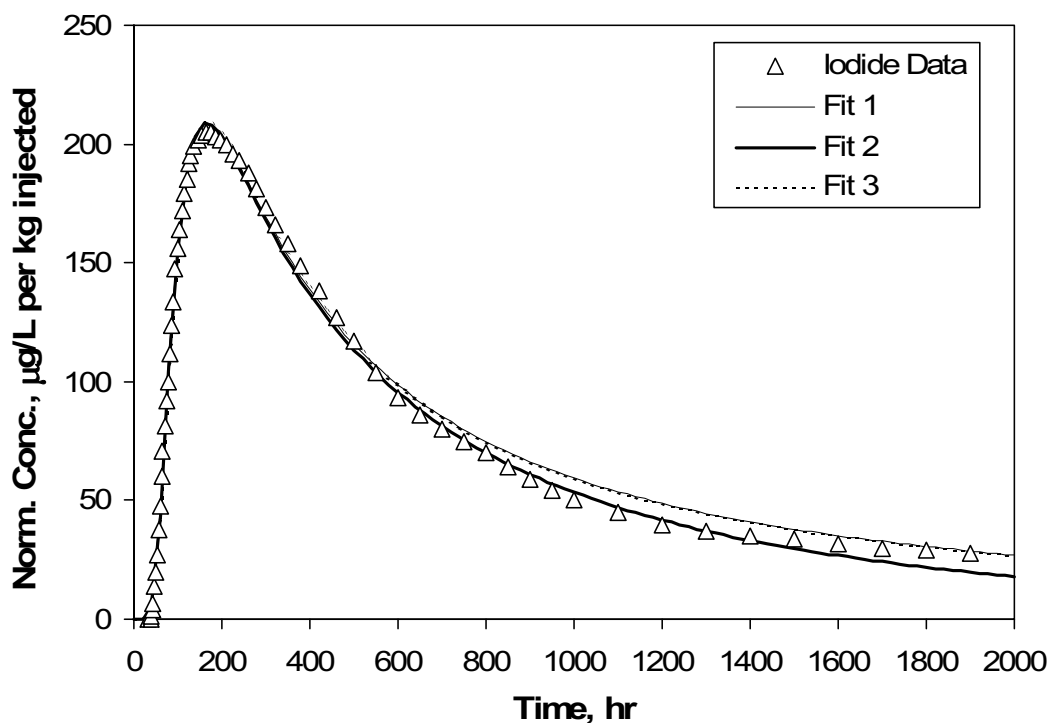
A detailed treatment of the limitations and uncertainties associated with the transport parameter estimates derived from C-wells tracer test interpretations is provided at the end of Appendix D. Limitations and sources of uncertainty included the following:

- Accuracy and precision of tracer chemical analyses, which are considered to have relatively minor influence on the test interpretations.
- Uncertainties associated with the following assumptions in the interpretive methods that were not strictly met or could not be verified:
 - Radial or linear (constant velocity) flow in a homogeneous, isotropic system, which results in highly uncertain effective flow porosity estimates.

- Steady flow conditions – there were degradations in pump performance and power outages that resulted in flow rate changes and interruptions.
 - Complete evacuation of tracers from the injection intervals in each test – this was quite unlikely, especially when recirculation was not employed.
 - Mean tracer residence times in the injection intervals were long enough that the apparent tracer travel times were dominated by the slow release of tracers from the injection well rather than by their travel time(s) in the aquifer.
 - The natural gradient had no influence on the tracer breakthrough curves.
 - There was no flow in the matrix.
 - Fractures are parallel-plate flow channels and that the matrix is either composed of rectangular blocks or spheres.
- Uncertainties associated with the nonuniqueness of test interpretations.

Most of these uncertainties cannot be quantitatively addressed. However, the uncertainty associated with the assumption of a very slow evacuation rate of tracers from the injection interval is addressed at length in Appendix D. The nonuniqueness of test interpretations is also quantitatively addressed in Appendix D, and it is summarized here because of its importance.

A prime example of nonuniqueness of test interpretations is that long tails in tracer responses can be interpreted as either being the result of large longitudinal dispersion or significant matrix diffusion. When only a single conservative tracer is used in a test, this distinction is essentially impossible to make. Figure 6.3-4 shows three RELAP V 2.0 (STN: 10551-2.0-00 [DIRS 159065]) fits to the iodide response in the Prow Pass tracer test in which 2,4,5-TFBA was also injected.



Output DTN: LA0304PR831231.001.

NOTE: Data points represent a subset of the actual data. Model parameters associated with the fits are listed in Table 6.3-5. Fits 1 and 3 essentially fall on top of each other.

Figure 6.3-4. RELAP Fits to Iodide Data from Prow Pass Tracer Test in which 2,4,5-TFBA was also Injected

These fits, which were obtained by arbitrarily fixing the Peclet number and then allowing the mean residence time, mass fraction, and matrix diffusion MTC to be adjusted to achieve a fit, are arguably equally good. However, the best-fitting parameters, listed in Table 6.3-5, vary by 2 to 4 orders of magnitude, and it is not even possible to distinguish between a single-porosity and a dual-porosity system (MTC can be zero).

In multiple-tracer tests, nonuniqueness of interpretations was minimized by simultaneously fitting the tracer responses using known ratios of diffusion coefficients as constraints on the relative matrix diffusion of different tracers. However, even after taking these measures, there is considerable nonuniqueness associated with tracer test interpretations.

A similar exercise in determining nonuniqueness of test interpretations was conducted for each of the multiple-tracer responses (i.e., two in the Prow Pass Tuff and two in the Bullfrog Tuff (two peaks in this case)). If an arbitrary criterion is established that any sum of squares of differences between model and data less than 1.5 times the minimum sum of squares difference is an equally good fit to the data, then the ranges of parameter values that provide equally good fits to the data sets are listed in Table 6.3-6. Fits having sum-of-squares differences of less than a factor of 1.5 times the minimum are essentially equally good in appearance; and when one considers that the best fits are dependent on data scatter and on variability in data point density in the breakthrough curves (e.g., more data in tails as opposed to peaks), then a good case can be

made that the fits are equally plausible. Figure 6.3-5 shows the fits to the iodide and 2,4,5-TFBA data from the Prow Pass tracer test that had the lowest and highest optimized sum-of-squares differences (with the highest still being within a factor of 1.5 of the lowest).

Although there are significant uncertainties in the parameter estimates of Table 6.3-6, the uncertainties are far smaller than when there is only a single tracer breakthrough curve to interpret (i.e., Table 6.3-5). For this reason, transport parameter estimates from multiple-tracer tests should be given more weight in the development of transport parameter distributions than parameter estimates from single-tracer tests. Additional discussion of this examination of nonuniqueness of test interpretations is provided in Appendix D5.3.

The transport parameter ranges of Tables 6.3-3 and 6.3-6, while not necessarily rigorously quantified, are considered to be very effectively captured in the parameter uncertainty distributions specified in *Saturated Zone Flow and Transport Model Abstraction* (SNL 2007 [DIRS 177390]). These transport parameter uncertainty distributions, which are ultimately propagated forward in TSPA, consistently encompass the ranges of estimates in Tables 6.3-3 and 6.3-6. The distributions even tend to be skewed such that the ranges obtained from saturated zone tracer testing often fall in the non-conservative ends of the distributions. For example, the flow porosity estimates of Table 6.3-3 are significantly higher than the lower limit obtained from the distributions of flowing interval spacing and fracture aperture, two parameters that combine to define the effective flow porosity in fractured tuffs in *Saturated Zone Flow and Transport Model Abstraction* (SNL 2007 [DIRS 177390]). Thus, the uncertainties inherent in transport parameter estimates obtained from tracer testing are typically propagated forward in TSPA in a conservative manner.

Table 6.3-5. Transport Parameters Obtained from RELAP Fits to Iodide Data Shown in Figure 6.3-4

Parameter	Fit 1	Fit 2	Fit 3
Mass Fraction	0.23	0.11	0.24
Mean Res. Time, τ , hr (linear flow)	50	700	9,000
Peclet number, Pe (linear flow)	17	1.3	0.1
Iodide MTC, $\frac{\phi}{b} \sqrt{D_m}$, $\text{sec}^{-1/2}$	0.01	0.0	0.0001

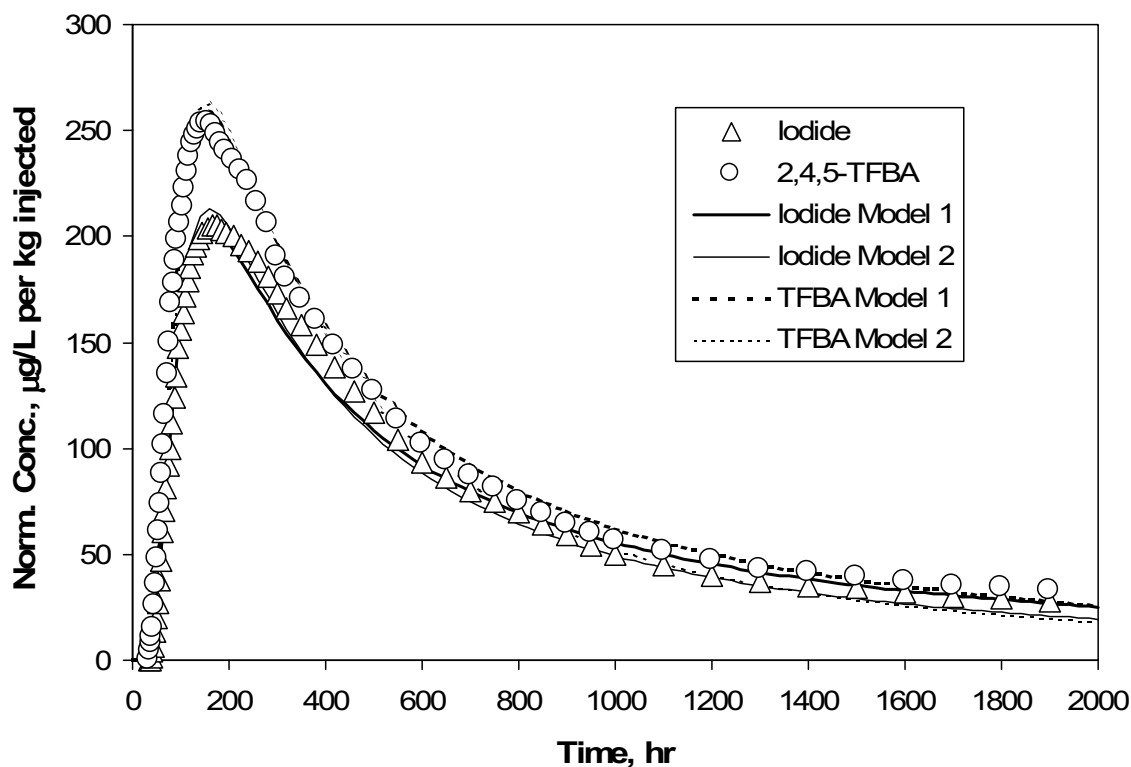
Output DTN: LA0304PR831231.001.

Table 6.3-6. Transport Parameter Ranges from Multiple-Tracer Tests at the C-Wells

Parameter	BF (Peak 1)	BF (Peak 2)	PP (I-TFBA)	PP (Br-PFBA)
Mass Fraction	0.11 to 0.13	0.56 to 0.7	0.17 to 0.3	0.56 to 0.82
Mean Res. Time, τ , hr (linear flow)	320 to 420	700 to 1,800	340 to 1,340	600 to 1,900
Peclet number, Pe (linear flow)	5 to 8	0.9 to 2.4	0.6 to 2.6	0.6 to 1.9
Halide MTC, $\frac{\phi}{b} \sqrt{D_m}$, $\text{sec}^{-1/2}$	0.000837 to 0.00224	0.000245 to 0.000775	0.000775 to 0.00122	0.000632 to 0.00122

Output DTN: LA0304PR831231.001.

BF=Bullfrog; PFBA=pentafluorobenzoic acid; PP=Prow Pass; TFBA= trifluorobenzoic acid.



Output DTN: LA0304PR831231.001.

NOTE: Data points represent a subset of the actual data. Bold curves represent the best fits to data. The sum of squares differences between data and models are within a factor of 1.5 of each other.

Figure 6.3-5. RELAP Fits to the Iodide and 2,4,5-TFBA Data from the Prow Pass Tracer Test

6.4 HYDROLOGIC PROPERTIES OF THE ALLUVIUM (ATC AND NYE COUNTY SITE 22)

6.4.1 Introduction

This section of the report (1) summarizes the hydraulic tests conducted at the ATC (NC-EWDP-19D, 19IM1, and 19IM2) and at Nye County Site 22 (NC-EWDP-22S, 22PA, and 22PB) and the interpretive analyses performed on the test data; (2) discusses the implications of the test interpretations, including implications for conceptual flow modeling in the alluvium and hydrologic parameter estimates; and (3) discusses the uncertainties and limitations associated with the hydrologic properties determined from the test analyses. Details of hydraulic testing at the ATC and Site 22 are provided in Appendix F. With the exception of one drawdown curve presented to illustrate an interpretation of a hydraulic test (Figure 6.4-1), the hydraulic test data are not presented in this section. The reader is referred to Appendix F for detailed presentation and discussion of the test data.

6.4.2 Summary of Hydraulic Testing to Determine Hydrologic Properties

Table 6.4-1 summarizes the hydraulic testing conducted at the ATC over a two-year period from July 2000 to July 2002, and Table 6.4-2 summarizes the hydraulic testing conducted at Site 22 over a 1.5-year period from March 2002 to September 2003. Most of the testing at the ATC was conducted in a single-well configuration in NC-EWDP-19D before NC-EWDP-19IM1 and 19IM2 were completed. The hydraulic tests at Site 22 were all cross-hole tests in which 22PA and 22PB were used as observation wells.

The single-well tests at the ATC included separate tests in which each of the four intervals completed in the alluvium in NC-EWDP-19D were isolated (by inflatable packers) and pumped, as well as a test in which the four intervals completed in the alluvium were simultaneously pumped as a single interval. These tests provided valuable insights into the relative transmissivities of the four screened intervals completed in the alluvium at this location as well as insights into the general characteristics of the alluvium flow system. However, later cross-hole hydraulic testing conducted after 19IM1 and 19IM2 were completed indicated that well losses in 19D resulted in poor quantitative estimates of storativity and transmissivity in the single-well tests. Therefore, storativity and transmissivity in the alluvium were estimated exclusively from water-level drawdowns measured in 19IM2 during pumping of 19D (19IM1 was also monitored, but the data were nonqualified (non-Q)). The storativity and transmissivity estimates were based on a single test in which 19D was pumped from all four combined intervals completed in the alluvium while 19IM2 was monitored in a configuration in which all four alluvium intervals were combined.

The cross-hole hydraulic tests at Site 22 involved simultaneous pumping of all four combined intervals in NC-EWDP-22S as well as isolated interval pumping of each of the four individual well screens in 22S. These tests provided hydraulic conductivity and storativity estimates in each of the intervals as well as valuable insights into the vertical hydraulic communication between the test intervals. This information supports a much more detailed conceptual understanding of the behavior of the flow system at this location than at the ATC because of the lack of isolated interval crosshole hydraulic tests at the ATC.

Although not considered a hydraulic test, a borehole gravimeter survey of NC-EWDP-19D in September 2000 provided direct estimates of in situ bulk density and hence indirect estimates of total porosity as a function of depth at the ATC location. Total porosity of the alluvium was also estimated from storativity and barometric efficiency estimates derived from hydraulic tests. These total porosity estimates serve as useful upper bounds for alluvium effective flow porosity in transport models. Details are provided in Appendix F.

6.4.3 Hydraulic Test Interpretation Methods

All single-well tests conducted in NC-EWDP-19D had drawdown curves that conformed to the Neuman (1975 [DIRS 150321]) unconfined-aquifer solution for a single-porosity system, and they were, therefore, interpreted using this solution. However, quantitative storativity and transmissivity estimates from cross-hole drawdown responses in 19IM2 when 19D was pumped were obtained using the Theis (1935 [DIRS 150327]) confined-aquifer solution for a

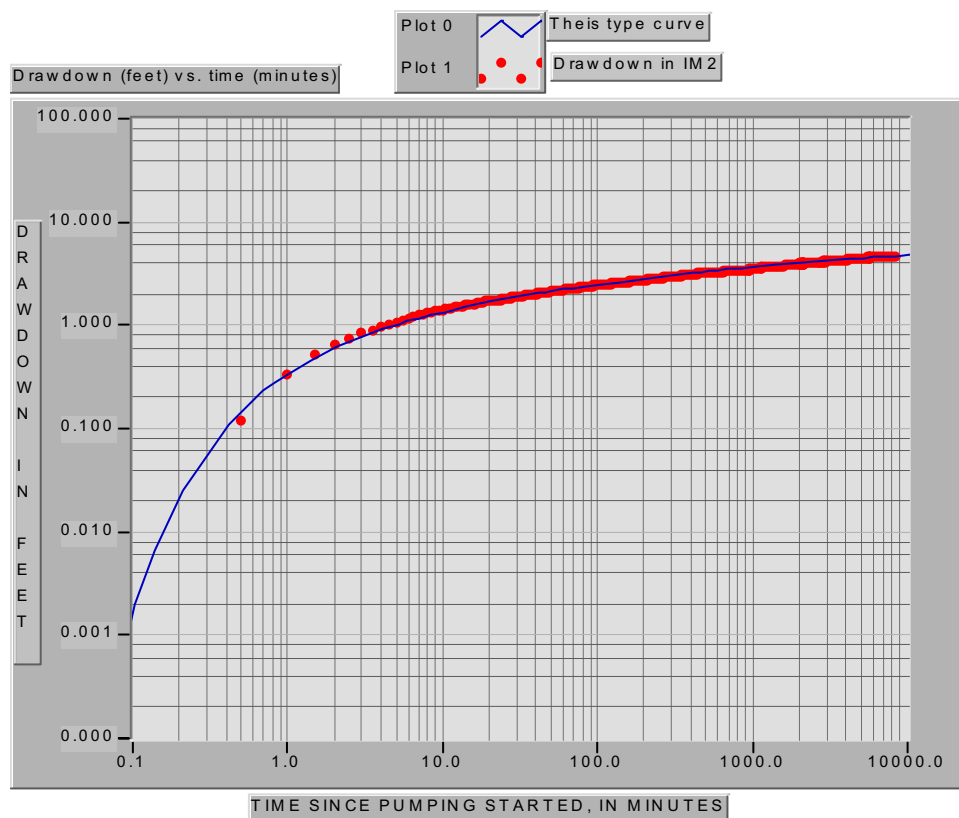
single-porosity system (Section 6.4.4). The match of the Theis (1935 [DIRS 150327]) solution to the drawdown in this cross-hole hydraulic test is shown in Figure 6.4-1.

Table 6.4-1. Highlights of Testing at the ATC and Site 22 to Determine Alluvium Hydrologic Properties (See Appendix F for Complete Description of Tests)

Dates	Testing Summary
July 2000	Single-well hydraulic test in all four combined intervals completed in the alluvium in NC-EWDP-19D
August 2000	Single-well hydraulic test in fourth screened interval from the top of NC-EWDP-19D (isolated)
September 2000	Single-well hydraulic test in third screened interval from the top of NC-EWDP-19D (isolated)
September 2000	Borehole gravimeter survey to obtain direct estimates of in situ bulk density and indirect estimates of in situ total porosity as a function of depth
October 2000	Single-well hydraulic test in uppermost screened interval (isolated) of NC-EWDP-19D
October to November 2000	Single-well hydraulic test in second screened interval from the top of NC-EWDP-19D (isolated)
December 2001	Single-well hydraulic test in which screens 5-7 of NC-EWDP-19D (completed in rocks underlying the alluvium) were pumped while screen 4 and combined screens 1-3 were monitored for drawdown
January 2002	Single-well hydraulic test in which screen 5 of NC-EWDP-19D was pumped while screen 4, combined screens 6-7, and combined screens 1-3 were monitored for drawdown
January 2002	Single-well hydraulic test in which screen 4 of NC-EWDP-19D was pumped while screen 3, combined screens 5-7, and combined screens 1-2 were monitored for drawdown
January 2002	Cross-hole hydraulic test in which combined screens 1-4 (all screens completed in the alluvium) of NC-EWDP-19D were pumped while all four alluvium intervals in 19IM1 and 19IM2 were isolated and monitored for drawdown
January to February 2002	Cross-hole hydraulic test in which combined screens 1-4 (all screens completed in the alluvium) of NC-EWDP-19D were pumped while all four alluvium intervals in 19IM1 were isolated and monitored and all four alluvium intervals in 19IM2 were combined and monitored as a single interval (for drawdown)
May to July 2002	Monitoring of barometric pressure and water levels in NC-EWDP-19D to determine barometric efficiency

Table 6.4-2 Highlights of Testing at Nye County Site 22 to Determine Alluvium Hydrologic Properties (see Appendix F for Complete Description of Tests)

Dates	Testing Summary
March 2002	Cross-hole hydraulic test in which all four combined alluvium intervals in 22S were pumped with 22PA and 22PB used as observation wells.
August 2003	Cross-hole hydraulic test in which zone 1 of 22S was pumped with 22PA and 22PB used as observations wells.
August 2003	Cross-hole hydraulic test in which zone 2 of 22S was pumped with 22PA and 22PB used as observations wells.
September 2003	Cross-hole hydraulic test in which zone 3 of 22S was pumped with 22PA and 22PB used as observations wells.
September 2003	Cross-hole hydraulic test in which zone 4 of 22S was pumped with 22PA and 22PB used as observations wells. Note that zone 4 of 22S was completed in a volcanic breccia rather than an alluvium.



Source: DTN: GS020908312316.002 [DIRS 162679] (data).

Output DTN: GS031008312316.002 (analysis).

NOTE: English units are shown in the figure because the analysis was conducted in English units. However, parameter estimates are reported in metric units to downstream users.

Figure 6.4-1. Fit to the Theis (1935 [DIRS 150327]) Confined-Aquifer Solution of the Drawdown in NC-EWDP-19IM2 Resulting from Pumping NC-EWDP-19D at 109 gpm

At Nye County Site 22, each of the cross-hole isolated interval pump tests were interpreted using the Hantush-Jacob leaky aquifer solution (Hantush, 1956 [DIRS 165169]), which was implemented using the commercially-available software MathcadTM. Additionally, because hydraulic responses were observed in intervals above and/or below the pumped interval in each test, a more general two-aquifer model and/or a three-aquifer model were also used to interpret the test data. A three-aquifer model was used for zones 2 and 3, which had hydraulic responses above and below, and a two-aquifer model was used for zone 4 because there were no responses below this zone. These models should not be considered true alternative conceptual models to the leaky aquifer model, but rather extensions of the latter model to relax some of its assumptions (e.g., only one adjacent aquifer, no drawdown in adjacent aquifer). Solutions to these more complex models involved solving the governing simultaneous differential equations in Laplace space and then numerically inverting the solutions to the time domain. The solution and inversion processes were accomplished using MathCadTM. The leaky aquifer solution was fitted to the hydraulic test drawdown curves using an automated least-squares minimization algorithm in MathCad. The two- and three-aquifer solutions were manually fitted to the data using both visual plots and a least-squares calculation to guide the process.

For each pump test of an isolated interval at Site 22, the hydraulic parameter estimates obtained from each of the three conceptual models were compared for consistency, and in the case of the two- and three-aquifer models, the parameter estimates obtained for actively-pumped aquifers were compared to the estimates obtained for these same aquifers when they were adjacent to pumped aquifers. Likewise, estimates of vertical leakage parameters for confining layers between pumped and non-pumped aquifers obtained from analyzing each of the individual pump tests were compared for consistency. Also, the cross-hole pump test of the four combined intervals in 22S was interpreted using the three-aquifer model (with the upper two aquifers lumped as a single aquifer because they had good hydraulic communication), and the resulting hydraulic parameter estimates were compared with estimates obtained from the analyses of the individual zone pump tests. Finally, an unconfined aquifer semi-analytical solution was used as an alternative conceptual model to analyze the pump tests of the two uppermost intervals in 22S to assess how sensitive the alluvium hydraulic parameter estimates are to the conceptual model assumed and also to assess whether a reasonable interpretation could be made using an alternative conceptual model. This integrated and overlapping approach was taken because good agreement between estimates of the same hydraulic parameters from different pump tests adds confidence to the hydraulic parameter estimates. The approach also provides a more unified and self-consistent interpretation of flow system behavior, and it qualitatively addresses nonuniqueness and uncertainties in the test interpretations.

6.4.4 Hydraulic Test Interpretations: Conceptual Flow Model Implications

The single-well hydraulic tests in NC-EWDP-19D all indicated that the alluvium in the immediate vicinity of this well behaves as an unconfined porous medium. However, the fact that the Theis (1935 [DIRS 150327]) confined-aquifer solution provided a good match to the water-level drawdowns observed in NC-EWDP-19IM2 when 19D was pumped suggests that the alluvium at the ATC location behaved as a confined porous medium flow system when a larger volume was interrogated than in the single-well tests. Unfortunately, because isolated interval cross-hole testing was not conducted at this site and most of the flow during the composite interval test occurred in the lower two intervals in 19D, it is not possible to determine with any certainty the depth of the layer(s) providing confinement. It is possible that the well losses in the single-well tests precluded observations that would have indicated a confined system in the isolated interval single-well tests. The possibility was also considered that the drawdown in 19IM2 was so small in the cross-hole test relative to the saturated thickness at this observation well (approximately 2%) that the response followed that of a confined aquifer even though the aquifer was unconfined. However, attempts to fit the Neuman (1975 [DIRS 150321]) (Neuman.vi V 1.0, STN: 10972-1.0-00 [DIRS 162754]) unconfined aquifer solution to the drawdown response indicated that the test had been conducted long enough to exhibit the flattening in drawdown at late times that would be expected if the aquifer were unconfined. Because this flattening did not occur, it appears likely that a confining layer influenced the response near 19IM2.

The relative drawdown responses of 19IM1 and 19IM2 during cross-hole hydraulic testing qualitatively suggest that the preferred orientation of horizontal anisotropy of hydraulic conductivity in the alluvium at the ATC is in the northeast-southwest direction (i.e., the direction from 19IM2 to 19D). Quantitative estimates of horizontal anisotropy orientation and ratio were not possible because there were only two observation wells and because the 19IM1 data are non-Q.

Because of the more extensive isolated-interval cross-hole testing at Nye County Site 22, it was possible to obtain a much better picture of the flow system at this location than at the ATC. The cross-hole hydraulic tests at Site 22 indicated that the upper two alluvium intervals behaved effectively as a single unconfined aquifer with a vertical anisotropy ratio (ratio of horizontal to vertical hydraulic conductivity) of about 2. Leaky aquifer and unconfined aquifer conceptual model solutions matched the drawdown data from these two test intervals equally well, and the resulting horizontal and vertical hydraulic conductivity estimates were in good agreement, with the leaky aquifer parameter estimates essentially confirming the unconfined character of the shallow flow system. However, the third test interval from the surface (the deepest alluvium interval at this location) exhibited a cross-hole hydraulic response consistent with the presence of significant confining layers above and below the interval. These confining layers had vertical hydraulic conductivities anywhere from a factor of 12 to 30 less than the horizontal conductivity of the test interval. Subsequent cross-hole tracer testing in the second interval from the surface at Site 22 indicated a horizontal hydraulic conductivity anisotropy ratio of 2.5 to 3 with a greater conductivity in the north-south direction (see Section 6.5.5).

Based on the Site 22 cross-hole hydraulic test results and the limited observations at the ATC, a reasonable generalized conceptual model of flow in the saturated alluvium south of Yucca Mountain is that of an unconfined aquifer with a relatively small vertical anisotropy ratio (2 to 3) near the water table with a transition to leaky-confined or confined aquifer behavior with a correspondingly large vertical anisotropy ratio (10 or more) beneath the shallowest confining layer. The horizontal hydraulic conductivity at both the ATC and Site 22 locations was greater in the north-south direction than in the east-west direction.

Horizontal hydraulic conductivity appeared to increase slightly with depth at the ATC and decrease slightly with depth at Site 22. However, the contrasts between shallow and deep conductivity at both locations were relatively small. At Site 22, the apparent contrast may be partly a result of anisotropy, as the deeper observation intervals were oriented further away from north-south than the shallower observation intervals. At any rate, it does not appear to be justified to assume any sort of variation of hydraulic conductivity with depth in the alluvium (for instance, a decrease with depth as a result of increasing overburden with depth). Rather, it appears that, at least for the depths of interest for the Yucca Mountain flow system, variations in hydraulic conductivity are primarily a result of layered heterogeneity.

6.4.5 Hydraulic Test Interpretations: Hydrologic Parameter Estimates

The storativity, transmissivity, and hydraulic conductivity estimates obtained from analyzing the drawdown response in NC-EWDP-19IM2 as a result of pumping all four combined alluvium intervals in NC-EWDP-19D using the Theis (1935 [DIRS 150327]) confined-aquifer solution are 0.00045, 306 m²/day, and 2.3 m/day, respectively (Appendix F, Section F2). The estimate of

hydraulic conductivity assumes an interval thickness of 133 m, which is the total thickness of the saturated alluvium from the water table to the bottom of the deepest screen completed in the alluvium in NC-EWDP-19D. Vertical transmissivity and hydraulic conductivity were not estimated from the test results because the cross-hole hydraulic response conformed to that of a confined aquifer (i.e., no vertical flow) rather than an unconfined aquifer.

Hydraulic parameter estimates from most of the interpretive analyses of the Site 22 hydraulic test data are summarized in Table 6.4-3. The definitions of the parameters are provided at the bottom of this table, and they are also depicted in Figure 6.4-2. In general, the interpretations indicate that the upper ~90 m of saturated alluvium at this location has a horizontal hydraulic conductivity of ~11 to 14 m/day and a vertical anisotropy ratio (K_h/K_z) of about 1.5 to 2. The lower ~75 m of saturated alluvium at this location has a considerably lower horizontal hydraulic conductivity (3.7 m/day for zone 3) and a vertical anisotropy ratio of 12 to 30. Test interval 3 is effectively confined by alluvium layers of low vertical hydraulic conductivity above and below (although the confinement from below could be provided by the top of the underlying volcanic breccia unit). The horizontal hydraulic conductivity of the volcanic breccia underlying the alluvium at Site 22 is about 10 to 11 m/day, which is comparable to that of the upper alluvium.

A short-duration cross-hole pumping test at NC-EWDP-10S (located along Fortymile Wash about 2 miles north-northeast of Site 22 and using borehole 10P as an observation well) indicated a horizontal hydraulic conductivity in the single alluvium zone at this location of about 3 m/day (Swanson 2006 [DIRS 179627]), which is comparable to the horizontal conductivity deduced at both the ATC and in the deepest alluvium zone at Site 22. This test was not analyzed by project staff, so it is not discussed elsewhere in this analysis report.

The entire saturated alluvium section at Site 22 has a composite horizontal hydraulic conductivity of about 5 m/day with a vertical anisotropy ratio of ~13. This composite horizontal hydraulic conductivity is taken to be $K_h = \sum_{i=1,3,5} \frac{K_{hi} b_i}{b_{Total}}$ (Freeze and Cherry 1979 [DIRS 101173],

p. 34), where K_{hi} = horizontal hydraulic conductivity of layer i , b_i = thickness of layer i , and $i = 1,3,5$ indicates that the layers considered are from the top of test zone 1 to the bottom of the confining layer between zones 3 and 4 at Site 22. Similarly, the composite vertical hydraulic

conductivity used to estimate the vertical anisotropy ratio is taken to be $K_v = \sum_{i=1,3,5} \frac{b_{Total}}{b_i / K_{vi}}$

(Freeze and Cherry 1979 [DIRS 101173], p. 34). The bases for the equations in the two preceding sentences are discussed in Section F7 of Appendix F. The composite estimates assume that horizontal hydraulic conductivities in the layers between test zones are the same as the estimated vertical hydraulic conductivities of these layers and that the vertical conductivities within the test zones are the same as the estimated horizontal conductivities of these zones (i.e., isotropy is assumed within each layer). These assumptions likely result in underestimation of the composite horizontal hydraulic conductivity and possibly also underestimation of the composite vertical anisotropy ratio because there is likely some vertical anisotropy within each layer. Nevertheless, if the alluvium is lumped as one continuous unit in the SZ flow model, these composite parameter estimates are appropriate values to compare with parameters obtained from calibration of the site-scale flow model (at the Site 22 location). Alternatively, one might consider a conductivity of ~12 to 13 m/day (the largest horizontal conductivity measured in any

Table 6.4-3. Summary of the Hydraulic Parameter Estimates for Nye County Site 22

Parameter Notation	Zone 1 Pumping Test		Zone 2 Pumping Test		Zone 3 Pumping Test		Zone 4 Pumping Test		All Four Zones Pumping Test	Range	Average	NWRPO, 03 [DIRS 178565 Table 2]	NWRPO, 2004 [DIRS 178566 Table 3]
	Leaky Aquifer	Two-Aquifer System	Leaky Aquifer	Three-Aquifer System	Leaky Aquifer	Three-Aquifer System	Leaky Aquifer	Two-Aquifer System					
χ_0, d^{-1}	-	0.15	0.15	-	-	-	-	-	0.15	0.15	0.15	-	-
$T_1, m^2/d$	264	280	280	-	-	-	-	-	-	264-280	316	-	242
s_1	.0013	.0017	.0017	-	-	-	-	-	-	.0013-.0017	.0016	-	.00116
χ_{1-2}, d^{-1}	-	0.10	0.10	-	0.10	-	-	-	-	0.10	0.10	-	-
$T_2, m^2/d$	-	600	600	325	400	-	450	-	-	325-600	475	550	427
s_2	-	0.003	0.003	.00061	0.0006	-	0.003	-	-	.0006-.003	-	.00031	.00035
χ_{2-3}, d^{-1}	-	0.01	0.01	0.01	0.01	-	0.01	-	0.01	0.01	0.01	-	-
$T_3, m^2/d$	-	170	170	133	133	133	133	180	130	130-180	153	237	139
s_3	-	0.0003	0.0003	0.0003	0.0003	.00021	.00021	-	0.0003	.0002-.0003	.00026	.00002	.0001
χ_{3-4}, d^{-1}	-	-	-	-	-	-	0.0026	0.0018	0.02	.0018-.0026	0.0022	-	0.0035
$T_4, m^2/d$	-	-	-	-	-	-	250	200	250	200-250	225	269	185
s_4	-	-	-	-	-	-	0.0003	0.0003	0.0003	.0003-.00035	.00031	.00023	.00021
$\chi_0 + \chi_{1-2}, d^{-1}$	0.25	-	-	-	-	-	-	-	-	-	-	-	0.31
$\chi_{01-2} + \chi_{2-3}, d^{-1}$	-	-	-	0.12	-	-	-	-	-	-	-	-	0.059
$\chi_{2-3} + \chi_{3-4}, d^{-1}$	-	-	-	-	-	0.0126	-	-	-	-	-	-	0.0119
$T_1+T_2, m^2/d$	-	-	-	-	-	-	-	-	1000	-	-	-	-
s_{1-2}	-	-	-	-	-	-	-	-	0.003	-	-	-	-

Output DTN: LA0701EK150304.001 (estimates provided in the 5 MathCad™ files of this DTN).

χ_0 = ratio of the hydraulic conductivity in m/day and thickness in m of the layer above zone 1.

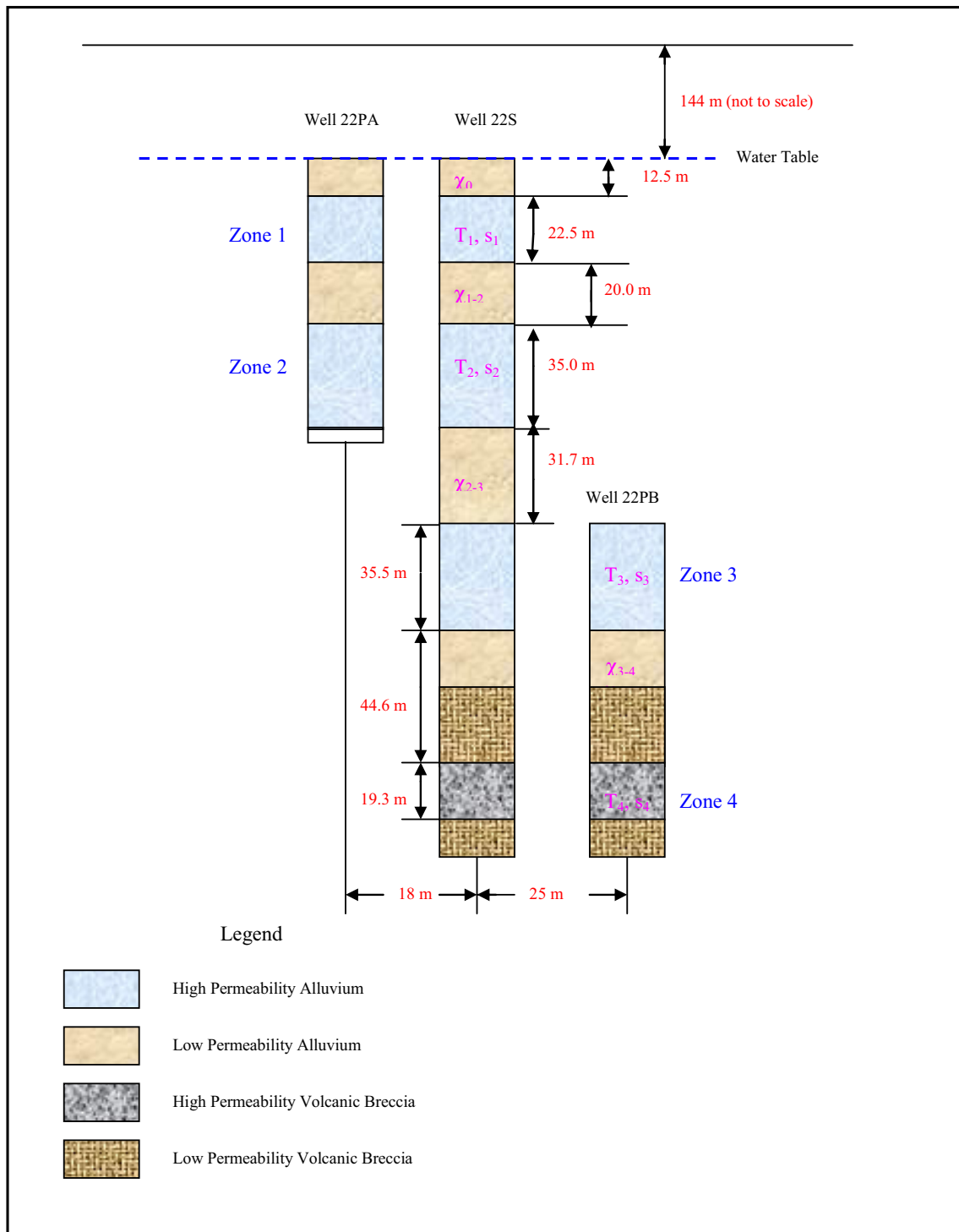
T_i = transmissivity of zone i in m^2/day .

s_i = storativity of zone i.

χ_{i-j} = ratio of the vertical hydraulic conductivity (m/day) to thickness (m) of the layer between zone i and zone j.

T_1+T_2 = transmissivity of the combined zone 1 and zone 2.

s_{1-2} = storativity of the combined zone 1 and zone 2.



NOTE: For illustration purposes only. This schematic assumes multiple-aquifer conceptual model – see Appendix F for depiction of multiple-layer conceptual model). See Table 6.4-3 for definition of symbols.

Figure 6.4-2. Schematic Depiction of the Hydraulic Parameters Estimated at NC-EWDP Site 22 in Relation to the Well Completions and Stratigraphy

individual zone) to be a reasonable upper bound estimate of the composite horizontal hydraulic conductivity at Site 22 given that a direct measurement of horizontal conductivities in the layers between test zones was not possible. This allows for the possibility that the layers between zones have large vertical anisotropy ratios (providing vertical confinement, but allowing considerable horizontal flow).

The estimate of total porosity in the alluvium obtained from storativity and barometric efficiency estimates at the ATC was approximately 0.41 (Appendix F, Section F3). Total porosity estimates from borehole gravimetry ranged from approximately 0.18 to approximately 0.29, depending on depth in the alluvium NC-EWDP-19D (Appendix F, Section F4). The estimates from borehole gravimetry are considered more accurate and reliable than those from storativity and barometric efficiency.

6.4.6 Limitations and Uncertainties

Analytic or semi-analytic solutions provide first-order estimates of hydrologic parameters consistent with both the limited knowledge of the nature and extent of subsurface heterogeneities in the alluvium at the scale of the ATC and Site 22 well complexes and the manner in which hydrologic parameter estimates are used in the SZ site-scale flow model (SNL 2007 [DIRS 177391]). The semi-analytical methods assume that each test interval has one average transmissivity and storativity value. Similarly, the SZ site-scale flow model (SNL 2007 [DIRS 177391]) assumes that single, average, intrinsic, hydrologic property values (e.g., permeability, porosity) apply to the alluvium over large spatial areas in the SZ flow system. Furthermore, the hydrologic parameters derived from ATC and Site 22 testing are not used as direct inputs in the SZ site-scale flow model, but rather they are used primarily for qualitative/corroborative consistency checks with the hydrologic parameters derived from calibrations of the SZ site-scale flow model.

Uncertainties in estimates of storativity, transmissivity, and hydraulic conductivity were not quantitatively analyzed because these parameter estimates were not used directly in the SZ site-scale flow model (SNL 2007 [DIRS 177391], Sections 6.6, 6.7 and 7); they were used only qualitatively/corroboratively in the flow model. Estimates of transmissivity and storativity at the ATC should be considered no more accurate than for the fractured volcanics (Section 6.2.7) (i.e., within at best a factor of 3 for transmissivity and an order of magnitude for storativity). Horizontal hydraulic conductivity at the ATC was calculated by dividing the transmissivity determined in the cross-hole test between NC-EWDP-19IM2 and NC-EWDP-19D by essentially the entire thickness of the saturated alluvium at this location. In reality, the thickness of the alluvium actually conducting flow may have been less than this total thickness (as suggested by the fact that the drawdown response in 19IM2 conformed to that of a confined aquifer, indicating that some layers in the alluvium may not have conducted flow). Although uncertainties in parameter estimates at both the ATC and Site 22 were not formally quantified, horizontal hydraulic conductivity estimates for different test intervals at Site 22 are considered more accurate (less uncertain) than at the ATC because multiple estimates obtained from different isolated-interval pump tests and from different analysis methods (including different conceptual models for the shallow alluvium) were in good agreement. The integrated interpretive approach taken for these hydraulic tests adds confidence to the parameter estimates at Site 22 and to the overall conceptual model of flow deduced from the hydraulic tests.

Only a qualitative estimate of the principal axis of a horizontal anisotropy ellipse for hydraulic conductivity in the alluvium (northeast to southwest) was possible from the cross-hole hydraulic test results at the ATC, and no estimate of the anisotropy ratio was possible. However, at Site 22, tracer test results (see Section 6.5.5) indicated a horizontal hydraulic conductivity anisotropy ratio of 2.5 to 3, with a greater conductivity in the north-south direction. The use of only two observation wells at each location certainly limits the confidence that can be assigned to any estimate of horizontal anisotropy. It is cautiously concluded that the principal axis of the horizontal hydraulic conductivity ellipse at both the ATC and Site 22 appears to be oriented more north-south than east-west (i.e., in the general direction of inferred flow), and an anisotropy ratio of about 3:1 appears reasonable.

The conceptual model that emerges from the combined consideration of hydraulic testing results at the ATC and Site 22 is that of an unconfined aquifer at shallow depths coupled with leaky-confined or confined aquifer behavior below the first significant confining layer. However, because of the limited amount of testing that has been conducted, the depth at which the shallowest major confining layer is likely to be encountered at different locations and the lateral extent of such layers must be considered very uncertain. Geochemical data at the ATC and Site 22 loosely corroborate (certainly do not refute) this alluvium conceptual model (see Section F.8).

Given the intended use of the hydrologic parameters derived from this scientific analysis in the SZ site-scale flow model (for qualitative/corroborative consistency checks), significant uncertainties associated with the parameter estimates are considered acceptable. Composite horizontal hydraulic conductivity estimates at three different locations along Fortymile wash (ATC, Site 22, and Site 10, with the latter being unqualified) span from about 2.3 to 5 m/day, with an upper bound estimate of about 12 to 13 m/day in any individual flow interval. However, the existence of horizontal zones of low vertical hydraulic conductivity that act as confining layers are suggested by hydraulic responses in isolated interval hydraulic tests.

6.5 TRANSPORT PROPERTIES OF ALLUVIUM (ATC AND NYE COUNTY SITE 22)

6.5.1 Introduction

This section (1) summarizes the tracer tests conducted at the ATC and Nye County Site 22 and the interpretive analyses performed on the test data; (2) discusses the implications of the test interpretations, including transport parameter estimates and implications for conceptual transport modeling in the alluvium; and (3) discusses the limitations and uncertainties associated with the transport properties determined from the test analyses.

6.5.2 Summary of ATC and Site 22 Tracer Testing, Including Objectives and Strategies

Three single-well injection-withdrawal tracer tests were conducted in the saturated alluvium in the uppermost screened interval of NC-EWDP-19D between December 2000 and April 2001 (Appendix G, Section G4), and two single-well injection-withdrawal tracer tests and two cross-hole tracer tests were conducted in the alluvium of the second interval from the surface at Site 22 between December 2004 and October 2005 (Appendix G, Section G5). The test interval at 19D ranged from approximately 14 m to 23 m (45 ft to 75 ft) below the water table (Figure 6.1-9),

and the test interval at Site 22 ranged from approximately 54 m to 89 m (178 ft to 293 ft) below the water table (Figure 6.1-10). In each of the single-well tests, two nonsorbing solute tracers with different diffusion coefficients were simultaneously injected (a halide and a fluorinated benzoate [FBA] dissolved in 5,700 L to 11,000 L of groundwater), followed immediately by the injection of a much larger volume (76,000 L to 83,000 L) of tracer-free groundwater called “chase” water. The chase water was intended to push the tracers into the aquifer so as to minimize the influence of the wellbore and gravel pack on the test results. The three tests at the ATC were conducted in essentially the same manner except for the time allowed to elapse between the cessation of chase water injection and the initiation of pumping, the so-called “rest” or “shut-in” period. The rest period was systematically varied from approximately 0.5 hr, to approximately 2 days, to approximately 30 days, after which the well was pumped back and water samples were collected to analyze for tracers. Likewise, the two single-well tests at Site 22 were conducted in essentially identical manner except the rest periods were approximately 3 days and 30 days. The different rest periods were employed to allow estimates of ambient groundwater velocity (see Section 6.5.5 for details). Pumping was continued until the majority of the tracer mass had been recovered. Flow interruptions were intentionally introduced during the pumping phase of two of the three tests at the ATC to determine if they had any effect on the responses of the tracers. The tracers and test conditions in the single-well tests are summarized in Table 6.5-1 for the ATC and in Table 6.5-2 for Site 22. A fourth single-well test was conducted at the ATC in the deepest interval in NC-EWDP-19D using a single FBA in early 2002, but this test was not used for transport parameter estimation because the FBA was not paired with a halide to allow diffusion into stagnant water to be evaluated and because additional tests with different rest periods were not conducted to allow estimates of ambient groundwater velocity.

The objectives of the single-well tracer tests were:

- To determine whether the alluvium behaves as a single- or a dual-porosity transport system based on the differences in the responses of the halide and FBA tracers in the same test (discussion in Section 6.3.2)
- To obtain estimates of diffusive mass transfer parameters (if a dual-porosity system is indicated) based on the magnitude of the differences between the halide and FBA tracer responses in tests of different rest periods)
- To obtain estimates of the ambient flow velocity in the alluvium based on the responses of the tracers in the tests of different rest periods.

Table 6.5-1. Summary of Tracers and Test Conditions in the Three Single-Well Tracer Tests in NC-EWDP-19D

Rest Period (Test)	0.5 hr	2 days	30 days
Dates	1/5/01 to 1/12/01	12/1/00 to 12/18/00	1/27/01 to 4/25/01
Tracers (injection concentration)	2,4-DFBA (0.46 g/L) Cl ⁻ (0.62 g/L NaCl) 640-nm microspheres	2,6-DFBA (0.46 g/L) I ⁻ (0.64 g/L KI)	PFBA (0.46 g/L) Br ⁻ (0.63 g/L NaBr)
Injection rate (L/min [gpm])	56.8 [15.0]	56.8 [15.0]	56.8 [15.0]
Average pumping rate (L/min [gpm])	50.3 [13.3]	41.3 [10.9]	51.67 [13.65]
Pumping duration (days)	7	14	54
Total liters [gallons] pumped	511,500 [135,100]	814,000 [215,000]	4,020,000 [1,062,000]
Tracer recovery (FBA)	0.864	0.928	0.913

Output DTN: LA0303PR831231.002.

Sources: DTNs: GS020708312316.001 [DIRS 162678] (injection and discharge rates); UN0109SPA008IF.006 [DIRS 162442] (0.5-hr tracer concentration data); UN0102SPA008KS.003 [DIRS 162614] (2-day tracer concentration data); UN0109SPA008KS.007 [DIRS 162615] (30-day PFBA concentration data); UN0109SPA008KS.008 [DIRS 162616] (30-day bromide concentration data); Stetzenbach 2001 [DIRS 180730] (2-day tracer injection masses); Farnham 2001 [DIRS 180732] (0.5-hr tracer injection masses), 2001 [DIRS 180733] (30-day tracer injection masses).

NOTES: Pumping duration is rounded to the nearest day. Total volumes pumped are approximate.

DFBA = difluorobenzoate; FBA = fluorinated benzoate; gpm = gallons per minute; PFBA = pentafluorobenzoate.

Table 6.5-2. Summary of Tracers and Test Conditions in the Two Single-Well Tracer Tests in NC-EWDP-22S

Rest Period (Test)	3 days	30 days
Dates	12/3/04 to 12/10/04	12/13/04 to 1/26/05
Tracers (injection concentration)	PFBA (0.25 g/L) I ⁻ (0.75 g/L NaI)	2,3,4,5-TeFBA (0.25 g/L) I ⁻ (0.75 g/L NaI)
Average Injection/chase rate (L/min [gpm])	67.8 [17.9]	58.7 [15.5]
Average pumping rate (L/min [gpm])	178.7 [47.2]	179.8 [47.5]
Pumping duration (days)	4.3	13
Total liters [gallons] pumped	1,110,000 [292,000]	3,370,000 [890,000]
Tracer recovery (I⁻)	1.0	0.98

Sources DTNs: LA0612PR831231.001 [DIRS 178733] (3-day data), LA0612PR831231.002 [DIRS 178735] (30-day data).

NOTES: Pumping duration for 30-day test is rounded to the nearest day. Total volumes pumped are approximate.

PFBA = pentafluorobenzoate; TeFBA = tetrafluorobenzoate.

Details of the single-well tracer testing strategy, including a discussion of pretest model predictions that illustrates how the results from the different tests could be used to achieve the above objectives, are provided in Appendix G.

Two cross-hole tracer tests were conducted at Nye County Site 22 from January to October 2005. The first test involved the injection of several tracers into the second interval from the surface in two different wells (22PA and 22PC) while the same interval was continuously pumped in 22S (see Figures 6.1-8 and 6.1-10). The two injection wells were located in approximately orthogonal directions to each other relative to 22S (22PA is north, and 22PC is east), so flow and transport anisotropy could be evaluated. The second cross-hole tracer test was conducted in the

same configuration as the first test, but only two tracers, iodide ion and perrhenate ion, and one injection interval, the second interval from the surface in 22PA, were used.

The objectives of the first cross-hole test were to (1) further evaluate alternative conceptual transport models in the saturated alluvium, building on the information obtained from the single-well tracer tests, (2) evaluate flow porosity and flow anisotropy in the alluvium, and (3) obtain estimates of transport parameters for solutes and colloids in the saturated alluvium. The second test was conducted primarily to evaluate whether perrhenate transport is retarded relative to iodide in the saturated alluvium. Perrhenate was used in this test as a surrogate for pertechnetate, which is the predominant technetium species predicted to be present in oxidizing groundwaters at Yucca Mountain. ^{99}Tc is one of the radionuclides that have been identified as potentially contributing significantly to future offsite doses because of its high solubility and weak sorption behavior.

The tracers injected into the second screened interval in 22PA in the first cross-hole test included two nonsorbing solutes (bromide ion and 2,4,5 TFBA) and a weakly sorbing cation tracer (lithium ion). These tracers were all injected simultaneously (co-dissolved in groundwater from 22S). Nonsorbing FBAs were also injected into the second screened interval from the surface in 22PC (2,6 DFBA) and into the first screened interval from the surface in 22PA (2,5 DFBA). The last tracer was injected to determine if there was any significant downward vertical flow through the alluvium induced by pumping from the deeper depth in 22S. Carboxylate modified polystyrene latex (CML) microspheres (200-nm diameter, and dyed with a fluorescent yellow dye to allow them to be distinguished from background colloids) were injected into the second screened interval of 22PA approximately ten days after the solute tracers to serve as colloid tracers. The sorption parameters for lithium and the filtration parameters for the microspheres were determined by comparing the cross-hole responses of these tracers to that of the two nonsorbing solutes. Table 6.5-3 provides a summary of the injection masses and volumes of the different tracers in both cross-hole tests at Site 22. The observed tracer recoveries are also summarized in this table.

For all cross-hole tracer injections, a steady flow field was established between the injection wells and the production well prior to the tracers being injected, and the tracer solution was followed by a small volume of untraced “chase” water. This “chase” water was intended to “push” the tracers out of the injection wellbore and into the formation to minimize the possibility that they might linger in the wellbore, which would result in biased estimates of transport parameters. The production well was pumped at a steady rate of approximately 47.5 gallons per minute (180 L/min) during both tests, including throughout the tracer injections and chases. Additional details of cross-hole tracer testing at Site 22 are provided in Appendix G., Section G5.

Table 6.5-3. Tracer Characteristics, Injection Masses, Injection Concentrations, and Fractional Recoveries in the Two Cross-Hole Tracer Tests at Site 22

Parameter	2,4,5 TFBA	Bromide	Lithium	2,6 DFBA
Solute Tracers – Test 1^a				
Free water diffusion coefficient at infinite dilution, D_f (cm ² /s)	7.2×10^{-6b}	2.1×10^{-5c}	1.0×10^{-5c}	7.5×10^{-6b}
Expected Sorption	None	None	Weak (ion exchange)	None
Solute Tracers – Test 1^a (Continued)				
Target and directly measured injection mass (kg)	8.500	23.002	18.457 ^d	8.500
Injection mass based on measured injection concentration and volume (kg)	8.232	21.504	18.060	8.116
Approximate injection volume (L)	1,000	1,000	1,000	1,000
Tracer fractional recovery ^e	0.93 to 0.96 (0.06)	0.78 to 0.84 (0.03)	0.092	0.91 (0.14)
CML Microsphere Tracers – Test 1^f				
Parameter	0.2-μm CML microspheres (yellow)			
Calculated free water diffusion coefficient, (cm ² /s)	2.15×10^{-8g}			
Number of spheres injected	4.65×10^{14}			
Injection concentration (number/L)	4.65×10^{11}			
Approximate injection volume (L)	1000			
Tracer fractional recovery	0.011			
Solute Tracers – Test 2				
Parameter	Iodide	Perrhenate		
Free water diffusion coefficient at infinite dilution, D_f (cm ² /s)	2.1×10^{-6c}	1.46×10^{-5h}		
Expected Sorption	None	None or very weak		
Target and directly measured injection mass (g)	4,233.13	68.123		
Injection mass based on measured injection concentration and volume (kg)	3,375.77	59.740		
Approximate injection volume (L)	1,000	1,000		
Tracer fractional recovery	0.78	0.84		

Sources: DTNs:LA0612PR831231.003 [DIRS 178736] (Test 1 solutes), LA0612PR831231.004 [DIRS 178738] (Test 2), LA0612PR831231.005 [DIRS 178739] (Test 1 microspheres).

CML=carboxylate-modified latex; TFBA=trifluorobenzoic acid or trifluorobenzoate; DFBA=difluorobenzoic acid or difluorobenzoate.

^a 2,5 DFBA was also injected into the uppermost screen of 22PA, but it was never detected in 22S, so it is not listed here.

^b Benson and Bowman 1994 [DIRS 122788], p. 1125; 1996 [DIRS 153427].

^c Newman 1973 [DIRS 148719], p. 230, Table 75-1; based on ionic conductances at infinite dilution.

^d Lithium was injected as 25.0 kg LiBr, 97.0 kg LiCl and 1.99 kg LiOH.

^e Ranges for TFBA and bromide reflect uncertainty in mass-based vs. concentration-based normalizations. (see Appendix G, Section G5.1, for discussion of these normalizations). Numbers in parentheses indicate the recovery that occurred during the second cross-hole tracer test, which is included in the totals. Lithium concentrations were not measured during the second cross-hole test.

^f The microsphere injection was initiated 10 days after the solute tracers were injected.

^g Calculated using Stokes-Einstein equation (Bird et al. 1960 [DIRS 103524]).

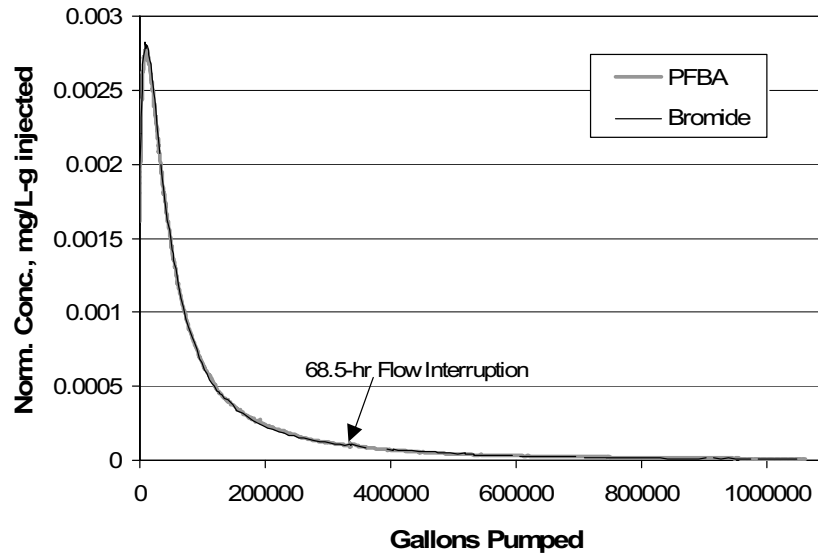
^h Lide 2006 [DIRS 178081].

6.5.3 Single-Well Tracer Test Results

Figure 6.5-1 shows the normalized solute tracer responses in the single-well tracer test at 19D with a rest period of approximately 30 days. It is apparent that the two solute tracers had essentially identical responses (within experimental error) in this test. The tracer responses were also identical in the other two single-well tests (Appendix G). However, Figure 6.5-2 shows that the tracer responses were highly dependent on the rest period of each test. These differences cannot be attributed to diffusion processes because the responses of the tracers with different diffusion coefficients were identical in each individual test. The differences must, therefore, be attributed to the different times that the tracers were allowed to drift in the ambient flow field in each test.

The response of the polystyrene microspheres injected in the 19D single-well test with a 0.5-hr rest period, and the estimates of colloid detachment rate constants obtained from this response are discussed in Appendix G.

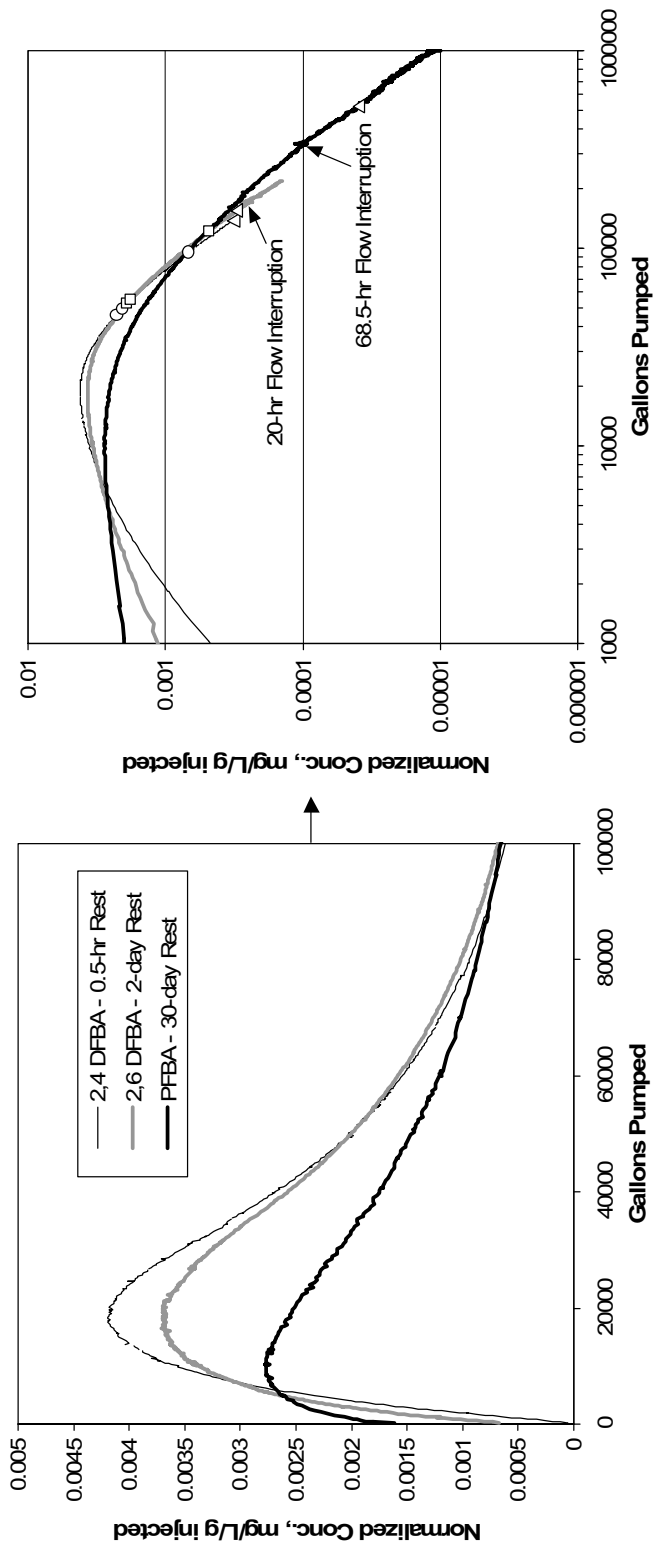
Figure 6.5-3 shows the normalized solute tracer responses in the single-well tracer test at 22S with a rest period of approximately 30 days. It is apparent that, in this tracer test, there is a significant difference between the responses of the two nonsorbing tracers with different diffusion coefficients. Thus, diffusion between flowing and stagnant water is inferred from the results of this test. However, as Figure 6.5-4 shows, there is also a significant difference between the responses of the same tracer (iodide) in the two tests with different rest periods. These differences cannot be accounted for by diffusion alone (particularly the shorter time to peak concentration in the longer-rest-period test), so tracer drift in the ambient flow field also influenced the single-well tracer responses at this location.



Sources: DTNs:UN0109SPA008KS.007 [DIRS 162615] (PFBA), UN0109SPA008KS.008 [DIRS 162616] (Br).
 Output DTN: LA0303PR831231.002. (volumes).

NOTE: The tracer responses are almost identical, so it is difficult to distinguish between the two responses. The figure is plotted in English units because the data were obtained in those units. However, parameter estimates are reported in metric units to downstream users.

Figure 6.5-1. Normalized Concentrations of Tracers in Production Water from NC-EWDP-19D as a Function of Gallons Pumped after a Rest Period of Approximately 30 Days

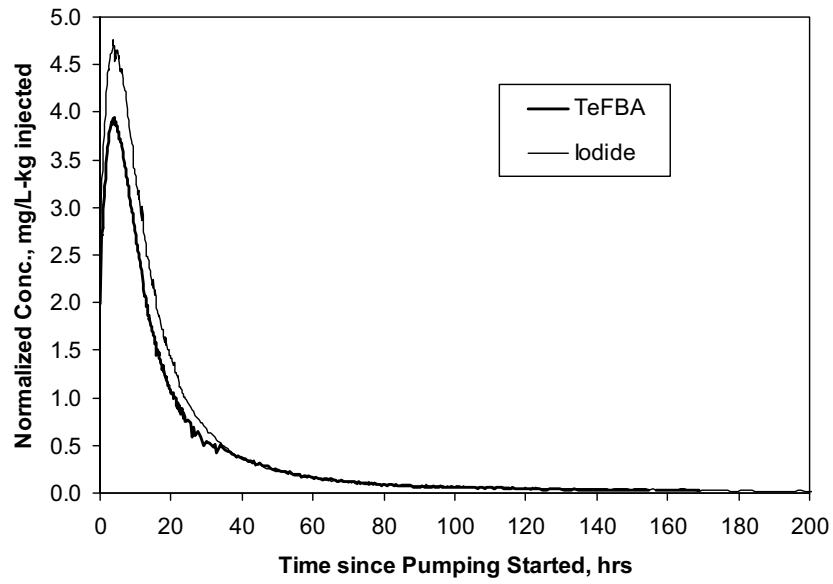


Sources: DTNs: UN0109SPA008IF.006 [DIRS 162442] (2,4-DFBA), UN0102SPA008KS.003 [DIRS 162614] (2,6-DFBA), UN0109SPA008KS.007 [DIRS 162615] (PFBA).

Output DTN: LA0303PR831231.002. (volumes).

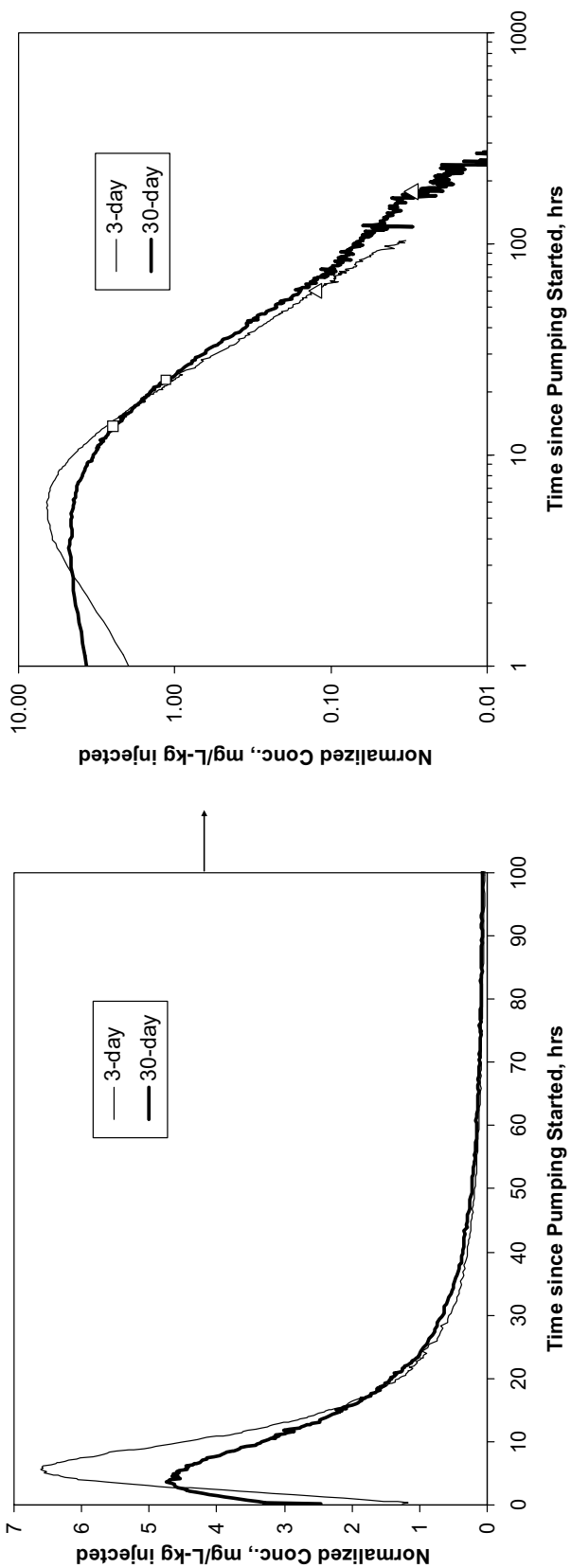
NOTE: On the right-hand plot, circles indicate volumes associated with mean arrival times (for each tracer response), squares indicate volumes associated with alternate mean arrival times, and triangles indicate volumes associated with "late" arrival times. The left-most symbol is always associated with the 0.5-hr rest-period test, and the right-most symbol is associated with the 30-day rest-period test. The bases for these different arrival times/volumes are discussed in detail in Appendix G. The figure is plotted in English units because the data were obtained in those units. However, parameter estimates are reported in metric units to downstream users.

Figure 6.5-2. Normalized Concentrations of Fluorinated Benzoates as a Function of Gallons Pumped in Each of the Three Single-Well Tracer Tests in NC-EWDP-19D



Source: DTN:LA0612PR831231.002 [DIRS 178735].

Figure 6.5-3. Normalized Concentrations of Tracers in Production Water from NC-EWDP-22S as a Function of Time after a Rest Period of Approximately 30 Days



Sources: DTNs: LA0612PR831231.001 [DIRS 178733] (3-day), LA0612PR831231.002 [DIRS 178735] (30-day).

NOTE: On the right-hand plot, squares indicate volumes associated with mean arrival times (for each tracer response), and triangles indicate volumes associated with "late" arrival times. The left-most symbol is always associated with the 3-day rest-period test, and the right-most symbol is associated with the 30-day rest-period test. The bases for these different arrival times/volumes are discussed in detail in Section G4.2.

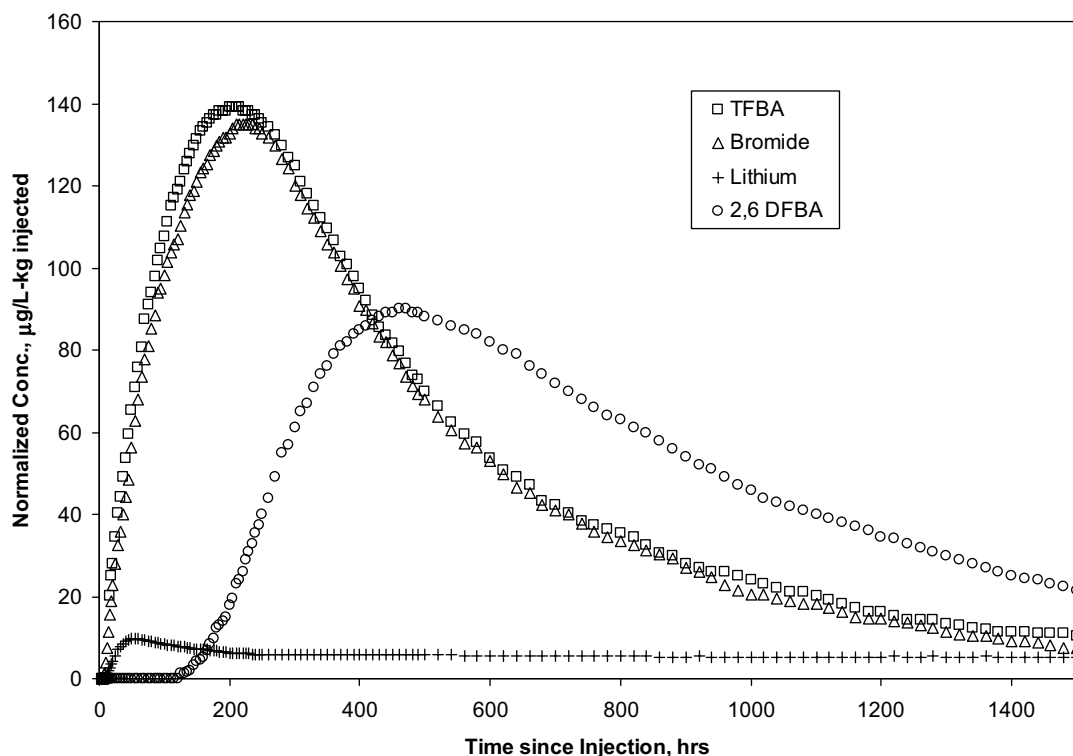
Figure 6.5-4. Normalized Concentrations of Iodide as a Function of Pumping Time in the Two Single-Well Tracer Tests in NC-EWDP-22S

6.5.4 Site 22 Cross-Hole Tracer Test Results

Figure 6.5-5 shows the breakthrough curves (normalized concentrations vs. time) of the solute tracers injected into the second screened intervals in 22PA and 22PC in the first cross-hole tracer test at Nye County Site 22. The data points of this figure represent an “abstraction” of the actual breakthrough curve data because the actual data are too numerous and result in too much weighting of the breakthrough curves tails (where most of the data lie) to be suitable for model fitting.

The tracer injection masses determined by direct mass measurements (i.e., measured weights of tracers added to injection solutions) and indirect concentration measurements (as measured by analyzing injection solutions and multiplying the measured concentrations by injection volumes) in the Site 22 cross-hole tests were in relatively poor agreement. The reasons for the relatively large differences in the apparent injection masses are unknown, but possible explanations (in addition to simple dilution errors) include (1) there was poor mixing of the tracer injection solution at the time it was sampled in the field, (2) some of the fluorinated benzoate tracers were not completely dissolved in the carboys containing concentrated solutions (prepared in the laboratory) or in the injection tanks at the time of sampling (would affect FBAs only), or (3) there was some minor spillage or sloshing of tracers as they were poured into the main injection tank from the carboys. In the following discussion, the tracer concentrations normalized using the direct mass measurements and the indirect concentration measurements are referred to as the “mass-based” and “concentration-based” normalizations, respectively.

The normalized concentrations of Figure 6.5-5 are mass-based normalizations for all tracers except bromide. Using a concentration-based normalization for bromide results in the smallest possible difference between the breakthrough curves of the 2,4,5 TFBA and bromide, which results in the least amount of apparent diffusion between flowing and stagnant water in the tracer test. When a concentration-based normalization is used for TFBA and a mass-based normalization for bromide, the differences between the normalized breakthrough curves of these tracers is maximized, so the deduced amount of diffusion between flowing and stagnant water is maximized. Regardless of which combination of normalizations is used, the 2,4,5 TFBA breakthrough curve always has an earlier and higher peak normalized concentration than the bromide (Figure 6.5-5 is the smallest possible separation), which is consistent with some diffusion occurring between flowing and stagnant water in the alluvium.



Source: DTN: LA0612PR831231.003 [DIRS 178736].

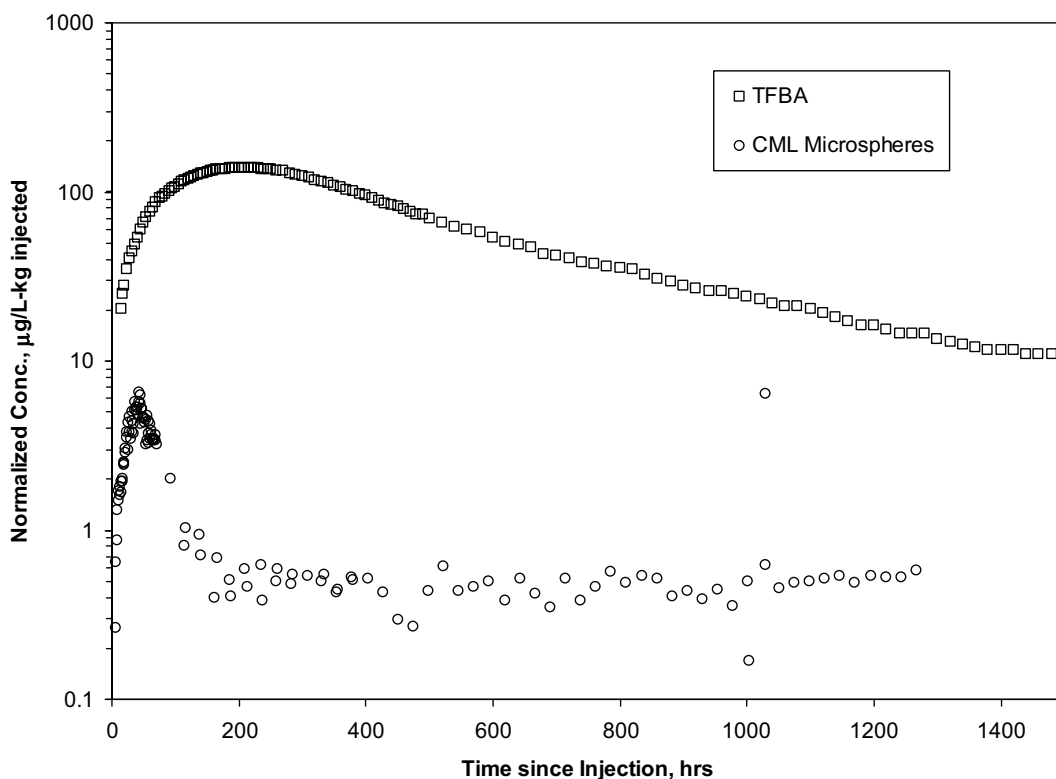
NOTE: All tracer concentrations except for bromide are normalized to directly-measured injection masses. Bromide concentrations are normalized to injection mass deduced from measured injection concentration.

Figure 6.5-5. Normalized Breakthrough Curves of 2,4,5 TFBA, Bromide, Lithium (all from 22PA), and 2,6 DFBA (from 22PC) in the First Cross-Hole Tracer Test at Site 22

Figure 6.5-6 shows the normalized breakthrough curve of the CML microspheres relative to the 2,4,5 TFBA breakthrough curve in the first cross-hole tracer test. These two tracers were injected into the same interval in 22PA, although the microspheres were injected 10 days later than the solutes. It is clear that the microspheres experienced significant filtration in the test interval, although it is also apparent that they had a long, low concentration breakthrough curve tail indicative of some detachment of filtered microspheres in the aquifer.

The 2,5 DFBA injected into the uppermost screened interval in 22PA was never detected in the water produced from 22S. This result suggests that vertical flow and transport through the alluvium is probably somewhat hindered relative to horizontal flow and transport, which is consistent with the hydraulic test interpretations that indicate the shallow alluvium at Site 22 (over the two shallowest intervals) has a horizontal-to-vertical hydraulic conductivity ratio of at least 1.5 to 2 (Section 6.4 and Appendix F). If the flow system were homogeneous and isotropic, the expected 2,5 DFBA travel time in the vertical direction from the bottom of zone 1 to the top of zone 2 (a distance of about 20 m) would be about 30 days. This estimate assumes a vertical hydraulic conductivity of ~12 m/day (based on the zone 2 hydraulic test interpretation), a drawdown difference of ~0.1 m between zones 1 and zone 2 (observed when zone 2 was pumped), and a flow porosity of 0.1 (based on the tracer test interpretations discussed below);

i.e., travel time = $L/(K\Delta H/L)/\eta$, where L = distance, K = hydraulic conductivity, ΔH = head or drawdown difference, and η = flow porosity = $20 \text{ m} / (12 \text{ m/day} \times (0.1/20) \text{ m/m} / 0.1 = \sim 33$ days. Given the observed horizontal tracer travel time of less than 10 days between wells 22PA and 22S, one would expect the 2,5 DFBA arrival time at 22S to be no more than about $30 + 10 = 40$ days in a homogeneous, isotropic system. The fact that there was no 2,5 DFBA arrival at 22S in over 60 days of pumping (and also no arrival in another ~ 45 days of pumping during the second cross-hole tracer test) indicates that the flow system must have a lower effective vertical hydraulic conductivity relative to horizontal hydraulic conductivity. If the vertical travel distance were 20 m (the distance from the bottom of zone 1 to the top of zone 2), a lower bound estimate of the horizontal-to-vertical hydraulic conductivity ratio would be about 3:1 based on the fact that there was no arrival in over 100 days of pumping. However, if the vertical travel distance were greater than the minimum distance of 20 m, then the lower bound estimate of the conductivity ratio would be smaller. Also, the possibility that the 2,5 DFBA arrived at 22S in concentrations too low to detect cannot be discounted given that the 2,5 DFBA injection mass was only about 18% of the injection mass of the 2,4,5 TFBA and 2,6 DFBA and that peak tracer concentrations tend to decrease approximately as $1/\text{travel time}$.



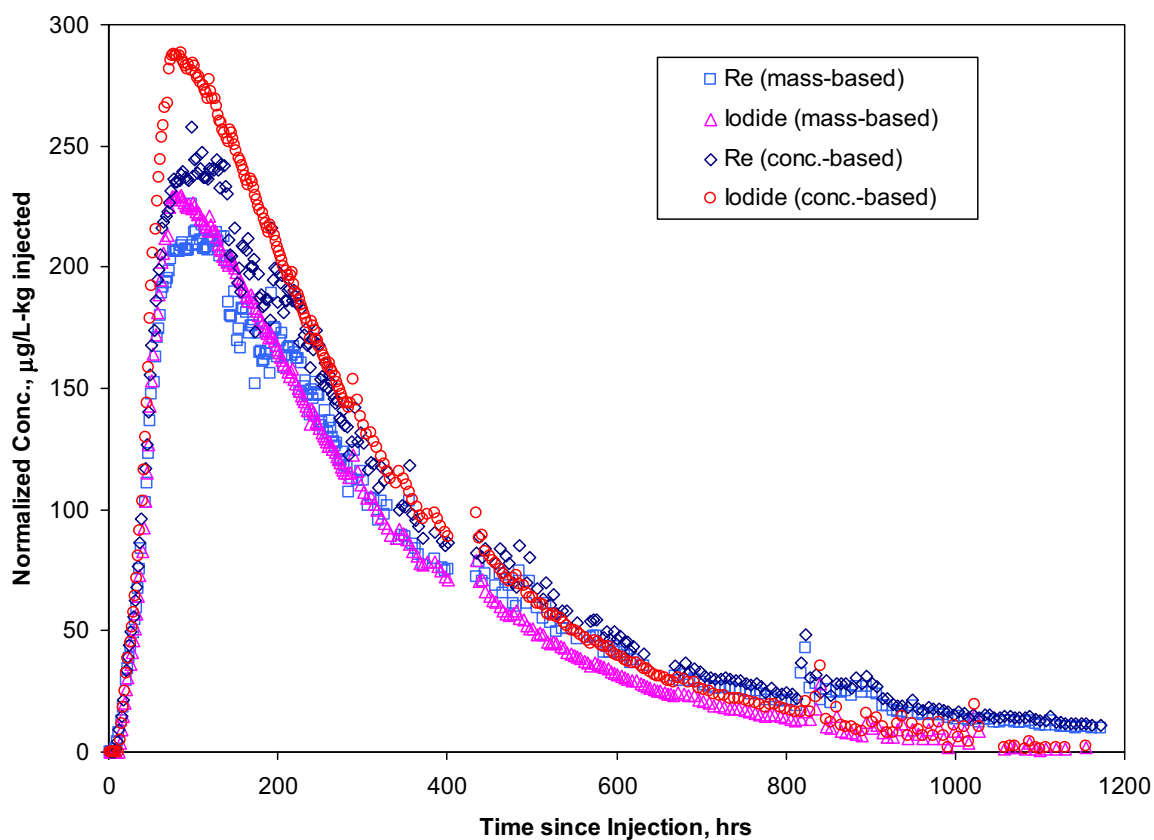
DTN: LA0612PR831231.005 [DIRS 178739] (microspheres); LA0612PR831231.003 [DIRS 178736] (TFBA) .

NOTE: Note the log normalized concentration scale. The very high microsphere data point at about 1,050 hours was reanalyzed and verified to be valid; this high concentration may have been the result of an undocumented flow perturbation.

Figure 6.5-6. Mass-Based Normalized Breakthrough Curves of 2,4,5 TFBA and CML Microspheres in the First Cross-Hole Tracer Test at Site 22

Figure 6.5-7 shows the mass-based and concentration-based normalized breakthrough curves of the iodide and perrhenate in the second cross-hole tracer test conducted between 22PA and 22S (abstracted data used for interpretive analyses are presented later). It is apparent that there were significant discrepancies in the injection masses determined from the direct and indirect measurement methods mentioned above in this test as well. It is also apparent that the analyzed rhenium concentrations have significant scatter associated with them. The fact that the concentration-based normalizations of both tracers are significantly larger (even more so than in the first test) than their respective mass-based normalizations suggests that the tracers were probably diluted in the field more than intended.

Regardless of whether mass- or concentration-based normalizations are used, the perrhenate breakthrough curve has a later peak concentration and a higher tail than the iodide breakthrough curve. Both of these characteristics are consistent with either greater diffusion of perrhenate into stagnant water in the system or sorption of perrhenate in the stagnant porosity after diffusion into this porosity. Given that perrhenate has a smaller diffusion coefficient than iodide (Table 6.5-3), the latter explanation seems more likely.



Source: DTN: LA0612PR831231.004 [DIRS 178738].

Figure 6.5-7. Mass-Based and Concentration-Based Normalized Breakthrough Curves of Iodide and Perrhenate in the Second Cross-Hole Tracer Test at Site 22

6.5.5 Tracer Test Interpretations: Estimates of Ambient Flow Velocity in Alluvium

Four methods were used to obtain groundwater velocity estimates from the single-well tracer tests at the ATC, and three of these were also used to estimate groundwater velocities from single-well tracer tests at Site 22. The three methods used at both locations involved relatively simple spreadsheet calculations that, given various simplifying assumptions, solve for groundwater velocities consistent with the observed differences in the following:

1. Peak tracer concentration arrival times
2. “Late” tracer arrival times, defined as the times in each test when the fractional tracer mass recovery was equal to the final recovery in the test having the lowest overall mass recovery.

“Mean” arrival times of tracer mass recovered at the same arbitrarily selected high fractional recovery in each test. Note that these three times also correspond to volumes pumped, and the latter can provide a more meaningful basis of comparison between tests when pumping rates vary in different tests. The peak, late, and mean arrival times (and corresponding volumes) for each test are listed in Table 6.5-4. The points on the tracer breakthrough curves corresponding to the mean and late arrival times in each test are identified in the right-hand plots of Figures 6.5-2 and 6.5-4.

The fourth method of estimating ambient groundwater velocity, which was applied only to the ATC tracer test data, involved detailed analytical calculations of tracer migration during the tests by linking together solute transport solutions for the injection, rest, and pumping phases that assume a two-dimensional homogeneous and isotropic aquifer. This method also provided estimates of effective flow porosity and longitudinal dispersivity in the alluvium, although these estimates are not well constrained.

The details of the calculations associated with four estimation methods are provided in Appendix G. Table 6.5-5 lists the results obtained for both the groundwater velocity, v_{GW} , and the specific discharge, v_S ($=\eta v_{GW}$), as a function of assumed flow porosity (η) by all four methods of estimation for the ATC. Table 6.5-6 lists the same estimates obtained from the first three methods for Site 22. Of the first three methods, the peak analysis method offers the smallest estimates, and the analysis of late-arriving mass (high recovery) offers the largest estimate at both locations. The range of the estimates from the three methods used at both sites spans about a factor of three for a given assumed value of flow porosity. The velocity estimate from the linked analytical solutions is in good agreement with the peak analysis method at the ATC.

An additional estimate of ambient flow velocity at Site 22 was obtained by analyzing the responses of nonsorbing tracers in 22S after a 159-day stoppage of flow between the two cross-hole tracer tests that were conducted at this location. This analysis, which is described in detail in Section G5.3, yielded a seepage velocity estimate of 9.25 m/yr. The corresponding specific discharge estimates for different assumed flow porosities are listed at the bottom of Table 6.5-6.

Table 6.5-4. Times and Pumped Volumes Associated with Each of the Single-Well Tracer Test Arrival Times Used in the Different Methods of Estimating Groundwater Velocities

	Arrival Time (hr)/Volume (L [gal])		
	0.5 hr	2 days	30 days
19D Rest Period:			
Peak arrival	24 / 76,000 [20,000]	30.5 / 76,000 [20,000]	12.2 / 38,600 [10,200]
Late arrival ^a	168 / 511,000 [135,000]	225 / 556,000 [147,000]	639 / 1,780,000 [471,000]
Mean arrival ^b	52 / 161,000 [42,500]	71 / 178,000 [46,500]	109 / 344,000 [91,000]
Alternate mean arrival ^c	61.5 / 189,000 [50,000]	81 / 201,000 [53,000]	149 / 469,000 [124,000]
22S Rest Period:	3 days	30 days	
Peak arrival	5.6 / 60,000 [15,900]	3.8 / 41,000 [10,800]	
Late arrival ^d	57 / 611,000 [161,400]	169 / 1,820,000 [481,700]	
Mean arrival ^e	12.6 / 135,000 [35,700]	20.9 / 225,500 [59,600]	

Sources: DTNs: UN0109SPA008IF.006 [DIRS 162442] (19D, 0.5 hr); UN0102SPA008KS.003 [DIRS 162614] (19D, 2 days); UN0109SPA008KS.007 [DIRS 162615] (19D, 30 days); LA0612PR831231.001 (22S, 3 days) [DIRS 178733]; LA0612PR831231.002 (22S, 30 days) [DIRS 178735].

Output DTNs: LA0303PR831231.002 (19D); LA0701PR150304.001 (22S).

^a Time/volume associated with approximately 86.4% mass recovery in each test at 19D (the final recovery in the 0.5-hr rest period test, which had the lowest final recovery of any test).

^b Mean arrival time calculated by truncating all tracer response curves at approximately 86.4% recovery in each test.

^c Alternate mean arrival time calculated by extrapolating the tracer response curves in the 0.5-hr rest period test to 91.3% and truncating the response curves in the 2-day rest period test to 91.3% recovery (the final recovery in the 30-day rest period test).

^d Time/volume associated with approximately 96.7% mass recovery in each test at 22S.

^e Mean arrival time calculated by truncating all tracer response curves at 96.7% recovery in each test at 22S.

Table 6.5-5. Specific Discharges and Groundwater Velocities Estimated from the Different Ambient Flow Velocity Analysis Methods as a Function of Assumed Flow Porosity at 19D

Assumed Flow Porosity ^a	Specific Discharge (m/yr) / Groundwater Velocity (m/yr)		
	0.05	0.18	0.3
Peak Arrival Analysis	1.2 / 24.5	2.4 / 13.1	3.0 / 9.9
Late Arrival Analysis ^b	3.9 / 77.1	7.3 / 40.4	9.4 / 31.3
Mean Arrival Analysis ^c	2.0 / 40.3	3.8 / 20.9	4.9 / 16.4
Mean Arrival Analysis ^d	2.5 / 49.1	4.6 / 25.8	6.0 / 20.2
Linked Analytical Solutions	1.5 / 15 with a flow porosity of 0.10 and a longitudinal dispersivity of 5 m.		

Output DTN: LA0303PR831231.002.

^a The three values are approximately the lowest, expected, and highest values of the alluvium flow porosity used in Yucca Mountain performance assessments (SNL 2007 [DIRS 177390]).

^b Time/Volume associated with approximately 86.4% recovery in each test (the final recovery in the 0.5-hr rest period test, which had the lowest final recovery of any test).

^c Mean arrival time calculated by truncating all tracer response curves at approximately 86.4% recovery in each test.

^d Alternative mean arrival time calculated by extrapolating the tracer response curves in the 0.5-hr rest period test to 91.3% and truncating the response curves in the 2-day rest-period test to 91.3% recovery (the final recovery in the 30-day rest-period test).

Table 6.5-6. Specific Discharges and Seepage Velocities at 22S Estimated from Different Drift Analysis Methods as a Function of Assumed Flow Porosity

Assumed Flow Porosity ^a	Specific Discharge (m/yr) / Seepage Velocity (m/yr)		
	0.05	0.18	0.3
Single-Well Peak Arrival Analysis	0.47 / 9.5	0.89 / 5.0	1.2 / 3.9
Single-Well Late Arrival Analysis ^b	2.2 / 43.8	4.2 / 23.1	5.4 / 17.9
Single-Well Mean Arrival Analysis ^c	0.82 / 16.4	1.6 / 8.6	2.0 / 6.7
Analysis of Cross-Hole Tracer Responses after 159-day Flow Interruption	0.46 / 9.25	1.7 / 9.25	2.8 / 9.25

Output DTNs: LA0701PR150304.001 (single-well tests); LA0701PR150304.004 (cross-hole test).

^a The three values are approximately the lowest, expected, and highest values of the alluvium flow porosity used in Yucca Mountain performance assessments (SNL 2007 [DIRS 177390]).

^b Time/Volume associated with approximately 96.7% recovery in each test.

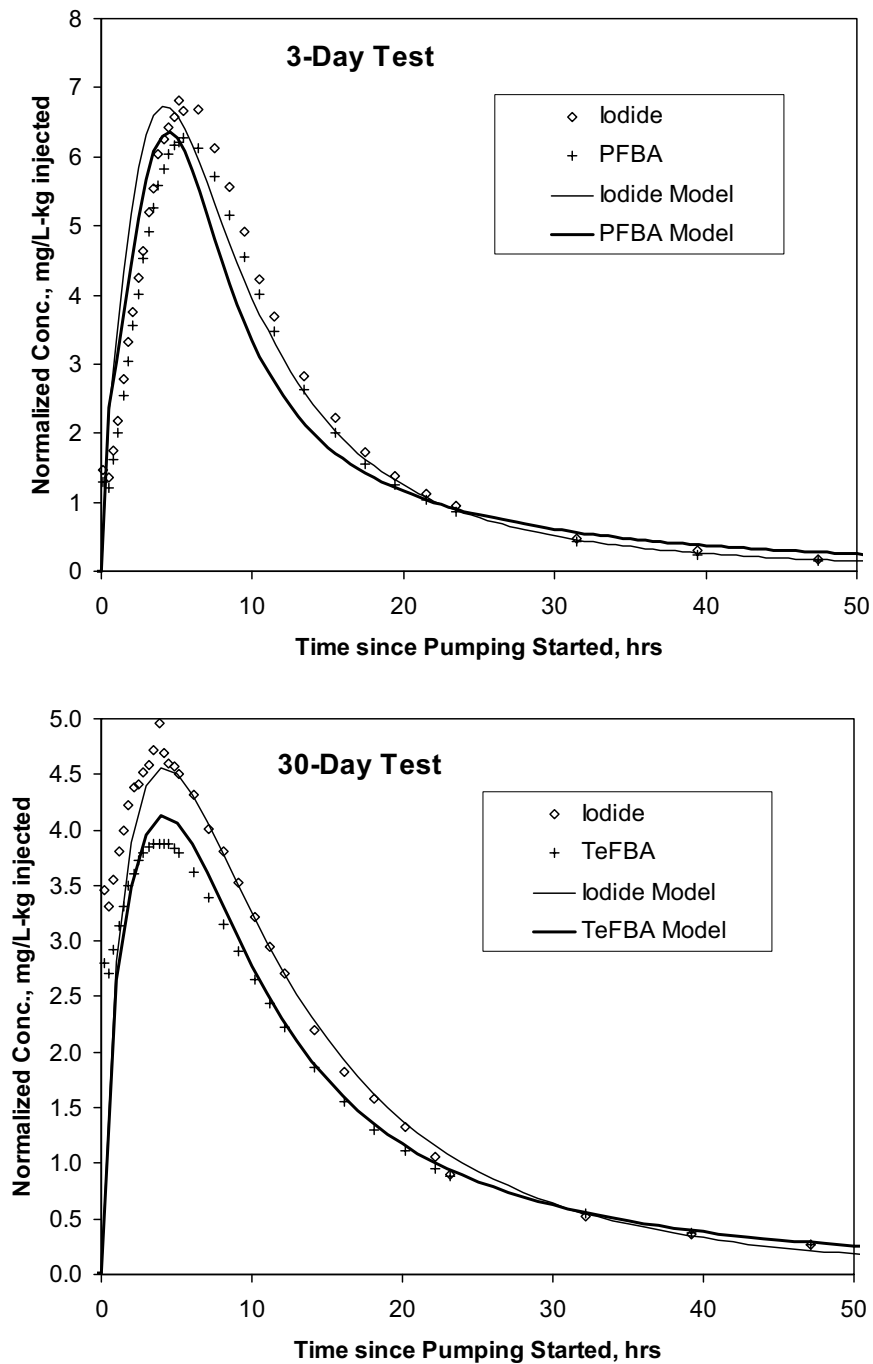
^c Mean arrival time calculated by truncating the two tracer response curves at 96.7% recovery in each test.

6.5.5 Tracer Test Interpretations: Conceptual Transport Model Implications

As with the C-wells tracer tests, the alluvium tracer tests at Site 22 were interpreted using a combination of the RELAP V2.0 (STN: 10551-2.0-00 [DIRS 159065]) and MULTRAN V 1.0 (STN: 10666-1.0-00 [DIRS 159068]) computer codes. The single-well tracer tests were interpreted using MULTRAN, and the cross-hole tracer tests were interpreted using RELAP. The MULTRAN interpretations of the single-well tracer tests were conducted to estimate parameters describing diffusion between flowing and stagnant water in the alluvial flow system. Figure 6.5-8 shows simultaneous MULTRAN fits to the tracer test responses in the two single-well tests at Site 22 using the same diffusive mass transfer parameters for each test. The single-well tests at the ATC were not quantitatively interpreted because they showed no evidence of dual-porosity behavior, so test interpretations were limited to the ambient flow velocity estimates discussed in the previous section. The RELAP interpretations of the Site 22 cross-hole tests were conducted to provide estimates of diffusion parameters, flow porosities, flow anisotropy, colloid (microsphere) filtration and detachment parameters, and retardation/sorption parameters for lithium and perrhenate in the alluvium. Details of the analyses are provided in Section G5.

The cross-hole tracer responses between 22PA and 22S were interpreted assuming multiple flow pathways contributed to the observed breakthrough curves. This assumption was supported by inflections in the time derivatives of the nonsorbing tracer breakthrough curves (see Figure G-41) and by the inability to fit the early portion of the breakthrough curves assuming a single flow pathway. Figure 6.5-9 shows a simultaneous multi-pathway RELAP fit to the nonsorbing tracer responses between 22PA and 22S in the first cross-hole tracer test. Figure 6.5-10 shows a simultaneous RELAP fit to the iodide and perrhenate responses in the second tracer test. The two flow pathways providing good fits to the responses in the second test corresponded very closely to the first two pathways in the first tracer test, suggesting that the third pathway was not accessed by tracers in the second test. That the third pathway was activated in the first test but not in the second test because of the very high density of the tracer

solution in the first test (specific gravity of greater than 1.12), which probably resulted in density-driven flow in the vicinity of the injection wellbore that did not occur in the second test.

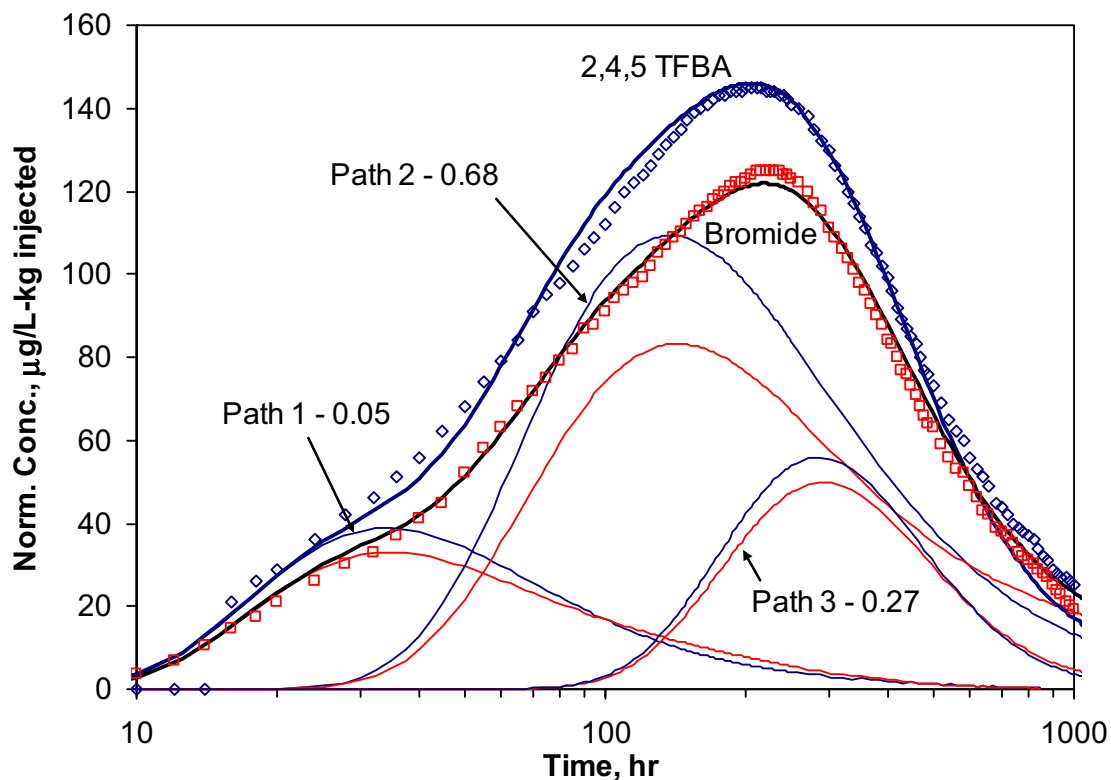


Sources: DTNs: LA0612PR831231.001 [DIRS 178733] (3-day test data), LA0612PR831231.002 [DIRS 178735] (30-day test data), and LA0701PR150304.007 (output).

NOTE: Details of the fitting procedure are provided in Appendix G, and model parameters are listed in Table G-11.

Figure 6.5-8. MULTRAN Model Matches to the 22S Single-Well Tracer Test Breakthrough Curves

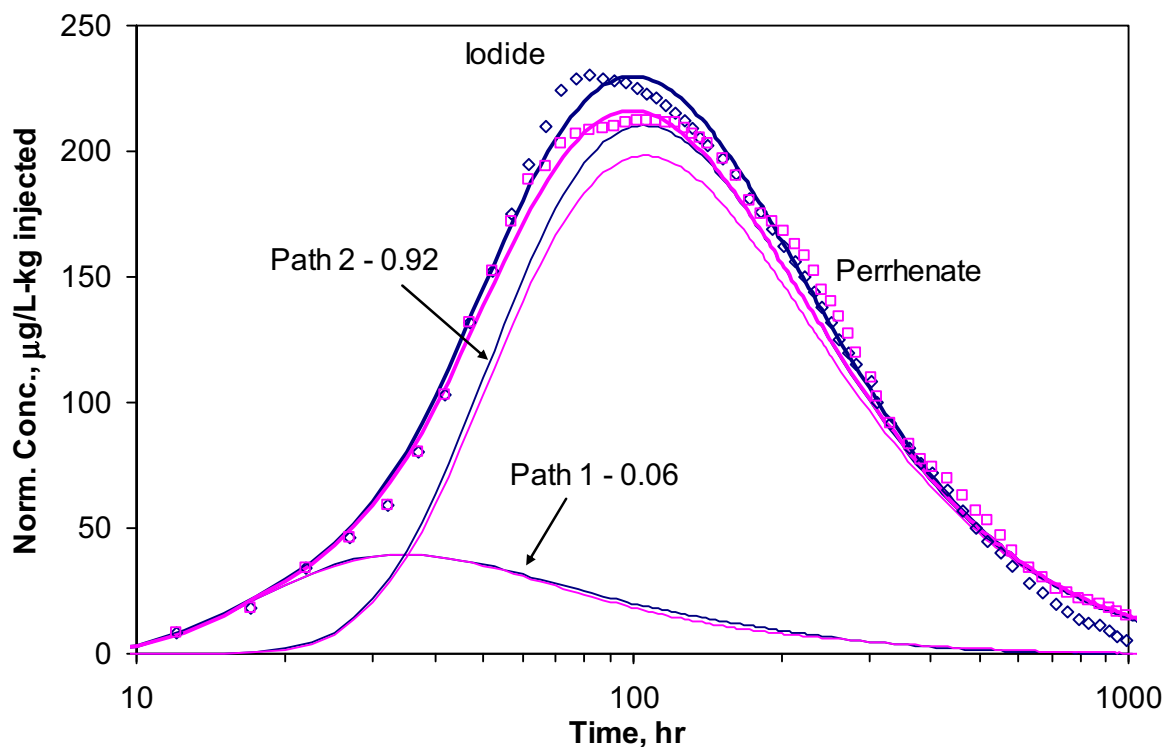
This density-driven flow likely caused some of the tracer solution to “sink” into pathways that were not accessed in the second test. RELAP fits to the lithium and microsphere responses between 22PA and 22S and to the 2,6 DFBA response between 22PC and 22S in the first cross-hole test are presented and discussed in Section G5 of Appendix G. The microsphere filtration and detachment parameters deduced from RELAP are listed in Table 6.5-7. The deduced retardation factors and partition coefficients (K_d values) for lithium are discussed and compared with laboratory-derived K_d estimates in Section G5.4.3. The conclusion from this comparison is that the laboratory K_d values would probably result in underestimation of field-scale sorption/retardation in the alluvium if used in large-scale predictive transport models.



Output DTN: LA0701PR150304.006.

NOTE: These normalizations yield the maximum possible difference between the TFBA and bromide breakthrough curves – as opposed to the minimum possible differences in Figure 6.5-5. The tracer mass fractions in each pathway are indicated on the plot. All pathways have dual-porosity behavior. The bold black curves are the sums of the three individual model pathway curves. Model parameters are listed in Table G-15. The simulated tracer responses associated with the individual pathways are indicated by the thin colored lines.

Figure 6.5-9. Composite Three-Pathway RELAP Fits to the First 1,000 Hours of the 2,4,5 TFBA (Concentration-Based Normalizations) and Bromide (mass-based normalization) Breakthrough Curves at Site 22



Output DTN: LA0701PR150304.003.

NOTE: The bold curves are the sum of the two individual model pathway curves. Model parameters are listed in Table G-18 of Appendix G.

Figure 6.5-10. Two-Pathway RELAP Fits to the Iodide and Perrhenate (mass-based normalization) Breakthrough Curves in the Second Cross-Hole Tracer Test at Site 22

Although there was no apparent diffusion between flowing and stagnant water in the single-well tracer tests at the ATC, the single-well and cross-hole tracer test results and interpretations at Site 22 collectively indicate dual-porosity transport behavior in the alluvium at this location. However, the diffusion time and length scales are relatively short compared to those of the fractured volcanics, and an important conclusion is that, over the time and distance scales of importance for performance assessment calculations, the tracer test interpretations suggest that the alluvium will behave as a single-porosity transport system with an effective porosity equal to the sum of the flowing and stagnant porosities deduced from the tracer tests. The short diffusion time and distance scales are more consistent with a diffusion-into-grains (or blocks) conceptual model than a diffusion-into-layers conceptual model. However, longer diffusion time scales cannot be ruled out in the alluvium because of the short time and distance scales of the tracer tests relative to performance assessment time scales. It is possible that the tests were strongly influenced by diffusion into blocks within flow pathways, but the flow pathways were large enough in thickness or diameter (i.e., channels) that longer-time-scale diffusion into stagnant water surrounding the pathways was not observed. Estimates of transport parameters that can be used directly in solute transport models derived from the best-fitting model parameters associated with the MULTRAN and RELAP model fits are listed in Table 6.5-8. Additional discussion of these ranges and how they were derived is provided in Appendix G.

An important result from the second cross-hole tracer test at Site 22 is that perrhenate transport appears to be attenuated relative to iodide in the saturated alluvium at this location. Because the free-water diffusion coefficient of perrhenate is smaller than that of iodide, the only logical explanation for this apparent attenuation is retardation of the perrhenate in either the flowing or stagnant porosity of the alluvium. The RELAP fits to the breakthrough curves suggest that the latter is more likely. However, regardless of whether the perrhenate retardation occurred in the flowing or stagnant porosity, the apparent sorption behavior is significant because it suggests that the perrhenate interacted with alluvium surfaces in ways (including, perhaps, some reduction of Re(VII) to Re(IV)) that might also occur for pertechnetate. Pertechnetate is assumed to be a nonsorbing species in Yucca Mountain performance assessment calculations, and this result for perrhenate, while not necessarily conclusive, certainly suggests that there may be favorable conditions in the saturated alluvium for at least partial sorption/attenuation of pertechnetate.

Table 6.5-7. CML Microsphere Filtration Parameters

	Parameter	Pathway 1	Pathway 2	Pathway 3
Minimum Diffusion Case	Mass fraction, f (minimum diffusion)	0.05	0.58	0.33
	k_{fit} (1/hr)	0.16	0.048	>0.04
	k_{res}^b (1/hr)	0.0011	0.00034	-
Maximum Diffusion Case	Mass fraction, f (maximum diffusion)	0.05	0.68	0.27
	k_{fit} (1/hr)	0.16	0.048	>0.045
	k_{res}^b (1/hr)	0.0011	0.00034	-

Output DTNs: LA0701PR150304.002 (minimum diffusion) and LA0701PR150304.006 (maximum diffusion).

NOTE: These parameters for multi-pathway fits to the microsphere response using the nonreactive transport parameters deduced from the fits to the TFBA and bromide breakthrough curves assuming the minimum and maximum possible amounts of matrix diffusion. Other transport parameters used to obtain the fits are given in Tables G-14 (minimum diffusion case) and G-15 (maximum diffusion case).

Table 6.5-8. Transport Parameter Estimates Deduced from Tracer Tests in Saturated Alluvium

Parameter	Lower Bound	Best Estimate	Upper Bound
Effective flow porosity ^a	0.036	0.121	0.187
Longitudinal dispersivity, m ^b	1.6	5	10
Horizontal flow anisotropy ratio (N-S principal axis) ^c	2.5	3.1	10.7
MTC, $\frac{\phi}{b} \sqrt{D_m}$, for halide (sec ^{-1/2}) ^d	0 (0.00016)	-	0.001
Characteristic diffusion time scale, (L ² /8D _m), hr ^d	0 (14.1)	-	1,125
Ratio of stagnant to flowing water volumes ^d	0 (0.3)	-	1.9

Output DTNs: LA0701PR150304.002, LA0701PR150304.003, LA0701PR150304.006, and LA0701PR150304.007.

NOTE: All estimates come from cross-hole tracer testing at Nye County Site 22 except for the lower bounds of the diffusion parameters (last 3 rows).

^a Calculated using Eq. D-6, Appendix D, Section D4.8.5, but with the production rate modified to account for flow anisotropy estimated from tracer responses. That is, instead of uniform radial flow at 47.5 gallons per minute (gpm), it was assumed that there was a flow rate of 71.25 gpm in the direction of 22PA and 23.75 gpm in the direction of 22PC, which is consistent with the ~3:1 flow anisotropy in the N-S direction. The lower bound is based on using the mean residence assuming radial flow in the fastest flow pathway between 22PA and 22S, and the upper bound is based on the mean residence time assuming linear flow in the second flow pathway between 22PA and 22S. The best estimate approximately corresponds to radial anisotropic flow for both 22PA (second pathway) and 22PC to 22S. See discussion in Section G5.4.

^b Lower bound assumes radial flow in third flow pathway of first cross-hole test, and upper bound assumes linear flow in second pathway in second cross-hole test. Best estimate is based on assuming radial flow in all first and second pathway analyses.

^c Lower bound based on ratio of linear flow residence time between 22PC and 22S and linear flow residence time in second pathway between 22PA and 22S. Upper bound based on ratio of radial flow residence time between 22PC and 22S and radial flow residence time in first pathway between 22PA and 22S. Best estimate based on ratio of radial flow residence time between 22PC and 22S and radial flow residence time in second pathway between 22PA and 22S.

^d MTC=diffusion mass transfer coefficient. Lower bound based on apparent single-porosity behavior in third-pathway of first cross-hole test (when minimum differences between bromide and TFBA are assumed) and also on the very minor differences in the iodide and PFBA responses in the first single-well tracer test at 22S, and on the negligible differences in halide and FBA responses in the single-well tests at the ATC. Numbers in parentheses for the lower bound are the lowest value from a dual-porosity pathway analysis. Upper bound is based on the maximum value observed in any of the tracer tests. However, for the ratio of stagnant to flowing water volumes, larger values cannot be ruled out because of the relatively short time scales of the tracer tests. See text for definitions of the individual parameters that comprise the MTC.

6.5.6 Laboratory Testing to Support Field Tracer Tests

A number of laboratory tests were conducted to support planned cross-hole tracer testing efforts at the ATC (Appendix H). These tests focused on the batch sorption characteristics and column transport behavior of lithium ion, which was to be used as a reactive tracer in cross-hole tracer testing. The motivation for comparing lithium sorption parameters obtained in laboratory and field tests was the same as that discussed in Section 6.3.6 for laboratory testing conducted in support of C-wells tracer testing: favorable comparisons of laboratory- and field-derived transport parameters of nonradioactive tracers lend credibility to the practice of using laboratory-derived radionuclide transport parameters in field-scale predictive simulations.

Laboratory testing conducted in support of ATC tracer testing included:

- Batch sorption tests to determine lithium sorption parameters associated with various depth intervals at the ATC and their dependence on mineralogical characteristics of the alluvium
- Lithium bromide and PFBA tracer tests in columns packed with alluvium from NC-EWDP-19D to determine lithium transport characteristics as a function of lithium injection concentration.

Details of the conduct and results of these laboratory tests are provided in Appendix H. These tests are not discussed further here because the field tracer test involving lithium ion was never conducted.

A small set of lithium batch sorption tests with 22S water and alluvium from the second screened interval from the surface of 22PC were conducted to support the cross-hole tracer testing efforts at Site 22. The results of these tests are presented in Section G5.4.3 of Appendix G, where the field- and laboratory-derived partition coefficients (K_d values) for lithium are discussed and compared. In summary, although the laboratory data set is quite limited compared to that for the ATC, the results suggest that apparent lithium sorption was greater in the field tracer test than in the laboratory batch tests.

6.5.7 Limitations and Uncertainties

The estimates of groundwater velocity and specific discharge in the alluvium at the ATC and Site 22 in Tables 6.5-1 and 6.5-2 vary over a range of about a factor of 3 for a given flow porosity assumption, and over a range of about a factor of 10 for all reasonable flow porosity assumptions. These estimates are in reasonably good agreement with estimates obtained using potentiometric head and hydraulic conductivity data and also with an estimate obtained from analyzing the responses of nonsorbing tracers used in cross-hole tracer testing at Site 22 after a 159-day flow interruption, so the one-order-of-magnitude range in the values is considered to be a reasonable reflection of the uncertainty associated with the estimates.

The limitations, uncertainties and general remarks regarding the alluvium field tracer test results are essentially identical to those discussed in Section 6.3.7 (for the tracer tests in fractured volcanic tuffs at the C-wells complex).

An additional uncertainty that applies to the alluvium cross-hole tracer tests is the uncertainty associated with the injection masses of the tracers that were used to normalize the tracer concentrations for the interpretive analyses. As discussed in Section 6.5.4, there was a significant lack of agreement between directly-measured injection masses and injection masses deduced from injection concentration measurements that did not occur for the tracer tests at the C wells or for the single-well tracer tests at the ATC and Site 22. This uncertainty introduces additional uncertainty into the transport parameter estimates deduced from the cross-hole tracer tests in the alluvium. However, we do not believe that this uncertainty raises doubts about the dual-porosity nature of the alluvium, as the relative shapes of the tracer breakthrough curves and

the lithium transport behavior are both consistent with dual-porosity transport regardless of the uncertainties in the normalizations of the tracer breakthrough curves.

Another uncertainty associated with the alluvium tracer test interpretations is the inherent and unquantifiable uncertainty associated with the conclusion that diffusion time and distance scales are quite small and that the alluvium should therefore behave as a single-porosity transport system over much larger time and distance scales than the tracer tests. The possibility exists that the time and distance scales of the tracer tests may have been too short to observe significant diffusion out of flowing pathways and into relatively extensive layers or blocks of stagnant or near-stagnant alluvium in the flow system. Furthermore, the uncertainties associated with the tracer injection masses (above) make any assessment of larger diffusion time and length scales essentially impossible using the available data from Site 22. However, it should be noted that the mass-fraction-weighted sum of the flowing and stagnant porosities from the two pathways between 22PA and 22S in the second cross-hole tracer test (the test without density-driven flow issues) is slightly greater than 0.2, which is probably quite close to the total porosity of the alluvium (considered to have a maximum value of around 0.3). Thus, while we cannot rule out the possibility of longer diffusion time and distance scales in the alluvium than the tracer tests indicated, the tracer test interpretations are consistent with tracers accessing the majority of the total porosity in the flow system.

7. CONCLUSIONS

7.1 SUMMARY OF SCIENTIFIC ANALYSIS

This scientific report documents the results of numerous in situ field hydraulic and tracer tests conducted in the SZ near Yucca Mountain over the past 10 years. These tests were conducted to verify or validate conceptual models of flow and transport in the SZ and to obtain field-scale estimates of flow and transport parameters to support the development of parameter distributions used in process and TSPA models. The tests also provide an enhanced understanding of the performance of the various components of the saturated zone barrier, which, in turn increases confidence in the process and TSPA models. This report also documents the results of several laboratory experiments conducted to help constrain field tracer test interpretations and to provide comparisons between field- and laboratory-derived sorption parameters for the lithium ion, which is a weakly sorbing tracer.

The most significant conclusions from in situ field testing with regard to barrier capability of the saturated zone are the following:

- For flow modeling purposes, the saturated volcanic tuffs near Yucca Mountain can be treated as an equivalent porous medium. The fracture networks in the tuffaceous rocks are connected well enough that hydraulic responses are similar to those observed in porous media. However, the flow system exhibits layered heterogeneity with layers of high permeability often associated with relatively narrow fractured intervals. Also, larger-scale hydraulic characteristics of the saturated tuffs are strongly influenced by structural features such as faults. Hydraulic parameters derived from cross-hole testing in the fractured volcanics are summarized in Section 6.2, Tables 6.2-2 through 6.2-4.
- Horizontal anisotropy in hydraulic conductivity in the saturated fractured volcanic tuffs near Yucca Mountain, as determined from drawdown responses in distant wells during the 1996 to 1997 long-term pumping test in UE-25 c#3, is oriented roughly north-south (direction of greatest conductivity) with an anisotropy ratio of about 4:1. A cumulative distribution function for anisotropy ratio assuming a north-south orientation of anisotropy is provided in Section 6.2.6, Figure 6.2-3.
- Solute tracer responses in cross-hole tracer tests at the C-wells were consistent with a dual-porosity conceptual transport model. In this model, solute migration occurs primarily in flowing fractures. The solutes are effectively attenuated by diffusion into stagnant water in the porous rock matrix (matrix diffusion). Solute transport parameters derived from cross-hole tracer testing at the C-wells are summarized in Section 6.3, Table 6.3-3.
- Apparent sorption of an ion-exchanging tracer (lithium) was generally greater in field tracer tests in the volcanic tuffs than in laboratory tests using the same materials. These results suggest that laboratory sorption parameters will tend to result in overestimation of radionuclide transport rates in the tuffs. Comparisons of field and laboratory lithium sorption parameters are provided in Section 6.3, Table 6.3-4.

- Polystyrene microsphere responses in cross-hole tracer tests at the C-wells suggest that filtration processes effectively attenuate a large percentage of the microspheres over relatively short distances. However, some of the filtered microspheres later detach from fracture surfaces and continue to migrate. Also, flow transients appear to be capable of initiating detachment. Estimates of microsphere transport parameters derived from the C-wells tracer tests are provided in Table 6.3-3.
- Hydraulic testing in the saturated alluvium at the Nye County ATC and Site 22 locations south of Yucca Mountain has indicated that the alluvium behaves as an unconfined aquifer (with vertical anisotropy ratio of about 2 to 3) at shallow depths and then transitions to a leaky-confined or confined aquifer system (with a vertical anisotropy ratio of greater than 10) beneath the first significant confining layer. The results indicate that subhorizontal confining or semi-confining layers exist in the alluvium, but insufficient data exist to predict their depth and lateral extent as a function of location. Composite horizontal hydraulic conductivity estimates from cross-hole hydraulic testing in the alluvium are on the order of 2 to 5 m/day, with individual isolated zones having horizontal conductivities as high as 12 to 13 m/day (Section 6.4).
- Single-well injection-withdrawal tracer testing in the saturated alluvium in the uppermost screened interval of NC-EWDP-19D and in the second screened interval from the surface in NC-EWDP-22S have yielded estimates of specific discharge that range from about 1 m to 10 m/yr at the 19D location and from about 0.5 to 5.5 m/yr at 22S (Section 6.5.4). Although single-well injection-withdrawal tracer testing at NC-EWDP-19D indicated single-porosity transport behavior at this location, both single-well and cross-hole tracer test results at Nye County Site 22 indicated dual-porosity behavior at this site. However, the tracer responses at Site 22 were consistent with relatively short characteristic time and length scales for diffusion into stagnant porosity, which suggests that, for solute transport over relatively long time and distance scales, the alluvium should effectively behave as a single-porosity system with an effective flow porosity equal to the sum of the flowing and stagnant water porosities deduced from tracer testing (Section 6.5.5).
- Apparent sorption of an ion-exchanging tracer (lithium) was greater in the cross-hole tracer test in the alluvium at Nye County Site 22 than in laboratory tests using the same materials. This result suggests that laboratory sorption parameters will tend to result in overestimation of radionuclide transport rates in the saturated alluvium (Section 6.5.6 and Appendix G, Section G5.4.3).
- The polystyrene microsphere response in the alluvium tracer testing at Nye County Site 22 suggests that filtration rate constants and retardation factors of microspheres, and, by inference, natural colloids, are probably greater in the alluvium than in the fractured volcanics near Yucca Mountain (Section 6.5.5 and Appendix G, Section G5.2).

- Section 7.4 lists specific locations in Section 6 and in the appendices where the reader can find discussions of uncertainties associated with hydrologic and transport parameters derived from SZ in situ testing. These uncertainties are incorporated into probability distributions for parameters documented primarily in *SZ Flow and Transport Model Abstraction* (SNL 2007 [DIRS 177390]).

The SZ included FEPs supported by this scientific analysis are listed in Section 6.1.2 of this report, which also indicates where in the report the FEPs are addressed.

The specific acceptance criteria that relate to this report are discussed in Section 4.2.

7.2 APPLICABLE ACCEPTANCE CRITERIA

The following information describes how this analysis addresses the acceptance criteria in *Yucca Mountain Review Plan, Final Report* (NRC 2003 [DIRS 163274], Sections 2.2.1.3.8.3 and 2.2.1.3.9.3). Only those acceptance criteria applicable to this report (Section 4.2) are discussed. In most cases, the applicable acceptance criteria are not addressed solely by this report; rather, the acceptance criteria are fully addressed when this report is considered in conjunction with other analysis and model reports that describe flow and transport in the saturated zone.

7.2.1 Acceptance Criteria from Section 2.2.1.3.8.3, *Flow Paths in the Saturated Zone*

Acceptance Criterion 1: *System Description and Model Integration Are Adequate*

- **Subcriterion (2)**—Sections 6.2 and 6.4 (and Appendices C and F) adequately describe and identify aspects of hydrology, geology, physical phenomena, and couplings, that may affect flow paths in the saturated zone. Conditions and assumptions supporting the abstraction of flow paths in the saturated zone are readily identified and supported in these two sections. Section 6.2 and Appendix C describe the hydraulic tests conducted and analyses performed on the test data, and extrapolates test results to estimate hydrogeologic properties of the volcanic rocks. Section 6.4 and Appendix F present hydrogeologic properties of the alluvium through interpretation of test results. Volcanic and alluvium hydrogeologic properties affect flow paths in the saturated zone.
- **Subcriterion (3)**—The assumptions, technical bases, data, and models incorporated in this report are appropriate and consistent with those supporting other abstractions because they are derived from tests and experiments directly applicable to the saturated zone at Yucca Mountain as described in Sections 6.2 and 6.4 (and Appendices C and F). Descriptions and technical bases provided in Sections 6.2 and 6.4, and in Appendices C and F) are transparent and traceable (Section 4.1 for data references) for items that support the total system performance assessment and abstraction for flow paths in the saturated zone.
- **Subcriterion (10)**—This document has been developed under *Quality Assurance Requirements and Description* (QARD) (DOE 2006 [DIRS 177092]).

Acceptance Criterion 2: *Data Are Sufficient for Model Justification*

- **Subcriterion (1)**—The description of how the geological and hydrological data were used to develop conceptual models and parameters that are used to support evaluation of flow paths in the saturated zone is adequately justified. The adequacy of the descriptions of how the data were used, interpreted, and appropriately synthesized into the parameters is summarized in Sections 6.2.2 through 6.2.6 and 6.4.2 through 6.4.5. Details are provided in Appendix C, Sections C1 through C4, C6, Appendix F, Sections F1 and F2. Section C1 discusses early studies that were conducted to define hydrostratigraphic units, flow patterns, effects of the different geologic features, geologic properties of the rocks, and the results of an open-hole test in the C-wells. Section C2 provides descriptions of equipment used and indicates that the equipment received extensive performance evaluation during prototype hydraulic tests. Section C3 provides detailed data, results, and interpretations of the hydraulic tests including the conceptual models considered and tested. Hydraulic properties of the volcanic rocks for the various hydrogeologic intervals at the C-wells are discussed in Section C4. Section C6 describes how reviews of a number of published studies are used in conjunction with reanalyzing the data to suggest a distribution of anisotropy ratios. The tests to determine hydraulic properties of the alluvium are described and their results adequately justified in detail in Section 6.4 and Appendix F, including single-well hydraulic testing (Section F1) and cross-hole hydraulic testing (Section F2).
- **Subcriterion (2)**—Sufficient data have been collected as discussed in Sections 6.2 and 6.4 on the natural system to establish boundary conditions for the abstraction of flow paths in the saturated zone. The discussions in Appendix C, Sections C1, C3, C6; and Appendix F, Section F4 show that the data employed from earlier studies and recent studies are sufficient to establish boundary conditions used in the abstraction of flow paths in the saturated zone.
- **Subcriterion (3)**—Data on the geology and hydrology of the saturated zone used in the total system performance assessment abstraction are based on appropriate techniques as discussed in detail in Sections 6.2 and 6.4, and in Appendices C and F. These techniques included site-specific field measurements and process-level modeling studies described in Sections 6.2 and 6.4, and in Appendices C and F. Sensitivity of parameters and uncertainty in the data were addressed in the analyses. A formal analysis of sensitivity to anisotropy in horizontal hydraulic conductivity is described in Appendix C, Section C6.4, FEHM Sensitivity Study. Other sensitivity considerations are discussed in Sections 6.2.7, 6.4; Appendix C, Section C5; and Appendix F.
- **Subcriterion (4)**—Sufficient information is provided in Sections 6.2.4, 6.2.6, and 6.4, as well as in Appendix C, Sections C4, C6; and Appendix F to substantiate the conclusions that the proposed conceptual groundwater modeling approach and model are applicable to site conditions. Confidence that the model is applicable to site conditions is provided by the extensive justifications of the methods and parameters used. Summaries of the conceptual models considered for fractured volcanics and the alluvium are presented in Sections 6.2.4 and 6.4.4, respectively.

Acceptance Criterion 3: *Data Uncertainty Is Characterized and Propagated Through the Model Abstraction*

- **Subcriterion (1)**—Technically defensible models that adequately account for uncertainties and risk are employed. Sections 6.2.6, 6.2.7, and 6.4, as well as Appendix C, Sections C5, C6; and Appendix F, discuss uncertainties and variabilities of the data and models. Sections 6.2.7 and C5 evaluate the uncertainties associated with the test data, analyses, methods, assumptions, and values of hydraulic properties of the volcanic rocks determined from test analyses and discusses why the simplifications used in the models are appropriate for estimating hydrogeologic parameters and uncertainty associated with them (which affect groundwater velocities and transport times). By addressing uncertainty in these parameters, assurance is provided that the groundwater velocities and transport times, and, consequently, the risk will not be underestimated. Section 6.4 and Appendix F discuss uncertainties related to alluvium zone deposits data, models, and assumptions. For example, this section describes why results from single-hole hydraulic testing results were replaced with cross-hole hydraulic and tracer tests for determination of hydraulic properties of the alluvium in the saturated zone to more accurately predict the flow.
- **Subcriterion (3)**—Uncertainty in parameter development for conceptual models, process-level models, and alternative conceptual models was considered in Sections 6.2.4, 6.2.6, and 6.4, as well as in Appendix C, Sections C5, C6; and Appendix F, for developing the abstraction of flow paths in the saturated zone. This was accomplished through considerations of data sensitivity and the use of conservative limits. Discussions in these sections identify uncertainties in saturated zone flow parameters that could affect the analyses.

Acceptance Criterion 4: *Model Uncertainty Is Characterized and Propagated Through the Model Abstraction*

- **Subcriterion (1)**—Alternative modeling consistent with available data and current scientific understanding is considered in Sections 6.2 and 6.4, and in Appendices C and F. The results and limitations are appropriately considered in the models that support the abstraction.
- **Subcriterion (2)**—Conceptual model uncertainties are adequately defined and documented in Sections 6.2.6, 6.2.7, and 6.4, as well as in Appendix C, Sections C5, C6 and Appendix F, and their effects on conclusions regarding performance are properly assessed. Model uncertainties and limitations are discussed in Sections 6.2.7 and C5. Particularly, the uncertainties associated with the assumption that the aquifer behaves as an equivalent porous medium even though the flow system consists of a fracture network are discussed. Uncertainty in anisotropy ratios is examined in Sections 6.2.6 and C6. Conceptual flow models are also supported by site data. The most appropriate conceptual model of flow in the volcanics (predominant flow through the fracture network) is derived in Section 6.2.4 (and C7) based on consideration of all the C-wells hydrologic test results. Section 6.4 and Appendix F address the hydrogeologic properties of the alluvium and describe the measures that were taken (cross-hole hydraulic testing) to

improve estimates of alluvium transmissivity and horizontal hydraulic conductivity that were obtained from initial single-well hydraulic tests.

- **Subcriterion (3)**—Consideration of conceptual model uncertainty is consistent with available site characterization data, field measurements, and process-level modeling studies as discussed in Sections 6.2.2 through 6.2.6, 6.4, with details provided in Appendix C, Sections C1 through C4, C6; Appendix F, Sections F1 and F2; see the responses to Acceptance Criteria 1 (1) and (3). Uncertainties in the report are summarized in Section 7.3.
- **Subcriterion (4)**—Appropriate alternative modeling approaches discussed in Sections 6.2.4, 6.2.6, and 6.4 (also Appendix C, Sections C3, C6; and Appendix F) are consistent with available data and current scientific knowledge, and appropriately consider their results and limitations, using tests and analyses that are sensitive to the processes modeled. Sections 6.2.3 and C3 describe different conceptual models that were obtained for the different test intervals in the fractured tuffs at the C-wells based on the analyses of the interval responses to pumping. Depending on these responses, either a confined Equivalent Porous Medium (EPM), confined fissure block, unconfined EPM, or a leaky confined EPM model was selected as being most appropriate for the various intervals. In Section 6.2.6, anisotropy ratio analyses performed employ two different methods with different approaches considered for each (also described in Section C6.2.5. Section 6.4 indicates that the analytical solutions used for individual test interpretations were selected primarily on the basis of the conformance of the test responses to idealized responses predicted by alternative solutions/conceptual models.

Acceptance Criterion 5: *Model Abstraction Output Is Supported by Objective Comparisons*

- **Subcriterion (4)**—Sensitivity analyses that cover ranges of hydrogeologic parameter estimates consistent with site data, field experiments, and tests are discussed in Sections 6.2 and 6.4 (also in Appendices C and F). Corresponding ranges are provided for the major hydrogeologic parameters in support of the abstraction of flow paths in the saturated zone.

7.2.2 Acceptance Criteria from Section 2.2.1.3.9.3, *Radionuclide Transport in the Saturated Zone*

Acceptance Criterion 1: *System Description and Model Integration Are Adequate*

- **Subcriterion (1)**—The analyses described in Sections 6.3 and 6.5 (and in Appendices D and G) adequately incorporate important physical phenomena and couplings, and use consistent and appropriate assumptions to support the saturated zone transport abstraction process. Section 6.3 (and Appendix D) provides a thorough discussion of transport properties of fractured tuffs including field tracer tests, lithium sorption tests, diffusion cell experiments, transport calculations, and model analysis. Section 6.5 (and Appendix G) analyzes transport properties of the alluvium. In Appendix G, it is shown that three conceptual alluvium transport models were considered for the alluvium, and transport parameters were estimated from results of tracer tests.

- **Subcriterion (2)**—Sections 6.3 and 6.5 (and Appendices D and G) provide adequate descriptions of the aspects of hydrology, geology, geochemistry, physical phenomena, and couplings that may affect radionuclide transport in the saturated zone. The descriptions include field tracer tests and laboratory experiments (Appendices E and H) designed to provide additional confidence in the model and in the physical and geochemical processes affecting radionuclide transport. Conditions and assumptions supporting the abstraction of radionuclide transport in the saturated zone are readily identified in Sections 6.3.3, 6.5.4, D4, D5, G1, and G4, and they are consistent with the body of data presented.
- **Subcriterion (3)**—Assumptions used in Sections 6.3 and 6.5 (and in Appendices D and G) for transport in the saturated zone are consistent with the total system performance assessment abstractions of radionuclide transport in the saturated zone. The detailed descriptions of the transport models and site data to which they were fitted and the associated technical bases provide transparent and traceable support for the abstraction of radionuclide transport in the saturated zone.
- **Subcriterion (5)**—Sections 6.3 and 6.5 (and Appendices D and G) provide sufficient data and technical bases for the inclusion of features and processes related to radionuclide transport in the saturated zone supporting the total system performance assessment abstraction. Section 6.3 (and Appendix D) analyzes the results of cross-hole tracer tests in the fractured volcanics and experiments and conceptual models employed to predict the results. Sections 6.5.3 through 6.5.5 present the results and interpretations of three single-well injection-withdrawal tests in the alluvium. Several laboratory experiments that have been conducted to support the ATC testing effort are discussed in Appendix H.
- **Subcriterion (6)**—This document has been developed under the QARD (DOE 2006 [DIRS 177092]).

Acceptance Criterion 2: *Data Are Sufficient for Model Justification*

- **Subcriterion (1)**—Geological, hydrological, and geochemical values used in the license application are adequately justified in Sections 6.3 and 6.5 (described in detail in Appendices D and G). Adequate descriptions of how the data were used, interpreted, and appropriately synthesized into the parameters are provided in those two sections. Detailed descriptions of the methods for obtaining data, interpretations of the data, and limitations on use of the data are provided in Sections 6.3 and 6.5 (and in Appendices D and G) and in the supporting documents listed in Section 4.1 from which the data were taken.
- **Subcriterion (2)**—Sufficient data have been collected on the characteristics of the natural system, as summarized in Sections 6.3 and 6.5 (described in detail in Appendices D and G), to establish boundary conditions for transport analyses supporting the total system performance assessment abstraction of radionuclide transport in the saturated zone. Section 6.3, Appendices D, and E describe the different transport boundary conditions used for interpreting the field and laboratory experiments for fractured

volcanics. Sections 6.5, Appendices G, and H discuss the different transport boundary conditions applicable to the field and laboratory experiments conducted in alluvium deposits.

- **Subcriterion (3)**—Data presented in Sections 6.3 and 6.5 on the geology, hydrology, and geochemistry of the saturated zone, including the influence of structural features, fracture distributions, fracture properties, and stratigraphy are based on appropriate techniques. These techniques include laboratory studies of lithium sorption and transport (Appendices E and H), borehole gravimetry logging measurements for porosity (Appendix F), diffusion cell experiments (Appendix D), site-specific field tracer tests (single well and cross-hole) and process-level modeling studies. Sensitivity and uncertainty analyses performed as discussed in Sections 6.3 and 6.5 to support the total system performance assessment abstraction are adequate to determine the need for additional data.

Acceptance Criterion 3: *Data Uncertainty Is Characterized and Propagated Through the Model Abstraction*

- **Subcriterion (1)**—Models use parameter values, assumed ranges, probability distributions, and bounding assumptions that are technically defensible, and reasonably account for uncertainties and variabilities. Sections 6.3.7, 6.5.5, 6.5.7; Appendix D, Sections D1, D3, D4, D5; Appendix E, Section E10; Appendix G, Sections G3 and G4 provide sensitivity and uncertainty estimations and analyses for various aspects of transport parameters.
- **Subcriterion (2)**—Sections 6.3 and 6.5 (with details in Appendices D, Sections D1 and D6, E, Sections E1, E2, E3, E4; G, Sections G1, G2, G3, G4; H, Sections H1 and H2 provide evidence that estimated flow and transport parameters are appropriate and valid, based on techniques that include laboratory studies of transport, borehole gravimetry logging measurements for porosity, diffusion cell experiments, site-specific field tracer tests (single well and cross-hole), lithium sorption tests, and process-level modeling studies conducted under conditions relevant to the saturated zone at Yucca Mountain. Models are demonstrated in Sections 6.3, D3, D4, and G1 to adequately predict field transport test results.
- **Subcriterion (4)**—Appendix D, Section D4 and Appendix G discuss how parameter values for different transport processes, including matrix diffusion, dispersion, and ground-water mixing, are based on reasonable assumptions about aquifer properties and ground-water volumetric fluxes.
- **Subcriterion (5)**—Sections 6.3, 6.5, Appendices D, Sections D1, D3, D4; E, Section E2; G, Sections G1, G3, and G4 show how adequate representations of uncertainty were developed in parameters for conceptual models, process-level models, and alternative conceptual models considered in this report and supporting the abstraction of radionuclide transport in the saturated zone. Both sensitivity analyses and conservative limits were used as discussed in those sections.

Acceptance Criterion 4: *Model Uncertainty Is Characterized and Propagated Through the Model Abstraction*

- **Subcriterion (1)**—Alternative modeling approaches of features, events, and processes are considered in Sections 6.3 and 6.5 (and in Appendices D and G) and are consistent with available data and current scientific understanding, and the results and limitations are appropriately considered in the abstraction. Appendix D Sections D3, D5, and Appendix G, Section G1 particularly, discuss conceptual models considered and justify the selection of the appropriate models.
- **Subcriterion (2)**—Conceptual model uncertainties are adequately defined and documented, and effects on conclusions regarding performance are properly assessed in Sections 6.3.7, 6.5.7, Appendices D, Sections D1, D3, D4, D5; E, Sections E2 and E4; G, Sections G3 and G4.
- **Subcriterion (3)**—Consideration of conceptual model uncertainty is consistent with available site characterization data, laboratory experiments, field measurements, and process-level modeling studies shown throughout Sections 6.3 and 6.5 (and Appendices D and G).
- **Subcriterion (4)**—Appropriate alternative modeling approaches discussed in Sections 6.3 and 6.5 and, more specifically, in Appendix D, Sections D3, D5, and Appendix G, Section G1, are consistent with available data and current scientific knowledge, and appropriately consider their results and limitations using tests and analyses that are sensitive to the processes modeled. For example, for radionuclide transport through fractures in volcanic rocks and porous media in alluvium, the report adequately considers alternative modeling approaches to develop its understanding of distributions and ranges of transport properties in the saturated zone.

7.3 OUTPUTS

Table 7-1 lists the output data for this scientific report. The data will be used primarily to support the development of CDFs for various flow and transport parameters used in TSPA simulations. These CDFs are documented in the *SZ Flow and Transport Model Abstraction* report (SNL 2007 [DIRS 177390]). The horizontal hydraulic conductivity anisotropy ratio described in Section 6.2.6 is used to support flow model calibrations described in *Saturated Zone Site-Scale Flow Model* (SNL 2007 [DIRS 177391]). Also, transport parameters and tracer breakthrough curves from C-wells tracer testing (Sections 6.3 and Appendix D) are used in the model validation section of *Site-Scale Saturated Zone Transport Model* (SNL 2007 [DIRS 177392]) and in the development of colloid transport parameter distributions in *Saturated Zone Colloid Transport* (BSC 2004 [DIRS 170006]).

The steps involved in processing the input data listed in Table 4-1 to arrive at the output data listed in Table 7-1 is often quite involved and is unique to each output DTN. Appendix I lists all the steps associated with this process for Figure C-21 (an example for a hydraulic test interpretation) and for Figure 6.3-3 (an example for a tracer test interpretation). Additionally, Appendix F, section F6, contains a thorough description of the process of interpreting the hydraulic tests at Nye County Site 22. The examples of Appendix I and the description in

Section F6 are provided for the benefit of the reader who is interested in following this process for any given table or figure appearing in this report (including all appendices). However, the reader is cautioned that each interpretation will be slightly different, and that all steps for any given figure or table are not necessarily represented in Appendix I or in Section F6.

Table 7-1. Output Data

Data Description	Data Tracking Number	Location of Output DTNs in This Report
Filtered UE-25 ONC-1 water levels, May 1996 to November 1996	GS030208312314.001	Sections C6.1.2, C6.2.1, Figures C-41, C-42, C-43, C-44 Tables C-10, C-12
Filtered UE-25 WT#3, UE-25 WT#14, and USW H-4 water levels, May 1996 to December 1996	GS030208312314.002	Sections C6.1.2, C6.2.1 Figures C-41, C-42, C-43, C-44 Tables C-10, C-12
Cooper-Jacob Transmissivity and Storativity Analysis of Wells UE-25 ONC-1, UE-25 WT#3, UE-25 WT#14, And USW H4	SN0409T0502203.002	Tables 6.2-3, 6.2-4 Figure C-41 Tables C-10, C-12
PDF and CDF for in north-south/east-west anisotropy ratio in fractured volcanics	SN0302T0502203.001	Sections 6.2.6 and C6.3 Figures 6.2-3 and C-46
Analysis of hydrologic properties of fractured tuffs (C-wells complex)	GS031008312314.004	Tables 6.2-1, 6.2-2, C-1 to C-9 and C-12 Figures 6.2-2 to 6.2-4, C-1 to C-45 (except for C-26 and C-41);
Analysis of hydraulic testing, ATC	GS031008312316.002	Figures 6.4-1, F-2, F-4 to F-8, F-10 to F-13, and F-23 to F-24; Sections F1.2 to F1.5, F2, F2.1, F3, and F4
Analysis of hydraulic testing at NC-EWDP Site 22	LA0701EK150304.001	Table 6.4-3 Figures and Tables throughout Section F6
Analysis of tracer testing, C-wells, Bullfrog, and Tram	GS031008312315.002	Figures D-1, D-3 to D-8, D-12 to D-13, and D-15 to D-16; Tables D-2 to D-3
Analysis of tracer testing, ATC	GS031008312316.003	Figures G-27 to G-29 and G-31 Sections G4.2.4 and G4.5
Simulations/modeling of field tracer tests	LA0303PR831231.003	Figures 6.3-2, 6.3-3, D-26 to D-30, and E-40 to E-41 Tables 6.3-3 and D-6 to D-9
Fitting or simulations of lithium sorption to C-wells tuffs.	LA0303PR831341.003	Figures E-2 to E-9 and E-37 Table E-4
Cation exchange capacity calculations for C-wells tuffs	LA0303PR831341.001	Figure E-10 Table E-5
DIFFCELL V 2.0 (STN: 10557-2.0-00 [DIRS 159063]) simulations of diffusion cell data	LA0303PR831362.001	Figures E-12 to E-19 Tables E-6 and E-18
Simulations of crushed C-wells tuff column experiments	LA0303PR831361.003	Figures E-20 to E-28 and E-38 Table E-7

Table 7-1. Output Data (Continued)

Data Description	Data Tracking Number	Location of Output DTNs in This Report
Simulations of C-wells fractured core experiments	LA0303PR831361.004	Figures E-31 to E-36 and E-41 Tables E-14 to E-18
Calculations to obtain values reported in tables and figures (generally combinations of other values reported or unit conversions)	LA0303PR831231.005	Tables 6.3-3, 6.3-4, D-6 to D-8, D-10 to D-11, E-14 to E-17, G-4 (note this DTN has a typo in Fig. G-4), and E-41 Table H-5
Predictions of transport behavior in single-well and cross-hole tracer tests in the saturated alluvium at the ATC	LA0303PR831231.001	Section G3 Figures G-2 to G-3, G-5 to G-8, and G-16 to G-17 Tables G-1 to G-3
Predictions of transport behavior in cross-hole tracer tests in single-porosity media	LA0403PR831231.001	Figures G-9 to G-10, G-12, and G-14 to G-15 Table G-4
Calculations to estimate ambient groundwater velocity at NC-EWDP-19D from single-well tracer test responses	LA0303PR831231.002	Section G4.2.1 Figures 6.5-1, 6.5-2, G-19 to G-20, and G-23 Tables 6.5-4, 6.5-5 and G-7 to G-8
Calculations to determine microsphere detachment rate constant in a single-well tracer test in saturated alluvium at NC-EWDP-19D	LA0303PR831352.001	Section G4.6
Estimates of specific discharge and seepage (drift) velocity at NC-EWDP Site 22 based on single-well tracer responses	LA0701PR150304.001	Section G5.3 Tables 6.5-4, 6.5-6, G-9
RELAP V2.0 interpretations of bromide, 2,4,5 TFBA, 2,6 DFBA and microsphere breakthrough curves in first cross-hole tracer test at NC-EWDP Site 22	LA0701PR150304.002	Figures G-42, G-43, G-45, G-46, and G-49 Tables 6.5-7, 6.5-8, G-14, G-16, G-17, G-20, and G-21
RELAP V2.0 interpretations of iodide and rhenium (as perrhenate) breakthrough curves in second cross-hole tracer test at NC-EWDP Site 22	LA0701PR150304.003	Figures 6.5-10, G-50, G-51 Tables 6.5-8, G-18, G-19, and G-20
Estimates of specific discharge and seepage (drift) velocity at NC-EWDP Site 22 based on responses of crosshole test #1 tracers after extended flow interruption	LA0701PR150304.004	Section G5.3 Table 6.5-6 Figure G-52
RELAP V2.0 interpretations of bromide, 2,4,5 TFBA, and microsphere breakthrough curves in first cross-hole tracer test at NC-EWDP Site 22 assuming the largest possible differences between the normalized concentrations of bromide and 2,4,5 TFBA	LA0701PR150304.006	Figures 6.5-9, G-44, G-47 Tables 6.5-7, 6.5-8, G-15, G-17, G-20, and G-21
MULTRAN V1.0 simulations of solute tracer responses between NC-EWDP-22PA and -22S in the first crosshole tracer test at NC-EWDP Site 22 and of solute tracer responses in the first and second single-well tracer tests at NC-EWDP Site 22	LA0701PR150304.007	Figures 6.5-9, G-32, G-33, and G-48 Tables 6.5-8, G-11, G-12, G-17, and G-20
Determination of cation exchange parameters from EQUILFIT V 1.0 (STN: 10668-1.0-00 [DIRS 159064]) fits to cation concentration data from lithium batch sorption measurements onto alluvium from different intervals in NC-EWDP-19P and -19D	LA0303PR831341.002	Figure H-32 Table H-10
Simulations of column transport experiments in alluvium from NC-EWDP-19D	LA0303PR831361.002	Figures H-31 and H-33 to H-35 Table H-12

Table 7-1. Output Data (Continued)

Data Description	Data Tracking Number	Location of Output DTNs in This Report
C-wells tracer test sensitivity calculations	LA0304PR831231.001	Figures 6.3-4, 6.3-5 and D-31 to D-38 Tables 6.3-5, 6.3-6 and D-13 to D-14

NOTE: ATC=Alluvial Testing Complex; DTN=data tracking number; STN=software tracking number.

7.4 UNCERTAINTIES

Discussions of uncertainties associated with the flow and transport parameters presented in this report can be found in the following sections:

- Hydraulic testing and test interpretations in saturated fractured volcanics at the C-wells are discussed in detail in Section 6.2.7 (also Appendix C, Section C5).
- Anisotropy of horizontal hydraulic conductivity in the fractured volcanics are discussed in Section 6.2.6.
- Tracer testing and test interpretations at the C-wells are discussed in detail in Section 6.3.7 (also Appendix D, Section D5).
- Hydraulic testing and test interpretations in the saturated alluvium at the ATC and Nye County Site 22 are discussed in Section 6.4.6 (also Appendix F, Section F4 for the ATC, and Sections F7 and F8 for general discussion that applies to both locations).
- Tracer testing and test interpretations at the ATC and Nye County Site 22 are summarized in Section 6.5.6 and discussed in detail in Appendix G, Section G4.4 (for groundwater velocity or specific discharge estimates) and in Section G8.

Uncertainty distributions for SZ flow and transport parameters are provided in the *SZ Flow and Transport Abstraction Model* report (SNL 2007 [DIRS 177390]). The rationale for documenting the uncertainty distributions in the model abstraction report rather than in this scientific analysis is that the distributions are based only in part on the parameters (and their uncertainties) presented in this report. The only exception is that the uncertainty distribution for the north-south and east-west anisotropy ratio of horizontal hydraulic conductivity in the fractured volcanics is derived entirely from the information presented in this scientific analysis (Section 6.2.6 and Appendix C, Section C6).

Literature data, expert elicitation input, and peer review input were considered in the development of parameter distributions because of the limited spatial representation of the SZ offered by the C-wells and alluvium hydraulic and tracer tests. Also, the time and distance scales of the C-wells and alluvium tests were relatively small compared to time and distance scales of performance assessment calculations. One exception is the long-term C-wells hydraulic test that led to the uncertainty distribution for hydraulic conductivity anisotropy ratio over an approximately 21-km² area. Thus, the flow and transport parameters derived from the C-wells and alluvium in-situ tests represent only discrete points in continuous distributions of parameter values spatially distributed throughout the SZ, and that potentially have scale dependencies that

would not be revealed by C-wells and alluvium in-situ testing. The parameter uncertainty distributions in the SZ model abstraction report (SNL 2007 [DIRS 177390]) are consistent with and supported by the parameters presented in this report, but they generally consist of a much wider range of potential values because of representativeness and scale of the field tests.

INTENTIONALLY LEFT BLANK

8. INPUTS AND REFERENCES

The following is a list of the references cited in this document. Column 1 represents the unique six digit numerical identifier (the Document Input Reference System number), which is placed in the text following the reference callout (e.g., BSC 2002 [DIRS 171585]). The purpose of these numbers is to assist in locating a specific reference. Within the reference list, multiple sources by the same author (e.g., BSC 2002) are sorted alphabetically by title.

8.1 DOCUMENTS CITED

- 103597 Altman, W.D.; Donnelly, J.P.; and Kennedy, J.E. 1988. *Peer Review for High-Level Nuclear Waste Repositories: Generic Technical Position*. NUREG-1297. Washington, D.C.: U.S. Nuclear Regulatory Commission. TIC: 200651.
- 103750 Altman, W.D.; Donnelly, J.P.; and Kennedy, J.E. 1988. *Qualification of Existing Data for High-Level Nuclear Waste Repositories: Generic Technical Position*. NUREG-1298. Washington, D.C.: U.S. Nuclear Regulatory Commission. TIC: 200652.
- 164635 Anghel, I.; Turin, H.J.; and Reimus, P.W. 2002. "Lithium Sorption to Yucca Mountain Tuffs." *Applied Geochemistry*, 17, (6), 819-824. New York, New York: Pergamon. TIC: 254046.
- 162534 Bachmat, Y.; Mandel, S.; and Bugayevski, M. 1988. "A Single-Well Tracer Technique for Evaluating Aquifer Parameters, I. Theoretical Work." *Journal of Hydrology*, 99, (1-2), 143-163. Amsterdam, The Netherlands: Elsevier. TIC: 254194.
- 105038 Bear, J. 1979. *Hydraulics of Groundwater*. New York, New York: McGraw-Hill. TIC: 217574.
- 156633 Becker, M.W. and Charbeneau, R.J. 2000. "First-Passage-Time Transfer Functions for Groundwater Tracer Tests Conducted in Radially Convergent Flow." *Journal of Contaminant Hydrology*, 40, (4), 299-310. New York, New York: Elsevier. TIC: 251009.
- 122788 Benson, C.F. and Bowman, R.S. 1994. "Tri- and Tetrafluorobenzoates as Nonreactive Tracers in Soil and Groundwater." *Soil Science Society of America Journal*, 58, (4), 1123-1129. Madison, Wisconsin: Soil Science Society of America. TIC: 246741.
- 153427 Benson, C.F. and Bowman, R.S. 1996. "Erratum, Tri- and Tetrafluorobenzoates as Nonreactive Tracers in Soil and Groundwater." *Soil Science Society of America Journal*, 60, 1780. Madison, Wisconsin: Soil Science Society of America. TIC: 246741.

- 101193 Bentley, C.B.; Robison, J.H.; and Spengler, R.W. 1983. *Geohydrologic Data for Test Well USW H-5, Yucca Mountain Area, Nye County, Nevada. Open-File Report 83-853*. Denver, Colorado: U.S. Geological Survey. ACC: NNA.19870519.0098.
- 103524 Bird, R.B.; Stewart, W.E.; and Lightfoot, E.N. 1960. *Transport Phenomena*. New York, New York: John Wiley & Sons. TIC: 208957.
- 101194 Bish, D.L. 1989. Evaluation of Past and Future Alterations in Tuff at Yucca Mountain, Nevada, Based on the Clay Mineralogy of Drill Cores USW G-1, G-2, and G-3. LA-10667-MS. Los Alamos, New Mexico: Los Alamos National Laboratory. ACC: NNA.19890126.0207.
- 113856 Bolt, G.H. and Bruggenwert, M.G.M., eds. 1978. *Soil Chemistry, A. Basic Elements*. Developments in Soil Science 5A. 2nd Revised Edition. New York, New York: Elsevier. TIC: 243742.
- 156639 Borchardt, G. 1995. "Smectites." Chapter 14 of *Minerals in Soil Environments*. 2nd Edition. Dixon J.B. and Weed, S.B., eds. SSSA Book Series, No. 1. Madison, Wisconsin: Soil Science Society of America. TIC: 237222.
- 162675 Bouwer, H. 1978. *Groundwater Hydrology*. McGraw-Hill Series in Water Resources and Environmental Engineering. New York, New York: McGraw-Hill. TIC: 244844.
- 156645 Bowman, R.S. 1984. "Evaluation of Some New Tracers for Soil Water Studies." *Soil Science Society of America Journal*, 48, (5), 987-993. Madison, Wisconsin: Soil Science Society of America. TIC: 251011.
- 156646 Brunauer, S.; Emmett, P.H.; and Teller, E. 1938. "Adsorption of Gases in Multimolecular Layers." *Journal of American Chemical Society*, 60, 309-319. Washington, D.C.: American Chemical Society. TIC: 224534.
- 156647 Brusseau, M.L.; Hu, Q.; and Srivastava, R. 1997. "Using Flow Interruption to Identify Factors Causing Nonideal Contaminant Transport." *Journal of Contaminant Hydrology*, 24, (3/4), 205-219. New York, New York: Elsevier. TIC: 250759.
- 172175 BSC (Bechtel SAIC Company) 2001. *Data Qualification Report: Water Level Data from Nye County Wells for Use on the Yucca Mountain Project*. TDR-NBS-HS-000016 REV 00. Las Vegas, Nevada: Bechtel SAIC Company. ACC: MOL.20011218.0002.
- 171585 BSC 2002. *Test Plan for Alluvial Testing Complex – Single-Well, Multi-Well, and Laboratory Studies*. SITP-02-SZ-003 REV 01 ICN 01. Las Vegas, Nevada: Bechtel SAIC Company. ACC: MOL.20020509.0351.

- 170014 BSC 2004. *Probability Distribution for Flowing Interval Spacing*. ANL-NBS-MD-000003 REV 01. Las Vegas, Nevada: Bechtel SAIC Company. ACC: DOC.20040923.0003.
- 168361 BSC 2004. *Q-List*. 000-30R-MGR0-00500-000-000 REV 00. Las Vegas, Nevada: Bechtel SAIC Company. ACC: ENG.20040721.0007.
- 170015 BSC 2004. *Recharge and Lateral Groundwater Flow Boundary Conditions for the Saturated Zone Site-Scale Flow and Transport Model*. ANL-NBS-MD-000010 REV 01. Las Vegas, Nevada: Bechtel SAIC Company. ACC: DOC.20041008.0004.
- 170006 BSC 2004. *Saturated Zone Colloid Transport*. ANL-NBS-HS-000031 REV 02. Las Vegas, Nevada: Bechtel SAIC Company. ACC: DOC.20041008.0007.
- 170042 BSC 2004. *Saturated Zone Flow and Transport Model Abstraction*. MDL-NBS-HS-000021 REV 02. Las Vegas, Nevada: Bechtel SAIC Company. ACC: DOC.20041028.0003.
- 170037 BSC 2004. *Saturated Zone Site-Scale Flow Model*. MDL-NBS-HS-000011 REV 02. Las Vegas, Nevada: Bechtel SAIC Company. ACC: DOC.20041122.0001.
- 178672 BSC 2006. *Impacts of Solubility and Other Geochemical Processes on Radionuclide Retardation in the Natural System – Rev 01*. Las Vegas, Nevada: Bechtel SAIC Company. ACC: MOL.20060105.0022.
- 177375 BSC 2006. *Technical Work Plan for Saturated Zone Flow and Transport Modeling*. TWP-NBS-MD-000006 REV 02. Las Vegas, Nevada: Bechtel SAIC Company. ACC: DOC.20060519.0002.
- 165281 Bussod, G. 2001. LA-EES-1-NBK-98-005, UZ Transport Test Notebook 2. Scientific Notebook SN-LANL-SCI-038-V1. ACC: MOL.20010830.0382.
- 165123 Callahan, T. 2001. LA-CST-NMTECHA-NBK-96-001, Laboratory Investigation YMP C-Wells Reactive Tracers Test. Scientific Notebook SN-LANL-SCI-028-V1. ACC: MOL.20010830.0385.
- 156649 Callahan, T.J. 2001. *Laboratory Investigations and Analytical and Numerical Modeling of the Transport of Dissolved Solutes Through Saturated Fractured Rock*. Ph.D. dissertation. Socorro, New Mexico: New Mexico Institute of Mining and Technology. TIC: 251010.
- 156648 Callahan, T.J.; Reimus, P.W.; Bowman, R.S.; and Haga, M.J. 2000. "Using Multiple Experimental Methods to Determine Fracture/Matrix Interactions and Dispersion of Nonreactive Solutes in Saturated Volcanic Tuff." *Water Resources Research*, 36, (12), 3547-3558. Washington, D.C.: American Geophysical Union. TIC: 250760.

- 101322 Caporuscio, F.; Vaniman, D.; Bish, D.; Broxton, D.; Arney, B.; Heiken, G.; Byers, F.; Gooley, R.; and Semarge, E. 1982. Petrologic Studies of Drill Cores USW-G2 and UE25b-1H, Yucca Mountain, Nevada. LA-9255-MS. Los Alamos, New Mexico: Los Alamos National Laboratory. ACC: NNA.19870519.0041.
- 102046 Carr, M.D.; Waddell, S.J.; Vick, G.S.; Stock, J.M.; Monsen, S.A.; Harris, A.G.; Cork, B.W.; and Byers, F.M., Jr. 1986. *Geology of Drill Hole UE25p#1: A Test Hole Into Pre-Tertiary Rocks Near Yucca Mountain, Southern Nevada*. Open-File Report 86-175. Menlo Park, California: U.S. Geological Survey. ACC: HQS.19880517.2633.
- 102495 Castor, S.B.; Tingley, J.V.; and Bonham, H.F., Jr. 1994. "Pyritic Ash-Flow Tuff, Yucca Mountain, Nevada." *Economic Geology*, 89, 401-407. El Paso, Texas: Economic Geology Publishing. TIC: 234278.
- 105075 Chipera, S.J. and Bish, D.L. 1995. "Multireflection RIR and Intensity Normalizations for Quantitative Analyses: Applications to Feldspars and Zeolites." *Powder Diffraction*, 10, (1), 47-55. Newtown Square, Pennsylvania: Joint Committee on Powder Diffraction Standards. TIC: 222001.
- 156651 Cohen, J.B.; Najita, J.; Karasaki, K.; and Simmons, A. 1996. *Conceptual Model Development of Saturated Zone Flow in the Vicinity of C-Holes, Yucca Mountain, Nevada*. Berkeley, California: Lawrence Berkeley National Laboratory. ACC: MOL.19961122.0314.
- 101588 Compton, R.R. 1962. *Manual of Field Geology*. New York, New York: John Wiley and Sons. TIC: 209518.
- 150245 Cooper, H.H., Jr. and Jacob, C.E. 1946. "A Generalized Graphical Method for Evaluating Formation Constants and Summarizing Well-Field History." *Transactions, American Geophysical Union*, 27, (IV), 526-534. Washington, D.C.: American Geophysical Union. TIC: 225279.
- 101040 Craig, R.W. and Robison, J.H. 1984. *Geohydrology of Rocks Penetrated by Test Well UE-25p#1, Yucca Mountain Area, Nye County, Nevada*. Water-Resources Investigations Report 84-4248. Denver, Colorado: U.S. Geological Survey. ACC: NNA.19890905.0209.
- 100131 D'Agnese, F.A.; Faunt, C.C.; Turner, A.K.; and Hill, M.C. 1997. *Hydrogeologic Evaluation and Numerical Simulation of the Death Valley Regional Ground-Water Flow System, Nevada and California*. Water-Resources Investigations Report 96-4300. Denver, Colorado: U.S. Geological Survey. ACC: MOL.19980306.0253.
- 143278 Dabros, T. and Van de Ven, T.G.M. 1982. "Kinetics of Coating by Colloidal Particles." *Journal of Colloid and Interface Science*, 89, (1), 232-244. Orlando, Florida: Academic Press. TIC: 224945.

- 156652 Dabros, T. and van de Ven, T.G.M. 1983. "On the Effects of Blocking and Particle Detachment on Coating Kinetics." *Journal of Colloid and Interface Science*, 93, (2), 576-579. New York, New York: Academic Press. TIC: 224944.
- 100027 Day, W.C.; Dickerson, R.P.; Potter, C.J.; Sweetkind, D.S.; San Juan, C.A.; Drake, R.M., II; and Fridrich, C.J. 1998. *Bedrock Geologic Map of the Yucca Mountain Area, Nye County, Nevada*. Geologic Investigations Series I-2627. Denver, Colorado: U.S. Geological Survey. ACC: MOL.19981014.0301.
- 101557 Day, W.C.; Potter, C.J.; Sweetkind, D.S.; Dickerson, R.P.; and San Juan, C.A. 1998. *Bedrock Geologic Map of the Central Block Area, Yucca Mountain, Nye County, Nevada*. Miscellaneous Investigations Series Map I-2601. Washington, D.C.: U.S. Geological Survey. ACC: MOL.19980611.0339.
- 162674 De Wiest, R.J.M. 1965. *Geohydrology*. New York, New York: John Wiley & Sons. TIC: 254221.
- 100722 Dean, J.A. 1992. *Lange's Handbook of Chemistry*. 14th Edition. New York, New York: McGraw-Hill. TIC: 240690.
- 102781 Dickerson, R.P. and Drake, R.M., II 1998. "Structural Interpretation of Midway Valley, Yucca Mountain, Nevada." *High-Level Radioactive Waste Management, Proceedings of the Eighth International Conference, Las Vegas, Nevada, May 11-14, 1998*. Pages 254-256. La Grange Park, Illinois: American Nuclear Society. TIC: 237082.
- 178771 Downing, R. 2003. Nye County Nuclear Waste Repository Project Office Pump Tests. Scientific Notebook 147. Pages Cover, TOC, Pages 14-74.
- 156653 Eckstein, Y.; Yaalon, D.H.; and Yariv, S. 1970. "The Effect of Lithium on the Cation Exchange Behaviour of Crystalline and Amorphous Clays." *Israel Journal of Chemistry*, 8, 335-342. Jerusalem, Israel: Laser Pages Publishing. TIC: 251012.
- 171918 Eddebarh, A.A. 2004. "Anisotropy Distribution." Interoffice memorandum from A.A. Eddebarh (BSC) to P. Reimus, October 5, 2004, 1004043437. ACC: MOL.20041005.0224.
- 100633 Ervin, E.M.; Luckey, R.R.; and Burkhardt, D.J. 1994. *Revised Potentiometric-Surface Map, Yucca Mountain and Vicinity, Nevada*. Water-Resources Investigations Report 93-4000. Denver, Colorado: U.S. Geological Survey. ACC: NNA.19930212.0018.
- 162811 Fahy, M. 1997. "Masses Recovered from Tracer Testing at C-Wells." E-mail from M. Fahy to A. Randall, July 21, 1997. ACC: MOL.20030515.0196.

- 137456 Fahy, M.F. 1997. "Dual-Porosity Analysis of Conservative Tracer Testing in Saturated Volcanic Rocks at Yucca Mountain in Nye County, Nevada." *International Journal of Rock Mechanics and Mining Sciences*. 34, (3-4). Amsterdam, The Netherlands: Elsevier. TIC: 237601.
- 180732 Farnham, I. 2001. ATC Laboratory and Field Studies [final closure]. Scientific Notebook UCCSN-UNLV-019, Volume 2. Pages TOC-100. ACC: MOL.20020129.0121.
- 180733 Farnham, I. 2001. ATC Laboratory and Field Studies [final closure]. Scientific Notebook UCCSN-UNLV-019, Volume 3. Pages TOC-102. ACC: MOL.20020129.0122.
- 157319 Farrell, D.A.; Armstrong, A.; Winterle, J.R.; Turner, D.R.; Ferrill, D.A.; Stamatakos, J.A.; Coleman, N.M.; Gray, M.B.; and Sandberg, S.K. 1999. *Structural Controls on Groundwater Flow in the Yucca Mountain Region*. San Antonio, Texas: Center for Nuclear Waste Regulatory Analyses. TIC: 254265.
- 100146 Faunt, C.C. 1997. *Effect of Faulting on Ground-Water Movement in the Death Valley Region, Nevada and California*. Water-Resources Investigations Report 95-4132. Denver, Colorado: U.S. Geological Survey. ACC: MOL.19980429.0119.
- 118941 Ferrill, D.A.; Winterle, J.; Wittmeyer, G.; Sims, D.; Colton, S.; Armstrong, A.; and Morris, A.P. 1999. "Stressed Rock Strains Groundwater at Yucca Mountain, Nevada." *GSA Today*, 9, (5), 1-8. Boulder, Colorado: Geological Society of America. TIC: 246229.
- 102009 Fetter, C.W. 1993. *Contaminant Hydrogeology*. Upper Saddle River, New Jersey: Prentice Hall. TIC: 240691.
- 156668 Fetter, C.W. 2001. *Applied Hydrogeology*. 4th Edition. Upper Saddle River, New Jersey: Prentice Hall. TIC: 251142.
- 101173 Freeze, R.A. and Cherry, J.A. 1979. *Groundwater*. Englewood Cliffs, New Jersey: Prentice-Hall. TIC: 217571.
- 105454 Frizzell, V.A., Jr. and Shulters, J. 1990. *Geologic Map of the Nevada Test Site, Southern Nevada*. Miscellaneous Investigations Series Map I-2046. Denver, Colorado: U.S. Geological Survey. TIC: 200459.
- 156826 Galloway, D. and Rojstaczer, S. 1988. "Analysis of the Frequency Response of Water Levels in Wells to Earth Tides and Atmospheric Loading." *Proceedings, Fourth Canadian/American Conference on Hydrogeology, Fluid Flow, Heat Transfer, and Mass Transport in Fractured Rocks, Banff, Alberta, Canada, June 21-24, 1988*. Hitchon, B. and Bachu, S., eds. Pages 100-113. Dublin, Ohio: National Water Well Association. TIC: 222289.

- 101045 Geldon, A.L. 1993. *Preliminary Hydrogeologic Assessment of Boreholes UE-25c #1, UE-25c #2, and UE-25c #3, Yucca Mountain, Nye County, Nevada.* Water-Resources Investigations Report 92-4016. Denver, Colorado: U.S. Geological Survey. ACC: MOL.19960808.0136.
- 100396 Geldon, A.L. 1996. *Results and Interpretation of Preliminary Aquifer Tests in Boreholes UE-25c #1, UE-25c #2, and UE-25c #3, Yucca Mountain, Nye County, Nevada.* Water-Resources Investigations Report 94-4177. Denver, Colorado: U.S. Geological Survey. ACC: MOL.19980724.0389.
- 156827 Geldon, A.L.; Earle, J.D.; and Umari, A.M.A. 1997. *Determination of Barometric Efficiency and Effective Porosity, Boreholes UE-25, c#1, UE-25 c#2, and UE-25 c#3, Yucca Mountain, Nye County, Nevada.* Water-Resources Investigations Report 97-4098. Denver, Colorado: U.S. Geological Survey. ACC: MOL.19980226.0570.
- 129721 Geldon, A.L.; Umari, A.M.A.; Earle, J.D.; Fahy, M.F.; Gemmell, J.M.; and Darnell, J. 1998. *Analysis of a Multiple-Well Interference Test in Miocene Tuffaceous Rocks at the C-Hole Complex, May-June 1995, Yucca Mountain, Nye County, Nevada.* Water-Resources Investigations Report 97-4166. Denver, Colorado: U.S. Geological Survey. TIC: 236724.
- 161163 Geldon, A.L.; Umari, A.M.A.; Fahy, M.F.; Earle, J.D.; Gemmell, J.M.; and Darnell, J. 2002. *Results of Hydraulic Tests in Miocene Tuffaceous Rocks at the C-Hole Complex, 1995 to 1997, Yucca Mountain, Nye County, Nevada.* Water-Resources Investigations Report 02-4141. Denver, Colorado: U.S. Geological Survey. TIC: 253755.
- 178622 Gilmore, K. 2005. Nye County Nuclear Waste Repository Project Office, Well ID # NC-EWDP-22 Site Tracer Tests. Scientific Notebook 166. Cover, Table of Contents, Pages 1-142 and 144-156.
- 178621 Gilmore, K. 2005. Nye County NWRPO NC-EWDP-22 Site Tracer Tests. Scientific Notebook 164. Cover and Pages 1-43.
- 101046 Graves, R.P.; Tucci, P.; and O'Brien, G.M. 1997. *Analysis of Water-Level Data in the Yucca Mountain Area, Nevada, 1985-95.* Water-Resources Investigations Report 96-4256. Denver, Colorado: U.S. Geological Survey. ACC: MOL.19980219.0851.
- 101132 Grisak, G.E. and Pickens, J.F. 1980. "Solute Transport Through Fractured Media, 1. The Effect of Matrix Diffusion." *Water Resources Research*, 16, (4), 719-730. Washington, D.C.: American Geophysical Union. TIC: 222056.
- 156830 Guimerà, J. and Carrera, J. 2000. "A Comparison of Hydraulic and Transport Parameters Measured in Low-Permeability Fractured Media." *Journal of Contaminant Hydrology*, 41, (3-4), 261-281. New York, New York: Elsevier. TIC: 251013.

- 156831 Haggerty, R. and Gorelick, S.M. 1995. "Multiple-Rate Mass Transfer for Modeling Diffusion and Surface Reactions in Media with Pore-Scale Heterogeneity." *Water Resource Research*, 31, (10), 2383-2400. Washington, D.C.: American Geophysical Union. TIC: 244502.
- 156832 Haggerty, R.; McKenna, S.A.; and Meigs, L.C. 2000. "On the Late-Time Behavior of Tracer Test Breakthrough Curves." *Water Resources Research*, 36, (12), 3467-3479. Washington, D.C.: American Geophysical Union. TIC: 250770.
- 165169 Hantush, M.S. 1956. "Analysis of Data from Pumping Tests in Leaky Aquifers." *Transactions, American Geophysical Union*, 37, (6), 702-714. Washington, D.C.: American Geophysical Union. TIC: 255072.
- 161160 Hantush, M.S. 1966. "Analysis of Data from Pumping Tests in Anisotropic Aquifers." *Journal of Geophysical Research*, 71, (2), 421-426. Washington, D.C.: American Geophysical Union. TIC: 225281.
- 178665 Hantush, M.S. 1960. "Modification of the Theory of Leaky Aquifers." *Journal of Geophysical Research*, 65, (11), 3713-3725. Washington, D.C.: American Geophysical Union. TIC: 223145.
- 156833 Happel, J. and Brenner, H. 1965. *Low Reynolds Number Hydrodynamics with Special Applications to Particulate Media*. Englewood Cliffs, New Jersey: Prentice-Hall. TIC: 251939.
- 100814 Harrar, J.E.; Carley, J.F.; Isherwood, W.F.; and Raber, E. 1990. *Report of the Committee to Review the Use of J-13 Well Water in Nevada Nuclear Waste Storage Investigations*. UCID-21867. Livermore, California: Lawrence Livermore National Laboratory. ACC: NNA.19910131.0274.
- 117358 Hiemenz, P.C. 1986. *Principles of Colloid and Surface Chemistry*. 2nd Edition, Revised and Expanded. Undergraduate Chemistry Volume 9. Lagowski, J.J., ed. New York, New York: Marcel Dekker. TIC: 246392.
- 179650 Horne, R.N. 1995. *Modern Well Test Analysis: A Computer-Aided Approach*. 2nd Edition. Palo Alto, California: Petroway. On Order.
- 156835 Israelachvili, J.N. 2000. *Intermolecular and Surface Forces*. 2nd Edition. San Diego, California: Academic Press. TIC: 251020.
- 156836 Jenson, V.G. and Jeffreys, G.V. 1977. *Mathematical Methods in Chemical Engineering*. 2nd Edition. Orlando, Florida: Academic Press. TIC: 251165.
- 156837 Johnson, G.W. 1994. *Labview Graphical Programming, Practical Applications in Instrumentation and Control*. New York, New York: McGraw-Hill. TIC: 251938.

- 164666 Kasenow, M. 2002. *Determination of Hydraulic Conductivity from Grain Size Analysis, with Errata and Grain-Size Analysis Supplement CDROM*. Highlands Ranch, Colorado: Water Resources Publications. TIC: 254721.
- 179421 Klute, A. and Dirksen, C. 1986. "Hydraulic Conductivity and Diffusivity: Laboratory Methods." Chapter 28 of *Methods of Soil Analysis: Part 1 Physical and Mineralogical Methods*. Klute, A., ed. 2nd Edition. Madison, Wisconsin: Soil Science Society of America. TIC: 217566.
- 101049 Lahoud, R.G.; Lobmeyer, D.H.; and Whitfield, M.S., Jr. 1984. *Geohydrology of Volcanic Tuff Penetrated by Test Well UE-25b #1, Yucca Mountain, Nye County, Nevada*. Water-Resources Investigations Report 84-4253. Denver, Colorado: U.S. Geological Survey. ACC: NNA.19890511.0117.
- 171587 LANL 2002. *Software Management Report (SMR) for Multran Version 1.0*. SDN: 10666-SMR-1.0-00. Los Alamos, New Mexico: Los Alamos National Laboratory. ACC: MOL.20021021.0385.
- 179420 LANL-INC-DP-140, R0. Constant Head Saturated Hydraulic Conductivity Measurements on Repacked Core Samples. Los Alamos, New Mexico: Los Alamos National Laboratory. ACC: MOL.20040506.0269.
- 144612 LeCain, G.D.; Anna, L.O.; and Fahy, M.F. 2000. *Results from Geothermal Logging, Air and Core-Water Chemistry Sampling, Air-Injection Testing, and Tracer Testing in the Northern Ghost Dance Fault, Yucca Mountain, Nevada, November 1996 to August 1998*. Water-Resources Investigations Report 99-4210. Denver, Colorado: U.S. Geological Survey. TIC: 247708.
- 156839 Levenspiel, O. 1972. *Chemical Reaction Engineering*. 2nd Edition. New York, New York: John Wiley & Sons. TIC: 224877.
- 178081 Lide, D.R., ed. 2006. *CRC Handbook of Chemistry and Physics*. 87th Edition. Boca Raton, Florida: CRC Press. TIC: 258634.
- 105457 Lobmeyer, D.H.; Whitfield, M.S., Jr.; Lahoud, R.G.; and Bruckheimer, L. 1983. Geohydrologic Data for Test Well UE-25b#1, Nevada Test Site, Nye County, Nevada. Open-File Report 83-855. Denver, Colorado: U.S. Geological Survey. ACC: NNA.19890922.0285.
- 150250 Lohman, S.W. 1972. *Ground-Water Hydraulics*. Professional Paper 708. Washington, D.C.: U.S. Geological Survey. ACC: NNA.19891220.0169.
- 100465 Luckey, R.R.; Tucci, P.; Faunt, C.C.; Ervin, E.M.; Steinkampf, W.C.; D'Agnes, F.A.; and Patterson, G.L. 1996. *Status of Understanding of the Saturated-Zone Ground-Water Flow System at Yucca Mountain, Nevada, as of 1995*. Water-Resources Investigations Report 96-4077. Denver, Colorado: U.S. Geological Survey. ACC: MOL.19970513.0209.

- 178614 Maas, C. 1986. "The Use of Matrix Differential Calculus in Problems of Multiple-Aquifer Flow." *Journal of Hydrology*, (88), 43-67. Amsterdam, The Netherlands: Elsevier. TIC: 259004.
- 101805 Maldonado, F. and Koether, S.L. 1983. *Stratigraphy, Structure, and Some Petrographic Features of Tertiary Volcanic Rocks at the USW G-2 Drill Hole, Yucca Mountain, Nye County, Nevada*. Open-File Report 83-732. Denver, Colorado: U.S. Geological Survey. ACC: NNA.19870506.0143.
- 156840 Maloszewski, P. and Zuber, A. 1984. "Interpretation of Artificial and Environmental Tracers in Fissured Rocks with a Porous Matrix." *Isotope Hydrology 1983, Proceedings of an International Symposium on Isotope Hydrology in Water Resources Development, Organized by the International Atomic Energy Agency in Co-operation with the United Nations Educational, Scientific and Cultural Organization and Held in Vienna, 12-16 September 1983*. Vienna, Austria: International Atomic Energy Commission. TIC: 236592.
- 148312 Maloszewski, P. and Zuber, A. 1985. "On the Theory of Tracer Experiments in Fissured Rocks with a Porous Matrix." *Journal of Hydrology*, 79, 333-358. Amsterdam, The Netherlands: Elsevier. TIC: 222390.
- 156841 Maloszewski, P.; Herrmann, A.; and Zuber, A. 1999. "Interpretation of Tracer Tests Performed in Fractured Rock of the Lange Bramke Basin, Germany." *Hydrogeology Journal*, 7, 209-218. New York, New York: Springer-Verlag. TIC: 250778.
- 156842 Ming, D.W. and Dixon, J.B. 1987. "Quantitative Determination of Clinoptilolite in Soils by a Cation-Exchange Capacity Method." *Clays and Clay Minerals*, 35, (6), 463-468. New York, New York: Pergamon Press. TIC: 251015.
- 156843 Ming, D.W. and Mumpton, F.A. 1995. "Zeolites in Soils." Chapter 18 of *Minerals in Soil Environments*. 2nd Edition. Dixon, J.B. and Weed, S.B., eds. SSSA Book Series, No. 1. Madison, Wisconsin: Soil Science Society of America. TIC: 237222.
- 101146 Moench, A.F. 1989. "Convergent Radial Dispersion: A Laplace Transform Solution for Aquifer Tracer Testing." *Water Resources Research*, 25, (3), 439-447. Washington, D.C.: American Geophysical Union. TIC: 238283.
- 148784 Moench, A.F. 1995. "Convergent Radial Dispersion in a Double-Porosity Aquifer with Fracture Skin: Analytical Solution and Application to a Field Experiment in Fractured Chalk." *Water Resources Research*, 31, (8), 1823-1835. Washington, D.C.: American Geophysical Union. TIC: 233132.
- 139151 National Research Council. 1996. *Rock Fractures and Fluid Flow, Contemporary Understanding and Applications*. Washington, D.C.: National Academy Press. TIC: 235913.

- 101148 Neretnieks, I. 1980. "Diffusion in the Rock Matrix: An Important Factor in Radionuclide Retardation." *Journal of Geophysical Research*, 85, (B8), 4379-4397. Washington, D.C.: American Geophysical Union. TIC: 221345.
- 150321 Neuman, S.P. 1975. "Analysis of Pumping Test Data from Anisotropic Unconfined Aquifers Considering Delayed Gravity Response." *Water Resources Research*, 11, (2), 329-342. Washington, D.C.: American Geophysical Union. TIC: 222414.
- 101464 Neuman, S.P. 1990. "Universal Scaling of Hydraulic Conductivities and Dispersivities in Geologic Media." *Water Resources Research*, 26, (8), 1749-1758. Washington, D.C.: American Geophysical Union. TIC: 237977.
- 156849 Newman, B.D.; Fuentes, H.R.; and Polzer, W.L. 1991. "An Evaluation of Lithium Sorption Isotherms and Their Application to Ground-Water Transport." *Ground Water*, 29, (6), 818-824. Worthington, Ohio: Water Well Journal Publishing. TIC: 203790.
- 148719 Newman, J. 1973. *Electrochemical Systems*. Englewood Cliffs, New Jersey: Prentice-Hall. TIC: 210201.
- 163274 NRC (U.S. Nuclear Regulatory Commission) 2003. *Yucca Mountain Review Plan, Final Report*. NUREG-1804, Rev. 2. Washington, D.C.: U.S. Nuclear Regulatory Commission, Office of Nuclear Material Safety and Safeguards. TIC: 254568.
- 170243 NRC 2004. *Risk Insights Baseline Report*. Washington, D.C.: U.S. Nuclear Regulatory Commission, Office of Nuclear Material Safety and Safeguards. ACC: MOL.20040629.0235.
- 179629 NWRPO (Nuclear Waste Repository Project Office) 2002. *Early Warning Drilling Program Phase IV Drilling and Well Construction Work Plan*. Work Plan 5, Rev. 3. Pahrump, Nevada: Nye County, Nuclear Waste Repository Project Office. ACC: MOL.20030520.0083.
- 178607 NWRPO (Nye County Nuclear Waste Repository Project Office) 2002. Technical Procedure: Pumping/Injection Tests of Packed-Off Zones in Unscreened Open Boreholes or in Multiple Screen Boreholes With or Without Observation Wells. TP-10.0. Pahrump, Nevada: Nye County Nuclear Waste Repository Project Office.
- 165947 NWRPO 2003. "Program Management." Pahrump, Nevada: Nye County Nuclear Waste Repository Project Office. Accessed December 12, 2003. ACC: MOL.20031212.0014. http://www.nyecounty.com/Program_mgmnt.htm
- 178608 NWRPO 2005. *Technical Procedure: Procedures for Operating Westbay Mosdax Groundwater Monitoring Equipment in Nye County Wells*. TP-9.2. Pahrump, Nevada: Nye County Nuclear Waste Repository Project Office.

- 156859 Nye County Nuclear Waste Repository Project Office. 1995. *Borehole UE-25 ONC #1 and USW NRG-4 Drilling and Instrumentation Report, Yucca Mountain, Nevada, September 1, 1995, Nye County Independent Scientific Investigation Program.* Pahrump, Nevada: Nye County Nuclear Waste Repository Project Office. ACC: MOL.19960910.0231.
- 101279 O'Brien, G.M.; Tucci, P.; and Burkhardt, D.J. 1995. *Water Levels in the Yucca Mountain Area, Nevada, 1992.* Open-File Report 94-311. Denver, Colorado: U.S. Geological Survey. ACC: NNA.19940627.0003.
- 150265 Papadopoulos, I.S. 1967. "Nonsteady Flow to a Well in an Infinite Anisotropic Aquifer." *Hydrology of Fractured Rocks, Proceedings of the Dubrovnik Symposium, October 1965. 1*, 21-31. Gentbrugge, Belgium: Association Internationale d'Hydrologie Scientifique. TIC: 223152.
- 150323 Papadopoulos, S.S. and Cooper, H.H., Jr. 1967. "Drawdown in a Well of Large Diameter." *Water Resources Research*, 3, (1), 241-244. Washington, D.C.: American Geophysical Union. TIC: 225288.
- 178743 Patterson, G.L. and Striffler, P.S. 2006. "Vertical Variability in Saturated Zone Hydrochemistry Near Yucca Mountain, Nevada." Proceedings of the 11th International High-Level Radioactive Waste Management Conference (IHLRWM), April 30 - May 4, 2006, Las Vegas, Nevada. Pages 390-394. La Grange Park, Illinois: American Nuclear Society. TIC: 258345.
- 178566 Questa Engineering Company 2004. *Analysis of Aquifer Pump Tests in Individual Well Zones at Site 22 near Yucca Mountain, Nevada.* NWRPO-2004-02. Pahrump, Nevada: Nye County, Nuclear Waste Repository Project Office. ACC: MOL.20070111.0004.
- 178565 Questa Engineering Corporation 2003. *Preliminary Analysis of Pump-Spinner Tests and Pump Test in Well NC-EWDP-22S, Near Yucca Mountain, Nevada.* NWRPO-2002-006. Pahrump, Nevada: Nye County, Nuclear Waste Repository Project Office. ACC: MOL.20031023.0064.
- 165125 Reimus, P. 2000. General C-Wells Notebook and Microsphere Analyses for C-Wells. Scientific Notebook SN-LANL-SCI-214-V1. ACC: MOL.20000413.0220; MOL.20000824.0084.
- 165124 Reimus, P. 2000. LA-CST-CW-NBK-98-001, YMP C-Wells Rocks. Scientific Notebook SN-LANL-SCI-146-V1. ACC: MOL.20010308.0191.
- 164625 Reimus, P. 2000. LA-CST-CW-NBK-98-003, YMP C-Wells Sorption. Scientific Notebook SN-LANL-SCI-006-V1. ACC: MOL.20010308.0193.
- 165121 Reimus, P. 2000. LA-CST-CW-NBK-98-004, YMP C-Wells Diffusion Cells. Scientific Notebook SN-LANL-SCI-007-V1. ACC: MOL.20010308.0195.

- 162852 Reimus, P. 2000. LANL C-Wells Prow Pass Field Notebook. Scientific Notebook SN-LANL-SCI-233-V1. ACC: MOL.20000824.0066.
- 163760 Reimus, P. 2003. Laboratory Testing in Support of Saturated Zone Investigations. Scientific Notebook SN-LANL-SCI-280-V1. ACC: MOL.20030227.0286.
- 165129 Reimus, P. 2003. LA-CST-NBK-98-011, Modeling and Interpretation of Transport Tests. Scientific Notebook SN-LANL-SCI-255-V1. ACC: MOL.20020206.0093; MOL.20031027.0086; MOL.20031027.0087.
- 101474 Reimus, P.W. 1995. *The Use of Synthetic Colloids in Tracer Transport Experiments in Saturated Rock Fractures*. Ph.D. dissertation. LA-13004-T. Los Alamos, New Mexico: Los Alamos National Laboratory. TIC: 240694.
- 162855 Reimus, P.W. 2000. C-Wells Bullfrog Multiple Tracer Test Notebook. Scientific Notebook SN-LANL-SCI-223-V1. ACC: MOL.20000818.0075.
- 164624 Reimus, P.W. 2000. LA-EES-4-NBK-96-003(b), C-Wells Bullfrog Multiple Tracer Test. Scientific Notebook for SN-LANL-SCI-224-V1. ACC: MOL.20000824.0094.
- 165126 Reimus, P.W. 2000. QA Notebook for C-Wells Tracer Testing (PFBA/C#2 Test). Scientific Notebook SN-LANL-SCI-217-V1. ACC: MOL.20000818.0063.
- 165127 Reimus, P.W. 2000. QA Notebook Iodide/C#1 Tracer Test. Scientific Notebook SN-LANL-SCI-218-V1. ACC: MOL.20000818.0071.
- 165128 Reimus, P.W. 2003. Single-Well and Cross-Hole Alluvial Tracer Testing. Scientific Notebook SN-LANL-SCI-251-V1. ACC: MOL.20030313.0331; MOL.20030313.0332; MOL.20030313.0333; MOL.20030313.0334.
- 154705 Reimus, P.W. and Haga, M.J. 1999. *Analysis of Tracer Responses in the BULLION Forced-Gradient Experiment at Pahute Mesa, Nevada*. LA-13615-MS. Los Alamos, New Mexico: Los Alamos National Laboratory. TIC: 249826.
- 101154 Robinson, B.A. 1994. "A Strategy for Validating a Conceptual Model for Radionuclide Migration in the Saturated Zone Beneath Yucca Mountain." *Radioactive Waste Management and Environmental Restoration*, 19, (1-3), 73-96. Yverdon, Switzerland: Harwood Academic Publishers. TIC: 222513.
- 108567 Robinson, R.A. and Stokes, R.H. 1965. *Electrolyte Solutions, The Measurement and Interpretation of Conductance, Chemical Potential and Diffusion in Solutions of Simple Electrolytes*. 2nd Edition (Revised). Washington, D.C.: Butterworth. TIC: 242575.

- 107944 Rush, F.E.; Thordarson, W.; and Bruckheimer, L. 1983. *Geohydrologic and Drill-Hole Data for Test Well USW H-1, Adjacent to Nevada Test Site, Nye County, Nevada*. Open-File Report 83-141. Denver, Colorado: U.S. Geological Survey. ACC: HQS.19880517.1835.
- 100075 Sawyer, D.A.; Fleck, R.J.; Lanphere, M.A.; Warren, R.G.; Broxton, D.E.; and Hudson, M.R. 1994. "Episodic Caldera Volcanism in the Miocene Southwestern Nevada Volcanic Field: Revised Stratigraphic Framework, ⁴⁰Ar/³⁹Ar Geochronology, and Implications for Magmatism and Extension." *Geological Society of America Bulletin*, 106, (10), 1304-1318. Boulder, Colorado: Geological Society of America. TIC: 222523.
- 101291 Scott, R.B. and Castellanos, M. 1984. Stratigraphic and Structural Relations of Volcanic Rocks in Drill Holes USW GU-3 and USW G-3, Yucca Mountain, Nye County, Nevada. Open-File Report 84-491. Denver, Colorado: U.S. Geological Survey. ACC: NNA.19870519.0095.
- 156862 Skagius, K. and Neretnieks, I. 1986. "Porosities and Diffusivities of Some Nonsorbing Species in Crystalline Rocks." *Water Resources Research*, 22, (3), 389-398. Washington, D.C.: American Geophysical Union. TIC: 225291.
- 174109 SNL (Sandia National Laboratories) 2007. *Hydrogeologic Framework Model for the Saturated Zone Site-Scale Flow and Transport Model*. MDL-NBS-HS-000024 REV 01. Las Vegas, Nevada: Sandia National Laboratories. ACC: DOC.20070411.0003.
- 177396 SNL 2007. *Radionuclide Transport Models Under Ambient Conditions*. MDL-NBS-HS-000008 REV 03. Las Vegas, Nevada: Sandia National Laboratories.
- 177390 SNL 2007. *Saturated Zone Flow and Transport Model Abstraction*. MDL-NBS-HS-000021 REV 04. Las Vegas, Nevada: Sandia National Laboratories.
- 177391 SNL 2007. *Saturated Zone Site-Scale Flow Model*. MDL-NBS-HS-000011 REV 03. Las Vegas, Nevada: Sandia National Laboratories.
- 177392 SNL 2007. *Site-Scale Saturated Zone Transport*. MDL-NBS-HS-000010 REV 03. Las Vegas, Nevada: Sandia National Laboratories.
- 177397 SNL 2007. *Particle Tracking Model and Abstraction of Transport Processes*. MDL-NBS-HS-000020 REV 03. Las Vegas, Nevada: Sandia National Laboratories.
- 101297 Spengler, R.W.; Byers, F.M., Jr.; and Warner, J.B. 1981. *Stratigraphy and Structure of Volcanic Rocks in Drill Hole USW-G1, Yucca Mountain, Nye County, Nevada*. Open-File Report 81-1349. Denver, Colorado: U.S. Geological Survey. ACC: NNA.19870406.0222.
- 180315 Spiegel, M. R. 1968. *Mathematical Handbook of Formulas and Tables*. Schaum's Outline Series in Mathematics. New York, New York: McGraw-Hill. On Order

- 180316 Spiegel, M. R. 1971. *Advanced Mathematics for Engineers and Scientists*. Schaum's Outline Series in Mathematics. New York, New York: McGraw-Hill. On Order
- 117341 Stehfest, H. 1970. "Algorithm 368, Numerical Inversion of Laplace Transforms." *Journal of the Association for Computing Machinery*, 13, (1), 47-49. New York, New York: Association for Computing Machinery. TIC: 246873.
- 180730 Stetzenbach, K. 2001. ATC Laboratory and Field Studies [final closure]. Scientific Notebook UCCSN-UNLV-019, Volume 1. ACC: MOL.20020129.0120.
- 156863 Stetzenbach, K.J. and Thompson, G.M. 1983. "A New Method for Simultaneous Measurement of Cl^- , Br^- , NO_3^- , SCN^- , and I^- at Sub-ppm Levels in Ground Water." *Ground Water*, 21, (1), 36-41. Worthington, Ohio: Water Well Journal Publishing. TIC: 252098.
- 150754 Streltsova-Adams, T.D. 1978. "Well Hydraulics in Heterogeneous Aquifer Formations." Volume 11 of *Advances in Hydroscience*. Chow, V.T., ed. Pages 357-423. New York, New York: Academic Press. TIC: 225957.
- 164623 Sullivan, E.J. 2002. Laboratory Testing in Support of Alluvial Tracer Testing. Scientific Notebook SN-LANL-SCI-213-V1. ACC: MOL.20021015.0198.
- 179627 Swanson, D. 2006. "Nye County Report Titled, 'Analysis of 48-Hour Aquifer Pump Test at Site 10 Near Yucca Mountain, Nevada'." Letter from D. Swanson (Nye County NWRPO) to Distribution, May 31, 2006, 0531065457, 06-216-DS (L), with enclosure. ACC: MOL.20060627.0049.
- 101160 Tang, D.H.; Frind, E.O.; and Sudicky, E.A. 1981. "Contaminant Transport in Fractured Porous Media: Analytical Solution for a Single Fracture." *Water Resources Research*, 17, (3), 555-564. Washington, D.C.: American Geophysical Union. TIC: 225358.
- 150327 Theis, C.V. 1935. "The Relation Between the Lowering of the Piezometric Surface and the Rate and Duration of Discharge of a Well Using Ground-Water Storage." *Transactions of the American Geophysical Union Sixteenth Annual Meeting, April 25 and 26, 1935, Washington, D.C.* Pages 519-524. Washington, D.C.: National Academy of Science, National Research Council. TIC: 223158.
- 100830 Thompson, J.L. 1989. "Actinide Behavior on Crushed Rock Columns." *Journal of Radioanalytical and Nuclear Chemistry, Articles*, 130, (2), 353-364. Lausanne, Switzerland: Elsevier. TIC: 222698.
- 103200 Thordarson, W.; Rush, F.E.; Spengler, R.W.; and Waddell, S.J. 1984. Geohydrologic and Drill-Hole Data for Test Well USW H-3, Yucca Mountain, Nye County, Nevada. Open-File Report 84-149. Denver, Colorado: U.S. Geological Survey. ACC: NNA.19870406.0056.

- 179628 TP-7.0, Rev. 3. *Drill Site Management*. Pahrump, Nevada: Nye County Nuclear Waste Repository Project Office.
- 125967 Treher, E.N. and Raybold, N.A. 1982. *The Elution of Radionuclides Through Columns of Crushed Rock from the Nevada Test Site*. LA-9329-MS. Los Alamos, New Mexico: Los Alamos National Laboratory. ACC: NNA.19920922.0021.
- 100422 Triay, I.R.; Meijer, A.; Conca, J.L.; Kung, K.S.; Rundberg, R.S.; Strietelmeier, B.A.; and Tait, C.D. 1997. *Summary and Synthesis Report on Radionuclide Retardation for the Yucca Mountain Site Characterization Project*. Eckhardt, R.C., ed. LA-13262-MS. Los Alamos, New Mexico: Los Alamos National Laboratory. ACC: MOL.19971210.0177.
- 113901 Tsang, Y.W. 1992. "Usage of "Equivalent Apertures" for Rock Fractures as Derived from Hydraulic and Tracer Tests." *Water Resources Research*, 28, (5), 1451-1455. Washington, D.C.: American Geophysical Union. TIC: 245891.
- 101060 Tucci, P. and Burkhardt, D.J. 1995. *Potentiometric-Surface Map, 1993, Yucca Mountain and Vicinity, Nevada*. Water-Resources Investigations Report 95-4149. Denver, Colorado: U.S. Geological Survey. ACC: MOL.19960924.0517.
- 164543 Umari, A.M.J.; Geldon, A.; Patterson, G.; Gemmell, J.; Earle, J.; and Darnell, J. 1994. "Use of an Analog Site Near Raymond, California, to Develop Equipment and Methods for Characterizing a Potential High-Level, Nuclear Waste Repository Site at Yucca Mountain, Nevada." *High Level Radioactive Waste Management, Proceedings of the Fifth Annual International Conference, Las Vegas, Nevada, May 22-26, 1994*. 4, 2413-2422. La Grange Park, Illinois: American Nuclear Society. TIC: 210984.
- 162858 Umari, M.J. 2002. Performing Various Hydraulic and Tracer Tests Using Prototype Pressure Transducer and Packer Assemblies. Scientific Notebook SN-USGS-SCI-036-V1. ACC: MOL.20020520.0364; MOL.20020520.0368; MOL.20020520.0367; MOL.20020520.0368; MOL.20020520.0369; MOL.20020520.0370; MOL.20020520.0371; MOL.20020520.0372; MOL.20020520.0373; MOL.20020520.0374; MOL.20020520.0375; MOL.20020520.0376; MOL.20020520.0377; MOL.20020520.0378; MOL.20020520.0379; MOL.20020520.0380; MOL.20020520.0381; MOL.20020520.0382.
- 164573 Umari, M.J.; Earle, J.; and Darnell, J. 2003. Alluvium Testing Complex. SN-USGS-SCI-123-V1 through V8. ACC: MOL.20010613.0239; MOL.20010613.0240; MOL.20010613.0241; MOL.20021028.0352; MOL.20030821.0216; MOL.20030821.0217; MOL.20030821.0218; MOL.20030821.0219; MOL.20031021.0281; MOL.20031021.0282; MOL.20031021.0284.
- 154495 USGS (U.S. Geological Survey) n.d. Bulk Density. Denver, Colorado: U.S. Geological Survey. ACC: NNA.19940406.0076.

- 144579 Valocchi, A.J. 1985. "Validity of the Local Equilibrium Assumption for Modeling Sorbing Solute Transport Through Homogeneous Soils." *Water Resources Research*, 21, (6), 808-820. Washington, D.C.: American Geophysical Union. TIC: 223203.
- 156868 van Genuchten, M.Th.; Wierenga, P.J.; and O'Connor, G.A. 1977. "Mass Transfer Studies in Sorbing Porous Media: III. Experimental Evaluation with 2,4,5-T." *Soil Science Society of America Journal*, 41, 278-285. Madison, Wisconsin: Soil Science Society of America. TIC: 251016.
- 156867 Vaughn, D.E.W. 1978. "Properties of Natural Zeolites." *Natural Zeolites, Occurrence, Properties, Use, A Selection of Papers Presented at Zeolite, 76, an International Conference on the Occurrence, Properties, and Utilization of Natural Zeolites, Tucson, Arizona, June 1976*. Sand, L.B. and Mumpton, F.A., eds. Pages 353-371. New York, New York: Pergamon Press. TIC: 206755.
- 100833 Weast, R.C. and Astle, M.J., eds. 1981. *CRC Handbook of Chemistry and Physics*. 62nd Edition. Boca Raton, Florida: CRC Press. TIC: 240722.
- 101366 Whitfield, M.S., Jr.; Thordarson, W.; and Eshom, E.P. 1984. *Geohydrologic and Drill-Hole Data for Test Well USW H-4, Yucca Mountain, Nye County, Nevada*. Open-File Report 84-449. Denver, Colorado: U.S. Geological Survey. ACC: NNA.19870407.0317.
- 129796 Winterle, J.R. and La Femina, P.C. 1999. *Review and Analysis of Hydraulic and Tracer Testing at the C-Holes Complex Near Yucca Mountain, Nevada*. San Antonio, Texas: Center for Nuclear Waste Regulatory Analyses. TIC: 246623.
- 104211 YMP (Yucca Mountain Site Characterization Project) 1998. *Saturated Zone C-Hole Tracer Testing*. Field Work Package FWP-SB-97-008, Rev. 1. Las Vegas, Nevada: Yucca Mountain Site Characterization Office. ACC: MOL.19981029.0058.
- 110491 Zyvoloski, G.A.; Robinson, B.A.; Dash, Z.V.; and Trease, L.L. 1997. *Summary of the Models and Methods for the FEHM Application—A Finite-Element Heat- and Mass-Transfer Code*. LA-13307-MS. Los Alamos, New Mexico: Los Alamos National Laboratory. TIC: 235587.

8.2 CODES, STANDARDS, REGULATIONS, AND PROCEDURES

- 176567 10 CFR 50. 2006. Energy: Domestic Licensing of Production and Utilization Facilities. Internet Accessible.
- 180319 10 CFR 63. 2007. Energy: Disposal of High-Level Radioactive Wastes in a Geologic Repository at Yucca Mountain, Nevada. Internet Accessible.
- AP-SIII.2Q, *Qualification of Unqualified Data*.

177092 DOE (U.S. Department of Energy) 2006. *Quality Assurance Requirements and Description*. DOE/RW-0333P, Rev. 18. Washington, D.C.: U.S. Department of Energy, Office of Civilian Radioactive Waste Management.
ACC: DOC.20060602.0001.

IM-PRO-002, *Control of the Electronic Management of Information*.

IM-PRO-003, *Software Management*.

LP-2.29Q-BSC, *Planning For Science Activities*.

SCI-PRO-002, *Planning for Science Activities*.

SCI-PRO-003, *Document Review*.

SCI-PRO-005, *Scientific Analyses and Calculations*.

8.3 SOURCE DATA, LISTED BY DATA TRACKING NUMBER

155860 GS010508312315.001. Concentrations of Difluorobenzoic Acid and Pyridone from Tracer Tests Conducted at the C-Well Complex, 1/8/97 - 7/11/97.
Submittal date: 06/01/2001.

179647 GS010608312314.001. Transducer, Barometer and Flowmeter Data Collected from April 2, 1997 to December 31, 1997 in Support of Hydraulic and Tracer Tests at the C-Hole Complex, Yucca Mountain, Nevada. Submittal date: 06/21/2001.

157067 GS010799992315.001. Injection and Production Flow Rates for the LANL Prow Pass Test, 11/30/98 through 1/27/99. Submittal date: 07/25/2001.

158690 GS011008314211.001. Interpretation of the Lithostratigraphy in Deep Boreholes NC-EWDP-19D1 and NC-EWDP-2DB Nye County Early Warning Drilling Program.
Submittal date: 01/16/2001.

162911 GS011108312322.006. Field and Chemical Data Collected between 1/20/00 and 4/24/01 and Isotopic Data Collected between 12/11/98 and 11/6/00 from Wells in the Yucca Mountain Area, Nye County, Nevada. Submittal date: 11/20/2001.

162678 GS020708312316.001. NC-EWDP-19D, ATC Single-Hole Hydraulic Testing Associated with the July 7, 2000 to April 26, 2001 Tracer Study.
Submittal date: 09/10/2002.

162679 GS020908312316.002. Flow Rates, Pressures, and Temperatures for Hydraulic and Tracer Testing at the NC-EWDP-19D, NC-EWDP-19IM1, and NC-EWDP-19IM2 Alluvial Testing Complex from December 18, 2001 to March 22, 2002.
Submittal date: 09/30/2002.

- 162680 GS020908312316.003. Background Pressures and Temperatures During Barometric Monitoring at the NC-EWDP-19D, NC-EWDP-19IM1, and NC-EWDP-19IM2 Alluvial Testing Complex from May 1, 2002 through July 3, 2002. Submittal date: 10/15/2002.
- 163483 GS030108314211.001. Interpretation of the Lithostratigraphy in Deep Boreholes NC-EWDP-18P, NC-EWDP-22SA, NC-EWDP-10SA, NC-EWDP-23P, NC-EWDP-19IM1A, and NC-EWDP-19IM2A, Nye County Early Warning Drilling Program, Phase III. Submittal date: 02/11/2003.
- 179648 GS031108312314.005. Revised Pumping Test Data Collected at the C-Hole Complex, September 28, 1995 (Pre-Test Data) and January through April, 1996. Submittal date: 08/03/2004.
- 179422 GS040108312322.001. Field and Chemical Data Collected Between 10/4/01 and 10/3/02 and Isotopic Data Collected Between 5/19/00 and 5/22/03 from Wells in the Yucca Mountain Area, Nye County, Nevada. Submittal date: 06/07/2004.
- 179434 GS040808312322.006. Field, Chemical, and Isotope Data for Spring and Well Samples Collected Between 03/01/01 and 05/12/04 in the Yucca Mountain Area, Nye County, Nevada. Submittal date: 11/15/2004.
- 174114 GS040908314211.001. Interpretation of the Lithostratigraphy in Deep Boreholes NC-EWDP-24P and NC-EWDP-29P, Nye County Early Warning Drilling Program, Phase IV B. Submittal date: 10/26/2004.
- 179423 GS060808312272.003. Analysis of Pore Water Samples Extracted from Sonic Core for the Period from February 2005 to May 2005. Submittal date: 08/10/2006.
- 148173 GS931008312313.016. Results and Interpretation of Preliminary Aquifer Tests in Boreholes UE-25C #1, UE-25C #2, and UE-25C #3, Yucca Mountain, Nye County, Nevada. Submittal date: 09/29/1993.
- 164801 GS960108312313.001. 280 Gallon per Minute Pump Test at the C-Hole Complex. Submittal date: 01/24/1996.
- 180534 GS960708312312.009. Water-Level Altitude Data From the Continuous Network, 1995. Submittal date: 07/30/1996.
- 159235 GS960808312315.001. Data Obtained from the Analysis of the Iodide-Tracer-Test Water Samples Collected During the 2/13/96 Convergent-Tracer Test Conducted at the C-Well Complex. Submittal date: 08/12/1996.
- 159240 GS970308312314.001. Pumping Test Data Collected at the C-Well Complex, 5/7/96 - 12/31/96. Submittal date: 03/07/1997.

- 161273 GS970308312314.002. Water-Level Altitude Data from Four Wells in the Continuous Network, May through December, 1996. Submittal date: 03/13/1997.
- 159241 GS970708312314.005. Pump Test Data Collected at the C-Well Complex, 1/8/97 - 6/15/97. Submittal date: 07/22/1997.
- 144468 GS970708312314.006. Water-Level Altitude Data from Four Wells in the Continuous Network, December 1996 through March 1997. Submittal date: 07/22/1997.
- 147068 GS981008312314.002. Pump Test Data Collected at the C-Wells Complex 1/8/97 - 3/31/97. Submittal date: 10/28/1998.
- 144464 GS981008312314.003. Pumping Test Data Collected at the C-Well Complex, 5/7/96 - 12/31/96. Submittal date: 10/28/1998.
- 159238 GS990208312315.001. Tracer Recovery Data from Testing in the Prow Pass Interval. Submittal date: 02/11/1999.
- 140115 GS990408312315.002. Transducer, Barometric Pressure and Discharge Data Collected from 4/18/98 through 11/24/98 in Support of the Ongoing Hydraulic and Tracer Tests Being Conducted at the UE-25 C-Well Complex, Nevada. Submittal date: 04/06/1999.
- 156043 LA0007PR831231.001. Bullfrog Reactive Tracer Test Data. Submittal date: 07/21/2000.
- 162623 LA0201JS831321.001. Alluvial Test Complex X-Ray Diffraction Results. Submittal date: 01/16/2002.
- 162627 LA0201JS831341.001. Alluvial Test Complex Cation Exchange Capacity Batch Study, Wells 19D and 19P Alluvium; 10/31/00, 06/12/01, 08/12/01. Submittal date: 01/16/2002.
- 162629 LA0201JS831361.001. Alluvial Test Complex Column Study, Well 19D Alluvium and Water, 12/13/00. Submittal date: 01/24/2002.
- 166205 LA0201JS831361.005. Alluvial Test Complex Column Study, Well 19D Alluvium and Water, 02/22/01. Submittal date: 01/29/2002.
- 162630 LA0201JS831361.007. Alluvial Test Complex Column Study, Well 19D Alluvium and Water, 04/02/01. Submittal date: 01/29/2002.
- 162613 LA0201JS831421.001. Grain Size Analysis of Alluvium Samples from Wells 19D and 19P of the Alluvial Test Complex. Submittal date: 01/30/2002.

- 162625 LA0201JS831421.002. BET Surface Area Measurements for 19D and 19P Alluvium Samples. Submittal date: 01/30/2002.
- 162431 LA0207PR831352.001. Microsphere Data from Single-Well Tracer Testing at NC-EWDP-19D1 (ATC). Submittal date: 07/30/2002.
- 162607 LA0212PR831231.001. Breakthrough Curves of Iodide in Saturated Fractured Cores from the C Wells. Submittal date: 01/30/2003.
- 162608 LA0212PR831231.002. Breakthrough Curves of Sodium, Calcium, Copper, Iodide, and Chloride in Saturated Fractured Cores from the C Wells. Submittal date: 01/21/2003.
- 162609 LA0212PR831231.003. Breakthrough Curves of Lithium, Bromide, and PFBA in Saturated Fractured Cores from the C Wells. Submittal date: 01/21/2003.
- 166215 LA0212PR831231.005. Breakthrough Curves of Sodium, Iodide, Calcium, and Chloride in Saturated Fractured Cores from the C Wells. Submittal date: 01/21/2003.
- 162603 LA0301PR831231.001. Bromide and Lithium Abundance Data from Column Studies of Crushed Central Bullfrog Tuff, UE-25 C#2 at 2406 ft. with Filtered J-13 Water. Submittal date: 02/25/2003.
- 162628 LA0302JS831341.001. Final Cation Concentrations in Libr Batch Sorption Experiments Involving Alluvium from Wells NC-EWDP-19D and NC-EWDP-19P. Submittal date: 03/06/2003.
- 162605 LA0302PR831231.001. Batch Experiments to Measure Bromide and PFBA Sorption onto C-Wells Tuffs. Submittal date: 03/06/2003.
- 162604 LA0302PR831341.001. Cation Exchange Capacity Measurements on C-Wells Tuffs Involving Displacement of Li and Other Cations by Cs. Submittal date: 03/06/2003.
- 162781 LA0303PR831232.001. Major Ion Chemistry of NC-EWDP-19D1 Waters Used in Batch Sorption and Column Transport Experiments. Submittal date: 03/12/2003.
- 171859 LA0401PR831231.001. Tabulations of Data Used in Tracer Test Interpretations. Submittal date: 01/29/2004.
- 171899 LA0410PR831231.001. Normalized Tracer Concentrations and Recoveries in C-Wells Tracer Tests. Submittal date: 10/04/2004.
- 179428 LA0501PR831231.001. Saturated Hydraulic Conductivity Data for Repacked Alluvium from NC-EWDP-19PB. Submittal date: 01/07/2005.

- 175878 LA0511PR831361.001. Alluvium Grain Density at the NC-EWDP-19D (ATC) Location. Submittal date: 11/22/2005.
- 178733 LA0612PR831231.001. Normalized Breakthrough Curves of Tracers from First Single-Well Tracer Test in NC-EWDP-22s, Conducted in December 2004. Submittal date: 12/05/2006.
- 178735 LA0612PR831231.002. Normalized Breakthrough Curves of Tracers from Second Single-Well Tracer Test in NC-EWDP-22s, Conducted in December 2004 and January 2005. Submittal date: 12/05/2006.
- 178736 LA0612PR831231.003. Normalized Breakthrough Curves of Tracers from First Cross-Hole Tracer Test at NC-EWDP Site 22, Conducted Between January and October 2005. Submittal date: 12/05/2006.
- 178738 LA0612PR831231.004. Normalized Breakthrough Curves of Tracers from Second Cross-Hole Tracer Test at NC-EWDP Site 22, Conducted Between August and October 2005. Submittal date: 12/06/2006.
- 178739 LA0612PR831231.005. Raw Data and Normalized Breakthrough Curves of Microspheres in First Cross-Hole Tracer Test at NC-EWDP Site 22, Conducted Between January and March 2005. Submittal date: 12/06/2006.
- 178745 LA0612PR831231.006. Measurements of Downhole Specific Conductance (Converted to Normalized Tracer Concentrations) at NC-EWDP Site 22 During and After Tracer Injections in Dec. 2004 and Jan. 2005. Submittal date: 12/06/2006.
- 179620 LA0701SL150304.001. Sulfide Mineral Occurrences in Yucca Mountain Core and Cutting Samples. Submittal date: 02/08/2007.
- 179625 LA0703PR150304.001. Lithium Batch Sorption Data using Groundwater from NC-EWDP-22S and Alluvium from Two Intervals in NC-EWDP-22PC. Submittal date: 03/05/2007.
- 181198 LA0705PR150304.002. June 1995 C-Wells Pressure Data. Submittal date: 05/22/2007.
- 181201 LA0705PR150304.003. June 1995 C-Wells Flow Rate Data. Submittal date: 05/22/2007.
- 181210 LA0705PR150304.004. June 1995 C-Wells Non-Q Data. Submittal date: 05/22/2007.
- 181211 LA0705PR150304.005. Nye County Pressure and Temperature Data from Hydraulic and Tracer Testing in NC-EWDP Site 22 Zone 2. Submittal date: 05/25/2007.

- 181212 LA0705PR150304.006. Nye County Pressure and Temperature Data from Westbay[®] transducer comparisons. Submittal date: 05/30/2007.
- 181202 LA0705PR150304.007. Well Completion Diagrams for NC-EWDP-19IM2, NC-EWDP-22S, NC-EWDP-22PA, NC-EWDP-22PB, and NC-EWDP-22PC. Submittal date: 05/30/2007.
- 181203 LA0705PR150304.008. NC-EWDP-22S Pump Test Westbay Data. Submittal date: 05/30/2007.
- 181204 LA0705PR150304.009. Nye County Pressure and Temperature Data from Westbay Transducers at NC-EWDP Site 22 from 7/31/2003 to 8/7/2003. Submittal date: 05/30/2007.
- 181205 LA0705PR150304.010. NC-EWDP-22S Zone #2 Pump Test Westbay Data. Submittal date: 05/30/2007.
- 181207 LA0705PR150304.011. NC-EWDP-22S Zone #3 Pump Test Westbay Data. Submittal date: 05/30/2007.
- 181208 LA0705PR150304.012. NC-EWDP-22S Zone #4 Pump Test Westbay Data. Submittal date: 05/30/2007.
- 129623 LA9909PR831231.004. Laboratory Data from C-Wells Core. Submittal date: 09/02/1999.
- 140134 LAPR831231AQ99.001. Prow Pass Reactive Tracer Test Field Data. Submittal date: 02/10/1999.
- 152554 MO0004QGFMPIK.000. Lithostratigraphic Contacts from MO9811MWDGFM03.000 to be Qualified Under the Data Qualification Plan, TDP-NBS-GS-000001. Submittal date: 04/04/2000.
- 179916 MO0007FLOWINTL.001. Data Qualification Report: Flowing Interval Data for Use on the Yucca Mountain Project. Submittal date: 7/25/2000.
- 151524 MO0007MAJIONPH.011. Major Ion Content of Groundwater from Selected Yucca Mountain Project Boreholes Extracted from ANL-NBS-HS-000021, Geochemical and Isotopic Constraints on Groundwater Flow Directions, Mixing and Recharge at Yucca Mountain, Nevada. Submittal date: 07/27/2000.
- 151530 MO0007MAJIONPH.013. Major Ion Content of Groundwater from Selected YMP and Other Boreholes Extracted from ANL-NBS-HS-000021, Geochemical and Isotopic Constraints on Groundwater Flow Directions, Mixing and Recharge at Yucca Mountain, Nevada. Submittal date: 07/27/2000.

- 153371 MO0012CATECHOL.000. Cation Exchange Capacity Data of C-Well Tuff from UE-25 C #1 and UE-25 C #2. Submittal date: 12/05/2000.
- 159243 MO0012DIFFCHOL.000. Tracer Movement Measured in C/CO. The Unit C/CO Represents the Effluent Concentration Divided by the Injection Concentration. Submittal date: 12/05/2000.
- 154765 MO0012FLOW25C3.001. Flow Meter Survey Data from Borehole UE-25 C#3 for Use on the Yucca Mountain Project. Submittal date: 12/15/2000.
- 153370 MO0012MINLCHOL.000. Mineral Abundance Data Using X-ray Diffraction Analyses of C-Well Tuffs from UE-25 C #1, and UE-25 C #2. Submittal date: 12/05/2000.
- 153368 MO0012PERMCHOL.000. Permeability Data (Using Filtered J-13 Water) from UE-25 C #1, UE-25 C #2, and UE-25 C #3. Submittal date: 12/05/2000.
- 153376 MO0012POROCHOL.000. Porosity Data (Using Deionized Water) from UE-25 C #1, UE-25 C #2, and UE-25 C #3. Submittal date: 12/05/2000.
- 153375 MO0012SORBCHOL.000. Sorbing Element Concentration Data of J-13 and C-3 Well Water from UE-25 C #1 and UE-25 C #2. Submittal date: 12/05/2000.
- 155267 MO0101NYE03734.073. Manual Water Level Data for EWDP Phase II Wells. Submittal date: 1/18/2001.
- 163480 MO0105GPLOG19D.000. Geophysical Log Data from Borehole NC EWDP 19D. Submittal date: 05/31/2001.
- 157066 MO0110BFROGREC.001. Bullfrog Test Recirculation Flow Rate Data. Submittal date: 10/17/2001.
- 157184 MO0112DQRWLNYE.014. Well Completion Diagram for Borehole NC-EWDP-19P. Submittal date: 12/04/2001.
- 157187 MO0112DQRWLNYE.018. Well Completion Diagram for Borehole NC-EWDP-19D. Submittal date: 12/05/2001.
- 168375 MO0203GSC02034.000. As-Built Survey of Nye County Early Warning Drilling Program (EWDP) Phase III Boreholes NC-EWDP-10S, NC-EWDP-18P, and NC-EWDP-22S - Partial Phase III List. Submittal date: 03/21/2002.
- 162617 MO0205UCC008IF.001. Concentration Data Set for 2, 4-Difluorobenzoic Acid (2,4-DFBA) Tracer Used for the Feb/Mar 2002 Single Well Tracer Test at the Alluvial Tracer Complex. Submittal date: 05/01/2002.

- 168378 MO0206GSC02074.000. As-Built Survey of Nye County Early Warning Drilling Program (EWDP) Phase III Boreholes, Second Set. Submittal date: 06/03/2002.
- 161274 MO0212SPANYESJ.149. Nye County Well ONC-1 Temperature and Pressure Data 03/01/1996 through 12/22/1997. Submittal date: 12/09/2002.
- 165876 MO0306NYE05259.165. Revised NC-EWDP-19IM1 Well Completion Diagram. Submittal date: 07/02/2003.
- 179376 MO0306NYE05264.170. Revised NC-EWDP-22S Well Completion Diagram. Submittal date: 07/03/2003.
- 179377 MO0306NYE05265.171. Revised NC-EWDP-22PA Well Completion Diagram. Submittal date: 07/03/2003.
- 179378 MO0306NYE05266.172. Revised NC-EWDP-22PB Well Completion Diagram. Submittal date: 07/03/2003.
- 164821 MO0308SPATRCRC.000. Concentration Data for “2,3,4,5-Tetrafluorobenzoic Acid” Used for Tracer Testing at the C-Well Complex. Submittal date: 08/19/2003.
- 168534 MO0401COV03168.000. Coverage: NCEWDPS. Submittal date: 01/27/2004.
- 171464 MO0408NYE05474.217. UE-25 ONC#1 Pressure and Temperature Data, April 1995 - November 1999. Submittal date: 08/30/2004.
- 177373 MO0411NYE06360.302. EWDP Manual Water Level Measurements through June 2004. Submittal date: 11/08/2004.
- 175275 MO0503GSC05025.000. As-Built Location of Nye County Early Warning Drilling Program (EWDP) Phase V Borehole Number NC-EWDP-22PC. Submittal date: 03/10/2005.
- 179599 MO0505NYE06464.314. NC-EWDP-22PC Well Completion Diagram. Submittal date: 05/16/2005.
- 175064 MO0508SEPFELA.002. LA FEP List and Screening. Submittal date: 08/22/2005.
- 180070 MO0703U25CHPTL.000. Borehole U-25 C-Hole Complex Packer and Transducer Locations. Submittal date: 03/21/2007.
- 172179 TMUE25C3000095.001. Geophysical Logs for UE-25 C#3. Submittal date: 11/14/1995.
- 162614 UN0102SPA008KS.003. Concentration Dataset for Tracers (2, 6-Difluorobenzoic Acid and Iodide) Used for 48 Hour Shut in Tracer Test at the Alluvial Tracer Complex in Nye County. Submittal date: 06/11/2001.

- 162442 UN0109SPA008IF.006. Concentration Dataset for Tracers (2,4-Difluorobenzoic Acid and Chloride) Used for the 30-Day Shut in Tracer Test at the Alluvial Tracer Complex in Nye County Nevada. Submittal date: 09/28/2001.
- 162615 UN0109SPA008KS.007. Concentration Dataset for Tracer (Pentafluorobenzoic Acid) Used for the 30Day-Shut in Tracer Test at the Alluvial Tracer Complex in Nye County Nevada. Submittal date: 09/21/2001.
- 162616 UN0109SPA008KS.008. Concentration Dataset for Tracer (Bromide) Used for the 30 Day-Shut in Tracer Test at the Alluvial Tracer Complex in Nye County Nevada. Submittal date: 09/21/2001.

8.4 OUTPUT DATA, LISTED BY DATA TRACKING NUMBER

GS030208312314.001. Filtered Water Level Data for UE-25 ONC-1. Submittal date: 02/28/2003.

GS030208312314.002. Filtered Water Level Data For USW-H4, UE-25 WT#3 and UE-25 WT#14. Submittal date: 02/28/2003.

GS031008312314.004. Hydraulic Parameters from Analysis of Hydraulic Tests Conducted in the Fractured Tuff at the C-hole Complex from 1995 to 1999. Submittal date: 10/09/2003.

GS031008312315.002. Transport Parameters from Analysis of Conservative (Non-Sorbing) Tracer Tests Conducted in the Fractured Tuff at the C-hole Complex from 1996 to 1999. Submittal date: 10/09/2003.

GS031008312316.002. Hydraulic Parameters from Analysis of Hydraulic Tests Conducted in the Alluvium at the Alluvial Testing Complex (ATC), and Total Porosity from Grain-size Distribution and from Background Monitoring. Submittal Date: 10/09/2003.

GS031008312316.003. Transport Parameters and Specific Discharge from Analysis of Single-Hole Tracer Tests Conducted in the Alluvium at the Alluvial Testing Complex (ATC), and Total Porosity from the Borehole-Gravimetry Survey at NC-EWDP-19D1. Submittal Date: 10/09/2003.

LA0303PR831231.001. Simulations Conducted to Predict Tracer Responses from Single-Well and Cross-Hole Tracer Tests at the Alluvial Testing Complex. Submittal date: 03/20/2003.

LA0303PR831231.002. Estimation of Groundwater Drift Velocity from Tracer Responses in Single-Well Tracer Tests at the Alluvial Testing Complex. Submittal date: 03/18/2003.

LA0303PR831231.003. Solute Data From ER-20-6#3 in the BULLION Forced-Gradient Field Tracer Test At The ER-20-6 Wells at NTS. Submittal date: 02/03/2003.

LA0303PR831231.005. Simple Calculations for SZ In-Situ Testing AMR. Submittal date: 03/19/2003.

LA0303PR831341.001. Calculations and Plots Associated with C-wells Cation Exchange Capacity Measurements. Submittal date: 04/08/2003.

LA0303PR831341.002. Model Interpretations of Alluvium Testing Complex Lithium Sorption Experiments. Submittal date: 04/16/2003.

LA0303PR831341.003. Model Interpretations of C-wells Lithium Sorption Experiments. Submittal date: 04/16/2003.

LA0303PR831352.001. Calculations to Determine Detachment Rate Constant of Microspheres in a Single-Well Tracer Test in Saturated Alluvium. Submittal date: 03/31/2003.

LA0303PR831361.002. Model Interpretations of ATC Alluvium-Packed Column Transport Experiments. Submittal date: 04/16/2003.

LA0303PR831361.003. Model Interpretations of C-wells Crushed Rock Column Experiments. Submittal date: 04/16/2003.

LA0303PR831361.004. Model Interpretations of C-wells Fractured Core Transport Experiments. Submittal date: 04/02/2003.

LA0303PR831362.001. Model Interpretations of C-wells Diffusion Cell Experiments. Submittal date: 04/02/2003.

LA0304PR831231.001. C-wells Tracer Test Sensitivity Calculations. Submittal date: 04/17/2003.

LA0403PR831231.001. Simulations Conducted to Generate a Spreadsheet that can be Used for Predictions of Mean, Peak, and First Tracer Arrival Times in Field Tracer Tests. Submittal date: 04/18/2004.

LA0403PR831231.001. Simulations Conducted to Generate a Spreadsheet that can be Used for Predictions of Mean, Peak, and First Tracer Arrival Times in Field Tracer Tests. Submittal date: 04/18/2004.

LA0701EK150304.001. Interpretations of 2002-2003 Cross-Hole Hydraulic Aquifer Tests Conducted at Nye County Site 22 (NC-EWDP Site 22). Submittal date: 01/30/2007.

LA0701PR150304.001. Estimates of Specific Discharge and Seepage (Drift) Velocity At NC-EWDP Site 22 Based on Single-Well Tracer Responses. Submittal date: 01/02/2007.

LA0701PR150304.002. RELAP V2.0 Interpretations of Lithium, Bromide, 2,4,5 TFBA, 2,6 DFBA and Microsphere Breakthrough Curves in First Cross-Hole Tracer Test at NC-EWDP Site 22. Submittal date: 01/02/2007.

LA0701PR150304.003. RELAP V2.0 Interpretations of Iodide and Rhenium (as Perrhenate) Breakthrough Curves in Second Cross-Hole Tracer Test at NC-EWDP Site 22. Submittal date: 01/02/2007.

LA0701PR150304.004. Estimates of Specific Discharge and Seepage (Drift) Velocity at NC-EWDP Site 22 Based on Responses of Crosshole Test #1 Tracers after Extended Flow Interruption. Submittal date: 01/02/2007.

LA0701PR150304.006. RELAP V2.0 Interpretations of Lithium, Bromide, 2,4,5 TFBA, and Microsphere Breakthrough Curves in First Cross-Hole Tracer Test at NC-EWDP Site 22 Assuming the Largest Possible Differences Between the Normalized Concentrations of Bromide and 2,4,5 TFBA. Submittal date: 01/02/2007.

LA0701PR150304.007. MULTRAN V1.0 Simulations of Solute Tracer Responses Between NC-EWDP-22PA And -22S In The First Crosshole Tracer Test at NC-EWDP Site 22 and of Solute Tracer Responses in the First and Second Single-Well Tracer Tests at NC-EWDP Site 22. Submittal date: 01/02/2007.

LA0704PR150304.001. Site 19 and 22 Geochemistry Profiles. Submittal Date: 04/26/2007.

SN0302T0502203.001. Saturated Zone Anisotropy Distribution Near the C-wells. Submittal date: 02/26/2003.

SN0302T0502203.001. Saturated Zone Anisotropy Distribution Near the C-wells. Submittal date: 02/26/2003.

SN0409T0502203.002. Cooper-Jacob Transmissivity and Storativity Analysis of Wells UE-25 ONC-1, UE-25 WT#3, UE-25 WT#14, And USW H4. Submittal date: 09/23/04.

SN0409T0502203.002. Cooper-Jacob Transmissivity and Storativity Analysis of Wells UE-25 ONC-1, UE-25 WT#3, UE-25 WT#14, And USW H4. Submittal date: 09/23/04.

8.5 SOFTWARE CODES

159064 *EQUILFIT* V. 1.0. 2002. Windows 2000/NT 4.0/98. STN: 10668-1.0-00.

- 159067 Software Code: *2WELLS_2D* VV1.0. 2002. PC, Windows 2000/NT 4.0/98. 10665-1.0-00.
- 159036 *2WELLS_3D* V. 1.0. 2002. WINDOWS 2000/NT 4.0/98. STN: 10667-1.0-00.
- 159063 Software Code: *DIFFCELL* VV2.0. 2002. PC, Windows 2000/NT. 10557-2.0-00.
- 159068 Software Code: *MULTRAN* VV1.0. 2002. PC, Windows 2000/NT 4.0. 10666-1.0-00.
- 159065 Software Code: *RELAP* VV2.0. 2002. PC, Windows 2000/NT. 10551-2.0-00.
- 159066 Software Code: *RETRAN* VV2.0. 2002. PC, Windows 2000/NT. 10552-2.0-00.
- 161725 *FEHM* V. 2.20. 2003. SUN 9.S. 5.7 & 5.8, Windows 2000, RedHat Linux 7.1. STN: 10086-2.20-00.
- 162668 *Filter.vi* V. 1. 2002. WINDOWS 2000/NT 4.0/98. STN: 10970-1-00.
- 162752 *MOENCH.vi*, Function(2) V. 1.0. 2002. WINDOWS 2000/NT 4.0/98. STN: 10582-1.0-00.
- 162754 *Neuman.vi* V. 1.0. 2002. WINDOWS 2000/NT 4.0/98. STN: 10972-1.0-00.
- 162750 *rcv2amos.exe and MOENCH.vi*, Function(1) V. 1.0. 2002. WINDOWS 2000/NT 4.0/98. STN: 10583-1.0-00.
- 162758 *Theis.vi* V. 1.0. 2002. WINDOWS 2000/NT 4.0/98. STN: 10974-1.0-00.
- 162749 *Injection_Pumpback.vi* V. 1. 2003. Windows 2000/98/NT 4.0. STN: 10675-1.0-00.
- 164432 *RECIRC.vi* V. 1.0. 2003. Windows 98/NT 4.0/2000. STN: 10673-1.0-00.
- 162756 *Streltsova-Adams.vi* V. 1. 2003. WINDOWS 2000/98/NT 4.0. STN: 10971-1.0-00.
- 161564 *PEST* V. 5.5. 2002. SUN O.S. 5.7 & 5.8, WINDOWS 2000, RedHat 7.3. STN: 10289-5.5-00.

INTENTIONALLY LEFT BLANK

APPENDIX A
QUALIFICATION OF EXTERNAL SOURCES

A1. INTRODUCTION

External sources have provided unqualified data that have been used as direct input to this document. The inputs from these sources are qualified for intended use within the document using the process found in SCI-PRO-005, *Scientific Analyses and Calculations* and the methods and attributes required for qualification of data per SCI-PRO-001, *Qualification of Unqualified Data*. The following information is provided for each source: the full reference citation, a description of the data used from the source, the extent to which the data demonstrate the properties of interest, the data qualification method(s) used, rationale for selection of method(s), acceptance criteria to determine if the data are qualified, and the decision as to the qualification of the data.

The process described above meets the requirements of SCI-PRO-005 and provides justification that the data used from these sources are considered to be qualified for intended use.

A2. EVALUATION OF SOME NEW TRACERS FOR SOIL WATER STUDIES

A2.1 REFERENCE

[DIRS 156645] **Bowman, R.S., 1984.** "Evaluation of Some New Tracers for Soil Water Studies." *Soil Science Society of America Journal*, 48, (5), 987-993. Madison, Wisconsin: Soil Science Society of America. TIC: 251011.

A2.2 DESCRIPTION OF EXTERNAL SOURCE DATA

The journal article by Bowman (1984 [DIRS 156645]) is cited in Section D1.2.1.3 as the source for the free-water diffusion coefficient of 2,4,5 trifluorobenzoic acid (TFBA), which was used as a tracer in a cross-hole tracer test conducted in the Prow Pass interval at the C-wells. Specifically, data presented by Bowman (1984 [DIRS 156645], Table 2) were used in conjunction with data for the free-water diffusion coefficient of iodide ion taken from a journal article by Skagius and Neretnieks (1986 [DIRS 156862]) to establish a *ratio* of 2,4,5 TFBA and iodide diffusion coefficients used in the interpretation of the tracer test described in Section D1.2.1.3. The absolute values of tracer diffusion coefficients are not important—only their ratio is used in the calculations.

A2.3 EXTENT TO WHICH THE DATA DEMONSTRATE THE PROPERTIES OF INTEREST

Bowman (1984 [DIRS 156645]) based his data on correlations of free-water diffusion coefficients and molecular/ionic size, and also as on limited diffusion coefficient data for fluorinated benzoates structurally similar to 2,4,5 TFBA. A single value was selected from Table 2 of the article (Bowman 1984 [DIRS 156645]) to represent the diffusion coefficient of 2,4,5 TFBA. The actual property of interest is the diffusion coefficient in the saturated rock matrix rather than the free-water diffusion coefficient, but it is assumed that the ratio of matrix diffusion coefficients is the same as the ratio of free-water diffusion coefficients (and only a ratio is used in the calculations). The results of the diffusion cell experiments described in Section E2 indicate that this is a very reasonable assumption.

Data Qualification Method: SCI-PRO-001, Attachment 3, Method 5 (Technical Assessment).

This method was selected because the data were published in a scientific journal and the data collection procedures are unavailable for review.

The qualification process attribute, selected from SCI-PRO-001, Attachment 4, is attribute 8. The Acceptance Criteria are: (1) the data were published in a recognized scientific journal, and (2) the data were subjected to the peer review process.

A2.4 DISCUSSION OF DATA WITH RESPECT TO ATTRIBUTES

Bowman (1984 [DIRS 156645]) published his work in *Soil Science Society of America Journal* (SSAJ), a professional scientific research journal dedicated to publications on soil science and geochemistry. It is sponsored and published by the Soil Science Society of America. Contributions to the journal are evaluated for scientific merit by thorough professional review. Peer review is an essential and integral aspect of the SSSAJ. The SSSAJ uses a double-blind review format. Authors are anonymous to reviewers and reviewers are anonymous to authors. The fundamental role of the reviewers is to advise the associate editor on the technical virtues, or lack thereof, of a manuscript submitted for publication, and the associate editor, in turn, provides recommendations to the technical editor regarding the suitability of the manuscript for publication in the journal. The author is notified of all reviewer comments in writing, and the manuscript is either accepted or rejected for publication. In most cases, acceptance is conditional on revising the manuscript (per reviewer and editor comments) as necessary to meet publication standards. Rejected manuscripts can typically be revised significantly to address reviewer and/or editor comments and then resubmitted for consideration for publication.

Decision: The criteria for qualification were satisfied and the data are qualified for its intended use.

A3. POROSITIES AND DIFFUSIVITIES OF SOME NONSORBING SPECIES IN CRYSTALLINE ROCKS

A3.1 REFERENCE

[DIRS 156862] **Skagius, K. and Neretnieks, I., 1986.** "Porosities and Diffusivities of Some Nonsorbing Species in Crystalline Rocks." *Water Resources Research*, 22, (3), 389-398. Washington, D.C.: American Geophysical Union. TIC: 225291.

A3.2 DESCRIPTION OF EXTERNAL SOURCE DATA

The Skagius and Neretnieks (1986 [DIRS 156862]) journal article is cited in Section D1.2.1.3 as the source for the free-water diffusion coefficient of iodide ion, which was used as a tracer in a cross-hole tracer test conducted in the Prow Pass interval at the C-wells. Specifically, data presented by Skagius and Neretnieks (1986 [DIRS 156862])) were used in conjunction with an estimate of the free-water diffusion coefficient of 2,4,5-TFBA taken from the Bowman (1984 [DIRS 156645]) article to establish a *ratio* of 2,4,5 TFBA and iodide diffusion coefficients used in the interpretation of the tracer test described in Appendix D, Section D1.2.1.3. The absolute

values of the tracer diffusion coefficients are not important – only their ratio is really used in the calculations.

A3.3 EXTENT TO WHICH THE DATA DEMONSTRATE THE PROPERTIES OF INTEREST

Skagius and Neretnieks (1986 [DIRS 156862]) report a single value (Tables 2 and 3) for the free-water diffusion coefficient of iodide ion. The actual property of interest is the diffusion coefficient in the saturated rock matrix rather than the free-water diffusion coefficient, but it is assumed that the ratio of matrix diffusion coefficients is the same as the ratio of free-water diffusion coefficients (and only a ratio is used in the calculations). The results of the diffusion cell experiments described in Section E2 suggest that this is a very reasonable assumption.

Data Qualification Method: SCI-PRO-001, Attachment 3, Method 5 (Technical Assessment).

This method was selected because the data were published in a scientific journal and the data collection procedures are unavailable for review.

The qualification process attribute, selected from SCI-PRO-001, Attachment 4, is attribute 8. The Acceptance Criteria are: (1) the data were published in a recognized scientific journal, and (2) the data were subjected to the peer review process.

A3.4 DISCUSSION OF DATA WITH RESPECT TO ATTRIBUTES

Skagius and Neretnieks (1986 [DIRS 156862]) published their work in *Water Resources Research*, a professional scientific research journal dedicated to “the social and natural sciences of water.” It has long been recognized as one of the premier technical journals in the world for hydrology and contaminant transport. It is sponsored and published by the American Geophysical Union. Contributions to the journal are evaluated for scientific merit by thorough professional review. Peer review is an essential and integral aspect of *Water Resources Research*. Each manuscript submission is assigned to an associate editor, who then assigns at least two independent technical reviewers with expertise on the subject matter to thoroughly review the manuscript. These reviews are done anonymously. The associate editor also, generally, conducts a less-detailed technical review of the manuscript. The reviewers advise the associate editor on the technical virtues, or lack thereof, of the manuscript, and the Associate Editor then makes a decision regarding the suitability of the manuscript for publication. The author is notified of manuscript acceptance or rejection, and is provided all reviewer comments in writing. In most cases, acceptance is conditional on revising the manuscript (per reviewer and editor comments) as necessary to meet publication and scientific standards. Rejected manuscripts can typically be revised significantly to address reviewer and/or editor comments and then resubmitted for consideration for publication.

Decision: The criteria for qualification were satisfied and the data are qualified for its intended use.

A4. ELECTROCHEMICAL SYSTEMS

A4.1 REFERENCE

- [DIRS 148719] **Newman, J. 1973.** *Electrochemical Systems*. Englewood Cliffs, New Jersey: Prentice-Hall. TIC: 210201.
- [DIRS 108567] **Robinson, R.A. and Stokes, R.H. 1965.** *Electrolyte Solutions, The Measurement and Interpretation of Conductance, Chemical Potential and Diffusion in Solutions of Simple Electrolytes*. 2nd Edition (Revised). Washington, D.C.: Butterworth. TIC: 242575.

A4.2 DESCRIPTION OF EXTERNAL SOURCE DATA

Electrochemical Systems (Newman 1973 [DIRS 148719], p. 230, Table 75-1) is cited in Appendix D as a source for the free-water diffusion coefficients of bromide and lithium ions. The *ratio* of the free-water diffusion coefficients of these ions was assumed to be equal to the ratio of their matrix diffusion coefficients for the interpretation of the C-wells cross-hole tracer tests in which both ions are used as tracers. Basing the ratio of matrix diffusion coefficients of lithium and bromide on free-water diffusion coefficient values is justified given that the free-water and matrix diffusion coefficient ratios for pentafluorobenzoate and bromide are almost identical based on the data in Table D-4 and the diffusion cell data of Section E.2. However, this ratio had to be modified to account for other factors.

Newman (1973 [DIRS 148719], Table 75-1) reports the bromide-to-lithium diffusion coefficient ratio is approximately 2:1. The ratio used in the analyses of the C-wells tracer was modified to 3:2 (with bromide larger) because the values reported by Newman (1973 [DIRS 148719], Table 75-1) are based on ionic conductances at *infinite dilution*, not on data or correlations applicable at the high ionic concentrations present in the tracer test solutions. The justification for using an effective ratio of 3:2 instead of 2:1 is that when a cation and an anion dominate the ionic strength of a solution (as in the case of Li^+ and Br^- in the tracer solutions), they cannot diffuse independently of each other because local charge balance must always be maintained. In the extreme case of having only one cation and one anion in solution (i.e., a binary electrolyte), the anion and cation would have exactly the same effective diffusion coefficient (a value that falls in between the diffusion coefficients of each ion at infinite dilution) because their charges cannot be separated. Given that there were other ions in solution besides Li^+ and Br^- , and that Li^+ and Br^- should have been diluted significantly in the flow system after tracer injection, a ratio of 3:2 was thought to be a reasonable interpolation between the 2:1 ratio at infinite dilution and the 1:1 ratio that would exist in a perfect binary solution of LiBr. The absolute values of the ion diffusion coefficients are not important for the tracer test analysis – only their ratio is used in the calculations.

A4.3 EXTENT TO WHICH THE DATA DEMONSTRATE THE PROPERTIES OF INTEREST

Newman (1973 [DIRS 148719], Table 75-1) reports values for free-water diffusion coefficients of many ions (including Li^+ and Br^-) based on ionic conductances at infinite dilution. Free-water diffusion coefficients of ions are always measured for cation-anion pairs rather than for

individual ions because individual ions cannot be spatially separated in solution (local charge balance cannot be violated). If the effective free-water diffusion coefficient of an ion pair is measured and the conductance of the solution is also measured, it is possible to determine the conductance that each individual ion contributes to the overall solution conductance. This determination is made by simultaneously solving Newman's equations 75-2 and 75-7 (1973 [DIRS 148719]) using the Nernst-Einstein relation (Newman 1973 [DIRS 148719], Eq. 75-6) to express the ionic diffusion coefficients in terms of ionic conductances. Typically, the measurements are repeated at several different concentrations of the ion-pair, and the results are extrapolated to zero concentration to obtain the ionic conductances at infinite dilution (which is what is usually reported in the literature). Once the ionic conductances are known for a specific ion pair, the ionic conductances of other ions can be easily determined by measuring the conductances of solutions in which one of the known ions is paired with the ion to be determined (the overall solution conductance is the sum of the ionic conductances). Ionic diffusion coefficients are then calculated from the ionic conductances using the Nernst-Einstein relation. This indirect method of determining ionic diffusion coefficients is employed because it is much easier to measure solution conductances than it is to measure diffusion coefficients of ion pairs.

Data Qualification Method: SCI-PRO-001, Attachment 3, Method 5 (Technical Assessment).

This method was selected because the data was published in a technical book and the data collection procedures are unavailable for review.

The qualification process attributes, selected from SCI-PRO-001, Attachment 4 are attributes 7 and 8. The Acceptance Criteria are: (1) the data have been widely used in other scholarly applications, and (2) the data have received scientific review during the publication process.

A4.5 DISCUSSION OF DATA WITH RESPECT TO ATTRIBUTES

Electrochemical Systems (Newman 1973 [DIRS 148719]) is a widely used and widely cited textbook recognized as an authoritative reference on electrochemical systems. Although he provides no specific citations, the ionic conductances and diffusion coefficients in his Table 75-1 (Newman 1973 [DIRS 148719]) are a compilation of values that can be found in many other reference books and peer-reviewed publications. Most of the ionic conductances in his table can be found in the classic reference book, *Electrolyte Solutions* (Robinson and Stokes 1965 [DIRS 108567]). It is quite likely that Newman (1973 [DIRS 148719]) compiled much of his Table 75-1 from the information in this source. In summary, the values of ionic conductance (and hence ionic diffusion coefficients) in Newman's Table 75-1 (1973 [DIRS 148719]) have been in widespread use for several decades, and they are generally accepted as established fact in the scientific literature on electrolyte solutions.

Decision: The criteria for qualification were satisfied and the data are qualified for its intended use.

INTENTIONALLY LEFT BLANK

APPENDIX B

WELLS

Table B-1. Wells Discussed in This Report and Their Abbreviations

Name	Abbreviation
NC-EWDP-4PA, NC-EWDP-4PB	N/A*
NC-EWDP-10S, NC-EWDP-10P	10S, 10P
NC-EWDP-15P	N/A
NC-EWDP-19D	19D
NC-EWDP-19IM1, NC-EWDP-19IM2	19IM1, 19IM2
NC-EWDP-19P	19P
NC-EWDP-19PB	19PB
NC-EWDP-22PA	22PA
NC-EWDP-22PB	22PB
NC-EWDP-22PC	22PC
NC-EWDP-22S	22S
UE-25 b#1	b#1
UE-25 c#1	c#1
UE-25 c#2	c#2
UE-25 c#3	c#3
UE-25 ONC-1	ONC-1
UE-25 p#1	p#1
UE-25 J-13	J-13
UE-25 WT#3	WT#3
UE-25 WT#13	WT#13
UE-25 WT#14	WT#14
UE-25 WT#17	WT#17
USW H-4	H-4
USW WT#1	WT#1
Washburn-1X	N/A

NOTE: N/A means that an abbreviation is not used for that well in this report.

INTENTIONALLY LEFT BLANK

APPENDIX C

**DETAILS OF HYDRAULIC TESTING AND TEST INTERPRETATIONS AT THE
C-WELLS COMPLEX**

C1. INTRODUCTION

The hydrologic properties of the fractured tuffs at Yucca Mountain were obtained as part of investigations of the hydrologic and geologic suitability of Yucca Mountain as a high-level nuclear waste repository by the U.S. Geological Survey (USGS) in cooperation with the U.S. Department of Energy. Five cross-hole hydraulic tests, some in conjunction with tracer tests, were conducted by the USGS at the C-wells complex in May and June 1995, February 1996, from May 1996 to November 1997, and between June and September 1998. The first test, conducted in May 1995, is documented by Geldon et al. (1998 [DIRS 129721]). The second through fourth tests (June 1995, February 1996, and May 1996 to November 1997) are documented by Geldon et al. (2002 [DIRS 161163]) and reproduced in this report. The fifth test, conducted between June and September 1998, is only described in this report.

This appendix describes the hydraulic tests conducted, the changes in water levels in monitoring wells as a result of pumping, and analyses performed on the C-wells hydraulic test data. Estimates of aquifer transmissivity, hydraulic conductivity, and storativity were obtained by analyzing the test data using various analytical (as opposed to numerical) solutions of the groundwater flow equation, which assume a radial flow regime to the pumping well, constant aquifer thickness, and a homogeneous and isotropic medium. In order to calculate anisotropy in the horizontal hydraulic conductivity, analytic solutions of the groundwater flow equation for homogeneous, anisotropic media were employed.

These analytic solutions provide first-order estimates of hydrologic parameters consistent with both the limited knowledge of the nature and extent of subsurface heterogeneities in the fractured volcanics at the scale of the C-wells complex and the manner in which hydrologic parameter estimates are used in the site-scale saturated zone (SZ) flow model. The analytical methods assume that the test interval has one average transmissivity and storativity value between the pumping well and the observation well. Similarly, the SZ flow model assumes that single average intrinsic hydrologic property (i.e., permeability, porosity) values apply to individual stratigraphic intervals over large spatial areas in the SZ flow system. Furthermore, the hydrologic parameters derived from C-wells testing are not used as direct inputs in the site-scale SZ flow model, but, rather, they are used primarily for qualitative/corroborative consistency checks with the hydrologic parameters derived from calibrations of the SZ flow model. Because of this qualitative end use of the parameter estimates, detailed analyses of the uncertainty and nonuniqueness of the estimates were not conducted.

At the C-wells complex, several analytic solutions to the groundwater flow equation were used. Following are the dominant modes of analysis used for each geohydrologic interval or aquifer. Details of these solutions and exceptions to the dominant modes presented here are found in Section C4. To analyze responses in the Calico Hills aquifer, which is at the water table, the Neuman (1975 [DIRS 150321]) unconfined-aquifer solution was used to successfully analyze five out of six responses in this aquifer among the various tests. To analyze the Prow Pass aquifer and the Upper Bullfrog and Lower Bullfrog aquifers, which are confined below the largely unconfined Calico Hills aquifer, either confined single-porosity (Theis 1935 [DIRS 150327]) or confined dual-porosity (Streltsova-Adams 1978 [DIRS 150754]) solutions were mostly used, depending upon whether the test duration was long enough for the fractured-rock aquifers to exhibit their dual-porosity character. To analyze the Upper Tram

aquifer, which is intersected by the known faults present at the bottom of the C-wells that provide a source of recharge or “leakage,” the leaky-confined Hantush (1956 [DIRS 165169]) solution was used successfully for all tests.

C1.1 EARLIER STUDIES

Before the in situ testing of the fractured tuffs at Yucca Mountain began in May 1995 (Geldon et al. 1998 [DIRS 129721]), studies were conducted to determine hydrogeologic intervals of the rocks, flow patterns, geologic influences, geologic properties of the rocks, and the hydraulic results of an open-hole test in one of the C-wells. Most of these studies have been published and are referred to in this section. Hydrogeologic intervals discussed in this report were identified by Geldon (1996 [DIRS 100396], pp. 9 to 69) on the basis of borehole geophysical logs, borehole flow surveys, cross-hole seismic tomography, and aquifer tests. Geophysical logs run in the C-wells include caliper, borehole-deviation, temperature, resistivity, gamma-gamma, acoustic, epithermal neutron, acoustic televiewer, and television logs (Geldon 1993 [DIRS 101045], pp. 14 to 18). Flow surveys run in the C-wells include tracejector, heat-pulse flowmeter, spinner, and oxygen-activation surveys (Geldon 1993 [DIRS 101045], pp. 14 to 18; 1996 [DIRS 100396], pp. 12 to 69). Tracejector surveys using radioactive iodide were run in the C-wells during hydraulic tests conducted in 1983 and 1984. Heat-pulse flowmeter surveys were run in 1991 without the boreholes being pumped. Spinner and oxygen-activation surveys were run in Borehole c#3 during the hydraulic test in June 1995 (described in Section A3.1). In 1993, a seismic tomogram was conducted between Boreholes c#2 and c#3 by Lawrence Berkeley National Laboratory (LBNL) for, and reported to, the USGS by written communication from E. Majer, LBNL (Geldon et al. 2002 [DIRS 161163], p. 2). That tomogram showed many of the hydrogeologic details evident from borehole lithologic and geophysical logs and flow surveys.

Hydrologic properties of the intervals in the C-wells and the manner in which they transmit water were determined provisionally by Geldon (1996 [DIRS 100396], pp. 12 to 69) from geophysical logs, laboratory analyses, and aquifer tests. A matrix-porosity profile for the C-wells was developed from a gamma-gamma log and nine values of core porosity obtained from c#1 in 1983 (Geldon 1993 [DIRS 101045], p. 62, Table 13). Geldon (1996 [DIRS 100396], pp. 9 to 69) developed a matrix-permeability profile for the C-wells from permeameter tests on 89 core samples obtained from the C-wells and four nearby boreholes between 1980 and 1984. Geldon (1996 [DIRS 100396], pp. 9 to 69) developed a hydraulic-conductivity profile for the C-wells by analyzing falling-head and pressure-injection tests done in c#1 in 1983. Transmissivity, hydraulic conductivity, and storativity of discrete intervals within the Calico Hills Formation and the Crater Flat Group were determined (Geldon 1996 [DIRS 100396], pp. 9 to 69) from analyses of a constant-flux injection test in c#2 and three hydraulic tests in c#2 and c#3 performed in 1984. Simultaneous monitoring of water-level and atmospheric-pressure fluctuations in 1993 established the barometric efficiency of the C-wells (Geldon et al. 1997 [DIRS 156827], p. 11). The open-hole hydraulic test determined the transmissivity, hydraulic conductivity, and storativity of the composite saturated thickness of Miocene tuffaceous rocks at the C-wells complex; lateral variations in hydrologic properties within a 3.2-km radius of the C-wells complex; and possible hydraulic connection between the tuffaceous rocks and the underlying regional aquifer composed of Paleozoic carbonate rocks (Geldon et al. 1998 [DIRS 129721], pp. 30 and 31).

A hydraulic test conducted at the C-wells complex from May 22 to June 12, 1995 (data reside in DTN: GS960108312313.001 [DIRS 164801]), indicated that the composite section of tuffaceous rocks in the vicinity of the C-wells has a transmissivity of 2,300 m²/day (square meters per day) and a storativity of 0.003 (Geldon et al. 1998 [DIRS 129721], p. 41). That test also indicated transmissivity values of 1,600 m²/day to 3,200 m²/day and storativity values of 0.001 to 0.003 for the rocks in individual boreholes (c#1, c#2, ONC-1, and USW H-4). Hydraulic tests conducted in 1984 indicated that those intervals have layered heterogeneity (Geldon 1996 [DIRS 100396], pp. 9 to 69).

C2. INSTRUMENTATION USED IN C-WELLS HYDRAULIC TESTING

Principal components of the equipment installed at the C-wells complex to conduct hydraulic tests from 1995 to 1997 are available commercially, but much of this hardware and software has not been used extensively because of its relatively recent development. Consequently, all of the equipment received extensive performance evaluation during prototype hydraulic tests conducted jointly with LBNL from 1992 to 1994 at a research site near Raymond, California. Modifications to system components and their assembly were made to address problems encountered during prototype testing and after the equipment was installed and initially used at the C-wells complex (Umari et al. 1994 [DIRS 164543], pp. 2,413 to 2,422). With few exceptions (discussed below), most system components performed to specifications, despite being operated almost continuously for more than two years.

C2.1 PACKERS

Dual-mandrel packers, manufactured by TAM International, Inc., were installed in c#1 and c#2 throughout the tests and in c#3 after August 1995. The packers are about 1.83-m long and have a deflated diameter of about 21.6 centimeters (cm) (see Geldon et al. 2002 [DIRS 161163], Figure 5). When inflated, the packers seal off the borehole to prevent upward or downward flow within the borehole, which effectively isolates “intervals” between the packers. Suspended on 7.30-cm-diameter tubing, each packer contains 12 pass-through tubes to allow packer-inflation lines and electrical cable to be installed in the borehole. The packers are inflated individually by injection of argon gas through 0.64-cm, stainless-steel tubing. Inflation pressures, which are about 1,034 kPa above hydrostatic pressure, range from about 2,758 kPa to 5,861 kPa at the depths at which packers were set in the C-wells from 1995 to 1997. Packer depths from 1995 to 1997, as measured from the land surface, are listed in Table C-1.

Table C-1. Location of Packers Emplaced in the C-Wells Complex for Hydraulic Tests, 1995 to 1997

Packer Number	Packer Depth (m below land surface)			
	UE-25 c#1	UE-25 c#2	UE-25 c#3	
			August 1995 to April 1996	April 1996 to November 1997
1	547.4 to 549.3	531.3 to 533.1	540.4 to 542.2	None
2	605.3 to 607.2	605.6 to 607.5	609.9 to 611.7	None
3	698.3 to 700.1	696.5 to 698.3	695.0 to 696.8	694.6 to 696.5
4	797.1 to 798.9	791.9 to 793.7	812.6 to 814.4	812.9 to 814.7
5	869.9 to 871.7	869.6 to 871.4	877.5 to 879.4	878.1 to 880.0

Source: DTN: MO0703U25CHPTL.000 [DIRS 180070].

Output DTN: GS031008312314.004 (Table 6.2-1).

NOTE: There were no packers in UE-25 c#3 before August 1995.

C2.2 TRANSDUCERS

Continuous records of pressures and temperatures in packed-off intervals during hydraulic tests were obtained using absolute pressure transducers (manufactured by Paroscientific, Inc), which record water pressure plus atmospheric pressure. The transducers used in the C-wells were strapped into brackets welded onto the 7.30-cm-diameter tubing on which the packers were suspended. Field determinations indicated a precision of 0.30 cm under pumping conditions and 0.061 cm under nonpumping conditions.

Although transducers were installed in all hydrogeologic intervals, several of the transducers failed after installation. Transducers operative during some or all of the hydraulic tests conducted from 1995 to 1997 and the locations of those transducers, as determined by subtracting recorded pressure heads from static water-level altitudes, are listed in Table C-2. Listed transducer altitudes have an accuracy of ± 0.3 m.

C2.3 BAROMETERS

A nonsubmersible, temperature-compensated pressure transducer, manufactured by Paroscientific, Inc., was used as a barometer during the 1995 to 1997 hydraulic tests. The barometer operated in a temperature-controlled office trailer at the C-wells complex. The factory-calibrated accuracy of this barometer is $\pm 0.005\%$ of its full operating range (103 kPa). The barometer was checked periodically against another barometer of the same type in the same office trailer.

C2.4 PUMPS

A 37-stage, 1,512 liters per minute (L/min) capacity, Centrilift submersible pump was used during the hydraulic test in June 1995. The pump was suspended in Borehole c#3 on 13.9-cm-diameter tubing. The pump intake depth was 450.1 m (48.0 m below the water-level altitude prior to pumping). The pump was powered by a 250-kW generator, and its frequency was regulated by a variable-speed controller. Water discharged by the pump was transported by a 15-cm-diameter pipeline to a leach field in Fortymile Wash, about 8 km from the C-wells complex.

Table C-2. Operative Transducers in the C-Wells, 1995 to 1997

Borehole	Interval	Transducer		
		Number	Depth (m)	Altitude (m)
UE-25 c#1	Prow Pass	2	552.09	578.51
	Upper Bullfrog	3	610.03	520.57
	Lower Bullfrog ^a	4	703.04	427.56
UE-25 c#2	Calico Hills	1	519.83	612.36
	Prow Pass	2	536.28	595.91
	Upper Bullfrog	3	610.70	521.49
	Lower Bullfrog ^a	4	701.58	430.61
UE-25 c#3	Calico Hills ^b	1	533.81	598.62
	Upper Bullfrog	3	614.49	517.93
	Lower Bullfrog ^c	4	708.93	423.49
	Upper Tram ^d	5	817.68	314.75

Sources: DTNs: GS031108312314.005 [DIRS 179648], GS981008312314.003 [DIRS 144464], GS981008312314.002 [DIRS 147068], GS010608312314.001 [DIRS 179647].

Output DTN: GS031008312314.004 (Table 6.2-2).

^aMonitored Lower Bullfrog and Upper Tram together, February to March 1996.

^bListed transducer locations are for August 1995 to March 1996. Prior to August 1995, a single transducer was installed in the Calico Hills interval at a depth of 441.12 m (altitude = 691.30 m) to monitor the composite geologic section in c#3. After April 1996, a new transducer was installed at a depth of 691.31 m (altitude = 441.11 m) to monitor the Calico Hills, Prow Pass, and Upper Bullfrog intervals combined.

^cOperative after April 1996.

^dMonitored Lower Bullfrog and Upper Tram together in February and March 1996; replaced in April 1996 by a transducer at a depth of 819.32 m (altitude = 313.11 m).

The original pump was replaced in August 1995 by a 43-stage, 756 L/min-capacity, Centrilt submersible pump. That pump, enclosed in a protective shroud, was offset from the main part of the 7.30-cm-diameter tubing on which the packers were suspended by a 22.9-m-long “Y-block” assembly (see Geldon et al. 2002 [DIRS 161163], Figure 6 for detailed drawing). The Y-block assembly was designed to allow wireline tool access past the pump for opening and closing sliding sleeves (screens installed to allow water movement to or from test intervals) and for placing a plug in the tubing to prevent recirculation of water through the pump shroud.

Although the Y-block assembly facilitated operations, its placement in the instrument string created problems that eventually caused pump performance to degrade beyond an acceptable level during hydraulic and tracer tests conducted in February and March 1996. Because the combined diameter of the Y-block assembly and main section of the instrument tubing (24.7 cm) was about the same as the borehole diameter below a depth of 463.4 m, the pump intake had to be set about 247 m above the top of the slotted section of pipe open in the test interval. Frictional head losses produced by water flowing through small openings (slots) in the intake tubing and through the tubing from the test interval to the pump intake caused the pump to operate at the limit of its designed performance range. Consequently, discharge decreased from 526.2 L/min when pumping started on February 8, 1996, to 370.8 L/min when pumping was terminated on March 29, 1996.

In April 1996, the pump-performance problem was addressed by (1) discarding the Y-block; (2) suspending a 72-stage, 756-L/min-capacity Centrifliff pump enclosed in a narrower shroud directly on the 7.30-cm-diameter tubing; (3) lowering the pump to within about 47 m of the interval to be tested; and (4) adding 6.1 m of slotted pipe in the test interval. From May 1996 to March 1997, the reconfigured pump assembly performed without major problems and sustained a relatively constant discharge of 560.4 to 590.4 L/min. Problems with one of the generators providing power to the pump caused the pump to operate erratically between March 26 and May 8, 1997, but the pump performed adequately again after the generator problem was resolved. These generator/pump problems had essentially no impact on the hydraulic test interpretations, as the responses in the C-wells were not quantitatively analyzed after March 26, 1997, and the responses in more distant wells were not significantly affected by the pumping perturbations.

C2.5 FLOWMETERS

A McCrometer turbine-type flowmeter was used during the hydraulic test in June 1995. Subsequently, the primary device used for monitoring discharge was a differential switched capacitor, vortex flowmeter manufactured by Endress and Hauser, measuring vortex frequency past a bluff body with signal output converted to voltage output across a temperature-controlled resistor.

The flowmeter signal was recorded at user-specified intervals by monitoring software installed on a personal computer in the office trailer at the C-wells complex (Section C2.6). The software program used a regression equation developed on the basis of the flowmeter calibration to convert the voltage signal from the flowmeter to a discharge rate.

C2.6 DATA ACQUISITION AND INSTRUMENT CONTROL

Data acquisition from and control of the transducers, barometer, flowmeter, and an automatic water sampler used for tracer tests was accomplished with the commercially available, graphic-language software program LabView (Johnson 1994 [DIRS 156837]). Installed on the personal computer in the office trailer, LabView enabled the PC monitor screen to look and act like an instrument panel.

Two separate “virtual instrument” routines were written for data acquisition and instrument control. One communicated with the transducers, barometer, and flowmeter; the other communicated with the automated water sampler during tracer tests. The two virtual instruments ran simultaneously, employed standard LabView functions for data acquisition and control, and performed no manipulations on the acquired data. Also, the acquired data in all cases constituted *input* data packages (DTNs) for this report; they are not product outputs. The only case in which raw acquired data was manipulated before being submitted to the Technical Data Management System (TDMS) was for flow meter readings, which were converted from voltages to flow rates in Excel spreadsheets prior to being submitted to the TDMS. These conversion calculations can be readily verified using simple formulas documented in the Yucca Mountain Project (YMP) RISweb system in records associated with data packages (see records roadmaps). For example, in the case of data package DTN: GS990408312315.002 [DIRS 140115], which contains flow rate data obtained during testing of the Prow Pass interval at the C-wells between 4/18/98 and 11/24/98, the supporting RISweb record (MOL.20010712.0251) contains the formulas supplied

by the calibration vendor for converting measured voltages to the flow rates that appear in the TDMS. These formulas were used in Excel spreadsheets contained on a CD-ROM referred to in another supporting record (MOL.20010712.0252). This approach was used consistently in going from raw data acquisition to data submittals for all hydraulic tests.

C3. RESULTS AND INTERPRETATIONS OF HYDRAULIC TESTS

The results and interpretations of the hydraulic tests discussed below include the conceptual models considered and tested.

C3.1 HYDRAULIC TESTS CONDUCTED BETWEEN JUNE 1995 AND NOVEMBER 1997

Three hydraulic tests were conducted at the C-wells complex from June 1995 to November 1997. During June 12 to June 22, 1995, well c#3 was pumped, without packers installed, and drawdown and recovery were measured in six hydrogeologic intervals (Figure C-5) separated by packers in wells c#1 and c#2 (Table C-1). From February 8 to February 13, 1996, c#3 was pumped, with packers inflated to isolate the Bullfrog-Tram interval, to establish a steady-state hydraulic gradient for a tracer test in the Bullfrog-Tram interval that continued until March 29, 1996. Drawdown was analyzed in the Bullfrog-Tram interval and in all other packed-off intervals of c#1 and c#2 that responded to pumping during the hydraulic test.

In the third hydraulic test, with packers inflated to isolate the Lower Bullfrog Tuff interval, c#3 was pumped for 553 days, from May 8, 1996 to November 12, 1997, before and during a series of tracer tests in the Lower Bullfrog interval. Drawdown was analyzed in this interval and in all other intervals of c#1 and c#2 that responded to pumping before mechanical problems developed on March 26, 1997. Drawdown was analyzed in UE-25 ONC-1 (ONC-1), USW H-4 (H-4), UE-25 WT#14 (WT#14), and UE-25 WT#3 (WT#3) for periods from 7 to 18 months to evaluate heterogeneity and scale effects in the Miocene tuffaceous rocks. Water levels in UE-25 p#1 (p#1), completed in Paleozoic carbonate rocks, were measured to detect a hydraulic connection between the Miocene tuffaceous rocks and the Paleozoic carbonate rocks in the vicinity of the C-wells.

C3.1.1 Analytical Methods

Although rock at the C-wells complex is fractured pervasively, hydrogeologic intervals respond to pumping in a manner consistent with an equivalent porous medium (EPM) (Geldon 1996 [DIRS 100396], pp. 12 to 69; Geldon et al. 1998 [DIRS 129721], pp. 29 to 31). To obtain estimates of hydrologic parameters, “type curves” from analytical solutions of drawdown versus time and distance corresponding to different conceptual aquifer flow models were matched to drawdown data in pumping tests. The following alternative aquifer models were considered for individual test intervals: EPM, confined fissure block, unconfined, and leaky confined. The analytical solution that provided the best match to a given data set with the least number of adjustable parameters was used for parameter estimation. Whenever it is stated in this section (Section C) that an interval responds as a given type of aquifer, this means the response is *consistent with* that type of aquifer and, therefore, that type of aquifer was assumed for parameter estimation purposes.

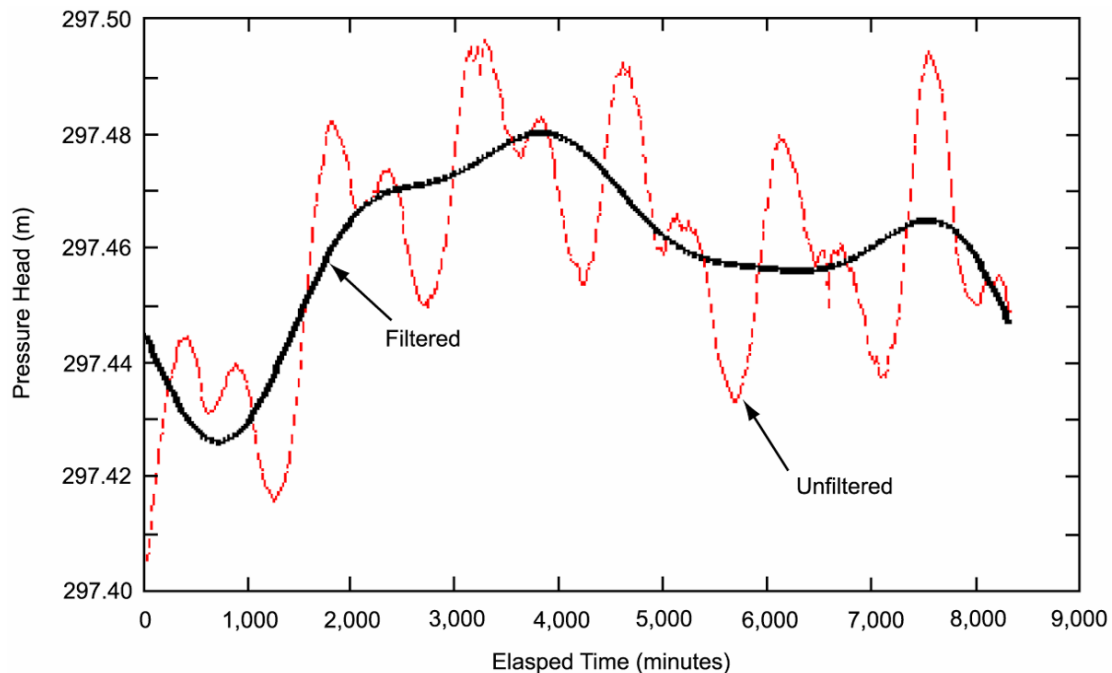
The Calico Hills interval in the vicinity of the C-wells complex typically responds to pumping as an anisotropic, unconfined aquifer, consistent with the fact that the water table occurs in this interval. With pervasive fracturing that apparently extends to the water table (Geldon et al. 2002 [DIRS 161163], p. 15), the Prow Pass and Upper Bullfrog intervals respond to pumping as either an unconfined, fissure-block, or confined aquifer. The Lower Bullfrog interval typically responds to pumping as a confined aquifer, consistent with the fact that it is isolated by layers of relatively unfractured, low-transmissivity rock. Apparently recharged by flow from fractures related to faults (identified on lithologic logs prepared by Richard W. Spengler and included in a report by Geldon (1993 [DIRS 101045], pp. 35 to 37, Table 4), the Upper Tram interval typically responds to pumping as a leaky, confined aquifer without confining bed storage.

Analytical methods used for hydraulic tests discussed in this section are those of Theis (1935 [DIRS 150327]) and Cooper and Jacob (1946 [DIRS 150245]) for infinite, homogeneous, isotropic, confined aquifers; Neuman (1975 [DIRS 150321]) for infinite, homogeneous, anisotropic, unconfined aquifers; and Streltsova-Adams (1978 [DIRS 150754]) for fissure-block aquifers. Geldon (1996 [DIRS 100396], pp. 21 to 69) discusses assumptions, equations, and application of these analytical methods in hydraulic tests at the C-wells complex. Analysis of drawdown in this study was restricted to observation wells because drawdown in pumping wells at the C-wells complex typically is too large and rapid to be explained solely by hydrologic properties of the pumped interval (Geldon 1996 [DIRS 100396], pp. 21 to 69). This observation can be illustrated by looking at the drawdown in c#3 at 464,000 minutes (322.22 days) after pumping began on May 8, 1996. That drawdown was 599 cm. With hydrologic properties computed for the Lower Bullfrog interval in c#1 and c#2 inserted into an approximation of the Theis (1935 [DIRS 150327]) equation, as given by Equation 19 of Lohman (1972 [DIRS 150250]), the drawdown in c#3 attributable to aquifer characteristics should have been no more than 69 cm to 72 cm after 322.22 days of pumping, or 12% of the actual recorded drawdown. Most of the drawdown in c#3 probably can be attributed to frictional head loss. Therefore, calculation of hydrologic properties from that drawdown is not reliable.

All of the analytical methods used in this study, except for the Neuman (1975 [DIRS 150321]) method, assume radial flow to the pumping well, and, therefore, ignore vertical flow (application of the Neuman fully penetrating-well solution, as was done in this report, to cases where pumping was in one interval and the analyzed drawdown response was in another, also ignores vertical flow). However, in hydraulic tests of the Bullfrog-Tram interval (February 1996) and the Lower Bullfrog interval (May 1996 to March 1997), drawdown was observed in the Calico Hills, Prow Pass, and Upper Bullfrog intervals, even though the sliding sleeves allowing direct communication between those intervals and the flow intake piping were not open. For water to reach the pumping well from the intervals that did not have open sliding sleeves, a downward component of flow must have occurred. The downward flow was assumed by the investigators to be much less than radial flow to the pumping well in order to analyze the drawdown from the nonopen intervals by the methods outlined here. Clearly, improved estimates of hydrologic parameters could be obtained using a three-dimensional numerical model to analyze the drawdowns in the nonpumped intervals by accounting for both horizontal and vertical flow. However, hydrologic properties calculated assuming radial flow have a reasonable level of confidence because they generally are consistent with quantitative results of the hydraulic test conducted in June 1995, which was designed such that flow from hydrogeologic intervals in c#1 and c#2 to c#3 would be largely radial.

C3.1.2 Earth Tides and Barometric Effects

Previous monitoring of water levels in observation wells before, during, and after hydraulic tests conducted in the C-wells indicated that all of those boreholes respond to Earth tides and atmospheric pressure changes. With frequencies of 0.9 cycles/day to 2.0 cycles/day (Galloway and Rojstaczer 1988 [DIRS 156826], p. 107, Table 2), Earth tides caused water levels in the C-wells to fluctuate as much as 12 cm during a 10-day hydraulic test conducted at the C-wells complex from May to June 1995 (Geldon et al. 1998 [DIRS 129721], Figure 21). Consequently, in the hydraulic testing described here, Earth-tide effects were removed from water levels, and cycles of the same frequency as Earth tides were removed from simultaneously recorded atmospheric pressures before computing the barometric efficiency of most borehole intervals. Earth-tide effects also were removed from the records of observation wells in which drawdown caused by pumping was expected to be obscured by Earth tides (Boreholes H-4, WT#14, WT#3, and p#1). The boreholes requiring an Earth-tide correction to water-level records were completed in Miocene tuffaceous rocks more than 1,500 m from c#3 or were completed in a different aquifer than that of the C-wells complex (i.e., in the Paleozoic carbonate rocks). Earth-tide effects were removed from records of water levels, and cycles of the same frequency as Earth tides were removed from simultaneously recorded atmospheric pressure by applying a low-pass filter with a cutoff frequency of 0.8 cycles/day to those records. As shown in Figure C-1, this filtering removes semi-diurnal changes in water levels while preserving longer-term trends.

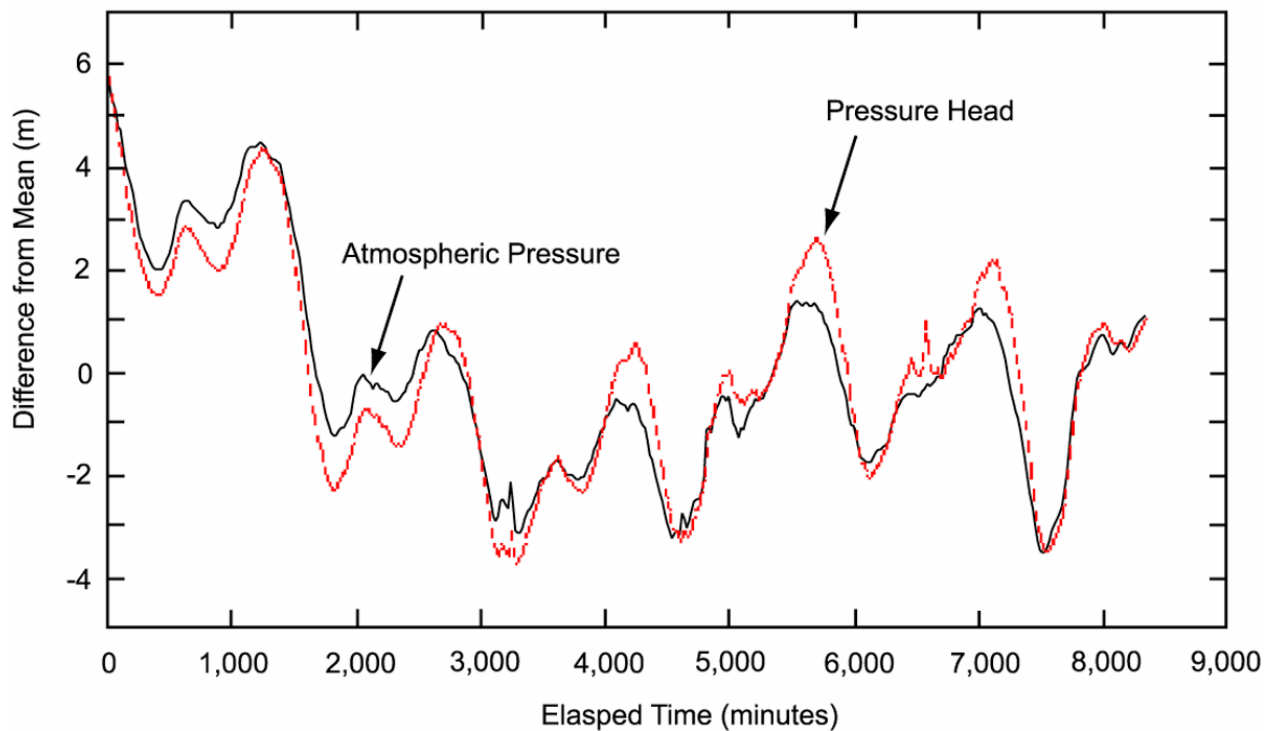


Source: Geldon et al. 2002 [DIRS 161163], Figure 7, p. 16.

NOTE: For illustration purposes only.

Figure C-1. Result of Filtering Out Earth Tides on UE-25 c#2 Lower Bullfrog Interval Pressure Heads, June 23 to 29, 1995

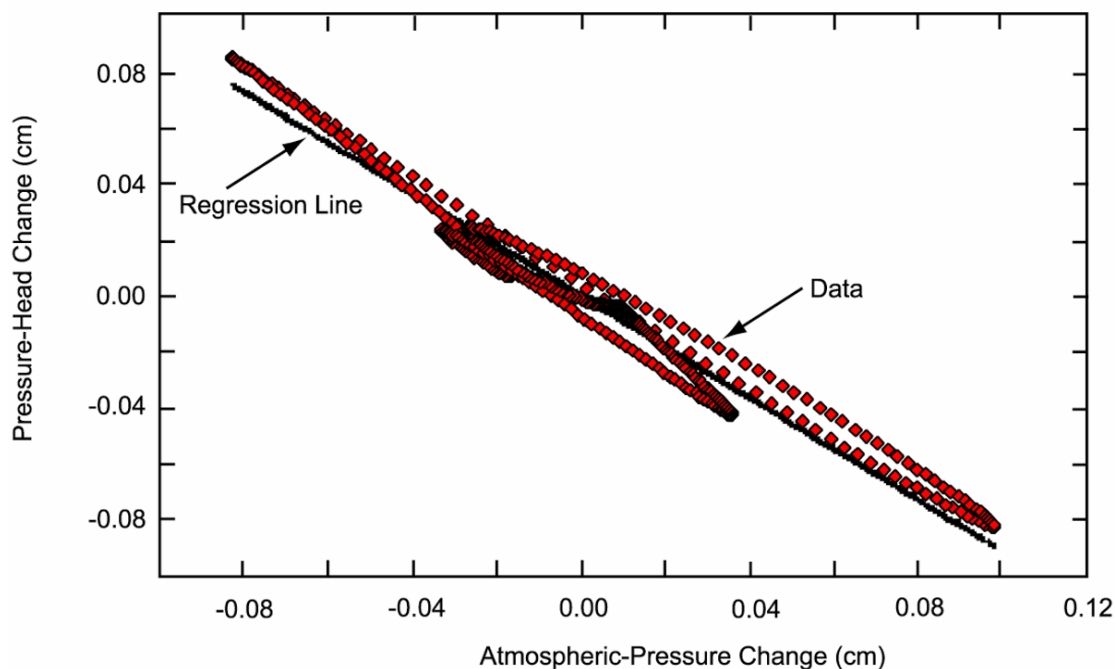
Changes in atmospheric pressure in the vicinity of the C-wells complex typically produce synchronous (but opposite) changes in water levels in boreholes (Figure C-2). The slope of a line fit to a plot of water-level change as a function of atmospheric-pressure change is called the barometric efficiency. Determination of the barometric efficiency of the Lower Bullfrog interval in c#2 is shown in Figure C-3. Barometric efficiency values of borehole intervals for which drawdown was computed during this study ranged from 0.75 to 0.99 (Table C-3). To compute barometrically corrected drawdown, barometric effects were removed from borehole records by subtracting the product of atmospheric-pressure change and barometric efficiency from the change in water level.



Source: Geldon et al. 2002 [DIRS 161163], Figure 8, p.17.

NOTE: For illustration purposes only.

Figure C-2. Difference of the Atmospheric Pressure from Its Mean Plotted Against the Opposite of the Difference of Concurrent Pressure Head from Its Mean



Source: Geldon et al. 2002 [DIRS 161163], Figure 9, p.17.

NOTE: For illustration purposes only.

Figure C-3. Filtered Pressure-head Change in UE-25 c#2 Lower Bullfrog Interval as a Function of Filtered Atmospheric-Pressure Change at the C-Wells Complex, June 23 to 29, 1995

Table C-3. Barometric Efficiency Values Determined for Borehole Intervals Monitored at the C-Wells Complex Through May 13, 1996

Borehole	Interval	Barometer Location	Period of Record	Barometric Efficiency	Regression Coefficient
UE-25 c#1	Prow Pass	C-wells	June 23 to 29, 1995	0.96	0.98
	Upper Bullfrog	C-wells	June 24 to 29, 1995	0.99	0.97
	Lower Bullfrog ^a	C-wells	June 23 to 29, 1995	0.97	0.98
	Bullfrog-Tram	C-wells	June 23 to 29, 1995	0.97	0.98
UE-25 c#2	Calico Hills	C-wells	June 23 to 29, 1995	0.93	0.94
	Prow Pass	C-wells	June 23 to 29, 1995	0.93	0.97
	Upper Bullfrog	C-wells	June 23 to 29, 1995	0.93	0.97
	Lower Bullfrog ^a	C-wells	June 23 to 29, 1995	0.91	0.96
	Bullfrog-Tram	C-wells	June 23 to 29, 1995	0.91	0.96
UE-25 c#3	Calico Hills ^b	C-wells	February 7 to 8, 1996	0.83	0.89
	Lower Bullfrog	C-wells	May 9 to 13, 1996	0.87	0.92
	Bullfrog-Tram	C-wells	N/A	0.94 ^c	N/A
UE-25 ONC-1	Prow Pass	ONC-1	July 1 to September 13, 1995	0.99	0.90
USW H-4	Prow Pass to Lithic Ridge	ONC-1	June 8 to 12, 1995	0.91	0.87

Table C-3. Barometric Efficiency Values Determined for Borehole Intervals Monitored at the C-wells Complex Through May 13, 1996 (Continued)

Borehole	Interval	Barometer Location	Period of Record	Barometric Efficiency	Regression Coefficient
UE-25 WT#14	Calico Hills	C-wells	June 4 to 12, 1995	0.89	0.94
UE-25 WT#3	Lower Bullfrog	C-wells	June 4 to 12, 1995	0.91	0.82
UE-25 p#1	Paleozoic carbonates	C-wells	January 1 to June 20, 1986	0.75	N/A

Sources: DTNs: LA0705PR150304.002 [DIRS 181198] (C-Wells), GS031108312314.005 [DIRS 179648], GS981008312314.003 [DIRS 144464], GS960708312312.009 [180534].

Output DTN: GS031008312314.004 (Table 6.2-3).

NOTE: N/A means that no record was used to calculate the barometric efficiency for the Bullfrog-Tram in c#3, per se. The barometric efficiency, in this case, was "estimated" by assuming that it was the average of the barometric efficiency for the Bullfrog-Tram in c#1 and c#2.

^aBarometric efficiency of Lower Bullfrog used also for Bullfrog-Tram in hydraulic test February 8 to 13, 1996.

^bBarometric efficiency of Calico Hills used also for Calico Hills-Upper Bullfrog in hydraulic test February 8 to 13, 1996.

^cBarometric efficiency estimated from values for Bullfrog-Tram in c#1 and c#2.

C3.1.3 Flow Distribution in the C-Wells

During hydraulic tests conducted in the C-wells in February 1996 and from May 1996 to November 1997, all hydrogeologic intervals in the C-wells being monitored responded to pumping, regardless of the interval being pumped. Leakage around packers could have occurred, although the packers were seated in nonrugose, sparsely fractured zones, but it is extremely unlikely that all packers failed to seal properly. A more likely explanation is that fractures beyond borehole walls are so interconnected that packers emplaced in the C-wells do not isolate the interval being pumped from other transmissive intervals within the volume of aquifer stressed by the pumping.

Spinner and oxygen-activation flow surveys (Figure C-4) were run in c#3 during the hydraulic test in June 1995 to determine the flow distribution in the C-wells under pumping conditions. However, those flow surveys failed to detect flow from the Prow Pass interval indicated by heat-pulse flowmeter surveys conducted without pumping in the C-wells in 1991 (Geldon 1996 [DIRS 100396], pp. 12 to 20). Oxygen activation logs, employing high-energy "fast" neutrons, can dynamically detect water movement inside and outside of casing. The technique consists of a short neutron-activation period followed by a longer data-acquisition period; flow is detected when the measured count-rate profile does not match the expected profile for a static environment. Results of the 1991 and 1995 flow surveys were combined algebraically to estimate a flow distribution during the hydraulic test in June 1995 (Table C-4). That flow distribution was adjusted for the hydraulic tests conducted in February 1996 and May 1996 to November 1997 (Table C-4) by inserting discharge and drawdown values recorded at the same elapsed time in the three hydraulic tests into Equation C-1c, which is an algebraic manipulation of Equations C-1a and C-1b:

$$s_1 = (P_1 Q_1 / (4\pi T)) W(u) \quad (\text{Eq. C-1a})$$

$$s_2 = (P_2 Q_2 / (4\pi T)) W(u) \quad (\text{Eq. C-1b})$$

$$P_2 = Q_1 P_1 s_2 / Q_2 s_1 \quad (\text{Eq. C-1c})$$

where

$u = r^2 S / 4 T t$ is a dimensionless parameter in which:

$r[\text{L}]$ = radial distance from pumping well

$S[\text{L}^0]$ = storativity

$T[\text{L}/\text{T}]$ = transmissivity of the tested interval in question, which is the same in Equations C-1a and C-1b

$t[\text{T}]$ = elapsed time from beginning of pumping.

$W(u) = \int_u^\infty (e^{-u}/u) du$; $W(u)$ is the well function, which can be a confined, unconfined, or leaky well function

$P_1[\text{L}^0]$ = the proportion of flow determined for a hydrogeologic interval during the hydraulic test in June 1995

$P_2[\text{L}^0]$ = the proportion of flow determined for a hydrogeologic interval during a hydraulic test in either February 1996 or May 1996 to November 1997, as appropriate

$Q_1[\text{L}^3/\text{T}]$ = the average discharge during the hydraulic test in June 1995

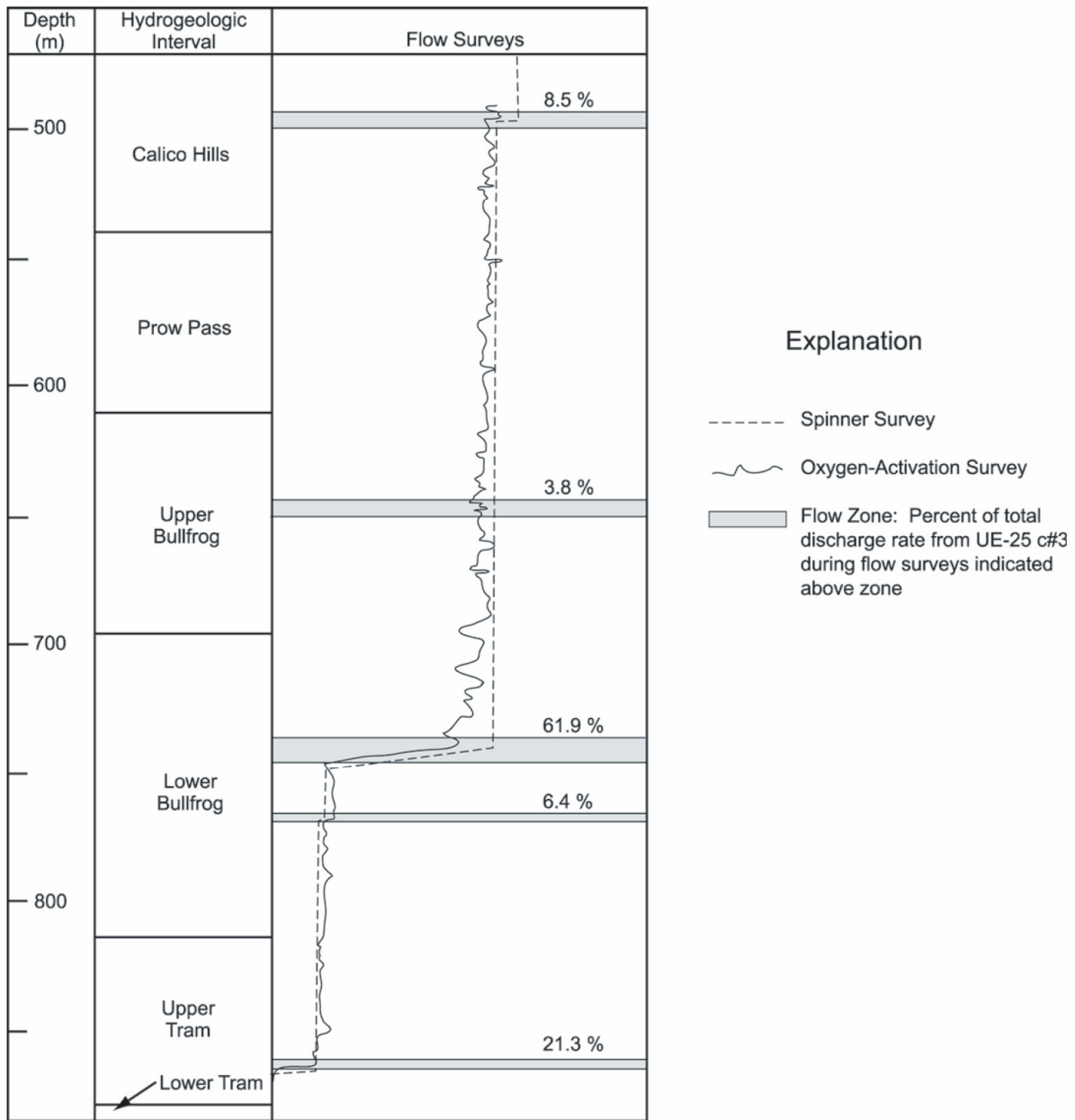
$Q_2[\text{L}^3/\text{T}]$ = the average discharge during a hydraulic test in February 1996 or May 1996 to November 1997, as appropriate

$s_1[\text{L}]$ = the drawdown in a hydrogeologic interval during the hydraulic test in June 1995

$s_2[\text{L}]$ = the drawdown in a hydrogeologic interval during a hydraulic test in either February 1996 or May 1996 to November 1997, as appropriate.

Equations C-1a and C-1b are based on the Theis equation (1935 [DIRS 150327], p. 520, Equation 4), except that s is used for drawdown instead of v , and Q is used for the discharge rate instead of F .

In the three hydraulic tests discussed in this report, the Lower Bullfrog interval consistently contributed about 70% of the flow from observation wells to the pumping well at the C-wells complex; the Upper Tram interval consistently contributed about 20% of that flow; and all other intervals combined contributed about 10% of the total flow. To analyze the drawdown in any hydrogeologic interval, the total discharge from c#3 first was multiplied by the percentage of flow contributed by the interval being analyzed to avoid calculating erroneously large values of transmissivity and storativity (both of which are directly proportional to discharge).



Source: DTN: MO0012FLOW25C3.001 [DIRS 154765].

Output DTN: GS031008312314.004.

Figure C-4. Flow Surveys in UE-25 c#3 During Hydraulic Testing in June 1995

Table C-4. Interval Discharges 5,800 Minutes after Pumping Started in Hydraulic Tests in UE-25 c#3, June 1995 to November 1997

Hydrogeologic Unit	June 1995			February 1996			May 1996 to November 1997		
	Dis-charge (L/min)	Draw-down (cm)	Flow (%)	Dis-charge (L/min)	Draw-down (cm)	Flow %	Dis-charge (L/min)	Draw-down (cm)	Flow (%)
UE-25 c#1									
Calico Hills	1,350	No data	3.8	507	No data	0.5 (est)	583.2	No data	1.1 (est)
Prow Pass	1,350	43.0	2.9	507	14.0	2.5	583.2	14.9	2.3
Upper Bullfrog	1,350	52.1	3.9	507	21.6	4.3	583.2	19.2	3.3
Lower Bullfrog	1,350	49.7	68.3	507	No data	No data	583.2	21.0	66.8
Bullfrog-Tram	1,350	No data	89.4	507	19.5	92.7	583.2	N/A	N/A
Upper Tram	1,350	No data	21.1	507	No data	No data	583.2	No data	26.5
Lower Tram	1,350	No data	trace	507	No data	trace	583.2	No data	trace
UE-25 c#2									
Calico Hills	1,350	351.7	3.8	507	16.4	0.5	583.2	43.0	1.1
Prow Pass	1,350	75.6	2.9	507	14.6	1.5	583.2	22.2	2.0
Upper Bullfrog	1,350	62.2	3.9	507	25.0	4.2	583.2	26.5	3.8
Lower Bullfrog	1,350	49.4	68.3	507	No data	No data	583.2	21.9	70.2
Bullfrog-Tram	1,350	No data	89.4	507	21.0	93.8	583.2	N/A	N/A
Upper Tram	1,350	283.2	21.1	507	No data	No data	583.2	No data	22.9
Lower Tram	1,350	239.6	trace	507	No data	trace	583.2	No data	trace

Sources: DTNs: MO0012FLOW25C3.001 [DIRS 1547 65], LA0705PR150304.002 [DIRS 181198], LA0705PR150304.003 [DIRS 181201] (qualified in Appendix R), GS031108312314.005 [DIRS 179648], GS970308312314.001 [DIRS 159240], GS981008312314.003 [DIRS 144464], and LA0705PR150304.004 [DIRS 181210] (corroborative only, drawdown in upper and lower Tram in June 1995).

Output DTN: GS031008312314.004 (Table 6.2-4).

NOTE: The Bullfrog-Tram refers to the combined Lower Bullfrog and Upper Tram intervals tested together as one unit during the February 1996 test. Flow proportion for the Bullfrog-Tram interval shown in June 1995 is the sum of values for the Lower Bullfrog and Upper Tram intervals.

est = estimated; N/A = not applicable.

C3.1.4 Monitoring Network

The monitoring network at the C-wells complex was selected after Borehole c#3 was chosen as the pumping well for all hydraulic tests conducted from 1995 to 1997 on the basis of its successful performance during two hydraulic tests conducted in 1984 (Geldon 1996 [DIRS 100396], pp. 48 to 68). Boreholes c#1 and c#2 were used as observation wells for the hydraulic tests conducted in June 1995 and February 1996. Boreholes ONC-1, H-4, WT#14, WT#3, and p#1 were also used as observation wells for the longer-term hydraulic test conducted from May 1996 to November 1997. Recording barometers were located at the C-wells complex during all hydraulic tests; a barometer located at borehole ONC-1 also was used during the third hydraulic test. (see Figure 6.1-3 for a map showing the location of the observation wells.)

Borehole c#3 is 900.4-m deep (Geldon 1993 [DIRS 101045], p. 2). The borehole is cased and grouted to a depth of approximately 417 m, just below the water table (Geldon 1993 [DIRS 101045], p. 7, Figure 3). During the hydraulic test in June 1995, c#3 did not contain

packers and was open from the Calico Hills Formation to the Lower Tram interval. After packers were emplaced in August 1995, manipulation of the packers, sliding sleeves, and slotted casing allowed selective hydraulic communication with only the Lower Bullfrog and Upper Tram intervals during hydraulic and tracer tests in February and March 1996, and with only the Lower Bullfrog interval from May 1996 to December 1997.

Borehole c#2 is 30.4 m from c#3 at the land surface (Geldon et al. 1998 [DIRS 129721], p. 3, Figure 1) and 910.1 m deep (Geldon 1993 [DIRS 101045], p. 2). It is cased and grouted to a depth of approximately 416.0 m (Geldon 1993 [DIRS 101045], p. 7, Figure 3). Five dual-mandrel packers, suspended on 7.30-cm-diameter tubing, were emplaced in the borehole to isolate hydrogeologic intervals throughout the period of testing discussed in this report. Manipulation of packers and sliding sleeves allowed hydraulic communication with six separate hydrogeologic intervals (Figure 6.1-5 and Table C-1) in June 1995, with the Lower Bullfrog and Upper Tram intervals in February and March 1996, and with the Lower Bullfrog interval from May 1996 to December 1997.

Borehole c#1 is 68.4 m from c#3 at the land surface (Geldon et al. 1998 [DIRS 129721], p. 3, Figure 1) and is 897.6 m deep (Geldon 1993 [DIRS 101045], p. 2). It is cased and grouted to a depth of approximately 417.9 m (Geldon 1993 [DIRS 101045], p. 7, Figure 3). Five dual-mandrel packers, suspended on 7.30-cm-diameter tubing, were emplaced in the borehole to isolate hydrogeologic intervals throughout the period of testing discussed in this report. Manipulation of packers and sliding sleeves allowed hydraulic communication with the Calico Hills, Prow Pass, Upper Bullfrog, and Lower Bullfrog intervals in June 1995, with the Lower Bullfrog and Upper Tram intervals in February and March 1996, and with the Lower Bullfrog interval from May 1996 to December 1997.

Borehole ONC-1 is 842.8 m from Borehole c#3 at the land surface and is 469.4 m deep (extending about 36.3 m below the water level in the borehole) (Nye County Nuclear Waste Repository Project Office 1995 [DIRS 156859], ONC-1 Drilling log). The borehole is telescoped downward and has a diameter of about 13 cm in the SZ. Seven packers inflated between the bottom of the casing and a depth of 410 m separate the unsaturated and SZs; another packer emplaced at a depth of 452 m divides the SZ into two intervals. The upper of the saturated-zone intervals is open in the Calico Hills Formation and the Prow Pass Tuff; the lower of those intervals is open in the Prow Pass Tuff. Absolute transducers, installed in all packed-off intervals, transmitted total (atmospheric plus hydraulic) pressures to a data logger every 15 to 20 minutes during the tests reported here. Data from the lowermost transducer, positioned at a depth of 458 m, were converted to pressure heads for analysis.

Borehole H-4, which is 2,245 m from Borehole c#3 at the land surface, is 1,219 m deep. The borehole diameter is 37.5 cm to a depth of 564 m and 22.2 cm below 564 m. Casing extends to a depth of 561 m; it is perforated below the water level, which was at an average depth of 518.3 m from 1985 to 1995. A packer emplaced at a depth of 1,181 m separates the Prow Pass, Bullfrog, and Tram Tuffs and the upper part of the Lithic Ridge Tuff from the lower part of the Lithic Ridge Tuff in the borehole. A 48-mm-diameter piezometer tube is installed in the upper part of the borehole, and a 62-mm-diameter piezometer tube is installed in the lower part of the borehole. (Graves et al. 1997 [DIRS 101046], pp. 4 to 5, Table 1; p. 100). Differential

transducers emplaced in the two monitored intervals transmitted hydraulic pressures to a data logger every 15 minutes during this study. Only the data from the upper interval were used.

Borehole WT#14, which is 2,249 m from Borehole c#3 at the land surface, is 399 m deep. The borehole has a diameter of 22.2 cm below the water table, which was at an average depth of 346.4 m from 1985 to 1995. The borehole is cased to a depth of 37 m and is open in the Topopah Spring Tuff and Calico Hills Formation. A 62-mm-diameter piezometer tube is installed in the borehole. (Graves et al. 1997 [DIRS 101046], pp. 4 to 5, Table 1; p. 84). A differential transducer emplaced in the piezometer tube transmitted hydraulic pressures to a data logger every 15 minutes during this study.

Borehole WT#3, which is 3,526 m from Borehole c#3 at the land surface, is 348 m deep. The borehole has a diameter of 22.2 cm below the water table, which was at an average depth of 300.5 m from 1985 to 1995. The borehole is cased to a depth of 12 m and is open in the Bullfrog Tuff. A 62-mm-diameter piezometer tube is installed in the borehole (Graves et al. 1997 [DIRS 101046], pp. 4 to 5, Table 1; p. 76). A differential transducer emplaced in the piezometer tube transmitted hydraulic pressures to a data logger every 15 minutes during this study.

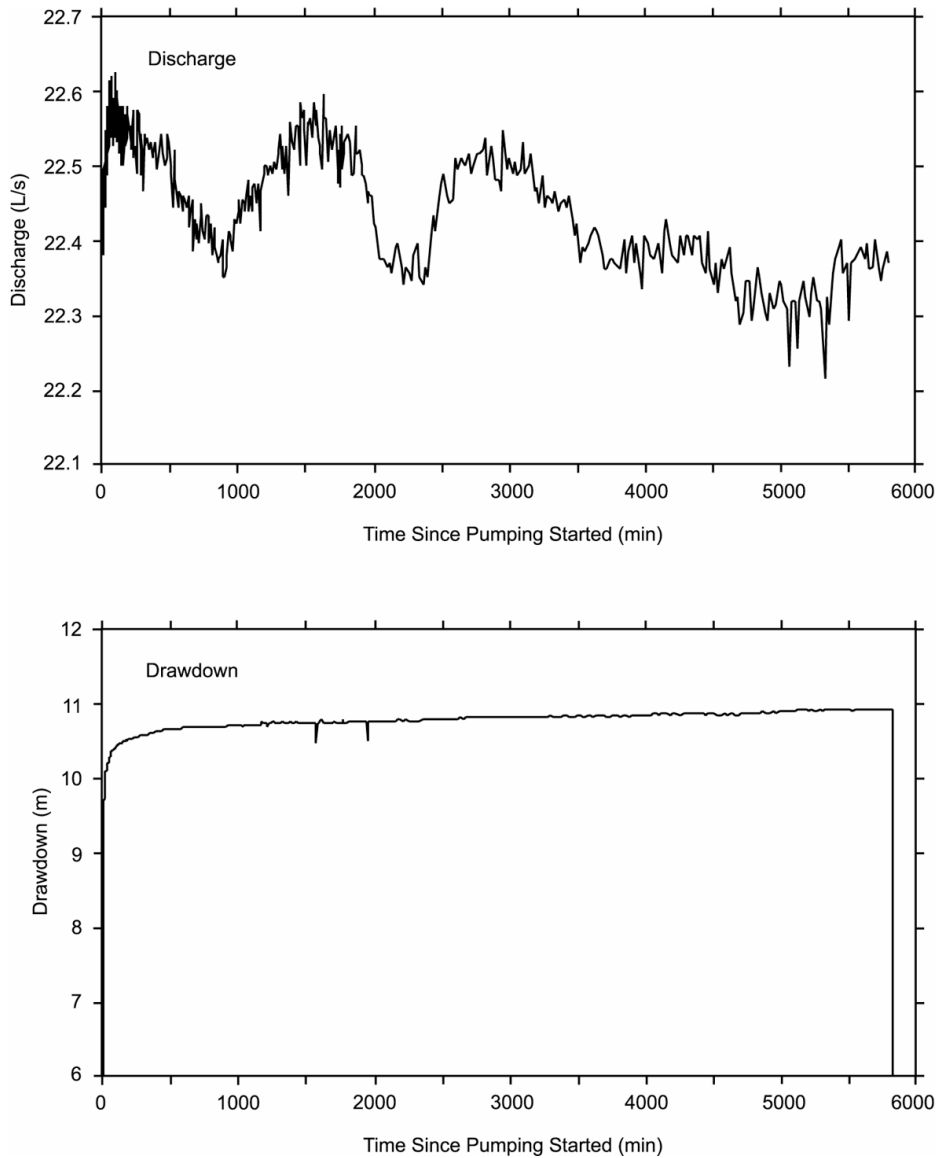
Borehole p#1, which is 630 m from Borehole c#3 at the land surface, is 1,805-m deep. The borehole diameter decreases from 37.5 cm to 15.6 cm with depth. Casing and cement emplaced to a depth of 1,297 m isolate the Miocene tuffaceous rocks in the upper part of the borehole from Paleozoic carbonate rocks in the lower part of the borehole. The water level for the Paleozoic carbonate rocks in p#1 was monitored through a 38-mm-diameter piezometer tube. The average depth to water in the piezometer tube was 361.8 m from 1985 to 1995. (Graves et al. 1997 [DIRS 101046], pp. 4 to 5, Table 1; p. 90). A differential transducer emplaced in the piezometer tube transmitted hydraulic pressures to a data logger every 60 minutes during this study.

C3.1.5 Description of Tests

A hydraulic test (DTNs: LA0705PR150304.002 [DIRS 181198], LA0705PR150304.003 [DIRS 181201] (qualified in Appendix R), and LA0705PR150304.004 [DIRS 181210]) was conducted in June 1995 to determine hydrologic properties of six hydrogeologic intervals (Figure C-5) at the C-wells complex (Table C-1) [a detailed description of the field tests is contained in *Performing Various Hydraulic and Tracer Test Using Prototype Pressure Transducer and Packer Assemblies* (Umari 2002 [DIRS 162858], Binder 3, Sections D-2 to D-6)]. The six intervals were isolated by packers in Boreholes c#1 and c#2. Sliding sleeves open in the packed-off intervals of the observation wells allowed hydraulic communication with the pumping well c#3, which was uncased and contained no packers to isolate intervals. Because of malfunctioning transducers, analyzable data were obtained only from the Prow Pass, Upper Bullfrog, and Lower Bullfrog intervals of c#1 and from the Calico Hills, Prow Pass, Upper Bullfrog, and Lower Bullfrog intervals of c#2.

The hydraulic test began on June 12 and ended on June 16, after 4.03 days of pumping. (Note that data were collected over thousands of elapsed minutes, the measure of time used by data-acquisition software and needed for hydraulic calculations. For the summarizing discussions here, those time intervals are expressed in hours and days.) Recovery was monitored

until June 29, by which date it appeared to be complete in all intervals. At an average discharge rate of 1350 L/min, drawdown in c#3 rapidly increased to a maximum of 10.9 m (Figure C-5). The pumping in c#3 produced drawdown ranging from 43.0 cm to 52.1 cm in intervals of c#1 (Figure C-6) and from 49.4 cm to 352 cm in intervals of c#2 (Figure C-7).

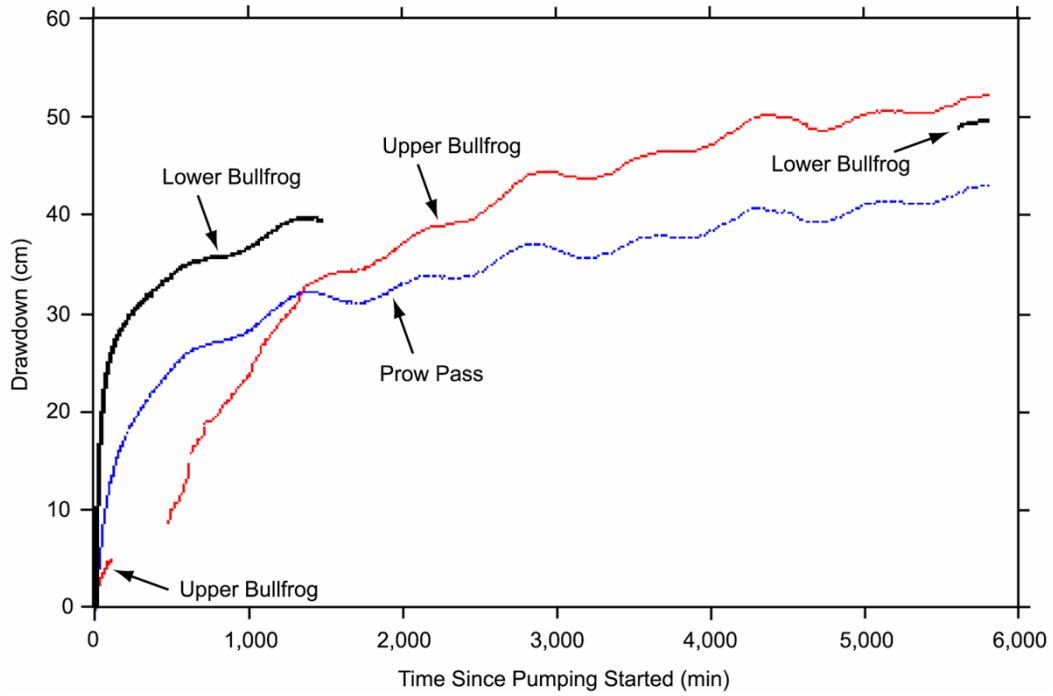


Sources: DTNs: LA0705PR150304.002 [DIRS 181198], LA0705PR150304.003 [DIRS 181201] (qualified in Appendix R).

Output DTN:GS031008312314.004.

NOTE: Discharge units in text are L/min.

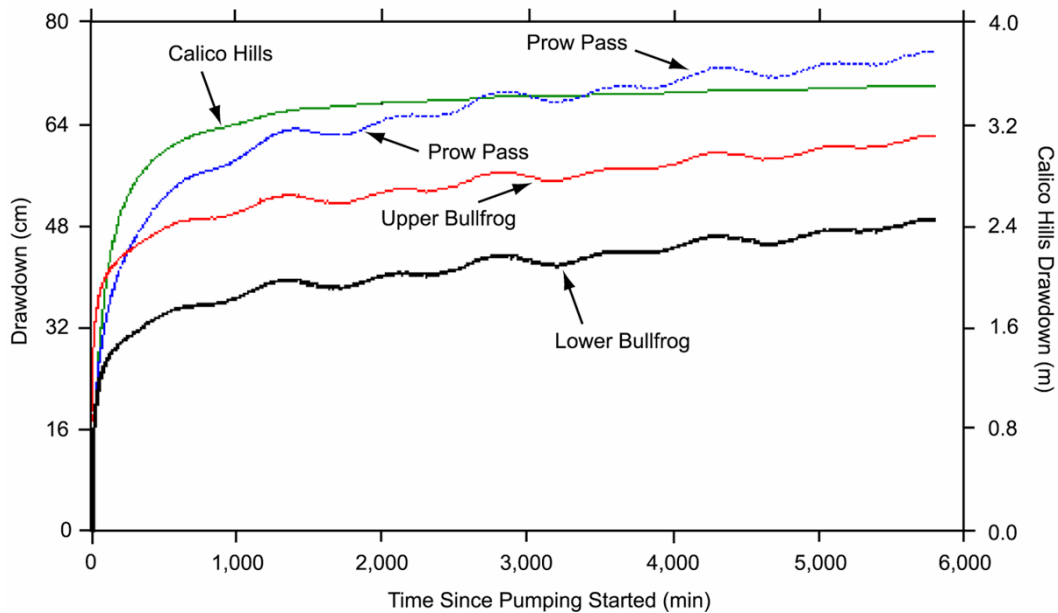
Figure C-5. UE-25 c#3 Discharge and Drawdown, June 12, 1995 (approximately 0 minutes), to June 16, 1995 (approximately 5,800 minutes)



Source: DTN: LA0705PR150304.002 [DIRS 181198].

Output DTN: GS031008312314.004.

Figure C-6. UE-25 c#1 Drawdown in June 1995



Source: DTN: LA0705PR150304.002 [DIRS 181198].

Output DTN: GS031008312314.004.

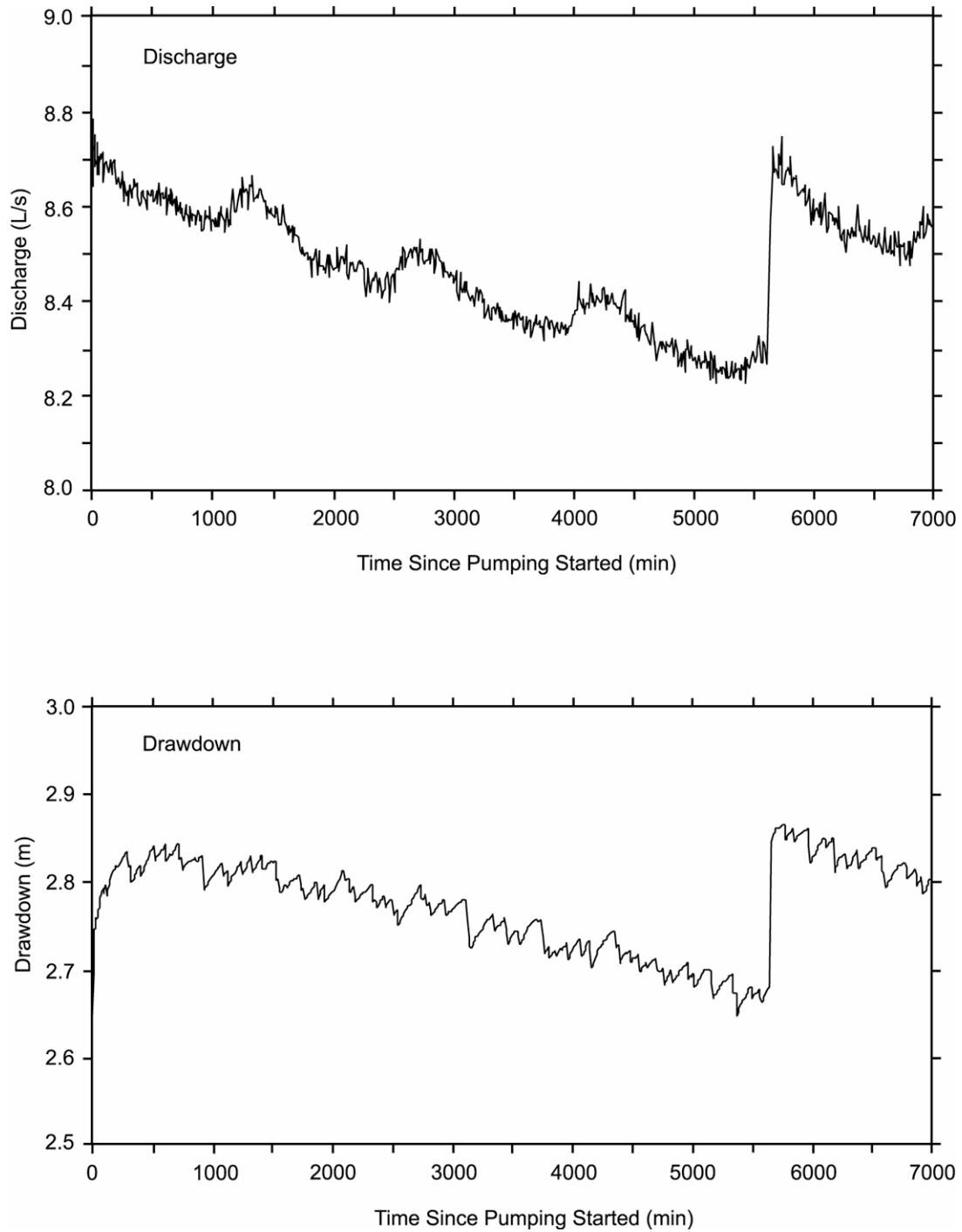
Figure C-7. UE-25 c#2 Drawdown in June 1995

The most permeable interval identified in the hydraulic test conducted in June 1995, the Lower Bullfrog interval, was chosen for subsequent tracer tests at the C-wells complex to increase the chance of successful transport of tracers between the injection and recovery wells. Because the transducer in the Lower Bullfrog interval of c#3 was not working, the packers between the Lower Bullfrog and Upper Tram intervals in all three of the C-wells were deflated, and the combined Lower Bullfrog and Upper Tram intervals (shown in Figure 6.1-5 as the Bullfrog-Tram interval) became the test interval for the following series of tests.

After testing pump performance in January 1996 and allowing water levels in the C-wells to recover, pumping began on February 8, 1996, to establish a steep, quasi-steady-state hydraulic gradient between c#2 (the injection well) and c#3 (the recovery well) for a conservative tracer test. Tracer injection on February 13 disturbed the hydraulic pressure in the injection interval for 12.5 hours and effectively terminated the analyzable drawdown record. The 4.85 days of drawdown recorded between the start of pumping and the injection of tracer on February 13 (when the hydraulic pressure in the injection interval was disturbed) were analyzed as an hydraulic test.

During the hydraulic test in February 1996, operation of the pump outside its optimal performance range caused discharge to decrease steadily, despite an adjustment of the pump speed on February 12, about 5,640 minutes (3.917 days) after pumping started. Prior to that adjustment, discharge decreased from 526.8 to 492.6 L/min. Adjusting the pump speed restored the discharge to 525 L/min, but discharge immediately began to decrease and was at 514.2 L/min when the tracer test started on February 13 (Figure C-8). Although average discharge after adjusting the pump speed was 6.0 L/min larger than before that adjustment, deviation from the average discharge of 509.4 L/min was just 3% for the entire period of pumping.

As shown in Figure C-8, the pumping produced as much as 2.86 m of drawdown in the Bullfrog-Tram interval of c#3 (96% of which occurred in the first 10 minutes). Adjustment of the pump speed caused a step-like increase of 0.19 m in c#3 drawdown, but it had no discernible effect on drawdown in the other C-wells. Although oscillatory, drawdown in c#1 steadily increased and ranged from 14.3 to 22.1 cm in the Prow Pass, Upper Bullfrog, and Bullfrog-Tram intervals (Figure C-9). Likewise, oscillatory drawdown in c#2 steadily increased and ranged from 14.9 to 25.3 cm in the Calico Hills, Prow Pass, Upper Bullfrog, and Bullfrog-Tram intervals (Figure C-10). Steady increases in observation-well drawdown together with small deviations from the average discharge enabled the observation-well drawdown for the entire period before tracer injection to be analyzable.

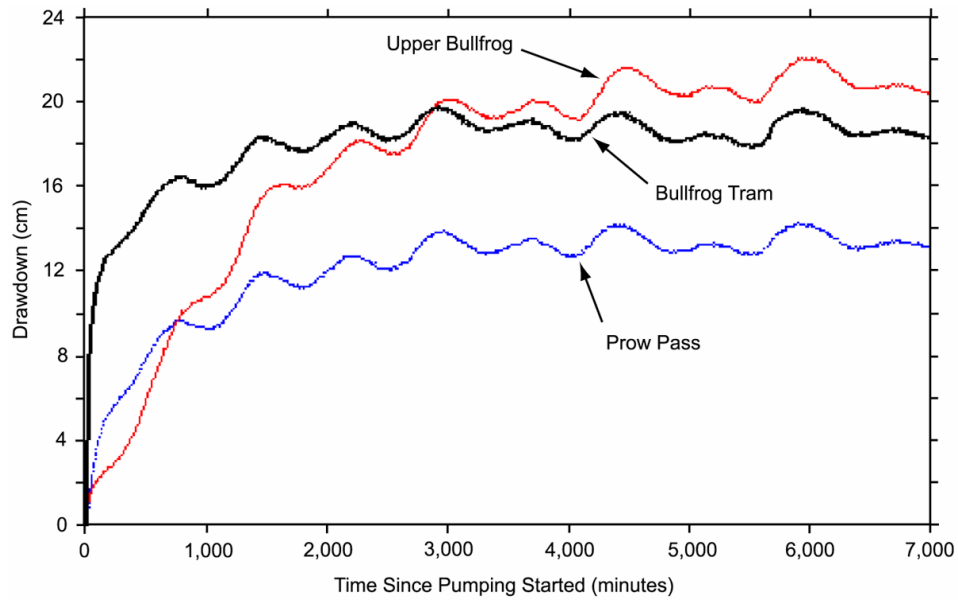


Source: DTN: GS031108312314.005 [DIRS 179648].

Output DTN: GS031008312314.004.

NOTE: Discharge units in text are L/min.

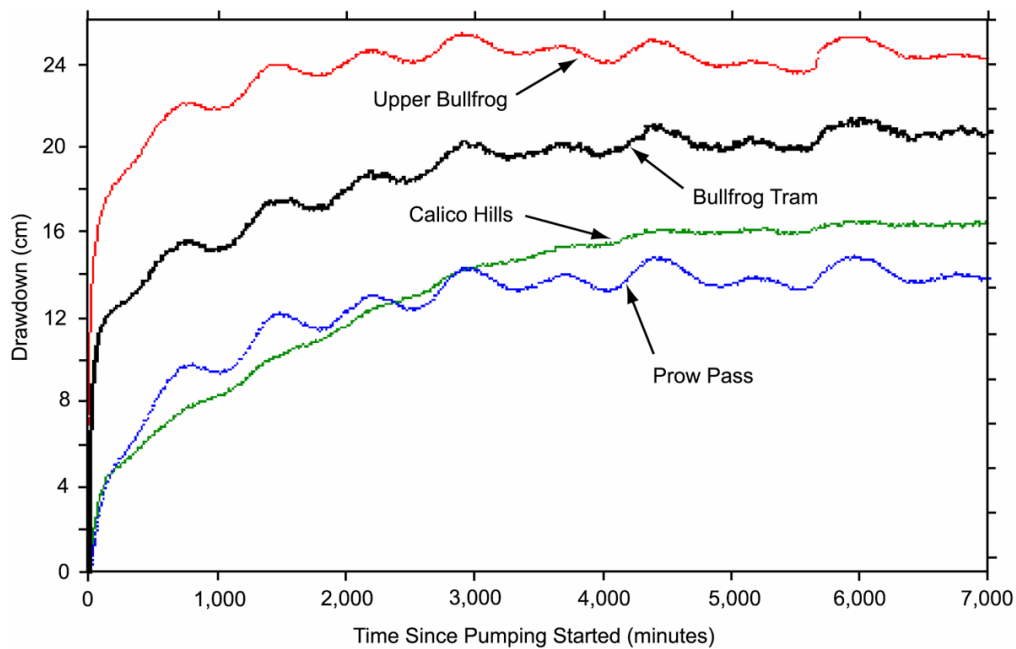
Figure C-8. UE-25 c#3 Discharge and Drawdown, February 8, 1996 (approximately 0 minutes), to February 13, 1996 (approximately 7,000 minutes)



Source: DTN: GS031108312314.005 [DIRS 179648].

Output DTN: GS031008312314.004.

Figure C-9. UE-25 c#1 Drawdown, February 8, 1996 (approximately 0 minutes), to February 13, 1996 (approximately 7,000 minutes)



Source: DTN: GS031108312314.005 [DIRS 179648].

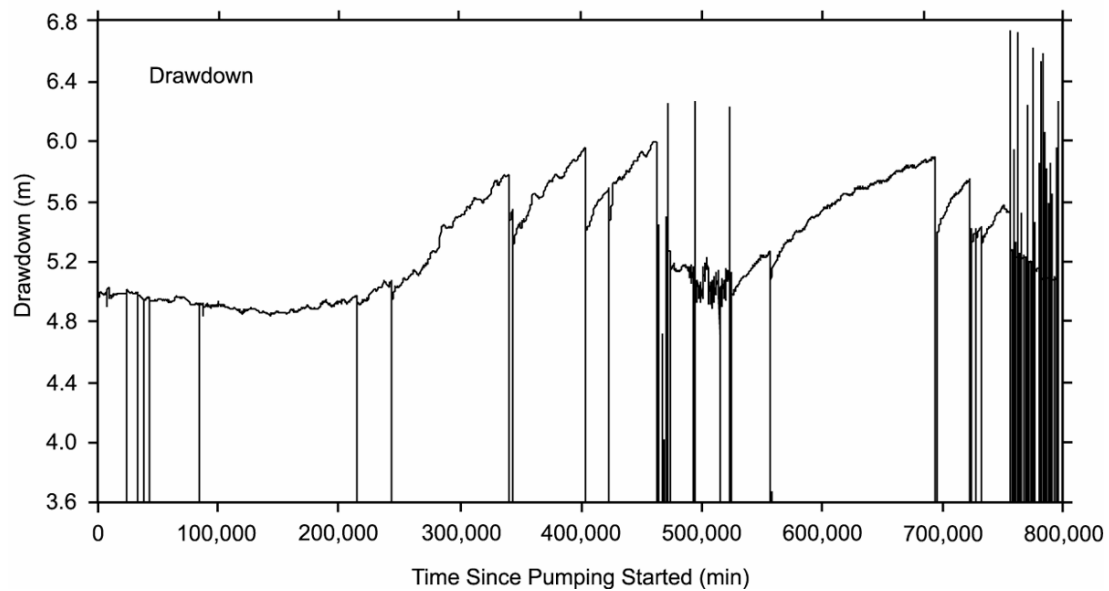
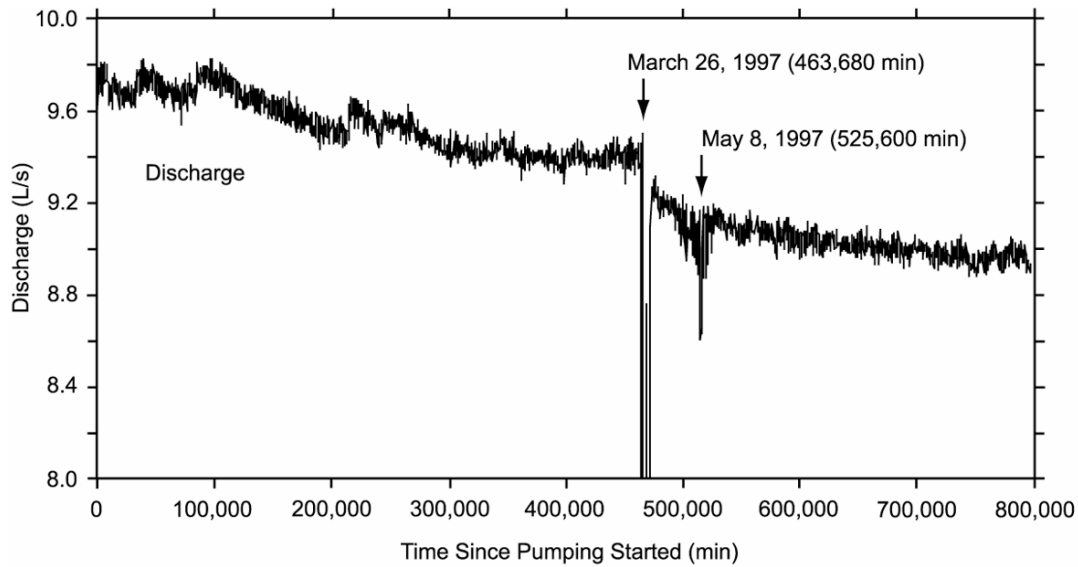
Output DTN: GS031008312314.004.

Figure C-10. UE-25 c#2 Drawdown, February 8, 1996 (approximately 0 minutes), to February 13, 1996 (approximately 7,000 minutes)

After the tracer test in the Bullfrog-Tram interval ended in March 1996, a new transducer was installed in the Lower Bullfrog interval of c#3, and packers in the borehole were reconfigured. Subsequently, it was possible to conduct hydraulic and tracer tests in the isolated Lower Bullfrog interval. With nearly continuous pumping, a series of tracer tests was conducted in that interval by the USGS and by Los Alamos National Laboratory from May 1996 to November 1997. Pumping in c#3 to establish a steep, quasi-steady-state hydraulic gradient for tracer tests in the Lower Bullfrog interval began May 8, 1996. From May 24, 1996, to March 26, 1997, the pump shut off 11 times because of problems with the generators that provided power to the site. Between March 26 and May 8, 1997, the pump operated erratically because of continued problems with one of the generators. Problems with the power supply caused the pump to shut off intermittently between May 30 and September 29, 1997, and at least once a day between October 15 and November 12, 1997. Pumping was terminated on November 12, 1997, 553.24 days after pumping started, and recovery was monitored until December 31, 1997.

Discharge between May 8, 1996, and March 26, 1997, initially oscillated between 576 and 588 L/min, eventually stabilized at about 564 L/min, and averaged 571.8 L/min (Figure C-11). After generator problems were resolved on May 8, 1997, discharge decreased steadily from 558 to 534 L/min on November 12, 1997, and averaged 540.6 L/min. The volume of water withdrawn between May 8, 1996, and November 12, 1997, was 440.2 million L, equivalent to an average discharge of 552.6 L/min.

As in previous hydraulic tests, drawdown in the pumped well was large and reached steady-state conditions rapidly (Figure C-11). Drawdown in the Lower Bullfrog interval of c#3 reached 4.8 m in 60 minutes and remained at 4.85 m to 5.0 m until October 16, 1996, 161.11 days (232,000 minutes) after pumping started. After March 26, the frequent pump shutoffs kept drawdown less than 5.9 m, except during the process of restarting the pump. Pump shutoffs typically caused rapid and complete or nearly complete recovery in c#3, but those effects were reversed just as rapidly when the pump was restarted. Tracer-test operations affected drawdown in the pumped well minimally. Recovery from pumping on December 12, 1997, approximately 30 days (42,965 minutes) after pumping stopped, was 99% of antecedent drawdown. The prolonged period of unsteady pump discharge after March 26, 1997, effectively ended the drawdown record that could be analyzed as a hydraulic test for all observation wells except ONC-1. The analyzable drawdown record from May 8, 1996, to March 26, 1997, is 322.32 days in duration. With 11 down times ranging from 2 minutes to 185 minutes, the pump was off for 10.82 hours (649 minutes), about 0.1% of the time, during that period.



Sources: DTNs: GS970308312314.001 [DIRS 159 240], GS970708312314.005 [DIRS 159241], GS981008312314.002 [DIRS 147068], GS010608312314.001 [DIRS 179647], GS981008312314.003 [DIRS 144464].

Output DTN: GS031008312314.004.

NOTE: Discharge units in text are L/min.

Figure C-11. UE-25 c#3 Discharge and Drawdown, May 8, 1996 (approximately 0 minutes), to November 12, 1997 (approximately 800,000 minutes)

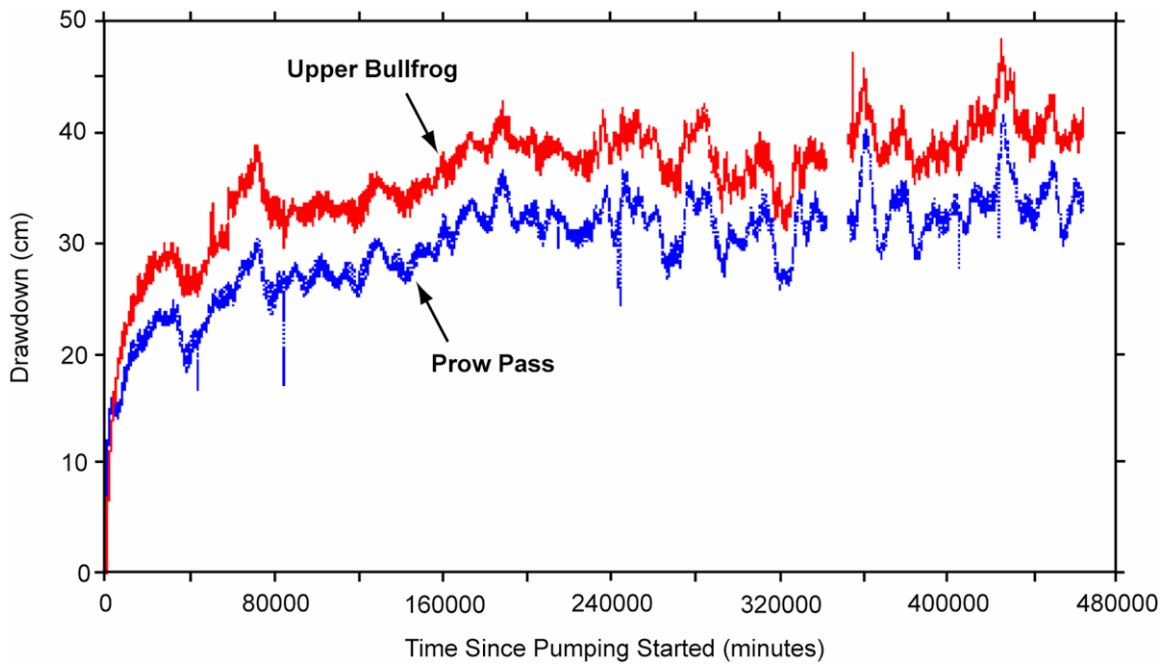
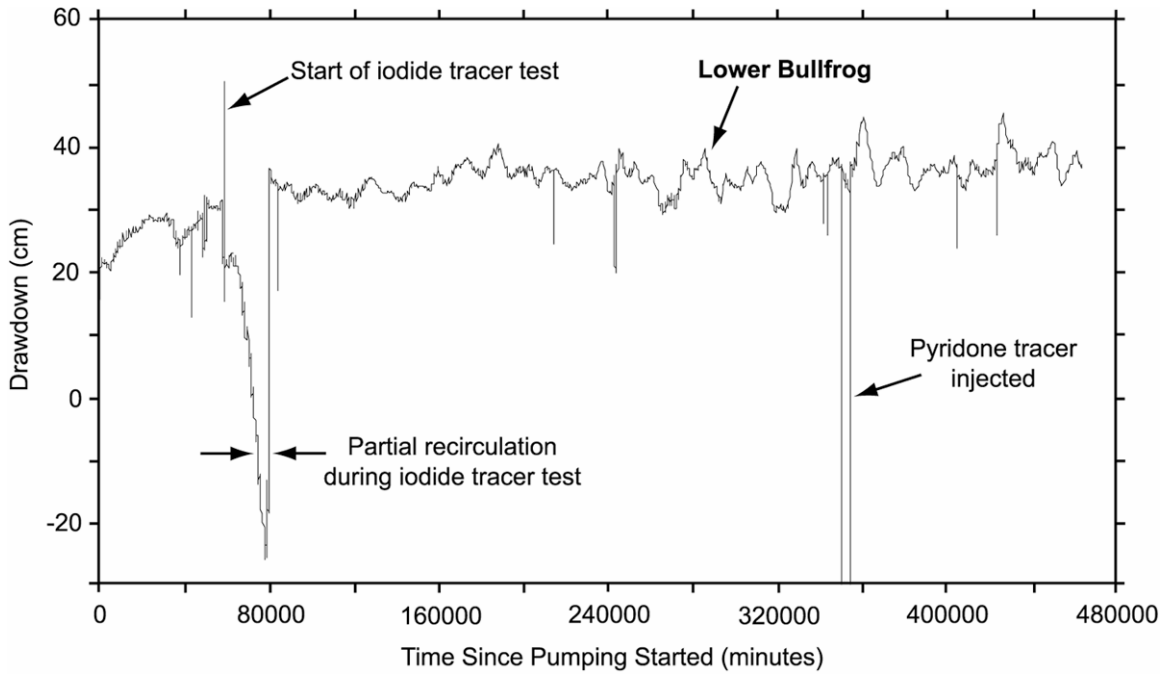
Drawdown in response to pumping the Lower Bullfrog interval of c#3 is known to have occurred in the Prow Pass, Upper Bullfrog, and Lower Bullfrog intervals of c#1 and in the Calico Hills, Prow Pass, Upper Bullfrog, and Lower Bullfrog intervals of c#2. Drawdown in all intervals of these boreholes generally increased steadily but was very oscillatory. Peak drawdown by

March 26, 1997, ranged from about 36 to 42 cm in intervals of c#1 (Figure C-12) and from about 35 to 51 cm in intervals of c#2 (Figure C-13).

Disruptions of drawdown in the Lower Bullfrog and other intervals of c#1 and c#2 occurred from pump shutoffs 11 times between May 1996 and March 1997. Pump shutoffs (most of the unlabeled downward spikes in Figures C-12 and C-13) generally resulted in 20% to 50% recovery of water levels. However, these effects dissipated 50 minutes to 500 minutes after the pump was restarted and did not affect analysis of the drawdown.

Recirculation of water during tracer tests conducted between May and November 1996 generally caused small decreases in drawdown in the Lower Bullfrog interval of c#1 or decreases followed by increases in drawdown in the Lower Bullfrog interval of c#2 at the start and end of recirculation, which generally lasted 70 minutes to 560 minutes. However, recirculation of water in c#1 from June 17 to July 3, 1996, to facilitate transport of iodide tracer between the injection and recovery wells caused drawdown in the Lower Bullfrog interval of c#1 to decrease in steps for 23,350 minutes (Figures C-12 and C-14a). Pumping water into c#1 faster than it could drain probably caused the drawdown to decrease. Periodic increases in the injection pump rate caused this decrease to occur in steps.

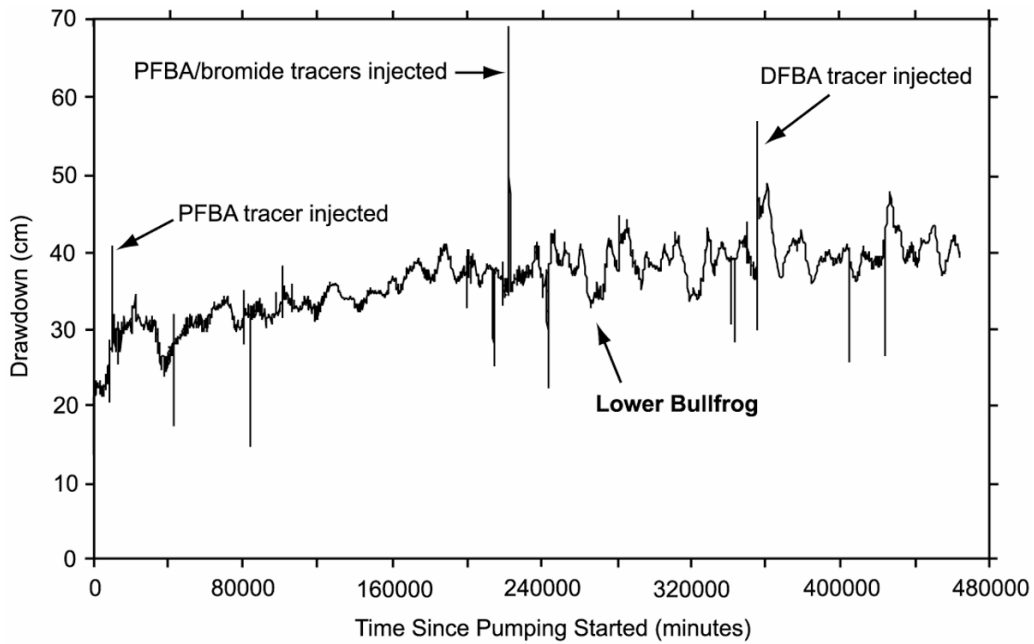
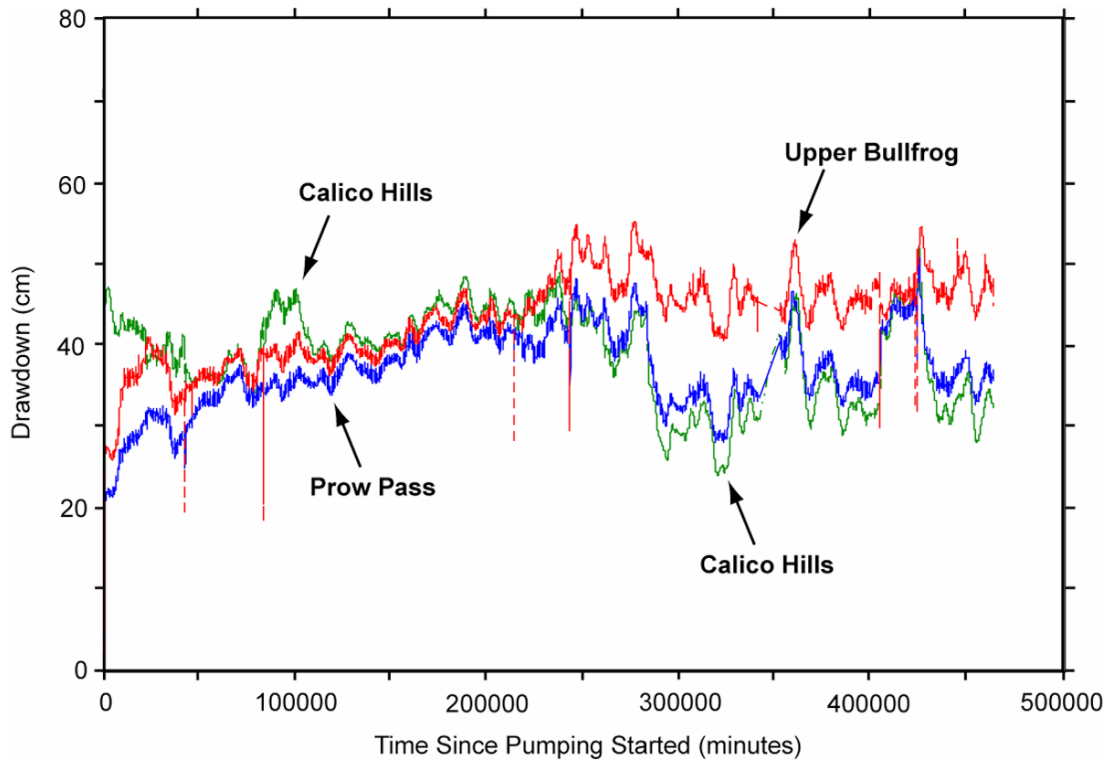
Tracer injection during four tests conducted between May 1996 and November 1997 caused increased drawdown in the Lower Bullfrog interval of c#1 or c#2 that generally lasted 180 minutes to 750 minutes. However, following injection of 2,6 difluorobenzoic acid tracer into c#2 on January 10, 1997, drawdown in the Lower Bullfrog interval of c#2 remained high for 8,360 minutes (Figures C-13 and C-14b). Changes in hydraulic head associated with the dense tracer injection solution also could have produced the observed water-level changes in c#2.



Sources: DTNs: GS970308312314.001 [DIRS 159 240], GS970708312314.005 [DIRS 159241], GS981008312314.002 [DIRS 147068]. GS981008312314.003 [DIRS 144464].

Output DTN: GS031008312314.004.

Figure C-12. UE-25 c#1 Drawdown, May 8, 1996 (approximately 0 minutes), to March 26, 1997 (approximately 470,000 minutes)

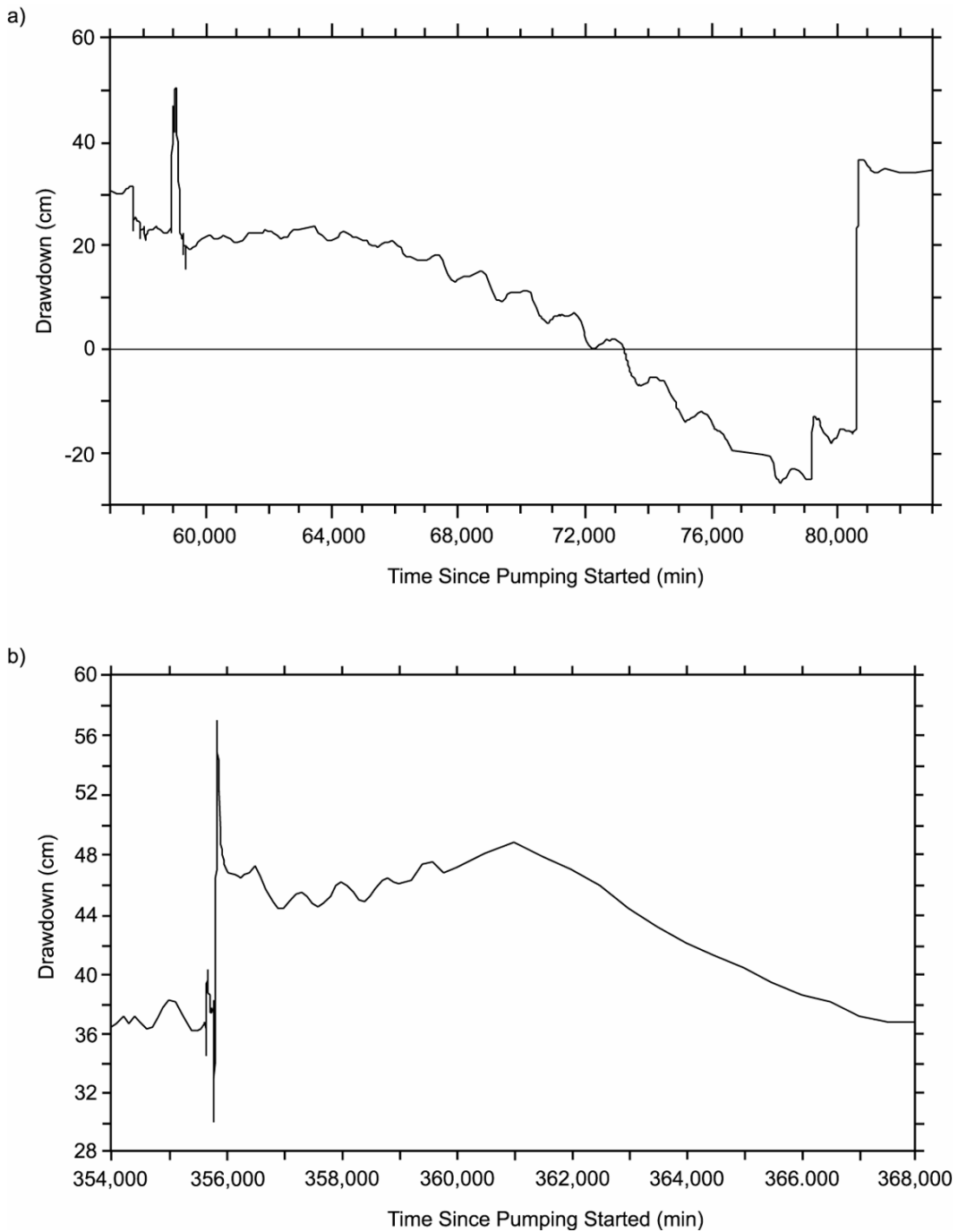


Sources: DTNs: GS970308312314.001 [DIRS 159240], GS970708312314.005 [DIRS 159241], GS981008312314.002 [DIRS 147068], GS981008312314.003 [DIRS 144464].

Output DTN: GS031008312314.004.

NOTE: PFBA=Pentafluorobenzoic acid; DFBA=2,6 difluorobenzoic acid.

Figure C-13. UE-25 c#2 Drawdown, May 8, 1996 (approximately 0 minutes), to March 26, 1997 (approximately 470,000 minutes)



Sources: DTNs: GS970308312314.001 [DIRS 159 240], GS970708312314.005 [DIRS 159241], GS981008312314.002 [DIRS 147068], GS981008312314.003 [DIRS 144464].

Output DTN: GS031008312314.004.

NOTE: a) Iodide tracer test in c#1, June 17, 1996 (approximately 57,000 minutes), to July 5, 1996 (approximately 83,000 minutes).
 b) 2,6 Difluorobenzoic acid tracer test in c#2, January 9, 1997 (approximately 354,000 minutes), to January 18, 1997 (approximately 368,000 minutes).

Figure C-14. Disturbance of Drawdown in Lower Bullfrog Interval of UE-25 c#1 and UE-25 c#2 by Tracer Tests in (a) 1996 and (b) 1997

Hypotheses regarding disturbances from tracer-test operations cannot be tested and, therefore, are presented only for consideration. It is important to note that (1) tracer-test operations conducted in one borehole generally did not affect drawdown in other boreholes and (2) disturbances from tracer-test operations did not affect analyses of drawdown in c#1 and c#2.

Events of unknown origin caused hydraulic heads in the Lower Bullfrog interval of c#1 and c#2 to rise 5 cm to 8 cm from June 1 to June 11, 1996 (a period of 14,800 minutes), and from November 6, 1996 to November 14, 1996 (a period of 11,900 minutes). Because six observation wells within 3.5 km of c#3 showed similar rises in hydraulic head, the events that produced these disturbances could not have been local in scale.

Shutting off the pump in c#3 on November 12, 1997, caused erratic responses in the Lower Bullfrog intervals of c#2 and c#1 that are not analyzable. Recovery in the Lower Bullfrog interval of c#1 reached a plateau from 8,000 minutes to 38,500 minutes after pumping stopped, after which it began increasing cyclically. On December 29, 1997, 46.53 days (67,000 minutes) after pumping stopped, recovery in the Lower Bullfrog interval of c#1 was about 95% of the antecedent drawdown (Figure C-15). The transducer in the Lower Bullfrog interval of c#2 was removed on December 9, 1997, at a time when readings from the transducer were erratic, and recovery was only about 70% of the antecedent drawdown.

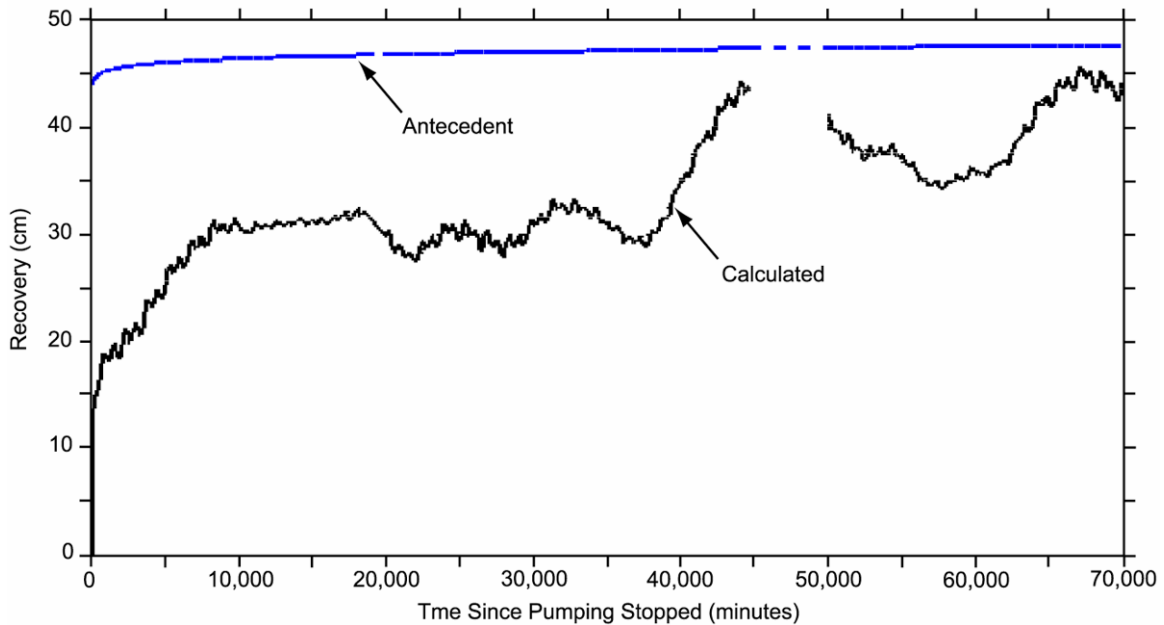
“Recovery” (as used in the previous paragraph and in Figure C-15) is a calculated value. First, the pattern of water-level decline prior to stopping the pump (antecedent water-level decline) is extrapolated beyond the time of stopping the pump. This extrapolated antecedent water-level decline is presented as the blue antecedent drawdown curve in Figure C-15. Then, for any point in time after pump stoppage, the “recovery” is calculated as the distance from the extrapolated antecedent water level to the recovered water level. So, “recovery” is larger than the distance that the water level has rebounded relative to where it was at the point of shutting off the pump.

Pumping in the Lower Bullfrog interval of c#3 from May 1996 to March 1997 caused drawdown in all four of the observation wells beyond the C-wells complex that are completed in Miocene tuffaceous rocks. As in c#1 and c#2, drawdown in the four outlying observation wells was very oscillatory. Drawdown in these wells was not affected by pump shutoffs or tracer test operations.

Drawdown in ONC-1, the nearest observation well to the C-wells, was detected 200 minutes after pumping started and increased steadily thereafter (Figure C-16). Peak drawdown by March 26, 1997, was about 28 cm to 30 cm. Peak drawdown when pumping ended on November 12, 1997, was about 36 cm to 37 cm. Recovery in ONC-1 followed a pattern similar to the Lower Bullfrog interval in c#1 (Figure C-15). On December 29, 1997, 46.875 days (67,500 minutes) after pumping stopped, recovery in ONC-1 was about 76% of the antecedent drawdown.

Borehole WT#3, the farthest observation well from the C-wells, responded like the C-wells and ONC-1 to the pumping in c#3 that began on May 8, 1996. Drawdown in WT#3 was detected 6.34 days (9,130 minutes) after pumping started (Figure C-17). Peak drawdown by March 26, 1997, was about 14 cm to 16 cm. Drawdown in WT#3 was more oscillatory than in the other observation wells after 166.67 days (240,000 minutes) of pumping. This behavior was

possibly because (1) WT#3 was much farther from the pumping well than the other observation wells and affected by environmental stresses that did not extend to the other wells, and (2) pumping-related water-level changes in WT#3 were much smaller than in the other observation wells and, therefore, harder to separate from barometric and Earth-tide effects.

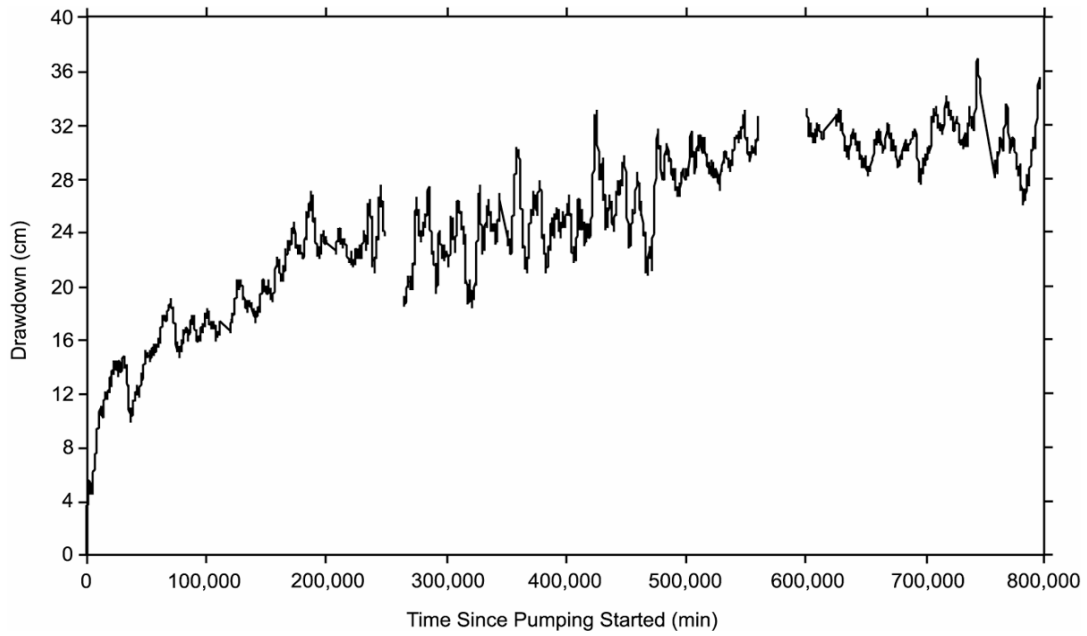


Source: DTN: GS010608312314.001 [DIRS 179647].

Output DTN: GS031008312314.004.

NOTE: Pump was turned off 11/12/97 at 15:59:50 PST.

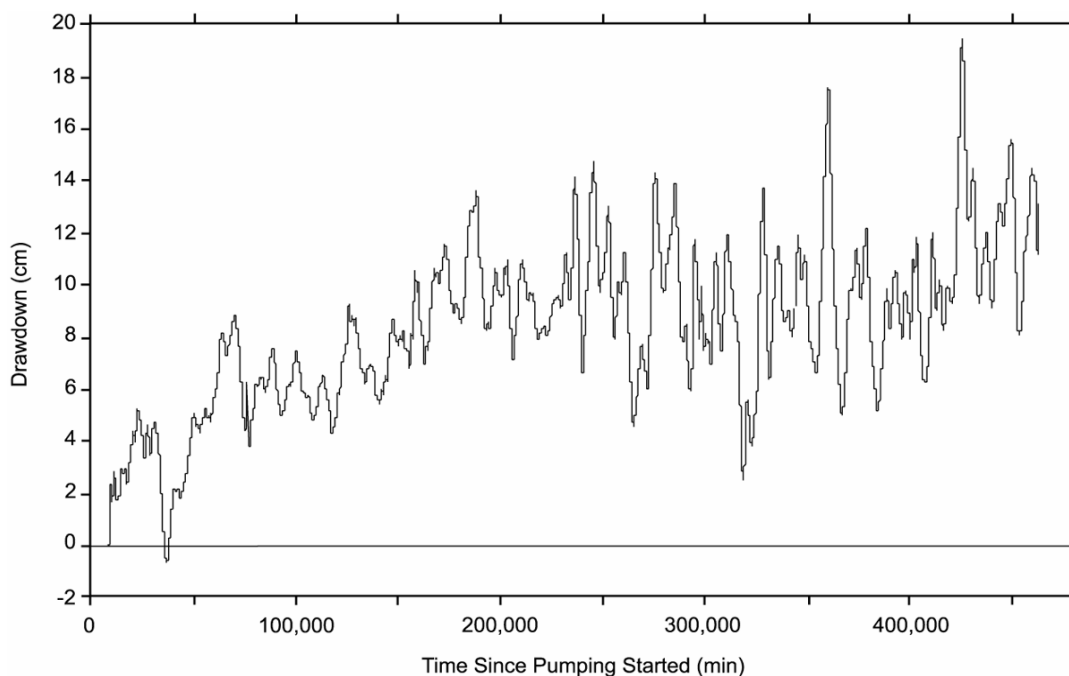
Figure C-15. UE-25 c#1 Lower Bullfrog Recovery, November 12, 1997 (approximately 0 minutes), to December 31, 1997 (approximately 70,000 minutes)



Source: DTN: MO0212SPANYESJ.149 [DIRS161274].

Output DTN: GS031008312314.004.

Figure C-16. Drawdown in UE-25 ONC-1, May 8, 1996 (approximately 0 minutes), to November 12, 1997 (approximately 800,000 minutes)



Source: DTNs: GS970308312314.002 [DIRS 161273], GS970708312314.006 [DIRS 144468].

Output DTN: GS031008312314.004.

Figure C-17. Drawdown in UE-25 WT#3, May 8, 1996 (approximately 0 minutes), to March 26, 1997 (approximately 480,000 minutes)

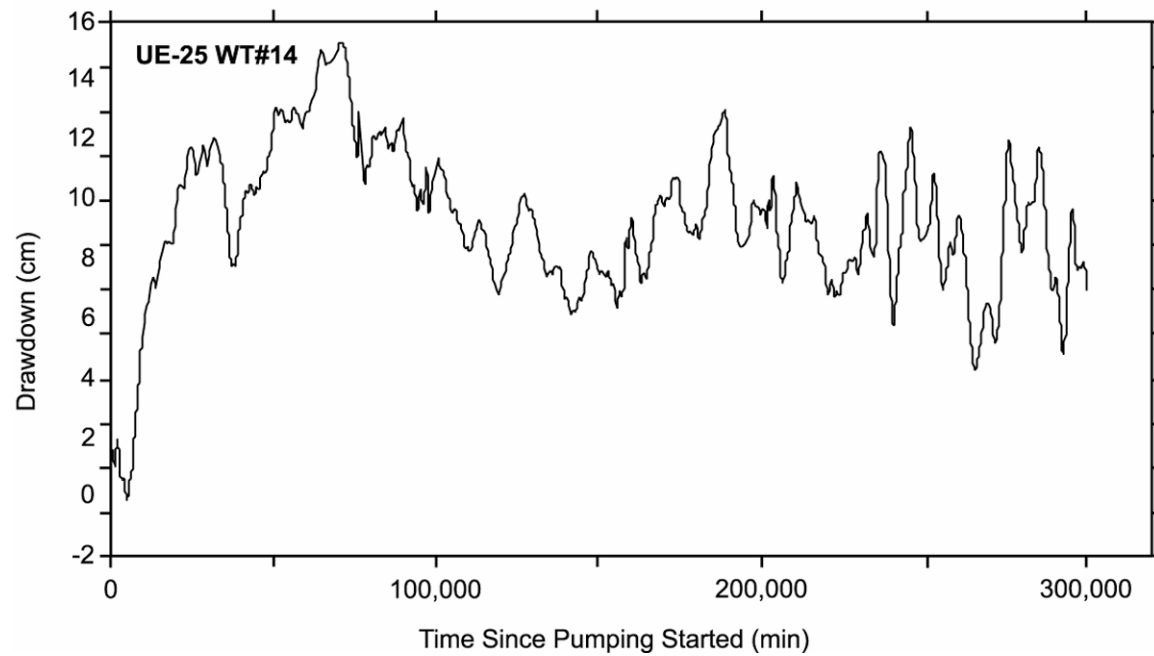
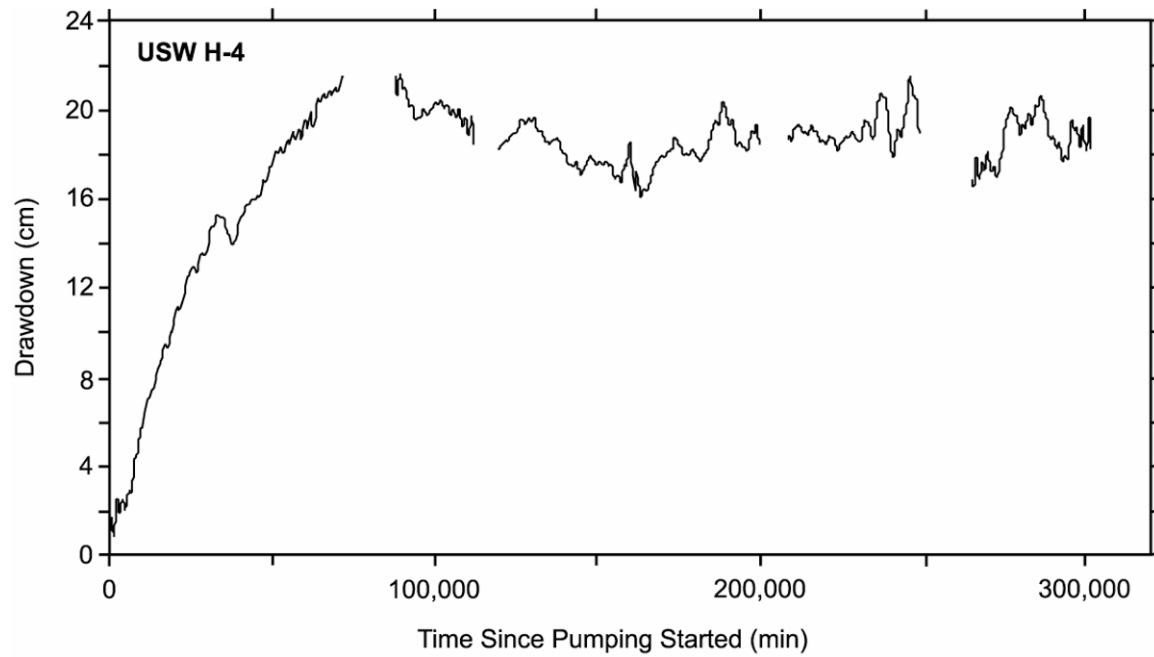
Unlike other observation wells monitored during the hydraulic test that began in May 1996, H-4 and WT#14 exhibited steady-state drawdown as pumping progressed (Figure C-18). Drawdown in both boreholes was delayed for about 5,000 minutes after pumping started, although very small, oscillatory water-level changes, possibly caused by borehole-storage release, occurred during this time. Between 5,000 minutes and 72,000 minutes after pumping started, drawdown increased steadily in response to pumping. Drawdown in H-4 peaked at about 22 cm; drawdown in WT#14 peaked at about 15 cm. After about 50 days (72,000 minutes) of pumping, fluxes from recharge boundaries, probably a transmissive fault, prevented further drawdown. As in a hydraulic test of the Tram interval in c#1 conducted in 1984 (Geldon 1996 [DIRS 100396], pp. 67 to 68), recharge boundaries affecting H-4 and WT#14 are inferred to be faults present near the observation wells. Numerous faults are located near H-4 (Day et al. 1998 [DIRS 101557]), and several segments of the Paintbrush Canyon fault are located near WT#14 (Dickerson and Drake 1998 [DIRS 102781]). Conversely, there are no known changes in stratigraphy or lithology between the C-wells and either H-4 or WT#14 that might be interpreted to create a hydraulic boundary.

C3.2 HYDRAULIC TESTS CONDUCTED IN 1998 AND 1999 (PROW PASS INTERVAL)

Pumping in c#2 to create a forced hydraulic gradient for tracer tests in the Prow Pass interval at the C-wells complex began June 2, 1998, and continued uninterrupted until September 22, 1998. Detailed description of the field tests is reported by Umari (2002 [DIRS 162858], Binder 12,

Sections M-20 to M-22). The pump in c#2 shut off for 70 minutes on September 22 as one of two packers at the bottom of the Prow Pass interval (number 3) was being deflated. Injection of water into c#3 to expedite tracer transport began June 11 and continued without interruption until September 2. The injection pump was off briefly on September 2 and 3 while injection tubing was removed from c#3. Tracers were injected into c#3 on June 17 and into c#1 on July 31.

Responses of c#1, c#3, and ONC-1 to pumping June 2 to June 11, in advance of the tracer tests, were analyzed as a constant-rate withdrawal (CRW) test. After water injection into c#3 began on June 11, the superimposed effects of pumping water from c#2, injecting water into c#3, injecting tracers into c#3 and c#1, operating a mixing pump in c#3 intermittently, and mechanical problems that affected pumping and injection rates made it difficult to analyze data from the C-wells quantitatively. However, ONC-1 was far enough away from the pumping and injection wells that a water-level rise in ONC-1 resulting from injecting water into c#3 clearly could be separated from relatively minor drawdown in the well caused by pumping c#2. The water-level rise in ONC-1 from June 11 to September 1 was analyzed as a constant-rate injection test.



Sources: DTNs: GS970308312314.002 [DIRS 161273], GS970708312314.006 [DIRS 144468].

Output DTN: GS031008312314.004.

Figure C-18. Drawdown in USW H-4 and UE-25 WT#14, May 8, 1996 (approximately 0 minutes), to December 3, 1996 (approximately 300,000 minutes)

C3.2.1 Performance Tests

Hydraulic and tracer tests in the Prow Pass interval were preceded by pump-performance, step-drawdown, and 1-day hydraulic tests conducted in c#2 and c#3 from April 21 to May 29, 1998. These tests were designed primarily to determine whether c#2 could be used as a pumping well for tracer tests and what the optimum pumping rate should be. These tests also were analyzed to determine values of hydrologic properties that would be expected from a longer hydraulic test planned to precede tracer tests in the Prow Pass interval. Fluctuations in water and atmospheric pressures between performance tests indicated barometric efficiency values (Table C-5) for the C-wells and ONC-1 that were used to analyze hydraulic tests (DTNs: GS990408312315.002 [DIRS 140115]; MO0212SPANYESJ.149 [DIRS 161274]) in the Prow Pass interval.

Table C-5. Barometric Efficiency in the C-Wells and UE-25 ONC-1

Interval	c#1	c#2	c#3	UE-25 ONC-1
Calico Hills	N/A	0.93	0.94	N/A
Prow Pass	0.96	0.93	1.0	0.99
Upper Bullfrog	0.99	0.93	≅1.0	N/A
Lower Bullfrog	0.97	N/A	N/A	N/A

Sources: DTNs: GS990408312315.002 [DIRS 140115] and MO0212SPANYESJ.149 [DIRS 161274].

Output DTN: GS031008312314.004 (Table 6.2-5).

N/A=not applicable.

C3.2.2 Analytical Methods

Analytical solutions were used to analyze data from hydraulic tests in the Prow Pass interval. Most of the data were analyzed using the method of Streltsova-Adams (1978 [DIRS 150754]) (Streltsova-Adams.vi V 1.0, STN: 10971-1.0-00 [DIRS 162756]) for a fissure-block aquifer. Analysis of data in this study was restricted to observation wells because most water-level changes in pumping wells at the C-wells complex are too large and rapid (Geldon 1996 [DIRS 100396], pp. 12 to 69) to be explained solely by hydrologic properties of the pumped interval.

C3.2.3 Constant-Rate Withdrawal Test

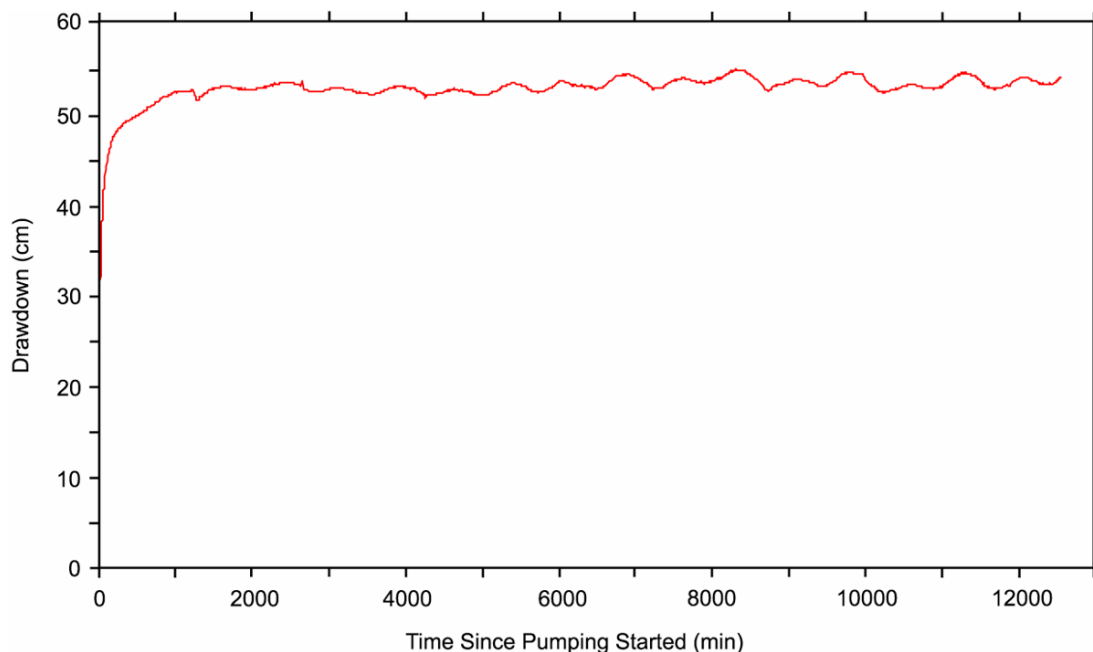
A CRW test in the Prow Pass interval started June 2, 1998. The pumping well for this test was c#2, and the observation wells for the test were c#1, c#3, and ONC-1.

Prior to starting the test, the packer in c#2 between the Prow Pass and Calico Hills intervals was deflated, and the two intervals, together, were pumped for 37 minutes at a rate of 34.2 L/min to fill tubing in the pumping well to the level of the flowmeter. After pumping stopped, the packer in c#2 between the Prow Pass and Calico Hills intervals was reinflated. With slight residual effects from the pretest pumping (which were removed to analyze the test), pumping for the CRW test in the Prow Pass began at 16:00 hours on June 2. Discharge averaged 19.8 L/min between June 2 and 11, a period of 12,500 minutes. Pumping water into c#1 on June 5 to attempt a tracer test, injecting argon gas into c#1 on June 9 to blow sediment out of the tracer injection valve, and testing the downhole mixing pump in c#3 on June 10 briefly disturbed

discharge from c#2 as well as pressures in c#1 and c#3. The CRW test was terminated on June 11, 1998, at 08:19 when operations began for a tracer test between c#3 and c#2.

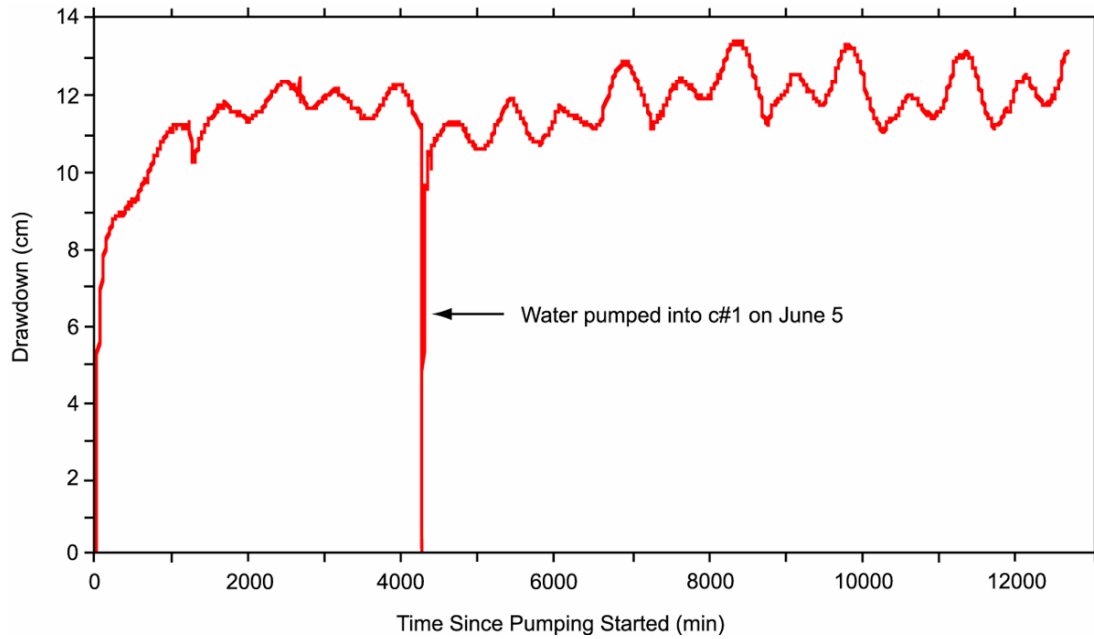
The pumping in c#2 caused 135 m of drawdown in the Prow Pass interval of c#2 three minutes after pumping started. However, the water level rebounded 22 m in the next nine minutes. Subsequently, drawdown increased steadily but slowly and was about 128 m after 12,500 minutes of pumping. On the basis of values of transmissivity and storativity determined in this and previous tests in which the drawdown in the Prow Pass in observation wells was analyzed, only 1.04% of the 128-m drawdown in the Prow Pass of the pumped well c#2, namely 1.34 m, is estimated to have resulted from stressing the aquifer. The remainder of the drawdown is attributed to head losses in the well bore.

The pumping in c#2 caused oscillatory drawdown in the Prow Pass interval of the observation wells. After 12,500 minutes of pumping, this drawdown was 54 cm in c#3 (Figure C-19), 12 cm in c#1 (Figure C-20), and 0.9 cm in ONC-1. Plotted on log-log scales, drawdown in the Prow Pass interval of c#1 and c#3 indicated delayed yield characteristic of a fissure-block aquifer (Streltsova-Adams 1978 [DIRS 150754]), Figures C-21 and C-22).



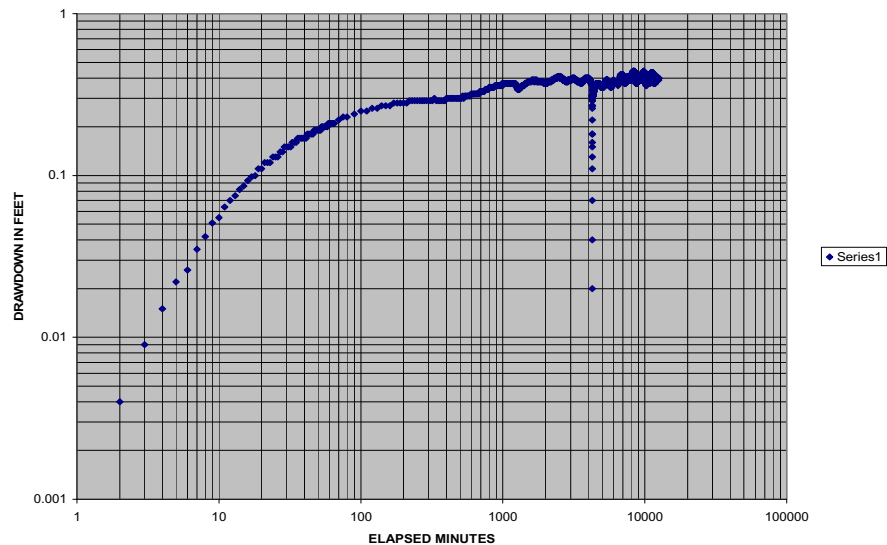
Output DTN: GS031008312314.004 (from Input DTN: GS990408312315.002 [DIRS 140115]).

Figure C-19. UE-25 c#3 Prow Pass Drawdown, June 2, 1998 (approximately 0 minutes), to June 11, 1998 (approximately 12,800 minutes)



Output DTN: GS031008312314.004 (from Input DTN: GS990408312315.002 [DIRS 140115]).

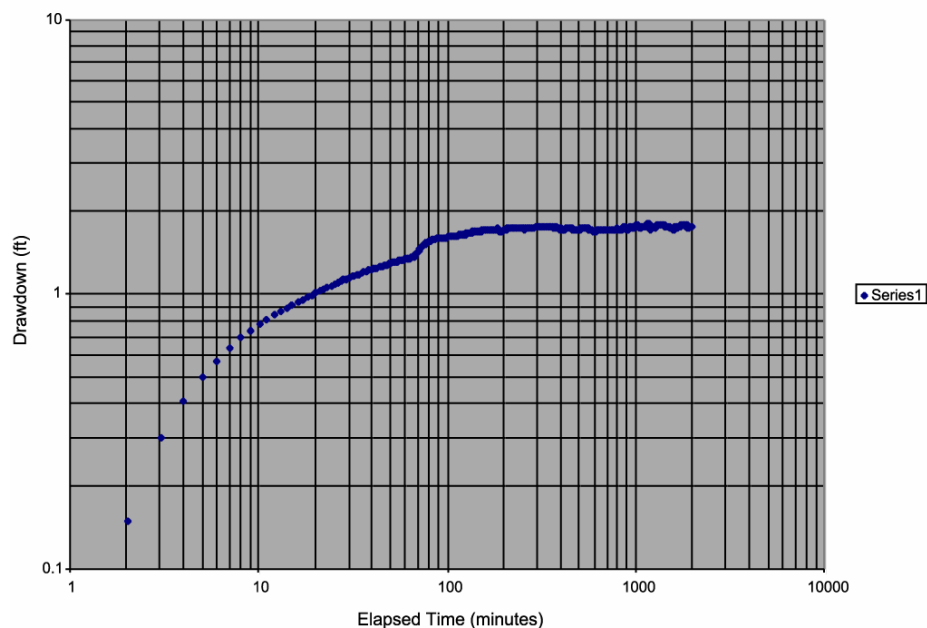
Figure C-20. UE-25 c#1 Prow Pass Drawdown, June 2, 1998 (approximately 0 minutes), to June 11, 1998 (approximately 12,800 minutes)



Output DTN: GS031008312314.004 (from Input DTN: GS990408312315.002 [DIRS 140115]).

NOTE: English units are shown in the figure because the analysis was conducted in English units. However, parameter estimates are reported in metric units to downstream users.

Figure C-21. Drawdown in the Prow Pass Interval of c#1 in Response to Pumping c#2, Starting June 2, 1998, Exhibiting Delayed Yield, Characteristic of a Fissure-Block Aquifer



Output DTN: GS031008312314.004 (from Input DTN: GS990408312315.002 [DIRS 140115]).

NOTE: English units are shown in the figure because the analysis was conducted in English units. However, parameter estimates are reported in metric units to downstream users.

Figure C-22. Drawdown in the Prow Pass Interval of c#3 in Response to Pumping c#2, Starting June 2, 1998, Exhibiting Delayed Yield, Characteristic of a Fissure-Block Aquifer

The pumping in c#2 indicated that the Calico Hills and Prow Pass intervals are connected by fractures beyond borehole walls because the Calico Hills responded to pumping in the Prow Pass wherever it was monitored. During the CRW test, the water level in the Calico Hills interval was drawn down as much as 19 cm in c#2 and 12 cm in c#3. In contrast, no drawdown was observed below the Prow Pass interval in c#2 and c#3 and below the Upper Bullfrog interval in c#1 during this test. The Upper Bullfrog drawdown in c#1 was 55 cm. The general lack of a response to pumping below the Prow Pass probably indicates that the highly permeable Lower Bullfrog and Upper Tram intervals in the C-wells were isolated from the Prow Pass interval during the CRW test.

The responses of the Calico Hills in the C-wells and the Upper Bullfrog in c#1 during pumping of the Prow Pass interval in c#2 made it necessary to apportion flow among the responding intervals to determine hydrologic properties. Lacking a flow survey for the test conditions, interval flow was determined by solving analytical equations simultaneously for interval discharge and transmissivity. To make the number of equations equal to the number of unknowns, it was assumed that (1) transmissivity values for the Calico Hills and Prow Pass intervals in the C-wells are constant, (2) the transmissivity of the Calico Hills is $5.6 \text{ m}^2/\text{day}$ (on the basis of previous hydraulic tests), and (3) flow laterally and vertically within the Calico Hills interval was the same in each of the C-wells during the test. These assumptions were based on analyses and interpretations of previous hydraulic tests, borehole flow surveys, borehole geophysical logs, and other information, which are discussed in Section C4.1 and in the report by Geldon (1996 [DIRS 100396], pp. 12 to 69).

Calculations indicated that the Prow Pass interval contributed 94% of the total flow in c#2 and c#3 but only 24% of the flow in c#1. The substantially different flow from the Prow Pass in c#1 does not seem reasonable because lithologic changes that might account for variable flow do not occur in the Prow Pass interval at the C-wells complex. It is more likely that flow from the Calico Hills interval, the interconnectivity between the Calico Hills and Prow Pass, or the transmissivity of either or both the Prow Pass and Calico Hills intervals is not constant throughout the C-wells complex. Unquantifiable uncertainty results from failure to apportion flow satisfactorily.

Hydrologic properties of the Prow Pass interval determined from analyses of drawdown during the CRW test are summarized in Table C-6. Input parameters (aquifer thickness, fracture half-spacing, interborehole distance, and discharge rate) needed in the analyses are also presented in Table C-6.

C3.2.4 Constant-Rate Injection Test

From June 11 to September 1, 1998, a period of 118,159 minutes, 676,973 L of water was pumped into c#3 to conduct tracer tests. The injection rate ranged from 1.92 L/min to 9.6 L/min before tracers were injected into c#3 on June 17, but it subsequently was stabilized by periodic valve adjustments. From June 11 to September 1, the injection rate averaged 5.7 L/min.

As water was being injected into c#3 from June 11 to September 1; 2,311,290 L of water were withdrawn from c#2 at an average rate of 19.8 L/min. Injecting water into c#3 caused the discharge from c#2 to oscillate within a range of 3.0 L/min. The discharge from c#2 ranged from 18 L/min to 21 L/min after water injection into c#3 started. Lowering the frequency of the pump in c#2 and increasing backpressure on it between August 3 and 31 decreased the discharge from c#2 to a range of 16.8 L/min to 19.8 L/min after August 31.

Table C-6. Hydrologic Properties of the Prow Pass Interval in the C-Wells and Input Parameters Used in Obtaining Them

Borehole	c#1	c#3	ONC-1
Test dates	June 2 to 11, 1998	June 2 to 11,1998	June 11 to September 1, 1998
Period of record (min)	12,500	12,500	≅140,000
Analyzed data	Drawdown	Drawdown	Water-level rise
Transmissivity (m ² /day)	30	30	30
Hydraulic conductivity, fractures (m/day)	1	0.8	2
Hydraulic conductivity, matrix (m/day)	0.000003	0.0002	0.00002
Storativity, fractures	0.00004	0.00004	0.0002
Storativity, matrix	0.0003	0.0004	0.002
Storativity ^a	0.0004	0.0004	0.002
Distance from pumping well, c#2(m)	82.6	28.7	≅843

Table C-6. Hydrologic Properties of the Prow Pass Interval in the C-Wells and Input Parameters Used in Obtaining Them (Continued)

Borehole	c#1	c#3	ONC-1
Transmissive thickness (m)	18.9	31.7	18.9
Fracture half-spacing (m)	0.34	2.0	0.34
Discharge from c#2 (L/min)	4.68 ^b	18.54	-5.7 ^c

Sources: DTNs: GS990408312315.002 [DIRS 140115] (Table 6.2-6) (c#1 and c#3 data); MO0408NYE05474.217 [DIRS 171464] (ONC-1 data) (corroborative data).

Output DTN: GS031008312314.004 (c#1 and c#3 parameters only).

NOTE: The ONC-1 column of this table is used for corroborative purposes only. The hydraulic test analyses indicate that the transmissivity obtained from the ONC-1 response is in good agreement with the transmissivity obtained from the c#1 and c#3 responses, which correspond to much smaller scales. However, the storativity obtained from analyzing the ONC-1 response is about an order-of-magnitude larger than the storativity from c#1 and c#3 responses.

^aCombined storativity: sum of fractures and matrix storativities.

^bAssumed to be 24% of the total discharge from c#2.

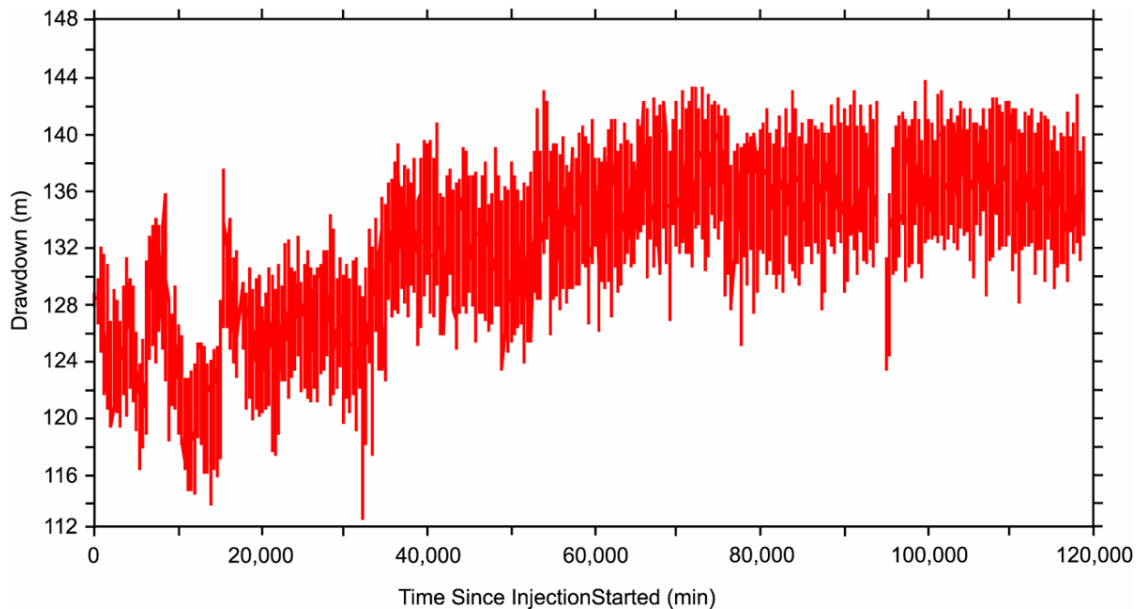
^cNegative discharge indicates an injection rate into c#3, leading to a water-level rise in ONC-1.

Water levels in the Prow Pass interval of c#2 oscillated as much as 10 m between readings due to injection of water into c#3. Although the water injection into c#3 caused drawdown in the Prow Pass interval of c#2 to decrease from 128 m to 115 m in the first 11 days after it began, pumping in c#2 eventually predominated over the superimposed effects of the water injection. From June 22 to September 1, the range in c#2 drawdown increased from 115 m to 125 m to 130 m to 143 m (Figure C-23).

Drawdown in the Prow Pass interval of c#3 decreased from +0.58 m to a range typically between -25 m and -30 m between June 11 and September 1 (the period of continuous injection of water into c#3 [Figure C-24]). This pronounced water-level rise was affected slightly by periodically adjusting the injection rate. Drawdown fluctuated markedly from +87 m to -32 m while tracers were injected into c#3 on June 17 and 18.

Drawdown in the Prow Pass interval of c#1 was disturbed significantly by tracer-test operations in c#3 and c#1 from June 11 to September 1. Injection of water into c#3 decreased drawdown in c#1 from 13 cm to 2.8 cm between June 11 and July 27, but drawdown subsequently increased and ranged from 4.0 cm to 7.9 cm by September 1 (Figure C-25). Injection of tracers into c#3 on June 17 increased drawdown from 8.9 cm to as much as 13 cm, whereas tracer injection in c#1 on July 31 decreased drawdown from +5.9 cm to -174 cm and then increased it to +10 cm. Removal of injection tubing from c#1 on June 26 to replace a cracking valve increased drawdown from 10 cm to 217 cm and then decreased it to -16 cm. Reinstallation of the tubing on July 13 increased drawdown from 5.5 cm to 10 cm and then decreased it to -1,150 cm.

Drawdown in ONC-1 decreased irregularly from +1.1 cm to -2.3 cm between June 11 and September 1 (Figure C-26). Sharply increased drawdown about 9,000 minutes after injection of water into c#3 began may be related to tracer injection into c#3 on June 17, although the timing of this spike does not correlate precisely with the timing of tracer injection in c#3.

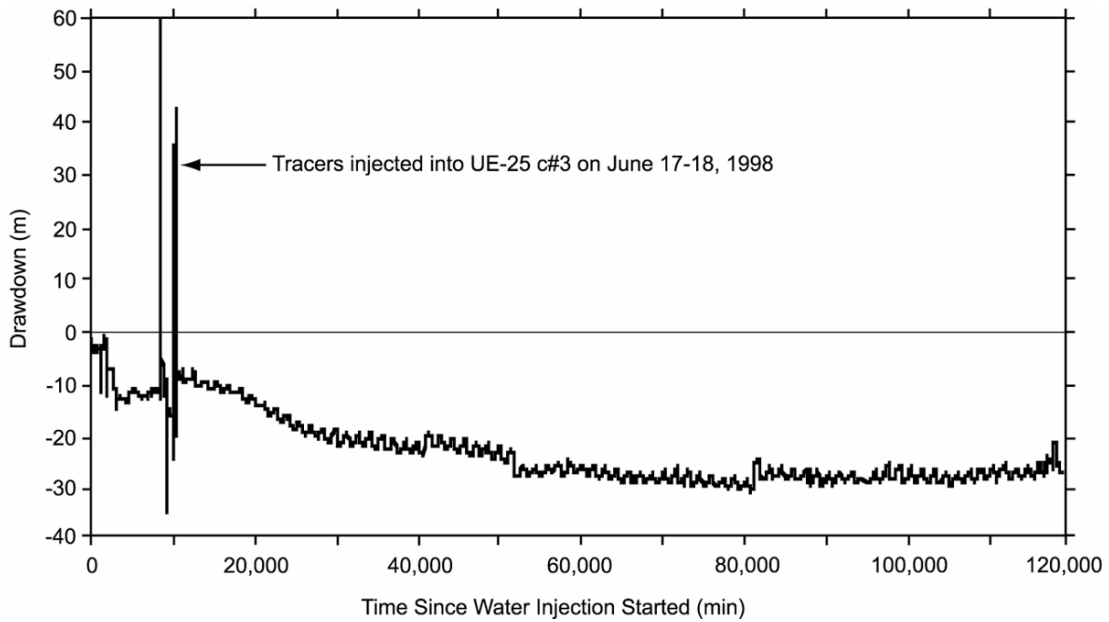


Source: DTN: GS990408312315.002 [DIRS 140115].

Output DTN: GS031008312314.004.

Figure C-23. UE-25 c#2 Prow Pass Drawdown, June 11, 1998 (approximately 0 minutes), to September 1, 1998 (approximately 120,000 minutes)

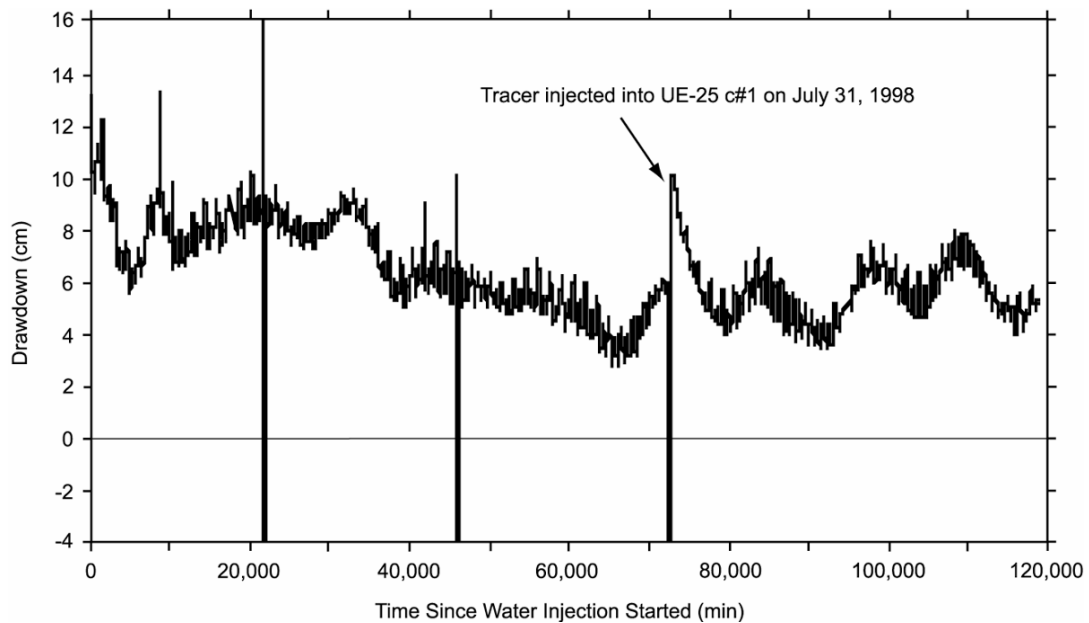
Water-level rises in the C-wells from June 11 to September 1, 1998, were very irregular and too disturbed by tracer-test operations to be analyzed quantitatively. However, the water-level rise in ONC-1 during this period (with superimposed drawdown from pumping c#2 removed) could be matched to the type curves of Streltsova-Adams (1978 [DIRS 150754]) (Streltsova-Adams.vi, V 1.0, STN: 10971-1.0-00 [DIRS 162756]) for a fissure-block aquifer. This analysis (presented in Table C-6) indicated a transmissivity of 30 m²/day, a fracture hydraulic conductivity of 2 m/day, insignificant matrix hydraulic conductivity, and a storativity of 0.002 (90% of which is in the matrix). The Prow Pass interval in ONC-1 and the C-wells have equally low permeability, but storativity is an order of magnitude larger between ONC-1 and the C-wells than at the C-wells complex.



Source: DTN: GS990408312315.002 [DIRS 140115].

Output DTN: GS031008312314.004.

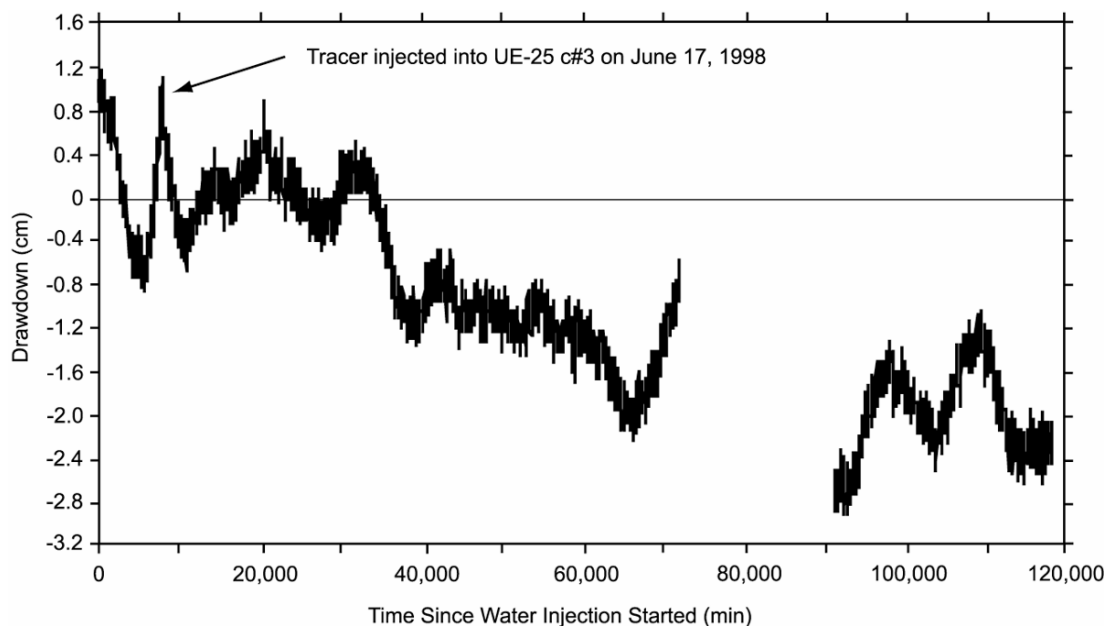
Figure C-24. UE-25 c#3 Prow Pass Drawdown, June 11, 1998 (approximately 0 minutes), to September 1, 1998 (approximately 120,000 minutes)



Source: DTN: GS990408312315.002 [DIRS 140115].

Output DTN: GS031008312314.004.

Figure C-25. UE-25 c#1 Prow Pass Drawdown, June 11, 1998 (approximately 0 minutes), to September 1, 1998 (approximately 120,000 minutes)



Source: DTN:MO0408NYE05474.217 [DIRS 171464] (corroborative data).

Figure C-26. UE-25 ONC-1 Prow Pass Drawdown, June 11, 1998 (approximately 0 minutes), to September 1, 1998 (approximately 120,000 minutes)

C4. HYDROLOGIC PROPERTIES

Hydraulic tests conducted at the C-wells complex from 1995 to 1997 revealed much about the ability of hydrogeologic intervals in the C-wells and the Miocene tuffaceous rocks in the vicinity to store and transmit water. However, it must be emphasized that hydrologic properties computed from these tests pertain only to the structural setting in which the tests were conducted. The Lower Bullfrog interval is the most permeable interval in the C-wells because it is located in these boreholes where two intersecting faults have caused intense fracturing. The Calico Hills interval is the least permeable interval in the C-wells, probably because it is the farthest interval vertically from faults that intersect these boreholes. The combination of its large distance from faults and its low degree of welding (and, thus, high ductility) result in the Calico Hills interval being the least fractured, and, hence, least transmissive interval at the C-wells. In a different structural setting, the Lower Bullfrog, Calico Hills, and other intervals of the Miocene tuffaceous rocks would be expected to have different hydrologic properties than indicated at the C-wells complex. For example, the Bullfrog Tuff yielded very little of the water produced from the Miocene tuffaceous rocks during a tracejector flow survey of p#1 (Craig and Robison 1984 [DIRS 101040]), and the Calico Hills Formation yielded 32% of the water produced from the Miocene tuffaceous rocks during a tracejector flow survey of b#1 (Lahoud et al. 1984 [DIRS 101049]).

Hydrologic properties for the various hydrogeologic intervals at the C-wells are discussed in the following subsections. With the exception of the Prow Pass interval, all of the hydrologic properties were derived from testing conducted prior to 1998. Properties of the Prow Pass interval were derived from testing conducted both prior to and during 1998. The 1998 testing involved pumping of only the Prow Pass interval.

In the analyses described in the following subsections, the interborehole distances were as given in Tables 6.1-1, C-6, and C-7; borehole diameters for all C-wells were assumed to be 27.94 cm (11 in), and aquifer thicknesses were as given under “transmissive thickness” in Tables C-6 and C-7.

C4.1 CALICO HILLS INTERVAL

The Calico Hills interval responded in most hydraulic tests, including one conducted from May to June 1984 (Geldon 1996 [DIRS 100396], pp. 12 to 69), as an unconfined aquifer. In four tests conducted from 1984 to 1997, the Calico Hills interval consistently was determined to be the least permeable interval in the C-wells (Table C-7). The hydraulic test in May and June 1984 indicated that the Calico Hills interval in c#1 has a transmissivity of 9 m²/day, a horizontal hydraulic conductivity of 0.2 m/day, a vertical hydraulic conductivity of 0.3 m/day, and a specific yield of 0.003 (Geldon 1996 [DIRS 100396], pp. 12 to 69). The hydraulic test in June 1995 indicated that the Calico Hills interval in c#2 has a transmissivity of 6 m²/day, a horizontal hydraulic conductivity of 0.1 m/day, and a storativity of 0.0002. Hydraulic tests conducted in February 1996 and from May 1996 to November 1997 generally supported the previous analyses. The specific yield of 0.4 obtained for the Calico Hills in c#2 from analyzing the May 8, 1996, response is much higher than expected for fractured rock [it can go up to 30% for unconsolidated materials (Bouwer 1978 [DIRS 162675], p. 30)]. A representative plot indicating a match between the data and one of the type curves of Neuman (1975 [DIRS 150321]) for an unconfined, anisotropic aquifer is shown in Figure C-27.

C4.2 PROW PASS INTERVAL

The Prow Pass interval generally responded to hydraulic tests conducted from June 1995 to November 1997 as a confined aquifer (Table C-7). The hydraulic test in June 1995 indicated that the Prow Pass interval in c#1 had a transmissivity of 60 m²/day, a hydraulic conductivity of 3 m/day, and a storativity of 0.0003. The same hydraulic test indicated that the Prow Pass interval in c#2 has a transmissivity of 40 m²/day, a hydraulic conductivity of 2 m/day, and a storativity of 0.0004. Analyses of hydraulic tests conducted in February 1996 and from May 1996 to March 1997 generally produced parameter values similar to those produced by the previous analyses, even when the February 1996 response was analyzed as an unconfined-aquifer response. A representative plot indicates a match between the data and the type curve by Theis (1935 [DIRS 150327]) for a confined aquifer (Figure C-28).

Hydraulic testing of the Prow Pass interval conducted in 1998 by pumping c#2 indicated a fissure-block aquifer with transmissivity of 30 m²/day in both c#1 and c#3. Fracture hydraulic conductivities derived from responses in c#1 and c#3 were 1 m/day and 0.8 m/day, respectively. Matrix hydraulic conductivities were negligible, and overall storativity was 0.0004, with most of that being attributed to the matrix. These parameter estimates are in good agreement with those derived from earlier testing in which the Prow Pass interval was not pumped directly (above). This result instills confidence in the ability to estimate hydrologic parameters for intervals that are not pumped directly but that respond to pumping other intervals. Even though comparable parameter values were obtained in c#1 by analyzing some of the test responses in the Prow Pass as either unconfined or fissure-block aquifer responses, the later interpretation is more logical because the Prow Pass interval is not at the water table.

Table C-7. Results of Hydraulic Tests in Borehole UE-25 c#3, June 1995 to November 1997

Starting Date	06/12/95	02/08/96	02/08/96 c#1	05/08/96	05/08/96	06/12/95	02/08/96 c#2	05/08/96	05/08/96
Calico Hills									
Analyzed data	None	None	N/A	None	N/A	Drawdown	Drawdown	Drawdown	N/A
Period of record (min)	N/A	N/A	N/A	N/A	N/A	5,800	7,000	464,100	N/A
Aquifer type	Unconfined	Unconfined	N/A	Unconfined	N/A	Unconfined	Confined	Unconfined	N/A
Transmissive thickness (m)	60.4	60.4	N/A	60.4	N/A	45.4	45.4	45.4	N/A
Distance from pumping well (m)	78.3	78.3	N/A	78.3	N/A	29.0	29.0	29.0	N/A
Average discharge (L/min)	51	2.52	N/A	6.0	N/A	51	2.52	6.0	N/A
Transmissivity (m ² /day)	9(est)	9(est)	N/A	9(est)	N/A	6	10	4	N/A
Horizontal hydraulic conductivity (m/day)	0.2(est)	0.2(est)	N/A	0.2(est)	N/A	0.1	0.2	0.08	N/A
Vertical hydraulic conductivity (m/day)	0.3(est)	0.3(est)	N/A	0.3(est)	N/A	ND	ND	0.01	N/A
Storativity (dimensionless)	ND	ND	N/A	ND	N/A	0.0002	0.0006	0.0003	N/A
Specific yield (dimensionless)	0.003(est)	0.003(est)	N/A	0.003(est)	N/A	ND	ND	0.4	N/A
Prow Pass									
Analyzed data	Drawdown	Drawdown	Drawdown	Drawdown	N/A	Drawdown	Drawdown	Drawdown	N/A
Period of record (min)	5,800	7,000	7,000	464,100	N/A	5,800	7,000	464,100	N/A
Aquifer type	Confined	Unconfined	Confined	Confined	N/A	Confined	Confined	Confined	N/A
Transmissive thickness (m)	18.9	18.9	18.9	18.9	N/A	23.8	23.8	23.8	N/A
Distance from pumping well (m)	81.1	81.1	81.1	81.1	N/A	28.6	28.6	28.6	N/A
Average discharge (L/min)	39	12.6	12.6	13.2	N/A	39	7.8	11.4	N/A
Transmissivity (m ² /day)	60	50	60	50	N/A	40	30	30	N/A
Horizontal hydraulic conductivity (m/day)	3	3	3	3	N/A	2	1	1	N/A
Vertical hydraulic conductivity (m/day)	ND	0.0001	ND	ND	N/A	ND	ND	ND	N/A
Storativity (dimensionless)	0.0003	0.0003	0.0004	0.0002	N/A	0.0004	0.003	0.0008	N/A
Specific yield (dimensionless)	ND	ND	ND	ND	N/A	ND	ND	ND	N/A
Upper Bullfrog									
Analyzed data	Recovery	Drawdown	N/A	Drawdown	N/A	Drawdown	Drawdown	Drawdown	N/A
Period of record (min)	5,700	7,000	N/A	464,100	N/A	5,800	7,000	464,100	N/A
Aquifer type	Confined	Unconfined	N/A	Fissure-block	N/A	Confined	Confined	Confined	N/A
Transmissive thickness (m)	46.0	46.0	N/A	46.0	N/A	24.1	24.1	24.1	N/A

Table C-7. Results of Hydraulic Tests in Borehole UE-25 c#3, June 1995 to November 1997 (Continued)

Starting Date	06/12/95	02/08/96	02/08/96 c#1	05/08/96	05/08/96	06/12/95	02/08/96 c#2	05/08/96	05/08/96
Upper Bullfrog (Continued)									
Distance from pumping well (m)	83.2	83.2	N/A	82.3	N/A	28.6	28.6	28.6	N/A
Average discharge (L/min)	52.8	22.2	N/A	19.2	N/A	52.8	21.6	21.6	N/A
Transmissivity (m ² /day)	90	40	N/A	50	N/A	100	100	80	N/A
Horizontal hydraulic conductivity (m/day)	2	0.8	N/A	1/0.00002*	N/A	4	4	3	N/A
Vertical hydraulic conductivity (m/day)	ND	0.5	N/A	ND	N/A	ND	ND	ND	N/A
Storativity (dimensionless)	0.00006	0.0009	N/A	0.0001/0.0009*	N/A	0.00003	0.00002	0.00002	N/A
Specific yield (dimensionless)	ND	0.002	N/A	ND	N/A	ND	ND	ND	N/A
Bullfrog-Tram									
Analyzed data	N/A	Drawdown	N/A	N/A	N/A	N/A	Drawdown	N/A	N/A
Period of record (min)	N/A	7,000	N/A	N/A	N/A	N/A	7,000	N/A	N/A
Aquifer type	N/A	Confined	N/A	N/A	N/A	N/A	Confined	N/A	N/A
Transmissive thickness (m)	N/A	112	N/A	N/A	N/A	N/A	51.2	N/A	N/A
Distance from pumping well (m)	N/A	86.3	N/A	N/A	N/A	N/A	29	N/A	N/A
Average discharge (L/min)	N/A	470.4	N/A	N/A	N/A	N/A	475.8	N/A	N/A
Transmissivity (m ² /day)	N/A	2,500	N/A	N/A	N/A	N/A	2,500	N/A	N/A
Horizontal hydraulic conductivity (m/day)	N/A	20	N/A	N/A	N/A	N/A	50	N/A	N/A
Vertical hydraulic conductivity (m/day)	N/A	ND	N/A	N/A	N/A	N/A	ND	N/A	N/A
Storativity (dimensionless)	N/A	0.0003	N/A	N/A	N/A	N/A	0.002	N/A	N/A
Specific yield (dimensionless)	N/A	ND	N/A	N/A	N/A	N/A	ND	N/A	N/A
Lower Bullfrog									
Analyzed data	Recovery	None	N/A	Drawdown	Drawdown	Drawdown	None	Drawdown	Drawdown
Period of record (min)	6,300	N/A	N/A	464,100	464,100	5,800	N/A	464,100	464,100
Aquifer type	Confined	Confined	N/A	Confined	Fissure-block	Confined	Confined	Confined	Fissure-block
Transmissive thickness (m)	62.8	62.8	N/A	62.8	62.8	29.9	29.9	29.9	29.9
Distance from pumping well (m)	85.6	85.6	N/A	85.6	85.6	29.3	29.3	29.3	29.3
Average discharge (L/min)	918	ND	N/A	382.2	382.2	918	ND	401.4	401.4
Transmissivity (m ² /day)	1,800	ND	N/A	1,600	1,300	1,900	ND	1,600	1,300

Table C-7. Results of Hydraulic Tests in Borehole UE-25 c#3, June 1995 to November 1997 (Continued)

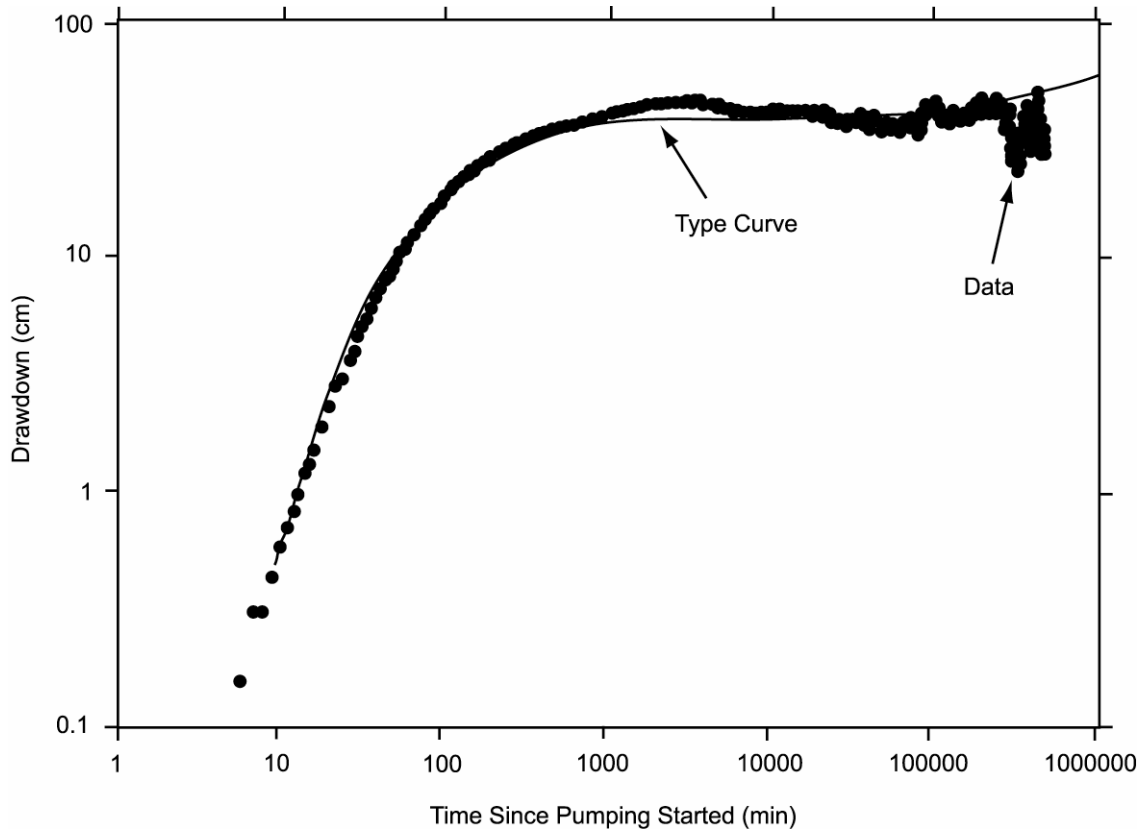
Starting Date	06/12/95	02/08/96	02/08/96 c#1	05/08/96	05/08/96	06/12/95	02/08/96 c#2	05/08/96	05/08/96
Lower Bullfrog (Continued)									
Horizontal hydraulic conductivity (m/day)	30	ND	N/A	30	20/0.0004*	60	ND	50	40/0.001*
Vertical hydraulic conductivity (m/day)	ND	ND	N/A	ND	ND	ND	ND	ND	ND
Storativity (dimensionless)	0.0004	ND	N/A	0.0002	0.0002/0.002*	0.003	ND	0.001	0.002/0.02*
Specific yield (dimensionless)	ND	ND	N/A	ND	ND	ND	ND	ND	ND
Upper Tram									
Analyzed data	None	None	N/A	None	N/A	None	None	None	N/A
Period of record (min)	N/A	N/A	N/A	N/A	N/A	N/A	N/A	N/A	N/A
Aquifer type	Leaky	Leaky	N/A	Leaky	N/A	Leaky	Leaky	Leaky	N/A
Transmissive thickness (m)	49.7	49.7	N/A	49.7	N/A	21.3	21.3	21.3	N/A
Distance from pumping well (m)	86.9	86.9	N/A	86.9	N/A	29.6	29.6	29.6	N/A
Average discharge (L/min)	284.4	284.4	N/A	151.2	N/A	284.4	ND	130.8	N/A
Transmissivity (m ² /day)	ND	ND	N/A	800	N/A	ND	ND	900	N/A
Horizontal hydraulic conductivity (m/day)	ND	ND	N/A	20	N/A	ND	ND	40	N/A
Vertical hydraulic conductivity (m/day)	ND	ND	N/A	ND	N/A	ND	ND	ND	N/A
Storativity (dimensionless)	ND	ND	N/A	0.0001	N/A	ND	ND	0.001	N/A
Specific yield (dimensionless)	ND	ND	N/A	ND	N/A	ND	ND	ND	N/A

Sources: DTNs: LA0705PR150304.002 [DIRS 181198], LA0705PR150304.003 [DIRS 181201] (qualified in Appendix R), GS970308312314.001 [DIRS 159240], GS970708312314.005 [DIRS 159241], GS981008312314.002 [DIRS 147068], GS981008312314.003 [DIRS 144464], GS010608312314.001 [DIRS 179647].

Output DTN: GS031008312314.004 (Table 6.2-7).

NOTE: First number is for fractures; second is for matrix.

ND=no data; N/A=not applicable; est=estimated to be the same as values obtained from a hydraulic test in May 1984.

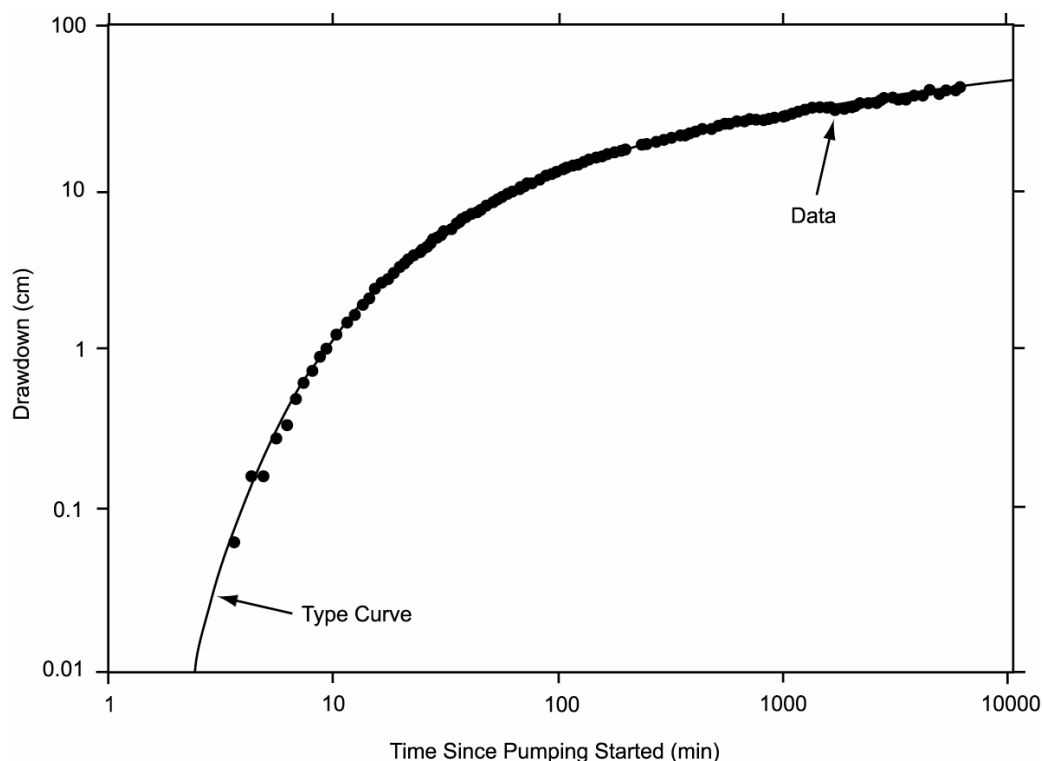


Sources: DTNs: GS970308312314.001 [DIRS 159 240], GS970708312314.005 [DIRS 159241],
GS981008312314.002 [DIRS 147068], GS981008312314.003 [DIRS 144464].

Output DTN: GS031008312314.004.

NOTE: The analysis used the Neuman (1975 [DIRS 150321]) method.

Figure C-27. Analysis of Drawdown in the Calico Hills Interval of UE-25 c#2, May 8, 1996 (approximately 0 minutes), to March 26, 1997 (approximately 470,000 minutes)



Sources: DTNs: LA0705PR150304.002 [DIRS 181198], LA0705PR150304.003 [DIRS 181201] (Qualified in Appendix R).

Output DTN: GS031008312314.004.

NOTE: The analysis used the Theis 1935 [DIRS 150327] method.

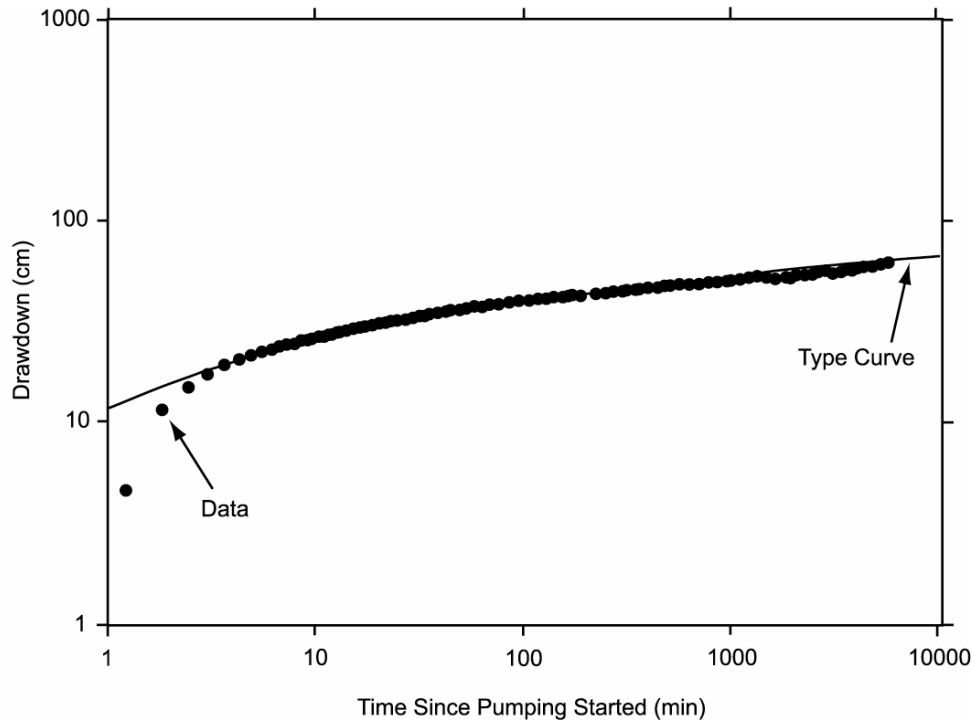
Figure C-28. Analysis of Drawdown in the Prow Pass Interval of UE-25 c#1, June 12 to 16, 1995

C4.3 UPPER BULLFROG INTERVAL

The Upper Bullfrog interval in c#2 responded to all hydraulic tests as a confined aquifer (Table C-7). Those tests consistently indicated a transmissivity of 80 m²/day to 100 m²/day, a hydraulic conductivity of 3 m/day to 4 m/day, and a storativity of 0.00002 to 0.00003. A representative plot indicates a match between the data and the type curve of Theis (1935 [DIRS 150327]) for a confined aquifer (Figure C-29).

The hydraulic test in June 1995 produced results for the Upper Bullfrog interval in c#1 consistent with results for that interval in c#2 (Table C-7). During longer tests conducted in February 1996 and May 1996, sufficient time elapsed to reveal the effects of fractures on flow between the Upper Bullfrog interval in c#1 and open intervals in the pumping well. Analyses of drawdown (complicated by downward flow through fractures) indicated smaller values of transmissivity and hydraulic conductivity and larger values of storativity than analyses of drawdown in which the effects of fractures were not evident (Table C-7). Hydrologic properties determined from hydraulic tests conducted in 1996 and 1997 using unconfined and fissure-block interpretations are less reliable than properties determined from the hydraulic test in June 1995 because of the sliding sleeve placement in the observation and pumping wells in the later tests. Unconfined and fissure-block responses are similar; however, a fissure-block interpretation is more logical for the

Upper Bullfrog aquifer than an unconfined interpretation because this aquifer is not at the water table. Also, the specific yield calculated from the unconfined solution, 0.002, seems unrealistically low.



Sources: DTNs: LA0705PR150304.002 [DIRS 181198], LA0705PR150304.003 [DIRS 181201] (Qualified in Appendix R).

Output DTN: GS031008312314.004.

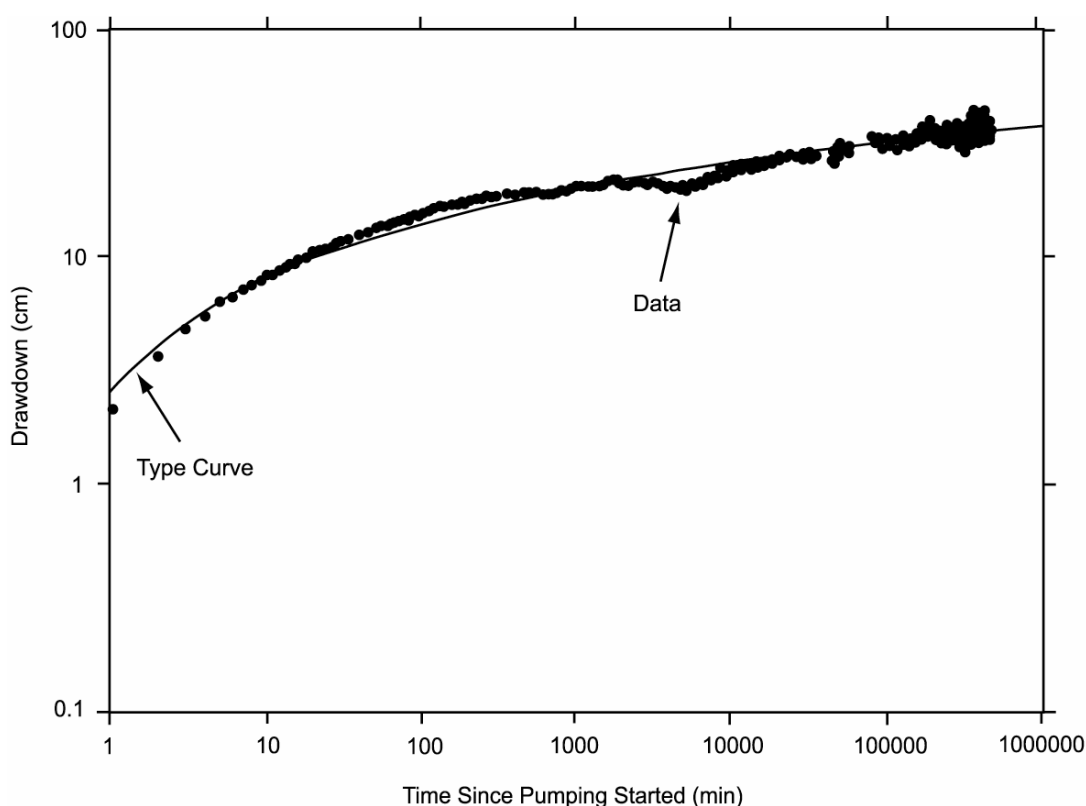
NOTE: The analysis used the Theis 1935 [DIRS 150327] method.

Figure C-29. Analysis of Drawdown in UE-25 c#2 Upper Bullfrog Interval, June 12 to 16, 1995

C4.4 LOWER BULLFROG INTERVAL

Undisturbed drawdown in the Lower Bullfrog interval of c#1 and c#2 during the hydraulic test conducted from May 1996 to November 1997 can be interpreted in several ways not evident from previous hydraulic tests of much shorter duration. Although previous tests indicated a confined-aquifer response, the test beginning in May 1996 progressed long enough to develop a double-humped drawdown curve characteristic of a fissure-block aquifer. From 158,000 minutes (110 days) after pumping started in May 1996 to the end of the analyzed record (464,100 minutes [312 days] after pumping started), drawdown in c#1 and c#2 was greater than anticipated on the basis of extrapolating the earlier drawdown for long periods (using the equation of Theis (1935 [DIRS 150327]) to extrapolate drawdown). The oscillatory pattern of drawdown in the C-wells after 158,000 minutes (110 days) of pumping can be interpreted to indicate that the spreading cone of depression encompassed volumes of the Lower Bullfrog interval that were alternately less transmissive or as transmissive as the Lower Bullfrog in the C-wells.

Values of transmissivity computed for the Lower Bullfrog interval are significantly different depending on whether the interval is considered a confined aquifer or a fissure-block aquifer (Table C-7). In c#1 and c#2, transmissivity is 1,600 m²/day if the Lower Bullfrog is analyzed as a confined aquifer (Figure C-30), and 1,300 m²/day if analyzed as a fissure-block aquifer (Figure C-31). Although the two analytical solutions produced equally plausible results, the fissure-block aquifer solution is consistent with a tracer test conducted from February to March 1996 that indicated dual porosity in the Bullfrog-Tram interval (Fahy 1997 [DIRS 137456], third {unnumbered} page). Also, the longer pumping required for the fissure-block aquifer response to develop and the lower transmissivity value determined from that response can be interpreted to confirm that less-transmissive rocks were reached as the cone of depression spread to increasingly distant areas during the hydraulic test that began in May 1996.



Sources: DTNs: GS970308312314.001 [DIRS 159 240], GS970708312314.005 [DIRS 159241], GS981008312314.002 [DIRS 147068], GS981008312314.003 [DIRS 144464].

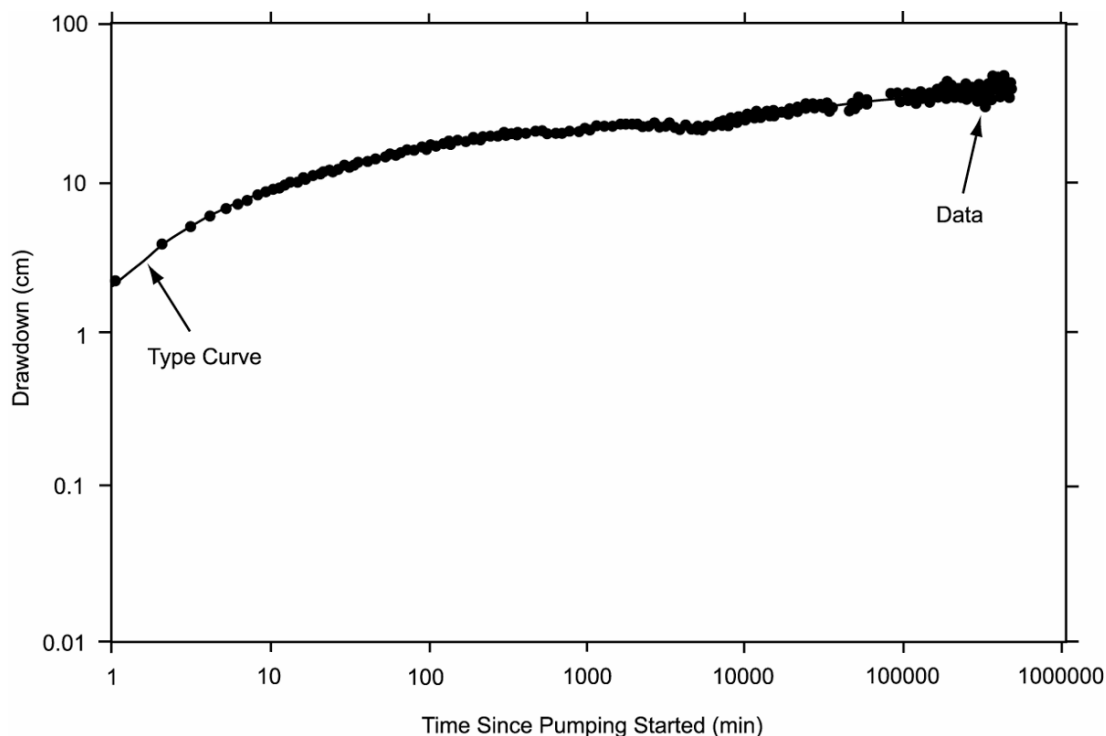
Output DTN: GS031008312314.004.

NOTE: The analysis used the Theis 1935 [DIRS 150327] method.

Figure C-30. Analysis of Drawdown in UE-25 c#1 Lower Bullfrog Interval, May 8, 1996, to March 26, 1997

Values of hydraulic conductivity and storativity are considerably larger in the rock mass between c#2 and c#3 than in the rock mass between c#1 and c#3. When analyzed as a confined aquifer, the hydraulic conductivity of the Lower Bullfrog interval is 50 m/day in c#2 and 30 m/day in

c#1, and its storativity is 0.001 in c#2 and 0.0002 in c#1. (These hydraulic conductivities and storativities of the interval in both boreholes are about the same as those of the fractures in the interval in both boreholes obtained when the Lower Bullfrog is analyzed as a fissure-block aquifer; Table C-7.)



Sources: DTNs: GS970308312314.001 [DIRS 159 240], GS970708312314.005 [DIRS 159241], GS981008312314.002 [DIRS 147068], GS981008312314.003 [DIRS 144464].

Output DTN: GS031008312314.004.

NOTE: For the analysis curve, the parameter $\tau/B = 0.05$. The analysis used the Streltsova-Adams (1978 [DIRS 150754]) method.

Figure C-31. Analysis of Drawdown in UE-25 c#1 Lower Bullfrog Interval, May 8, 1996, to March 26, 1997

C4.5 UPPER TRAM INTERVAL

The Upper Tram interval was known from earlier hydraulic tests (conducted in 1984) to respond to pumping as a leaky aquifer without confining bed storage because of recharge from faults that intersect the C-wells in that interval (Geldon 1996 [DIRS 100396], pp. 12 to 69). Although hydrologic properties of the Upper Tram (UT) interval could not be determined directly from hydraulic tests conducted during this study (because of transducer malfunction), they could be estimated by subtracting values of hydrologic properties determined for the Lower Bullfrog (LB) interval from those determined for the Bullfrog-Tram (BT) interval. This is deemed acceptable based on the assumption that flow during the Bullfrog-Tram test and the Lower Bullfrog test was radial in an equivalent porous medium that is homogeneous and isotropic, and composed of interconnected fractures.

The following equations (C-2 to C-4) were used:

$$T_{UT} = T_{BT} - T_{LB} \quad (\text{Eq. C-2})$$

$$S_{UT} = S_{BT} - S_{LB} \quad (\text{Eq. C-3})$$

$$K_{UT} = (K_{BT} \times b_{BT} - K_{LB} \times b_{LB})/b_{UT} \quad (\text{Eq. C-4})$$

where

T = transmissivity (L^2/T)

S = storativity (dimensionless)

K = hydraulic conductivity (L/T)

b = thickness (L).

Only hydrologic properties of the Lower Bullfrog interval determined by the Theis (1935 [DIRS 150327]) solution were used in these calculations because hydrologic properties of the Bullfrog-Tram interval (which includes the Lower Bullfrog) were determined by this method. These calculations indicated a transmissivity of 800 m^2/day , a hydraulic conductivity of 20 m/day , and a storativity of 0.0001 for the Upper Tram interval in c#1; and a transmissivity of 900 m^2/day , a hydraulic conductivity of 40 m/day , and a storativity of 0.001 for the Upper Tram interval in c#2 (Table C-7).

C4.6 MIOCENE TUFFACEOUS ROCKS: HYDROLOGIC PROPERTIES AND LARGE-SCALE HORIZONTAL ANISOTROPY

Indicative of hydraulic connection through a highly developed fracture network, diverse intervals of the Miocene tuffaceous rocks in six observation wells responded to the pumping in c#3 from May 1995 to November 1997 (Table C-8). The C-wells, ONC-1, and H-4 appear to be connected hydraulically through a northwest-trending zone of discontinuous faults that extends from Bow Ridge to Antler Wash (Geldon et al. 1998 [DIRS 129721], pp. 23 to 25, Figure 2; p. 31). The Paintbrush Canyon and related faults that intersect WT#14 and the C-wells probably enhance hydraulic communication between those boreholes. Hydraulic communication between the C-wells and WT#3 is probably enabled both stratigraphically and structurally because those boreholes were open during hydraulic tests in the same geologic unit (the Bullfrog Tuff) and are cut by the same faults (the Paintbrush Canyon and related faults).

Analyses of the drawdown in individual observation wells (Figures C-32 to C-35) provide hydrologic properties of the rock mass at the scale of the distance between those boreholes and c#3 (Table C-8). Analyses of drawdown in multiple observation wells, either as a function of time (normalized by dividing by the square of the distance between the observation and pumping wells) or as a function of distance at a specified time, allow computation of hydrologic properties of the tuffaceous rock mass in which all of the included observation wells are located.

Table C-8. Hydrologic Properties Computed from Observation Well Responses to Pumping in UE-25-c#3, May 1995 to November 1997

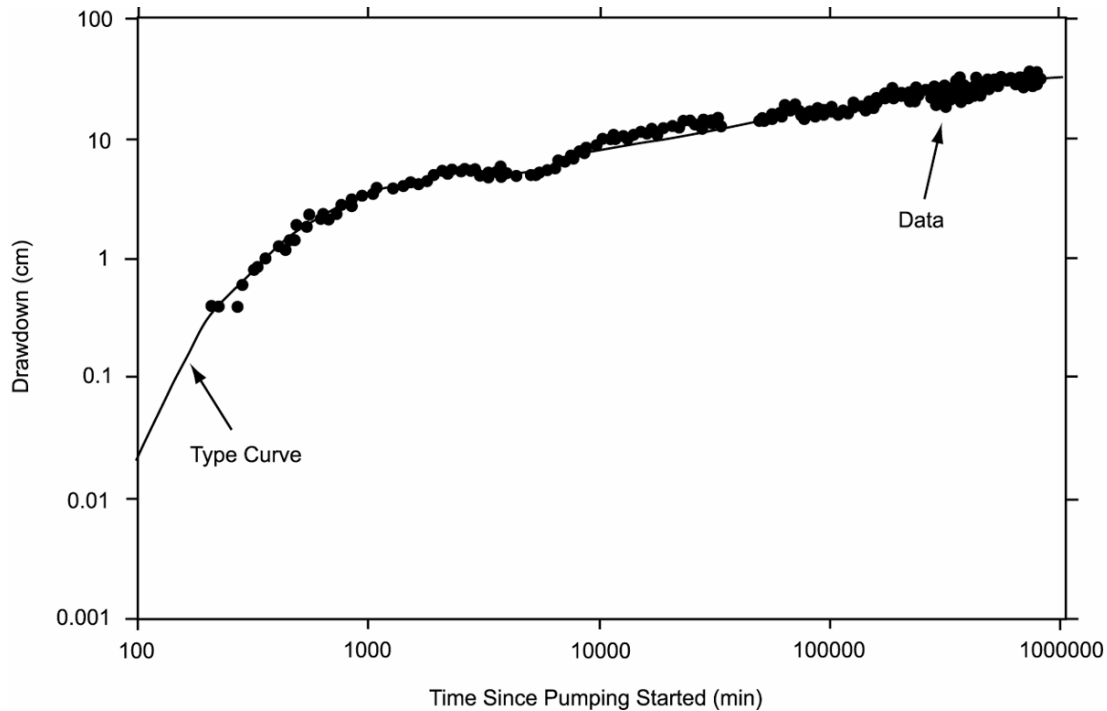
Borehole	c#2	c#2	c#1	c#1
Starting date of hydraulic test	05/22/95	05/08/96	05/22/95	05/08/96
Period of record (min)	14,400	464,100	11,400	464,100
Analyzed data	Drawdown	Drawdown	Recovery	Drawdown
Geologic units in monitored interval	Calico Hills to Tram	Calico Hills to Tram	Calico Hills to Tram	Calico Hills to Tram
Aquifer type	Unconfined	Variable	Unconfined	Variable
Transmissive thickness (m) ^a	165	144	252	238
Distance from pumping well (m)	29.0	29.0	82.6	82.9
Average discharge (L/min)	1074	571.8	1074	571.8
Transmissivity (m ² /day)	2,100	2,400–2,600	1,800	2,200–2,600
Horizontal hydraulic conductivity (m/day)	13	16–18	7	9–11
Vertical hydraulic conductivity (m/day)	1.7	Not estimated	0.3	Not estimated
Storativity (dimensionless)	0.003	0.003–0.004	0.001	0.002
Specific yield (dimensionless)	0.2	Not estimated	0.01	Not estimated
Borehole	UE-25 ONC-1	USW H-4	UE-25 WT#14	UE-25 WT#3
Starting date of hydraulic test	05/08/96	05/08/96	05/08/96	05/08/96
Period of record (min)	796,663	72,000	72,000	463,500
Analyzed data	Drawdown	Drawdown	Drawdown	Drawdown
Geologic units in monitored interval	Prow Pass	Prow Pass to Lithic Ridge	Topopah Spring and Calico Hills	Bullfrog
Aquifer type	Fissure-block	Confined	Confined	Confined
Transmissive thickness (m)	193 (est)	276	Not estimated	47.5 (estimated)
Distance from pumping well (m)	843	2,245	2,249	3,526
Average discharge (L/min)	552.6	583.2	583.2	575.4
Transmissivity (m ² /day)	1,000	700	1,300	2,600
Horizontal hydraulic conductivity (m/day)	5/.002 ^b	2	Not estimated	56
Storativity (dimensionless)	0.001/0.01 ^b	0.002	0.002	0.002

Sources: DTNs: GS960108312313.001 [DIRS 164801] (Corroborative only), LA 0705PR150304.002 [DIRS 181198], LA0705PR150304.003 [DIRS 181201] (Qualified in Appendix R), GS970308312314.001 [DIRS 159240], GS970708312314.005 [DIRS 159241], GS981008312314.002 [DIRS 147068], GS981008312314.003 [DIRS 144464], GS970308312314.002 [DIRS 161273], GS970708312314.006 [DIRS 144468], MO0212SPANYESJ.149 [DIRS 161274].

Output DTN: GS031008312314.004 (Table 6.2-8).

^aThe sum of transmissive thicknesses of component geologic units is shown in Table C-7 for the corresponding test.

^bThe first number is for fractures; the second is for matrix (values of transmissivity and hydraulic conductivity listed for UE-25 ONC-1 and USW H-4 differ from those obtained from a hydraulic test conducted from May 22 to June 1, 1995, but the values determined from the longer test beginning in May 1996 are considered more reliable).



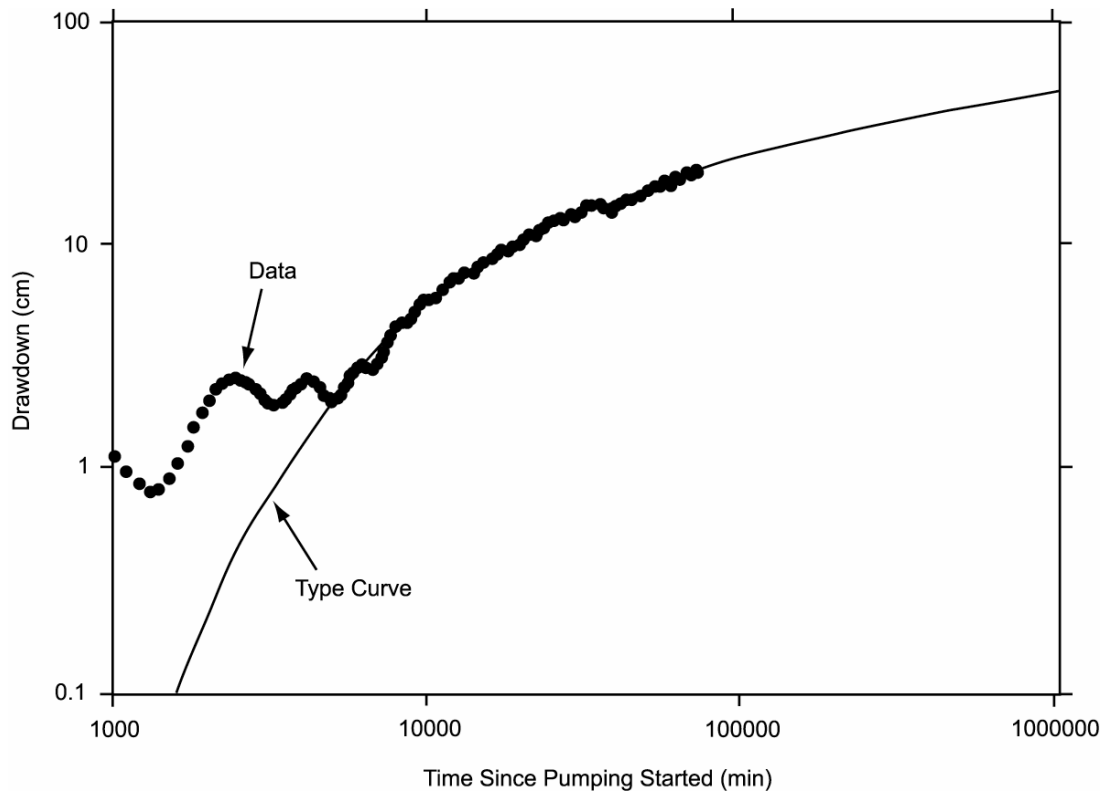
Source: DTN: MO0212SPANYESJ.149 [DIRS 161274].

Output DTN: GS031008312314.004.

NOTE: For the analysis curve, the parameter $\tau/B = 0.05$. The analysis used the Streltsova-Adams 1978 [DIRS 150754] method.

Figure C-32. Analysis of Drawdown in UE-25 ONC-1, May 8, 1996, to November 12, 1997

Observation wells showed clear responses to the pumping, allowing computation of hydrologic parameters. Despite being 843 m from c#3, ONC-1 responded to pumping after only 200 minutes because it is in the same structural block as the C-wells (between the Bow Ridge and Paintbrush Canyon faults), and is connected by fractures related to northwest-striking faults. That fracture connection is reflected in a characteristic fissure-block aquifer response. From 200 minutes to 2,000 minutes (up to 1.4 days), flow from fractures caused drawdown to increase as a function of log time. From 2,000 minutes to 6,000 minutes (1.4 days to 4 days), drawdown remained relatively constant as flow occurred from the rock matrix into fractures. After 6,000 minutes (4 days), drawdown increased again as a function of log time as flow from both the fractures and matrix occurred. Drawdown conformed to the type curve of Streltsova-Adams (1978 [DIRS 150754]; see Figure C-32). Transmissivity computed from the type-curve match equals $1,000 \text{ m}^2/\text{day}$. If the transmissive thickness between the C-wells complex and ONC-1 is assumed to vary linearly between known thicknesses in c#2 and H-4, then it can be estimated to be about 193 m in ONC-1. Dividing transmissivity by the estimated transmissive thickness indicates a fracture hydraulic conductivity of 5 m/day . In comparison, the hydraulic conductivity of the matrix (Table C-8) is insignificant. Computed storativity for the fractures in ONC-1 is 0.001, which is a tenth of the computed storativity of the matrix.



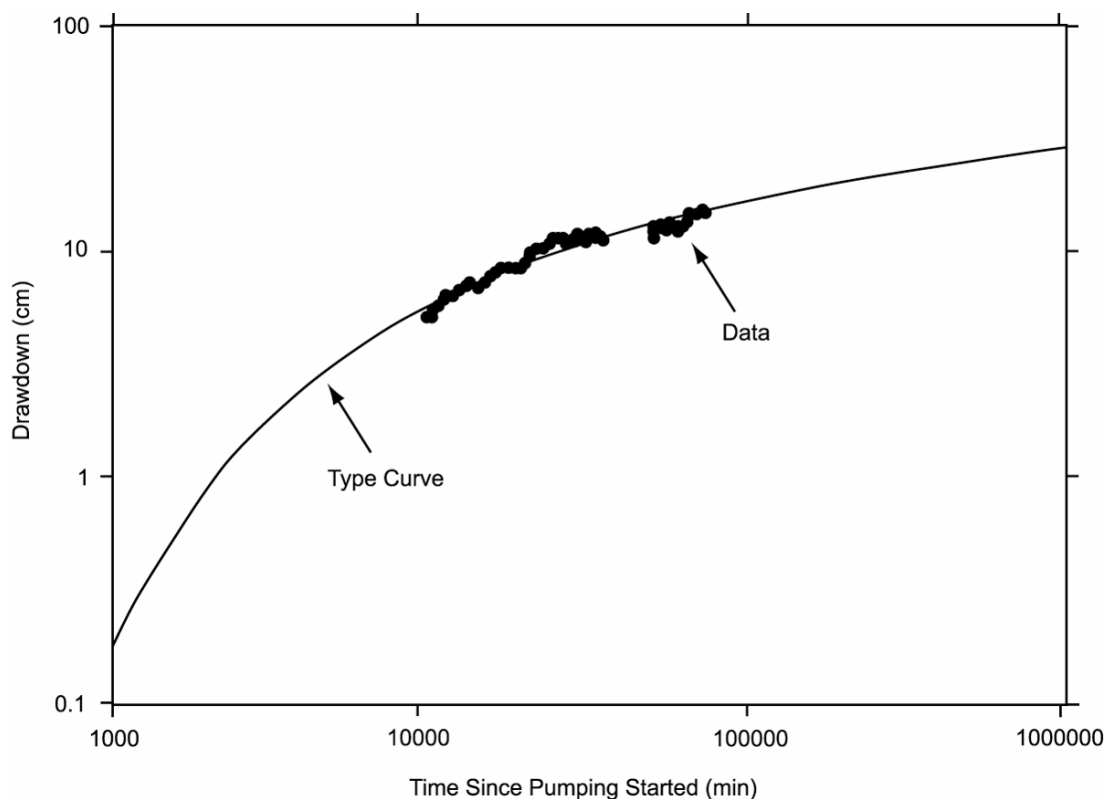
Sources: DTNs: GS970308312314.002 [DIRS 161273], GS970708312314.006 [DIRS 144468].

Output DTN: GS031008312314.004.

NOTE: The analysis used the Theis 1935 [DIRS 150327] method.

Figure C-33. Analysis of Drawdown in USW H-4, May 8, 1996, to June 27, 1996

Because of its location 2,245 m from c#3, Borehole H-4 took 5,000 minutes (3.5 days) to respond to pumping. Even though an extensive effort had been made to remove the effects of Earth tides and barometric changes on water-level fluctuations, the process is approximate and residual effects are still visible in the H-4 water-level record up to 5,000 minutes. After 5,000 minutes, the effect of pumping c#3 at H-4 became discernible above the residual water-level fluctuations, and the drawdown became analyzable (Figure C-33). From 5,000 to 72,000 minutes (3.5 to 50 days) after pumping started, drawdown in H-4 conformed to the type curve of Theis (1935 [DIRS 150327]) for a confined aquifer (Figure C-33). After 72,000 minutes (50 days), drawdown became relatively constant, probably in response to flux from a nearby fault boundary. The preboundary drawdown indicated transmissivity of $700 \text{ m}^2/\text{day}$ and storativity of 0.002 (Table C-8). Dividing transmissivity by the transmissive thickness obtained from a flow survey (Whitfield et al. 1984 [DIRS 101366]) indicated a hydraulic conductivity of 2 m/day . The location of the recharge boundary could not be ascertained because only H-4 was affected by that boundary, and the analytical solution to determine the location of a boundary (Lohman 1972 [DIRS 150250], pp. 57 to 61) requires that at least two wells be affected by the same boundary.



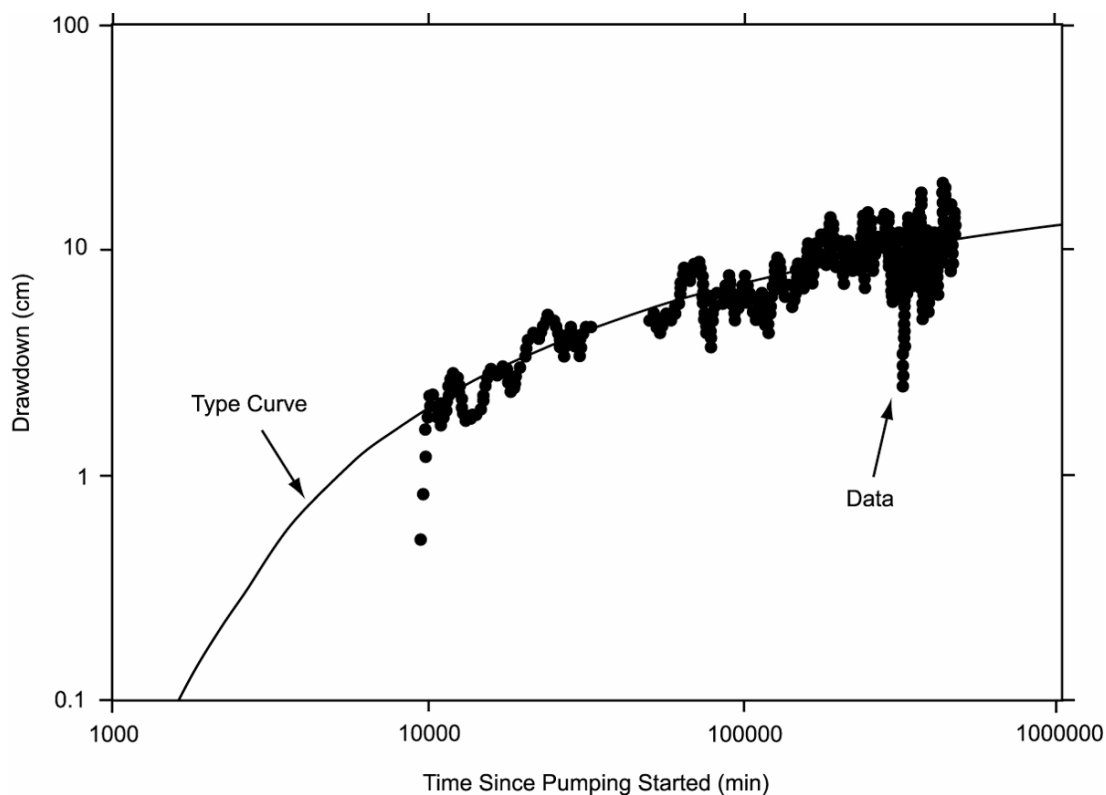
Sources: DTNs: GS970308312314.002 [DIRS 161273], GS970708312314.006 [DIRS 144468].

Output DTN: GS031008312314.004.

NOTE: The analysis used the Theis 1935 [DIRS 150327] method.

Figure C-34. Analysis of Drawdown in UE-25 WT#14, May 8, 1996, to June 27, 1996

Located a nearly identical distance (2,249 m) from c#3, Borehole WT#14 took slightly longer (5,250 minutes or 3.7 days) to respond to pumping. From 3.7 days to just over 6 days (5,250 to 9,000 minutes), a transition from borehole-storage release to release of water from the aquifer occurred. From 6 to 50 days (9,000 to 72,000 minutes) after pumping started, drawdown in WT#14 conformed to the type curve of Theis (1935 [DIRS 150327]) for a confined aquifer (Figure C-34). After that time, drawdown became strongly oscillatory, but those broad oscillations in the data deviated about a relatively constant value. Both the period of transition from borehole-storage release (5,250 to 9,000 minutes) and the strongly oscillatory drawdown period (after 72,000 minutes) are not shown in Figure C-34, which is intended to show only the portion of the record that conforms to the confined Theis (1935 [DIRS 150327]) solution. The late-time data are interpreted to represent less-than-ideal response to a recharge boundary. The preboundary drawdown indicates transmissivity of 1,300 m²/day and storativity of 0.002 (Table C-8). Hydraulic conductivity and the location of the boundary could not be determined because of insufficient data.



Sources: DTNs: GS970308312314.002 [DIRS 161273], GS970708312314.006 [DIRS 144468].

Output DTN: GS031008312314.004.

NOTE: The analysis used the Theis 1935 [DIRS 150327] method.

Figure C-35. Analysis of Drawdown in UE-25 WT#3, May 8, 1996, to March 26, 1997

Borehole WT#3 is located 3,526 m from c#3 and took more than 6 days (9,130 minutes) to respond to pumping. Thereafter, drawdown in WT#3 was oscillatory, but the data could be fit to the type curve of Theis (1935 [DIRS 150327]) for a confined aquifer (Figure C-35). The oscillations, which are substantially larger than those occurring at the other distant observation wells are likely caused by a combination of factors: (1) a possible low-quality transducer signal; (2) excessive distance from the pumping well (at 3,526 km, WT#3 is the farthest of the distant observation wells from the C-hole complex); and (3) residual Earth-tide and barometric-pressure effects remaining, even after substantial, but approximate, efforts to remove them. The solution indicated a transmissivity of 2,600 m²/day and a storativity of 0.002 (Table C-8). Dividing transmissivity by the length of the open interval in WT#3 (47.5 m) indicated a hydraulic conductivity of 56 m/day. Actual hydraulic conductivity probably is smaller than the calculated value because the thickness of transmissive rock between the C-wells complex and WT#3 probably exceeds the length of the open interval.

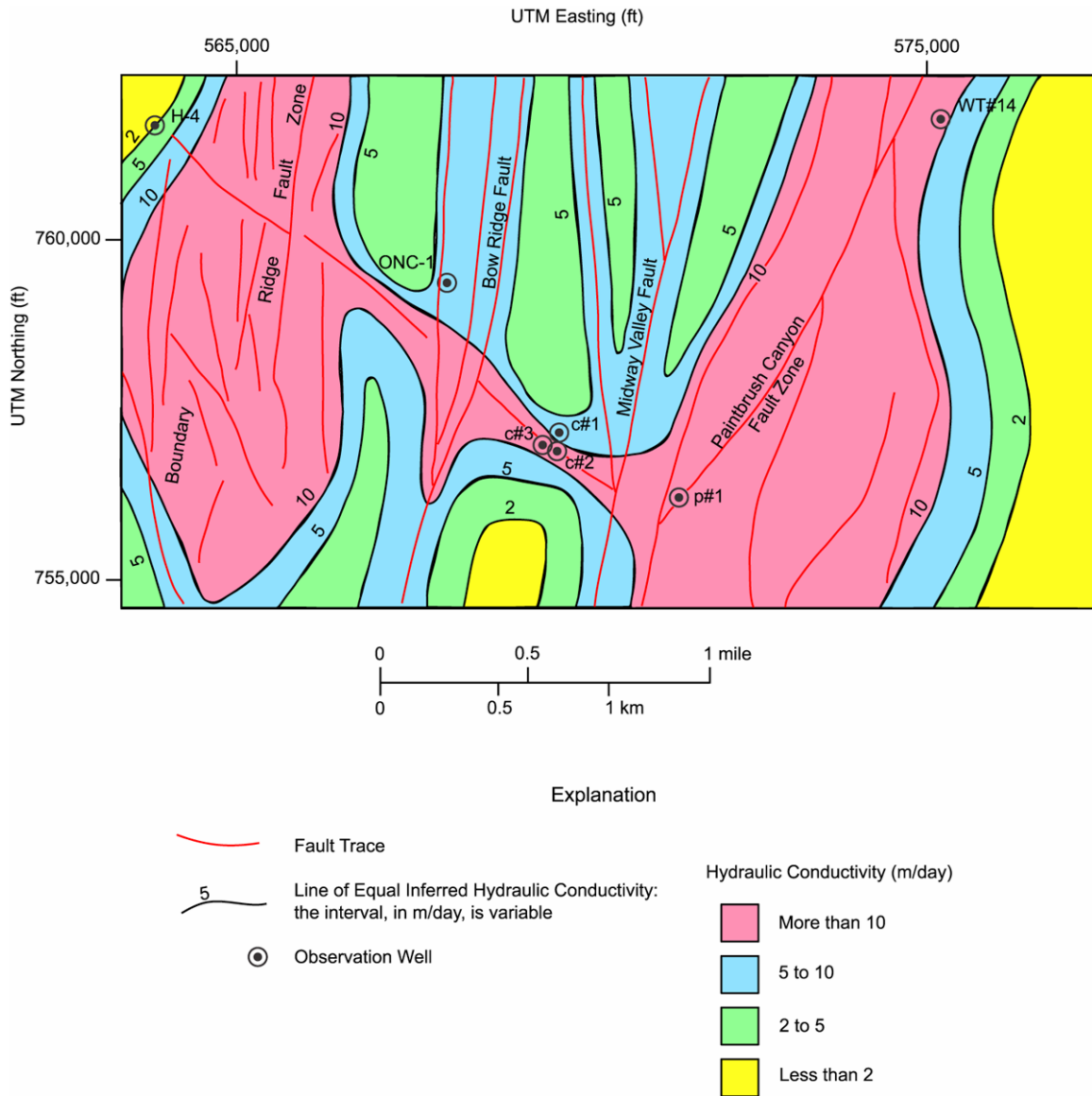
The transmissivity of the Miocene tuffaceous rocks appears to decrease northwestward in the area containing the observation wells used in the hydraulic test that began in May 1996. Depending on the analytical solutions used, transmissivity could be interpreted to decrease from 2,600 m²/day in the vicinity of WT#3 to about 2,000 m²/day in the vicinity of the C-wells. The

transmissivity of the Miocene tuffs is 1,300 m²/day in the vicinity of WT#14, 1,000 m²/day in the vicinity of ONC-1, and 700 m²/day in the vicinity of H-4.

The distribution of hydraulic conductivity in the tuffs in the vicinity of the C-wells complex appears to be structurally controlled. Hydraulic conductivity in c#2 decreases sharply from a range of 20 to 60 m/day in the Upper Tram and Lower Bullfrog intervals to a range of 0.08 m/day to 0.2 m/day in the Calico Hills interval as the vertical distance from faults that intersect the boreholes increases (Table C-7). Average hydraulic conductivity of the Miocene tuffaceous rocks in c#2 is twice that of c#1 (Table C-8), possibly because c#2 is located nearer to the subsurface intersection of the north-striking Paintbrush Canyon or Midway Valley faults and a northwest-striking fault (shown in Figure C-36) that underlies the gap through the northern part of Bow Ridge. If spatial relations between faults and hydraulic conductivity at the C-wells complex are combined with values of hydraulic conductivity determined from analyses of drawdown in ONC-1, WT#3, and H-4 (Table C-8), then a possible distribution of hydraulic conductivity for the Miocene tuffaceous rocks in the vicinity of the C-wells can be inferred (Figure C-36). Clearly, this distribution is not unique; just one possible scenario that attempts to extrapolate areally the correlation between vertical proximity of geohydrologic units at the C-hole complex to faults and the hydraulic conductivities of these units. When that correlation is applied areally, relative to known geologic structures in the area, while honoring the hydraulic conductivities obtained at the C-hole complex itself and the distant observation wells (ONC-1, H-4, WT#14, and WT#3), one obtains Figure C-36.

In the 21-km² area encompassed by observation wells used in hydraulic tests at the C-wells complex from 1995 to 1997, the storativity of Miocene tuffaceous rocks in those observation wells uniformly is 0.001 to 0.003 (Table C-8). Analysis of drawdown in observation wells not affected by boundaries as a function of the time divided by the square of the distance from the pumping well (Figure C-37) indicates that the average storativity of the tuffs in the observation area is 0.002. This same analysis indicates that the average transmissivity of the Miocene tuffaceous rocks in the area is 2,200 m²/day. Derivation of a single analytical solution for c#1, c#2, ONC-1, and WT#3 confirms that the Miocene tuffaceous rocks, at least as far north as lower Midway Valley in the structural block delineated by the Paintbrush Canyon, Bow Ridge, and Dune Wash faults, are a single aquifer in which flow is influenced by the same structural and stratigraphic factors.

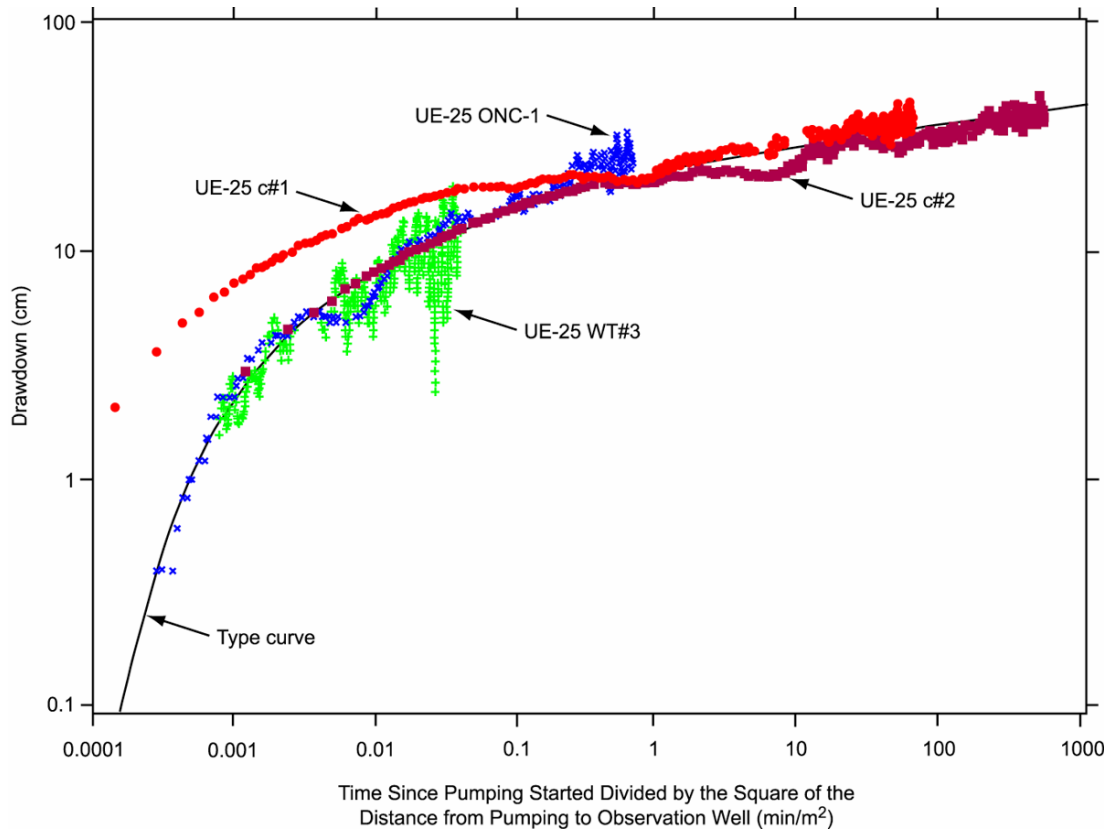
Plots of drawdown in observation wells as a function of distance 30,000 minutes, 100,000 minutes, 200,000 minutes, 305,000 minutes, and 463,000 minutes (21 days, 69 days, 139 days, 212 days, and 322 days) after pumping started in May 1996 (drawdown contours at 30,000 minutes and 463,000 minutes shown in Figure C-38) confirm an ovoid pattern of drawdown aligned with faults extending from Bow Ridge to Antler Wash detected during the hydraulic test conducted from May 22 to June 1, 1995 (Geldon et al. 1998 [DIRS 129721], pp. 23 to 25, Figure 2; p. 31). Analyzed by the method of Cooper and Jacob (1946 [DIRS 150245]), plots of drawdown as a function of distance (Figure C-39) indicate values of transmissivity ranging from 2,100 to 2,600 m²/day and values of storativity ranging from 0.0005 to 0.002 (Table C-9).



Sources: DTNs: GS970308312314.001 [DIRS 159 240], GS970708312314.005 [DIRS 159241], GS981008312314.002 [DIRS 147068], GS981008312314.003 [DIRS 144464], GS010608312314.001 [DIRS 179647], GS970308312314.002 [DIRS 161273], GS970708312314.006 [DIRS 144468], MO0212SPANYESJ.149 [DIRS 161274].

Output DTN: GS031008312314.004.

Figure C-36. Inferred Distribution of Hydraulic Conductivity of Miocene Tuffaceous Rocks in the Vicinity of the C-Wells



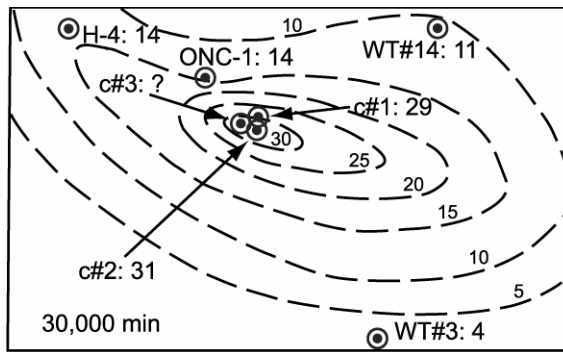
Sources: DTNs: GS970308312314.001 [DIRS 159 240], GS970708312314.005 [DIRS 159241], GS981008312314.002 [DIRS 147068], GS981008312314.003 [DIRS 144464], GS010608312314.001 [DIRS 179647], GS970308312314.002 [DIRS 161273], GS970708312314.006 [DIRS 144468], MO0212SPANYESJ.149 [DIRS 161274].

Output DTN: GS031008312314.004.

Figure C-37. Analysis of Drawdown in Observation Wells as a Function of Time Divided by the Square of the Distance from Pumping Well, UE-25 c#3

Because the higher transmissivity and lower storativity values resulting from the 30,000- and 100,000-minute analyses in Table C-9 give way to more stable and consistent lower transmissivity and higher storativity values from later-time analyses, the later values appear to be more reliable. In comparison, the same type of analysis of drawdown in observation wells as a function of distance 10 days (14,000 minutes) after pumping started in May 1995 had indicated a transmissivity of 2,300 m²/day and storativity of 0.003 (Geldon et al. 1998 [DIRS 129721], p. 29). Distance-drawdown and time-drawdown analyses discussed in this section converge on similar solutions.

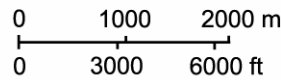
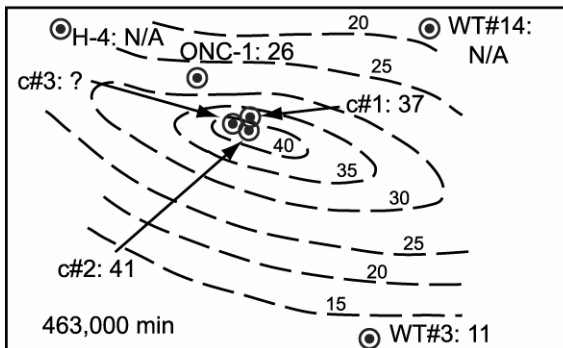
The ovoid pattern of drawdown aligned with faults extending from Bow Ridge to Antler Wash detected during the hydraulic test conducted from May 22 to June 1, 1995 (Geldon et al. 1998 [DIRS 129721], pp. 23 to 25, Figure 2; p. 31) and confirmed in this study (Figure C-38) indicates large-scale anisotropy caused by heterogeneity and structure. Large-scale transmissivity is higher in the direction of the long axis of the ovoid and lower in the direction perpendicular to it.



Explanation

WT#3: 11 Observation Well Number: Drawdown (cm)
 N/A: not applicable because drawdown is affected by a recharge boundary

— 25 — Line of Equal Drawdown (5-cm interval)



Sources: DTNs: GS970308312314.001 [DIRS 159 240], GS970708312314.005 [DIRS 159241], GS981008312314.002 [DIRS 147068], GS981008312314.003 [DIRS 144464], GS010608312314.001 [DIRS 179647], GS970308312314.002 [DIRS 161273], GS970708312314.006 [DIRS 144468], MO0212SPANYESJ.149 [DIRS 161274].

Output DTN: GS031008312314.004.

NOTE: The upper panel shows the drawdown distribution 30,000 minutes (20.8 days) after pumping started; the lower panel shows the distribution 463,000 minutes (321.5 days) after pumping started.

The reason for the question mark in the figure is that the drawdown in the aquifer at the location of the pumped well, c#3, is unknown; only the apparent drawdown in the well, which contains a lot of friction head, is known.

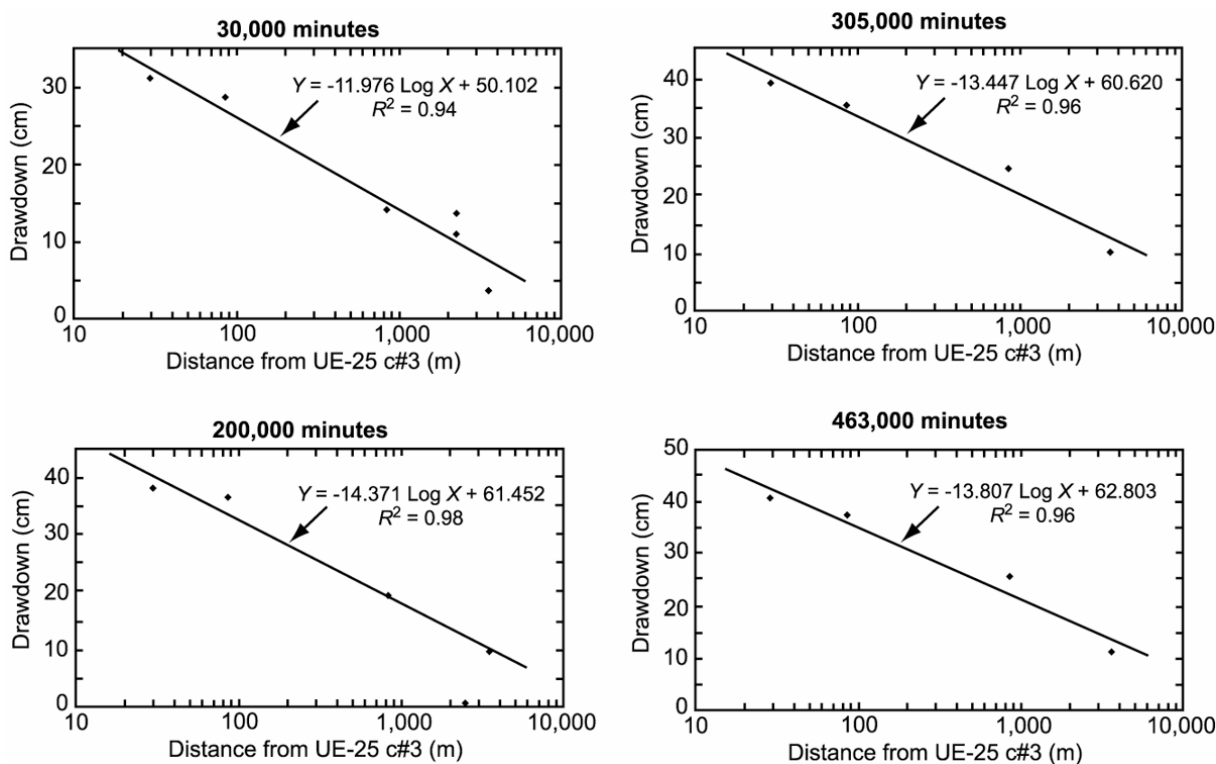
Figure C-38. Distribution of Drawdown in Observation Wells at Two Times after Pumping Started in UE-25 c#3 on May 8, 1996

Table C-9. Hydrologic Properties Determined from Drawdown in Observation Wells as a Function of Distance from the Pumping Well UE-25 c#3, May 1996 to November 1997

Time Since Pumping Started (min)	Transmissivity (m ² /day)	Storativity
30,000	2,600	0.0005
100,000	2,500	0.0009
200,000	2,100	0.002
305,000	2,300	0.001
402,000	2,200	0.001
463,000	2,200	0.001

Sources: DTNs: GS970308312314.001 [DIRS 159 240], GS970708312314.005 [DIRS 159241], GS981008312314.002 [DIRS 147068], GS981008312314.003 [DIRS 144464], GS010608312314.001 [DIRS 179647], GS970308312314.002 [DIRS 161273], GS970708312314.006 [DIRS 144468], MO0212SPANYESJ.149 [DIRS 161274].

Output DTN: GS031008312314.004 (Table 6.2-9).



Sources: DTNs: GS970308312314.001 [DIRS 159 240], GS970708312314.005 [DIRS 159241], GS981008312314.002 [DIRS 147068], GS981008312314.003 [DIRS 144464], GS010608312314.001 [DIRS 179647], GS970308312314.002 [DIRS 161273], GS970708312314.006 [DIRS 144468], MO0212SPANYESJ.149 [DIRS 161274].

Output DTN: GS031008312314.004.

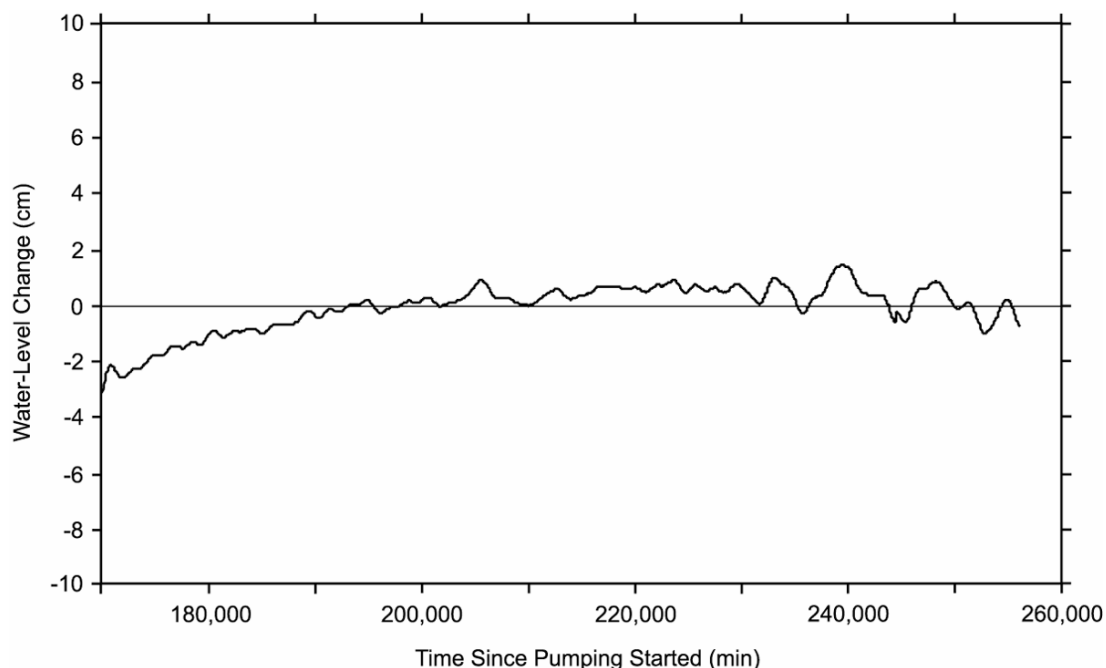
NOTE: The panels show the drawdown analyses at 30,000 minutes (upper left), 200,000 minutes (lower left), 305,000 (upper right), and 463,000 minutes (lower right) after pumping started.

Figure C-39. Analyses of Drawdown in Observation Wells as a Function of Distance from the Pumping Well at Various Times after Pumping Started in UE-25 c#3

C4.7 PALEOZOIC CARBONATE ROCKS

Borehole p#1 was monitored during hydraulic tests in 1995 and 1996 to detect hydraulic connection between the Miocene tuffaceous rocks and Paleozoic carbonate rocks in the vicinity of the C-wells. Hydraulic connection previously had been indicated by hydraulic head measurements in p#1 and by borehole flow surveys in the C-wells. Measurements made as p#1 was being drilled in 1983 detected a 22-m difference in hydraulic heads for the Paleozoic carbonate rocks and Miocene tuffaceous rocks in p#1 (Craig and Robison 1984 [DIRS 101040]), which indicated a potential for water to flow from the lower to the upper of those hydrogeologic units. Flow surveys conducted in the C-wells in 1991 detected upward flow in the lower parts of those boreholes (Geldon 1996 [DIRS 100396], pp. 12 to 69) that most likely originated in the Paleozoic carbonate rocks because the intervening tuffaceous rocks generally behave as a confining unit (Luckey et al. 1996 [DIRS 100465], p. 18, Figure 7).

Although p#1 was monitored for 10 days (14,400 minutes) after pumping started in May 1995 (Geldon et al. 1998 [DIRS 129721]), and for about 180 days (256,200 minutes) after pumping started in May 1996, drawdown in the Paleozoic carbonate rocks was not detected (Figure C-40). This lack of drawdown could indicate that the water being pumped was drawn laterally from the Miocene tuffaceous rocks. Alternatively, the water could have been drawn upward from Paleozoic carbonate rocks without causing drawdown in the underlying aquifer if the Paleozoic rocks have a large storage capacity. Hydraulic connection between the Miocene tuffaceous rocks and Paleozoic carbonate rocks could not be confirmed or refuted by monitoring water levels in p#1 during the study reported here.



Sources: DTNs: GS970308312314.002 [DIRS 161273], GS970708312314.006 [DIRS 144468].

Output DTN: GS031008312314.004.

NOTE: Water-level change is relative to the water level in p#1 prior to start of pumping in c#3 on May 8, 1996.

Figure C-40. Water-Level Changes in UE-25 p#1, September 3 to November 2, 1996

C5. LIMITATIONS AND UNCERTAINTIES

All analytical methods used in this study to determine hydrologic properties from drawdown or recovery responses assume that the aquifer is an equivalent porous medium. Although the flow system consists of a fracture network rather than a porous medium, the pressure responses conform quite well to type curves derived for either porous media or uniformly fractured media (Strelsova-Adams 1978 [DIRS 150754]). Thus, the fracture network at the C-wells is apparently interconnected in such a way that the fractured tuffs respond to pumping as “an equivalent porous medium.” Another fundamental assumption is that flow to the pumping well is derived from an aquifer of infinite extent. The many faults near the C-wells complex that potentially function as either recharge or barrier boundaries make the concept of an infinite aquifer difficult to support. However, only observation wells that lay between faults bounding the structural block in which the C-wells are located were considered in the analyses, so boundary effects, while not completely eliminated, should have been minimized. Drawdown in H-4 and WT#14 obviously was affected by recharge boundaries.

All the analytical methods used in this study assume a constant thickness for the interval for which drawdown is being analyzed, whereas, in reality, the intervals have variable thicknesses. This is a necessary simplification, and extreme care was taken to define transmissive intervals in each well and a meaningful resulting assumed-interval thickness between the pumped and observation well.

In addition, all the analytical methods used in this study, except for the Neuman (1975 [DIRS 150321]) method, assume radial flow to the pumping well, and, therefore, ignore vertical flow (application of the Neuman fully penetrating-well solution, as was done in this report, to cases where pumping was in one interval and the analyzed drawdown response was in another, also ignores vertical flow). The flow from intervals other than the one being pumped that was detected during hydraulic tests in February 1996 and May 1996 to November 1997 indicates that flow during those tests actually was three-dimensional. To obtain hydrologic parameter estimates in nonpumped intervals, it was necessary to assume an equivalent radial volumetric flow rate in these intervals. These estimates of equivalent radial flow were quite uncertain, and they could have resulted in significant errors in hydrologic parameter estimates in nonpumped intervals. However, parameter estimates based on an assumed radial flow in nonpumped intervals were generally in good agreement with estimates obtained from open-hole pumping of c#3 in May through June 1995, and also from later pumping of the intervals when they were isolated (e.g., estimates for the Prow Pass interval when the Lower Bullfrog was pumped in 1996 to 1997 were in good agreement with estimates obtained when the Prow Pass interval was pumped directly in 1998). Thus, the approach taken seems to have yielded reasonable hydrologic parameter estimates in the cases in which it could be verified with a more direct measurement.

All the analytical techniques used in this study required input parameters that had to be determined or approximated for hydrogeologic intervals or boreholes in which drawdown was monitored. Included in those parameters are the distance of the interval or borehole from the pumping well, the transmissive thickness of the interval or borehole, the barometric efficiency of the interval or borehole, the proportion of flow from a given hydrogeologic interval, and the fracture spacing within a hydrogeologic interval. Errors in deriving any of those input parameters could have changed calculated hydrologic properties considerably.

Uncertainties and nonuniqueness in estimates of storativity, transmissivity, and hydraulic conductivity were not quantitatively analyzed because these parameter estimates were not used directly in the SZ site-scale flow model (BSC 2004 [DIRS 170037], Sections 6.6, 6.7, and 7); they were used only qualitatively/corroboratively in the flow model. Based on the ranges of transmissivity estimates obtained for a given hydrogeologic interval by different methods using either the drawdown or recovery data from the C-wells hydraulic tests (Tables C-6 and C-7) or the drawdown data from distant wells that responded to pumping c#3 in 1996 to 1997 (see Section C6.2, Tables C-10 and C-11), the transmissivity estimates determined in this analysis can be considered accurate to within about a factor of 1.5 for high-transmissivity intervals (lower Bullfrog and upper Tram Tuffs) and within a factor of 2.5 for low transmissivity intervals (Calico Hills, Prow Pass, and upper Bullfrog Tuffs). The factor of 2.5 also applies to the assemblage of volcanic tuffs between the C-wells and distant wells. Storativity estimates can be considered accurate to only within an order of magnitude or so. These ranges of transmissivity and storativity estimates are a result of the use of different theoretical models to fit the data (confined porous medium, confined/fissure block, unconfined), and also the data set analyzed (different tests, drawdown vs. recovery curves). However, relative values of transmissivity estimates (that is, the ratios of transmissivities of different flow intervals) can be considered more accurate because errors and biases should be reasonably consistent for estimates obtained by the same analyst using similar assumptions and methods (as is the case here). Estimates of hydraulic conductivity are more uncertain than transmissivity estimates because hydraulic

conductivity is calculated by dividing the transmissivity by either the known thickness of transmissive intervals within a test interval, the entire thickness of the test interval, or an assumed thickness of transmissive rock between the observation and pumping wells. In many cases, the transmissive thickness was unknown, so it was only possible to obtain bounding estimates of the hydraulic conductivity. Even when hydraulic conductivity could be estimated, it was done with limited confidence. For example, it is impossible to know whether the hydraulic conductivity of the Lower Bullfrog interval in c#1 really is about half that in c#2 or whether these calculated hydraulic conductivity values result from dividing approximately the same transmissivity in each borehole by an assumed transmissive thickness twice as large in c#1 as in c#2.

C6. SATURATED ZONE ANISOTROPY NEAR THE C-WELLS COMPLEX

C6.1 INTRODUCTION

Understanding SZ flow and transport near the high-level nuclear waste repository at Yucca Mountain is critical to a successful license application. Because radionuclides released from the repository at Yucca Mountain must travel through the saturated fractured tuff and the saturated alluvium before reaching the compliance boundary, it is important to characterize the hydrogeologic properties of the down-gradient media. Since the completion of the site-characterization wells in 1983, several single- and cross-hole tracer and pumping tests have been conducted to gain a better understanding of the hydrogeology of the region. A number of published studies have assigned transmissivities, storativities, and anisotropy ratios to the SZ in this area (Farrell et al. 1999 [DIRS 157319]), 1999 [DIRS 118941]; Winterle and La Femina 1999 [DIRS 129796]). In this scientific analysis report, reviews of the above mentioned studies are used in conjunction with independent re-analyses of the data to suggest a distribution of anisotropy ratios to be used in the finite-element, heat and mass transfer (FEHM) stochastic flow model of the SZ (Zyvoloski et al. 1997 [DIRS 110491]).

C6.1.1 Background

A geologic description of the C-wells complex and the surrounding area can be found in several publications (including Geldon et al. 1998 [DIRS 129721], Table 1, Figures 3 and 5; Farrell et al. 1999 [DIRS 157319]; Ferrill et al. 1999 [DIRS 118941]; Winterle and La Femina 1999 [DIRS 129796]). Nevertheless, one geologic characteristic bears mentioning. Based on in situ stress-field analyses, the maximum horizontal geologic stress runs north-northeast (azimuth between 25° and 30° east of north). Therefore, any fractures oriented in this direction tend to dilate and present potential preferential flow pathways (Farrell et al. 1999 [DIRS 157319], p. 4-1; Ferrill et al. 1999 [DIRS 118941], p. 1). This finding supports some of the calculated principal directions of anisotropy discussed below, but not all.

Although many hydraulic tests have been conducted at the C-wells complex, only the long-term pumping test from May 8, 1996, through November 12, 1997, yielded data suitable for estimating the hydrologic properties of the medium on a broad scale beyond the immediate vicinity of the C-wells. These data may help to estimate an overall anisotropy ratio for the area. Specifically, changes in local groundwater elevations due to pumping at the C-wells complex were monitored at several distant wells, the locations of which are shown in Figure 6.1-4 (only

H-4, ONC-1, WT#3, and WT#14 exhibited sufficient drawdown for an anisotropy analysis). Well c#3 has traditionally served as the pumping well because of its record of consistent production rates.

Although several cross-hole hydraulic tests have been conducted by USGS investigators, only the long-term pumping test yielded data suitable for calculating a nonlocal anisotropy ratio. For this test, well c#3 was packed around the Lower Bullfrog interval, and water levels were monitored at H-4, ONC-1, WT#3, and WT#14. Data collected during this test were used to calculate transmissivity and storativity at each well—parameters necessary to analytically estimate an anisotropy ratio for the area. Although water levels were monitored at other wells, none yielded data suitable for an analytic treatment of anisotropy.

C6.1.2 Technical Approaches

Water-level data for wells H-4, WT#3, and WT#14 were obtained from the DTN: GS970308312314.002 [DIRS 161273]. Data from well ONC-1 were collected by Nye County under the Nye County Nuclear Waste Repository Project Office (NWRPO) QA program (QAP) (NWRPO 2003 [DIRS 165947], Program Management, Quality Assurance Program). Nye County requires that the NWRPO establish and maintain a documented QAP that meets the requirements of American National Standards Institute/American Society of Mechanical Engineers NQA-1 and the criteria of 10 CFR 50 (2002 [DIRS 165855], Appendix B). These data are available under DTN: MO0212SPANYESJ.149 [DIRS 161274].

Winterle and La Femina (1999 [DIRS 129796]) reduced and filtered the drawdown data for the above wells to obtain estimates of hydrologic parameters over the affected area. In the analyses presented here, the filtering of data from wells H-4, WT#3, WT#14, and ONC-1 was accomplished with Filter.vi (STN: 10970-1-00 [DIRS 162668]). These filtered drawdown data are identified by Output DTNs: GS030208312314.001 and GS030208312314.002.

The first analytical anisotropy analysis in this report was calculated in Microsoft ExcelTM using the standard formulation offered by Hantush (1966 [DIRS 161160]); the second uses a modification of the method of Papadopoulos (1967 [DIRS 150265]) combined with the PEST parameter-estimation program, Version 5.5 (STN: 10289-5.5-00 [DIRS 161564]). Winterle and La Femina (1999 [DIRS 129796]) used AQTESOLV, Version 2.12, marketed by HydroSOLVE, Inc., to analyze pump tests. This analysis report used analytical solutions of Theis (1935 [DIRS 150327]) or Streltsova-Adams (1978 [DIRS 150754]) for analyses of the responses at the four observation wells to pumping at c#3. These analyses were performed using Theis.vi (STN: 10974-1-00 [DIRS 162758]) and Streltsova-Adams.vi (STN: 10971-1-00 [DIRS 162756]), respectively.

C6.2 ESTIMATING ANISOTROPY

Interpretation of well test data with analytical solutions consists of inferring the hydrologic properties of the system from its measured responses based on, among other things, an assumed flow geometry (i.e., radial). The problem becomes more complicated, however, when the system geometry cannot be specified with reasonable certainty. In a layered sedimentary system lacking extreme heterogeneity, flow might reasonably be expected to be radial during an hydraulic test. When hydraulic tests are conducted at some arbitrary point within a three-dimensional fractured rock mass, however, the flow geometry is convoluted. Radial flow would occur only if the test were performed in a single uniform fracture of effectively infinite extent or within a network of fractures confined to a planar body in which the fractures were so densely interconnected that the network behaves like an equivalent porous medium. More likely, flow would be nonradial and variable, as fracture terminations and additional fracture intersections were reached. The nonradial nature of the cone of depression near Yucca Mountain is illustrated in Figure C-38. Despite all of this, analytic solutions provide important requisite first-order answers commensurate with the spatial distribution of the available hydrogeologic and geophysical data, and that can only be improved by numerical modeling if that data distribution is enhanced by substantial new data-gathering efforts.

Through the fractured tuff near Yucca Mountain, there are significant heterogeneity and hydrologic properties that not only vary spatially but also differ depending upon the direction in which they are measured (both horizontally and vertically). In this analysis, transmissivity and storativity are the key parameters defining large-scale anisotropy, and their measured values reflect the heterogeneity of the media. The concept of anisotropy is typically associated with a homogeneous medium—a criterion not met here. Nevertheless, there are clearly spatial and directional variations in transmissivity, and the notion remains that, over a large enough representative elementary volume, there exists a preferential flow direction that can be termed “anisotropy.”

Data from the long-term pumping test conducted from May 8, 1996, to November 12, 1997, can be used to evaluate the anisotropy of the C-wells complex and vicinity because transmissivity and storativity can be calculated at four distant wells (H-4, ONC-1, WT#3, and WT#14). The hydrologic properties measured at these wells are used to develop an estimate for the anisotropy ratio. Data from the other C-wells (c#1 and c#2) were not used in the anisotropy analysis because, according to Farrell et al. (1999 [DIRS 157319], p. 4-9):

- Over the small scale of observation at the C-wells, pump-test results are likely dominated by discrete fractures (i.e., inhomogeneities)
- Three-dimensional flow effects are likely
- Recirculation from simultaneous tracer tests obscured results.

Furthermore, because anisotropy is conceptually difficult to define for heterogeneous media, it is more easily described as an average preferential flow over as large a representative elementary volume as possible. Thus, it makes little sense to attempt to define anisotropy over an heterogeneous area as small as that of the C-wells.

C6.2.1 Data Filtering and Reduction

Because drawdown was measured at great distances from the pumping well (up to 3,526 m between WT#3 and c#3), natural variations in groundwater levels obscured responses due to pumping and had to be filtered out before the drawdown data could be analyzed. Drawdowns were corrected for Earth-tide effects (head fluctuations of up to 0.12 m) and atmospheric pressure change (head fluctuation of up to 0.25 m). First, the water levels were processed with a low-pass filter (Filter.vi V 1.0, STN: 10970-1-00 [DIRS 162668]) to remove oscillations with a frequency greater than 0.8 cycles per day to eliminate Earth-tide effects and semi-diurnal barometric-pressure effects, leaving only the effects of long-term weather-related barometric-pressure changes. The barometric record from the C-wells complex, which was assumed to apply to all the wells, was also filtered to remove frequencies greater than 0.8 cycles per day to eliminate semi-diurnal barometric-pressure fluctuations, leaving only long-term weather-related barometric pressure changes. Using barometric efficiency values of the wells, the effects of long-term, weather-related, barometric-pressure changes were removed from the filtered water levels, leaving only the effect of c#3 pumping. The filtered and barometrically corrected water-level data for the four observation wells can be found in Output DTNs: GS030208312314.001 and GS030208312314.002. The water-level data for H-4, WT#3, and WT#14 were obtained from DTN: GS970308312314.002 [DIRS 161273], and the water levels for ONC-1 were obtained from DTN: MO0212SPANYESJ.149 [DIRS 161274]. The barometric record used for the above processing was from the C-wells complex (DTN: GS981008312314.003 [DIRS 144464]).

Winterle and La Femina (1999 [DIRS 129796], pp. 3-4 to 3-6) also applied a second stage of filtering to the long-term pumping test to remove barometric effects that reached the aquifer through the unsaturated zone by accounting for the time lag and attenuation that occurs in the unsaturated zone. Second-stage barometric pressure effects were filtered using a 2.6-day running average, multiplied by an attenuation factor of 0.6, and lagged by a period of 0.42 days.

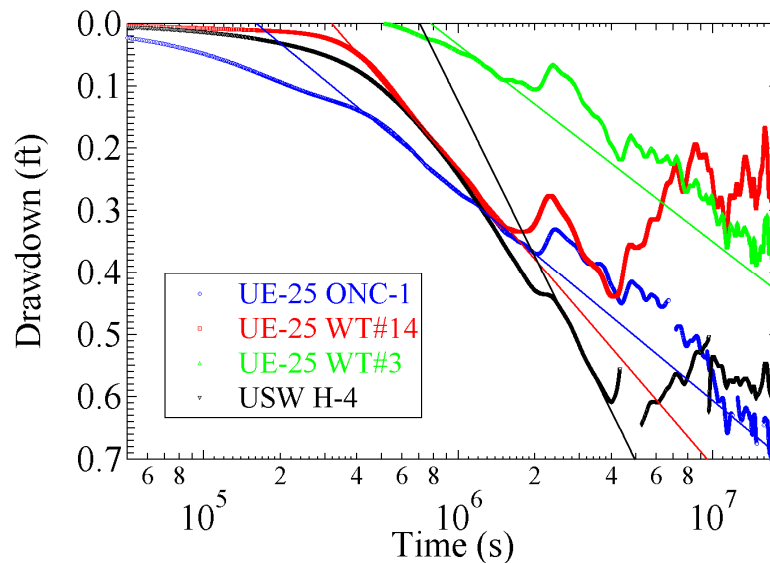
The derivative of the filtered drawdowns with respect to the log of time was calculated for H-4, WT#3, WT#14, and ONC-1 to establish the optimum range of data to fit with the straight-line method of Cooper and Jacob (1946 [DIRS 150245]). The flattest (zero-slope) portion of the resulting curve is deemed the best location for a linear fit to the drawdown data.

C6.2.2 Transmissivity and Storativity Calculations

In the first analysis of this section, the Cooper-Jacob (1946 [DIRS 150245]) method applied to filtered and derivative-analyzed data is used to calculate transmissivities and storativities. The key to a reasonable estimate of anisotropy is an accurate assessment of transmissivity and storativity at each monitoring well. Figure C-41 is a plot of the filtered drawdowns fit with the Cooper-Jacob straight-line method to the appropriate portion of the derivative curve. Note the inconsistent slope of the fit to drawdown in well H-4 resulting in a significantly lower transmissivity at this well. Transmissivity and storativity values are presented in Table C-10.

In the second analysis methodology of this report, which uses the modified Papadopoulos-PEST method, the response of each of observation wells H-4, WT#14, and WT#3 is analyzed using the homogeneous, isotropic method of Theis (1935 [DIRS 150327]) (Theis.vi V 1.0,

STN: 10974 1 00 [DIRS 162758]) for confined aquifers, and the response of observation well ONC-1 is analyzed using the homogeneous, isotropic method of Streltsova-Adams (1978 [DIRS 150754]) (Streltsova-Adams.vi, V 1.0, STN: 10971-1.0-00 [DIRS 162756]) for fissure-block aquifers—both type-curve-fitting techniques—to obtain transmissivity and storativity values. Three analyses were made: one with transmissivities constrained to 1,000 m²/day, the other with the transmissivities and storativities as listed in Table C-8, and the third with transmissivities and storativities obtained from analyzing the filtered and barometrically corrected water levels processed for this report and described in the first paragraph of Section C6.2.1. The three sets of values are used to produce three sets of anisotropy magnitudes and directions as discussed below.



Sources: DTNs: GS970308312314.002 [DIRS 161273]; MO0212SPANYESJ.149 [DIRS 161274]. Output DTNs: GS030208312314.001, GS030208312314.002 (filtered data).

Output DTN: SN0409T0502203.002.

NOTE: The straight lines were fit to relatively small portions of each drawdown curve selected because they had the most constant derivatives (i.e., the least noisy portions of the curves). Fitting a straight line to larger portions of the curves could result in slopes and, hence, estimated transmissivities that differ by nearly a factor of two.

Figure C-41. Straight-Line Fits to the Filtered and Derivative-Analyzed Data at the Four Monitoring Wells

Table C-10. Transmissivities and Storativities Calculated by the Cooper-Jacob Method Using the Filtered and Derivative-Analyzed Data

Well	Cooper-Jacob ^a Analysis	
	T (m ² /day)	S (-)
UE-25 ONC-1	1465	0.009
UE-25 WT#3	1566	0.003
UE-25 WT#14	1043	0.002
USW H-4	598	0.002

Sources: DTNs: GS970308312314.002 [DIRS 161273];
MO0212SPANYESJ.149 [DIRS 161274].

Output DTNs: GS030208312314.0 01, GS030208312314.002
(filtered data).

Output DTN: SN0409T0502203.002.

^aThe Cooper-Jacob (1946 [DIRS 150245]) method was used in the analysis.

C6.2.3 Previously Reported Results

Winterle and La Femina (1999 [DIRS 129796], Section 4.5) processed the long-term pumping data with AQTESOLV, and their transmissivity and storativity results (obtained with the Theis (1935 [DIRS 150327]) method) are shown in Table C-11. Considering the differences in the Cooper-Jacob (1946 [DIRS 150245]) and Theis (1935 [DIRS 150327]) analysis methods, as well as differences in data reduction methods, the Winterle and La Femina (1999 [DIRS 129796], p. 4-25) transmissivities agree reasonably well with the results from the analyses shown in Table C-10. The drawdown data from the long-term pumping test in Section C4.6 and from Winterle and La Femina (1999 [DIRS 129796], p. 4-25) were also analyzed using the Theis method, and these results are reproduced in Table C-11. With the exception of WT#3, the transmissivities are in good agreement with those of Winterle and La Femina (1999 [DIRS 129796], p. 4-25). The difference of more than a factor of 2 in the transmissivity of WT#3 can probably be attributed to differences in data reduction methods, which lead to greater differences in parameter estimates when the overall drawdown is relatively small (as it is for WT#3).

Table C-11. Transmissivities and Storativities of Distant Wells for the Long-Term Pumping Test

Well	Transmissivity and Storativity Results			
	T (m ² /day) ^a	S (-) ^a	T (m ² /day) ^b	S (-) ^b
UE-25 ONC1	1,340	0.008	1,000	0.001
UE-25 WT#3	1,230	0.005	2,600	0.002
UE-25 WT#14	1,330	0.002	1,300	0.002
USW H-4	670	0.002	700	0.002

Sources: ^aWinterle and La Femina 1999 [DIRS 129796], p. 4-25.

^bBased on Section C4.6

C6.2.4 ONC-1 Data

The ONC-1 drawdown data were acquired by the Nye County Nuclear Waste Repository Project Office (NWRPO) under the NWRPO QAP, which was established to meet the requirements of American National Standards Institute/American Society of Mechanical Engineers NQA 1 and the criteria in 10 CFR Part 50 (2002 [DIRS 165855]). These data are qualified in Appendix M of this analysis report for their intended use in the determination of anisotropy in horizontal hydraulic conductivity (documented in this section of Appendix C and in Section 6.2.6).

C6.2.5 Anisotropy Ratios

Anisotropy ratio analyses performed for this report employ the analytical solution of Hantush (1966 [DIRS 161160]) or a modification of the analytic solution of Papadopoulos (1967 [DIRS 150265]) combined with PEST (STN: 10289-5.5-00 [DIRS 161564]). The analyses of Winterle and La Femina (1999 [DIRS 129796], p. 4-24) and Ferrill et al. (1999 [DIRS 118941], p. 6) used the Papadopoulos (1967 [DIRS 150265]) method. Although all techniques assume homogeneous confined aquifers with radial flow to the pumping well, some deviations from these assumptions may still yield reasonable estimates of anisotropy. In particular, these methods require as input transmissivity, storativity, and the locations of a minimum of three monitoring wells. With this information, anisotropy ratios and principal directions may be calculated. Results from all analyses are presented in Table C-12.

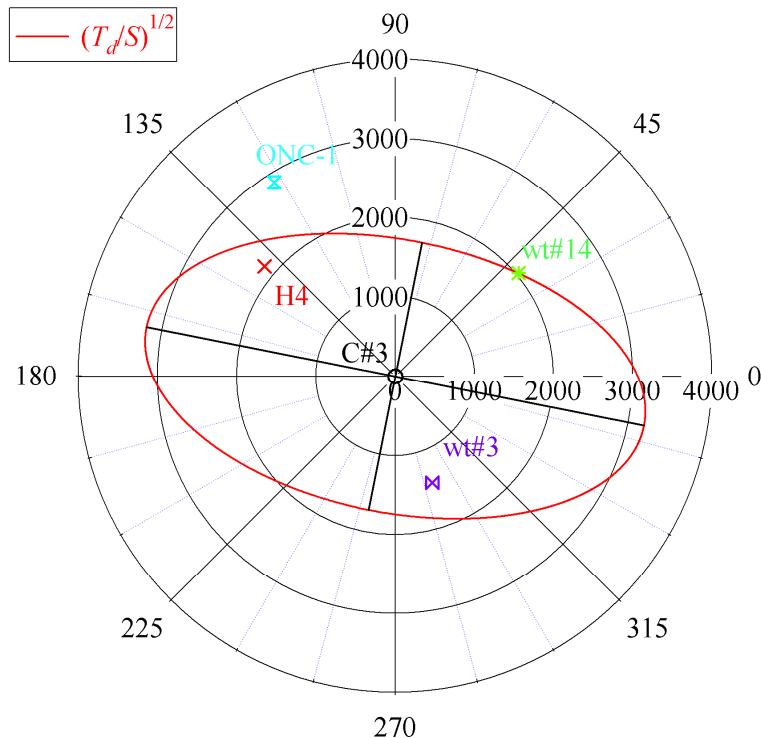
Using transmissivities and storativities from Table C-10 with the Hantush (1966 [DIRS 161160]) method yields an anisotropy ratio of 3.3 at principal direction 15° east of north. The data from H-4 were excluded from this analysis (as they were in the Winterle and La Femina (1999 [DIRS 129796]) and Ferrill et al. (1999 [DIRS 118941]) analyses) because including the data resulted in an undefined (negative) anisotropy ratio.

In the modified Papadopoulos-PEST method, three approaches were considered. In the first approach and in order to satisfy the homogeneous, anisotropic assumption of Papadopoulos (1967 [DIRS 150265]), which requires that all the observation-well responses produce the same transmissivity (to honor the homogeneity assumption), Theis (1935 [DIRS 150327]) (Theis.vi V 1.0, STN: 10974-1-00 [DIRS 162758]) type-curve fits for H-4, WT#3, WT#14, and a Streltsova-Adams (1978 [DIRS 150754]) (Streltsova-Adams.vi V 1.0, STN: 10971-1.0-00 [DIRS 162756]) type-curve fit for ONC-1 were constrained to produce the intermediate transmissivity value of 1,000 m²/day (the unconstrained values listed in Table C-8 ranged from 700 m²/day for H-4 to 2,600 m²/day for WT#3). These constrained fits produce storativities of 0.0023, 0.0052, 0.0026, and 0.0013 for wells H-4, WT#3, WT#14, and ONC-1, respectively. From these constrained fits, ratios of the directional transmissivity over storativity, T_d/S , were obtained after an article by Papadopoulos (1967 [DIRS 150265]). The square roots of these ratios were plotted on a polar plot with the pumping well, c#3, at the center.

It is important to note that while the Theis (1935 [DIRS 150327]) well function was used to develop the anisotropy ratios in this report, there is no reason why the well function cannot be replaced by another appropriate function. For example, if the medium responds as a fissure-block system, the fissure-block well function of Streltsova-Adams (1978 [DIRS 150754]) may be used. Because anisotropy analyses assume that drawdown is proportional to the well

function $W(u)$ through the relation $s = (Q/(4\pi T))W(u)$, where Q is the pumping rate, substitution of other well functions should not affect the anisotropy calculation methodology.

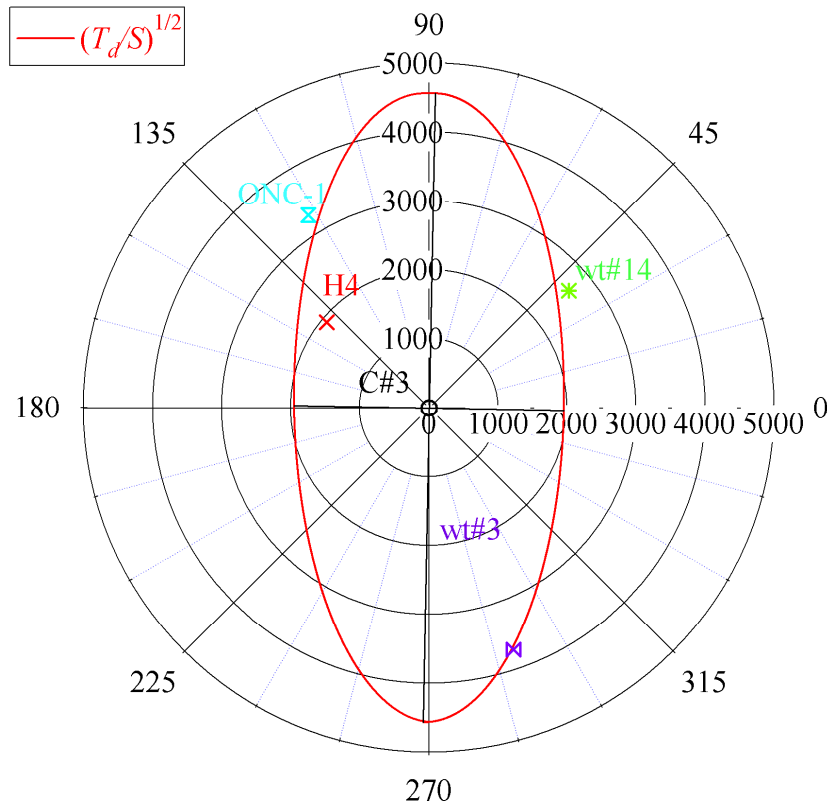
The modified Papadopoulos-PEST method (1967 [DIRS 150265]) then fits an ellipse, centered at the pumping well, through the $(T_d/S)^{1/2}$ data. This fitting was done with PEST V 5.5 (STN: 10289-5.5-00 [DIRS 161564]), in conjunction with a Microsoft Excel spreadsheet (*PEST-callable Excel Spreadsheet for Anisotropy Calculations in ANL-NBS-HS-000039*. ACC: MOL.20040901.0189), which calculates the shortest distance from each of the $(T_d/S)^{1/2}$ data points to the constructed ellipse (a notebook reference will be provided). PEST is instructed to vary the long and short axes of the ellipse and the principal direction to minimize the distances of all four $(T_d/S)^{1/2}$ data points from the ellipse. The ellipse in Figure C-42 is the optimal PEST ellipse. For this fit, PEST indicates that the direction of anisotropy is 79° west of north (with a 95% confidence interval of 75° to 82°), and that the magnitude of anisotropy is 3.5:1 (with a 95% confidence interval of 2.7:1 to 4.3:1). This direction of anisotropy is consistent with the geologic evidence of the Antler Wash series of fractures and faults running northwest from the C-wells to H-4. Two types of anisotropy are present within the study area: one is the NE-SW uniformly distributed anisotropy caused by regional stresses, and another is a NW-SE anisotropy related to the Antler Wash fault zone. The well H-4 is located along Antler Wash, northwest from the C-wells. When the well H-4 is included in the analysis, the results are greatly affected by Antler Wash and represent the NW-SE anisotropy related to this system. When the well H-4 is not included in the analysis, the results represent the NE-SW uniformly distributed anisotropy caused by regional stresses.



Sources: DTNs: GS970308312314.002 [DIRS 161273]; MO0212SPANYESJ.149 [DIRS 161274].
 Output DTNs: GS030208312314.001, GS030208312314.002 (filtered data).
 Output DTN: GS031008312314.004.

Figure C-42. Optimal Papadopulos-PEST Ellipse Fit to the Square Root of the Ratio of Directional Transmissivity to Storativity for USW H-4, UE-25 WT#3, UE-25 WT#14, and UE-25 ONC-1 for the 1,000 m²/day Transmissivity Fit for All Wells

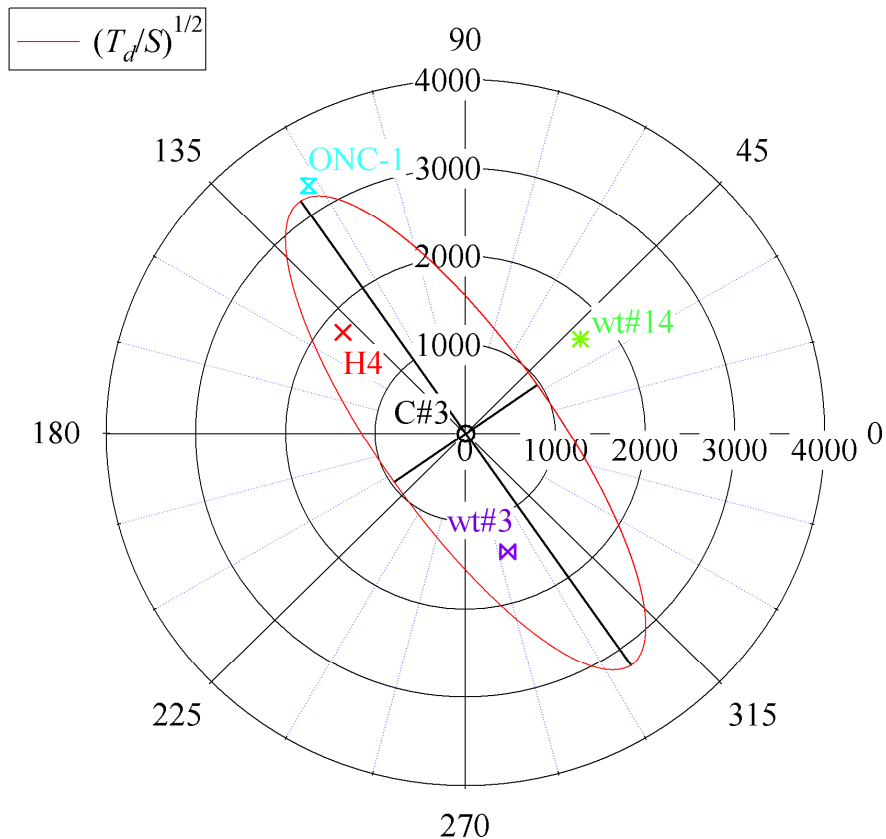
In the second modified Papadopulos-PEST approach, an optimal PEST ellipse was obtained for the unconstrained transmissivity values from Table C-8, although it violates the homogeneity requirement inherent in the Papadopulos (1967 [DIRS 150265]) method. The values for T and S are 700 m²/day and 0.002, respectively, for well H-4; 2,600 m²/day and 0.002 for WT#3; 1,300 m²/day and 0.002 for WT#14; and 1,000 m²/day and 0.001 for ONC-1. From these nonconstrained fits, ratios of the directional transmissivity over storativity, T_d/S, were obtained following the Papadopulos (1967 [DIRS 150265]) technique. The square roots of these ratios were plotted on a polar plot with the pumping well, c#3, at the center (Figure C-43). For this fit, PEST V 5.5 (STN: 10289-5.5-00 [DIRS 161564]) indicates that the direction of anisotropy is 1.1° east of north (with a 95% confidence interval of 0.5° to 1.7°) and that the magnitude of anisotropy is 5.5:1 (with a 95% confidence interval of 5.2:1 to 5.8:1).



Sources: DTNs: GS970308312314.002 [DIRS 161273]; MO0212SPANYESJ.149 [DIRS 161274]
 Output DTNs: GS030208312314.001, and GS030208312314.002 (filtered data).
 Output DTN: GS031008312314.004.

Figure C-43. Optimal Modified-Papadopoulos Ellipse Fit to the Square Root of the Ratio of Directional Transmissivity to Storativity for USW H-4, UE-25 WT#3, UE-25 WT#14, and UE-25 ONC-1 Using PEST for Variable (700 to 2,600 m²/day, Not in Order of Listed Wells) Transmissivities for the Four Wells

In the third modified Papadopoulos-PEST approach, an optimal PEST ellipse was obtained for unconstrained transmissivity values resulting from Theis (1935 [DIRS 150327]) (Theis.vi V 1.0, STN: 10974-1-00 [DIRS 162758]) type-curve fits for H-4, WT#3, WT#14, and Streltsova-Adams (1978 [DIRS 150754]) (Streltsova-Adams.vi V 1.0, STN: 10971-1.0-00 [DIRS 162756]) type-curve fits for ONC-1, using the filtered water-level data described in the first paragraph under Section C6.2.1. The unconstrained values for T and S resulting from analyzing the filtered data are 700 m²/day and 0.0024, respectively, for well H-4; 861 m²/day and 0.0045 for WT#3; 743 m²/day and 0.0029 for WT#14; and 1,230 m²/day and 0.0012 for ONC-1. From these values, ratios of the directional transmissivity over storativity, T_d/S , were obtained after Papadopoulos (1967 [DIRS 150265]). The square roots of these ratios were plotted on a polar plot with the pumping well, c#3, at the center (Figure C-44). For this fit, PEST V 5.5 (STN: 10289-5.5-00 [DIRS 161564]) indicates that the direction of anisotropy is 34.7° west of north (with a 95% confidence interval of 31.7° to 37.7°) and that the magnitude of anisotropy is 11.3:1 (with a 95% confidence interval of 9.3:1 to 13.9:1).



Sources: DTNs: GS970308312314.002 [DIRS 161273]; MO0212SPANYESJ.149 [DIRS 161274].
 Output DTNs: GS030208312314.001, and GS030208312314.002 (filtered data).
 Output DTN: GS031008312314.004.

Figure C-44. Optimal Modified-Papadopoulos Ellipse Fit to the Square Root of the Ratio of Directional Transmissivity to Storativity for USW H-4, UE-25 WT#3, UE-25 WT#14, and UE-25 ONC-1, using PEST, for Variable (700–1,230 m²/day) Transmissivities Obtained from Filtered Water Levels for the Four Wells

Using the analytical solution of Papadopoulos (1967 [DIRS 150265]), which assumes an homogeneous, confined aquifer, Ferrill et al. (1999 [DIRS 118941], p. 7) report an anisotropy ratio of 17:1 with principal direction at azimuth 30° (east of north).

The anisotropy ratio of Winterle and La Femina (1999 [DIRS 129796], p. 4-23) is listed in the last row of Table C-12 as 5 at 33° east of north. It should be noted that the difference in reported anisotropy between Ferrill et al. (1999 [DIRS 118941], p. 7) and Winterle and La Femina (1999 [DIRS 129796], p. 4-23) was solely due to a change in transmissivity for well WT#14, which decreased from 1,370 to 1,330 m²/day due to a difference in technique for correcting barometric pressures. The sensitivity of the analytical solution is demonstrated by the 3% change in transmissivity manifesting itself as a 70% decrease in the anisotropy ratio to 5:1.

Although not listed in Table C-12, the Hantush (1966 [DIRS 161160]) technique was applied to the transmissivities and storativities of Section C4.6, yielding an undefined anisotropy ratio (i.e.,

the transmissivities do not define an ellipse). However, when the modified Papadopulos-PEST analysis methodology was applied to these transmissivities and storativities, the anisotropy ratio was estimated as 5.5, as indicated in the third row of Table C-12. With the varied results, it is clear that the anisotropy ratio is highly sensitive to the locations and transmissivities of the monitoring wells. Three of the principal directions of anisotropy presented in Table C-12 vary between 15° and 33°. These values agree favorably with the geologically interpreted value of between 25° and 30°, the principal directional trend of faults in the Yucca Mountain area. In the methods producing these values, H-4 was not included in the analysis, and, hence, the resulting anisotropy values appear to not be affected by the Antler Wash structure; rather, they may be showing the underlying uniformly distributed anisotropy.

Table C-12. Calculated and Reported Anisotropies and Principal Directions

Data Set Used (Method)	T_{\max} (m ² /day)	T_{\min} (m ² /day)	Anisotropy ^a	Azimuth ^a
Table C-10 (Hantush) ^b	2,455	751	3.3	15°E
$T = 1,000$ m ² /day (Papadopulos-PEST) ^c	1,863	537	3.5	79°W
$T = 700 - 2,600$ m ² /day (Papadopulos-PEST) ^c	3,272	599	5.5	1°E
$T = 700 - 1,230$ m ² /day (Papadopulos-PEST) ^c	3,047	271	11.3	35°W
Ferrill et al. ^d	5,400	315	17	30°E
Winterle and La Femina ^e	2,900	580	5	33°E

Sources: DTNs: GS970308312314.002 [DIRS 161273]; MO0212SPANYESJ.149 [DIRS 161274].
Output DTNs: GS030208312314.001, and GS030208312314.002 (filtered data).

Output DTNs: GS031008312314.004 (Table 6.2-12), SN0409T0502203.002.

^aReported values.

^bHantush 1966 [DIRS 161160]

^cPapadopulos 1967 [DIRS 150265]

^dFerrill et al. 1999 [DIRS 118941]

^eWinterle and La Femina 1999 [DIRS 129796].

Winterle and La Femina (1999 [DIRS 129796], p. 4-25) claim a low degree of confidence in their anisotropy ratio because the problem is poorly constrained (e.g., data from only the minimum number of wells necessary for a solution is used; the medium is not homogeneous; the flow is not radial; and the aquifer may not be confined). Data from well H-4 were only used in the modified Papadopulos-PEST method. When data from H-4 were not used, it was because the transmissivity for this well was consistently about half of the other wells (note that both of the analytical solutions of Hantush (1966 [DIRS 161160]) and Papadopulos (1967 [DIRS 150265]) require that all wells have equal or nearly equal transmissivities). The rationale for excluding H-4 from the horizontal anisotropy analysis, in some cases, was also based on the Geldon et al. (1998 [DIRS 129721], p. 31) suggestion that a preferential flow path exists between well H-4 and the C-wells. However, inclusion of the H-4 data in the modified Papadopulos-PEST method and constraining the transmissivity to 1,000 m²/day (as described above) produced a direction of anisotropy consistent with the alignment of this preferential pathway. It is also noted that after approximately 50 days of pumping, water levels in wells H-4 and WT#14 stopped responding to pumping and actually began to increase, a phenomenon attributed to a recharge or high transmissivity boundary to the east or northeast of WT#14, which could potentially be a transmissive fault. This water-level increase was never observed in well ONC-1, even after 237 days of monitoring. This result implies that not all of the assumptions used in the anisotropy

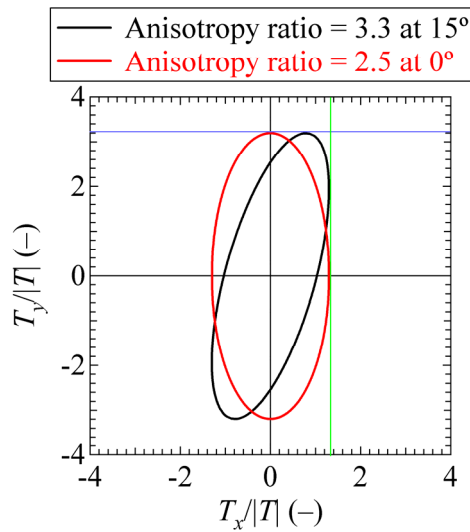
analysis are justifiable. Overall, this conclusion should serve to underscore the level of uncertainty in reported anisotropy ratios.

Considering the range of values demonstrated by the various anisotropy calculations, the results in Table C-12 help characterize a parameter that was not targeted explicitly for measurement when the data ultimately used to calculate it were obtained.

C6.3 INTERPRETATION AND ASSIGNMENT OF THE ANISOTROPY DISTRIBUTION

Well-test analysis is the process of estimating hydrologic parameters of interest (in this case, transmissivity and storativity) from measured drawdown data, and is known as an inverse (or parameter-estimation) problem. An inherent quality of inverse problems is that the parameters estimated via this process have some degree of uncertainty associated with their values. More importantly, when solving an inverse problem, a family of solutions should be matched to the data. Because there are typically infinitely many solutions that fit the data, reporting only a single value imparts no real information. It is much more important to examine the range of solutions and to evaluate the sensitivity of each parameter to the solution. In other words, uncertainty must be quantified. To date, there have been no attempts to assign confidence intervals to the estimated parameters. Comparing the well test results of previous researchers helps to emphasize the dependence of the estimated hydrologic parameters upon the solution technique and input data used. Analytical techniques alone cannot provide a measure of confidence in their reported solution. Therefore, it is left to scientific judgment to assign a distribution of anisotropy ratios based upon the available scientific evidence.

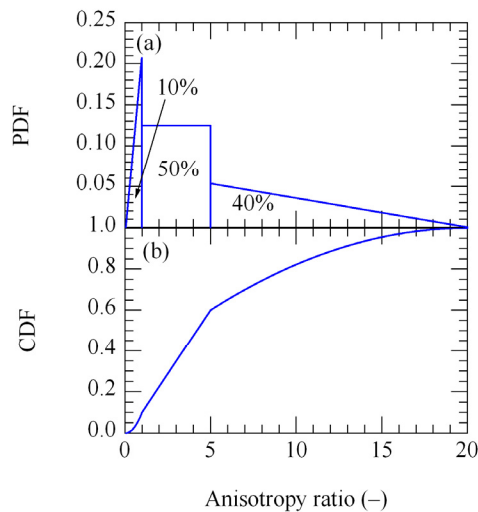
Practically speaking, an anisotropy ratio must be selected for each of the 200 stochastic model realizations used as input to the SZ site-scale flow model, which is implemented using the software code FEHM. Because the current version of FEHM (V. 2.20, STN: 10086-2.20-00 [DIRS 161725]) can only implement anisotropy oriented in a north-south direction, principal directions discussed above are not applicable in the model. The net result of being unable to specify a principal direction is that uncertainty in the anisotropy ratio can only increase. For example, the analytical result for anisotropy using the Cooper-Jacob (1946 [DIRS 150245]) method is 3.3 at 15° east of north. A projection that orients the principal direction north-south (0°) results in a new anisotropy ratio of 2.5. As illustrated in Figure C-45, this value was calculated by dividing the maximum y value on the anisotropy ellipse oriented 15° east of north (horizontal blue line at top) by its maximum x value (vertical green line at right). Similarly, the projected north-south anisotropy ratio for an anisotropy ratio of 5 oriented 33° east of north is 1.5. Uncertainty in the analytically calculated anisotropy ratio is propagated in the projected anisotropy ratio and magnified as a function of the uncertainty in the principal direction. In fact, this line of reasoning suggests that it is possible for the projected north-south anisotropy ratio to be significantly less than one.



Output DTN: GS031008312314.004.

Figure C-45. Anisotropy Ratio of 3.3 at 15° East of North Projected onto a North-South Anisotropy Ratio (0°) Resulting in a Projected Anisotropy Ratio of 2.5

Based on consultations between Sandia National Laboratories (SNL) staff, USGS staff, and the YMP Parameters Team, as well as results from the analytical anisotropy analyses, Figure C-46 (a) represents the best estimate of the probability density function (PDF) for the anisotropy ratio in the SZ near the C-wells complex (Eddebarh 2004 [DIRS 171918]). Figure C-46 (b) is the corresponding cumulative distribution function.



Output DTN: SN0302T0502203.001.

Figure C-46. Probability Density Function (a) and Corresponding Cumulative Distribution Function (b) for the North-South/East-West Anisotropy Ratio Used in FEHM Input Files

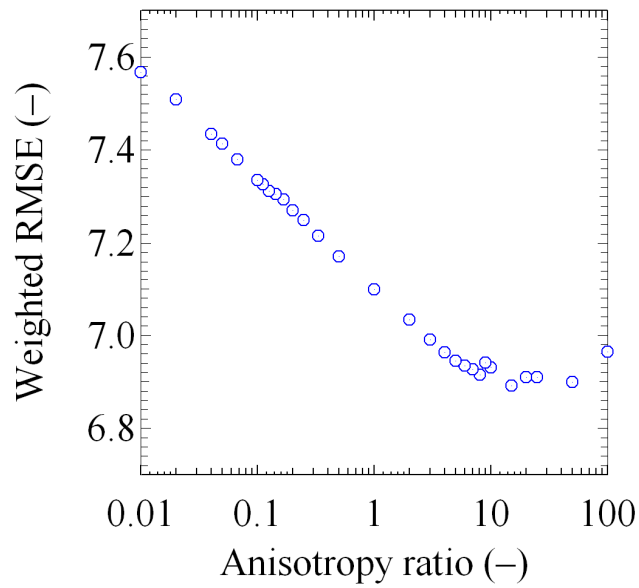
There are three noteworthy points based on three distinct regions of the anisotropy ratio distribution (Output DTN: SN0302T0502203.001):

- *Anisotropy ratio between 5 and 20.* The maximum anisotropy ratio of 20:1 is physically based. Although features such as high transmissivity zones and fractures may yield very large anisotropy ratios locally, globally, their effects are attenuated. That is, over the area of the saturated-zone model, $45 \times 30 \text{ km}^2$, an anisotropy ratio of 20 is the expected upper bound. Additionally, the highest calculated anisotropy ratio reported is 17:1 (Ferrill et al. 1999 [DIRS 118941], p. 7). The 5.5 anisotropy ratio calculated by the second approach of the modified Papadopoulos-PEST method lies in this range near its highest probability point. Therefore, between 5 and 20, a triangularly distributed anisotropy ratio is constructed that decreases to zero probability at 20. Given that 3 of the 6 estimates of anisotropy ratio in Table 6.2-4 fall between 5 and 20, and one of these three estimates is just barely greater than 5 (5.5), a 40% probability is assigned to this portion of the PDF.
- *Anisotropy ratio between 0.05 and 1.* Discussions among Sandia National Laboratories and USGS staff established that, although it is likely the SZ is anisotropic with principal direction approximately northeast, it is possible the media could be isotropic, as well as a small probability that the principal direction could be significantly different from northeast. Correspondingly, anisotropies less than one are possible, and the minimum anisotropy ratio is set equal to the inverse of the maximum, 1:20, with a triangularly distributed 10% probability decreasing to zero at a ratio of 0.05. The 3.5 anisotropy ratio calculated by the first approach of the modified Papadopoulos-PEST method, when adjusted according to Figure C-45, falls in this range.
- *Anisotropy ratio between 1 and 5.* A uniformly distributed 50% probability is assigned to the range of anisotropy ratios between 1 and 5. This interval comprises the most likely values of anisotropy ratios with no specific value more likely than another.

Figure C-46 (a and b) is the best estimate for the PDF and the cumulative distribution function, respectively, of north-south anisotropy ratios in the SZ to be used as input to the SZ site-scale flow model.

C6.4 FEHM SENSITIVITY STUDY

One last point worthy of mention is that a sensitivity analysis of FEHM V 2.20 (STN: 10086-2.20-00 [DIRS 161725]) results to the anisotropy ratio demonstrated that the modeled heads are insensitive to the input anisotropy ratio. However, inferred groundwater transport times and flow pathways, which, ultimately, are more important for radionuclide transport predictions than heads, are more sensitive to the anisotropy ratio. Figure C-47 illustrates how varying the anisotropy ratio affects the weighted root-mean-square error (RMSE) between measured and FEHM modeled heads. The RMSE ranges only between 6.9 and 7.6. Although this short range demonstrates relative insensitivity of the modeled heads to the anisotropy ratio, it is encouraging to note that the minimum RMSE corresponds to an anisotropy ratio of 20.



NOTE: For information purposes only.

Figure C-47. Weighted Root-Mean-Square Error (RMSE) between Measured Heads and FEHM Modeled Heads Subject to a Range of Anisotropy Ratios between 0.01 and 100

C6.5 CONCLUSIONS

Although analytical and graphical techniques can produce a single, specific anisotropy ratio, this value is sensitive to both the solution technique and the analyst's interpretation of the data (e.g., what filtering parameters were used or how the slopes of drawdown were calculated). A wide distribution of anisotropy ratios is suggested to account for the significant uncertainty in this hydrologic property. Each run of FEHM V 2.20 (STN: 10086-2.20-00 [DIRS 161725]) must have a single value of anisotropy assigned to the anisotropy zone of the model area, and, though this is unrealistic (no single value of anisotropy truly applies to such a large heterogeneous area), drawing an anisotropy ratio from the specified distribution and running FEHM stochastically should effectively account for the uncertainty in this model parameter. Additionally, because the current version of FEHM cannot specify the principal direction of anisotropy, the range of possible north-south anisotropies is increased to consider this fact.

C7. SUMMARY OF CONCEPTUAL MODELS AND PARAMETERS

Hydraulic tests conducted by the USGS in Miocene tuffaceous rocks at the C-wells complex, Yucca Mountain, Nevada, between May 1995 and November 1997 determined flow characteristics in six saturated-zone hydrogeologic intervals. North- and northwest-striking faults intersect boreholes of the C-wells complex, defining hydrogeologic intervals by spatially related faults and fracture zones. Flow within those intervals comes from diversely oriented fractures and from the interstices of variably welded ash-flow, ash fall, and reworked tuff. The tuffs in the immediate vicinity of the C-wells act as a single aquifer. About 70% of flow seen in hydraulic tests was contributed by the Lower Bullfrog interval, and another 20% came from the Upper Tram interval. Identified hydrogeologic units, and related hydrologic properties, cannot be extended far beyond the immediate vicinity of the C-wells complex due to control of those intervals by fault and fracture zones.

In several hydraulic tests from 1995 to 1997, Borehole c#3 of the C-wells complex was used as the pumping well. Boreholes c#1 and c#2 (tens of meters distant) were used as observation wells. Each of the wells of the complex is about 900 m deep, and all are open below surface casings to the penetrated formations. Additional boreholes were used as observation wells in some of the hydraulic tests, including ONC-1, H-4, WT#14, WT#3, and p#1. The observation wells were completed in various intervals seen also in the holes of the C-wells complex; p#1 was completed in Paleozoic carbonate rocks. Those observation wells were sited 630 to 3,526 m from c#3, allowing some extrapolation of hydraulic characteristics from the C-wells location. The hydraulic tests were conducted to determine: (1) properties of the composite saturated-zone section in the C-wells; (2) hydrologic properties of the six intervals in those holes; and (3) heterogeneity in the tuffs, including the influence of faults. Monitoring in Borehole p#1 was intended to establish whether the tuffs are connected hydraulically to the Paleozoic carbonate rocks (a regional aquifer), estimated to lie some 455 m below the C-wells.

The series of hydraulic tests began with short-term test episodes. The 10-day test of May 1995 pumped Borehole c#3 at an average rate of 1,074 L/min and produced pumping-well drawdown of 7.76 m. Drawdown in observation wells ranged from 0 to 42 cm. The June 1995 test lasted four days and used packers to isolate the six saturated-zone hydrogeologic intervals of the C-wells complex. After pumping at a rate of 1,350 L/min, drawdown in the pumping well

was 10.9 m, and drawdown in monitored intervals of observation wells c#1 and c#2 ranged from 43 to 352 cm. The five-day test of February 1996 used packers to isolate and pump the Lower Bullfrog and Upper Tram intervals at a rate of 510 L/min. All monitored intervals responded to that pumping. Drawdown in the pumping well was 2.86 m, and drawdown in c#2 and c#1 ranged from 14 to 25 cm.

A long-term test in which the Lower Bullfrog interval was isolated was conducted over more than 550 days starting in May 1996. All monitored intervals again responded to pumping (at a rate of 552 L/min). Drawdown reached nearly 6 m by late March 1997 when some disruption due to pump shutoffs occurred. Drawdown in all observation wells was strongly oscillatory, with peak drawdown in the C-wells complex observation holes of 35 to 51 cm. Drawdown in distant observation wells began after hours to days of pumping and ranged from 15 to 37 cm. No drawdown had been observed in p#1 (completed in the carbonate aquifer) by December 1996.

In all of these tests, significant, rapid drawdown and recovery in the pumping well far exceeded amounts that could be predicted from hydrologic properties calculated from observation-well drawdown in the same tests. Much of that excess likely can be attributed to frictional head loss (“borehole skin”) in the pumping well. Thus, analysis of pumping-well drawdown data may lead to misleading values for the transmissivity and hydraulic conductivity of the aquifer due to effects of turbulence in the well bore and attendant well losses.

Hydrogeologic intervals in the C-wells exhibit layered heterogeneity. The response in the Calico Hills interval is consistent with an unconfined aquifer; responses in the Prow Pass and Upper Bullfrog intervals are consistent with either an EPM or a fissure-block confined aquifer; response in the Lower Bullfrog interval is consistent with a fissure-block confined aquifer; and the response in the Upper Tram interval is consistent with a leaky confined aquifer receiving flow from cross-cutting faults. Transmissivity increases downhole from a range of 4 m²/day to 10 m²/day in the Calico Hills interval to a range of 1,300 m²/day to 1,600 m²/day in the Lower Bullfrog interval. This trend is reversed near the bottom of the wells (i.e., in the Upper Tram Interval, transmissivity is 800 m²/day to 900 m²/day). Likewise, hydraulic conductivity increases downhole from about 0.2 m/day in the Calico Hills interval to a range of 20 m/day to 50 m/day in the Lower Bullfrog and Upper Tram intervals. Storativity generally increases downhole; for example, in c#2 it increases from a range of about 0.0002 to 0.0004 in the Calico Hills and Prow Pass intervals to a range of 0.001 to 0.002 in the Lower Bullfrog and Upper Tram intervals. Order-of-magnitude differences, though, are evident between wells of the C-wells complex and nearby observation wells. These vertical distributions of hydrologic properties reflect the greater influence of faults and related fractures toward the bottom of the boreholes.

During hydraulic tests at the C-wells complex, drawdown occurred in all monitored intervals of those holes and in observation wells, regardless of the interval being pumped. The hydraulic connection across lithostratigraphic contacts likely results from interconnected faults, fractures, and intervals with large matrix permeability. The Miocene tuffaceous rocks thereby act as a single aquifer within a portion of the structural block bounded by the Paintbrush Canyon and Dune Wash faults as well as by faults cutting Boundary Ridge (extending at least as far north as lower Midway Valley). This aquifer encompasses a 21-km² area surrounding the C-wells complex.

Drawdown data from monitored wells during the long-term hydraulic test matched the type curve for a confined aquifer and indicated a transmissivity of 2,200 m²/day and a storativity of 0.002 for the tuffs in the region around the C-wells complex. Plots of drawdown in observation wells as a function of distance during the same test showed a transmissivity of 2,100 m²/day to 2,600 m²/day and a storativity of 0.0005 to 0.002. Analyses of drawdown in the C-wells and in outlying observation wells indicated a northwestward decrease in transmissivity from 2,600 m²/day in WT#3 to about 2,000 m²/day at the C-wells and, eventually, to 700 m²/day in H-4. (Hydraulic conductivity is smallest toward the crest of Yucca Mountain and toward Jackass Flats.) Distributions of drawdown likewise were influenced strongly by northwest- and north-striking faults, as was hydraulic conductivity. Drawdown in observation well ONC-1 showed a fissure-block aquifer response during the long-term test, possibly due to a northwesterly zone of discontinuous faults that extends beneath Bow Ridge and Antler Wash. Drawdown in other observation wells reached a steady state after some 50 days of pumping, again likely in response to faults and fracture zones. Hydraulic conductivity ranges areally from less than 2 m/day to more than 10 m/day, and is largest where prominent north-striking faults are closely spaced or intersected by northwest-striking faults. Relatively large hydraulic conductivity occurs beneath Fran Ridge, Bow Ridge, and Boundary Ridge.

Collective consideration of all the C-wells hydrologic test results suggests that the most appropriate conceptual model for flow in the saturated volcanic tuffs near Yucca Mountain is one in which flow occurs predominantly through fractures, with these fractures tending to form better-connected networks in the horizontal direction than in the vertical direction, resulting in some apparent stratification of flow (that is, greater horizontal hydraulic conductivity than vertical hydraulic conductivity). Besides hydraulic test results, other lines of evidence suggesting some degree of horizontal stratification are the significant upward vertical hydraulic gradient in the volcanic tuffs and the apparent lack of mixing of waters in the tuffs with water from the underlying carbonate aquifer at the C-wells. This upward gradient and the lack of vertical mixing, which are observed at other locations around Yucca Mountain as well, presumably could not be sustained if it were not for some confinement of flow in the vertical direction. However, hydraulic responses in intervals above and below pumped intervals at the C-wells clearly indicate that there is some hydraulic communication vertically within the tuffs. This point is mentioned because the use of analytical solutions for confined aquifers to estimate hydrologic parameters for some intervals may give the impression that some intervals are completely confined. A more accurate conceptualization is that, over larger scales, the vertical hydraulic conductivity in the fractured tuffs is considerably smaller than the horizontal hydraulic conductivity, resulting in an effective anisotropy favoring horizontal flow over vertical flow.

Flow surveys at the C-wells and in other wells in the fractured tuffs indicate that not all fractures in the SZ contribute significantly to flow, and they also suggest that flowing intervals appear to be much less extensive in the vertical direction than the stratigraphic intervals in which they are contained. Thus, the concept of assigning bulk hydrologic properties to entire stratigraphic intervals may be somewhat misleading, and it may be more appropriate to consider the concept of flowing intervals that are spatially separated but nevertheless interconnected at larger scales. Faults undoubtedly play an important role in the larger-scale interconnectedness of flowing intervals. In addition, because faults tend to be steeply dipping near Yucca Mountain, they may have an important influence on effective hydrologic properties in the vertical direction over large scales in the SZ.

Uncertainties in hydrologic parameter estimates, including uncertainties associated with the data-analysis methods, are discussed in detail in Section C5. When all of the contributing uncertainties are considered, transmissivity and storativity estimates for individual hydrogeologic intervals at the C-wells are considered accurate to within a factor of 2.5 for transmissivity (1.5 for the lower Bullfrog and upper Tram Tuffs) and within an order of magnitude for storativity. Hydraulic conductivity estimates are considered to be somewhat less accurate because of the inherent uncertainty in the assumed transmissive thickness of a given test interval.

The responses of WT#3, WT#14, ONC-1, and in some cases H-4, to the long-term hydraulic test were analyzed for anisotropy of the hydraulic conductivity. When H-4 was not included in the analysis, the principal directions of anisotropy vary between 15°E and 33°E. These values agree favorably with the geologically interpreted value of between 25°E and 30°E, the principal directional trend of faults in the Yucca Mountain area. Because the methods producing these values do not include H-4 results, the resulting anisotropy values do not appear to be affected by the northwesterly trending Antler Wash structure; rather, they may be showing the underlying uniformly distributed anisotropy. When H-4 was included in the analysis of anisotropy, the influence of the northwesterly trending Antler Wash structure is seen, and the resulting principal directions of anisotropy range from 79°W to 1°E.

Based on these analyses, a PDF was derived for north-south/east-west anisotropy in horizontal hydraulic conductivity in the fractured volcanics (Figure C-46). This PDF reflects the uncertainty in horizontal anisotropy associated with the analysis of the long-term hydraulic test data. The PDF assigns a probability of 0.9 to a north-south orientation of the anisotropy “ellipse,” with a 0.5 probability of the anisotropy ratio ranging from 1 to 5 and a 0.4 probability of the ratio ranging from 5 to 20. Although this is a relatively wide range of possible anisotropy ratios, flow simulations indicated little sensitivity of modeled heads to the full range of ratios. However, flow rates would be expected to be more sensitive to the assumed anisotropy ratio, and the range of specific discharges used in performance assessments reflect this uncertainty.

APPENDIX D

**DETAILS OF TRACER TESTING AND TRACER TEST INTERPRETATIONS AT THE
C-WELLS COMPLEX**

D1. NONSORBING TRACER TESTS AT THE C-WELLS

Nonsorbing tracer tests conducted at the C-wells complex included: (1) iodide injection into the combined Bullfrog-Tram interval; (2) injection of pentafluorobenzoic acid (PFBA) into the Lower Bullfrog interval, (3) injection of iodide into the Lower Bullfrog interval; (4) injection of 2,6 Difluorobenzoic acid (DFBA) into the Lower Bullfrog interval; (5) injection of 3-carbamoyl-2-pyridone (Pyridone) into the Lower Bullfrog interval; (6) injection of iodide and 2,4,5 trifluorobenzoic acid (TFBA) into the Prow Pass formation; and (7) injection of 2,3,4,5 tetrafluorobenzoic acid (TeFBA) into the Prow Pass formation.

The purpose of testing with nonsorbing tracers was to obtain estimates of flow porosity and longitudinal dispersivity of the Bullfrog and the Prow Pass Tuffs. The approach to developing parameters was to conduct multiple tests in a cross-hole system and use different mathematical solutions to interpret the results. Consequently, uncertainties and the sensitivity of the system were better understood.

Iodide, benzoic acids (including DFBA, TFBA, TeFBA, and PFBA), and pyridone can be analyzed by high-performance liquid chromatography (HPLC) with either ultraviolet (UV) absorbance detection or fluorescence detection (pyridone). This method was selected not only because it is precise and sensitive but also because the groundwater samples can be injected directly into the instrument, allowing analyses to be conducted easily in the field for immediate test results.

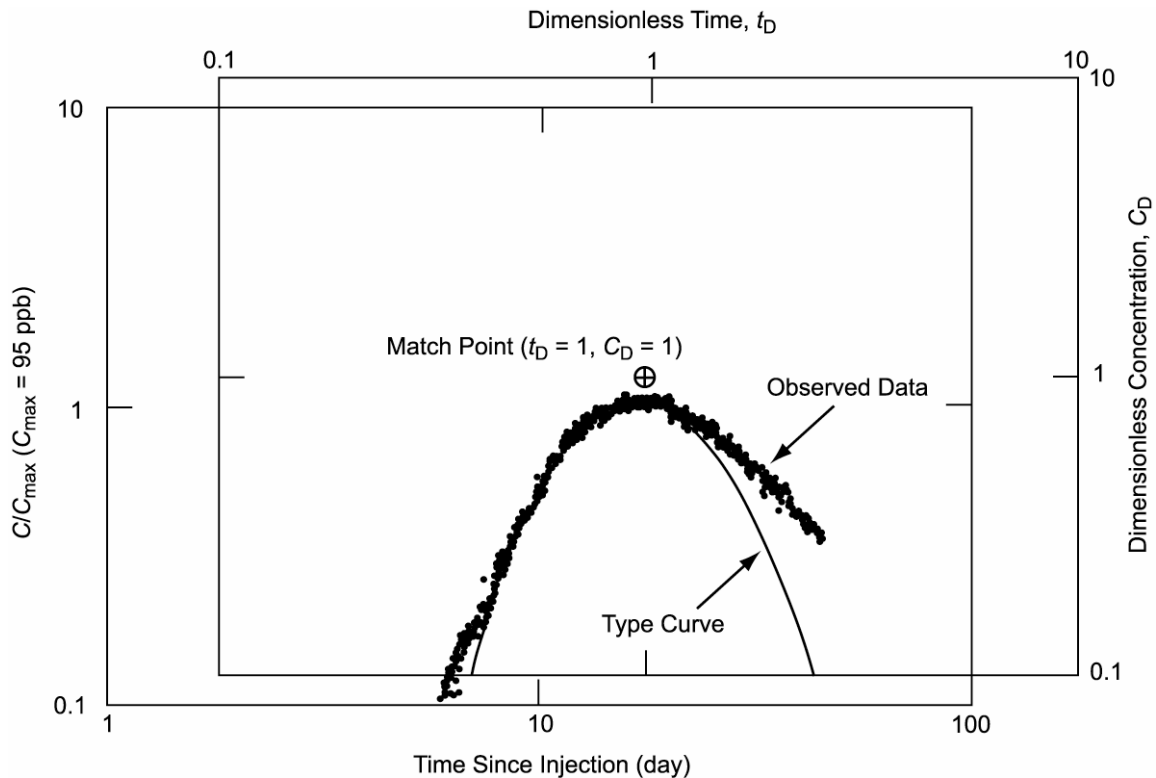
All nonsorbing tracer tests were analyzed by the Moench (1989 [DIRS 101146]; 1995 [DIRS 148784]) single- and dual-porosity analytical solutions to the advection-dispersion equation or by superposition of these solutions. Both solutions are implemented using the MOENCH.vi Function(1) code in conjunction with the *rcv2amos.exe* routine (STN: 10583-1.0-00 [DIRS 162750]) and the MOENCH.vi, Function(2), V 1.0 code (STN: 10582-1.0 [DIRS 162752]). The first software package implements the published dimensionless solutions. The second allows for curve matching to actual, dimensional, tracer breakthrough curves. The input parameters required by the Moench (1989 [DIRS 101146]; 1995 [DIRS 148784]) single-porosity and dual-porosity solutions are:

- Production rate, q_o (L/min)
- Distance from the production to injection well, r_L (m)
- Aquifer thickness, h (m)
- Radius of production well, r_w ; and injection well, r_i (m)
- Thickness where mixing occurs in the production well, h_w (m)
- Thickness where mixing occurs in the injection well, h_i (m)
- Mass of tracer injected, M (g)

- Volume of water in which the mass of tracer is dissolved prior to entering the aquifer, V (L)
- Time for the tracer slug to enter the aquifer, t_{inj} (s)
- Flow porosity, ϕ_f , and matrix porosity, ϕ (matrix porosity is also referred to, interchangeably, as “storage porosity” in Appendix B)
- Longitudinal dispersivity, α_L , in the form of a Peclet number ($Pe = r_L/\alpha_L$) (m)
- Retardation coefficients representing linear, reversible adsorption R in the fractures and R' in the matrix (always assumed to be 1.0 for conservative tracers)
- Dimensionless diffusion coefficient, γ , which is a function of the effective coefficient of diffusion from the fractures into the matrix, D' , and of h , ϕ_f , R , q_o , and the radius, b' , of theoretical sphere-shaped matrix blocks of the dual-porosity aquifer
- Dimensionless storage parameter, σ , which is a function of ϕ_f , ϕ , R , and R'
- Dimensionless skin parameter, SK , which is a function of the mass transfer coefficient, k_s , representing the continuity of diffusive flux across the “skin” (such as mineral fracture-surface coatings separating fractures from matrix blocks), and of D' and b' .

In a radially convergent flow field, the volume of interest is a cylinder centered at the production borehole and extending to the injection borehole. Moench (1989 [DIRS 101146]) assumes that the injection borehole is well mixed and that the tracer is distributed over a specified fraction of the borehole interval length (i.e., the “mixing length”).

Radially convergent, flow-type curves were generated for a range of Peclet numbers. These single-porosity and dual-porosity type curves are in the form of log—log plots of dimensionless concentration, $C_D = C/C_i$, where C_i = average concentration in injection borehole after tracer injection, versus dimensionless time, $t_D = t/(\pi h \phi (r_L^2 - r_w^2)/q_o)$, where the denominator is referred to as the advective transport time, t_a . The observed field tracer breakthrough data are presented in the form of log—log plots of normalized concentration, C/C_{max} (where the concentration is normalized by the maximum observed concentration), versus time since injection. By overlaying the type curve and dimensionless breakthrough curve and matching the rising portions of the two curves, an estimate of the advective transport time, t_a , is obtained when the match point ($C_D = 1$, $t_D = 1$) is projected onto the log-time axis of the dimensionless field breakthrough curve (e.g., D-1, which shows this process for the tracer test described in Section D1.1.1). In addition, because dimensionless time is defined as the ratio of time since injection to the advective transport time, the value of t_a is equal to the time since injection, indicated on the time axis of the breakthrough curve, corresponding to $t_D = 1$. The Peclet number is also estimated based on the type curve match. In the dual-porosity solution, diffusion is minimal on the rising limb of the breakthrough curve, but it was calculated on the falling limb. The tail of the observed data was matched to a theoretical dual-porosity breakthrough curve with diffusion processes in which the controlling parameters include the γ and σ terms. The physical parameters that are estimated are the matrix porosity, ϕ , and the dimensionless diffusion coefficient, γ .



Source: DTN: GS960808312315.001 [DIRS 159235] (data).

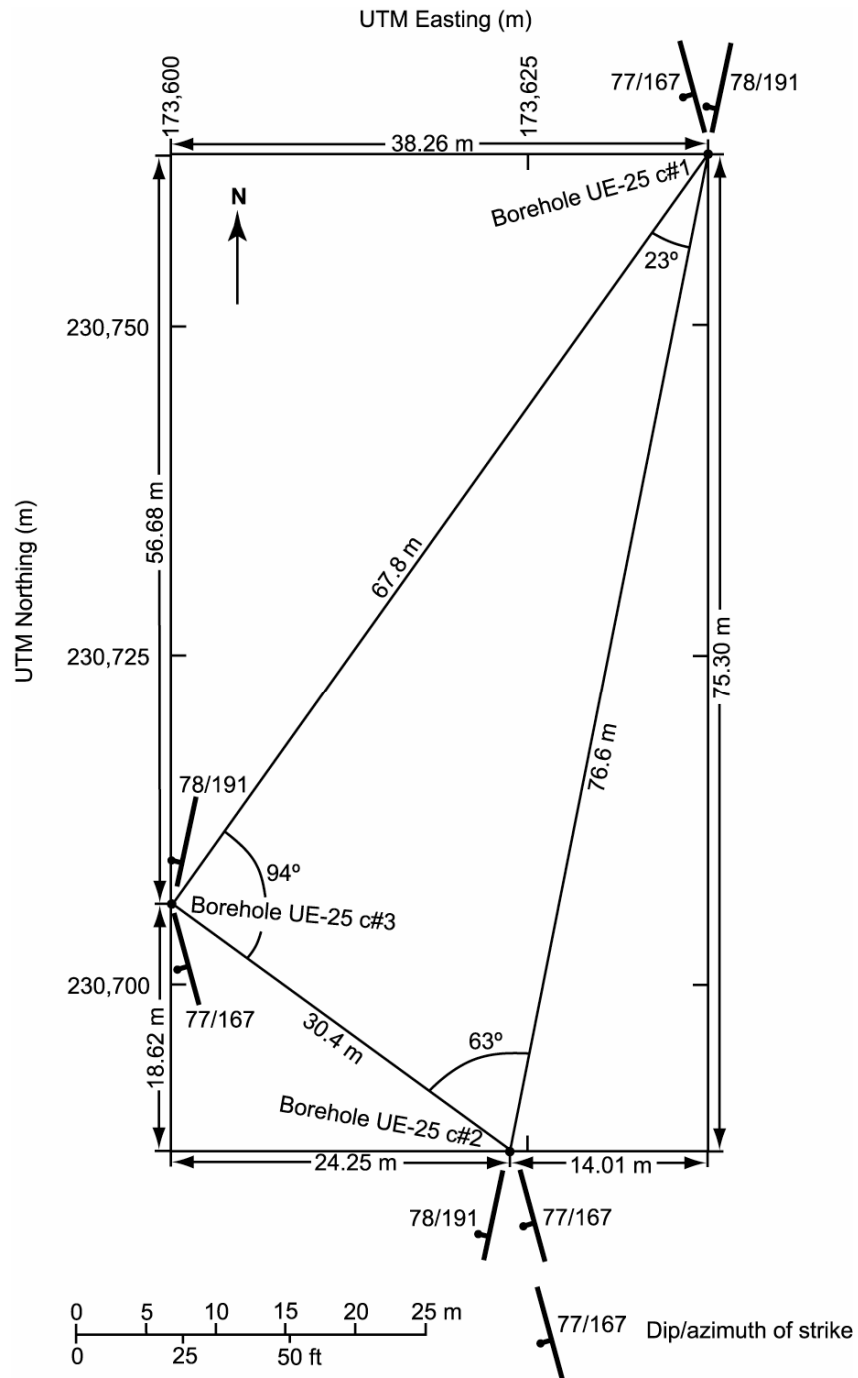
Output DTN: GS031008312315.002 (analysis).

NOTE: The Peclet number $Pe = 11$.

Figure D-1. Type-Curve Match for Iodide Injection into UE-25 c#2

Some of the analyses of nonsorbing tracer tests in this report used the single-porosity Moench solution, some used the dual-porosity solution, and some used a combination of both, depending on the type of test. This was done to explore the effectiveness of a particular solution method in matching a particular set of data. When both the single- and dual-porosity solutions were used, the t_a and Peclet number were first obtained from the match of the single-porosity type curves to the rising limb of the data curve; then Moench's dual-porosity solution was used to obtain estimates of gamma and sigma by fitting to the whole data curve.

To constrain the range of parameter values (such as of flow porosity) that can result from various possible interpretations of tracer tests, the fracture characteristics of the formations in which tracer testing was conducted should be considered. Fracture orientations in the Lower Bullfrog were based on televiwer data reported by Geldon (1996 [DIRS 100396], pp. 14 to 17, Table 6) and obtained in the 1980s when the boreholes were drilled. Two orientations are statistically significant. The dip and strike of the fracture planes are: 77/167 and 78/191 (first number is degrees from horizontal, and second number is degrees from due north in a clockwise direction; the two orientations are shown in Figure D-2, relative to the sides of the C-wells triangle). The fractures at the C-wells complex are moderately to steeply inclined, trend in a northerly direction, and have a probable nonuniform spacing. If transport is along fractures and faults, then the orientation data represent the possible directions of transport that may be occurring at the small scale in any interpretation.



Source: Geldon (1993 [DIRS 101045], p. 6 for well locations); Geldon (1996 [DIRS 100396], pp. 74 to 119 for fracture information).

Figure D-2. Dominant Bullfrog Tuff Fracture Sets in Each of the C-Wells

D1.1 RESULTS AND INTERPRETATIONS OF NONSORBING TRACER TESTS: BULLFROG AND TRAM FORMATIONS

D1.1.1 Iodide Tracer Test in the Lower Bullfrog/Upper Tram Interval

Following establishment of a quasi-steady-state hydraulic gradient by pumping the recovery borehole (c#3) for about 7,000 minutes, the first convergent tracer test at the C-wells complex was initiated in the Bullfrog-Tram Tuff interval on February 13, 1996, under convergent flow field conditions (Umari 2002 [DIRS 162858], Binder 4, Section F-12; Binder 5, Sections G-4 to G-12, H-1 to H-7; Binder 6, Sections H-1 to H-7 and H-10 to H-11). Tracer solution was injected into the Bullfrog-Tram interval of Borehole c#2 for 28 minutes at an average rate of 24.6 (liters per minute [L/min]) (6.5 gallons per minute [gpm]). This test was conducted in the most transmissive interval in the C-wells (the Bullfrog-Tram interval), over the shortest interborehole distance (from Borehole c#2 to Borehole c#3), and using the simplest flow field (a convergent flow field) to enhance the possibility of successful tracer recovery.

The tracer solution consisted of 5.9 kilograms (kg) of sodium iodide (of which 5 kg were iodide) dissolved in 500 liters (L) (132 gal) of water from Borehole c#3 (Umari 2002 [DIRS 162858]). The tracer solution was chased with 182 L (48 gal) of water from c#3, which was pumped into Borehole c#2 to ensure evacuation of the injection string (Umari 2002 [DIRS 162858]).

The chemical constituent used as a tracer was iodide with an injection concentration of 10,200 parts per million (ppm). The iodide injection from c#2 on February 13, 1996, has been discussed by Fahy (1997 [DIRS 137456], second and third unnumbered pages). Iodide concentrations in water sampled during the tracer test were obtained by a reverse-phase, HPLC in conjunction with a UV-absorption detector (Stetzenbach and Thompson 1983 [DIRS 156863], pp. 36 to 41). The field-determined detection limit for iodide was 3 µg/L. The precision of the HPLC analytical technique, as determined by comparing replicate analyses, was 2.3% for the field-determined concentrations and 1.61% for laboratory-determined concentrations.

Iodide breakthrough occurred 5.07 days after injection. The peak concentration occurred 17.75 days after injection. The test was terminated 45.1 days after injection. The iodide mass recovered was estimated as 2.347 kg, 47% of the injected mass (Fahy 1997 [DIRS 137456], second and third unnumbered pages).

The tracer test was complicated by progressively decreasing discharge from the recovery well, which was caused by a mechanically failing pump. The pump discharge decreased from 510 L/min (134.7 gpm) on February 13, 1996, to 372 L/min (98.3 gpm) on March 29, 1996. For analysis of the tracer test, the median value of 444 L/min (117.3 gpm) was used as the discharge rate (the decline in discharge rate was approximately linear with time and the discharge measurements were obtained at equal time increments, so the median and mean of all measurements were essentially the same). Despite these problems, a breakthrough curve, with breakthrough and peak arrival times readily discernible, was clearly established by March 29, 1996.

Interpretation of Test

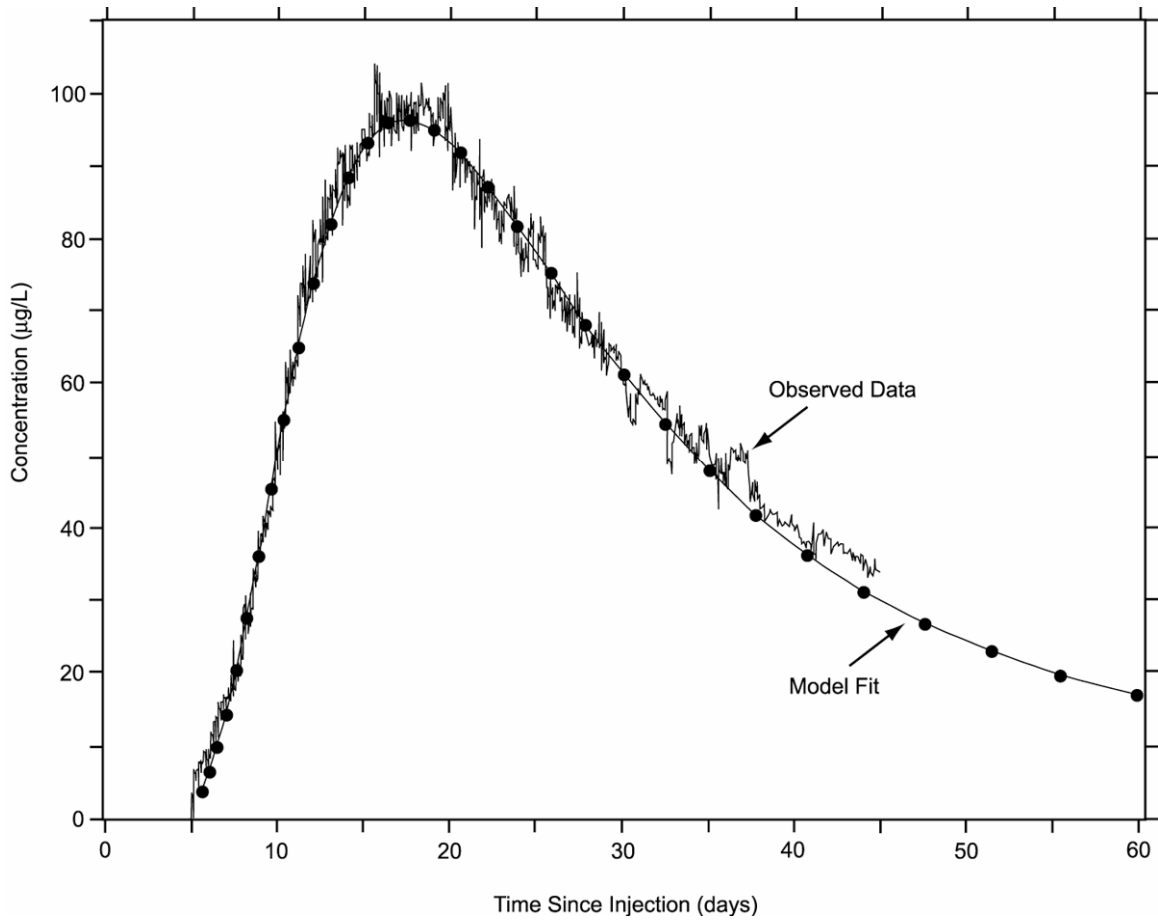
Both the single- and dual-porosity Moench (1989 [DIRS 101146]; 1995 [DIRS 148784]) solutions were used to interpret the iodide test in the Bullfrog-Tram interval. The rising limb was first analyzed using the single-porosity solution, as presented in Figure D-1, to obtain the flow porosity and Peclet number. The dual porosity solution was then used with these parameter values to fit the whole curve and obtain the matrix porosity. Input parameters and results are the following:

- Discharge equal to the median value of 444 L/min (117.3 gpm).
- Aquifer thickness equal to the transmissive thickness of the Bullfrog-Tram interval between Boreholes c#2 and c#3 (168 ft (51.2 m)). The transmissive thickness is less than the average packed-off interval thickness because significant water production occurred over only a fraction of the total interval thickness, as previously reported in Geldon (1996 [DIRS 100396], pp. 12 to 20). This test, the 2,6 DFBA test in the lower Bullfrog interval (Section D1.1.2), and the pyridone test in the lower Bullfrog interval (Section D1.1.3) were the only tracer tests in which the aquifer thickness was assumed to be less than the total interval thickness on the basis of flow logging information.
- Peclet number of 11 to 12, which corresponds to a longitudinal dispersivity of approximately 2.5 m.
- Advection transport time of 17.75 days (calculated from peak concentration; Figure D-1).
- The flow porosity, ϕ_f , was estimated as 0.086. This porosity estimate is high if only fractures are considered as the flow pathways. Typical fracture porosities are of the order of 0.01 maximum (Freeze and Cherry 1979 [DIRS 101173], p. 408)].
- The complete curve match (Figure D-3) results in an estimate of the matrix porosity of 0.19.

The high flow porosity values above indicate that either (1) a composite flow pathway occurred for the iodide (a combination of both fractures and matrix), or (2) flow heterogeneity resulted in much longer transport times than would be expected under ideal radial convergent flow conditions in a homogeneous, isotropic medium. In the first case, the solute is hypothesized as traveling through a connected-fracture-network segment, then through a segment of matrix until it reaches the next connected-fracture-network segment. In the second case, flow to the production well is seen as being nonuniformly distributed in the flow domain, with a relatively small amount of flow coming from the direction of the injection well. The matrix porosity estimated is reasonable, based on geophysical logging conducted at the C-wells complex (Geldon 1996 [DIRS 100396], pp. 12 to 69).

The software program PEST V 5.5 (STN: 10289-5.5-00 [DIRS 161564]) was used to corroborate tracer solution results and to obtain optimal parameter values based on the iodide test results. The PEST optimization started with the visual graphical match to the breakthrough

curve presented in Figure D-3 for which $Pe = 11$, $\sigma = 2.0$, and $\gamma = 0.04$. Three PEST runs were conducted with each of these parameters changed from the above values while the others were held constant. In the first run, PEST was given $Pe = 11$, $\sigma = 1.0$ (intentionally “perturbed” from its good-visual-fit value of 2.0), and $\gamma = 0.04$; PEST was allowed to change only σ . At the end of this run, PEST converged on an optimal value of $\sigma = 1.7175$ and an associated confidence interval for σ . In the second run, PEST was given the values $Pe = 8$ (intentionally perturbed from its good-visual-match value of 11), $\sigma = 1.7175$, and $\gamma = 0.04$; PEST was allowed to change only Pe . At the end of this run, PEST converged on an optimal value of $Pe = 11.478$ and an associated confidence interval for Pe . In the third run, PEST was given the values $Pe = 11.478$, $\sigma = 1.7175$, and $\gamma = 1.0$ (intentionally perturbed from its good-visual-fit value of 0.04); PEST was allowed to change only γ . At the end of this run, PEST converged on an optimal value of $\gamma = 0.03565$ and an associated confidence interval for γ . The above optimal values, their associated confidence intervals, and the fit to the actual breakthrough curve that they produce are presented in Figure D-4.

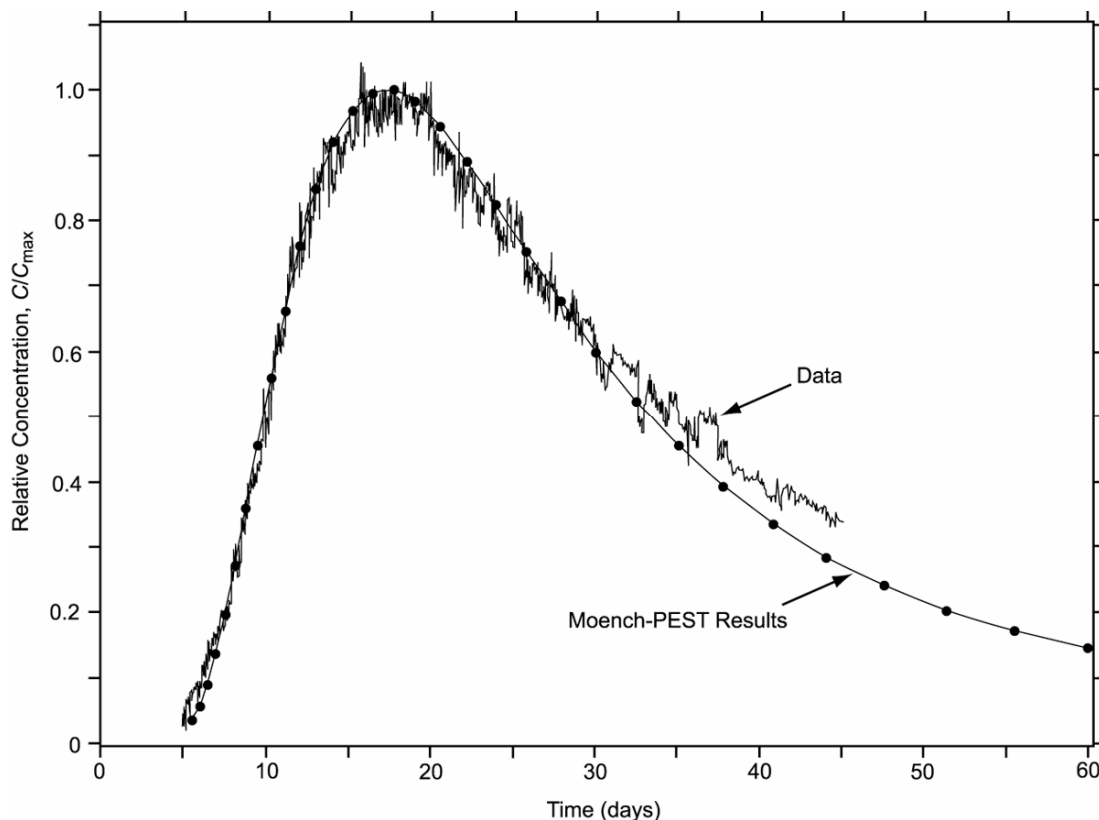


Source: DTN: GS960808312315.001 [DIRS 159235] (data).

Output DTN: GS031008312315.002 (analysis).

NOTE: Estimated parameters are Peclet number, $Pe = 11$; dispersivity, $\alpha L = 2.6$ m (8.5 ft); flow porosity, $\phi_f = 0.086$; and matrix porosity, $\phi' = 0.19$. The dots on the model fit curve have no significance. ("Model fit" refers to the match of the analytical solution to the data.)

Figure D-3. Preliminary Moench Analytical Solution Fit for Iodide Injection in UE-25 c#2



Source: DTN: GS960808312315.001 [DIRS 159235] (data).

Output DTN: GS031008312315.002 (analysis).

NOTE: The breakthrough curve was matched by the PEST V 5.5 (STN: 10289-5.5-00 [DIRS 161564]) program with initial estimates from a manual match. The optimal PEST results, with 95% confidence intervals in parentheses, are $Pe = 11.478$ (11.2276 to 11.7284), $R = 1.0$, $\sigma = 1.71746$ (1.4353 to 1.99962), and $\gamma = 0.0356464$ (0 to 0.12744), and the other estimated parameters are dispersivity $\alpha_L = 2.52$ m (8.28 ft), flow porosity $\phi = 0.087$, and matrix porosity $\phi' = 0.163$. The dots on the model fit curve have no significance.

Figure D-4. Breakthrough Curve for February 13, 1996, Iodide Tracer Test

The visual graphical match and the optimized PEST V 5.5 (STN: 10289-5.5-00 [DIRS 161564]) parameters are in good agreement. The Peclet number and dispersivity estimates vary by approximately 4%, as can be seen by comparing the values listed in the notes under Figures D-3 and D-4. The flow porosity estimates vary by less than 1%. The visual-graphical-match matrix-porosity estimate is 0.19, and the PEST estimate is 0.163.

The difference in values is attributed to the different weights assigned to fitting/matching portions of the breakthrough curve. The rising limb is used exclusively in the visual graphical match to estimate the Peclet number and the advective transport time, and then the advective transport time is used to estimate the flow porosity. The PEST V 5.5 (STN: 10289-5.5-00 [DIRS 161564]) approach uses all of the data, both rising- and falling-limb, and optimizes the fit to these data. This results in a slightly different fit than the visual graphical match. Tables D-2 and D-3 in Section D3 (summary section) list the parameter values obtained from all of the nonsorbing tracer testing described in Section D1.

D1.1.2 Difluorobenzoic Acid Tracer Test in the Lower Bullfrog Interval

On January 10, 1997, a purely convergent conservative tracer test was initiated from c#2 to c#3 in the Lower Bullfrog interval at an average rate of 568 L/min (Umari 2002 [DIRS 162858] Binder 7, Sections J-6 to J-12 and K-1 to K-9; Binder 8, Sections J-6 to J-12 and K-1 to K-9; Binder 9, Sections J-6 to J-12, K-1 to K-9, K-11 to K-12, and L-3). Approximately 11.35 kg of 2,6 DFBA mixed with 795 L (210 gal) of c#3 water were injected into the Lower Bullfrog Tuff in Borehole c#2, followed by 238 L (62.9 gal) of chase water. A total of 1,798 L (475 gal) of fluid was injected, the first portion of which was the fluid in the injection string preceding the injectate solution. The average injection rate was 31.2 L/min (8.2 gpm), with a range of 28.8 L/min to 33.0 L/min (7.6 gpm to 8.8 gpm). The average progressive-cavity pump (injection pump) pressure measured at the surface was 1.541 megapascals (MPa) (223.6 psi), with a range of 1.5 MPa to 1.6 MPa (215 psi to 230 psi). The chemical constituent used as a tracer in this test was 2,6 DFBA. Chemical analysis indicated that the 2,6 DFBA injectate solution had a concentration of 15,560 mg/L. The field-determined detection limit for DFBA was 40 µg/L. The precision of the HPLC analytical technique, as determined by comparing replicate analyses, was ±10%.

Breakthrough occurred at c#3 on January 15, 1997, 5.07 days after injection. The peak concentration occurred 13.5 days after injection. The mass recovered is estimated as 7.6 kg, which is approximately 67% of the injected mass (Fahy 1997 [DIRS 162811]).

Interpretation of Test

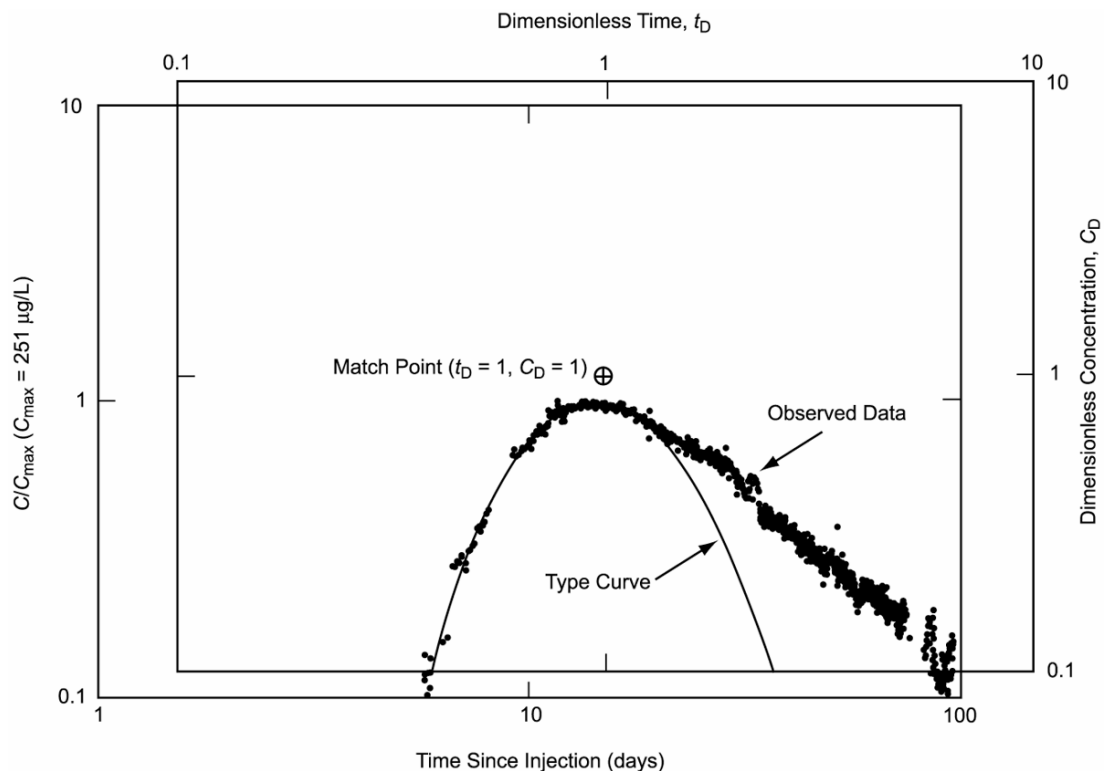
Interpretation of the DFBA test using the Moench (1995 [DIRS 148784]) dual-porosity analytical solution for radially convergent flow produced the following results.

- Discharge rate and transmissive thickness used for the analysis were 568 L/min and 51.2 m, respectively. The transmissive thickness is less than the average packed-off interval thickness because significant water production occurred over only a fraction of the total interval thickness, as previously reported by Geldon (1996 [DIRS 100396], pp. 12 to 20).
- Peclet number between 12 and 15 (Figures D-5, D-6, and D-7).
- Advection transport time between 12 and 16.5 days.
- Flow porosity between 0.072 and 0.099 (Figures D-6 and D-7).
- Matrix porosity between 0.088 and 0.132, and a longitudinal dispersivity value between 1.94 m (6.37 ft) and 2.43 m (7.96 ft): (Figures D-6 and D-7).

The range of values reflects two approaches for obtaining a curve match using a dual-porosity solution. In the first approach, the rising limb of the breakthrough curve plus the very early portion of the tail of the breakthrough curve were matched to obtain a Peclet number of 12, a flow porosity of 0.099, a matrix porosity of 0.088, and a dispersivity of 2.43 m (7.96 ft). Figures D-5 and D-6 show the resulting curve fits on plots with log–log and linear–linear axes scales,

respectively. At longer times, the data and curve fits diverge, possibly indicating secondary arrivals from longer residence time flow pathways. In the second curve-matching approach, both the rising limb and the entire tail of the breakthrough curve were considered equally in the curve-fitting process, resulting in the curve fits of Figure D-7 with corresponding parameter values of $Pe = 15.0$ (longitudinal dispersivity = 1.94 ft), $\sigma = 1.7$, and $\gamma = 0.12$ (equivalent to a flow porosity of 0.072 and a matrix porosity of 0.132). In both curve-matching approaches, the parameter estimates were obtained from visual matches to the breakthrough data.

The program PEST V 5.5 (STN: 10289-5.5-00 [DIRS 161564]) was applied to the DFBA test results by starting with the visual graphical match to the breakthrough curve presented in Figure D-7, for which $Pe = 15.0$, $\sigma = 1.7$, and $\gamma = 0.12$.



Source: DTN: GS010508312315.001 [DIRS 155860] (data).

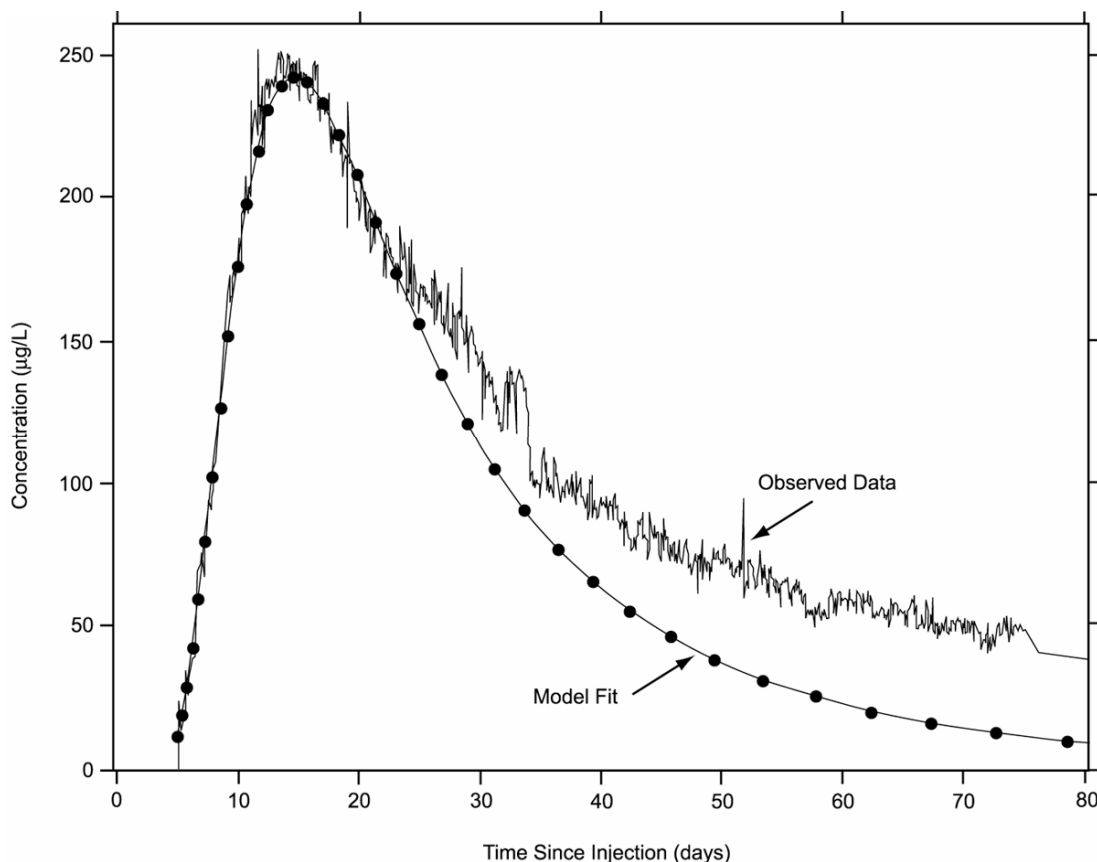
Output DTN: GS031008312315.002 (analysis).

NOTE: The Peclet number $Pe = 12$. Only the rising limb of the observed data was fit because the falling limb could be the result of secondary arrivals.

Figure D-5. Type Curve Fit for 2,6 DFBA Injection in UE-25 c#2

The latter set of parameter values were then used as initial guesses in three PEST V 5.5 (STN: 10289-5.5-00 [DIRS 161564]) runs, each conducted with one of the three parameters (Pe , σ , and γ) changed from the above values while the other parameters were held constant. In the first run, PEST was given $Pe = 15$, $\sigma = 3.0$ (intentionally “perturbed” from its good-visual-fit value of 1.7), and $\gamma = 0.12$; PEST was allowed to change only σ . At the end of this run, PEST converged on an optimal value of $\sigma = 1.8776$ and an associated

confidence interval for sigma. In the second run, PEST was given the values $Pe = 8$ (intentionally “perturbed” from its good-visual-fit value of 15.0), $\sigma = 1.8776$, and $\gamma = 0.12$; PEST was allowed to change only Pe . At the end of this run, PEST converged on an optimal value of $Pe = 15.8$ and an associated confidence interval for Pe . In the third run, PEST was given the values $Pe = 15.8$, $\sigma = 1.8776$, and $\gamma = 1.0$ (intentionally perturbed from its good-visual-fit value of 0.12); PEST was allowed to change only γ . At the end of this run, PEST converged on an optimal value of $\gamma = 0.11793$ and an associated confidence interval for γ . The above optimal values, their associated confidence intervals, and the fit to the actual breakthrough curve that they produce are presented in Figure D-8.



Source: DTN: GS010508312315.001 [DIRS 155860] (data).

Output DTN: GS031008312315.002 (analysis).

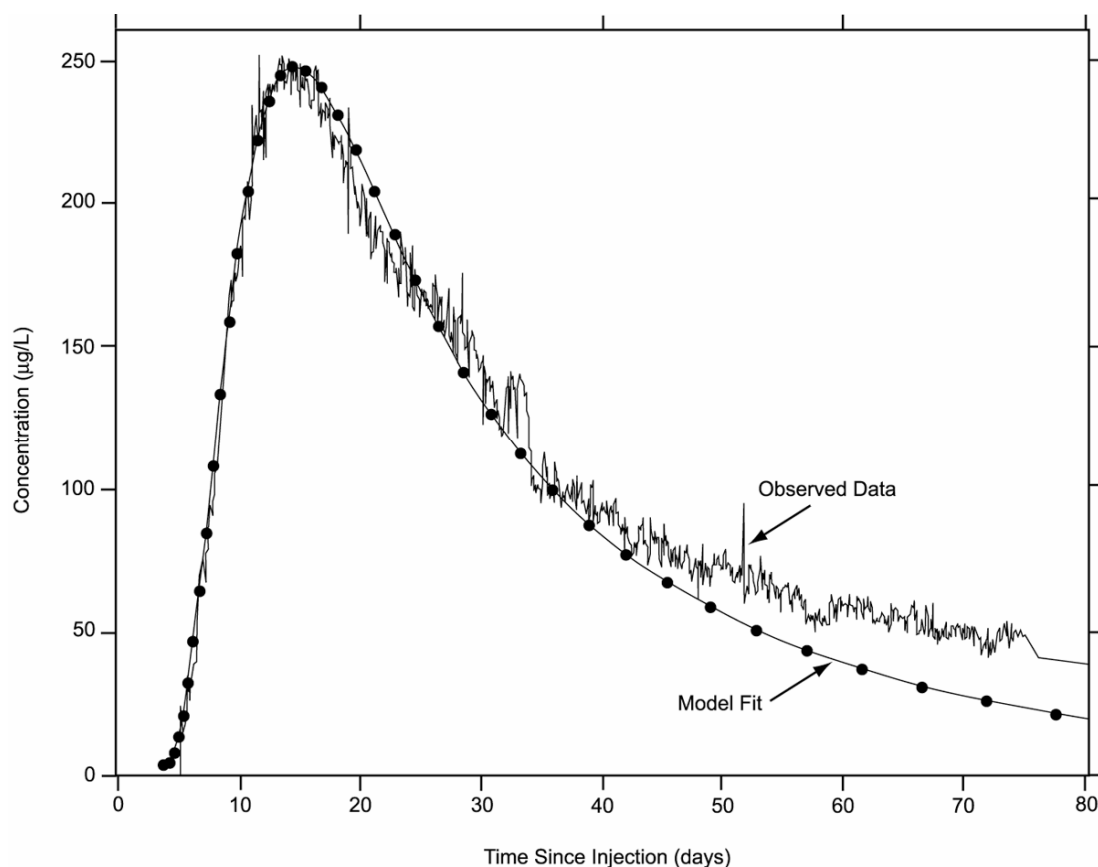
NOTE: The fit 1 estimated parameters are Peclet number $Pe = 12$, dispersivity $\alpha_L = 2.4$ m (7.96 ft), flow porosity $\phi_f = 0.099$, and matrix porosity $\phi = 0.088$. Only the rising limb of the observed data was fit because the falling limb could be the result of secondary arrivals. The dots on the model fit curve have no significance. (“Model fit” refers to the match of the analytical solution to the data.)

Figure D-6. Fit 1 Preliminary Moench Analytical Solution for 2,6 DFBA Injection in UE-25 c#2

The visual-graphical match and the optimized PEST V 5.5 (STN: 10289-5.5-00 [DIRS 161564]) parameters are in good agreement. The Peclet number and dispersivity estimates vary by approximately 5%, as can be seen by comparing the values listed in the notes under Figures D-7 and D-8. The flow porosity estimates are identical. The visual-graphical-match matrix porosity estimate is 0.132, and the PEST estimate is 0.146.

D1.1.3 Pyridone Tracer Test in the Lower Bullfrog Interval from c#1 to c#3

On January 9, 1997, approximately 3.018 kg of 3-carbamoyl-2-pyridone (pyridone), mixed with 795 L (210 gal) of Borehole c#3 water, was injected into Borehole c#1, followed by 252 L (66.6 gal) of chase water to test the Lower Bullfrog interval (Umari 2002 [DIRS 162858], Binder 7, Sections J-6 to J-12 and K-1 to K-9; Binder 8, Sections J-6 to J-12, and K-1 to K-9; Binder 9, Sections J-6 to J-12, K-1 to K-9, K-11 to K-12, and L-3). This injection was made while c#3 was being pumped at an average rate of 572 L/min (151.1 gpm).



Source: DTN: GS010508312315.001 [DIRS 155860] (data).

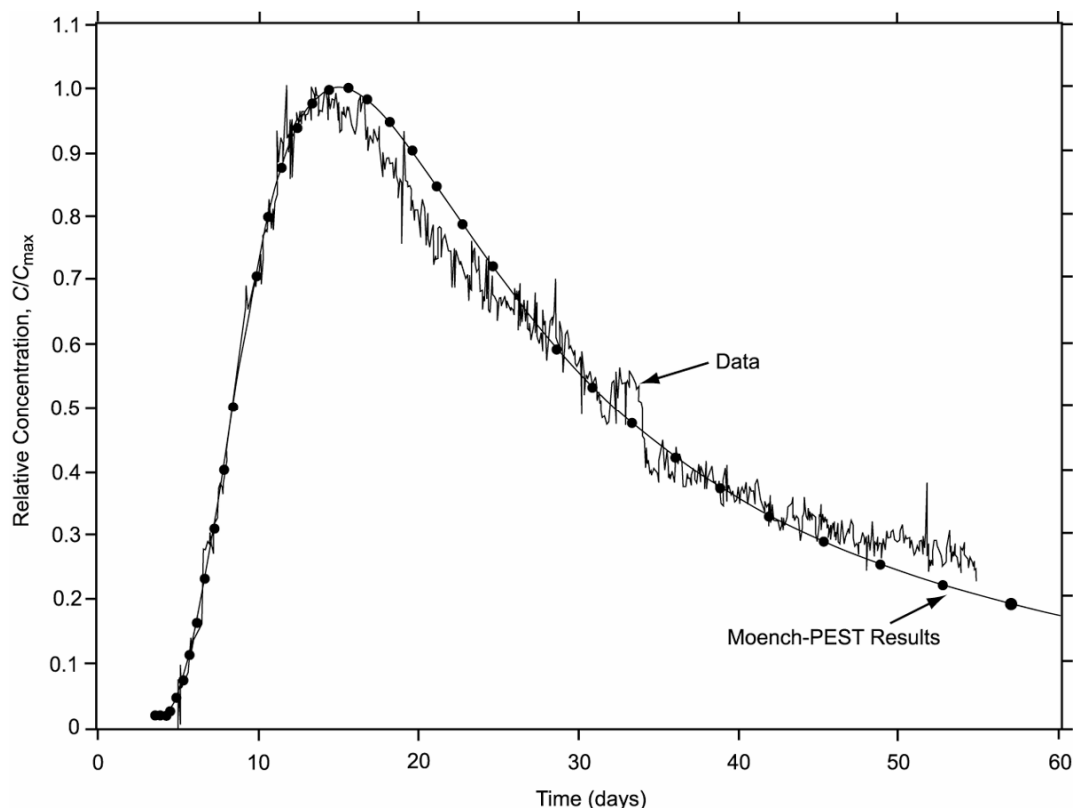
Output DTN: GS031008312315.002 (analysis).

NOTE: The fit 2 estimated parameters are Peclet number $Pe = 15$, dispersivity $\alpha_L = 1.9$ m (6.37 ft), flow porosity $\phi_f = 0.072$, and matrix porosity $\phi = 0.132$. The dots on the model fit curve have no significance. ("Model fit" refers to the match of the analytical solution to the data.)

Figure D-7. Fit 2 Preliminary Moench Analytical Solution for 2,6 DFBA Injection in UE-25 c#2

A total of 2,082 L (550 gal) of fluid were injected, the first portion of which was the fluid in the injection string preceding the injectate solution. The average injection rate was 22.8 L/min (6.1 gpm), with a range of 16.8 L/min to 37.2 L/min (4.4 gpm to 9.8 gpm). The average progressive-cavity pump (injection pump) pressure, measured at the surface, was 1.743 MPa (252.8 psi), with a range of 0.3 MPa to 2 MPa (50 psi to 300 psi). Chemical analysis indicated that the pyridone injectate solution had an average concentration of 2,998 mg/L (2,998,000 µg/L). The field-determined detection limit for pyridone was 0.1 µg/L. The

precision of the HPLC/fluorometry analytical technique, as determined by comparing replicate analyses, was $\pm 10\%$.



Source: DTN: GS010508312315.001 [DIRS 155860] (data).

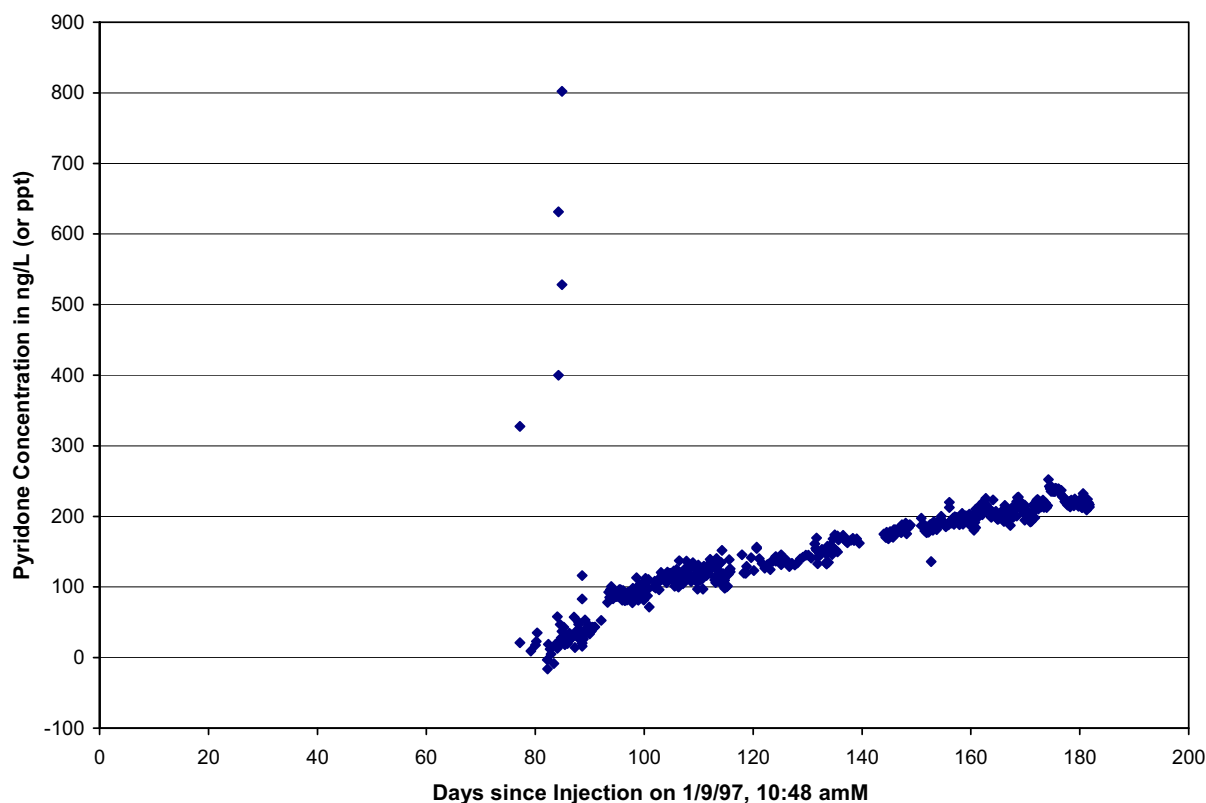
Output DTN: GS031008312315.002 (analysis).

NOTE: The breakthrough curve was matched by the PEST V 5.5 (STN: 10289-5.5-00 [DIRS 161564]) program with initial estimates from a manual match. The optimal PEST results, with 95% confidence intervals in parentheses, are $Pe = 15.7954$ (15.4998 to 16.091), $R = 1.0$, $\sigma = 1.87763$ (1.65457 to 2.10068), and $\gamma = 0.117934$ (0.01741397 to 0.218454), and the other estimated parameters are dispersivity $\alpha_L = 1.83$ m (6.01 ft), flow porosity $\phi_f = 0.072$, and matrix porosity $\phi = 0.146$. The dots on the Moench-PEST results curve have no significance.

Figure D-8. Breakthrough Curve for January 10, 1997, DFBA Tracer Test

Breakthrough at c#3 occurred on March 27, 1997, 77 days after injection (Figure D-9). The concentration of pyridone continued to increase, but at a gradually-decreasing rate until the end of the test (the test was terminated on November 12, 1997, before a clear peak was observed). Except for isolated very high concentrations at the time of breakthrough, the maximum concentration of Pyridone reached was $0.252 \mu\text{g/L}$ (parts per billion [ppb]), or 252 ng/L (ppt) as of July 10, 1997, which was determined by laboratory analyses with detection limits lower than $0.1 \mu\text{g/L}$. Because the pyridone test was terminated before a peak concentration was reached, no quantitative interpretation of the test was attempted.

The precision of the pyridone concentration measurements vary. For concentrations less than 100 ng/L , errors exceeded $\pm 10\%$, based on replicate sample analyses. For concentrations of pyridone greater than 100 ng/L , replicate errors were less than or equal to $\pm 10\%$.



Source: DTN: GS010508312315.001 [DIRS 155860].

NOTE: Pyridone concentrations continued to increase for another 124 days beyond the last data point shown on this plot (until November 12, 1997), but the data beyond July 10, 1997 do not appear in the above DTN and are unqualified.

Figure D-9. Breakthrough Curve for Pyridone Injection in UE-25 c#1

D1.1.4 PFBA and Iodide Tracer Tests in the Lower Bullfrog Interval

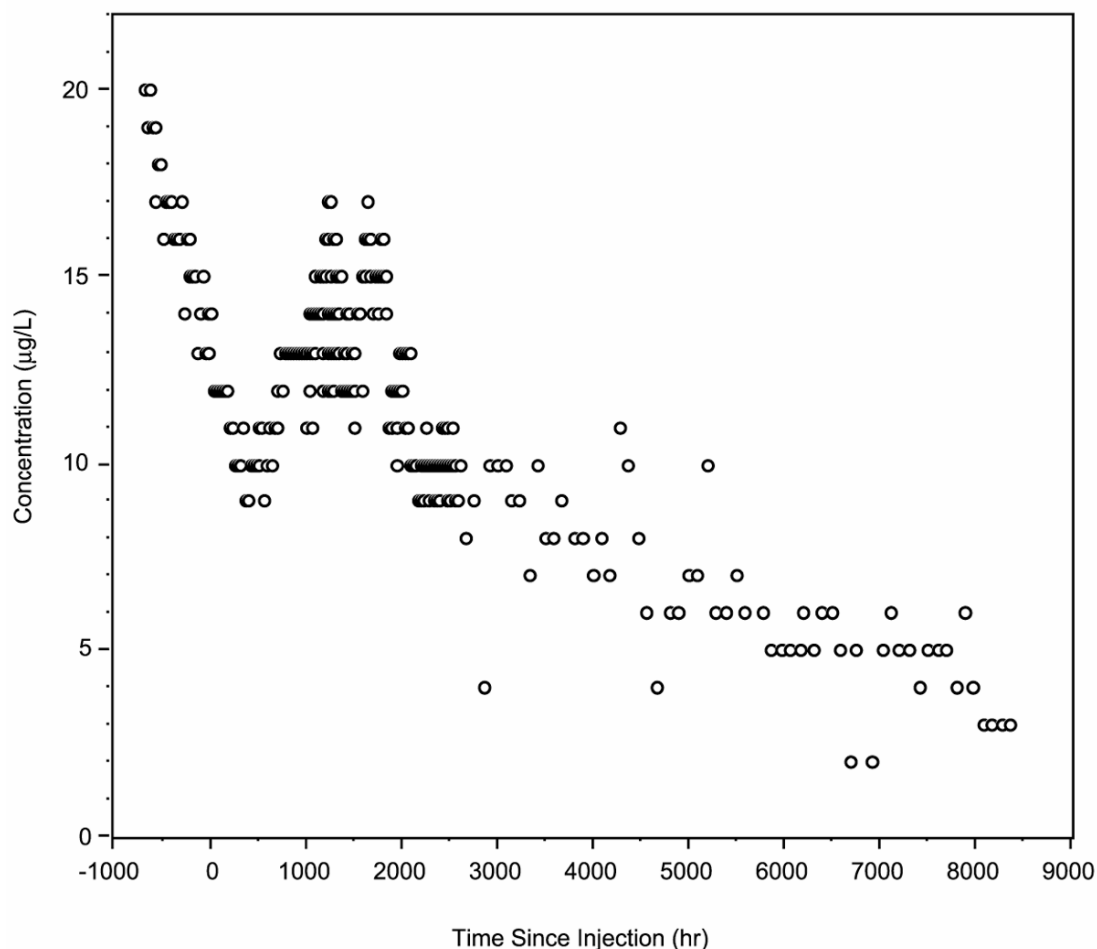
In cooperation with the U.S. Geological Survey, Los Alamos National Laboratory conducted two “pilot” tracer tests, each involving the injection of a single nonsorbing tracer in the Lower Bullfrog interval during 1996. These tests were conducted primarily to determine which well, c#1 or c#2, would serve as a better injection well for the planned multiple-tracer test. The primary motivation was the concern that the responses of both sorbing and colloid tracers might be highly attenuated or excessively delayed relative to nonsorbing tracers, which could make test durations impractically long. Thus, it was desirable to determine which potential injection well yielded the quickest and highest-concentration responses at the production well, c#3. It was not taken for granted that the best response would be from c#2, the injection well closest to c#3, because c#1 and c#3 are more closely aligned with the predominant fracture strike direction at the C-wells than c#2 and c#3.

The first pilot tracer test involved the injection of approximately 10 kg of PFBA into the lower Bullfrog interval in well c#2 on May 15, 1996. This same interval in c#3 was pumped continuously at about 575 L/min throughout the test (starting on May 8, 1996, prior to tracer

injection). The PFBA was dissolved in approximately 1,000 L of groundwater from c#3. The test was conducted under partial recirculation conditions with about 20 L/min of the water produced from c#3 (approximately 3.5% of production rate) being continuously reinjected into c#2. The recirculation was initiated approximately 24 hr before tracer injection to establish a steady flow field, and it was continued for 23 days after injection. The tracer solution was plumbed into the recirculation loop such that there were no flow interruptions during injection. Information pertaining to the PFBA pilot test is documented by Reimus (2000 [DIRS 165126]).

The second pilot test involved the injection of about 12.7 kg of iodide (approximately 15 kg of sodium iodide dissolved in approximately 1,000 L of groundwater from c#3) into the Lower Bullfrog interval in c#1. It was conducted in a manner very similar to the PFBA pilot test and was initiated on June 18, 1996. The recirculation rate in this test was about 15 L/min (approximately 2.6% of production rate), and recirculation continued for approximately 16 days after injection. Production from c#3 was maintained at approximately 575 L/min throughout the test, the same as that of the PFBA pilot test. Information pertaining to the iodide pilot test is documented by Reimus (2000 [DIRS 165127]).

It was clear a few days after the injection of iodide into c#1 that the PFBA response from c#2 was much more conducive to multiple-tracer testing than the iodide response from c#1. The results of the PFBA test are relevant to the interpretation of the multiple-tracer test conducted in the Lower Bullfrog interval, so they are discussed in Section D4 of this report along with the results of the multiple-tracer test. The iodide response between c#1 and c#3 is shown in Figure D-10. This response is complicated by the initially high and gradually declining iodide background concentrations, which are attributed to the residual iodide in the aquifer from the February 13, 1996, injection of iodide into the Bullfrog-Tram interval in c#2. However, there is clear evidence of a peak occurring about 2 months after injection. The estimated iodide recovery from the c#1 injection by October 1, 1996, (after correcting for the declining background by assuming that it followed an exponential decay) was approximately 13% of the injected iodide mass (DTN: LA0410PR831231.001 [DIRS 171899]). In contrast, the PFBA recovery from c#2 was about 72% on October 1, 1996 (DTN: LA0410PR831231.001 [DIRS 171899]). Neither the PFBA nor the iodide pilot tracer tests were interpreted quantitatively.



Source: DTN: LA0007PR831231.001 [DIRS 156043] (data).

NOTE: The breakthrough curve is a result of injection of approximately 12.7 kg of iodide into c#1 on June 18, 1996; the declining background prior to and immediately after injection is due to recovery of iodide from a February 1996 iodide injection into c#2; and the estimated recovery from c#1 accounting c#2 background was approximately 13% through June 1, 1997.

Figure D-10. Breakthrough Curve for Iodide Injection in UE-25 c#1

D1.2 RESULTS AND INTERPRETATIONS OF NONSORBING TRACER TESTS: PROW PASS FORMATION

D1.2.1 2,4,5 Trifluorobenzoic Acid and Iodide Test from c#3 to c#2

On June 17, 1998, a partial-recirculation nonsorbing tracer test was initiated from c#3 to c#2 by injecting approximately 14.83 kg of 2,4,5 trifluorobenzoic acid (TFBA) and 12.26 kg of iodide (in the form of sodium iodide) into the Prow Pass interval of c#3 while c#2 was pumped at the rate of approximately 5.2 gpm (19.7 L/min). The concentration of 2,4,5 TFBA was 14,239 ppm in the injected slug, and that of iodide 14,307 ppm. Of the 5.2 gpm (19.7 L/min) pumped from c#2, 1.5 gpm (5.7 L/min) was continuously reinjected into the Prow Pass interval of c#3 (Umari 2002 [DIRS 162858], Binder 13, Sections M-29 to M-36; Binder 14, Sections M-29 to M-36, M-40, M-43 to M-44).

Approximately 40 hours after the injection, breakthrough of both tracers occurred in c#2. The peak for the 2,4,5 TFBA occurred 6.74 days after injection, and the peak for iodide at 7 days after injection (Figure D-11).

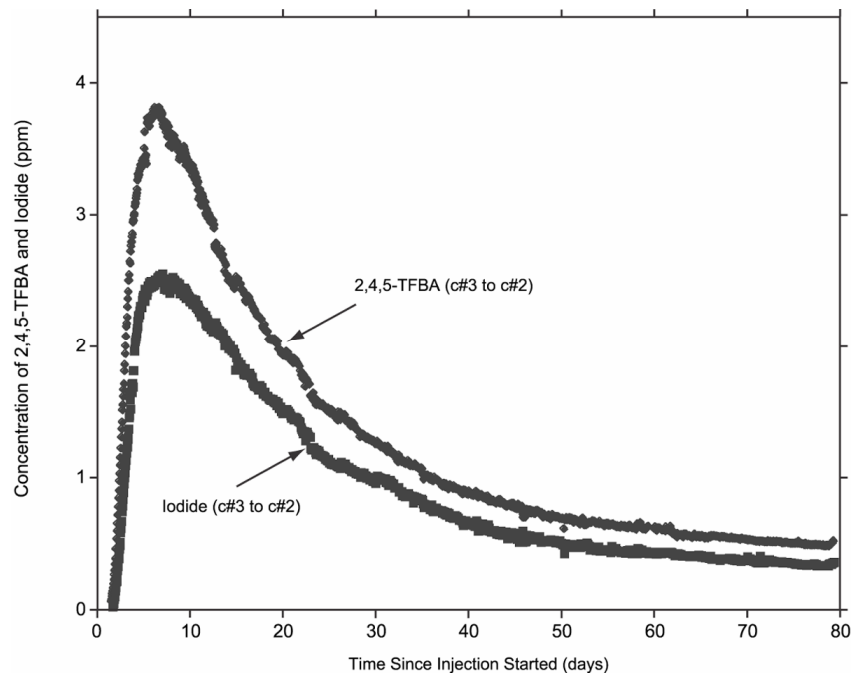
The iodide and 2,4,5 TFBA breakthrough curves were analyzed using the single- and dual-porosity analytical solutions of the advection-dispersion equation as given in Moench (1989 [DIRS 101146]; 1995 [DIRS 148784]). These solutions were used, as is, for a hypothetical purely convergent flow field, and they were also lagged and superposed to obtain the solution for the actual partial-recirculation flow field (Section D1.2.1.2). The curves were first analyzed assuming Moench's single-porosity solution for both the convergent and the partially recirculating flow-field assumptions, using the entire curves for the matches to obtain the flow porosity and longitudinal dispersivity. In this case, the aquifer is considered to be an equivalent porous medium made up of a network of fractures, some of them continuous, and some potentially discontinuous with connecting segments of matrix (Fahy 1997 [DIRS 137456], fourth and fifth {unnumbered} pages). The porosity of this network of fractures and connecting segments of matrix, through which flow of solutes occurs, is referred to herein as "flow porosity" (Fahy 1997 [DIRS 137456], fourth and fifth {unnumbered} pages). The curves were then analyzed assuming a dual-porosity system, also using the entire curves for the match. In addition to the above network of fractures and connecting segments of matrix, the dual-porosity medium is conceptualized as having a storage component consisting of dead-end fractures and the part of the matrix not contributing to the flow network.

The flow porosity and longitudinal dispersivity are different for each of the solutions presented. The retardation coefficient used for all solutions was 1.0, assuming that iodide and 2,4,5 TFBA are considered nonsorbing with respect to the Prow Pass Tuff. All of the solutions used the following input parameters:

- Production rate of 19.7 L/min (5.2 gpm; represents the average rate for the test).
- Aquifer thickness of 61 m (200 ft, packed-off interval, rounded to one significant figure) (Umari 2002 [DIRS 162858], Binder 10, Section L-11, pp. 70 to 71, Section L-9, pp. 57 to 58). In this case, the entire interval thickness was assumed to be transmissive despite the fact that earlier hydraulic tests (in 1995 and 1996 – Table C-7) had indicated that only a portion of the interval may be significantly transmissive. The earlier hydraulic tests were considered to have significant uncertainty because the Prow Pass interval was never isolated for hydraulic testing as it was for tracer testing in 1998 and 1999.
- Distance between injection and production wells of 29 m (95.15 ft) (Table A-6).
- Radii of injection and production wells of 13.97 cm (5.5 in.) (assumed for rugose, variable-diameter open-hole portion of C-wells where all testing was conducted, based on C-wells caliper logs (Geldon 1993 [DIRS 101045], p. 10).
- Borehole mixing length of 30.5 m (100 ft; assumed, as discussed below).
- Recirculation rate of 5.7 L/min (for the partially recirculation solution).

D1.2.1.1 Single-Porosity, Purely Convergent Interpretation

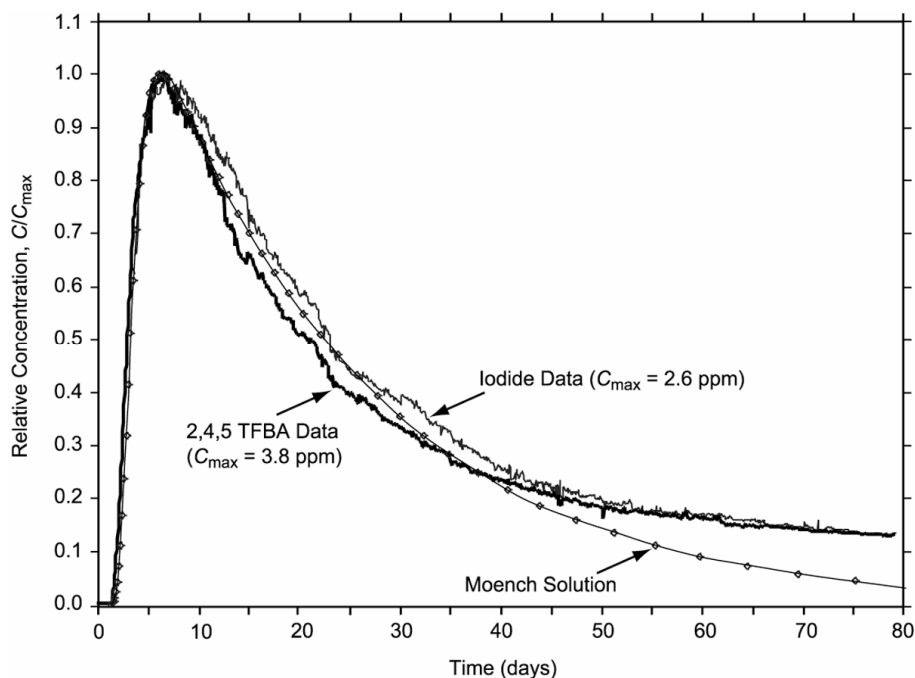
The single-porosity, purely convergent solution is obtained directly from the Moench (1989 [DIRS 101146]) solution to the advection-dispersion equation. A best visually matching single-porosity solution corresponding to flow porosity and longitudinal dispersivity values of 0.0007 and 1.45 m, respectively, is presented in Figure D-12, along with the iodide and 2,4,5 TFBA breakthrough curves. All breakthrough curves, such as the ones in Figure D-12, were normalized by dividing the measured concentrations by the maximum concentration, C_{\max} , rather than by the concentration of the injected mass slug, C_0 . Longitudinal dispersivity is a measure of the media's ability to disperse a solute along streamlines. Transverse dispersivity, which represents the media's ability to disperse a solute in a direction perpendicular to streamlines, is not obtainable from this analysis method and flow geometry. The longitudinal dispersivity of 1.45 m and the 29-m flow length correspond to a Peclet number of 20. Only one curve fit is shown in Figure D-12 because a single-porosity solution is capable of simulating only a single breakthrough curve for tracers with different diffusion coefficients.



Source: DTN: GS990208312315.001 [DIRS 159238] (data).

NOTE: C#2 and C#3 refer to UE-25 c#2 and UE-25 c#3, respectively.

Figure D-11. Breakthrough Curves for 2,4,5 TFBA and Iodide Tracer Test from UE-25 c#3 to UE-25 c#2



Source: DTN: GS990208312315.001 [DIRS 159238] (data).

Output DTN: GS031008312315.002 (analysis).

NOTE: Flow porosity = 0.0007, storage porosity was not applicable because a single-porosity medium was assumed, and longitudinal dispersivity = 1.45 m. The dots on the Moench solution curve have no significance.

Figure D-12. Breakthrough Curve for June 17, 1998, 2,4,5 TFBA and Iodide Tracer Test Matched by the Single-Porosity, Purely Convergent Moench Solution

The matched values of longitudinal dispersivity and flow porosity may be sensitive to the mixing lengths assumed for the injection and pumped wells. The mixing lengths represent those lengths within the boreholes through which the tracer enters or exits the aquifer. The 30.5-m mixing length assumed for all solutions is based on the thickness of the transmissive interval within the packed-off Prow Pass interval in c#3 (Table C-6), and is consistent with the hydrogeology of the interval (Geldon 1996 [DIRS 100396], pp. 9 to 69).

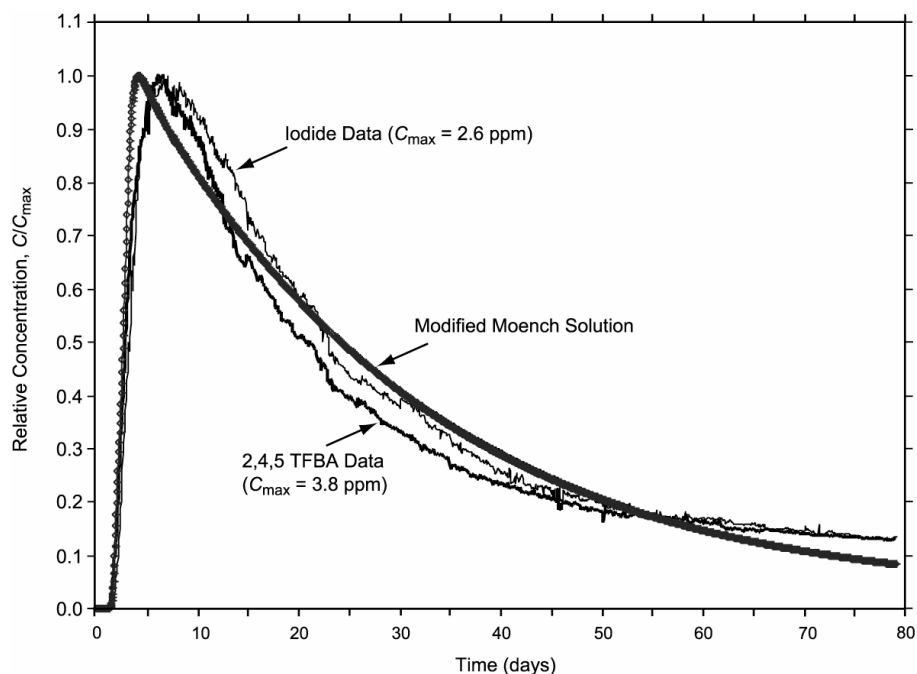
The residence time of the tracer slug within the borehole is directly proportional to the mixing length. Data collected during the tracer injection indicate that the borehole was flushed in 8.5 hrs (the concentration in the injected interval was measured in the field and found to rise from below detection limit to 2,721 ppm and then back to below detection limit in 8.5 hrs, 8:00 A.M. to 4:30 P.M.) (Umari 2002 [DIRS 162858], Binder 13, p. 91). When the mixing length is reduced to 0.3 m and only the rising limb of the actual breakthrough curve is matched to the theoretical breakthrough curve from the single-porosity solution of Moench (1989 [DIRS 101146], assuming minimal diffusion during the rising limb), a longitudinal dispersivity value of 4.27 m and a flow porosity value of 0.0016 are obtained as fitting parameters. Changing the mixing length from 30.5 m to 0.3 m constitutes a two-orders-of-magnitude change in this parameter. Corresponding to this change in the assumed mixing length, the estimates of longitudinal dispersivity and flow porosity change from 1.45 m and 0.0007 (for a 30.5-m mixing length) to 4.3 m and 0.0016 (for a 0.3-m mixing length). This is a three-fold change of longitudinal

dispersivity and a two-fold change of flow porosity, both less than one order of magnitude. The estimated parameters, therefore, are not very sensitive to the mixing length.

The above porosity value of 0.0007 is in the range of 0.00001 to 0.01 cited in the literature to represent fracture porosity (see, for example, Freeze and Cherry 1979 [DIRS 101173], p. 408). This implies that the flow network for this test in the Prow Pass Tuff is composed predominantly of fractures.

D1.2.1.2 Single-Porosity, Partially Recirculating Interpretation

When the purely convergent flow field of Figure D-12 is replaced by a partially recirculating flow field, the resulting solution to the advection-dispersion equation changes from the curve labeled “Moench solution” in Figure D-12 to the curve labeled “Modified Moench solution” shown in Figure D-13. The difference between the two solutions reflects the difference in flow field representation and in the fitted values of longitudinal dispersivity and flow porosity used (or implied) for each solution. Two elements of partial recirculation are represented in the partial-recirculation solution, which is obtained using the RECIRC.vi V 1.0 code (STN: 10673-1.0-00 [DIRS 164432]). Rather than straight converging rays into the production well, the partially recirculating flow field streamlines within the capture zone of the production well emanate from the injection well and curve towards the production well (Figure D-14a). The streamlines shown in Figure D-14a are lines of equal stream function values, in which the stream function of the partial-recirculation field is calculated as the sum of the stream functions of a 19.8 L/min sink (production rate) and a 5.7 L/min source (recirculation rate) in a confined aquifer of constant thickness (two-dimensional flow). The volume of rock between pairs of these curved streamlines emanating from the injection well and curving towards the production well constitute distinct pathways for the solute (tracer) to take from the injection to the production well. Three such inter-streamline pathways emanating from the injection well and curving towards the production well (Figure D-14a) are assumed for the partial-recirculation analysis in this section. These pathways, labeled Interstreamline pathway 1, 2, and 3 in Figure D-14a, and the three nonlabeled pathways, which are mirror images of them around the horizontal line of symmetry, carry all of the tracer mass from injection to production well. Symmetry allows that the analysis be restricted to only three of the six interstreamline pathways emanating from the injection well and curving towards the production well, namely Interstreamline pathway 1, 2, and 3, and that half of the mass of the tracer and half of the reinjection flow rate be carried by these three pathways. The Moench (1989 [DIRS 101146]) single-porosity, purely convergent solution is viewed as the solution of the advection-dispersion equation along a single straight pathway (Figure D-14b). This solution for a particular longitudinal dispersivity value and flow porosity is applied to each of the above three distinct pathways. Because the Moench solution is for a strictly convergent flow field, its application to the first-diverging-then-converging flow pattern within Interstreamline pathway 1, 2, and 3 in Figure D-14a is an approximation and will introduce some error. A proper delay factor (the advective transport time calculated from the volume of rock of each pathway, the flow rate within the pathway, and the assumed porosity) is used to account for the differences in lengths, or swept volumes, of these pathways relative to the straight purely convergent pathway, and the injected mass is distributed among the three pathways in proportion to the flow in each of them.



Source: DTN: GS990208312315.001 [DIRS 159238] (data).

Output DTN: GS031008312315.002 (analysis).

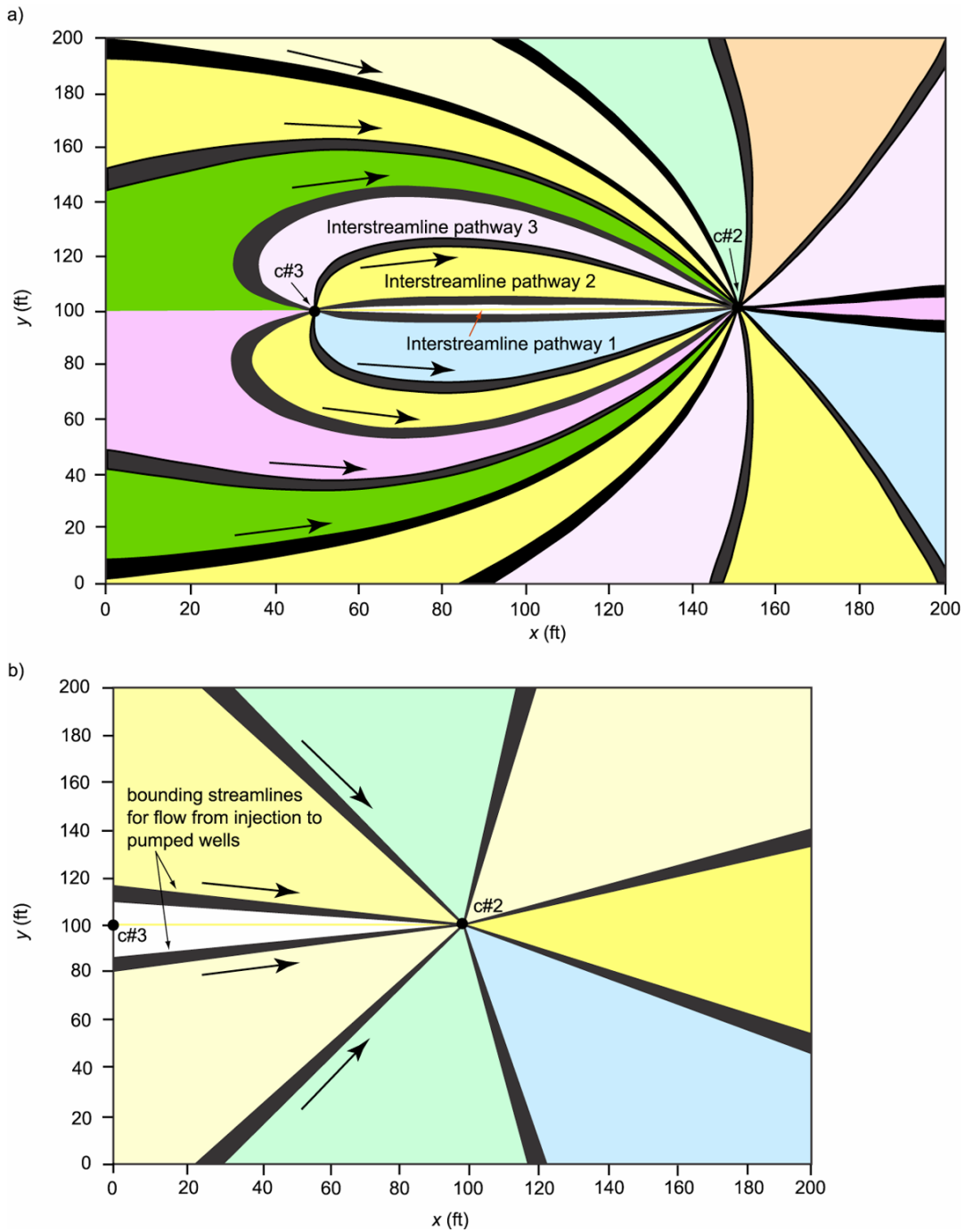
NOTE: Three inter-streamline pathways were assumed with delay factors of 2.01 days, 2.99 days, and 3.11 days. The flow porosity = 0.00045, storage porosity was not applicable because a single-porosity solution was assumed, and longitudinal dispersivity = 0.27 m ($Pe = 107$). Borehole mixing length was 30.5 m.

Figure D-13. Breakthrough Curve for June 17, 1998, 2,4,5 TFBA and Iodide Tracer Test Matched by the Single-Porosity, Partial-Recirculation Solution Derived from Moench

The solutions from Moench (1989 [DIRS 101146]) for a particular longitudinal dispersivity value, flow porosity, and an instantaneous-slug injection are then superimposed with appropriate delay factors (defined above) to obtain what is considered to be the system's unit response function. The summed curve represents what is seen at the pumped well in response to an instantaneous input function at the injection well in a partial-recirculation flow field.

The second element of partial recirculation is that the reinjected water contains a small amount of tracer; therefore, the tracer is continuously reintroduced into the aquifer. For the calculations presented here, it was assumed that this lag duration is approximately 1 hr, which was the estimated time for travel of the recirculated fluid in the 2.5-cm (1-in) coil-tubing return line (YMP 1998 [DIRS 104211], Attachment 5, p. 2) from the production well, c#2, to the injection well, c#3 (536 m [1,760 ft] at 5.7 L/min [1.5 gpm]) (Umari 2002 [DIRS 162858], Binder 10, 57th page of binder – pages are not numbered sequentially). The input concentration curve at the injection well is, therefore, constructed by starting with the breakthrough curve at the pumped (or extraction) well and then lagging it by the “lag duration.” The input concentration curve at the injection well is then convolved (Levenspiel 1972 [DIRS 156839], Chapter 9) with the unit response function to produce the calculated partial-recirculation breakthrough curve at the production well. Different flow porosity and longitudinal dispersivity values are used in a trial and error process to iteratively repeat the process described above until the calculated

partial-recirculation breakthrough curve is as visually close as possible to the measured breakthrough curve.



NOTE: Figures generated using RECIRC.vi (V. 1.0, STN: 10673-1.0-00 [DIRS 164432]). English units are shown in the figure because the analysis was conducted in English units.

Figure D-14. Streamlines for (a) Partial-Recirculation Flow Field and (b) Purely Convergent Flow Field

Using the iterative parameter-matching process described above, a longitudinal dispersivity of 0.27 m ($Pe = 107.4$) and a flow porosity of 0.00045 were selected as optimal for the single-porosity, partial-recirculation case (as opposed to the 1.45 m and 0.0007 optimal values found earlier for the single-porosity, purely convergent solution). These parameters result in the calculated partial-recirculation breakthrough curve presented in Figure D-13.

The delay factors for the three inter-streamline pathways inherent in the calculation of the breakthrough curve of Figure D-13 were initially assumed to be 1.83 days for the first pathway, 3.5 days for the second, and 7.5 days for the third (these are the advective transport times calculated from the volume of rock of each pathway, the assumed porosity, and the flow rate within the pathway).

However, use of these delay factors (as defined above) produced a calculated breakthrough curve that did not visually match the actual curve. The visual match was substantially improved by changing the delay factors to 2.01 days, 2.99 days, and 3.11 days, which resulted in the calculated breakthrough curve of Figure D-13. Because these three delay factors are not the ones indicated by the volumes of rock calculated for the three inter-streamline pathways, they are interpreted to represent the uncertainty in either the single-flow porosity value or in the assumed streamline pattern and resulting rock volumes. If the streamline pattern with associated rock volumes is assumed correct, then the delay factors of 2.01, 2.99, and 3.11 days correspond to storage porosities of 0.0005, 0.0004, and 0.0002 for the three inter-streamline pathways, respectively. However, because different porosities for the three pathways are not compatible with the underlying homogeneity assumption, the three porosities are taken to provide a range of uncertainty for the single-porosity estimate of 0.00045 used for all partial recirculation cases.

The results shown in Figures D-12 and D-13 indicate that if the breakthrough curves of 2,4,5 TFBA and iodide are analyzed as if they result from a purely convergent flow field, ignoring that the real flow field is partially recirculating, some error in the derived parameters results. A longitudinal dispersivity of 1.45 m is obtained when purely convergent conditions are assumed, five times the 0.27 m obtained when the partial-recirculation flow field is recognized. The flow porosity of 0.0007 obtained for purely convergent conditions is 56% higher than the flow porosity of 0.00045 obtained for partial recirculation.

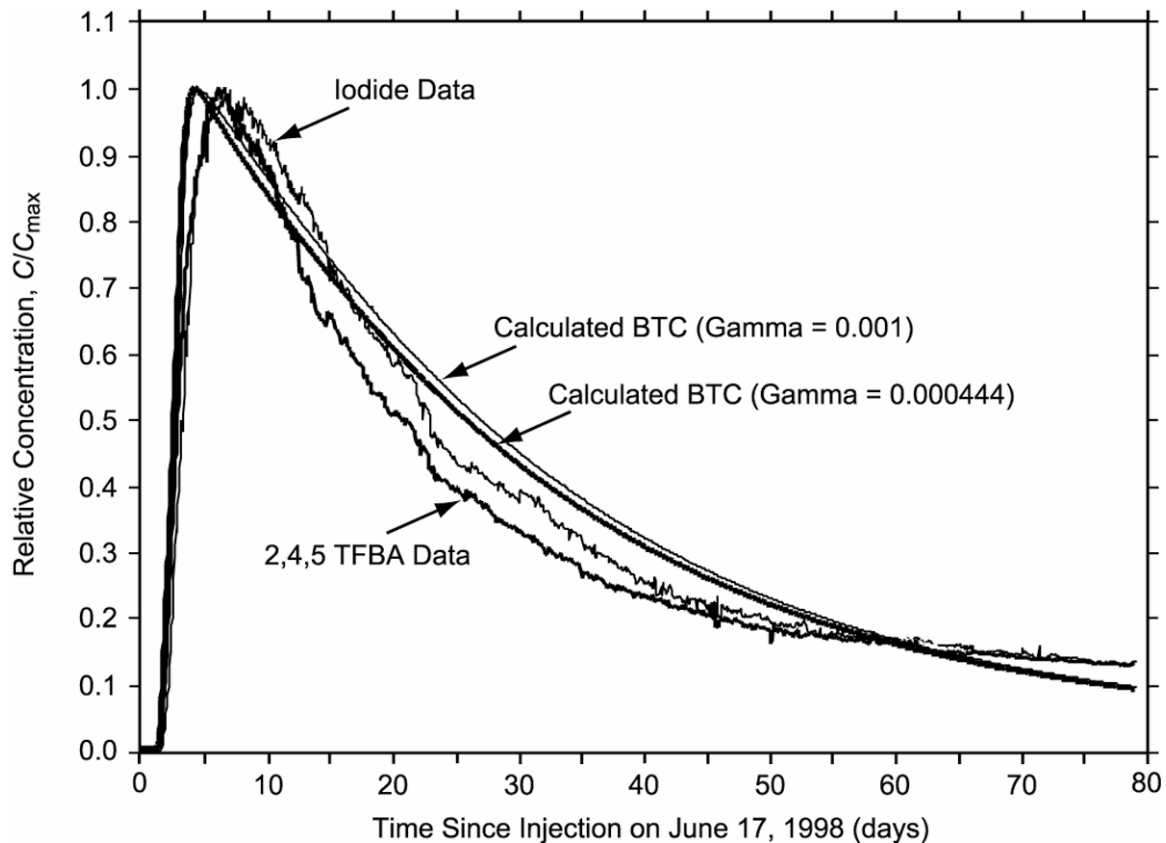
The partial-recirculation solution shown in Figure D-13, and others in the remainder of Section D1.2 are not as good fits to the actual tracer breakthrough curves as the purely convergent solution of Figure D-12, even though the latter ignores the flow field created by partial recirculation. This could either mean that the explicit representation of the partial-recirculation flow field is not important and that the test can be analyzed successfully as a purely convergent tracer test, or that the homogeneous and isotropic representation of the partial-recirculation flow field presented here does not capture the real partial-recirculation flow field. Perhaps increasing the number of the inter-streamline pathways beyond three to, in effect, “discretize” the flow field more finely would improve the fits. This increased discretization was not attempted.

D1.2.1.3 Dual-Porosity, Partially Recirculating Interpretation

In the dual-porosity case, the medium is comprised of flow and storage components. The flow component is conceptualized as a flow network of (1) continuous fractures and (2) discontinuous fractures with interconnecting segments of matrix. The porosity of the flow component of the medium is referred to as the “flow porosity.” The storage component is assumed to consist of dead-end fractures and the part of the matrix not contributing to the flow network. The porosity of the storage component of the medium is referred to as the “storage porosity” (within Appendix B of this report, “matrix porosity” means the same thing as “storage porosity”). The flow network is represented by a longitudinal dispersivity and a flow porosity, and the storage component is represented by a storage porosity and a dimensionless matrix diffusion coefficient.

The calculated dual-porosity, partial recirculation solution is predicated upon the single-porosity, partial-recirculation solution presented earlier, i.e., a longitudinal dispersivity of 0.27 m and a flow porosity of 0.00045. Two calculated breakthrough curves obtained for a storage porosity of 0.001 and two dimensionless matrix diffusion coefficients (γ), namely 0.000444 and 0.001, are presented in Figure D-15 along with the actual breakthrough curves of 2,4,5 TFBA and iodide.

The free-water molecular diffusion coefficients of 2,4,5 TFBA and iodide are 8.0×10^{-6} cm²/s and 18.0×10^{-6} cm²/s, respectively (Bowman 1984 [DIRS 156645], Table 2; Skagius and Neretnieks 1986 [DIRS 156862], Tables 2 and 3), which corresponds to a ratio of 1:2.25 (TFBA: iodide). When a solution is placed in a porous medium and it diffuses into the matrix, the extent of matrix diffusion is represented by the dimensionless matrix diffusion parameter, γ , defined in Moench (1995 [DIRS 148784], p. 1826, Table 1). According to Moench (1995 [DIRS 148784], p. 1826, Table 1), the ratio of the dimensionless matrix diffusion parameter, γ , for the two tracers is the same as the ratio of their free-water molecular diffusion coefficients. The γ values of 0.000444 and 0.001 were chosen for Figure D-15 because they have the same ratio as the γ values of 2,4,5 TFBA and iodide, namely 1:2.25. Figure D-15 shows the effects on matrix diffusion, as represented by the two calculated breakthrough curves, of changing the free-water diffusion coefficient by a factor of 2.25 for a fixed storage porosity of 0.001 and the fixed flow rate of the test. The effect of increasing the free-water diffusion coefficient, which increases γ , is a delay of the calculated breakthrough curve for higher γ relative to the breakthrough curve for lower γ . This “differential matrix diffusion delay” is seen as a horizontal offset between the two calculated breakthrough curves in Figure D-15 and later figures. The larger the difference in γ between the two curves, the larger the differential matrix diffusion delay.



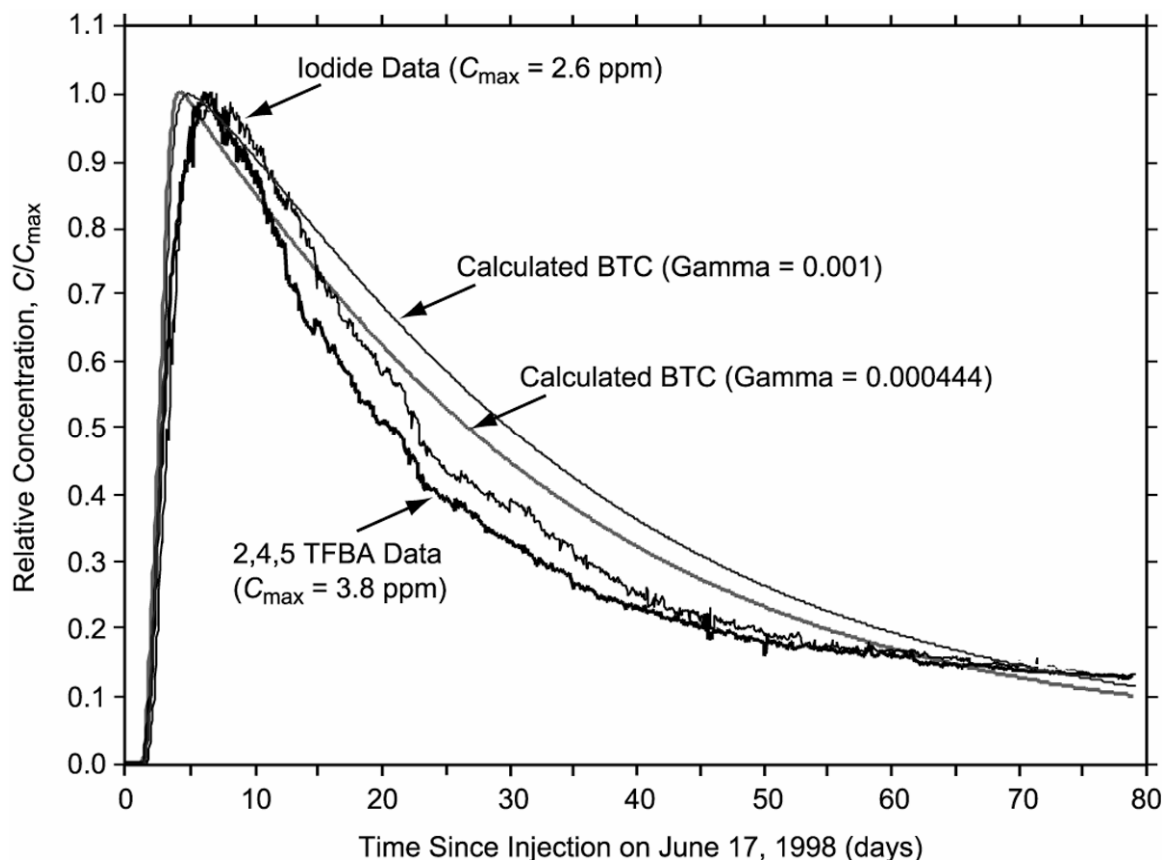
Source: DTN: GS990208312315.001 [DIRS 159238] (data).

Output DTN: GS031008312315.002 (analysis).

NOTE: The breakthrough curves were matched by the dual-porosity, partial-recirculation solution derived from Moench (1995 [DIRS 148784]) with storage porosity of 0.001 and dimensionless diffusion coefficients, gamma, of 0.000444 and 0.001. Three inter-streamline pathways were assumed to have delay factors of 2.01 days, 2.9 days, and 3.11 days. Longitudinal dispersivity = 0.27 m (0.9 ft).

Figure D-15. Breakthrough Curve for June 17, 1998, 2,4,5 TFBA and Iodide Tracer Test Matched with a Lower Storage Porosity and a Higher Diffusion Coefficient

In addition, it is seen from a comparison of Figures D-15 and D-16 that this differential matrix diffusion delay for a particular pair of free-water diffusion coefficients (or gamma values) increases with increasing storage porosity. Figure D-16, which uses the same pair of gamma values used in Figure D-15, shows that when the storage porosity is increased from the 0.001 value of Figure D-15 to 0.01, the differential matrix diffusion delay is markedly larger than that in Figure D-15.



Source: DTN: GS990208312315.001 [DIRS 159238] (data).

Output DTN: GS031008312315.002 (analysis).

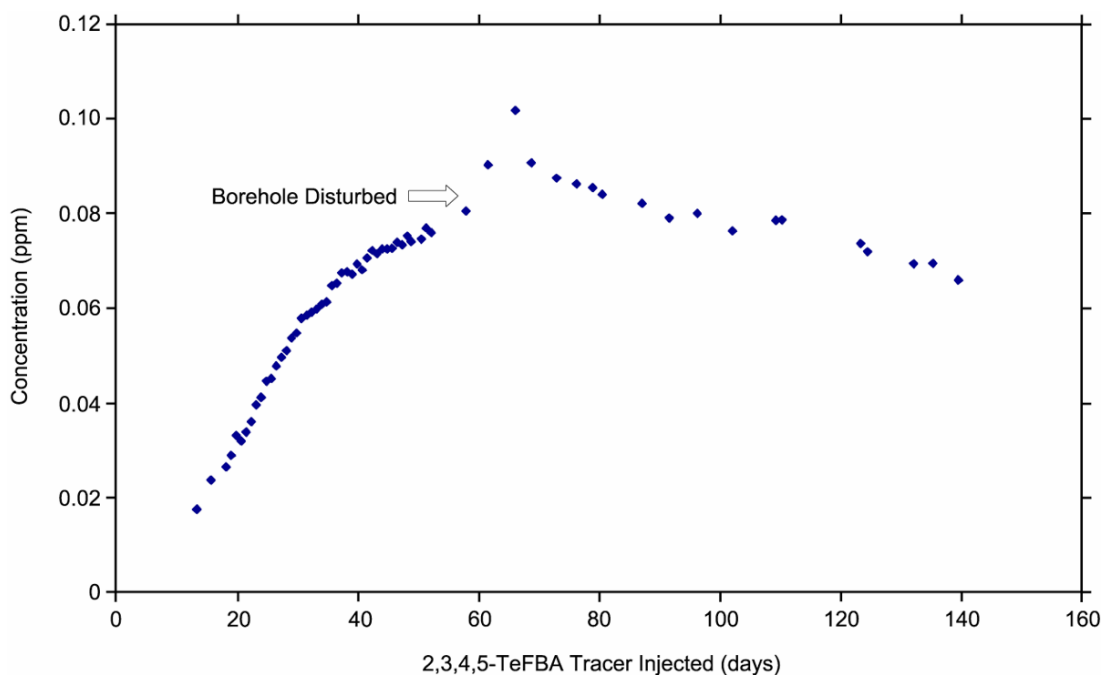
NOTE: The breakthrough curves were matched by the dual-porosity, partial-recirculation solution derived from Moench (1995 [DIRS 148784]) with storage porosity of 0.01 and dimensionless diffusion coefficients, gamma, of 0.000444 and 0.001. Three inter-streamline pathways were assumed with delay factors of 2.01 days, 2.9 days, and 3.11 days. The flow porosity was 0.00045, and the longitudinal dispersivity was 0.27 m.

Figure D-16. Breakthrough Curve for June 17, 1998, 2,4,5 TFBA and Iodide Tracer Test Matched with a Higher Storage Porosity and a Higher Diffusion Coefficient

The differential matrix diffusion delay between calculated breakthrough curves in Figure D-16 is similar to that between the actual 2,4,5 TFBA and iodide, suggesting a storage porosity value of approximately 0.01. This result is combined with earlier ones to indicate a dual-porosity medium with a flow porosity of 0.00045 (with an uncertainty range of 0.0002 to 0.0005), a storage porosity of 0.01, and a longitudinal dispersivity of 0.27 m. The flow porosity and longitudinal dispersivity characterize a flow network within this medium comprised of (1) continuous fractures and (2) discontinuous fractures with interconnecting segments of matrix. The storage porosity characterizes a storage component of the conceptualized dual-porosity medium consisting of dead-end fractures and the part of the matrix not contributing to the flow network.

D1.2.2 2,3,4,5 Tetrafluorobenzoic Acid Test from c#1 to c#2

On July 31, 1998, the nonsorbing tracer 2,3,4,5 tetrafluorobenzoic acid (2,3,4,5 TeFBA) was injected in the Prow Pass interval of c#1 while c#2 continued to be pumped at the rate of approximately 19.3 L/min (5.1 gpm) (Umari 2002 [DIRS 162858], Binder 13, Sections M-23 to M-25; Binder 14, Section M-40; Binder 15, Section M-34). Breakthrough of this tracer occurred on August 17, 1998, in the water pumped out of c#2, and the concentration eventually rose to a maximum of around 90 parts per billion, approximately 65 days after tracer injection (Figure D-17). The results of this tracer test were used to qualitatively assess flow heterogeneity at the C-wells (Table D-1)



Source: DTN: MO0308SPATRCRC.000 [DIRS 164821].

Figure D-17. Breakthrough Curve for 2,3,4,5 TeFBA Tracer Test in Prow Pass from UE-25 c#1 to UE-25 c#2

D2. FLOW ANISOTROPY AT THE SCALE OF THE C-WELLS FROM NONSORBING TRACER ARRIVAL TIMES

The comparisons of tracer responses resulting from injections into well c#1 and into either well c#2 or c#3 (while pumping the other well) provided some insights into flow heterogeneity/ anisotropy at the scale of the C-wells. Table D-1 lists the ratios of peak arrival times or first arrival times for nonsorbing tracers between c#1 and the production well (either c#2 or c#3) and between c#2 and c#3 for all tests in which a comparison was possible. For a homogeneous, isotropic medium, the arrival times under radial flow conditions are expected to vary as r_L^2 , the distance squared between injection and production well (Guimerà and Carrera 2000 [DIRS 156830], Equation 6). The ratios of r_L^2 values corresponding to each case are also listed in Table D-1. If the ratio of arrival times is less than the ratio of distances squared, then the direction from c#1 to the production well is a preferred flow orientation; on the other

hand, if the ratio of arrival times is greater than the ratio of distances squared, then the direction from c#2 to c#3 is a preferred flow orientation. Furthermore, the ratio of arrival times divided by the ratio of distances squared can be taken as a measure of the flow anisotropy ratio for the two different directions relative to the production well (note that these two directions are not strictly orthogonal). The ratios of tracer arrival times and r_L^2 values are in reasonably good agreement in all three cases, with apparent flow anisotropy ratios (c#1 to production well direction divided by c#2-c#3 direction) varying from 0.77 to 1.42. These relatively small ratios suggest that flow anisotropy at the scale of the C-wells may be relatively small despite the apparent orientation of the fracture network in the general direction of c#1 to c#2 (Geldon 1993 [DIRS 101045], pp. 43 to 51). The apparent flow anisotropy ratios deduced from the tracer arrival times should be carefully distinguished from the flow anisotropy ratios derived in Section A6, which were based on drawdown observations over much larger scales.

Table D-1. Ratios of Observed Tracer Arrival Times and Distances Squared, as well as Apparent Flow Anisotropy Ratios, for C-Wells Nonsorbing Tracer Tests

Tests (Injection Well)	Time _{c#1} / Time _{c#2-c#3} ^a	r_L^2 _{c#1} / r_L^2 _{c#2-c#3} ^a	Anisotropy Ratio ^a
Bullfrog: PFBA (c#2) and iodide (c#1) ^b	6	8.5	1.42
Bullfrog: 2,6-DFBA (c#2) and pyridone (c#1) ^c	11	8.5	0.77
Prow Pass: iodide and 2,4,5-TFBA (c#3) and 2,3,4,5-TeFBA (c#1) ^d	10	8.3	0.83

Sources: DTNs: GS010508312315.001 [DIRS 155 860]; GS990208312315.001 [DIRS 159238]; LA0007PR831231.001 [DIRS 156043] (data); Borehole separation distances taken from Table 6.1-1.

Output DTN: LA0303PR831231.005.

NOTES: Because the borehole separation distances are unqualified data, the anisotropy ratios are provided for information purposes only. The uncertainties in the anisotropy ratios are quite large because vertical tracer transport distances, which were not accounted for in the calculations, could have been comparable to or even greater than the horizontal travel distances between the boreholes. c#1, c#2, and c#3 are abbreviations for Boreholes UE-25 c#1, UE-25 c#2, and UE-25 c#3. r_L^2 is the distance squared between injection and production wells.

^aTime_{c#1} and r_L^2 _{c#1} are the time and distance, respectively, between c#1 and the production well (either c#2 or c#3, depending on the test), and Time_{c#2-c#3} and r_L^2 _{c#2-c#3} are the time and distance, respectively between c#2 and c#3. Columns 2 and 3 give the ratios of these times and distances. Ratio is for c#1 to production well direction divided by c#2 to c#3 direction. For the anisotropy ratio, a value greater than 1.0 indicates that the c#1 to production well direction is the preferred flow orientation.

^bBoth tests conducted with 2.5% to 3.5% recirculation into injection well. Peak tracer arrivals compared.

^cBoth tests conducted with no recirculation. First tracer arrivals compared.

^dc#3-to-c#2 test conducted with 30% recirculation; c#1-to-c#2 test conducted with no recirculation. Peak tracer arrivals compared.

DFBA= difluorobenzoic acid or difluorobenzoate; PFBA= pentafluorobenzoic acid or pentafluorobenzoate; TFBA= trifluorobenzoic acid.

D3. SUMMARY OF CONCEPTUAL MODELS AND PARAMETERS FROM NONSORBING TRACER TESTS AT THE C-WELLS

Uncertainty in the values of longitudinal dispersivity, flow porosity, and matrix (or storage) porosity result from physical processes, such as the scale-dependence of dispersivity (when comparing tracer tests conducted from Borehole c#1 to those conducted between Boreholes c#2 and c#3), as well as from variability in the transport characteristics of the tracer materials. However, there is good agreement in dispersivity values obtained from tracer tests conducted

between Boreholes c#2 and c#3 in the Bullfrog and Tram intervals. Peclet numbers range from 11 to 15; therefore, the longitudinal dispersivities are similar (Table D-2).

The breakthrough times are identical for the iodide and the DFBA tracer tests (Table D-2), and the advective transport times are within 10%. Therefore, the inferred flow porosities are similar, which implies that similar flow pathways are used by the tracers in those tests. These differences can be explained by the different thicknesses of the zones tested: the iodide tracer test was conducted in the combined Bullfrog-Tram zone, and the DFBA tracer test was conducted in the Lower Bullfrog zone.

The parameter estimates are robust because the visual-graphic match is close to the PEST fit (which is based on the dual-porosity analytical solution.) The differences are less than 5% for all parameters except matrix porosity, and these estimates vary by only 0.03.

The estimated flow porosities suggest that the pathways between Boreholes c#2 and c#3 in the Bullfrog and Tram intervals are not well-connected. This possibility is supported by the interpretation of the higher-than-expected flow porosities for the Bullfrog and Tram Tuffs. The microsphere responses (Section D4) are consistent with this interpretation. The arrival of the microspheres at the recovery borehole indicates the existence of a connected pathway, somewhere, with an aperture at least 0.36 μm (the diameter of the spheres).

Table D-2. Summary of Results and Transport Properties for the Bullfrog and Tram Tuffs from Nonsorbing Tracer Tests

	Iodide Test from c#2 to c#3 in Bullfrog-Tram	DFBA Test from c#2 to c#3 in Lower Bullfrog	Pyridone Test from c#1 to c#3 in Lower Bullfrog
Breakthrough (days)	5.07	5.07	56.3
Peak concentration ($\mu\text{g/L}$)	99.5	251	0.210 (final value)
Peclet number	11	12 to 15	11
Dispersivity (m)	2.6	2.4 to 1.9	6.2
Flow porosity, ϕ (%)	8.6	9.9 to 7.2	
Matrix (or storage) porosity, ϕ (%)	19	8.8 to 13.2	

Sources: DTNs: GS960808312315.001 [DIRS 159235] (Iodide data) and GS010508312315.001 [DIRS 155860] (DFBA and Pyridone data).

Output DTN:GS031008 312315.002 (analysis).

NOTES: c#1, c#2, and c#3 are abbreviations for Boreholes UE-25 c#1, UE-25 c#2, and UE-25 c#3, respectively.

DFBA= difluorobenzoic acid or difluorobenzoate.

This report presents the first unequivocal tracer testing from Borehole c#1 to c#3 in the Lower Bullfrog test and from c#1 to c#2 in the Prow Pass test. The preliminary results suggest that the arrival time from c#1 to c#3, 56.3 days, is consistent with the arrival time from c#2 to c#3, 5.07 days, because, as implemented in the Moench (1989 [DIRS 101146]) solution, the arrival time is directly proportional to the square of the distance between injection and production wells (Section D2).

Tracer testing in the Prow Pass interval (Table D-3) showed different transport characteristics than those obtained in the Bullfrog and Tram intervals. The flow porosity was found to be 0.00045 in the Prow Pass as opposed to 0.072 to 0.099 in the Bullfrog and Tram Tuffs (Table D-2). This result indicates that the flow network in the Prow Pass is dominated by interconnected fractures (fracture porosity is in the range from 0.00001 to 0.01), whereas in the Bullfrog and Tram, it was dominated by discontinuous fractures with interconnecting segments of matrix. Alternatively, the flow heterogeneity in the Bullfrog and Tram Tuffs may have been such that a vast majority of the water produced from c#3 came from locations that were not in communication with the injection wells (i.e., only a small amount of the production flow rate came from the direction of the injection wells).

Longitudinal dispersivity in the Prow Pass Tuff testing at the scale of the distance between c#2 and c#3 was calculated as 0.27 m, whereas it was 1.9 m to 2.6 m in the Bullfrog and Tram intervals at the same scale. A relatively small dispersivity is consistent with a flow network dominated by interconnected fractures (Prow Pass), and a relatively large dispersivity is consistent with a flow network dominated by discontinuous fractures with interconnecting segments of matrix (Bullfrog and Tram) because the more the actual microscopic flow pathways are different from the macroscopic, averaged, flow pathway, the larger is the longitudinal dispersivity. Clearly, a flow network dominated by discontinuous fractures with interconnecting segments of matrix (Bullfrog and Tram) would have more microscopic flow pathways than a flow network dominated by interconnected fractures (Prow Pass).

The storage porosity (or matrix porosity) calculated for the Prow Pass Tuff was 0.01 (Table D-3), whereas it was 0.088 to 0.19 for the Bullfrog and Tram (Table D-2). A small storage porosity is consistent with a dual-porosity medium dominated by interconnected fractures (Prow Pass). In such a medium, the storage component, which is assumed to consist of dead-end fractures and the part of the matrix not contributing to the flow network, would be dominated by fractures, which have very small porosities. Similarly, a large storage porosity is consistent with a dual-porosity medium dominated by discontinuous fractures with interconnecting segments of matrix (Bullfrog and Tram). In such a medium, the porosity of the storage component (dead-end fractures and the part of the matrix not contributing to the flow network) would be dominated by the large porosity of the matrix component of storage.

Table D-3. Summary of Results and Transport Properties in a Partly Recirculating Tracer Test from Borehole c#3 to c#2 and from Borehole c#1 to c#2, Prow Pass Tuff

Parameter	2,4,5 TFBA & Iodide: c#3 to c#2		2,3,4,5 TeFBA: c#1 to c#2
	Breakthrough (days)	1.67	
Peak concentration (ppm)	TFBA : 3.7 Iodide : 2.7		0.09
	Single-Porosity, Partial Recirculating Solution	Dual-Porosity, Partial Recirculating Solution	
Longitudinal dispersivity (m)	0.27	0.27	
Peclet number	107.4	107.4	
Flow porosity, ϕ_f	0.00045	0.00045	
Gamma (dimensionless matrix diffusion coefficient)	N/A	0.000444, 0.001(TFBA and Iodide, respectively)	
Storage porosity, ϕ'	N/A	0.01	

Sources: DTNs: GS990208312315.001 [DIRS 159238] and MO0308SPATRCRC.000 [DIRS 164821] (data).
Output DTN: GS031008312315.002 (analysis).

NOTE: c#1, c#2, and c#3 are abbreviations for Boreholes UE-25 c#1, UE-25 c#2, and UE-25 c#3, respectively.
Borehole mixing length was assumed to be 30.5 m.

N/A = Not Applicable. TFBA = trifluorobenzoic acid.

D4. MULTIPLE TRACER TESTS WITH SORBING SOLUTES AND COLLOID TRACERS AT THE C-WELLS

D4.1 INTRODUCTION AND OBJECTIVES

This section describes the conduct and interpretation of two cross-hole tracer tests between c#2 and c#3 in which multiple solute tracers and colloid tracers (carboxylate-modified latex (CML) microspheres) were simultaneously injected. One test was conducted in the Lower Bullfrog Tuff and the other was conducted in the Prow Pass Tuff (referred to as the Bullfrog test and the Prow Pass test, respectively). The objectives of the multiple-tracer tests in the fractured tuffs at the C-wells included the following:

- Testing/validating the applicability of a dual-porosity conceptual transport model (Section D4.2) in the saturated, fractured volcanic tuffs that underlie Yucca Mountain
- Obtaining estimates of key transport parameters in the flow system, including parameters for colloid transport
- Assessing the applicability of laboratory-derived tracer transport parameters to field-scale transport predictions.

The latter objective is important because radionuclides cannot be tested in the field, so favorable comparisons of laboratory- and field-scale transport of nonradioactive tracers can lend credibility to the practice of using laboratory-derived radionuclide transport parameters in field-scale predictive simulations.

This section also summarizes laboratory experiments that were conducted to support the C-wells field test interpretations and to provide the comparisons between laboratory-derived transport parameters and field-scale transport parameters. Special emphasis is given to the sorption behavior of the lithium ion, which was used as a sorbing tracer in the field tracer tests.

D4.2 DUAL-POROSITY CONCEPTUAL TRANSPORT MODEL

A consistent observation in all hydrogeologic units below the water table at the C-wells is that bulk permeabilities (determined from aquifer tests) exceed matrix permeabilities (determined from laboratory core measurements) by 2 to 6 orders of magnitude (Geldon 1993 [DIRS 101045], pp. 58 to 64; Geldon 1996 [DIRS 100396], pp. 69 to 71). This ratio of bulk to matrix permeabilities suggests that flow in the Miocene tuffs at the C-wells occurs predominantly in fractures. However, matrix porosities in the C-wells range from about 0.10 to 0.35 (Geldon 1993 [DIRS 101045], pp. 58 to 64), so most of the water in these rocks is stored in the pores of the matrix. Radionuclide and tracer transport in fractures, therefore, could be attenuated by diffusive mass transfer between the fractures and the rock matrix, a process known as matrix diffusion. Matrix diffusion in fractured systems has been discussed and modeled at length by Neretnieks (1980 [DIRS 101148], pp. 4,379 to 4,397), Grisak and Pickens (1980 [DIRS 101132]), Tang et al. (1981 [DIRS 101160], pp. 555 to 564), Maloszewski and Zuber (1984 [DIRS 156840]; 1985 [DIRS 148312]), and Moench (1995 [DIRS 148784]). A system exhibiting fracture and matrix flow frequently is called a “dual-porosity, dual-permeability” system. When the matrix permeability is small compared to the fracture permeability (e.g., smaller by a factor of 100 or more), the matrix permeability can be assumed to be negligible in transport calculations, and the system is often referred to as simply a “dual-porosity” system. It has been suggested elsewhere that the saturated zone in the vicinity of Yucca Mountain should behave as a dual-porosity system (Robinson 1994 [DIRS 101154]). This concept has important transport implications, particularly for sorbing radionuclides, because it suggests that solutes moving through fractures will have access to a very large surface area for sorption once they diffuse out of fractures and into adjacent matrix pores.

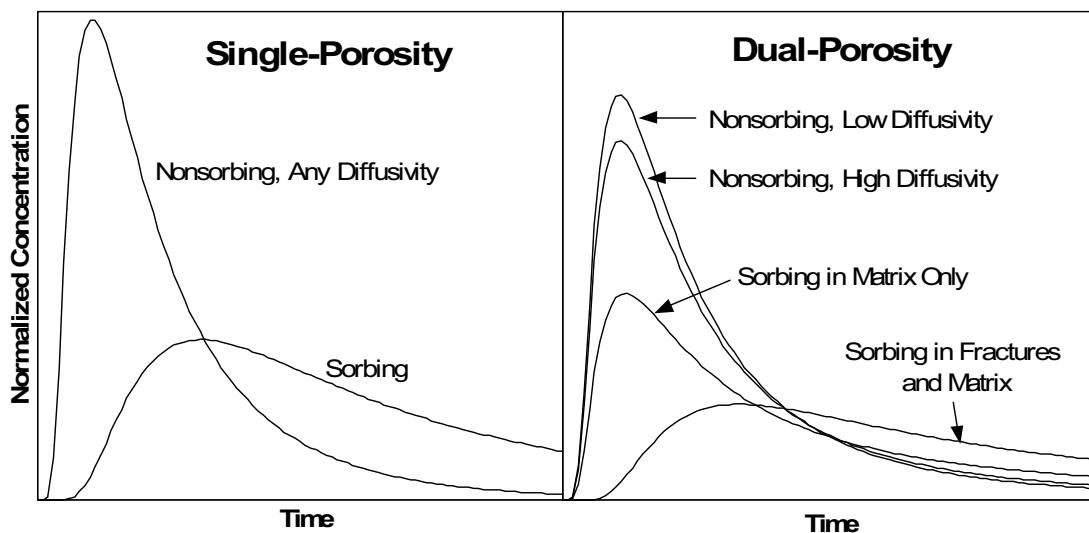
D4.3 TRACER TESTING STRATEGY

To accomplish all of the test objectives mentioned in Section D4.1 in a reasonable time, cross-hole, forced-gradient tracer tests were conducted in which three different solute tracers having different physical and chemical properties were simultaneously injected into the lower Bullfrog and Prow Pass flow systems. By dissolving the tracers in the same solution and simultaneously introducing them, it was ensured that they all experienced the same flow field and, hence, initially followed identical flow pathways through the system. This assurance is especially important in field tests where it can be extremely difficult to reproduce exact flow conditions for different tracer injections because of equipment problems and possible irreversible changes in the system (e.g., well development, biofouling, unsteady drawdown, etc.). The test interpretations were then based on comparing the responses of the different tracers. The tracers used in each test included two nonsorbing solutes having different diffusion coefficients (bromide and penta-fluoro-benzoate) and a weakly sorbing, ion-exchanging solute (lithium ion). The bromide and pentafluorobenzoate were verified to be nonsorbing in a limited set of batch adsorption experiments involving the seven different C-wells tuff lithologies listed in Tables D-16 and D-17 (DTN: LA0302PR831231.001 [DIRS 162605]). CML polystyrene

microspheres were also injected in both tests to serve as colloid tracers. These microspheres have negatively charged hydrophilic surfaces at pH greater than 5, which tends to minimize their attachment to rock surfaces (Reimus 1995 [DIRS 101474], p. 35, Table 3.6). The properties of all tracers are summarized in Table D-4, along with the injection masses and concentrations used in the tracer tests.

The rationale for using multiple solute tracers in cross-hole tests is illustrated in Figure D-18. The left plot of this figure shows hypothetical solute tracer responses (log normalized concentration versus log time) for a cross-hole tracer test with a short injection pulse in a single-porosity system. There is no distinction between nonsorbing tracers with different diffusion coefficients in this plot because there is no secondary porosity for the tracers to diffuse into and, hence, no separation of their responses. The sorbing tracer response is delayed in time and lower in concentration than the nonsorbing tracers. In contrast, the right plot of Figure D-18 shows hypothetical solute tracer responses for a test in a dual-porosity system. In this case, there is a separation between nonsorbing tracers with different diffusion coefficients, with the higher diffusivity tracer exhibiting a lower peak concentration and a longer tail than the lower diffusivity tracer. This separation occurs because the higher-diffusivity tracer diffuses more readily into the matrix than the lower-diffusivity tracer, resulting in a lower recovery at early times but a longer tail due to subsequent diffusion back out of the matrix after the tracer pulse has passed.

Figure D-18 also shows two possible responses for a sorbing tracer: (1) one with sorption occurring in the matrix and (2) one with sorption occurring in the fractures and the matrix (if the fractures have sorptive mineral coatings or are filled with sorptive granular material). In the matrix-only case, the sorbing tracer response is attenuated in peak concentration but not significantly in time relative to the nonsorbing tracers, whereas in the latter case both a concentration and a time attenuation are apparent. The minimal time attenuation of the sorbing tracer relative to the nonsorbing tracers in the matrix-only sorption case is primarily a result of the relatively short duration of a typical cross-hole tracer test relative to characteristic times of diffusion into the matrix; as transport times increase, the time and concentration attenuation of a sorbing tracer relative to nonsorbing tracers should increase.



NOTE: For illustration purposes only. The figure illustrates how multiple tracers can be used to distinguish between single- and dual-porosity systems (Reimus 2003 [DIRS 165129], Attachment A, pp. A-198 to A-208). As cross-hole transport times increase, the “nonsorbing, high diffusivity” and “sorbing, matrix only” peaks on the right-hand plot will begin to arrive later than the “nonsorbing, low diffusivity” peak. The curves were generated using the RELAP V 2.0 code (STN: 10551-2.0-00 [DIRS 159065]) with arbitrary input parameters intended to qualitatively illustrate the differences between tracer responses in single- and dual-porosity media. The inputs and outputs of the simulations were not submitted to the TDMS and do not have a DTN.

Figure D-18. Hypothetical Cross-Hole Responses of Tracers with Different Physical and Chemical Characteristics in Single- and Dual-Porosity Media

Table D-4. Tracer Characteristics, Injection Masses, and Injection Concentrations in the Two Multiple-Tracer Tests

Parameters	Solute Tracers		
	PFBA	Bromide	Lithium
Free water diffusion coefficient, D_f (cm^2/s) ^a	7.2×10^{-6} ^b	2.1×10^{-5} ^c	1.0×10^{-5} ^c
Sorption ^d	None ^d	None ^d	Weak (ion exchange)
Bullfrog test injection mass (kg)	12.1	165.6	14.39
Bullfrog test injection concentration (mg/L) ^e	1,000	13,800	1,200
Prow Pass test injection mass (kg)	12.0	30.6	16.0 ^f
Prow Pass test injection concentration (mg/L) ^g	2,000	5,100	2,670

Table D-4. Tracer Characteristics, Injection Masses, and Injection Concentrations in the Two Multiple-Tracer Tests (Continued)

CML Microsphere Tracers			
Tracer (fluorescent dye color)	Test	Injection Amount ^(j)	Injection Concentration ^(k)
0.36- μm CML microspheres (yellow) ^h	Bullfrog	3.6×10^{14} spheres	4.6×10^{10} spheres/L
0.64- μm CML microspheres (blue) ⁱ	Prow Pass	3.0×10^{14} spheres	5.1×10^{10} spheres/L
0.28- μm CML microspheres (orange) ⁱ	Prow Pass	2.1×10^{14} spheres	3.5×10^{10} spheres/L
0.28- μm CML microspheres (yellow)	Prow Pass	2.1×10^{14} spheres	3.5×10^{10} spheres/L

Sources: DTNs: LA0007PR831231.001 [DIRS 156043] (Bullfrog Test); LAPR831231AQ99.001 [DIRS 140134] (Prow Pass Test); LA0302PR831231.001 [DIRS 162605]; LA0401PR831231.001 [DIRS 171859].

NOTES: ^aCallahan et al. (2000 [DIRS 156648], Table 7) found that diffusion coefficients in rock matrices had the same ratio as free water diffusion coefficients for PFBA and bromide.

^bBenson and Bowman (1994 [DIRS 122788], p. 1,125; 1996 [DIRS 153427], p. 1,780).

^cNewman (1973 [DIRS 148719], p. 230, Table 75-1); based on ionic conductances at infinite dilution.

^dBased on results of laboratory batch sorption experiments (DTN: LA0302PR831231.001 [DIRS 162605]).

^eTracers were dissolved in approximately 12,000 L of groundwater from c#3 (DTN: LA0401PR831231.001 [DIRS 171859]).

^fLithium was injected as 33.3 kg LiBr and 80.8 kg LiCl (Reimus 2000 [DIRS 162855]).

^gTracers were dissolved in approximately 6,000 L of groundwater from c#2 (DTN: LA0401PR831231.001 [DIRS 171859]).

^hThe microsphere injection was initiated 3.5 hours after the start of injection of solute tracers in the Bullfrog test. The microsphere and solute injections ended at the same time. (Reimus 2000 [DIRS 162855]).

ⁱThese microspheres were injected 2 days prior to solute tracers in the Prow Pass test (dispersed in approximately 6,000 L of groundwater from c#2) to avoid the possible destabilization of the microspheres in the high-ionic strength injection solution containing the solute tracers (Reimus 2000 [DIRS 162852]).

^jBased on average concentration measured in a dilution of a known volume fraction of the microsphere stock solution injected. Sources: concentration measurements (Reimus 2000 [DIRS 165125]); preparation of dilutions for Bullfrog test (Reimus 2000 [DIRS 162855]); preparation of dilutions for Prow Pass test (Reimus 2000 [DIRS 162852]); and summary of calculations (DTN: LA0401PR831231.001 [DIRS 171859], also Reimus 2003 [DIRS 165129], pp. 115 to 116; Attachment A, pp. A-1 to A-6).

^kInjection concentrations calculated by dividing number of spheres injected by injection volumes of 12,000 L \times (6.5/10) = 7,800 L (Bullfrog test) and 6,000 L (Prow Pass test). The factor of 6.5/10 for the Bullfrog test accounts for the fact that the microspheres were injected for only 6.5 hours of the total of 10 hrs that the 12,000 L was injected.

CML=carboxylate-modified latex; PFBA=pentafluorobenzoic acid or pentafluorobenzoate.

The hypothetical responses in Figure D-18 suggest that a multiple tracer test involving the simultaneous injection of nonsorbing solute tracers with different diffusion coefficients and a sorbing tracer should allow qualitative discrimination between a single-porosity system and a dual-porosity system. That is, if nonsorbing tracers of different diffusion coefficients have different responses and/or if a sorbing tracer has a peak concentration that occurs at about the same time as a nonsorbing tracer but with a lower concentration, then a dual-porosity system is suggested. This approach was taken by Maloszewski et al. (1999 [DIRS 156841]), although they used only multiple nonsorbing tracers in a fractured sandstone/quartzite/slate system. Furthermore, if a dual-porosity response is observed and one knows the relative diffusion coefficients of the two nonsorbing tracers, it should be possible to determine how much of the apparent dispersion in the responses is due to true hydrodynamic dispersion and how much is due to matrix diffusion. Both of these processes have the effect of broadening the response curves or increasing the tailing of the tracers, but only matrix diffusion can cause a separation of the responses of the two tracers. The magnitude of the separation can be used to distinguish

quantitatively between the effects of matrix diffusion and hydrodynamic dispersion, resulting in unambiguous estimates of mean residence times, dispersion coefficients, and matrix diffusion parameters in a tracer test.

Effective sorption parameters associated with the response of a simultaneously injected sorbing tracer can then be estimated by assuming that the sorbing tracer experiences the same mean residence time, longitudinal dispersivity, and matrix diffusion (subject to its diffusion coefficient) as the nonsorbing tracers. In this case, only the sorption parameter(s) need be adjusted to obtain a fit/match to the sorbing tracer response. Likewise, colloid filtration/attachment and detachment parameters can be obtained by assuming that the CML microspheres experience the same mean residence times and longitudinal dispersivities as the nonsorbing solute tracers. For the microspheres, matrix diffusion is assumed to be negligible because of their large size and small diffusivity relative to the solutes.

D4.4 CONDUCT OF TRACER TESTS

The cross-hole tracer tests were conducted between wells c#2 and c#3, which are separated by about 30 m at the surface (Figure D-2). c#2 was used as the tracer injection well and c#3 as the production well in the lower Bullfrog Tuff (Reimus 2000 [DIRS 162855]; [DIRS 164624]). In the Prow Pass Tuff, c#3 was the injection well, and c#2 was the production well (Reimus 2000 [DIRS 162852]). The natural gradient at the C-wells site, though quite flat, is believed to be oriented in the direction from c#3 to c#2 (Figure D-2), so tracer movement in the Bullfrog test was against the gradient, and in the Prow Pass test, it was with the gradient. Prior to injecting tracers, a weak-dipole flow field was established in each test by reinjecting a fraction of the water pumped from the production well into the injection well. The production and recirculation flow rates are summarized in Table D-5. The weak-dipole flow configuration was chosen over a convergent flow configuration (no recirculation) to ensure that tracers were “flushed” out of the injection wellbore instead of relying on the flow field induced by pumping the production well to draw tracers out of the wellbore. Pressure transducers continuously monitored pressures between the packers, above the upper packer, and below the lower packer in each well during the tests. Because of the drastic differences in transmissivity of the two test intervals, the water level drawdown in the Prow Pass interval (62 m) was over an order of magnitude greater than the drawdown in the Bullfrog interval (5 m) despite the fact that the production rate in the Bullfrog test was approximately 30 times greater than in the Prow Pass test.

After establishing a reasonably steady weak-dipole flow field, as indicated by stable water levels in the packed-off intervals, the recirculation of produced water into the injection well was replaced by the injection of a groundwater solution containing the three solute tracers. The tracer solution was injected at the same flow rate as the recirculation and without any interruption to the flow, and when the injection was complete, recirculation was immediately resumed without interruption. Thus, there were no pressure or flow transients introduced to the system as a result of tracer injection. Recirculation of produced water was discontinued after 40 days in the Bullfrog test, but it was maintained throughout the Prow Pass test. The Bullfrog test was conducted for 337 days, and the Prow Pass test was conducted for 127 days.

Table D-5. Average Production and Recirculation Rates During the Bullfrog and Prow Pass Tracer Tests and Summary of Flow Interruptions During the Prow Pass Test

Test	Production Rate (L/min)	Recirculation Rate (L/min)	Recirculation Ratio
Bullfrog ^a	568	19 (zero after 40 days)	0.033
Prow Pass ^b	19	5.7	0.3
Prow Pass Test Flow Interruptions: ^c			
Interruption	Flow Shut Off	Flow Turned On	Duration (hr)
1	11/14/98, ~9:00 am	11/14/98, ~11:00 pm	~14
2	11/23/98, ~9:00 am	11/30/98, ~4:00 pm	~175
3	12/21/98, ~9:00 am	1/4/99, ~11:00 pm	~337

Sources: DTNs: GS970308312314.001 [DIRS 159240], GS970708312314.005 [159241] (Bullfrog production rates); MO0110BFROGREC.001 [DIRS 157066] (Bullfrog recirculation rates); GS010799992315.001 [DIRS 157067] (Prow Pass production and recirculation rates).

^a Injection well was c#2, production well was c#3. Test initiated in October 1996.

^b Injection well was c#3, production well was c#2. Test initiated in September 1998.

^c Microsphere tracers were injected on 9/23/98, and solute tracers were injected on 9/25/98.

The Prow Pass test featured three different flow interruptions (two intentional) during the tailing portion of the test. The times and durations of these interruptions are summarized in Table D-5. The first interruption was unplanned and occurred as a result of a diesel generator failure. The latter two interruptions were intentional and coincided with the Thanksgiving and Christmas-New Year holiday breaks, respectively. In addition to the practical consideration of not staffing the remote field site over the holidays, these flow interruptions offered the opportunity to obtain independent confirmation of matrix diffusion in the flow system. If a flow interruption is introduced during the tailing portion of a tracer test in a dual-porosity medium when tracers are diffusing back out of the matrix, then an increase in nonsorbing tracer concentrations should result when flow is resumed.

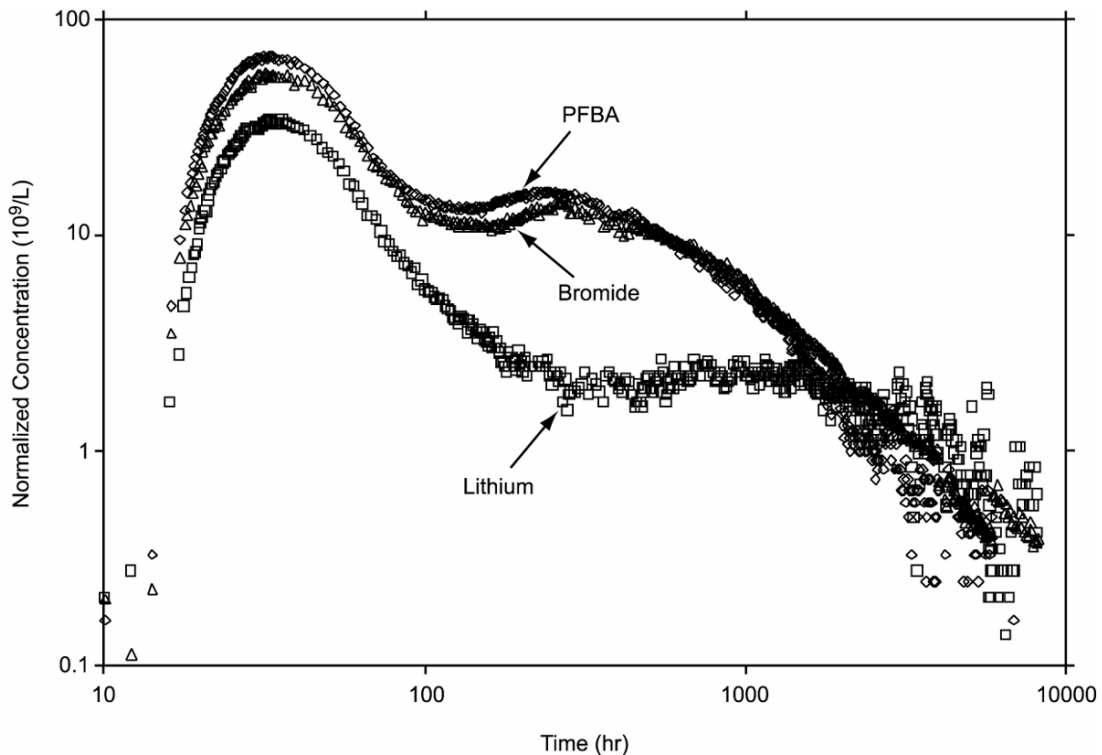
Water samples were collected at the production well throughout both tests using an automatic sampler. The sampling interval was gradually increased as the tests progressed. Sampling of the injection interval was not possible in the Bullfrog test, but a sampling loop that was designed to continuously mix the injection interval in c#3 was implemented in the Prow Pass test. Unfortunately, the submersible pump used to bring water to the surface generated more heat than could be efficiently removed from the loop, so the use of the loop for mixing had to be abandoned to prevent overheating of the downhole instrumentation. However, the loop was used 40 days into the Prow Pass test to obtain samples over a 10-hr period to assess how well the injection wellbore had been purged of tracers by the reinjection of production water.

Groundwater samples were analyzed for bromide (Br^-) by liquid chromatography (with a conductivity detector) and for lithium (Li^+) by inductively coupled-plasma, atomic-emission-spectroscopy at Los Alamos National Laboratory. PFBA was analyzed by HPLC (with a UV-absorbance detector), also at Los Alamos. The fluorescent CML microspheres were analyzed by flow cytometry.

D4.5 TRACER TEST RESULTS

Figure D-19 shows the normalized concentrations of the three solute tracers at the production well as a function of time during the Bullfrog test. All concentrations are normalized to the injection masses of tracers ($\mu\text{g/L}\text{-kg}$ injected or $\text{L}^{-1} \times 10^9$). The axes in Figure D-19 have logarithmic scales so that the details of the breakthrough curves can be seen throughout the entire test. The fractional recoveries of the tracers over the duration of the test were 0.74 for PFBA, 0.69 for bromide, and 0.39 for lithium (DTN: LA0410PR831231.001 [DIRS 171899]). Figure D-20 shows the response of the 360-nm diameter CML microspheres relative to the PFBA response in the Bullfrog tracer test. It is apparent that, while the microspheres arrived slightly earlier than the PFBA, they were significantly attenuated relative to the PFBA throughout the test. The fractional recovery of microspheres during the test was 0.145 (DTN: LA0410PR831231.001 [DIRS 171899]).

The most striking feature of the tracer breakthrough curves (Figures D-19 and D-20) is their bimodal shape. It is believed that the double-peak responses were the result of at least two distinct fracture-flow pathways between the injection and production wells located at different depths within the relatively long (approximately 100 m) test interval. The flow survey information in Figure 6.1-2 suggests that there were probably two principal zones of outflow during tracer injection and recirculation in c#2 (see the triangles indicating percentages of flow during open-hole pumping). Because of the lack of mixing in the injection interval, the tracer solutions, which were injected directly below the top packer and were approximately 2% more dense than the groundwater, probably sank rapidly to the bottom of the interval (approximately 200 kg of tracers dissolved in approximately 12,000 L (or kg) of groundwater would have resulted in an approximately 2% increase in water density). Under these conditions, the majority of the tracer mass would be expected to exit c#2 from the lower flow zone; and, indeed, the majority of the tracer mass (60%) was associated with the second tracer peak. The first peak was apparently the result of a small percentage (approximately 12%) of the tracer mass exiting c#2 from the upper flow zone. This zone was apparently more conductive (as suggested by the greater percentage of flow during open-hole pumping) and much better connected hydraulically to c#3 than the lower zone, as the transport time between the wells in this zone was much shorter. Additional evidence to support this hypothesis is obtained by comparing the PFBA response of Figure D-19 with the response of the same tracer injected into c#2 six months prior to the start of the multiple tracer test. Figure D-21 shows that the PFBA breakthrough curve in the earlier test was a more conventional single-peak response with a peak arrival time that coincided with the arrival time of the second peak in the latter test. The earlier test was conducted in the same interval between c#2 and c#3 and under the same flow conditions as the multiple-tracer test. The only noteworthy difference between the two tests, besides the additional tracers in the second test, was that only approximately 1,000 L of tracer solution was injected in the first test, whereas approximately 12,000 L was injected in the second. The larger volume in the second test was due to the large mass of LiBr that was dissolved to ensure a quantifiable response of lithium ion. Given that the volume of the injection interval (volume between the two packers) was approximately 4,300 L, it seems logical that the approximately 1,000 L of tracer solution injected in the first test would have sunk rapidly and exited the borehole via only the lower flow zone. In contrast, the approximately 12,000 L of tracer solution injected in the second test (approximately 3 interval volumes) would have eventually “filled up” the interval, and a small fraction of the tracer mass apparently accessed the upper flow zone.

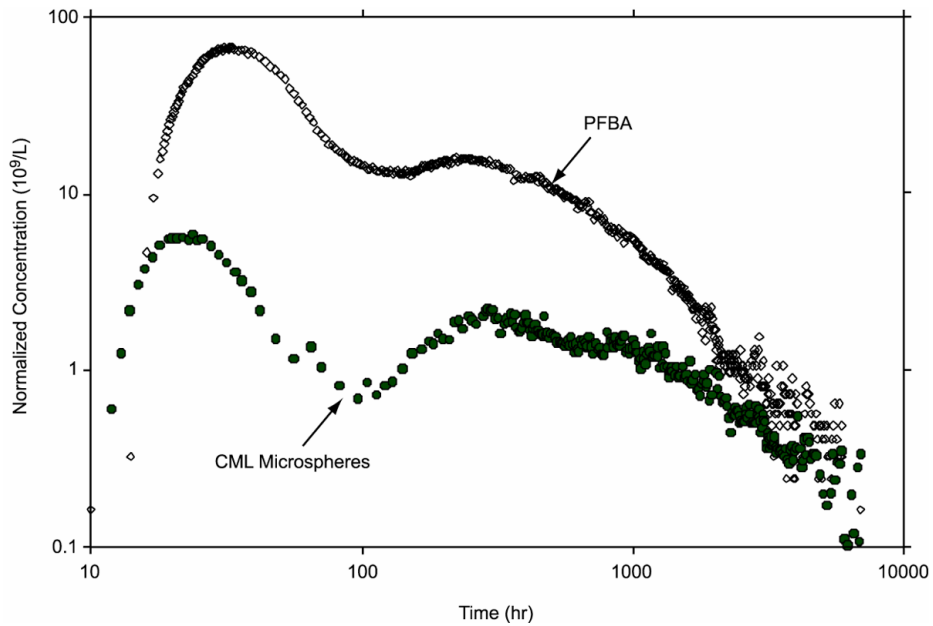


Sources: DTNs: LA0007PR831231.001 [DIRS 156043] (raw data), LA0410PR831231.001 [DIRS 171899] (normalized concentrations).

NOTE: Log-log scales are used for the axes so that the bimodal nature of the tracer responses can be seen more clearly.

Figure D-19. Normalized Tracer Concentrations Versus Time in the Bullfrog Tuff Tracer Test Conducted from October 1996 to September 1997

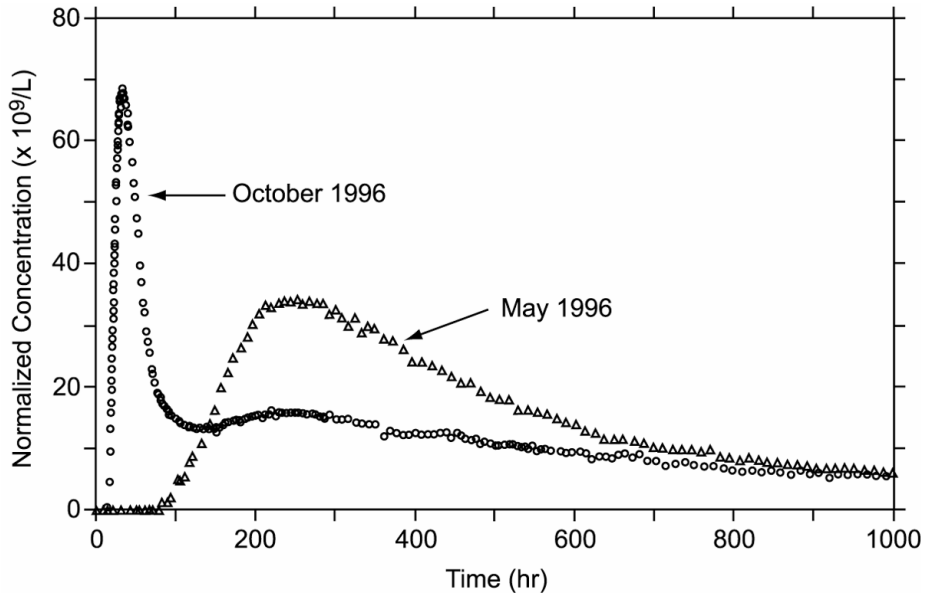
PFBA concentrations in the earlier test were monitored for just over 3,000 hr with a total fractional recovery of 0.72; at 3,000 hr into the second test, the total PFBA fractional recovery was 0.60 (DTN: LA0410PR831231.001 [DIRS 171899]). Thus, the tracer recovery in the former test was actually higher than in the latter test despite the early tracer arrival in the latter test. This observation, plus the fact that the shapes of the common peaks of the two tests are different, suggest that a considerable fraction of the mass injected in the latter test followed additional pathways not accessed in the first test. Although the possibility of additional recovery of PFBA from the first test in the second test cannot be ruled out, it is not plausible that the PFBA from the first test could have caused either the first or second PFBA peak in the second test because all of the other tracers used in the second test (which were not injected in the first test) exhibited a bimodal response.



Sources: DTNs: LA0007PR831231.001 [DIRS 156043] (raw data), LA0410PR831231.001 [DIRS 171899] (normalized concentrations).

NOTE: Log-log scales are used for the axes so that the bimodal nature of the tracer responses can be seen more clearly.

Figure D-20. Normalized Concentrations of PFBA and 360-nm-Diameter Carboxylate-Modified Polystyrene Latex Microspheres in the Bullfrog Tuff Tracer Test



Sources: DTNs: LA0007PR831231.001 [DIRS 156043] (raw data), LA0410PR831231.001 [DIRS 171899] (normalized concentrations).

NOTE: The test conditions were the same in both tests, but the injection solution volume was approximately 1,000 L in the May test and approximately 12,000 L in the October test.

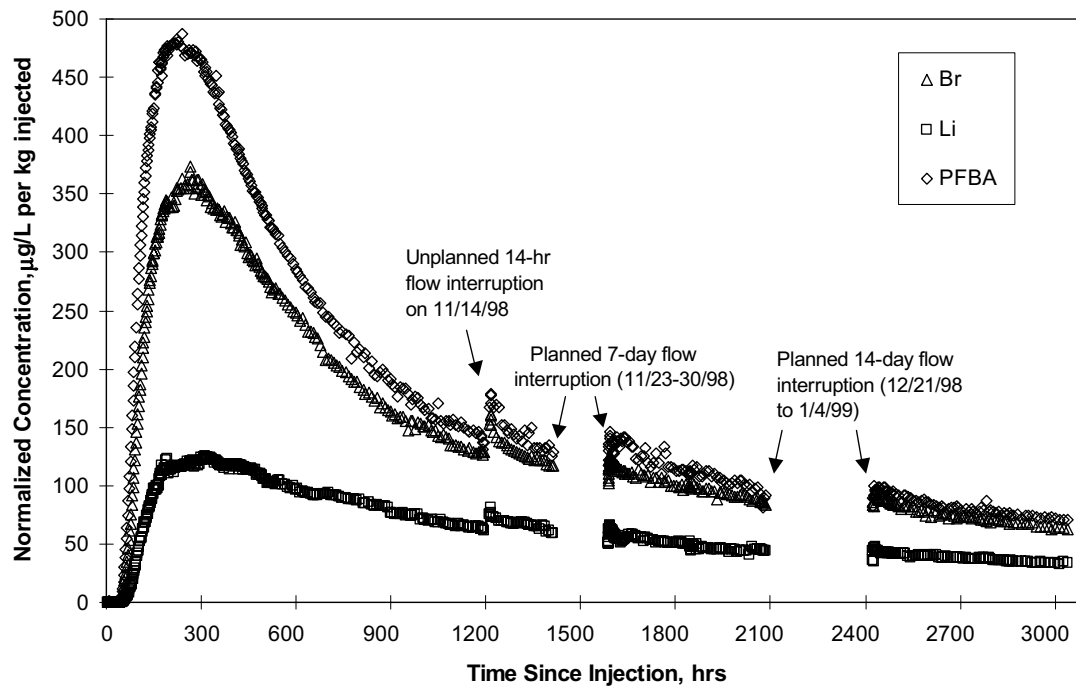
Figure D-21. Comparison of Normalized PFBA Responses in the Bullfrog Tuff Resulting from Tracer Injections in May 1996 and October 1996

Figure D-22 shows the normalized concentrations of the three solute tracers at the production well as a function of time during the Prow Pass test. In contrast to the Bullfrog test, the responses in this test had a more conventional single-peak shape. Figure D-22 also shows that there was indeed an increase in the tracer concentrations upon resumption of flow after each of the three interruptions. The fractional recoveries of the solute tracers over the duration of the test were 0.52 for PFBA, 0.43 for bromide, and 0.19 for lithium ion (DTN: LA0410PR831231.001 [DIRS 171899]). The Figure D-22 axes have a linear scale as opposed to the logarithmic scale used in Figure D-19 for the Bullfrog test.

It is apparent in Figures D-19 and D-22 that there is considerable separation between the peak normalized concentrations of bromide and PFBA in the two tracer tests, with PFBA always having a higher normalized concentration in each peak. It is also apparent that the tails of the responses of these two tracers converge, with a suggestion of a crossover at late times. However, the appearance of a second peak in the Bullfrog test precluded a crossover after the first peak, and the Prow Pass test was not conducted long enough to see a definitive crossover. Referring to Figure D-18, these breakthrough-curve features are qualitatively consistent with a dual-porosity transport system. The lithium responses in the first peak of the Bullfrog test and in the Prow Pass test are highly attenuated in normalized concentration compared to the nonsorbing tracers, although they are not significantly attenuated in time. Again referring to Figure D-18, these responses are qualitatively consistent with a dual-porosity transport system in which most of the sorption is occurring in the matrix (after diffusive mass transfer from the fractures), with possibly a small amount of sorption also occurring on fracture surfaces. In the case of the second peak in the Bullfrog test, the lithium response is attenuated both in concentration and in time, which is consistent with sorption occurring in both the matrix and on fracture surfaces.

The responses of the CML microspheres relative to PFBA in the Prow Pass test are shown in Figure D-23, which has a logarithmic normalized concentration axis because of the very low normalized concentrations of the microspheres. The fractional recoveries of microspheres in this test were 0.0033 for the 640-nm-diameter blue microspheres, 0.0012 for the 280-nm-diameter orange microspheres, and, effectively, zero for the 280-nm-diameter yellow microspheres (DTN: LA0410PR831231.001 [DIRS 171899]). The response of the yellow microspheres is not shown in Figure D-23 because these microspheres, effectively, never arrived at the production well. The 280-nm-diameter orange and 640-nm-diameter blue microspheres were injected 2 days before the solutes, whereas the 280-nm-diameter yellow microspheres were injected simultaneously with the solutes. It is likely that the high ionic strength of the injection solution (approximately 0.4 M) caused the yellow microspheres to attach to rock surfaces much more readily than the other microspheres, which were injected in untraced groundwater (ionic strength equals approximately 0.003 M). It is also interesting to note that the peak concentrations of blue and orange microspheres occurred at about the same time that solutes began arriving at c#2, and then the microspheres rapidly decreased in concentration as the solute concentrations increased. This behavior may be purely coincidental, or it may hint that the increased ionic strength associated with the solutes caused the remaining microspheres to attach more readily to rock surfaces. The microsphere “spikes” occurring at about 1,000 hr into the test (Figure D-23) actually correspond to a few days after the c#3 mixing/sampling loop was run, which suggests that the pressure and flow transients caused by the mixing may have mobilized/detached some microspheres. The timing of this response was consistent with the arrival time of the microspheres after injection into c#3 on September 23, 1998. A second spike in microsphere

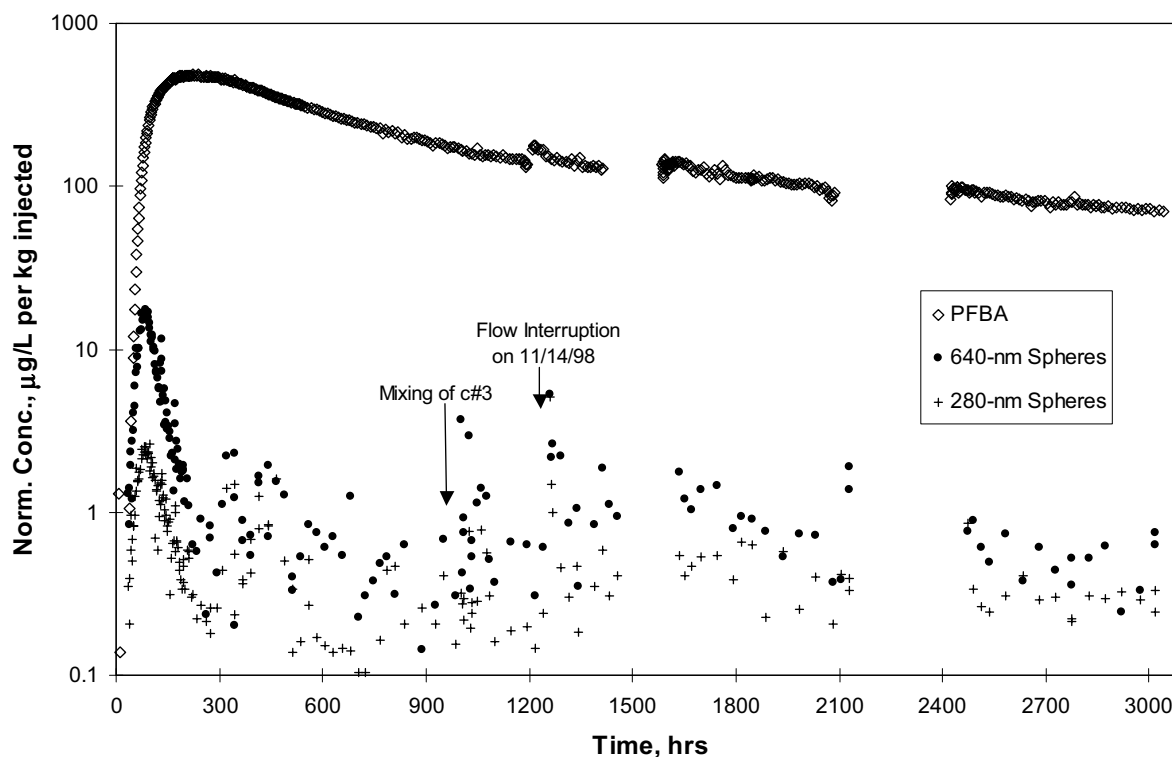
concentrations occurred the day after the unplanned flow interruption on November 14, 1998 (Figure D-23), which further supports the hypothesis that flow and pressure transients may have resulted in microsphere detachment.



Sources: DTNs: LAPR831231AQ99.001 [DIRS 140134] (raw data), LA0410PR831231.001 [DIRS 171899] (normalized concentrations).

NOTE: "Spheres" in the legend refers to CML microspheres.

Figure D-22. Normalized Tracer Concentrations versus Time in the Prow Pass Tracer Test Conducted from September 1998 to January 1999



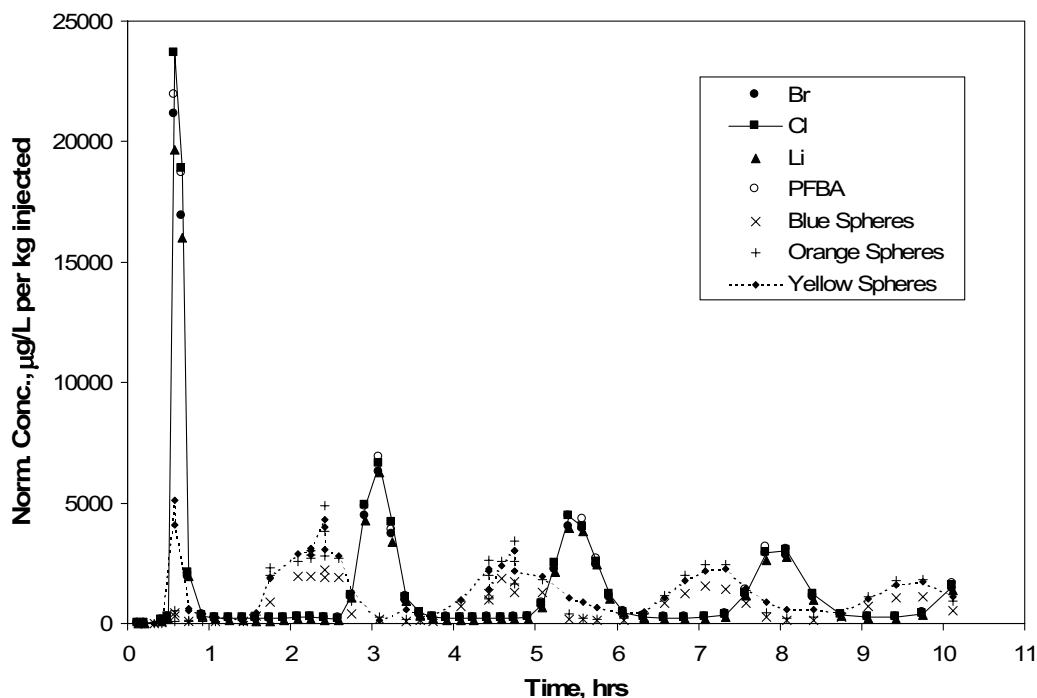
Sources: DTNs: LAPR831231AQ99.001 [DIRS 140134] (raw data), LA0410PR831231.001 [DIRS 171899] (normalized concentrations).

NOTE: "Spheres" in the legend refers to CML microspheres. The 280-nm-diameter spheres are the orange-dyed microspheres injected two days prior to the solutes. The 280-nm-diameter yellow-dyed spheres that were injected with the solutes were not recovered.

Figure D-23. Normalized Concentrations of PFBA and Carboxylate-Modified Polystyrene Latex Microspheres in the Prow Pass Tracer Test

The sampling loop in c#3 in the Prow Pass test afforded the opportunity to see how well tracers had been "flushed" from the injection borehole after the test had been running for approximately 40 days. The sampling loop was run for approximately 11 hours, and over 50 samples were collected at the surface during this time. The "responses" from the injection interval are shown in Figure D-24. These responses clearly indicate that there was a "slug" of concentrated tracer solution remaining in the interval and that this slug circulated around the sampling loop/borehole several times during the 11 hours of loop operation, dispersing as it circulated (indicated by the lowering and broadening of tracer peaks). Interestingly, the microspheres appear to precede the solutes each time the tracers cycle through the loop, which suggests that there was some as yet unexplained spatial separation of microspheres and solutes in the borehole. The total mass of any given tracer associated with the slugs was less than 0.1% of the mass that was injected, so the injection interval had been reasonably well purged of all tracers. This result is important because it shows that the unaccounted-for tracer mass in the overall test is not the result of mass being left behind in the injection borehole, but rather it is mass that is being "lost" by other means (e.g., flow into the matrix that never makes it to the production borehole, stagnation points, losses due to density-driven flow). Given the flow rate through the sampling loop and the volumes of the injection interval and piping, the timing of the slug(s) suggested that they had

been near the bottom of the interval where the pump intake was located. This result is consistent with the expectation that some of the dense tracer solution would have sunk to the bottom of the interval and remained there if there was no flow to push it out.



Sources: DTNs: LAPR831231AQ99.001 [DIRS 140134] (raw data), LA0410PR831231.001 [DIRS 171899] (normalized concentrations).

NOTE: "Spheres" in the legend refers to CML microspheres. The tracers remaining in the injection interval were apparently highly stratified, probably at the bottom of the interval. Total masses remaining in the injection interval were less than 0.1% of the total injection mass of each tracer.

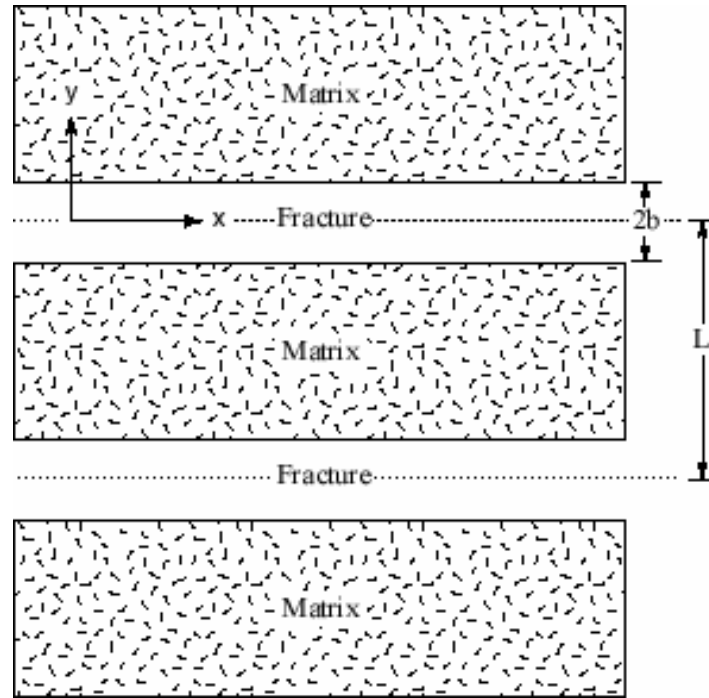
Figure D-24. Tracer Concentrations Mixing Loop 40 Days after Tracer Injection in UE-25 c#3 in the Prow Pass Tracer Test

D4.6 TRACER TEST INTERPRETIVE MODELING APPROACH

D4.6.1 Solute Tracers

To obtain estimates of solute transport parameters in the flow system, the semi-analytical dual-porosity transport code RELAP (REactive transport LAPlace transform inversion computer code) V 2.0 (STN: 10551-2.0-00 [DIRS 159065]) was used to fit simultaneously the solute tracer responses. RELAP, which is described in detail by Reimus and Haga (1999 [DIRS 154705], Appendix B), essentially combines the Laplace-domain dual-porosity transport equations derived by Maloszewski and Zuber (1984 [DIRS 156840], Appendix; 1985 [DIRS 148312]) (modified to account for linear sorption) with Laplace-domain transfer functions that describe a finite-pulse injection, wellbore mixing, and recirculation. Similar approaches have been used by others (Moench 1989 [DIRS 101146], 1995 [DIRS 148784]; Becker and Charbeneau 2000 [DIRS 156633], pp. 299 to 310). Maloszewski and Zuber (1984

[DIRS 156840], Appendix; 1985 [DIRS 148312]) assumed that tracer transport in fractures was described by the one-dimensional advection-dispersion equation with one-dimensional diffusion occurring into the surrounding matrix perpendicular to the flow direction in fractures. This simplified flow-system geometry assumed by RELAP is shown in Figure D-25. The solution embodied in the code assumes parallel-plate fractures of constant aperture, $2b$, and constant spacing, L , no concentration gradients across the fracture aperture, and a steady flow rate in fractures.



NOTE: For illustration purposes only. Matrix and fractures extend infinitely in z direction.

Figure D-25. System Geometry Assumed in the RELAP and MULTRAN Codes

The equations describing dual-porosity transport under these conditions are the following based on work by Maloszewski and Zuber (1984 [DIRS 156840], Appendix):

Fracture:

$$R_f \frac{\partial C_f}{\partial t} + v_f \frac{\partial C_f}{\partial x} - D_f \frac{\partial^2 C_f}{\partial x^2} - \frac{\phi D_m}{b\eta} \frac{\partial C_m}{\partial y} \Big|_{y=b} = 0 \quad (\text{Eq. D-1})$$

Matrix:

$$R_m \frac{\partial C_m}{\partial t} - D_m \frac{\partial^2 C_m}{\partial y^2} = 0 \quad (\text{Eq. D-2})$$

subject to the following initial and boundary conditions:

$$C_f(x,0) = 0 \quad (\text{Eq. D-1a})$$

$$C_f(x,0) = C_p \text{ from } t = 0 \text{ to } t = t_{\text{pulse}} \text{ (i.e., pulse input)} \quad (\text{Eq. D-1b})$$

$$C_f(\infty, t) = 0 \quad (\text{Eq. D-1c})$$

$$C_m(y, x, 0) = 0 \quad (\text{Eq. D-2a})$$

$$C_m(b, x, t) = C_f(x, t) \quad (\text{Eq. D-2b})$$

$$\left. \frac{\partial C_m}{\partial y} \right|_{y=\frac{L}{2}} = 0 \text{ (finite matrix) or } C_m(\infty, x, t) = 0 \text{ (semi - infinite matrix)} \quad (\text{Eq. D-2c})$$

where

C_f = tracer concentration in solution in fractures, $\mu\text{g}/\text{cm}^3$

C_m = tracer concentration in solution in matrix, $\mu\text{g}/\text{cm}^3$

C_p = pulse concentration, $\mu\text{g}/\text{cm}^3$

v_f = fluid velocity in fractures (in x direction), cm/s

D_f = dispersion coefficient in fractures, cm^2/s

D_m = molecular diffusion coefficient in matrix, cm^2/s

R_f = retardation factor in fractures = $1 + A_{\text{sp}} k_A$ (or $1 + \frac{2}{b} k_A$) for open parallel-plate fractures). Alternatively, for fractures that are filled with aquifer material, $R_f = 1 + \frac{\rho_f}{\eta} K_d$

R_m = retardation factor in matrix = $1 + \frac{\rho_B}{\phi} K_d$

K_d = sorption partition coefficient = mass of tracer sorbed per unit *mass* of aquifer material divided by solution concentration of tracer at equilibrium, cm^3/g

$k_A = K_d/A_{\text{sp}}$ sorption partition coefficient on a unit surface area basis (i.e., mass of tracer sorbed per unit *surface area* of aquifer material divided by solution concentration of tracer at equilibrium – K_d is defined above, and A_{sp} is defined below), cm^3/cm^2

A_{sp} = surface area per unit mass of material in fractures or on fracture walls, cm^2/g

ρ_f = bulk density in fractures, g/cm^3

ρ_B = bulk density in matrix, g/cm^3

η = porosity within fractures

ϕ = matrix porosity

b = fracture half aperture, cm

L = spacing between centerlines of adjacent fractures, cm.

The transformation of Equations D-1 and D-2 to the Laplace domain and their subsequent solution in the Laplace domain and inversion of the solution back to the time domain are described by Reimus and Haga (1999 [DIRS 154705], Appendix B). Equations D-1 and D-2 reduce to a single-porosity system if the matrix porosity, ϕ , (or the matrix diffusion coefficient, D_m) is set equal to zero. RELAP V 2.0 (STN: 10551-2.0-00 [DIRS 159065]) provides a simultaneous least-squares fit to up to four tracer data sets by automatically adjusting the following parameters (which arise from the dimensionless forms of the governing equations):

- Mean fluid residence time in fractures (τ)
- Peclet number ($Pe = r_L/\alpha$, where r_L = distance between wells, m, and α = dispersivity in fractures, m)
- Mass fraction of tracers participating in the test (f)
- Matrix diffusion mass-transfer coefficient, $\frac{\phi}{b}\sqrt{D_m}$, which is obtained from the Laplace transformations of Equations D-1 and D-2
- Characteristic fracture spacing, L
- Fracture retardation factor, R_f
- Matrix retardation factor, R_m .

The fractional mass participation (f) is used as an adjustable parameter because low mass recoveries are frequently observed in field tracer tests in fractured rock (e.g., Reimus and Haga 1999 [DIRS 154705], Appendix B), presumably due to (1) dense tracer solutions “sinking” out of the zone of influence of pumping, (2) a significant volumetric flow of tracer solution into the matrix within the injection wellbore (this tracer mass will not make it to the production well during the tracer test because of the very low flow velocities in the matrix), or (3) the loss of tracer mass due to stagnation points induced either by recirculation or by the superposition of the induced flow field on the ambient flow field. Although these phenomena can affect absolute tracer responses, they should not, in principle, affect the relative responses of different tracers that are injected simultaneously.

The interpretation of the tracer responses in each test involved first fitting the two nonsorbing tracer responses by simultaneously adjusting all of the parameters listed above with the constraint that the matrix diffusion coefficient, D_m , for bromide was three times that of PFBA (and therefore the matrix diffusion mass transfer coefficient, $\phi D_m^{1/2}/b$, was approximately 1.7 times that of PFBA). This factor-of-three difference is based on the experimental diffusion

cell results discussed in Section E2. R_f and R_m were held equal to 1 for the two nonsorbing tracers. This fitting procedure implicitly assumed that both tracers had exactly the same mean residence time, Peclet number, mass fraction participation, and characteristic fracture spacing during the tracer tests, which is justified because the tracers were injected simultaneously and, thus, should have experienced the same flow system and same flow conditions.

For the Bullfrog test, the two sets of tracer peaks were fitted sequentially with the second peak being fitted after accounting for the contribution of the tail from the first peak. The analytical solution parameters were allowed to vary independently for each peak, as the peaks were assumed to represent different flow pathways with different transport characteristics. Although the tracer injection duration in the Bullfrog test was about 10 hr, it was assumed that for the first peak there was a delay of 4 hr, followed by a 6-hr injection of tracer into the pathways that resulted in the first peak. The rationale for this assumption was that there was no early peak in the earlier PFBA test (Figure D-21), which involved an injection of less than one hour, so it seemed logical to assume that the earliest injected tracer solution did not follow the earliest-arriving pathways. A 4-hr delay time was chosen because the injected-tracer-solution volume exceeded the injection-interval volume by this time, and it was felt that this was a reasonable criterion for when at least a portion of the tracer solution should have begun moving through the early arriving pathways.

In contrast to the Bullfrog test, the fitting procedure for the Prow Pass test was very straightforward, as only one set of tracer peaks was observed. However, because RELAP V 2.0 (STN: 10551-2.0-00 [DIRS 159065]) is based on a semi-analytical Laplace transform inversion method, it was not capable of simulating the flow transients associated with the flow interruptions during the latter part of the test. To simulate these transients, the computer code MULTRAN (multicomponent transport) V 1.0 (STN: 10666-1.0-00 [DIRS 159068]) was used. MULTRAN is an implicit alternating-direction, two-dimensional, finite-difference code that accounts for cation exchange (involving up to three exchanging cations), charge balance, and multicomponent diffusion in a dual-porosity transport system (Section C.3.2.2). The best-fitting transport parameters obtained from RELAP fits to the tracer data up until the time of the flow interruptions were used in MULTRAN to extend the simulations throughout the entire test.

Once best simultaneous fits to the nonsorbing tracer responses in both tests were obtained, the lithium responses associated with each distinct tracer peak were fitted with RELAP V 2.0 (STN: 10551-2.0-00 [DIRS 159065]) by adjusting R_f and R_m while holding all other parameters equal to the values that provided the best fits to the nonsorbing tracers. However, D_m for lithium was assumed to be two-thirds that of bromide (and approximately 2 times that of PFBA), rather than about half that of bromide as indicated in Table D-4, because lithium and bromide would tend to diffuse together to maintain local charge balance (see Appendix A3 for further discussion). Rate-limited sorption was not considered in the field tests because the response times were all quite long relative to typical rates of ion exchange.

RELAP V 2.0 (STN: 10551-2.0-00 [DIRS 159065]) provided a good match to the lithium response associated with the second peak in the Bullfrog test and also to the lithium response in the Prow Pass test. However, in the case of the first peak in the Bullfrog test, RELAP consistently overestimated the normalized concentrations in the lithium tail when the leading edge of the lithium response was fitted well. The inability to fit the response of an

ion-exchanging tracer using a linear equilibrium sorption model (K_d model) had been previously encountered when trying to fit cation responses from both laboratory-scale fracture-transport experiments (Section E3.2) and crushed-rock column experiments (Section E3.1). In these previous studies, it was observed that cation-exchanging tracers transport with less apparent sorption than K_d models predict when the tracer injection concentration is high relative to the ionic strength of the groundwater (that is, when the total cation equivalents in the system are dominated by the cation tracer). Under these conditions, some of the cation tracer mass tends to elute with the anion tracers to maintain local charge balance in the system. When tracer concentrations are sufficiently dilute, local charge balance can be maintained by exchanging cations, and a K_d model tends to approximate more closely the observed transport behavior. In the Bullfrog test, the injection concentration of lithium was approximately 0.1 M, whereas the ionic strength of the C-wells groundwater was approximately 0.003 M; therefore, the conditions of a very high cation injection concentration relative to the groundwater ionic strength were met. MULTRAN V1.0 (STN: 10666-1.0-00 [DIRS 159068]) provided much better predictions of cation transport data in laboratory-scale dual-porosity systems under these conditions than RELAP because it explicitly accounts for ion-exchange reactions, multicomponent diffusion, and local charge balance (Section E3.2.2). For this reason, MULTRAN was employed to match the lithium data in the first peak of the Bullfrog test using the mean residence time, Peclet number, and matrix-diffusion, mass-transfer coefficient obtained from the best RELAP fit to the nonsorbing tracer data and allowing the lithium ion-exchange parameters to be varied to fit the lithium data. Lithium was assumed to exchange with sodium and calcium ions based on the results of cation exchange capacity measurements conducted on C-wells tuffs (Section E1.2).

It should be noted that the relatively low tracer concentrations observed at the production well in the Bullfrog test do not necessarily reflect the concentrations that existed in the fractures in which transport occurred; it is very likely that a significant amount of dilution occurred in the production borehole. Thus, concentrations could have remained quite high in the fractures that conducted tracers, satisfying conditions for weakly sorbing transport of the lithium ion. For the second lithium peak of the Bullfrog test and for the Prow Pass test, concentrations in the fractures apparently were dilute enough during the much longer residence times associated with these responses that the lithium transport behavior could be reasonably approximated by a K_d model.

D4.6.2 Colloid Tracers (Microspheres)

As with the solutes, the microsphere responses in the tracer tests were interpreted using the RELAP V 2.0 (STN: 10551-2.0-00 [DIRS 159065]) code to fit the data. The differential equations used to describe microsphere transport were:

$$\frac{\partial C}{\partial t} + v_f \frac{\partial C}{\partial x} - D \frac{\partial^2 C}{\partial x^2} + k_{\text{filt}} C - k_{\text{res}} S = 0 \quad (\text{Eq. D-3})$$

$$\frac{1}{b} \frac{\partial S}{\partial t} - k_{\text{filt}} C + k_{\text{res}} S = 0 \quad (\text{Eq. D-4})$$

where

- C = colloid concentration in solution, no./L
 S = colloid concentration on surfaces, no./cm²
 v_f = flow velocity in fractures, cm/s
 D = dispersion coefficient, cm²/s
 k_{filt} = filtration rate constant (1/s) = λv_f , where λ = filtration coefficient (1/cm)
 k_{res} = resuspension rate constant, 1/cm-s
 x, t = independent variables for distance and time, respectively.

These equations assume that microspheres are confined to fractures because they are too large to diffuse significantly into the porous rock matrix. The RELAP V 2.0 (STN: 10551-2.0-00 [DIRS 159065]) semi-analytical solution is capable of representing Equations D-3 and D-4 by making use of its rate-limited sorption features and setting the matrix porosity equal to zero (to eliminate matrix diffusion). It was assumed that the mass fractions, mean residence times, and Peclet numbers that provided the best fits to the nonsorbing solute responses also applied to the microspheres. Any size exclusion chromatography effects (Hiemenz 1986 [DIRS 117358], pp. 42 to 45) that would have resulted in a shorter mean residence time for the microspheres compared to the solutes were assumed to be accounted for by not allowing the microspheres to diffuse into the matrix. Thus, the only adjustable parameters in the analysis were a forward first-order filtration-rate constant and a first-order reverse-filtration-rate constant (also called a resuspension or detachment-rate constant). The product of the latter and the fracture aperture was actually obtained by dividing the best-fitting filtration rate constant by a best-fitting retardation factor minus 1 (i.e., $b k_{\text{res}} = k_{\text{filt}} / (R_f - 1)$).

Initially, attempts to fit the microsphere response associated with the first peak in the Bullfrog test were made by assuming only irreversible filtration with no resuspension/detachment. Although this approach was capable of fitting the timing and normalized concentration of the first microsphere peak, it resulted in a much shorter tail than the data indicated. Therefore, to account for the tail, a small fraction of the filtered microspheres was assumed to detach. A fit to the tail was obtained by adjusting both the fraction of microspheres detaching and the detachment rate constant (only a single-forward filtration-rate constant was assumed for all the microspheres in the first peak). Mathematically, these adjustments are equivalent to making the following changes to equation D-4:

$$\frac{1}{b} \frac{\partial S}{\partial t} - f_1 k_{\text{filt}} C + k_{\text{res}} S = 0 \quad (\text{Eq. D-4a})$$

where

- f_1 = fraction of colloids that are *reversibly attached* or reversibly filtered (if $f_1 = 1.0$, all colloids are reversibly filtered and equation D-4a becomes identical to equation D-4)
 S = concentration of *reversibly attached* colloids on surfaces, no./cm².

A fit to the second microsphere peak in the Bullfrog test was obtained in the same manner. However, in this case, the forward filtration rate constant had to be adjusted large enough so that, essentially, all of the microspheres were filtered as they moved through the system. This approach was necessary because any microspheres moving through the system without being filtered were predicted to arrive too early to match the observed response (note that the second microsphere peak occurred after the second nonsorbing solute peaks; Figure D-20). Unfiltered microspheres moving through the second set of pathways were predicted to arrive at about the same time as the low point in concentration between the two peaks. Thus, to account for the second microsphere peak, it was necessary to assume that a substantial fraction of the microspheres in the second set of pathways were reversibly filtered. The peak itself was fit by assuming a fraction of the microspheres experienced one detachment rate, and the tail was fit by assuming a separate fraction experienced another detachment rate. The remaining microspheres were assumed to not detach at all. This approach implies that there is a distribution of detachment rate constants, a possibility that has been discussed by Dabros and Ven de Ven (1982 [DIRS 143278], pp. 232 to 244); 1983 [DIRS 156652], pp. 576 to 579). The forward rate constant associated with each of these mass fractions was set equal to the minimum rate constant necessary to ensure that nearly all of the microspheres were filtered before making it through the system. Mathematically, these adjustments are equivalent to making the following changes to equations D-3 and D-4:

$$\frac{\partial C}{\partial t} + v_f \frac{\partial C}{\partial x} - D \frac{\partial^2 C}{\partial x^2} + k_{\text{filt}} C - k_{\text{res},1} S_1 - k_{\text{res},2} S_2 = 0 \quad (\text{Eq. D-3a})$$

$$\frac{1}{b} \frac{\partial S_1}{\partial t} - f_1 k_{\text{filt}} C + k_{\text{res},1} S_1 = 0 \quad (\text{Eq. D-4b})$$

$$\frac{1}{b} \frac{\partial S_2}{\partial t} - f_2 k_{\text{filt}} C + k_{\text{res},2} S_2 = 0 \quad (\text{Eq. D-4c})$$

where, f_1 = fraction of *reversibly attached* colloids detaching with detachment rate constant $k_{\text{res},1}$,

f_2 = fraction of *reversibly attached* colloids detaching with detachment rate constant $k_{\text{res},2}$, (if $f_1 + f_2 = 1.0$, all colloids are reversibly attached), and

S_1 and S_2 = concentrations of *reversibly attached* colloids on surfaces that detach according to detachment rate constants $k_{\text{res},1}$ and $k_{\text{res},2}$, respectively, no./cm².

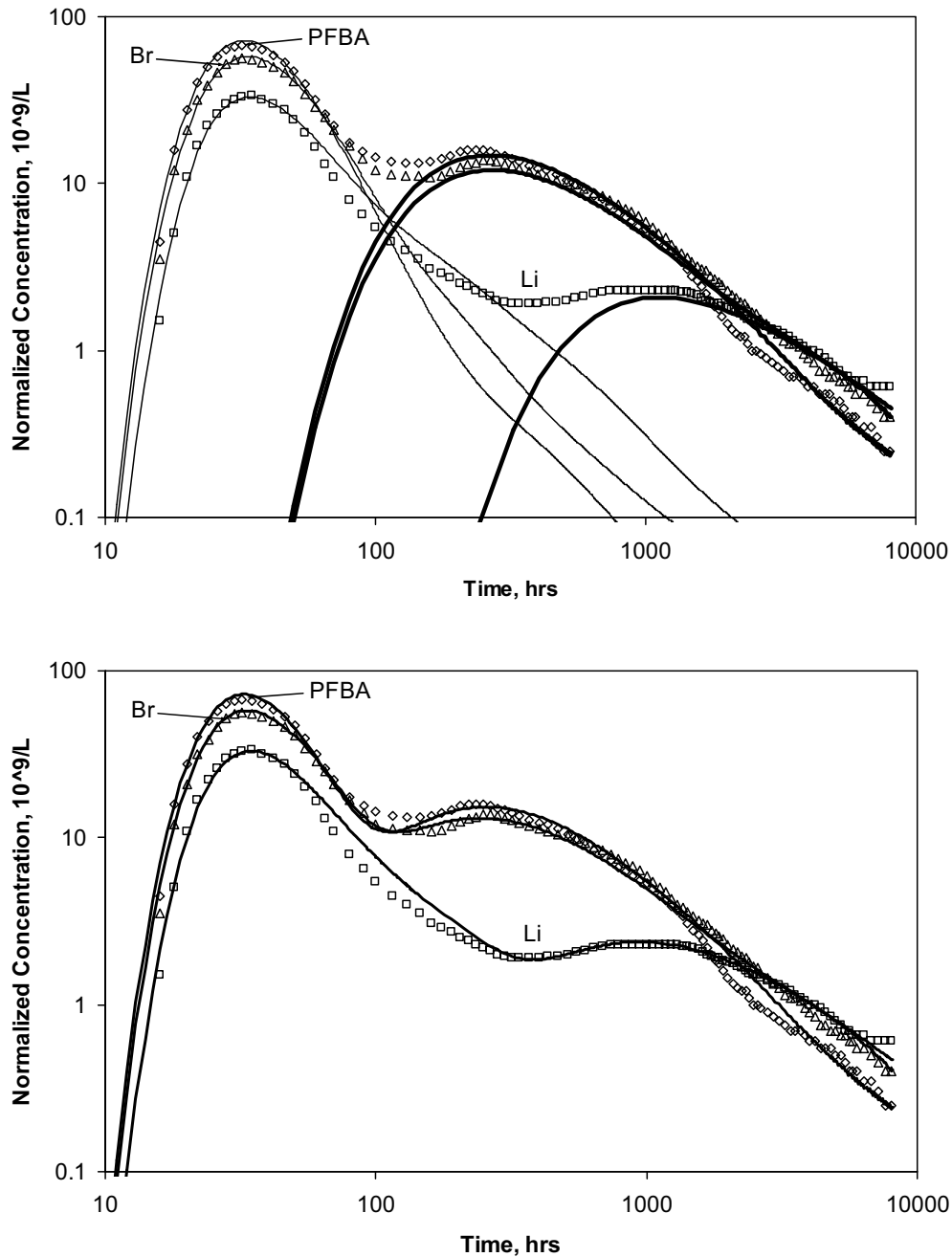
In the Prow Pass test, only a single filtration and detachment-rate constant were needed to fit the responses of each microsphere, provided the “spikes” associated with the flow transients could be ignored. No attempt was made to fit these spikes.

D4.7 TRACER TEST INTERPRETATIONS

D4.7.1 Solute Tracers

The best RELAP/MULTRAN fits to the solute tracer breakthrough curves in the Bullfrog test are shown in Figure D-26. As discussed above, RELAP V 2.0 (STN: 10551-2.0-00 [DIRS 159065]) was used to fit the nonsorbing tracer responses and the lithium response in the second peak, and MULTRAN V 1.0 (STN: 10666-1.0-00 [DIRS 159068]) was used to fit the lithium response in the first peak (MULTRAN fits to the bromide and PFBA data are also shown for the first peak in Figure D-26). The RELAP fits were obtained assuming a constant production rate of 568 L/min and a constant recirculation rate of 19 L/min (3.3% of production), despite the fact that recirculation in the field test was stopped after 40 days. Both tracer peaks occurred well before recirculation was terminated, so the only portion of the test that was incorrectly interpreted was the latter tailing portion of the second peak. Separate simulations comparing the results of MULTRAN runs with and without recirculation after 40 days indicated that the assumption of continued recirculation after 40 days had negligible effect on the fits or the values of the fitted parameters.

The best-fitting parameters from RELAP V 2.0 (STN: 10551-2.0-00 [DIRS 159065]) for the Bullfrog test are listed in Table D-6. Separate estimates of τ and Pe are provided, depending on whether linear flow (constant flow velocity between injection and production well) or radial flow (flow velocity inversely proportional to distance from production well) is assumed to occur in the test interval. RELAP is capable of providing estimates for these parameters under either assumption (the quality of the fits and the other fitted parameters are not affected). In a heterogeneous, confined aquifer with fully penetrating wells (i.e., no flow in the vertical direction), the flow velocity to a single production well with no recirculation into an injection well is expected to vary between linear and radial (National Research Council 1996 [DIRS 139151], pp. 252 to 261). Thus, if it is assumed that the test interval was reasonably confined, presenting the two values of τ and Pe in Table D-6 is a rough way of bounding these parameter estimates as a result of flow-field uncertainty. Although the Bullfrog flow system was not perfectly confined, this approach should still yield reasonable bounds for τ and Pe , as the flow velocities in pathways carrying tracers from c#2 to c#3 should have started out relatively high due to the recirculation into c#2, gone through a minimum, and then increased again in the vicinity of c#3. Thus, the weak dipole should have resulted in a flow pattern that was intermediate between linear and radial flow.



Sources:DTNs: LA0007PR831231.001 [DIRS 156043] (data), LA0410PR831231.001 [DIRS 171899] (normalized concentrations).

Output DTN: LA0303PR831231.003 (interpretive fits).

NOTE: The upper plot shows individual fits to first and second tracer peaks (MULTRAN V 1.0 (STN: 10666-1.0-00 [DIRS 159068]) and RELAP V 2.0 (STN: 10551-2.0-00 [DIRS 159065]), respectively, and the lower plot shows composite fits. For clarity, the data points shown are a subset of the actual data. The best-fitting model parameters are provided in Table D-6.

Figure D-26. RELAP and MULTRAN Fits to the Tracer Response Curves in the Bullfrog Tuff Tracer Test

Table D-6. RELAP Model Parameters Providing the Best Fits to the Bullfrog Tracer Test Data

Parameter	Pathway 1	Pathway 2
Mass fraction, f	0.115	0.60
Mean residence time, τ , for linear flow (hr)	36	1020
Peclet number, Pe , for linear flow	6.5	1.6
Mean residence time, τ , for radial flow (hr)	30	630
Peclet number, Pe , for radial flow	9.3	2.8
$\frac{\phi}{b} \sqrt{D_m}$ for bromide ($s^{-1/2}$) ^a	0.0015	0.000469
Fracture spacing (cm)	∞ (2.4) ^b	4.4
Lithium fracture retardation factor, R_f	1	4
Lithium matrix retardation factor, R_m	7.5 ^c	20

Output DTNs: LA0303PR831231.003; LA0303PR831231.005.

NOTE: Pathway 1 and Pathway 2 are associated with the first and second tracer peaks, respectively. The fits are shown in Figure D-26 (MULTRAN V 1.0 (STN: 10666-1.0-00 [DIRS 159068]) was used to fit first lithium peak in Figure D-26).

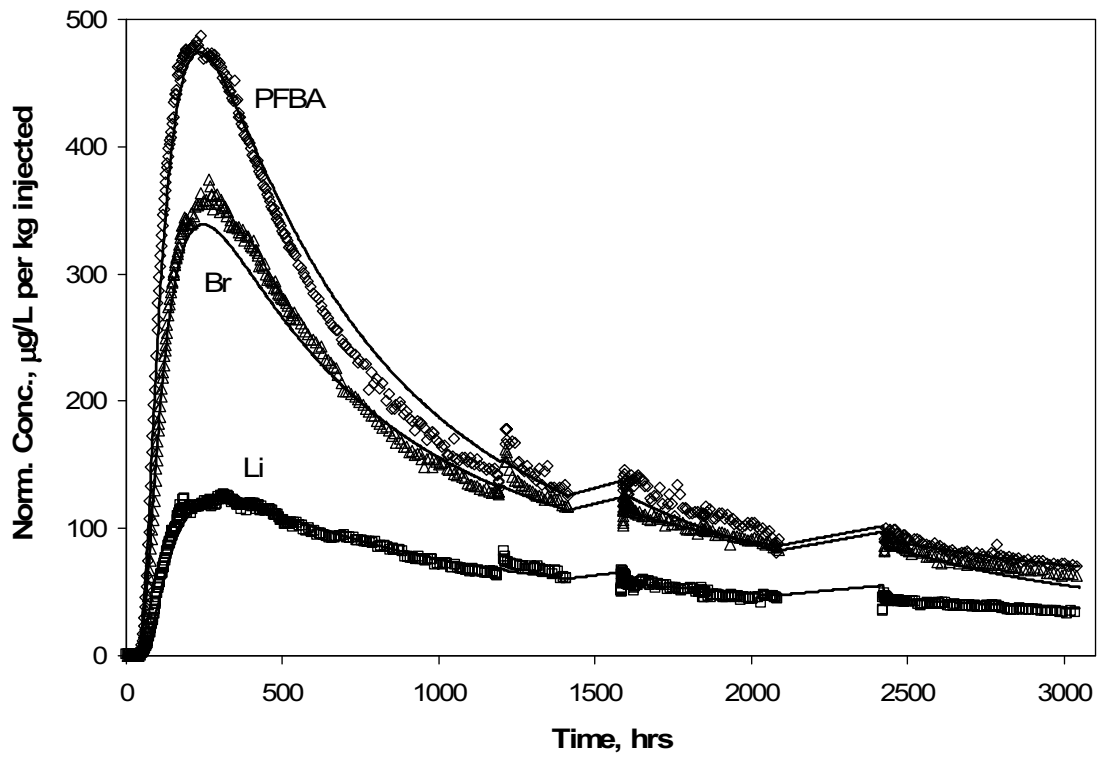
MTC=mass transfer coefficient.

^aThe mass transfer coefficient, $MTC = \frac{\phi}{b} \sqrt{D_m}$, for PFBA is 0.577 times that for bromide.

^bThe number in parentheses is the minimum fracture spacing that yields the same results as an infinite fracture spacing.

^cLithium response associated with first tracer peak was poorly fitted by RELAP V 2.0 (STN: 10551-2.0-00 [DIRS 159065]), so MULTRAN was used to obtain a better fit, which is shown in Figure D-26.

Figure D-27 shows the best RELAP/MULTRAN fits to the Prow Pass solute tracer test data, and Table D-7 gives the best-fitting RELAP V 2.0 (STN: 10551-2.0-00 [DIRS 159065]) parameters (obtained by simulating the first 1,200 hr of the test, prior to the first flow interruption). MULTRAN V 1.0 (STN: 10666-1.0-00 [DIRS 159068]) was used after the first flow interruption to interpret the remainder of the test using the best-fitting parameters from RELAP to extend the simulations. Because the tracer concentrations were significantly higher in this test than in the Bullfrog test, it was possible to determine the responses of the cations (sodium and calcium) that exchanged with lithium during the test. (The background concentrations of the exchanging cations were too high relative to their signals in the Bullfrog test to determine their responses.) Figure D-28 shows the responses of lithium, sodium, and calcium ions in the Prow Pass test, expressed as meq/L versus time. MULTRAN fits to the data are also included in Figure D-28. Although not shown here, it was confirmed that the total cation and anion charges balanced each other, as they must, throughout the test (DTN: LA0410PR831231.001 [DIRS 171899]).



Sources:DTNs: LAPR831231AQ99.001 [DIRS 140134] (raw data), LA0410PR831231.001 [DIRS 171899] (normalized concentrations).

Output DTN: LA0303PR831231.003 (interpretive fits).

NOTE: The best-fitting model parameters are provided in Table D-7.

Figure D-27. RELAP/MULTRAN Fits to the Tracer Response Curves in the Prow Pass Tuff Tracer Test

Table D-7. RELAP Parameters Providing the Best Fits to the First 1200 Hours of Prow Pass Tracer Test Data

Parameter	Parameter Value
Mass fraction, f	0.72
Mean residence time, τ , for linear flow (hr)	1210
Peclet number, Pe , for linear flow	1.3 ^a
Mean residence time, τ , for radial flow (hr)	610
Peclet number, Pe , for radial flow	2.3 ^a
$\frac{\phi}{b} \sqrt{D_m}$ for bromide ($s^{-1/2}$) ^b	0.00095
Fracture spacing (cm)	∞ (6.4) ^c
Lithium fracture retardation factor, R_f	1
Lithium matrix retardation factor, R_m	12

Output DTNs: LA0303PR831231.003; LA0303PR831231.005.

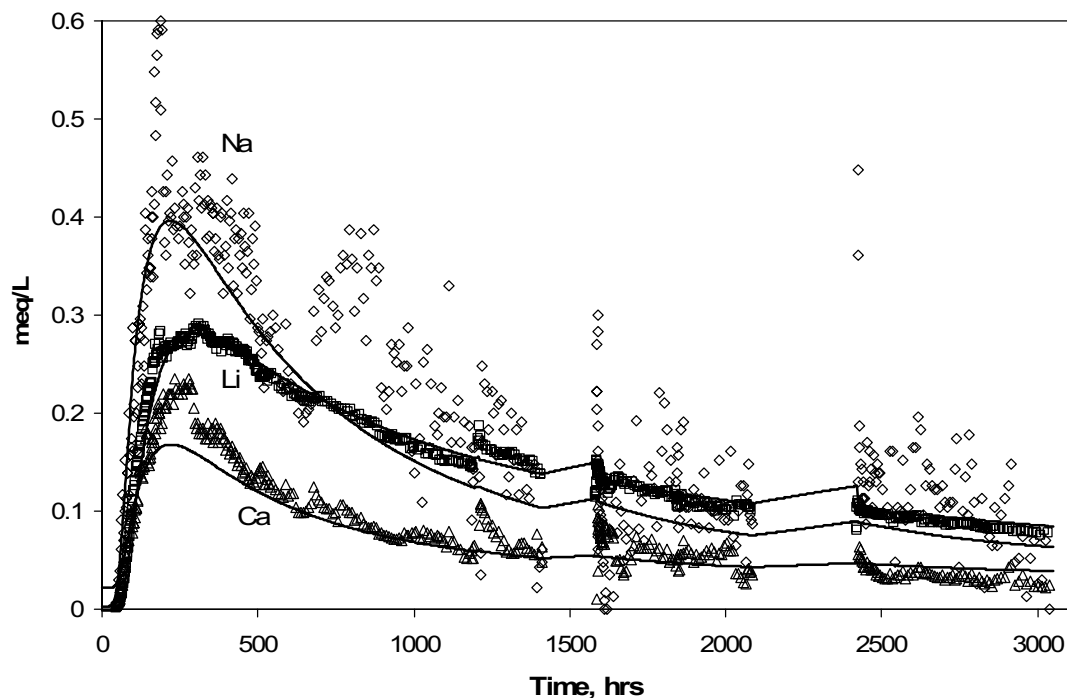
NOTE: The fits (extended by MULTRAN V 1.0 (STN: 10666-1.0-00 [DIRS 159068]) simulations) are shown in Figure D-27.

^a The Peclet numbers were adjusted to correct for the theoretical dispersion caused by the partial recirculation flow field (see text). Peclet numbers obtained directly from RELAP V 2.0 (STN: 10551-2.0-00 [DIRS 159065]) were 0.9 (linear flow) and 1.9 (radial flow).

^b The mass transfer coefficient, $MTC = \frac{\phi}{b} \sqrt{D_m}$, for PFBA is 0.577 times that for bromide.

^c The number in parentheses is the minimum fracture spacing that yields the same results as infinite fracture spacing.

MTC=mass transfer coefficient.



Sources: DTNs: LAPR831231AQ99.001 [DIRS 140134] (raw data), LA0410PR831231.001 [DIRS 171899] (meq/L).
Output DTN: LA0303PR831231.003 (interpretive fits).

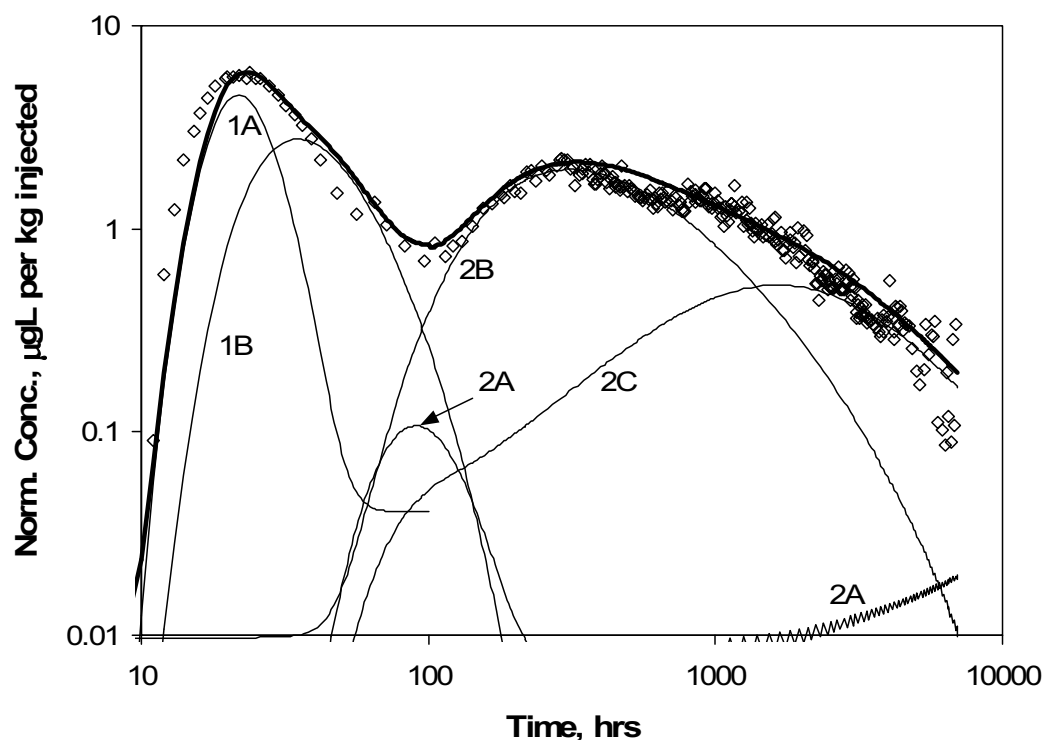
NOTE: Scatter for sodium is due to the background, which has been subtracted, being large relative to the signal.

Figure D-28. MULTTRAN Fits to Cation Responses in the Prow Pass Tracer Test

D4.7.2 Colloid Tracers (Microspheres)

The fit(s) to the Bullfrog test microsphere data are shown in Figure D-29. The “pathways” labeled 1A and 1B represent the nondetaching (or very slowly detaching) and detaching fractions, respectively, of the microspheres following the pathway(s) that resulted in the first solute peak. Pathways 2A, 2B, and 2C in Figure D-29 represent the nondetaching (or very slowly detaching) and the two detaching fractions, respectively, of the microspheres following the pathway(s) that resulted in the second solute peak. The fitted mass fractions and filtration parameters associated with the “subpathways” in Figure D-29 are given in Table D-8.

The predicted first arrival of microspheres precedes their actual first arrival by 2 to 3 hr. This result can be attributed to the fact that a 4-hr delay was not assumed for the injection of microspheres into the pathways that resulted in the first tracer peaks (as it was for the solutes). No delay was assumed for the microspheres because the microsphere injection began about 3.5 hr after the solutes were injected. If the solutes did not begin entering the pathways resulting in the first tracer peaks until after the microspheres were injected, then it would be reasonable to assume that the microspheres should have entered those pathways at the same time as the solutes.



Sources: DTNs: LA0007PR831231.001 [DIRS 156043] (raw data), LA0410PR831231.001 [DIRS 171899] (normalized concentrations).

Output DTN: LA0303PR831231.003 (interpretive fits).

NOTE: Diamonds are microsphere data points. Numbers followed by letters indicate flow pathways discussed in text and listed in Table D-8. Bold line is the sum of all the pathways.

Figure D-29. RELAP Fits to CML Microsphere Response in Bullfrog Tuff Tracer Test

Table D-8. Microsphere Filtration and Detachment Parameters Associated with the Fits Shown in Figure D-29

Parameter	Path 1A	Path 1B	Path 2A	Path 2B	Path 2C
Mass fraction, f	0.111	0.004	0.42	0.07	0.11
k_{filt} (1/hr)	0.175	0.175	0.04	0.04	0.04
λ^a (1/cm)	0.0017	0.0017	0.0084	0.0084	0.0084
bk_{res}^b (1/hr)	0.000219 ^c	1.08	0.000201 ^c	0.211	0.00755

Output DTNs: LA0303PR831231.003; LA0303PR831231.005.

NOTE: Other transport parameters used to obtain the fits are given in Table D-6. Subpathways 1A and 1B represent a mass fraction split of Pathway 1 from Table D-6, and subpathways 2A, 2B, and 2C represent a mass fraction split of Pathway 2 from Table D-6. The parameter f_1 in equation D-4a is $0.004/0.115 = 0.035$ for pathway 1 and the parameters f_1 and f_2 in equations D-3a, D-4b, and D-4c are $f_1 = 0.07/0.6 = 0.117$ and $f_2 = 0.11/0.6 = 0.183$ for pathway 2.

^a λ calculated as k_{filt}/v_f , where v_f = average linear velocity determined from mean fluid residence time.

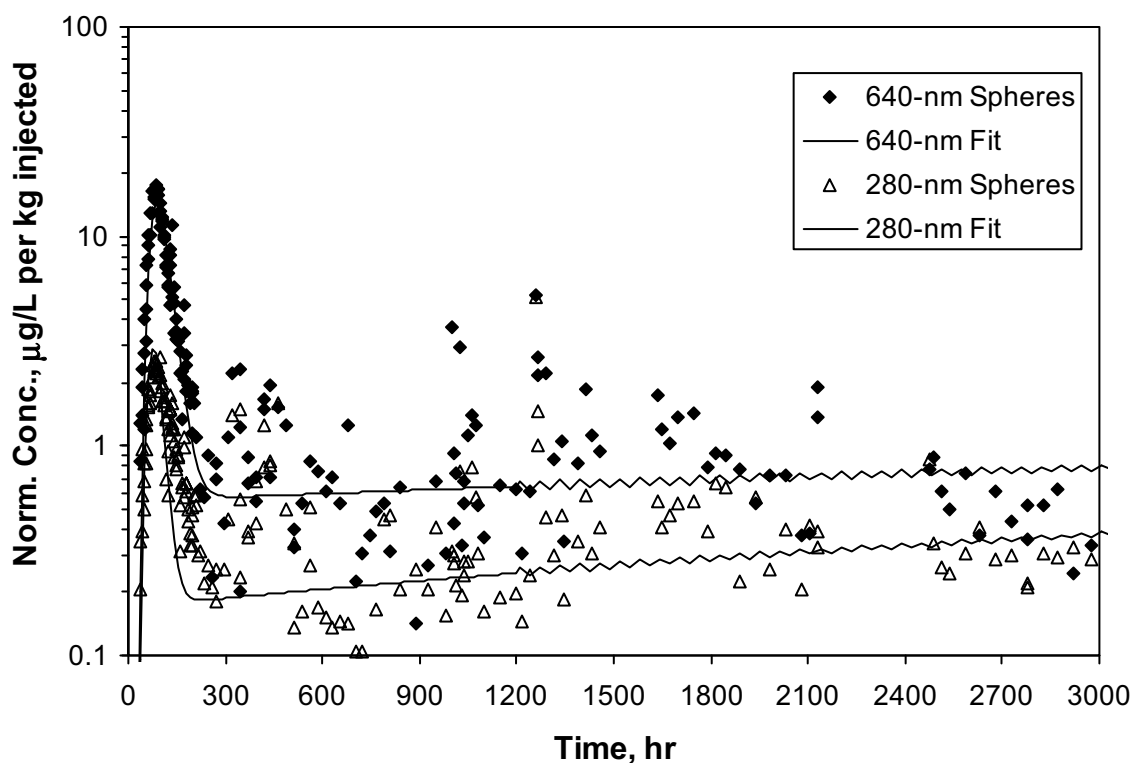
^b b = fracture half aperture in cm. The fitted detachment rate constant is this lumped parameter.

^c Maximum detachment rate constant; cannot distinguish between this value and zero, so microspheres could be very slowly detaching or not detaching at all.

However, if the microspheres experienced a delay similar to the solutes, then their predicted first arrival would actually be slightly later than the observed first arrival. In fact, in this case, the first arrival would coincide almost exactly with the first arrival of solutes. Thus, the uncertainty associated with when the microspheres actually began entering the flow system causes uncertainty in the predicted first arrival of the microspheres.

The fits to the Prow Pass test microsphere data are shown in Figure D-30, and the corresponding best-fitting filtration and detachment rate constants are listed in Table D-9. The fits suggest that the small peaks in this test were the result of a very small fraction of microspheres that moved through the flow system unfiltered, and the long tails were the result of small detachment rate constants. The filtration-rate constant listed in Table D-9 for the 280-nm-diameter yellow microspheres was not obtained from fitting, but rather it was the smallest filtration coefficient that resulted in a peak concentration of microspheres at or below detection limits. This number can be considered a lower-bound estimate of the yellow-microsphere filtration coefficient because any larger value will result in more filtration and an even lower recovery. Unlike the Bullfrog test, only a single filtration and detachment rate constant were needed to effectively fit the microsphere responses in the Prow Pass test. As mentioned in Section D4.6.2, no attempt was made to fit the “spikes” in microsphere concentration that occurred after flow transients.

It should be pointed out that the interpretations of the microsphere responses presented in the preceding paragraphs, particularly for the Bullfrog test, are by no means unique. First, it is quite likely that there exists a continuous distribution of filtration and detachment rate constants rather than a few discrete ones, as assumed in the above analyses. Such a distribution could arise from a distribution of colloid surface properties and/or physical and chemical heterogeneities in fracture surfaces (Dabros and Van de Ven 1982 [DIRS 143278], pp. 232 to 244; 1983 [DIRS 156652], pp. 576 to 579). It is also possible that colloid filtration and detachment are not linear first-order processes as assumed in Equations D-3 and D-4. Rather, they might be better described as nonlinear and/or stochastic processes. Finally, as mentioned above, the interpretation of the microsphere response relative to the solutes is complicated by the fact that, with the exception of the 280-nm-diameter yellow microspheres in the Prow Pass test, the microsphere injections were not started at exactly the same times as the solute injections (they were started about 3.5 hours later in the Bullfrog test and about 2 days earlier in the Prow Pass test). In addition to causing uncertainty as to when the microspheres actually began moving into flow pathways (relative to the solutes), the differences in injection times may have resulted in the microspheres not being distributed into flow pathways in exactly the same proportion as the solutes (i.e., a different source term). If different assumptions were made about the distribution of microspheres between the two major sets of pathways in the Bullfrog test, different filtration parameters would be obtained.



Sources: DTNs: LAPR831231AQ99.001 [DIRS 140134] (raw data), LA0410PR831231.001 [DIRS 171899] (normalized concentrations).

Output DTN: LA0303PR831231.003 (interpretive fits).

NOTE: The jagged appearance of the fits starting at approximately 1,000 hr is the result of instabilities in the Laplace transform inversion algorithm of RELAP V 2.0 (STN: 10551-2.0-00 [DIRS 159065]). "Spheres" in the legend refers to CML-microspheres.

Figure D-30. RELAP Fits to the CML Microsphere Responses in the Prow Pass Tracer Test

Table D-9. Filtration and Detachment Rate Constants for the CML Microspheres in the Prow Pass Tuff Tracer Test

Parameter	Microspheres		
	640-nm Blue	280-nm Orange	280-nm Yellow
k_{filt} (1/hr)	0.043	0.07	0.2 ^a
λ (1/cm)	0.0087	0.014	0.041
bk_{res} ^b (1/hr)	0.000154	0.000251	0.0002

Output DTN: LA0303PR831231.003.

NOTE: Mass fractions are assumed to be the same as for solutes (Table D-7).

^a Minimum value that is consistent with the lack of appearance of these spheres at the production well. The actual filtration rate constant could be much higher.

^b Maximum values; cannot distinguish between these values and zero. See also footnote b of Table D-8.

D4.8 DISCUSSION OF FIELD TRACER TEST RESULTS

Estimates of transport parameters that can be used directly in solute transport models were derived from the best-fitting parameters in Tables D-6 and D-7. These parameter estimates are presented in Table D-10 as ranges of values consistent with the tracer test interpretation(s). Additional discussion of these ranges and how they were derived is provided in the following sections. This parameter estimation exercise has several important implications for radionuclide transport in fractured volcanic tuffs near Yucca Mountain.

Table D-10. Transport Parameter Estimates Deduced from the Bullfrog and Prow Pass Multiple-Tracer Tests

Parameter	Prow Pass		Bullfrog	
	Lower Bound	Upper Bound	Lower Bound	Upper Bound
Effective flow porosity (Equation D-6, Section D4.8.5)	0.003	0.006	0.003 ^a	0.031 ^a
Longitudinal dispersivity, m^b	13.0	61.5	3.2	62.5
MTC, $\frac{\phi}{b} \sqrt{D_m}$, for radionuclides ($s^{-1/2}$) ^c	0.00054	0.00095	0.00027	0.0015
Fracture aperture (cm)	0.18	1.05	0.081	1.31
Fracture spacing (cm)	6.4	∞	4.4	∞
Ratio of stagnant to flowing water volumes	3.1	∞	2.1	∞

Output DTN: LA0303PR831231.005.

NOTE: These values above are provided as ranges of values; see text for explanations.

^a These estimates assume that 75% of the production flow was associated with flow pathways that resulted in the first tracer peak and 25% was associated with the second tracer peak (based on flow survey information (DTN: GS931008312313.016 [DIRS 148173]); see Figure 6.1-2).

^b Lower bounds assume Peclet numbers for radial flow and 30-m travel distance; upper bounds assume Peclet numbers for linear flow and interval thicknesses as travel distances (see Table 6.1-1 for actual borehole separations and interval thicknesses).

^c Assumes that bromide and PFBA effectively bound molecular sizes and diffusion coefficients of radionuclide solution species.

MTC=mass transfer coefficient; PFBA= pentafluorobenzoic acid or pentafluorobenzoate.

D4.8.1 Conceptual Transport Model

Even without quantitative parameter estimation, it is clear that the tracer responses in both the Bullfrog and Prow Pass tests are consistent with a dual-porosity conceptual transport model for the fractured volcanic tuffs. It is simply not possible to account for the differences in the bromide and PFBA responses or the relatively small time attenuation but significant concentration attenuation of the lithium response relative to the nonsorbing tracers (in the Prow Pass test and the first peak of the Bullfrog test) without invoking diffusion between flowing fractures and stagnant matrix water. Some diffusion into stagnant water within fractures (e.g., dead-end fractures or along rough fracture walls) cannot be ruled out. However, if the stagnant water were primarily in fractures, the surface area for sorption would be limited, and it is unlikely that there would be as much concentration attenuation of lithium relative to the nonsorbing solutes as observed in the tracer tests. The large surface-area-to-volume ratio necessary to result in the large observed concentration attenuation of lithium seems plausible only if a significant fraction of the stagnant water is in matrix pores.

The quantitative estimates of the lumped mass transfer parameter, $\frac{\phi}{b}\sqrt{D_m}$ for bromide in Tables D-6 and D-7 are based on the assumption that bromide has a diffusion coefficient a factor of three greater than PFBA. This assumption is based on matrix diffusion coefficients measured in laboratory diffusion cell tests, which are discussed in Section E2. It is worth noting that RELAP V 2.0 (STN: 10551-2.0-00 [DIRS 159065]) simulations in which a finite matrix was assumed (i.e., a finite spacing between fractures) offered a slightly better fit to the tracer responses associated with the second peak of the Bullfrog test than simulations assuming an infinite matrix. This result suggests that tracer molecules may have diffused far enough into the matrix to begin encountering molecules from neighboring fractures, which implies a relatively small fracture spacing. Alternatively, the tracers may have encountered diffusion boundaries (no-flux boundaries) within the matrix, which implies a significant increase in tortuosity or a decrease in interconnected porosity at some distance into the matrix from fracture surfaces. For the first peak in the Bullfrog test and for the Prow Pass test, a finite matrix offered no better fits to the tracer data than an infinite matrix. In these cases, it can only be stated that the fracture spacing must have exceeded some threshold value below which the tracer responses would have been significantly different than observed. The applicable threshold values for the first Bullfrog test peak and for the Prow Pass test were estimated by adjusting the fracture spacing in RELAP until the simulated tracer responses began to differ significantly from the simulated responses assuming an infinite matrix. The results are presented in Table D-10 as lower bounds for fracture spacing.

The tracer responses and the qualitative and quantitative conclusions about matrix diffusion that can be drawn from them illustrate very clearly the advantages of using multiple nonsorbing tracers with different diffusion coefficients in tracer tests to distinguish between alternative conceptual transport models. The individual responses of either bromide or PFBA could have been fit reasonably well assuming no matrix diffusion at all. Only when the responses of these tracers are considered together is it obvious that diffusive mass transfer must be invoked to explain the test results. Even long tails that plot linearly on log-log plots of tracer responses (power-law behavior), which are often said to infer matrix diffusion when single tracer responses are analyzed (Haggerty et al. 2000 [DIRS 156832], pp. 3,467 to 3,469), do not unequivocally substantiate diffusive mass transfer. Such responses can also be attributed to hydrodynamic dispersion that scales with residence time (due to the recirculating flow field or effects of density-driven flow), stagnation points, and/or source-term effects (e.g., the slow release of tracers from the injection borehole). Furthermore, the fact that the lithium responses were significantly attenuated in concentration but not in time supports the concept that a significant amount of diffusion occurred into the matrix pores and not simply into stagnant water within the fracture network. This conclusion is very important for Yucca Mountain performance assessment because mass transfer between flowing fractures and the true matrix implies that a large amount of surface area will be available for sorption of radionuclides in the saturated, fractured tuffs.

D4.8.2 Fracture Apertures

An estimate of the average fracture aperture ($2b$) experienced by the tracers in the Bullfrog and Prow Pass tests can be obtained from the estimate of the lumped, diffusive, mass-transfer parameter, $\phi D_m^{1/2}/b$ provided independent estimates of matrix porosity, ϕ , and matrix diffusion coefficients, D_m , are available. Using estimates of ϕ determined from laboratory measurements and D_m for bromide and PFBA from diffusion cell tests (Section E2), estimates of $2b$ range from 0.081 to 1.31 cm in the Bullfrog Tuff and from 0.18 to 1.05 cm in the Prow Pass Tuff, as listed in Table D-10. Because the long tracer test intervals in each test both included more than one major lithology (Figure 6.1-2), it was necessary to estimate $2b$ for each major lithologic unit in each interval. The fact that there is a positive correlation between matrix porosity and matrix diffusion coefficient results in a relatively large range of aperture estimates. If it is assumed that the flow pathways associated with the first tracer peak in the Bullfrog test were in the central Bullfrog unit and the pathways associated with the second tracer peak were in the lower Bullfrog unit, then the aperture estimates in these two units correspond to the two extremes listed in Table D-10. These aperture estimates based on tracer responses should be distinguished from friction loss or cubic-law aperture estimates obtained from hydraulic responses (Tsang 1992 [DIRS 113901], pp. 1,451 to 1,455), although they should be the most appropriate aperture estimates to use for transport calculations.

D4.8.3 Ratios of Stagnant Water to Flowing Water Volumes

Estimates of the ratio of stagnant water volume to flowing water volume in the flow system(s) can be calculated from estimates of fracture spacings obtained from RELAP V 2.0 (STN: 10551-2.0-00 [DIRS 159065]) simulations and the matrix porosities and fracture apertures used in the RELAP simulations (ratio = $\phi(L/2b - 1)$). Ranges of these estimates are listed in Table D-10. The upper-bound ratios for both tracer tests are listed as infinite because all tracer responses could be fitted reasonably well, assuming infinite fracture spacing. The lower bounds in Table D-10 were obtained using fracture spacings that yielded slightly better fits to the tracer responses than the fits obtained assuming an infinite fracture spacing. These ratios plus one can be considered physical retardation factors for nonsorbing species in the flow system when flow rates are low enough that there is ample time for solutes to diffuse throughout the stagnant water in the system (Robinson 1994 [DIRS 101154]).

D4.8.4 Lithium Sorption Behavior

Tables D-6 and D-7 list the best-fitting values of the lithium fracture and matrix retardation factors (R_f and R_m , respectively) for the Bullfrog and Prow Pass tests. The R_f values are 1 for both the Prow Pass test and for the first peak in the Bullfrog test, implying negligible retardation within the fractures and sorption only in the matrix. A fracture retardation factor of 1 does not necessarily imply that sorption did not occur on fracture surfaces; it merely suggests that the majority of the lithium sorption occurred after a diffusive mass-transfer step to sorptive surfaces in the matrix. For the second peak in the Bullfrog test, the lithium response was best fitted with $R_f = 4$ and $R_m = 20$, implying some sorption in fractures and a large amount of sorption in the matrix.

Matrix K_d values were deduced from the fitted matrix retardation factors by simple rearrangement of the expression defining the retardation factor:

$$K_d = \frac{\phi}{\rho_B} (R_m - 1) \quad (\text{Eq. D-5})$$

Because the K_d values depend on the matrix porosity, values are listed in Table D-11 for each lithologic unit that transport may have occurred in for each test (matrix porosities from Section E.2, Table E-6, were used in Equation D-5). For a given retardation factor, the corresponding K_d value is always higher in a unit with higher matrix porosity. The R_m value associated with the first lithium peak in the Bullfrog test (Table D-6) was obtained by fitting the rising limb of the lithium response using RELAP V 2.0 (STN: 10551-2.0-00 [DIRS 159065]). However, because it was necessary to use MULTRAN V 1.0 (STN: 10666-1.0-00 [DIRS 159068]) to achieve a reasonable fit to the tail of the response (see above), the K_d value for this peak was estimated from the ion-exchange parameters that yielded the best fit to the lithium data (see Section E.3.1.3 for a discussion of using ion-exchange parameters to fit lithium responses in laboratory experiments) rather than from the R_m value obtained from RELAP. The best-fitting, ion-exchange parameters suggested a nonlinear sorption isotherm for lithium in the matrix; hence, K_d values are reported in Table D-11 for lithium concentrations of both approximately 600 mg/L (low K_d value) and approximately 0.5 mg/L (high K_d value). This range of concentrations should reasonably bound the concentrations experienced in the field test.

Laboratory batch measurements of lithium sorption onto crushed tuff from C-wells cores indicated a dependence of K_d values on both lithium concentrations and the mineralogy associated with the different lithologies (Section E1). The concentration dependence in each case could be represented by a classic nonlinear isotherm in which K_d values decreased as lithium solution concentrations increased. There was also a strong dependence of lithium K_d values on the smectite and zeolite content of the tuffs (Anghel et al. 2002 [DIRS 164635], pp. 822 to 824, Section 3.2). The range of laboratory-derived K_d values associated with each unit that could have participated in the Bullfrog and Prow Pass tests is listed in Table D-11 next to each corresponding field-derived K_d value.

The lithium K_d values deduced from the field tracer tests (assuming any given lithologic unit) are consistently higher than the corresponding K_d values measured at the lowest lithium concentrations in the laboratory. These results suggest that the use of laboratory-derived K_d values to predict sorbing species transport in the saturated fractured tuffs near the C-wells location would tend to underpredict the amount of sorption experienced by the species in the field. The fact that the field K_d values tended to be greater than the laboratory K_d values suggests that lithium may have come into contact with alteration minerals in the field that were not present or were depleted in the lab rock samples. Any loosely adhering alteration minerals (e.g., clays) that may have been present in the core samples would very likely have been lost during crushing and wet sieving of the material when it was prepared for the batch sorption experiments.

Table D-11. Lithium Partition Coefficients Derived from Field Tracer Tests and Laboratory Measurements

Parameter	Field K_d (mL/g)	Laboratory K_d^a (mL/g)
Prow Pass matrix K_d assuming Central Prow Pass Tuff	0.66	0.13 (0.26 at infinite dilution)
Prow Pass matrix K_d assuming Lower Prow Pass Tuff	1.68	0.084 (0.44 at infinite dilution)
Bullfrog matrix K_d in Pathway 1 assuming Central Bullfrog Tuff ^b	0.58–4.1 (nonlinear) ^c	0.19 (0.44 at infinite dilution)
Bullfrog matrix K_d in Pathway 1 assuming Lower Bullfrog Tuff ^b	0.58–4.1 (nonlinear) ^c	0.32 (1.64 at infinite dilution)
Bullfrog matrix K_d in Pathway 2 assuming Central Bullfrog Tuff ^b	0.74	0.19 (0.44 at infinite dilution)
Bullfrog matrix K_d in Pathway 2 assuming Lower Bullfrog Tuff ^b	3.04	0.32 (1.64 at infinite dilution)

Output DTN: LA0303PR831231.005.

NOTE: These lithium partition coefficients (K_d values) were derived from field tracer tests assuming transport in different lithologies within the test intervals.

^a Values at “infinite dilution” obtained from Langmuir isotherm fits to the data (asymptotic slope at very low concentrations (i.e., $K_L S_{max}$ – see Section C.1.2 for definitions). Other values obtained from a simple linear fit to the entire range of data.

^b “Pathway 1” refers to pathways that resulted in the first tracer peak in the Bullfrog reactive tracer test, and “Pathway 2” refers to pathways that resulted in the second peak in this test. K_d values were calculated from the smallest matrix retardation factors obtained from alternative interpretations of the test.

^c The first number corresponds to a K_d value calculated at approximately 600 mg/L Li^+ using the three-component cation exchange model parameters yielding the best fit to the first lithium peak (see Section C.3.1.3 for description of three-component model); the second number corresponds to a K_d value calculated at 0.5 mg/L Li^+ concentration using the same model parameters. In obtaining the field parameters, a matrix porosity of 0.10 was assumed in the MULTRAN V 1.0 (STN: 10666-1.0-00 [DIRS 159068]) simulations (approximately equal to that of the Central Bullfrog Tuff). The K_d values for pathway 1 would increase if a greater matrix porosity was assumed, and they would decrease if a smaller matrix porosity was assumed.

D4.8.5 Effective Flow Porosity

Contaminant transport predictions are generally very sensitive to assumed flow porosities because transport rates are directly proportional to the specific discharge divided by flow porosity. The effective flow porosity in a cross-hole tracer test without recirculation can be estimated from the following equation, which assumes a steady-state, two-dimensional (confined with fully penetrating well), homogeneous and isotropic flow system (Guimera and Carrera 2000 [DIRS 156830], Equation 6):

$$\eta = \frac{Q\tau}{\pi r_L^2 T} \quad (\text{Eq. D-6})$$

where

η = effective flow porosity

Q = production flow rate, m^3/hr

τ = mean residence or transport time, hr

r_L = distance between wells, m

T = formation thickness (assumed to be interval length).

With recirculation, the situation is complicated by the fact that there is a hypothetical stagnation point; hence, the mean tracer residence time theoretically approaches infinity. However, the interpretive method described in this report allows for incomplete tracer mass recoveries that could result from stagnation, so a finite estimate of the mean tracer residence time can always be obtained. Guimera and Carrera (2000 [DIRS 156830]) discuss an alternative method of estimating effective flow porosity from peak, rather than mean, tracer arrival times in tests with partial recirculation. However, their method was derived for system Peclet numbers (r_L/α) ranging from 10 to 100, which are considerably larger than the Peclet numbers obtained in the C-wells multiple-tracer tests (1.3 to 9.3); therefore, their method was not applied here.

For the mean tracer arrival times and flow conditions in the C-wells tracer tests, Table D-10 gives the effective flow porosities calculated using Equation D-6 for the Bullfrog and Prow Pass tests. The upper and lower bounds given in Table D-10 were calculated using the mean tracer residence times calculated assuming linear and radial flow, respectively (values in Tables D-6 and D-7). Also, in the Bullfrog test, it was assumed that 75% of the total production flow rate was associated with the first tracer peak and 25% was associated with the second tracer peak (based on flow survey information suggesting that a large amount of flow occurred in the upper part of the injection interval in c#2; DTN: GS931008312313.016 [DIRS 148173]).

The relatively large effective porosity estimates obtained from Equation D-6 could be due to heterogeneities in the flow field. Flow is undoubtedly not radial, as assumed in the above equations, but rather it very likely follows tortuous pathways between the injection and production wells. Furthermore, it is conceivable that a single high-conductivity feature, such as a large, open fracture or fault, could transmit the vast majority of the flow to the production well. If this feature does not pass near the injection well, the effective flow rate drawing tracers to the production well will be greatly reduced relative to what would occur in a radial flow field.

D4.8.6 Longitudinal Dispersivity

Longitudinal dispersivity estimates from cross-hole tracer tests generally have considerable uncertainty due to (1) uncertainty in the actual tracer transport distance (the actual flow pathways followed by tracers are unknown); (2) whether the flow field is radial, linear, or some combination; (3) the amount of apparent dispersion caused by nonidealities such as a poorly mixed injection wellbore or density/buoyancy effects; and (4) the amount of apparent dispersion caused by recirculation or the ambient flow field. It is beyond the scope of this report to address in detail the possible effects of each of these uncertainties on the longitudinal dispersivity estimates provided in Table D-10. These estimates can be considered “upper and lower bounds” that were obtained as follows.

1. The maximum transport distance, r_L , was assumed to be the distance from the top of one packed-off interval in the production well to the bottom of the packed-off interval in the injection well (80 to 100 m) while the minimum transport distance was assumed to be the linear distance between the wells (approximately 30 m).

2. The radial and linear Peclet numbers were used to obtain estimates of the dispersivity for the two cases above ($\alpha = r_L/Pe$), and the most extreme values were used for the upper and lower bounds.
3. The RELAP V 2.0 code (STN: 10551-2.0-00 [DIRS 159065]) simulated a gradual release of tracer from the borehole to the formation by assuming a well-mixed interval, resulting in an exponential decay in tracer concentration in the wellbore. The decay time constant was determined from the volume of the packed-off interval divided by the injection/recirculation rate. Thus, the slow release of tracers from the injection well did not bias the dispersivity (or mean residence time) estimates.
4. An attempt to “subtract out” the apparent dispersion caused by recirculation in the Prow Pass test was made by the following (Reimus 2003 [DIRS 165129], pp. 123 to 129).
 - a. Obtaining a simulated tracer response for a cross-hole test with the appropriate amount of recirculation in a homogeneous, isotropic medium using the 2WELLS_2D V 1.0 computer code (STN: 10665-1.0-00 [DIRS 159067])
 - b. Calculating the variance of the particle residence times in (a)
 - c. Calculating the variance of tracer response in the actual field test from $\sigma^2 = 2 \frac{\tau^2}{Pe}$ where σ^2 is the variance
 - d. Subtracting the variance in (b) from the variance in (c) to obtain the variance due to “true hydrodynamic dispersion”, σ_T , in the flow system (this assumes that the variance due to recirculation and the variance due to true dispersion are additive, which assumes that the two processes giving rise to the total variance are independent)
 - e. Rearranging the above expression to obtain the Peclet number and, hence, dispersivity, that represents true hydrodynamic dispersion; i.e., $Pe = 2 \frac{\tau^2}{\sigma_T^2}$.

Corrections for dispersion caused by recirculation in the Bullfrog test were assumed to be negligible because 2WELLS_2D V 1.0 (STN: 10665-1.0-00 [DIRS 159067]) simulations indicated that the variance in tracer transport times for 3.5% recirculation was very small (Reimus 2003 [DIRS 165129], Attachment A).

D4.8.7 Colloid Transport

The microsphere filtration and detachment rate constants deduced from the Bullfrog and Prow Pass tracer tests can potentially be used as estimates of filtration and detachment rate constants for natural colloids that could facilitate the transport of radionuclides strongly adsorbed to colloids. However, it must be kept in mind that the CML microspheres do not have the same physical and chemical properties as natural inorganic colloids [see the SZ colloid transport report

(BSC 2004 [DIRS 170006], Section 6.8)]. The SZ colloid transport report summarizes laboratory experiments (BSC 2004 [DIRS 170006], Section 6.8), in which it was shown that 330-nm-diameter CML microspheres transported with the same attenuation or less attenuation through saturated fractures than 100-nm-diameter silica spheres, suggesting that microsphere filtration and detachment rate constants may be conservative if used to predict silica colloid transport in fractured media.

Perhaps of greater importance than the microsphere filtration and detachment rate constants derived from the field tests is the fact that the microsphere responses qualitatively indicate that (1) colloid detachment from fracture surfaces is a process that clearly occurs in fractured tuffs, and (2) colloid detachment is apparently enhanced by flow transients. These qualitative results suggest that it is not sufficient to consider only colloid filtration when assessing colloid-facilitated radionuclide transport, but that colloid detachment and its dependence on other variables must also be considered and could possibly dominate the transport behavior of colloids. It is beyond the scope of this report to discuss how the dependence of colloid detachment on other variables should be incorporated into transport models. However, colloid detachment, in general, can be accounted for in models with simple first-order kinetics expressions.

D5. LIMITATIONS AND UNCERTAINTIES ASSOCIATED WITH TRANSPORT PARAMETER ESTIMATES

D5.1 LIMITATIONS AND UNCERTAINTIES INHERENT IN TRACER TESTING

Several factors contributed to the uncertainty in transport parameters derived from tracer test interpretations. First, there are data uncertainties which are related to the accuracy and precision of the tracer chemical analyses, including both random and systematic errors. Random errors were estimated to be small because the breakthrough-curve data are not widely scattered and show well-defined trends. The most significant sources of systematic errors would have been day-to-day differences in analytical instrument operation and in analytical standard preparation over extended periods of time. However, repeat measurements on separate days indicate that these errors were also minimal.

During the iodide tracer test in the Bullfrog-Tram interval (February to April 1996), the pump gradually failed, resulting in a decreasing flow rate during the entire test, which changed from 526 L/min (139 gpm) at the beginning to 371 L/min (98 gpm) at the end (Umari 2002 [DIRS 162858], Binder 5, Section G-10, pp. 65 to 77). This violated the assumption of a steady-state flow field in the Moench (1989 [DIRS 101146]) semi-analytic method employed to analyze the tracer test results. This source of uncertainty was eliminated for subsequent tests by replacing the pump.

There was uncertainty regarding the extent to which the tracers were evacuated from the injection intervals to the aquifer in each test. The very long injection intervals (ranging from 75 m to almost 200 m) and the lack of down-hole mixing contributed to this uncertainty. Slow release of tracers from the injection intervals could have contributed to tailing in the solute tracer responses that would have been interpreted as dispersion or matrix diffusion when only one nonsorbing tracer was used. Attempts to reduce this uncertainty in the Prow Pass tests were made by deploying a down-hole system capable of mixing the tracer solution after its injection

into the borehole. Although the down-hole mixing system worked only marginally, it is believed that lingering of tracer in the injection borehole was minimized because recirculation of 30% of the water produced from c#2 during the Prow Pass test should have served to “flush” tracers out of the injection interval.

The influence of the natural gradient that exists at the C-wells on tracer recovery at the pumped well is a source of uncertainty. Determinations of the capture zone of the pumped well, and how it is altered by the existence of a natural gradient depend on the assumptions made regarding flow heterogeneity and anisotropy. Mass not recovered by the pumped well is potentially the result of pathways other than the postulated radially convergent or partially recirculating streamlines toward the pumped well. However, it could also be a result of some of the tracer mass moving through the matrix rather than fractures; transport through the matrix would be so slow that the mass would not be expected to appear in the production well during the time of the tracer tests.

A limitation of all tracer tests conducted at the C-wells is that they produce estimates only of longitudinal dispersivity, not transverse dispersivity (because sampling occurs only at the production well and is not spatially distributed). In addition, the estimate of flow porosity has the uncertainty of an unknown travel distance between the tracer injection and production points in the boreholes (i.e., the source and the sink locations). This travel distance was bounded by assuming a minimum of the straight-line distance between the injection and production wells and a maximum of the formation thickness, defined by the distance between packers in the injection and the pumped intervals.

D5.2 UNCERTAINTIES ASSOCIATED WITH TEST INTERPRETATION METHODS

When estimating transport parameters using a semi-analytical solution to the advection-dispersion equation, such as the Moench (1989 [DIRS 101146]) solution or the RELAP V 2.0 computer code (STN: 10551-2.0-00 [DIRS 159065]) employed in this study, several assumptions are made. The medium is assumed to be homogeneous and isotropic, and the flow regime is assumed to be either radial or linear (i.e., having a velocity that varies as $1/r$ or having a constant velocity between injection and production well). Also, the aquifer is assumed to be two-dimensional (flow only in the two horizontal dimensions without a vertical component); to the extent that these assumptions do not reflect the true nature of the media, the transport parameter estimates will be erroneous. However, the information necessary to implement more sophisticated models that explicitly account for flow and transport heterogeneity does not exist. Even data to support stochastically generated hydraulic conductivity distributions in numerical models are scarce to nonexistent. Thus, the interpretive approaches used in this report reflect the level of knowledge of flow and transport heterogeneity at the scale of the tracer tests. Uncertainty associated with assuming either radial or linear flow (when the actual nature of the flow field could be somewhere in between) is addressed in the multiple tracer-test interpretations by reporting mean residence times and Peclet numbers for both radial and linear flow assumptions.

The Moench (1989 [DIRS 101146]; 1995 [DIRS 148784]) and RELAP V 2.0 (STN: 10551-2.0-00 [DIRS 159065]) semi-analytical solutions are mathematically very similar.

However, differences in the methodologies and assumptions used in the implementation of the models to interpret tracer responses result in differences in the resulting transport parameter estimates. Highlights of the differences in the two approaches are the following.

1. The first approach (Moench 1989 [DIRS 101146]; 1995 [DIRS 148784]; Section D1) involves normalizing tracer concentrations to the maximum (peak) tracer concentration, whereas the second approach (RELAP, Section D4.6) involves normalizing tracer concentrations to the injection mass. The first method results in matching the shapes of breakthrough curves (or differences in shapes when there are multiple tracers), while the second is aimed at matching not only shapes, but also peak normalized concentrations and total recoveries. Thus, the second method has some additional fitting constraints that result in different transport parameter estimates compared to the first method.
2. Both methods use essentially the same mathematical model to account for the tracer residence time in the injection borehole (i.e., a well-mixed interval with an exponential decay in tracer concentration). However, the mean residence time in the borehole was allowed to be much larger when running simulations using the first method (Section D1) compared to the second method (Section D4.6). A larger residence time in the injection borehole effectively adds dispersion to the simulated response curves, which results in a smaller flow-system dispersivity when the tracer data are fitted. Thus, the longitudinal dispersivity estimates from the first method tend to be lower than from the second method.

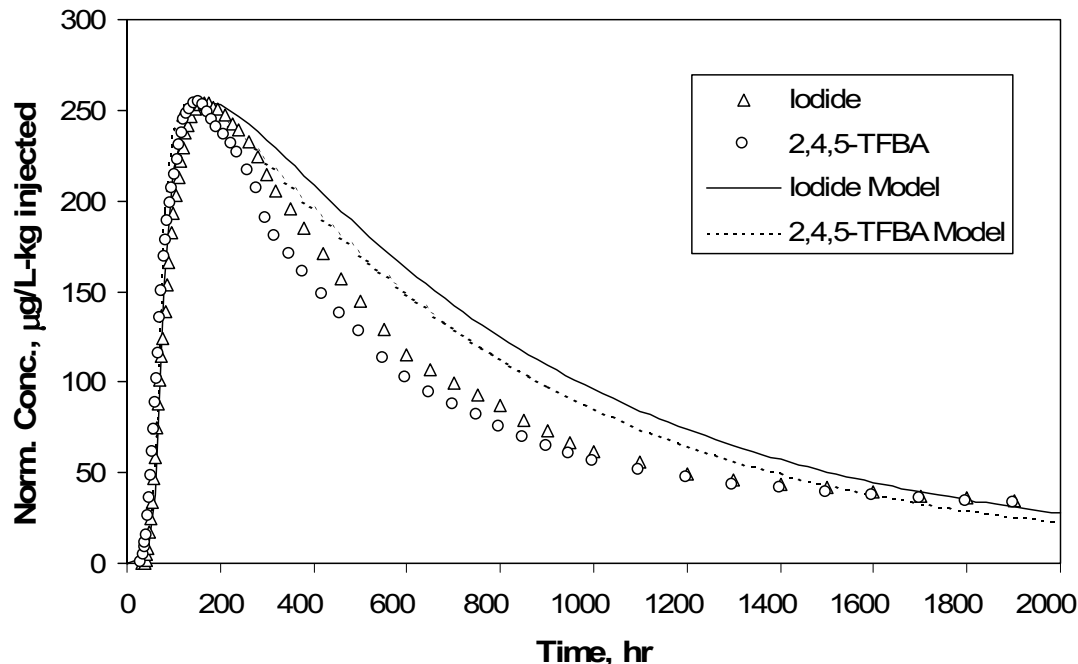
To assess the different results obtained from the two approaches qualitatively, the RELAP V 2.0 (STN: 10551-2.0-00 [DIRS 159065]) computer code was used to interpret the iodide and 2,4,5-TFBA tracer test in the Prow Pass Tuff. The Moench solution (Moench 1995 [DIRS 148784]) interpretation of this test is presented in Section D1.2.1. First, the parameters obtained from the Moench model analysis were used in RELAP to see how well the two solutions agree when using the same inputs. It can be shown through algebraic manipulations

that the mass transfer coefficient $\frac{\phi}{b} \sqrt{D_m}$ in RELAP is equivalent to $6 b' \sqrt{\frac{\sigma' \gamma'}{\tau}}$ in the Moench solution (Moench 1995 [DIRS 148784]), where b' = radius of spheres that represent matrix blocks (into which diffusion occurs), σ' = dimensionless storage parameter = $\frac{\phi}{\phi_f}$, and $\gamma' = \frac{D_m \tau}{\phi_f (b')^2}$. ϕ_f is the fracture porosity in this case, and τ is defined as $\frac{\pi h \phi_f (r_L^2 - r_w^2)}{Q}$, where h is

the aquifer thickness, r_L is the distance between the injection and production wells, r_w is the radius of the production well, and Q is the volumetric flow rate from the production well. Additionally, an injection borehole “mixing length” of 30.5 m was used in the Moench solution analysis of Section D1.2.1. This mixing length can be shown to translate to an injection borehole time constant of approximately 0.0023 hr^{-1} in the RELAP solution (time constant = $\frac{4 Q r_i}{2 \pi r_L} \left(\frac{1}{\pi r_i^2 h_i} \right)$, where r_i = injection well radius and h_i = mixing length

(Moench 1989 [DIRS 101146]). Using these input parameters, along with a Peclet number of 100 (i.e., a longitudinal dispersivity of 0.29 m), the RELAP code yields the fits shown in Figure D-31 (the mean residence time and mass fraction were adjusted to obtain these fits). The longitudinal dispersivity reported in Section D1.2.1 was 0.27 m. The tracer responses and fits in Figure D-31 are adjusted so that they all have the same maximum concentration, which is consistent with the analysis used in Section D1.2.1. A comparison of Figure D-31 and Figure D-16 shows that the two methods yield almost indistinguishable results when the same input parameters are used.

The injection borehole time constant of 0.0023 hr^{-1} used in the above analysis translates to a mean tracer residence time in the borehole of $1/0.0023$, or approximately 435 hr. This residence time is at odds with the tracer concentration measurements in the injection borehole described in Section D1.2.1.1, where it is stated that the borehole was effectively flushed of tracer in approximately 8.5 hr. The fact that the tracer was flushed from the borehole in such a short time is not surprising given that there was a continuous injection of approximately 1.5 gpm (approximately 5.7 L/min) of groundwater into the injection zone following the injection of tracers. A mean residence time of approximately 9 hrs is calculated by dividing the volume of the injection interval (approximately 3,000 L) by the 5.7 L/min flow rate. For these reasons, a second RELAP simulation was conducted in which it was assumed that the injection borehole

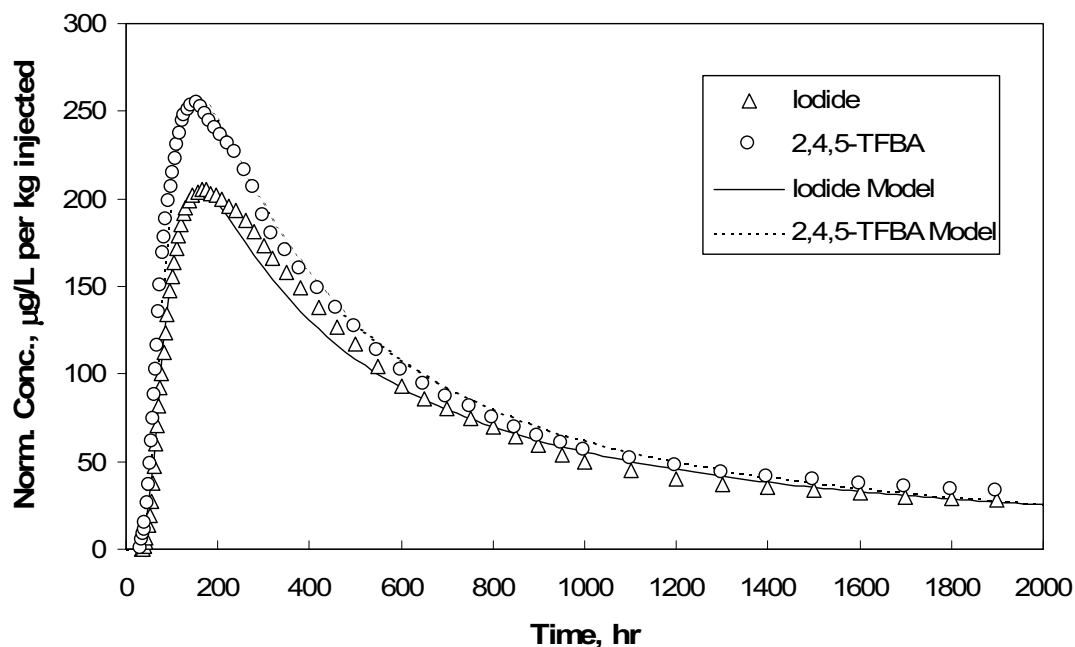


Output DTN: LA0304PR831231.001.

NOTE: Data points represent a subset of the actual data. Data and curves are adjusted so that they all have the same maximum normalized concentration (see Figure D-16 for comparison). The same parameters obtained from the Moench solution in Section D1.2.1 were used. "Model" refers to a fit generated by the RELAP code.

Figure D-31. RELAP Fits to the Iodide and 2,4,5-TFBA Responses in the Prow Pass Tuff Tracer Test Assuming an Injection Zone Time Constant of 0.0023 hr^{-1}

time constant was 0.11 hr^{-1} ($(5.7)(60)/3,000$). This is the same time constant value that was used in the analysis of the PFBA and bromide tracer test conducted in the Prow Pass Tuff described in Section D4.7.1. The resulting RELAP fits to the tracer data are shown in Figure D-32, where in this case the tracer concentrations are normalized to tracer injection mass, as in Section D4. The RELAP transport parameters for the simulations of Figures D-31 and D-32 are listed in Table D-12. Also listed in this table are the parameters obtained from RELAP fits to the PFBA and bromide data in the Prow Pass Tuff, discussed in Section D4.7. This test was conducted in the same configuration and with the same flow rates as the iodide and 2,4,5-TFBA test, although the volume of the tracer solution injected was considerably larger. Clearly, there is a very large difference in the mean residence times and Peclet numbers of the simulations with significantly different borehole time constants, although the iodide mass transfer coefficients, $\frac{\phi}{b} \sqrt{D_m}$, are in reasonably good agreement in all simulations.



Output DTN: LA0304PR831231.001.

NOTE: Data points represent a subset of the actual data. "Model" refers to a fit generated by the RELAP code.

Figure D-32. RELAP Fits to the Iodide and 2,4,5-TFBA Responses in the Prow Pass Tuff Tracer Test Assuming an Injection Borehole Time Constant of 0.11 hr^{-1}

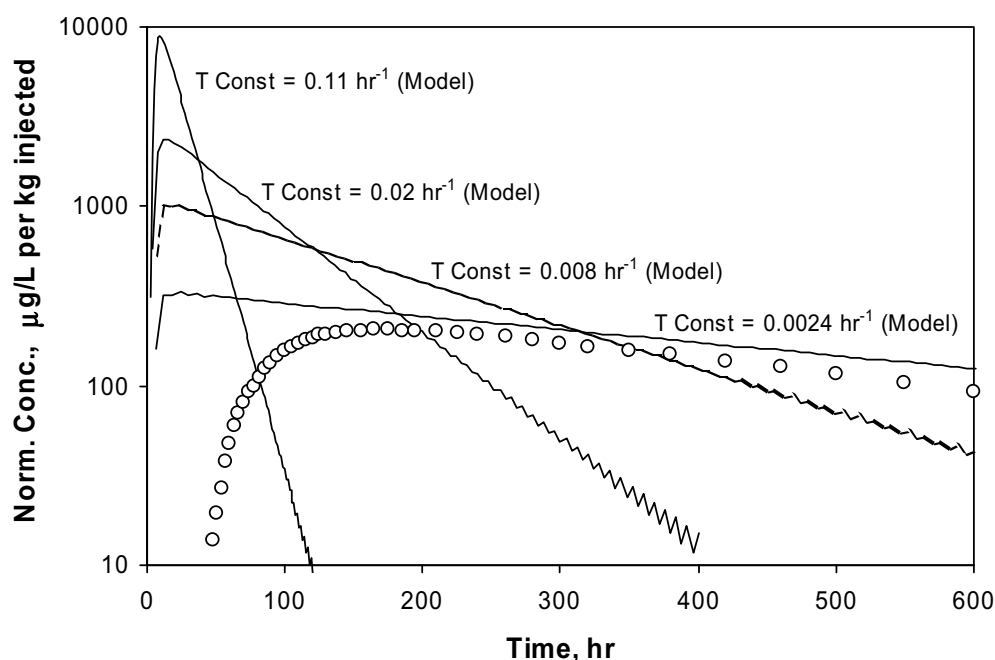
The reason for the large differences in mean residence times and Peclet numbers in Table D-12, particularly between the two interpretations of the iodide and 2,4,5-TFBA test, becomes clear when one considers the implications of the different borehole mixing assumptions. Figure D-33 shows tracer responses calculated by RELAP V 2.0 (STN: 10551-2.0-00 [DIRS 159065]) in a hypothetical system with a mean residence time in the aquifer (not the injection borehole) of 1 hr, a Peclet number of 100, and no matrix diffusion. With this choice of parameters, the responses are due almost entirely to tracer residence time in the injection borehole. The tails of the responses are linear on a semi-log plot because tracer concentrations in a well-mixed region decay exponentially. The curve with the largest time constant corresponds to the tracer residence time distribution in the borehole for the RELAP fits of Figure D-32, and the curve with the smallest time constant shows the residence time distribution associated with the fits of Figure D-31. The iodide response in the Prow Pass tracer test is also shown in Figure D-33. It is apparent that the curve with the smallest time constant has a tail that matches the tracer data quite well. Thus, to match the entire breakthrough curve, it is only necessary to impose a lag on the borehole response (accounted for by a finite residence time in the flow system), with only a very small amount of additional dispersion or matrix diffusion in the flow system necessary to optimize the fit. However, as the borehole time constants get larger, it becomes necessary to impose a greater lag and account for more dispersion or matrix diffusion in the flow system to achieve a match to the data.

Table D-12. Transport Parameters Estimates from RELAP Fits of Figures D-31, D-32, and from the Fits to the PFBA and Bromide Responses in the Prow Pass Tuff

Parameter	I, TFBA Figure D-31	I, TFBA Figure D-32	Br, PFBA Test
Borehole Time Constant, α , hr^{-1}	0.0023	0.11	0.11
Mean Res. Time, τ , hr (linear flow)	55	520	1210
Peclet number, Pe (linear flow)	100	1.6	0.9
MTC, $\frac{\phi}{b} \sqrt{D_m}$, $\text{s}^{-1/2}$	0.00161	0.001	0.000949

Output DTN: LA0304PR831231.001.

MTC=mass transfer coefficient; PFBA= pentafluorobenzoic acid or pentafluorobenzoate; TFBA= trifluorobenzoic acid



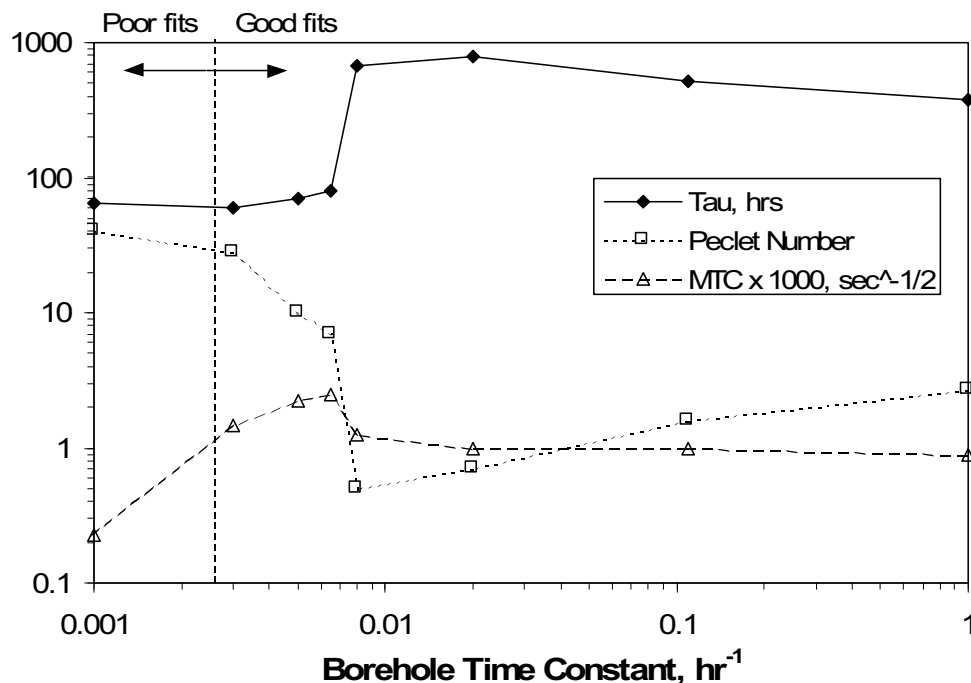
Output DTN: LA0304PR831231.001.

NOTE: Data points represent a subset of the actual data. Iodide data from the Prow Pass Tuff tracer test (Figures D-31 and D-32) are shown for comparison. See Section D4.7 for discussion. "Model" refers to a fit generated by the RELAP code.

Figure D-33. Tracer Responses as a Function of Injection Borehole Time Constant in a Hypothetical Flow System with a Mean Residence Time of 1 hr in the Aquifer, a Peclet Number of 100, and No Matrix Diffusion

Figure D-34 shows the mean residence times (in the aquifer), Peclet numbers, and mass transfer coefficients, $\frac{\phi}{b} \sqrt{D_m}$ or mass transfer coefficient (MTC), that provided best fits to the combined iodide and 2,4,5-TFBA tracer data sets as a function of borehole time constant. The fits were equally good until the time constant became less than about 0.0025 hr^{-1} , which roughly corresponds to the time constant used in Figure D-31. There is a sharp transition at a time constant of approximately 0.007 hr^{-1} , where residence times increase and Peclet numbers

decrease dramatically. This transition corresponds to the point where the tracer residence time in the borehole can no longer account for the majority of the dispersion in the tracer curves. Figure D-34 shows that the MTC does not vary nearly as much as the mean residence time and Peclet number, although it goes through a maximum at the transition point because of an attempt to account for tracer dispersion with increased matrix diffusion. This result is important because it indicates that despite the dramatic differences in mean residence time and Peclet number as a function of borehole time constant, matrix diffusion is always necessary to explain the tracer responses (at least until borehole residence times become so low that all fits are poor). Furthermore, the estimates of matrix diffusion parameters do not vary all that much. Thus, the various interpretations, while significantly different in mean residence time and Peclet number, are all consistent with a dual-porosity conceptualization of the fractured volcanics.



Output DTN: LA0304PR831231.001.

NOTE: Units on y axis depend on the curve.

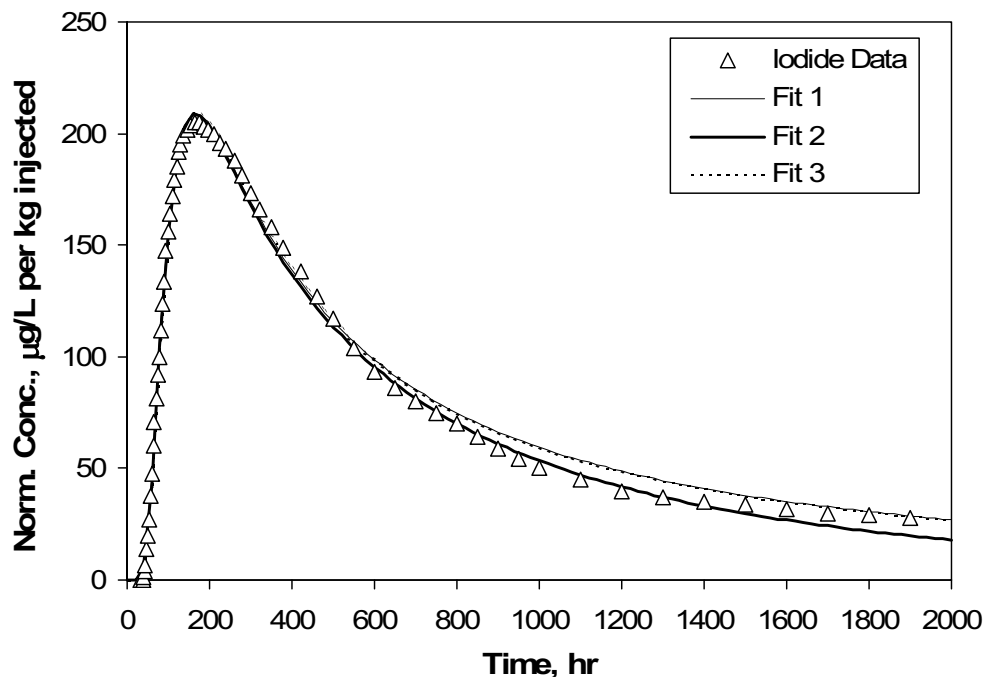
Figure D-34. Mean Residence Time (τ), Peclet Number, and MTC ($\times 1,000$) as a Function of Borehole Time Constant from RELAP Fits to the Iodide and 2,4,5-TFBA Data of Figure D-32

D5.3 UNCERTAINTIES ASSOCIATED WITH NONUNIQUENESS OF TEST INTERPRETATIONS

Nonuniqueness of tracer test interpretations must be considered before uncertainties in transport parameters derived from tracer tests can be fully addressed. A prime example of nonuniqueness is that long tails in tracer responses can be interpreted as either being the result of a large amount dispersion (assumed to be longitudinal but transverse dispersion may also play a role) or significant matrix diffusion. In the nonsorbing tracer tests, nonuniqueness was addressed by using PEST V 5.5 (STN: 10289-5.5-00 [DIRS 161564]) to obtain optimal transport parameter

estimates and to estimate confidence intervals associated with the parameters. In the multiple tracer tests, nonuniqueness of interpretations was minimized by simultaneously fitting the tracer responses using known ratios of diffusion coefficients as constraints on the relative matrix diffusion of different tracers. However, even after taking these measures, there is considerable nonuniqueness associated with tracer test interpretations.

First, nonuniqueness associated with the interpretation of responses of single tracers is addressed. Figure D-35 shows three RELAP V 2.0 (STN: 10551-2.0-00 [DIRS 159065]) fits to the iodide response in the Prow Pass tracer test shown in Figure D-32. These fits, which were obtained by arbitrarily fixing the Peclet number and then allowing the mean residence time, mass fraction, and MTC to be adjusted to achieve a fit, are arguably equally good. However, the best-fitting parameters, listed in Table D-13, vary by 2 to 4 orders of magnitude, and it is not even possible to distinguish between a single-porosity and a dual-porosity system (MTC can be zero). Clearly, nonuniqueness associated with interpreting single tracer responses is excessive and probably unacceptable for the purpose of transport parameter estimation.



Output DTN: LA0304PR831231.001.

NOTE: Data points represent a subset of the actual data. Parameters associated with the fits are listed in Table D-13. Fits 1 and 3 essentially fall on top of each other.

Figure D-35. RELAP Fits to Iodide Data from Prow Pass Tracer Test

Table D-13. Transport Parameters Obtained from RELAP Fits to Iodide Data Shown in Figure D-35

Parameter	Fit 1	Fit 2	Fit 3
Mass Fraction	0.23	0.11	0.24
Borehole Time Constant, hr ⁻¹	0.11	0.11	0.11
Mean Res. Time, τ , hr (linear flow)	50	700	9000
Peclet number, Pe (linear flow)	17	1.3	0.1
Iodide MTC, $\frac{\phi}{b} \sqrt{D_m}$, s ^{-1/2}	0.01	0.0	0.0001

Output DTN: LA0304PR831231.001.

A similar exercise in determining nonuniqueness of test interpretations was conducted for each of the multiple tracer responses (i.e., two in the Prow Pass Tuff and two in the Bullfrog Tuff (two peaks in this case)). Although the absolute best-fitting parameters in each case, as determined by minimizing the sum of squares of differences between the semi-analytical solution and data, are reported in Sections D1 and D4, there is still considerable nonuniqueness of the fits. If we arbitrarily establish a criterion that any sum of squares of differences less than 1.5 times the minimum is an equally good fit to the data, then the ranges of parameter values that provide equally good fits to the data sets are listed in Table D-14. Fits having sum-of-squares differences of less than a factor of 1.5 times the minimum are essentially equally good in appearance; and when one considers that the best fits are dependent on data scatter and on variability in data point density in the breakthrough curves (e.g., more data in tails as opposed to peaks), then a good case can be made that the fits are equally plausible. The parameter ranges were determined by varying each parameter in Table D-14 manually over a wide range of values while letting all other parameters in Table D-14 be adjusted to achieve fits to the data sets. Figure D-36 shows the fits to the iodide and 2,4,5-TFBA data from the Prow Pass tracer test (Figure D-32) that had the lowest and highest optimized sum-of-squares differences (with the highest still being within a factor of 1.5 of the lowest). Another “parameter” that was varied in the exercise was the ratio of the diffusion coefficients of halides (bromide and iodide) and fluorobenzoates (PFBA and TFBA) in the multiple tracer tests. This ratio is somewhat uncertain, especially in rock matrices, because most literature values are based on free water measurements. However, the values of the other transport parameters were found to be quite insensitive to this ratio when it was varied over a reasonable range.

Table D-14. Transport Parameter Ranges from Multiple-Tracer Tests at the C-wells

Parameter	BF, Peak 1	BF, Peak 2	PP, I-TFBA	PP, Br-PFBA
Mass Fraction	0.11 to 0.13	0.56 to 0.7	0.17 to 0.3	0.56 to 0.82
Mean Res. Time, τ , hr (linear flow)	320 to 420	700 to 1,800	340 to 1,340	600 to 1,900
Peclet number, Pe (linear flow)	5 to 8	0.9 to 2.4	0.6 to 2.6	0.6 to 1.9
Halide MTC, $\frac{\phi}{b} \sqrt{D_m}$, s ^{-1/2}	0.000837 to 0.00224	0.000245 to 0.000775	0.000775 to 0.00122	0.000632 to 0.00122

Output DTN: LA0304PR831231.001.

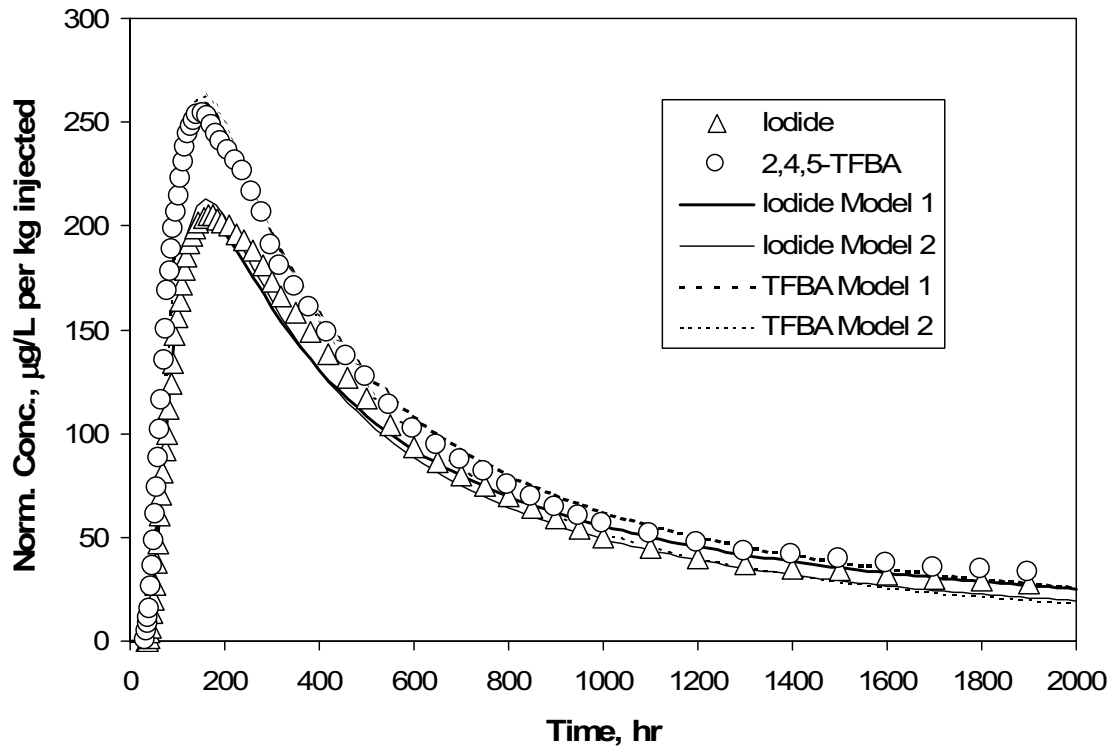
BF=Bullfrog; PFBA= pentafluorobenzoic acid or pentafluorobenzoate; PP=Prow Pass; TFBA= trifluorobenzoic acid.

It is important to note that the ranges of parameter values in Table D-14 are not completely independent of each other. That is, when one parameter value is taken from the high end of its range, another may have to be taken from near the low end of its range to achieve a good fit. This is especially true of the mean residence time and Peclet number, which have a very strong inverse correlation. Figure D-37 shows the relationship between best-fitting values of Peclet number and mean residence time for the four multiple-tracer tests at the C-wells. All of the points plotted in this figure are associated with equally good fits to the data according to the criterion stated in the previous paragraph. The range of mean residence times is significantly lower for the data set with the largest Peclet numbers compared to the three data sets with smaller Peclet numbers. This result was found to be true in general (i.e., the range of mean residence times was smaller for hypothetical tracer responses with less longitudinal dispersion).

Figure D-38 shows that the best-fitting mass fractions are positively correlated with the best-fitting mean residence times for the iodide and 2,4,5-TFBA responses in the Prow Pass Tuff. This result and Figure D-37 imply a negative correlation of mass fraction with Peclet number. These same trends were obtained for all other multiple-tracer tests. Interestingly, the

MTC, $\frac{\phi}{b} \sqrt{D_m}$, was poorly correlated with any of the other transport parameters. In fact, the extremes of MTC values were generally associated with values of other parameters not near the ends of their respective ranges. Also, the range of MTC values never included zero, which indicates that a dual-porosity system is always implied from the fits.

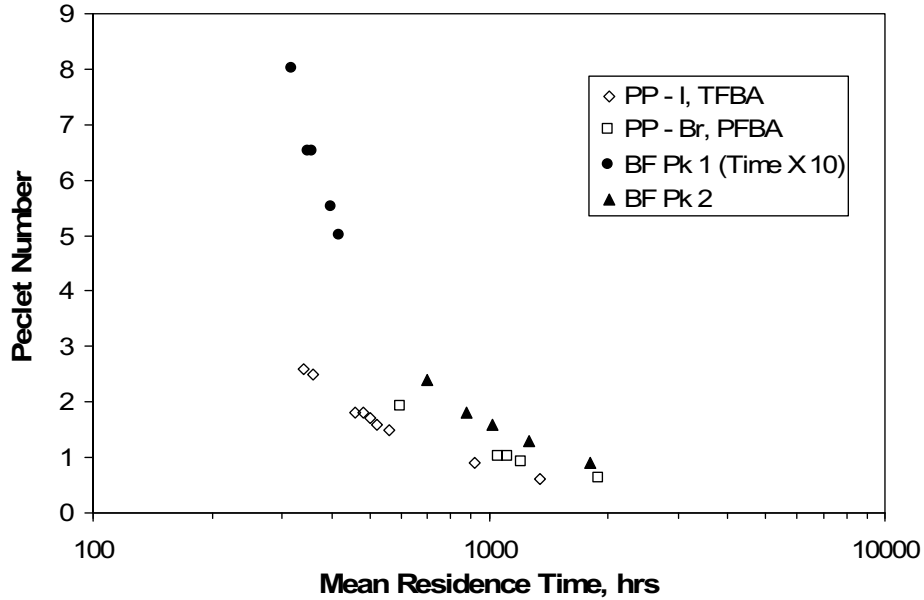
The parameter ranges in Table D-14 reflect considerable uncertainty associated with the nonuniqueness of interpretive fits for multiple tracer tests. These ranges, in general, are comparable in magnitude to the ranges of derived parameter values provided in Table D-10, which were based on uncertainties in tracer travel distances and radionuclide diffusion coefficients, as well as the range of parameter values obtained from different tests in the same interval. The ranges in Table D-10 would have to be expanded somewhat to account for the additional uncertainty associated with the nonuniqueness of fits. Expanding these ranges by multiplying the lower value of any parameter in Table D-10 by 0.5 and the upper value by 2 would effectively capture this additional uncertainty.



Output DTN: LA0304PR831231.001.

NOTE: Data points represent a subset of the actual data. Bold curves represent the best fits to data. The sum of squares differences between data and curves are within a factor of 1.5 of each other. "Model" refers to a fit generated by the RELAP code.

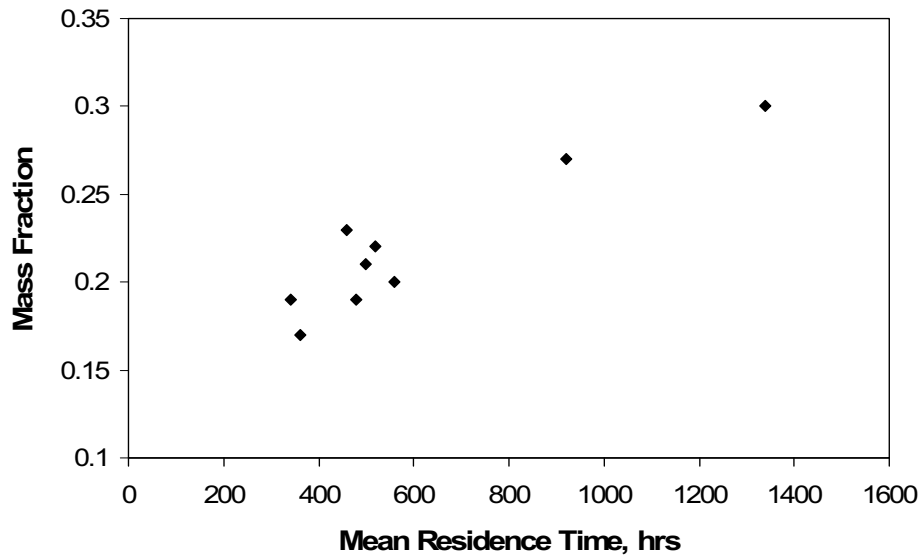
Figure D-36. RELAP Fits to the Iodide and 2,4,5-TFBA Data from the Prow Pass Tracer Test



Output DTN: LA0304PR831231.001.

NOTE: PP refers to Prow Pass; BF refers to Bullfrog. The residence times (but not Peclet numbers) are multiplied by 10 for peak 1 of the Bullfrog Tuff tracer test.

Figure D-37. Correlation Between Best-Fitting Peclet Numbers and Mean Residence Times for the Multiple-Tracer Tests at the C-Wells



Output DTN: LA0304PR831231.001.

Figure D-38. Correlation Between Best-Fitting Mass Fractions and Mean Residence Times for the Multiple-Tracer Tests at the C-Wells

A few points are worthy of mention regarding uncertainty associated with nonuniqueness of the semi-analytical solution fits to obtain transport parameter estimates:

1. Although there is considerable uncertainty associated with model fits to multiple-tracer data sets, the uncertainty is far less than the uncertainty associated with fits to single-tracer data sets (compare Tables D-13 and D-14). Also, all the fits to multiple-tracer data sets indicated a dual-porosity system (in which flow occurs primarily through fractures but with a significant volume of stagnant or near-stagnant water in the matrix that is in diffusive communication with the flowing water), while fits to single-tracer data sets cannot effectively distinguish between a single- and dual-porosity transport system.
2. This uncertainty analysis and discussion is by no means complete. Other factors must be considered when doing a rigorous uncertainty analysis. A couple of additional considerations that go beyond the scope of this report are:
 - When fitting multiple data sets, one must be careful to not inadvertently give one set more weight than the others in the fitting procedure. Inappropriate weighting can occur, for instance, when one data set has significantly more data points than the other(s) or when one set has much larger numerical values than the other(s). Approaches to dealing with this problem include (1) various weighting schemes, (2) making the number of data points the same for all data sets (by dropping some data from the larger data sets), or (3) normalizing the sum-of-squares errors for each data set by dividing by the number of points fitted for each set. Each of these approaches introduces some arbitrary bias into the fitting procedure, which introduces bias into the errors associated with the parameter estimates. In this report, we use approach (3).
 - The fitting criteria (or objective function) are very important and can have a significant influence on both parameter estimates and error estimates. For instance, one will obtain different answers if the sum-of-squares differences between semi-analytical solution and data are minimized vs. minimizing the sum-of-squares differences between the log of the data and the solution. In this report, it was chosen to minimize the straight sums-of-squares differences rather than the differences in any transformations of the data and solution values.

Although the transport parameter uncertainty analysis is not necessarily complete or entirely quantitative, it is important to point out that the uncertainties in the parameter estimates obtained from tracer testing are considered to be very effectively, and even conservatively, captured in *Saturated Zone Flow and Transport Model Abstraction* (BSC 2004 [DIRS 170042]). Thus, conservatism is ultimately built into the downstream propagation of transport parameter uncertainties in the TSPA.

D6. CONCLUDING REMARKS ABOUT FIELD TRACER TESTS

It is recognized that the tracer-test interpretations using primarily semi-analytical solution methods that assume an idealized geometry and steady flow rates are a considerable simplification of reality. Numerical models could certainly be used to account for greater system heterogeneity. Also, more sophisticated semi-analytical representations of dual-porosity systems, such as the multirate-diffusion solution of Haggerty and Gorelick (1995 [DIRS 156831], pp. 2,383 to 2,400), could be applied. However, the information available to support these more sophisticated representations of the flow and transport system is sparse to nonexistent. Furthermore, the agreement between the relatively simple semi-analytical solutions (either the Moench 1989 [DIRS 101146]; 1995 [DIRS 148784]) solution or RELAP (LANL 2002 [DIRS 159065]) and the tracer responses are considered to be very good. The only additional interpretive complexity needed to explain any portion of the tracer-test data sets was the multicomponent transport and ion exchange capabilities of the MULTRAN V 1.0 (STN: 1066-1.0-00 [DIRS 159068]) code needed to match the lithium response in the first peak of the Bullfrog tracer test. Although the introduction of additional interpretive complexity could improve the agreement between solution and data, it appears that all of the critical features of the tracer responses are effectively captured, and the introduction of additional complexity, especially in light of the minimal information to support it, is not justified.

One must also keep in mind that the tracer-test results are intended to support predictive calculations that span much larger time and distance scales than represented by the test. With this in mind, it is desirable to capture the important transport processes with as concise an interpretation as possible so that others can incorporate a relatively simple conceptual model on a local scale into a more sophisticated flow model that captures the important hydraulic features of the larger-scale flow system. It is believed that the C-wells tracer tests and their interpretations presented in this report accomplish this objective.

INTENTIONALLY LEFT BLANK

APPENDIX E

**LABORATORY TESTING CONDUCTED TO SUPPORT INTERPRETATIONS OF
TRACER TESTS AT THE C-WELLS COMPLEX**

E1. BATCH TESTING OF LITHIUM SORPTION TO C-WELLS TUFFS

E1.1 MATERIALS AND METHODS

The batch lithium sorption experiments were conducted as follows (full details of the sorption measurements are provided in “YMP C-Wells Sorption” (Reimus 2000 [DIRS 164625]):

- C-wells core from a stratigraphic unit of interest was crushed, pulverized, and passed through a 500- μm sieve but retained on a 75- μm sieve.
- A specified amount of crushed tuff was added to polycarbonate (polyallomer) Oak Ridge centrifuge tubes. In some experiments, the tuff and centrifuge tubes were autoclaved prior to contacting the tuff with the lithium solution.
- The tuff was preconditioned with filter-sterilized (0.2- μm filter) J-13 well water.
- A specified amount of lithium-bearing water (either from well J-13 or well c#3) was added to the preconditioned tuff, and the mixture was continuously shaken for 24 hr to 72 hr at either 25°C or 38°C. Previous studies had indicated that lithium sorption equilibrium onto C-wells tuffs was reached in approximately 1 hr (Newman et al. 1991 [DIRS 156849], pp. 818 to 824), so 24 hr should have been sufficient to achieve equilibration between solid and solution.
- After equilibration, the tubes were centrifuged and a portion of the supernate was filtered (0.2- or 0.4- μm filter) for tracer analysis to determine the tracer concentration remaining in solution. Lithium was analyzed by inductively coupled plasma-atomic emission spectrometry (ICP-AES).
- The mass of tracer sorbed to the tuff was determined by mass balance, with corrections if necessary, to account for sorption to the container walls, which was measured in control experiments in which tuff was omitted.
- All measurements were made in duplicate or triplicate.

Sorption isotherms were determined under several different experimental conditions:

- 1:1 solution:solid ratio in J-13 water at 25°C
- 1:1 solution:solid ratio in J-13 water at 38°C
- 2:1 solution:solid ratio in J-13 water at 25°C
- 4:1 solution:solid ratio in C-3 water at 38°C
- 4:1 solution:solid ratio in J-13 water at 25°C
- 4:1 solution:solid ratio in J-13 water at 38°C.

The two temperatures were intended to approximate the range of conditions under which sorption would occur in either the laboratory or the field [the groundwater temperature in the Bullfrog Tuff at the C-wells ranges from about 38°C to 45°C (Geldon 1993 [DIRS 101045], pp. 68 to 70, Figures 31 to 33)].

At the time of these studies, groundwater from the C-wells complex was not consistently available, so groundwater from well J-13, located 4 km southeast of the C-wells complex, was used as a surrogate in most tests. J-13 well water is well-characterized and has become a de facto standard groundwater for use in Yucca Mountain sorption studies (Harrar et al. 1990 [DIRS 100814], pp. 6.6 to 6.7; Triay et al. 1997 [DIRS 100422], pp. 11, 16, and 45). A comparison of J-13 and C-wells groundwater chemistry shows that the two waters are both sodium bicarbonate dominated and, in all regards, quite similar (Table E-1). Lithium solutions for sorption tests were prepared by dissolving reagent-grade lithium bromide in either c#3 or J-13 well water. All solutions were filter-sterilized before use.

Table E-1. Comparison of Major Ion Chemistry of J-13 and c#3

Species	Concentration ($\mu\text{g/mL}$)	
	J-13	c#3
Ca	12.0	11.0
Cl	7.1	7.2
K	5.0	1.9
Mg	2.1	0.4
Na	42.0	55.0
SiO ₂	47.0	53.0
SO ₄	17.0	22.0
HCO ₃	124.0	137.0
pH	7.2	7.7

Sources: DTNs: MO0007MAJIONPH.013 [DIRS 151530] (J-13);
MO0007MAJIONPH.011 [DIRS 151524] (c#3).

A few tests were conducted in a sodium bicarbonate solution having the same ionic strength as J-13 well water but without the calcium and other cations present in J-13 well water. Lithium sorption in this solution was noticeably greater than in J-13 well water, presumably because of the absence of cations that compete with lithium for sorption sites (primarily calcium). The results of these experiments are reported in a scientific notebook by Callahan (2001 [DIRS 165123]), but not in this appendix.

Ion-exchange theory suggests that the actual ion-exchange process is rapid and will reach equilibrium quickly; in natural systems, apparent equilibration rates are limited by diffusion of ions through the solution to the mineral surface (Bolt et al. 1978 [DIRS 113856], pp. 54 to 90). In a well-mixed system, such as a shaken centrifuge tube, diffusion is not limiting, and equilibration should be achieved quickly. A previous study of lithium sorption to the Prow Pass member of the Crater Flat Tuff found that sorption equilibrium was reached within 1 hr,

confirming this hypothesis (Newman et al. 1991 [DIRS 156849], pp. 818 to 824). For consistency with other sorption studies and for scheduling convenience, a minimum equilibration period of 24 hours was adopted for these studies.

Tuffs from seven different lithologies were tested, including two samples of the same unit (the central Bullfrog Tuff) from two different holes (c#1 and c#2), to allow an assessment of spatial heterogeneity in lithium-sorption parameters. The experimental matrix of tuffs, groundwaters, temperatures, and solid-solution ratios is summarized in Table E-2. Figure E-1 shows the sampling locations of the C-wells core used in the experiments. This figure is essentially identical to Figure 6.1-2 except that the triangles indicating flow zones in the wells have been replaced with triangles identifying locations of core samples used in the batch experiments.

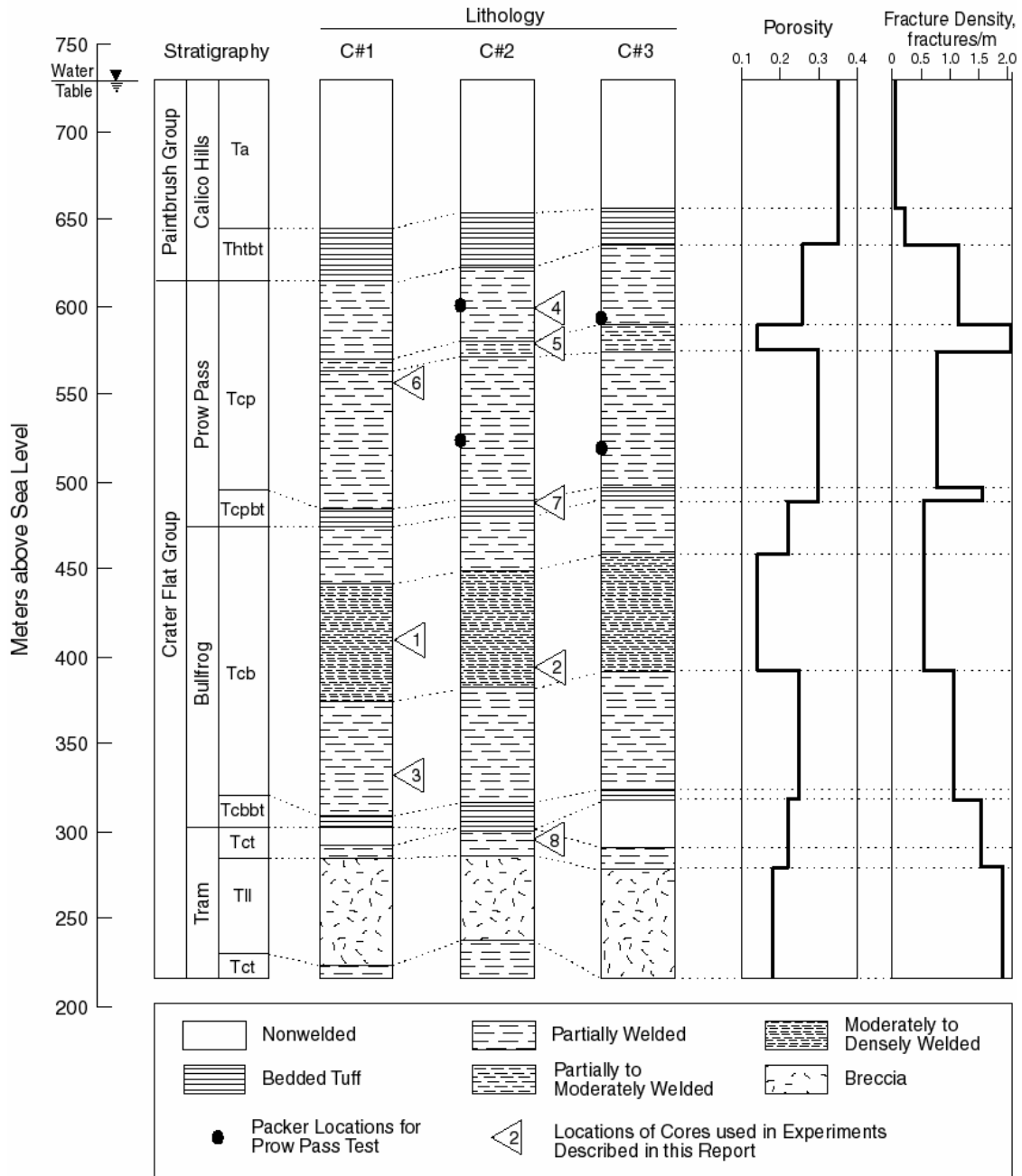
Batch-sorption experiments were also conducted on each of the tuffs to determine whether pentafluorobenzoate (PFBA) and bromide sorbed to them. The bromide experiments were actually conducted simultaneously with the lithium experiments, as lithium was added to the solutions as lithium bromide. The starting bromide concentrations ranged from approximately 10 parts per million (ppm) to approximately 1,000 ppm. The PFBA experiments were conducted at a single concentration (1 ppm). These experiments were conducted on each rock type at 25°C. There was no measurable sorption of PFBA or bromide on any of the tuffs (DTN: LA0302PR831231.001 [DIRS 162605]).

Table E-2. Summary of C-Wells Experimental Batch Lithium Sorption Test Matrix

Tuff (Lithology, Borehole, Depth (m))	Water (Well ID)	Solution: Solid (mL:g)	Temperature (°C)
Central Bullfrog, c#1, 715 m (1)	J-13	2:1	25
	J-13	2:1	38
Central Bullfrog, c#2, 734 m (2)	J-13	1:1	25
	J-13	1:1	38
	c#3	4:1	38
Lower Bullfrog, c#1, 795 m (3)	J-13	4:1	25
	J-13	4:1	38
	J-13	2:1	25
Upper Prow Pass, c#2, 533 m (4)	J-13	4:1	25
	J-13	4:1	38
	J-13	2:1	25
Central Prow Pass, c#2, 553 m (5)	J-13	4:1	25
	J-13	4:1	38
	J-13	2:1	25
Lower Prow Pass, c#1, 573 m (6)	J-13	4:1	25
	J-13	4:1	38
	J-13	2:1	25
Bedded Prow Pass, c#2, 643 m (7)	J-13	4:1	25
	J-13	4:1	38
	J-13	2:1	25
Upper Tram, c#2, 839 m (8)	J-13	4:1	25
	J-13	4:1	38
	J-13	2:1	25

Source: DTN: MO0012SORBCHOL.000 [DIRS 153375].

NOTE: The numbers in parentheses correspond to the numbers in Figure E-1 (the locations where core was collected from the C-wells).



Sources: Geldon 1993 [DIRS 101045], pp. 35 to 37, 43 to 51, and 58 to 64, for lithology, stratigraphy, porosity, and fracture density information. Umari 2002 [DIRS 162858], Binder 10, Section L-11, pp. 70 to 71, Section L-9, pp. 57 to 58, for packer locations. Reimus 2000 [DIRS 165124], pp. E1 to E10, M1 to M14, Q1 to Q20, W1 to W15, X1 to X14, AB1 to AB11, and AC1 to AC17, for locations of core samples.

NOTE: The numbers in the figure correspond to the numbers in Table E-2. Also shown are approximate locations of packers for the tracer tests in the Prow Pass Tuff.

Figure E-1. C-Wells Hydrogeology Showing Sampling Locations of All Cores Used in the Laboratory Experiments Described in Sections E1, E2, and E3

The mineralogy of the tuffs used in the batch-sorption experiments is listed in Table E-3. The mineralogy was determined from quantitative X-ray diffraction analyses. The tuffs differ primarily in their smectite and zeolite (clinoptilolite and mordenite) content, both of which have high cation-exchange capacities and would be expected to sorb lithium quite strongly compared to other minerals present in the rocks (Anghel et al. 2002 [DIRS 164635], Section 3.2, pp. 822 to 824).

Table E-3. X-Ray Diffraction Results for Tuffs from Prow Pass, Bullfrog, and Tram Units

Tuff	Depth (m)	Concentration (wt %)				
		Smectite	Clinoptilolite	Mordenite	Analcime	Calcite
Central Bullfrog, c#1	715	2 ± 1	—	—	—	2 ± 1
Central Bullfrog, c#2	734	5 ± 2	—	—	—	—
Lower Bullfrog, c#1	795	9 ± 3	4 ± 1	3 ± 1	12 ± 1	4 ± 1
Upper Prow Pass, c#2	533	—	—	—	—	Trace
Central Prow Pass, c#2	553	2 ± 1	—	—	—	2 ± 1
Lower Prow Pass, c#1	573	2 ± 1	—	—	—	—
Bedded Prow Pass, c#2	643	—	—	20 ± 4	39 ± 2	—
Upper Tram, c#2	839	1 ± 1	—	—	—	—

Sources: DTNs: MO0012MINLCHOL.000 [DIRS 153370]; LA9909PR831231.004 ([DIRS 129623] for Central Bullfrog c#2 only (qualified for use in this report in Appendix J).

NOTE: c#1, c#2, and c#3 are abbreviations for Boreholes UE-25 c#1, UE-25 c#2, and UE-25 c#3, respectively. Trace: trace abundance of less than 0.5 wt %. Only the main sorptive mineral fractions are listed; the balance of the tuffs was mostly quartz and feldspar with small amounts of hematite, mica/illite, and/or kaolinite. Dashes indicate “not measured.”

A lithium-specific cation-exchange-capacity (CEC) method was developed to quantify the lithium affinity for the selected tuffs. The method involved two steps: saturation of the exchange sites with lithium, followed by displacement of the lithium and other cations with cesium. The mineralogical composition of the samples was preserved as close as possible to the field conditions; therefore, no pretreatment was applied to remove carbonate or organic matter. The method involved the following steps (Anghel et al. 2002 [DIRS 164635], Section 3.2, pp. 822 to 824).

- The tuff samples were crushed and wet-sieved with J-13 well water to a particle-size range between 75 µm to 500 µm. Then approximately 5 g of each tuff was weighed into a 50-mL centrifuge Teflon tube. Each tuff sample was tested in triplicate.
- The samples were saturated three times with 30 mL of 0.8 N LiBr–0.2 N LiOAc solution to ensure replacement of cations present on mineral surface sites with lithium. The pH of the solution was maintained at approximately 8.2 to prevent dissolution of calcite. After each LiBr addition, the tubes were sonicated to disperse the centrifuged sediment, and then the samples were shaken for 30 min.
- The samples were centrifuged at 10,000 rpm for 15 min to achieve a good separation of solids and solution. The supernatant from each lithium-sorption step was combined and analyzed for sodium, potassium, calcium, and magnesium.

- After the Li-sorption steps, the tuff present in each centrifuge tube was washed three times with 30 mL of 1 N CsCl to remove the sorbed lithium. The combined supernate from centrifuging was analyzed for lithium, sodium, calcium, potassium, and magnesium. Residual lithium saturating solution remaining in the centrifuge tubes was accounted for by analyzing for bromine and making the appropriate correction. Cesium has more affinity for zeolites, and it should, therefore, displace more cations than lithium. In many cases, cesium sorption gives a measure of the total CEC (lithium measurements of the aliquots give the CEC for lithium–cesium exchange).

The method described yields two different CEC results: (1) CEC–LiT, the total CEC available to lithium, estimated from the total cations displaced by lithium in the saturation step; and (2) CEC–CsT, the total CEC available to cesium, estimated from the total cations displaced by cesium in the displacement step. CEC–CsT can be further subdivided into CEC–CsLi based on the lithium displaced by cesium, and CEC–CsNat, based on the native cations (sodium, potassium, calcium, magnesium) displaced by cesium. Each of these results is expressed in milliequivalents per 100 g of dry tuff.

E1.2 RESULTS AND DISCUSSION

During the course of the experiments, it became apparent that lithium sorption was essentially independent of solution:solid ratio, temperature, and water composition (J-13 or c#3) over the range of conditions studied. Therefore, the data sets for a given tuff lithology were combined to estimate sorption parameters. Three common isotherm models, defined as follows, were fitted to the data for each tuff.

(1) Linear Isotherm:

$$S = K_d C \quad (\text{Eq. E-1})$$

where

S = equilibrium sorbed concentration ($\mu\text{g/g}$)
 C = equilibrium solution concentration ($\mu\text{g/mL}$)
 K_d = linear distribution coefficient (mL/g).

(2) Freundlich Isotherm:

$$S = K_F C^n \quad (\text{Eq. E-2})$$

where

K_F = Freundlich coefficient ($\text{mL}/\mu\text{g})^n(\mu\text{g/g})$
 n = Freundlich exponent (dimensionless).

(3) Langmuir Isotherm:

$$S = \frac{K_L S_{\max} C}{1 + K_L C} \quad (\text{Eq. E-3})$$

where

K_L = Langmuir coefficient (mL/ μ g)

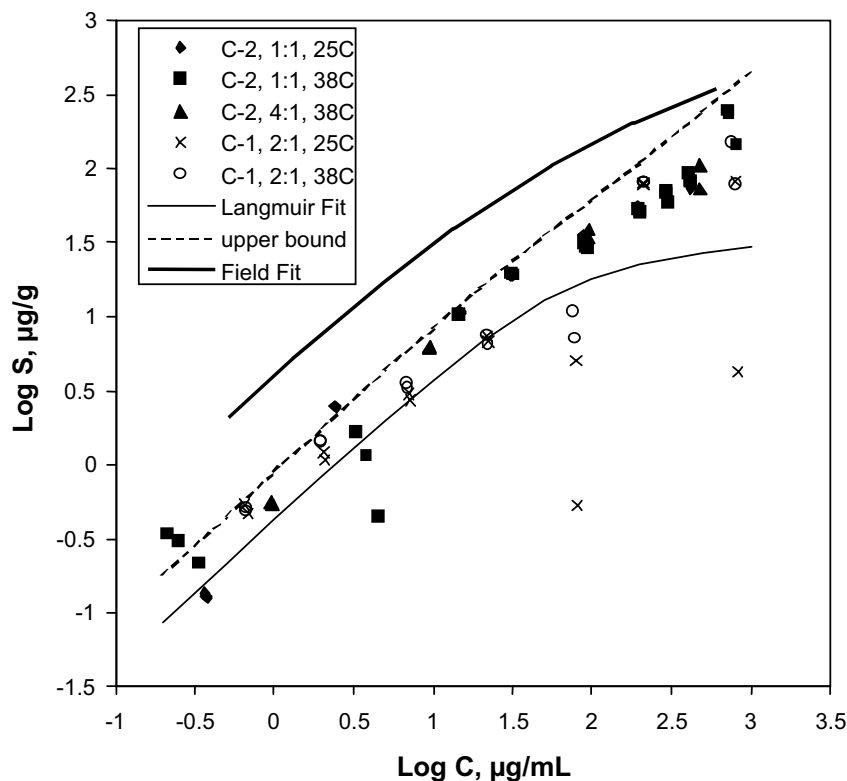
S_{\max} = maximum attainable solid sorption capacity (μ g/g).

Figures E-2 to E-8 show the experimental data for each tuff plotted as log-equilibrium-sorbed concentration, S (μ g/g), versus log-solution concentration, C (μ g/mL). A Langmuir isotherm consistently yielded better visual fits to the data than the other isotherms, so a fitted Langmuir isotherm is also shown in each figure. The Langmuir isotherm is the only one that captures the curvature of the data when graphed on log-log axes. Furthermore, only the Langmuir isotherm recognizes the finite sorptive capacity of the solid matrix; the other models imply potential infinite sorption. A previous study of lithium sorption to the Prow Pass member of the Crater Flat Tuff also revealed Langmuir behavior (Newman et al. 1991 [DIRS 156849], pp. 818 to 824). The Langmuir, Freundlich, and linear isotherm parameters associated with the data in Figures E-2 to E-8 are given in Table E-4. It is concluded that a Langmuir isotherm provides the best representation of lithium sorption onto C-wells tuffs. However, a detailed statistical analysis to quantify how much better this representation is relative to the other isotherms (or whether it is statistically better) was not conducted. Statistical analyses were not conducted to determine whether there were significant isotherm differences as a function of temperature, solid-solution ratio, or core taken from different locations in the same lithological unit (i.e., the Central Bullfrog Tuff from c#1 or c#2). However, it appears from Figures E-2 to E-8 that any of these differences should have been minimal.

The error bounds shown in Figures E-2 to E-8 reflect the propagation of analytical errors associated with lithium concentration measurements in the solutions before and after contact with the sorbing tuffs (Reimus 2003 [DIRS 165129], p. 126). These bounds are shown relative to the fitted Langmuir isotherms, not relative to individual data points. The bounds were calculated assuming a 10% relative standard deviation in the lithium concentration measurements, which is high for ICP-AES measurements but it also serves to account for other experimental errors, such as imperfect separations of solid and solution phases during centrifugation. Errors increase as concentrations increase because there is a lower percentage of lithium sorbing at higher concentrations and, hence, a smaller relative difference between measured initial and final solution concentrations. It is apparent that the scatter in the data sets often exceeds the analytical error bounds, suggesting greater than 10% error in some of the measurements.

In Figures E-2 to E-6, the lithium isotherm associated with the ion-exchange parameters used in MULTRAN V 1.0 (STN: 1066-1.0-00 [DIRS 159068]) to obtain a good match to either the first lithium peak in the Bullfrog Tuff tracer test (Figure D-26) or the lithium response in the Prow Pass Tuff tracer test (Figure D-27) are plotted along with the laboratory data and the Langmuir isotherm fits to the laboratory data. In all cases, the isotherms derived from the simulations of the field data indicate greater lithium sorption in the field than the best-fitting Langmuir isotherms derived from the laboratory experiments. A likely explanation for this result is that the lithium in the field tests came into contact mineral surfaces that were not present or were under-represented in the small-scale laboratory tests. "Field" isotherms are not shown in Figures E-7 and E-8 because the Bedded Prow Pass and Upper Tram Tuff lithologies were not part of the packed-off intervals in the reactive tracer tests.

The fitted Langmuir isotherms corresponding to all seven C-wells tuff lithologies are plotted together in Figure E-9. By comparing Figure E-9 to the X-ray diffraction results of Table E-3, it is apparent that the two tuffs demonstrating the greatest affinity for lithium (Bedded Prow Pass and Lower Bullfrog) are also the tuffs that have the greatest smectite and/or zeolite contents. A quantitative relationship between lithium sorption and tuff mineralogy is discussed further below.

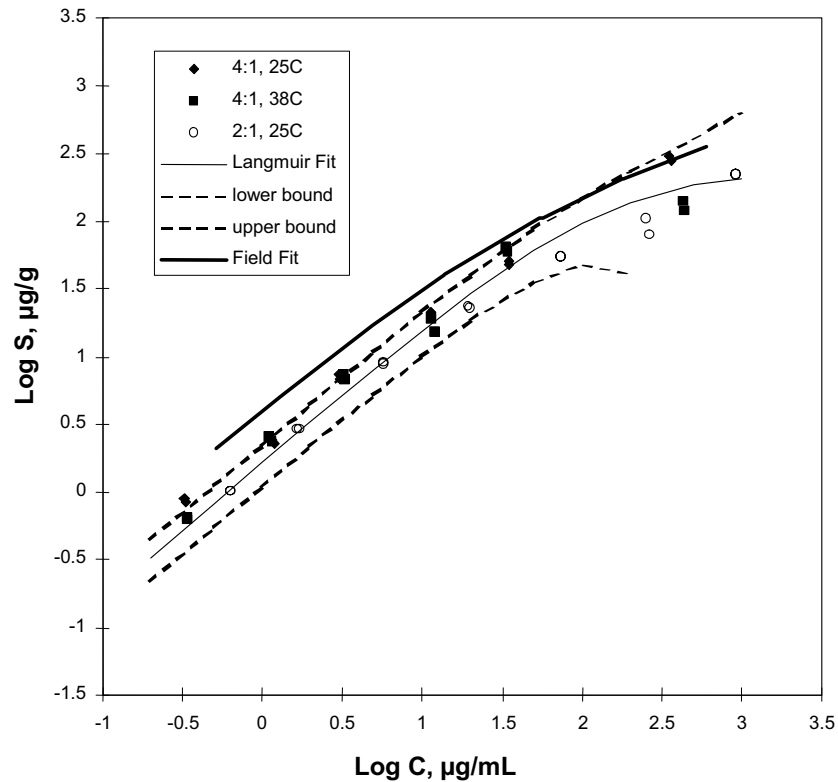


Source: DTN: MO0012SORBCHOL.000 [DIRS 153375] (data).

Output DTN: LA0303PR831341.003 (isotherm fits).

NOTE: C-1 and C-2 refer to UE-25 c#1 and c#2, respectively. The legend indicates the borehole (c#1 or c#2) from which the tuff came, the solution:solid ratio (mL:g), and the temperature of the experiments. The dashed line is an upper error bar associated with a 10% experimental error (this error bar is plotted relative to the Langmuir isotherm line – lower error bound is off-scale over the entire range of data). The method for calculating the error bars is described by Reimus (2003 [DIRS 165129], p. 126). J-13 well water was used in all experiments except for “C-2, 4:1, 38C.” Water from c#3 was used for “C-2, 4:1, 38C.” The lithium concentration range in the Bullfrog Tuff field test spanned from less than 0.1 µg/mL up to 1,200 µg/mL. The line labeled “Field Fit” is the isotherm corresponding to the MULTRAN V 1.0 (STN: 1066-1.0-00 [DIRS 159068]) “fit” to the first lithium peak in the Bullfrog Tuff field tracer test (Figure D-26).

Figure E-2. Lithium Sorption Data and Fitted Langmuir Isotherm for the Central Bullfrog Tuff

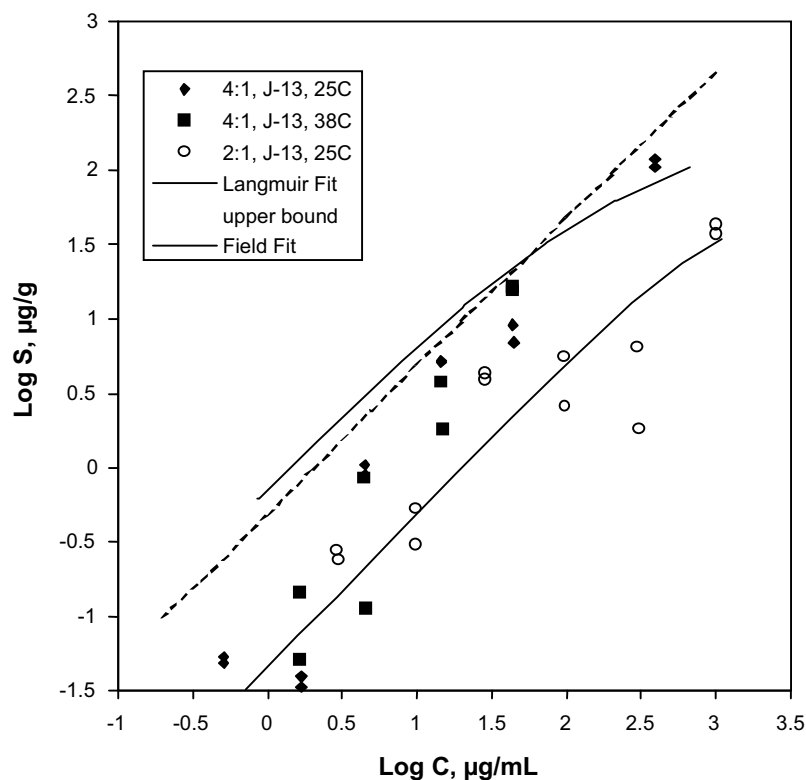


Source: DTN: MO0012SORBCHOL.000 [DIRS 153375] (data).

Output DTN: LA0303PR831341.003 (isotherm fits).

NOTE: The legend indicates the solut ion:solid ratio (mL:g) and the temperature of the experiments. The dashed lines are error bars associated with a 10% experimental error (these error bars are plotted relative to the Langmuir isotherm line). The method for calculating the error bars is by Reimus (2003 [DIRS 165129], p. 126). The lower bound at the highest concentrations is off scale. J-13 well water was used in all experiments. The lithium concentration range in the Bullfrog Tuff field test spanned from less than 0.1 µg/mL up to 1,200 µg/mL. The line labeled "Field Fit" is the isotherm corresponding to the MULTRAN V 1.0 (STN: 1066-1.0-00 [DIRS 159068]) "fit" to the first lithium peak in the Bullfrog Tuff field tracer test (Figure D-26).

Figure E-3. Lithium Sorption Data and Fitted Langmuir Isotherm for the Lower Bullfrog Tuff (c#1, 795 m Below Land Surface)

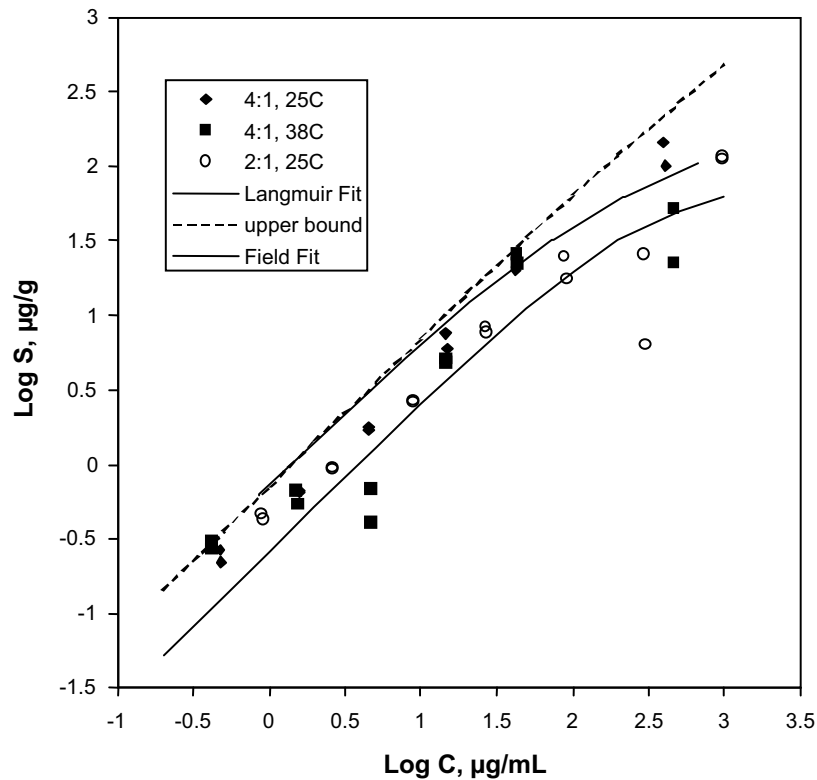


Source: DTN: MO0012SORBCHOL.000 [DIRS 153375] (data).

Output DTN: LA0303PR831341.003 (isotherm fits).

NOTE: The legend indicates the solut ion:solid ratio (mL:g) and the temperature of the experiments. The dashed line is an upper error bar associated with a 10% experimental error (this error bar is plotted relative to the Langmuir isotherm line – lower error bound is off-scale over entire range of data). The method for calculating the error bars is by Reimus (2003 [DIRS 165129], p. 126). J-13 well water was used in all experiments. The lithium concentration in the Prow Pass Tuff field test ranged from less than 0.1 µg/mL up to 2,700 µg/mL. The line labeled "Field Fit" is the isotherm corresponding to the MULTRAN V 1.0 (STN: 1066-1.0-00 [DIRS 159068]) "fit" to the lithium data in the Prow Pass Tuff field tracer test (Figure D-27).

Figure E-4. Lithium Sorption Data and Fitted Langmuir Isotherm for the Upper Prow Pass Tuff (c#2, 533 m Below Land Surface)

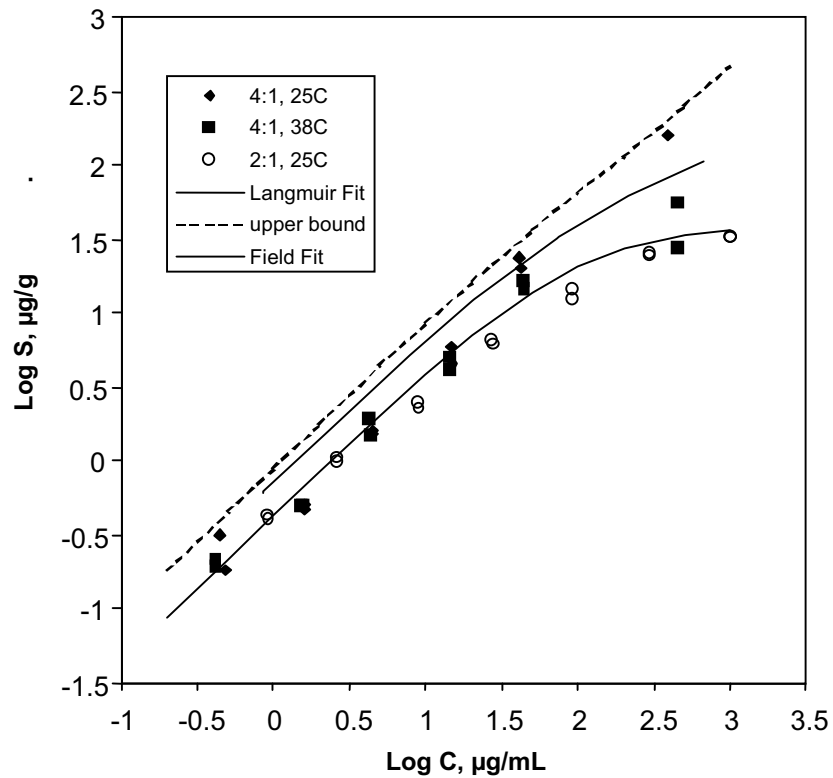


Source: DTN: MO0012SORBCHOL.000 [DIRS 153375] (data).

Output DTN: LA0303PR831341.003 (isotherm fits).

NOTE: The legend indicates the solution:solid ratio (mL:g) and the temperature of the experiments. The dashed line is an upper error bar associated with a 10% experimental error (this error bar is plotted relative to the Langmuir isotherm line – lower error bound is off-scale over entire range of data). The method for calculating the error bars is by Reimus (2003 [DIRS 165129], p. 126). J-13 well water was used in all experiments. The lithium concentration in the Prow Pass Tuff field test ranged from less than 0.1 µg/mL up to 2,700 µg/mL. The line labeled “Field Fit” is the isotherm corresponding to the MULTRAN V 1.0 (STN: 1066-1.0-00 [DIRS 159068]) “fit” to the lithium data in the Prow Pass Tuff field tracer test (see Figure D-27).

Figure E-5. Lithium Sorption Data and Fitted Langmuir Isotherm for the Central Prow Pass Tuff (c#2, 553 m Below Land Surface)

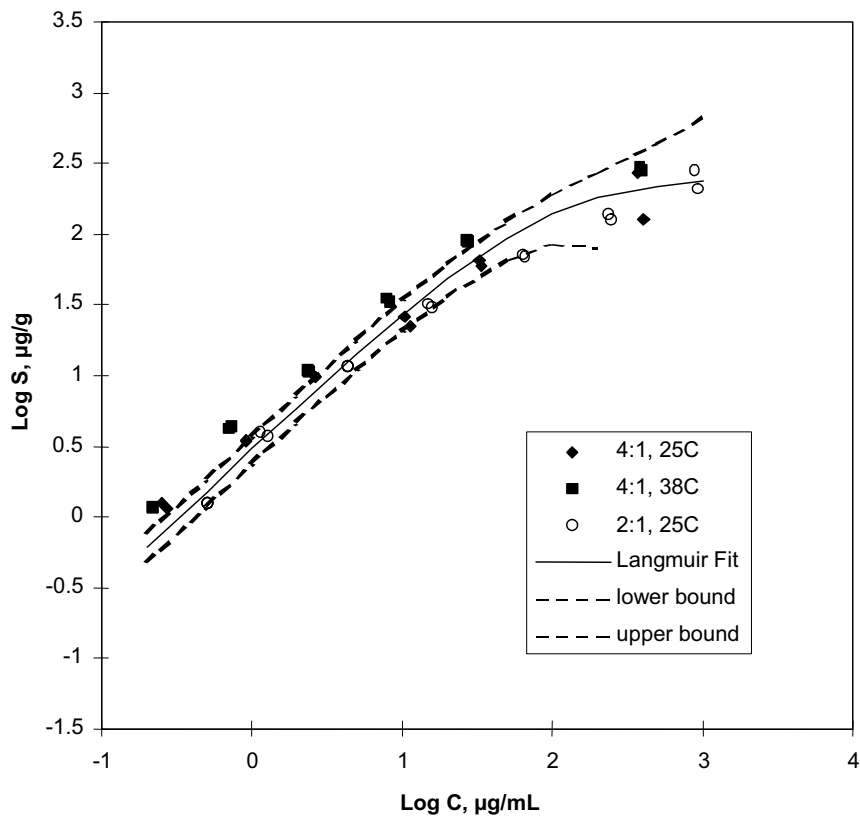


Source: DTN: MO0012SORBCHOL.000 [DIRS 153375] (data).

Output DTN: LA0303PR831341.003 (isotherm fits).

NOTE: The legend indicates the solution:solid ratio (mL:g) and the temperature of the experiments. The dashed line is an upper error bars associated with a 10% experimental error (this error bar is plotted relative to the Langmuir isotherm line – lower error bound is off-scale over entire range of data). The method for calculating the error bars is by Reimus (2003 [DIRS 165129], p. 126). J-13 well water was used in all experiments. The lithium concentration in the Prow Pass Tuff field test ranged from less than 0.1 µg/mL up to 2,700 µg/mL. The line labeled “Field Fit” is the isotherm corresponding to the MULTRAN V 1.0 (STN: 1066-1.0-00 [DIRS 159068]) “fit” to the lithium data in the Prow Pass Tuff field tracer test (Figure D-27).

Figure E-6. Lithium Sorption Data and Fitted Langmuir Isotherm for the Lower Prow Pass Tuff (c#1, 573 m Below Land Surface)

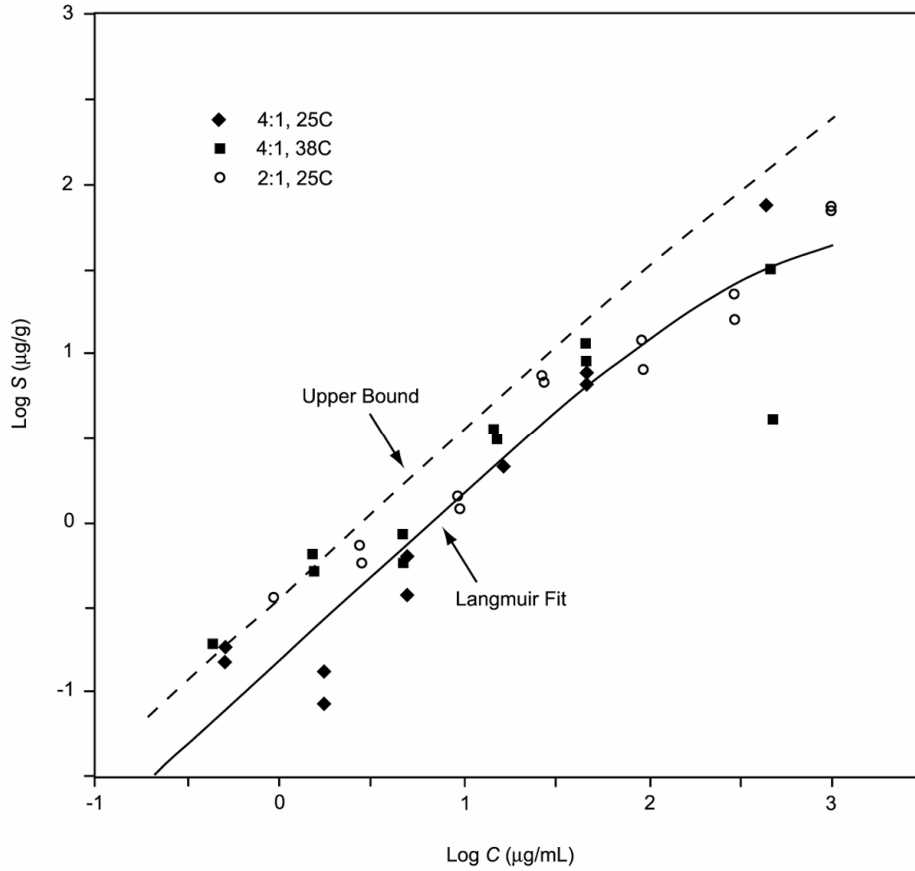


Source: DTN: MO00012SORBCHOL.000 [DIRS 153375] (data).

Output DTN: LA0303PR831341.003 (isotherm fits).

NOTE: The legend indicates the solution:solid ratio (mL:g) and the temperature of the experiments. The dashed lines are error bars associated with a 10% experimental error (these error bars are plotted relative to the Langmuir isotherm line). The method for calculating the error bars is by Reimus (2003 [DIRS 165129], p. 126). The lower bound at the highest concentrations is off scale. J-13 well water was used in all experiments.

Figure E-7. Lithium Sorption Data and Fitted Langmuir Isotherm for the Bedded Prow Pass Tuff (c#1, 643 m Below Land Surface)

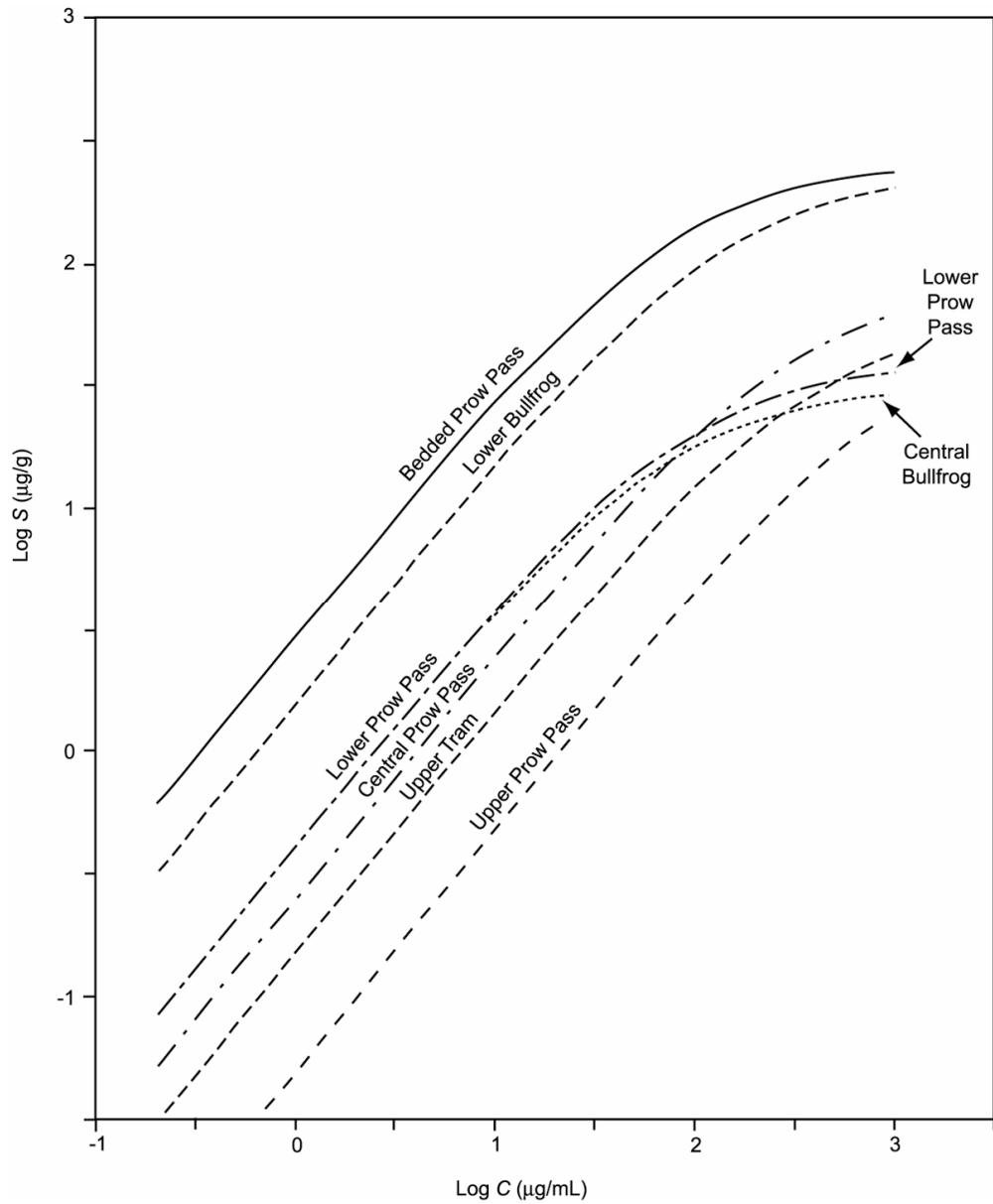


Source: DTN: MO0012SORBCHOL.000 [DIRS 153375] (data).

Output DTN: LA0303PR831341.003 (isotherm fits).

NOTE: The legend indicates the solution:solid ratio (mL:g) and the temperature of the experiments. The dashed line is an upper error bar associated with a 10% experimental error (these error bars are plotted relative to the Langmuir isotherm line - lower error bound is off-scale over entire range of data). The method for calculating the error bars is described by Reimus (2003 [DIRS 165129], p. 126). J-13 well water was used in all experiments.

Figure E-8. Lithium Sorption Data and Fitted Langmuir Isotherm for the Upper Tra m Tuff (c#2, 839 m Below Land Surface)



Output DTN: LA0303PR831341.003.

NOTE: The lithium concentration range in the field test in the central and lower Bullfrog Tuff spanned from less than 0.1 µg/mL up to 1,200 µg/mL. The concentration range in the Prow Pass Tuff field test ranged from less than 0.1 µg/mL up to 2,700 µg/mL.

Figure E-9. Fitted Langmuir Isotherms for the Seven C-Wells Tufts

Table E-4. Lithium Sorption Isotherm Parameters Associated with the Different C-wells Tuffs

Unit	Langmuir		Freundlich		Linear
	K_L (L/mg)	S_{max} ($\mu\text{g/g}$)	K_F ($\text{mL}/\mu\text{g})^n(\mu\text{g/g})$	n	K_d (mL/g)
Central Bullfrog, c#1 + c#2 ^a	0.014	31.4	0.70	0.79	0.186
Lower Bullfrog, c#1	0.0070	233.9	2.26	0.75	0.321
Upper Prow Pass, c#2	0.00094	53.1	0.075	1.03	0.068
Central Prow Pass, c#2	0.0031	83.3	0.48	0.80	0.131
Lower Prow Pass, c#1	0.011	39.8	0.48	0.78	0.084
Bedded Prow Pass, c#2	0.012	254.9	4.17	0.69	0.383
Upper Tram, c#2	0.0026	59.8	0.27	0.78	0.072

Output DTN: LA0303PR831341.003 (also from Anghel et al. 2002 [DIRS 164635], Section 3.2, pp. 822 to 824).

NOTE: c#1 and c#2 are abbreviations for Boreholes UE-25 c#1 and UE-25 c#2, respectively.

^aSorption data from c#1 and c#2 tuffs are lumped together to obtain parameter estimates. K_L and S_{max} were 0.0053 L/mg and 110 $\mu\text{g/g}$, respectively, for the Central Bullfrog Tuff from c#2 alone (used in crushed tuff column experiments of Section E3).

Results of the CEC measurements on the seven-tuff samples are presented in Figure E-10 and Table E-5. In all cases, the total CEC available to cesium (CEC-CsT) exceeds that available to lithium (CEC-LiT). This result is not surprising; the hydrated ionic radius of cesium (0.33 nm) is smaller than that of lithium (0.38 nm) (Israelachvili 2000 [DIRS 156835], p. 55), which permits cesium access to internal exchange sites in zeolites that are not available to lithium. More surprising is the consistent observation that cesium displaces more lithium during the displacement step than lithium displaced other cations during initial saturation (i.e., CEC-CsLi greater than CEC-LiT). This phenomenon, a “lithium excess” during the displacement step, was also reported by Eckstein et al. (1970 [DIRS 156653], pp. 341 to 342). They attributed this lithium excess to a separate process that occurs in addition to normal cation exchange: selective and specific adsorption of lithium, particularly to amorphous silicates and to edges and broken bonds of nonexpanding clay minerals. Eckstein et al. (1970 [DIRS 156653]) state that “it [is] difficult or even doubtful that a ‘true’ value for the exchange capacity can be given for any specific clay.” They further conclude that “the sum of cations replaced by Li will usually give a better value for the exchange capacity than the amount of Li retained and replaced by $\text{Ca}(\text{OAc})_2$.”

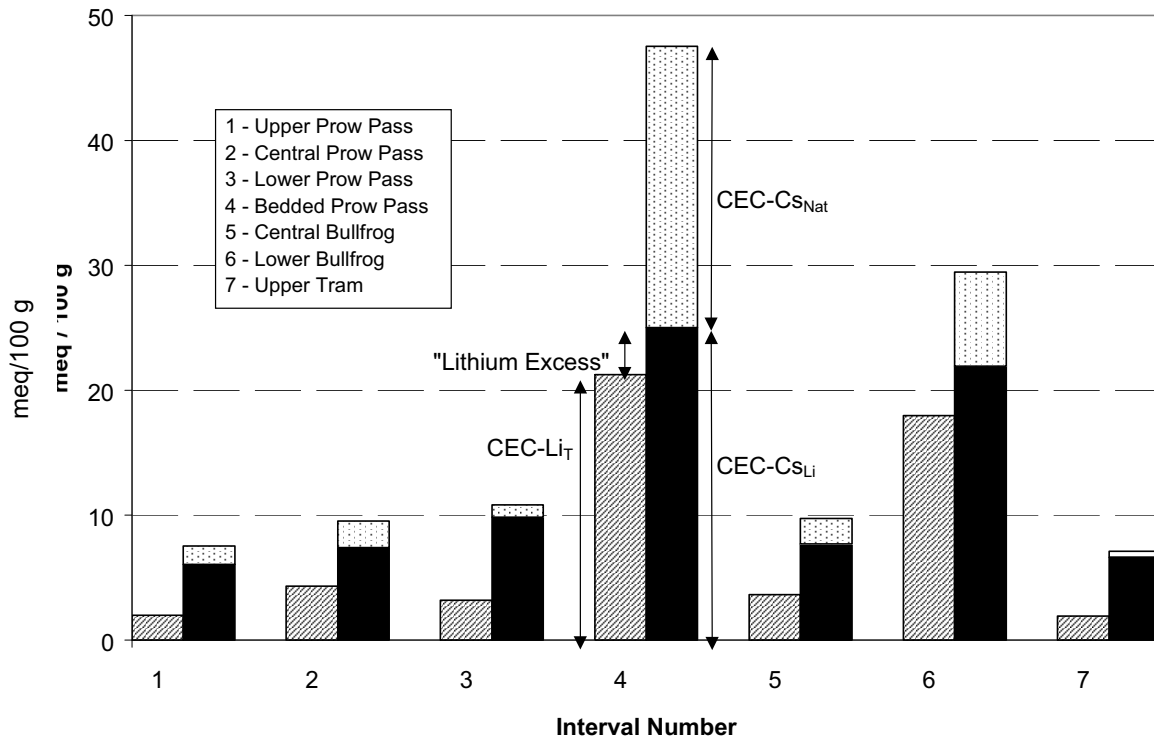
Inspection of the mineralogy of the samples, presented in Table E-3, indicates that the primary minerals likely to participate in cation exchange include smectite and the zeolite minerals clinoptilolite and mordenite. Although analcime has a high theoretical CEC (Ming and Mumpton 1995 [DIRS 156843], pp. 873 to 911), kinetic factors prevent significant cation exchange at normal environmental temperatures (Vaughan 1978 [DIRS 156867], pp. 353 to 371). To test whether a simple two-mineral model could explain the observed measurements, a multivariable linear regression was conducted on the CEC results, using measured smectite and (clinoptilolite + mordenite) fractions (f_{smec} , $f_{clin/mord}$) as independent variables, and three CEC estimates as the dependent variables. In all cases, the model yielded the following results:

$$CEC-Li_T = 106 \pm 8 \text{ meq}/100\text{g} \cdot f_{smec} + 99 \pm 3 \text{ meq}/100\text{g} \cdot f_{clin/mord} + 1.5 \pm 0.3 \text{ meq}/100\text{g}, R^2 = 0.997$$

$$CEC-C_{sLi} = 103 \pm 13 \text{ meq}/100\text{g} \cdot f_{smec} + 95 \pm 5 \text{ meq}/100\text{g} \cdot f_{clin/mord} + 6.1 \pm 0.5 \text{ meq}/100\text{g}, R^2 = 0.990$$

$$CEC-C_{sT} = 90 \pm 13 \text{ meq}/100\text{g} \cdot f_{smec} + 199 \pm 5 \text{ meq}/100\text{g} \cdot f_{clin/mord} + 7.7 \pm 0.5 \text{ meq}/100\text{g}, R^2 = 0.997.$$

where R^2 = coefficient of regression (sum of squares regression divided by sum of squares total).



Sources: DTNs: MO0012CATECHOL.000 [DIRS 153371] (CEC-Li data); LA0302PR831341.001 [DIRS 162604] (CEC- cesium data).

Output DTN: LA0303PR831341.001.

NOTE: Interval numbers in legend do not correspond to numbers in Table E-2 or Figure E-1. Explanation of bar patterns provided for interval 4 applies to all intervals.

Figure E-10. Cation-exchange Capacity Results for the Seven Different C-Well Tuff Intervals

Table E-5. Cation-exchange Capacity Measurements for C-wells Tuffs

Sample ^a	Cation-exchange Capacity (meq/100g)				
	CEC-Li _T	CEC-Cs _{Nat}	CEC-Cs _{Li}	CEC-Cs _T	Lithium Excess
Upper Prow Pass (1)	2.0 ± 0.5	1.5 ± 0.1	6.1 ± 0.8	7.5	4.1
Central Prow Pass (2)	4.3 ± 0.1	2.1 ± 0.0	7.4 ± 0.4	9.5	3.1
Lower Prow Pass (3)	3.2 ± 0.4	1.0 ± 0.9	9.8 ± 1.9	10.8	6.6
Bedded Prow Pass (4)	21.3 ± 0.1	22.5 ± 0.4	25.0 ± 1.4	47.5	3.8
Central Bullfrog (5) ^b	3.7 ± 0.1	2.0 ± 0.5	7.7 ± 0.6	9.7	4.1
Lower Bullfrog (6)	18.0 ± 0.2	7.5 ± 0.4	21.9 ± 0.2	29.5	4.0
Upper Tram (7)	1.9 ± 0.1	0.5 ± 0.2	6.6 ± 0.5	7.1	4.7

Sources: DTNs:MO0012CATECHOL.000 [DIRS 153371] (C EC-Li data); LA0302PR831341.001 [DIRS 162604] (CEC- cesium data).

Output DTN: LA0303PR831341.001.

NOTE: Range shown is ± one standard deviation. Refer to text for definitions.

^aNumbers correspond to numbers in Figure E-10.

^bOnly the Central Bullfrog Tuff from c#1 was analyzed for CEC.

The exchange factors for the individual minerals can be compared to literature values of 110 ± 23 meq/100 g for smectite (Borchardt 1995 [DIRS 156639], Chapter 14) and 220 meq/100 g for clinoptilolite and mordenite (Ming and Mumpton 1995 [DIRS 156843]). Starting with the model for *CEC-Li_T*, the specific exchange capacity for smectite matches the reported value from Borchardt (1995 [DIRS 156639], Chapter 14), whereas the modeled capacity for the zeolite minerals is less than half that reported by Ming and Mumpton (1995 [DIRS 156843]). This discrepancy is consistent with the inaccessibility of some of the internal zeolite exchange sites to the relatively large lithium ion. The *CEC-Li_T* model includes a relatively small constant term, indicating that almost all of the observed behavior can be explained by smectite and clinoptilolite/mordenite cation exchange. Comparing this model to the *CEC-Cs_{Li}* model, we see that the major difference lies in the constant term; the larger constant term in the second model reflects the observed lithium excess. The similarity of the other two terms demonstrates that the Li-excess effect is not a result of exchange onto either smectite or clinoptilolite/mordenite; additional correlation analysis shows that the lithium excess is not proportional to any of the mineral phases identified by quantitative x-ray diffraction. These observations, combined with the overall uniformity of the lithium excess among these widely varying tuff samples, lead one to agree with Eckstein et al. (1970 [DIRS 156653], pp. 341 and 342) and attribute the lithium excess to a noncation-exchange sorption process.

The final model for *CEC-Cs_T* reveals a similar specific CEC for smectite as found in the literature and the previous models but shows a much higher specific CEC for the zeolite minerals, which is more in line with published values (Ming and Mumpton 1995 [DIRS 156843]). This demonstrates the accessibility to the smaller cesium ion of internal exchange sites that were apparently unavailable to lithium. The constant term in this model is the sum of the constant terms in the *CEC-Li_T* and *CEC-Cs_{Li}* models.

To a first approximation, it can be seen that the two samples that sorb lithium most strongly have the highest isotherms in Figure E-9 and the largest K_d and K_F values in Table E-4. These two rocks also showed the highest CEC values. To quantify the sorption relationships more

rigorously, the linearization of the nonlinear Freundlich isotherm was undertaken, and K_{lin} was calculated. K_{lin} is an effective distribution coefficient with uniform units, identical to those of K_d . For this purpose, the equal-area linearization of van Genuchten et al. (1977 [DIRS 156868], pp. 278 to 285) was used:

$$K_{lin} = \frac{2K_F C_{max}^{n-1}}{n+1} \quad (\text{Eq. E-4})$$

where C_{max} is the maximum solution concentration of interest; in this case, 1,000 mg/L, and K_F and n are taken from Table E-4. Using the same multivariate linear regression methods described above, K_{lin} can be modeled as a function of smectite and clinoptilolite/mordenite content:

$$K_{lin} = 2.28 \pm 0.45 \text{ L/kg} \cdot f_{smec} + 2.46 \pm 0.18 \text{ L/kg} \cdot f_{clin/mord} + 0.09 \pm 0.02 \text{ L/kg}, r^2 = 0.981.$$

This model does not fit the data quite as well as the CEC models described above but, nevertheless, demonstrates that lithium sorption can be estimated fairly accurately for these tuffs, given smectite, clinoptilolite, and mordenite concentrations. The small constant term in the model indicates that the contribution of other minerals to lithium sorption is quite low.

E1.3 CONCLUSIONS FROM BATCH LITHIUM SORPTION STUDIES

Lithium ion sorption onto devitrified tuffs from the saturated zone near Yucca Mountain follows nonlinear isotherm behavior. Both the lithium sorption parameters and the lithium-specific cation-exchange capacities of the tuffs are highly correlated with the clay (smectite) content and the zeolite (clinoptilolite + mordenite) content of the tuffs. Multiple linear regression analyses show that these two classes of minerals account for the majority of the observed lithium exchange. Regression of cesium cation-exchange data yields results that are consistent with the accessibility of the smaller cesium ion to internal zeolite exchange sites that lithium cannot access. The cesium CEC data also suggest that some of the lithium sorption to the tuffs can be attributed to a noncation-exchange process. The results of this study support the development and use of mineralogy-based models for predicting cation sorption in the saturated zone near Yucca Mountain.

E2. DIFFUSION CELL EXPERIMENTS

E2.1 MATERIALS AND METHODS

Six diffusion cell experiments were conducted to determine diffusion coefficients of PFBA and bromide ion in five different C-wells tuff matrices [details are in YMP C-Wells Diffusion Cells (Reimus 2000 [DIRS 165121])]. Estimates of matrix diffusion coefficients are important because they can greatly reduce uncertainty in interpreting and predicting both field-scale and laboratory-scale tracer experiments. One of the tests was a repeat experiment using a different core from the same interval as another test (the lower Prow Pass Tuff). This test was conducted to determine the reproducibility and variability of the experiments. The five different intervals tested in the diffusion cell experiments represented all of the major lithologies in either the

Bullfrog field tracer test or the Prow Pass field tracer test (see Table E-6 for specific intervals tested).

A schematic drawing of the experimental diffusion cell apparatus is illustrated in Figure E-11. The apparatus consists of two Plexiglas reservoirs, one large and one small, separated by a “pellet” of tuff, which is cut/cored from C-wells core and incorporated into either a flat epoxy cast or a room-temperature vulcanizing silicone cast of the same thickness as the pellet. After saturating the tuff, experiments were initiated by carefully pouring a solution containing PFBA and LiBr into the large reservoir and tracer-free solution into the small reservoir. The pressures in the two reservoirs were kept approximately equal to minimize advective flow through the tuff, thus ensuring that tracer movement through the tuff was by diffusion only. The small reservoir was kept well mixed with a magnetic stir bar and flushed continuously at a relatively low flow rate. The flush water was collected in an automatic fraction collector, and fractions were analyzed for tracers to establish breakthrough curves through the tuff from which diffusion coefficients could be estimated. As in the other laboratory experiments, PFBA and bromide were analyzed by liquid chromatography, and lithium was analyzed by ICP-AES. Filtered J-13 well water or synthetic J-13 well water (a sodium/calcium bicarbonate solution having the same ionic strength as J-13 well water – refer to Reimus 2000 [DIRS 165121] for details) were used in all experiments.

The porosities of the tuffs were measured by subtracting dry weights from saturated weights of intact tuff samples and dividing by the volumes of the samples (measured by water displacement). Porosity measurements were used to obtain unambiguous estimates of diffusion coefficients in the tuff matrices (see equations below). Hydraulic conductivities/permeabilities of the tuffs were also measured by imposing a known head difference across the tuff pellets, either before or after a diffusion experiment was conducted. The flow through the pellets at the imposed head difference was measured by weighing the water that flowed through the pellet over a specified amount of time.

Hydraulic conductivities were then calculated from the following equation (Freeze and Cherry 1979 [DIRS 101173], p. 335, Equation 8.24):

$$K = - \frac{QL}{A \Delta H} \quad (\text{Eq. E-5})$$

where

K = hydraulic conductivity, cm/s

ΔH = water height (head) difference across pellet, cm

A = surface area of pellet, cm²

Q = volumetric flow rate through pellet, mL/s

L = thickness of pellet, cm.

Permeabilities were calculated from hydraulic conductivities using the following well-known formula (Freeze and Cherry 1979 [DIRS 101173], pp. 26 to 30):

$$k = (1.013 \times 10^{11}) \frac{K \mu}{\rho g} \quad (\text{Eq. E-6})$$

where

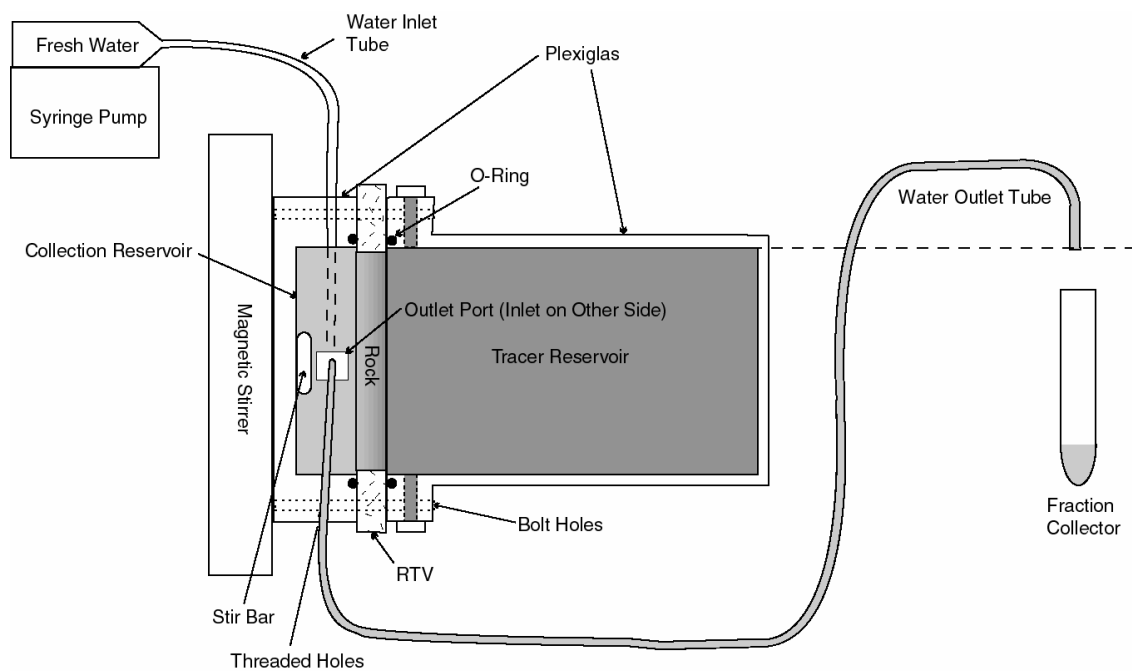
k = permeability, millidarcys (mD)

μ = water viscosity, g/cm-s (1.00 centipoise or 0.01 g/cm-s at 20°C (Weast and Astle 1981 [DIRS 100833], p. F-42))

ρ = water density, g/cm³ (0.998 g/cm³ at 20°C (Weast and Astle 1981 [DIRS 100833], p. F-11))

g = acceleration due to gravity, cm/s² (980 cm/s² on Earth (Weast and Astle 1981 [DIRS 100833], p. F-144))

and the constant 1.013×10^{11} has units of mD/cm².



NOTE: For illustration purposes only.

Figure E-11. Diffusion Cell Experimental Apparatus

To estimate diffusion coefficients, it was assumed that the tracers moved according to one-dimensional diffusive transport through the tuff pellets. The one-dimensional diffusion equation is:

$$\frac{\partial c}{\partial t} = \frac{D}{R} \frac{\partial^2 c}{\partial x^2} \quad (\text{Eq. E-7})$$

where

c = tracer concentration in tuff pellet, $\mu\text{g/mL}$
 D = diffusion coefficient, cm^2/s
 R = retardation factor (1 for nonsorbing solutes),
 x = position within tuff pellet ($x = 0$ at inlet reservoir), cm
 t = time, s .

Although analytical solutions to this simple partial differential equation exist for simple boundary conditions (Jenson and Jeffreys 1977 [DIRS 156836], pp. 291 to 295), the time-dependent concentration boundary conditions at the inlet and outlet reservoirs in the diffusion cell experiments demand a numerical solution. Thus, Equation E-7 was solved using an implicit finite-difference technique. The equations describing the tracer concentrations in the inlet and the outlet reservoirs (the first and last finite difference nodes), respectively, were:

$$\frac{\partial c_i}{\partial t} = \frac{\phi \pi r^2 D}{V_i} \frac{\partial c}{\partial x} \Big|_{x=0} \quad (\text{Eq. E-8})$$

$$\frac{\partial c_o}{\partial t} = - \frac{\phi \pi r^2 D}{V_o} \frac{\partial c}{\partial x} \Big|_{x=L} - \frac{q}{V_o} c_o \quad (\text{Eq. E-9})$$

where

c_i = tracer concentration in inlet reservoir, $\mu\text{g/mL}$
 c_o = tracer concentration in outlet reservoir, $\mu\text{g/mL}$
 V_i = volume of inlet reservoir, mL
 V_o = volume of outlet reservoir, mL
 q = flush rate of outlet reservoir, mL/s
 ϕ = porosity of tuff
 r = radius of tuff “pellet”, cm
 L = thickness of tuff “pellet”, cm .

The numerical solution of Equations E-7, E-8, and E-9 was obtained using computer code DIFFCELL V. 2.0 (STN: 10557-2.0-00 [DIRS 159063]). This code allows the user to specify changes in the flush rate, q , with time, which was necessary to simulate the manner in which the experiments were conducted.

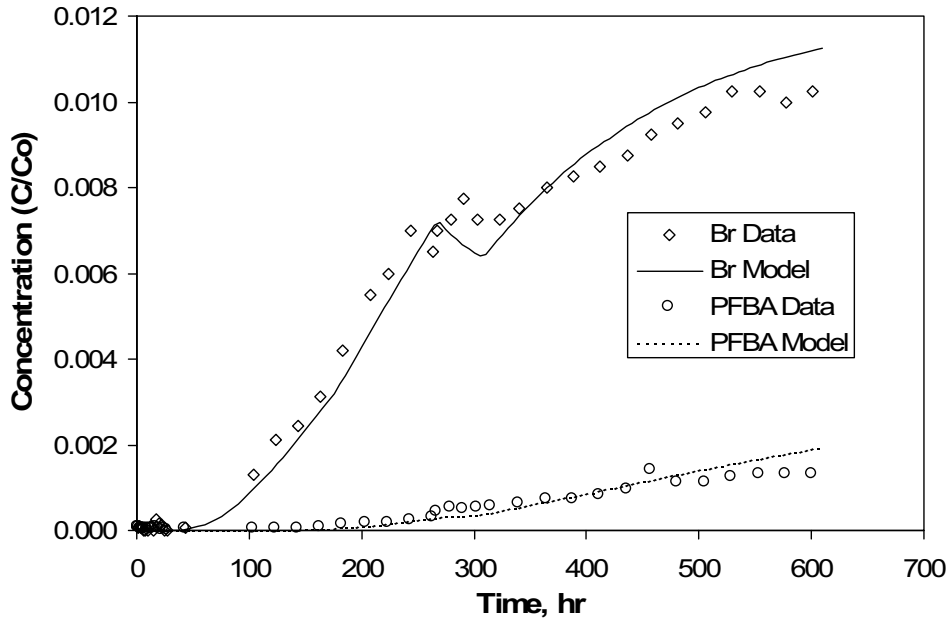
E2.2 RESULTS AND DISCUSSION

Figures E-12 through E-17 show the breakthrough curves of the bromide and PFBA in each of the six diffusion cells along with “fits” to the data obtained using DIFFCELL V. 2.0 (STN: 10557-2.0-00 [DIRS 159063]). The “fits” are not actual least-squares fits; rather, they were obtained by manual adjustment of the diffusion coefficients until a reasonable match to the data was obtained. The apparent discontinuities in some of the data sets and the corresponding model predictions are a consequence of changes in the flush rate through the outlet reservoirs. A decrease in concentration occurs when the flush rate is increased and vice-versa.

The resulting estimates of tracer diffusion coefficients in each diffusion cell are given in Table E-6 (measured tuff porosities, pellet thicknesses, and tuff permeabilities are also listed in this table). It is apparent that there is about an order of magnitude range of diffusion coefficients in the various tuff lithologies. Figures E-18 and E-19 show the bromide diffusion coefficients in the tuff matrices as a function of porosity and permeability, respectively, for the five different C-wells tuffs. Although the diffusion coefficients are not well correlated with porosity, they are quite well correlated with permeability (on a log-log scale). This result suggests that permeability may be a good predictor of matrix diffusion coefficients. Such correlations could prove useful for estimating matrix diffusion coefficients, as diffusion coefficients are typically more difficult to measure than matrix properties such as permeabilities.

Table E-6 shows that excellent agreement was obtained between the two diffusion cell experiments conducted for the same lithology (the lower Prow Pass Tuff). This result suggests that the experiments have reasonably good reproducibility, although certainly more experiments should be conducted in the same lithologies before measurement uncertainty and tuff variability can be properly assessed.

Although the PFBA and bromide diffusion coefficients are significantly different in the different tuffs, the ratios of the diffusion coefficients are approximately the same in each tuff. This result suggests that advection through the tuff pellets was successfully eliminated, as any advection would result in different ratios in different tests. The factor of approximately 3 difference in the diffusion coefficients of the PFBA and bromide is the basis for assuming a factor of 3 difference in all of the field and laboratory tracer-test interpretations in this report.

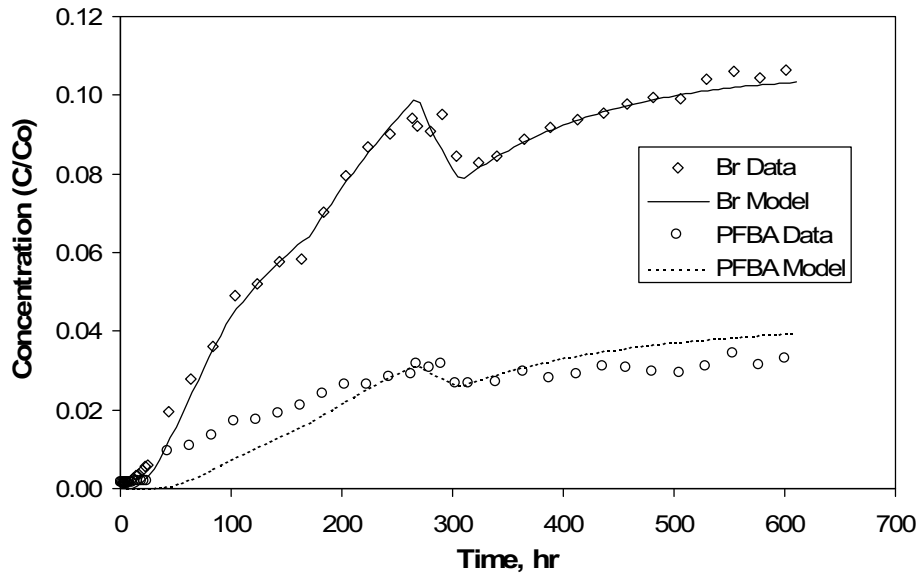


Source: DTN: MO0012DIFFCHOL.000 [DIRS 159243] (data).

Output DTN: LA0303PR831362.001 (DIFFCELL fits).

NOTE: Diffusion coefficients are given in Table E-6.

Figure E-12. Diffusion Cell Data (Tracer Concentrations in Outlet Reservoir Normalized to Starting Concentrations in Inlet Reservoir, C_o) and DIFFCELL Fits for Bromide and PFBA in the Central Bullfrog Tuff

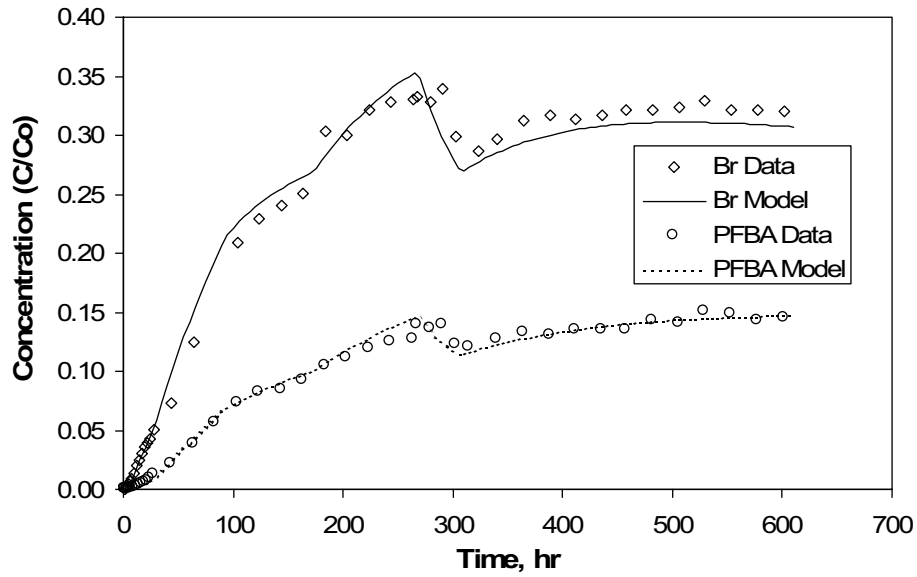


Source: DTN: MO0012DIFFCHOL.000 [DIRS 159243] (data).

Output DTN: LA0303PR831362.001 (DIFFCELL fits).

NOTE: Diffusion coefficients are given in Table E-6.

Figure E-13. Diffusion Cell Data (Tracer Concentrations in Outlet Reservoir Normalized to Starting Concentrations in Inlet Reservoir, C_o) and DIFFCELL Fits for Bromide and PFBA in the Lower Bullfrog Tuff

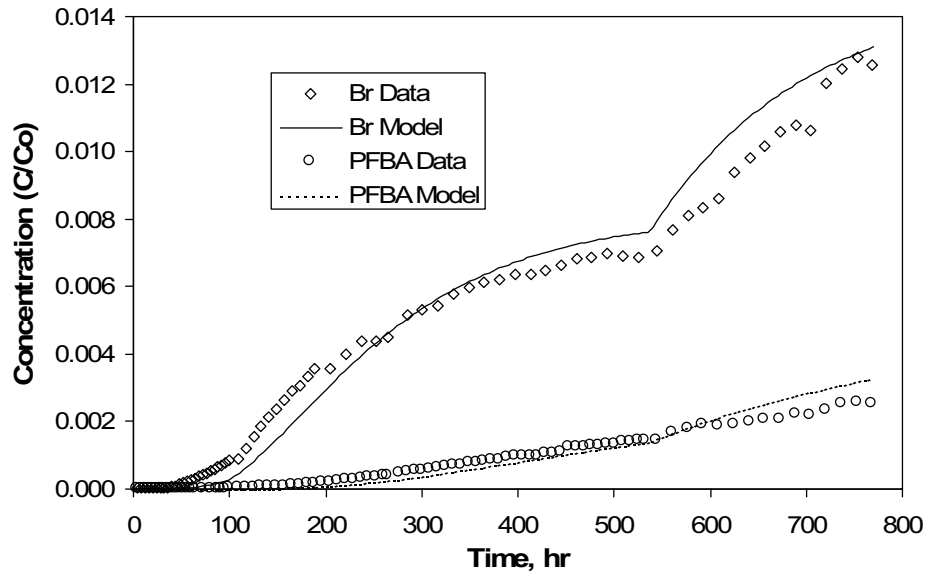


Source: DTN: MO0012DIFFCHOL.000 [DIRS 159243] (data).

Output DTN: LA0303PR831362.001 (DIFFCELL fits).

NOTE: Diffusion coefficients are given in Table E-6.

Figure E-14. Diffusion Cell Data (Tracer Concentrations in Outlet Reservoir Normalized to Starting Concentrations in Inlet Reservoir, C_o) and DIFFCELL Fits for Bromide and PFBA in the Upper Prow Pass Tuff

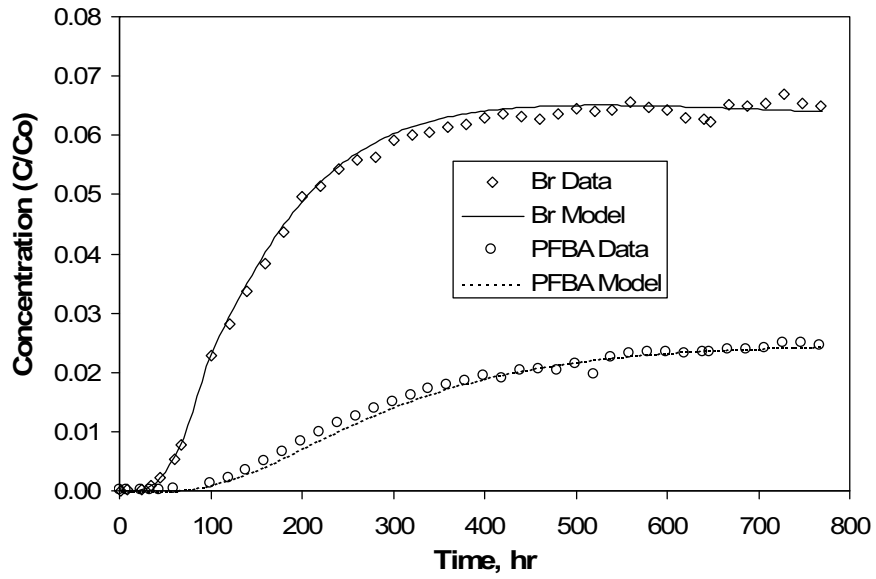


Source: DTN: MO0012DIFFCHOL.000 [DIRS 159243] (data).

Output DTN: LA0303PR831362.001 (DIFFCELL fits).

NOTE: Diffusion coefficients are given in Table E-6.

Figure E-15. Diffusion Cell Data (Tracer Concentrations in Outlet Reservoir Normalized to Starting Concentrations in Inlet Reservoir, C_o) and DIFFCELL Fits for Bromide and PFBA in the Central Prow Pass Tuff

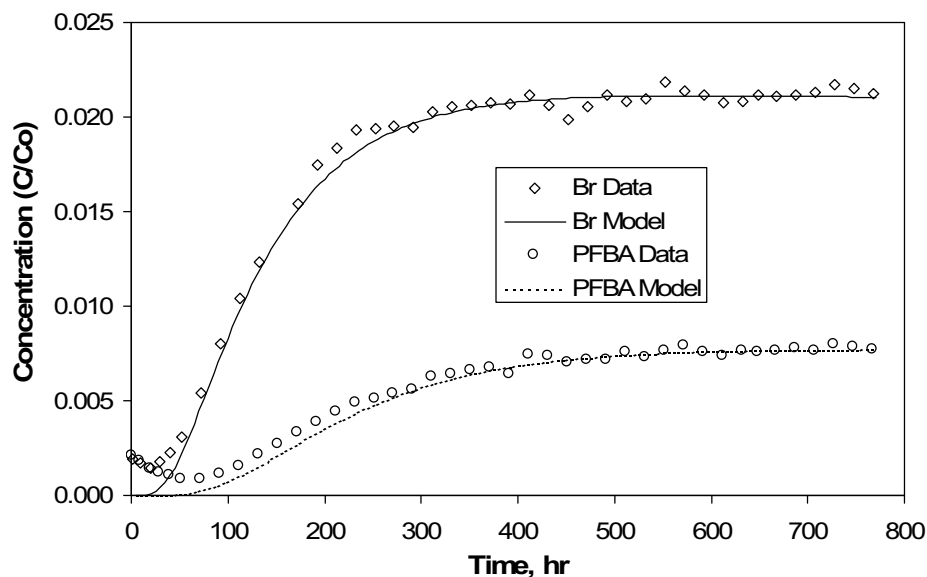


Source: DTN: MO0012DIFFCHOL.000 [DIRS 159243] (data).

Output DTN: LA0303PR831362.001 (DIFFCELL fits).

NOTE: Diffusion coefficients are given in Table E-6.

Figure E-16. First Diffusion Cell Data (Tracer Concentrations in Outlet Reservoir Normalized to Starting Concentrations in Inlet Reservoir, C_o) and DIFFCELL Fits for Bromide and PFBA in the Lower Prow Pass Tuff



Source: DTN: MO0012DIFFCHOL.000 [DIRS 159243] (data).

Output DTN: LA0303PR831362.001 (DIFFCELL fits).

NOTE: Diffusion coefficients are given in Table E-6.

Figure E-17. Second Diffusion Cell Data (Tracer Concentrations in Outlet Reservoir Normalized to Starting Concentrations in Inlet Reservoir, C_0) and DIFFCELL Fits for Bromide and PFBA in the Lower Prow Pass Tuff

Table E-6. Measured Porosities, Permeabilities, and Matrix Diffusion Coefficients of Bromide and PFBA in C-wells Tuffs

Tuff ^a	Porosity	Permeability (mDarcy)	Thickness ^b (cm)	Diffusion Coefficient (cm ² /s × 10 ⁶) ^c		Br/PFBA (Ratio)
				Br	PFBA	
Central Bullfrog (1)	0.094	0.00107	1.12	0.42	0.12	3.5
Lower Bullfrog (3)	0.298	0.0949	0.79	1.0	0.35	2.86
Upper Prow Pass (4)	0.272	4.72	0.98	6.2	2.0	3.1
Central Prow Pass (5)	0.138	0.000786	1.23	0.38	0.13	2.92
Lower Prow-1 (6) ^d	0.288	0.455	2.27	3.0	1.1	2.73
Lower Prow-2 (6) ^d	0.288	0.455	1.82	2.8	1.0	2.8

Sources: DTNs: MO0012POROCHOL.000 [DIRS 153376] (porosity); MO0012PERMCHOL.000 [DIRS 153368] (permeability); MO0012DIFFCHOL.000 [DIRS 159243] (diffusion cells).

Output DTN: LA0303PR831362.001 (DIFFCELL results – diffusion coefficients).

NOTE: Synthetic J-13 well water was used for the experiments involving the first three tuffs. Filtered J-13 well water was used in the other three experiments.

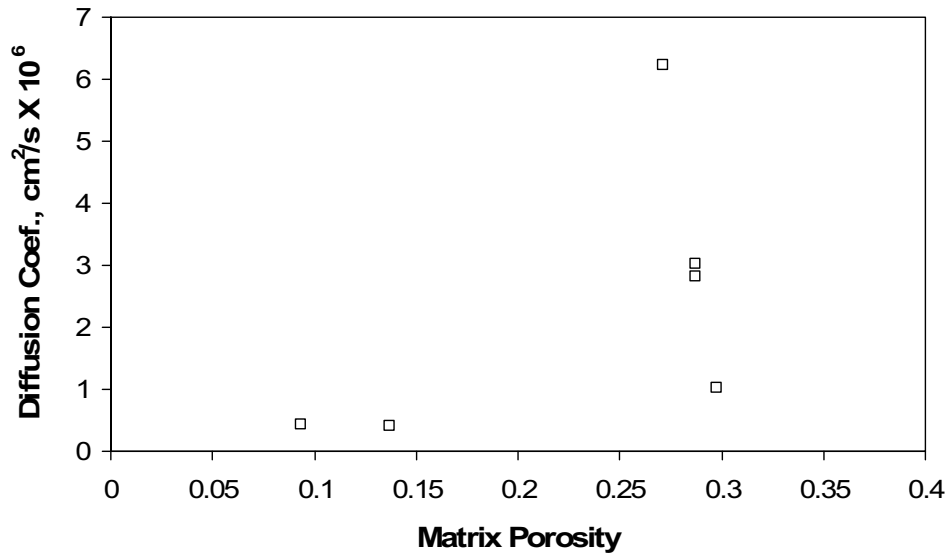
^aNumbers in parentheses correspond to numbers in Figure E-1 (locations where core was collected from the C-wells) and in Table E-2 (where actual depths associated with the cores are listed).

^bThickness, L , of tuff pellet.

^c Measured matrix diffusion coefficients are equal to values in these columns multiplied by 10^{-6} .

^dExperiments were conducted using two separate tuff pellets from the Lower Prow Pass Tuff.

PFBA=pentafluorobenzoic acid or pentafluorobenzoate.

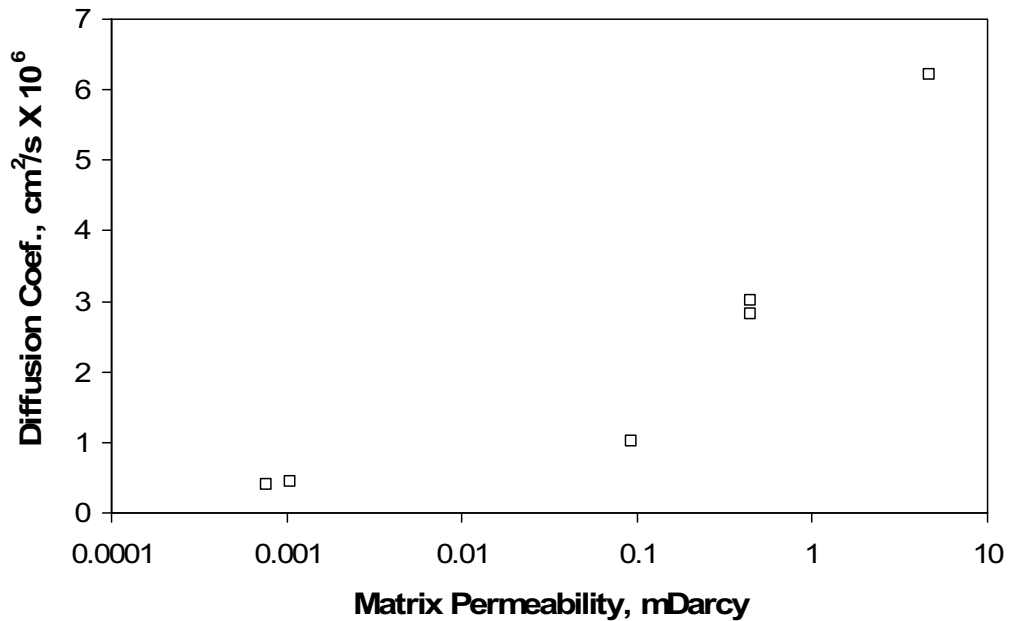


Source: DTN: MO0012POROCHOL.000 [DIRS 153376] (porosity data).

Output DTN: LA0303PR831362.001 (diffusion coefficients).

NOTE: Porosity and diffusion coefficient for bromide are listed in Table E-6.

Figure E-18. Bromide Diffusion Coefficients Versus Tuff Porosity for All C-Wells Diffusion Cell Experiments



Source: DTN: MO0012PERMCHOL.000 [DIRS 153368] (permeability data).

Output DTN: LA0303PR831362.001 (diffusion coefficients).

NOTE: Permeability and diffusion coefficient are listed in Table E-6.

Figure E-19. Bromide Diffusion Coefficients Versus Tuff Permeability for All C-Wells Diffusion Cell Experiments

E3. LABORATORY STUDIES OF LITHIUM TRANSPORT IN CRUSHED TUFF COLUMNS AND FRACTURED CORES

Several laboratory transport experiments were conducted to study lithium transport under flowing conditions in both columns packed with crushed C-wells tuff and fractured C-wells cores (Reimus 2003 [DIRS 163760], Attachments A, B1, and B2). The crushed-tuff column experiments were conducted to compare lithium sorption parameters under flowing conditions to batch-sorption measurements. The fractured-core experiments were conducted to study lithium transport under more realistic fracture flow conditions where matrix diffusion and sorption in the matrix should also influence transport. The crushed-tuff experiments are described in Section E3.1, and the fractured-core experiments are described in Section E3.2.

E3.1 CRUSHED-TUFF COLUMN EXPERIMENTS

E3.1.1 Experimental Methods

A series of transport experiments was conducted in plexiglass columns 91.44 cm in length and 0.62 cm in diameter (Reimus 2003 [DIRS 163760], Attachment A). The columns were packed with crushed central Bullfrog Tuff (from location number 2 in Figure E-1) that had been wet-sieved to a size range between 75 μ m and 500 μ m. A wet slurry technique was used to pack the columns. Column porosity was measured at approximately 57% (average of two columns), and dry bulk density was calculated at 1.14 g/mL by assuming a mineral density of 2.65 g/mL, which are typical values for columns prepared in this fashion (Treher and Raybold 1982 [DIRS 125967], pp. 8 to 9; Thompson 1989 [DIRS 100830], pp. 353 to 364). Two columns were prepared identically. The column apparatus included a constant-rate pump, a valve to switch between a reservoir containing J-13 "background" water and a solution of lithium bromide in J-13 well water, and an automatic fraction collector at the downstream end of the column. Each experiment began by pumping approximately 180 mL (roughly 12 pore volumes) of J-13 well water through the column at a specified flow rate to equilibrate the tuff with the groundwater. The input was then switched to a lithium bromide solution, which was maintained for approximately three pore volumes before being switched back to tracer-free groundwater. Effluent samples were analyzed for lithium and bromide using liquid chromatography (detection limits were 0.10 mg L⁻¹ for Li⁺ and 0.005 mg L⁻¹ for Br⁻). Bromide was used as a nonsorbing tracer to determine mean residence times and dispersivities in the columns as well as to serve as a nonsorbing tracer against which lithium retardation could be gauged.

A total of five experiments were conducted in the two columns, with the tracer concentrations and flow rate both being varied. In three of the five column experiments, the responses of Li⁺ and Br⁻ were monitored until concentrations returned to background levels; in the other two experiments, concentrations were monitored only until they leveled off at the inlet concentrations. The experimental conditions are summarized in Table E-7. The different tracer concentrations were intended to investigate potential effects of lithium sorption nonlinearity, and the different flow rates were intended to reveal rate-limited effects, such as sorption nonequilibrium or diffusion-controlled sorption rates. All tests were conducted at 25°C.

Table E-7. Results of RELAP Fits to Rising Limbs of Lithium and Bromide Breakthrough Curves in Crushed Tuff Columns

Column	Figure	Flow Rate (mL/hr)	Lithium Concentration (mg/L)	τ (hr)	Pe	R_f	k_f (1/hr)	Da
1 ^a	E-20	2.2	23.5	7.6	250	2.0 (2.0)	3.1	24
1	E-21	1.6	23.5	10.3	260	2.0 (2.0)	3.7	38
1 ^a	E-22	9.7	20.1	1.8	580	1.8 (1.7)	8.8	16
2 ^a	E-23	2.2	5.9	7.7	870	2.3 (2.3)	22	169
2	E-24	1.6	5.9	10.4	750	2.3 (2.25)	4.6	48

Source: DTN: LA0301PR831231.001 [DIRS 162603] (for flow rates and concentrations).

Output DTN: LA0303PR831361.003 (RELAP results).

NOTE: τ = residence time; Pe = Peclet number; R_f = retardation factor; k_f = rate constant for sorption onto the column material; and Da = Damkohler number ($= k_f \tau$), which represents the ratio of reaction rate to advection rate in the columns. R_f values in parentheses indicate the best-fitting retardation factors when equilibrium sorption was assumed (i.e., very fast sorption kinetics).

^aDenotes experiments in which tracer concentrations were monitored until background levels were reached.

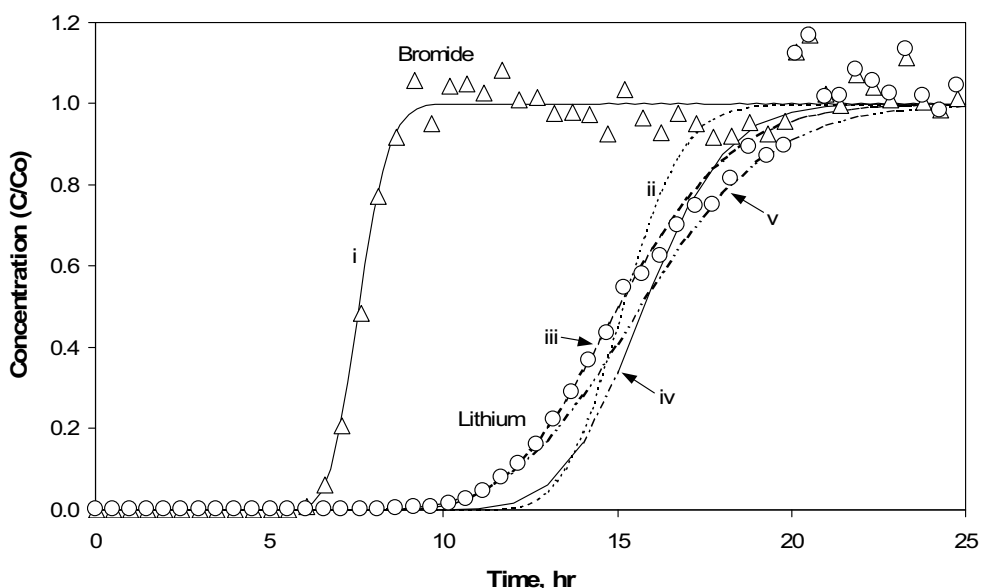
E3.1.2 Interpretive Methods

The bromide responses in the experiments were interpreted using the RELAP V 2.0 computer code (STN: 10551-2.0-00 [DIRS 159065]) to obtain estimates of mean residence times and dispersivities/Peclet numbers in the columns. RELAP was also used to fit the rising limbs of the lithium responses in each experiment to obtain an estimate of the lithium retardation factor in the columns. The rate-limited sorption features of RELAP were also used to obtain an estimate of the rate constant (k_f) describing lithium sorption onto the column packing material. The rate constants were obtained by relaxing the equilibrium sorption assumption and adjusting the rate constants for each data set until the RELAP fits were optimized. Damkohler numbers ($k_f \tau$), which represent the ratio of reaction rate to advection rate in the columns, were calculated for each experiment. Damkohler numbers significantly greater than one indicate a system that can be treated as being at equilibrium locally (Valocchi 1985 [DIRS 144579], pp. 808 to 820).

It was apparent that while RELAP V 2.0 (STN: 10551-2.0-00 [DIRS 159065]) could fit the arrival of lithium, it could not fit the tails of the lithium responses when concentrations were monitored until they returned to background levels. The tails exhibited a behavior suggesting that a portion of the lithium eluted with the bromide as if it were a nonsorbing tracer. This behavior can occur when an ion-exchanging cation such as lithium comprises the majority of the cation equivalents in the tracer solution, which was certainly the case in the higher-concentration LiBr experiments. Essentially, if the CEC of the tuff and the exchange equilibria are not sufficient to exchange all of the lithium injected into a column, then some of the lithium must elute with the bromide to maintain charge balance in the solution exiting the column. Thus, for the tests in which the lithium was fully eluted from the columns, the MULTRAN V 1.0 computer code (STN: 10666-1.0-00 [DIRS 159068]), which is capable of explicitly modeling cation exchange and maintaining solution charge balance, was used to interpret the lithium responses (see Section E3.2.2 for description of the code).

E3.1.3 Results and Interpretations

The rising limbs of the breakthrough curves for the five experiments along with the RELAP V 2.0 (STN: 10551-2.0-00 [DIRS 159065]) fits to the data are shown in Figures E-20 through E-24. The best-fitting parameters are listed in Table E-7. Although significant improvements to the RELAP fits of the lithium breakthrough curves were obtained by assuming finite sorption rates, the relatively large Damkohler numbers listed in Table E-7 suggest that the local equilibrium assumption is reasonably valid in the columns. Furthermore, this assumption should be even more valid in field experiments where tracer residence times are much longer than in the columns. Figure E-20 shows the results of fitting the lithium response curve from one of the experiments assuming a nonlinear (Langmuir) sorption isotherm with parameters obtained from batch sorption testing ($K_L = 0.0058 \text{ mL}/\mu\text{g}$ and $S_{\max} = 106 \mu\text{g/g}$ for the Bullfrog Tuff from c#2 used in these columns). It is apparent that the RELAP fits are not improved by assuming a nonlinear isotherm. The RETRAN V 2.0 computer code (STN: 10552-2.0-00 [DIRS 159066]) was used for the nonlinear simulations.



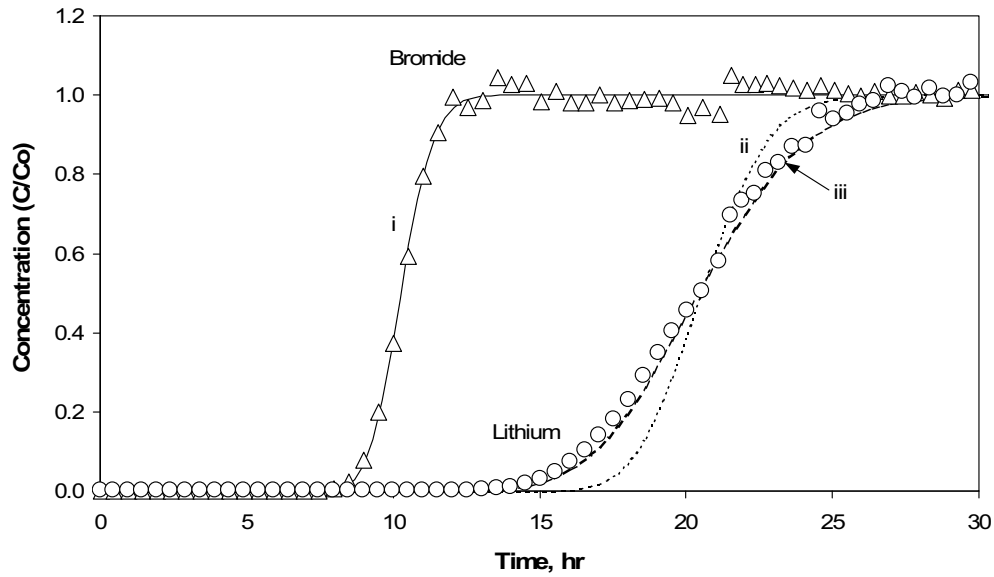
Source: DTN: LA0301PR831231.001 [DIRS 162603] (data).

Output DTN: LA0303PR831361.003 (fits).

NOTE: The curves above are numbered as follows:

- (i) Fit to bromide data with a Pelet number of 250
 - (ii) Fit to lithium data assuming linear isotherm ($R_F = 2.0$) with equilibrium sorption
 - (iii) Fit to lithium data assuming linear isotherm with a forward rate constant of 3.1 1/hr (and $R_F = 2.0$)
 - (iv) Fit to lithium data assuming a Langmuir isotherm with equilibrium sorption
 - (v) Fit to lithium data assuming a Langmuir isotherm with a forward rate constant of 3.2 1/hr.
- Langmuir isotherm parameters: $K_L = 0.0058 \text{ mL}/\mu\text{g}$ and $S_{\max} = 105.8 \mu\text{g/g}$ (batch isotherm values obtained for lithium on central Bullfrog Tuff from UE-25 c#2).

Figure E-20. Bromide and Lithium Breakthrough Curves in Column 1 at a Flow Rate of 2.2 mL/hr and Corresponding RELAP and RETRAN Fits to Data



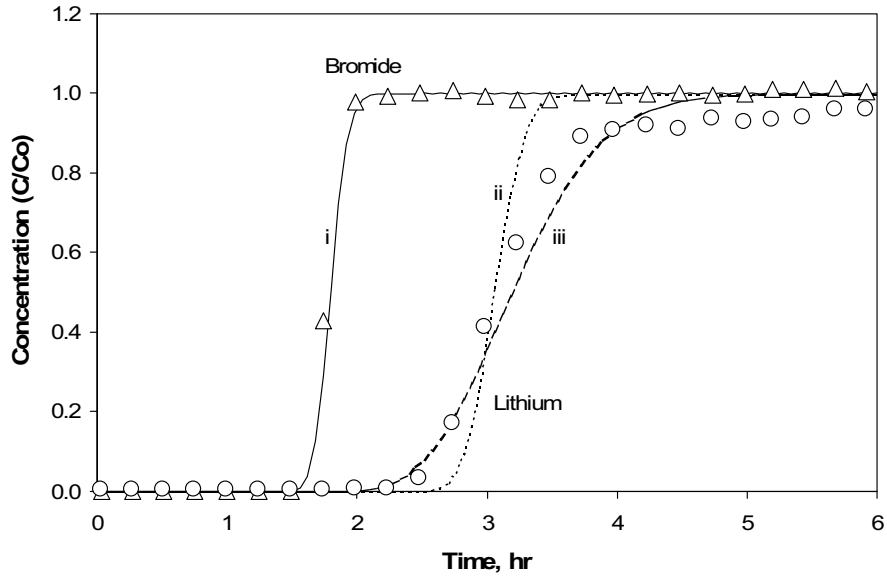
Source: DTN: LA0301PR831231.001 [DIRS 162603] (data).

Output DTN: LA0303PR831361.003 (fits).

NOTE: The curves above are numbered as follows:

- (i) Fit to bromide data with a Peclet number of 260
- (ii) Fit to lithium data assuming linear isotherm ($R_F = 2.0$) with equilibrium sorption
- (iii) Fit to lithium data assuming linear isotherm with a forward rate constant of 3.7 1/hr (and $R_F = 2.0$).

Figure E-21. Bromide and Lithium Breakthrough Curves in Column 1 at a Flow Rate of 1.6 mL/hr and Corresponding RELAP Fits to Data



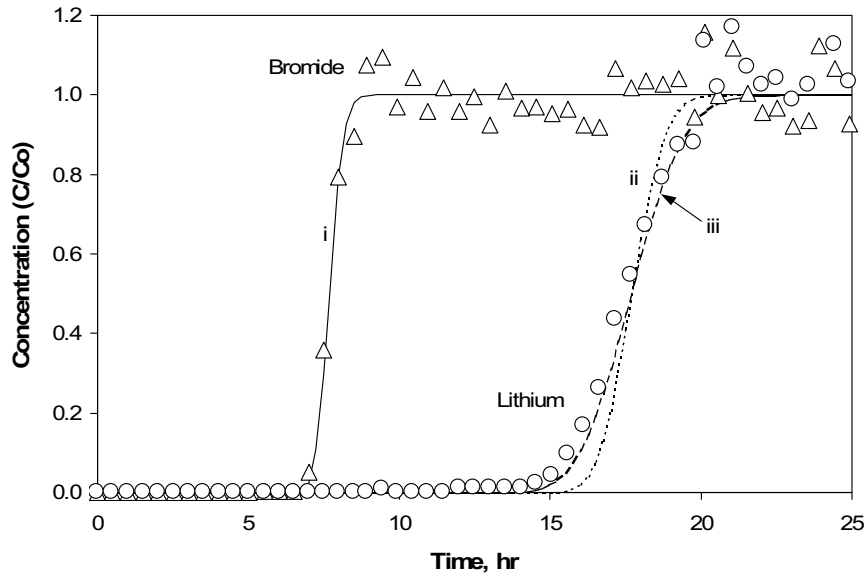
Source: DTN: LA0301PR831231.001 [DIRS 162603] (data).

Output DTN: LA0303PR831361.003 (fits).

NOTE: The curves above are numbered as follows:

- (i) Fit to bromide data with a Peclet number of 580
- (ii) Fit to lithium data assuming linear isotherm ($R_F = 1.7$) with equilibrium sorption
- (iii) Fit to lithium data assuming linear isotherm with a forward rate constant of 8.8 1/hr (and $R_F = 1.8$).

Figure E-22. Bromide and Lithium Breakthrough Curves in Column 1 at a Flow Rate of 9.7 mL/hr and Corresponding RELAP Fits to Data



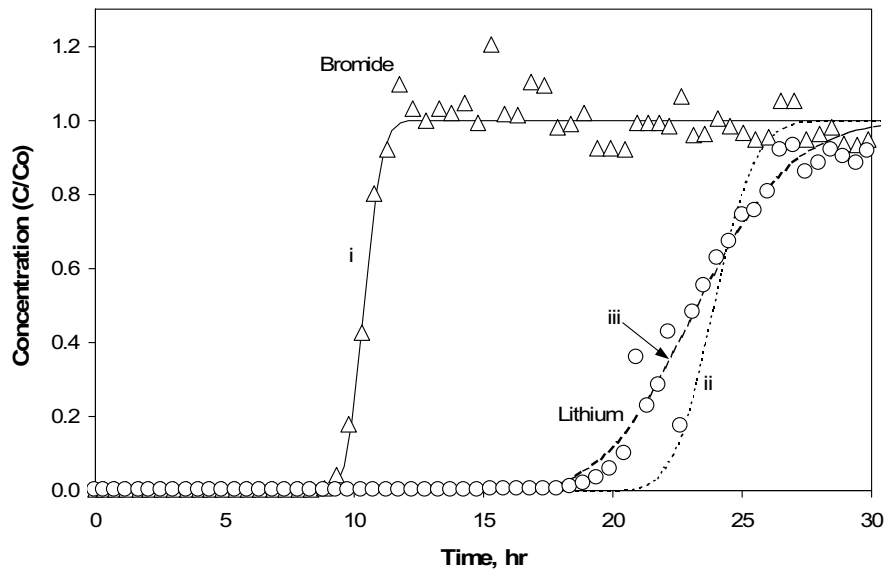
Source: DTN: LA0301PR831231.001 [DIRS 162603] (data).

Output DTN: LA0303PR831361.003 (fits).

NOTE: The curves above are numbered as follows:

- (i) Fit to bromide data with a Peclet number of 870
- (ii) Fit to lithium data assuming linear isotherm ($R_F = 2.3$) with equilibrium sorption
- (iii) Fit to lithium data assuming linear isotherm with a forward rate constant of 22 1/hr (and $R_F = 2.3$).

Figure E-23. Bromide and Lithium Breakthrough Curves in Column 2 at a Flow Rate of 2.2 mL/hr and Corresponding RELAP Fits to Data



Source: DTN: LA0301PR831231.001 [DIRS 162603] (data).

Output DTN: LA0303PR831361.003 (fits).

NOTE: The curves above are numbered as follows:

- (i) Fit to bromide data with a Peclet number of 750
- (ii) Fit to lithium data assuming linear isotherm ($R_F = 2.3$) with equilibrium sorption
- (iii) Fit to lithium data assuming linear isotherm with a forward rate constant of 4.6 1/hr (and $R_F = 2.25$).

Figure E-24. Bromide and Lithium Breakthrough Curves in Column 2 at a Flow Rate of 1.6 mL/hr and Corresponding RELAP Fits to Data

Table E-7 shows that lithium retardation factors (R_{FS}) for the tests with lower tracer concentrations ranged from 2.2 to 2.3, with a mean of 2.25; whereas R_{FS} for the higher concentration tests ranged from 1.7 to 2.0, with a mean of 1.87. The observed decreased R_F at higher concentrations is consistent with a nonlinear sorption isotherm. For the Langmuir isotherm, the R_F can be shown to be (Fetter 1993 [DIRS 102009], pp. 122 to 123):

$$R_F = 1 + \frac{\rho_B}{\theta} \left(\frac{K_L S_{\max}}{(1 + K_L C)^2} \right) \quad (\text{Eq. E-10})$$

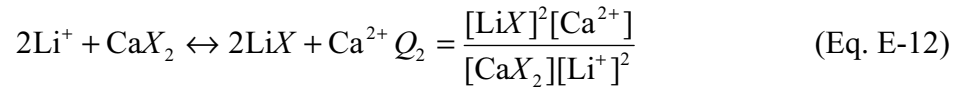
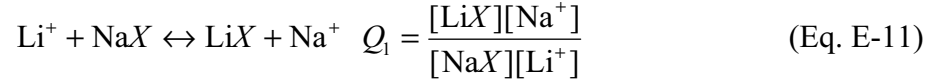
where

ρ_B is the dry bulk density of the medium (g/mL)

θ is the volumetric moisture content, or porosity for a saturated medium.

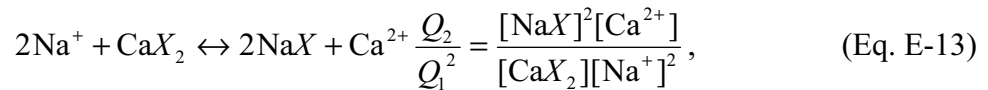
By solving Equation E-10 with the batch Langmuir parameters obtained for the Central Bullfrog Tuff used in the column experiments ($K_L = 0.0053$ mL/ μ g and $S_{\max} = 110$ μ g/g – see Table E-4 footnote) and column values for ρ_B and θ , retardation factor predictions of 2.11 are obtained for the lower concentration tests and 1.95 for the higher concentration tests. Overall these predictions match the R_F values of Table E-7 very well, differing by 7% or less for both concentration levels. The MULTRAN V 1.0 (STN: 10666-1.0-00 [DIRS 159068]) fits to the

full data sets for the three experiments in which tracer concentrations were monitored until they returned to background levels are shown in Figures E-25 to E-27. The Q_1 and Q_2 values listed in these figures correspond to the “selectivity coefficients” for the following cation-exchange reactions (LANL 2002 [DIRS 171587], MOL.20021021.0385, Section 2):



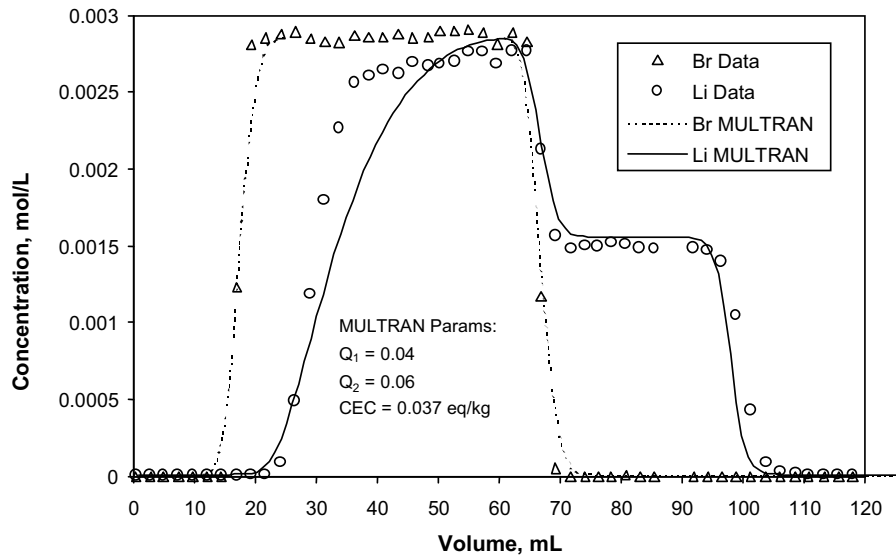
where X = a negatively charged surface site.

In addition to these reactions, MULTRAN V 1.0 (STN: 10666-1.0-00 [DIRS 159068]) also accounts for the exchange between sodium and calcium ions, and it solves the surface cation-exchange balance equation for a three-component system (LANL 2002 [DIRS 171587], MOL.20021021.0385, Section 2):



$$\text{CEC} = \frac{\rho_B}{\phi} ([\text{LiX}] + [\text{NaX}] + 2[\text{CaX}_2]) \quad (\text{Eq. E-14})$$

The measured CEC for the Bullfrog Tuff (Section E1.2) was used as the CEC value in the simulations, and the selectivity coefficients Q_1 and Q_2 were adjusted to fit the lithium data. However, without sodium and calcium concentration data, it was not possible to obtain a unique fit to the lithium responses. In fact, the lithium responses could be fit equally well assuming lithium exchange with only sodium or only calcium. Thus, the Q_1 and Q_2 values presented in Figures E-25 through E-27 should be considered as only one of many possible combinations that could fit the lithium data equally well. However, it is not the values of these parameters that are important but rather the recognition that cation-exchange equilibria must be explicitly accounted for to explain the observed transport behavior of the lithium. For comparison, a RELAP V 2.0 (STN: 10551-2.0-00 [DIRS 159065]) “fit” to the data from Figure E-25 is shown in Figure E-28. It is clear that the single-component equilibrium K_d -model fit cannot capture the tailing behavior of the lithium. These results could have important implications for field tracer tests conducted in porous media that have a small sorption capacity for cation-exchanging tracers.

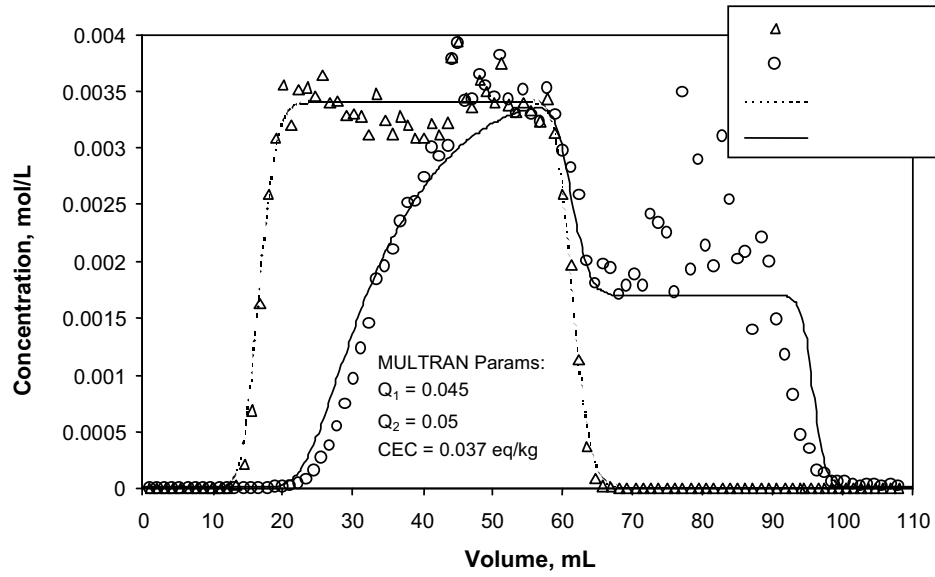


Source: DTN: LA0301PR831231.001 [DIRS 162603] (data).

Output DTN: LA0303PR831361.003 (fits).

NOTE: "MULTRAN Params" refers to the parameter values used in MULTRAN V 1.0 (STN: 10666-1.0-00 [DIRS 159068]) to obtain the simulated curves.

Figure E-25. MULTRAN Fits to Complete Bromide and Lithium Breakthrough Curves from High-Concentration Experiment Conducted at 9.7 mL/hr in Column 1 (Figure E-22)

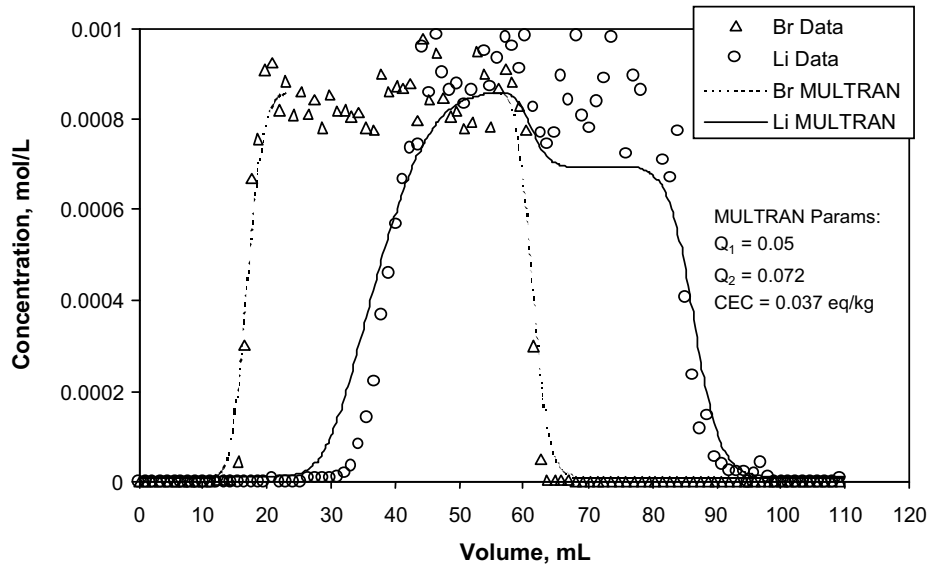


Source: DTN: LA0301PR831231.001 [DIRS 162603] (data).

Output DTN: LA0303PR831361.003 (fits).

NOTE: "MULTRAN Params" refers to the parameter values used in MULTRAN V 1.0 (STN: 10666-1.0-00 [DIRS 159068]) to obtain the simulated curves.

Figure E-26. MULTRAN Fits to Complete Bromide and Lithium Breakthrough Curves from High-Concentration Experiment Conducted at 2.2 mL/hr in Column 1 (Figure E-20)

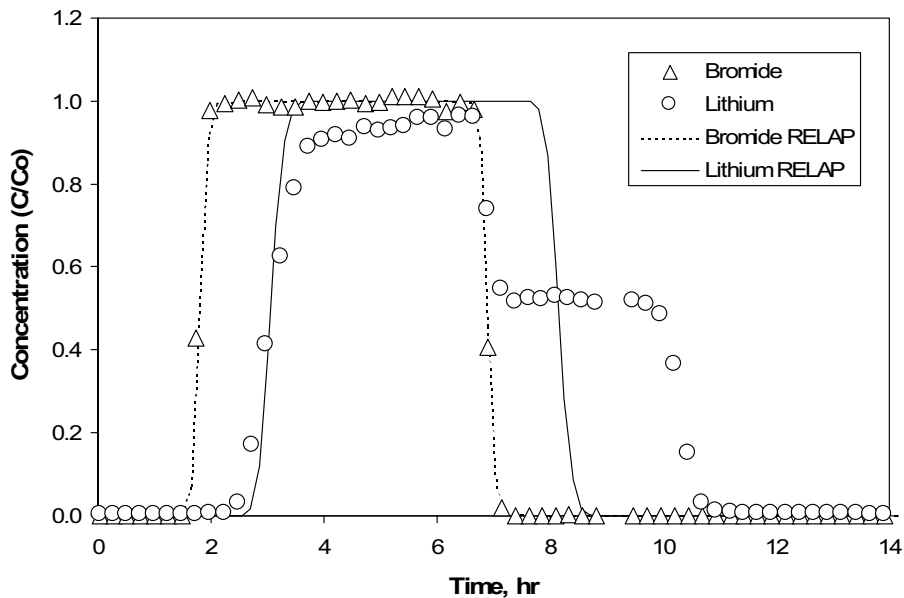


Source: DTN: LA0301PR831231.001 [DIRS 162603] (data).

Output DTN: LA0303PR831361.003 (fits).

NOTE: "MULTRAN Params" refers to the parameter values used in MULTRAN V 1.0 (STN: 10666-1.0-00 [DIRS 159068]) to obtain the simulated curves.

Figure E-27. MULTRAN Fits to Complete Bromide and Lithium Breakthrough Curves from Low-Concentration Experiment Conducted at 2.2 mL/hr in Column 2 (Figure E-23)



Source: DTN: LA0301PR831231.001 [DIRS 162603] (data).

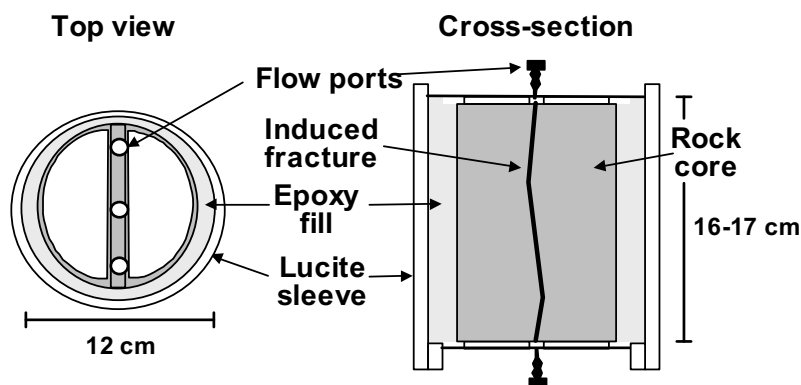
Output DTN: LA0303PR831361.003 (fits).

Figure E-28. RELAP Fits to Complete Bromide and Lithium Breakthrough Curves from Experiment Conducted at 9.7 mL/hr in Column 1 (Figure E-25 Shows the MULTRAN Fits)

E3.2 FRACTURED-CORE EXPERIMENTS

E3.2.1 Experimental Methods

Fractured-core transport experiments were conducted on four separate cores obtained from the C-wells following the procedure by Callahan et al. (2000 [DIRS 156648], pp. 3547 to 3558). The experiments are documented in detail by Reimus (2003 [DIRS 163760], Attachments B1 and B2). The cores were obtained from locations 3, 4, 5, and 6 in Figure E-1. In the following discussion, the cores from the upper, central, and lower flow zones of the Prow Pass Tuff (locations 4, 5, and 6, respectively) will be referred to as cores 1, 2, and 3, respectively. The core from the lower flow zone of the Bullfrog Tuff will be referred to as core 4. The mineralogy of the cores is given in Table E-3. Core 4 (lower flow zone of the Bullfrog Tuff) contained the highest percentage of clay and zeolite minerals, 9 ± 3 wt % smectite, 4 ± 1 wt % clinoptilolite, and 13 ± 1 wt % analcime. A single fracture was mechanically induced in each of the four cores. The cores were laid on a cement floor and a four-pound hammer and chisel were used to induce an axial fracture running the length of the core. The cores were then encased in an epoxy and Plexiglas column apparatus following the Callahan et al. (2000 [DIRS 156648]) procedure. Figure E-29 shows a schematic illustration of a column experimental system.



NOTE: For illustration purposes only. Three flow ports on each end of the core allowed access to the inlet and outlet regions; the central flow ports were used to connect the cores to a syringe pump and fraction collector via a 0.8-mm-diameter tubing. The lengths of the cores varied, but the diameters of all cores were 9.5 cm.

Figure E-29. Schematic Illustration of a Fractured Rock Core Experimental System

The tracer experiments conducted in each core are summarized in Tables E-8 through E-13. As described by Callahan et al. (2000 [DIRS 156648]), cores 1 and 2 each featured three experiments in which iodide was used as a nonsorbing tracer at three different flow rates. The objective of these experiments was to obtain estimates of matrix-diffusion, mass-transfer parameters in the cores by using RELAP to fit simultaneously the iodide responses at each flow rate. All four cores also featured at least two multiple-tracer experiments that were conducted and interpreted very similarly to the C-wells field tracer tests. Each experiment involved the injection of a pulse containing PFBA, lithium bromide (LiBr), and, in some cases, sodium iodide (NaI). Five multiple-tracer experiments were conducted in core 1. Two of these experiments were intended to be replicates, and they yielded very similar results, indicating good experimental reproducibility. Only two multiple-tracer tests were conducted in each of the other

three cores. The flow rate in at least one of the multiple-tracer experiment in each core was approximately an order of magnitude lower than the flow rate(s) in the other multiple-tracer experiment(s). Flow rates were varied over this large range so that the effect of experiment time scale on matrix diffusion processes could be assessed in fracture systems of constant geometry. The fractures were thoroughly flushed after each experiment so that residual tracer concentrations were minimized in subsequent experiments.

A steady-state flow field was established in each core by continuously injecting degassed, filtered groundwater obtained from well J-13. A pulse of tracer solution (tracers dissolved in J-13 well water) was then injected. After injection of the tracer pulse, continuous injection of tracer-free J-13 well water was resumed. The effluent was monitored for the tracer ions as well as for Na^+ and Ca^{2+} using ion chromatography for Br^- and PFBA and ICP-AES for analysis of Li^+ , Na^+ , and Ca^{2+} . Iodide was analyzed either using an ion-selective electrode or ion chromatography. The quantitative detection limits were 0.05 mg/L for Li^+ , Na^+ , and Ca^{2+} ; 0.04 mg/L for Br^- ; 0.02 mg/L for I^- ; and 0.02 mg L^{-1} for PFBA. Na^+ and Ca^{2+} were analyzed so that cation-exchange equilibria could be more rigorously quantified than in the crushed-tuff column experiments described in Section E3.1. Copper complexed with ethylenediamine tetraacetic acid was used as a tracer in some of the experiments to determine its potential to serve as a weakly sorbing tracer in field tests. In some of the tests (Tables E-9 through E-13), flow was interrupted for a time after the tracer concentrations had been tailing to verify diffusive mass transfer in the cores (Brusseau et al. 1997 [DIRS 156647], pp. 205 to 219; Callahan et al. 2000 [DIRS 156648]). This strategy was similar to that used in the Prow Pass multiple-tracer field test (Section D4.4).

Table E-8. Experimental Conditions for the Iodide Fracture Transport Tests, Upper Prow Pass Tuff Core (Core 1)

Experimental Parameters			
Core length, L (m)	0.161		
Core width, w (m)	0.095		
Matrix porosity, nm	0.272		
Hydraulic aperture, Bh (m) ^a	0.14×10^{-3}		
Iodide tests:	Test 1	Test 2	Test 3
Volumetric flow rate, Q (mL/hr)	2.2	19.6	8.7
Injection duration, t_p (hr)	28.02	3.08	7.23
Injection concentration, C_o (mg/L)	1,000	1,000	1,000
Flow interruption period, time since start of injection (hr)	N/A ^b	N/A ^b	N/A ^b
Flow rate after restart, Q (mL/hr)	N/A ^b	N/A ^b	N/A ^b
Mass recovery (%)	86	96	94

Source: Reimus 2003 [DIRS 163760], Attachment B1.

^a Determined from a constant head permeameter method.

^b N/A: Not applicable; flow was not interrupted during these tests.

Table E-9. Experimental Conditions for the Multiple-Tracer Fracture Transport Tests, Upper Prow Pass Tuff Core (Core 1)

Experimental Parameters	Test 1	Test 2	
Volumetric flow rate, Q (mL/hr)	3.8	3.9	
Injection duration, t_p (hr)	14.97	15.22	
Injection concentration, C_o (mg/L)	192 (Li ⁺) 0 (Na ⁺) 0 (Ca ²⁺) 1,728 (Br ⁻) 300 (I ⁻) 635 (PFBA)	192 (Li ⁺) 0 (Na ⁺) 0 (Ca ²⁺) 1,728 (Br ⁻) 300 (I ⁻) 635 (PFBA)	
Background groundwater concentration, C_i (mg/L)	0.64 (Li ⁺) 46.7 (Na ⁺) 12.8 (Ca ²⁺) 3.63 (Br ⁻) 1.8 (I ⁻) 1.11 (PFBA)	1.79 (Li ⁺) 45.4 (Na ⁺) 12.8 (Ca ²⁺) 10.7 (Br ⁻) 0.55 (I ⁻) 3.86 (PFBA)	
Flow interruption period, time since start of injection (hr)	87.3 to 137.3	87.1 to 137.2	
Flow rate after restart, Q (mL/hr)	3.96	3.99	
Mass recovery (%)	89 (Li ⁺) 89 (Br ⁻) 92 (I ⁻) 95 (PFBA)	89 (Li ⁺) 89 (Br ⁻) 86 (I ⁻) 95 (PFBA)	
Experimental Parameters	Test 3	Test 4	Test 5
Volumetric flow rate, Q (mL hr ⁻¹)	0.51	7.9	6.3
Injection duration, t_p (hr)	156.85	19.0	10.5
Injection concentration, C_o (mg/L)	159 (Li ⁺) 394 (Na ⁺) 0 (Ca ²⁺) 1,870 (Br ⁻) 296 (I ⁻) 641 (PFBA) 145 (Cu ²⁺) 699 (EDTA)	1,010 (Li ⁺) 59.1 (Na ⁺) 0 (Ca ²⁺) 11,400 (Br ⁻) N/A ^a (I ⁻) 766 (PFBA)	216 (Li ⁺) 250 (Na ⁺) 0 (Ca ²⁺) 2,528 (Br ⁻) N/A ^a (I ⁻) 766 (PFBA) 192 (Cu ²⁺) 1,131 (EDTA)
Background groundwater concentration, C_i (mg/L)	0.08 (Li ⁺) 51.8 (Na ⁺) 13.2 (Ca ²⁺) 10.87 (Br ⁻) < 0.4 (I ⁻) 2.07 (PFBA)	0.08 (Li ⁺) 45 (Na ⁺) 13.3 (Ca ²⁺) < 0.02 (Br ⁻) < 0.4 (I ⁻) < 0.005 (PFBA)	0.53 (Li ⁺) 45 (Na ⁺) 13.3 (Ca ²⁺) 0.98 (Br ⁻) < 0.4 (I ⁻) < 0.005 (PFBA)
Flow interruption period, time since start of injection (hr)	689 to 904	19.8 to 21.2, 49.9 to 64.2	44.0 to 64.0
Flow rate after restart, Q (mL/hr)	0.51	8.05, 8.04	6.46
Mass recovery (%)	83 (Li ⁺) 94 (Br ⁻) 82 (I ⁻) 94 (PFBA)	89 (Li ⁺) 89 (Br ⁻) N/A ^a (I ⁻) 95 (PFBA)	89 (Li ⁺) 89 (Br ⁻) N/A ^a (I ⁻) 95 (PFBA)

Source: Reimus 2003 [DIRS 163760], Attachment B1.

^a N/A: not applicable; iodide was not injected in these tests.

EDTA=ethylenediamine tetraacetic acid; PFBA=pentafluorobenzoic acid or pentafluorobenzoate.

Table E-10. Experimental Conditions for the Iodide Fracture Transport Tests, Central Prow Pass Tuff Core (Core 2)

Experimental Parameters			
Core length, L (m)	0.173		
Core width, w (m)	0.095		
Matrix porosity, n_m	0.138		
Hydraulic aperture, B_h (m) ^a	0.13×10^{-3}		
	Test 1	Test 2	Test 3
Volumetric flow rate, Q (mL/hr)	19.7	49.3	11.3
Injection duration, t_p (hr)	4.0	1.47	6.05
Injection concentration, C_o (mg/L)	1,000	1,000	1,000
Flow interruption period, time since start of injection (hr)	N/A ^b	N/A ^b	N/A ^b
Flow rate after restart, Q (mL/hr)	N/A ^b	N/A ^b	N/A ^b
Mass recovery (%)	89	98	84

Source: Reimus 2003 [DIRS 163760], Attachment B2.

^a Determined from a constant head permeameter method.

^b N/A: not applicable; flow was not interrupted during these tests.

Table E-11. Experimental Conditions for the Multiple-Tracer Fracture Transport Tests, Central Prow Pass Tuff Core (Core 2)

Experimental Parameters	Test 1	Test 2
Volumetric flow rate, Q (mL/hr)	5.9	0.44
Injection duration, t_p (hr)	12.3	170
Injection concentration, C_o (mg/L)	216 (Li ⁺) 205 (Na ⁺) 0 (Ca ²⁺) 2,528 (Br ⁻) N/A ^a (I ⁻) 766 (PFBA) 192 (Cu ²⁺) 1131 (EDTA)	159 (Li ⁺) 301 (Na ⁺) 0 (Ca ²⁺) 1,870 (Br ⁻) 296 (I ⁻) 641 (PFBA) 145 (Cu ²⁺) 699 (EDTA)
Background groundwater concentration, C_i (mg/L)	0.08 (Li ⁺) 45 (Na ⁺) 13.3 (Ca ²⁺) < 0.02 (Br ⁻) < 0.4 (I ⁻) < 0.005 (PFBA)	0.55 (Li ⁺) 75.1 (Na ⁺) 10.0 (Ca ²⁺) 1.97 (Br ⁻) 0.9 (I ⁻) 0.98 (PFBA)
Flow interruption period, time since start of injection (hr)	42.9 to 62.9	799 to 999
Flow rate after restart, Q (mL/hr)	5.95	0.44
Mass recovery (%)	84 (Li ⁺) 90 (Br ⁻) N/A ^a (I ⁻) 95 (PFBA)	68 (Li ⁺) 97 (Br ⁻) 97 (I ⁻) 102 (PFBA)

Source: Reimus 2003 [DIRS 163760], Attachment B2.

^a N/A: not applicable; iodide was not injected in these tests.

EDTA=ethylenediamine tetraacetic acid; PFBA=pentafluorobenzoic acid.

Table E-12. Experimental Conditions for the Multiple-Tracer Fracture Transport Tests, Lower Prow Pass Tuff Core (Core 3)

Experimental Parameters		
Core length, L (m)	0.116	
Core width, w (m)	0.095	
Matrix porosity, n_m	0.288	
Hydraulic aperture, B_h (m) ^a	0.16×10^{-3}	
	Test 1	Test 2
Volumetric flow rate, Q (mL/hr)	11.4	0.46
Injection duration, t_p (hr)	14.5	340
Injection concentration, C_o (mg/L)	159 (Li ⁺) 331 (Na ⁺) 1.2 (Ca ²⁺) 1870 (Br ⁻) 296 (I ⁻) 641 (PFBA) 145 (Cu ²⁺) 699 (EDTA)	165 (Li ⁺) 310 (Na ⁺) 0 (Ca ²⁺) 1930 (Br ⁻) 299 (I ⁻) 681 (PFBA) 150 (Cu ²⁺) 699 (EDTA)
Background groundwater concentration, C_i (mg/L)	0.08 (Li ⁺) 44.6 (Na ⁺) 13.3 (Ca ²⁺) < 0.02 (Br ⁻) < 0.35 (I ⁻) < 0.005 (PFBA)	4.41 (Li ⁺) 67.2 (Na ⁺) 16.4 (Ca ²⁺) 60.1 (Br ⁻) 9.49 (I ⁻) 16.2 (PFBA)
Flow interruption period, time since start of injection (hr)	43.6 to 68.6	792 to 992
Flow rate after restart, Q (mL/hr)	11.4	0.47
Mass recovery (%)	97.2 (Li ⁺) 95.7 (Br ⁻) 98.4 (I ⁻) 99.3 (PFBA)	72.4 (Li ⁺) 87.3 (Br ⁻) 84.2 (I ⁻) 80.1 (PFBA)

Source: Reimus 2003 [DIRS 163760], Attachment B1.

^a Determined from a constant head permeameter method.

EDTA=ethylenediamine tetraacetic acid; PFBA=pentafluorobenzoic acid.

Table E-13. Experimental Conditions for the Multiple-Tracer Fracture Transport Tests, Lower Bullfrog Tuff Core (Core 4)

Experimental Parameters	Test 1	Test 2
Volumetric flow rate, Q (mL/hr)	5.0	0.47
Injection duration, t_p (hr)	34.0	335.0
Injection concentration, C_o (mg/L)	165 (Li^+) 342 (Na^+) 0 (Ca^{2+}) 1930 (Br^-) 299 (I^-) 681 (PFBA) 150 (Cu^{2+}) 699 (EDTA)	192 (Li^+) 0 (Na^+) 0 (Ca^{2+}) 1728 (Br^-) 300 (I^-) 635 (PFBA)
Background groundwater concentration, C_i (mg/L)	0.04 (Li^+) 51.1 (Na^+) 11.0 (Ca^{2+}) 0.14 (Br^-) 0.07 (I^-) 0.14 (PFBA)	4.41 (Li^+) 67.2 (Na^+) 16.4 (Ca^{2+}) 60.1 (Br^-) 9.49 (I^-) 16.2 (PFBA)
Flow interruption period, time since start of injection (hr)	67.2 to 87.2	79 to 992
Flow rate after restart, Q (mL/hr)	5.05	0.47
Mass recovery (%)	57 (Li^+) 96 (Br^-) 86 (I^-) 99 (PFBA)	85 (Li^+) 103 (Br^-) 86 (I^-) 91 (PFBA)

Source: Reimus 2003 [DIRS 163760], Attachment B2.

EDTA=ethylenediamine tetraacetic acid; PFBA=pentafluorobenzoic acid.

E3.2.2 Interpretive Methods

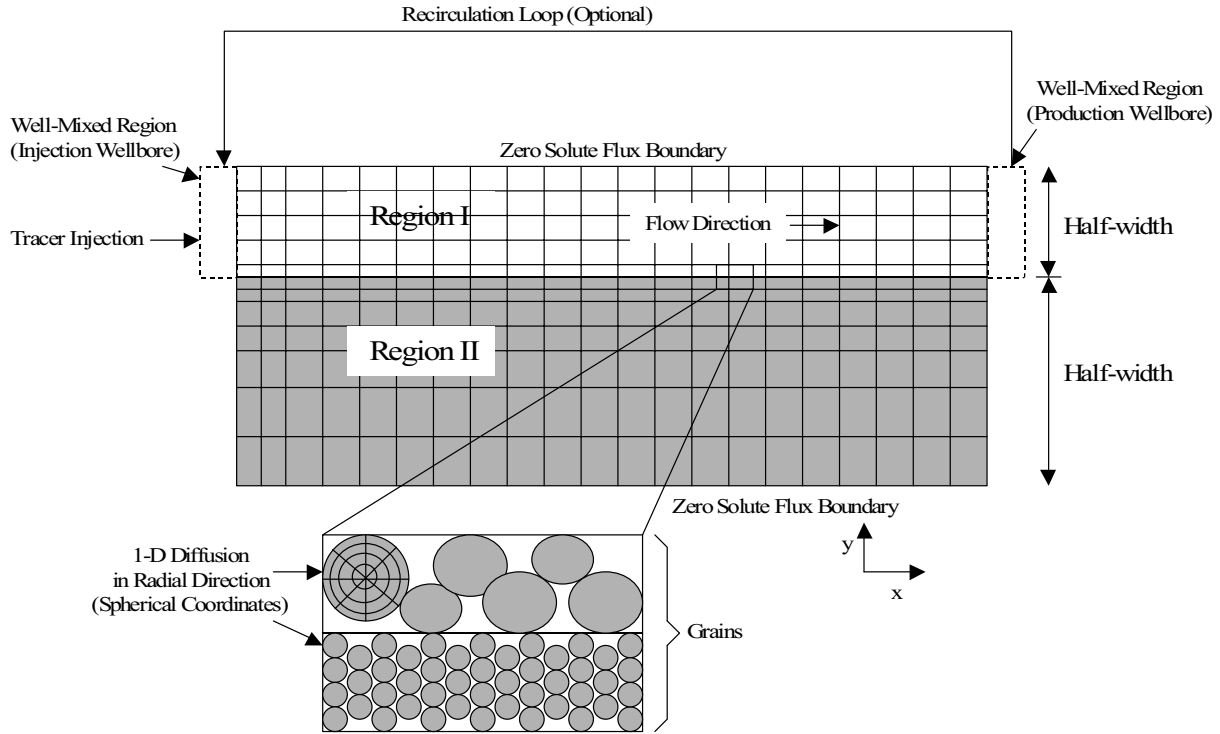
The RELAP V 2.0 (STN: 10551-2.0-00 [DIRS 159065]) code was used to interpret the nonsorbing iodide, bromide, and PFBA tracer responses. For the iodide-only experiments conducted in cores 1 and 2, the responses at the three different flow rates were simultaneously fitted, assuming the same Peclet number and matrix diffusion mass transfer coefficient (mass transfer coefficient [MTC] = $\phi D_m^{1/2}/b$) in each test, and a mean residence time (τ) that was inversely proportional to flow rate. This procedure assumes that the MTC and Peclet number have no flow rate or time scale dependence.

For the multiple-tracer tests, the bromide and PFBA responses were simultaneously fitted, assuming that bromide had a matrix diffusion coefficient a factor of three greater than PFBA (this same assumption was used in the field tracer-test interpretations). However, because of the difficulties encountered in fitting the lithium responses in the crushed-tuff column experiments, and the fact that Na^+ and Ca^{2+} were analyzed in addition to Li^+ in the fractured-core experiments, it was decided to use the MULTRAN V 1.0 (STN: 10666-1.0-00 [DIRS 159068]) code

(described below) rather than RELAP V 2.0 (STN: 10551-2.0-00 [DIRS 159065]) to interpret the lithium responses. The values of τ , Pe , and MTC that provided the best RELAP fits to the bromide and PFBA responses were used as inputs to MULTRAN (for tests conducted at different flow rates in the same core, τ was adjusted such that it was inversely proportional to flow rate and Pe was held constant for all tests). The parameters Q_1 and Q_2 were then adjusted to fit the Li^+ , Na^+ , and Ca^{2+} data while holding the CEC values equal to the measured CEC values.

MULTRAN V 1.0 (STN: 10666-1.0-00 [DIRS 159068]) employs an implicit-in-time, alternating-direction, finite-difference method to solve the two-dimensional numerical equations describing multicomponent transport of sorbing and nonsorbing solutes in a single- or dual-porosity medium. Figure E-30 illustrates the assumed simulation domain and shows an example spatial discretization. Advective transport, simulated by solving the advection-dispersion equation, is assumed to occur only in the x -direction in region I. The first and last nodes in the x -direction in this region are simulated as well-mixed regions that correspond to either boreholes in field experiments or flow manifolds in laboratory experiments. ReInjection of part or all of the solution entering the last node back into the first node can be specified to simulate recirculating conditions in tracer experiments. Only diffusive transport is assumed to occur in the y -direction in both regions I and II, with the code having the capability to simulate different diffusion coefficients in the different regions. Finally, within each region, additional diffusive transport can be simulated into “grains,” which are assumed to be spherical. These grains can be assigned a lognormal distribution of diameters with specified mean and variance. The user can control the spatial discretization within each region and within the grains.

The user also can eliminate certain portions of the domain shown in Figure E-30 simply by specifying that they have zero porosity. For instance, if one wishes to simulate a single-porosity medium, it is only necessary to specify a zero porosity for region II and zero porosity for the grains in region I. This approach was taken to simulate the crushed-tuff column transport experiments described in Section E3.1 because the columns were packed with a relatively uniform material that had no apparent secondary porosity. Reducing the simulation effectively to a one-dimensional system (region I) greatly simplifies numerical computations.



NOTE: For illustration purposes only. Blocks are finite-difference cells that are solved at their midpoints. Region I is the high-permeability layer (advective transport in x-direction, diffusive in y-direction); region II is the low-permeability layer (diffusive transport in y-direction only).

Figure E-30. Schematic Illustration of MULTRAN Simulation Domain

Each time-step of a MULTRAN V 1.0 (STN: 10666-1.0-00 [DIRS 159068]) simulation is broken into four computational segments conducted sequentially, as follows (LANL 2002 [DIRS 171587], MOL.20021021.0385, Section 2):

- (1) Solution of the advection-dispersion equation in the x-direction in region I:

$$\frac{\partial c}{\partial t} = -v_x \frac{\partial c}{\partial x} + D \frac{\partial^2 c}{\partial x^2} \quad (\text{Eq. E-15})$$

where

c = molar concentration, moles/L

v_x = velocity in x direction, cm/s

D = dispersion coefficient, cm^2/s ($D = \alpha v_x$, α = dispersivity, cm).

- (2) Solution of the multicomponent diffusion equation(s) and the local electroneutrality equation in the y-direction in regions I and II (coupled):

- a. *Multicomponent diffusion equation for all species except species n (Newman 1973 [DIRS 148719], p. 228):*

$$\frac{\partial c_i}{\partial t} = D_i \nabla^2 c_i - \sum_j \frac{z_j}{z_i} (D_j - D_n) \nabla \cdot (t_i \nabla c_i) \quad (\text{Eq. E-16})$$

where

c_i = molar concentration of species i , moles/L

D_i = diffusion coefficient of species i , cm^2/s

∇ = del operator

∇^2 = Laplacian operator

$$t_i = \frac{z_i^2 u_i c_i}{\sum_j z_j^2 u_j c_j} = \text{transference number of species } i$$

z_i = charge of species i

$u_i = \frac{D_i}{RT}$ = mobility of species i , where R = gas constant and T = temperature (K)

n = species being determined using electroneutrality equation.

b. *Electroneutrality equation for species n :*

$$z_n c_n = - \sum_{j \neq n} z_j c_j \quad (\text{Eq. E-17})$$

- (3) Solution of the multicomponent diffusion equation(s) and the local electroneutrality equation in the radial direction in the grains of both regions I and II (same as step 2, but using spherical coordinates).
- (4) Chemical re-equilibration of the entire system with respect to cation exchange. This step is accomplished by solving Equations E-11 through E-14 at each node in the simulation domain to ensure that the equilibrium expressions and the surface cation balance are locally satisfied. The system is assumed to always be at chemical equilibrium (i.e., reaction kinetics assumed to be fast relative to transport rates).

E3.2.3 Results and Interpretations

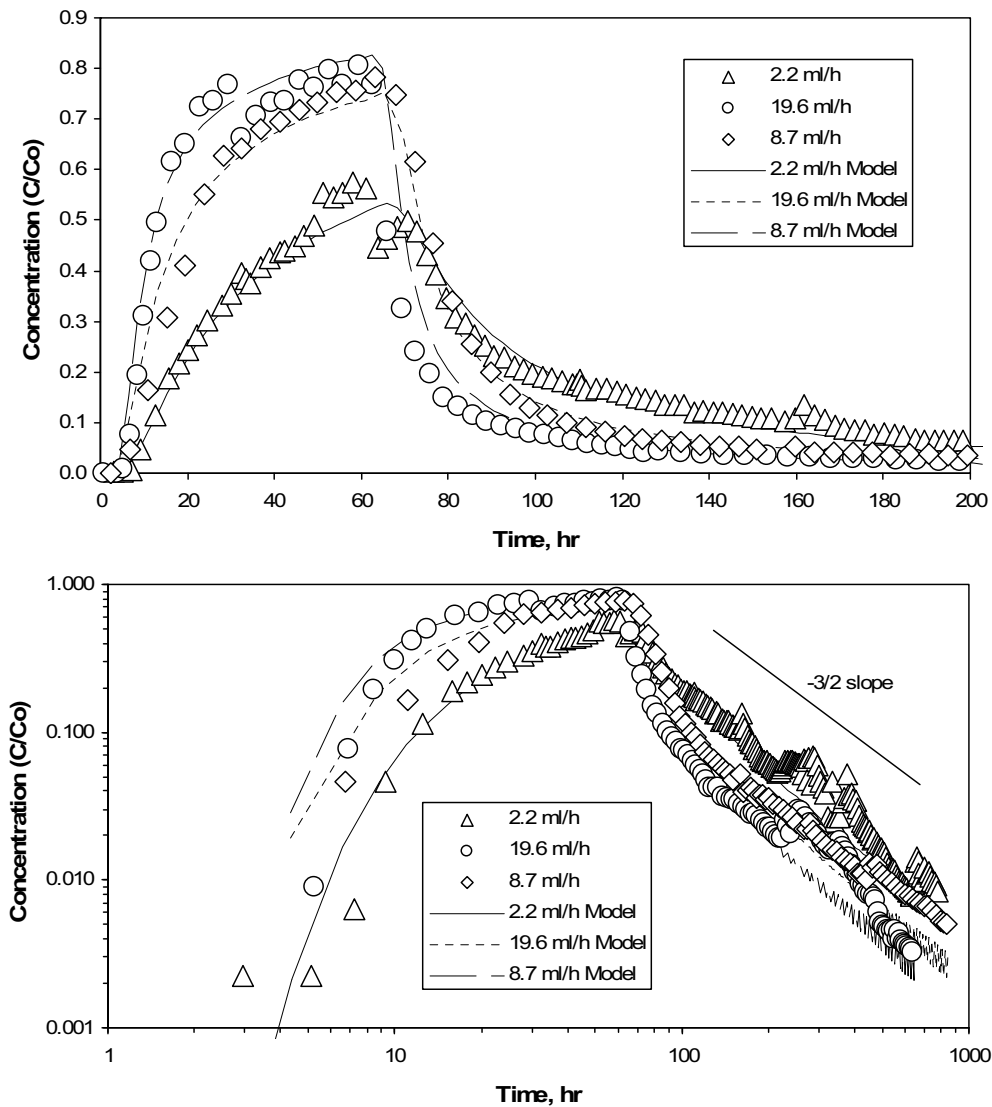
The experimental data and interpretive fits for the iodide-only tests conducted in cores 1 and 2 (three in each core) are shown in Figures E-31 and E-32, respectively. Tables E-14 and E-15 list the transport parameters associated with the fits shown in these figures. It is apparent that RELAP offered good simultaneous fits to the three data sets.

The experimental data and associated MULTRAN V 1.0 (STN: 10666-1.0-00 [DIRS 159068]) fits for Tests 1 and 3 in the Upper Prow Pass Tuff core (Core 1) are shown in Figure E-33. MULTRAN fits to the multiple-tracer tests in Cores 2, 3, and 4 (two tests in each core) are shown in Figures E-34, E-35, and, E-36, respectively. Table E-16 lists the transport parameters associated with the fits to the tracer responses in Cores 1 and 2, and Table E-17 lists the parameters associated with the fits to the responses in Cores 3 and 4. The Br^- and PFBA responses in the two tests in each core were first fitted simultaneously using RELAP V 2.0

(STN: 10551-2.0-00 [DIRS 159065]) (i.e., a total of four responses were fitted simultaneously, two from each test). The RELAP fits were executed only up to the time of a flow interruption (which was introduced in several of the tests). For these fits, the Peclet numbers and tracer matrix-diffusion parameters were constrained to be the same for both tests, and the mean residence times were constrained to be inversely proportional to the flow rates in the tests. The fracture spacing was also manually varied to improve the simultaneous fits to the tracer responses; this was justified because the residence times in the low-flow-rate tests were long enough for tracers to potentially diffuse to the epoxy sealing the periphery of the fractured cores, which should serve as a diffusion boundary. The parameters resulting from the RELAP fits were then used in MULTRAN with only the ion-exchange parameters, Q_1 and Q_2 , being varied to achieve a match to the Li^+ , Na^+ , and Ca^{2+} responses.

Figures E-33 through E-36 indicate that MULTRAN V 1.0 (STN: 10666-1.0-00 [DIRS 159068]) was able to simulate very effectively the responses of all tracers in each multiple-tracer test in each core. The finite fracture spacing used in both the RELAP V 2.0 (STN: 10551-2.0-00 [DIRS 159065]) and MULTRAN simulations was found to be essential for obtaining a reasonable simultaneous fit to the tracer responses at the two significantly different flow rates in each core, suggesting that diffusion boundaries played an important role at the lower flow rates.

The matrix-diffusion, MTCs for Br^- in the first two cores were surprisingly much smaller than the MTCs obtained for iodide in these two cores. In theory, these two halides should have very similar diffusion properties. However, the apparent dispersivities and deduced fracture apertures in the two cores were both larger in the multiple-tracer tests than in the iodide-only tests. Larger apertures directly decrease MTCs, and larger dispersivities indirectly decrease MTCs because greater dispersion results in longer-tailed and lower-peaked tracer responses, both of which matrix diffusion also produces. The greater apparent dispersion and lower apparent matrix diffusion in the multiple-tracer tests relative to the iodide-only tests cannot be explained. However, it is possible that microbial growth or small geometry changes in the flow systems could have played a role because the iodide-only tests were conducted well before the multiple-tracer tests in both cores. An inherent fundamental difference in the transport behavior of Br^- and iodide can be ruled out because these two tracers behaved almost identically in the multiple-tracer tests in which both were injected simultaneously (8 of the 11 multiple tracer tests—Tables E-9 and E-11 to E-13). Another more subtle explanation could be that the iodide tests were conducted only at what would be considered the higher flow rates in the multiple-tracer tests, raising the possibility that tests conducted at higher flow rates could be biased toward greater apparent matrix diffusion because of a greater influence of diffusion into stagnant free water in the fractures or other time-scale effects (Section E4).

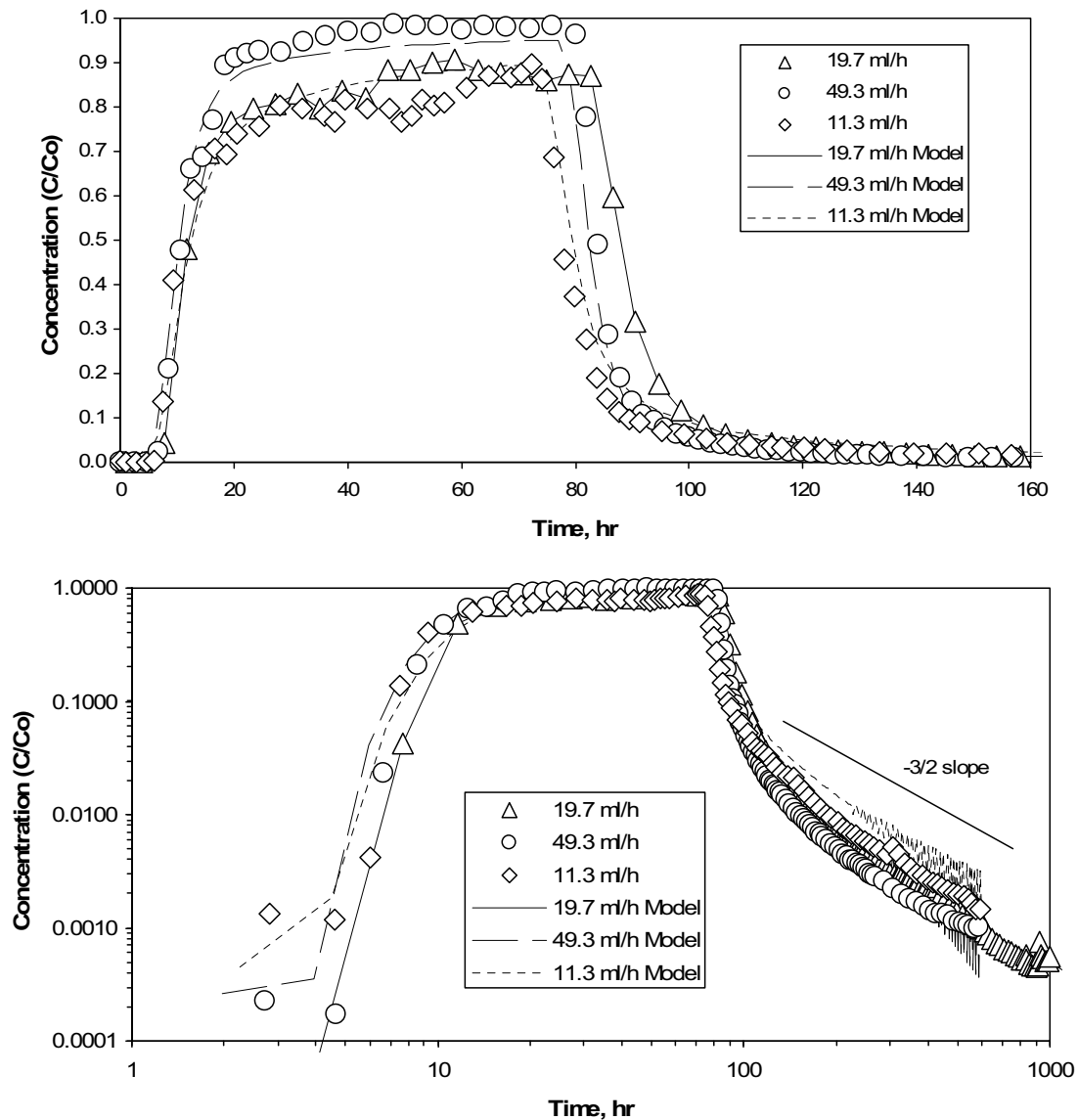


Source: DTN: LA0212PR831231.001 [DIRS 162607] (data).

Output DTN: LA0303PR831361.004 (fits).

NOTE: All three data sets were used to simultaneously fit τ , Pe , and MTC . Concentrations are normalized to injection concentration. Lower plot is same as upper plot except with log scales for the x- and y-axes. The $-3/2$ slope on the log-log plot is the expected slope for a system experiencing single-rate matrix diffusion. "Model" refers to the RELAP simulation/fits.

Figure E-31. Experimental and Simulation Results from the Three Iodide-Only Transport Tests in Core 1



Source: DTN: LA0212PR831231.001 [DIRS 162607] (data).

Output DTN: LA0303PR831361.004 (fits).

NOTE: All three data sets were used to simultaneously fit τ , Pe , and MTC . Concentrations are normalized to injection concentration. Lower plot is same as upper plot except with log scales for the x- and y-axes. The $-3/2$ slope on the log-log plot is the expected slope for a system experiencing single-rate matrix diffusion. "Model" refers to the RELAP simulation/fits.

Figure E-32. Experimental and Simulation Results from the Three Iodide-Only Transport Tests in Core 2

Table E-14. Simulation Results for the Three Iodide Tracer Tests in Upper Prow Pass Tuff Core (Core 1)

Fitted Transport Parameters ^a	Test 1	Test 2	Test 3
Solute mean residence time, τ (hr)	3.0	0.34	0.76
Peclet number, Pe	18		
Mass transfer coefficient, $MTC = \frac{\phi}{b} \sqrt{D_m}$ (hr ^{-0.5})	1.56 (Γ)		
Fracture aperture, $2b$ (cm) ^b	0.043		
Dispersivity in fracture, $\alpha = \frac{L}{Pe}$ (cm)	0.89		
Matrix diffusion coefficient, D_m ($\times 10^{-10}$ m ² /s) ^c	4.3 (Γ)		

Output DTNs: LA0303PR831361.0 04; LA0303PR831231.005.

^aThe three Γ data sets were fit simultaneously assuming Pe was the same for the three tests and τ was inversely proportional to the volumetric flow rate.

^bBased on the relationship $b = \frac{Q\tau}{Lw}$, where τ is the solute mean residence time.

^cDetermined from the MTC using the measured ϕ and the calculated b .

MTC=mass transfer coefficient

Table E-15. Simulation Results for the Three Iodide Tracer Tests in Central Prow Pass Tuff Core (Core 2)

Fitted Transport Parameters ^a	Test 1	Test 2	Test 3
Solute mean residence time, τ (hr)	0.48	0.19	0.84
Peclet number, Pe	24		
Mass transfer coefficient, $MTC = \frac{\phi}{b} \sqrt{D_m}$ (hr ^{-0.5})	0.518 (Γ)		
Fracture aperture, $2b$ (cm) ^b	0.058		
Dispersivity in fracture, $\alpha = \frac{L}{Pe}$ (cm)	0.72		
Matrix diffusion coefficient, D_m ($\times 10^{-10}$ m ² /s) ^c	3.2 (Γ)		

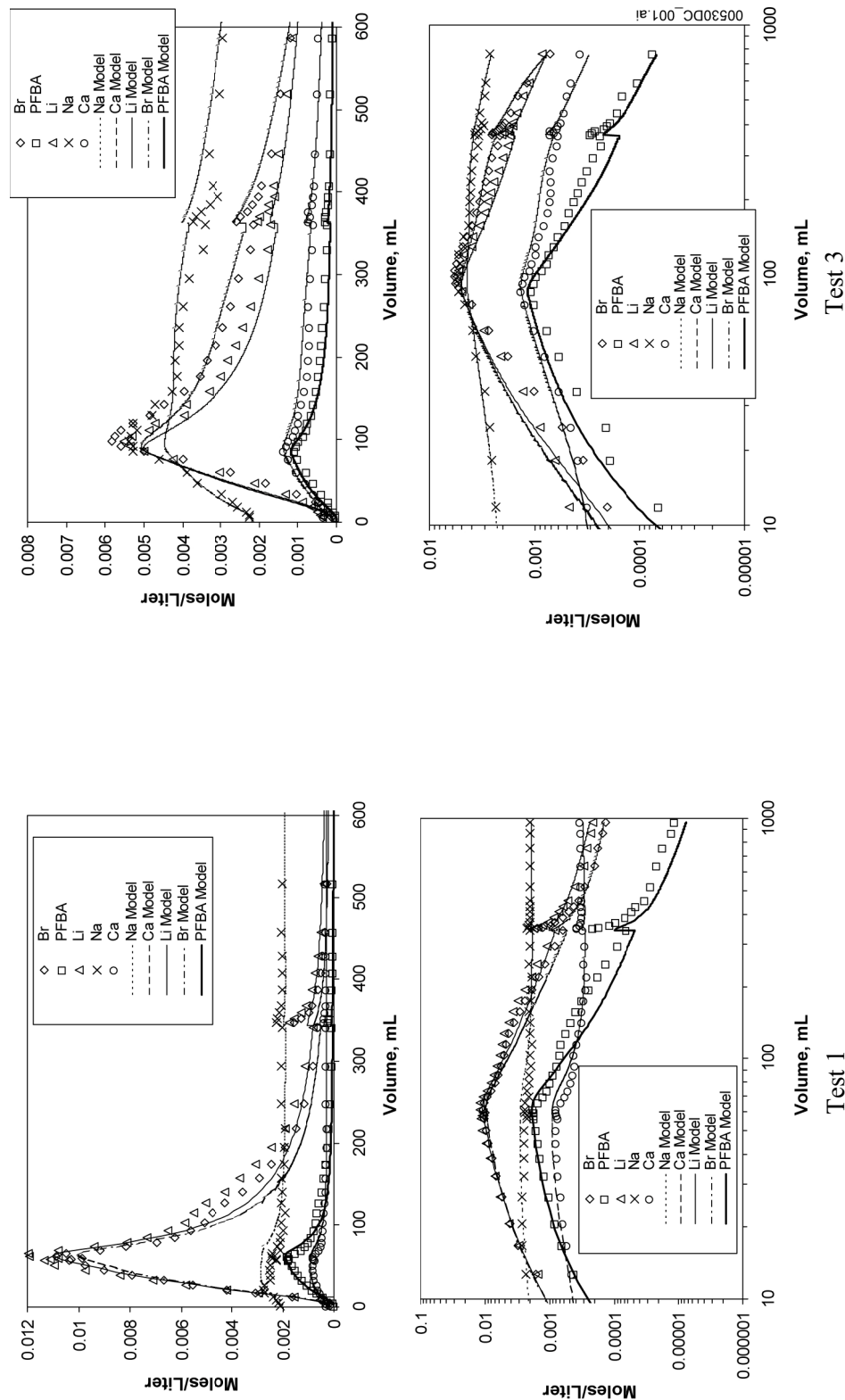
Output DTNs: LA0303PR831361.0 04; LA0303PR831231.005.

^a The three Γ data sets were fit simultaneously assuming Pe was the same for the three tests and τ was inversely proportional to the volumetric flow rate.

^b Based on the relationship $b = \frac{Q\tau}{Lw}$, where τ is the solute mean residence time.

^c Determined from the MTC using the measured ϕ and the calculated b .

MTC=mass transfer coefficient.

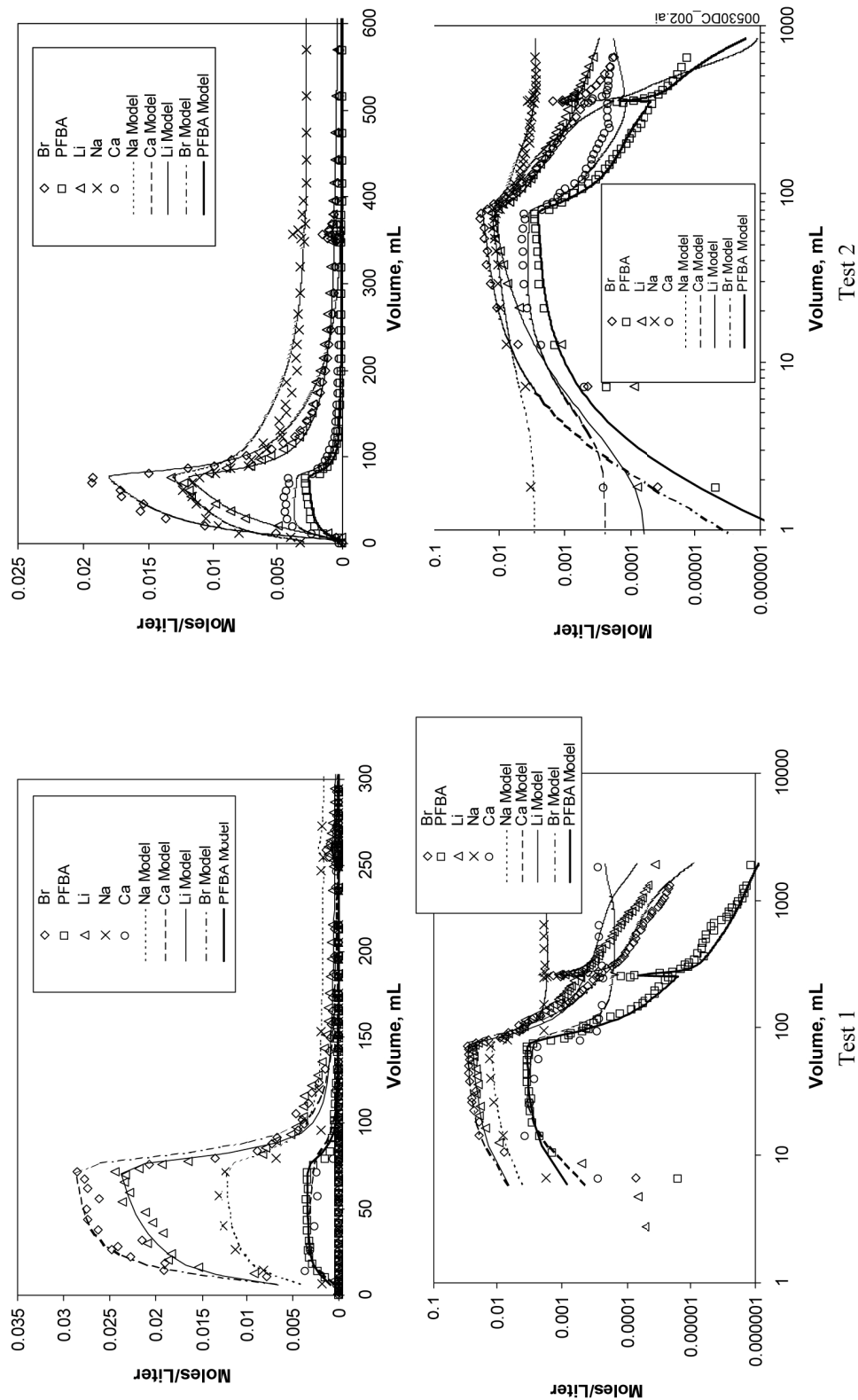


Sources: DTNs: LA0212PR831231.003 [DIRS 162609] (lithium, bromine, PFBA data); LA0212PR831231.005 [DIRS 166215] (sodium, calcium data).

Output DTN: LA0303PR831361.004 (simulations).

NOTE: The jumps in the concentrations and in the model curves correspond to flow interruptions in the tests. The flow rate in Test 1 (left) was 3.9 mL/h, and the flow rate in Test 3 (right) was 0.51 mL/h. The Br⁻ and PFBA data were fit simultaneously by constraining the D_m ratio for Br:PFBA to 3:1. "Model" refers to MULTRAN simulations.

Figure E-33. Experimental Data and MULTRAN Simulation Results for Multiple Tracer Tests 1 and 3 in the Upper Prow Pass Tuff Core (Core 1)

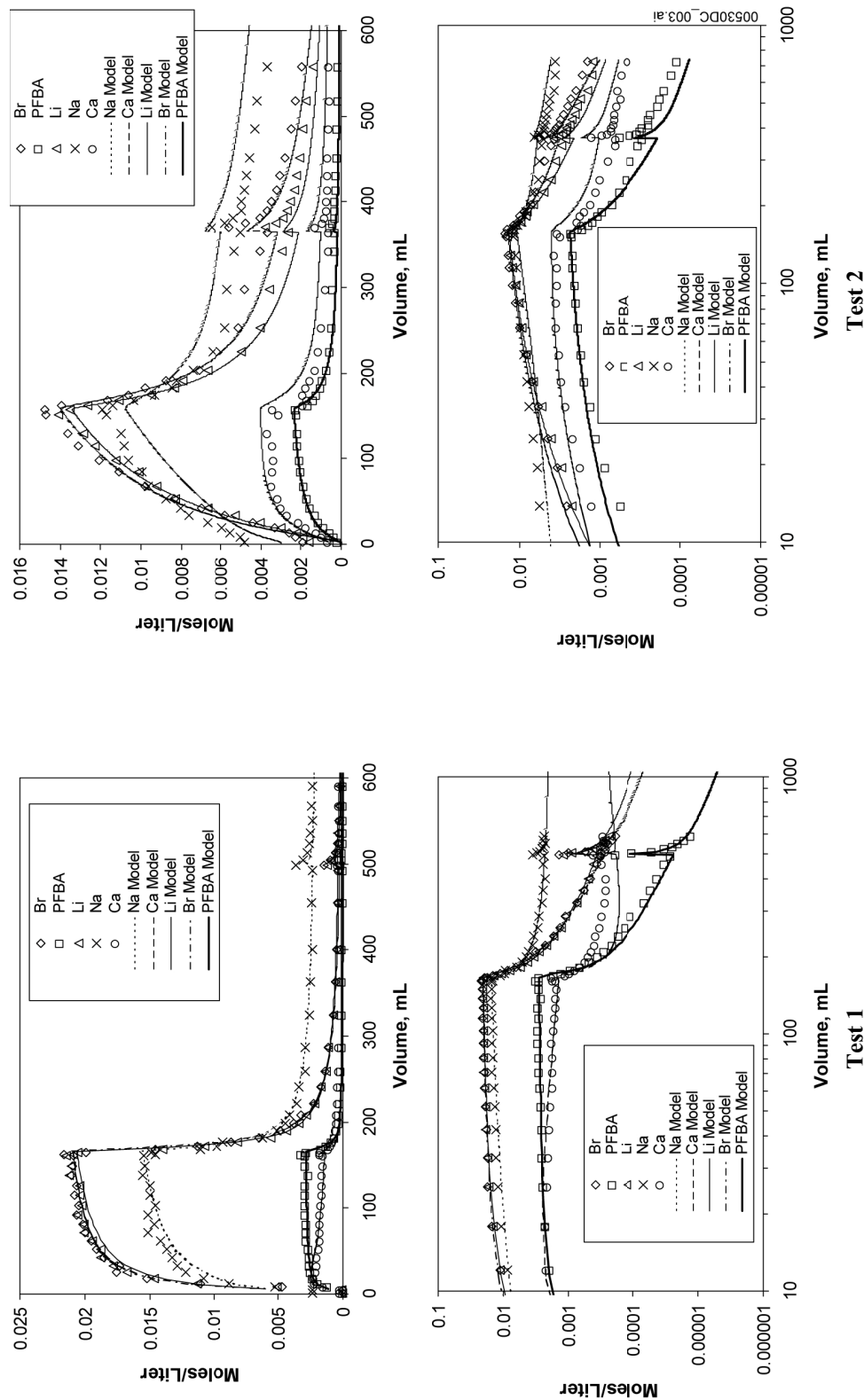


Sources: DTNs: LA0212PR831231.002 [DIRS 162608] (sodium, calcium data); LA0212PR831231.005 [DIRS 166215] (lithium, bromine, PFBA data).

Output DTN: LA0303PR831361.004 (simulations).

NOTE: The jumps in the concentrations and in the model curves correspond to flow interruptions in the tests. The flow rate in Test 1 (left) was 5.9 mL/h, and the flow rate in Test 2 (right) was 0.44 mL/h. The Br⁻ and PFBA data were fit simultaneously by constraining the D_m ratio for Br:PFBA to 3:1. "Model" refers to MULTRAN simulations.

Figure E-34. Experimental Data and MULTRAN Simulation Results for Multiple Tracer Tests 1 and 2 in the Central Prow Pass Tuff Core (Core 2)



Sources: DTNs: LA0212PR831231.002 [DIRS 162608] (sodium, calcium data); LA0212PR831231.003 [DIRS 162609] (lithium, bromine, PFBA data).

Output DTN: LA0303PR831361.004 (simulations).

NOTE: The jumps in the concentrations and in the model curves correspond to flow interruptions in the tests. The flow rate in Test 1 (left) was 11.4 mL/h, and the flow rate in Test 2 (right) was 0.46 mL/h. The Br- and PFBA data were fit simultaneously by constraining the D_m ratio for Br:PFBA to 3:1. "Model" refers to MULTRAN simulations.

Figure E-35. Experimental Data and MULTRAN Simulation Results for Multiple Tracer Tests 1 and 2 in the Lower Prow Pass Tuff Core (Core 3)

Table E-16. Best-Fit Model Parameters for the Multiple-Tracer Tests Conducted in Cores 1 and 2

Modeling Parameters	Core 1, Test 1	Core 1, Test 3	Core 2, Test 1	Core 2, Test 1
Porosity of matrix	0.27	0.27	0.14	0.14
Solute mean residence time, τ (hr) ^a	5.4	40.2	1.95	26.1
Peclet number, Pe ^a	4.0	4.0	3.5	3.5
Dispersivity in fracture, $\alpha = \frac{L}{Pe}$ (cm)	4.0	4.0	5.0	5.0
Li^+ Retardation factor, R ^a	2.25	1.1	4.2	5.9
Li^+ Partition coefficient, K_d (L/kg)	0.17	0.014	0.19	0.30
Mass transfer coefficient ^a , $MTC = \frac{\phi}{b} \sqrt{D_m}$ (hr ^{-0.5})	0.80 (Br ⁻) 0.46 (PFBA)	0.80 (Br ⁻) 0.46 (PFBA)	0.21 (Br ⁻) 0.12 (PFBA)	0.21 (Br ⁻) 0.12 (PFBA)
Fracture aperture, $2b$ (cm) ^b	0.134	0.134	0.07	0.07
Distance to diffusion boundary (fracture half spacing), (cm)	1.9	1.9	0.9	0.9
Matrix diffusion coefficient ^c , D_m ($\times 10^{-10}$ m ² /s)	11.0 (Br ⁻) 3.7 (PFBA)	11.0 (Br ⁻) 3.7 (PFBA)	0.8 (Br ⁻) 0.27 (PFBA)	0.8 (Br ⁻) 0.27 (PFBA)
CEC (meq/kg), Measured	19.9	19.9	43.2	43.2
Q_1 ^d	0.05	0.025	10.2	6.0
Q_2 ^d	0.079	0.04	3.0	0.45

Source: DTN: MO00012POROCHOL.000 [DIRS 153376] (for porosity).

Output DTNs: LA0303PR831361.004 (model results); LA0303PR831231.005.

NOTE: Cores 1 and 2 are shown in Figures E-31 through E-34.

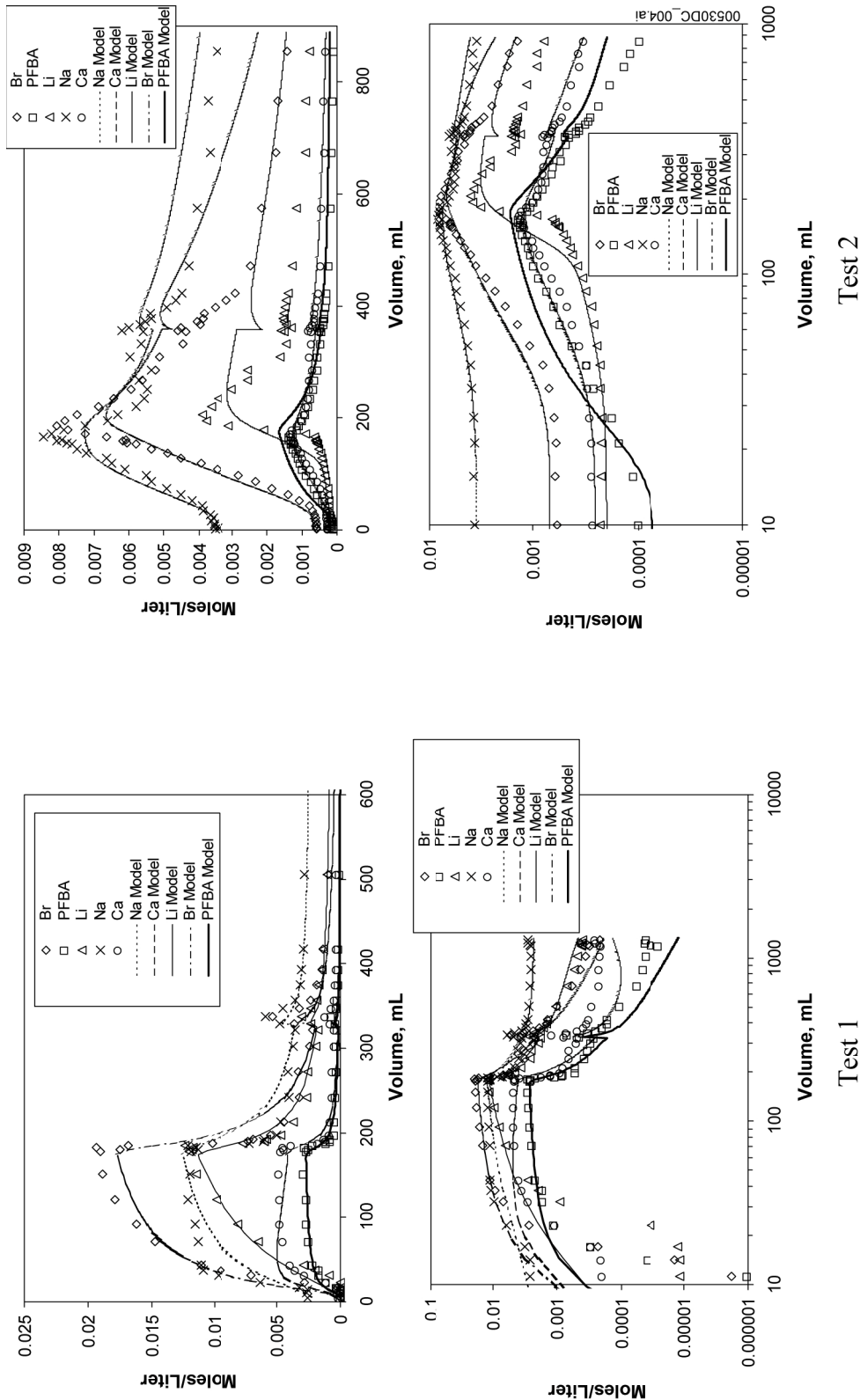
^a Parameters obtained using RELAP to fit simultaneously the Br⁻ and PFBA data from the two tests for a given core with the constraint that the D_m ratio for Br⁻:PFBA was 3:1. The matrix diffusion coefficient for Li⁺ was assumed to be two-thirds the value for Br⁻.

^b Based on the relationship $b = \frac{Q\tau}{Lw}$, where τ is the solute mean residence time.

^c Determined from the MTC using the measured ϕ and the calculated b .

^d Equilibrium ion-exchange coefficients, obtained using MULTRAN to manually "fit" the Li⁺, Na⁺, and Ca²⁺ data for each test.

MTC = mass transfer coefficient; PFBA = pentafluorobenzoic acid or pentafluorobenzoate.



Sources: DTNs: LA0212PR831231.002 [DIRS 162608] (sodium, calcium data – Test 1); LA0212PR831231.005 [DIRS 166215] (sodium, calcium data – Test 2); LA0212PR831231.003 [DIRS 162609] (lithium, bromine, PFBA data).

Output DTN: LA0303PR831361.004 (simulations).

NOTE: The jumps in the concentrations and in the model curves correspond to flow interruptions in the tests. The flow rate in Test 1 (left) was 4.85 mL/h, and the flow rate in Test 2 (right) was 0.47 mL/h. The Br⁻ and PFBA data were fit simultaneously by constraining the D_m ratio for Br:PFBA to 3:1. "Model" refers to MULTRAN simulations.

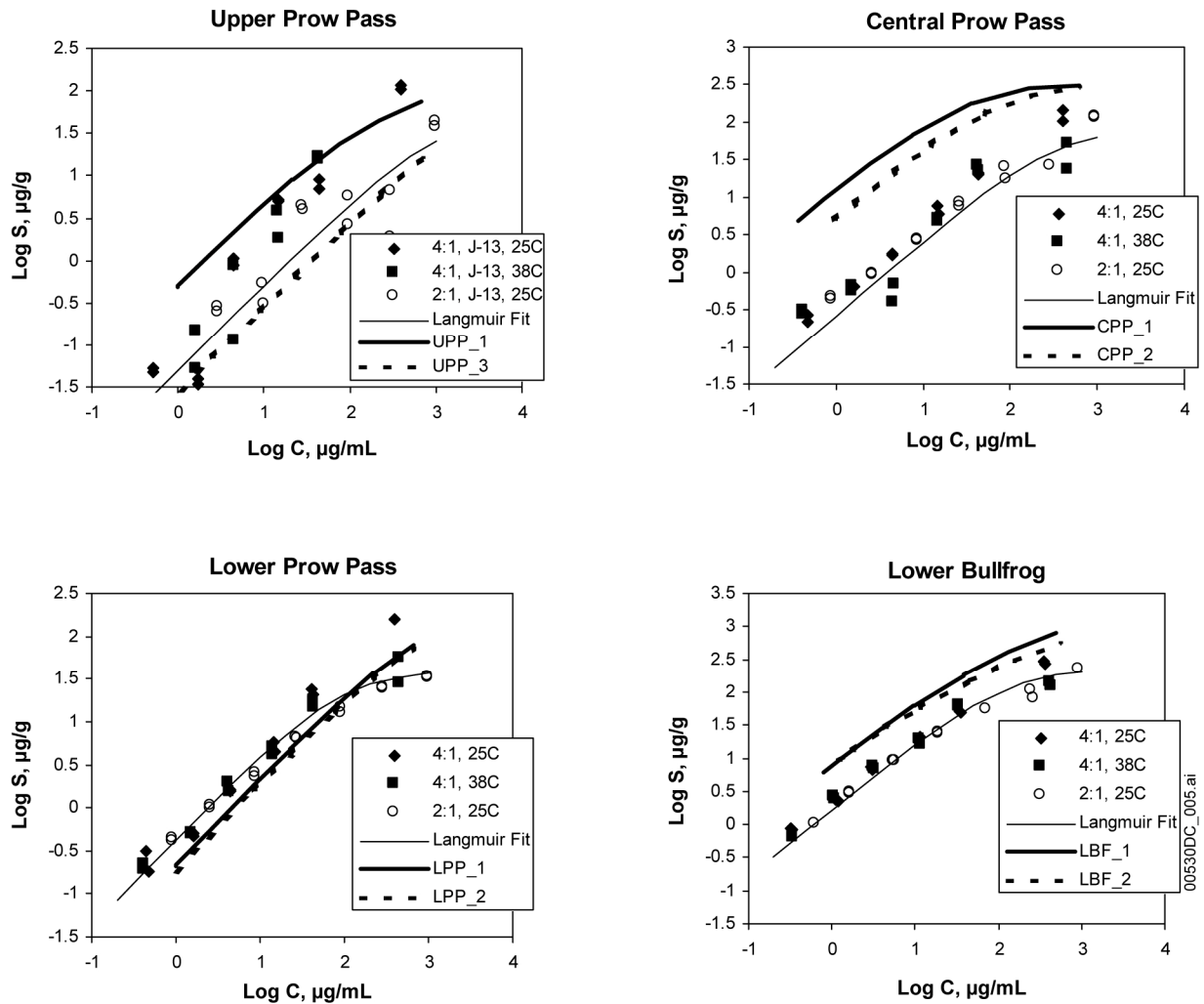
Figure E-36. Experimental Data and MULTRAN Simulations Results for Multiple Tracer Tests 1 and 2 in the Lower Bullfrog Tuff Core (Core 4).

The ion exchange parameters, Q_1 and Q_2 , exhibited a curious decreasing trend from the first to the second multiple-tracer test in each core, suggesting that some Li^+ may have become irreversibly sorbed in the first test and reduced the sorption capacity for Li^+ in subsequent tests. This speculation is consistent with the incomplete recovery of Li^+ in each test. In any case, the Li^+ sorption isotherms calculated from the ion-exchange parameters deduced from MULTRAN V 1.0 (STN: 10666-1.0-00 [DIRS 159068]) fits were generally higher than or comparable to the sorption isotherms derived from batch Li^+ sorption experiments (Figure E-37).

It is important to point out that the best-fitting values of the ion-exchange parameters Q_1 and Q_2 in the MULTRAN V 1.0 (STN: 10666-1.0-00 [DIRS 159068]) simulations were somewhat sensitive to the background concentrations specified for all three cations in the system. These background concentrations were chosen to match the concentrations measured in the first one or two samples collected in each experiment (prior to the arrival of the tracers), which generally differed slightly from one experiment to the next in a given core. There were also significant differences in the relative amounts of cations and the overall ionic strengths of the tracer solutions used in different experiments, which could have affected the experimental and simulation results. One notable difference in the cation mix occurred as a result of using either NaOH or LiOH to neutralize the PFBA in the tracer solutions (if a stoichiometric amount of OH^- was not added, the pH of the tracer solutions was <2). These differences in cation mix and ionic strength were accounted for in the MULTRAN inputs, but any “memory” effects resulting from the use of significantly different tracer solutions in consecutive experiments, which could affect the pre-experiment mix of cations sorbed to mineral surfaces, were not accounted for. It is possible that if these factors had been accounted for, the Q_1 and Q_2 values from consecutive experiments may have been in better agreement.

It was also found that reasonable matches to the cation responses in the cores could be obtained using almost any value of the CEC greater than some threshold, provided that Q_1 and Q_2 were both adjustable. This nonuniqueness problem was avoided by setting the CEC values in all MULTRAN V 1.0 (STN: 10666-1.0-00 [DIRS 159068]) simulations equal to the laboratory measurements for each tuff. However, if the effective CEC value had been reduced for each subsequent experiment in each core (because of some irreversible sorption of Li^+), then the Q_1 and Q_2 values would have been higher in the later experiments, which would have brought them into better agreement with the values in earlier experiments.

Although not all of the experimental and simulation results can be completely explained, Figure E-38 shows that the use of the multicomponent ion-exchange MULTRAN V 1.0 (STN: 10666-1.0-00 [DIRS 159068]) code offers a significant improvement over the single-component RELAP V 2.0 (STN: 10551-1.0-00 [DIRS 159065]) code in simulating the responses of ion-exchanging tracers in dual-porosity systems. This improvement is especially pronounced when there is a large amount of sorption in the matrix, as there is for the Lower Bullfrog Tuff core (Figure E-38).



Source: DTN: MO0012SORBCHOL.000 [DIRS 153375] (data).

Output DTN: LA0303PR831341.003 (isotherms).

Figure E-37. Comparison of Li^+ Isotherms Calculated from Best-Fitting MULTRAN Parameters (Designated by XXX_Y, where Y is the Fractured Core Test Number) and Obtained in Batch Sorption Experiments for the Four Different C-Wells Tufts Used in the Fracture Experiments

Table E-17. Best-Fit Transport Parameters for the Multiple-Tracer Tests Conducted in Cores 3 and 4

Transport Parameters	Core 3, Test 1	Core 3, Test 2	Core 4, Test 1	Core 4 ^a , Test 2
Porosity of matrix	0.29	0.29	0.30	0.30
Solute mean residence time, τ (hr) ^b	0.55	13.6	2.0	21.3
Peclet number, Pe^b	4.5	4.5	130	130
Dispersivity in fracture, $\alpha = \frac{L}{Pe}$ (cm)	2.6	2.6	0.09	0.09
Li^+ Retardation factor, R^b	1.3	1.6	9.2	8.2
Li^+ Partition coefficient, K_d (L/kg)	0.046	0.092	1.33	1.16
Mass transfer coefficient ^b , $MTC = \frac{\phi}{b} \sqrt{D_m}$ (hr ^{-0.5})	1.32 (Br ⁻) 0.76 (PFBA)	1.32 (Br ⁻) 0.76 (PFBA)	1.45 (Br ⁻) 0.84 (PFBA)	1.45 (Br ⁻) 0.84 (PFBA)
Fracture aperture, $2b$ (cm) ^c	0.057	0.057	0.049	0.049
Distance to diffusion boundary (fracture half spacing), (cm)	4.4	4.4	4.6	4.6
Matrix diffusion coefficient ^d , D_m ($\times 10^{-10}$ m ² /s)	4.6 (Br ⁻) 1.5 (PFBA)	4.6 (Br ⁻) 1.5 (PFBA)	3.8 (Br ⁻) 1.3 (PFBA)	3.8 (Br ⁻) 1.3 (PFBA)
CEC (meq/kg), Measured	31.9	31.9	179.7	179.7
Q_1^e	0.1	0.085	6.0	0.2 ^e
Q_2^e	0.08	0.035	0.3	0.12 ^e

Source: DTN: MO00012POROCHOL.000 [DIRS 153376] (for porosity).

Output DTNs: LA0303PR831361.004 (simulation results), LA0303PR831231.005.

NOTE: Cores 3 and 4 are shown in Figures E-35 and E-36.

^a The MULTRAN V 1.0 (STN: 10666-1.0-00 [DIRS 159068]) "fit" shown for Core 4, Test 2 in Figure E-36 was actually obtained assuming sorption in both the fracture and the matrix. The fracture was assumed to have a porosity of 0.9, a CEC of 200 meq/kg, $K_1 = 5.0$, and $K_2 = 50.0$. The matrix had a CEC of 179.7 meq/kg, and $K_1 = K_2 = 0.0223$. The resulting fit was somewhat better than the fit assuming sorption only in the matrix.

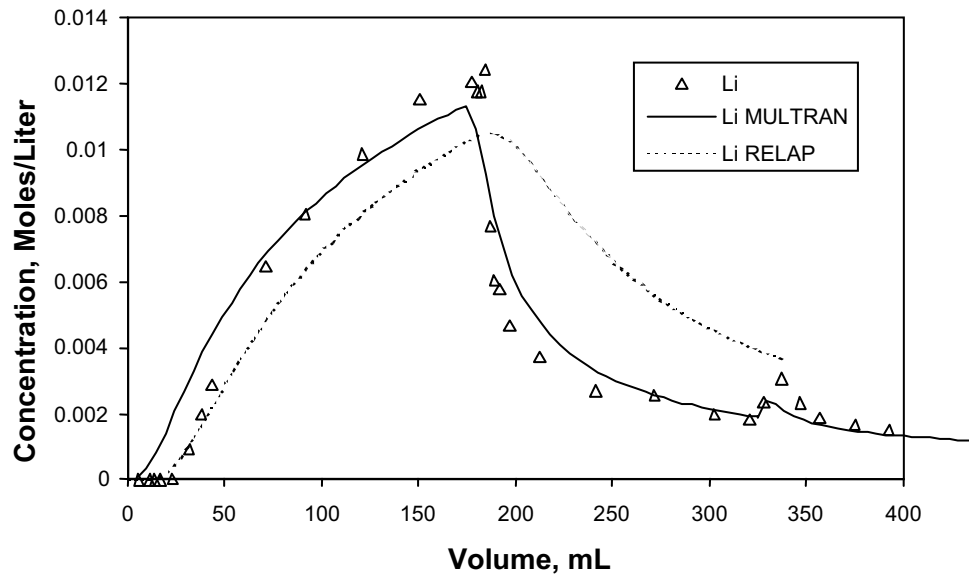
^b Parameters obtained using RELAP V 2.0 (STN: 10551-2.0-00 [DIRS 159065]) to simultaneously fit the Br⁻ and PFBA data from the two tests for a given core with the constraint that the D_m ratio for Br⁻:PFBA was 3:1. The matrix diffusion coefficient for Li⁺ was assumed to be 2/3 the value for Br⁻.

^c Based on the relationship $b = \frac{Q\tau}{Lw}$, where τ is the solute mean residence time.

^d Determined from the MTC using the measured ϕ and the calculated b .

^e Equilibrium ion exchange coefficients, obtained using MULTRAN V 1.0 (STN: 10666-1.0-00 [DIRS 159068]) to manually "fit" the Li⁺, Na⁺, and Ca²⁺ data for each test.

MTC=mass transfer coefficient;PFBA=pentafluorobenzoic acid or pentafluorobenzoate.



Source: DTN: LA0212PR831231.003 [DIRS 162609] (lithium data).

Output DTN: LA0303PR831361.003 (simulations).

Figure E-38. Comparison of the Fits of the MULTRAN Multicomponent Ion-Exchange Model and the Single-Component RELAP Code to the Lithium Transport Data in the First Multiple-Tracer Test in Core 4

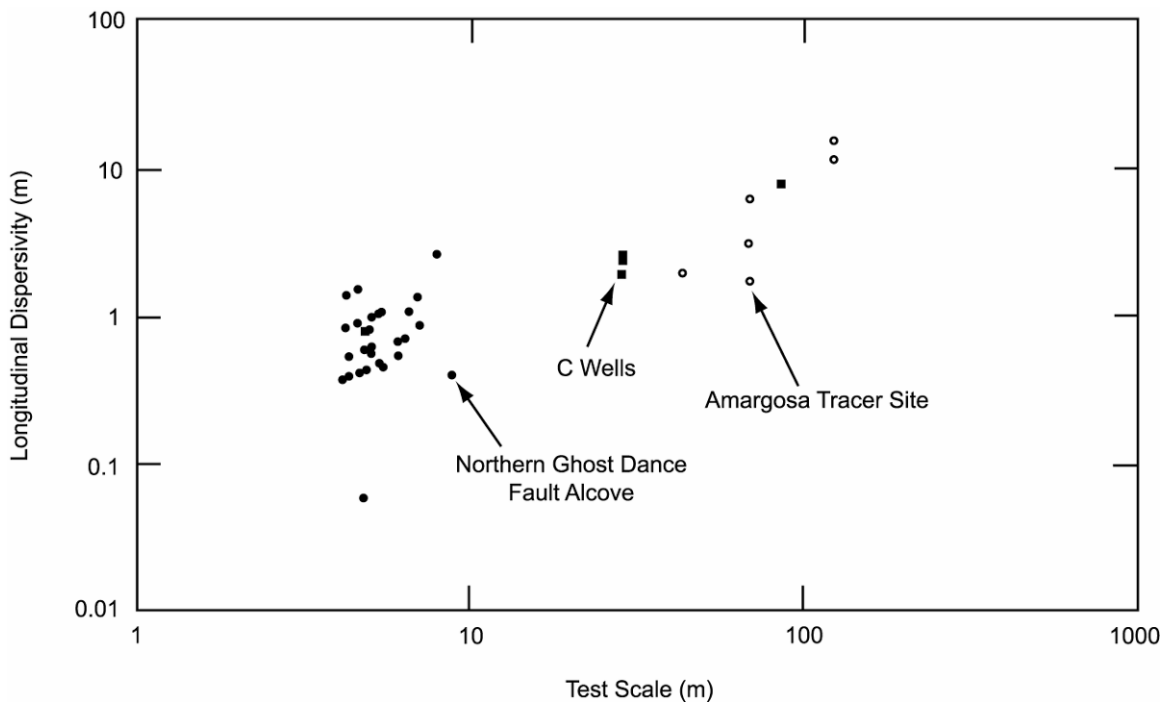
E3.3 CONCLUSIONS REGARDING LITHIUM TRANSPORT EXPERIMENTS

The lithium transport experiments in both crushed tuff columns and fractured tuff cores demonstrate the importance of accounting for multicomponent transport effects, particularly charge balance, when simulating and interpreting the transport behavior of an ion-exchanging cation tracer, especially when the tracer is the most abundant cation in solution. These experiments also indicate that sorption parameters derived from dynamic transport experiments tend to either agree quite well with those measured in batch sorption experiments or are somewhat greater than those measured in batch experiments (i.e., the batch experiments underpredict the amount of sorption observed in the dynamic transport experiments). This result is consistent with the comparison between field-derived sorption parameters and laboratory-derived batch sorption parameters (Section D4.8.4), and it lends additional credibility to the practice of using of laboratory-derived K_d values to predict radionuclide transport in saturated fractured tuffs near Yucca Mountain (suggesting that such predictions should, if anything, overestimate the transport rates of radionuclides).

E4. SCALE-DEPENDENCE OF TRANSPORT PARAMETERS IN FRACTURED TUFFS

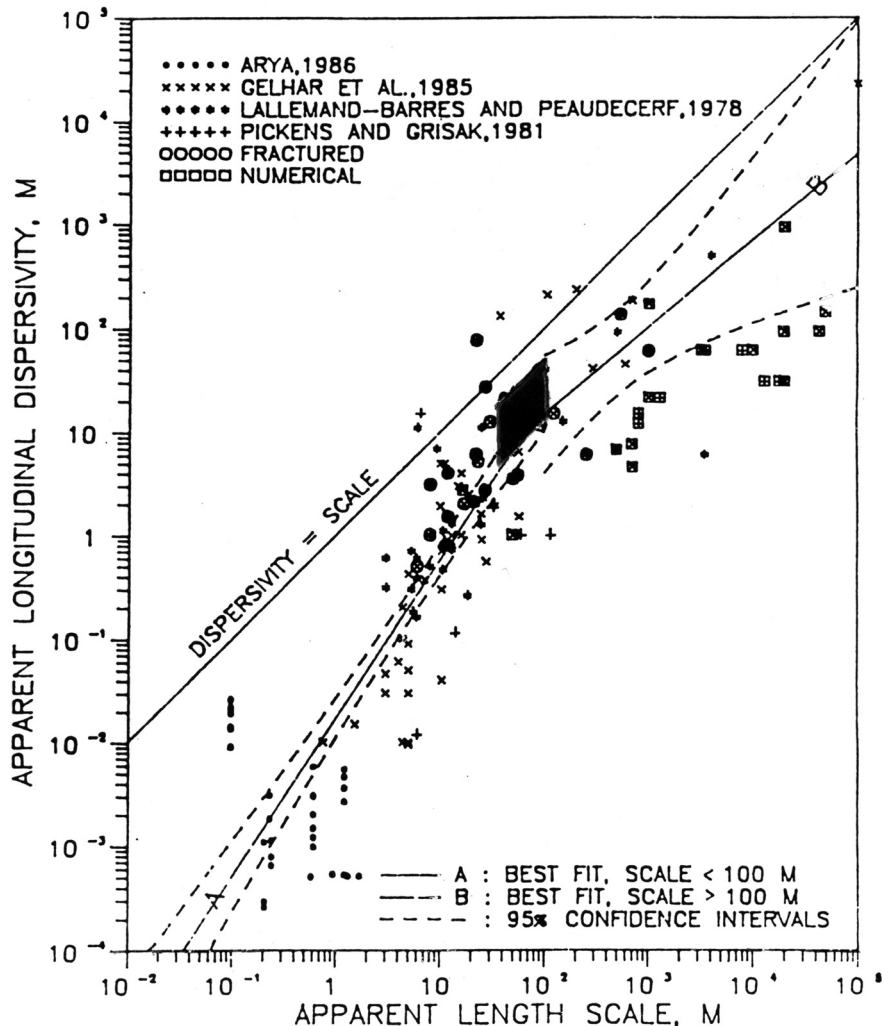
E4.1 SCALE-DEPENDENCE OF LONGITUDINAL DISPERSIVITY

A plot of the longitudinal dispersivity values as a function of test scale for several Nevada Test Site fractured-rock, tracer-test programs is shown in Figure E-39. The plot indicates that the longitudinal dispersivity increases with test scale that ranges from less than one meter to over 100 meters. Figure E-40 shows the range of longitudinal dispersivities as a function of scale derived from the C-wells multiple-tracer tests (darkened area) superimposed on a plot of dispersivity versus scale prepared by Neuman (1990 [DIRS 101464], Figure 1). The lower end of the range of length scales associated with the darkened area corresponds to the interwell separation in the tracer tests, and the upper end corresponds to the test interval thickness (used as an upper bound for the transport distance).



Source: LeCain et al. 2000 [DIRS 144612], Figure 19.

Figure E-39. Longitudinal Dispersivity as a Function of Test Scale in Several Tracer Tests Conducted in the Vicinity of Yucca Mountain



Source: Plot taken from Neuman 1990 [DIRS 101464], Figure 1.

Output DTN: LA0303PR831231.003 (dispersivities from C-wells).

NOTE: The darkened box shows the range of values derived from the multiple-tracer field tests at the C-wells in which lithium ion was used as a sorbing tracer. The right edge of the box corresponds to the interwell separation distance, and the left edge of the box corresponds to the test interval thickness (taken to be the upper limit of transport distance).

Figure E-40. Plot of Longitudinal Dispersivity Versus Length Scale Showing the Range of C-Wells Values Derived from Interpretations of the Prow Pass and Bullfrog Multiple Tracer Tests in Which Lithium Ion Was Used as a Sorbing Tracer

E4.2 SCALE-DEPENDENCE OF MATRIX DIFFUSION

There is some question about whether matrix diffusion parameters measured in laboratory-scale experiments can be used reliably in field-scale transport predictions. To address this issue, it is first of interest to compare the matrix diffusion coefficients measured in the diffusion cell tests (Section E2) with the diffusion coefficients calculated from the fractured-core tests (Section E3.2). Table E-18 shows that the Br^- matrix diffusion coefficients deduced from the fractured-core experiments (from simultaneous RELAP V 2.0 (STN: 10551-2.0-00 [DIRS 159065]) fits to the Br^- and PFBA responses at two different flow rates in each fracture)

were consistently greater than the Br^- diffusion coefficients obtained from the diffusion cell experiments. This result could be explained by the fact that matrix diffusion in the fractured cores was really a combination of diffusion into stagnant free water in the fractures (e.g., into voids along the rough walls of the fracture surfaces or into stagnant regions between flowing channels) and true diffusion into the matrix, whereas diffusion in the diffusion cell experiments, by design, occurred only in the matrix. The RELAP computer code interprets both free-water and matrix diffusion as matrix diffusion, so any free-water diffusion will tend to increase estimates of matrix diffusion coefficients (Callahan 2001 [DIRS 156649], Chapter 5). The time scales of the diffusion cell measurements also tended to be longer than in the fractured cores, which would have resulted in greater tracer penetration of the matrices and, hence, a more representative measurement of true matrix diffusion.

It is also of interest to compare matrix-diffusion MTCs derived from the fractured-core experiments (Section E3.2) with MTCs derived from the C-wells field tracer tests (Section D4.7). Such a comparison is provided in Figure E-41, which shows the laboratory and field MTCs plotted as a function of time scale in the tests. The MTCs derived from the laboratory experiments are plotted as lines that span the range of tracer residence times in the cores. It is apparent that the residence times in the iodide-only core experiments were shorter than in the multiple-tracer experiments, and there is a corresponding increase in the deduced MTC values in the iodide experiments. The MTCs from the field experiments are also plotted as lines that span the range of tracer residence times obtained assuming either linear or radial flow fields. Separate lines are plotted for the two pathways that resulted in the two tracer peaks in the Bullfrog Tuff field test.

It is clear that the MTCs collectively exhibit a decreasing trend with tracer residence times in Figure E-41. This trend is consistent with the notion that as time scales increase, more of the apparent diffusion will be true matrix diffusion and less will be diffusion into stagnant free water. However, it is also likely that effective fracture apertures over the 30-meter scales of the field tests were much larger than in the approximately 0.2-meter-scale laboratory tests. Intuitively, one would expect that, as distance scales increase, there will be a higher probability of encountering larger-aperture fractures in which flow can occur. Larger apertures would have contributed to the decreasing trend of Figure E-41 because fracture apertures appear in the denominator of the MTC. Alternatively, matrix diffusion coefficients, which appear as a square-root term in the numerator of the MTC, would have to be nearly two orders of magnitude smaller in the field than in the lab to explain the trend of Figure E-41 if fracture apertures were held constant, which seems implausible. Similarly, matrix porosities, which appear in the numerator of the MTC, would have to be smaller by about a factor of 10 in the field to explain the observed trend if fracture apertures were held constant and matrix diffusion coefficients were assumed to be the same as in the lab experiments – also seemingly implausible.

One would expect an asymptotic lower limit to be reached eventually for the MTC in saturated fractured systems, given a long enough transport time or distance. However, for the C-wells field system, the transport data suggest that this asymptotic value, if it exists, was not reached for characteristic transport times of up to approximately 1,200 hrs or travel distances of approximately 30 m (Figure E-41).

All of the test results discussed here are consistent with diffusive mass transfer having a strong influence on the migration of solutes in fractured volcanic tuffs. However, at short time and distance scales, there may be a significant influence of diffusion into stagnant free water within fractures in addition to “true” matrix diffusion. Thus, matrix diffusion parameters obtained from laboratory tracer experiments should be used cautiously when predicting contaminant migration at larger scales in fractured media.

Table E-18. Comparison of Matrix Diffusion Coefficients Calculated from Fractured-Core Tracer Tests and from Diffusion-Cell Experiments

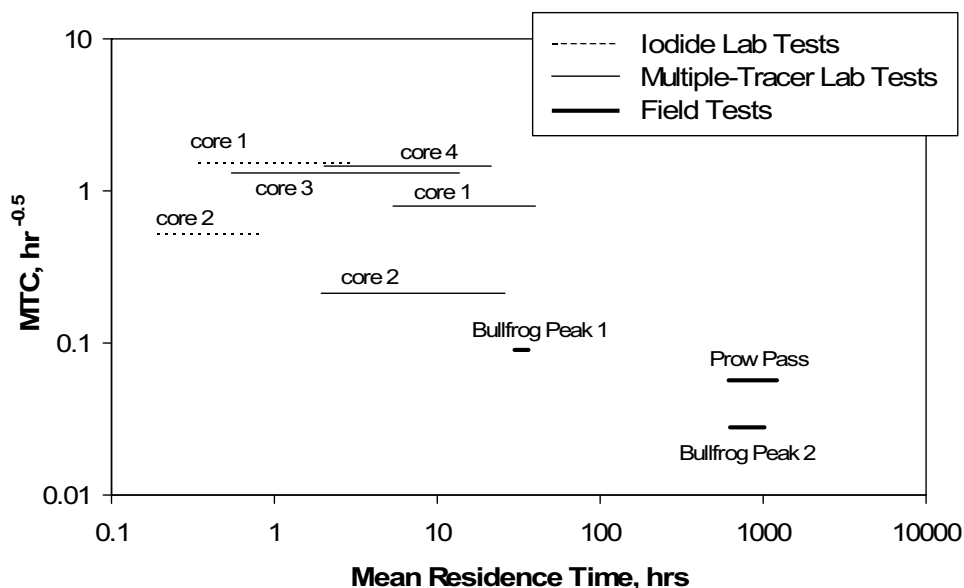
Core	Fractured Core $D_m(\text{Br}^-)$ (m^2/s) ^a	Diffusion Cell $D_m^*(\text{Br}^-)$ (m^2/s)
Upper Prow Pass (1)	11.0×10^{-10}	6.2×10^{-10}
Central Prow Pass (2)	0.8×10^{-10}	0.38×10^{-10}
Lower Prow Pass (3)	4.6×10^{-10}	$2.9 \times 10^{-10\text{b}}$
Lower Bullfrog (4)	3.8×10^{-10}	1.0×10^{-10}

Output DTNs: LA0303PR831362.001 (diffusion cells); LA0303PR831361.004 (fractured cores).

^a Determined from MTC using the measured matrix porosity and *b* determined from $b = Q\tau$ (see Tables E-16 and E-17).

^b Average of two measurements.

MTC=mass transfer coefficient.



Output DTNs: LA0303PR831231.003 (field data); LA0 303PR831361.004 (lab data); LA0303PR831231.005.

NOTE: The lines represent the field tests; endpoints of the lines reflect the uncertainty in the mean residence time depending on whether radial or linear flow is assumed.

The matrix diffusion mass transfer coefficient, MTC, is defined as $\frac{\phi}{b} \sqrt{D_m}$.

The experimental time scale here is the mean residence time.

Figure E-41. Matrix Diffusion Mass Transfer Coefficient as a Function of Experimental Time Scale in All C-Wells Laboratory and Field Multiple Tracer Tests

INTENTIONALLY LEFT BLANK

APPENDIX F

**DETAILS OF HYDRAULIC TESTING AND TEST INTERPRETATIONS AT THE
ALLUVIAL TESTING COMPLEX (ATC) AND NYE COUNTY SITE 22**

Hydrologic properties of the alluvium have been determined from single-well and cross-hole aquifer tests at the Alluvial Testing Complex (ATC), which is centered around well NC-EWDP-19D, located just outside the southwest corner of the Nevada Test Site (see Figure 6.1-6). The tests, which are described in detail in this section, were interpreted using analytical methods similar to those used for interpretation of the hydraulic tests in fractured tuffs at the C-wells (Section 6.2 and Appendix C). Specifically, the unconfined aquifer solution of Neuman (1975 [DIRS 150321]) and the confined aquifer solution of Theis (1935 [DIRS 150327]) were used to interpret the single-well and cross-hole hydraulic responses, respectively. Although other analytical solutions were considered, the test responses appeared to conform most closely to these two solutions, so they were used for the analyses.

The analytic solutions provide first-order estimates of hydrologic parameters consistent with both the limited knowledge of the nature and extent of subsurface heterogeneities in the alluvium at the scale of the ATC and the manner in which hydrologic parameter estimates are used in the site-scale saturated zone (SZ) flow model. The analytical methods assume that the test interval has one average transmissivity and storativity value. Similarly, the SZ flow model assumes that single average intrinsic hydrologic property (i.e., permeability, porosity) values apply to the alluvium over large spatial areas in the SZ flow system. Furthermore, the hydrologic parameters derived from ATC testing are not used as direct inputs in the site-scale SZ flow model, but rather they are used primarily for qualitative/corroborative consistency checks with the hydrologic parameters derived from calibrations of the SZ flow model. Because of this qualitative end use of the parameter estimates, detailed analyses of the uncertainty and nonuniqueness of the estimates were not conducted.

F1. ATC SINGLE-WELL HYDRAULIC TESTS

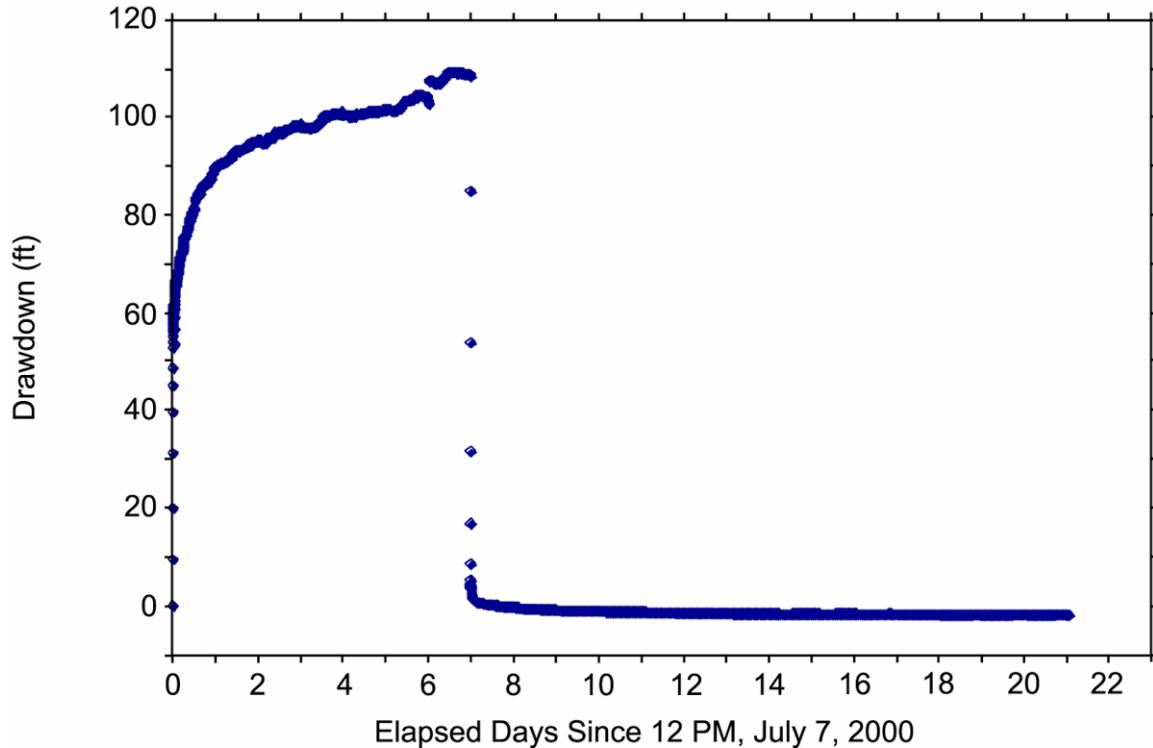
Single-well hydraulic testing of the saturated alluvium in well NC-EWDP-19D was conducted between July 2000 and November 2000. This section presents the results and interpretations of those tests. Detailed documentation of the tests is reported by Umari et al. (2003 [DIRS 164573]). The single-well test results are presented here primarily to provide some indication of the variability in hydraulic conductivity that occurs with depth at the ATC location and also to provide information on the alluvium aquifer characteristics (e.g., confined, unconfined). Analyses of single-well step-drawdown tests (Section F1.4), calculations of leakage between screens 4 and 5 in NC-EWDP-19D (Section F1.5), and interpretations of subsequent cross-hole hydraulic tests (Section F2) all indicate that hydraulic conductivity estimates derived from single-well testing in NC-EWDP-19D are biased low because of significant near-wellbore head losses and/or artificial near-wellbore leakage between adjacent intervals. However, it is assumed that the relative values of hydraulic conductivities obtained from different intervals in the single-well tests are valid for comparison purposes, which implicitly assumes that the near-wellbore head losses in each interval (as a fraction of total drawdown) are comparable.

F1.1 HYDRAULIC TEST OF THE FOUR COMBINED ALLUVIUM INTERVALS IN NC-EWDP-19D

On July 7, 2000, a single-well hydraulic test of the alluvium aquifer to a depth of 247.5 m (812 ft) below land surface was initiated in NC-EWDP-19D (referred to as 19D in the remainder of this document) to determine the transmissivity and hydraulic conductivity of the entire alluvium system at the 19D location. The construction of this well, including the location of all the screens discussed in this section, is summarized in Figure 6.1-8. The well was pumped for seven days, with production coming from the upper four screened intervals in 19D, for all of the intervals completed in the alluvium (a packer was inflated below the fourth screen to isolate the alluvium from the underlying tuffs). Prior to the completion of 19D, Nye County and U.S. Geological Survey/Los Alamos National Laboratory representatives agreed to install screens 5, 6, and 7 in the tuffaceous units encountered by the well bore to allow for possible testing of these intervals in the future. Depth to water just before the test was approximately 106 m (approximately 349 ft) below land surface, and the effective alluvium thickness tested was approximately 136 m (446 ft), which is the distance from the water table to the bottom of the fourth screened interval; the total saturated alluvium thickness is 141 m (463 ft). Recovery data were collected for 14 days after pumping stopped. The test was used, along with the isolated-interval tests that followed, to obtain preliminary estimates of transmissivity and horizontal hydraulic conductivity that were then improved with cross-hole testing. Also, during this test, distant wells (NC-EWDP-15P, NC-EWDP-4PA, NC-EWDP-4PB, and Washburn-1x) were monitored. The nearby piezometer NC-EWDP-19P was also monitored. No responses were detected at these wells. The wells discussed in this report will be referred to by their abbreviated forms.

During the combined-interval test, 19D was pumped at the rate of approximately 564 L/min (149 gallons per minute [gpm]); after seven days of pumping, the drawdown was approximately 33.5 m (110 ft). Comparable pumping rates in the Nye County 48-hour (hr) well-development aquifer test in which all seven screened intervals in 19D were allowed to produce water caused an order of magnitude less drawdown. This result indicates that the Tertiary volcanics and tuff below the alluvium had contributed significantly to that test.

Figure F-1 presents the drawdown data for the entire combined-interval test, including both the pumping and recovery periods. Pumping was started at 12:00 P.M. on July 7, 2000, and ended at 12:00 P.M. on July 14, 2000. The open alluvium interval was allowed to recover until 1:00 P.M. on July 28, 2000. The average pumping rate during the test was 564 L/min (149.11 gpm). The day markers in Figure F-1 are at 12:00 P.M., so the day-1 marker indicates 12:00 P.M. on July 8, 2000; the day-2 marker indicates 12:00 P.M. on July 9, 2000; and so forth. There were no changes in the pumping rate or any other configuration changes to cause the jump in drawdown seen at the 6-day marker. All drawdown values were calculated relative to the starting pressure head at 12:00 P.M. on July 7, 2000, registered by one of the two pressure transducers placed above the packer isolating the alluvium from the underlying tuffs (there were two transducers for redundancy; only one was used for drawdown measurements). Negative drawdown values during recovery indicate pressure heads higher than the starting pressure head. These negative drawdowns indicate that when the test was started on July 7, 2000, there was some residual drawdown relative to background water levels due to pumping associated with preparations for the test, including a step-drawdown test on July 6, 2000.



Source: DTN: GS020708312316.001 [DIRS 162678] (data).

NOTE: English units are shown in the figure because the analysis was conducted in English units. However, parameter estimates are reported in metric units to downstream users.

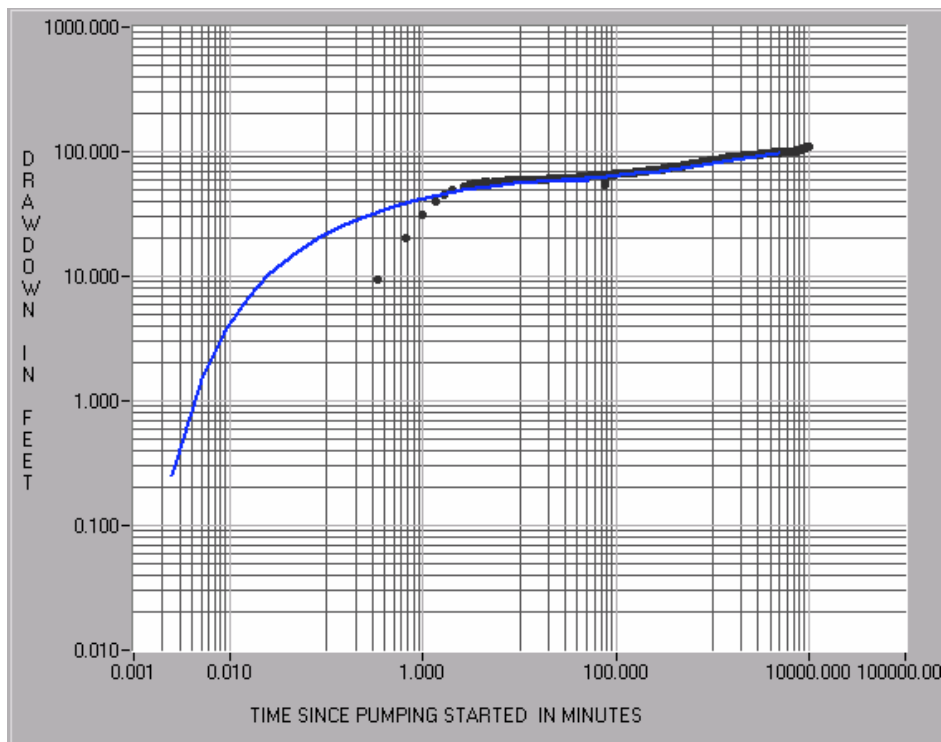
Figure F-1. Drawdown and Recovery Data Associated with the Pump Test of the Four Combined Alluvium Intervals in NC-EWDP-19D, July 2000

Figure F-2 presents a fit of the Neuman (1975 [DIRS 150321]) (Neuman.vi V 1.0, STN: 10972-1.0-00 [DIRS 162754]) fully penetrating unconfined aquifer analytic solution to the combined-interval test data. The Neuman solution gives a transmissivity value of $20.7 \text{ m}^2/\text{day}$ ($223 \text{ ft}^2/\text{day}$). If the thickness of the saturated alluvium from the water table to the bottom of the fourth screened interval 136 m (446 ft) is used, a hydraulic conductivity of approximately 0.5 ft/day is calculated. The type-curve matching procedure for the Neuman unconfined aquifer solution involves matching both the early and late portions of the drawdown data. In Figure F-2, these two portions of the matching type curve are graphically spliced together (the late portion of the type curve match is horizontally shifted to the left) to give the appearance of a single type curve. The latter portion of the early curve match and the early portion of the late curve match are not shown in Figure F-2. Both portions of this match are consistent with the transmissivity and hydraulic conductivity reported above. The slope of 1 for the early time data (less than 2 minutes) in Figure F-2 (log-log scale) is indicative of borehole storage (Papadopoulos and Cooper 1967 [DIRS 150323]), so these very early time data were not considered in the curve-matching procedure.

F1.2 HYDRAULIC TESTS OF ISOLATED ALLUVIUM INTERVALS IN NC-EWDP-19D

After the combined interval test, each of the four intervals in the alluvium in NC-EWDP-19D were isolated and hydraulically tested to obtain transmissivity and associated hydraulic conductivity. This interval testing program was initiated in an effort to evaluate heterogeneity in hydrologic properties over the thickness of the alluvium at the NC-EWDP-19D location to help determine the conceptual model of flow in the saturated alluvium south of Yucca Mountain.

The following description of the isolated-interval hydraulic tests is presented in order of screen depth, starting with screen #1, the top screen, and ending with screen #4, the bottom screen. The chronological order in which the tests were conducted was screens #4, #3, #1, and #2.



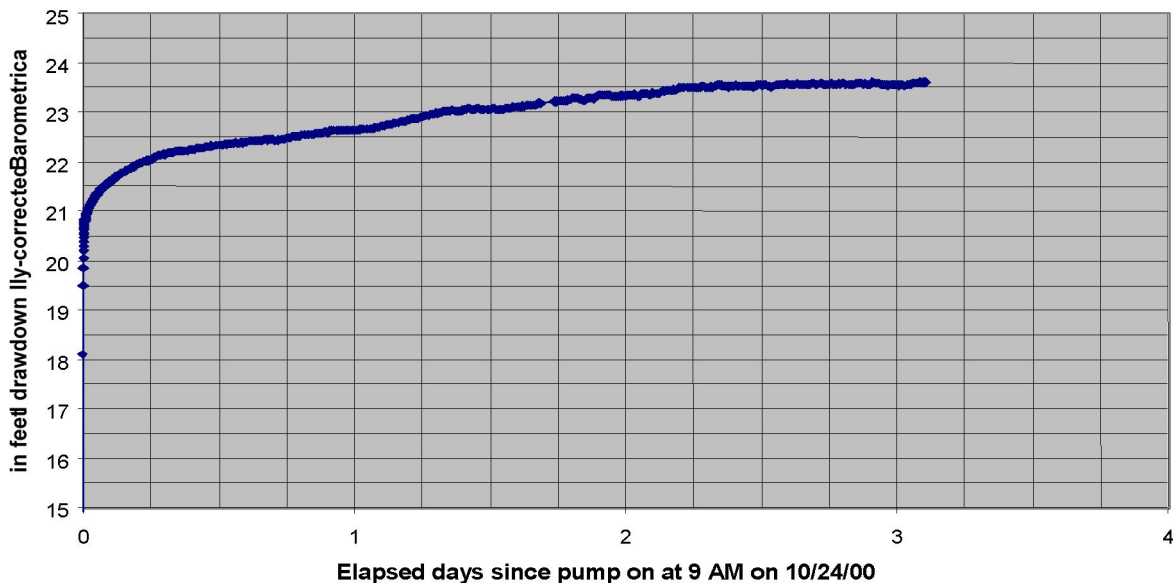
Source: DTN: GS020708312316.001 [DIRS 162678] (data).

Output DTN: GS031008312316.002 (analysis).

NOTE: The blue line is a composite curve showing both early- and late-time fits of July 7, 2000, open-hole drawdown data to Neuman's (1975 [DIRS 150321]) $\beta = 0.001$ type curve (latter portion of early time type curve and beginning portion of late-time type curve are truncated so that the two curves are joined into one continuous type curve). A value of $\beta = 0.001$ in the Neuman (1975 [DIRS 150321]) solution translates to a transmissivity of $20.7 \text{ m}^2/\text{day}$ ($223 \text{ ft}^2/\text{day}$). The early time data (less than 2 minutes) were not considered in the type-curve analysis because this early time response was attributed to borehole storage, not aquifer response. English units are shown in the figure because the analysis was conducted in English units. However, parameter estimates are reported in metric units to downstream users.

Figure F-2. Drawdown as a Function of Elapsed Time for the Combined Interval Hydraulic Test in NC-EWDP-19D Overlaid with the Neuman Unconfined Aquifer Type Curve Solution

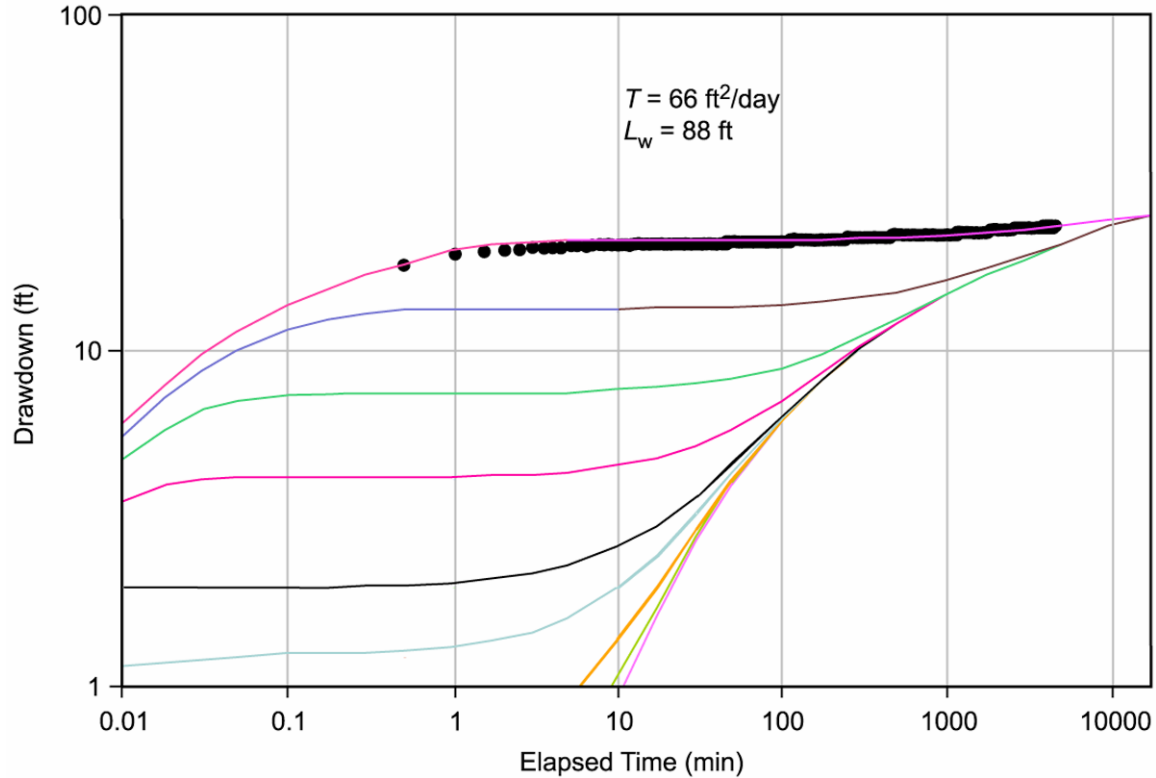
On October 24, 2000, a hydraulic test in the top interval in the alluvium, screen #1, was started in 19D. Pumping continued at a nominal rate of 61 L/min (16 gpm), with an average of 61.7 L/min (16.3 gpm), until October 27, 2000. Recovery was monitored until October 30, 2000. Figure F-3 presents the drawdown data from the test. Figure F-4 presents a fit of the Neuman (1975 [DIRS 150321]) (Neuman.vi V 1.0, STN: 10972-1.0-00 [DIRS 162754]) fully penetrating unconfined aquifer analytic solution to the data, which was obtained following the same procedure of matching the early- and late-time drawdown responses as in the combined-interval test, but with no horizontal shift required. The fully penetrating Neuman solution gives a transmissivity value of 6.1 m²/day (66 ft²/day) (see Section F1.3 for correction needed because screen #1 only partially penetrates the total saturated alluvium section).



Source: DTN: GS020708312316.001 [DIRS 162678], (data).

NOTE: English units are shown in the figure because the analysis was conducted in English units. However, parameter estimates are reported in metric units to downstream users.

Figure F-3. Drawdown as a Function of Time for the Hydraulic Test in Screen #1 of NC-EWDP-19D, October 24 to October 27, 2000



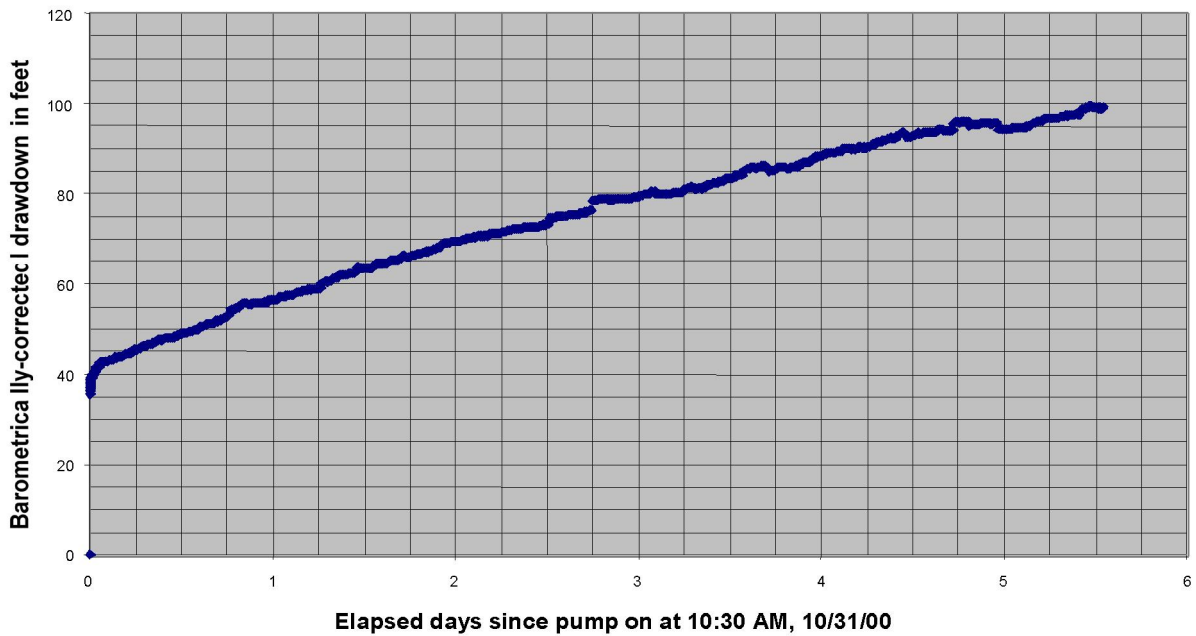
Source: DTN: GS020708312316.001 [DIRS 162678] (data).

Output DTN: GS031008312316.002 (analysis).

NOTE: The chosen type curve fits early- and late-time data simultaneously. L_w is defined in Section F1.3. English units are shown in the figure because the analysis was conducted in English units. However, parameter estimates are reported in metric units to downstream users.

Figure F-4. Drawdown versus Elapsed Time for the Hydraulic Test in Screen #1 of NC-EWDP-19D Overlaid with the Neuman Unconfined Aquifer Type Curves

On October 31, 2000, a hydraulic test in the second interval from the top in the alluvium, screen #2, was started in 19D. Pumping continued at a nominal rate of 17 L/min (19 gpm) until November 6, 2000. Recovery was monitored until November 9, 2000. Figure F-5 presents the drawdown data from the test. It is apparent that, unlike the other isolated interval hydraulic tests in 19D, the drawdown in screen #2 increased at a relatively constant rate. This interval was completed just below a clay-rich layer in the alluvium, and there is a possibility (unconfirmed) that the screen and gravel pack may have been gradually clogging with fines during the test. Figure F-6 presents a fit of the Neuman (1975 [DIRS 150321]) (Neuman.vi V 1.0, STN: 10972-1.0-00 [DIRS 162754]) fully penetrating unconfined aquifer analytic solution to the drawdown data from screen #2, which was obtained following the same procedure of matching the early- and late-time drawdown responses as in the combined-interval test, but with no horizontal shift required. The fully penetrating Neuman solution gives a transmissivity value of $0.70 \text{ m}^2/\text{day}$ ($7.5 \text{ ft}^2/\text{day}$) (Output DTN: GS031008312316.002) (see Section F1.3 for correction needed because screen #2 only partially penetrates the total saturated alluvium section).

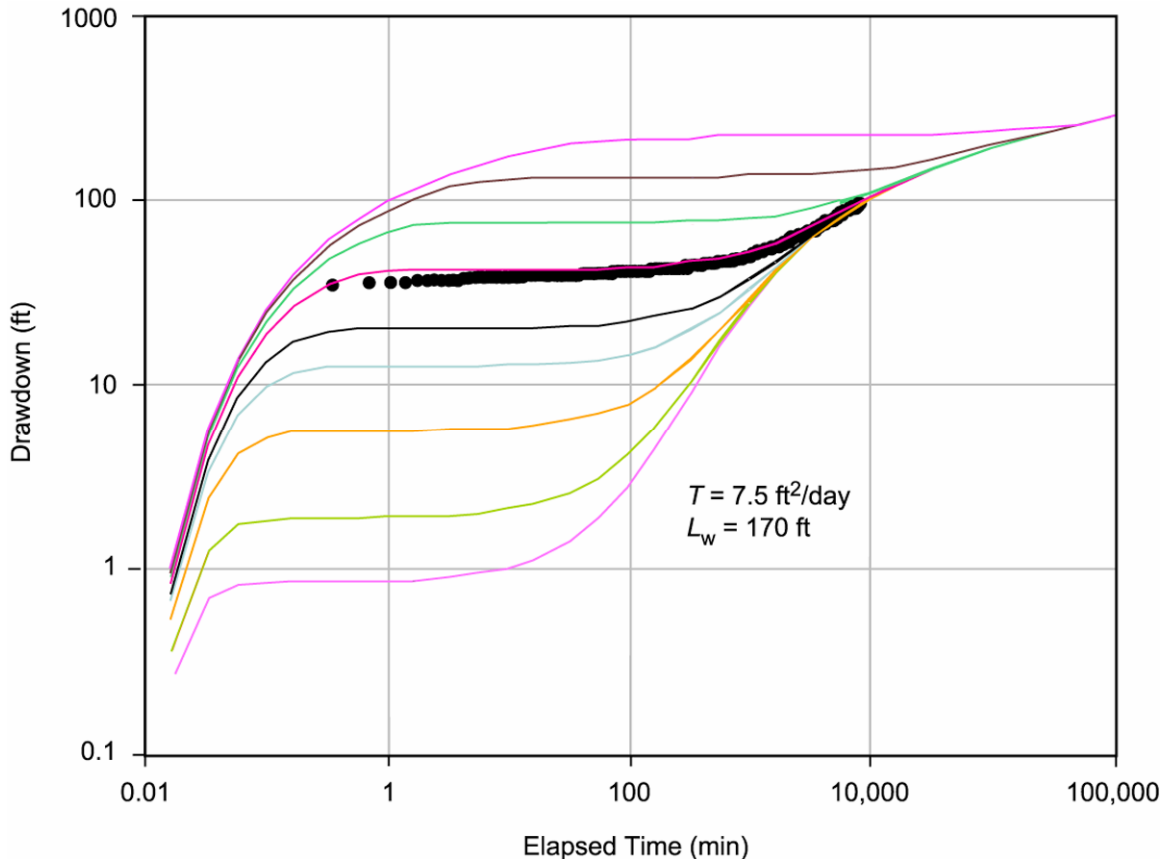


Source: DTN: GS020708312316.001 [DIRS 162678] (data).

Output DTN: GS031008312316.002 (analysis).

NOTE: English units are shown in the figure because the analysis was conducted in English units. However, parameter estimates are reported in metric units to downstream users.

Figure F-5. Drawdown as a Function of Time for the Hydraulic Test in Screen #2, NC-EWDP-19D, October 31 to November 6, 2000



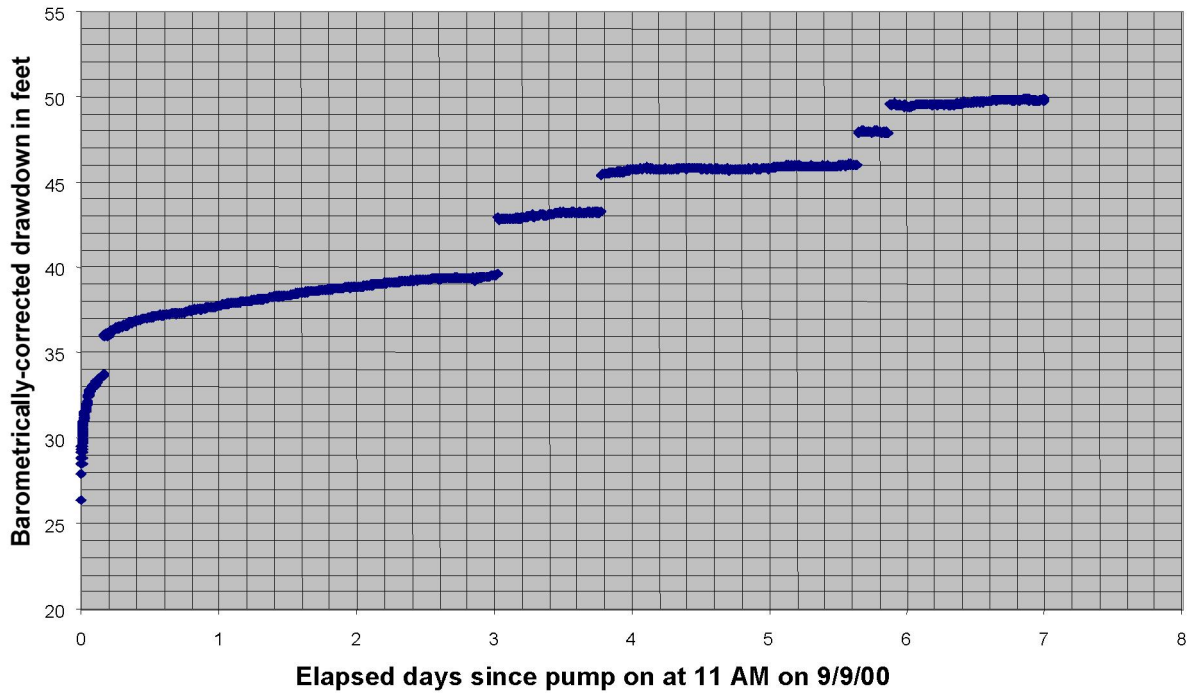
Source: DTN: GS020708312316.001 [DIRS 162678] (data).

Output DTN: GS031008312316.002 (analysis).

NOTE: The chosen type curve fits early- and late-time data simultaneously. L_w is defined in Section F1.3. English units are shown in the figure because the analysis was conducted in English units. However, parameter estimates are reported in metric units to downstream users.

Figure F-6. Drawdown as a Function of Time during the Hydraulic Test in Screen #2, NC-EWDP-19D, Overlaid with the Neuman Unconfined Aquifer Type Curves

On September 9, 2000, a hydraulic test in the second interval from the bottom in the alluvium, screen #3, was started in 19D. Pumping continued at a nominal rate of 314 L/min (83 gpm), with an average of 309.3 L/min (81.7 gpm), until September 16, 2000. Recovery was monitored until September 21, 2000. Figure F-7 presents the drawdown data from this test. The stair-step shape of the drawdown versus time curve suggests that the gravel pack was compacting at discrete times during this test, thus causing nearly instantaneous jumps in the drawdown. Figure F-8 presents a fit of the Neuman (1975 [DIRS 150321]) (Neuman.vi V 1.0, STN: 10972-1.0-00 [DIRS 162754]) fully penetrating unconfined aquifer analytic solution to the drawdown data from screen #3, which was obtained following the same procedure of matching the early- and late-time drawdown responses as in the combined-interval test, but with no horizontal shift required. The fully penetrating Neuman (1975 [DIRS 150321]) solution gives a transmissivity value of 20.7 m²/day (223 ft²/day) (see Section F1.3 for correction needed because screen #3 only partially penetrates the total saturated alluvium section).

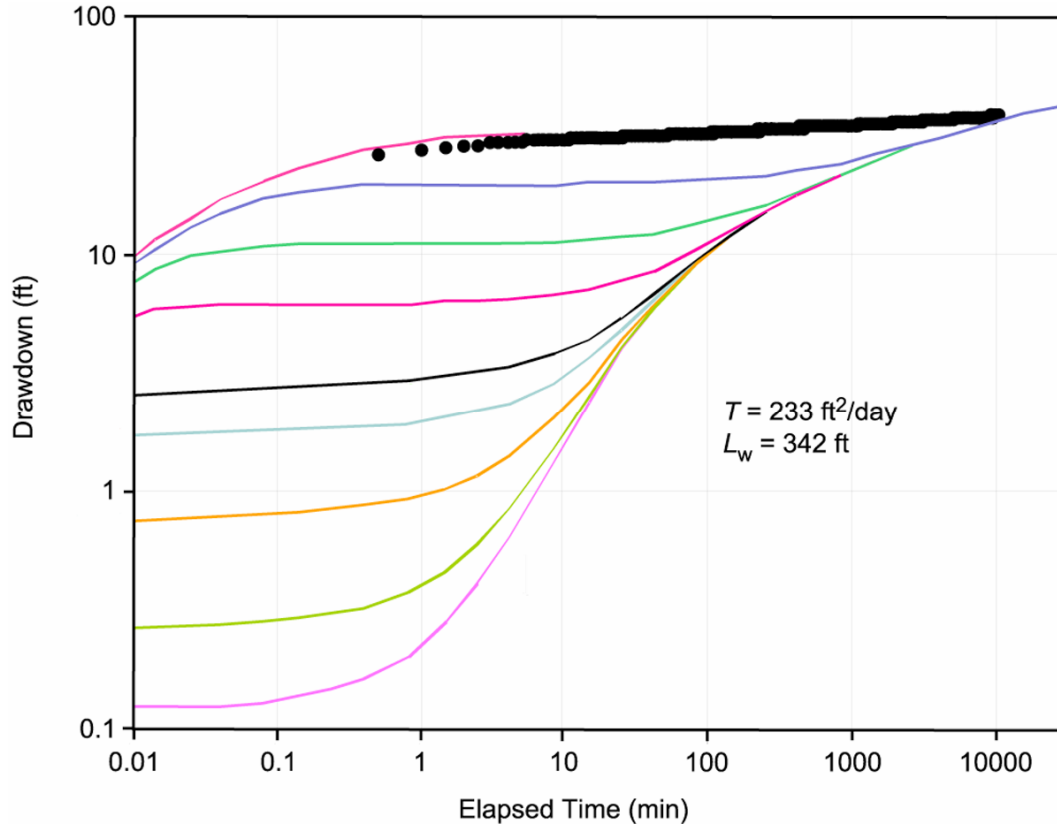


Source: DTN: GS020708312316.001 [DIRS 162678] (data).

Output DTN: GS031008312316.002 (analysis).

NOTE: English units are shown in the figure because the analysis was conducted in English units. However, parameter estimates are reported in metric units to downstream users.

Figure F-7. Drawdown as a Function of Elapsed Time for the Hydraulic Test in Screen #3 of NC-EWDP-19D, September 9 to September 16, 2000



Source: DTN: GS020708312316.001 [DIRS 162678] (data).

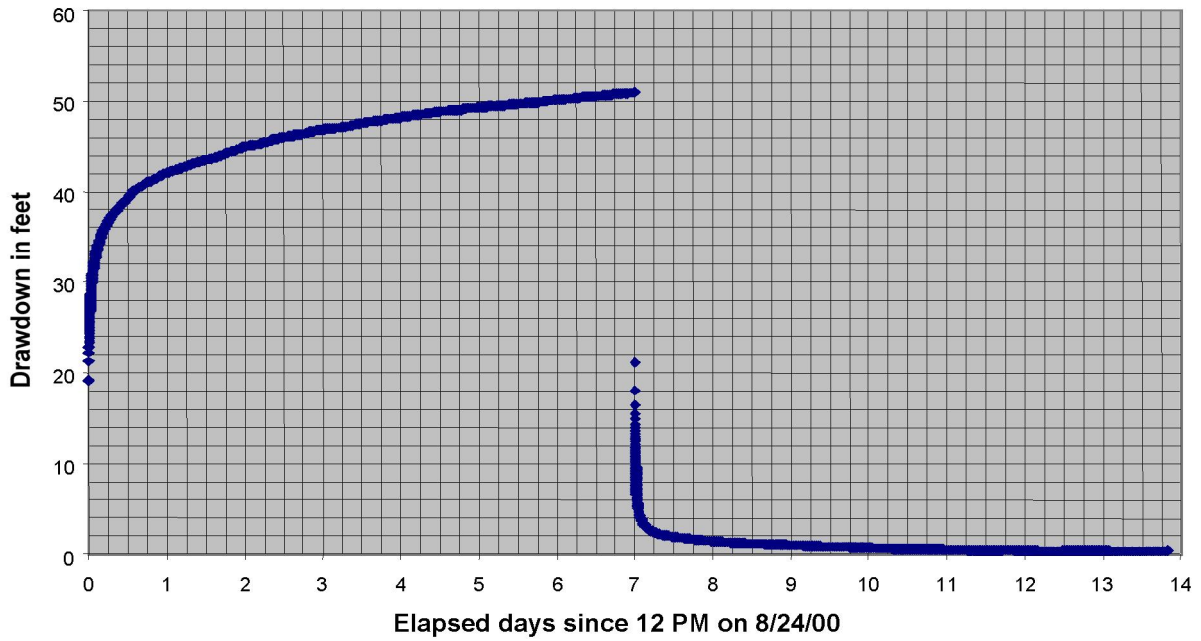
Output DTN: GS031008312316.002 (analysis).

NOTE: The chosen type curve fits early- and late-time data simultaneously. L_w is defined in Section F1.3. English units are shown in the figure because the analysis was conducted in English units. However, parameter estimates are reported in metric units to downstream users.

Figure F-8. Drawdown as a Function of Time during the Hydraulic Test in Screen #3, NC-EWDP-19D, Overlaid with the Neuman Unconfined Aquifer Type Curves

On August 24, 2000, a hydraulic test in the lower-most screen in the alluvium section of 19D, screen #4, was started. Pumping continued at the nominal rate of 299 L/min (79 gpm) until August 31, 2000, with an average of 299.8 L/min (79.2 gpm). Recovery was monitored from August 31, 2000, to September 7, 2000. Figure F-9 presents the drawdown data from this test, including both the pumping and recovery periods. Figure F-10 presents a fit of the Neuman (1975 [DIRS 150321]) (Neuman.vi V 1.0, STN: 10972-1.0-00 [DIRS 162754]) fully penetrating unconfined aquifer analytic solution to the drawdown data from screen #4, which was obtained following the same procedure of matching the early- and late-time drawdown responses as in the combined-interval test. The fully penetrating Neuman solution gives a transmissivity value of 28 m²/day (300 ft²/day) (Output DTN: GS031008312316.002) (see Section F1.3 for correction needed because screen #4 only partially penetrates the total saturated alluvium section).

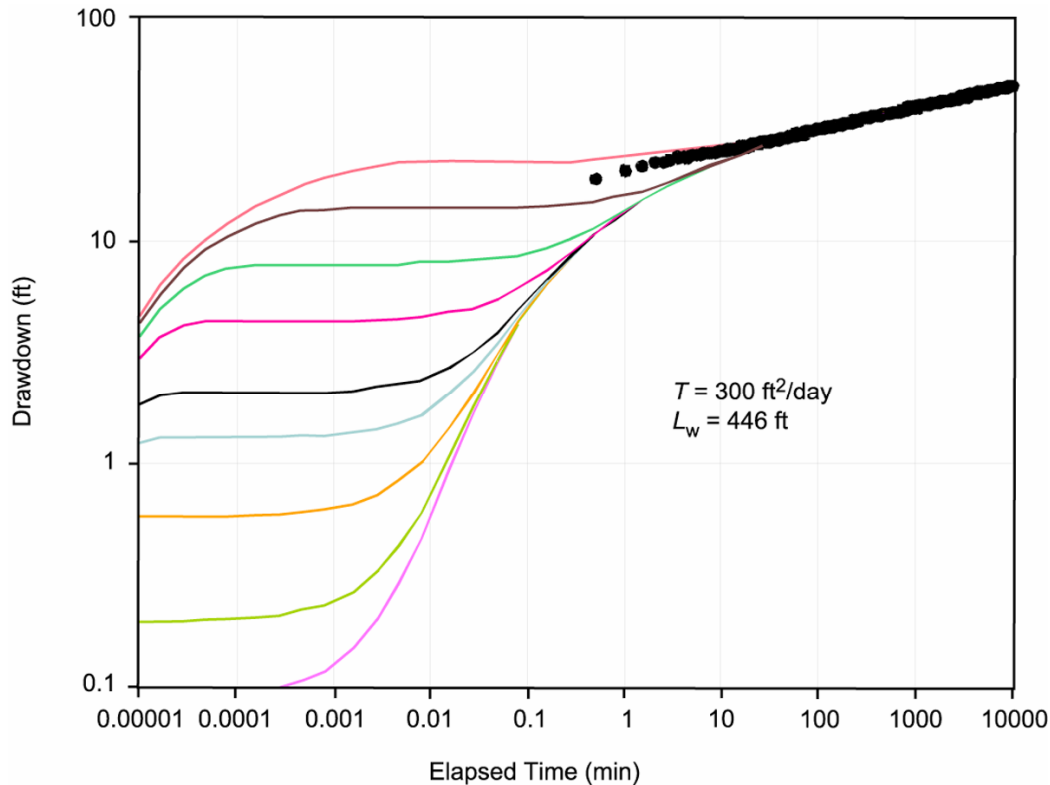
The drawdown in the combined screens #5, #6, and #7 interval as a function of elapsed time during the above test in screen #4 beginning on August 24, 2000, is presented in Figure F-19 in Section F1.5, where it is used to calculate the rate of leakage from below the alluvium into the screen #4 interval.



Source: DTN: GS020708312316.001 [DIRS 162678] (data).

NOTE: English units are shown in the figure because the analysis was conducted in English units. However, parameter estimates are reported in metric units to downstream users.

Figure F-9. Drawdown as a Function of Time for the Hydraulic Test in NC-EWDP-19D, Screen #4, August 24 to August 31, 2000



Source: DTN: GS020708312316.001 [DIRS 162678] (data).

Output DTN: GS031008312316.002 (analysis).

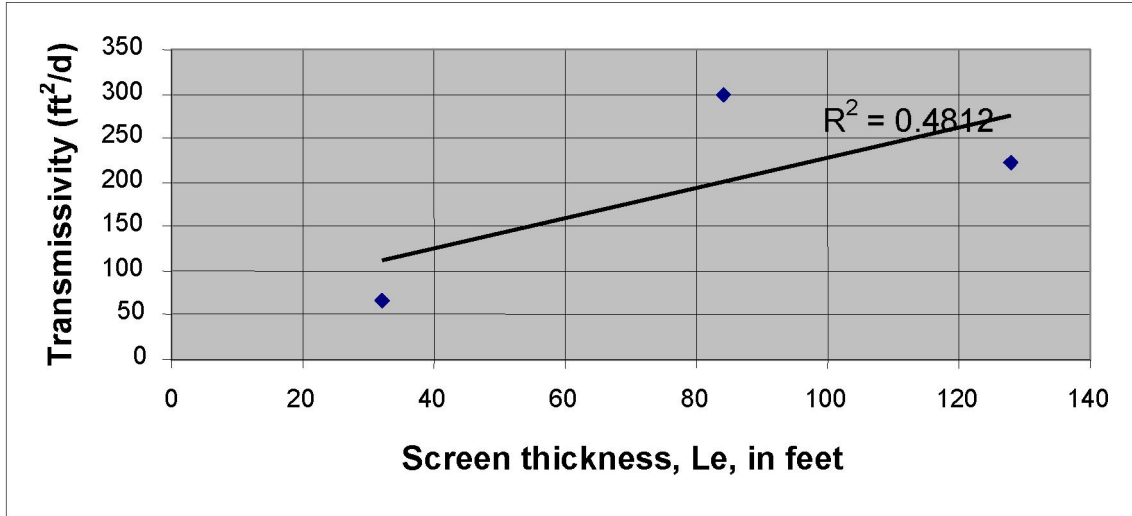
NOTE: The matching type curve has been shifted horizontally to emphasize the match to the late-time data. The early-time data were also matched by this type curve, although, unlike in Figure F-2, the early-time and late-time type curve (Neuman 1975 [DIRS 150321]) matches are not “spliced” together to show a single composite fit. L_w is defined in Section F1.3. English units are shown in the figure because the analysis was conducted in English units. However, parameter estimates are reported in metric units to downstream users.

Figure F-10. Drawdown as a Function of Time during the Hydraulic Test in Screen #4, NC-EWDP-19D, Overlaid with the Neuman Unconfined Aquifer Type Curves

F1.3 SUMMARY OF SINGLE-WELL HYDRAULIC TESTS IN ALLUVIUM IN NC-EWDP-19D

The hydraulic tests in 19D, screens 1 through 4, were analyzed using the fully penetrating Neuman (1975 [DIRS 150321]) (Neuman.vi V 1.0, STN: 10972-1.0-00 [DIRS 162754]) unconfined aquifer solution because all four individual screens, as well as the combined intervals, exhibited characteristic unconfined aquifer responses. Because each of the screens did not fully penetrate the unconfined alluvial aquifer, they should be analyzed by the partially penetrating Neuman solution. However, there is no Yucca Mountain Project-qualified software to perform this analysis, so the transmissivity, T , values resulting from the Neuman fully penetrating solution should be corrected to account for the length of the screen, L_e , and the depth from the water table to the bottom of the screen being tested, L_w (see, for example, Bouwer 1978 [DIRS 162675], pp. 79 to 82, 114 to 117). An empirical relationship was sought between transmissivity and each of L_e and L_w by plotting transmissivity versus L_e (Figure F-11) and transmissivity versus L_w/b in Figure F-12, where b is the total unconfined alluvial aquifer

thickness (136 m or 446 ft). The results from screen #2 are not included in Figures F-11 and F-12 because they don't follow the trend of the results from the other screens, probably because the screen #2 interval is highly affected by a clay layer at the same horizon. Figure F-13 is a plot of transmissivity versus L_w/b showing results from all four screens.

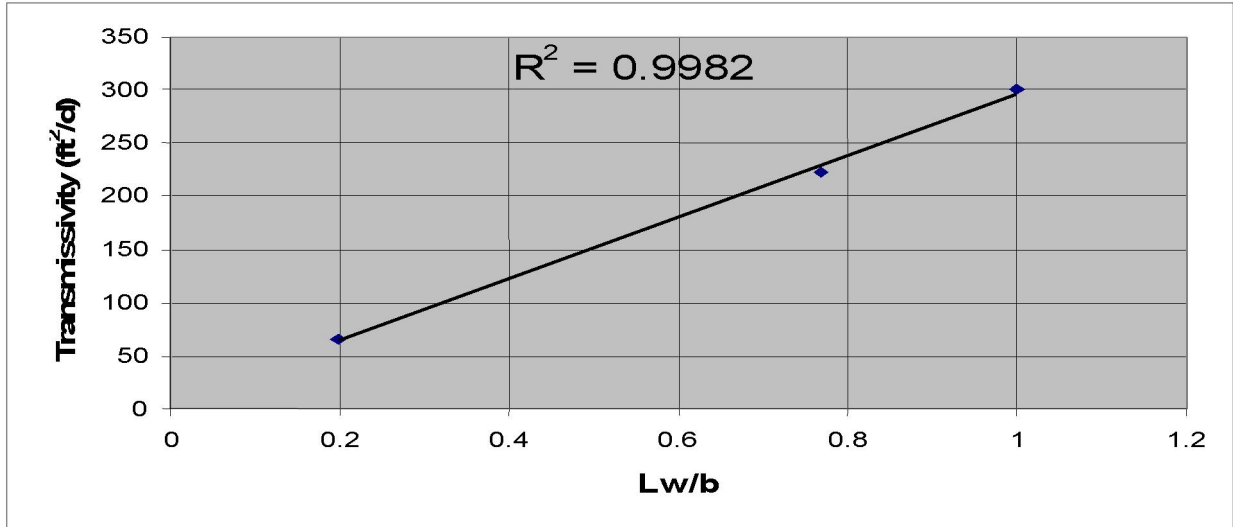


Source: DTN: GS020708312316.001 [DIRS 162678] (data).

Output DTN: GS031008312316.002 (analysis).

NOTE: English units are shown in the figure because the analysis was conducted in English units. However, parameter estimates are reported in metric units to downstream users.

Figure F-11. Transmissivity of Screens #1, #3, and #4 of NC-EWDP-19D as a Function of Screen Thickness

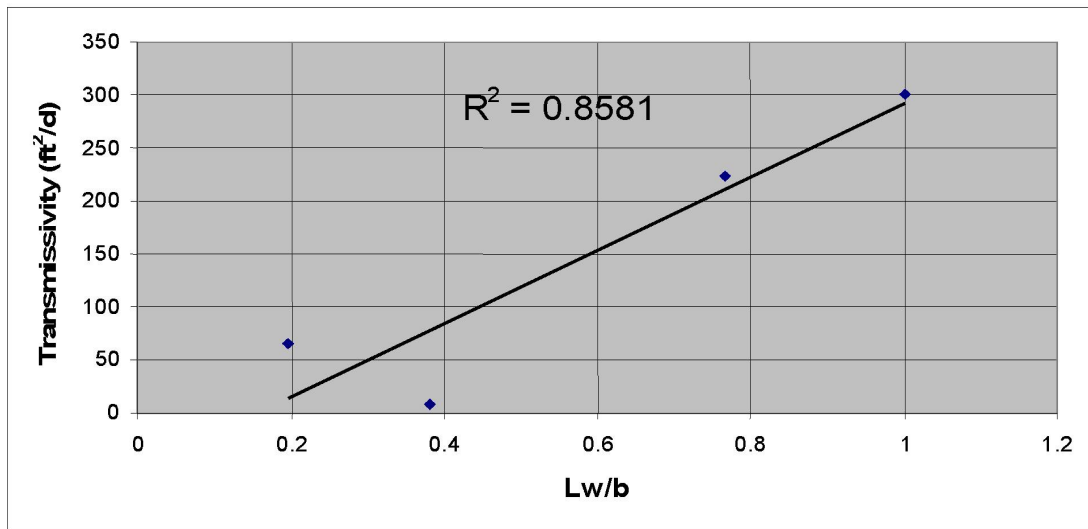


Source: DTN: GS020708312316.001 [DIRS 162678] (data).

Output DTN: GS031008312316.002 (analysis).

NOTE: English units are shown in the figure because the analysis was conducted in English units. However, parameter estimates are reported in metric units to downstream users.

Figure F-12. Transmissivity of Screens #1, #3, and #4 of NC-EWDP-19D as a Function of Distance from Water Table to Bottom of Screen Divided by Distance from Water Table to Bottom of Screen #4



Source: DTN: GS020708312316.001 [DIRS 162678] (data).

Output DTN: GS031008312316.002 (analysis).

NOTE: English units are shown in the figure because the analysis was conducted in English units. However, parameter estimates are reported in metric units to downstream users.

Figure F-13. Transmissivity of Screens #1, #2, #3, and #4 of NC-EWDP-19D as a Function of Distance from Water Table to Bottom of Screen Divided by Distance from Water Table to Bottom of Screen #4

It can be seen from Figures F-11 and F-12 that the hydraulic test results from screens #1, #3, and #4 indicate that transmissivity calculated with the fully penetrating solution is a very weak function of L_e ($R^2 = 0.4812$) but is very strongly correlated ($R^2 = 0.9982$) with L_w/b , and, therefore, with L_w . In fact, Figure F-12, and even Figure F-13, can be viewed as an empirical relationship derived from ATC single-well hydraulic testing for correction of the partially penetrating transmissivity values that give a value for transmissivity of 28 m²/day (300 ft²/day) as their upper limit when the aquifer is fully penetrated, i.e. at $L_w/b = 1$. Thus, the transmissivity values obtained in the hydraulic tests of screens #1, #3, and #4 are all consistent with an overall transmissivity of 28 m²/day (300 ft²/day) for the saturated alluvium at 19D (Output DTN: GS031008312316.002). The transmissivity value of 28 m²/day (300 ft²/day) from the 8/24/00 screen #4 test is essentially the same as the transmissivity from the fully penetrating open-hole test started on July 7, 2000 (20.7 m²/day or 223 ft²/day), considering that the borehole was slugged to increase its capacity between the two tests. Using an aquifer thickness equal to the distance from the water table to the bottom of screen #4 (136 m or 446 ft), an overall transmissivity value of 28 m²/day (300 ft²/day) represents a hydraulic conductivity of 0.20 m/day (0.67 ft/day) (Output DTN: GS031008312316.002).

Because of the large head losses discussed in the next section, the results from single-well hydraulic testing at 19D are considered to have a high degree of uncertainty in their absolute values. It is recommended instead that values of transmissivity, and associated hydraulic conductivity, obtained from cross-hole testing at the ATC, which is discussed in Section F2, be used for the saturated alluvium.

F1.4 STEP-DRAWDOWN TESTS TO DETERMINE HEAD LOSSES

A step-drawdown test was conducted prior to the hydraulic test in each interval. On July 6, 2000, prior to the open-alluvium hydraulic test starting on July 7, a step-drawdown test was conducted in the open-alluvium in well 19D. Two methods were attempted to analyze the data as presented below.

The drawdown in the well itself (as opposed to the drawdown in the aquifer at the well wall) is given by the following equation (modified from Bouwer 1978 [DIRS 162675], p. 83, Equation 4.38):

$$s = B \cdot Q + C \cdot Q^n \quad (\text{Eq. F-1})$$

where

- s = the drawdown
- Q = the pumping rate
- B , C , and n are coefficients.

$B \cdot Q$ represents the laminar flow that describes groundwater flow movement occurring in the aquifer and $C \cdot Q^n$ represents the turbulent flow and associated head losses caused by water entering the borehole on its way from the aquifer to the pump intake. Jacob assumed $n = 2$ (Bouwer 1978 [DIRS 162675], p. 83, Equation 4.39) to obtain:

$$s = B \cdot Q + C \cdot Q^2 \quad (\text{Eq. F-2})$$

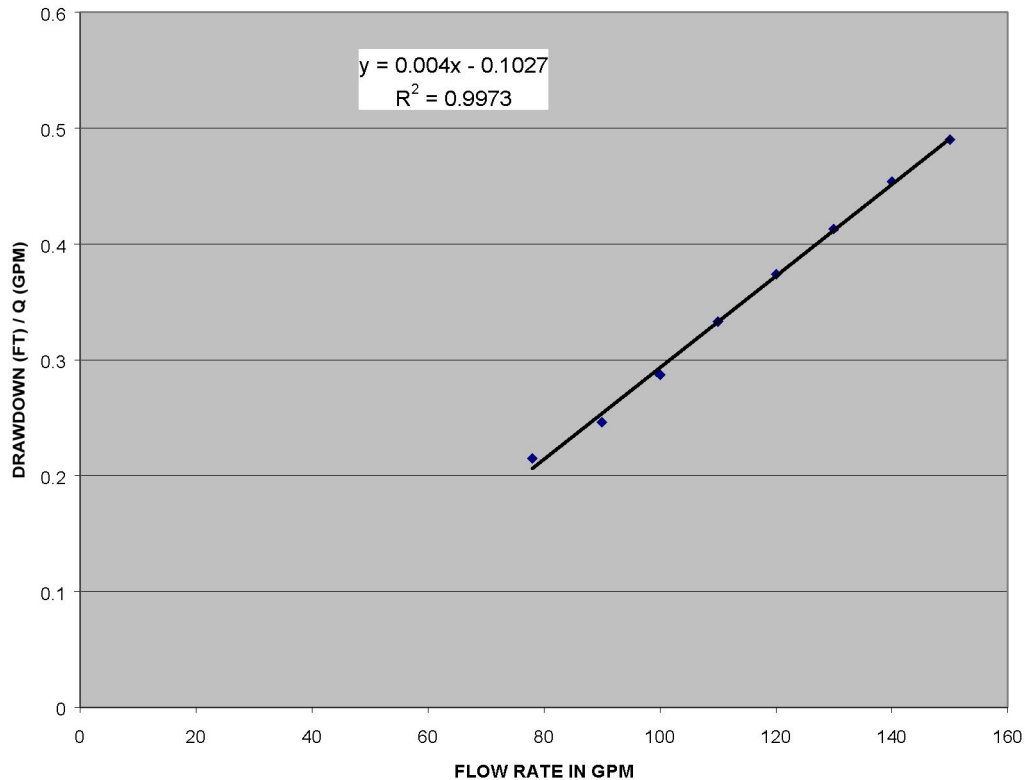
The idea is to calculate B and C and then to calculate the fractional efficiency as the laminar drawdown divided by total (laminar plus turbulent) drawdown. Efficiency would, thus, be $B \cdot Q / (B \cdot Q + C \cdot Q^2)$, if equation F-1 is used, and $B \cdot Q / (B \cdot Q + C \cdot Q^2)$, if equation F-2 is used.

Calculations based on both equations were carried out on the data from the July 6, 2000, step-drawdown test in the open alluvium that indicate a negative value of B (a similar result is obtained when analyzing a step-drawdown test conducted in screen #4 on January 7, 2002). This result, of course, is incorrect because a negative B leads to an indeterminate efficiency calculation. Calculation of B is demonstrated below for the July 6, 2000, step-drawdown test.

Dividing equation F-2 by Q to obtain

$$\frac{s}{Q} = B + C \cdot Q \quad (\text{Eq. F-3})$$

indicates that a plot of s/Q versus Q yields a linear relationship with an intercept of B and a slope of C . Figure F-14 is such a plot for the above step-drawdown test. It can be seen from the figure that the intercept B is -0.1027 and the slope C is 0.004. Since the laminar flow component, $B \cdot Q$, cannot be negative, the negative value for B is taken to indicate that $B \cdot Q$ is approximately zero.



Source: DTN: GS020708312316.001 [DIRS 162678] (data).

NOTE: Each data point represents an average of several drawdown and flow rate measurements at each nominal pump rate. English units are shown in the figure because the analysis was conducted in English units. However, parameter estimates are reported in metric units to downstream users.

Figure F-14. Step-Drawdown Test in the Open Alluvium of NC-EWDP-19D, July 6, 2000

The cause of this problem is believed to be that the step-drawdown test was carried out at a flow-rate range too high to permit calculation of the laminar groundwater flow component, $B \cdot Q$. In the flow-rate range for the test, 295 to 568 L/min (78 to 150 gpm), the turbulent head losses, $C \cdot Q^2$, were so large that they dominated the much smaller laminar-flow-caused drawdown, $B \cdot Q$, which, at the accuracy of the test results, is approximately zero. To have been able to calculate the laminar component and, therefore, quantify well efficiency, the step-drawdown test would have had to be run at a much lower range of flow rates than the range used, namely 295 to 568 L/min (78 to 150 gpm). However, the pump used, which was required for pumping up to 606 L/min (160 gpm) in the open-alluvium test and which was used in the screens #4 and #3 isolated interval tests, had a minimum operational rate of approximately 291 L/min (77 gpm).

Because the 19D well efficiency could not be calculated from the step-drawdown tests conducted in it, the efficiency was estimated by comparing results from single-well hydraulic tests in that well with those of cross-hole tests. Single-well tests indicated a transmissivity of 28 m²/day (300 ft²/day) for the saturated alluvium at 19D (Output DTN: GS031008312316.002) (Section F1.3), whereas cross-hole testing indicated a transmissivity of 306 m²/day (3,300 ft²/day) (Output DTN: GS031008312316.002) by analyzing the response in observation well 19IM2 (Section F2).

Drawdown is related to Q and transmissivity, T , by the relationship:

$$s = \frac{Q}{4\pi T} W(u) \quad (\text{Eq. F-4})$$

where

$u = r^2 S / 4Tt$, in which:

r [L] = radial distance from the pumping well

S [L⁰] = storativity

t [T] = elapsed time from the beginning of pumping

and

$W(u) = \int_0^\infty (e^{-u}/u) du$; $W(u)$ is the well function for a confined aquifer, or, in modified form, for an unconfined or leaky aquifer.

Equation F-4 is the same relationship as in the paper by Theis (1935 [DIRS 150327], p. 520, Equation 4) except that s is used for drawdown instead of v , and Q is used for the discharge rate instead of F .

Assuming that head losses in observation well 19IM2 in the cross-hole test when well 19D was being pumped (Section F2) to be negligible relative to those in the pumped well, the value of 306 m²/day (3,300 ft²/day) is considered to be the true transmissivity value of the alluvium aquifer at the ATC (Output DTN: GS031008312316.002). Therefore, in the single-well tests at well 19D, by substituting 306 m²/day (3,300 ft²/day) into equation F-4, the drawdown in the aquifer itself due to laminar flow is:

$$s_{\text{laminar}} = \frac{Q}{4\pi(306)} W(u) \quad (\text{Eq. F-5})$$

The actual drawdown in well 19D is the total drawdown (laminar plus turbulent) that was used to calculate a T of 28 m²/day (300 ft²/day), which when substituted into equation F-4 yields:

$$s_{\text{laminar}} + s_{\text{turbulent}} = \frac{Q}{4\pi(28)} W(u) \quad (\text{Eq. F-6})$$

The well function, $W(u)$, in equations F-5 and F-6 is the same because it pertains to the same well and time history. Q is also the same; it is the actual pumping rate for the single-well testing.

The well efficiency for 19D (Output DTN: GS031008312316.002) is now calculated by dividing equation F-5 by equation F-6:

$$\text{Efficiency} = \frac{s_{\text{laminar}}}{s_{\text{laminar}} + s_{\text{turbulent}}} = \frac{28}{306} = 0.091 = 9.1\% \quad (\text{Eq. F-7})$$

F1.5 DETERMINATION OF LEAKAGE FROM SCREENS #5, #6, AND #7 TO SCREEN #4

After single-well hydraulic and tracer tests in well 19D, screen #4 had been selected to conduct cross-hole tracer testing by pumping 19D and injecting tracers into 19IM1 and 19IM2. For that reason, it was desirable to determine the upward contribution of the intervals below the alluvium (screens #5, #6, and #7 in 19D) to the water withdrawn from screen #4 in 19D during such a cross-hole tracer test (see Figure 6.1-8 for location of screens and other lithologic information). Such contribution from the intervals below the alluvium would be promoted by the natural upward gradient at the site and the creation of a substantial additional vertical gradient by pumping screen #4 in 19D and lowering its hydraulic head. Knowledge of this contribution is necessary for the correct analysis of the results from cross-hole tracer testing in screen #4, especially for effective porosity. The flow rate that should be used in calculating the effective porosity when analyzing the results of cross-hole tracer testing should be the portion of the pumped rate that is actually provided by screen #4 of the alluvium, that is, excluding the portion contributed by the intervals below the alluvium.

To determine the component of flow from below screen #4, three “confirmatory” hydraulic tests were conducted in 19D. The results from these three tests will first be presented below, followed by an analysis to determine the leakage rate from below the screen #4 interval.

In the first confirmatory test from December 18 to 20, 2001, the combined interval below the alluvium containing screens #5, #6, and #7 was pumped at the nominal rate of 356 L/min (94 gpm) for 48 hr. During the test, the screen #4 interval and the combined interval containing screens #1, #2, and #3 were monitored. The drawdown in the combined screens #5, #6, and #7 interval as a function of elapsed time is shown in Figure F-15.

In the second confirmatory test from January 4 to 6, 2002, the screen #5 interval also (like the screens #5, #6, and #7 interval test) was pumped at the nominal rate of 356 L/min (94 gpm) for 48 hr. During the test, the combined screens #6 and #7 interval, the screen #4 interval, and the combined screens #1, #2, and #3 interval were monitored. The drawdown in the screen #5 interval as a function of elapsed time is shown in Figure F-16.

In the third confirmatory test from January 8 to 10, 2002, the screen #4 interval was pumped at the nominal rate of 254 L/min (67 gpm) for 48 hr. During the test, the combined screens #5, #6, and #7 interval, the screen #3 interval, and the combined screens #1 and #2 interval were monitored. The drawdown in the screen #4 interval as a function of elapsed time is shown in Figure F-17.

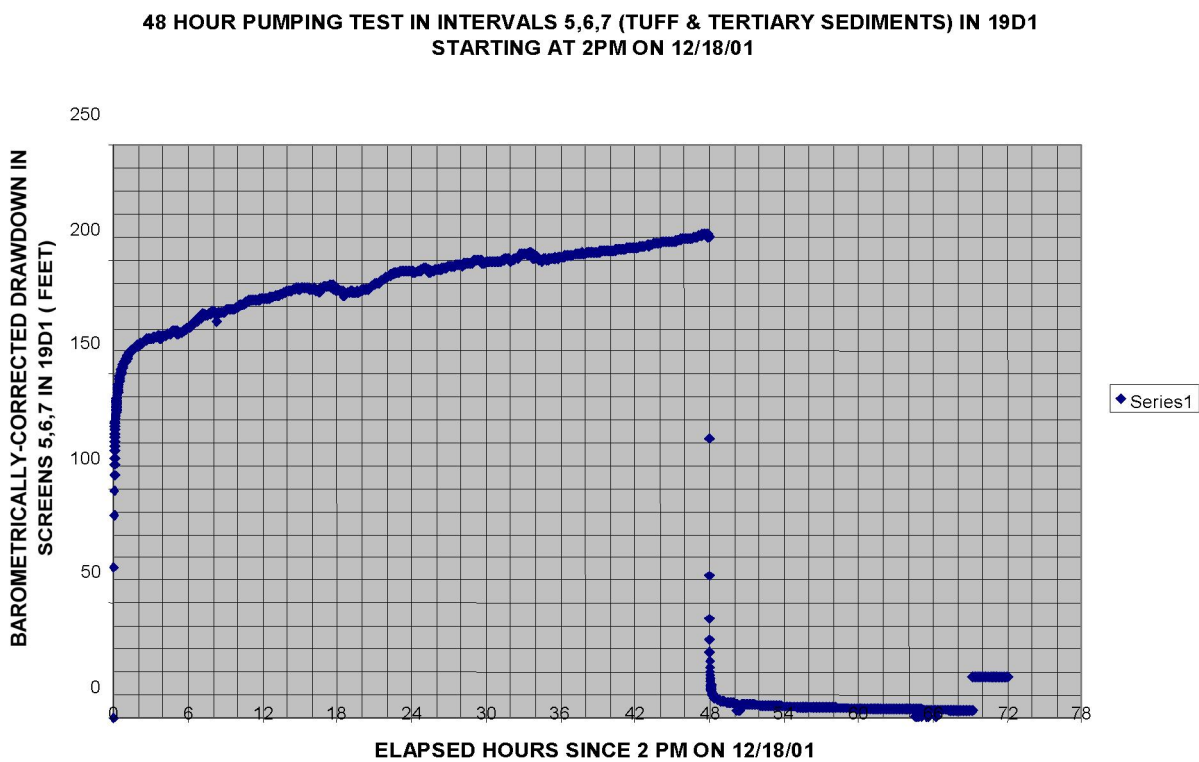
Also for this confirmatory test in screen #4, the recovery for the screens #5, #6, and #7 interval is shown in Figure F-18 because it is needed in the following analysis of leakage.

To determine the component of flow from below screen #4 to withdrawal from screen #4, a comparison was made of the drawdown in screens #5, #6, and #7 when they were pumped at 356 L/min (94 gpm) in the December 18, 2001, test (Figure F-15) with the drawdown in screens #5, #6, and #7 in response to pumping screen #4 in the August 24, 2000, “screen #4” test (Figure F-19).

Figure F-20 presents the comparison. The responses are very similar with a ratio of 153 in the drawdown values. These are both drawdowns in the same intervals (i.e., screens #5, #6, and #7): one in response to direct pumping at 356 L/min (94 gpm) and the other in response to an unknown leakage rate from screens #5, #6, and #7 to screen #4. Thus,

$$\frac{s_{5,6,7(12/18/01)}}{s_{5,6,7(8/24/00)}} = 153 \quad (\text{Eq. F-8})$$

where $s_{5,6,7(12/18/01)}$ is the drawdown for the combined screens #5, #6, and #7 interval on December 18, 2001, and so forth.

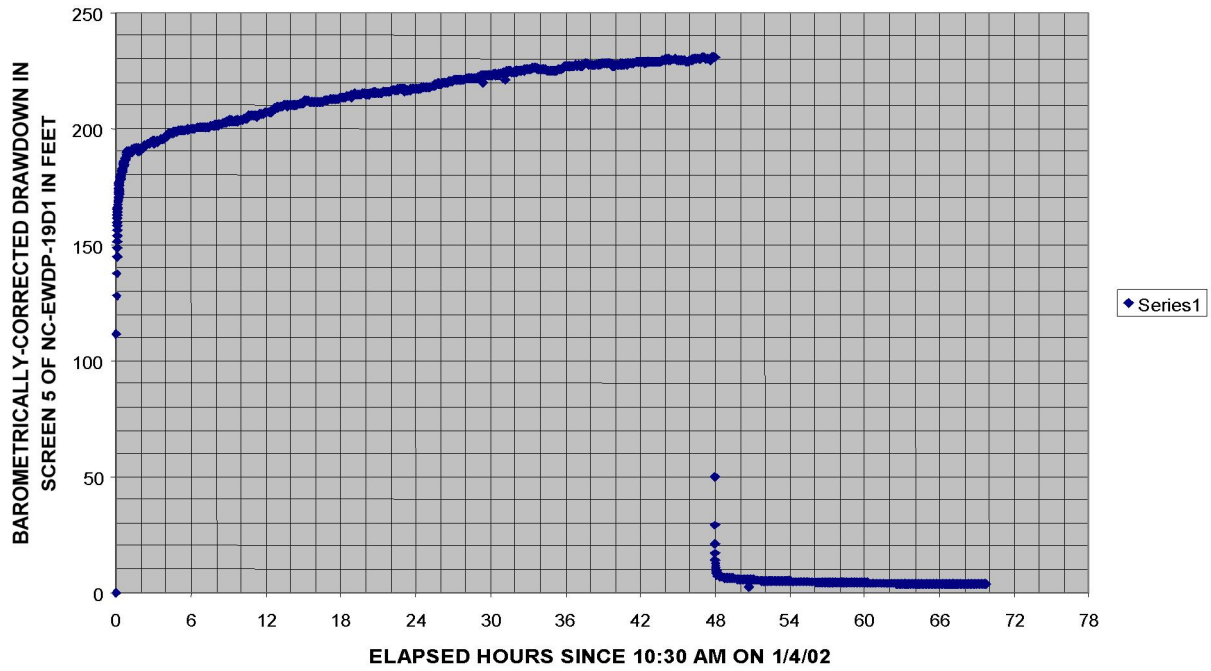


Source: DTN: GS020908312 316.002 [DIRS 162679] (data).

NOTE: English units are shown in the figure because the analysis was conducted in English units. However, parameter estimates are reported in metric units to downstream users.

Figure F-15. Drawdown versus Elapsed Time Since Pumping Started for the Confirmatory Hydraulic Test in Which the Combined Screens #5, #6, and #7 Interval in NC-EWDP-19D was Pumped

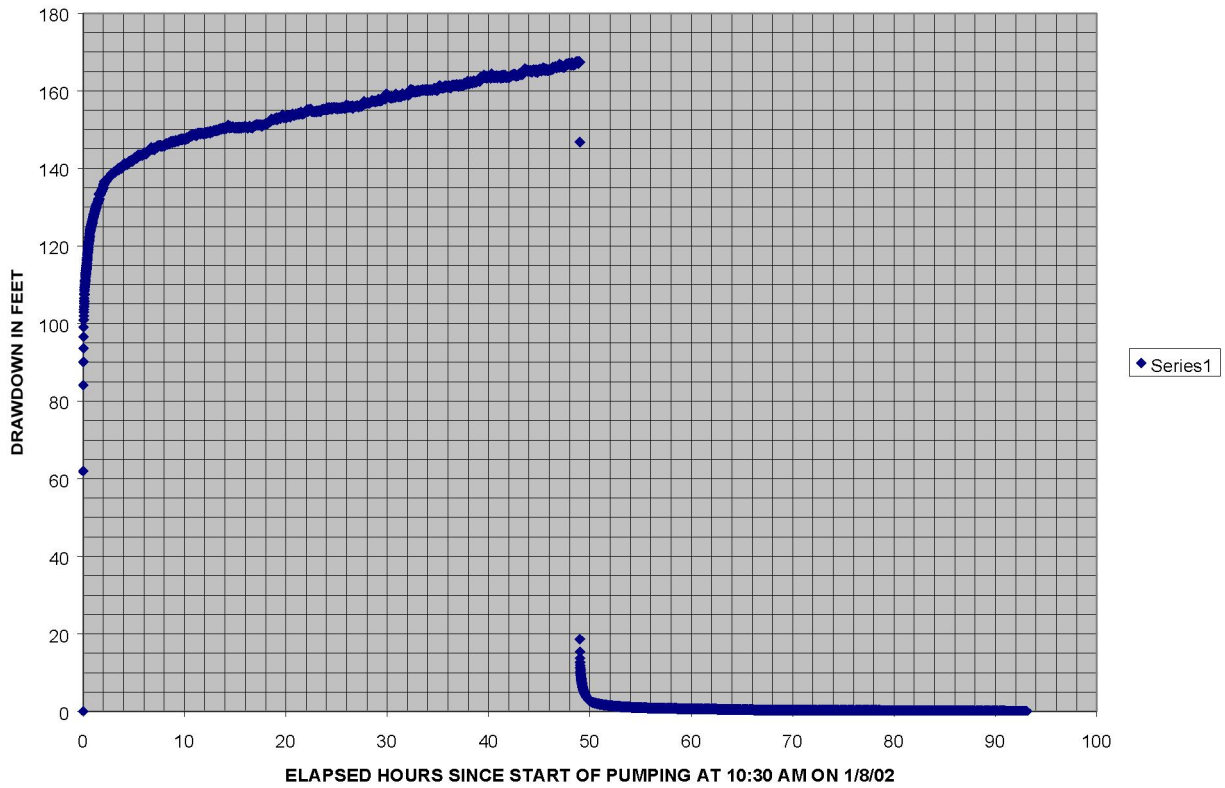
48 HOUR TEST IN SCREEN #5 OF NC-EWDP-19D1 STARTING AT 10:30 AM ON 1/4/02



Source: DTN: GS020908312316.002 [DIRS 162679] (data).

NOTE: English units are shown in the figure because the analysis was conducted in English units. However, parameter estimates are reported in metric units to downstream users.

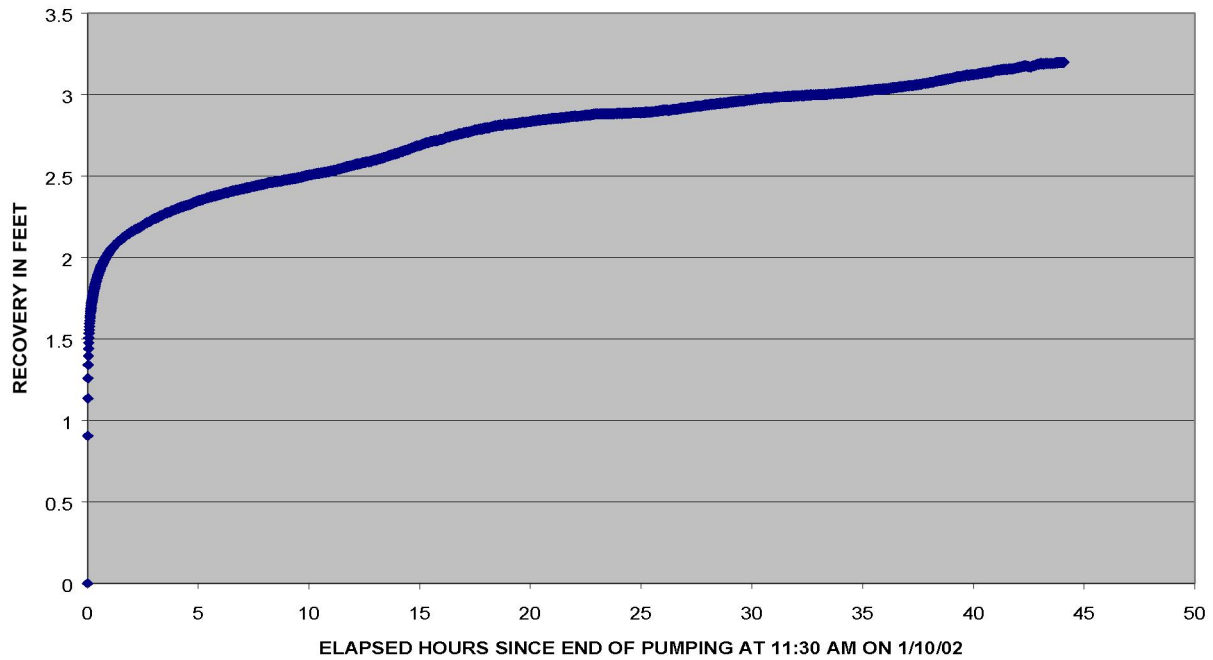
Figure F-16. Drawdown as a Function of Elapsed Time for the Confirmatory Hydraulic Test in Which the Screen #5 Interval in NC-EWDP-19D was Pumped



Source: DTN: GS020908312316.002 [DIRS 162679] (data).

NOTE: English units are shown in the figure because the analysis was conducted in English units. However, parameter estimates are reported in metric units to downstream users.

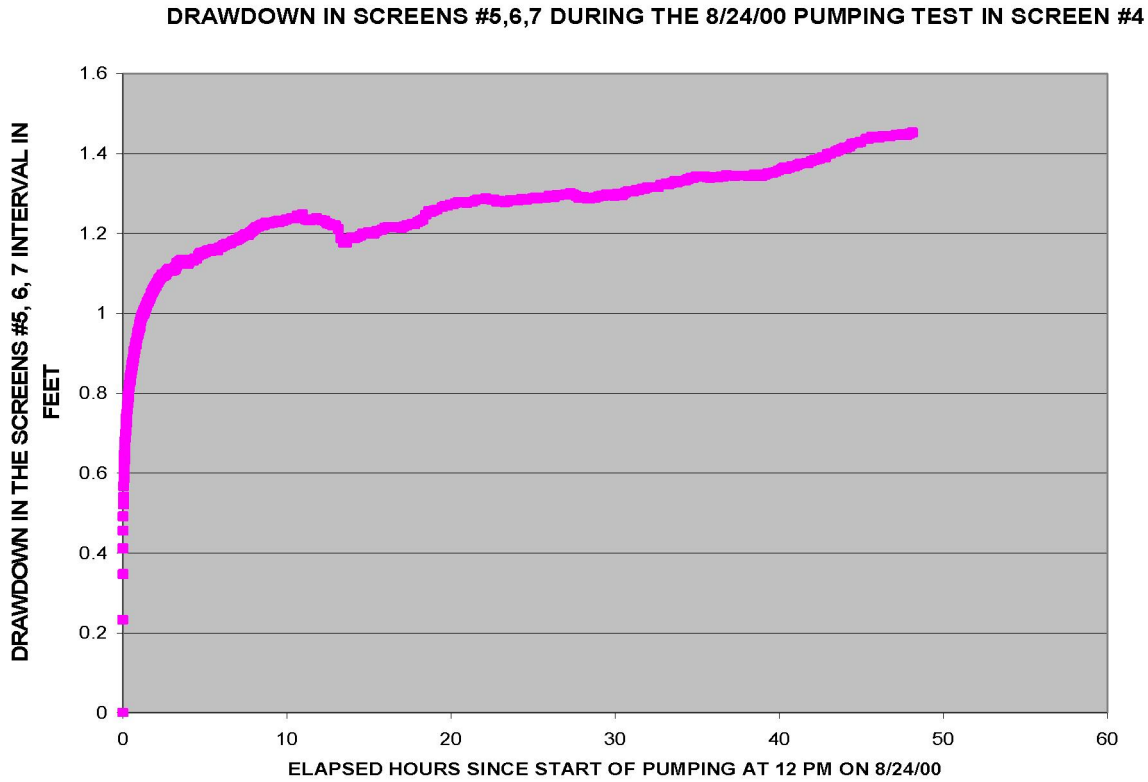
Figure F-17. Drawdown as a Function of Elapsed Time in Screen #4 during Pumping and Recovery in the Confirmatory Hydraulic Test in that Screen, January 8 to 10, 2002



Source: DTN: GS020908312316.002 [DIRS 162679] (data).

NOTE: English units are shown in the figure because the analysis was conducted in English units. However, parameter estimates are reported in metric units to downstream users.

Figure F-18. Recovery versus Elapsed Time for the Screens #5, #6, and #7 Interval during the Confirmatory Hydraulic Test in Screen #4 of NC-EWDP-19D, January 8 to 10, 2002



Source: DTN: GS020708312316.001 [DIRS 162678] (data).

NOTE: English units are shown in the figure because the analysis was conducted in English units. However, parameter estimates are reported in metric units to downstream users.

Figure F-19. Drawdown in the Screens #5, #6, and #7 Interval during the August 24 to 31, 2000, Pumping Test in Screen #4



Sources: DTNs: GS020708312316.001 [DIRS 162678] and GS020908312316.002 [DIRS 162679] (data).

NOTE: English units are shown in the figure because the analysis was conducted in English units. However, parameter estimates are reported in metric units to downstream users.

Figure F-20. Comparing Drawdown in the Screens #5, #6, and #7 Interval While It Was Pumped During the December 18, 2001, Test with the Drawdown in the Same Interval during the August 24 to 31, 2000, Pumping Test in Screen #4

A correction should be made, however, to the drawdown in the screens #5, #6, and #7 interval during the December 18, 2001, test, based on the approximately 9% well efficiency of 19D, as determined by equation F-7. This efficiency indicates that the laminar component of the drawdown occurring in the aquifer is only 9% of the total drawdown recorded in the screens #5, #6, and #7 interval of 19D when that interval was directly pumped during the December 18, 2001, test. In other words, using a prime to indicate laminar drawdown in the aquifer and multiplying the drawdown by the well efficiency (decimal equivalence 0.09) in order to calculate 9% of drawdown is mathematically expressed as,

$$s'_{5,6,7(12/18/01)} = (0.09)s_{5,6,7(12/18/01)} \tag{Eq. F-9}$$

On the other hand, negligible head losses are assumed in the screens #5, #6, and #7 interval when it was not pumped directly but leaked to the screen #4 interval when the latter was pumped in the August 24, 2000, test—that is, if no drawdown is subtracted for well inefficiency, then s prime equals s , which is mathematically expressed as

$$s'_{5,6,7(8/24/00)} = s_{5,6,7(8/24/00)} \quad (\text{Eq. F-10})$$

Therefore, the ratio of drawdowns occurring in the aquifer itself for the above two contrasted tests is

$$\frac{s'_{5,6,7(12/18/01)}}{s'_{5,6,7(8/24/00)}} = (0.09) \frac{s_{5,6,7(12/18/01)}}{s_{5,6,7(8/24/00)}} = (0.09)(153) = 13.77 \quad (\text{Eq. F-11})$$

Assuming that the transmissivity of the screens #5, #6, and #7 interval is the same during the August 24, 2000, and December 18, 2001, tests, the ratio of the two drawdown responses, which is 13.77, should be the same as the ratio of the flow rates that produced them—that is, from equation F-4 (Theis 1935 [DIRS 150327]),

$$s'_{5,6,7(12/18/01)} = \frac{356}{4\pi T} W(u) \quad (\text{Eq. F-12})$$

and

$$s'_{5,6,7(8/24/00)} = \frac{Q_{5,6,7(8/24/00)}}{4\pi T} W(u) \quad (\text{Eq. F-13})$$

where $Q_{5,6,7(8/24/00)}$ is the “withdrawal” rate from the screens #5, #6, and #7 interval that occurred while pumping screen #4; that is, the leakage from screens #5, #6, and #7 to screen #4 during the August 24 to 31, 2000 test. Dividing equation F-12 by equation F-13 gives

$$\frac{s'_{5,6,7(12/18/01)}}{s'_{5,6,7(8/24/00)}} = \frac{356}{Q_{5,6,7(8/24/00)}} \quad (\text{Eq. F-14})$$

or, using the value for the ratio of 13.77 from equation F-11,

$$Q_{5,6,7(8/24/00)} = \frac{356}{13.77} = 25.8 \text{ L/min or (6.83 gpm)} \quad (\text{Eq. F-15})$$

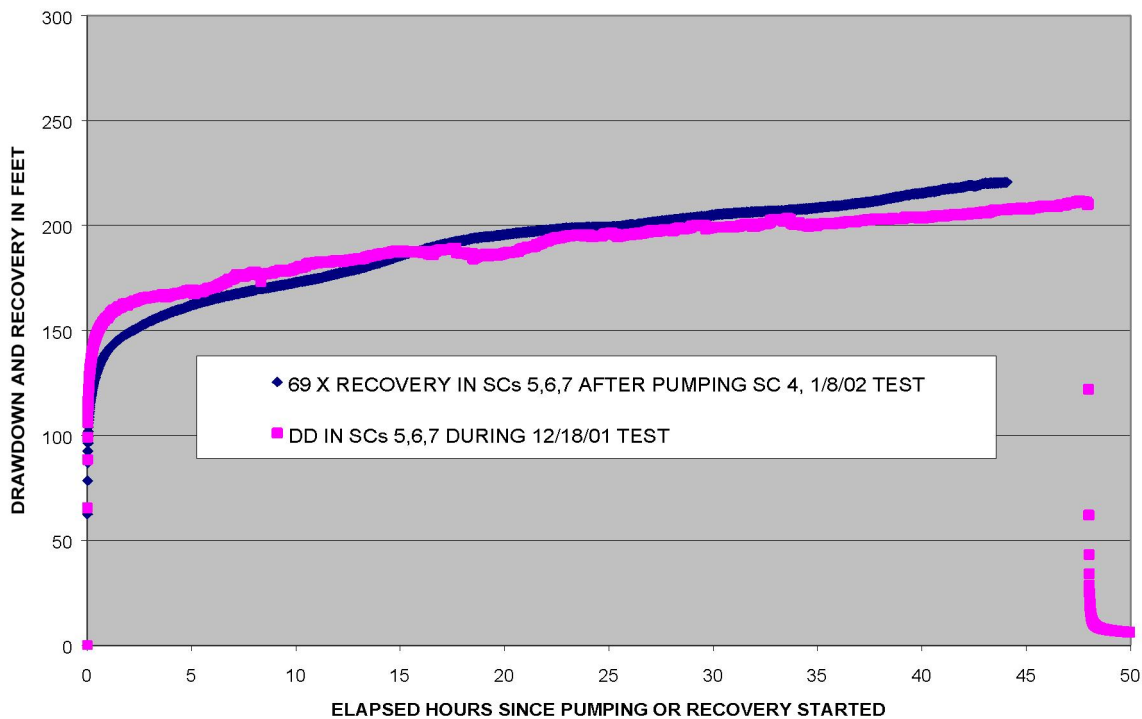
In other words, when screen #4 was pumped at the rate of 299 L/min (79 gpm) during the August 24, 2000, test, 25.8 L/min (6.83 gpm) of the 299 L/min (79 gpm) withdrawn (or 8.65%) actually came from the screens #5, #6, and #7 interval.

The same analysis can be done by comparing the drawdown in the screens #5, #6, and #7 interval when it was pumped in the December 18, 2001 test (Figure F-15) with the recovery in the same interval in response to pumping the screen #4 interval in the January 8, 2002, test (Figure F-18).

Figure F-21 presents the comparison. The responses are very similar with a ratio of 69 in the drawdown values—that is,

$$\frac{s_{5,6,7(12/18/01)}}{s_{5,6,7(1/8/02)}} = 69 \quad (\text{Eq. F-16})$$

These are both drawdowns in the same intervals (i.e., the combined screens #5, #6, and #7) – one in response to direct pumping at 356 L/min (94 gpm) and the other in response to an unknown leakage rate from screens #5, #6, and #7 to screen #4.



Source: DTN: GS020908312316.002 [DIRS 162679] (data).

NOTE: English units are shown in the figure because the analysis was conducted in English units. However, parameter estimates are reported in metric units to downstream users.

Figure F-21. Comparing Drawdown in the Screens #5, #6, and #7 Interval While It Was Pumped During the December 18, 2001 Test with the Recovery in the Same Interval after Cessation of Pumping in Screen #4 during the January 8, 2002 Test

Negligible head losses are assumed in the screens #5, #6, and #7 interval when it was not pumped directly but leaked to the screen #4 interval when the latter was pumped in the January 8, 2002, test—that is,

$$s'_{5,6,7(1/8/02)} = s_{5,6,7(1/8/02)} \quad (\text{Eq. F-17})$$

Assuming that the transmissivity of screens #5, #6, and #7 is the same during the December 18, 2001, and January 8, 2002, tests, the ratio of the two drawdown responses, which is 38.8, should be the same as the ratio of the flow rates that produced them—that is, from equation F-4 (Theis 1935 [DIRS 150327], p. 520, Equation 4),

$$s'_{5,6,7(12/18/01)} = \frac{356}{4\pi T} W(u) \quad (\text{Eq. F-18})$$

which is the same as equation F-12 (Theis 1935 [DIRS 150327], p. 520, Equation 4), and

$$s'_{5,6,7(1/8/02)} = \frac{Q_{5,6,7(1/8/02)}}{4\pi T} W(u) \quad (\text{Eq. F-19})$$

where $Q_{5,6,7(1/8/02)}$ is the “withdrawal” rate from the screens #5, #6, and #7 interval occurring during the pumping of screen #4 (that is, the leakage from screens #5, #6, and #7 to screen #4) during the January 8, 2002, test. Dividing equation F-18 by equation F-19 (Theis 1935 [DIRS 150327], p. 520, Equation 4) gives

$$\frac{s'_{5,6,7(12/18/01)}}{s'_{5,6,7(1/8/02)}} = \frac{356}{Q_{5,6,7(1/8/02)}} \quad (\text{Eq. F-20})$$

Substituting $0.09 s_{5,6,7(12/18/01)}$ for $s'_{5,6,7(12/18/01)}$ from equation F-9, and $s_{5,6,7(1/8/02)}$ for $s'_{5,6,7(1/8/02)}$ from equation F-17, into equation F-20, and then further substituting 69 from equation F-16 for the resulting ratio of $s_{5,6,7(12/18/01)} / s_{5,6,7(1/8/02)}$, results in:

$$Q_{5,6,7(1/8/02)} = 356 / (0.09 \times 69) = 57.3 \text{ L/min (15.14 gpm)} \quad (\text{Eq. F-21})$$

In other words, when screen #4 was pumped at the rate of 254 L/min (67 gpm) during the January 8, 2002 test, 57.3 L/min (15.14 gpm) of the 254 L/min (67 gpm) withdrawn (or 22.6%) actually came from the screens #5, #6, and #7 interval.

The increase in calculated leakage from screens #5, #6, and #7 to screen #4 in the January 8, 2002, test, 22.6%, compared to the calculated leakage in the August 24, 2000, test, 8.65%, is a result of the drop of efficiency of Borehole 19D (at least in screen #4) in the time period between the two tests. When the screen #4 drawdown of the January 8, 2002, test is analyzed by the Neuman (1975 [DIRS 150321] (Neuman.vi V 1.0, STN: 10972-1.0-00 [DIRS 162754]) solution, a transmissivity of 4.4 m²/day (48 ft²/day) is obtained compared with the 28 m²/day (300 ft²/day) obtained by analyzing the August 24, 2000, screen #4 interval test. Both of these transmissivities were estimated without accounting for leakage from screens #5 to #7 to screen #4; if leakage were accounted for, the transmissivities would be somewhat smaller. This result indicates that the 19D (screen #4) well efficiency during the January 8, 2002, test could have been as low as 16% (4.4/28) of the well efficiency during the August 24, 2000, test. Loss of well efficiency causes increased drawdown in the pumped interval, screen #4, which causes an increase in the upward gradient, and resultant leakage, from screens #5, #6, and #7 to screen #4.

Based on the two analyses above that compare the drawdown in the screens #5, #6, and #7 interval when it was directly pumped during the December 18, 2001, test with the drawdown in the screens #5, #6, and #7 interval in response to pumping screen #4 in both the August 24, 2000, and January 8, 2002, tests, it is concluded that up to 23% (upper envelope of 8.65% and 22.6%) of the flow rate may have been a contribution from the screens #5, #6, and #7 interval when pumping screen #4 in 19D (DTNs: GS020708312316.001 [DIRS 162678]; GS020908312316.002 [DIRS 162679]; and Output DTN: GS031008312316.002).

F2. ATC CROSS-HOLE HYDRAULIC TESTING

Two cross-hole hydraulic tests were conducted at the ATC in January 2002. In both tests, borehole 19D was pumped in the open-alluvium section while 19IM1 and 19IM2 were used as monitoring wells. The surface configuration of the three wells is shown in Figure 6.1-7, and Figure 6.1-8 shows the construction/completion of the wells. Cross-hole hydraulic responses in 19IM1 were not analyzed quantitatively for this scientific analysis report because data collection in this well was not conducted in strict accordance with Yucca Mountain Project Quality Assurance procedures.

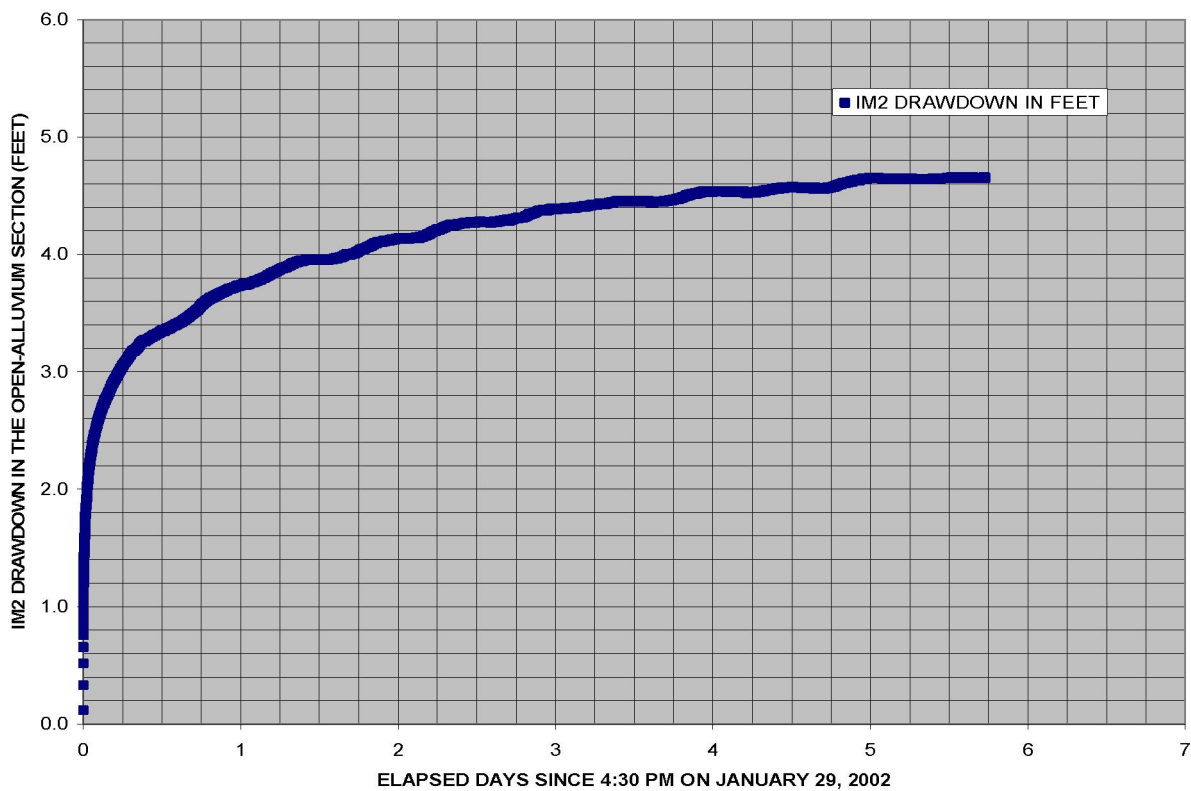
In the first cross-hole hydraulic test, conducted from January 26 to 28, 2002, in 19D, both 19IM1 and 19IM2 were packed off, each isolating four intervals in the alluvium section. In the January 29 to February 4, 2002, test, 19IM1 was packed off while 19IM2 had only one packer inflated isolating the alluvium section from the intervals below it. Only results from the January 29 to February 4, 2002, test are presented in this report because the total transmissivity of the alluvium is less ambiguously obtained in this test than in the earlier test with isolated intervals in the observation wells.

The drawdown in the alluvium section of 19IM2 resulting from pumping the same section in well 19D at 109 gpm from January 29 to February 4, 2002, is presented in Figure F-22. This drawdown exhibits the characteristics of a confined aquifer, and the fit to the type curve of Theis (1935 [DIRS 150327]) (Neuman.vi V 1.0, STN: 10972-1.0-00 [DIRS 162754]) is presented in Figure F-23. The fact that the response at 19IM2 is that of a confined aquifer, whereas the response of single-well testing in 19D conformed to the Neuman (1975 [DIRS 150321]) unconfined response, indicates that there may be a unit causing confinement at 19IM2 that pinches out at 19D. The possibility was considered that the drawdown in 19IM2 was so small relative to the saturated thickness at this observation well (approximately 2%) that the response followed that of a confined aquifer even though the aquifer was unconfined. However, attempts to fit the Neuman (1975 [DIRS 150321]) (Neuman.vi V 1.0, STN: 10972-1.0-00 [DIRS 162754]) unconfined aquifer solution to the drawdown response indicated that the test had been conducted long enough to exhibit the flattening in drawdown at late times that would be expected if the aquifer were unconfined. Because this flattening did not occur, it appears likely that a confining layer influenced the response near 19IM2.

The fit to the Theis (1935 [DIRS 150327]) curve presented in Figure F-23 results in an estimated transmissivity value of 306 m²/day (3,300 ft²/day) (Output DTN: GS031008312316.002) and a storativity of 0.00045 (Output DTN: GS031008312316.002). The transmissivity estimate is approximately an order-of-magnitude higher than the 28 m²/day (300 ft²/day) value obtained from single-well testing in 19D (Section F1.2). This difference is the result of large head losses

in the single-well testing, and the ratio of the single-well to the cross-hole transmissivities is shown in the discussion leading to equation F-7 to be the efficiency of well 19D. The tested interval in 19IM2 from the water table to the bottom of screen #4 is approximately 133 m (437 ft). Therefore, the hydraulic conductivity is $306 \text{ m}^2/\text{day}/133 \text{ m}$ ($3,300 \text{ ft}^2/\text{day}/437 \text{ ft}$), which is approximately 2.3 m/day (7.5 ft/day) (Output DTN: GS031008312316.002).

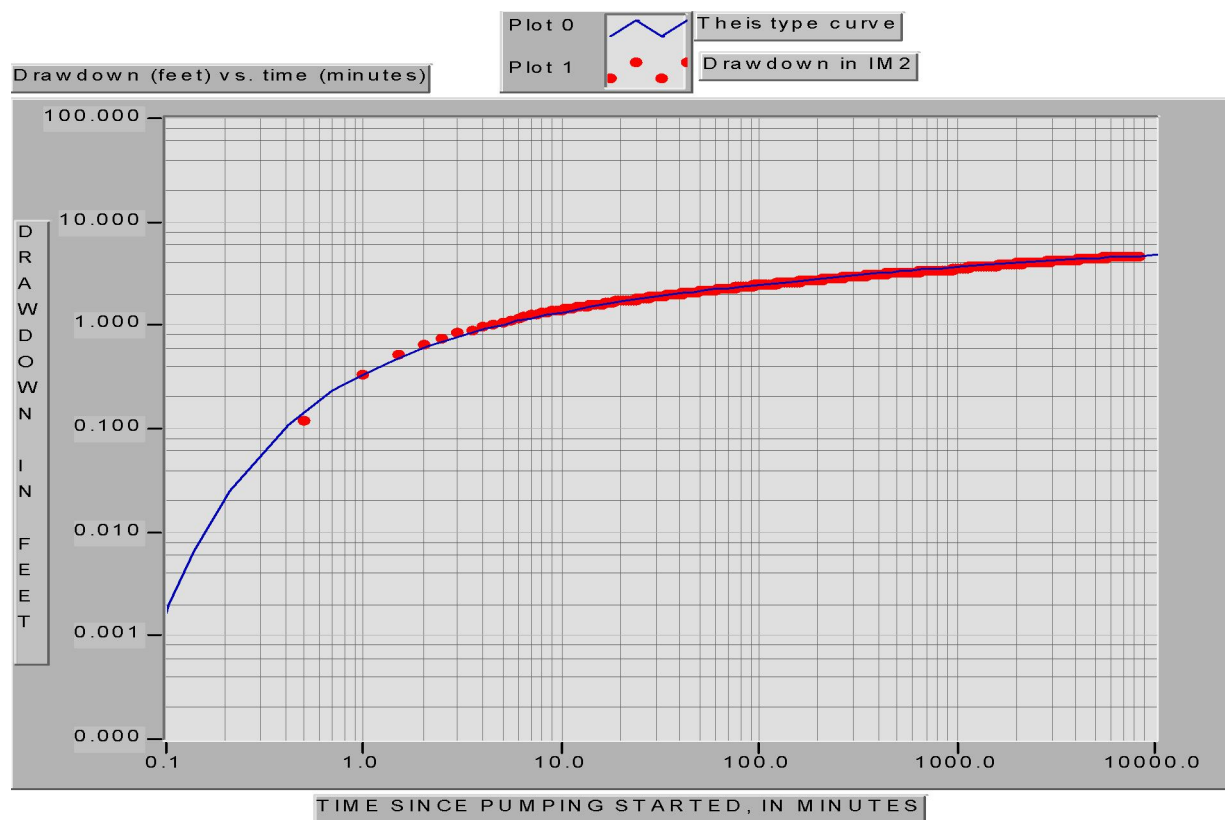
The storativity estimate above allows calculation of the specific storage needed for calculation of total porosity in Section F3. The above storativity estimate of 0.00045 is for the entire open-alluvium thickness at 19IM2, which is 133.1 m (436.6 ft) (depth to bottom of sand at the bottom of screen #4, 242.5 m (795.6 ft), minus depth to water, 109 m (359 ft)). These numbers give a value for the specific storage, S_s , of $0.00045/133.1 \text{ m} = 0.00000338 \text{ m}^{-1}$ ($0.00045/436.6 \text{ ft} = 0.000001031 \text{ ft}^{-1}$) (Output DTN: GS031008312316.002).



Source: DTN: GS020908312316.002 [DIRS 162679] (data).

NOTE: English units are shown in the figure because the analysis was conducted in English units. However, parameter estimates are reported in metric units to downstream users.

Figure F-22. Drawdown in the Open-Alluvium Section of Observation Well NC-EWDP-19IM2 While Pumping NC-EWDP-19D at the Nominal Rate of 109 gpm



Source: DTN: GS020908312316.002 [DIRS 162679] (data).

Output DTN: GS031008312316.002 (analysis).

NOTE: English units are shown in the figure because the analysis was conducted in English units. However, parameter estimates are reported in metric units to downstream users.

Figure F-23. Fit to the Theis Confined-Aquifer Solution of the Drawdown in NC-EWDP-19IM2 Resulting from Pumping NC-EWDP-19D at 109 gpm

F2.1 QUALITATIVE DISCUSSION OF HORIZONTAL ANISOTROPY OF THE HYDRAULIC CONDUCTIVITY

The drawdown pattern at 19IM1 and 19IM2 in response to pumping 19D in both of the above cross-hole tests clearly indicated anisotropy in the horizontal hydraulic conductivity. It showed that the direction of the major principal hydraulic conductivity tensor is oriented in the northeast to southwest direction (Output DTN: GS031008312316.002). With only two observation wells, however, the degree of horizontal anisotropy and its precise orientation cannot be quantified. It should be noted that because the apparent transmissivity between 19D and IM2 was greater than the transmissivity between -19D and 19IM1, the estimate of well efficiency in Section F1.5 would have been greater if the transmissivity between 19D and 19IM1 had been used instead of the transmissivity between 19D and 19IM2.

F3. TOTAL POROSITY ESTIMATED FROM SPECIFIC STORAGE AND BAROMETRIC EFFICIENCY

An estimate of total porosity was obtained by combining the specific storage value from cross-hole testing, namely $S_s = 0.00000338 \text{ m}^{-1}$ ($0.000001031 \text{ ft}^{-1}$) (Section F2), with a value of barometric efficiency, BE , obtained from analyzing background water-level monitoring. Calculation of total porosity is done through use of a relationship derived for a confined aquifer in De Wiest (1965 [DIRS 162674], p. 191, Equation 4.77). This equation is also presented in Geldon et al. (1997 [DIRS 156827], p. 15, Equation 14) and attributed to Jacob. Using the notation of Geldon et al. (1997 [DIRS 156827]) and rearranging terms of his equation, an expression for total porosity, θ , can be written as:

$$\theta = \frac{S_s(BE)}{\gamma\beta} \quad (\text{Eq. F-22})$$

where

γ = the unit weight of water = 1000 kg/m^3 ($0.434 \text{ lb/in}^2/\text{ft}$ [62.496 lb/ft^3]) (Lohman 1972 [DIRS 150250], constants in Equations 20 and 21).

β = the compressibility of water = $4.69 \times 10^{-9} \text{ m}^2/\text{kg}$ ($3.3 \times 10^{-6} \text{ in}^2/\text{lb}$ [$2.29167 \times 10^{-8} \text{ ft}^2/\text{lb}$]) (Lohman 1972 [DIRS 150250], constants in Equations 20 and 21).

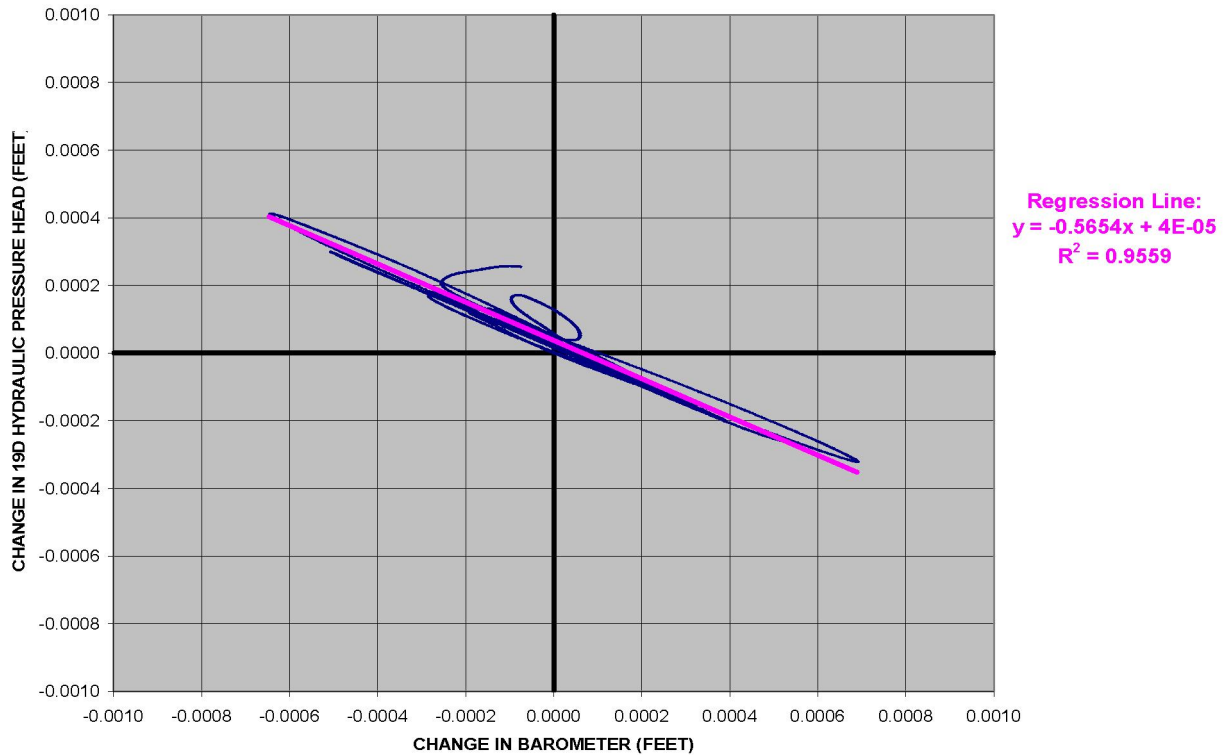
The barometric efficiency, BE , was obtained by analyzing background water-level monitoring conducted between May 1 and July 3, 2002 (DTN: GS020908312316.003 [DIRS 162680]).

The atmospheric pressure is first subtracted from the absolute-pressure transducer values to obtain the hydraulic pressure (represented in equivalent feet of water.) The hydraulic pressure and atmospheric pressure (also represented as equivalent feet of water) records for the period of monitoring (DTN: GS020908312316.003 [DIRS 162680]) are then filtered (Output DTN: GS031008312316.002; Software: Filter.vi V 1.0, STN: 10970-1.0-00 [DIRS 162668]) to remove all oscillations with frequencies higher than 0.8 cycles/day. This step removes the effects of all semidiurnal atmospheric pressure changes and all earth tides on the hydraulic-pressure record. It also removes the semidiurnal atmospheric pressure fluctuations from the atmospheric-pressure record. What remains are the low-frequency atmospheric pressure fluctuations associated with weather systems and the oscillations they cause in the hydraulic pressure record. The changes in the low-frequency hydraulic pressure record is then plotted against the changes in the low-frequency atmospheric pressure record, as shown in Figure F-24.

The slope of the best-fit line through the data in Figure F-24 is -56.54%, indicating that for any incremental change in the atmospheric pressure at the 19D location, a corresponding change in the hydraulic pressure occurs, which is opposite in sign to the atmospheric pressure change and equal to 56.54% of its magnitude. In other words, the barometric efficiency, BE , of the aquifer at the 19D location is 56.54%, or 0.5654 (Output DTN: GS031008312316.002).

Substituting $BE = 0.5654$ from above and $S_s = 0.00000338 \text{ m}^{-1}$ ($0.000001031 \text{ ft}^{-1}$) (from Section F2) into equation F-22 (along with the values for γ and β listed under that equation) gives (Output DTN: GS031008312316.002):

$$\theta = \frac{(0.00000338 \text{ m}^{-1})(0.5654)}{(1000 \text{ kg/m}^3)(4.69 \times 10^{-9} \text{ m}^2/\text{kg})} = 0.407 = 40.7\% \quad (\text{Eq. F-23})$$



Source: DTN: GS020908312316.003 [DIRS 162680] (data).

Output DTN: GS031008312316.002 (analysis).

NOTE: English units are shown in the figure because the analysis was conducted in English units. However, parameter estimates are reported in metric units to downstream users.

Figure F-24. Relation of Low-Frequency Hydraulic-Pressure Change in NC-EWDP-19D to Low-Frequency Atmospheric-Pressure Change at the NC-EWDP-19D Location: Data and Regression Line

The largest total porosity value obtained from grain-size distributions in well 19D is 0.33, occurring at the 152- to 154-m (500- to 505-ft) depth interval (DTN: LA0201JS831421.001 [DIRS 162613], Output DTN: GS031008312316.002). The largest total porosity value obtained from the Borehole Gravity Meter survey done in NC-EWDP-19D, presented in Section F4, is 0.29, occurring at approximately 198 m (650 ft) of depth. The above values would indicate that the upper limit for total porosity in the alluvium at the 19D location ranges from 29% to approximately 40%. (The total porosity from grain-size distribution is obtained through the relation, $\text{Porosity} = 0.255(1 + 0.83^C)$, where C , the coefficient of uniformity, is the ratio of the 60th grain-size percentile to the 10th percentile.) (Kasenow 2002 [DIRS 164666], p. 72).

There are many assumptions involved in the derivation of equation F-22 (De Wiest 1965 [DIRS 162674], pp. 189 to 191). Uncertainties in the estimate of total porosity using this equation depend primarily on the extent to which these assumptions hold true in the saturated alluvium. Unfortunately, the data and information necessary to evaluate the validity of these assumptions were not available. Barometric efficiency was believed to be determined quite accurately from the large number of barometer and water-level measurements, and the storativity estimate obtained from cross-hole hydraulic testing at the ATC is considered less uncertain than the assumptions inherent in equation F-22. A formal analysis of uncertainty in the porosity estimate was not conducted.

F4. TOTAL POROSITY ESTIMATED FROM BOREHOLE GRAVIMETRY AT NC-EWDP-19D

Standard suites of geophysical logs were conducted during and after completion of all wells at the ATC. In addition, borehole gravimetry (BHGM) logging of 19D was conducted by EDCON, Inc. in September 2000 (DTN: MO0105GPLOG19D.000 [DIRS 163480]). BHGM logs provide bulk density as a function of depth, from which total porosity as a function of depth can be estimated if grain density is known or assumed. The total porosities deduced from BHGM logging are reported here because they serve as useful upper bounds for effective flow porosity in the alluvium. These estimates can be compared with the estimates of flow porosity obtained from analysis of single-well tracer tests in the alluvium, which are presented in Section G4. Other estimates of total porosity in the alluvium, obtained from specific storage and barometric efficiency and from grain size distributions, are discussed in Section F3.

For a water-saturated sample of alluvium, the mass of solids plus the mass of water is equal to the total mass of the sample, i.e.:

$$V_s \rho_s + V_v \rho_w = \rho_b V_T \quad (\text{Eq. F-24})$$

where

V_s = volume of solids

ρ_s = density of solids (grain density)

V_v = volume of voids (filled with water for a saturated medium)

ρ_w = density of water, ρ_b is the saturated (wet) bulk density of the sample

V_T = total volume of the sample.

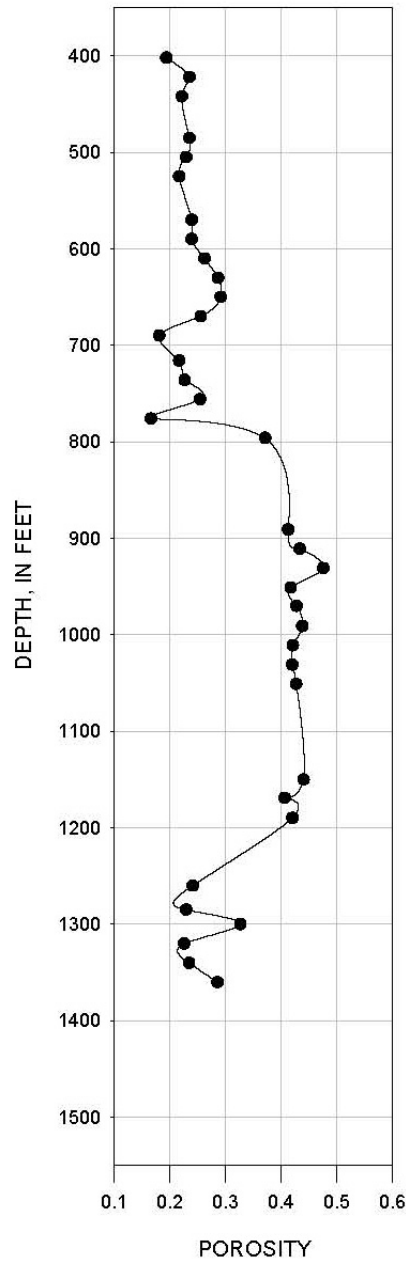
By algebraic manipulation, the porosity, ϕ , which is defined as V_v/V_T , can be obtained from equation F-24 as:

$$\phi = V_v/V_T = (\rho_s - \rho_b)/(\rho_s - \rho_w) \quad (\text{Eq. F-25})$$

Using equation F-25 with $\rho_s = 2.52 \text{ g/cm}^3$ (USGS n.d. [DIRS 154495]) and $\rho_w \cong 1.0 \text{ g/cm}^3$ (ranges from 0.9986 g/cm^3 at 18°C to 0.9959 g/cm^3 at 29°C ; (Dean 1992 [DIRS 100722], p. 5.87)), one can calculate ϕ from various values of ρ_b . For the minimum ρ_b of 2.082 g/cm^3 and the maximum ρ_b of 2.244 g/cm^3 in the alluvium section at 19D (DTN: MO0105GPLOG19D.000

[DIRS 163480]), a maximum porosity of 0.29 and a minimum porosity of 0.18 (Output DTN: GS031008312316.003) are obtained from equation F-25.

Using the entire set of bulk densities for the entire section of 19D logged by the BHGM (DTN: MO0105GPLOG19D.000 [DIRS 163480]) for ρ_b in equation F-25 and the values of ρ_s and ρ_w , given above, total porosities as a function of depth are obtained as shown in Figure F-25.



Source: DTN: MO0105GPLOG19D.000 [DIRS 163480].

Output DTN: GS031008312316.003.

NOTE: The figure is plotted in English units because the data were obtained in those units. However, parameter estimates are reported in metric units to downstream users.

Figure F-25. Total Porosities as a Function of Depth below Land Surface at NC-EWDP-19D, Obtained from the Borehole Gravity Meter (BHGM) Survey Conducted in September 2000

F5. SUMMARY OF HYDROLOGIC PARAMETERS IN ALLUVIUM FROM HYDRAULIC TESTING AT THE ATC

The single-hole testing indicated an overall transmissivity for the alluvium of 28 m²/day (300 ft²/day) with an associated hydraulic conductivity of 0.20 m/day (0.67 ft/day) (Output DTN: GS031008312316.002). This is a horizontal hydraulic conductivity value with no directional dependence. The transmissivity and hydraulic conductivity estimates were also estimated without assuming any near-wellbore head losses, which apparently were very significant, possibly because of the narrow slots in the well screens and the relatively small particle size of the sand packs in 19D, among other reasons (well efficiency is determined to be 9.1% [Output DTN: GS031008312316.002]; see Section F1.4, Equation F-7). Thus, the true transmissivity and hydraulic conductivity are believed to be approximately an order-of-magnitude higher than the single-hole *apparent* values.

Vertical hydraulic conductivities could not be estimated from the single-well testing, although they were presumably small, because none of the intervals above or below the isolated intervals in the hydraulic tests showed any pressure response during pumping (with the exception of interval #5 in the tuffs, which responded slightly to pumping interval #4). Also, there was minimal response in 19P when pumping any of the intervals in 19D except for screen #1 and the combined-interval test.

Estimates of transmissivity and horizontal hydraulic conductivity were greatly improved after cross-hole hydraulic testing was conducted at the 19D location (Section F2). The cross-hole tests indicated a transmissivity of 306 m²/day (3,300 ft²/day) (hydraulic conductivity of 2.0 m/day [6.7 ft/day]), which is about an order of magnitude higher than the transmissivity and hydraulic conductivity values obtained from single-well hydraulic tests. Because of well losses in 19D (well efficiency of 9.1%), the cross-hole transmissivity value of 306 m²/day (3,300 ft²/day) is considered to be much more representative of the saturated alluvium in the vicinity of 19D than the single-well transmissivity values of approximately 28 m²/day (approximately 300 ft²/day). The cross-hole tests also provided storativity estimates as well as qualitative information on horizontal anisotropy of hydraulic conductivity in the saturated alluvium.

F.6 RESULTS AND ANALYSES OF THE HYDRAULIC TEST DATA AT NYE COUNTY SITE 22

F6.1 INTRODUCTION

This section documents the analysis of the pumping tests at the Nye County Site 22 complex located just east of Fortymile Wash approximately 5 miles north-north-west of Amargosa Valley and about 3 miles northeast of the ATC site (see Figure 6.1-6; Amargosa Valley is labeled "Lathrop Wells" in this figure). Five pumping tests were conducted at this site, and the data from all five tests were analyzed to produce estimates of transmissivity and storativity of the different intervals of the alluvium and underlying volcanic breccia, as well as the leakage parameters between these intervals. The estimated transmissivity and leakage parameter values were used to calculate horizontal and vertical hydraulic conductivities within the different

intervals of the alluvium and volcanic breccia. The average horizontal and vertical hydraulic conductivity of the alluvium at this location was also estimated.

The site consists of 4 wells: NC-EWDP-22S, NC-EWDP-22PA, NC-EWDP-22PB, and NC-EWDP-22PC, although only the first three wells were used in hydraulic testing because 22PC was not drilled until after the hydraulic tests were completed. Figure 6.1-8 shows the layout of the Site 22 complex, and Figure 6.1-10 shows the well completions and stratigraphy at the site. The site was established as a part of Phase III of the Nye County Early Warning Drilling Program (EWDP).

Well NC-EWDP-22S, referred to as well 22S in this appendix, was drilled in October 2001 to a total depth of 364.7 m and is completed with four screened intervals. Each screen is sand packed. The data on the screen and sand pack depths and heights is summarized in Table F-1. The first three screens from the land surface screens are completed within the alluvium or valley-fill deposits consisting of silty sand with gravel. The fourth (and deepest) screen is located in a volcanic breccia (or conglomerate). The lithologic data for the well 22S location are from the well NC-EWDP-22SA, which is an abandoned borehole located immediately next to 22S. The lithostratigraphy data for the well 22SA are from DTN: GS030108314211.001 [DIRS 163483]. The lithologic logs provide no evidence for considering the intervals between the screens as confining units. In contrast to the ATC, where a significant upward vertical pressure gradient exists, water level data from the different zones at site 22 indicate essentially no vertical pressure gradient (DTN: MO0411NYE06360.302 [DIRS 177373]). This result suggests that the screened intervals are hydraulically well connected (Questa Engineering Corporation 2003 [DIRS 178565]). As will be discussed in detail later, the adjacent intervals demonstrated fast response when only one interval was pumped, providing additional support to the good hydraulic connection concept. Based on the lithologic data in the adjacent Nye County wells 24P, 29P, 23P, and 10SA (DTNs: GS040908314211.001 [DIRS 174114] and GS030108314211.001 [DIRS 163483]), the alluvium deposits extend several kilometers from the 22 Site. This suggests that no boundary effects would be observed in the short duration pumping tests performed at the site.

Well NC-EWDP-22PA, referred to as well 22PA in this appendix, was drilled in January 2002 to a total depth of 237.7 m and is completed with two screened intervals. The data on the screen and sand pack depths and heights is summarized in Table F-1. These two screens correspond to the first and second screened intervals in well 22S.

Well NC-EWDP-22PB, referred to as well 22PB in this appendix, was drilled in February 2002 to a total depth of 365.7 m and is completed with two screened intervals. The data on the screen and sand pack depths and heights is summarized in Table F-1. These two screens correspond to the third and fourth screened intervals in well 22S.

Five pumping tests were conducted from well NC-EWP-22S in 2002 and 2003. Wells 22 PA and 22PB served as observation wells during these tests. The field data consists of pressures and temperatures in each zone of all 3 wells as a function of time as well as pumping rates during the tests. Pressure and temperature data were collected before each pumping test to characterize the background conditions, during the pumping test, and following the pumping test (recovery period).

Table F-1. Zones and Screen Depths in Site 22 Wells

Well Name	Well Zone	Sand Pack Depth Interval, m bgs	Sand Pack Height, m	Screen Top to Bottom Depth, m bgs	Screen Height, m
22S	1	156.5-178.7	22.2	159.0-177.2	18.2
	2	198.7-233.6	35.0	201.5-231.8	30.2
	3	265.3-300.8	35.5	268.3-298.7	30.4
	4	345.4-364.7	19.3	347.5-359.7	12.2
22PA	1	155.1-178.9	23.9	158.7-176.7	18.0
	2	198.0-237.7	39.7	201.6-231.6	30.0
22PB	3	265.4-301.5	36.1	268.6-298.6	30.0
	4	343.0-365.7	22.7	347.6-359.6	12.0

Source: DTN: LA0705PR150304.007 [DIRS 181202].

The first pumping test was conducted in March of 2002. All four zones in well 22S were simultaneously pumped in this test. The test was preceded by spinner tests and background observations. The test began on March 19, 2002. It was interrupted once for about 1 hour after 19 hours of pumping due to a pump shut down and was resumed for another 5 hours after that. Recovery was observed for about 15 hours. The pumping rate was apportioned to the four screened intervals in 22S in accordance with the spinner test results (see Table F-2). The MOSDAX™ pressure sensor readings recorded during this test are available from DTN: LA0705PR150304.008 [DIRS 181203].

The data in DTN LA0705PR150304.008 [DIRS 181203] are unqualified. The data qualification is described in Appendix N. The data are qualified for use in this analysis only. The pumping test interpretation was conducted for the Nye County Department of Natural Resources and Federal Facilities Nuclear Waste Repository Project Office under Grant # DE-FC28-02RW12163 by Questa Engineering Corporation. The field data, analyses, and interpretation are documented in *Preliminary Analysis of Pump-Spinner Tests and Pump Test in Well NC-EWDP-22S, Near Yucca Mountain, Nevada* (Questa Engineering Corporation 2003 [DIRS 178565]).

The 4 subsequent pumping tests were conducted in August to September of 2003. Only one zone in the well 22S was pumped in each test. Each test was preceded by background observations. The pumping was conducted for about 11 hours and was followed by observation of the recovery. The MOSDAX™ pressure sensor readings recorded during these tests are available from DTNs: LA0705PR150304.009 [DIRS 181204], LA0705PR150304.010 [DIRS 181205], LA0705PR150304.011 [DIRS 181207], and LA0705PR150304.012 [DIRS 181208]. The data in these DTNs are unqualified. The data qualification is described in Appendix N. These data are qualified for use in this analysis only.

The pumping test interpretation was conducted for the Nye County Department of Natural Resources and Federal Facilities Nuclear Waste Repository Project Office under Grant # DE-FC28-02RW12163 by Questa Engineering Corporation. The field data, analyses, and interpretation are documented in *Analysis of Aquifer Pump Tests in Individual Well Zones at Site 22 Near Yucca Mountain, Nevada* (Questa Engineering Corporation 2004 [DIRS 178566]). The first pumping test in the series of isolated interval tests began on August 5, 2003, with Zone 1 in 22 S pumped at the rate of 43.5 gpm. The second test began on August 12, 2003, with Zone 2 in

22 S pumped at the rate of 44.1 gpm. The third test began on September 9, 2003 with Zone 3 in 22 S pumped at the rate of 27.1 gpm, and the last test began on September 23 of 2003 with Zone 4 in 22 S pumped at the rate of 20.5.gpm.

Table F-2. Summary of the Pumping Test Duration and Rates

Test Date	Pumping Period Duration (hrs)	Recovery Period Duration (hrs)	Pumping Rate in m ³ /day (gpm)			
			Zone 1	Zone 2	Zone 3	Zone 4
03-19-02 8:40:00 AM	19.33*	–	240.39 (44)	288.90 (53)	125.37 (23)	70.86 (13)
08-05-03 5:24:00 AM	11.06	45.42	237.12 (43.5)	–	–	–
08-12-03 5:21:20 AM	11.14	37.47	–	240.39 (44.1)	–	–
09-09-03 5:48:50 AM	10.73	14.62	–	–	147.72 (27.1)	–
09-23-03 5:36:30 AM	10.86	15.13	–	–	–	111.75 (20.5)

Output DTN LA0701EK150304.001

NOTE: *The pump was shut down for an hour after 19.33 hrs of pumping and the pumping period data after the pumping was resumed were not used as well as the recovery period data.

The analysis presented in this section is based on the same input data (pressure readings, pumping rates, and well information) as the analyses presented in *Preliminary Analysis of Pump-Spinner Tests and Pump Test in Well NC-EWDP-22S, Near Yucca Mountain, Nevada* (Questa Engineering Corporation 2003 [DIRS 178565]) and in *Analysis of Aquifer Pump Tests in Individual Well Zones at Site 22 Near Yucca Mountain, Nevada* (Questa Engineering Corporation 2004 [DIRS 178566]). However, the processing of the input data was conducted independently and the data interpretation methods are different, as will be discussed below. The results obtained in this analysis are compared to the results obtained in *Preliminary Analysis of Pump-Spinner Tests and Pump Test in Well NC-EWDP-22S, Near Yucca Mountain, Nevada* (Questa Engineering Corporation 2003 [DIRS 178565]) and in *Analysis of Aquifer Pump Tests in Individual Well Zones at Site 22 Near Yucca Mountain, Nevada* (Questa Engineering Corporation 2004 [DIRS 178566]) below as appropriate.

F6.2 INPUT DATA AND INITIAL DATA PROCESSING

As discussed above, the input data were taken from the input DTNs: LA0705PR150304.008 [DIRS 181203], LA0705PR150304.009 [DIRS 181204], LA0705PR150304.010 [DIRS 181205], LA0705PR150304.011 [DIRS 181207], and LA0705PR150304.012 [DIRS 181208]. The data in the DTNs consist of a number of files generated by the MOSDAX data acquisition system. Each file has a header with the test identification information and a description of probes and actual readings consisting of the date and time of reading and the pressures and temperatures measured at the corresponding probes. The data are divided into a few time periods. Two sets of data are provided for each time period. The data in the first set (pressures and temperatures) are for well 22S and zone 1 in well 22PA. This set will be referred to as Set 1. The data in the second set (pressures and temperatures) are for well 22PA zone 2 and well 22PB zone 3 and zone 4. This

set will be referred to as Set 2. Not all the times of measurement are the same in these 2 sets. The atmospheric pressure and temperature were recorded in both sets.

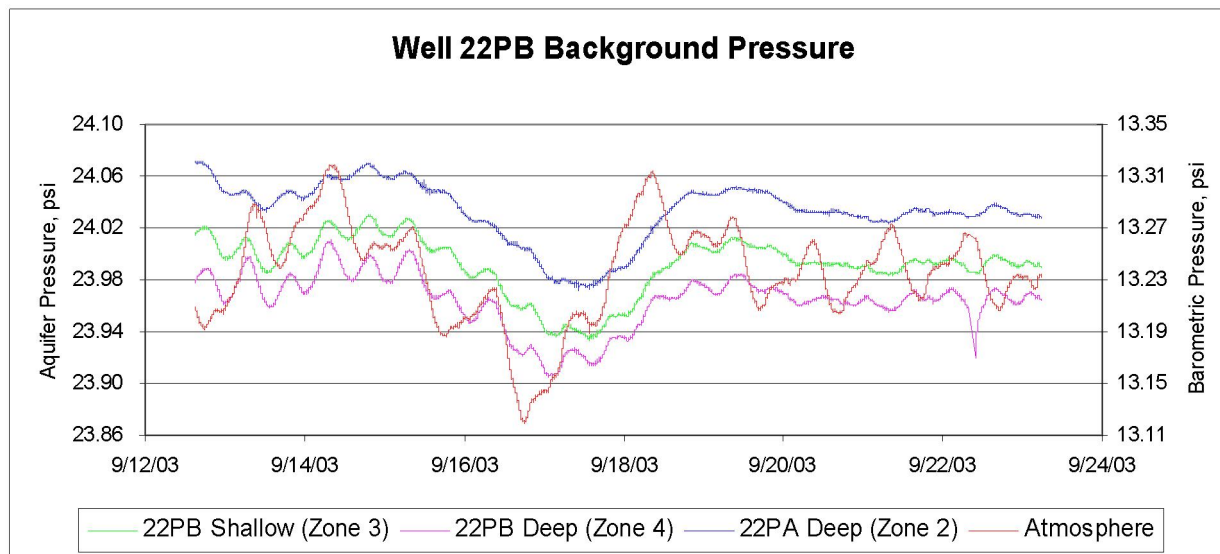
The initial data processing consisted of combining all the data related to one pumping test in one Excel file. The Excel file contains all the original files recorded for a pumping test in a form of a separate worksheet. The name of the worksheet is the same as the name of the original file in the input DTNs. The data from these worksheets are then combined by sets. The *Set 1 Background* and *Set 2 Background* worksheets contain all the data for the corresponding set recorded prior to the beginning of the pumping test and represent the background conditions. These worksheets were not generated for the case when all 4 zones were pumped. The *Set 1 Pumping* and *Set 2 Pumping* worksheets contain all the data for the corresponding set recorded shortly before the beginning of the pumping test and the data recorded during the pumping test and the recovery period. A separate Excel file, *2003 Background Data.xls*, was created to combine all the background data available for the 3 pumping tests (zone 2, zone 3, and zone 4 pumping tests) conducted in August to September of 2003.

The preliminary data analysis consisted of a few steps. First, the background data were analyzed. Then the pressure data collected during the pumping test and recovery were converted to the equivalent piezometric elevations expressed as drawdown. The background pressure and temperature data and pumping/recovery drawdown data were analyzed to develop adequate conceptual models to be used in the data interpretation.

F6.3 BACKGROUND DATA ANALYSIS

The Set 2 atmospheric and aquifer pressure data collected before each pumping test conducted in 2003 are shown in the Figure F-26. The data in this figure are for the period of time before the pumping test in zone 4. The other background data express the same behavior. The Set 1 data for the corresponding periods have large data gaps and are not shown. However all the available background data are used in the correlation analysis described below.

Visual analysis of the background pressure data indicates that the pressures in all 4 zones behave in a very similar fashion, except zone 4 pressures demonstrate slightly more fluctuation than the other zones (Figure F-26). There is a time lag of 9 hrs to 12 hrs between the atmospheric pressure and aquifer pressures, which is consistent with diurnal (twice daily) cycling manifested as a tendency to see high aquifer pressures when atmospheric pressures hit diurnal lows and low aquifer pressures when atmospheric pressures hit diurnal highs. There is no visually identifiable time lag between the pressures in the different zones. The aquifer pressure responses are attenuated by about 3 times relative to the atmospheric pressure fluctuations. Similar conclusions are reached in *Analysis of Aquifer Pump Tests in Individual Well Zones at Site 22 Near Yucca Mountain, Nevada* (Questa Engineering Corporation 2004 [DIRS 178566]). The behavior of the aquifer pressures and temperatures suggests a very good connection between all four zones.



Output DTN: LA0701EK150304.001.

NOTE: The pressures in zone 3 shown in the figure are the actual (measured) pressures in psi minus 0.70 psi. This allows for showing all the pressures in the same plot using the same relative scale as for the barometric pressure. Zone 1, not shown, exhibited similar behavior to the other zones.

Figure F-26. Background Pressures Prior to Zone 4 Pumping

The correlation analysis was performed using all the background pressure data collected in the 2003 series of pumping tests. As discussed above, the Set 2 data includes zone 2, zone 3, and zone 4 in the 22PA and 22PB monitoring wells. The results of the correlation analysis are provided in output DTN: LA0701EK150304.001, *2003 Background Data.xls*. Set 1 is less complete and has many gaps. Also, the Set 1 pressure transducers had a much larger dynamic range than the Set 2 transducers (250 psi vs. 30 psi), which resulted in much lower measurement precision for the Set 1 transducers. Whereas Set 2 transducers could record pressures in increments of less than 0.001 psi, the Set 1 transducers could only record in increments of about 0.0075 psi (about 8 times less precision). Thus, there was inherently lower measurement precision in zone 1 of 22PA and zones 1, 2, 3, and 4 in 22S than in the other observation well zones.

The built-in Excel functions *CORREL*, *INTERCEPT*, and *SLOPE* were used in the correlation analysis. The correlation coefficients between the different zones are summarized in Table F-3. There is a very good correlation among all the zones, as expected based on the visual analysis of the data. Figure F-27 shows the results of correlation analyses between zones 2 and 3 and between zones 2 and 4. The correlation between aquifer pressures and atmospheric pressures is only 0.56 when no time lag is applied to the aquifer data. Similar conclusions were reached in *Analysis of Aquifer Pump Tests in Individual Well Zones at Site 22 Near Yucca Mountain, Nevada* (Questa Engineering Company 2004 [DIRS 178566], Section 2.6).

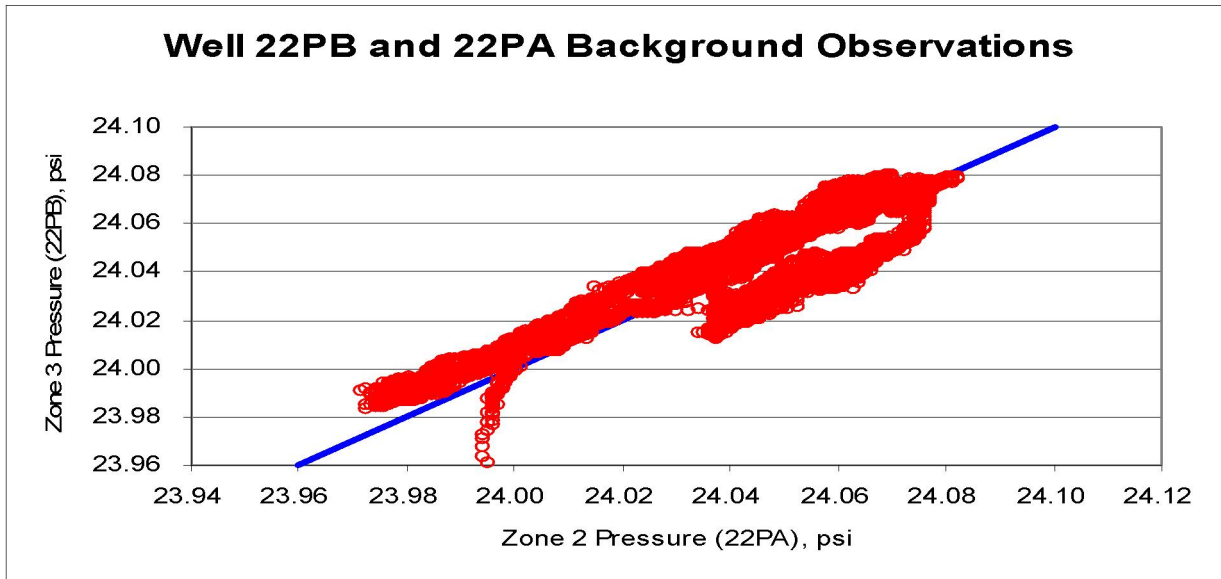
Table F-3. Results of the Correlation and Linear Regression Analysis Using Background Pressures in the Different Aquifer Zones

Estimated Parameters	Pressures (Zones 2 and 3)		Pressures (Zones 2 and 4)		Pressures (Zones 3 and 4)	
Correlation coefficient	0.89		0.93		0.95	
Linear Regression Parameters	$p_2 = a \cdot p_3 + c$	$p_3 = a \cdot p_2 + c$	$p_2 = a \cdot p_4 + c$	$p_4 = a \cdot p_3 + c$	$p_3 = a \cdot p_4 + c$	$p_4 = a \cdot p_3 + c$
Slope	1	1	1.052	0.83	0.99	0.80
Intercept	0	0	-1.166	4.017	0.27	4.805

Output DTN: LA0701EK150304.001.

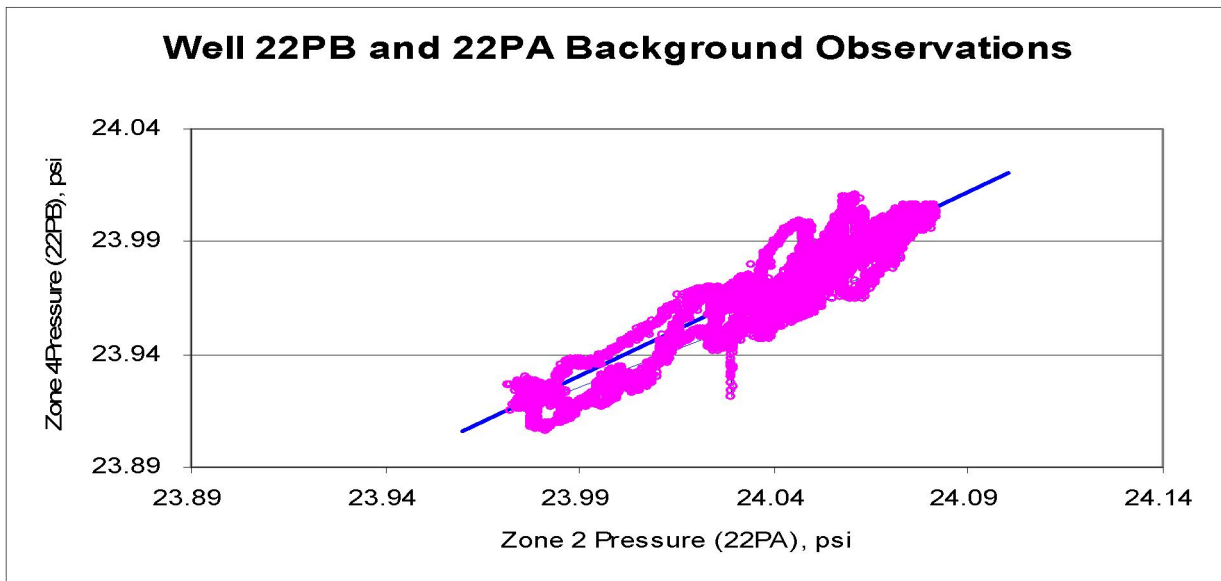
NOTE: p_2 , p_3 , and p_4 are the background pressure in zone 2, 3, and 4 correspondingly.

(a) Correlation Between Zone 2 and Zone 3 Pressures



Legend: Red circles represent the pressure data and blue solid line is the linear regression line.

(b) Correlation between Zone 2 and Zone 4 Pressures



Legend: Purple circles represent the pressure data and blue solid line is the linear regression line.

Output DTN: LA0701EK150304.001.

Figure F-27. Correlation between the Pressures in Different Zones

Because of the very good correlation between the pressures in the different aquifer zones and the low correlation between the atmospheric and aquifer pressures (when not accounting for the time lag), it was concluded that it was justified to use the linear regression relationships between aquifer zones to account for ambient aquifer pressure changes that are superimposed on responses to pumping (or recovery). If such correction is required, the pressure changes since

the beginning of a pumping test in a zone unaffected by pumping should be subtracted from the pressure changes in the affected zones in the case of zones 1, 2, and 3. In case of zone 4 the changes in an unaffected zone 1, 2, or 3 should be multiplied by 0.83 before being subtracted. If zone 4 data are used to correct zone 1, 2, or 3 data, then the changes in zone 4 pressures should be multiplied by 1.05 before being subtracted. Similar conclusions were reached in *Analysis of Aquifer Pump Tests in Individual Well Zones at Site 22 Near Yucca Mountain, Nevada* (Questa Engineering Corporation 2004 [DIRS 178566]), where the factor for correcting zone 4 pressures using zone 3 data was 0.7, and the factor for correcting zone 3 pressures using zone 4 data was 1.4. Another alternative would be using specially designed software allowing for correcting the aquifer pressure using barometric pressure and adjustable time lag. However, there is no qualified software that can perform these functions.

F6.4 PUMPING TEST DATA ANALYSIS

During the pumping tests from zones 2, 3, and 4, the probes corresponding to Set 2 were not synchronized with the probes corresponding to Set 1. This lack of synchronization is described in *Analysis of Aquifer Pump Tests in Individual Well Zones at Site 22 Near Yucca Mountain, Nevada* (Questa Engineering Corporation 2004 [DIRS 178566]) and is obvious from the pressure data analysis. The information provided in *Preliminary Analysis of Pump-Spinner Tests and Pump Test in Well NC-EWDP-22S, Near Yucca Mountain, Nevada* (Questa Engineering Corporation 2003 [DIRS 178565]) and *Analysis of Aquifer Pump Tests in Individual Well Zones at Site 22 Near Yucca Mountain, Nevada* (Questa Engineering Corporation 2004 [DIRS 178566]), as well as the analysis of pressure changes in well 22S, were used to identify the beginning of the pumping and recovery periods for each Set in each test. The time lag between Sets was the smallest in the zone 2 pumping test (up to 60 sec) and the greatest in zone 4 pumping test (up to 280 sec). The dates and times corresponding to the beginning of the pumping and recovery periods are summarized in Table F-2 for all 5 pumping tests based on the data in Set 1. The time lags between the data in Set 1 and the data in Set 2 are: 30 sec, 130 sec, and 230 sec. The corresponding time lags in *Analysis of Aquifer Pump Tests in Individual Well Zones at Site 22 Near Yucca Mountain, Nevada* (Questa Engineering Corporation 2004 [DIRS 178566]) are: 30 sec, 130 sec, and 240 sec. The time lag was selected based on the best fit between the time-drawdown curves obtained during both pumping and recovery.

Once the beginning of a pumping test was identified in each set, it was assigned relative time equal to 0. The drawdowns in all zones were assigned 0 at this point in time. The drawdowns at any given time were calculated as the difference between the pressure at that time and the pressure at the beginning of pumping converted to the equivalent water head units. The same conversion factor as in *Analysis of Aquifer Pump Tests in Individual Well Zones at Site 22 Near Yucca Mountain, Nevada* (Questa Engineering Corporation 2004 [DIRS 178566]), equal to 0.43275 psi/ft, was used to convert pressures in psi to the equivalent water head in feet. This conversion factor is based on the nominal water density of 998.203 kg/m³ at 20°C (Fetter 2001 [DIRS 156668], Appendix 14). The temperature of ground water in the monitoring wells ranged from 24°C to 28°C. The maximum change in pressure during the pumping tests was about 1 psi. Based on a water density of 996.232 kg/m³ at 28°C, the difference between the maximum drawdown at 28°C and at 20°C is 0.0046 ft, which is less than the transducer resolution of 0.01 ft (Questa Engineering Corporation 2004 [DIRS 178566]). Thus, the use of the water density at 20°C to convert from pressure in psi to head in feet does not introduce significant errors. The

equivalent water heads were then converted to metric units. The same calculations were performed for the recovery periods, except the drawdowns were assigned the opposite sign. As a result, the pumping and recovery data can be shown on the same plot. The recovery data were not used in the case when all 4 zones were pumped since the recovery was affected by the pump shutdown during the pumping period.

Only the drawdowns in the monitoring wells were used in the hydraulic parameter estimation presented below. It was shown in *Preliminary Analysis of Pump-Spinner Tests and Pump Test in Well NC-EWDP-22S, Near Yucca Mountain, Nevada* (Questa Engineering Corporation 2003 [DIRS 178565]) and *Analysis of Aquifer Pump Tests in Individual Well Zones at Site 22 Near Yucca Mountain, Nevada* (Questa Engineering Corporation 2004 [DIRS 178566]) that the pumping well efficiency is very low (15% to 30%) and changes from one test to another. Under these conditions, using drawdowns in the pumping well (well 22S) for test interpretation is meaningless. The pumping well drawdowns were used to estimate well efficiency only.

The input data to this analysis are in output DTN: LA0701EK150304.001, *Zone 1.xls*, *Zone 2.xls*, *Zone 3.xls*, *Zone 4.xls*, and *All Zones.xls*.

F6.5 DATA ANALYSIS

Before discussing the data interpretations, it is important to discuss that there are two alternative conceptualizations of the flow system that are both consistent with the interpretative approach. These two conceptualizations are illustrated schematically in Figures F-28(a) and F-28(b), with the differences being highlighted in Figure F-28(c). The first conceptualization is called the multiple-aquifer conceptual model, in which it is assumed that each screened interval at Site 22 (defined by the top and bottom of the sand packs associated with each well screen) is completed within a separate aquifer that has the same thickness as the screened interval. These aquifers are assumed to be separated by intervening layers of less permeable material that provide some degree of confinement and have thicknesses defined by the distances between the bottom of one sand pack (or the water table in the case of the shallowest layer) to the top of the next sand pack down (or the bottom of the well in the case of the deepest layer). Thus, all material in the same depth range as a screened interval is considered an aquifer, and all material not within the depth range of a screened interval is considered a (semi-)confining layer. In the second conceptualization (Figure 28(b)), called the multiple-layer model, the system is assumed to consist of four aquifers that have no intervening layers that provide significant confinement. The boundaries between the aquifers are either the midpoints between the screened intervals, or, in the case of the bottom two aquifers, the interface between the alluvium and the volcanic breccia. In this conceptualization, any apparent confinement between screened intervals is interpreted as a low vertical hydraulic conductivity within the horizontally-oriented layers.

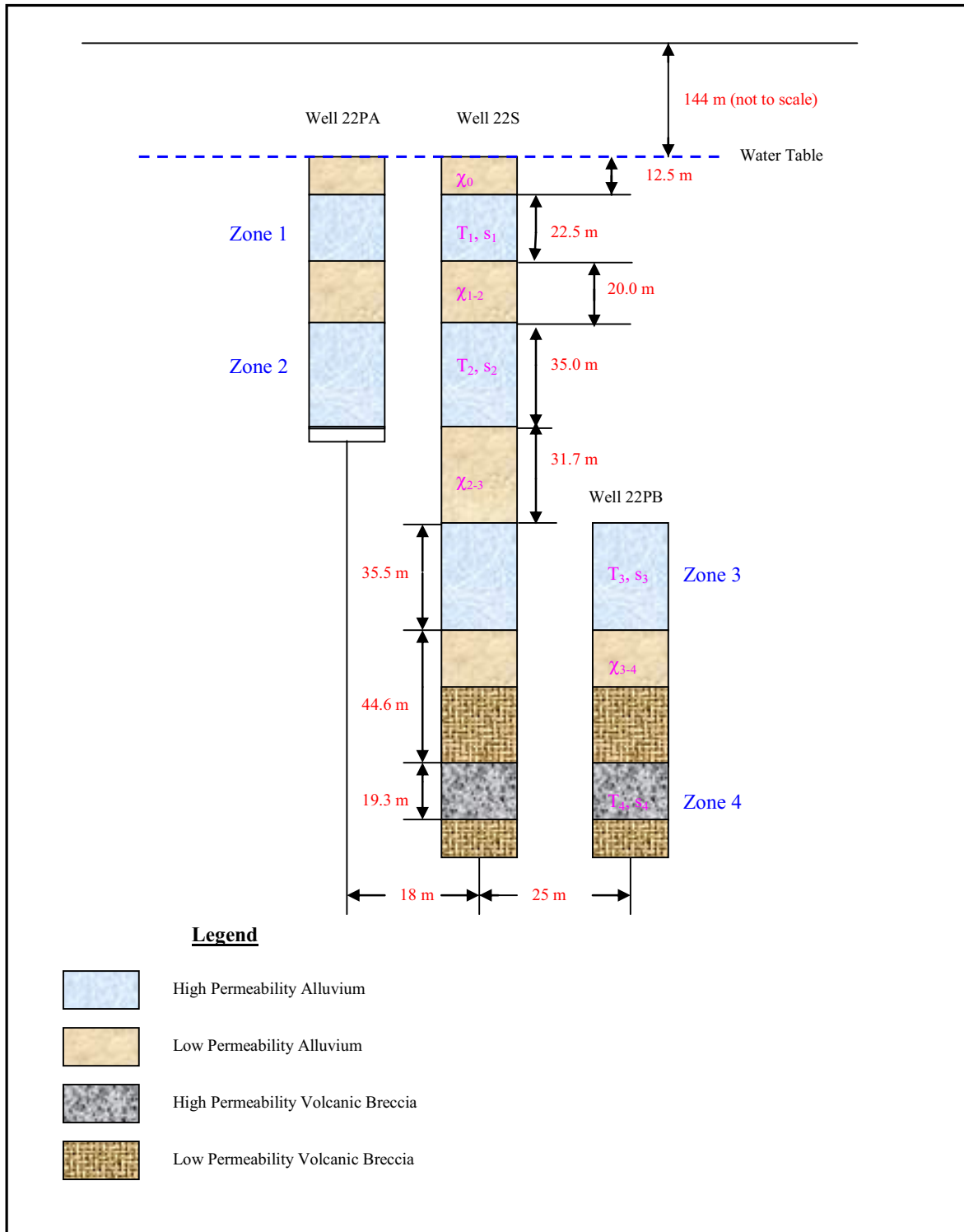
Within the context of these general conceptualizations, three separate conceptual mathematical models are applied to obtain three separate sets of hydraulic parameter estimates: (1) a confined leaky aquifer model, (2) a two-aquifer (or two-layer) model, and (3) a three-aquifer (or three-layer) model. Each of the models (described in more detail below) assumes that each zone of the system is homogeneous. Vertical anisotropy is represented using either a leakance parameter B [units of length] or a parameter χ [units of 1/time]. In the multiple-aquifer system conceptualization (Figure F-28(a)), χ represents the vertical hydraulic conductivity divided by

the thickness of the confining layer. In the multiple-layer system conceptualization (Figure F-28(b)), χ represents hydraulic conductivity in the vertical direction divided by the distance between the mid points of the pumped and adjacent aquifers. The estimation of B or χ for each conceptual mathematical model is explained below.

The mathematical solutions to the governing equations for each conceptual mathematical model are identical for both general conceptualizations (multiple aquifer or multiple layer); the only difference is in the way in which the deduced model parameters are interpreted. The transmissivities associated with each screened interval are divided by different aquifer thicknesses to yield different horizontal hydraulic conductivity estimates in the two conceptualizations. Additionally, the vertical hydraulic communication parameters (discussed below) are interpreted as reflecting either vertical hydraulic conductivity through the confining layers in the case of the multiple-aquifer conceptualization or vertical hydraulic conductivity between the midpoints of two adjacent screened intervals in the case of the multiple-layer conceptualization. Thus, the two conceptual models result in somewhat different horizontal and vertical hydraulic conductivity estimates despite the fact that the same mathematical models are used to estimate transmissivity and storativity. The differences in the resulting parameter estimates reflect uncertainty in system knowledge, as there are no a priori data indicating whether one conceptualization is better or more likely than the other.

The drawdowns versus time from the start of pumping or recovery for the five pumping tests are shown in Figures F-29 through F-39. In the case of each isolated-interval pump test, there is one observation point in 22PA or 22PB in the zone pumped and 3 observation points in the remaining zones (there are also observations in the corresponding intervals in 22S, but these were not used in the analyses for the reasons stated above). For the test involving pumping of all four combined zones, the responses in zones 1, 3 and 4 are plotted and analyzed. In this case, the response in zone 1 is taken to reflect a composite response for combined intervals 1 and 2, as the analyses of the isolated zone tests indicated good vertical communication between these two intervals, suggesting they could be treated as a single aquifer (details provided below).

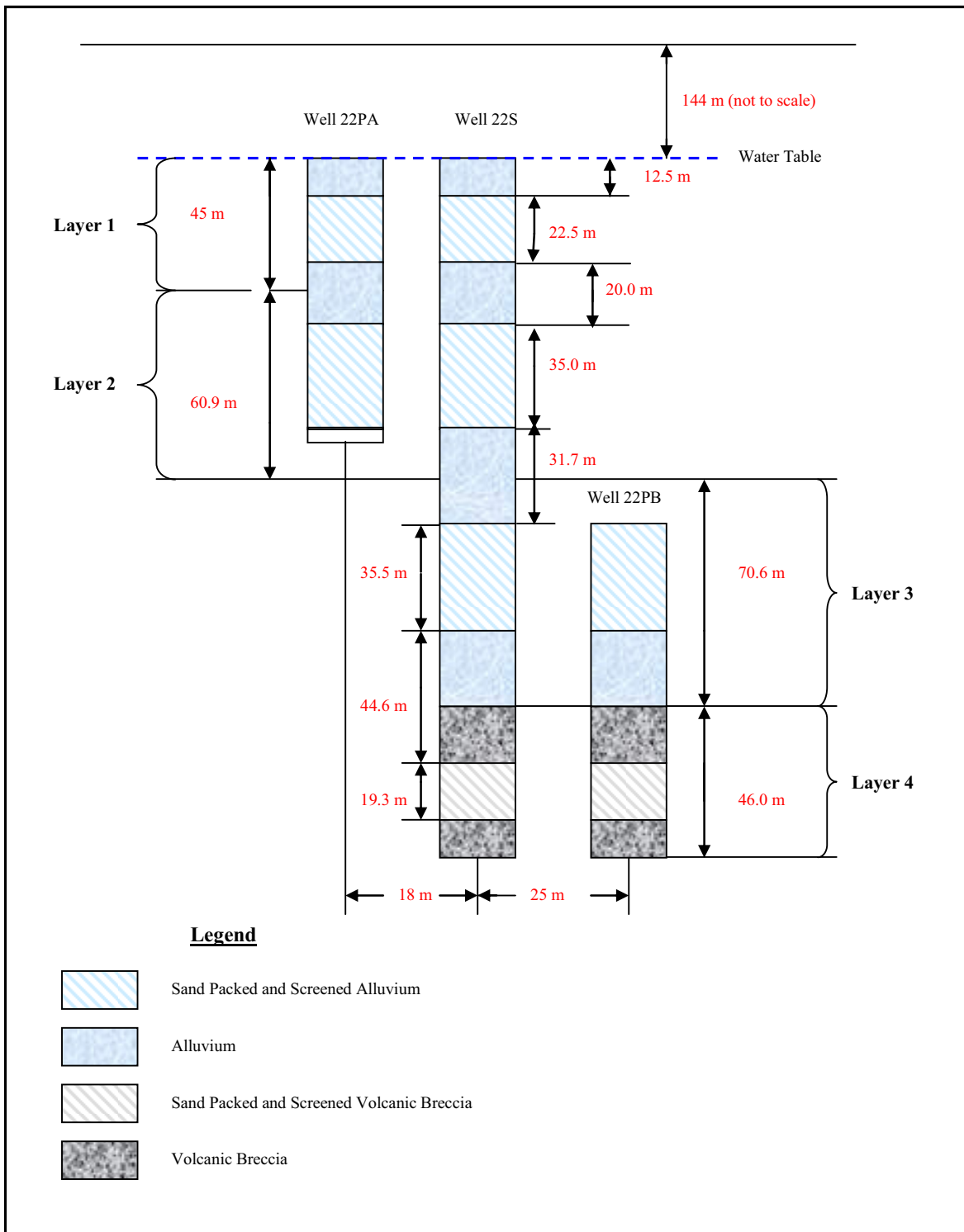
(a) Multiple-Aquifers Conceptual Model



NOTE: For illustration purposes only.

Figure F-28. Site 22 Schematic in the Vertical Cross Section

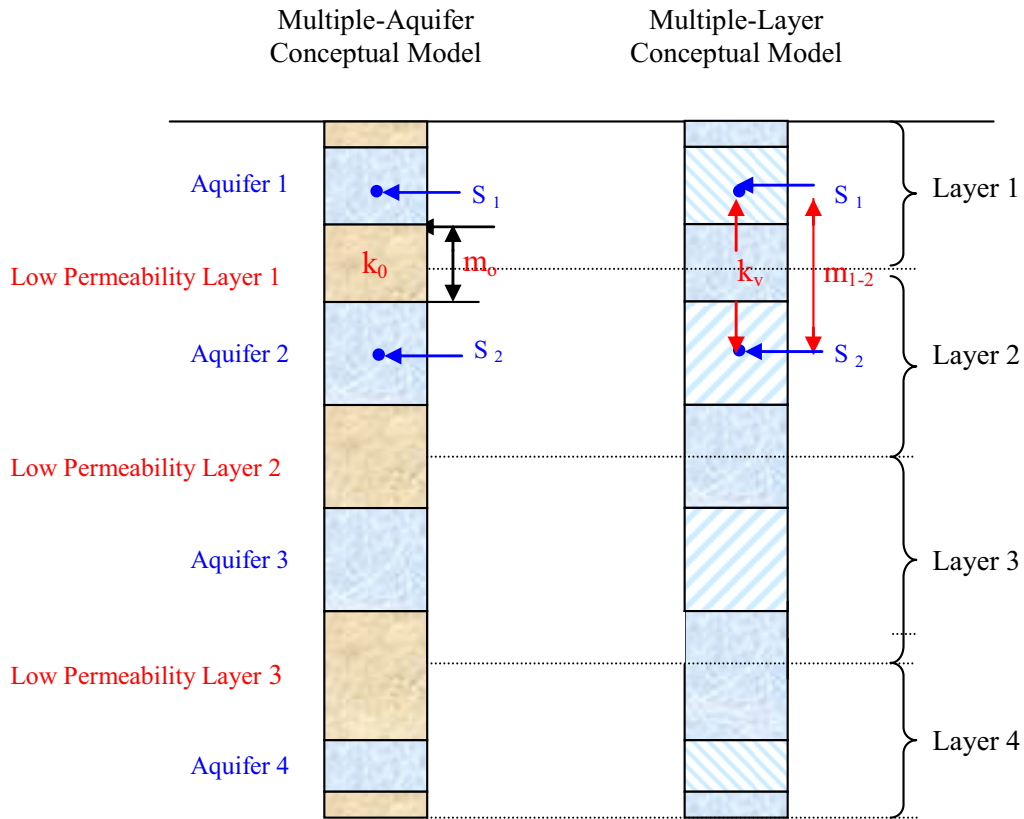
(b) Multiple-Layers Conceptual Model



NOTE: For illustration purposes only.

Figure F-28. Site 22 Schematic in the Vertical Cross Section (for illustration purposes only) (Continued)

(c) Differences in the Vertical Flow Representation in Multiple-Aquifer and Multiple-Layer Conceptual Models



$$\chi_{1-2} = \frac{k_0}{m_0} \qquad \chi_{1-2} = \frac{k_v}{m_{1-2}}$$

$$q_{1-2} = (S_1 - S_2)\chi_{1-2}$$

- k_0 is the hydraulic conductivity of the low permeability layer
- m_0 is the thickness of the low permeability layer
- k_v is the vertical hydraulic conductivity
- m_{1-2} is the distance between the mid points of the two adjacent layers
- S_1 is the averaged drawdown over the aquifer (layer) thickness in Aquifer 1 (Layer 1)
- S_2 is the averaged drawdown over the aquifer (layer) thickness in Aquifer 2 (Layer 2)
- q_{1-2} is the vertical flux between the two adjacent aquifers (layers)

NOTE: For illustration purposes only.

Figure F-28. Site 22 Schematic in the Vertical Cross Section (Continued)

Visual analysis of the data shown in Figures F-29 through F-40 suggests the following:

- The drawdowns in the observation wells reach steady-state or close to a steady-state condition shortly after the pumping (recovery) begins.
- The drawdowns in the observation wells in the pumped interval are relatively small.
- The drawdowns in the intervals adjacent to the pumping interval are very small. However, based on the available data, the intervals immediately adjacent to the pumped interval appear to respond to pumping.
- In most cases, the pumping and recovery data in the pumped interval are in good agreement. The ambient fluctuations of the aquifer pressures in the pumped interval are significantly smaller than the pressure drops due to the pumping. There are some differences between pumping and recovery data in adjacent intervals because the ambient pressure fluctuations become comparable to the pressure drop induced by pumping.
- The observed responses of the system described above are consistent with the concept of the system being well hydraulically connected. The small response in the adjacent zones suggests either vertical anisotropy in hydraulic conductivity or the presence of lower permeability layers between the pumped intervals. The steady-state or close to steady-state condition indicates the presence of inflow from adjacent zones and possibly from the water table in the case of the upper two zones.

F6.5.1 Leaky Aquifer Conceptual Model

This model assumes a single aquifer that is semi-confined or leaky. As such, it represents a special case of the multiple-aquifer conceptualization in which only one aquifer is considered. The results from this model can also be interpreted in the context of the multiple-layer conceptualization. However, because the model is almost universally applied assuming that the test interval is an aquifer, not part of a layer, the parameter estimates from this model in the remainder of this appendix are always presented as aquifer parameters (e.g., hydraulic conductivities are calculated from transmissivities using only the screened interval thickness, not the layer thicknesses of Figure F-28b). The confining layers below and above the aquifer are permeable and water can be transmitted across the confining layers from the overlying and underlying aquifers. The heads in the adjacent aquifers are assumed to be unaffected by pumping (the drawdowns are either zero or very small). This assumption is appropriate because during the pumping tests, the observed drawdowns in the adjacent zones were small. The storage of the confining layers is also assumed to be negligible. This assumption is valid when the observation times are greater than t_{cr} which is calculated as the product of 0.036 and the ratio of low permeability layer storativity and parameter χ (Fetter 2001 [DIRS 156668], p.158, Equation 5.16). The results from *Analysis of Aquifer Pump Tests in Individual Well Zones at Site 22 Near Yucca Mountain, Nevada* (Questa Engineering Corporation 2004 [DIRS 178566]) were used to estimate t_{cr} . The storativity of the low permeability layer was assumed to be the same as the storativity of the adjacent zone. This should result in overestimating t_{cr} because the storativity of a low permeability layer should be smaller than the storativity of an aquifer. For the uppermost zone, t_{cr} is 0.194 min (storativity of 0.00116 and χ of 0.31day^{-1}). For the lower zone, t_{cr} is

4.37 min (storativity of 0.0001 and χ of 0.0119 day⁻¹). The pressure observations were made using 10-s time increments. Correspondingly, the observations that occurred before t_{cr} include 1 data point and 26 data points out of about 3,800 data points in the uppermost and lower cases, respectively. It is concluded that assuming negligible storativity of the low permeability layers is appropriate.

The parameters of this model are:

- Transmissivity of the main aquifer, T_i , [L²/T]
- Storativity of the main aquifer, s_i , [-]
- Leakage factor B_i , [L]

The parameter B_i is related to the parameters χ_i (confining layer above the main aquifer) and χ_{i+1} (confining layer below the main aquifer) by the following equation:

$$B_i^2 = \frac{T_i}{\chi_i + \chi_{i+1}} \quad (\text{Eq. F-26})$$

The solution for the leaky aquifer conceptual model is known as the Hantush-Jacob solution (Hantush 1956 [DIRS 165169]). The following equations describe the drawdowns (S_i) in the leaky confined aquifer as a function of time elapsed since pumping/recovery (t):

$$S_i(t) = \frac{Q_i}{4\pi T_i} W(u, r) \quad (\text{Eq. F-27})$$

$$u = \frac{R^2 s_i}{4t T_i} \quad r = \frac{R}{B_i}$$

$$W(u, r) = \int_u^\infty \exp\left(-x - \frac{r^2}{4x}\right) \frac{dx}{x}$$

where Q_i is the constant pumping rate and R is the distance from the pumping well to the monitoring well (or the radius of the pumping well). $W(u, r)$ is known as the leaky aquifer well function.

F6.5.2 Two-Aquifer System with Drawdowns Accounted for in Both Aquifers

This model assumes that the adjacent aquifer located below or above the main aquifer responds to the pumping in the main aquifer. The other assumptions are the same as in the case of the leaky aquifer conceptual model. The parameters of this model are:

- Transmissivity of the main aquifer, T_i , [L²/T]
- Storativity of the main aquifer, s_i , [-]
- Transmissivity of the adjacent aquifer, T_{i+1} , [L²/T]
- Storativity of the adjacent aquifer, s_{i+1} , [-]
- Leakage parameter χ_i [T⁻¹]

- Leakage parameter χ_{i-1} [T^{-1}]
- Leakage parameter χ_{i+1} [T^{-1}].

The parameter, χ_{i+1} , represents the connection of the adjacent aquifer to the 3rd aquifer that may contribute water to this aquifer, but which is not affected by pumping of the main aquifer. The parameter χ_{i-1} represents the connection of the main aquifer to the adjacent aquifer that may contribute water to this aquifer, but which is not affected by pumping of the main aquifer. In the case of an isolated system, χ_{i-1} and χ_{i+1} are equal to 0. In the case of semi-open system, either χ_{i-1} or χ_{i+1} is not zero, or both of them are not zero.

The equations for non-steady multiple-aquifer flow towards a well are formulated by Maas (1986 [DIRS 178614]). In the case of two aquifers, the Maas (1986 [DIRS178614]) equations can be written as:

$$s_i \frac{\partial s_i}{\partial t} = T_i \nabla S_i + \chi_i (S_{i+1} - S_i) - \chi_{i-1} S_i$$

and (Eq. F-28)

$$s_{i+1} \frac{\partial s_{i+1}}{\partial t} = T_{i+1} \nabla S_{i+1} + \chi_i (S_i - S_{i+1}) - \chi_{i+1} S_{i+1},$$

$$\nabla S_i = \frac{1}{R} \frac{\partial}{\partial R} \left(R \frac{\partial s_i}{\partial R} \right) \quad \nabla S_{i+1} = \frac{1}{R} \frac{\partial}{\partial R} \left(R \frac{\partial s_{i+1}}{\partial R} \right)$$

where S_i and S_{i+1} are drawdowns in the main and adjacent aquifers correspondingly.

The boundary conditions are:

$$R \frac{\partial s_i}{\partial R} \Big|_{R \rightarrow r_{well}} = \frac{Q_i}{2\pi T_i} \quad \text{and} \quad R \frac{\partial s_{i+1}}{\partial R} \Big|_{R \rightarrow r_{well}} = \frac{Q_{i+1}}{2\pi T_{i+1}} \quad (\text{Eq. F-29a})$$

$$S_1 \Big|_{r \rightarrow \infty} = 0, \quad \text{and} \quad S_2 \Big|_{r \rightarrow \infty} = 0 \quad (\text{Eq. F-29b})$$

where r_{well} is the radius of the pumping well and Q_i is the pumping rate from the main aquifer. In a general case, an adjacent aquifer may be pumped as well with the pumping rate Q_{i+1} . If it is not pumped, Q_{i+1} is set equal to zero.

The system of equations F-28, F-29a, and F-29b has an analytical solution in only a few special cases. One of these is when the system is closed ($\chi_{i+1} = \chi_{i-1} = 0$) and $T_i/s_i = T_{i+1}/s_{i+1}$ (Hantush 1960 [DIRS 178665]).

Equations F-28, F-29a, and F-29b can be rewritten using Laplace transforms as shown below to eliminate the time derivative and obtain a system of ordinary differential equations that can be solved analytically.

$$s_1 p \tilde{S}_1 = T_1 \nabla \tilde{S}_1 + \chi_{1-2} (\tilde{S}_2 - \tilde{S}_1) - \chi_0 \tilde{S}_1 \quad (\text{Eq. F-30a})$$

and

$$s_2 p \tilde{S}_2 = T_2 \nabla \tilde{S}_2 + \chi_{1-2} (\tilde{S}_1 - \tilde{S}_2) - \chi_{2-3} \tilde{S}_2 \quad (\text{Eq. F-30b})$$

with boundary conditions (Equation F-31):

$$r \left. \frac{d\tilde{S}_1}{dr} \right|_{r \rightarrow r_{\text{well}}} = \frac{Q_1}{2\pi T_1}, \quad r \left. \frac{d\tilde{S}_2}{dr} \right|_{r \rightarrow r_{\text{well}}} = \frac{Q_2}{2\pi T_2} \quad (\text{Eq. F-31a})$$

and

$$\tilde{S}_1 \Big|_{r \rightarrow \infty} = 0, \quad \text{and} \quad \tilde{S}_2 \Big|_{r \rightarrow \infty} = 0 \quad (\text{Eq. F-31b})$$

where \tilde{S}_i and \tilde{S}_{i+1} are Laplace transforms of the drawdowns S_i and S_{i+1} and p is the Laplace transform variable.

For the general case of a multiple-aquifer flow system, the solution is the set of equations described by Maas (1986 [DIRS 178614]). The two-aquifer system is a simplified case that has the analytical solution described below. The derivation of the solution is presented in Appendix P.

The solution to Equation F-30 with the boundary conditions of Equation F-31 is:

$$\tilde{S}_i = C_1 K_0(b_1 R) + C_2 K_0(b_2 R)$$

and

(Eq. F-32)

$$\tilde{S}_{i+1} = C_1 \beta_1 K_0(b_1 R) + C_2 \beta_2 K_0(b_2 R)$$

$$b_1^2 = \frac{1}{2} \left(\frac{\kappa_1}{T_i} + \frac{\kappa_2}{T_{i+1}} \right) + \sqrt{\frac{1}{4} \left(\frac{\kappa_1}{T_i} + \frac{\kappa_2}{T_{i+1}} \right)^2 - \frac{\kappa_2 \kappa_1 - \chi_i^2}{T_i T_{i+1}}}$$

$$b_2^2 = \frac{1}{2} \left(\frac{\kappa_1}{T_i} + \frac{\kappa_2}{T_{i+1}} \right) - \sqrt{\frac{1}{4} \left(\frac{\kappa_1}{T_i} + \frac{\kappa_2}{T_{i+1}} \right)^2 - \frac{\kappa_2 \kappa_1 - \chi_i^2}{T_i T_{i+1}}}$$

$$\beta_1 = \frac{\kappa_1 - T_i b_1^2}{\chi_i} \quad \beta_2 = \frac{\kappa_1 - T_i b_2^2}{\chi_i}$$

$$\kappa_1 = s_i p + \chi_i + \chi_{i-1}$$

$$\kappa_2 = s_{i+1} p + \chi_i + \chi_{i+1}$$

$$C_1 = \frac{Q_i/T_i \beta_2 - Q_{i+1}/T_{i+1}}{2\pi(\beta_2 - \beta_1)} \quad C_2 = \frac{Q_{i+1}/T_{i+1} - Q_i/T_i \beta_1}{2\pi(\beta_2 - \beta_1)}$$

where K_0 is the modified Bessel function of the second kind.

The actual drawdowns $S_i(t)$ and $S_{i+1}(t)$ can be obtained by applying the inverse Laplace transform. A method of inversion commonly used in hydrogeology is Stehfest's (1970 [DIRS 117341]) method. The formula for the inverse Laplace transform is:

$$S_j(t) = \frac{\ln(2)}{t} \sum_{n=1,10} v_n \frac{\tilde{S}_j(p_n)}{p_n}, \quad j=i \text{ and } i+1 \quad (\text{Eq. F-33})$$

$$p_n = \frac{\ln(2)}{t} n$$

$$v_n = (-1)^{5+n} \sum_{k=\frac{n+1}{2}}^{\min(5,n)} \frac{k^5 (2k)!}{(5-k)! k! (n-k)! (2k-n)!}$$

F6.5.3 Three-Aquifer System with Drawdowns Accounted for in All Three Aquifers

This model assumes that three aquifers respond to pumping one of the aquifers. The other assumptions are the same as in the two-aquifer system conceptual model. The parameters of this model are:

- Transmissivity of the main aquifer, T_i , [L^2/T]
- Storativity of the main aquifer, s_i , [-]
- Transmissivity of the adjacent aquifer, T_{i-1} , [L^2/T]
- Storativity of the adjacent aquifer, s_{i-1} , [-]
- Transmissivity of the second adjacent aquifer or an aquifer below or above the adjacent one, T_{i+1} , [L^2/T]
- Storativity of the second adjacent aquifer or an aquifer below or above the adjacent one, s_{i+1} , [-]
- Leakage parameter χ_i [T^{-1}]
- Leakage parameter χ_{i+1} [T^{-1}]
- Leakage parameter χ_{i-1} [T^{-1}].

The parameter χ_{i-1} represents the connection of the adjacent aquifer to the 4th aquifer that may contribute water to this aquifer, but which is not affected by pumping of the main aquifer. In the case of an isolated system $\chi_{i-1} = 0$.

The same approach as in the two-aquifer case is used to derive solutions for this conceptual model. The equations for non-steady multiple-aquifer flow towards a well are formulated by Maas (1986 [DIRS 178614]). In the case of three aquifers, the Maas (1986 [DIRS 178614]) equations in Laplace space can be written as:

$$s_{i-1}p\tilde{S}_{i-1} = T_{i-1}\nabla\tilde{S}_{i-1} + \chi_i(\tilde{S}_i - \tilde{S}_{i-1}) - \chi_{i-1}\tilde{S}_{i-1} \quad (\text{Eq. F-34})$$

$$s_i p S_i = T_i \nabla \tilde{S}_i + \chi_i(\tilde{S}_{i-1} - \tilde{S}_i) + \chi_{i+1}(\tilde{S}_{i+1} - \tilde{S}_i)$$

$$s_{i+1}p\tilde{S}_{i+1} = T_{i+1}\nabla\tilde{S}_{i+1} + \chi_{i+1}(\tilde{S}_i - \tilde{S}_{i+1})$$

The boundary conditions are:

$$R \left. \frac{\partial \tilde{S}_{i-1}}{\partial R} \right|_{R \rightarrow r_{well}} = \frac{Q_{i-1}}{2\pi T_{i-1}} \quad (\text{Eq. F-35})$$

$$R \left. \frac{\partial \tilde{S}_i}{\partial R} \right|_{R \rightarrow r_{well}} = \frac{Q_i}{2\pi T_i}$$

$$R \left. \frac{\partial \tilde{S}_{i+1}}{\partial R} \right|_{R \rightarrow r_{well}} = \frac{Q_{i+1}}{2\pi T_{i+1}}$$

where Q_i is the pumping rate from the main aquifer. In a general case defined by the boundary conditions in equation F-35, the adjacent aquifers may be pumped as well with the pumping rates Q_{i-1} and Q_{i+1} . If they are not pumped, Q_{i-1} and Q_{i+1} are set equal to zero. Also, any of the three aquifers can be the main one. For example, if the first aquifer is the main one, then Q_{i-1} is set equal to the pumping rate from this aquifer and Q_i and Q_{i+1} are set equal to 0.

The three-aquifer system is a simplified case of the solution provided by Maas (1986 [DIRS 178614]), and it has the analytical solution described below. The derivation of the solution is presented in Appendix P.

The solution of the system (Equation F-34) with the boundary conditions (Equation F-35) is:

$$\tilde{S}_{i-1} = C_1 K_0(b_1 R) + C_2 K_0(b_2 R) + C_3 K_0(b_3 R)$$

$$\tilde{S}_i = C_1 \beta_1 K_0(b_1 R) + C_2 \beta_2 K_0(b_2 R) + C_3 \beta_3 K_0(b_3 R) \quad (\text{Eq. F-36})$$

$$\tilde{S}_{i+1} = C_1 \beta'_1 K_0(b_1 R) + C_2 \beta'_2 K_0(b_2 R) + C_3 \beta'_3 K_0(b_3 R)$$

$$\text{Where, } \beta_j = \frac{\kappa_1 - T_{i-1} b_j^2}{\chi_i}, \quad \beta'_j = \frac{\kappa_1 - T_{i-1} b_j^2}{\kappa_3 - T_{i+1} b_j^2} \frac{\chi_{i+1}}{\chi_i} \quad j=1,3$$

$$\kappa_1 = s_{i-1} p + \chi_i + \chi_{i-1} \quad \kappa_2 = s_i p + \chi_i + \chi_{i+1} \quad \kappa_3 = s_{i+1} p + \chi_{i+1}$$

$$b_1^2 = \kappa_3 (f_1 \cos(\frac{\phi}{3}) - \frac{A}{3})$$

$$b_2^2 = \kappa_3 (-f_1 \cos(\frac{\phi}{3} + \frac{\pi}{3}) - \frac{A}{3})$$

$$b_3^2 = \kappa_3 (-f_1 \cos(\frac{\phi}{3} - \frac{\pi}{3}) - \frac{A}{3})$$

$$f_1 = 2\sqrt{\frac{-\alpha}{3}} \quad \alpha = -\frac{A^2}{3} + B$$

$$A = \frac{1}{T_{i+1}} + \frac{\kappa_2}{T_i \kappa_3} + \frac{\kappa_1}{T_{i-1} \kappa_3} \quad B = \frac{\kappa_1}{\kappa_3 T_{i-1} T_{i+1}} + \frac{\kappa_2}{T_i T_{i+1} \kappa_3} + \frac{\kappa_1 \kappa_2}{T_{i-1} T_i \kappa_3^2} - \frac{\chi_i^2}{\kappa_3^2 T_{i-1} T_i} - \frac{\chi_{i+1}^2}{\kappa_3^2 T_i T_{i+1}}$$

$$\phi = -a \tan\left(\frac{f_2}{\sqrt{-f_2^2 + 1}}\right) + 1.5708$$

$$f_2 = -\gamma \frac{4}{f_1^3}$$

$$\gamma = 2\left(\frac{A}{3}\right)^3 - \frac{AB}{3} + G$$

$$G = \frac{\chi_i^2 \kappa_3 - \kappa_1 \kappa_2 \kappa_3 + \chi_{i+1}^2 \kappa_1}{T_{i-1} T_i T_{i+1} \kappa_3^3}$$

$$C_1 = \frac{Q_{i-1}}{2\pi T_{i-1}} - C_2 - C_3$$

$$C_2 = \left[\frac{Q_i}{2\pi T_i} + (\beta_1 - \beta_3) C_3 - \beta_1 \frac{Q_{i-1}}{2\pi T_{i-1}} \right] / (\beta_2 - \beta_1)$$

$$C_3 = \frac{\frac{\beta_2 - \beta_1}{2\pi} \left(\frac{Q_{i+1}}{T_{i+1}} - \beta_1' \frac{Q_{i-1}}{T_{i-1}} \right) - \frac{\beta_2 - \beta_1'}{2\pi} \left(\frac{Q_i}{T_i} - \beta_1 \frac{Q_{i-1}}{T_{i-1}} \right)}{(\beta_1 - \beta_3)(\beta_2' - \beta_1') - (\beta_2 - \beta_1)(\beta_1' - \beta_3')}$$

Equation F-33 with j equal to $i-1$, i , and $i+1$ is used to obtain the actual drawdowns $S_{i-1}(t)$, $S_i(t)$, and $S_{i+1}(t)$.

F6.5.4 Hantush Inflection Point Method

The Hantush inflection point method (Hantush 1956 [DIRS 165169]) was used in *Analysis of Aquifer Pump Tests in Individual Well Zones at Site 22 Near Yucca Mountain, Nevada* (Questa Engineering Corporation 2004 [DIRS 178566]) to estimate leaky-aquifer parameters (transmissivity, storativity, and leakage factor). The major assumption of this method is that the steady-state conditions are reached and the steady-state drawdown S_{max} is known. The parameters are estimated from the following equations:

$$\exp\left(\frac{R}{B}\right)K_0\left(\frac{R}{B}\right) = 2.3 \frac{S_{inf}}{\zeta_{inf}} \quad (\text{Eq. F-37})$$

$$T = \frac{QK_0\left(\frac{R}{B}\right)}{2S_{max}\pi}$$

$$S = \frac{2t_{inf}T}{RB}$$

$$S_{inf} = \frac{1}{2} S_{max}$$

where T , s , and B are transmissivity, storativity, and leakage factor of the leaky aquifer, Q is the pumping rate, R is the distance to the monitoring well, t_{inf} is the time when S_{inf} (half of maximum drawdown or inflection point) was observed, and ζ_{inf} is the slope of the straight portion of the drawdown curve plotted using logarithmic scale for time and arithmetic scale for drawdowns.

F6.6 PARAMETER ESTIMATION

As can be seen from the discussion above, each conceptual model has its own set of parameters that may be estimated from the pumping test data.

In the case of the leaky aquifer, automatic parameter estimation is implemented by minimizing an objective function of these parameters. The objective function $F(T_i, s_i, B_i)$ is defined as:

$$F(T_i, s_i, B_i) = \sum_{j=1, N} [S_c(t_j) - S_m(t_j)]^2 \quad (\text{Eq. F-38})$$

where $S_c(t_j)$ is the drawdown in the pumped aquifer calculated using equation F-27 at the moment of time t_j , $S_m(t_j)$ is the drawdown measured at the time t_j , and N is the number of observations. The parameters T_i , s_i , and B_i that result in minimum value of F (best fit to the data) represent the estimated parameter values.

In the case of two-aquifer and three-aquifer systems, the parameters are adjusted manually to provide the best visual match to the data. This approach is taken because: (1) the number of unknown parameters is significantly larger in these cases (7 and 9 correspondingly) than for the leaky-aquifer solution, and (2) the data in the aquifers adjacent to the pumped aquifers are less

accurate. The simplified approach of correcting the pressures does not allow for excluding all the possible noises that affect the drawdowns in the adjacent zones. To provide a measure of the goodness of fit, the root mean square errors are calculated for the drawdowns in all the aquifers using the formula:

$$Err_i = \left[\sum_{j=1, N} [S_c^i(t_j) - S_m^i(t_j)]^2 / N \right]^{\frac{1}{2}} \quad (\text{Eq. F-39})$$

$i=1,2$ (2 aquifer system) and $i=1,3$ (3 aquifer system)

F6.7 IMPLEMENTATION OF THE ANALYSIS

All three mathematical models described above were implemented using MathCAD[®]. One MathCAD application was developed for each pumping test (output DTN: LA0701PR150304.001). The built-in MathCAD[®] functions, such as the Ko (modified Bessel) function, the calculation of integrals and factorials, data smoothing function, and minimization procedure were used.

Each application does the following:

- Reads the drawdown versus time data for pumping and recovery periods. These data are copied from the corresponding Excel file where the initial data processing was done, into a built-in Excel file within MathCAD[®]. The data are already corrected for the ambient pressure fluctuation (if needed). This is discussed in more detail when each test is considered below.
- Displays the input data.
- Defines the pumping rate(s) and the distance to the monitoring wells.
- Implements the calculations related to the leaky aquifer conceptual model, Equations F-26 and F-27.
- Defines the objective function using Equation F-38.
- Uses minimization procedure to estimate leaky-aquifer parameters T_i , s_i , and B_i .
- Displays the calculated versus measured drawdowns versus time and calculates root mean square error using Equation F-39 and $i=1$.
- Defines the input parameters required for the two-aquifer system conceptual model.
- Implements two-aquifer system calculations, Equations F-30, F-31, and F-32.
- Displays the calculated versus measured drawdowns versus time in the first and in the second aquifers and calculates root mean square errors using Equation F-39.

- Defines the input parameters required for the three-aquifer system conceptual model.
- Implements three-aquifer system calculations, Equations F-34, F-35, and F-36.
- Displays the calculated versus measured drawdowns versus time in the first, second, and third aquifers and calculate root mean square errors using Equation F-39.

The MathCAD[®] application developed for the pumping test when all four zones were pumped only implements the three-aquifer system solution as discussed in detail later in this appendix. The MathCAD[®] applications developed for the pumping tests from zones 2 and 3 implement the leaky aquifer and three-aquifer system solutions. The MathCAD[®] application developed for the zone 4 pumping test implements the leaky aquifer and two-aquifer system solutions. All three solutions are implemented in the MathCAD[®] application developed for the zone 1 pumping test.

In the discussion provided below the aquifer parameters are denoted in accordance with the Figure 28 notations. This is somewhat different from the general cases described in Equations F-26 through F-39. For example, the actual zone numbers are used instead of indexes $i-1$, i , and $i+1$.

F6.7.1 Pumping Test in Zone 1

During the pumping test from zone 1 the ambient fluctuations of the hydraulic heads were relatively small. The ambient fluctuations are the fluctuations observed in zone 4 that is separated from zone 1 by the two intermediate zones. As can be seen from Figure F-30, zone 4 appears to be unaffected by pumping and zones 2 and 3 show some response to pumping. The drawdown versus time data corresponding to the pumping and recovery periods are in good agreement in all 4 zones, indicating that ambient pressure fluctuations, which were different during the pumping and recovery periods, had negligible impact on the drawdown curves. Consequently, it was decided not to correct the drawdowns in zones 1, 2, and 3. The same conclusion was reached in *Analysis of Aquifer Pump Tests in Individual Well Zones at Site 22 Near Yucca Mountain, Nevada* (Questa Engineering Corporation 2004 [DIRS 178566]).

Zone 1 in 22S was pumped for 11 hrs and 3.5 min at a pumping rate of 237.1 m³/day (43.5 gpm). The recovery was observed for 45 hrs and 25 min. The observations in zone 1 are available for well 22PA located 18 m from the pumping well. The observations for zone 2 are in 22PA deep (18 m from the pumping well), and for zones 3 and 4 they are in 22PB shallow and deep (25 m from the pumping well). All three mathematical solutions were applied to the data, as described below. The resulting parameter estimates provided at the end of Section F6.7.5.

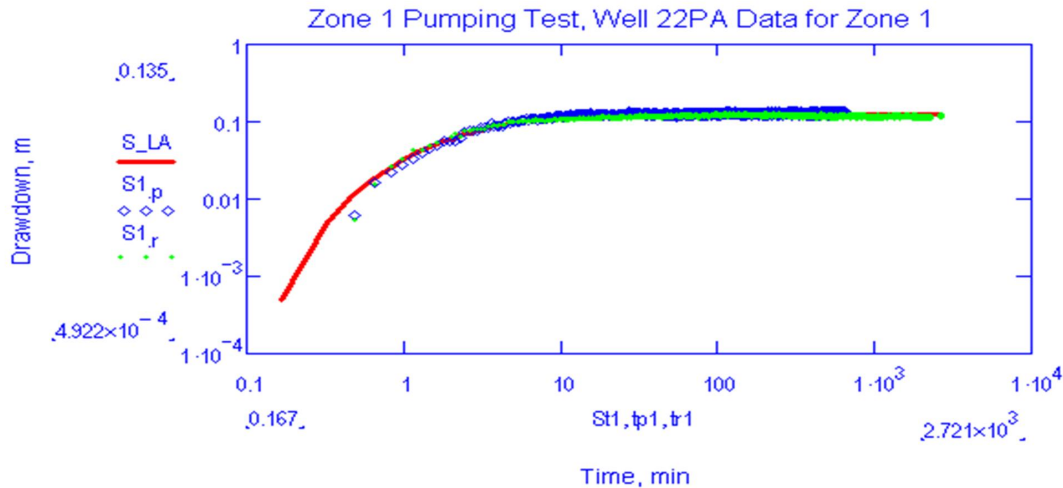
F6.7.1.1 Leaky Aquifer Solution

Based on the model assumptions (no drawdowns in adjacent aquifers), only the drawdown data for zone 1 (22PA shallow) are used in this analysis. The drawdowns observed during pumping and recovery periods in well 22PA shallow were combined. As a result, the vector S_m in equation F-38 includes both pumping and recovery data. The total number of observations is 10,700. The drawdowns S_c in equation F-38 are calculated in the same 10,700 time points as the observed drawdowns.

As described above, the leaky aquifer solution has three parameters. The parameter estimates obtained by minimizing the objective function defined in equation F-38 are:

$$\begin{aligned} T_1 &= 264.2 \text{ m}^2/\text{day} \\ s_1 &= 0.00132 \\ B_1 &= 32.5 \text{ m.} \end{aligned}$$

The measured and calculated drawdowns are shown in Figure F-29. The root mean square error is 6.3 mm.



Output DTN: LA0701EK150304.001 (produced by MathCAD application *Zone 1.xmcd*).

NOTE: Red solid line shows the calculated drawdowns; blue diamonds show the drawdowns during pumping period; green dots show the drawdowns during the recovery period; and the green solid line shows the smoothed data (averaged drawdowns).

Figure F-29. Zone 1 Pumping Test, Leaky Aquifer Solution

Based on the zone 1 thickness of 22.2 m, the hydraulic conductivity of zone 1 is 11.9 m/day. Based on equation F-26, $(\chi_{1-2} + \chi_0) = 0.25 \text{ day}^{-1}$. The high estimated storativity value indicates possible unconfined conditions in zone 1.

The parameter estimates reported in *Analysis of Aquifer Pump Tests in Individual Well Zones at Site 22 Near Yucca Mountain, Nevada* (Questa Engineering Corporation 2004 [DIRS 178566]) based on using the Hantush inflection point method (Hantush 1956 [DIRS 165169]) were:

$$\begin{aligned} T_1 &= 242 \text{ m}^2/\text{day} \\ s_1 &= 0.0016 \\ B_1 &= 29.9 \text{ m.} \end{aligned}$$

These values are in good agreement with the estimates obtained from the method described above.

F6.7.1.2 Two-Aquifer Solution

In this analysis it was assumed that the pumping of zone 1 affects zone 2 but does not affect zone 3. The same data for zone 1 (22PA shallow) are used in the data interpretation. In addition, the drawdown data for zone 2 (22PA deep) are used. The manually-adjusted parameters providing the best visual fit to the drawdowns in zones 1 and 2 are:

$$T_1 = 280 \text{ m}^2/\text{day}$$

$$s_1 = 0.0017$$

$$T_2 = 600 \text{ m}^2/\text{day}$$

$$s_2 = 0.003$$

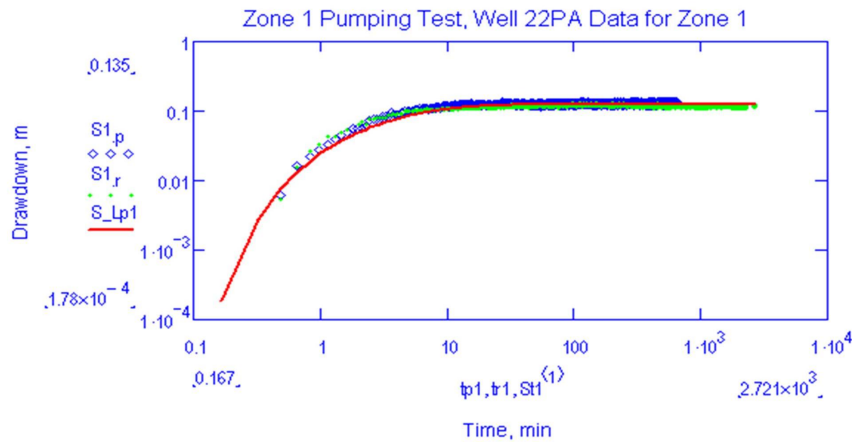
$$\chi_{1-2} = 0.10$$

$$\chi_{2-3} = 0.01$$

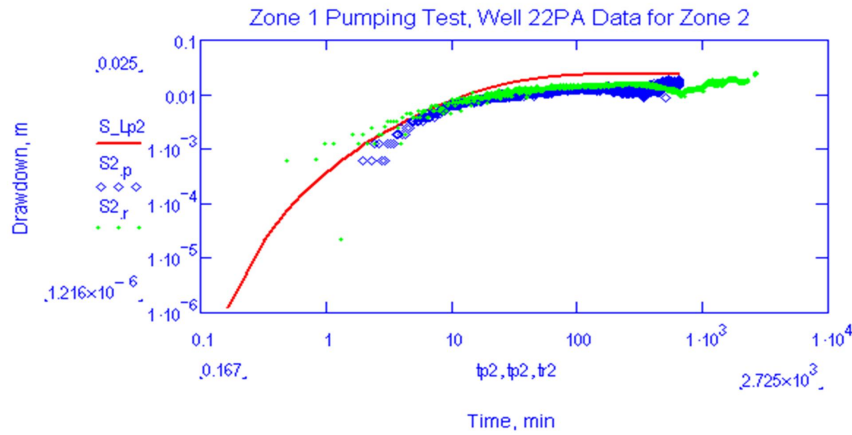
$$\chi_0 = 0.15.$$

The measured and calculated drawdowns in zones 1 and 2 are shown in Figure F-30. The root mean square error is 7.0 mm for zone 1 and 10.0 mm for zone 2.

(a) Zone 1



(b) Zone 2



Output DTN: LA0701EK150304.001 (produced by MathCAD application *Zone 1.xmcd*).

NOTE: Red solid line shows the calculated drawdowns; blue diamonds show the drawdowns during pumping period; and green dots show the drawdowns during the recovery period.

Figure F-30. Zone 1 Pumping Test, Two-Aquifer Solution

The transmissivity and storativity of zone 1 estimated from this model are slightly higher than in the leaky aquifer model. $(\chi_{1-2} + \chi_0) = 0.15 + 0.10 = 0.25 \text{ day}^{-1}$, which is the same as in the leaky aquifer model.

Based on the estimated χ_{1-2} value, the hydraulic conductivity of the layer between zones 1 and 2 (multiple-aquifer model) is 2 m/day, assuming that the thickness of this layer is 20 m. In the case of the multiple layer model, when there is assumed to be no low permeability layer, the estimated vertical hydraulic conductivity is 4.9 m/day assuming that the distance between zones 1 and 2 midpoints is 49 m.

It was not possible to fit the drawdown in zone 1 without introducing the parameter χ_0 . This means that the drawdowns in zone 1 are affected by flow from the water table. This result supports the concept of unconfined conditions in zone 1.

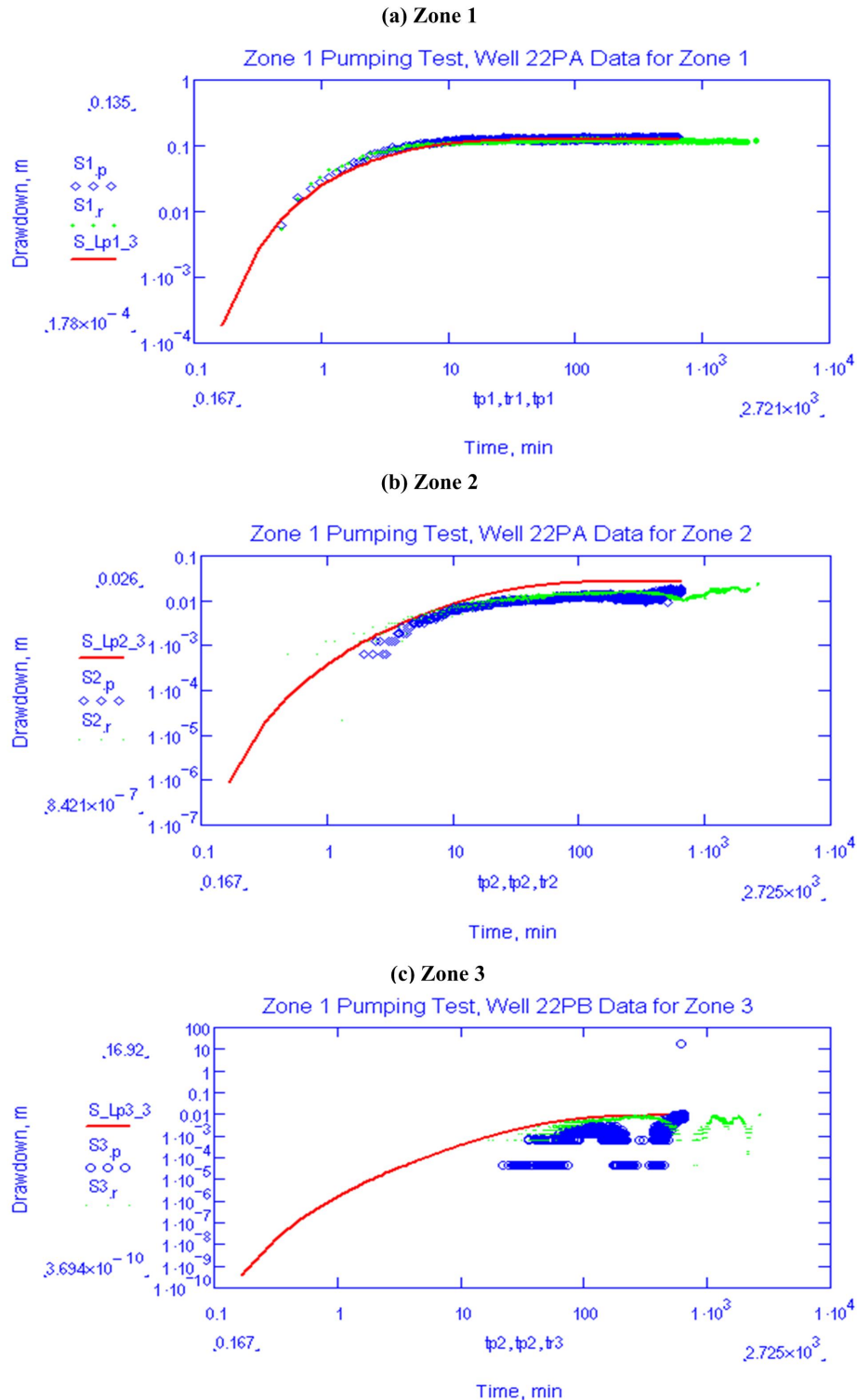
The high estimated storativity value for zone 2 indicates possible unconfined conditions in zone 2 as well. This result is consistent with the finding that the hydraulic conductivity of the low permeability layer between zones 1 and 2 (or vertical hydraulic conductivity in the two layers) is relatively high.

F6.7.1.3 Three-Aquifer Solution

In this analysis it was assumed that the pumping of zone 1 affects zones 2 and 3 but does not affect zone 4. The same data for zone 1 (22PA shallow) and zone 2 (22PA deep) are used in the data interpretation. In addition, the drawdowns in zone 3 (22PB shallow) are used. The manually-adjusted parameters providing the best visual fit to the drawdowns in zones 1, 2, and 3 are:

$$\begin{aligned}T_1 &= 280 \text{ m}^2/\text{day} \\s_1 &= 0.0017 \\T_2 &= 600 \text{ m}^2/\text{day} \\s_2 &= 0.003 \\T_3 &= 140 \text{ m}^2/\text{day} \\s_3 &= 0.0003 \\\chi_{1-2} &= 0.10 \\\chi_{-3} &= 0.01 \\\chi_0 &= 0.15.\end{aligned}$$

The measured and calculated drawdowns in zones 1, 2, and 3 are shown in Figure F-31. The root mean square error is 4.8 mm for zone 1, 13.0 mm for zone 2, and 6.1 mm for zone 3.



Output DTN: LA0701EK150304.001 (produced by MathCAD application *Zone 1.xmcd*).

NOTE: Red solid line shows the calculated drawdowns; blue diamonds show the drawdowns during pumping period; and green dots show the drawdowns during the recovery period.

Figure F-31. Zone 1 Pumping Test, Three-Aquifer Solution

F6.7.2 Pumping Test in Zone 2

Based on the observed ambient fluctuations of the hydraulic heads during the pumping test from zone 2 it was decided not to correct the drawdowns in zones 1, 3, and 4 (the considerations are similar to the ones described above for zone 1). The same conclusion was reached in *Analysis of Aquifer Pump Tests in Individual Well Zones at Site 22 Near Yucca Mountain, Nevada* (Questa Engineering Corporation 2004 [DIRS 178566]).

Zone 2 in 22S was pumped for 11 hrs and 8.5 min with the pumping rate of 240.4 m³/day (44.1 gpm). The recovery was observed for 37 hrs and 28 min. The observations in zone 2 are available for well 22PA located 18 m from the pumping well. The other observations are available for zone 1 in 22PA shallow (18 m from the pumping well) and zones 3 and 4 in 22PB shallow and deep (25 m from the pumping well). The two mathematical models used in the data interpretation are described below. The resulting parameter estimates are summarized in Table F-4, provided at the end of Section F6.7.5.

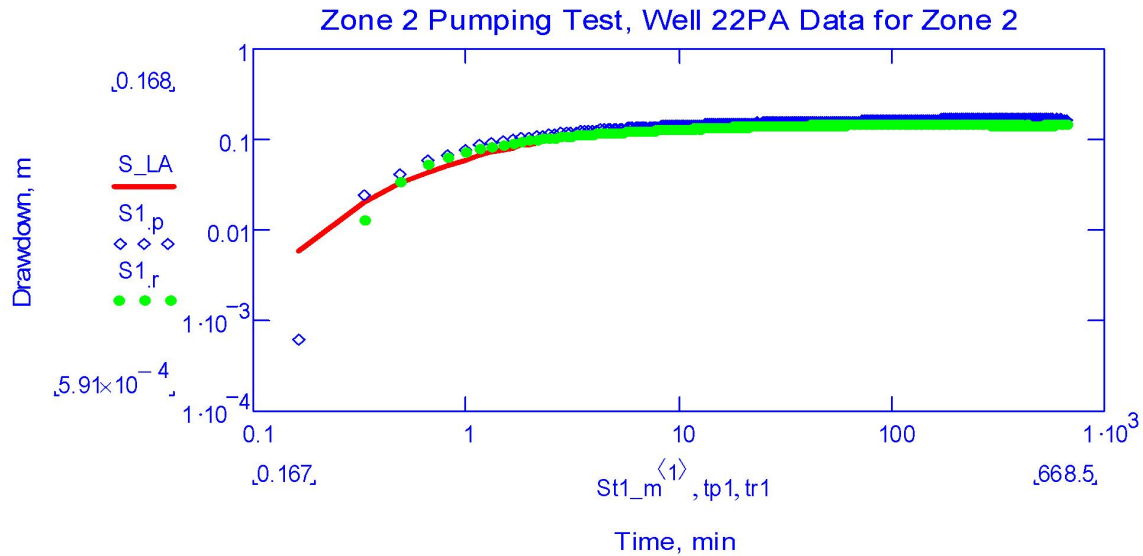
F6.7.2.1 Leaky Aquifer Solution

Based on the model assumptions (no drawdowns in the adjacent aquifers) only the drawdown data for zone 2 (22PA deep) are used in the data analysis. The drawdowns observed during pumping and recovery periods in the well 22PA deep were combined. As a result, the vector S_m in equation F-38 includes both, pumping and recovery data. The total number of observations is 7,973. The drawdowns S_c in equation F-38 are calculated for the same 7,973 time points as the observed drawdowns.

The leaky aquifer parameter estimates obtained by minimizing the objective function defined in Equation F-38 are:

$$\begin{aligned}T_2 &= 325 \text{ m}^2/\text{day} \\s_2 &= 0.00070 \\B_2 &= 54.8 \text{ m.}\end{aligned}$$

The measured and calculated drawdowns are shown in Figure F-32. The root mean square error is 13 mm.



Output DTN: LA0701EK150304.001 (produced by MathCAD application *Zone 2.xmcd*).

NOTE: Red solid line shows the calculated drawdowns; blue diamonds show the drawdowns during pumping period; and green dots show the drawdowns during the recovery period.

Figure F-32. Zone 2 Pumping Test, Leaky Aquifer Solution

Assuming a zone 2 thickness of 35 m (sand pack thickness), the hydraulic conductivity of zone 2 is 9.3 m/day. Based on Equation F-26, $(\chi_{1-2} + \chi_{2-3}) = 0.11 \text{ day}^{-1}$. This value is the same as the value estimated from the zone 1 pumping test.

The high estimated storativity value suggests it is likely that unconfined conditions exist in zone 2.

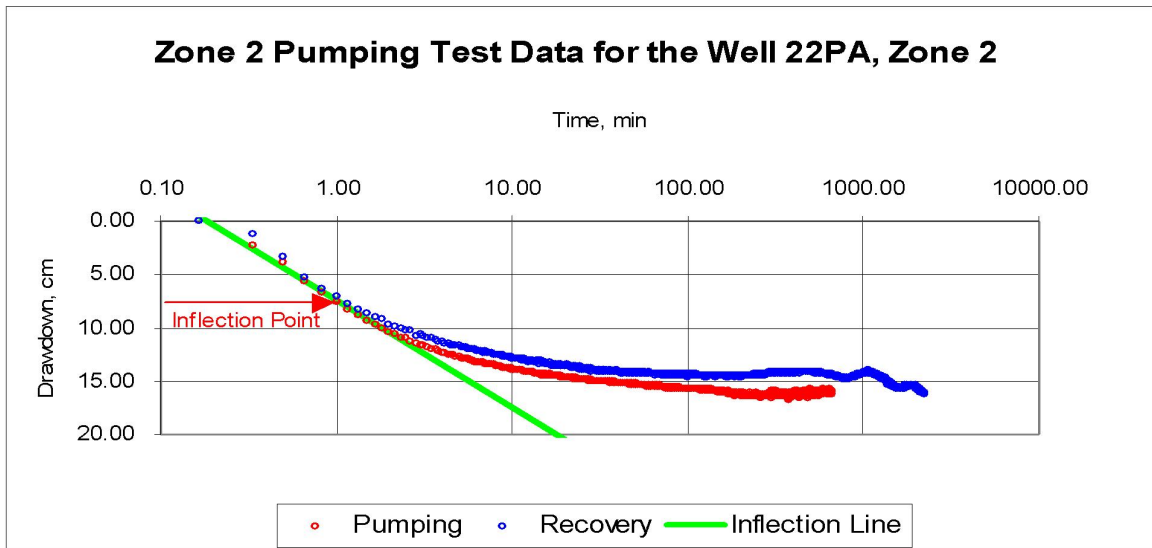
The estimated transmissivity and storativity of zone 2 are lower than the ones estimated from the zone 1 pumping test. The transmissivity and storativity are very sensitive to the absolute drawdown values. When zone 1 was pumped, the drawdowns in zone 2 were very small and affected by noise. This could have affected the estimation results. The parameters χ_{1-2} and χ_{2-3} are most sensitive to *differences* in the heads in zones 1 and 2 and these differences are less affected by noise in zone 2. Thus, the estimates of these parameters from pumping zones 1 and 2 are more consistent than the estimates of transmissivity and storativity.

The parameter estimates reported in *Analysis of Aquifer Pump Tests in Individual Well Zones at Site 22 Near Yucca Mountain, Nevada* (Questa Engineering Corporation 2004 [DIRS 178566]) based on using the Hantush inflection point method (Hantush 1956 [DIRS 165169]) were:

$$\begin{aligned} T_2 &= 427 \text{ m}^2/\text{day} \\ s_2 &= 0.00035 \\ B_2 &= 85.0 \text{ m.} \end{aligned}$$

These estimates are somewhat different (transmissivity and leakage factor are higher and storativity is lower) from those provided above. The inflection point method uses the slope of the straight portion of the drawdown curve and maximum (steady-state) drawdown to estimate

these parameters. As shown in Figure F-33, the estimates are greatly affected by the way the actual data are approximated by the straight line and by the maximum drawdown selected.



Output DTN: LA0701EK150304.001 (Zone 2.xls).

Figure F-33. Application of the Inflection Point Method to Zone 2 Pumping Test

The inflection line in this figure is drawn using linear regression and slope is calculated as the slope of the linear regression line. The maximum drawdown is assumed to be 0.15 m. The resulting parameters calculated using formulae (F-66) are:

$$\begin{aligned} T &= 299 \text{ m}^2/\text{day} \\ s &= 0.00054 \\ B &= 47.4 \text{ m.} \end{aligned}$$

These estimates are very close to the ones obtained using minimization of the objective function defined in equation F-38.

F6.7.2.2 Three-Aquifer Solution

In this analysis, it was assumed that the pumping of zone 2 affects zone 1 and zone 3 and does not affect zone 4. The same data for zone 2 (22PA deep) are used in the analysis. In addition, the drawdowns in zone 1 (22PA shallow) and in zone 3 (22PB shallow) are used. The manually-adjusted parameter estimates providing the best visual fit to the drawdowns in zones 1, 2, and 3 are:

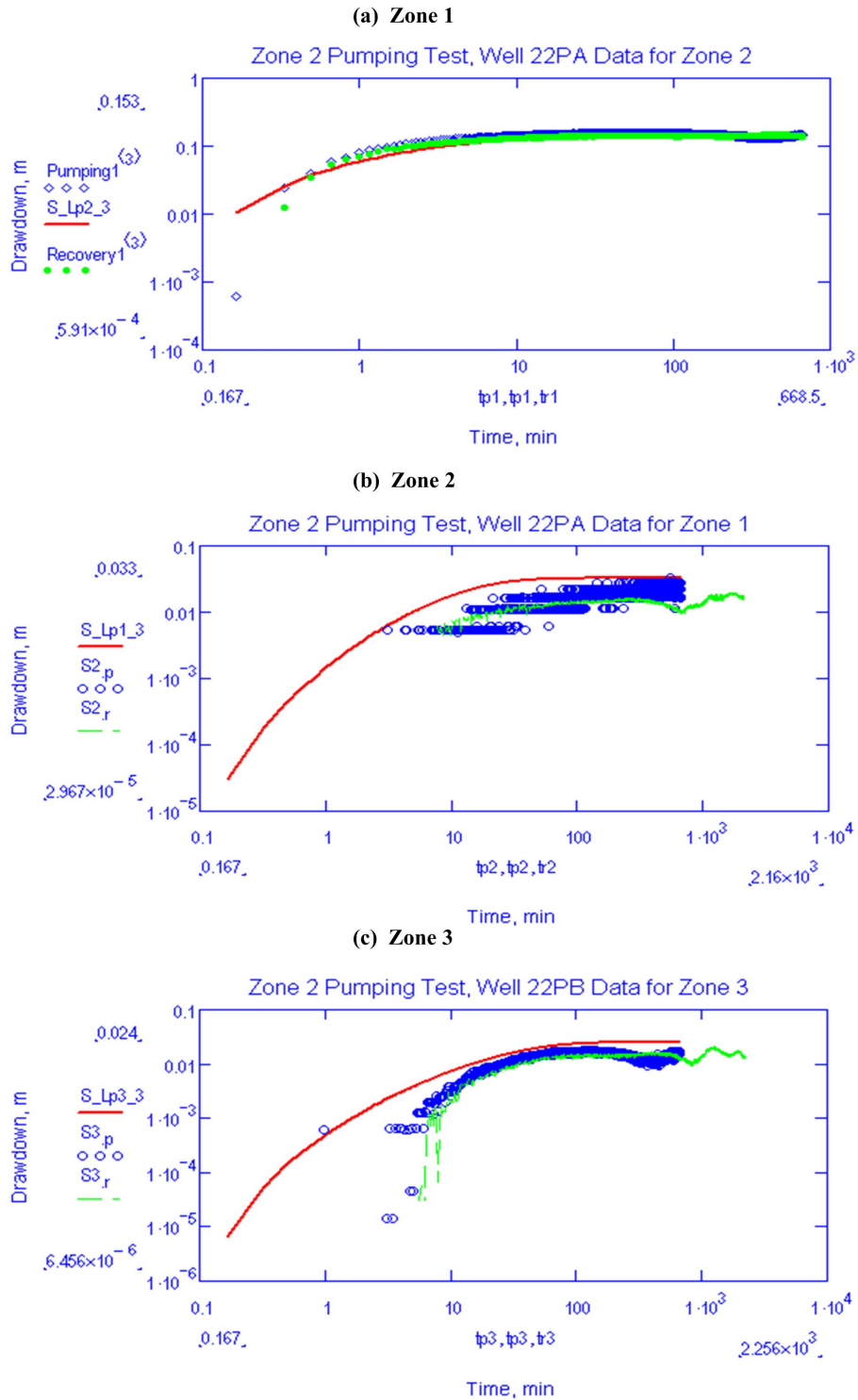
$$\begin{aligned} T_1 &= 280 \text{ m}^2/\text{day} \\ s_1 &= 0.0017 \\ T_2 &= 400 \text{ m}^2/\text{day} \\ s_2 &= 0.0007 \\ T_3 &= 170 \text{ m}^2/\text{day} \\ s_3 &= 0.0003 \end{aligned}$$

$$\chi_{1-2} = 0.10$$

$$\chi_{2-3} = 0.01$$

$$\chi_0 = 0.15.$$

The measured and calculated drawdowns in zones 1, 2, and 3 are shown in Figure F-34. The root mean square error is 13 mm for zone 2, 14.0 mm for zone 3, and 11 mm for zone 1.



Output DTN: LA0701EK150304.001 (produced by MathCAD application *Zone 2.xmcd*).

NOTE: Red solid line shows the calculated drawdowns; blue diamonds show the drawdowns during pumping period; and green dots show the drawdowns during the recovery period.

Figure F-34. Zone 2 Pumping Test, Three-Aquifer Solution

The estimated parameters are in good agreement with the estimates obtained for the leaky-aquifer solution and also with the parameters obtained from analyzing the zone 1 pumping test with the two- and three-aquifer solutions. Assuming a zone 2 thickness of 35 m, the hydraulic conductivity of zone 2 is 11.4 m/day.

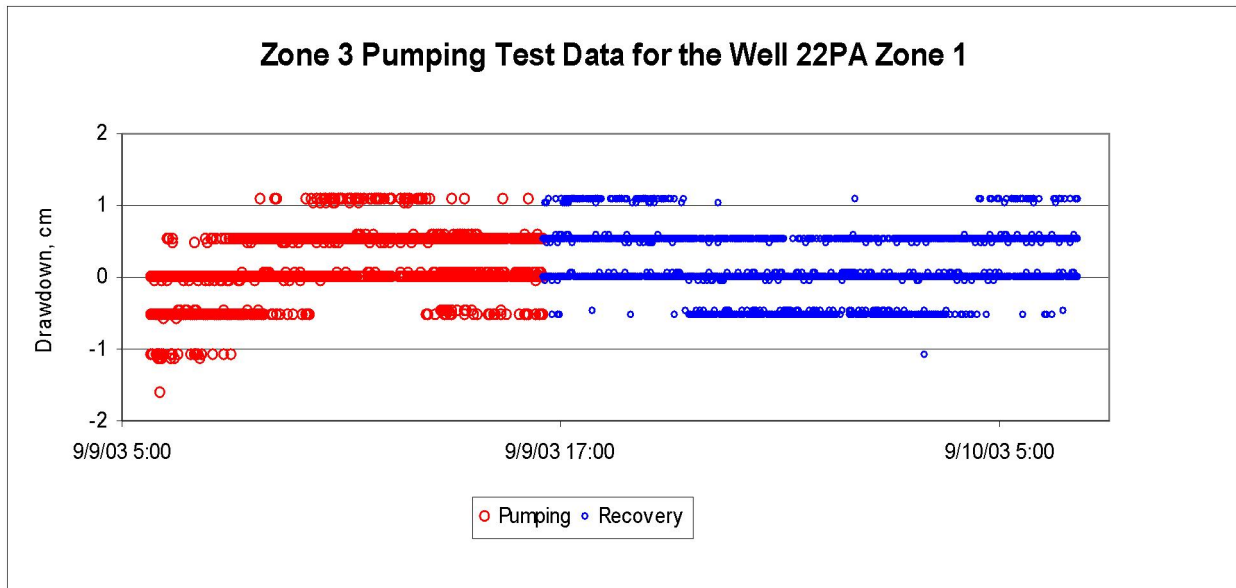
Based on the analyses of the zone 1 and zone 2 pumping tests, and particularly on the relatively large leakage or vertical hydraulic connection parameters estimated for each test, it can be concluded that the upper 80 m of the saturated zone at Site 22 (which includes zones 1 and 2) behave as if it is unconfined with a slightly higher horizontal hydraulic conductivity than a vertical conductivity. An unconfined aquifer solution applied to the Zone 1 and Zone 2 data using unqualified software corroborated that this is a valid conceptualization of the shallow portions of the saturated alluvium (see Section F6.4). Zones 1 and 2 are very similar in their hydraulic properties (hydraulic conductivity and storage) and have a good hydraulic connection. If the multiple-aquifer conceptualization is applied, the lower permeability layer between zones 1 and 2 is about 5 to 6 times less permeable than zones 1 and 2. If the multiple-layer conceptualization is used, which is probably more appropriate for a system exhibiting unconfined behavior, the vertical anisotropy ratio (ratio of horizontal to vertical conductivity) is 1.7 (assuming that the combined transmissivity of zone 1 and 2 is $600 + 280 = 880 \text{ m}^2/\text{day}$).

The vertical hydraulic connection between zones 2 and 3 is noticeably smaller than between zones 1 and 2. The parameter χ_{2-3} is 0.01 in all the analyses, which is one order of magnitude lower than χ_{1-2} . The thickness of the layer separating zones 2 and 3 is 31.7 m. Consequently, the hydraulic conductivity of this layer (assuming χ_{2-3} is 0.01 and using the multiple-aquifer conceptualization) is 0.317 m/day. The distance between the midpoints of zones 2 and 3 is 67 m, so the vertical hydraulic conductivity between layers 2 and 3 assuming the multiple-layer conceptual model is 0.67 m/day.

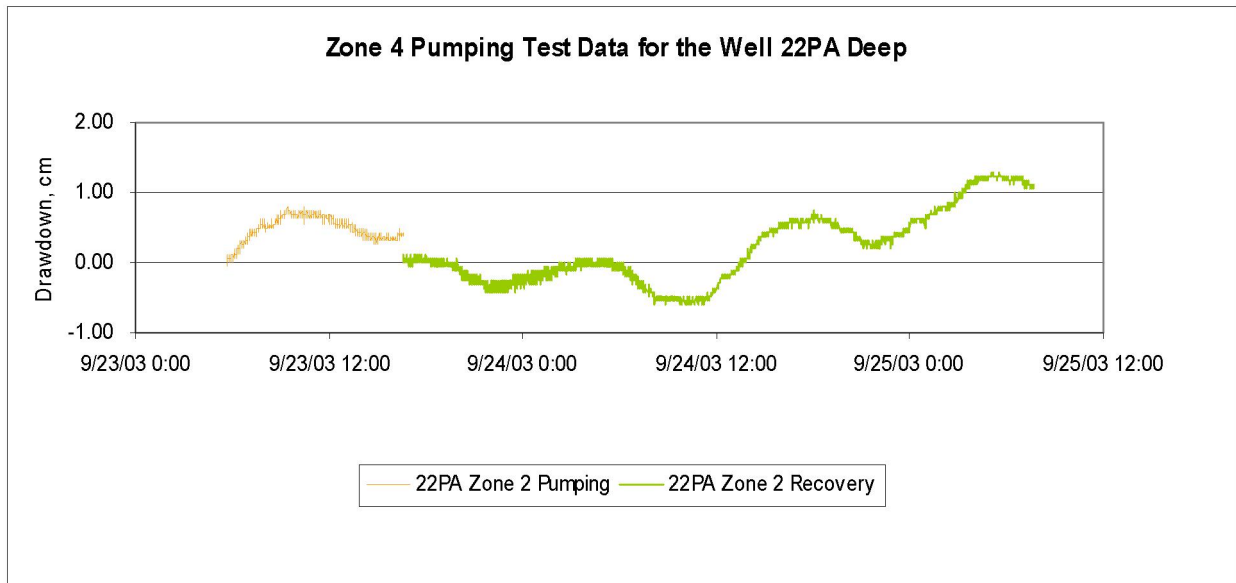
F6.7.3 Pumping Test in Zone 3

The observed ambient fluctuations of hydraulic heads in the non-pumped zones during the zone 3 pumping test were more pronounced than in the zone 1 and 2 pumping tests. Only zone 1 was unaffected by pumping. However, no corrections were made using zone 1 data because of the lower measurement precision of the zone 1 pressure transducer as a result of the larger dynamic measurement range of this transducer. The observations in zone 1 are shown in Figure F-35(a) to demonstrate this problem. For comparison, Figure F-35(b) shows the pressures in zone 2 in response to pumping zone 4 (zone 2 did not noticeably respond to pumping zone 4). *Analysis of Aquifer Pump Tests in Individual Well Zones at Site 22 Near Yucca Mountain, Nevada* (Questa Engineering Corporation 2004 [DIRS 178566]), assumed that zone 4 was not affected by pumping zone 3, and the data in zone 4 were used to correct the drawdowns in zone 3.

(a) Zone 1 Data during Zone 3 Pumping Test



(b) Zone 2 Data during Zone 4 Pumping Test



Output DTN: LA0701EK150304.001 (Zone 3.xls and Zone 4.xls).

Figure F-35. Ambient Fluctuations during the Zone 3 and Zone 4 Pumping Tests

Zone 3 in 22S was pumped for 10 hrs and 43.5 min at a pumping rate of 147.7 m³/day (27.1 gpm). The recovery was observed for 14 hrs and 37 min. The observations in zone 3 are available for well 22PB located 25 m from the pumping well. The other observations are in zone 2 in 22PA deep, zone 1 in 22PA shallow (both 18 m from the pumping well), and in zone 4 in 22PB deep (25 m from the pumping well). The analyses of the data using the leaky-aquifer and

the three-aquifer solutions are discussed below. The resulting parameter estimates are summarized in Table F-4, provided at the end of Section F6.7.5.

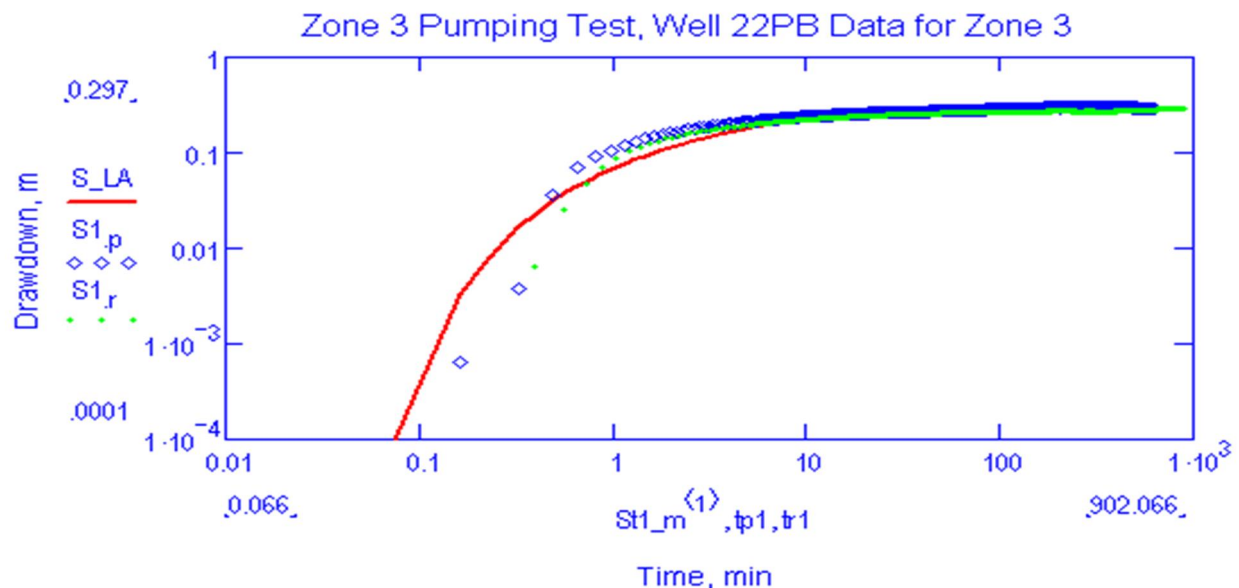
F6.7.3.1 Leaky Aquifer Solution

Based on the model assumption (no drawdowns in adjacent aquifers) only the drawdown data for zone 3 (22PB shallow) are used in the data analysis. The drawdowns observed during pumping and recovery periods in 22PB shallow were combined, so the vector S_m in equation F-38 includes both pumping and recovery data. The total number of observations is 9224. The drawdowns S_c are calculated for the same 9,224 times as the observed drawdowns S_m .

The leaky aquifer parameter estimates obtained by minimizing the objective function defined in equation F-38 are:

$$\begin{aligned} T_3 &= 132.7 \text{ m}^2/\text{day} \\ s_3 &= 0.000216 \\ B_3 &= 102.62 \text{ m.} \end{aligned}$$

The measured and calculated drawdowns are shown in Figure F-36. The root mean square error is 11 mm.



Output DTN: LA0701EK150304.001 (produced by MathCAD application *Zone 3.xmcd*).

NOTE: Red solid line shows the calculated drawdowns; blue diamonds show the drawdowns during pumping period; and green dots show the drawdowns during the recovery period.

Figure F-36. Zone 3 Pumping Test, Leaky Aquifer Solution

Based on the zone 3 thickness of 35.5 m, the hydraulic conductivity of zone 3 is 3.7 m/day. Based on the Equation F-26, $(\chi_{2-3} + \chi_{3-4}) = 0.0126 \text{ day}^{-1}$. The parameter χ_{2-3} is 0.01 day^{-1} based on the pumping tests from zone 1 and zone 2. Consequently, parameter χ_{3-4} is 0.0026 day^{-1} . The low storativity value suggests that there are confined conditions in zone 3.

The estimated parameter values for zone 3 are in good agreement with estimates obtained for zone 1 and zone 2 test interpretations.

Similar parameter estimates are reported in *Analysis of Aquifer Pump Tests in Individual Well Zones at Site 22 Near Yucca Mountain, Nevada* (Questa Engineering Corporation 2004 [DIRS 178566]) using the Hantush inflection point method (Hantush 1956 [DIRS 165169]). The results of that estimation were:

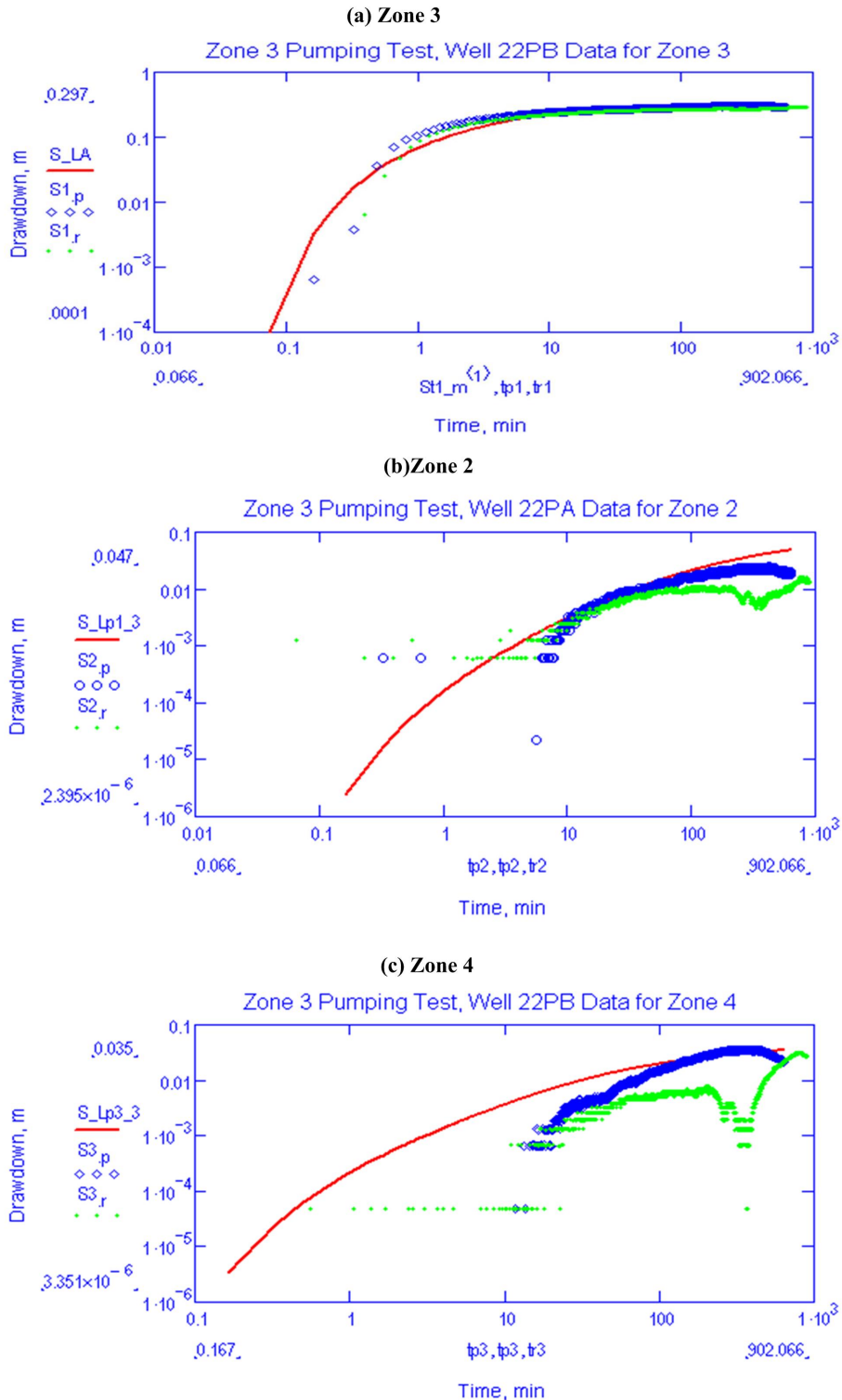
$$\begin{aligned}T_3 &= 139 \text{ m}^2/\text{day} \\s_3 &= 0.0001 \\B_3 &= 108.2 \text{ m}.\end{aligned}$$

F6.7.3.2 Three-Aquifer Solution

For this solution, it is assumed that the pumping of zone 3 affects zone 2 and zone 4 and does not affect zone 1. The same data for zone 3 (22PB shallow) are used in the analysis. In addition, the drawdowns in zone 2 (22PA deep) and in zone 4 (22PB deep) are used. The manually-adjusted parameter estimates providing the best visual fit to the drawdowns in zones 2, 3, and 4 are:

$$\begin{aligned}T_2 &= 450 \text{ m}^2/\text{day} \\s_2 &= 0.003 \\T_3 &= 133 \text{ m}^2/\text{day} \\s_3 &= 0.000216 \\T_4 &= 250 \text{ m}^2/\text{day} \\S_4 &= 0.0003 \\\chi_{2-3} &= 0.01 \\\chi_{3-4} &= 0.0026.\end{aligned}$$

The measured and calculated drawdowns in zones 2, 3 and 4 are shown in Figure F-37. The root mean square error is 12 mm for zone 3, 17.0 mm for zone 2, and 5.4 mm for zone 4.



Output DTN: LA0701EK150304.001 (produced by MathCAD application *Zone 3.xmcd*).

NOTE: Red solid line shows the calculated drawdowns; blue diamonds show the drawdowns during pumping period; and green dots show the drawdowns during the recovery period.

Figure F-37. Zone 3 Pumping Test, Three-Aquifer Solution

All the estimated parameters are in good agreement with the estimates discussed above.

These results support the previously-discussed conclusion that the hydraulic connection between zone 2 and 3 is noticeably lower than between zones 1 and 2. The hydraulic connection between zones 3 and 4 is even smaller than that between zones 2 and 3. The parameter χ_{3-4} is about 4 times smaller than parameter χ_{2-3} . The thickness of the layer separating zones 3 and 4 is 44.6 m. Consequently, if a multiple-aquifer conceptualization is used, the hydraulic conductivity of this layer (assuming χ_{3-4} is 0.0026) is 0.116 m/day. The distance between the midpoints of zones 3 and 4 is 72 m, so the vertical hydraulic conductivity between layers 3 and 4 assuming the multiple-layer conceptual model is 0.187 m/day.

F6.7.4 Pumping Test in Zone 4

The observed ambient fluctuations of hydraulic heads in the non-pumped zones during the zone 4 pumping test were more pronounced than in the zone 1 and zone 2 pumping tests. It was assumed that zone 2 was unaffected by pumping. Thus, the drawdowns in zones 3 and 4 were corrected using the pressure data from zone 2 (drawdowns in zone 2 were subtracted directly from the drawdowns in zone 3, and drawdowns in zone 2 times 0.83 were subtracted from the drawdowns in zone 4). A similar approach was taken in *Analysis of Aquifer Pump Tests in Individual Well Zones at Site 22 Near Yucca Mountain, Nevada* (Questa Engineering Corporation 2004 [DIRS 178566]), except that it was assumed that zone 3 was not affected by zone 4 pumping, so the zone 3 data were used to correct the drawdowns in zone 4.

Zone 4 in 22S was pumped for 10 hrs and 51.7 min with the pumping rate of 111.m³/day (20.5 gpm). The recovery was observed for 15 hrs and 7.5 min. Observations in zone 4 were obtained from well 22PB deep, located 25 m from the pumping well. Observations were also obtained for zone 1 in 22PA shallow, zone 2 in 22PA deep (18 m from the pumping well), and zone 3 in 22PB shallow (25 m from the pumping well). The model solutions used in the data analysis are described below. The resulting parameter estimates are summarized in Table F-4, provided at the end of Section F6.7.5. The three-aquifer solution was not considered because the response in zone 2 was too small. This is consistent with the previous interpretations that the layers between zones 2 and 3 and between zones 3 and 4 have relatively low permeability.

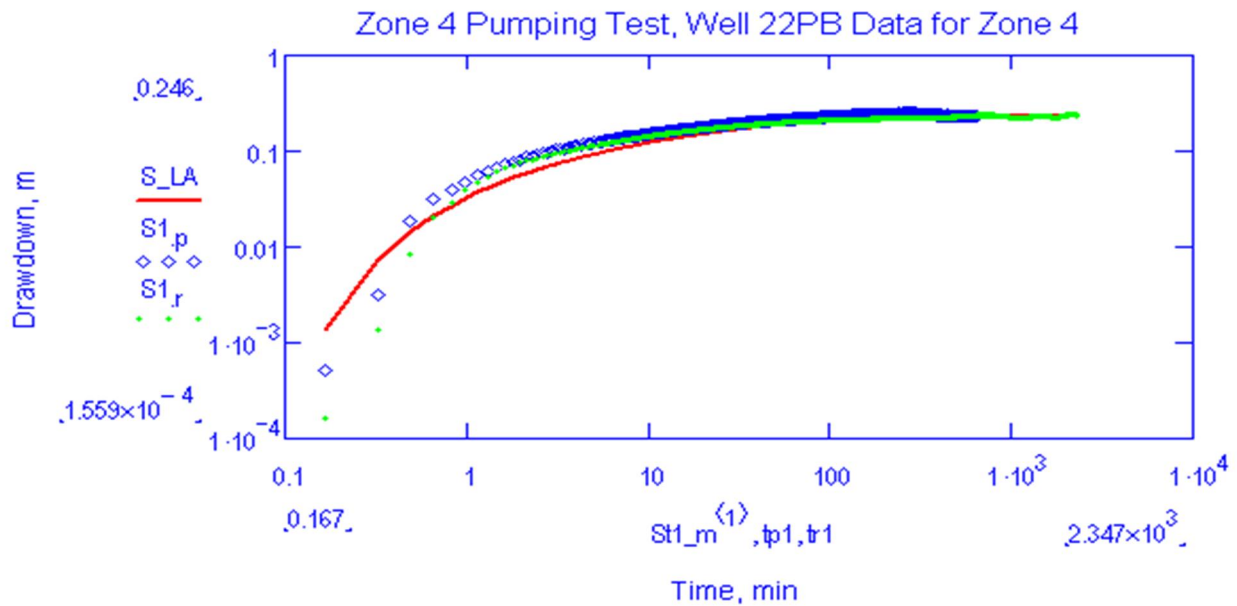
F6.7.4.1 Leaky Aquifer Solution

Based on the model assumptions (no drawdowns in the adjacent aquifers), only the drawdown data for zone 4 (22PB deep) are used in the data analysis. The drawdowns observed during pumping and recovery periods in well 22PB deep (corrected for ambient pressure fluctuations) were combined, so the vector S_m in equation F-38 includes both pumping and recovery data. The total number of observations is 10,740. The drawdowns S_c in Equation F-38 are calculated for the same 10,740 times as the observed drawdowns.

The leaky aquifer parameter estimates obtained by minimizing the objective function defined in equation F-38 are:

$$\begin{aligned} T_4 &= 200.0 \text{ m}^2/\text{day} \\ s_4 &= 0.00035 \\ B_4 &= 295.0 \text{ m.} \end{aligned}$$

The measured and calculated drawdowns are shown in Figure F-38. The root mean square error is 11 mm.



Output DTN: LA0701EK150304.001 (produced by MathCAD application *Zone 4.xmcd*).

NOTE: Red solid line shows the calculated drawdowns; blue diamonds show the drawdowns during pumping period; and green dots show the drawdowns during the recovery period.

Figure F-38. Zone 4 Pumping Test, Leaky Aquifer Solution

Assuming a zone 4 thickness of 19.3 m, the hydraulic conductivity of zone 4 is 10.4 m/day. Based on Equation F-26, $\chi_{3-4} = 0.0023 \text{ day}^{-1}$, which is in good agreement with the estimates obtained from the zone 3 analysis.

The parameter estimates reported in *Analysis of Aquifer Pump Tests in Individual Well Zones at Site 22 Near Yucca Mountain, Nevada* (Questa Engineering Corporation 2004 [DIRS 178566], Table 3) using Hantush inflection point method (Hantush 1956 [DIRS 165169]) are:

$$T_4 = 185 \text{ m}^2/\text{day}$$

$$s_4 = 0.00021$$

$$B_4 = 228.6 \text{ m.}$$

These values are in reasonably good agreement with the estimates obtained from the method described above.

F6.7.4.2 Two-Aquifer Solution

For this solution, it is assumed that the pumping of zone 4 affects zone 3 but does not affect zone 2. The data for zone 4 (22PB deep) and the ambient-pressure-corrected data for zone 3 (22PB shallow) were used in the data analysis. The manually-adjusted parameter estimates providing the best visual fit to the drawdowns in zones 3 and 4 are:

$$T_3 = 180 \text{ m}^2/\text{day}$$

$$s_3 = 0.00022$$

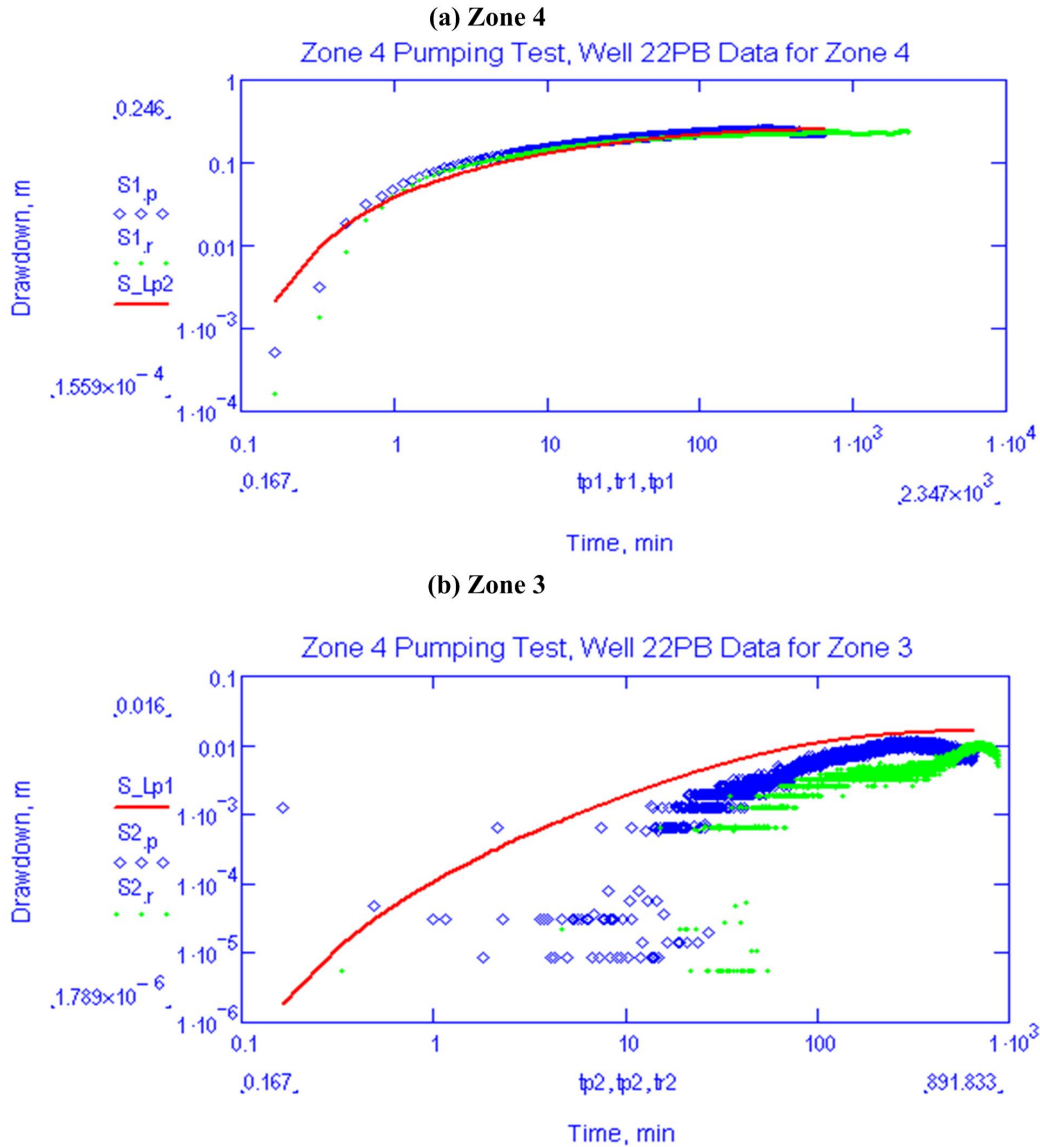
$$T_4 = 200 \text{ m}^2/\text{day}$$

$$s_4 = 0.0003$$

$$\chi_{2-3} = 0.01$$

$$\chi_{3-4} = 0.0018.$$

The measured and calculated drawdowns in zones 3 and 4 are shown in Figure F-39. The root mean square error is 13.0 mm for zone 4 and 5.9 mm for zone 3.



Output DTN: LA0701EK150304.001 (produced by MathCAD application *Zone 4.xmcd*).

NOTE: Red solid line shows the calculated drawdowns; blue diamonds show the drawdowns during pumping period; and green dots show the drawdowns during the recovery period.

Figure F-39. Zone 4 Pumping Test, Two-Aquifer Solution

The zone 4 transmissivity and storativity estimates from this analysis are in a good agreement with the previous estimates, but the value of χ_{3-4} is somewhat smaller than those discussed above.

F6.7.5 Pumping Test from All Four Combined Zones

A pumping test of the four combined zones in 22S took place in March 2002. The fraction of the total pumping rate allocated to each zone during this test was based on an open-hole spinner survey conducted prior to testing. The resulting pumping rates assumed in each zone were 240.4 m³/day (44 gpm), 288.9 m³/day (53 gpm), 125.4 m³/day (23 gpm), and 70.9 m³/day

(13 gpm) for zones 1, 2, 3, and 4, respectively. Pumping was interrupted after 19 hrs for about one hour and then it was resumed. Only the drawdown data obtained before this interruption were analyzed. The observations used in the analysis are from zone 1 in 22PA shallow (18 m from the pumping well), zone 3 in 22PB shallow (25 m from the pumping well), and zone 4 in 22PB deep (also 25 m from the pumping well). The three-aquifer solution was used to interpret the data. The resulting parameter estimates are summarized in Table F-4.

F6.7.5.1 Three-Aquifer Solution

To apply the three-aquifer solution, zones 1 and 2 were combined and assumed to be a single aquifer. The pumping tests from zones 1 and 2 indicated that these zones have very similar hydraulic properties and are well connected hydraulically. Consequently, combining these two zones is justified. The pumping rate from combined zones 1 and 2 was assumed to be equal to the sum of the individual zone pumping rates.

The manually-adjusted parameter estimates providing the best visual fit to the drawdowns in all three zones are:

$$T_{1+2} = 1,000 \text{ m}^2/\text{day}$$

$$s_{1-2} = 0.003$$

$$T_3 = 130 \text{ m}^2/\text{day}$$

$$s_3 = 0.0003$$

$$T_4 = 250 \text{ m}^2/\text{day}$$

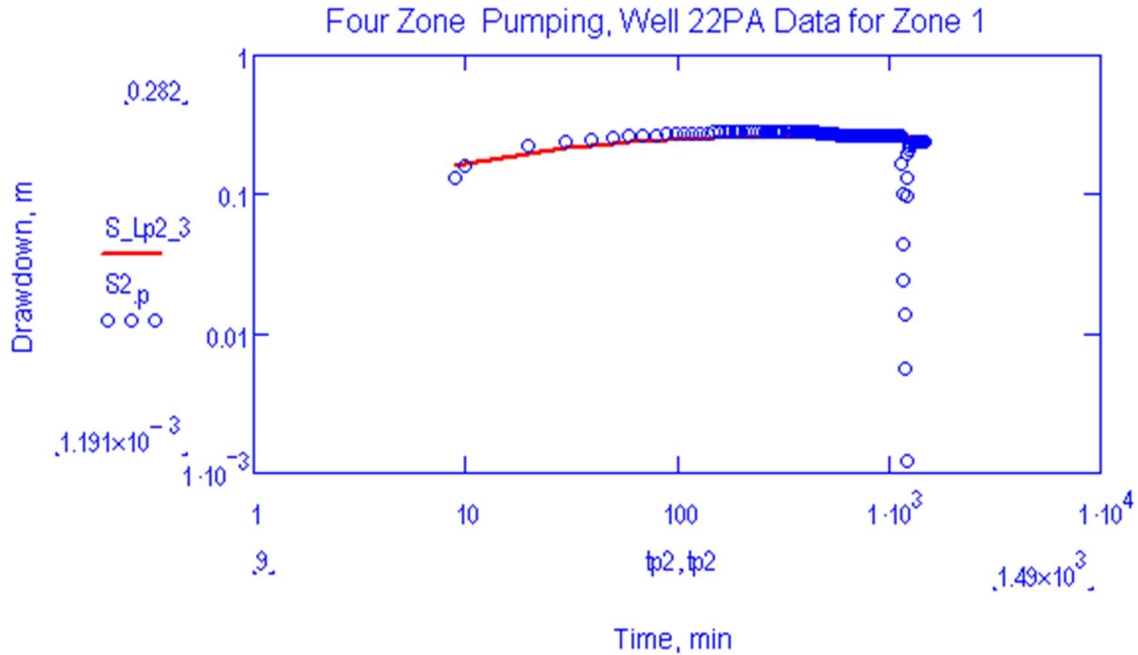
$$s_4 = 0.0003$$

$$\chi_{2-3} = 0.01$$

$$\chi_{3-4} = .02$$

$$\chi_0 = 0.15.$$

The measured and calculated drawdowns in zones 1+2, 3, and 4 are shown in Figure F-40. The root mean square error is 18.0 mm for zones 1 and 2, 14 mm for zone 3, and 14 mm for zone 4.



Output DTN: LA0701EK150304.001 (produced by MathCAD application *All Zones.xmcd*).

NOTE: Red solid line shows the calculated drawdowns and blue circles show the drawdowns during pumping period.

Figure F-40. Combined Zone Pumping Test, Three-Aquifer Solution

The estimated combined transmissivity of zones 1 and 2 is 1,000 m²/day. The combined thickness of zones 1 and 2, and the layer between them is 77.1 m. Consequently, the average hydraulic conductivity is 13.0 m/day. This value is in good agreement with previous estimates. The other parameter estimates are in a good agreement with the previous estimates as well (see Table F-4).

Table F-4. Summary of the Parameter Estimates for Nye County Site 22

Parameter Notation	Zone 1 Pumping Test			Zone 2 Pumping Test			Zone 3 Pumping Test			Zone 4 Pumping Test			All Four Zones Pumping Test	Range	Average	Questa Engineering Company 2003 [DIRS 178565], Table 2	Questa Engineering Company 2004 [DIRS 178566], Table 3
	Leaky Aquifer	Two-Aquifer System	Three-Aquifer System	Leaky Aquifer	Three-Aquifer System	Three-Aquifer System	Leaky Aquifer	Three-Aquifer System	Leaky Aquifer	Three-Aquifer System	Leaky Aquifer	Two-Aquifer System					
X_0, day^{-1}	—	0.15	0.15	—	0.15	—	—	—	—	—	—	—	0.15	0.15	—	—	—
$T_1, \text{m}^2/\text{day}$	264	280	280	—	280	—	—	—	—	—	—	—	—	276	316	242	—
s_1	.0013	.0017	.0017	—	.0017	—	—	—	—	—	—	—	—	—	.0016	.00116	—
X_{1-2}, day^{-1}	—	0.10	0.10	—	0.10	—	—	0.10	—	—	—	—	—	0.10	—	—	—
$T_2, \text{m}^2/\text{day}$	—	600	600	325	400	—	—	450	—	—	—	—	—	475	550	427	—
s_2	—	0.003	0.003	.00061	0.0006	—	—	0.003	—	—	—	—	—	—	.00031	.00035	—
X_{2-3}, day^{-1}	—	0.01	0.01	—	0.01	—	—	0.01	—	—	0.01	—	0.01	0.01	—	—	—
$T_3, \text{m}^2/\text{day}$	—	—	170	—	170	133	133	133	—	—	180	—	130	153	237	139	—
s_3	—	—	0.0003	—	0.0003	.00021	.00021	.000216	—	.00022	.00022	.00022	.0002	.00026	.00002	.0001	—
X_{3-4}, day^{-1}	—	—	—	—	—	—	—	0.0026	0.0023	0.0018	0.0018	—	.0018	0.0022	—	0.0035	—
$T_4, \text{m}^2/\text{day}$	—	—	—	—	—	—	—	250	200	200	200	200	200	225	269	185	—
s_4	—	—	—	—	—	—	—	0.0003	.00035	0.0003	0.0003	0.0003	.0003	.00031	.00023	.00021	—
$X_0 + X_{1-2}, \text{day}^{-1}$	0.25	—	—	—	—	—	—	—	—	—	—	—	—	—	—	0.31	—
$X_{01-2} + X_{2-3}, \text{day}^{-1}$	—	—	—	0.12	—	—	—	—	—	—	—	—	—	—	—	0.059	—

Table F-4. Summary of the Parameter Estimates for Nye County Site 22 (Continued)

Parameter Notation	Zone 1 Pumping Test		Zone 2 Pumping Test		Zone 3 Pumping Test		Zone 4 Pumping Test		All Four Zones Pumping Test	Range	Average	Questa Engineering Company 2003 [DIRS 178565], Table 2	Questa Engineering Company 2004 [DIRS 178566], Table 3
	Leaky Aquifer System	Two- Aquifer System	Leaky Aquifer System	Three- Aquifer System	Leaky Aquifer System	Three- Aquifer System	Leaky Aquifer System	Two- Aquifer System					
$X_{day}^{2-3} + X_{day}^{3-4}$	—	—	—	—	0.0126	—	—	—	—	—	—	—	0.0119
$T_1 + T_2$, m ² /day	—	—	—	—	—	—	—	—	1,000	—	—	—	—
s_{1-2}	—	—	—	—	—	—	—	—	0.003	—	—	—	—

Output DTN: LA0701EK150304.001.

NOTES: χ_0 = ratio of the hydraulic conductivity in m/day and thickness in m of the layer above zone 1; T_i = transmissivity of zone i in m²/d; s_i = storativity of zone i; X_{ij} = the ratio of the hydraulic conductivity in m/day and thickness in m of the layer between zones i and j; $T_1 + T_2$ = the transmissivity of the combined zone 1 and zone 2; s_{1-2} = s storativity of combined zone 1 and zone 2.

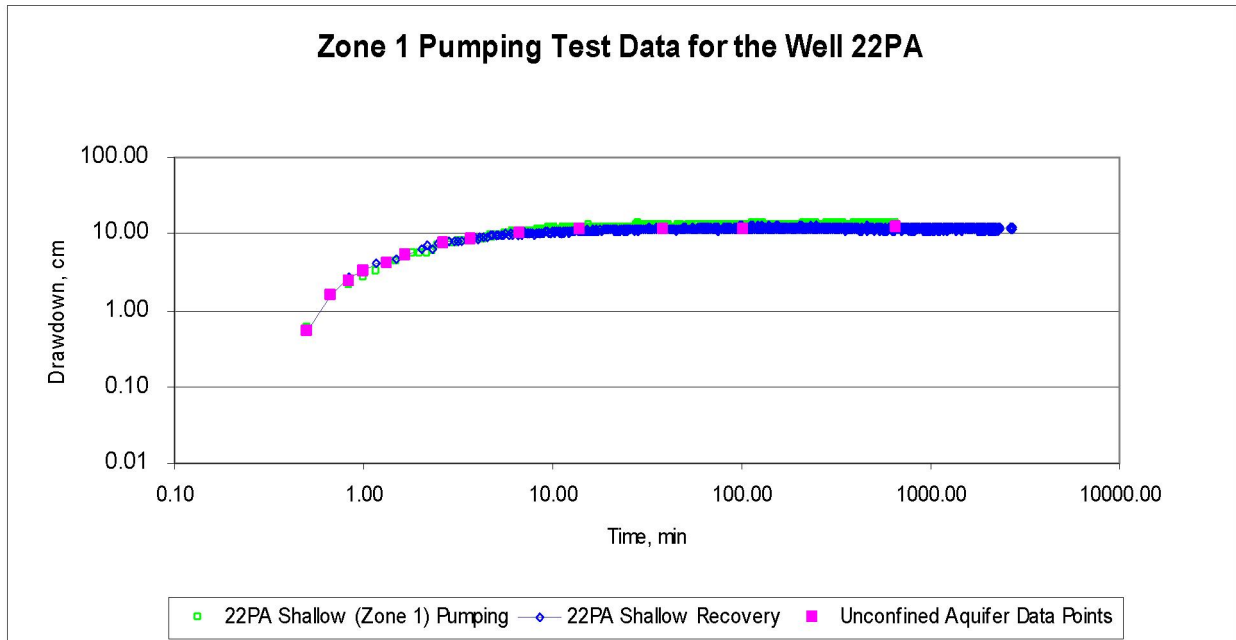
F6.8 CORROBORATION OF THE RESULTS USING ALTERNATIVE CONCEPTUAL MODEL

As discussed above, the results obtained for zones 1 and 2 suggest unconfined conditions in these two zones. Zones 1 and 2 have very similar hydraulic properties and are well connected hydraulically. An alternative conceptual model for these two zones is an unconfined aquifer model with vertical anisotropy. This model was implemented using the unqualified code AQTESOLV, which incorporates the Neuman solution for an unconfined homogeneous aquifer with non-fully penetrating pumping and observation wells (Neuman 1972 [DIRS150321]). The student version of this code is available from *Applied Hydrology* (Fetter 2001 [DIRS 156668]). This version has limitations on the number of data points it can accept and the methods it will implement.

Two analyses were conducted, as discussed below. In both cases, zones 1 and 2 were assumed to be a combined homogeneous aquifer with a thickness of 121.3 m (the distance from the water table to the top of zone 3).

F6.8.1 Pumping Test from Zone 1

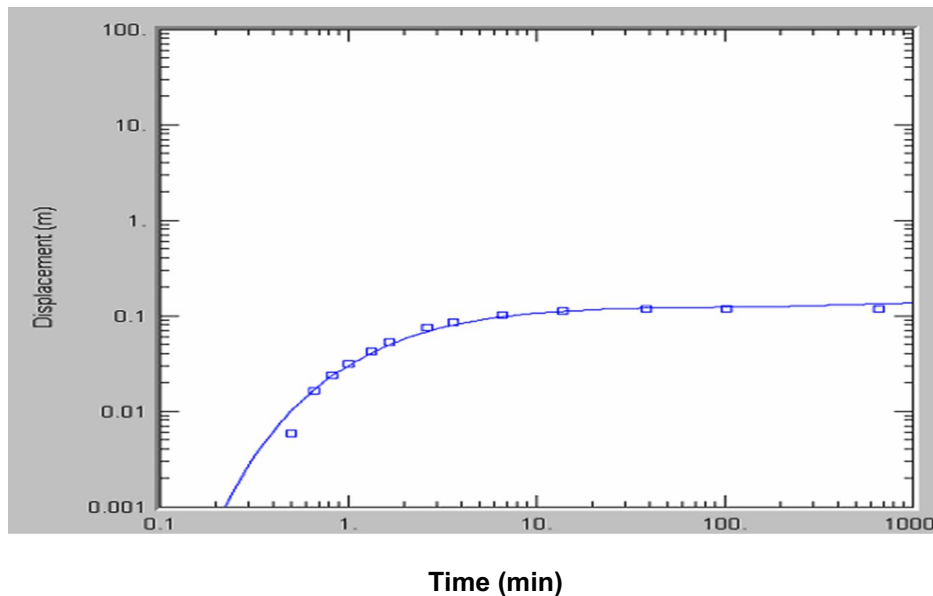
Zone 1 in well 22S was defined as a non-fully penetrating well with the top being 12.5 m below the water table and the bottom being 34.7 m below the water table (this corresponds to the zone 1 location). The monitoring well 22PA shallow (zone 1) was defined the same way. Twenty-five points were selected from the drawdown data to define the shape of the drawdown curve in 22PA shallow (see Figure F-41). These data were used in AQTESOLV calculations. The obtained match between the calculated and observed drawdowns is shown in Figure F-42. A good visual match is apparent for this conceptual model. The estimated combined transmissivity of zones 1 and 2 is $836 \text{ m}^2/\text{day}$. The vertical anisotropy ratio is 1.8. These estimates are in good agreement with the ones obtained from the multiple-aquifer and multiple-layer model solutions. The combined transmissivity of zone 1 and zone 2 based on these estimates ranges from $590 \text{ m}^2/\text{day}$ to $1,000 \text{ m}^2/\text{day}$. The vertical anisotropy ranges from 1.1 to 1.7 in the multiple-layer case.



Output DTN: LA0701EK150304.001 (*Zone 1.xls*).

NOTE: Red solid line shows the calculated drawdowns; blue diamonds show the drawdowns during pumping period; and green dots show the drawdowns during the recovery period. Drawdowns in well 22PA shallow, zone 1.

Figure F-41. Pumping Test from Zone 1, Unconfined Aquifer Conceptual Model



Output DTN: LA0701EK150304.001 (*Zone1 Unc.aqt*).

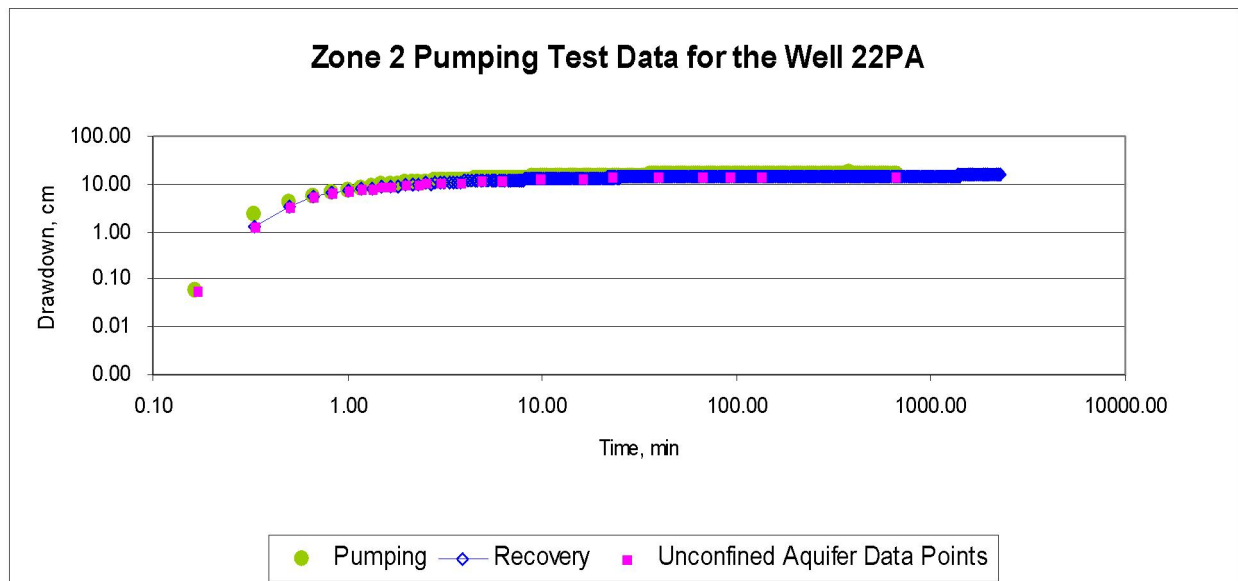
NOTE: Drawdowns in well 22PA shallow, zone 1.

Figure F-42. Pumping Test from Zone 1, Unconfined Aquifer Conceptual Model

F6.8.2 Pumping Test from Zone 2

Zone 2 in 22S was defined as a non-fully penetrating well with the top being 54.7 m below the water table and the bottom being 89.6 m below the water table (this corresponds to the zone 2 location). The monitoring well 22PA deep (zone 2) was defined the same way. Twenty-five points were selected from the drawdown data to define the shape of the drawdown curve in 22PA deep (see Figure F-43). These data were used in the AQTESOLV calculations. The obtained match between the calculated and observed drawdown is shown in Figure F-44. A good visual match is apparent for this conceptual model. The estimated combined transmissivity of zone 1 and 2 is $842 \text{ m}^2/\text{day}$, and the vertical anisotropy ratio is 1.8, which is very close to the parameter estimates from the zone 1 pumping test.

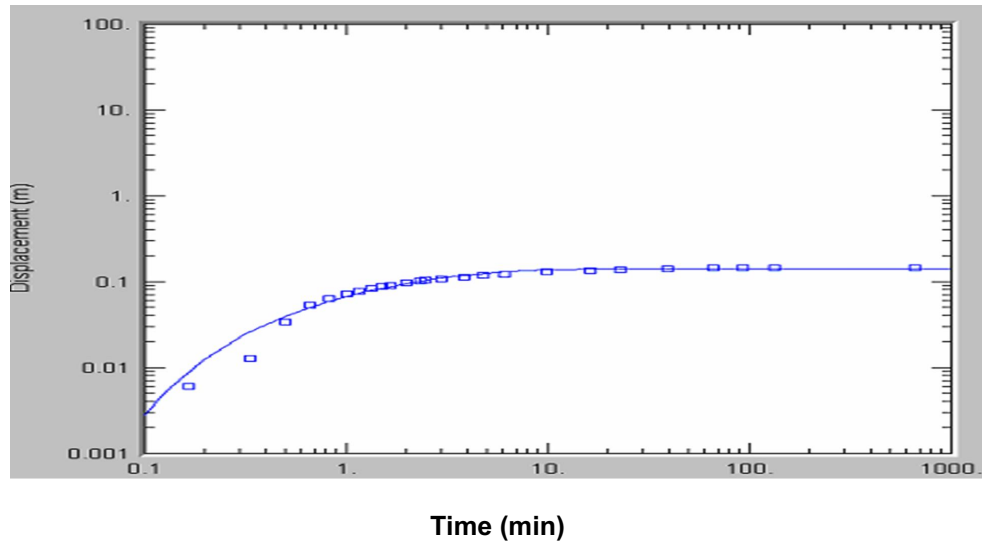
The good match of the unconfined aquifer solution to the zone 1 and zone 2 pump test data corroborate the multiple-aquifer and multiple-layer interpretations that these zones behave as part of the same unconfined aquifer.



Output DTN: LA0701EK150304.001 (Zone 2.xls).

NOTE: Drawdowns in well 22PA deep, Zone 2.

Figure F-43. Pumping Test from Zone 2, Unconfined Aquifer Conceptual Model



Output DTN: LA0701EK150304.001 (*Zone2 Unc.aqt*).

NOTE: Drawdowns in well 22PA shallow, zone 1.

Figure F-44. Pumping Test from Zone 1, Unconfined Aquifer Conceptual Model

F6.9 WELL EFFICIENCY ESTIMATION USING THE DRAWDOWN DATA IN THE PUMPING WELL (WELL 22S)

The following simplified approach was used to evaluate pumping well efficiency. The steady-state drawdown (S_{max}) in the pumping well in the case of a leaky aquifer conceptual model can be defined as (Hantush 1956 [DIRS 165169]):

$$S_{max} = \frac{Q}{2\pi T} K_0\left(\frac{r_w}{B}\right) \quad (\text{Eq. F-40})$$

where r_w is the pumping well radius and other parameters were previously defined. When r_w/B is small (less than 0.1), the following approximation can be used:

$$K_0\left(\frac{r_w}{B}\right) = -\log\left(\frac{r_w}{B}\right) + 0.116 \quad (\text{Eq. F-41})$$

and

$$S_{max} = \frac{Q}{2\pi T} \log\left(\frac{1.12B}{r_w}\right)$$

This approximation is applicable to all the pumping tests ($r_w/B \ll 0.1$ in all the cases). The simplified effects of the well skin and wellbore storage, can be accounted by introducing well efficiency coefficient ε . Equation F-41 can be then modified as:

$$S_{max} = \frac{Q}{2\pi T \varepsilon} \log\left(\frac{1.12B}{r_w}\right) \quad (\text{Eq. F-42})$$

Well efficiency can be estimated from equation F-42 as:

$$\varepsilon = \frac{Q}{2\pi TS_{\max}} \log\left(\frac{1.12B}{r_w}\right) \quad (\text{Eq. F-43})$$

Equation F-43 was used to estimate well efficiencies in all 5 pumping tests. The maximum drawdown in 22S observed in each test was used in these estimations. The calculations were done for the transmissivity ranges obtained from the multiple-aquifer and multiple-layer solutions. The leakage factor B was set equal to the leakage factor obtained from the corresponding leaky aquifer solution. In the case when all four zones were pumped, the combined transmissivity (sum of transmissivities in all four zones) was used. The leakage factor B was calculated using equation F-26 assuming that $\chi_{1-2}=0.15$ (influx from the water table) and $\chi_{2-3}=0.0$ (no flow boundary condition at the bottom). The resulting well efficiencies are provided below. The numbers in the parentheses are the well efficiencies estimated in *Analysis of Aquifer Pump Tests in Individual Well Zones at Site 22 Near Yucca Mountain, Nevada* (Questa Engineering Corporation 2004 [DIRS 178566]):

- Zone 1 Pumping Test: $\varepsilon=25.8\%$ to 27.5% (30%)
- Zone 2 Pumping Test: $\varepsilon=10.5\%$ to 17.8% (16%)
- Zone 3 Pumping Test: $\varepsilon=21.6\%$ to 29.9% (27%)
- Zone 4 Pumping Test: $\varepsilon=11.6\%$ to 14.6% (15%).

The average well efficiency weighted according to the individual zone thickness is 17.0%. The average well efficiency estimated in *Analysis of Aquifer Pump Tests in Individual Well Zones at Site 22 Near Yucca Mountain, Nevada* (Questa Engineering Corporation 2004 [DIRS 178566]) is 22%. The well efficiencies estimates in *Analysis of Aquifer Pump Tests in Individual Well Zones at Site 22 Near Yucca Mountain, Nevada* (Questa Engineering Corporation 2004 [DIRS 178566]) agree with the well efficiency ranges estimated using this simplified approach.

The well efficiency calculated based on all four zone pumping is 16.8%. This is in good agreement with the average efficiency calculated from the individual zone pumping test.

F6.10 SUMMARY OF THE SITE 22 HYDRAULIC TEST DATA INTERPRETATION

The interpretation of the pumping tests conducted at Site 22 was performed using different conceptual models and different methods. As a result, there are a number of estimates for each parameter. In some cases up to 6 estimates for a parameter are available (see Table F-4). The range of parameter estimates reflects the uncertainties in the system conceptualizations and in the mathematical solutions employed. A summary of the parameter estimates is provided below.

As discussed earlier, the transmissivity and storativity of each aquifer (layer) and the parameters χ_{1-2} , χ_{2-3} , and χ_{3-4} are the same regardless which system conceptualization (multiple-aquifers or multiple-layers) is assumed. However, the hydraulic conductivities are different because the aquifer thickness is different from the layer thickness (see Figure F-28). Similarly, the hydraulic conductivity of a low permeability layer between aquifers in the multiple-aquifer conceptualization may be different from the vertical hydraulic conductivity of a horizontal layer

in the multiple-layer conceptualization. The following formulae were used in calculating vertical hydraulic conductivities in the multiple-layer conceptual model:

$$k_{v1} = \chi_{1-2} m_{1-2} \quad (\text{Eq. F-44})$$

$$k_{v2} = k_{v1}$$

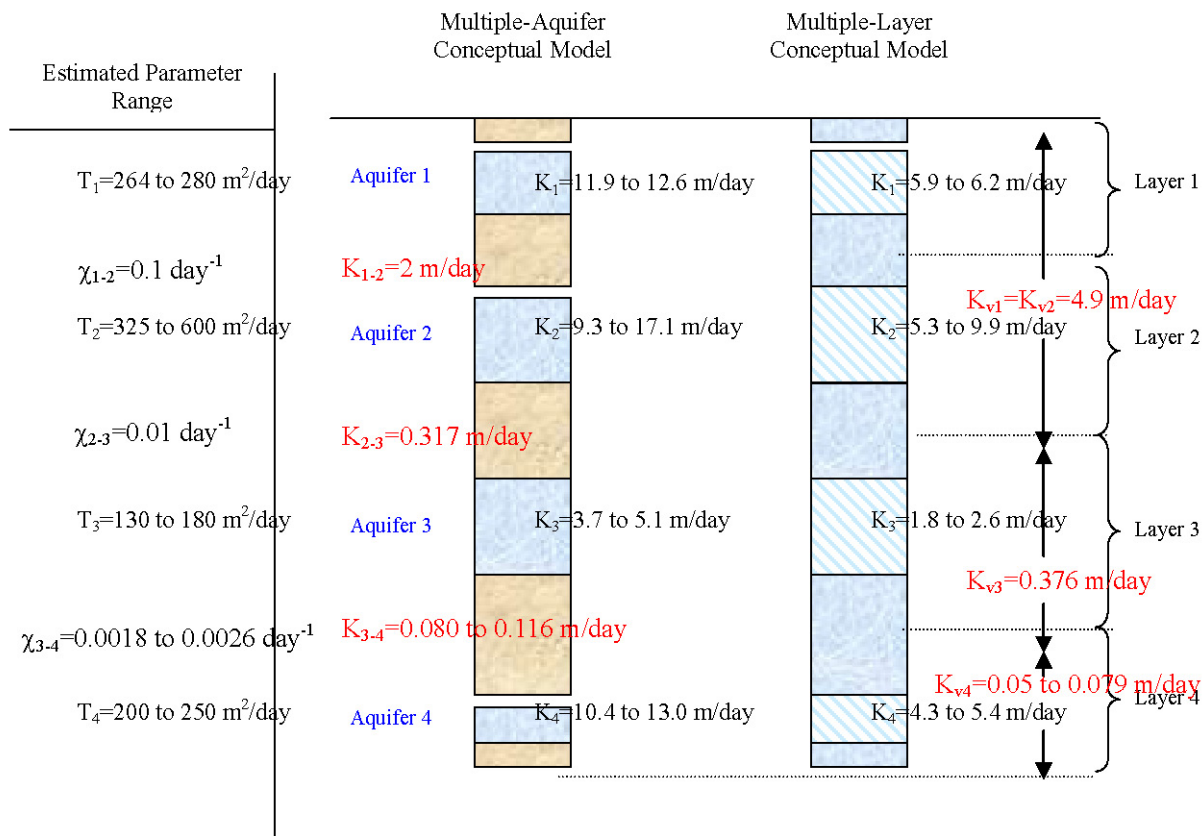
$$k_{v3} = \frac{k_{v2} m_3 \chi_{2-3}}{2k_{v2} - m_2 \chi_{2-3}}$$

$$k_{v4} = \frac{k_{v3} m_4 \chi_{3-4}}{2k_{v3} - m_3 \chi_{3-4}}$$

where m_{1-2} is the distance between the mid points of zone 1 and zone 2, m_3 is the layer 3 thickness, and m_4 is the layer 4 thickness. The range of hydraulic conductivities obtained for multiple-aquifer and multiple-layer models are shown in Figure F-45.

Five estimates of transmissivity were obtained for zone 1. The transmissivities range from 264 m²/day to 280 m²/day. The average transmissivity is 276 m²/day, assuming equal weight of each conceptual model. The transmissivity estimates for zone 1 obtained in *Preliminary Analysis of Pump-Spinner Tests and Pump Test in Well NC-EWDP-22S, Near Yucca Mountain, Nevada* (Questa Engineering Corporation 2003 [DIRS 178565]) and *Analysis of Aquifer Pump Tests in Individual Well Zones at Site 22 Near Yucca Mountain, Nevada* (Questa Engineering Corporation 2004 [DIRS 178566]) are 316 m²/day and 242 m²/day, respectively. The thickness of zone 1 is 22.2 m. Consequently, the hydraulic conductivity of zone 1 ranges from 11.4 m/day to 12.6 m/day assuming the multiple-aquifer system conceptualization. The average hydraulic conductivity is 12.4 m/d. The thickness of layer 1 is 45 m. Consequently, the hydraulic conductivity of layer 1 ranges from 5.9 m/day to 6.2 m/day assuming the multiple-layer system conceptualization with the transmissivity of zone 1 assigned to all of layer 1. The average hydraulic conductivity is 6.1 m/day.

Five estimates of transmissivity were obtained for zone 2. The transmissivities range from 325 m²/day to 600 m²/day. Assuming equal weight of each conceptual model, the average transmissivity is 475 m²/day. The transmissivity estimates of zone 2 obtained in *Preliminary Analysis of Pump-Spinner Tests and Pump Test in Well NC-EWDP-22S, Near Yucca Mountain, Nevada* (Questa Engineering Corporation 2003 [DIRS 178565]) and *Analysis of Aquifer Pump Tests in Individual Well Zones at Site 22 Near Yucca Mountain, Nevada* (Questa Engineering Corporation 2004 [DIRS 178566]) are 550 m²/day and 427 m²/day, respectively. The thickness of zone 2 is 35 m. Consequently, the hydraulic conductivity of zone 2 ranges from 9.3 m/day to 17.1 m/day assuming the multiple-aquifer system conceptualization. The average hydraulic conductivity is 13.6 m/day. The thickness of layer 2 is 60.9 m. Consequently, the hydraulic conductivity of layer 2 ranges from 5.3 m/day to 9.9 m/day assuming the multiple-layer system conceptualization with the transmissivity of zone 2 assigned to all of layer 2. The average hydraulic conductivity is 7.8 m/day.



Output DTN: LA0701EK150304.001.

Figure F-45. Hydraulic Conductivities Obtained for Multiple-Aquifer and Multiple-Layer Conceptual Models Based on the Estimated Parameter Ranges

The confining layer between zone 1 and zone 2 has a hydraulic conductivity of 2 m/day assuming that the thickness of this layer is 20 m. The parameter χ_{1-2} , from which the hydraulic conductivity of this layer is estimated, is 0.10 day⁻¹ to 0.11 day⁻¹. For the multiple-layer conceptualization, the vertical hydraulic conductivity estimate is 4.9 m/day for the two upper layers in the alluvium (Figure F-45).

Zones 1 and 2 are very well hydraulically connected, have similar hydraulic properties and exhibit unconfined aquifer behavior. It is concluded that zone 1 and zone 2 can be considered to be one unconfined aquifer with the average horizontal hydraulic conductivity of 7.1 m/day (multiple-layer conceptualization) and vertical anisotropy in hydraulic conductivity of 1.5. Because both zone 1 and zone 2 are unconfined, the storativity estimated from the conceptual models is considered a lumped parameter that has a value somewhere between the specific storage and specific yield. The specific yield can only be estimated in the case of an unconfined aquifer conceptual model since it is not a parameter of multiple-aquifer and multiple-layer conceptual models.

Six estimates of transmissivity were obtained for zone 3. The transmissivities range from 130 m²/day to 180 m²/day. Assuming equal weight of each conceptual model, the average transmissivity is 153 m²/day. The transmissivity estimates of zone 3 obtained in *Preliminary*

Analysis of Pump-Spinner Tests and Pump Test in Well NC-EWDP-22S, Near Yucca Mountain, Nevada (Questa Engineering Corporation 2003 [DIRS 178565]) and *Analysis of Aquifer Pump Tests in Individual Well Zones at Site 22 Near Yucca Mountain, Nevada* (Questa Engineering Corporation 2004 [DIRS 178566]) are 237 m²/day and 139 m²/day, respectively. The thickness of zone 3 is 35.5 m. Consequently, the hydraulic conductivity of zone 3 ranges from 3.7 m/day to 5.1 m/day assuming the multiple-aquifer system conceptualization. The average hydraulic conductivity is 4.3 m/day. This is significantly lower than the hydraulic conductivity of the two upper zones. The thickness of layer 3 is 70.6 m. Consequently, the hydraulic conductivity of layer 3 ranges from 1.8 m/day to 2.6 m/day assuming the multiple-layer system conceptualization with the transmissivity of zone 3 assigned to all of layer 3. The average hydraulic conductivity is 2.2 m/day. This is significantly lower than the hydraulic conductivity of the two upper zones.

The layer between zones 2 and 3 has a significantly lower hydraulic conductivity than the layer between zones 1 and 2. The vertical conductivity is 0.317 m/day assuming that the thickness of this layer is 31.7 m. The parameter χ_{2-3} , from which the hydraulic conductivity of this layer is estimated is 0.01 day⁻¹. In the case of the multiple-layer system conceptualization, the vertical hydraulic conductivity of layer 3 calculated using formula (F-71) is 0.376 m/day.

Zone 3 is separated from the upper portion of the alluvial deposits by a layer with a noticeably lower permeability, and it exhibits confined aquifer behavior. Consequently, the storativity estimates obtained from the different conceptual models represent the actual specific storage. The storativity values range from 0.00022 to 0.0003. The average storativity is 0.00026 based on six estimates. The storativity values of zone 3 obtained in *Preliminary Analysis of Pump-Spinner Tests and Pump Test in Well NC-EWDP-22S, Near Yucca Mountain, Nevada* (Questa Engineering Corporation 2003 [DIRS 178565]) and *Analysis of Aquifer Pump Tests in Individual Well Zones at Site 22 Near Yucca Mountain, Nevada* (Questa Engineering Corporation 2004 [DIRS 178566]) are 0.00002 and 0.0001, respectively.

Four estimates of transmissivity were obtained for zone 4. The transmissivities range from 200 m²/day to 250 m²/day. The average transmissivity is 225 m²/day, assuming equal weight of each conceptual model. The transmissivity values of zone 4 obtained in *Preliminary Analysis of Pump-Spinner Tests and Pump Test in Well NC-EWDP-22S, Near Yucca Mountain, Nevada* (Questa Engineering Corporation 2003 [DIRS 178565]) and *Analysis of Aquifer Pump Tests in Individual Well Zones at Site 22 Near Yucca Mountain, Nevada* (Questa Engineering Corporation 2004 [DIRS 178566]) are 269 m²/day and 185 m²/day, respectively. The thickness of zone 4 is 19.3 m. Consequently, the hydraulic conductivity of zone 4 ranges from 10.3 m/day to 13.0 m/day. The average hydraulic conductivity is 11.7 m/day. The thickness of layer 4 is 46 m. Consequently, the hydraulic conductivity of layer 4 ranges from 4.3 m/day to 5.4 m/day assuming the multiple-layer system conceptualization with the transmissivity of zone 4 assigned to all of layer 4. The average hydraulic conductivity is 4.9 m/day. This is very similar to the hydraulic conductivity of the two upper zones. Zone 4 is identified as volcanic breccia deposits. As such, it may have properties similar to the alluvial deposits.

The layer between zones 3 and 4 has even lower hydraulic conductivity than the layer between zones 2 and 3. The parameter χ_{3-4} , from which the hydraulic conductivity of this layer is estimated ranges from 0.0018 day⁻¹ to 0.0026 day⁻¹. The conductivity is estimated as

0.080 m/day to 0.115 m/day, assuming that the thickness of the layer is 44.6 m. For the multiple-layer conceptualization, the vertical hydraulic conductivity calculated using formula (F-71) ranges from 0.050 m/day to 0.079 m/day.

The storativity values of zone 4 range from 0.00030 to 0.00035. The average storativity is 0.00031 based on four estimates. The storativity values of zone 4 obtained in *Preliminary Analysis of Pump-Spinner Tests and Pump Test in Well NC-EWDP-22S, Near Yucca Mountain, Nevada* (Questa Engineering Corporation 2003 [DIRS 178565]) and *Analysis of Aquifer Pump Tests in Individual Well Zones at Site 22 Near Yucca Mountain, Nevada* (Questa Engineering Corporation 2004 [DIRS 178566]) are 0.00023 and 0.00021, respectively.

F7. CONCLUSIONS REGARDING HYDRAULIC PARAMETERS AND THE CONCEPTUAL FLOW MODEL IN THE SATURATED ALLUVIUM BASED ON HYDRAULIC TESTING

The hydraulic test data at Site 22 indicate that the upper ~90 m of saturated alluvium at this location behave as an unconfined aquifer with a horizontal hydraulic conductivity of ~11 m/day to 14 m/day and a vertical anisotropy ratio (K_h/K_z) of about 1.5 to 2 (the horizontal hydraulic conductivity is only ~6 m/day to 8 m/day if a layered conceptualization is applied and the combined transmissivity of zones 1 and 2 is assigned to all of layers 1 and 2. If zones 1 and 2 are considered to be separate aquifers that are separated by a semi-confining layer, the average horizontal hydraulic conductivity estimates of the individual zones are 12.4 and 13.6 m/day, respectively, and the vertical conductivity of the intervening layer is about 2 m/day. The lower ~75 m of saturated alluvium at this location has a considerably lower horizontal hydraulic conductivity (4.3 m/day for zone 3, assuming it is an isolated aquifer) with a vertical anisotropy ratio of at least 10 based on the vertical hydraulic conductivity estimate for the intervening alluvium material between zones 2 and 3 (a larger vertical anisotropy ratio is obtained if the vertical conductivity is based on the intervening material between zones 3 and 4). Test zone 3 is effectively confined by alluvium layers of low vertical hydraulic conductivity above and below (although the confinement from below could be provided by the top of the underlying volcanic breccia unit). The horizontal hydraulic conductivity of the volcanic breccia underlying the alluvium at Site 22 is estimated to be 11.7 m/day, which is comparable to that of the upper alluvium.

Cross-hole hydraulic responses to pumping all four alluvium test intervals simultaneously at the ATC resulted in a confined-aquifer response with a horizontal hydraulic conductivity estimate of ~2.5 m/day, which is about a factor of 5 lower than the two upper alluvium zones at Site 22, but comparable to the deepest alluvium zone at Site 22. Additionally, a short-duration cross-hole pumping test at NC-EWDP-10S (located along Fortymile Wash about 2 miles north-northeast of Site 22 and using borehole 10P as an observation well) indicated a horizontal hydraulic conductivity in the single alluvium zone at this location of about 3 m/day (Swanson 2006 [DIRS 179627]), which is comparable to the horizontal conductivity deduced at both the ATC and in the deepest alluvium zone at Site 22. This test was not analyzed by project staff, so it is not discussed elsewhere in this analysis report. The 10S-10P test was not conducted long enough to determine whether the aquifer at this location behaved as a confined or unconfined system, and the Nye County interpretation (Swanson 2006 [DIRS 179627]) indicated that there was a nearby constant head boundary encountered during the test. The entire saturated alluvium

section at 10S is only about 200-ft (60-m) thick, and the bottom of the alluvium test interval (screened interval) is only 130 ft (40 m) below the water table.

The entire saturated alluvium section at Site 22 has a composite horizontal hydraulic conductivity of about 5.0 m/day with a vertical anisotropy ratio of ~13. This composite horizontal hydraulic conductivity is taken to be $K_h = \sum_{i=1,3,5} \frac{K_{hi} b_i}{b_{Total}}$ (Freeze and Cherry 1979

[DIRS 101173], p. 34), where K_{hi} = horizontal hydraulic conductivity of layer i , b_i = thickness of layer i , and $i = 1,3,5$ indicates that the layers considered are from the top of test zone 1 to the bottom of the confining layer between zones 3 and 4 at Site 22. This equation is a mathematical statement of the well-known result that the sum of the transmissivities of multiple adjacent horizontal layers ($K_{hi} b_i$) is equal to the total transmissivity of the combined layers, and the composite horizontal hydraulic conductivity of the assemblage of layers is equal to the total transmissivity divided by the total combined thickness of the layers. In this case, the “layers” include both aquifers and confining layers using the multiple-aquifer system conceptualization discussed above. Similarly, the composite vertical hydraulic conductivity used to estimate the vertical anisotropy ratio is taken to be $K_v = \sum_{i=1,3,5} \frac{b_{Total}}{b_i / K_{vi}}$ (Freeze and Cherry 1979

[DIRS 101173], p. 34). This equation is readily derived from the following logical steps:

(i) For horizontal layers in series, rearrangement of Darcy’s equation (Freeze and Cherry 1979 [DIRS 101173], p. 16) yields, $K_v = \frac{Q b_{Total}}{A \Delta H_{Total}}$, where K_v = composite vertical hydraulic conductivity through all combined layers, Q = vertical volumetric flow rate through the layers, A = cross-sectional area perpendicular to flow, and ΔH_{Total} = head difference across all layers.

(ii) Given that the discharge rate (Q/A) through each individual layer (and through all combined layers) must be the same, and the total head difference across all layers is equal to the sum of the head differences across each individual layer, Darcy’s equation also yields $\Delta H_{Total} = \sum_i \Delta H_i = \sum_i \frac{Q}{A} \left(\frac{b_i}{K_{vi}} \right) = \frac{Q}{A} \sum_i \left(\frac{b_i}{K_{vi}} \right)$, where ΔH_i = head difference across layer i .

(iii) Combining (i) and (ii) yields $K_v = \sum_i \frac{b_{Total}}{b_i / K_{vi}}$, which is the equation given above for the composite vertical hydraulic conductivity (Freeze and Cherry 1979 [DIRS 101173], p. 34).

The hydraulic conductivity estimates presented in the previous section were used for these calculations. These composite estimates assume that horizontal hydraulic conductivities in the confining layers between aquifers are the same as the estimated vertical hydraulic conductivities of these confining layers and that the vertical conductivities within the aquifers (test zones) are the same as the estimated horizontal conductivities of these zones (i.e., isotropy is assumed within each “layer”). These assumptions likely result in underestimation of the composite horizontal hydraulic conductivity and possibly also underestimation of the composite vertical anisotropy ratio because there is likely some vertical anisotropy within each layer. Nevertheless,

if the alluvium is lumped as one continuous unit in the SZ flow model, these composite parameter estimates are appropriate values to compare with parameters obtained from calibration of the site-scale flow model (at the Site 22 location). Alternatively, one might consider a conductivity of ~ 14 m/day (the largest horizontal conductivity measured in any individual zone) to be a reasonable upper bound estimate of the composite horizontal hydraulic conductivity at Site 22 given that a direct measurement of horizontal conductivities in the layers between test zones was not possible. This allows for the possibility that the layers between zones have large vertical anisotropy ratios (providing vertical confinement, but allowing considerable horizontal flow).

The fact that the upper alluvium and lower alluvium at Site 22 behave according to different conceptual hydrologic models (unconfined vs. leaky-confined aquifers) underscores the heterogeneous nature of the saturated alluvium south of Yucca Mountain. Because Site 22 is the only alluvium location at which detailed cross-hole hydraulic testing has been conducted, extrapolating the local behavior at this site to other alluvium locations is very uncertain. However, the one cross-hole hydraulic test at the ATC also indicated confined-aquifer flow conditions in the alluvium, and the large upward hydraulic gradient at the ATC is consistent with the presence of confining layers in the alluvium at this location.

Based on the Site 22 hydraulic test results and the limited observations at the ATC, a reasonable generalized conceptual model of flow in the saturated alluvium is that of an unconfined aquifer with a relatively small vertical anisotropy ratio (2 to 3) near the water table with a transition to leaky-confined or confined aquifer behavior with a correspondingly large vertical anisotropy ratio (10 or more) beneath the shallowest confining layer. The depth at which the shallowest major confining layer is likely to be encountered (at different locations) and the lateral extent of such layers must be considered very uncertain at the present time. The layers offering the greatest confinement in the alluvium depositional setting south of Yucca Mountain are likely to be old lake beds or playas where fine sediments tend to accumulate, and these would be expected to occur at varying depths and over varying spatial extents depending on the details of the depositional history, past climate fluctuations, and how much structural reworking of the sediments has occurred. Layered cementation (e.g., by localized calcite precipitation) within the alluvium is another possible mechanism that could result in confining layers, but, as with the lakebed or playa mechanism, the depth and extent of such layers cannot be readily predicted.

Perhaps the most important implication of the 22S hydraulic test results for radionuclide transport in the alluvium is that vertical flow, and hence vertical dispersion of solutes, is likely to be limited by vertical anisotropy and/or horizontal layering within the flow system. The hydraulic test results, coupled with general observations of upward hydraulic gradients in the alluvium (although with different magnitudes at different locations), suggest that solutes that enter the alluvium near the water table are likely to remain near the water table, and solutes that enter deeper within the alluvium, especially if they are below an extensive confining layer, are likely to remain deeper.

F8. CORROBORATION OF THE ALLUVIUM CONCEPTUAL FLOW MODEL USING GEOCHEMICAL DATA

Groundwater samples have been collected and analyzed for major and minor constituents for many years and from numerous locations and depths in the saturated zone in the vicinity of Yucca Mountain. These efforts have resulted in a fairly comprehensive understanding of saturated zone flow pathways in the Yucca Mountain area that are useful for corroborating flow model predictions based on head data, hydraulic test data, and inferred boundary conditions from larger-scale regional models. Here a summary of how the geochemical data from the ATC and Site 22 support the conceptualization of flow at these two locations which was summarized in the previous section is provided. A detailed summary of the geochemical data and how it supports the SZ site scale flow model is provided in Appendices A and B of *Saturated Zone Site-Scale Flow Model* (SNL 2007 [DIRS 177391]). The reader is referred to those appendices for a more general discussion of geochemical data over the entire Yucca Mountain saturated zone flow system.

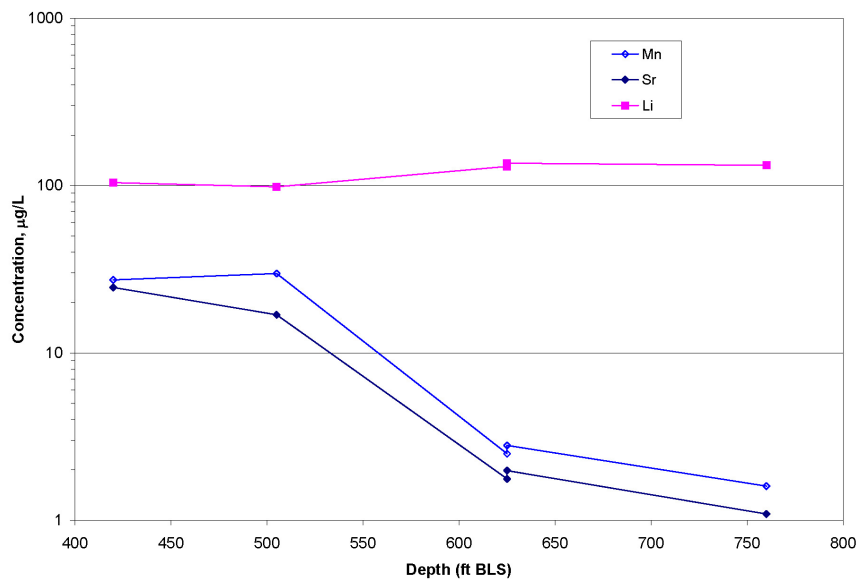
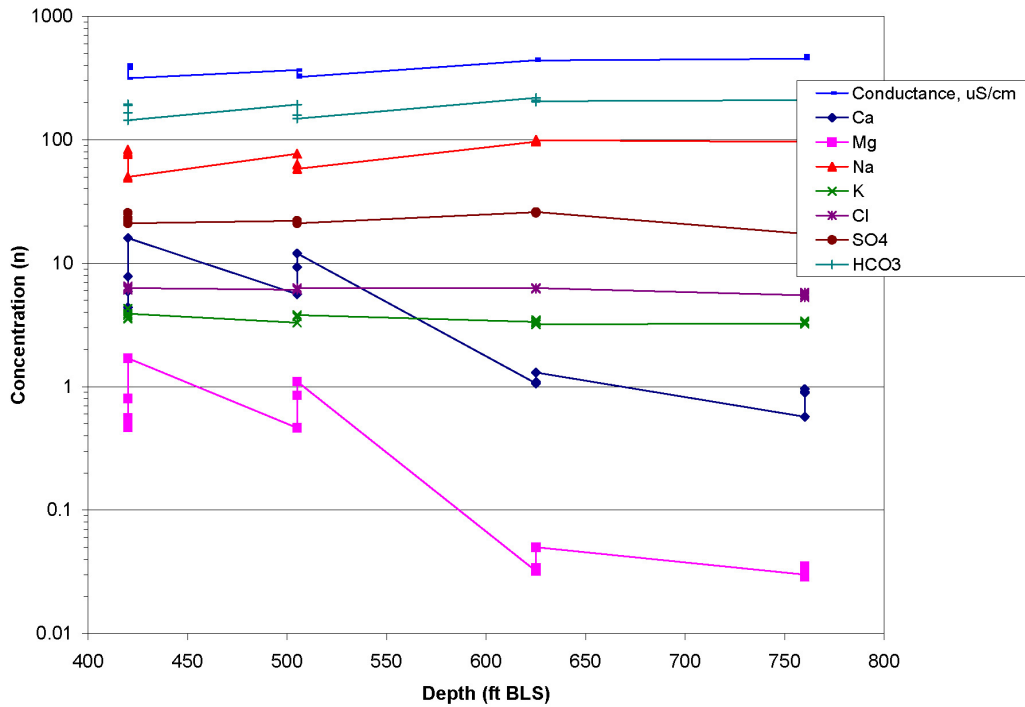
In addition to sampling the upper four zones in 19D and 19IM1 at the ATC site and the four zones in 22S plus the two zones in both 22PA and 22PB, pore water samples were extracted (by centrifugation) for geochemical analyses from the saturated sonic “core” that was obtained from boreholes 19PB and 22PC (Patterson et al. 2006 [DIRS 178743]). These sonic core samples provided much finer resolution geochemical depth profiles than is possible with bulk samples obtained from screened intervals in wells. However, because of limitations in the sonic coring technology, these boreholes extend to only the bottom of the second interval from the surface at both the ATC and Site 22 locations. Thus, the detailed geochemical profiles from the sonic cores exist only for approximately the upper half of the saturated alluvium at each location.

Figure F-46 shows depth profiles of major and minor ions in 19D and 19IM1, and Figure F-47 shows profiles from 19PB (upper half of alluvium at this location). It is apparent in Figure F-46 that there is a drop in multivalent cation concentrations and a noticeable increase in sodium concentrations with depth in the alluvium at this location (note the log concentration axes). Anion concentrations do not change as much with depth. A significant decrease in multivalent cation concentrations occurs somewhere between zones 2 and 3 in 19D and 19IM1, and there is a strong suggestion from the sonic core samples that the decrease starts near the bottom of 19PB (although the minor cation concentrations fluctuate quite a bit in the lower portion of 19PB, indicating possible finer-scale flow layering – see Figure F-47). The higher multivalent cation concentrations at shallow depths at the ATC location have been interpreted as an infiltration signature from Fortymile Wash, and the lower multivalent cation concentrations at greater depths are interpreted as a signature of water originating from near Yucca Mountain (Patterson et al. 2006 [DIRS 178743]). The depletion of multivalent cations in the deeper waters is attributed to the movement of water through clays and/or zeolites during its transit from upgradient location(s). Stable and natural radioactive isotope data (not presented here) don’t strongly support or refute this interpretation (although there is a hint of somewhat older waters as depth increases based on ^{14}C analysis).

The different cation signatures in the shallow and deep alluvium at the ATC suggest some stratification of the aquifer at this location. It is unfortunate that no isolated interval cross-hole hydraulic tests were conducted in the shallower zones at the ATC to test for the possible

existence of the confining layer between zones 2 and 3 that is suggested by the geochemical data. The fact that the combined-interval cross-hole hydraulic test at the ATC resulted in a confined aquifer response seems to suggest that a confining layer must exist near the top of the saturated section at this location. However, it must be remembered that the third and fourth zones from the surface produced most of the water in 19D when all the alluvium zones were pumped together, so the existence of a confining layer between zones 2 and 3 could have resulted in a confined aquifer response from pumping the combined intervals.

Figure F-48 shows depth profiles of major and minor ions from samples collected in 22S, 22PA, and 22PB, and Figure F-49 shows profiles from the 22PC sonic core over depths that correspond to the two shallower screened intervals in 22S. It is apparent that, other than a spike in concentration of many ions right at the water table (consistent with some evaporation) there is no significant difference with depth in the major ion geochemistry of the groundwater samples collected from screened intervals (Figure F-48) as at the ATC location. An infiltration signature similar to that at the ATC location is not apparent at Site 22 despite the fact that the latter location is just as close to Fortymile wash as is the ATC. The stable and natural radioactive isotope data corroborate this result. However, the higher resolution profiles from the 22PC sonic core indicate some trends in minor cation concentrations with depth as well as the possible existence of relatively narrow intervals that have different geochemical signatures than the groundwater immediately above and below them. The most obvious examples of the latter are at about 620 ft and 700 ft below ground surface, where monovalent cation, major anion, and minor cation concentrations spike slightly. There is also a general tendency for the minor cations to increase in concentration with depth throughout the 22PC profile. However, 22S, 22PA, and 22PB samples show no significant change in geochemistry between zones 2 and 3 or between zones 3 and 4, where the existence of confining layers are deduced from the hydraulic test results.

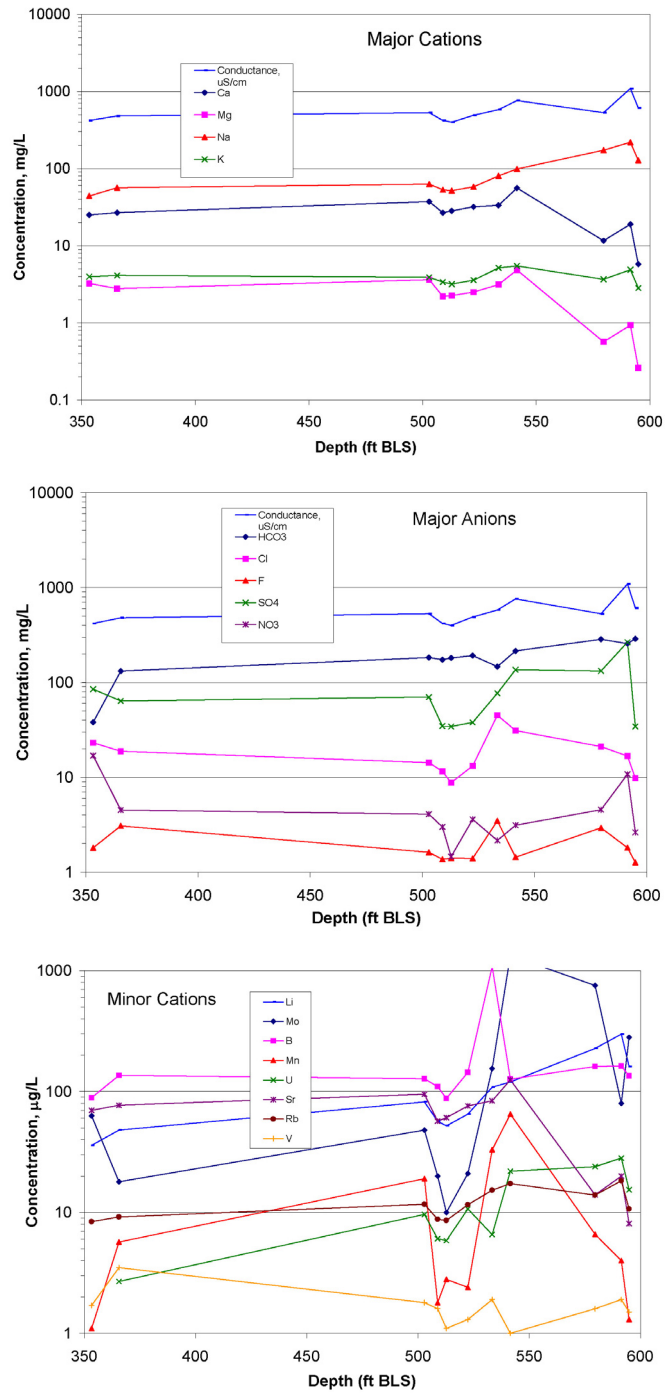


Sources: DTNs: GS011108312322.006 (19D data) [DIRS 162911], GS040108312322.001 (19IM1 data) [DIRS 179422].

Output DTN: LA0704PR150304.001.

NOTES: Depths correspond to the midpoints of screened intervals, and the data points do not distinguish between 19D and 19IM1. Plots show multiple samples from same interval when available. All divalent cations show a distinct decrease in concentration below zone 2 (505 ft), and sodium shows a corresponding increase below this depth, although this increase is not easy to see because of the generally high sodium concentrations and the log concentration axis. Note the log concentration scales.

Figure F-46. Geochemistry Depth Profiles of Major Cations and Anions (upper) and Minor Cations (lower) in Boreholes 19D and 19IM1

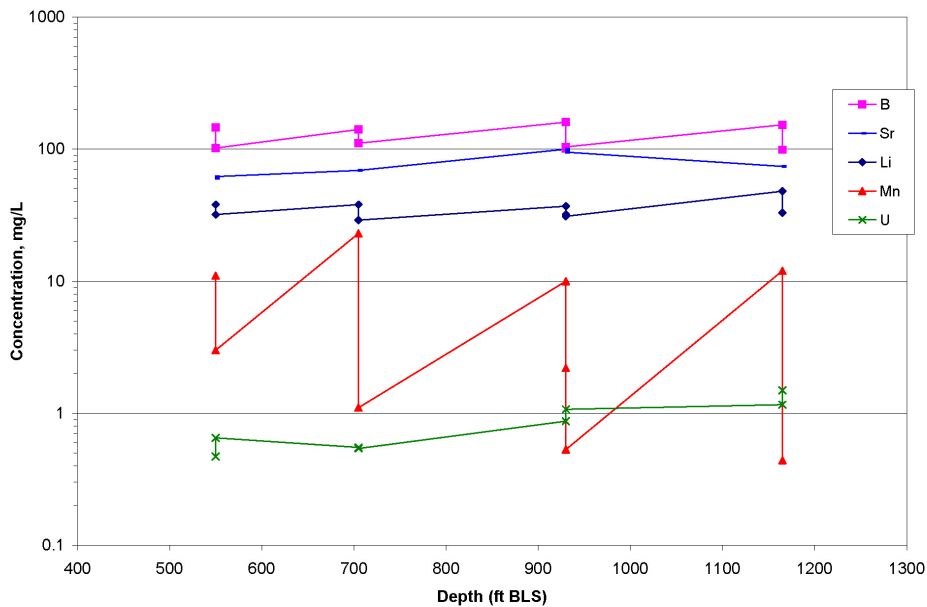
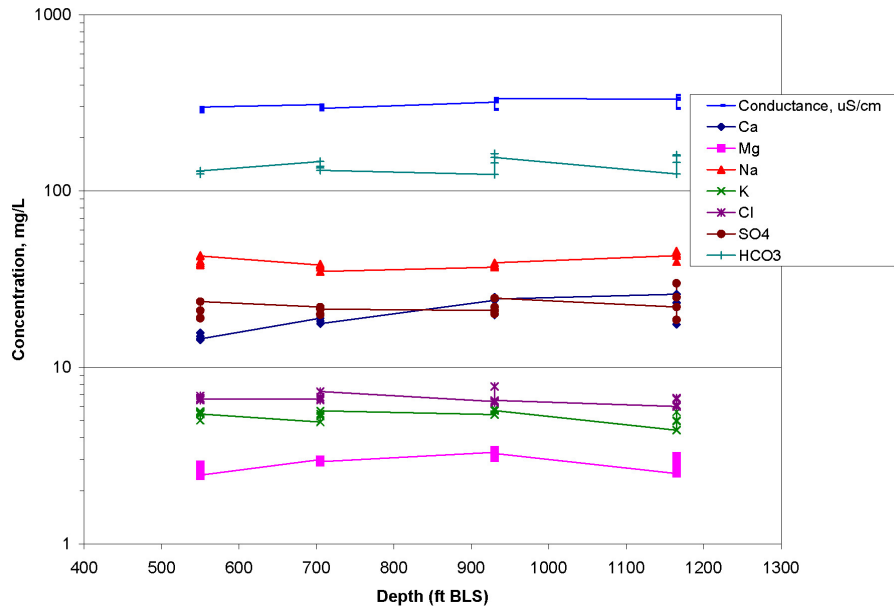


Source DTN: GS060808312272.003 [DIRS 179423].

Output DTN: LA0704PR150304.001.

NOTES: The data gap between 370 ft and 500 BLS provides a potentially false illusion of little variability in geochemistry over this depth range. There is some suggestion of changes in geochemistry that may be associated with flow stratification between 510 ft to 520 ft and 540 ft to 550 ft BLS and again between 540 ft to 550 ft and 580 ft to 590 ft BLS.

Figure F-47. Geochemistry Profiles of Major Cations, Major Anions, and Minor Cations in Samples from Sonic Borehole 19PB

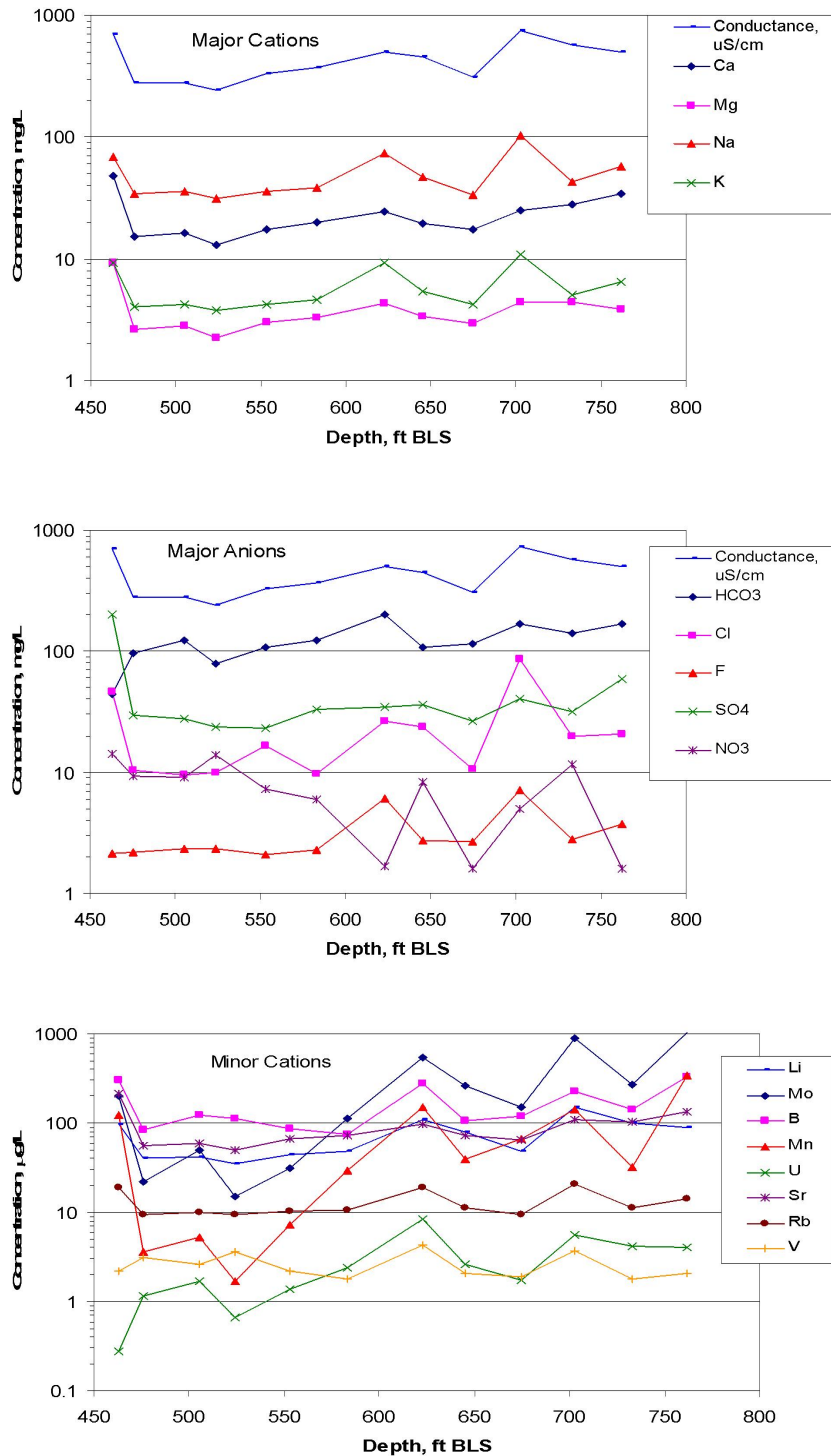


Source: DTNs: GS040108312322.001 (2002 data) [DIRS 179422], GS040808312322.006 (2003 data) [DIRS 179434].

Output DTN: LA0704PR150304.001.

NOTES: Depths correspond to the midpoints of screened intervals, and the data points do not distinguish between 22S, 22PA, and 22PB. The higher manganese concentrations at a given depth correspond to samples taken from 22S, and the lower manganese concentrations at the same depth correspond to samples taken from 22PA or 22PB. These results indicate that the presence (22S) or absence (22PA and 22PB) of steel in the borehole completions probably influences manganese concentrations. There are no obvious trends in concentrations with depth except a hint of increasing calcium concentrations with depth and a minor spike in strontium concentrations at ~940 ft BLS. Note the log concentration scales.

Figure F-48. Geochemistry Depth Profiles of Major Cations and Anions (upper) and Minor Cations (lower) in Boreholes 22S, 22PA, and 22PB



Source: DTN: GS060808312272.003 [DIRS 179423].

Output DTN: LA0704PR150304.001.

NOTE: Note the suggestion of flow stratification associated with the spikes in cation and anion concentrations at ~620 ft and ~700 ft BLS.

Figure F-49. Geochemistry Profiles of Major Cations, Major Anions, and Minor Cations in Samples from Sonic Borehole 22PC

Thus, while the geochemical data from the 22PC sonic borehole suggest the possible existence of some narrow layering shallow in the flow system, this layering apparently does not have enough contrast in hydraulic properties to result in a confined aquifer response in either of the two shallow screened intervals penetrated by 22PC. However, it must be kept in mind that 22PA, not 22PC, was used in hydraulic testing, and these two wells are located over 20 m away from each other in orthogonal directions from 22S, so it is possible that some local layering could exist in 22PC that is not present in 22PA. Also, it is apparent that if there are confining layers between zones 2 and 3 and between zones 3 and 4 at Site 22, as suggested by the cross-hole hydraulic test results, the geochemical data indicate that the waters flowing through the transmissive layers at these depths must have the same or very similar geochemical signatures.

In conclusion, the geochemical data at the ATC site generally support the conceptual model of flow in the alluvium that was discussed in the previous section, but the geochemical data at Site 22 are inconclusive in that they neither support nor refute this conceptual model. The sonic core data at both locations show some indications of relatively small-scale layering of flow in the upper portions of the saturated alluvium, but this layering, if it exists, is apparently not associated with strong confining layers but rather is reflected in aquifer tests as only a relatively small vertical anisotropy. An inherent limitation of geochemical data to test hydraulic models is that they are not necessarily genetically linked to hydrologic characteristics (i.e., geochemical characteristics may be caused by processes that do not affect hydrologic properties), and likewise, hydrologic contrasts need not alter chemical characteristics, especially at the local scale.

F.9 CORROBORATION OF THE ALLUVIUM CONCEPTUAL FLOW MODEL FROM SMALL-SCALE LABORATORY HYDRAULIC CONDUCTIVITY DATA

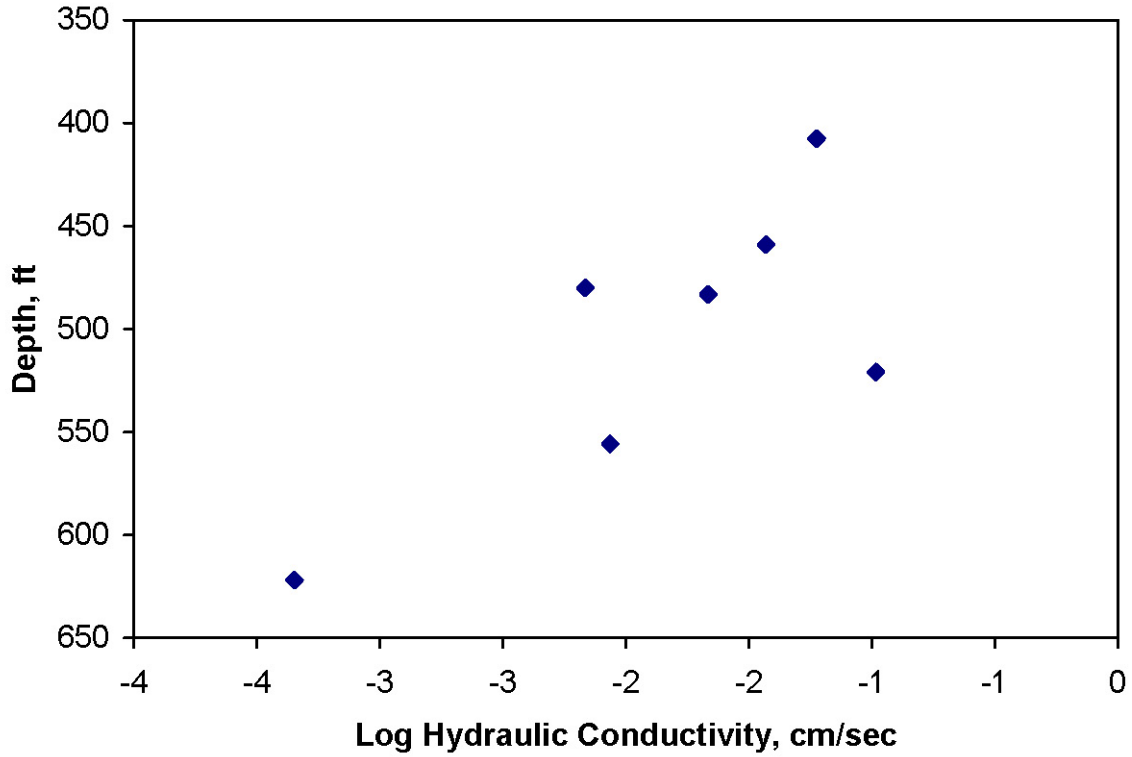
Some of the alluvium collected from sonic borehole NC-EWDP-19PB was repacked into polyvinyl chloride (PVC) tubes measuring approximately 1 ft long and 6 inches diameter (outer) for saturated hydraulic conductivity measurements. The sonic “core” had the advantage of not experiencing any mixing of the alluvium from different depths during extraction from the borehole, as typically occurs when soils are recovered during drilling operations. Consequently, very fine-scale layering and large pieces of alluvium that might otherwise be ground up during drilling are preserved.

In a collaborative effort between Los Alamos National Laboratory and the Nye County Department of Natural Resources, the PVC “permeameters” were moist-packed with alluvium taken from very narrow intervals of the sonic “core” (at most only a few feet of alluvium in the vertical direction). Material from seven different intervals was moist packed into the permeameters to achieve bulk densities that matched the in-situ bulk densities of the alluvium as determined by weighing the alluvium extracted from a known length (and hence volume) of “core” (dry packing did not achieve high enough bulk densities). After saturation, the permeability of the alluvium samples were measured using a constant head method in accordance with LANL-INC-DP-140, *Constant Head Saturated Hydraulic Conductivity Measurements on Repacked Core Samples* [DIRS 179420], which is based on laboratory methods described by Klute and Dirksen (1986 [DIRS 179421]).

The saturated hydraulic conductivities of the seven samples as a function of depth below surface in 19PB are plotted in Figure F-50 (note the log conductivity scale). This figure shows that the seven small-scale samples exhibit a range of hydraulic conductivities of over two orders of magnitude, which is greater than the range deduced from the relatively detailed interpretations of the hydraulic tests at Site 22 and consistent with a strongly-layered system. Unfortunately, no small-scale permeability measurements were conducted using “core” from sonic borehole NC-EWDP-22PC, which would more directly apply to Site 22.

It is noteworthy that the small-scale hydraulic conductivities of Figure F-50 all tend to be significantly smaller than the larger scale hydraulic conductivity deduced from the cross-hole field test at the ATC (about 2.3 m/day), and the lowest conductivity is much lower than any vertical or horizontal hydraulic conductivity deduced from testing at Site 22. Some of this result could be reflecting the fact that the greater alluvium horizontal hydraulic conductivities at the ATC were deeper than the bottom 19PB. However, the result also suggests that there could be some bias in the laboratory permeameter tests, including perhaps some column-packing artifacts or an inability to completely saturate the permeameters, which would lead to lower measured conductivities. Additionally, despite the fact that each samples was taken over only a few vertical feet of alluvium, the samples were still homogenized over that distance and therefore might provide a better measure of vertical conductivity than horizontal conductivity. Finally, there could be issues with the sample size and the number of samples being too small to effectively detect either the presence or the larger-scale behavior of the higher conductivity intervals in the alluvium (only about 5% of the saturated alluvium section of 19PB is represented in the samples tested).

It is concluded that the small-scale laboratory-based hydraulic conductivity data from NC-EWDP-19PB support the general concept of a layered heterogeneous alluvium flow system, although the laboratory-measured hydraulic conductivities are consistently lower than the field-measured hydraulic conductivities.



Source: DTN: LA0501PR831231.001 [DIRS 179428].

NOTES: As determined from laboratory permeameter measurements on sonic "core" that was packed to match the in-situ bulk density of the alluvium. The field-scale log hydraulic conductivity measured in cross-hole pump testing at this location was 0.36, over an order of magnitude larger than the largest measurement plotted.

Figure F-50. Log-saturated Hydraulic Conductivity as a Function of Depth below Land Surface in NC-EWDP-19PB

INTENTIONALLY LEFT BLANK

APPENDIX G

**DETAILS OF TRACER TESTING AND TRACER TEST INTERPRETATIONS IN
SATURATED ALLUVIUM SOUTH OF YUCCA MOUNTAIN**

G1. INTRODUCTION AND ALTERNATIVE CONCEPTUAL TRANSPORT MODELS

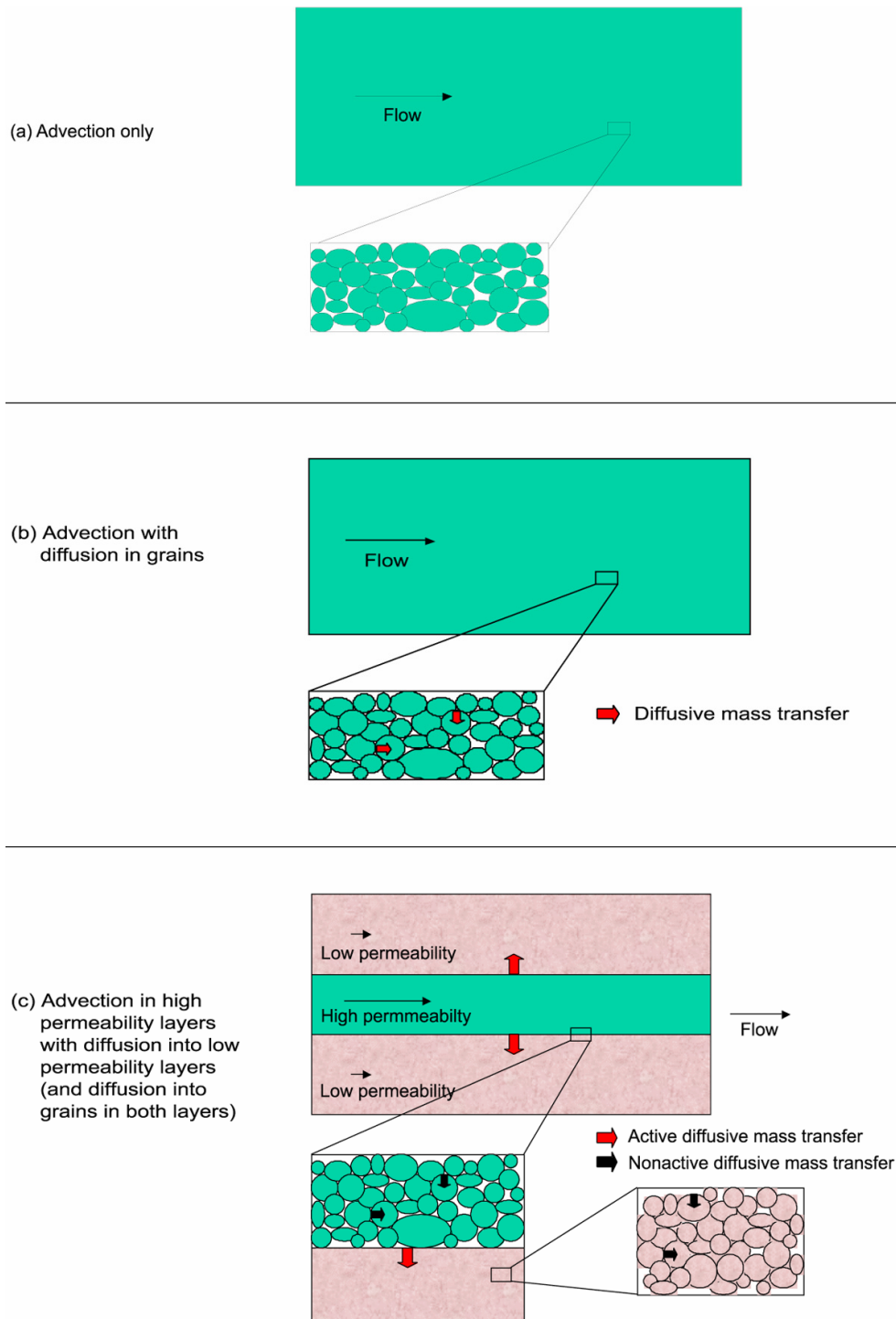
Three single-well injection-withdrawal tracer tests were conducted in screen #1 (the uppermost screened interval) of NC-EWDP-19D between December 2000 and April 2001 (see Figure 6.1-9 for a diagram showing well completion and lithology; note that well NC-EWDP-19D will be referred to by its abbreviated form [19D] in the remainder of this document; see Table B-1). A fourth single-well injection-withdrawal tracer test was conducted in screen #4 of 19D in February and March of 2002. This test is only briefly discussed in this report (Section D.4.5) because it was conducted for the purposes of comparing and contrasting parameter estimates obtained from single-well and cross-hole tests, but the cross-hole tests were never conducted. Detailed documentation of the first three tracer tests is reported by Umari et al. (2003 [DIRS 164573]) and Reimus (2003 [DIRS 165128]).

Two single-well injection withdrawal tracer tests and two cross-hole tracer tests were subsequently conducted at NC-EWDP Site 22 (involving wells -22S, -22PA, and -22PC; see Figure 6.1-10 for well completion diagrams and lithology) from December 2004 to October 2005. NC-EWDP Site 22 will be referred to as Site 22, and the individual wells will be referred to as 22S, 22PA, and 22PC in the remainder of this appendix. The primary objective of the tests at both 19D and Site 22 was to distinguish between alternative conceptual transport models for the saturated alluvium south of Yucca Mountain. Secondary objectives included obtaining estimates of key transport parameters associated with the appropriate conceptual transport model and independent estimates of ambient groundwater velocity at the two locations from the single-well tracer tests.

The three conceptual transport models considered for the saturated valley-fill deposits located south of Yucca Mountain prior to the tracer tests are depicted in Figure G-1 (with some additional variations/combinations). The first model assumes purely advective transport through a porous medium with no diffusive mass transfer into either the grains of the medium or between advective and nonadvective regions of the aquifer. This model does not necessarily imply a homogeneous flow field, but it does preclude a system with alternating layers of relatively narrow thickness and significant permeability contrasts. Such a conceptual model might be valid in a sandy aquifer with grains of relatively low porosity. The second model is similar to the first except that it assumes diffusive mass transfer into the grains of the porous medium. These grains have significant internal porosity, but the porosity is not well-connected over the scale of the grains; therefore, the grains transmit negligible flow. The third model assumes diffusive mass transfer between advective and nonadvective layers in the aquifer. In this model, the flow system is assumed to alternate between high and low conductivity layers, a simplified representation consistent with some depositional scenarios. Diffusive mass transfer in this case is only between the two layers, not into grains within the layers. However, one variation of this model is to assume that diffusion also occurs into grains in both the advective and nonadvective layers. This variation is, essentially, a combination of the second and third conceptual models, with an additional level of complexity allowing for diffusion in the nonadvective layer into both the inter- and intragranular pore spaces.

Pretest predictions of the single-well injection-withdrawal tracer tests conducted at 19D are presented in Section G2. Pretest predictions of cross-hole tracer test responses in the alluvium are provided in Section G3. The results and interpretations of the three single-well

injection-withdrawal tests conducted in 19D in FY 2001 are presented in Section G4, and the results and interpretations of the two single-well tracer tests conducted in 22S are presented in Section G5. Section G6 contains the results and interpretations of the two cross-hole tracer tests conducted at Site 22, and Section G7 provides a summary of the tracer testing results at both the 19D and Site 22 locations.



NOTE: For illustration purposes only. Red arrows in (c) indicate diffusive mass transfer options that were exercised in this scientific analysis, and black arrows indicate options that were not exercised.

Figure G-1. Schematic Illustration of Alternative Conceptual Transport Models for the Valley-Fill Deposits South of Yucca Mountain

G2. PRETEST PREDICTIONS OF SINGLE-WELL TRACER RESPONSES FOR EACH CONCEPTUAL MODEL

Prior to conducting the single-well tracer tests in 19D, the MULTRAN model (Section E3.2.2) was used to simulate tracer responses, assuming each of the three alternative conceptual models of Figure G-1. These pretest predictions also apply to the two single-well tracer tests in 22S, as the tests at both locations were conducted in essentially the same manner. Simulations were conducted for each of three planned single-well tracer tests: a zero rest-period test, a 2-day rest-period test, and a 30-day rest-period test (where “rest period” refers to the time period after injection that is allowed to elapse before starting to pump the well); note that the single-well tracer tests in 22S were planned to have 3- and 30-day rest periods. In each of the tests in 19D, it was anticipated that approximately 11,000 L (3,000 gallons) of tracer solution would be injected into the test interval followed by approximately 95,000 L (25,000 gallons) of tracer-free “chase” water to push the tracer solution out of the wellbore and gravel pack into the formation. The well would then be pumped for several days to several weeks after the prescribed rest period. Each of the three tracer tests was to include both a halide (bromide, chloride, or iodide) and a fluorinated benzoate so that any diffusion from flowing water into stagnant water could be identified from differences in the tracer responses. The single-well tracer tests in 22S differed from those in 19D primarily in that the tracer solution volumes were only approximately 6,000 L (1,500 gallons) instead of 11,000 gallons, and the injection and pumping rates were greater than in 19D (see later discussion).

In single-well simulations using MULTRAN V 1.0 (STN: 10666-1.0-00 [DIRS 159068]), only one end of the domain is modeled as a well-mixed borehole; the other end becomes a zero-concentration-gradient boundary. However, to minimize boundary effects, an initial calculation establishes a node spacing in the radial (r) direction that results in a tracer “plume” that never reaches the edge of the domain. Furthermore, the numerical calculations are carried out assuming cylindrical coordinates with flow only in the radial direction (with a flow velocity that varies as $1/r$), instead of Cartesian coordinates. Ambient flow during single-well tests, which is superimposed on the radial flow induced by injection into and pumping of the well, is not accounted for in MULTRAN because the code is designed primarily to predict and analyze differences in tracer responses resulting from differences in tracer diffusion coefficients and sorption properties, not to analyze the effects of ambient flow on tracer responses. Thus, the advection-dispersion equation in the flow direction solved by MULTRAN for single-well tests is (Bear 1979 [DIRS 105038], p. 247):

$$\frac{\partial c}{\partial t} = -V(r) \frac{\partial c}{\partial r} + \frac{1}{r} \frac{\partial}{\partial r} \left(rD \frac{\partial c}{\partial r} \right) \quad (\text{Eq. G-1})$$

where

- c = tracer concentration (mol/L)
- r = radial coordinate, cm
- $V(r)$ = flow velocity as a function of r (cm/hr)
- D = dispersion coefficient (cm²/hr).

Single-well tracer test responses for all three single-well tests were simulated for both a generic halide (bromide or iodide) and a generic fluorinated benzoate, with the assumption that the halide has a factor-of-three larger diffusion coefficient than the benzoate. The response of a counter cation (potassium was assumed in all cases) was also simulated, as well as the responses of the cations with which it exchanges (see Sections E3.1.3 and E3.2.2). Also, a flow interruption of several hours was simulated for the test with zero rest period to illustrate the additional information that can be obtained by doing a planned flow interruption during the latter portion of the test.

The MULTRAN V 1.0 (STN: 10666-1.0-00 [DIRS 159068]) simulations associated with the different conceptual transport models illustrate how the appropriate conceptual transport model can be best determined by comparing the responses of the nonsorbing tracers with different diffusion coefficients for each of the different rest periods. The differences in the responses of the tracers with different diffusion coefficients as a function of rest period can provide information on the relative volumes of flowing and stagnant water in the system, which is very important for determining the ability of the alluvium to attenuate the transport of nonsorbing radionuclides. The MULTRAN simulations also illustrate how cation responses (both injected and exchanged cations) could potentially provide useful information on cation-exchange-capacity and, hence, cation sorption in the system. The flow system parameters that were assumed for the three different conceptual models are listed in Table G-1. Other input parameters that do not pertain to the flow system are listed in Table G-2.

Figure G-2 illustrates the tracer responses that can be expected in each of the three tracer tests if a homogeneous, single-porosity medium is assumed (conceptual model of Figure G-1a). Only one response is shown because there is no difference between the predicted responses of the nonsorbing tracers of different diffusion coefficients or the predicted responses after the different rest periods. Although not shown in Figure G-2, there is also no change in predicted tracer concentrations immediately after a flow interruption. The lack of a difference between tracers, and between tracer responses for different rest periods, as well as the lack of a response after a flow interruption are all indications of very little or no diffusive mass transfer in the flow system.

Table G-1. Flow System Parameters Used in the Single-Well Simulations

Parameter	Figure G-1a Model	Figure G-1b Model	Figure G-1c Model
Porosity in advective layers	0.25	0.25	0.25
Porosity in nonadvective layers	N/A	N/A	0.25
Porosity of grains	N/A	0.15	N/A
Width of advective layers (cm)	N/A	N/A	10.0
Width of nonadvective layers (cm)	N/A	N/A	24.0
Grain diameter in advective layers (mm)	N/A	3.0 (2.2) ^a	N/A
Grain diameter in nonadvective layers (mm)	N/A	N/A	N/A
Halide diffusion coefficient in advective layers (cm ² /s) ^b	N/A	3 × 10 ⁻⁶	3 × 10 ⁻⁶
Halide diffusion coefficient in nonadvective layers (cm ² /s) ^b	N/A	N/A	1 × 10 ⁻⁶
Halide diffusion coefficient in grains (cm ² /s) ^b	N/A	1 × 10 ⁻⁶	N/A
Drift velocity (cm/s)	0 ^c	0 ^c	0 ^c

Output DTN: LA0303PR831231.001.

^a The number in parentheses is the standard deviation of ln (diameter) used for a lognormal distribution of grain sizes in one set of simulations (see text).

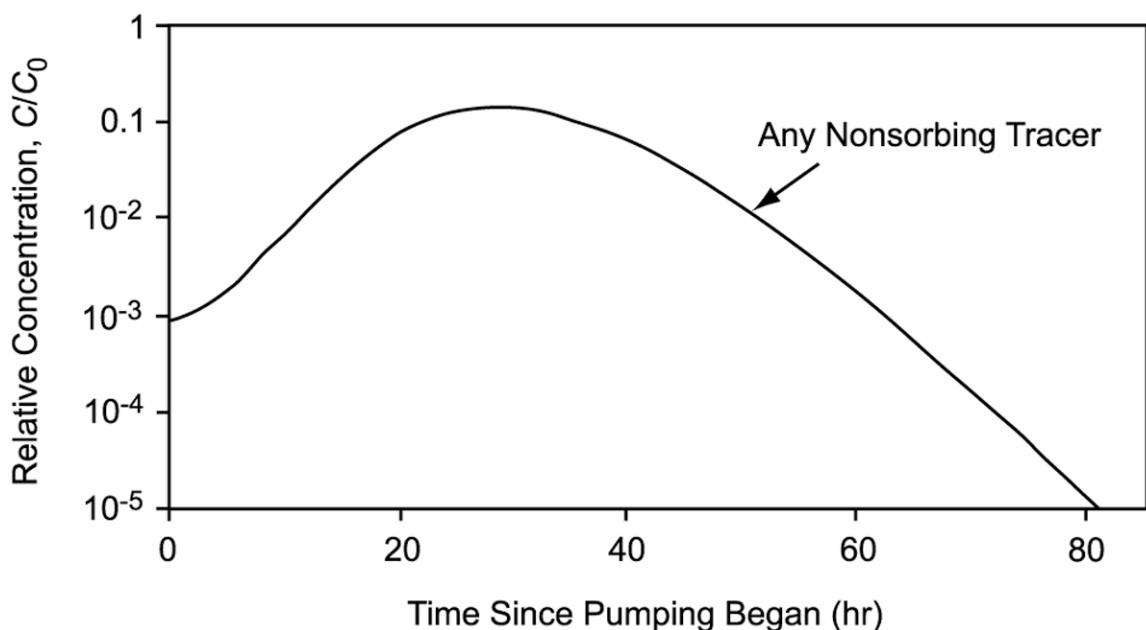
^b The fluorinated benzoate diffusion coefficient is always assumed to be one-third of the halide diffusion coefficient (Section E.2).

^c Drift velocity is assumed to be zero because of the small apparent hydraulic gradient in the vicinity of NC-EWDP-19D and NC-EWDP-22S.

Table G-2. Nonflow-System Input Parameters for the Single-Well Simulations

Parameter	Value
Volume of injection interval (including gravel pack) (L)	500
Radius of gravel pack (cm)	18
Duration of injection pulse (hr)	3
Duration of chase (hr)	28
Flow interruption duration (zero-rest-period test only) (hr)	24
Flow rate during injection and pumping (L/min [gpm])	approximately 57 [approximately 15]

Output DTN: LA0303PR831231.001.

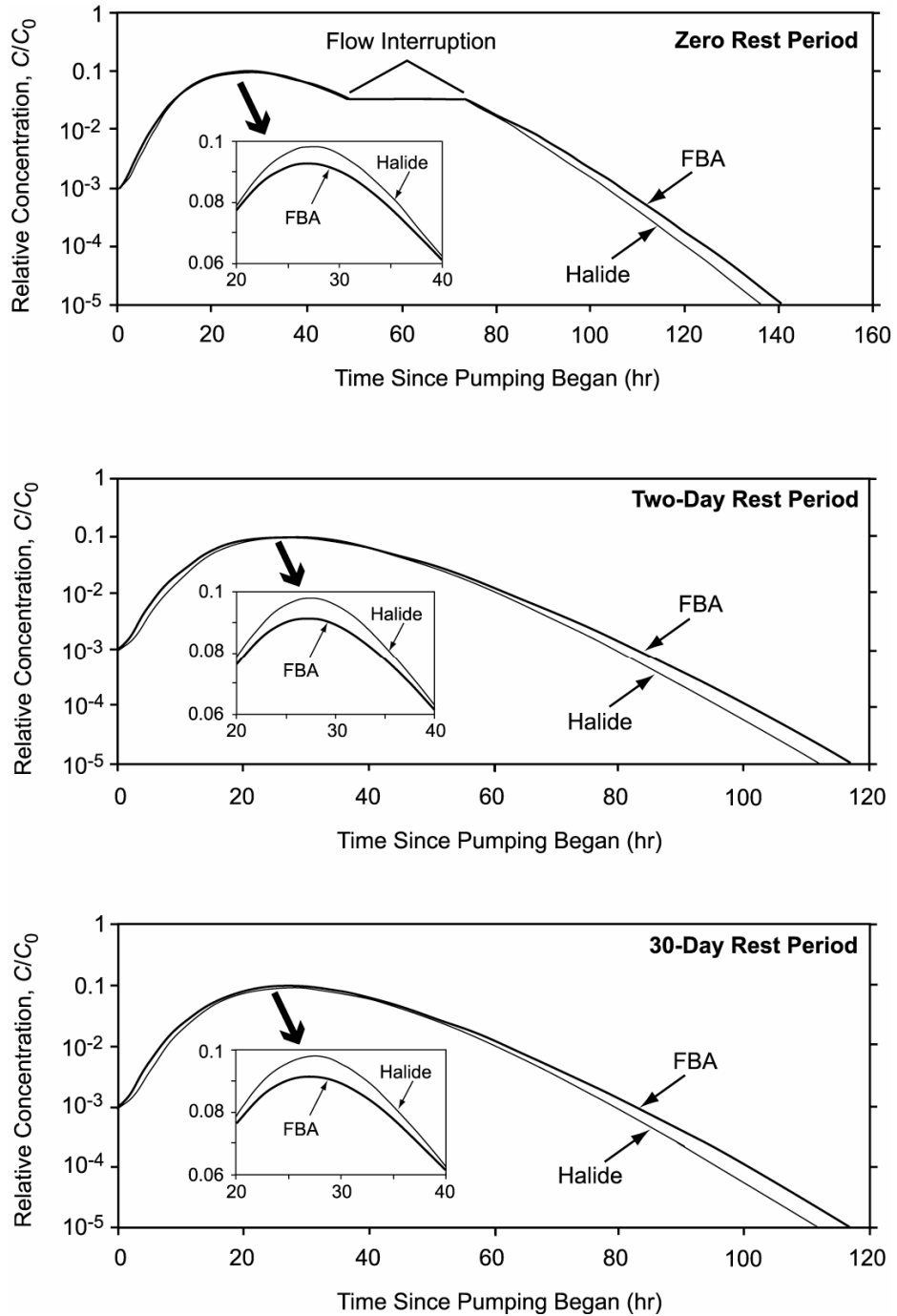


Output DTN: LA0303PR831231.001.

Figure G-2. Normalized Concentration Response of Any Nonsorbing Tracer in a Single-Well Test in a Porous Medium with No Diffusive Mass Transfer and/or No Stagnant Water (the Conceptual Model of Figure G-1a)

Figure G-3 shows the tracer responses (normalized to injection concentrations) that can be expected in each of the three single-well tracer tests if a homogeneous system with porous grains is assumed (conceptual model of Figure G-1b). In this case, a uniform grain diameter of 3 mm was assumed, which corresponds to the mass-weighted mean diameter of the material collected from four different intervals in 19P. A mass-weighted mean diameter was used because tracer storage capacity in grains is proportional to mass, not number of grains. Cuttings collected from 19D (D1) were not used for grain-size analysis because the mud-rotary-drilling method used in this hole tended to truncate the upper and lower ends of the size range. Figure G-3 shows that there is a slight difference in the responses of the halide and FBA in each test, with the halide having a slightly higher peak concentration and a shorter tail than the FBA. These differences qualitatively indicate that there is some diffusion into stagnant water in the system. However, the fact that the halide has a higher peak concentration and a shorter tail than the FBA indicates that the characteristic diffusion lengths must be relatively short. Both tracers effectively diffused throughout the grains during the time that they were injected and chased into the system, so the responses primarily reflect the diffusion rates of the tracers back out of the grains, which is faster for the halide. The tracer mass recoveries (not presented) were very high (over 95%) in all of these simulations, with the recoveries of the two tracers being essentially the same at the end of the simulations. The halide initially had a higher recovery than the FBA (during the peak) because it diffused more rapidly out of the grains, but the FBA recovery approached that of the halide as pumping continued into the tails of the responses. Given a long enough pumping period, the recoveries of both tracers would have approached 100%.

Another indication of the short diffusion lengths is the lack of an increase in tracer concentrations after the flow interruption in the test with no rest period. If a significant amount of tracer remained in the grains at the time of the flow interruption, an increase in concentration would be expected upon resumption of flow due to the tracer diffusing out of the grains during the rest period. An additional indication of the relatively short diffusion distances in the system is the fact that both the halide and the FBA have essentially the same response in the 2-day rest period test as the 30-day rest period test. This result suggests that the tracers were able to effectively diffuse throughout the grains during the 2-day rest period so that very little additional diffusion occurred during the 30-day rest period.



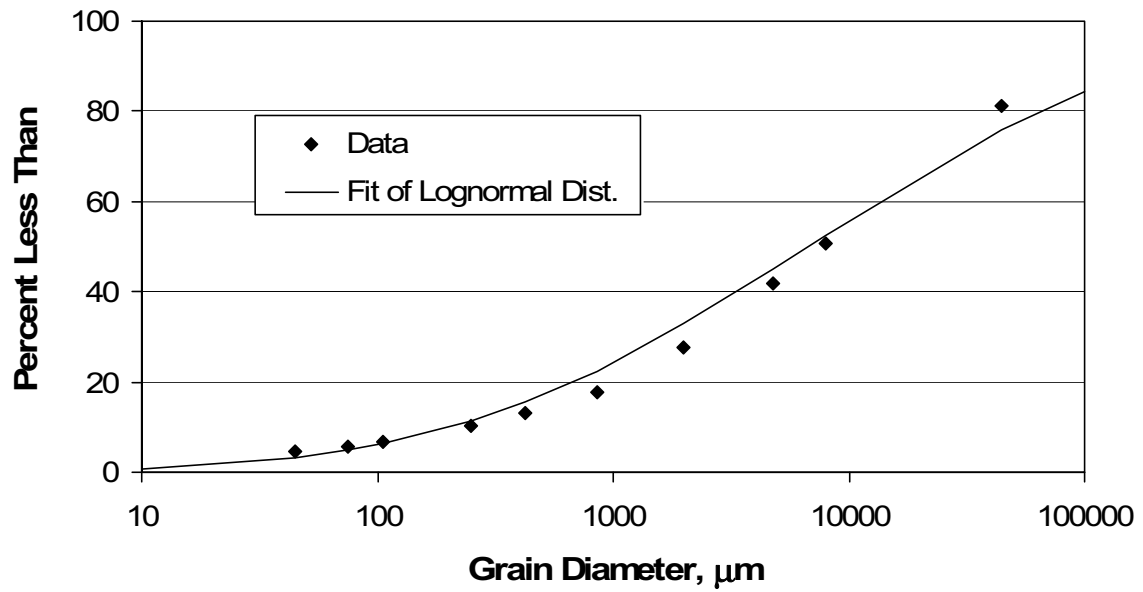
Output DTN: LA0303PR831231.001.

NOTE: The rest periods are zero (top), 2 days (middle), and 30 days (bottom); a 3-mm fixed grain diameter was used. X axis extends to 160 hr for zero-rest-period test because of 24 hours flow interruption.

Figure G-3. Normalized Concentration Responses of a Halide and a FBA in Single-Well Tests for the Conceptual Transport Model of Figure G-1b Using a Fixed Grain Diameter

Figure G-4 shows the measured grain-size distribution of the material collected from 19P. A qualitative fit of a lognormal distribution to the data is also shown. Clearly, there is a relatively wide distribution of grain sizes not accounted for when a single mean grain size is assumed, as in the simulations that generated the tracer responses shown in Figure G-3. Figure G-5 shows the results of incorporating the lognormal distribution of grain sizes shown in Figure G-4 into the MULTRAN V 1.0 (STN: 10666-1.0-00 [DIRS 159068]) simulations. The only difference between Figures G-3 and G-5 is that the grain size in the former is uniform (equal to the mean), whereas in the latter, it is varied over the lognormal distribution of Figure G-5. It is apparent that the inclusion of larger grain sizes in the simulations greatly increases the length of the tails of both tracers. Additional simulations confirmed that the elimination of the smaller grain sizes in the lognormal distribution had very little effect on the tracer responses. The increase in the lengths of the tails is a result of the greater diffusion distances associated with the larger grains. Because of the greater distances, it takes longer for the tracer mass to diffuse back out into the advective pathways, resulting in the extended tailing. The longer diffusion distances are also indicated by the noticeable increase in tracer concentrations after the flow interruption in the test with no rest period. Note that in all cases the FBA still has a longer/higher tail than the halide, indicating that the responses are still dominated by diffusion back out of the grains. The mass recoveries of both tracers were slightly lower than in the simulations of Figure G-3 (for the same pumping time). However, by the end of the simulations, both tracer recoveries were well over 95%.

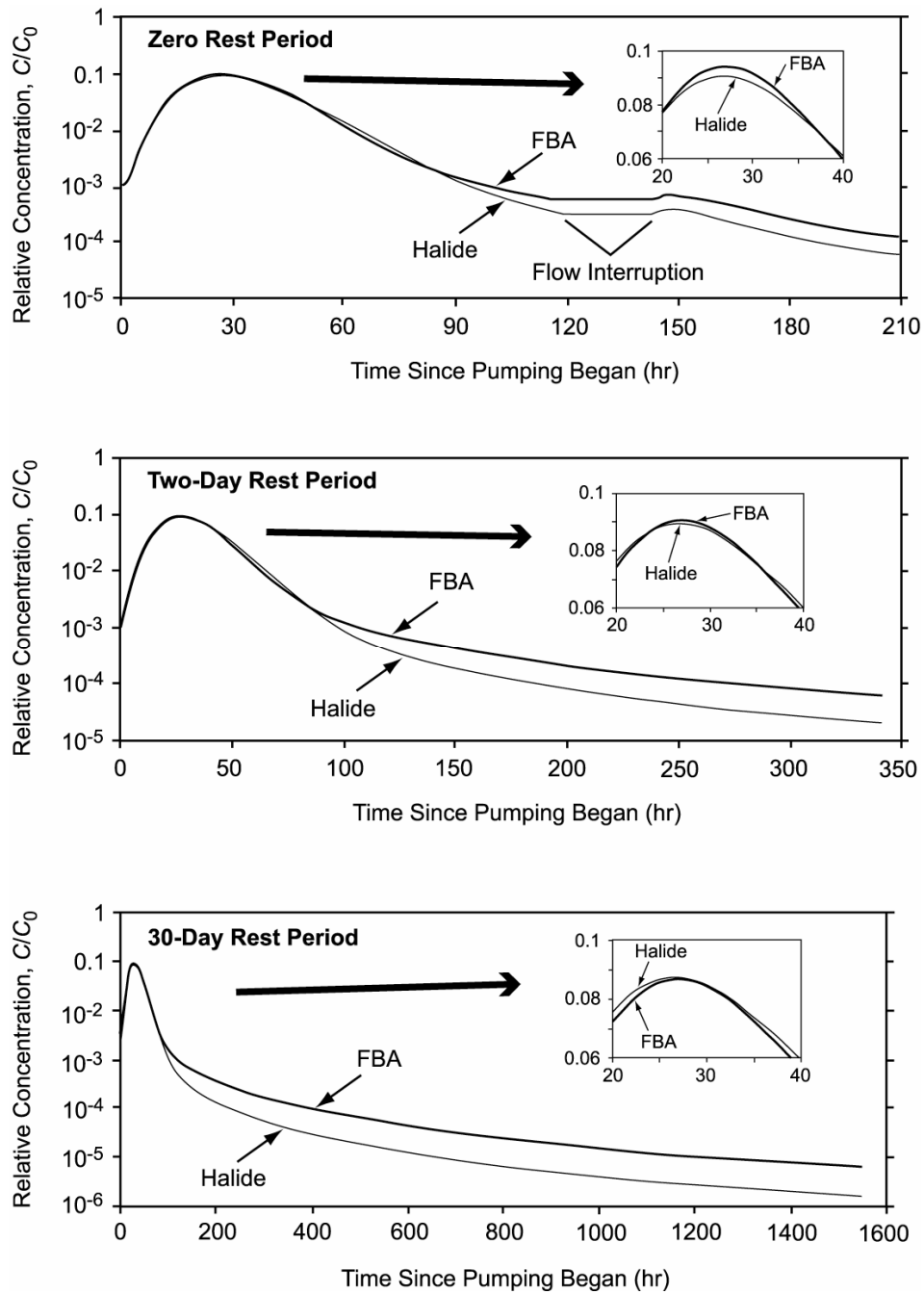
Figure G-6 shows the tracer responses that can be expected in each of the three single-well tracer tests if a layered dual-porosity system is assumed (Figure G-1c). Grains in both the advective and nonadvective regions were assumed to be nonporous for these simulations. The differences in the responses of the halide and the FBA in the tests, and the fact that the peak concentrations decrease while the lengths of the tails increase as the rest period increases all indicate relatively long diffusion lengths. However, in contrast to the results shown in Figures G-3 and G-5, the FBA has a higher peak concentration and a shorter/lower tail than the halide during the pumpback phase. This result is primarily due to the relatively wide advective flow pathways (10 cm), which tracers can only slowly diffuse out of because of the long distance to the nonadvective region. It is the slower diffusion of the FBA out of these advective pathways that is primarily responsible for the higher peak concentrations and lower tails of the FBA relative to the halide.



Source: DTN: LA0201JS831421.001 [DIRS 162613].

NOTE: The above data are a composite of four depth intervals.

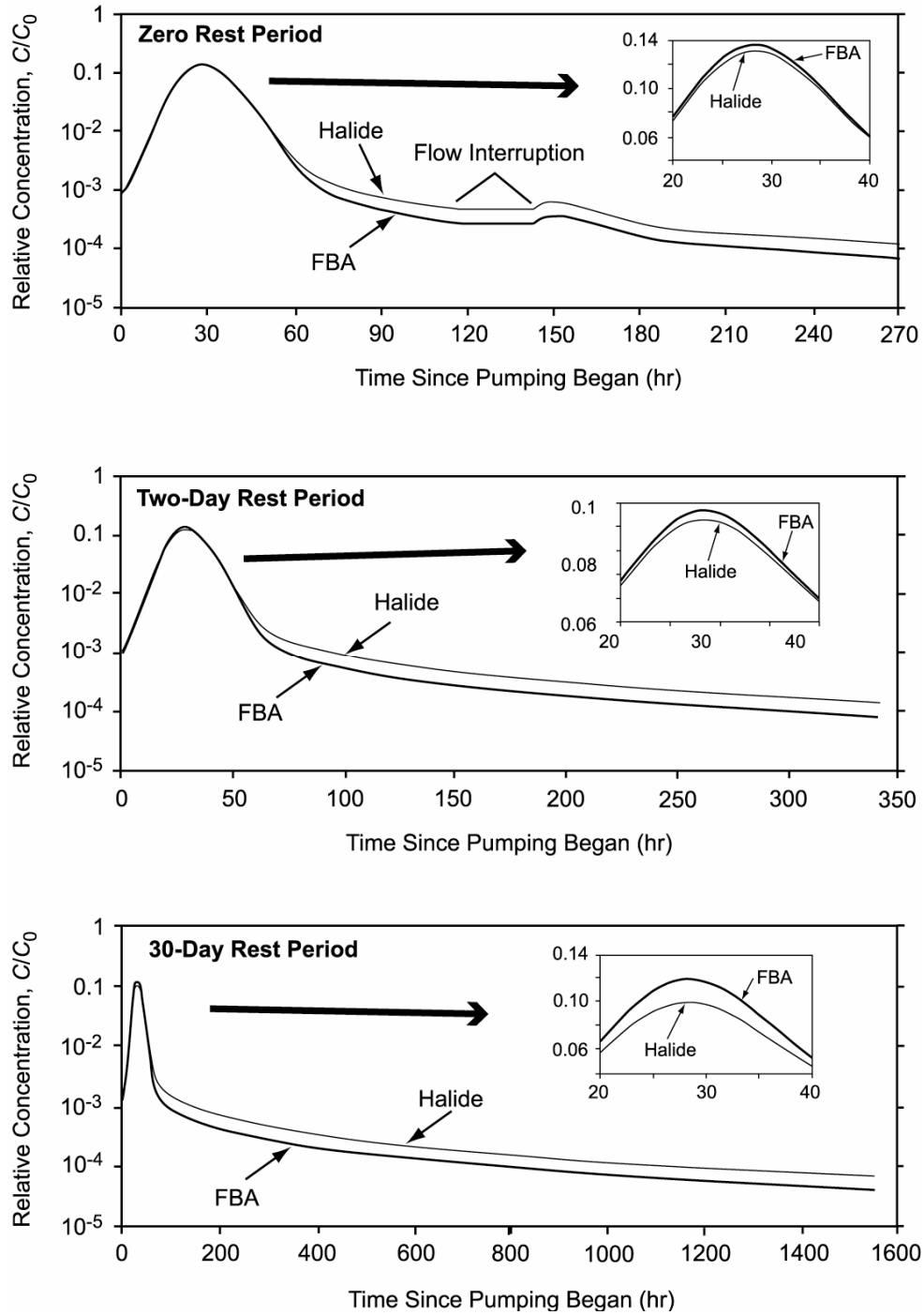
Figure G-4. Measured and Fitted Grain Size Distributions from NC-EWDP-19P



Output DTN: LA0303PR831231.001.

NOTE: The rest periods are zero (top) days, 2 days (middle), and 30 days (bottom); a mean grain diameter of 3 mm was used with a standard deviation for ln (diameter) of 2.2. X axes have different scales to reflect the different pumping durations planned for the three tests in 19D.

Figure G-5. Normalized Concentration Responses of a Halide and an FBA in Single-Well Tests for the Conceptual Transport Model of Figure G-1b Using a Grain Size Distribution

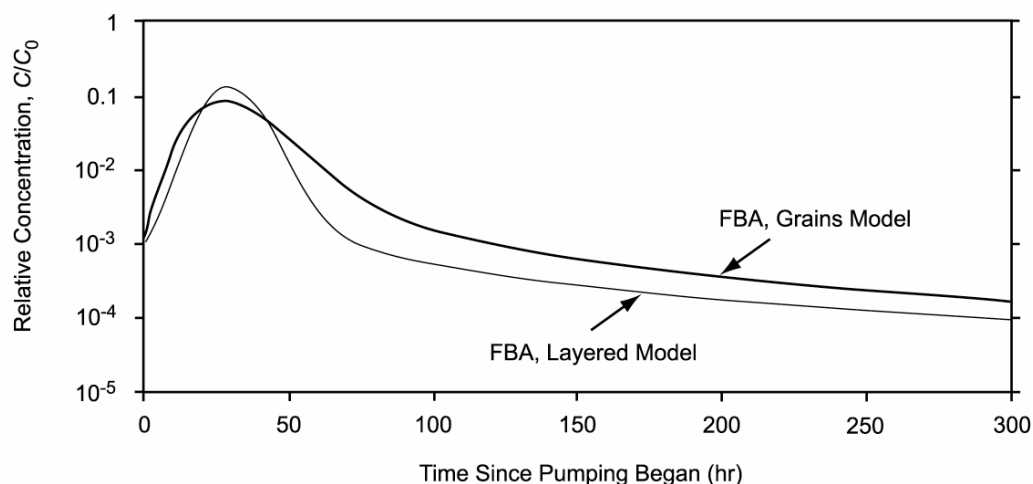


Output DTN: LA0303PR831231.001.

NOTE: The rest periods are zero (top) days, 2 days (middle), and 30 days (bottom). X axes have different scales to reflect the different pumping durations planned for the three tests in 19D.

Figure G-6. Normalized Concentration Responses of a Halide and an FBA in Single-Well Tests for the Conceptual Transport Model of Figure G-1c

The value of comparing the responses of the FBA and halide to help distinguish between alternative conceptual models is made apparent in Figure G-7, which shows the simulated responses of the FBA in the 2-day-rest period tests with the diffusion-into-grains model (Figure G-5) and the diffusion-into-layers model (Figure G-6). Other than a slightly broader peak in the diffusion-into-grains response (which could be attributed to hydrodynamic dispersion or tracer drift with the natural gradient), the two responses are very similar, and it would be difficult to distinguish between the two models on the basis of either one of these responses alone. However, by knowing whether the halide has a higher or lower tail, it will be possible to make a distinction between the models. The additional information obtained from the test with a longer rest period will also help in making this distinction. Also, quantitative estimates of diffusive mass-transfer rates and diffusion distances can be best made using the MULTRAN V 1.0 (STN: 10666-1.0-00 [DIRS 159068]) model to fit simultaneously the tracer responses from each test with the constraint that the halide has a factor-of-three larger diffusion coefficient than the FBA.



Output DTN: LA0303PR831231.001.

NOTE: The rest period was 2 days.

Figure G-7. Comparison of FBA Responses for the Layered Conceptual Model (Figure G-1c) and the Grain-Diffusion Model (Figure G-1b) with a Lognormal Distribution of Grain Sizes

Table G-3 summarizes the tracer-response characteristics from single-well tracer tests that are consistent with the different conceptual transport models of Figure G-1, including a diffusion-into-grains model (Figure G-1b) with a relatively wide distribution of grain sizes (see Figure G-4 and G-5). This table serves as a guide for how the appropriate conceptual transport model can be identified from the qualitative nature of the tracer responses in the three planned single-well tracer tests in 19D and also for the two planned single-well tracer tests in 22S.

Table G-3. Single-Well Tracer Test Response Characteristics Consistent with the Conceptual Models of Figure G-1

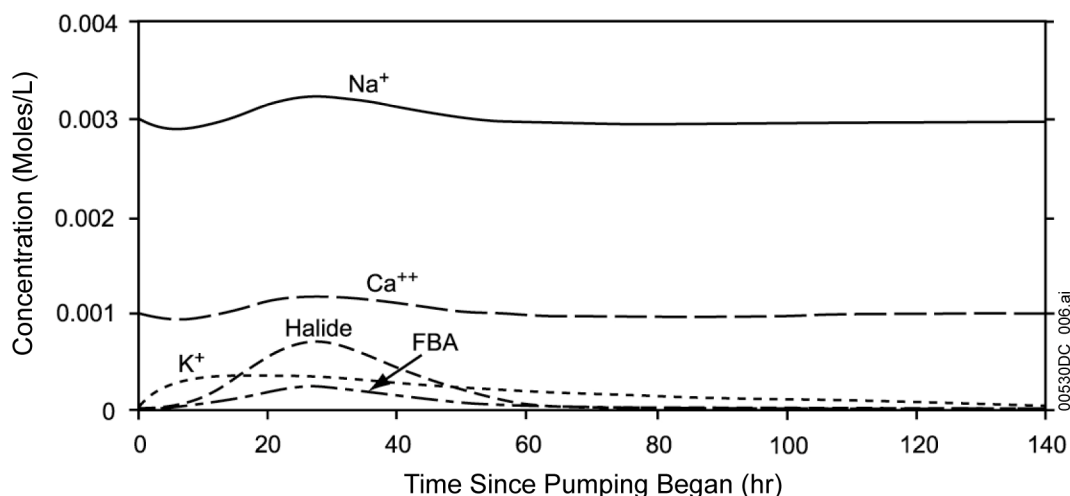
Conceptual Model	Single-Well Tracer Test Response Characteristics
Single-Porosity (Figure G-1a)	<ul style="list-style-type: none"> • All nonsorbing tracers have the same normalized concentration responses. • Response curves are independent of rest period (unless there is significant tracer drift during the rest period, but even then, there will be little or no difference in the response curves of different nonsorbing tracers). • No increase in tracer concentrations after a flow interruption in the tail of the response curves.
Diffusion into Small Grains—Short Diffusion Distances (Figure G-1b)	<ul style="list-style-type: none"> • Tracer with larger diffusion coefficient will tend to have higher peak concentration and lower tail concentration than tracer with smaller diffusion coefficient. • Relatively minor differences in response curves of each individual tracer as a function of rest period (unless there is significant tracer drift during the rest period). • Relatively minor increase in tracer concentrations after a flow interruption in the tail of the response curves.
Diffusion into Variable-Sized Grains—Combination of Short and Long Diffusion Distances, but Relatively Narrow Advective Flow Pathways (Figure G-1b, with grain size distribution of Figure G-4)	<ul style="list-style-type: none"> • Either tracer (large or small diffusion coefficient) could have the higher peak concentration, with the larger diffusion coefficient tracer tending to have the higher peak concentration as grain sizes decrease or rest periods increase. Tracer with smaller diffusion coefficient will tend to have the higher concentration in the tails of the responses. • Tracer with smaller diffusion coefficient will tend to have the higher concentration in the tails of the responses. • Noticeable differences in response curves of each individual tracer as a function of rest period, with longer, higher tails as rest period increases. • Significant increase in tracer concentrations after a flow interruption in the tail of the response curves.
Diffusion into Layers—Long Diffusion Distances and Relatively Wide Advective Flow Pathways (Figure G-1c)	<ul style="list-style-type: none"> • Tracer with smaller diffusion coefficient will tend to have higher peak concentration and lower tail concentration than tracer with larger diffusion coefficient. • Significant differences in response curves as a function of rest period, with longer, higher tails as rest period increases. • Significant increase in tracer concentrations after a flow interruption in the tail of the response curves.

Output DTN: LA0303PR831231.001.

NOTE: The characteristics in this table apply when tracer concentrations are normalized to injection concentrations.

Although sorption parameters for sorbing tracers are much more easily obtained from cross-hole tracer tests, Figure G-8 shows how information on cation sorption can also be obtained from a single-well tracer test. In this case, the counter-cation (assumed to be potassium ion) injected with the nonsorbing anion tracers exchanges with sodium and calcium, the two predominant cations in the system. The potassium ion initially responds more quickly than the nonsorbing anions because it traveled a shorter distance into the system during injection (due to ion exchange). This behavior results in an initial depression of the sodium and calcium concentrations because they displace potassium as the system is pumped back and also because charge balance must be maintained. As the anions respond, the concentrations of sodium and

calcium increase and peak at the same time as the anions. In principle, the magnitude of the fluctuations of the sodium and calcium concentrations, as well as the response of the counter-cation, can provide qualitative estimates of ion-exchange parameters for the counter-cation in the system.



Output DTN: LA0303PR831231.001.

NOTE: The Na^+ and Ca^{++} responses are the result of cation exchange with K^+ .

Figure G-8. Molar Responses of Injected Tracers (K^+ , Halide, FBA) and Naturally Occurring Cations (Na^+ and Ca^{++}) in the 2-Day-Rest-Period Test Assuming the Model of Figure G-1b

G3. PRETEST PREDICTIONS OF CROSS-HOLE TRACER TEST RESPONSES

After the single-well tracer tests in 19D were completed, Nye County drilled two additional wells (NC-EWDP-19IM1 and NC-EWDP-19IM2, known as 19IM1 and 19IM2) in the immediate vicinity of 19D to allow for cross-hole hydraulic and tracer testing. These wells were completed similarly to 19D so that they could be used interchangeably as production, injection, or observation wells. Cross-hole tracer tests were to be conducted immediately after cross-hole hydraulic testing was completed (Section F.2). However, water discharge and tracer injection permits issued by the State of Nevada were rescinded before tracer testing could be initiated. Two cross-hole tracer tests were eventually conducted in 2005 at Site 22 in collaboration with the Nye County Early Warning Drilling Program, which obtained both the water discharge and tracer injection permits at this location. The results of these tests are presented in Section G6. The remainder of this section provides pretest predictions that were originally conducted for the planned cross-hole tracer testing at the 19D location, but they apply equally well to the cross-hole tracer testing eventually conducted at Site 22.

The pretest predictions for the cross-hole tracer tests place emphasis on (1) expected tracer arrival times under various assumptions, and (2) predicted lithium transport behavior given results of lithium sorption testing onto alluvium in the laboratory. The predictions serve to satisfy environmental permitting requirements and address a Key Technical Issue raised by the U.S. Nuclear Regulatory Commission (KTI RT 2.04).

The cross-hole tracer tests were expected to provide additional information on diffusive mass-transfer properties and the appropriate conceptual transport model for the saturated valley-fill system. They were also expected to provide field estimates of several transport parameters for performance-assessment calculations that cannot be obtained from single-well tracer testing, including effective flow porosity, longitudinal dispersivity, sorption parameters, and colloid transport parameters. Because sorbing radionuclides of interest to Yucca Mountain performance assessments cannot be used in field tests, sorption parameters were to be obtained for a weakly sorbing cation tracer, lithium ion. Although lithium transport is not of immediate interest to the project, its field-sorption behavior was to be compared to its laboratory-sorption behavior to determine whether laboratory-derived parameters provide reasonable estimates of field-scale retardation. If that proved to be the case, or if the laboratory parameters resulted in underestimation of field-scale sorption, the Project would gain credibility in its approach of using laboratory-derived radionuclide sorption parameters in performance-assessment calculations. On the other hand, if the field transport behavior of lithium indicated that lithium was sorbing less than predicted from laboratory experiments, then conceptual models and parameterizations of radionuclide sorption might have to be revisited to account for differences between lab and field observations.

Cross-hole tracer-test predictions were conducted primarily to estimate how long a cross-hole test may take to conduct for scheduling and budgeting purposes. However, pretest predictions were also a requirement imposed by the State of Nevada to obtain an environmental permit for tracer injections. Emphasis was placed on the sensitivity of the predictions to variables such as interwell separation, interval thickness, flow porosity, production rate, longitudinal dispersivity, two-dimensional vs. three-dimensional flow conditions, and most importantly, lithium sorption parameters. Two-dimensional flow conditions refers to a situation where a well fully penetrates a confined aquifer and, therefore, there is no flow in the vertical direction, whereas three-dimensional flow conditions refer to a situation in which a well is open to only a small fraction of the thickness of an aquifer so that flow occurs in all three dimensions without being influenced by upper and lower boundaries (e.g., confining layers). These represent two extremes of flow conditions (in a homogeneous, isotropic medium) with respect to cross-hole tracer transport times.

Many of these sensitivities can be effectively captured using a simple analytical expression for nonsorbing tracer transport times in radial convergent flow to a pumping well in a two-dimensional homogeneous, isotropic medium (i.e., a rearrangement of equation D-6 from Section D4.8.5) (Guimera and Carrera 2000 [DIRS 156830], Equation 6):

$$\tau = \frac{\eta \pi r_L^2 T}{Q} \quad (\text{Eq. G-2})$$

where

τ = mean transport time, hr

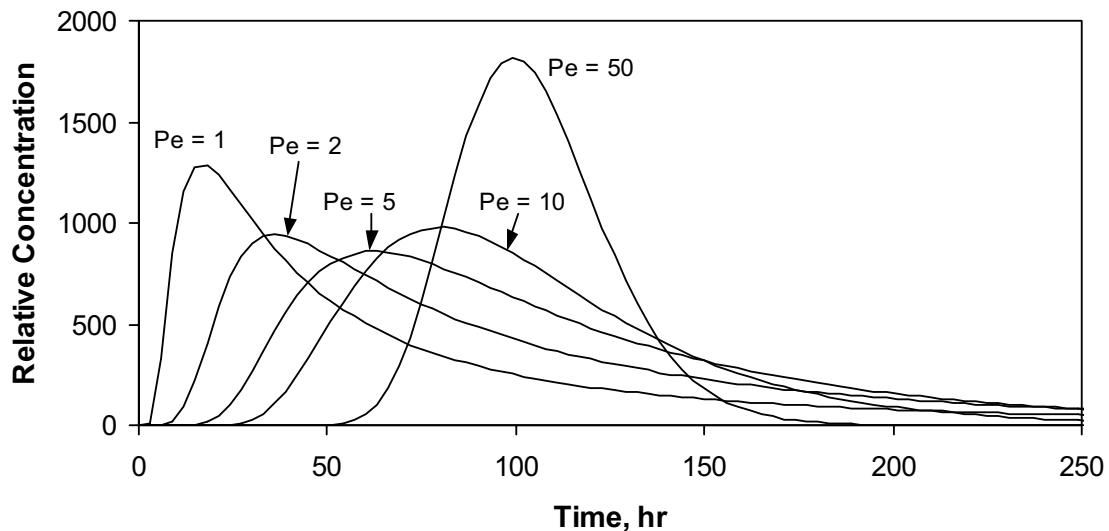
η = effective flow porosity

r_L = distance between injection and production wells, m

T = formation thickness, m
 Q = production flow rate, m³/hr.

Of course, any real flow system will never be completely homogeneous or isotropic, but this equation serves as a useful starting point for estimating transport times. It is clear that, all other things being equal, mean transport times will vary linearly with effective flow porosity and formation thickness, with the square of the distance between wells, and, inversely, with the production flow rate. Equation G-2 does not account for any delays associated with diffusion into stagnant water in the system, although these delays are not expected to affect first arrival times and peak arrival times of tracers significantly in the valley-fill deposits, which are of greater practical interest than the mean arrival time.

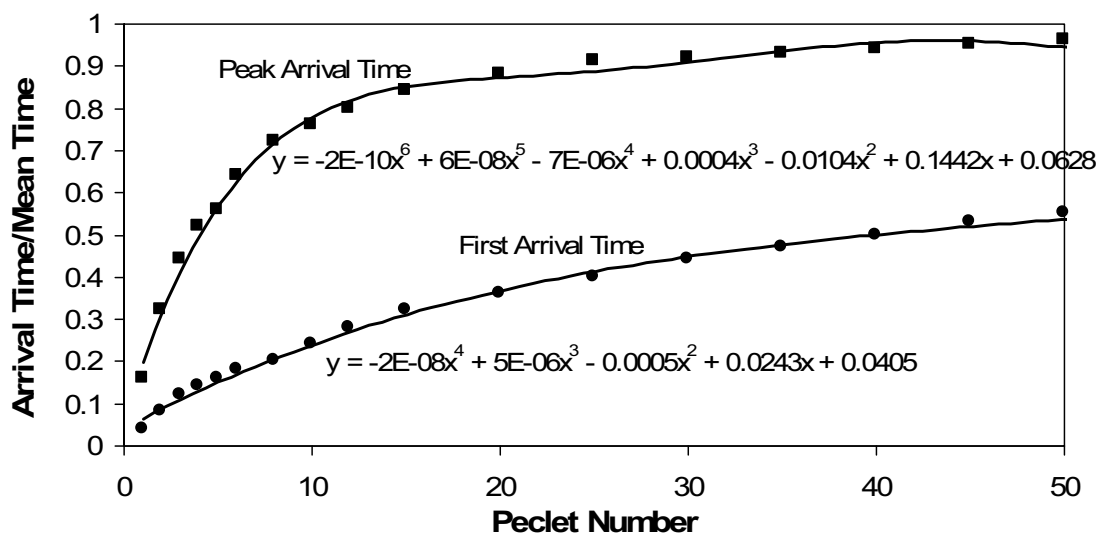
The first arrival times and peak arrival times of tracers were estimated as a function of mean transport time and dispersivity using the RELAP V 2.0 computer code (STN: 10551-2.0-00 [DIRS 159065]). A set of response curves showing the effect of dispersivity (or, more specifically, Peclet number, which is equal to the travel distance/dispersivity) on the first and peak arrival times for a given mean tracer residence time is shown in Figure G-9. The ratio of first arrival time to mean arrival time, and the ratio of peak arrival time to mean arrival time were both found to have a relatively smooth dependence on the Peclet number of the system. By obtaining a polynomial fit to these ratios as a function of Peclet number, the first and peak arrival times could be estimated from the mean arrival time obtained from equation G-2 for any assumed value of dispersivity. Plots of these ratios and the polynomial fits as a function of Peclet number are shown in Figure G-10.



Output DTN: LA0403PR831231.001.

NOTE: Peclet number is travel distance/dispersivity; mean arrival time is 100 hr; and flow is assumed to be linear, not radial.

Figure G-9. Relative Responses in a Single-Porosity Medium to a Pulse Function Input for Different Peclet Numbers



Output DTN: LA0403PR831231.001.

NOTE: Equations are polynomial fits to the "data." First arrival time is defined as the arrival time corresponding to 1% of the peak concentration.

Figure G-10. Ratios of First Arrival Time to Mean Arrival Time and Peak Arrival Time to Mean Arrival Time for Different Peclet Numbers

To obtain estimates of the mean, first, and peak arrival times for a sorbing tracer, the corresponding arrival times for a nonsorbing tracer can be multiplied by the retardation factor, R , given by (Freeze and Cherry 1979 [DIRS 101173], p. 404, Equation 9.14):

$$R = 1 + \frac{\rho_B}{\phi} K_d \quad (\text{Eq. G-3})$$

where

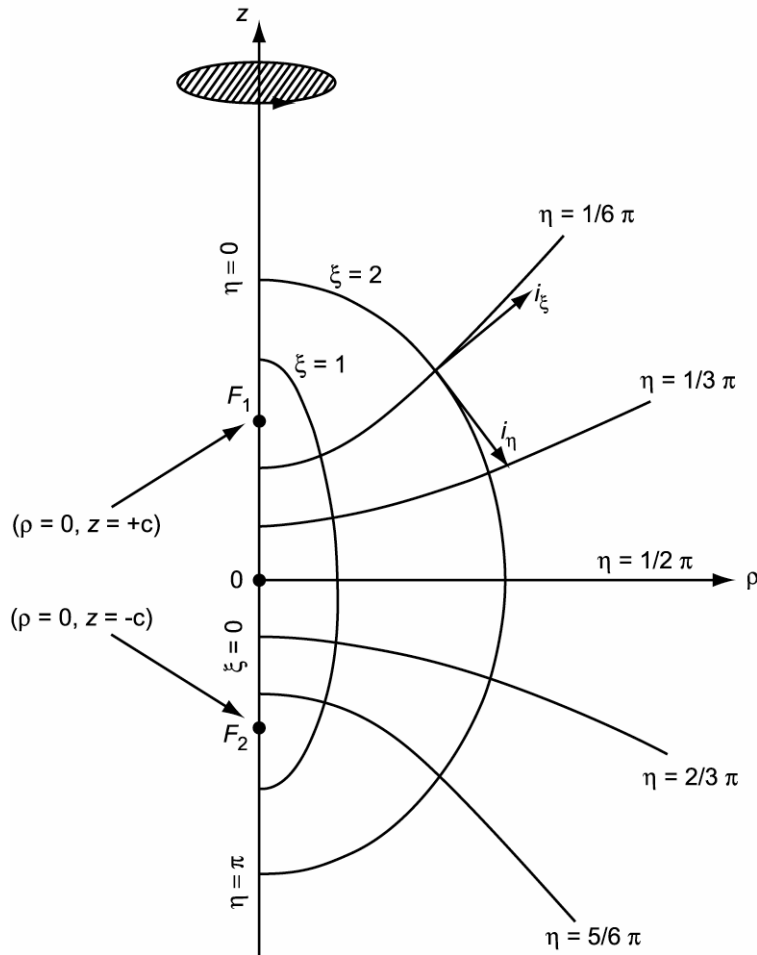
K_d = linear partition coefficient, mL/g
 ρ_B = bulk density of medium, g/cm³
 ϕ = porosity of medium.

To obtain an estimate of transport times in an unbounded three-dimensional flow system, the 2WELLS_3D V 1.0 computer code was used (STN: 10667-1.0-00 [DIRS 159036]). 2WELLS_3D is a particle-tracking code that simulates tracer transport between two wells in a homogeneous, isotropic medium. It assumes that flow streamlines between the injection and production well follow trajectories given by the prolate spheroidal coordinate system, shown in Figure G-11. This coordinate system reduces to spherical coordinates in the limit of $a = 0$ (i.e., a point source instead of a line source). A number of 2WELLS_3D simulations with zero dispersion were conducted to determine mean nonsorbing tracer residence times as a function of the ratio of well separation to interval length (i.e., length of screen or gravel pack). Because 2WELLS_3D superimposes tracer movement (as particles) onto an analytical solution of the three-dimensional flow field, there is, effectively, no numerical dispersion in the simulated tracer

responses. In the limit of a very large interval length relative to well separation, the arrival times approached those given by equation G-2 for radial flow in cylindrical coordinates; and in the limit of a very small interval length relative to well separation, the arrival times approached what would be expected for spherical flow [derivation found in Modeling and Interpretation of Transport Tests Scientific Notebook (Reimus 2003 [DIRS 165129], pp. 116 to 122)]:

$$\tau = \frac{4\eta\pi r_w^3}{3Q} \tag{Eq. G-4}$$

where the symbols are defined the same as in equation G-2.



Source: Happel and Brenner (1965 [D IRS 156833], Appendix A, Figure A-17.1(a)).

NOTE: η and ξ are coordinate designations by Happel and Brenner (1965 [DIRS 156833]); they have no relation to η and ξ elsewhere in this report.

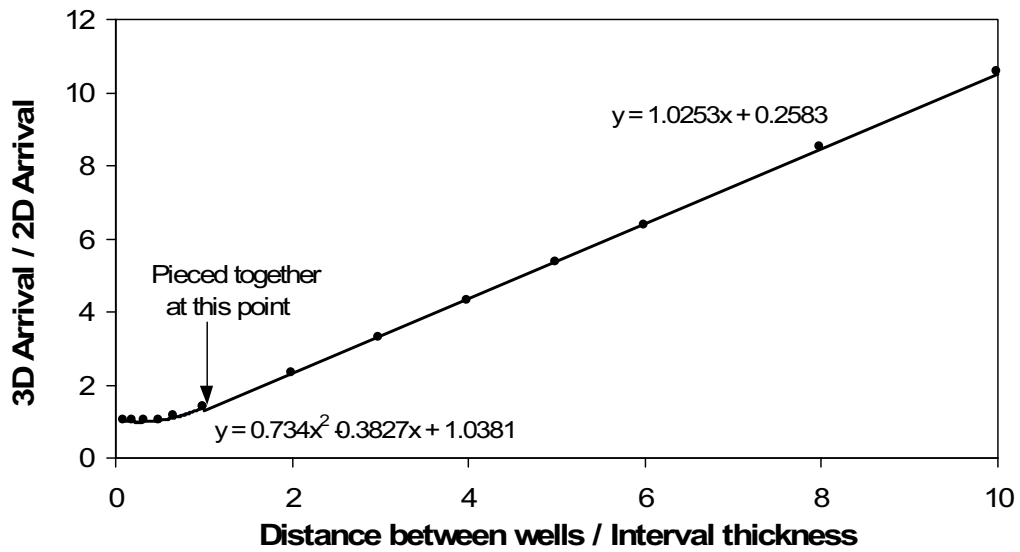
Figure G-11. Prolate Spheroidal Coordinate System Used for Unbounded Three-Dimensional Flow and Transport Calculations Using the 2WELLS_3D Code

The ratio of mean arrival time in unbounded three-dimensional flow to mean arrival time in two-dimensional flow was found to have a relatively smooth dependence on the ratio of well separation to interval length. This dependence and a piecewise fit to the simulated data are

shown in Figure G-12. Using the piecewise fit, it was possible to “correct” the mean arrival times resulting from equation G-2 to obtain corresponding arrival times for unbounded three-dimensional flow. The relationship shown in Figure G-12 was obtained from 2WELLS_2D V 1.0 (STN: 10665-1.0-00 [DIRS 159067]) and 2WELLS_3D V 1.0 (STN: 10667-1.0-00 [DIRS 159036]) simulations, assuming zero longitudinal and transverse dispersivity. However, the same correction factors were assumed to apply to the first and peak arrival times in cases where the dispersivity was not zero.

A final “correction” applied to the calculations described above was to account for shifts in first and peak tracer arrival times due to recirculation of produced water. Recirculation establishes a dipole flow pattern (Figure G-13) that causes some of the tracer mass to arrive earlier and some later than in the case of no recirculation. A correction factor for various recirculation ratios (ratios of recirculation flow rate to production flow rate) was obtained by simulating a series of tracer responses with different recirculation ratios using the 2WELLS_2D V 1.0 code (STN: 10665-1.0-00 [DIRS 159067]). This code is very similar to the 2WELLS_3D V 1.0 code (STN: 10667-1.0-00 [DIRS 159036]) except that it simulates cross-hole responses in two-dimensional flow using a cylindrical coordinate system instead of three-dimensional flow. These simulations assumed no longitudinal or transverse dispersion, so the travel-time shifts reflected only the changing flow patterns. As in the case of 2WELLS_3D, 2WELLS_2D superimposes tracer movement (as particles) onto an analytical solution of the two-dimensional flow field, so there is effectively no numerical dispersion in the simulated tracer responses. A subset of the resulting response curves is shown in Figure G-14. In reality, the response curves for the larger amounts of recirculation (greater than about 20%) should all have multiple tracer peaks that are equally spaced in time due to tracer recirculation. However, all but the first peak for each response curve was suppressed from the 2WELLS_2D output to clarify Figure G-14. With typical amounts of dispersion, these secondary peaks would be highly damped relative to the first peak anyway. Note that because there was no dispersion assumed for the simulations associated with Figure G-14, the first and peak arrival times nearly coincide. The correction factor for both first arrival times and peak arrival times was taken to be the ratio of peak recirculation arrival time to the peak arrival time without recirculation. These correction factors as a function of recirculation ratio, as well as a polynomial fit to the simulated data, are plotted in Figure G-15.

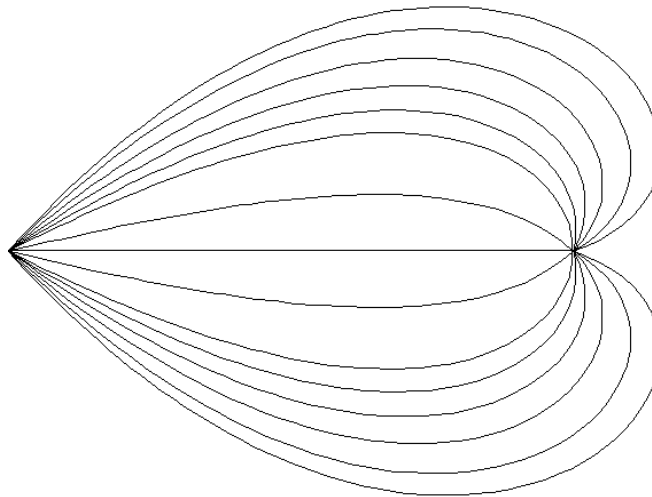
The methods described above for estimating first and peak arrival times while accounting for dispersion, sorption, unbounded three-dimensional flow, and recirculation ratio in cross-hole tracer tests are amenable to simple spreadsheet calculations once adequate expressions/fits are obtained for the dependence of the correction factors on the appropriate input parameters. A Microsoft Excel spreadsheet was set up for this purpose (Output DTN: LA0303PR831231.001). It should be noted that the spreadsheet calculations assume that the correction factors are linearly independent and commutative. That is, corrections are made by multiplying the mean arrival time (given by equation G-2) by each of the appropriate correction factors for a given set of test conditions.



Output DTN: LA0403PR831231.001.

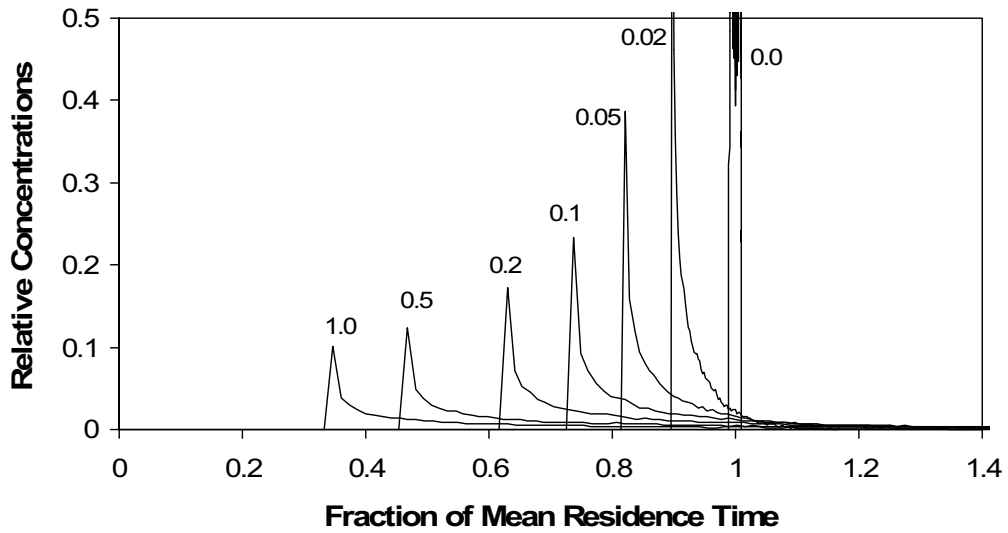
NOTE: A piecewise polynomial fit to the "data" is shown.

Figure G-12. Ratio of Mean Arrival Time in Unbounded Three-Dimensional Flow to Mean Arrival Time in Two-Dimensional Flow as a Function of Distance between Wells Divided by Interval Thickness



NOTE: For illustration purposes only. In the above pattern, the injection well is on the right, the production well is on the left, and the injection flow rate is 30% of the production flow rate. A homogeneous isotropic medium is assumed.

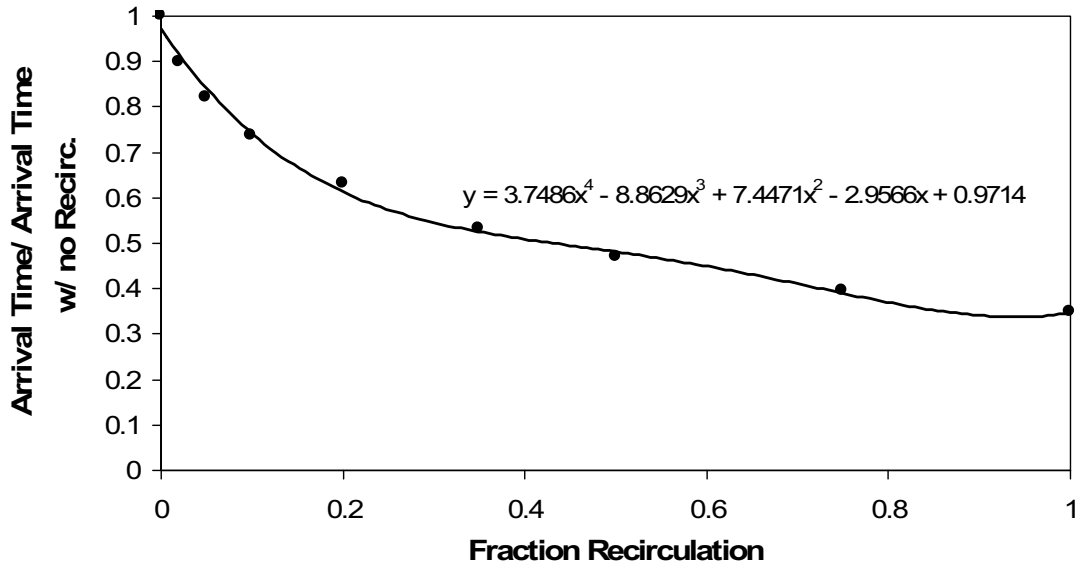
Figure G-13. Tracer Streamlines in a Weak Dipole Flow Pattern



Output DTN: LA0403PR831231.001.

NOTE: The numbers next to the curves above are the recirculation fractions; local dispersivity was set equal to zero; and secondary tracer peaks associated with tracer recirculation are not shown. The sharp early arrivals occur because of the zero longitudinal and transverse dispersion assumed in the simulations. The long tails are the result of a small number of flow streamlines having very long residence times.

Figure G-14. Predicted Nonsorbing Tracer Responses in a Two-Dimensional Homogeneous Isotropic Medium as a Function of the Recirculated Fraction of Produced Water



Output DTN: LA0403PR831231.001.

Figure G-15. Tracer Arrival Times as a Function of Fraction Recirculation in a Two-Dimensional Homogeneous Isotropic Medium

A final feature added to the Excel spreadsheet was the propagation of uncertainties of two key input parameters: flow porosity and well separation. Flow porosity is an uncertain parameter because it is an unknown property of the flow system, and well separation is uncertain because of vertical deviations that can occur during well drilling, which can result in significantly different separations at depth than planned. The propagation of these uncertainties was accounted for using standard error propagation methods and assuming that the uncertainties were not correlated (i.e., linearly independent). Without derivation, when these methods are applied to equation G-2, they yield the following result for the relative standard deviation of the transport time of a nonsorbing tracer as a function of standard deviation of the flow porosity and well separation [flow derivation found in Modeling and Interpretation of Transport Tests Scientific Notebook (Reimus 2003 [DIRS 165129])]:

$$\frac{\sigma_{\tau}}{\tau} = \sqrt{\frac{\sigma_{\eta}^2}{\eta^2} + 4 \frac{\sigma_{r_L}^2}{r_L^2}} \quad (\text{Eq. G-5})$$

where

σ_i = standard deviation of variable i

τ = mean residence time, hr

η = flow porosity

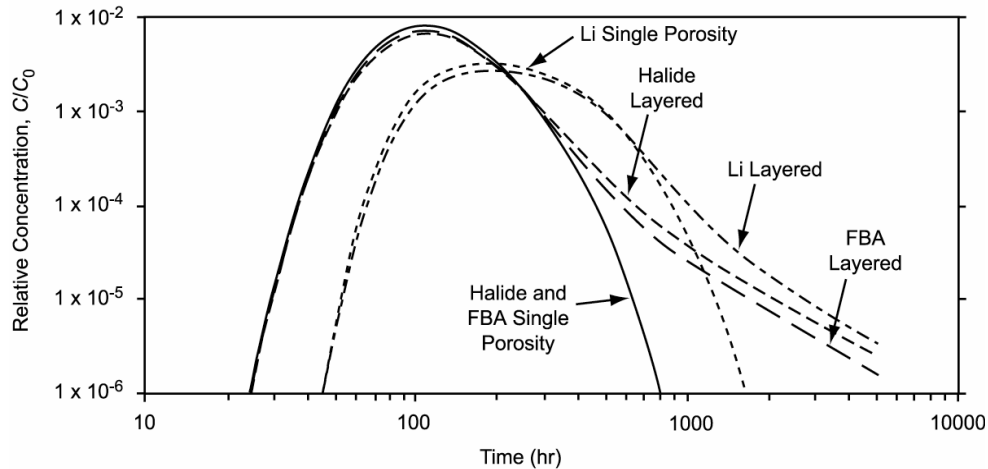
r_L = well separation, m.

To provide a measure of transport time uncertainties, the Excel spreadsheet calculates mean, first, and peak tracer transport times associated with $\pm \sigma_{\tau} \tau$ (i.e., transport times that are plus and minus one standard deviation from the best estimate).

An additional parameter of considerable uncertainty is the K_d sorption parameter for sorbing tracers. However, a formal propagation of uncertainty calculation for this parameter was not included in the spreadsheet. Rather, it is left to the analyst to evaluate this uncertainty by manually entering different K_d values and determining what effect these have on predicted transport times.

As mentioned at the beginning of this section, all simulations using the RELAP V 2.0 (STN: 10551-2.0-00 [DIRS 159065]), 2WELLS_2D V 1.0 (STN: 10665-1.0-00 [DIRS 159067]), and 2WELLS_3D V 1.0 (STN: 10667-1.0-00 [DIRS 159036]) codes assumed a single-porosity system with no diffusive mass transfer into nonadvective water. Two sets of paired MULTRAN V 1.0 (STN: 10666-1.0-00 [DIRS 159068]) simulations were conducted to illustrate the impact of relaxing this assumption on predicted cross-hole responses. One set used sorption parameters corresponding to the strongest lithium sorption that has been observed in laboratory batch sorption tests with 19P or 19D material, and the other set used parameters corresponding to the weakest lithium sorption observed. Of the two simulations in each pair, one used parameters corresponding to the single-porosity system for the single-well tracer test simulations (conceptual model of Figure G-1a) and the other used parameters corresponding to the layered flow system for the single-well simulations (Figure G-1c). The latter system had the greatest predicted mass loss from advective flow pathways of the three conceptual models shown in Figure G-1 in the single-well simulations. The predicted cross-hole responses of a halide, an

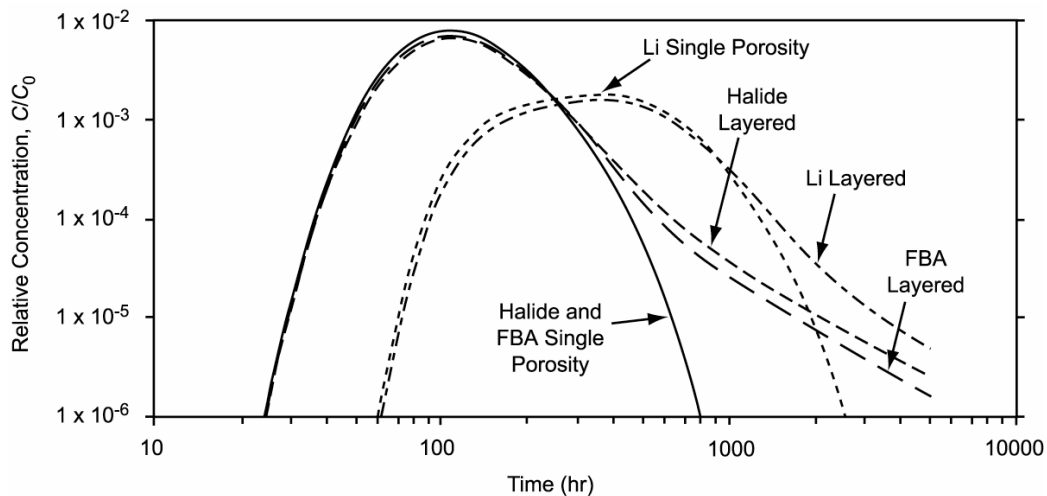
FBA, and lithium ion for each type of flow system are shown in Figures G-16 and G-17 for the cases of weak and strong lithium sorption, respectively. A mean tracer residence time of 150 hr (for nonsorbing tracers) and a Peclet number of 10 were arbitrarily chosen for the simulations. The injection concentrations were assumed to be 0.1 mole/L for LiBr (694 mg/L Li^+ , and 7,990 mg/L Br^-) and 0.01 mole/L for the FBA (1,500 mg/L to 2,000 mg/L depending on the specific FBA), and the injection pulse duration was assumed to be 10 hrs. There was no recirculation in the simulations. The 150-hr mean residence time corresponds to a relatively low effective flow porosity or a relatively high production flow rate in the valley-fill deposits if a well separation of 18 m (the approximate separation between 22PA and 22S) is assumed and if the flow intervals are assumed to be 30-m thick, which is approximately the gravel-pack thickness in the valley-fill deposits at Site 22. Table G-4 provides combinations of flow system parameters and production flow rates that result in mean nonsorbing tracer residence times of 150 hr based on equation G-2. It is apparent in Figures G-16 and G-17 that the differences in first and peak arrival times of any given tracer as a function of the system conceptualization (single porosity vs. layered system) are trivial. However, the first and peak arrival times for lithium are quite different in the two figures depending on whether weak (Figure G-16) or strong (Figure G-17) sorption is assumed. Also, the tails of the tracer responses are significantly different for the different system conceptualizations because the layered system has a secondary porosity that tracers diffuse into and out of, which results in the long tailing behavior typical of a dual-porosity system. The parameters assumed for the layered system are the same as those listed in Table G-1. The single-porosity system was assumed to have the same geometry and parameters as the layered system except that the nonadvective region was assigned a porosity of zero so that it played no part in tracer transport. The parameters used to describe cation exchange between lithium, sodium, and calcium are listed in the figure captions (see Equations E-11 and E-12 in Section E3.1.3). These parameters are representative of the smallest (Figure G-16) and largest (Figure G-17) amounts of lithium exchange observed in laboratory batch-sorption experiments conducted to date (see Section G6).



Output DTN: LA0303PR831231.001.

NOTE: Lithium sorption parameters are $Q_1 = 0.17$, $Q_2 = 0.019$ L/kg, cation-exchange-capacity (CEC) = 0.024 eq/kg (see Equations E-11, E-12, and E-14); the two systems have the same mean tracer residence time of 150 hr; and the peak lithium concentration occurs at about 190 hr, whereas the peak FBA and halide concentrations occur at about 110 hr.

Figure G-16. Predicted Cross-Hole Responses for a Halide, FBA, and Lithium Ion in a Single-Porosity System and a Layered System with Weak Lithium Sorption



Output DTN: LA0303PR831231.001.

NOTE: Lithium sorption parameters are $Q_1 = 0.35$, $Q_2 = 0.005$ L/kg, $CEC = 0.345$ eq/kg (see Equations E-11, E-12, and E-14); the two systems have the same mean tracer residence time of 150 hr; the peak lithium concentration occurs at about 390 hr, whereas the peak FBA and halide concentrations occur at about 110 hr; and the peak lithium concentration is approximately 1.75 times lower than in Figure G-16.

Figure G-17. Predicted Cross-Hole Responses for a Halide, FBA, and Lithium Ion in a Single-Porosity System and a Layered System with Strong Lithium Sorption

Table G-4. Combinations of Flow-System Parameters and Production Flow Rate that Result in a Mean Nonsorbing Tracer Residence Time of 150 Hours in a Cross-Hole Tracer Test

Well Separation (m)	Interval Thickness (m)	Flow Porosity	Production Flow Rate (L/min [gpm])
25	40	0.1	874 [231]
25	40	0.3	2,619 [692]
20	40	0.1	560 [148]
20	40	0.3	1,677 [443]
25	8	0.1	174 [46]
25	8	0.3	522 [138]
20	8	0.1	114 [30]
20	8	0.3	337 [89]

Output DTNs: LA0403PR831231.001; LA0303PR831231.005.

G4. RESULTS AND INTERPRETATION OF SINGLE-WELL TRACER TESTS IN ALLUVIUM

Three single-well injection-withdrawal tracer tests were conducted in the saturated alluvium of NC-EWDP-19D between December 2000 and April 2001, and two single-well tracer tests were conducted in the alluvium of NC-EWDP-22S in December 2004 and January 2005. Detailed documentation of the tracer tests in 19D is contained in Umari et al. (2003 [DIRS 164573]) and Reimus (2003 [DIRS 165128]). Documentation of the tracer tests in 22S is contained in this analysis report.

In each of the single-well tracer tests, two nonsorbing solute tracers with different diffusion coefficients were simultaneously injected (a halide and an FBA dissolved in the same solution). The three tests in 19D were conducted in essentially the same manner except for the time that was allowed to elapse between the cessation of tracer and chase water injection and the initiation of pumping – that is, the so-called “rest” or “shut-in” period. The rest period was systematically varied from approximately 0.5 hr, to approximately 2 days, to approximately 30 days in the 19D tests to vary the time allowed for tracers to diffuse into stagnant water in the flow system and for the tracers to migrate with the natural groundwater flow. The two tests in 22S were also conducted in identical manner except for the “rest” period, which was ~3 days and ~30 days, respectively. Test interpretations were based on comparing the responses of the different tracers in the same test and in different tests (“responses” refers to tracer concentrations normalized to injection mass as a function of time or volume pumped). As demonstrated in Section G2, the differences between the responses of two tracers with different diffusion coefficients in the same test and in tests with different rest periods can yield valuable information on diffusive mass transfer between flowing and stagnant water in the flow system and on the relative volumes of flowing and stagnant water in the system. In this section, it will be shown that differences in the responses of tracers with the same (or similar) diffusion coefficients in tests with different rest periods can provide information on ambient groundwater flow velocities in the flow system.

All three tests in 19D were conducted in the uppermost screened interval of the well, which ranges from approximately 15 to 21 m (50 to 70 ft) below the water table (gravel pack from approximately 14 m to 23 m (45 to 75 ft) below the water table). The static water table is

approximately 107 m (350 ft) below land surface at this location. The tracer solution volume injected in each test was approximately 11,000 L (2,900 gallons), and the volume of chase water (untraced water injected immediately after the tracer solution) was approximately 83,000 L (22,000 gal). The chase water was intended to push the tracers into the formation so as to minimize the influence of the wellbore and gravel pack on the test results. Actual distances penetrated by the tracer solution into the formation ultimately depend on the effective porosity of the formation and its spatial variability in hydraulic conductivity, which are uncertain quantities at this time.

The two tests in 22S were conducted in the second screened interval from the surface of the well, which ranges from approximately 57 to 87 m below the water table (gravel pack from approximately 55 to 90 m below the water table). The static water table is approximately 144 m (472 ft) below land surface at this location. The tracer solution volume injected in each test was approximately 5,700 L (1,500 gal), and the volume of chase water was approximately 76,000 L (20,000 gal).

The tracers used in each test and their injection concentrations and recoveries, the injection and withdrawal flow rates (averages), and the volumes pumped during each test are listed in Table G-5 for 19D and Table G-6 for 22S. Tracer solutions were prepared by adding tracers to groundwater that had been withdrawn from either 19D or 22S prior to any of the tests. Tracer concentrations were kept low and, at 19D, the solutions were heated to roughly match the ambient groundwater temperature to minimize density contrasts between the injection and chase solutions and the groundwater (the injection and chase water were not heated at 22S).

Table G-5. Summary of Tracers and Test Conditions in the Three Single-Well Tracer Tests in NC-EWDP-19D

Rest Period (Test)	0.5 hr	2 days	30 days
Dates	1/5/01 to 1/12/01	12/1/00 to 12/18/00	1/27/01 to 4/25/01
Tracers (injection concentration)	2,4-DFBA (0.46 g/L) Cl ⁻ (0.62 g/L NaCl) 640-nm microspheres	2,6-DFBA (0.46 g/L) I ⁻ (0.64 g/L KI)	PFBA (0.46 g/L) Br ⁻ (0.63 g/L NaBr)
Injection rate (L/min [gpm])	56.8 [15.0]	56.8 [15.0]	56.8 [15.0]
Average pumping rate (L/min [gpm])	50.3 [13.3]	41.3 [10.9]	51.67 [13.65]
Pumping duration (days)	7	14	54
Total liters [gallons] pumped	511,500 [135,100]	814,000 [215,000]	4,020,000 [1,062,000]
Tracer recovery (FBA)	0.864	0.928	0.913

Output DTN: LA0303PR831231.002.

Sources: DTNs: GS020708312316.001 [DIRS 162678] (injection and discharge rates); UN0109SPA008IF.006 [DIRS 162442] (0.5-hr tracer concentration data); UN0102SPA008KS.003 [DIRS 162614] (2-day tracer concentration data); UN0109SPA008KS.007 [DIRS 162615] (30-day PFBA concentration data); UN0109SPA008KS.008 [DIRS 162616] (30-day bromide concentration data); Stetzenbach 2001 [DIRS 180730] (2-day tracer injection masses); Farnham 2001 [DIRS 180732] (0.5-hr tracer injection masses); Farnham 2001 [DIRS 180733] (30-day tracer injection masses).

NOTES: Pumping duration is rounded to the nearest day. Total volumes pumped are approximate.

DFBA = difluorobenzoate; FBA = fluorinated benzoate; gpm = gallons per minute; PFBA = pentafluorobenzoate.

Table G-6. Summary of Tracers and Test Conditions in the Two Single-Well Tracer Tests in NC-EWDP-22S

Rest Period (Test)	3 days	30 days
Dates	12/3/04 to 12/10/04	12/13/04 to 1/26/05
Tracers (injection concentration)	PFBA (0.25 g/L) I ⁻ (0.75 g/L NaI)	2,3,4,5-TeFBA (0.25 g/L) I ⁻ (0.75 g/L NaI)
Average Injection/chase rate (L/min [gpm])	67.8 [17.9]	58.7 [15.5]
Average pumping rate (L/min [gpm])	178.7 [47.2]	179.8 [47.5]
Pumping duration (days)	4.3	13
Total liters [gallons] pumped	1,110,000 [292,000]	3,370,000 [890,000]
Tracer recovery (I ⁻)	1.0	0.98

Sources: DTNs: LA0612PR831231.001 [DIRS 178733] (3-day data), LA0612PR831231.002 [DIRS 178735] (30-day data).

NOTES: Pumping duration for 30-day test is rounded to the nearest day. Total volumes pumped are approximate. PFBA = pentafluorobenzoate; TeFBA = tetrafluorobenzoate.

G4.1 SINGLE-WELL TRACER TEST RESULTS

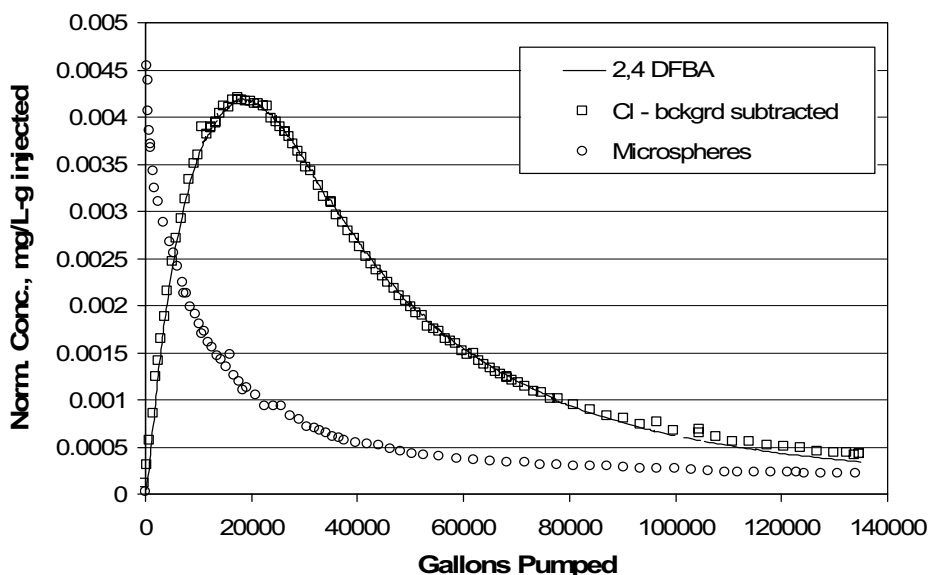
Figures G-18, G-19, and G-20 show the normalized tracer responses in the each of the three tracer tests in 19D. Figures G-21 and G-22 show the normalized tracer responses in the two tracer tests in 22S. At 19D, the two simultaneously-injected solute tracers had essentially identical responses (within experimental error) in each test. This result is consistent with very little diffusive mass transfer between flowing and stagnant water in the aquifer over the time scales of the tests. It is, therefore, consistent with a single-porosity conceptualization of the saturated alluvium. The flow interruptions during the tailing portions of the two longer tests provided additional evidence for very little diffusive mass transfer in the aquifer. If diffusive mass transfer were an important process, the tracer concentrations would have increased significantly immediately after the flow interruptions due to tracers diffusing out of stagnant water and into flowing water during the interruptions. The microspheres used in the shortest rest period test (Figure G-18) provided information on colloid filtration and detachment rates in the flow system (see Section G4.6).

At 22S (Figures G-21 and G-22), the two simultaneously-introduced solute tracers had notably different responses in each single-well test, indicating that there was probably some diffusion occurring between flowing and stagnant water in the aquifer at this location. Concentrations in automatically-collected samples and grab samples and also normalizations of the tracer concentrations using the measured tracer injection masses and the measured concentrations in the tracer injection solutions were in very good agreement in both tests, so it is unlikely that the differences in normalized concentrations were caused by systematic errors associated with sampling or errors in the deduced masses used in the normalizations. In each test, the tracer with the larger diffusion coefficient (iodide) had a higher normalized peak concentration than the tracer with the smaller diffusion coefficient (PFBA or TeFBA), and the difference between the peak concentrations was greater in the test with the longer rest-period. These responses are consistent with diffusion into stagnant water that has a relatively short diffusion distance scale. That is, it appears that both tracers were able to diffuse into the majority of the accessible stagnant water during their residence time in the formation, and the higher peak concentration of

the more diffusive tracer was the result of it diffusing *out of* the stagnant water faster than the less diffusive tracer. This interpretation is explored more quantitatively in Section G4.7.

Figure G-23 shows how the responses of the FBAs differed as a function of volume pumped in each of the three tracer tests in 19D. Because diffusion can be ruled out as having caused these differences (based on the nearly-identical normalized responses of the FBAs and halides), the most plausible explanation is that the differences are due to drift with natural groundwater flow during the different rest periods. These different responses and the assumption that they are due to drift form the basis of three separate methods of estimating drift or seepage velocities in the aquifer.

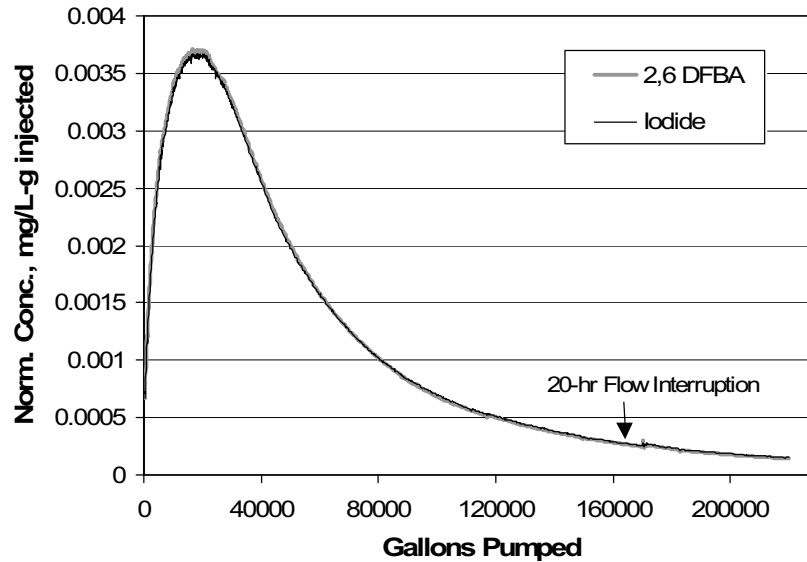
Figure G-24 shows the responses of iodide as a function of time in the two single-well tracer tests conducted in 22S. In this case, plotting the concentrations as a function of time provides a valid comparison of the breakthrough curves because the pumping rates in the two tests were nearly identical. It is apparent that the differences between the two iodide breakthrough curves are too large to be attributed entirely to diffusion. In particular, the shift in peak concentration to earlier times for the longer rest-period test is not consistent with diffusion as the only explanation for the different responses. As in the case of the 19D tracer responses, the most plausible explanation for these differences is drift with the natural groundwater flow during the different rest periods.



Sources: DTNs: UN0109SPA008IF.006 [DIRS 162442] (2,4-DFBA and Cl), LA0207PR831352.001 [DIRS 162431] (microspheres).

NOTE: Microspheres were 640-nm diameter carboxylate-modified latex (CML) polystyrene spheres tagged with a UV-excited fluorescent dye for detection. The figure is plotted in English units because the data were obtained in those units. However, parameter estimates are reported in metric units to downstream users.

Figure G-18. Normalized Concentrations of Tracers in Production Water from NC-EWDP-19D as a Function of Gallons Pumped after a Rest Period of Approximately 0.5 Hours

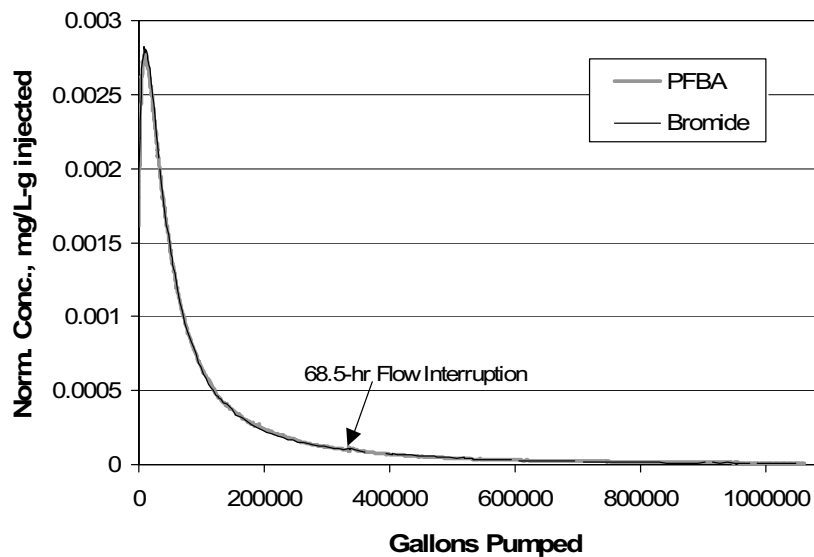


Source: DTN: UN0102SPA008KS.003 [DIRS 162614].

Output DTN: LA0303PR831231.002 (volumes).

NOTE: The tracer responses are almost identical, so it is difficult to distinguish between the two responses. The figure is plotted in English units because the data were obtained in those units. However, parameter estimates are reported in metric units to downstream users.

Figure G-19. Normalized Concentrations of Tracers in Production Water from NC-EWDP-19D as a Function of Gallons Pumped after a Rest Period of Approximately 2 Days

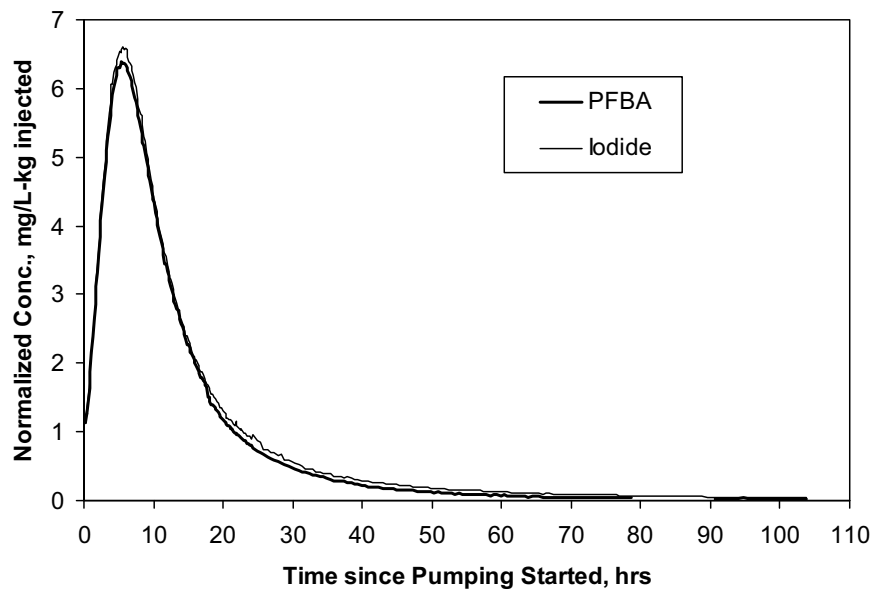


Sources: DTNs: UN0109SPA008KS.007 [DIRS 162615] (PFBA), UN0109SPA008KS.008 [DIRS 162616] (Br).

Output DTN: LA0303PR831231.002 (volumes).

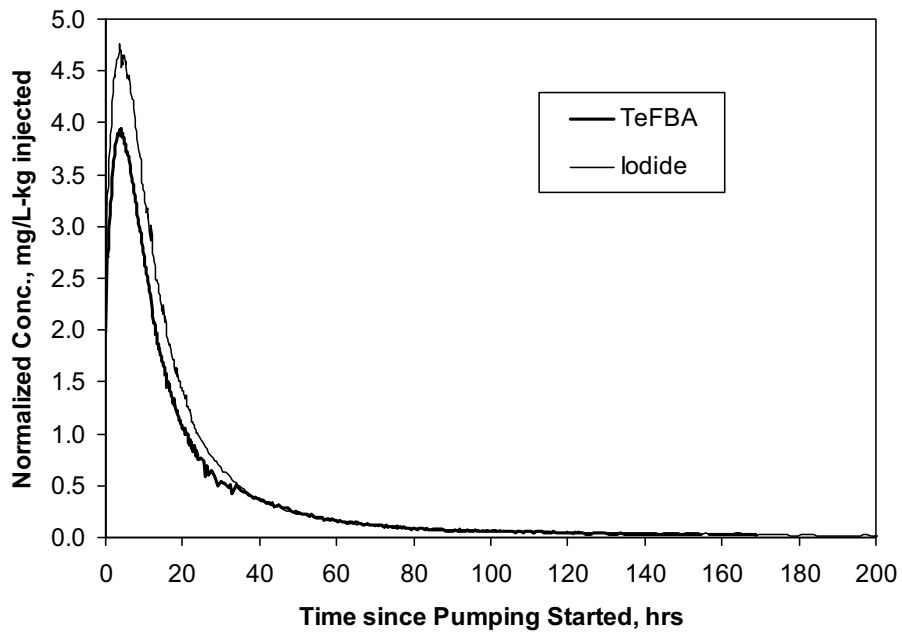
NOTE: The tracer responses are almost identical, so it is difficult to distinguish between the two responses. The figure is plotted in English units because the data were obtained in those units. However, parameter estimates are reported in metric units to downstream users.

Figure G-20. Normalized Concentrations of Tracers in Production Water from NC-EWDP-19D as a Function of Gallons Pumped after a Rest Period of Approximately 30 Days



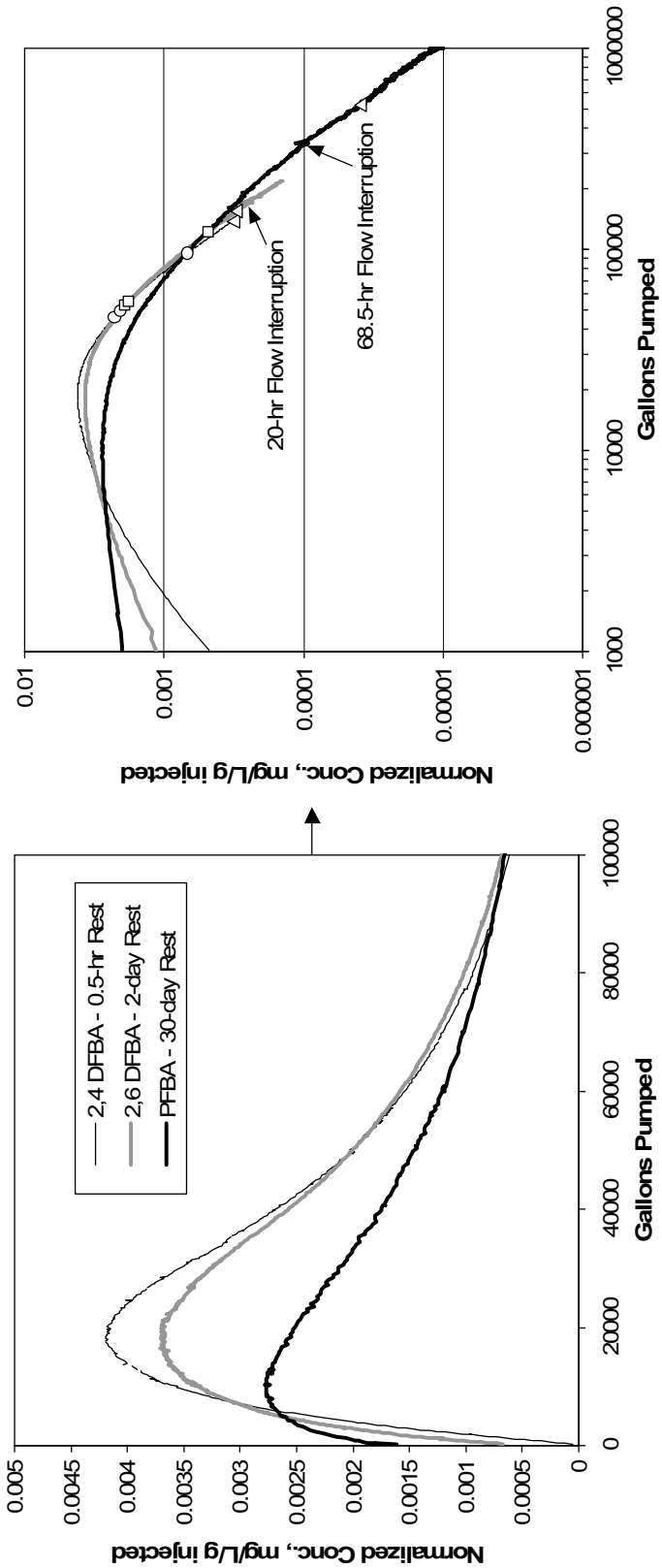
Source: DTN:LA0612PR831231.001 [DIRS 178733].

Figure G-21. Normalized Concentrations of Tracers in Production Water from NC-EWDP-22S as a Function of Time after a Rest Period of Approximately 3 Days



Source: DTN:LA0612PR831231.002 [DIRS 178735].

Figure G-22. Normalized Concentrations of Tracers in Production Water from NC-EWDP-22S as a Function of Time after a Rest Period of Approximately 30 Days

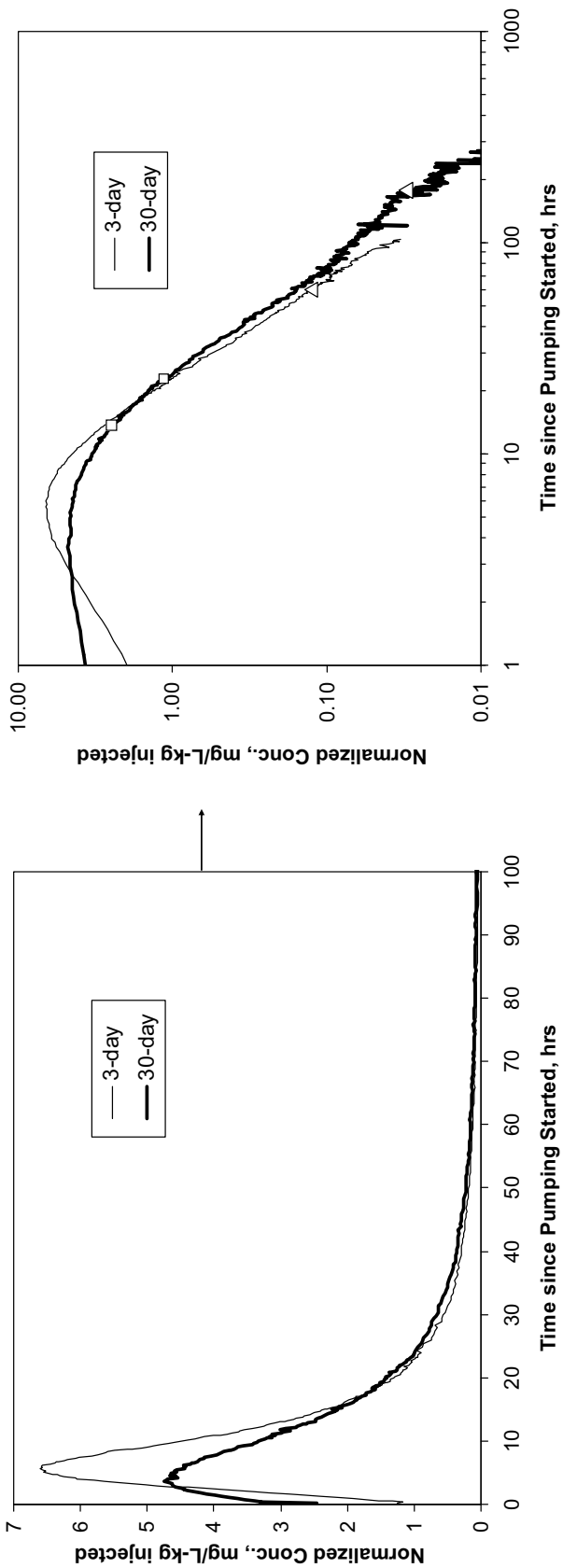


Sources: DTNs: UN0109SPA008IF.006 [DIRS 162442] (2,4-DFBA), UN01 02SPA008KS.003 [DIRS 162614] (2,6-DFBA), UN0109SPA008KS.007 [DIRS 162615] (PFBA).

Output DTN: LA0303PR831231.002 (volumes).

NOTE: On the right-hand plot, circles indicate volumes associated with mean arrival times (for each tracer response), squares indicate volumes associated with alternate mean arrival times, and triangles indicate volumes associated with "late" arrival times. The left-most symbol is always associated with the 0.5-hr rest-period test, and the right-most symbol is associated with the 30-day rest-period test. The bases for these different arrival times/volumes are discussed in detail in Section G4.2. The figure is plotted in English units because the data were obtained in those units. However, parameter estimates are reported in metric units to downstream users.

Figure G-23. Normalized Concentrations of Fluorinated Benzoates as a Function of Gallons Pumped in Each of the Three Single-Well Tracer Tests in NC-EWDP-19D



Sources: DTNs: LA0612PR831231.001 [DIRS 178733] (3-da y), LA0612PR831231.002 [DIRS 178735] (30-day).

NOTE: On the right-hand plot, squares indicate volumes associated with mean arrival times (for each tracer response), and triangles indicate volumes associated with "late" arrival times. The left-most symbol is always associated with the 3-day rest-period test, and the right-most symbol is associated with the 30-day rest-period test. The bases for these different arrival times/volumes are discussed in detail in Section G4.2.

Figure G-24. Normalized Concentrations of Iodide as a Function of Pumping Time in the Two Single-Well Tracer Tests in NC-EWDP-22S

G4.2 ESTIMATION OF GROUNDWATER VELOCITY

Four methods were used to obtain groundwater velocity estimates from the single-well tracer tests. The first three methods involve relatively simple spreadsheet calculations that, given various simplifying assumptions, solve for groundwater velocities that are consistent with the observed differences in the following:

1. Peak tracer concentration arrival times.
2. “Late” arrival times, defined as the times in each test at a given location when the fractional tracer mass recovery was equal to the final recovery in the test at that location having the lowest overall mass recovery. At 19D, the total mass recoveries in the three tests were 0.864, 0.928, and 0.913 (Table G-5), so the late arrival time in each test was the time at which the mass recovery was 0.864. At 22S, a mass recovery of 0.967 was used, which was the recovery associated with the last consecutively analyzed sample in the longer-rest-period test. The fluorinated benzoate breakthrough curves were used for the analyses of the 19D tests, and the iodide breakthrough curves were used for the analyses of the 22S tests.
3. “Mean” arrival times of tracer mass recovered at the same arbitrarily selected high fractional recovery in each test. For the 19D tests, two different fractional recoveries were selected to calculate mean arrival times: 0.864, the lowest fractional recovery in any of the tests, and 0.913, the fractional recovery in the 30-day-rest-period test. In the latter case, the tracer responses in the test with a mass recovery of 0.864 were extrapolated to 0.913 (see Section G4.2.3 for details) to allow a calculation of the mean arrival time. This alternative method of calculating the mean arrival time was employed because the 30-day test had the largest calculated mean arrival time, and it was, therefore, considered to have the greatest amount of information pertinent to groundwater velocity estimates. For the 22S tests, the mean time was calculated based on a fractional recovery of 0.967 in each test (i.e., the last 0.033 fraction of tracer mass was not included in the calculation). Again, the fluorinated benzoate breakthrough curves were used for the analyses of the 19D tests, and the iodide breakthrough curves were used for the analyses of the 22S tests.

Note that these times also correspond to volumes pumped, and because the pumping rates varied in the different tests at 19D, the relationship between times and volumes is different for each test at this location. The peak, late, and mean arrival times (and corresponding volumes) for each test are listed in Table G-7. The points on the tracer breakthrough curves corresponding to the mean and late arrival times in each test are identified in the right-hand plot of Figure G-23 for the 19D tests, and in the right-hand plot of Figure G-24 for the 22S tests. The fourth method, which was only applied to the 19D test data, involved detailed analytical calculations of tracer migration during the tests by linking together solute transport solutions that assume a two-dimensional homogeneous and isotropic aquifer.

Because the peak tracer concentrations occurred earliest in the tests with the longest rest period at both locations, the tracer mass corresponding to the peak probably moved upgradient during injection and then drifted back toward the well during the rest period. In contrast, the tracer

mass corresponding to times at which fractional recoveries were high (i.e., mass recovered far out in the tails of the responses) probably moved downgradient during injection and arrived late because of the competing effects of drift that moved the tracer further from the well and pumping the tracers toward the well. The mean tracer arrival time represents a compromise between these two cases, as the mean is influenced by both early and late-arriving tracer mass. However, for asymmetric long-tailed distributions, the mean is more strongly influenced by late-arriving mass than early arriving mass, so it was assumed that the differences in mean arrival times were due mainly to tracer mass that had moved downgradient during injection.

Table G-7. Times and Pumped Volumes Associated with Each of the Single-Well Tracer Test Arrival Times Used in the Different Methods of Estimating Groundwater Velocities

	Arrival Time (hr)/Volume (L [gal])		
	0.5 hr	2 days	30 days
19D Rest Period:			
Peak arrival	24 / 76,000 [20,000]	30.5 / 76,000 [20,000]	12.2 / 38,600 [10,200]
Late arrival ^a	168 / 511,000 [135,000]	225 / 556,000 [147,000]	639 / 1,780,000 [471,000]
Mean arrival ^b	52 / 161,000 [42,500]	71 / 178,000 [46,500]	109 / 344,000 [91,000]
Alternate mean arrival ^c	61.5 / 189,000 [50,000]	81 / 201,000 [53,000]	149 / 469,000 [124,000]
22S Rest Period:			
Peak arrival	5.6 / 60,000 [15,900]		3.8 / 41,000 [10,800]
Late arrival ^d	57 / 611,000 [161,400]		169 / 1,820,000 [481,700]
Mean arrival ^e	12.6 / 135,000 [35,700]		20.9 / 225,500 [59,600]

Sources: DTNs: UN0109SPA008IF.006 [DIRS 162442] (19D, 0.5 hr); UN0102SPA008KS.003 [DIRS 162614] (19D, 2 days); UN0109SPA008KS.007 [DIRS 162615] (19D, 30 days); LA0612PR831231.001 [DIRS 178733] (22S, 3 days); LA0612PR831231.002 [DIRS 178735] (22S, 30 days).

Output DTNs: LA0303PR831231.002 (19D); LA0701PR150304.001 (22S).

^a Time/volume associated with approximately 86.4% mass recovery in each test at 19D (the final recovery in the 0.5-hr rest period test, which had the lowest final recovery of any test).

^b Mean arrival time calculated by truncating all tracer response curves at approximately 86.4% recovery in each test.

^c Alternate mean arrival time calculated by extrapolating the tracer response curves in the 0.5-hr rest period test to 91.3% and truncating the response curves in the 2-day rest period test to 91.3% recovery (the final recovery in the 30-day rest period test).

^d Time/volume associated with approximately 96.7% mass recovery in each test at 22S.

^e Mean arrival time calculated by truncating all tracer response curves at 96.7% recovery in each test at 22S.

In all four estimation methods, it is assumed that injection into and pumping from the well results in a two-dimensional radial flow field in which the flow velocity varies as $1/r$:

$$v(r) = \frac{Q}{2h\eta\pi r} \quad (\text{Eq. G-6})$$

where

$v(r)$ = linear velocity as a function of radial position, m/hr

Q = injection or production flow rate, m^3/hr (negative number for production)

h = interval thickness, m

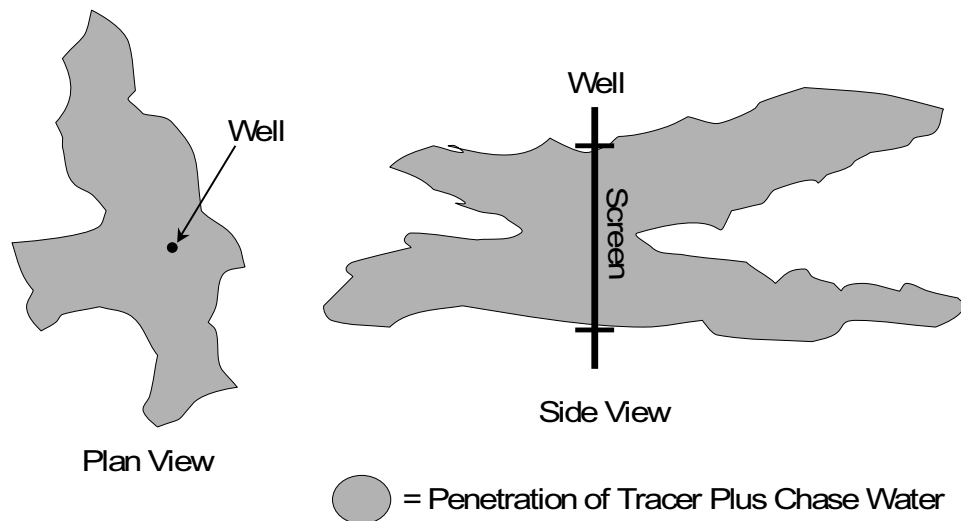
η = flow porosity

r = radial distance from the well, m.

For the first three methods, the ambient groundwater flow is superimposed on the radial flow induced by injection or pumping, and it is assumed to be present during the rest period when there is no radial flow component. The ambient flow is assumed to be unidirectional.

Flow fields resulting from injection and pumping will not be ideally radial unless the aquifer is perfectly homogeneous, isotropic, and two-dimensional. Figure G-25 shows a hypothetical representation of how injected tracer solution and chase water might be distributed in the aquifer immediately after injection. Figure G-25 represents only one of many possibilities for how heterogeneity might affect tracer distribution in the system, and all of these possibilities must be considered equally likely given the present knowledge of the flow system. Although it may not be strictly correct, the radial flow assumption is qualitatively consistent with the picture of heterogeneity shown in Figure G-25 because the flow velocity will maintain an approximately $1/r$ dependence as long as the flow cross-sectional area “fans out” such that it increases approximately linearly with r . Only highly channelized flow that does not increase significantly in cross-sectional area with r will have a velocity that does not decrease as approximately $1/r$. In pipeline flow, the extreme case of channelized flow, there is no dependence of velocity on r .

Alternatively, if the system is not two-dimensional, the flow cross-sectional area could increase with more than a linear dependence on r , with the extreme case being spherical flow where the velocity decreases as $1/r^2$ (at sufficiently large distances from the well). However, this latter possibility was ignored because (1) there is qualitative evidence (both lithologic and from hydraulic testing) of layering in the aquifer that could cause considerable vertical confinement, and (2) the injection volumes were small enough relative to the interval thickness and potential flow porosities that the tracer injection distances into the formation should have been relatively short compared to what it would take to approximate a spherical flow condition.

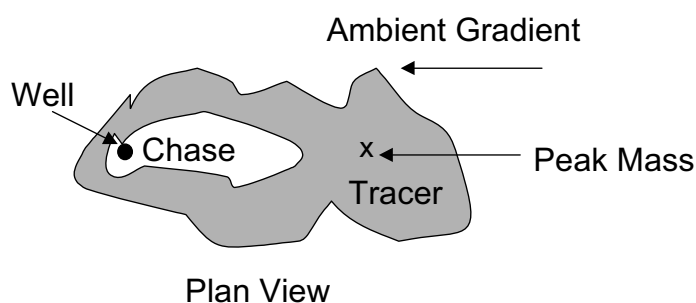


NOTE: For illustration purposes only.

Figure G-25. Depiction of How Tracer and Chase Water Might Be Distributed after Injection into a Heterogeneous Porous Medium

G4.2.1 Peak-Arrival-Time Analysis

For the analysis comparing the peak tracer arrival times, the mass contributing to the peak was assumed to move directly upgradient during injection. That is, the radial flow pushing the mass was assumed to be in the exact opposite direction as the ambient groundwater flow (Figure G-26). Any estimate of groundwater drift velocity using this assumption should be considered a lower bound because the peak mass will have the *greatest decrease* in arrival time as the rest period is increased when the mass is injected directly upgradient. Trigonometric calculations show that if the tracer mass corresponding to the peak concentration were injected at some angle relative to the ambient gradient direction, the groundwater velocity would have to be greater to result in the same decrease in arrival time (assuming a reasonably homogeneous system).



NOTE: For illustration purposes only. The shape of the distribution is not important; the key assumption is that the tracer mass associated with the peak concentration is located directly up-gradient.

Figure G-26. Depiction of Assumed Tracer Mass Distribution Immediately after Injection

Given the assumption of the peak tracer mass moving strictly upgradient, the distance that the tracer mass moved into the formation during the injection and chase phase is given by derivations of Equations G-7 to G-16 are documented in a scientific notebook by Reimus (2003 [DIRS 165129]):

$$r_{inj} = \sqrt{\frac{(0.5 V_{tracer} + V_{chase})}{\pi \eta h}} - v_{GW} \frac{(0.5 V_{tracer} + V_{chase})}{Q_{inj}} \quad (\text{Eq. G-7})$$

where

- r_{inj} = upgradient injection distance, m
- V_{tracer} = volume of tracer solution injected, m^3
- V_{chase} = volume of chase water injected, m^3
- v_{GW} = groundwater velocity (seepage velocity), m/hr
- Q_{inj} = injection flow rate, m^3/hr
- h = interval thickness, m
- η = flow porosity.

The first term in equation G-7 accounts for the distance injected under pure radial flow conditions, and the second term accounts for the drift back toward the well during injection. Only half of the tracer solution volume is used in equation G-7 because it is assumed that the tracer mass resulting in the peak should have corresponded to approximately the midpoint of the injection volume. However, the calculations are not sensitive to this assumption because the tracer solution volume in all tests was small relative to the chase volume.

The radial distance, r_{rest} , between the peak tracer mass and the well at the end of the rest period is given by:

$$r_{\text{rest}} = r_{\text{inj}} - v_{\text{GW}} t_{\text{rest}} \quad (\text{Eq. G-8})$$

where t_{rest} = duration of the rest period, hr.

The time required to pump the peak tracer mass back to the well after the rest period, t_{pump} , is calculated from the following integral:

$$t_{\text{pump}} = \int_{r_{\text{rest}}}^0 \frac{dr}{v(r)} \quad (\text{Eq. G-9})$$

where

$$v(r) = -\frac{|Q_{\text{pump}}|}{2h\eta\pi r} - v_{\text{GW}}$$

Q_{pump} = production flow rate, m^3/hr .

The solution to this integral (with $v(r)$ from equation G-6 inserted and using the appropriate upper and lower limits) is (Weast and Astle 1981 [DIRS 100833], p. A-36, Equations 84 and 85):

$$t_{\text{pump}} = \left[-\frac{r}{v_{\text{GW}}} + \frac{|Q_{\text{pump}}|}{2\pi\eta h v_{\text{GW}}^2} \ln \left(\frac{|Q_{\text{pump}}|}{2\pi\eta h} + v_{\text{GW}} r \right) \right]_{r=r_{\text{rest}}}^{r=0} \quad (\text{Eq. G-10})$$

t_{pump} can be converted to a volume corresponding to the arrival time of the peak concentration using:

$$V_{\text{pump}} = t_{\text{pump}} |Q_{\text{pump}}| \quad (\text{Eq. G-11})$$

The pertinent equations above were encoded into an Excel spreadsheet for the analysis (Output DTNs: LA0303PR831231.002 (19D) and LA0701PR150304.001 (22S)). The only unknown variables for each of the tests were the groundwater velocity, v_{GW} , and the flow porosity, η , both of which were assumed to be the same in all tests at a given location. The procedure for obtaining an estimate of v_{GW} involved selecting η and then varying v_{GW} by trial-and-error until

the calculated peak arrival volumes in the three tests had approximately the same ratios as in the actual field tests. It was considered more important to match the ratios of times than to match the actual times, although the calculated times were generally in reasonable agreement with the actual times, once the ratios were matched. In the case of the 19D tests, greater emphasis was placed on matching the volume ratio between the 30-day-rest-period test and the approximately 0.5-hr-rest-period test than on matching the volume ratios in any other pair of tests, particularly the two shorter tests. The uncertainty associated with a groundwater velocity estimate obtained from the two shorter duration tests at 19D was considered to be far greater than estimates obtained using the 30-day test results because of the much greater time allowed for drift to take place in the 30-day test. For this reason, only one short-rest-period test was conducted at 22S, and a rest period of 30 days was employed for the longer test.

The process of estimating v_{GW} was repeated for three different values of η - 0.05, 0.18, and 0.3. These values are approximately the lowest, expected (mean), and highest values, respectively, used for alluvium flow porosity in Yucca Mountain performance assessment simulations (BSC 2004 [DIRS 170042]). The value of v_{GW} was different in each case because of the dependence of equations G-7 and G-10 on η . For each case, a specific discharge, v_s , was calculated from v_{GW} using $V_s = \eta v_{GW}$.

G4.2.2 Analysis of Late Arrival Times (Associated with High Fractional Tracer Recoveries)

The analysis of late arrival times (arrival times associated with high fractional tracer recoveries) was similar to the analysis of peak arrival times except that the tracer mass associated with the late arrival time was assumed to have been injected downgradient rather than upgradient. This assumption seems reasonable, given that any mass injected upgradient should arrive earlier than the mean tracer arrival time, not later. Analogous to the peak arrival-time analysis, it was assumed that the mass was injected directly downgradient (in the same direction as the ambient groundwater flow). Any estimate of groundwater velocity using this assumption should be considered an upper bound because the late-arriving mass will have the *greatest increase* in arrival time as the rest period is increased if the mass is injected directly downgradient.

For the tests at 19D, the times/volumes associated with the final recovery in the approximately 0.5-hr-rest-period test (0.864), which had the lowest recovery of the three tests, were used as the basis of comparison of the late arrival times for the three tests. Although this is a somewhat arbitrary definition of the late arrival time because it depends on when pumping was stopped in the approximately 0.5-hr-rest-period test, it was considered to be the most objective measure because times associated with recoveries greater than 0.864 would require an extrapolation of the tracer responses in the 0.5-hr test. Clearly, if the 0.5-hr test had been pumped longer, the late arrival times in the tests would have all been greater, and the estimates of groundwater velocities would be slightly different. However, the pumped volumes associated with the arrival times would also have been greater, which would tend to have a moderating effect on the changes in velocity estimates. For the tests at 22S, the times/volumes associated with a fractional recovery of 0.967 were used in the late-arrival-time analysis.

The analysis requires that equations G-7, G-8, and G-9 be modified as shown in equations G-12, G-13, and G-14, respectively.

$$r_{inj} = \sqrt{\frac{(V_{tracer} + V_{chase})}{\pi\eta h}} + v_{GW} \frac{(V_{tracer} + V_{chase})}{Q_{inj}} \quad (\text{Eq. G-12})$$

$$r_{rest} = r_{inj} + v_{GW} t_{rest} \quad (\text{Eq. G-13})$$

$$t_{pump} = \left[\frac{r}{v_{GW}} + \frac{|Q_{pump}|}{2\pi\eta h v_{GW}^2} \ln \left(\frac{|Q_{pump}|}{2\pi\eta h} - v_{GW} r \right) \right]_{r=r_{rest}}^{r=0} \quad (\text{Eq. G-14})$$

The modifications are primarily changes in sign associated with the v_{GW} terms because the groundwater drift velocity is now assumed to push the tracer mass further from the well during injection and slow down the movement of the mass toward the well during pumping. Also, the mass associated with the high fractional recovery is assumed to be on the leading edge of the tracer injection volume rather than at the midpoint of the volume (Equation G-12). One additional difference between the peak- and late-arrival analyses that does not involve equation modifications is that the flow interruption times were added to t_{rest} for the late-arrival analyses because the tracer mass associated with the latter analyses arrived after the flow interruptions.

As with the peak arrival time analyses, v_{GW} was varied to achieve matches to the ratios of the arrival volumes, rather than the actual volumes. However, unlike the peak analyses, the calculated volumes were typically much smaller than the actual volumes associated with the late recoveries. The most likely reason for this discrepancy is that this simple analysis does not account for any hydrodynamic dispersion during any of the three test phases (injection, rest period, withdrawal). Dispersion during each of these three phases could have significantly increased late-recovery arrival times relative to those calculated without dispersion because a fraction of the tracer mass should always disperse further away from the well at any given time. However, if it is assumed that dispersion during each test had approximately the same effect on the tracer plume (disregarding the expected slight increase in dispersion for the longest test), then a comparison of the ratios of the late arrival times should still yield a reasonable estimate of groundwater velocity.

G4.2.3 Mean-Arrival-Time Analysis

The mean tracer arrival-time analysis was essentially identical to the analysis of the late-recovery arrival time, with the only exception being that the mass associated with the mean tracer mass was assumed to be at the midpoint of the tracer injection volume rather than at the leading edge. Thus, equation G-12 is modified to

$$r_{inj} = \sqrt{\frac{(0.5 V_{tracer} + V_{chase})}{\pi\eta h}} + v_{GW} \frac{(0.5 V_{tracer} + V_{chase})}{Q_{inj}} \quad (\text{Eq. G-15})$$

The primary difference between the mean and late arrival time analyses was in how the times/volumes used for comparison with the calculations were obtained from the actual field tracer data. For the late-recovery time analysis, it was a simple matter to extract the

times/volumes associated with a specific (though arbitrary) tracer recovery. However, for the mean analysis, it was necessary to calculate a meaningful estimate of the mean arrival time/volume from the data. Without 100% tracer recovery, it is impossible to calculate a true mean, so a mean for comparison purposes was calculated by truncating the tracer responses at a high fractional recovery that all the tests at a given location achieved. The mean volume was calculated by:

$$\mu = \frac{\sum_i (f_i - f_{i-1}) V_{\text{pump } i}}{\sum_i (f_i - f_{i-1})} \quad (\text{Eq. G-16})$$

where

μ = mean volume, m³

f_i = mass fraction recovered at volume $V_{\text{pump } i}$

f_{i-1} = mass fraction recovered at volume $V_{\text{pump } i-1}$

However, because the mean times/volumes are sensitive to the tails of the tracer response curves, an alternative method of calculating the mean arrival time was devised to include all the data from the 30-day-rest-period test at 19D, which had the largest mean of the three tests at this location and, therefore, was considered to contain the greatest amount of information pertinent to ambient groundwater velocities. Although this method required that the data from the approximately 0.5-hr rest-period-test be extrapolated until the fractional recovery in that test matched the final recovery in the 30-day test (0.913), the extrapolation was considered justified in light of the additional information contained in the tracer responses from the 30-day test. Also, it was desirable to determine the sensitivity of the ambient groundwater velocity estimates to different methods of calculating the mean arrival time. For the tests at 22S, a fractional recovery of 0.967 (used for the late-arrival-time method) was considered large enough that extrapolation to higher recoveries was not necessary.

The extrapolation of the approximately 0.5-hr test data at 19D was accomplished by doing the mathematical equivalent of linearly extending the tail of the tracer response curve on a log-log plot. The means were then recalculated using equation G-16. The recalculated means for all three tests at 19D increased significantly relative to the means calculated from the breakthrough curves that were truncated at a fractional tracer recovery of 0.864. However, the mean for the 30-day test increased by the greatest percentage (about 36% compared to 18% and 15% for the approximately 0.5-hr and 2-day tests, respectively). The (re)calculated mean for the approximately 0.5-hr test was found to be relatively insensitive to the slope of the line used to extrapolate the tracer data. This insensitivity was probably due to the relatively steep slope of the tail of the response curve in this test.

G4.2.4 Linked Analytical Solutions (19D Single-Well Tracer Tests Only)

Three different analytical solutions of the advection-dispersion equation, with appropriate boundary conditions representing the three distinct single-well tracer test phases (injection/chase, drift, and pump back) were combined into one Personal Computer-based Windows program

with a user interface called Injection-Pumpback.vi V 1.0 (STN: 10675-1-00 [DIRS 162749]). Injection-Pumpback.vi is a “LabView” program where LabView is the graphical-programming language “G” as implemented by National Instruments, Inc. The linked analytical solutions were intended to provide an alternative, more rigorous method of estimating groundwater drift velocities in the alluvium from single-well tracer tests than the analytical approaches described in Sections G4.2.1 through G4.2.3. This method was also intended to provide estimates of other transport parameters derived from single-well tracer testing in the alluvium (flow porosity, dispersivity) given an assumption of a homogeneous and isotropic flow system. The method was chosen instead of numerical modeling approaches because of the relative simplicity of the analysis and the desire to avoid numerical dispersion that occurs in numerical models. A description of the three analytical solutions that constitute the program Injection-Pumpback.vi and the application of the program to analyze the three injection-pumpback tracer tests conducted in Borehole 19D follows.

The tracer injection and chase phase was analyzed using simple flow displacement calculations combined with a one-dimensional uniform-flow solution of the advection-dispersion equation by Crank (Bear 1979 [DIRS 105038], p. 266, Equation 7-123) to determine the location and width of the “tracer ring” resulting from the outward radial flow. The inner radius of the ring was calculated directly from the volume of chase water injected, and the one-dimensional solution was then used to determine the width and, hence, outer radius, of the ring. This approach is only approximate because the one-dimensional column solution assumes a constant velocity flow field, whereas a divergent radial flow field has a decreasing velocity with increasing distance from the injection well. In the one-dimensional column solution, dispersion of the “plume” results in the leading and trailing edges of the plume being essentially equidistant from the plume center of mass. However, in an outward radial flow field, the leading edge will tend to be closer to the center of mass than the trailing edge because of the velocity decrease in the radial direction. Given this approximation, the analysis of the tracer injection and chase phase is conducted as follows.

The column solution by Crank (Bear 1979 [DIRS 105038]) is given by:

$$C_{CR}(x, t) = \frac{M/\eta}{(4\pi D_h t)^{1/2}} \exp\left\{-\frac{x'^2}{4D_h t}\right\} \quad (\text{Eq. G-17})$$

where

$C_{CR}(x, t)$ = concentration of solute at a point x meters from the point of tracer injection (top of the column) at t minutes after injection (kg/m^3)

M = mass of tracer injected per unit cross-sectional area in kilograms (kg/m^2)

η = flow porosity

D_h = coefficient of hydrodynamic dispersion (longitudinal) as given by equation G-18 (m^2/s)

x' = distance in meters from the top of the column (where the tracer slug is introduced at time $t=0$) to the centroid of the slug at time t as given by equation G-19 (m)

$t = 27.6$ hours (for this application), the time it took to inject the tracer volume, 10,600 L (2,800 gal), followed by the chase volume, 83,000 L (22,000 gal), at an injection rate of 56.8 L/min (15 gpm).

If molecular diffusion is ignored, D_h (m^2/min) is given by (Bear 1979 [DIRS 105038], p. 264):

$$D_h = \alpha_L |q| / \eta \quad (\text{Eq. G-18})$$

where

α_L = longitudinal dispersivity (m)

q = specific discharge in cubic meters per minute for a unit area of one meter squared (m/s).

For one-dimensional flow in a column, x' is given by Bear (1979 [DIRS 105038], p. 266, Equation 7-120):

$$x' = x - (q/\eta) t \quad (\text{Eq. G-19})$$

where

x = distance from top of column (m).

Equations G-17 to G-19, representing movement of a tracer slug in a one-dimensional column experiment, were modified to represent outwardly divergent flow from an injection well as follows. The radial distance from the center of the well, r , was converted to an equivalent linear column length x by calculating the length of a column whose volume is equivalent to that of a cylinder centered at the well with height equal to the test-interval thickness, h , and with radius r . This cylinder has radial cross-sectional areas increasing from a minimum of $2\pi r_w h$ at the well, (where $r = r_w$ (the well radius, m)), to $2\pi r h$ at a radius of r from the center of the well. The equivalent column is defined as having a constant cross-sectional area of $2\pi r_w h$ (representing the cross-sectional area of the aquifer in contact with the well) and a volume equal to that of the cylinder. For the same porosity, this equivalent column would contain the same volume of water as the cylinder.

The volume of the above cylinder, V_{CYL} , is given by:

$$V_{CYL} = \pi r^2 h \quad (\text{Eq. G-20})$$

where

h = interval thickness (m).

The volume of the equivalent linear column, V_{COL} , is:

$$V_{COL} = A_{COL} x \quad (\text{Eq. G-21})$$

where

A_{COL} = cross-sectional area of the column (m^2), which is $2\pi r_w h$, by definition.

Setting V_{CYL} equal to V_{COL} and A_{COL} equal to $2\pi r_w h$ in equations G-20 and G-21, and solving for x , results in equation G-22:

$$x = \pi r^2 h / 2\pi r_w h = r^2 / (2r_w) \quad (\text{Eq. G-22})$$

where

r_w = injection well radius (m).

So, for a particular radius r , equation G-22 is used to calculate the equivalent linear column distance, x . This value of x is used to calculate x' in equation G-19, and then equation G-17 is used to calculate the concentration $C_{CR}(x,t)$ (kg/m^3), according to Crank (Bear 1979 [DIRS 105038], p. 266, Equations 7-120 and 7-123). $C_{CR}(x,t) = C_{CR}(r,t)$, obtained in this manner, describes the change of concentration as a function of radial distance from the injection well.

The specific discharge, q (m/s), used in equations G-18 and G-19, is obtained by dividing the injection rate, $Q_{INJ} = 56.8$ L/min (15 gpm), by the cross-sectional area of the aquifer in contact with the well, $2\pi r_w h$:

$$q = Q_{INJ} / (2\pi r_w h) \quad (\text{Eq. G-23})$$

By defining a threshold concentration at which a sharp edge of the tracer ring starts at its inner circumference and ends at its outer circumference (5 mg/L or 5×10^{-9} kg/m^3 for this analysis), a width can be determined for the tracer ring from the modified equation G-17. In summary, the modified solution has been used to define the width of the tracer ring (formed by the chase fluid pushing the tracer outward from the well) as a function of the assumed effective porosity and longitudinal dispersivity. The tracer ring is then positioned with its inner radius at a distance r_C (radius of chase zone) calculated from the assumed effective porosity and known volume of chase water, V_c (r_C from $V_c = 83,000$ L [22,000 gal] = $\pi r_C^2 h \eta$), and with its width as determined from the analytical solution by Crank (Bear 1979 [DIRS 105038], p. 266, Equation 7-123). The superposition of the ambient groundwater flow on the outward-radial flow caused by tracer injection and chase was ignored (i.e., it was assumed that the injection and chase dominated the flow field). Given that the tracer injection and chase phase in all the single-well tests was relatively short compared to the drift plus pumpback phase, this approximation should not preclude obtaining reasonable estimates of groundwater velocity for the purposes of comparing with the analytical methods of Sections G4.2.1 through G4.2.3. Figure G-27 shows a LabView depiction of the tracer “plume” after injection and chase.

A two-dimensional analytical solution of the advection-dispersion equation for a tracer slug injected in a uniform flow field (Bear 1979 [DIRS 105038], as given in Bachmat et al. (1988 [DIRS 162534], p. 149, Equation 11) was used to calculate tracer movement during the “drift” phase of each single-well test:

$$C_i(x_1, y_1, t_1) = \frac{M_1 / h\eta}{4\pi(\alpha_L \alpha_T)^{1/2} V_o t_1} \exp\left\{-\frac{1}{4V_o t_1} \left[\frac{(x_1 - V_o t_1)^2}{\alpha_L} + \frac{y_1^2}{\alpha_T} \right]\right\} \quad (\text{Eq. G-24})$$

where

$C_i(x_1, y_1, t_1)$ = concentration at one of the grid blocks (with transformed coordinates (x_1, y_1) – see below) in Figure G-28 resulting from drift of a mass M_1 kg initially positioned at the centroid of the particular wedge, wedge i ($i = 1$ through 18) of Figure G-27. Wedge numbering is not unique and the index “ i ” is only used here to indicate enumeration of wedges.

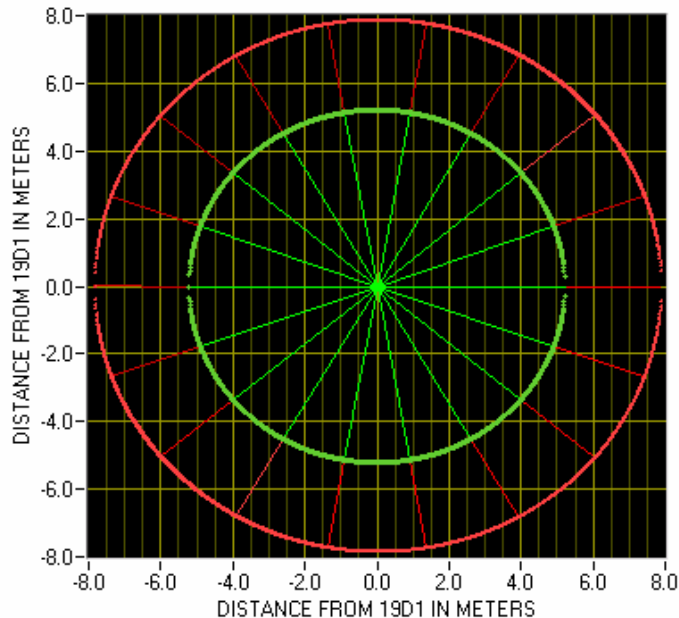
x_1 and y_1 are the coordinates of this grid block relative to an orthogonal system centered at the centroid of wedge i . For this orthogonal coordinate system, the positive x_1 axis is oriented parallel to streamlines of the ambient flow field and in the direction of flow.

α_L = longitudinal dispersivity (m)

α_T = transverse dispersivity (m)

V_o = interstitial velocity caused by the ambient gradient (m/s)

t_1 = duration of drift allowed before pumpback (hr).

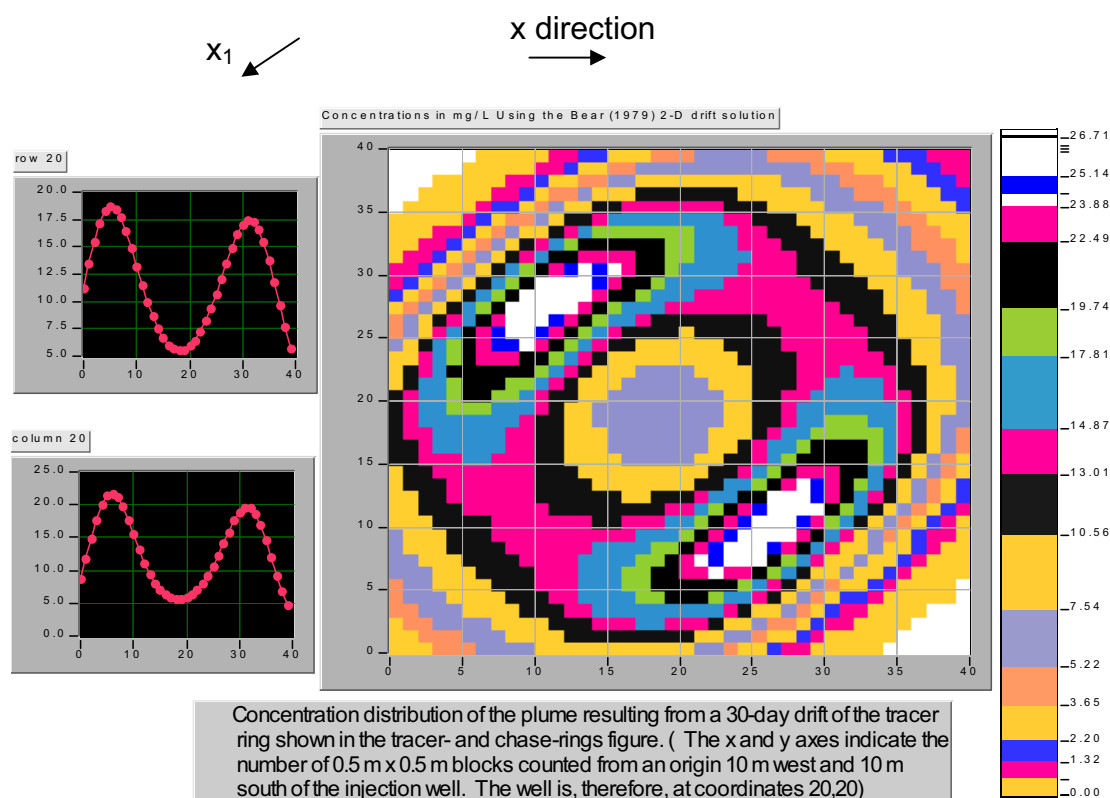


Sources: DTNs: GS020708312316.001 [DIRS 162678] (data); GS020908312316.002 [DIRS 162679] (data).

Output DTN: GS031008312316.003 (analysis).

Figure G-27. Tracer Ring (Red-Hatched Area) and Chase Ring (Green-Hatched Area) around the Injection Well NC-EWDP-19D

In essence, equation G-24 is solved in the transformed coordinate system to obtain the distribution of tracer mass resulting from the drift of tracer initially located in each of the wedge-shaped volume elements of Figure G-27. Then, the solutions for all 18 wedge-shaped volume elements are superimposed to obtain the overall distribution of tracer mass after the drift phase. The relatively coarse discretization of the tracer mass at the centroid of the 18 wedges of Figure G-24 at the beginning of the drift phase is an inherent approximation in the method. The resultant concentration field representing the drifted plume is shown in Figure G-28.



Sources: DTNs: GS020708312316.001 [DIRS 162678] (data); GS020908312316.002 [DIRS 162679] (data); UN0109SPA008IF.006 [DIRS 162442] (conc.); UN0109SPA008KS.007 [DIRS 162615] (conc.); UN0109SPA008KS.008 [DIRS 162616] (conc.).

Output DTN: GS031008312316.003 (analysis).

NOTE: The x and y axes indicate the number of blocks counted from an origin 10 m west and 10 m south of the injection well; the blocks are 0.5 m on a side; and the well is, therefore, at coordinate (20, 20). Concentrations are calculated using the Bear (1979 [DIRS 105038]) two-dimensional drift solution. The x-y plots to the left of the main two-dimensional plot show the tracer concentration distribution along linear profiles in the east-west (top) and north-south (bottom) directions through the grid point corresponding to the location of the well (20, 20). The x_1 direction is the direction of ambient flow.

Figure G-28. Concentration Distribution of Tracer Plume Resulting from a 30-Day Drift of the Tracer Ring Shown in Figure G-27

For each block, the total concentration, $C_1 + C_2 + C_3 + \dots + C_{18}$, is multiplied by the volume of the block, $0.5\text{m} \times 0.5\text{m} \times h$, times the porosity, η , to obtain the mass of the tracer slug, M_{slug} , used at that block for the pumpback phase. A radial solution of the advection-dispersion equation for a cross-hole convergent tracer test with slug injection (Moench 1989 [DIRS 101146], pp. 440 to 443; 1995 [DIRS 148784], pp. 1,824 to 1,827) was then used to calculate tracer movement during the pumpback phase of each test.

The mass in each of the 0.5 m × 0.5 m blocks of the calculation grid of Figure G-28 was considered a slug injection in a convergent flow field towards the pumped well located at coordinates 20, 20 of the figure.

Moench (1989 [DIRS 101146], pp. 440 to 443; 1995 [DIRS 148784], pp. 1,824 to 1,827) used the Laplace transform method to solve the following dimensionless governing advection-dispersion equation for horizontal, radial flow in a homogeneous, double-porosity aquifer:

$$\frac{1}{Pe r_D} \frac{\partial^2 C_D}{\partial r_D^2} + \frac{1}{r_D} \frac{\partial C_D}{\partial r_D} - \frac{2R}{(1-r_{wD}^2)} q'_D = \frac{2R}{(1-r_{wD}^2)} \frac{\partial C_D}{\partial t_D} \quad (\text{Eq. G-25})$$

where

$Pe = r_L/\alpha_L$, the Peclet number, and r_L = distance from the tracer injection point (normally a well) to the pumped well

$r_D = r/r_L$ is the dimensionless radial distance from the pumping well, where r is the dimensional distance from the pumping well

C_D = dimensionless concentration, which for a slug injection is given by $C_D = C/C_i$, where C = concentration at r , and C_i = reference concentration given by $C_i = M_{\text{slug}} / [\pi h \eta (r_L^2 - r_w^2)]$ in which r_w = radius of the pumping well

$r_{wD} = r_w/r_L$, the dimensionless well radius

t_D = dimensionless time, t/t_a , where t_a is the advection transport time given by $t_a = (\pi r_L^2 h \eta)/Q$ in which Q = pumping rate

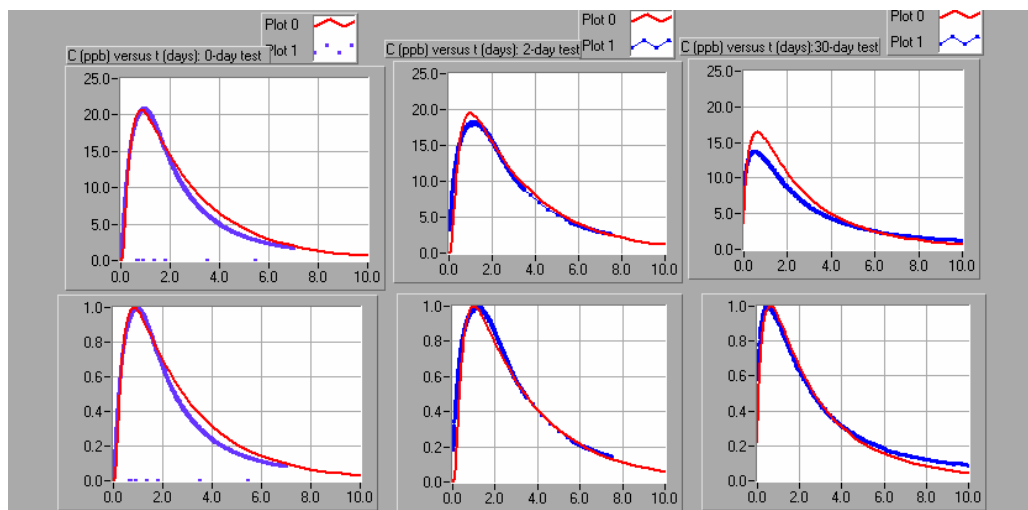
R = retardation factor

q'_D = dimensionless distributed sources or sinks of tracer due to diffusion of the tracer into stagnant porosity.

Moench (1989 [DIRS 101146], pp. 440 to 443; 1995 [DIRS 148784], 1824 to 1827) provided a FORTRAN program, *rcv2amos.exe* V 1.0 (STN: 10583-1.0-00 [DIRS 162750]), that computes the Laplace transform of equation G-25 and then the inverse Laplace transform to finally give dimensionless concentration, C_D , versus dimensionless time, t_D , at the pumped well in the form of two numerical arrays. The C_D versus t_D dimensionless theoretical breakthrough curve is then converted to a dimensional curve of C versus t using the above relation. Injection-Pumpback.vi V 1.0 (STN: 10675-1-00 [DIRS 162749]) uses *rcv2amos.exe* to obtain the effect at the pumping well of a slug of mass M_{slug} placed at each block of the calculation grid of Figure G-28. It then superposes all of these solutions to obtain the final effect at the pumping well of a slug of mass M_{slug} placed at each block of the calculation grid of Figure G-28, and then superposes all of these solutions to obtain the final calculated breakthrough. The superposition of the ambient groundwater flow on the radial flow caused by the pumping well was ignored (i.e., it was assumed that the pumping dominated the flow field). This approximation clearly introduces some error to the analysis. However, given that the curve-matching procedure discussed below is heavily influenced by tracer data obtained early in the pumpback phase of each test (the tracer peaks occur within a day), the error should not preclude reasonable estimates of groundwater velocity for the purposes of comparing with the analytical methods of Sections G4.2.1 through G4.2.3.

The complete analysis involves adjusting the flow porosity, longitudinal dispersivity, transverse dispersivity, and specific discharge in all three computational stages (keeping them the same in each stage) until simulated tracer responses offer a reasonable match to the observed tracer responses in each single-well test. The results of such a match to the three injection-pumpback tracer responses in well 19D are shown in Figure G-29. The analysis indicates a flow porosity value of 0.10, a longitudinal dispersivity of 5 m, and a specific discharge of 1.5 m/yr (Output DTN: GS031008312316.003). Although a rigorous sensitivity analysis to evaluate the uniqueness of the solution was not conducted, many combinations of parameter values were considered, and there appeared to be qualitative convergence to these values. The top three plots in Figure G-29 present dimensional (actual) concentrations, whereas the bottom three plots present concentrations normalized relative to maximum concentrations. The assumed input parameter combination yields a reasonable fit to all three single-well tracer data sets.

The flow porosity value of 0.10 should be less than the total porosity and is, therefore, consistent with three estimates of total porosity presented in different sections of this report: (1) a value of 0.29 obtained from the Borehole Gravity Meter survey in 19D, presented in Section D.4; (2) a value of 0.41 obtained from estimates of barometric efficiency and specific storage, presented in Section D.3; and (3) a value of 0.33 obtained from grain-size-distribution analysis, presented in Section D.3.



Sources: DTNs: UN0109SPA008IF.006 [DIRS 162442] (0 -day test), UN0102SPA008KS.003 [DIRS 162614] (2-day test), UN0109SPA008KS.007 [DIRS 162615] (30-day test).

Output DTN: GS031008312316.003 (analysis).

NOTE: The plots are fits of three injection-pumpback tracer tests with theoretical curves that result from three solutions to the advection-dispersion equation for the three phases of injection, drift, and pumpback. The red curves are the model fits and the blue curves are the data curves. The three top graphs are actual concentrations versus elapsed days, and the bottom three graphs are normalized concentrations versus elapsed days. The parameters used in the calculations are: flow porosity = 0.1; matrix porosity = 0.0; longitudinal dispersivity = 5.05 m; transverse dispersivity = 1.00 m; test interval thickness = 9.75 m (32.0 ft); tracer volume injected = 10,600 L (2,800 gal); chase volume injected = 83,000 L (22,000 gal); injection rate 56.8 L/min = (15.0 gpm); mass injected = 5.0 kg; natural gradient = 0.002 m/m; T for gradient = 20.0 m^2/d ; and specific discharge = 1.5 m/year; the Q values for the 0-, 2-, and 30-day tests are 13.41, 11.00, and 13.50, respectively.

Figure G-29. Fitting the Injection-Pumpback Tracer Tests in Screen #1 of NC-EWDP-19D Using the Linked-Analytical Solutions Method

G4.3 GROUNDWATER VELOCITY ANALYSIS RESULTS

Table G-8 lists the results obtained for both v_{GW} and the specific discharge, $v_s (= \eta v_{GW})$ at the 19D location, as a function of assumed flow porosity (η) by all four methods of estimation. Similarly, Table G-9 lists the results obtained by the first three estimation methods at the 22S location. As expected, of the first three methods, the peak analysis method offers the smallest estimates, and the analysis of late-arriving mass (high recovery) offers the largest. The range of estimates from the three methods spans about a factor of three for a given assumed value of flow porosity. The 19D velocity estimate from the linked analytical solutions is in very good agreement with the peak analysis method. The peak-analysis method yields a velocity estimate of 17.5 m/yr (specific discharge of 1.75 m/yr), as compared to 15 m/yr (1.5 m/yr specific discharge) from the linked analytical solutions, when a flow porosity of 0.10 is assumed (the flow porosity obtained from the linked analytical solutions).

For the 22S location, groundwater specific discharge was independently estimated from hydraulic gradient and hydraulic conductivity data to compare with the estimates of Table G-9. These independent estimates of specific discharge were based on water levels in nearby wells (for gradient estimates) and on the local hydraulic conductivity in screen #2 at Site 22 from cross-hole hydraulic testing (Appendix F). Because water levels were essentially identical in all of the Site 22 wells (to within measurement error), the hydraulic gradient estimates were based on water level differences between wells 10S, 22S, and 19IM2, which are aligned along Fortymile wash in what is believed to be the principal direction of groundwater flow (Figure 6.1-6). The hydraulic gradients between each of the three possible well pairs were used as high, medium, and low estimates of the hydraulic gradient at Site 22. The hydraulic gradient multiplied by the hydraulic conductivity from cross-hole hydraulic testing yields an estimate of specific discharge. The high, medium, and low estimates are listed in Table G-10. It should be noted that the estimates in Table G-10 are non-Q and are presented for comparison purposes only because the water levels used to calculate the hydraulic gradients are unqualified Nye County data.

It is apparent that the specific discharge estimates from Table G-10 are slightly larger than those from Table G-9, although the ranges of values in the two tables overlap (0.5 m/yr to 5.4 m/yr for Table G-9, and 3.1 to 12.4 m/yr for Table G-10). The differences could be due to the fact that the local hydraulic gradient at Site 22 is somewhat different than any of the estimates based on the water levels in wells that are separated by several km. Also, the analytical methods involve several assumptions (see Section G.4.2) that undoubtedly do not hold true in a real system. Some of the limitations and uncertainties associated with the analytical methods are discussed in Section G4.4.

Table G-8. Specific Discharges and Seepage Velocities at 19D Estimated from the Different Drift Analysis Methods as a Function of Assumed Flow Porosity

Assumed Flow Porosity ^a	Specific Discharge (m/yr) / Seepage Velocity (m/yr)		
	0.05	0.18	0.3
Peak Arrival Analysis	1.2 / 24.5	2.4 / 13.1	3.0 / 9.9
Late Arrival Analysis ^b	3.9 / 77.1	7.3 / 40.4	9.4 / 31.3
Mean Arrival Analysis ^c	2.0 / 40.3	3.8 / 20.9	4.9 / 16.4
Mean Arrival Analysis ^d	2.5 / 49.1	4.6 / 25.8	6.0 / 20.2
Linked Analytical Solutions	1.5 / 15 with a flow porosity of 0.10 and a longitudinal dispersivity of 5 m.		

Output DTN: LA0303PR831231.002.

^a The three values are approximately the lowest, expected, and highest values of the alluvium flow porosity used in Yucca Mountain performance assessments (BSC 2004 [DIRS 170042]).

^b Time/Volume associated with approximately 86.4% recovery in each test (the final recovery in the 0.5-hr rest period test, which had the lowest final recovery of any test).

^c Mean arrival time calculated by truncating all tracer response curves at approximately 86.4% recovery in each test.

^d Alternative mean arrival time calculated by extrapolating the tracer response curves in the 0.5-hr rest period test to 91.3% and truncating the response curves in the 2-day rest period test to 91.3% recovery (the final recovery in the 30-day rest period test).

Table G-9. Specific Discharges and Seepage Velocities at 22S Estimated from Different Drift Analysis Methods as a Function of Assumed Flow Porosity

Assumed Flow Porosity ^a	Specific Discharge (m/yr) / Seepage Velocity (m/yr)		
	0.05	0.18	0.3
Peak Arrival Analysis	0.47 / 9.5	0.89 / 5.0	1.2 / 3.9
Late Arrival Analysis ^b	2.2 / 43.8	4.2 / 23.1	5.4 / 17.9
Mean Arrival Analysis ^c	0.82 / 16.4	1.6 / 8.6	2.0 / 6.7

Output DTN: LA0701PR150304.001.

^a The three values are approximately the lowest, expected, and highest values of the alluvium flow porosity used in Yucca Mountain performance assessments (BSC 2004 [DIRS 170042]).

^b Time/Volume associated with approximately 96.7% recovery in each test.

^c Mean arrival time calculated by truncating the two tracer response curves at 96.7% recovery in each test.

Table G-10. Specific Discharge and Seepage Velocity Estimates at 22S Using Different Natural Gradient Estimates and Assuming a Hydraulic Conductivity of 12 m/day from Cross-Hole Hydraulic Testing at Site 22

Assumed Flow Porosity ^a	Specific Discharge (m/yr) / Seepage Velocity (m/yr)		
	0.05	0.18	0.3
Gradient between 22S and 19IM2 (0.00279 m/m)	12.2 / 244	12.2 / 67.8	12.2 / 40.7
Gradient between 10S and 19IM2 (0.00196 m/m)	8.6 / 172	8.6 / 47.7	8.6 / 28.6
Gradient between 10S and 22S (0.00069 m/m)	3.0 / 60.5	3.0 / 16.8	3.0 / 10.1

Output DTN: LA0701PR150304.005 (non-Q; used for comparative purposes).

^a The three values are approximately the lowest, expected, and highest values of the alluvium flow porosity used in Yucca Mountain performance assessments (BSC 2004 [DIRS 170042]).

G4.4 DISCUSSION OF GROUNDWATER-VELOCITY ANALYSES

Some significant uncertainties are associated with each of the estimation methods for v_{GW} and v_S described in this report. Although it would be of interest to determine which of the methods provides the best estimate, a detailed analysis of uncertainties was not conducted. In the discussion that follows, qualitative comments are provided on several uncertainties, and some advantages and potential pitfalls of the different methods are discussed.

The linked-analytical-solution method offers the advantage of providing estimates of flow porosity and longitudinal dispersivity, which are very important parameters for repository performance assessment, in addition to providing flow velocity estimates. Although the parameter estimates in Table G-8 for this method were obtained after many trials using various values of flow porosity, dispersivity, and groundwater flow velocity to fit the three tracer responses simultaneously, an exhaustive sensitivity analysis to evaluate the uniqueness of the matches was not conducted. With such an analysis, it is possible that other combinations of flow porosity, dispersivity, and groundwater-flow velocity could yield essentially equally good matches to the tracer responses.

The value of longitudinal dispersivity obtained from the linked analytical solutions (5 m) intuitively seems large given that calculated injection distances from the well should have been only about 5 m to 6 m with a flow porosity of 0.1. This large dispersivity probably reflects that the aquifer was not truly homogeneous and isotropic as assumed, and a large dispersivity was the only way the analytical solutions could account for tracer plume spreading that occurred due to flow heterogeneity.

The impact of ignoring tracer drift during the injection and pumpback phases of testing for the linked-analytical-solution method is not clear. The error introduced by this assumption may be important for the two tests with the shortest rest periods, as the injection and pumpback phases were collectively longer than the rest period in both tests. The remaining discussion is focused on the other three estimation methods, although some aspects of it also apply to the linked-analytical-solution method.

The peak-analysis method would intuitively seem to have considerable uncertainty associated with it because of the inability to determine whether the tracer mass associated with the peak remained upgradient of the well during the rest period or if it drifted back downgradient of the well during the rest phase. The former case was assumed here, as it provides the lowest estimate of groundwater velocity and specific discharge. If the latter case were assumed, the estimated velocity would have been about twice the estimates obtained by the other methods instead of about half the other estimates. Another uncertainty associated with the peak-analysis method is that at least part of the shift in the peak-arrival time/volume may have been due to hydrodynamic dispersion in the system rather than pure advection (as was assumed). A considerable amount of dispersion during the rest phase could have shifted the peak-arrival time without significant translation of the tracer plume's "center of mass" due to advection. However, some advection is necessary for dispersion to occur.

Both the analyses of late-arrival times and mean-arrival times are potentially highly sensitive to diffusion into stagnant water and to density-driven flow resulting from density contrasts between

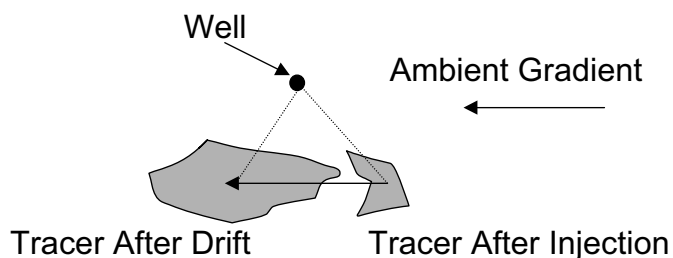
the injection solution and the ambient groundwater. Both of these phenomena can dramatically increase tailing in the tracer response curves and, hence, increase the late-arrival or mean-arrival times/volumes. Although the nearly identical responses of the tracers with different diffusion coefficients in all the tests (though to a lesser degree in the 22S tests) suggest that diffusion did not play an important role in the observed tailing behavior in the tests, density contrasts cannot be ruled out. If the tracer solution was more or less dense than the ambient groundwater during injection (due to either concentration or temperature differences), a portion of the tracer mass could have moved upward or downward into nearly stagnant regions of the aquifer by density-driven flow. Under these conditions, a portion of the tracer mass could remain in the aquifer for an extended period of time because pumping will not rapidly “draw” the tracer out of the nearly stagnant regions. Despite the disadvantages mentioned above, the peak-analysis method offers an advantage in this situation because the peak-arrival time should be relatively unaffected by such “artificial” tailing behavior. It should be noted that the effects of density-driven flow should have been less in the 22S tests than the 19D tests because the overall tracer injection concentrations were nearly a factor of two lower at 22S.

Assuming that diffusion can either be neglected or corrected for, and that the effects of density contrasts are negligible, the mean-arrival-time analysis would intuitively seem to be the method least affected by hydrodynamic dispersion in the system. In theory, dispersion should not affect the mean-arrival time, whereas it will affect the other arrival times. However, the mean-arrival-analysis method has the disadvantage that complete recoveries are seldom achieved in field tracer tests, so the mean must generally be estimated somewhat arbitrarily from either a truncated or an extrapolated distribution, as in the analyses described in this report for 19D.

Finally, some practical considerations associated with hypothetically possible test results are worth discussing. Consider a case in which the heterogeneity in aquifer hydraulic conductivity in the vicinity of the well is such that the entire tracer mass moves upgradient of the well during injection. In this situation, it is possible that both the mean and late arrival volumes could be *less* than the sum of the injection and chase volumes (this was clearly not the case in the 19D and 22S tests). Under these circumstances, the test analyst will have to recognize that the equations used in both the late- and mean-arrival analyses should be modified to account for groundwater flow moving the tracer mass back toward the well. The late-arrival-analysis method will also be very sensitive to dispersion in this case.

If the tracer mass moves primarily perpendicular to the direction of ambient groundwater flow during injection but slightly upgradient, the peak-, late-, and mean-arrival methods all have the potential to underestimate groundwater velocities because drift may only slightly alter the separation distance between the tracer mass and the well before pumping starts (Figure G-30). Each of the three analytical methods will work best if the “center of mass” of the tracer plume is injected either directly upgradient or downgradient. Intuitively, it also seems likely that the uncertainty associated with all the methods should decrease as the difference between the rest periods of the tests, and, hence, the difference in the amount of drift in the tests, increases. An increase in the difference in drift should result in a greater difference in each of the arrival times, which should make the analyses less sensitive to subtle differences in the injection/withdrawal procedures or other nonidealities in the tests.

Additional insights into uncertainties associated with the estimation methods could probably be obtained by (1) generating random-stochastic-hydraulic-conductivity fields having statistics consistent with the current knowledge of the alluvium, and then (2) numerically simulating injection-withdrawal tests in these fields (for various assumed drift velocities). These methods could ultimately yield more refined estimates of groundwater velocities in the alluvium.



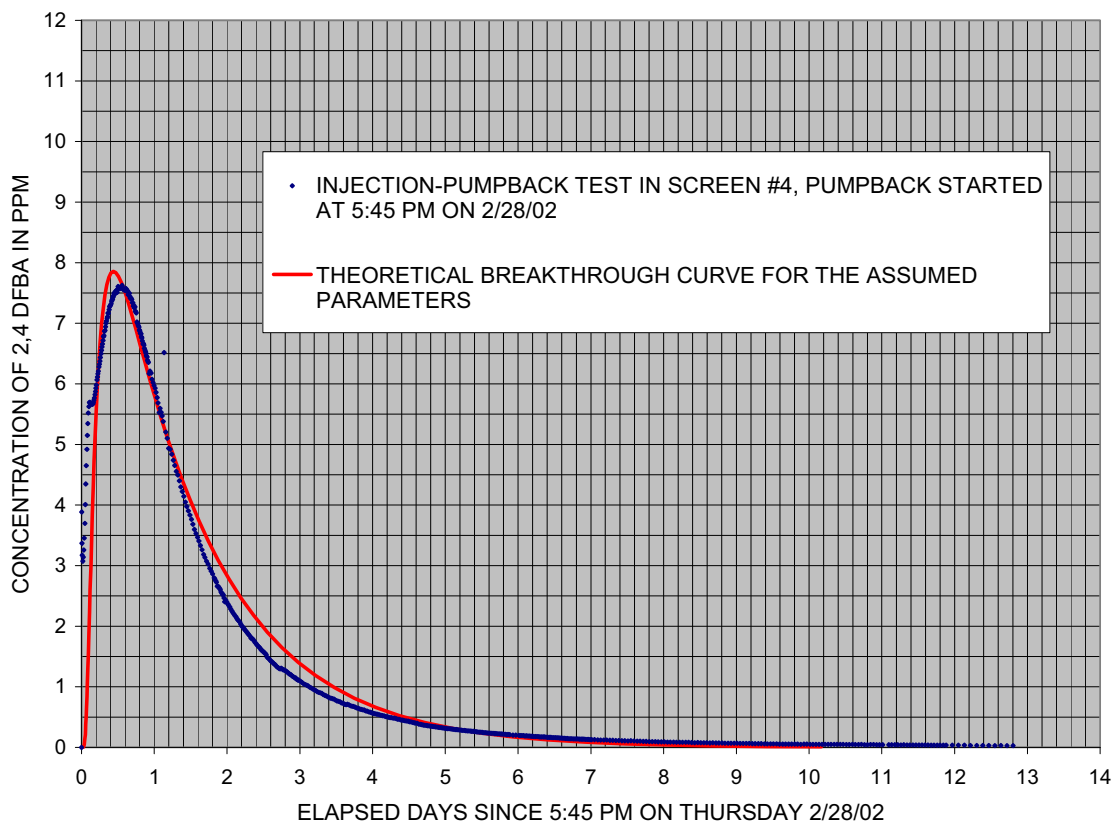
NOTE: For illustration purposes only. The dashed lines connect the well with the center of mass of the tracer "plume" before and after the rest period.

Figure G-30. Depiction of a Tracer Injection Scenario That Could Result in Underestimation of Groundwater Velocity

G4.5 SUMMARY OF GROUNDWATER-VELOCITY ANALYSES

Four methods of estimating groundwater velocities from multiple single-well injection-withdrawal tracer tests conducted with varying rest periods in the saturated alluvium south of Yucca Mountain, Nye County, Nevada are presented in this report. All four were applied to the single-well tracer test data at 19D, and three were applied to the single-well tracer test data at 22S. The resulting estimates of groundwater velocity and specific discharge vary over a range of about a factor of 3 for a given assumed flow porosity, and by about a factor of 10 for a reasonable range of flow porosities. The estimates of specific discharge at 19D range from 1.2 m to 9.4 m per year, which is comparable to specific discharges being used in Yucca Mountain performance assessments (obtained from the calibrated site scale SZ Flow Model). Flow porosity and longitudinal dispersivity estimates of 0.10 m and 5 m, respectively (Output DTN: GS031008312316.003), were obtained for the 19D location using a linked-analytical-solution method. Estimates of specific discharge at 22S range from 0.5 m to 5.4 m per year, which compares reasonably well with estimates of 3.1 m to 12.4 m per year based on hydraulic gradient and hydraulic conductivity estimates at 22S.

The same aquifer parameter values obtained from analyzing the three injection-pumpback tracer tests in screen #1 of 19D were in the above linked-analytical-solutions to generate a theoretical breakthrough curve to compare with to the actual breakthrough curve from the 19D, screen #4 injection-pumpback tracer test (detailed documentation reported by Umari et al. 2003 [DIRS 164573]). The results are shown in Figure G-31. The close match indicates that the same aquifer parameters that were suitable for screen #1 in well 19D also appear to be suitable for screen #4 in the same well.



Source: DTN: MO0205UCC008IF.001 [DIRS 162617] (data).

Output DTN: GS031008312316.003 (analysis).

Figure G-31. Comparison of the Theoretical Breakthrough Curve from the Linked-Analytical-Solutions Method to the Actual Breakthrough Curve from the Injection-Pumpback Tracer Test in Screen #4 of NC-EWDP-19D

G4.6 ESTIMATE OF COLLOID DETACHMENT RATE CONSTANT FROM MICROSPHERE RESPONSE IN SINGLE-WELL TEST IN 19D

A rough estimate of the effective detachment rate constant for the 640-nm-diameter polystyrene microspheres that were injected in the zero-rest-period single-well tracer test at 19D (Figure G-18) was made as follows. First, the assumption was made that after 90 hr of pumping, the microsphere response is entirely the result of detachment from the alluvium. At this time, about 72% of the solutes had been recovered but only 26% of the microspheres (the final recoveries were 87% and 32%, respectively). In fact, there may have been some spheres recovered after 90 hr that were not truly detaching (they were just making their way out of the system without ever having become attached), so counting these as being detached spheres increases the estimate of the detachment rate constant.

The following simple mass action equation was assumed to apply:

$$Q C = k_r M [(1 - f_{\text{sphere}}) - (1 - f_{\text{solute}})] \quad (\text{Eq. G-26})$$

where

C = concentration of spheres in water produced from well, number/L

Q = production rate from well = 3066 L/hr

k_r = detachment rate constant, 1/hr

M = total number of spheres injected (a known value)

f_{sphere} = fraction of spheres recovered (so $(1 - f_{\text{sphere}})$ is the fraction not recovered)

f_{solute} = fraction of solutes recovered.

Equation G-26 assumes that the spheres remaining on the alluvium surfaces are equal to the total number of spheres injected times the fraction of spheres not recovered $(1 - f_{\text{sphere}})$ minus the fraction of solutes not recovered $(1 - f_{\text{solute}})$. Subtracting $(1 - f_{\text{solute}})$ from $(1 - f_{\text{sphere}})$ is a correction that accounts for the fraction of spheres that would not have been recovered at a given time, even if they did not interact with alluvium surfaces. The quantity $[(1 - f_{\text{sphere}}) - (1 - f_{\text{solute}})]$ averages about 0.5 over the last 77 hr of the test (0.46 at 90 hr and 0.545 at 167 hr).

Rearranging equation G-26 to solve for k_r yields the following:

$$k_r = \left(\frac{Q}{[(1 - f_{\text{sphere}}) - (1 - f_{\text{solute}})]} \right) \left(\frac{C}{M} \right). \quad (\text{Eq. G-27})$$

The quantity C/M is the normalized concentration plotted in Figure G-18. It has a value of approximately 0.0000002/L during the latter portion of the test. Using the average pumping rate during the test of 3066 L/hr, equation G-27 yields a value of 0.0012/hr for k_r (Output DTN: LA0303PR831352.001). This estimate of the detachment-rate constant can be considered high (upper bound) because dC/dt slowly decreased as the test proceeded and the fractional recovery of solutes increased faster than the microsphere recovery (which means that the estimate of the number of spheres remaining on the surfaces according to equations G-26 and G-27 actually increased with time—a physical impossibility). The latter contradiction could be remedied by simply setting $(1 - f_{\text{solute}})$ equal to zero, which would lower the detachment-rate constant estimate by about 30%.

G.4.7 ANALYSIS OF DIFFUSION IN SINGLE-WELL TRACER TESTS AT 22S

The two single-well tracer tests at 22S exhibited notable separation of the normalized breakthrough curves of the two nonsorbing tracers with different diffusion coefficients (iodide and FBAs – see Figures G-21 and G-22) in each individual test. The observed separations were significantly greater than in the 19D single-well tests. The good agreement between the measured concentrations in automatically-collected samples and grab samples and also between concentrations normalized with respect to directly-measured injection masses (i.e., measured weights of tracers added to injection solutions) and with respect to masses deduced from measured injection concentrations (i.e., determined by analyzing injection solutions for tracers and multiplying the measured concentrations by injection volumes) suggests that systematic sampling errors and errors in deduced injection masses (used in the normalizations) are unlikely explanations for the observed separations in the tracer breakthrough curves. It is, therefore,

concluded that the observed separations reflect diffusion between flowing and stagnant water in the aquifer.

To conduct a semi-quantitative assessment of diffusion in the site 22 flow system, the MULTRAN V1.0 code (STN: 10666-1.0-00 [DIRS 159068]) was used to simulate the single-well tracer tests in flow systems with both the conceptual models of Figures G-1(b) and G-1(c). As discussed in Section G4.2, the MULTRAN model simulates radial outward and inward flow during the injection and pumping phases, respectively, of a single-well test, but it does not account for ambient groundwater flow, or drift, in the flow system during the rest period or any other phases of a test. Thus, the only way to account for the additional plume spreading that occurs during longer drift period tests is to increase the longitudinal dispersivity during the injection and pumpback phases in MULTRAN. Consequently, the longitudinal dispersivities from the MULTRAN interpretations of the single-well tracer tests should not be interpreted as meaningful longitudinal dispersivities.

Figure G-32 shows simultaneous fits to the tracer breakthrough curves in each single-well test at 22s using the conceptual model of Figure G-1(b), with diffusion into spherical grains or “blocks” of varying size with a mean radius of 0.3 cm, and a standard deviation of the log of the block radii of 0.5. Other model parameters are listed in Table G-11. The model curves shown in Figure G-32 were not obtained using an automated numerical optimization algorithm, but rather they are trial-and-error “fits” obtained by manually adjusting the dispersivity, block size (radius of spherical blocks), block internal porosity, flowing porosity, and diffusion coefficients within the blocks. As such, these fits should not be considered optimized, and they only serve to illustrate that the observed differences in the tracer breakthrough curves are qualitatively consistent with the conceptual model of Figure G-1(b) with variable block sizes. The emphasis in the “fitting” process was on matching the tracer peak concentrations and the relative features of the tracer breakthrough curves (i.e., their relative peak heights, where they approach each other or cross-over), rather than on absolute matches. The slight mismatches between the data and model curves, particularly with respect to the timing of the peaks and the tailing behavior can likely be attributed to the lack of drift simulation in the MULTRAN code. The use of an adjustable longitudinal dispersivity in MULTRAN (see above) to account for tracer plume spreading during the drift period apparently does not approximate the effects of drift very well. It should be noted that assuming a constant block size resulted in poorer matches to the breakthrough curves than assuming a variable block size, so it appears that the multiple diffusion rates and diffusion distances offered by the variable block sizes constitute a more representative conceptualization of the flow system.

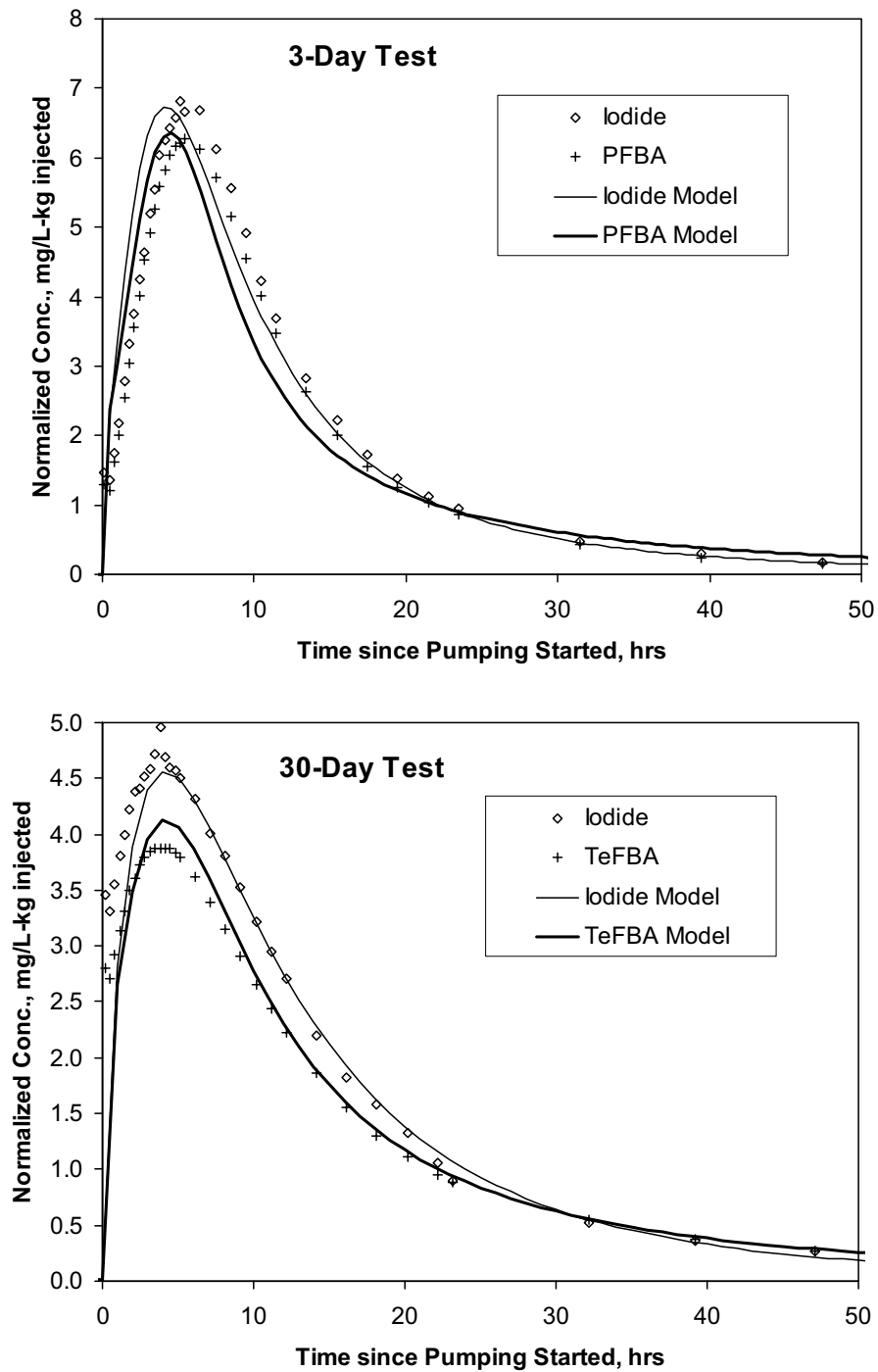
It should be noted that four of the five parameters that were adjusted to obtain a good model fit (excluding longitudinal dispersivity) combine synergistically to define both a characteristic time scale and a mass transfer coefficient for diffusion between flowing and stagnant water in the flow system. These two lumped parameters govern the diffusive mass transfer behavior of the system, so the adjustment of the four model parameters effectively reduces to the adjustment of these two lumped parameters to fit the data. The block radius (R) and the diffusion coefficient within blocks (D_m) combine to define a characteristic time scale for diffusion ($t_{ch} = R^2/2D_m$), which is essentially a measure of the time it takes for the flowing and stagnant water domains to “equilibrate” with respect to solute diffusion gradients. When advective time scales are significantly greater than t_{ch} , solutes will experience single-porosity transport behavior with an

effective porosity equal to the sum of the flowing and stagnant water porosities. All four parameters combine to define a mass transfer coefficient, MTC , for diffusion between the flowing and stagnant water domains, given by $\frac{\phi_b \sqrt{D_m}}{R\phi_f / 3(1-\phi_f)} = \frac{3\phi_b(1-\phi_f)}{\phi_f \sqrt{t_{ch}}}$, where ϕ_b = block

internal porosity, ϕ_f = flowing porosity, and spherical blocks are assumed. The ratio of stagnant to flowing water porosity in the system, r_{sf} , is given by $\frac{(1-\phi_f)\phi_b}{\phi_f}$, so the diffusive mass transfer

coefficient can also be written as $\frac{3r_{sf}}{\sqrt{2t_{ch}}}$. Allowing the block radius, R , to take on a range of

values (defined by the standard deviation of the log of block radius) effectively introduces an additional adjustable parameter (the standard deviation). The addition of this parameter can only improve the model fit, but the improvement must be significant to justify the addition.



Sources: DTNs: LA0612PR831231.001 [DIRS 178733] (3-day test data), LA0612PR831231.002 [DIRS 178735] (30-day test data), and LA0701PR150304.007 (output).

NOTE: The data points are grab sample normalized concentrations. Model parameters are listed in Table G-11.

Figure G-32. MULTRAN Model Matches to the 22S Single-well Tracer Test Breakthrough Curves using the Diffusion-into-Blocks Conceptual Model

Table G-11. MULTRAN Model Parameters Associated with the Matches to the 22S Single-well Tracer Test Breakthrough Curves Shown in Figure G-32 (diffusion-into-blocks model)

Model Parameter	Parameter Value
Longitudinal Dispersivity, m	2 / 8 ^a
Flowing Porosity	0.25
Porosity in Blocks	0.1
Iodide Diffusion Coefficient in Blocks (D_m), cm ² /s	3×10^{-7}
Mean Block Radius (R), cm	0.31
Std. Dev. of Log Block Radius	0.5
Characteristic Diffusion Time Scale ($R^2/2D_m$), hr	44.5
Diffusive Mass Transfer Coefficient, $\frac{\phi_b \sqrt{D_m}}{R\phi_f / 3(1-\phi_f)}$, hr ^{-1/2}	0.095
Ratio of Stagnant to Flowing Water Porosity	0.3

Output DTN: LA0701PR150304.007.

^aValues correspond to first test and second test, respectively.

Figure G-33 shows simultaneous fits to the tracer breakthrough curves in each single-well test at 22S using the conceptual model of Figure G-1(c), with diffusion between flowing and stagnant “layers” in a flow system. Model parameters are listed in Table G-12. As in the case of the conceptual model of Figure G-1(b) (Figure G-32), the model curves shown in Figure G-33 are not numerically optimized fits, but rather they are trial-and-error “fits” obtained by manually adjusting the dispersivity, layer thicknesses, layer porosities, and diffusion coefficients within the layers. The matches to the data in Figure G-33, though qualitatively reasonable, appear to be somewhat poorer than those in Figure G-32. However, a comparison of the conceptual models based on these differences is somewhat biased because the diffusion-into-blocks model includes multiple diffusion rates and distance scales (because of the range of block radii), whereas the layered model has only a single set of diffusion parameters. The additional adjustable parameter associated with the standard deviation in block sizes in the diffusion-into-blocks model provides much greater flexibility in matching the observed data than the layered model with a single effective diffusion rate and diffusion distance. For the diffusion-into-layers model, the characteristic time scale for diffusion, t_{ch} is given by $L^2/8D_m$, where L is the thickness of the non-flowing layers, and D_m is the diffusion coefficient in the non-flowing layers, and the mass transfer coefficient, MTC , is given by $\frac{\phi_l \sqrt{D_m}}{\phi_f (b + L/2)}$, where ϕ_l is the porosity within the non-flowing layer, ϕ_f is the flowing porosity, and b is half the thickness of the flowing layers.

As Tables G-11 and G-12 indicate, the best-fitting diffusion-into-grains and the diffusion-into-layers conceptual models both have relatively small ratios of stagnant to flowing water volumes (both less than 1.0). Also, the time scales for diffusion into the stagnant water are relatively short (less than 2 days) compared to the time scales of the rest periods in both tracer tests. These characteristics are necessary for the iodide to have higher peak concentrations than the FBAs, which occurs because diffusion into the accessible stagnant porosity essentially depletes the concentrations of both tracers in the flowing porosity by about the same relative amount during the rest periods of the tests, and the iodide diffuses back out of the stagnant porosity more quickly than the FBAs. While both the diffusion-into-blocks and

diffusion-into-layers conceptual models match the tracer breakthrough curves reasonably well, the very short time and distance scales suggest that the former model is more plausible than the latter for solute transport in the saturated alluvium. The layer thicknesses necessary to have such short time scales with realistic solute diffusion coefficients are on the order of 2 mm for flowing layers and 6 mm for non-flowing layers. These are seemingly much too narrow to correspond to layer thicknesses in a material that has grain sizes much larger than this.

Thus, it is concluded from the 22S single-well tracer testing results that the diffusion-into-blocks (or grains) conceptual dual-porosity model is most applicable for the saturated alluvium at this location. However, the very short diffusion time and distance scales suggest that the alluvium should behave as a single-porosity system over the much longer time and distance scales associated with performance assessment. That is, the flowing and stagnant porosities should effectively act as a combined flowing porosity for solute transport in the alluvium, with the solute transport velocity being less than the groundwater velocity in the flowing porosity by a factor of $(\text{flowing porosity})/(\text{flowing}+\text{stagnant porosity})$, which is 0.53 for the diffusion-into-grains model and 0.77 for the diffusion-into-layers model. Of course, these conclusions must be tempered with the realization that the volume of the aquifer interrogated in the single-well tests was relatively small (on the order of 20,000 gal to 30,000 gal based on the tracer and chase water volumes and allowing for some plume spreading) and certainly can't be considered representative of km scales. Also, if the permeable layers were more than just a few cm thick, diffusion into adjacent low-permeability layers could have been masked by diffusion into grains within the permeable layers over the relatively short time scales of the tests. Thus, it is possible that over much longer time scales, additional diffusion between thicker alternating high and low permeability layers would have been observed.

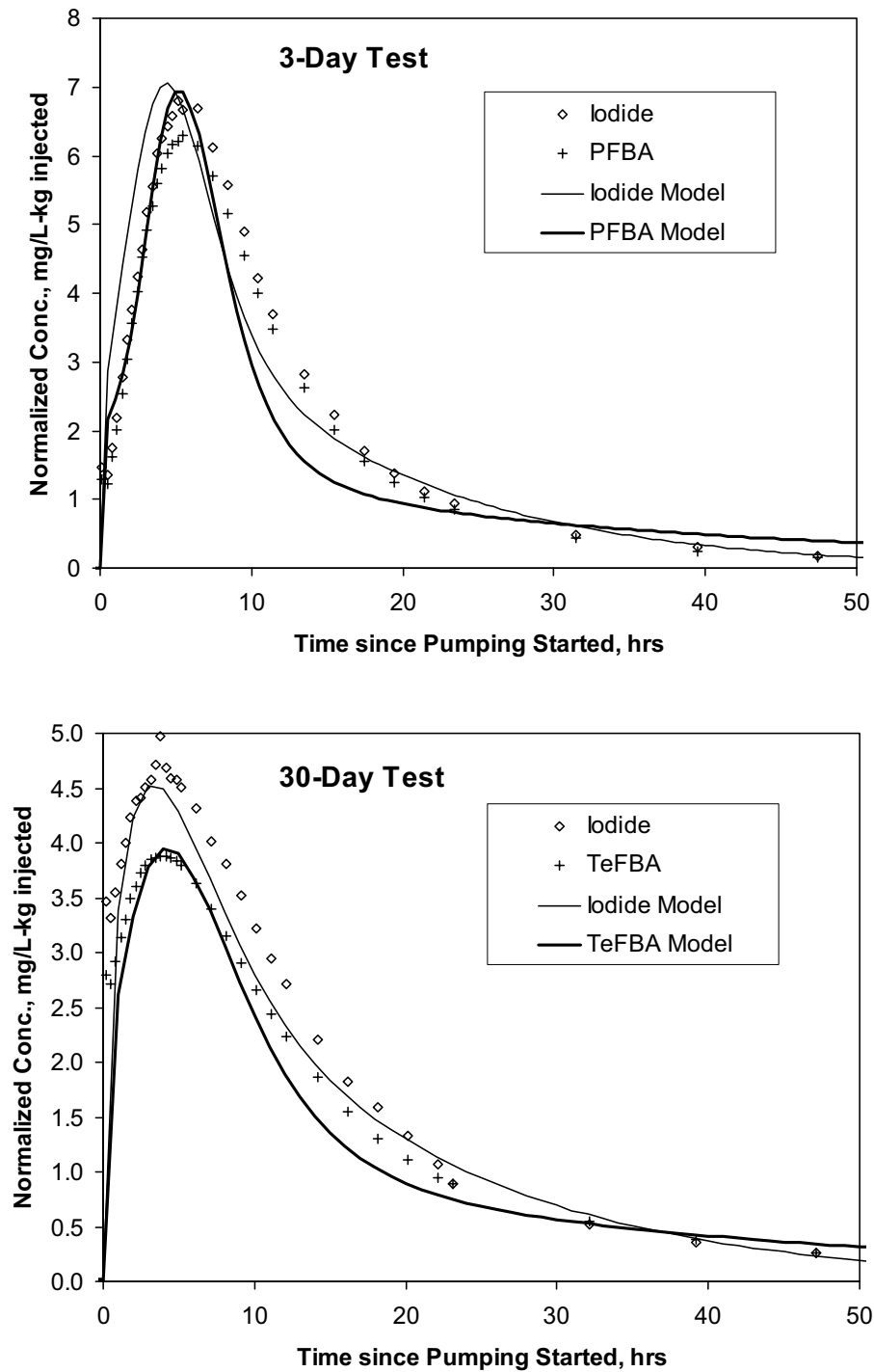
G4.8 CONCLUSIONS FROM SINGLE-WELL TRACER TESTING IN ALLUVIUM

The single-well tracer tests at 19D showed no evidence of dual-porosity transport behavior based on the lack of any separation of the halide and FBA tracer breakthrough curves. However, the single-well tracer test results at 22S were consistent with a dual-porosity, diffusion-into-blocks conceptual transport model with relatively short characteristic time and distance scales for diffusion. These were short enough that single-porosity transport behavior with an effective flowing porosity equal to the flowing plus stagnant porosity would be predicted for solutes over performance assessment time and distance scales. However, the caveats identified in the last three sentences of the previous paragraph should be kept in mind.

Differences in the tracer responses for the different rest periods in the three tests at 19D can be attributed to groundwater drift during the rest periods. At 22S, the differences in tracer responses between the two tests are also dominated by groundwater drift, although they can't be exclusively attributed to drift. Further evidence for a single-porosity flow/transport system at 19D was provided by the lack of an increase in tracer concentrations after flow interruptions during the tailing portions of the tracer responses in the two tests featuring flow interruptions.

Four methods were used to estimate groundwater drift velocities from the three single-well tracer tests in 19D, and three of these methods were also used to estimate groundwater velocities from the two single-well tests at the 22S location. The resulting estimates of specific discharge range from 1.2 m/yr to 9.4 m/yr at 19D and from 0.5 m/yr to 5.4 m/yr at 22S, with the estimates

depending on the method used for analysis and the assumed flow porosity (lower flow porosities yield lower estimates). These estimates are in reasonably good agreement with estimates obtained using potentiometric head and hydraulic conductivity data. It is doubtful that these estimates would be improved significantly by more sophisticated modeling without more detailed information on the distribution of tracer mass after the injection and rest phases of the single-well tests. However, the generation of random-stochastic-hydraulic-conductivity fields having statistics consistent with the current knowledge of the alluvium, followed by the numerical simulation of injection-withdrawal tests within these fields (for various assumed drift velocities), would probably yield considerable additional information on the uncertainties associated with the estimation methods.



Source: DTN: LA0612PR831231.001 [DIRS 178733] (3-day test data), LA0612PR831231.002 [DIRS 178735] (30-day test data), and LA0701PR150304.007 (output).

NOTE: The data points are grab sample normalized concentrations.

Figure G-33. MULTRAN Model Matches to the 22S Single-well Tracer Test Breakthrough Curves Using the Diffusion-into-Layers Conceptual Model

Table G-12. MULTRAN Model Parameters Associated with the Matches to the 22S Single-well Tracer Test Breakthrough Curves Shown in Figure G-33 (diffusion-into-layers model)

Model Parameter	Parameter Value
Longitudinal Dispersivity, m	2 / 12 ^a
Flow Porosity	0.077
Porosity in Non-Flowing Layer	0.1
Iodide Diffusion Coefficient in Non-Flowing Layer (D_m), cm ² /s	5×10^{-7}
Flowing Layer Thickness, cm	0.2
Non-Flowing Layer Thickness (L) cm	0.45
Characteristic Diffusion Time Scale ($L^2/8D_m$), hr	14.1
Diffusive Mass Transfer Coefficient, $\frac{\phi_f \sqrt{D_m}}{\phi_f (b + L/2)}$, hr ^{-1/2}	0.170
Ratio of Stagnant to Flowing Water Porosity	0.9

Output DTN: LA0701PR150304.007.

^aValues correspond to first test and second test, respectively.

G5. RESULTS AND INTERPRETATION OF CROSS-HOLE TRACER TESTS IN SATURATED ALLUVIUM AT NC-EWDP SITE 22

Two cross-hole tracer tests were conducted in the saturated alluvium in the second screened interval from the surface at Nye County Site 22 in 2005 (the same interval in which the single-well tracer tests were conducted at this location – see Section G4). The first test involved the injection of several tracers into this interval in two different wells (22PA and 22PC) while the same interval was continuously pumped in 22S (see Figures 6.1-8 and 6.1-10). The two injection wells were located in approximately orthogonal directions to each other relative to 22S (22PA is north, and 22PC is east), so flow and transport anisotropy could be evaluated. Also, another nonsorbing tracer was injected into the first screened interval in 22PA, which was completed at a shallower depth than the pumped interval. The second cross-hole tracer test was conducted in the same configuration as the first test, but only two tracers, iodide ion and perrhenate ion, and one injection interval, the second interval from the surface in 22PA, were used.

The objectives of the first cross-hole test were to (1) further evaluate alternative conceptual transport models in the saturated alluvium, building on the information obtained from the single-well tracer tests, (2) evaluate flow anisotropy in the alluvium, both horizontal and vertical, and (3) obtain estimates of transport parameters for solutes and colloids in the saturated alluvium. The second test was conducted primarily to evaluate whether perrhenate transport is retarded relative to iodide in the saturated alluvium. Perrhenate was used in this test as a surrogate for pertechnetate, which is the predominant technetium species predicted to be present in oxidizing groundwaters at Yucca Mountain, and ⁹⁹Tc is one of the radionuclides that have been identified as potentially contributing significantly to future offsite doses because of its high solubility and weak sorption behavior. Both pertechnetate and perrhenate are predicted to be reduced to species of much lower solubility and significant sorption under reducing groundwater conditions, and perrhenate should be slightly harder to reduce based on standard tables of electrochemical potentials of half reactions (Lide 2006 [DIRS 178081], p. 8-24). Thus, if perrhenate were significantly retarded relative to a nonsorbing tracer (e.g., iodide), it would

suggest that local reducing conditions may exist in the alluvium that would also be capable of reducing, and thus retarding, pertechnetate.

The tracers injected into the second screened interval in 22PA in the first cross-hole test included two nonsorbing solutes (bromide ion and 2,4,5 TFBA) and a weakly sorbing cation tracer (lithium ion). These tracers were all injected simultaneously (co-dissolved in groundwater from 22S). Nonsorbing FBAs were also injected into the second screened interval from the surface in 22PC (2,6 DFBA) and into the first screened interval from the surface in 22PA (2,5 DFBA). This last tracer was injected to determine if there was any significant downward vertical flow through the alluvium induced by pumping from the deeper depth in 22S. Carboxylate modified polystyrene latex (CML) microspheres (200-nm diameter, and dyed with a fluorescent yellow dye to allow them to be distinguished from background colloids) were injected into the second screened interval of 22PA approximately ten days after the solute tracers to serve as colloid tracers. The delay in injecting the microspheres was to avoid the high ionic strength of the solute injection solution, which could have caused the microspheres to aggregate or to attach to the media surfaces more readily than in the much lower ionic strength ground water. The sorption parameters for lithium and the filtration parameters for the microspheres were to be determined by comparing the cross-hole responses of these tracers to that of the two nonsorbing solutes. Table G-13 provides a summary of the injection masses and volumes of the different tracers in both cross-hole tests at Site 22. The observed tracer recoveries are also summarized in Table G-13.

The 2,5 DFBA was never detected in 22S, so it is not discussed further and not included in Table G-13. This result suggests that vertical flow and transport through the alluvium at Site 22 is probably somewhat hindered relative to horizontal flow and transport, which is consistent with the hydraulic test interpretations that indicate the shallow alluvium at Site 22 (over the two shallowest intervals) has a horizontal-to-vertical hydraulic conductivity ratio of at least 1.5 to 2 (Section 6.4 and Appendix F). If the flow system were homogeneous and isotropic, the expected 2,5 DFBA travel time in the vertical direction from the bottom of zone 1 to the top of zone 2 (a distance of about 20 m) would be about 30 days. This estimate assumes a vertical hydraulic conductivity of ~ 12 m/day (based on the zone 2 hydraulic test interpretation), a drawdown difference of ~ 0.1 m between zones 1 and zone 2 (observed when zone 2 was pumped), and a flow porosity of 0.1 (based on the tracer test interpretations discussed below); i.e., travel time = $L / (K\Delta H / L) / \eta$, where L = distance, K = hydraulic conductivity, ΔH = head or drawdown difference, and η = flow porosity = $20 \text{ m} / (12 \text{ m/d} \times (0.1/20) \text{ m/m} / 0.1 = \sim 33$ days. Given the observed horizontal tracer travel time of less than 10 days between wells 22PA and 22S, one would expect the 2,5 DFBA arrival time at 22S to be no more than about $30 + 10 = 40$ days in a homogeneous, isotropic system. The fact that there was no 2,5 DFBA arrival at 22S in over 60 days of pumping (and also no arrival in another ~ 45 days of pumping during the second cross-hole tracer test) indicates that the flow system must have a lower effective vertical hydraulic conductivity relative to horizontal hydraulic conductivity. If the vertical travel distance were 20 m (the distance from the bottom of zone 1 to the top of zone 2), a lower bound estimate of the horizontal-to-vertical hydraulic conductivity ratio would be about 3:1 based on the fact that there was no arrival in over 100 days of pumping. However, if the vertical travel distance were greater than the minimum distance of 20 m, then the lower bound estimate of the conductivity ratio would be smaller. Also, the possibility that the 2,5 DFBA arrived at 22S in concentrations too low to detect cannot be discounted given that the 2,5 DFBA injection mass

was only about 18% of the injection mass of the 2,4,5 TFBA and 2,6 DFBA and that peak tracer concentrations tend to decrease approximately as 1/travel time.

For all tracer injections, a steady flow field was established between the injection wells and the production well (indicated by steady downhole pressures) prior to the tracers being injected, and the tracer solution was followed by a small volume of untraced “chase” water. This “chase” water was intended to “push” the tracers out of the injection wellbore and into the formation to minimize the possibility that they might linger in the wellbore, which would result in biased estimates of transport parameters. The chases were small enough in volume and duration that they should have had a negligible effect on the steady flow fields except very close to the injection interval. The production well was pumped at a steady rate of approximately 47.5 gal/min (180 L/min) during both tests, including throughout the tracer injections and chases.

Table G-13. Tracer Characteristics, Injection Masses, Injection Concentrations, and Fractional Recoveries in the Two Cross-Hole Tracer Tests at Site 22

Solute Tracers – Test 1^a				
Parameter	2,4,5 TFBA	Bromide	Lithium	2,6 DFBA
Free water diffusion coefficient at infinite dilution, D_f (cm^2/s)	$7.2 \times 10^{-6\text{ b}}$	$2.1 \times 10^{-5\text{ c}}$	$1.0 \times 10^{-5\text{ c}}$	$7.5 \times 10^{-6\text{ b}}$
Expected Sorption	None	None	Weak (ion exchange)	None
Target and directly measured injection mass (kg)	8.500	23.002	18.457 ^d	8.500
Injection mass based on measured injection concentration and volume (kg)	8.232	21.504	18.060	8.116
Approximate injection volume (L)	1,000	1,000	1,000	1,000
Tracer fractional recovery ^e	0.93 to 0.96 (0.06)	0.78 to 0.84 (0.03)	0.092	0.91 (0.14)
CML Microsphere Tracers – Test 1^f				
Parameter	0.2-μm CML microspheres (yellow)			
Calculated free water diffusion coefficient, (cm^2/s)	$2.15 \times 10^{-8\text{ g}}$			
Number of spheres injected	4.65×10^{14}			
Injection concentration (number/L)	4.65×10^{11}			
Approximate injection volume (L)	1000			
Tracer fractional recovery	0.011			
Solute Tracers – Test 2				
Parameter	Iodide	Perrhenate		
Free water diffusion coefficient at infinite dilution, D_f (cm^2/s)	$2.1 \times 10^{-6\text{ c}}$	$1.46 \times 10^{-5\text{ h}}$		
Expected Sorption	None	None or very weak		
Target and directly measured injection mass (g)	4,233.13	68.123		
Injection mass based on measured injection concentration and volume (kg)	3,375.77	59.740		

Table G-13. Tracer Characteristics, Injection Masses, Injection Concentrations, and Fractional Recoveries in the Two Cross-Hole Tracer Tests at Site 22 (Continued)

Solute Tracers – Test 2 (Continued)		
Parameter	Iodide	Perrhenate
Approximate injection volume (L)	1,000	1,000
Tracer fractional recovery	0.78	0.84

Sources: DTNs: LA0612PR831231.003 [DIRS 178736] (Test 1 solutes), LA0612PR831231.004 [DIRS 178738] (Test 2), and LA0612PR831231.005 [DIRS 178739] (Test 1 microspheres).

^a 2,5 DFBA was also injected into the uppermost screen of 22PA, but it was never detected in 22S, so it is not listed here.

^b Benson and Bowman 1994 [DIRS 122788], p. 1,125; 1996 [DIRS 153427], p. 1,780.

^c Newman 1973 [DIRS 148719], p. 230, Table 75-1; based on ionic conductances at infinite dilution.

^d Lithium was injected as 25.0 kg LiBr, 97.0 kg LiCl and 1.99 kg LiOH.

^e Ranges for TFBA and bromide reflect uncertainty from mass-based vs. concentration-based normalizations. Numbers in parentheses indicate the recovery that occurred during the second cross-hole tracer test, which is included in the totals. Lithium concentrations were not measured during the second cross-hole test.

^f The microsphere injection was initiated 10 days after the solute tracers were injected.

^g Calculated using Stokes-Einstein equation (Bird et al. 1960 [DIRS 103524], Equation 16.5-4 on p. 514).

^h Lide 2006 [DIRS 178081], pp. 5-76 to 5-78.

NOTE: CML=carboxylate-modified latex; TFBA=trifluorobenzoic acid or trifluorobenzoate; DFBA=diffuorobenzoic acid or diffuorobenzoate.

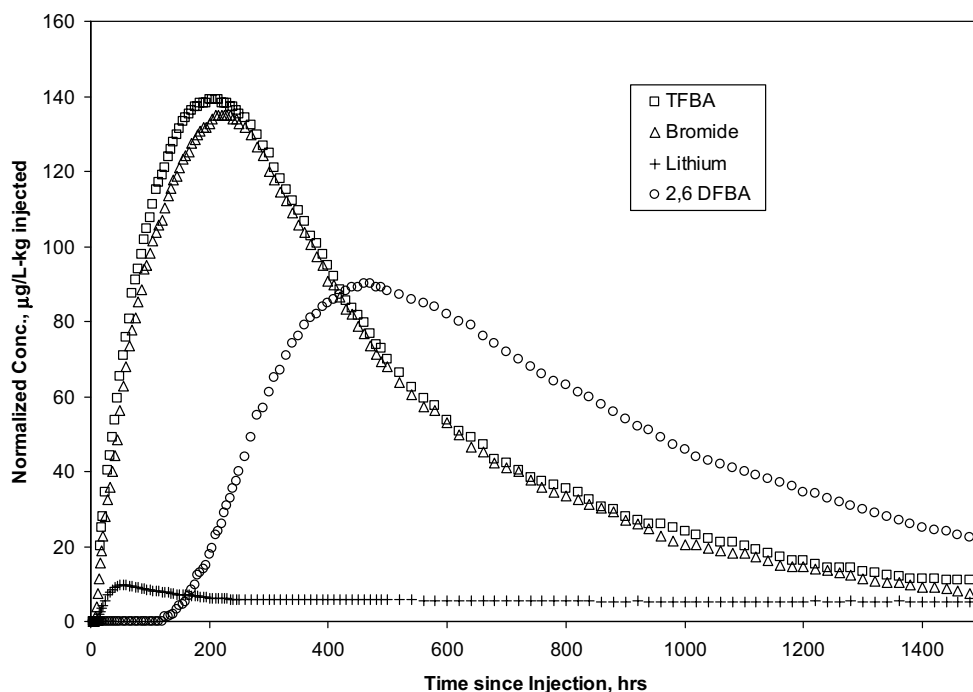
G5.1 CROSS-HOLE TRACER TEST RESULTS

Figure G-34 shows the breakthrough curves (normalized concentrations vs. time) of the solute tracers injected into the second screened intervals in 22PA and 22PC in the first cross-hole tracer test. The data points of this figure represent an “abstraction” of the actual breakthrough curve data because the actual data are too numerous and result in too much weighting of the breakthrough curves tails (where most of the data lie) to be suitable for model fitting. Unlike the single-well tracer tests, in which the injected tracer masses determined from direct mass measurements (i.e., measured weights of tracers added to injection solutions) and indirect mass measurements (i.e., determined by analyzing injection solutions and multiplying the measured concentrations by injection volumes) were in very good agreement, the injection masses determined by these two methods in the first cross-hole test were in relatively poor agreement. The masses from indirect concentration measurements were always smaller than the masses measured directly from the weights of the tracers (see Table G-13), suggesting that the tracers may have been diluted more than intended in the field (field volume measurements were not highly accurate). However, the ratios of the injected tracer masses measured by the two methods were also in relatively poor agreement, which calls into question a simple dilution error that would leave the ratios unaffected. These injection mass discrepancies result in significant uncertainty in the tracer test interpretations because any errors in tracer injection masses will result in raising or lowering the entire corresponding normalized tracer breakthrough, and the interpretations, particularly regarding diffusion processes, are based largely on *differences* in the normalized tracer breakthrough curves.

The reasons for the relatively large differences in the apparent injection masses are unknown, but possible explanations (in addition to simple dilution errors) include (1) there was poor mixing of the tracer injection solution at the time it was sampled in the field, (2) some of the fluorinated benzoate tracers were not completely dissolved in the carboys containing concentrated solutions (prepared in the laboratory) or in the injection tanks at the time of sampling (would affect FBAs

only), or (3) there was some minor spillage or sloshing of tracers as they were poured into the main injection tank from the carboys. Normally, one would consider directly-measured masses to be more accurate than masses indirectly determined from concentration measurements, but if (2) or (3) occurred, the concentration measurements might provide a better measure of the masses. In the following discussion, the tracer concentrations normalized using the direct mass measurements and the indirect concentration measurements are referred to as the “mass-based” and “concentration-based” normalizations, respectively.

The normalized concentrations of Figure G-34 are mass-based normalizations for all tracers except bromide. Using the concentration-based normalization for bromide results in the smallest possible difference between the breakthrough curves of the 2,4,5 TFBA and bromide, which also results in the least amount of deduced diffusion between flowing and stagnant water in the tracer test. Figure G-35 shows bromide breakthrough curves for the different normalizations, and Figure G-36 shows the 2,4,5 TFBA breakthrough curves for the different normalizations (2,6 DFBA mass-based normalized concentrations are also shown on this figure). It is clear that, for this cross-hole tracer test, there are significant differences in the nonsorbing tracer breakthrough curves depending on which normalization method is used, and these different normalizations will result in significant differences in the deduced diffusive properties of the alluvium (see below).

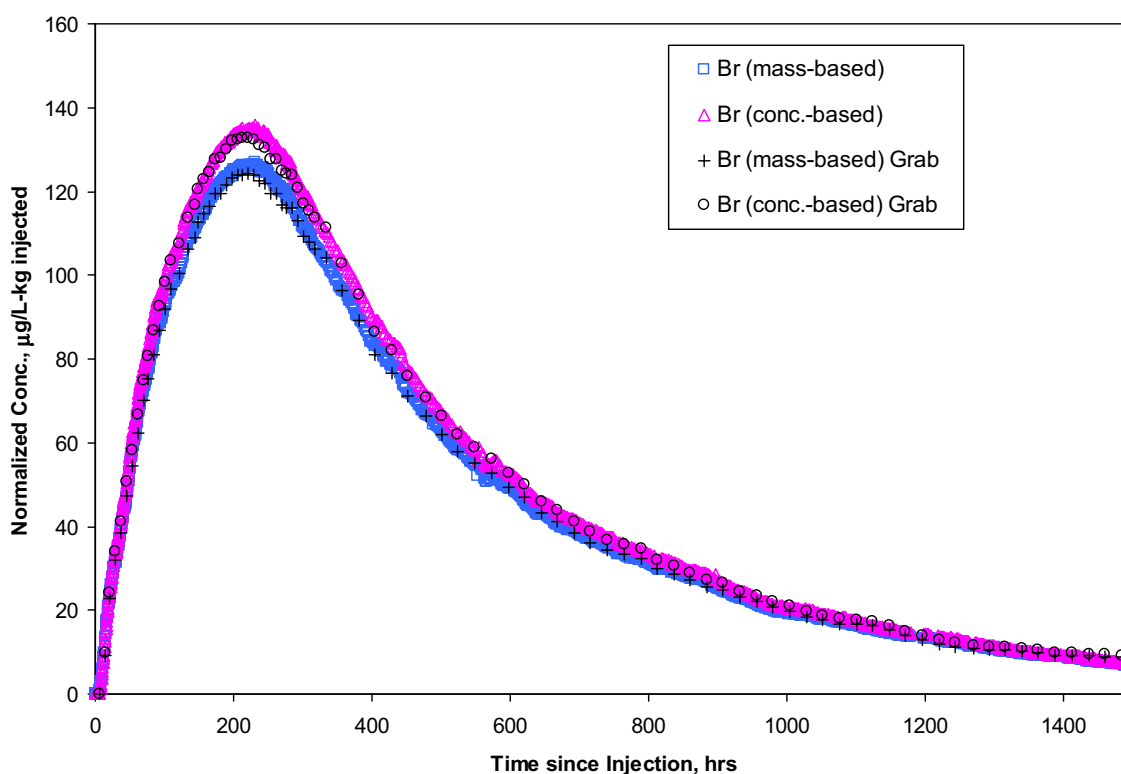


Source: DTN: LA0612PR831231.003 [DIRS 178736].

NOTE: All tracer concentrations except for bromide are normalized to directly-measured injection masses. Bromide concentrations are normalized to injection mass deduced from measured injection concentration.

Figure G-34. Normalized Breakthrough Curves of 2,4,5 TFBA, Bromide, Lithium (all from 22PA), and 2,6 DFBA (from 22PC) in the First Cross-Hole Tracer Test at Site 22

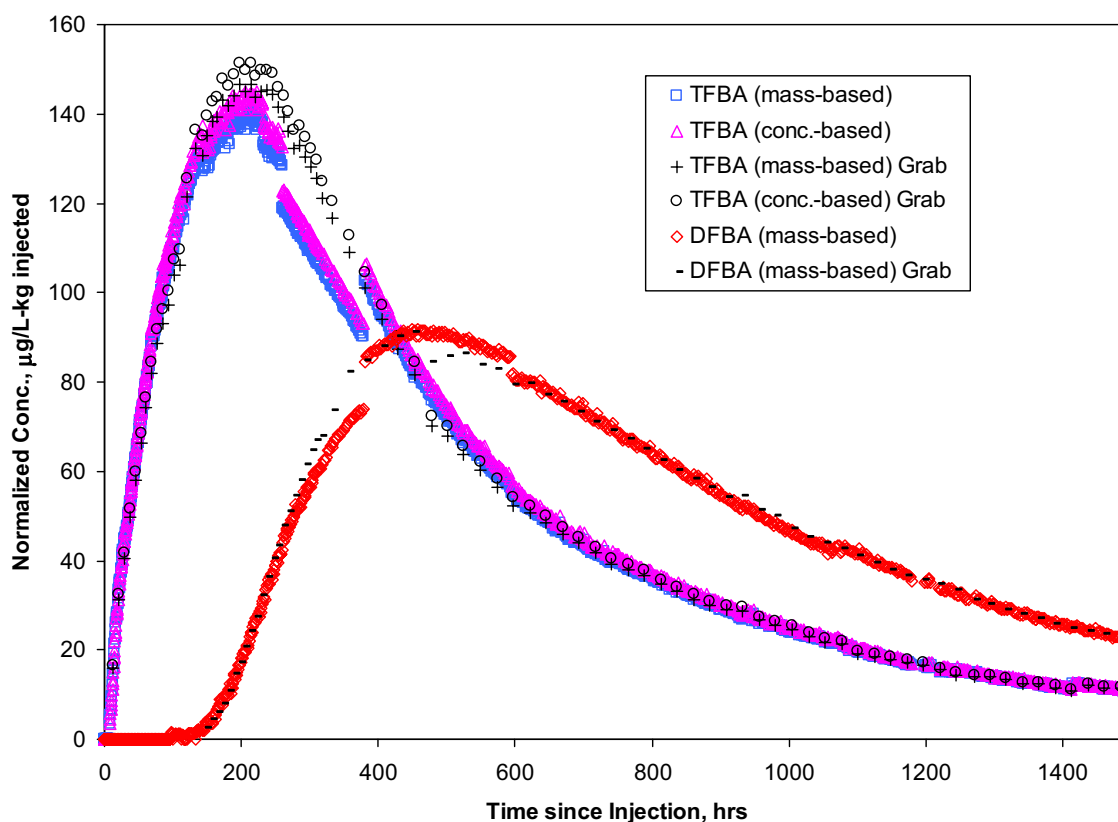
Figure G-37 shows the normalized breakthrough curve of the CML microspheres relative to the 2,4,5 TFBA breakthrough curve in the first cross-hole tracer test. These two tracers were injected into the same interval in 22PA, although the microspheres were injected 10 days later than the solutes. It is clear that the microspheres experienced significant filtration in the test interval, although it is also apparent that they had a long, low concentration breakthrough curve tail indicative of some detachment of filtered microspheres in the aquifer. The 2,5 DFBA injected into the uppermost screened interval in 22PA was never detected in the water produced from 22S. This result suggests that vertical flow and transport through the alluvium is probably somewhat hindered relative to horizontal flow and transport, which is consistent with the hydraulic test interpretations that indicate the alluvium at Site 22 behaves primarily as a leaky, confined aquifer in the individual test intervals (Appendix F).



Source: DTN: LA0612PR831231.003 [DIRS 178736].

NOTE: The black symbols are grab samples, and the colored symbols are automatically-collected samples.

Figure G-35. Mass-Based and Concentration-Based Normalized Breakthrough Curves of Bromide in the First Cross-Hole Tracer Test at Site 22

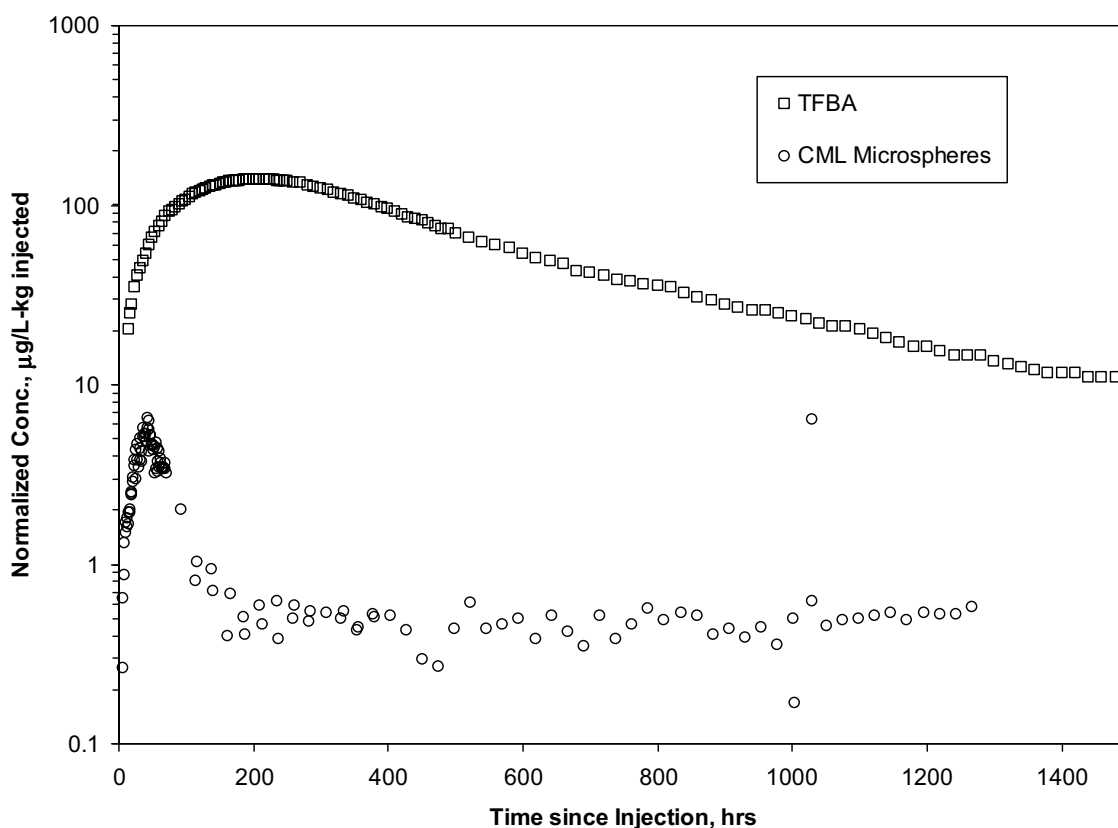


Source: DTN: LA0612PR831231.003 [DIRS 178736].

NOTE: The 2,6 DFBA mass-based normalized breakthrough curve is also shown. The black symbols are for grab samples, and the colored symbols are for automatically-collected samples. Note that the analyses of the grab samples confirm that the portions of the breakthrough curves that appear to be offset for the automatic samples are probably artifacts of analyzing different batches of samples at different times (with different instrument calibration curves, etc.). These offsets were therefore smoothed out when the "abstracted" data used for fitting were developed.

Figure G-36. Mass-Based and Concentration-Based Normalized Breakthrough Curves of 2,4,5 TFBA in the First Cross-Hole Tracer Test at Site 22

Figure G-38 shows the mass-based and concentration-based normalized breakthrough curves of the iodide and perrhenate in the second cross-hole tracer test conducted between 22PA and 22S (abstracted data used for interpretive analyses are presented later). It is apparent that there were significant discrepancies in the mass-based versus concentration-based normalizations in this test as well. It is also apparent that the analyzed rhenium concentrations have significant scatter associated with them. The fact that the concentration-based normalizations of both tracers are significantly larger (even more so than in the first test) than their respective mass-based normalizations, and that the ratios of the deduced tracer injection masses are similar for the two normalization methods, suggests that the tracers were probably diluted in the field more than intended.

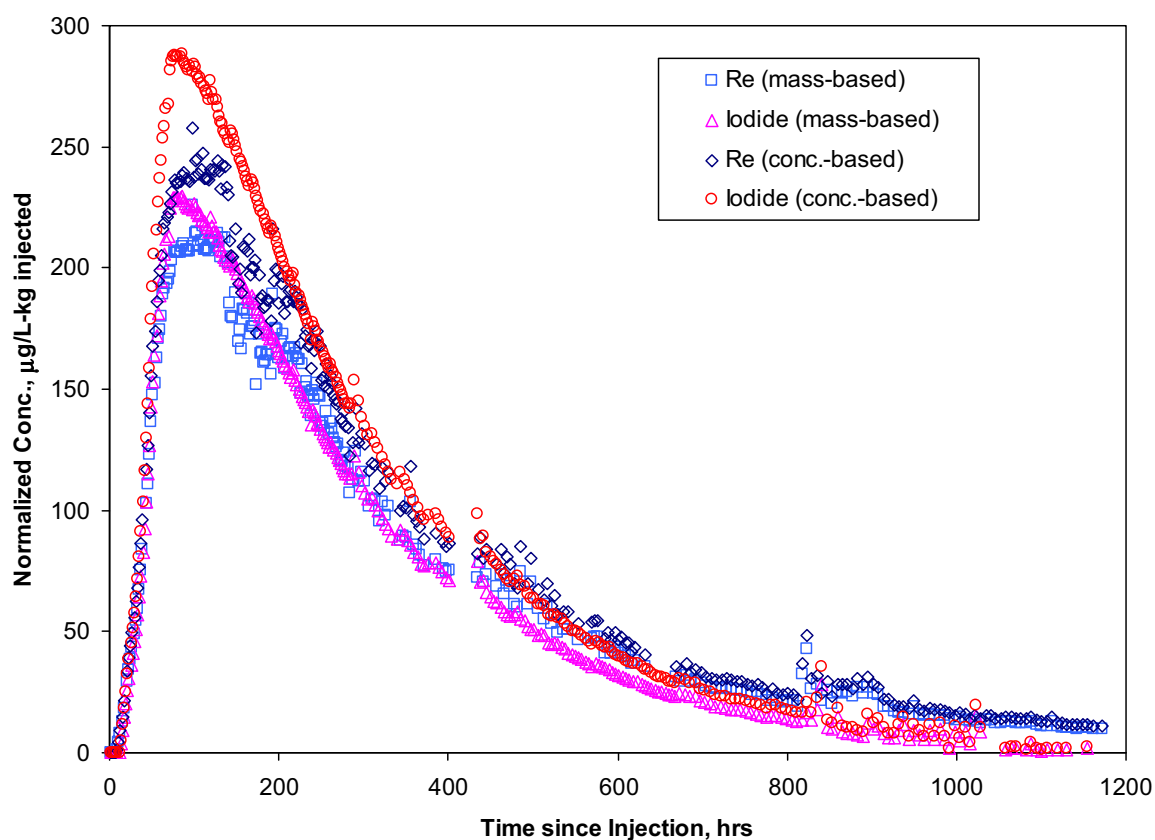


Sources: DTNs: LA0612PR831231.005 [DIRS 178739] (microspheres); LA0612PR831231.003 [DIRS 178736] (TFBA).

NOTES: Note the log normalized concentration scale. The very high microsphere data point at about 1,050 hr was reanalyzed and verified to be valid; this high concentration may have been the result of an undocumented flow perturbation.

Figure G-37. Mass-Based Normalized Brea kthrough Curves of 2,4,5 TFBA and CML microspheres in the First Cross-Hole Tracer Test at Site 22

Regardless of whether mass- or concentration-based normalizations are used, the perrhenate breakthrough curve has a later peak concentration and a higher tail than the iodide breakthrough curve. Both of these characteristics are consistent with either greater diffusion of perrhenate into stagnant water in the system or sorption of perrhenate in the stagnant porosity after diffusion into this porosity. Given that perrhenate should have a smaller diffusion coefficient than iodide (Table G-13), the latter explanation seems more likely. This possibility is discussed in more detail in the next section.



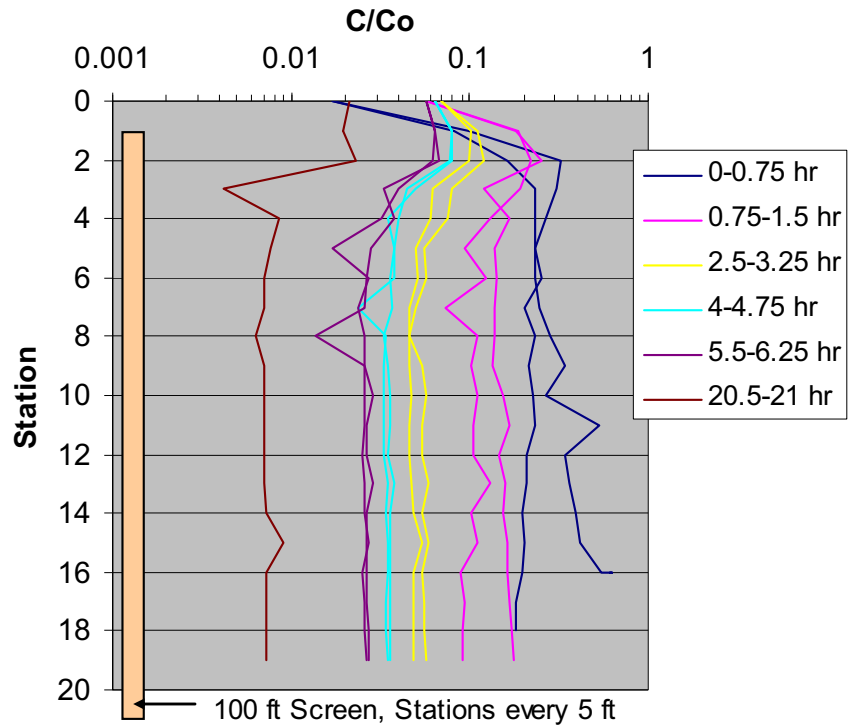
Source: DTN: LA0612PR831231.004 [DIRS 178738].

Figure G-38. Mass-Based and Concentration-Based Normalized Breakthrough Curves of Iodide and Perrhenate in the Second Cross-Hole Tracer Test at Site 22

During the injection of the concentrated multiple-solute tracer solution into the second interval from the surface in 22PA in the first cross-hole tracer test, a downhole probe was used to measure specific conductance as a function of time and depth in the injection interval. These measurements were performed for approximately 21 hours after the tracer injection to monitor the decline in conductance, and hence the decline in tracer concentrations in the borehole. A calibration curve of C/C_0 (tracer concentration divided by starting concentration) vs. conductance was obtained by performing conductance measurements on a series of dilutions of the injection solution, and this was used to relate measured conductances to C/C_0 in the borehole. Figure G-39 shows “profiles” of C/C_0 as a function of depth (five-foot intervals) and time in the borehole, and Figure G-40 shows how the concentrations at a given depth decreased with time over the 21 hours of monitoring.

The concentration profiles of Figure G-39 indicate that there is minimal stratification of the tracer solution in the borehole at any given time, but rather the tracer concentrations appear to be declining quite uniformly throughout the injection interval over time. The lack of stratification could be attributable in part to mixing caused by probe movement in the borehole, as the probe (1.66-in diameter) occupied most of the cross-sectional area of the borehole (nominally 2-in

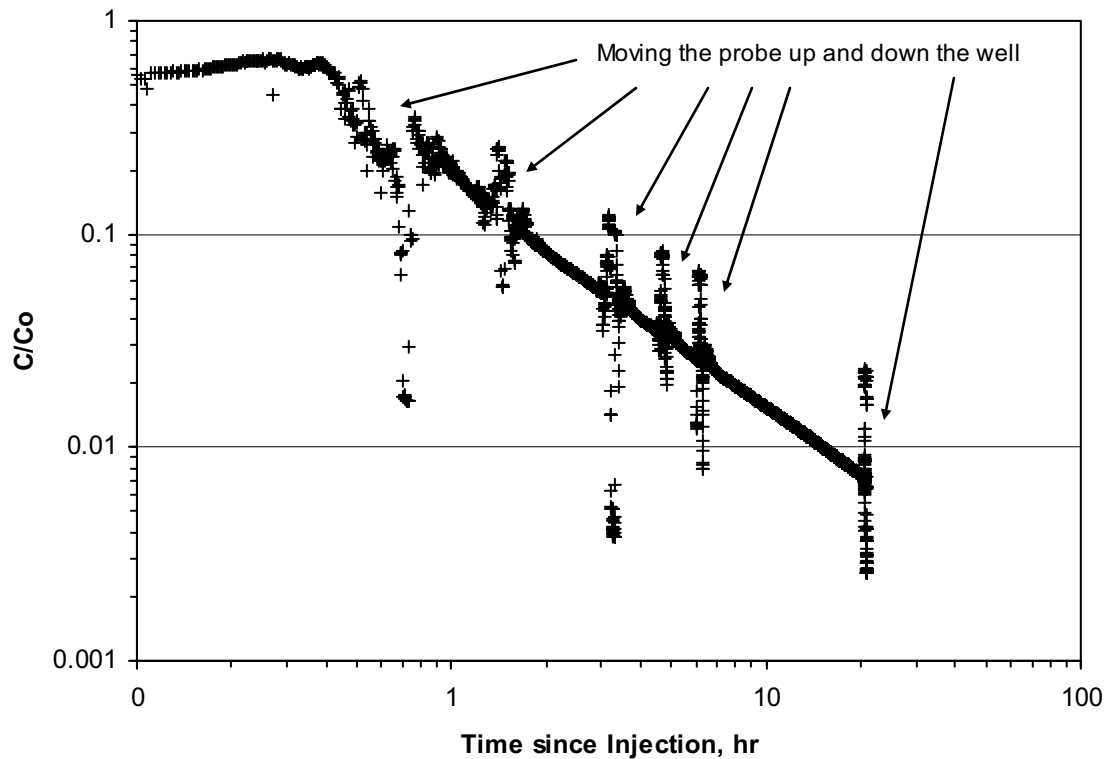
diameter). The linear decline in tracer concentrations on the log-log plot of Figure G-40 is somewhat unexpected in that, for an ideally-mixed borehole, one would expect a linear decline in $\log(C/C_0)$ with time (not log time). This result clearly indicates that the borehole was not ideally mixed and/or that the flow regime through the borehole changed with time (most likely a combination of both). The fact that the decline in concentrations slowed down with time relative to what would be expected in a well-mixed borehole could indicate that the initial decline in concentrations was influenced strongly by density-driven flow of the tracer solution, which had a calculated specific gravity of more than 1.12 and would therefore have been expected to “sink” in the borehole and aquifer. The first profile of Figure G-39 (0 to 0.75 hr) shows some evidence of an initially higher concentration at the bottom of the screened interval that rapidly declined. By the time of the second profile, the tracer concentrations were less than 20% of their initial concentrations, and density-driven flow would therefore have slowed significantly. The driving force for density-driven flow would have decreased with time as the tracer concentrations in the borehole decreased. Because of these nonidealities, the measured concentration decline was not used to estimate an ambient flow velocity through the borehole as is done in a borehole dilution test (Freeze and Cherry 1979 [DIRS 101173], pp. 429 to 430). However, the measured rate at which the tracers left the borehole was used to estimate the injection borehole decay constant used in RELAP interpretative modeling of the tracer test (Section G5.2), and it also helped rule out the possibility that the tracers lingered in the vicinity of the injection borehole for a long enough time to significantly influence the test interpretations.



Source: DTN: LA0612PR831231.006 [DIRS 178745].

NOTE: "Stations" are every five feet (grid lines are every 10 ft). The probe was not lowered into the lower 10 feet of the interval because of the presence of "muck" at the bottom.

Figure G-39. Depth Profiles of Tracer C/Co (based on specific conductance) as a Function of Time in 22PA after Tracer Injection



Source: DTN: LA0612PR831231.006 [DIRS 178745].

Figure G-40. Tracer C/Co (based on specific conductance) as a Function of Time at 82.9 m below the Water Table in 22PA after Tracer Injection (Station 16 in Figure G-39)

G5.2 CROSS-HOLE TRACER TEST INTERPRETATIONS

Because there was no solid defensible basis for choosing either the mass-based or concentration-based normalizations of bromide or 2,4,5 TFBA concentrations as being more accurate or representative in the first cross-hole tracer test at Site 22, two sets of interpretative analyses of this test were conducted; one using the normalized breakthrough curves that yielded the largest possible differences between the tracer breakthrough curves and another that yielded the smallest possible differences between the curves. The set of curves with the larger differences would yield maximum diffusion parameter estimates for the alluvium, and the curves with the smaller differences would yield the minimum diffusion parameter estimates.

RELAP V2.0 (STN: 10551-2.0-00 [DIRS 159065]) was used to simultaneously fit both sets of bromide and TFBA breakthrough curves, as well as all the other tracer breakthrough curves (mass-based normalizations for all other tracers) in the first cross-hole test. For details of the RELAP code and how it is used to simultaneously fit tracer breakthrough curves the reader is referred to Section D4.6.1. However, it should be noted that, for dual-porosity fits, the individual parameters that comprise the diffusive mass transfer coefficient, $\frac{\phi}{b} \sqrt{D_m}$, have slightly different interpretations in alluvium than in fractured systems. In alluvium, ϕ is the

porosity within the stagnant domain (as opposed to the matrix porosity), D_m is the diffusion coefficient within the stagnant porosity, and b is the ratio of the volume of the flowing porosity to the interfacial area between the flowing and stagnant porosity (as opposed to the fracture half aperture). It can be readily confirmed that $\frac{\phi}{b}\sqrt{D_m} = \frac{\phi_b\sqrt{D_m}}{R\phi_f/3(1-\phi_f)}$ for the diffusion-into-grains

conceptual model of the alluvium, and $\frac{\phi}{b}\sqrt{D_m} = \frac{\phi_l\sqrt{D_m}}{\phi_f(b+L/2)}$ for the diffusion-into-layers conceptual model.

Before attempting the RELAP fits, it was first noted that the rising limbs of the bromide and TFBA breakthrough curves (Figure G-34) had the unconventional appearance of being steepest at the point of initial breakthrough with gradually decreasing slopes until the peak concentration was reached and even a hint of one or two nearly linear segments between the initial breakthrough and the peak. Figure G-41 shows the derivative of the bromide concentrations with respect to time as a function of time in the early portion of the tracer test. The derivatives at any given time were calculated using the following 20-point moving-average formula, which served to smooth out the derivative data without compromising any of the information contained in the data:

$$\left(\frac{dC}{dt}\right)_i = \frac{\text{Average}(C_i, C_{i+19}) - \text{Average}(C_{i-20}, C_{i-1})}{\text{Average}(t_i, t_{i+19}) - \text{Average}(t_{i-20}, t_{i-1})}$$

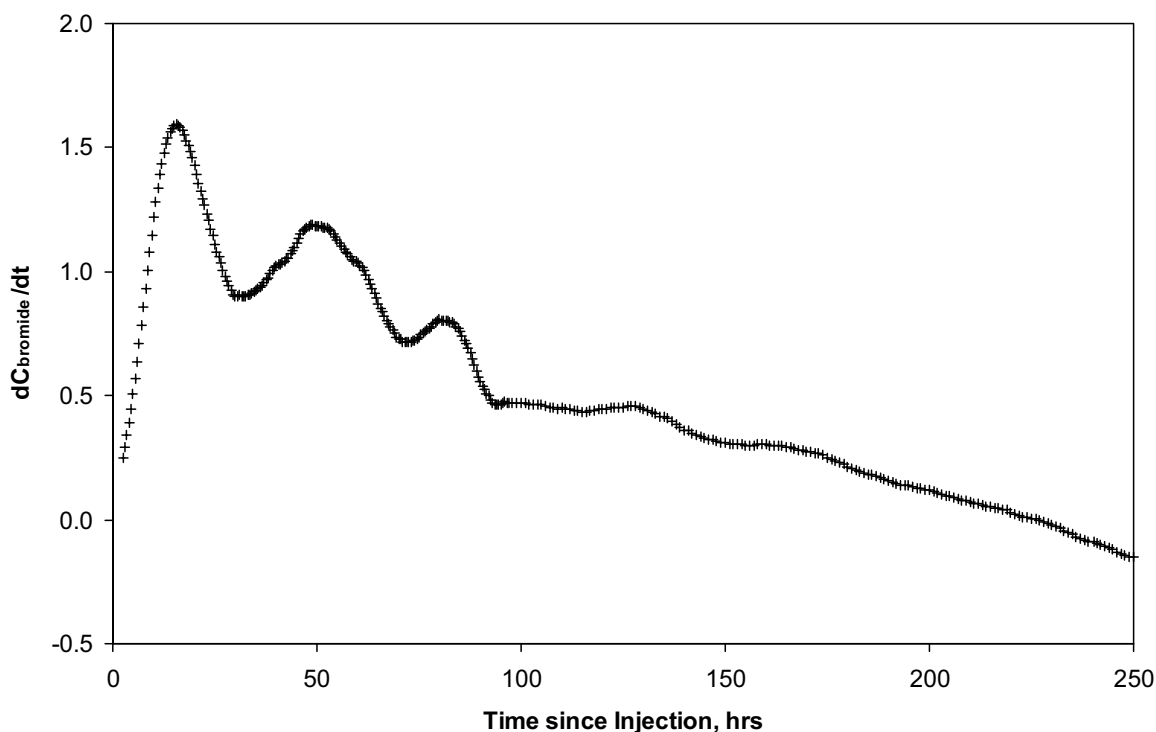
where, C = concentration

t = time

i = data point corresponding to the time at which the derivative is calculated.

$\text{Average}(A_x, A_y)$ = average of A (concentration or time) for consecutive data points x through y (relative to the current data point i).

Three distinct maxima are shown on Figure G-41. Multiple maxima are not generally observed from breakthrough curves that result from a single dominant flow pathway. Furthermore, model fits of the data using only a single advective-dispersive pathway do not match the early portion of the breakthrough curve (Figure G-42). These two lines of evidence combined strongly suggest separate arrival of the tracers along separate flow pathways in the flow system. The derivative of concentration curve (Figure G-41) suggests that three pathways were dominant.



Source: DTN: LA0612PR831231.003 [DIRS 178736].

NOTE: The three prevalent peaks are interpreted as corresponding to separate tracer arrivals associated with different flow pathways.

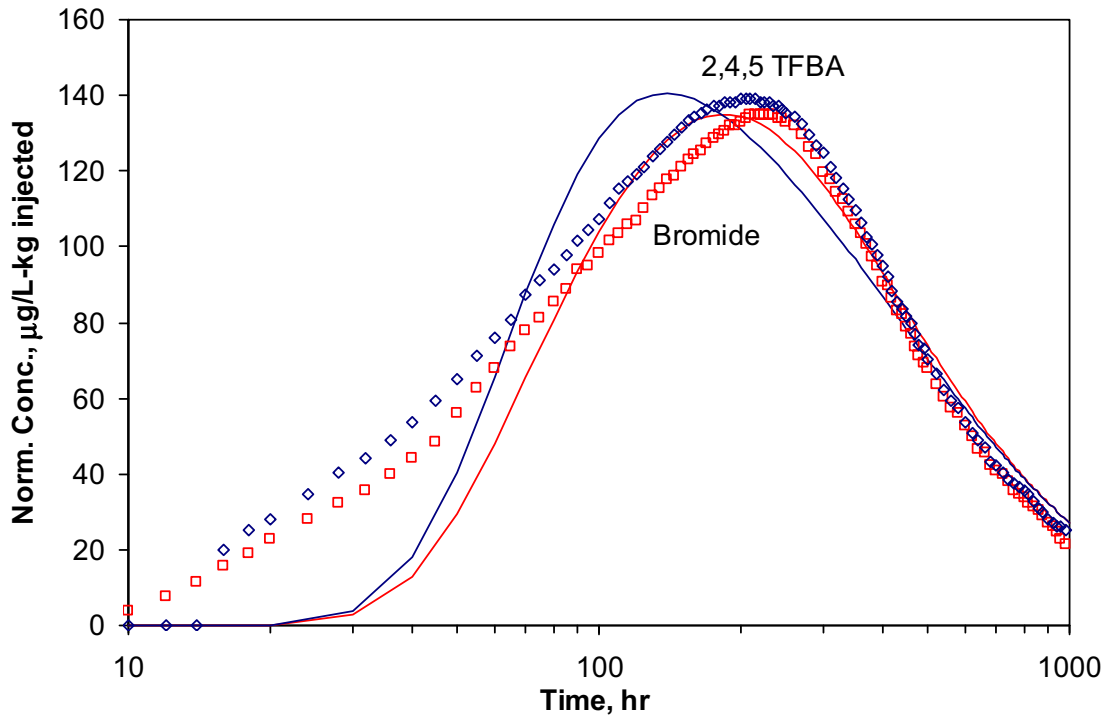
Figure G-41. Derivative of Bromide Concentration with Respect to Time as a Function of Time since Injection in the First Cross-Hole Tracer Test at Site 22

For these reasons, the bromide and TFBA breakthrough curves were simultaneously fitted as three separate breakthrough curves in a sequential manner with RELAP. The earliest arrivals were fitted first, and then the model curves resulting from these fits were subtracted from the observed breakthrough curves and the differences were fitted. This process was repeated so that the overall fits to the bromide and TFBA breakthrough curves consisted of the sum of the three separate fits corresponding to the three separate flow pathways suggested by Figure G-41. The multiple pathway fits to the bromide and TFBA breakthrough curves with the minimum and maximum possible differences are shown in Figures G-43 and G-44. The model parameters corresponding to these fits are provided in Tables G-14 and G-15, respectively. The dual-porosity pathways were simulated assuming a “diffusion-into-layers” conceptual model because RELAP does not have a diffusion-into-blocks capability.

Figure G-43 and Table G-14 also show the results of a single-porosity RELAP fit to the 2,6 DFBA breakthrough curve, which represents transport between 22PC and 22S. A single-porosity model was used to fit these data because there were no other tracer responses that could be used to estimate diffusion parameters. A single-porosity assumption was considered justified because the third Br-TFBA pathway in the case of the minimum possible differences between these tracer concentrations was interpreted as having no diffusion (i.e., single-porosity

behavior), and of the three pathways, this one most closely matched the timing and shape of the 2,6 DFBA breakthrough curve. A single flow pathway was found to be sufficient to achieve a good fit to the 2,6 DFBA data.

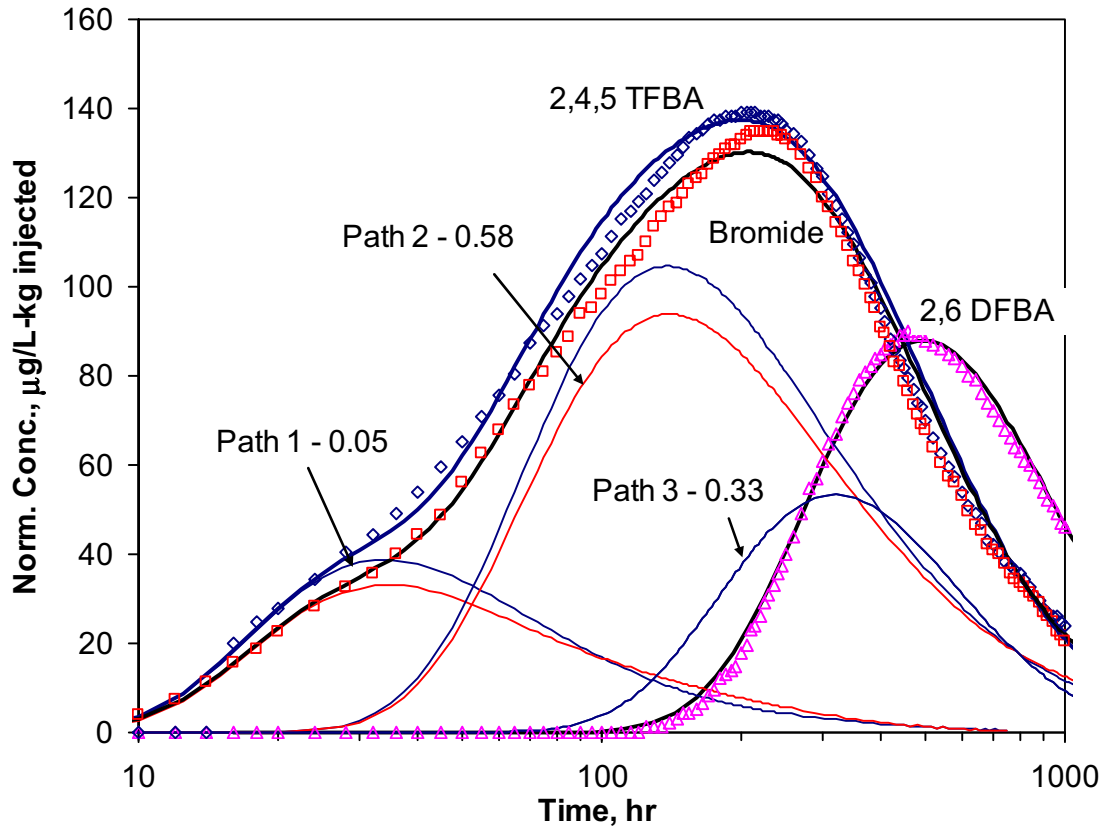
The fitting procedure for the bromide and TFBA was essentially the same as that used to fit the C-wells tracer breakthrough curves, as described in Section D4.6.1 (i.e., the mean residence time, Peclet number, and participating tracer mass fraction were constrained to be the same for all tracers, and the ratio of the tracer diffusion coefficients was fixed to be the ratio of their free-water diffusion coefficients). It is apparent from the model parameters in Tables G-14 and G-15, that dual-porosity behavior (i.e., diffusion between flowing and stagnant porosity) was assumed in all three pathways in the case of the maximum possible bromide and TFBA differences, and in two of the three pathways for the minimum possible bromide and TFBA differences. Thus, regardless of which combination of bromide and TFBA normalized concentrations are used, dual-porosity behavior appears to be necessary to explain the nonsorbing tracer responses in the first cross-hole tracer test.



Output DTN: LA0701PR150304.002.

NOTE: Note the log time scale.

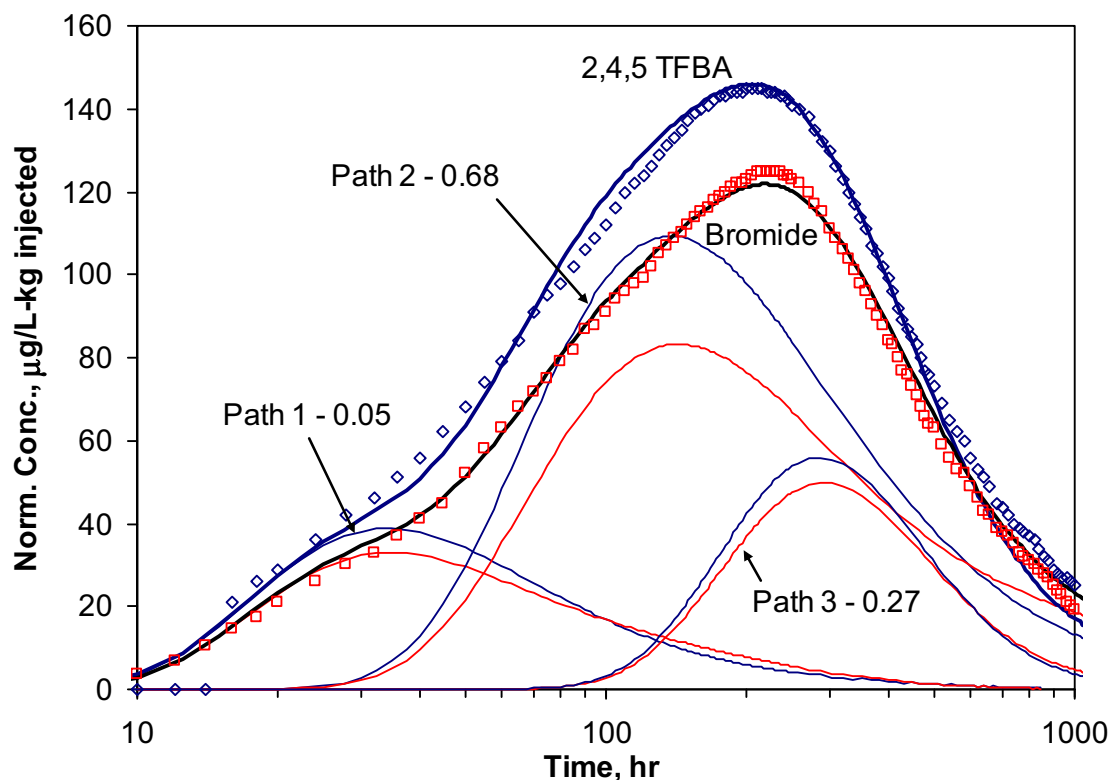
Figure G-42. Fit of a Single-Pathway Model (solid lines) to the First 1,000 Hours of the 2,4,5 TFBA (blue diamonds, mass-based normalization) and Bromide (red squares, concentration-based normalization) Breakthrough Curves at Site 22



Output DTN: LA0701PR150304.002.

NOTES: The tracer mass fractions in each pathway are indicated on the plot. The third pathway fitting the TFBA and bromide data is a single-porosity pathway (tracers have identical predicted behavior). Only one pathway was needed to fit the 2,6 DFBA breakthrough curve. The bold black curves are the sums of the three individual model pathway curves. Model parameters are listed in Table G-14. The simulated tracer responses associated with the individual pathways are indicated by the thin colored lines.

Figure G-43. Composite Three-pathway RELAP Fits to the First 1,000 Hours of the 2,4,5 TFBA (blue diamonds, mass-based normalization), 2,6 DFBA (magenta triangles, mass-based normalization) and Bromide (red squares, concentration-based normalization) Breakthrough Curves at Site 22



Output DTN: LA0701PR150304.006.

NOTES: The tracer mass fractions in each pathway are indicated on the plot. All pathways have dual-porosity behavior. The bold black curves are the sums of the three individual model pathway curves. Model parameters are listed in Table G-15. The simulated tracer responses associated with the individual pathways are indicated by the thin colored lines.

Figure G-44. Composite Three-Pathway RELAP Fits to the First 1,000 Hours of the 2,4,5 TFBA (blue diamonds, concentration-based normalization) and Bromide (red squares, mass-based normalization) Breakthrough Curves at Site 22

Table G-14. RELAP Model Parameters Yielding Fits to the Solute Responses for the Three Pathways in the First Cross-hole Tracer Test at Site 22 for the Case with the Minimum Possible Differences between the TFBA and Bromide Breakthrough Curves and for the Single Pathway Interpreted for DFBA (Figure G-43)

Parameter	22PA to 22S (2,4,5 TFBA)			22PC to 22S (2,6 DFBA)
	Pathway 1	Pathway 2	Pathway 3	Single Pathway
Mass fraction, f	0.05	0.58	0.33	0.88
Mean residence time, τ , for linear flow (hr)	100	490	560	900
Peclet number, Pe , for linear flow	2.1	1.8	5	4.6
Mean residence time, τ , for radial flow (hr)	67	313	452	716
Peclet number, Pe , for radial flow	3.5	3.1	7.3	6.8
$\frac{\phi}{b} \sqrt{D_m}$ for bromide ($s^{-1/2}$) ^a	0.001	0.00032	0	N/A

Table G-14. RELAP Model Parameters Yielding Fits to the Solute Responses for the Three Pathways in the First Cross-hole Tracer Test at Site 22 for the Case with the Minimum Possible Differences between the TFBA and Bromide Breakthrough Curves and for the Single Pathway Interpreted for DFBA (Figure G-43)

Parameter	22PA to 22S (2,4,5 TFBA)			22PC to 22S (2,6 DFBA)
	Pathway 1	Pathway 2	Pathway 3	Single Pathway
Ratio of stagnant to flowing water porosity	0.7	0.9	N/A	N/A
Characteristic diffusion time scale ($L^2/8D_m$), hr	68.1	1125	N/A	N/A
Lithium flowing porosity retardation factor, R_f	1.25	1.7	10.5	N/A
Lithium stagnant porosity retardation factor, R_s	33	800	N/A	N/A

Output DTN: LA0701PR150304.002.

NOTE: TFBA and bromide curves associated with fitted pathways 1 to 3 are shown on Figure G-43. The lithium fit is shown in Figure G-46.

^a The mass transfer coefficient, $MTC = \frac{\phi}{b} \sqrt{D_m}$, for TFBA is ~0.58 times that for bromide.

MTC=mass transfer coefficient; TFBA = Trifluorobenzoic acid or trifluorobenzoate.

Table G-15. RELAP Model Parameters Yielding Fits to the TFBA, Bromide, and Lithium Responses in the First Cross-Hole Tracer Test at Site 22 for the Case with the Maximum Possible Differences between the TFBA and Bromide Breakthrough Curves (Figure G-44)

Parameter	22PA to 22S		
	Pathway 1	Pathway 2	Pathway 3
Mass fraction, f	0.05	0.68	0.27
Mean residence time, τ , for linear flow (hr)	100	400	400
Peclet number, Pe , for linear flow	2.1	2.2	8
Mean residence time, τ , for radial flow (hr)	67	270	346
Peclet number, Pe , for radial flow	3.5	3.6	11.3
$\frac{\phi}{b} \sqrt{D_m}$ for bromide ($s^{-1/2}$) ^a	0.001	0.00089	0.00022
Ratio of stagnant to flowing water porosity	0.7	1.9	0.63
Characteristic diffusion time scale ($L^2/8D_m$), hr	68.1	627	1125
Lithium flowing porosity retardation factor, R_f	1.3	1.9	5
Lithium stagnant porosity retardation factor, R_s	32	135	900

Output DTN: LA0701PR150304.006.

NOTE: TFBA and bromide curves associated with fitted pathways 1-3 are shown on Figure G-44. The lithium fit is shown in Figure G-47.

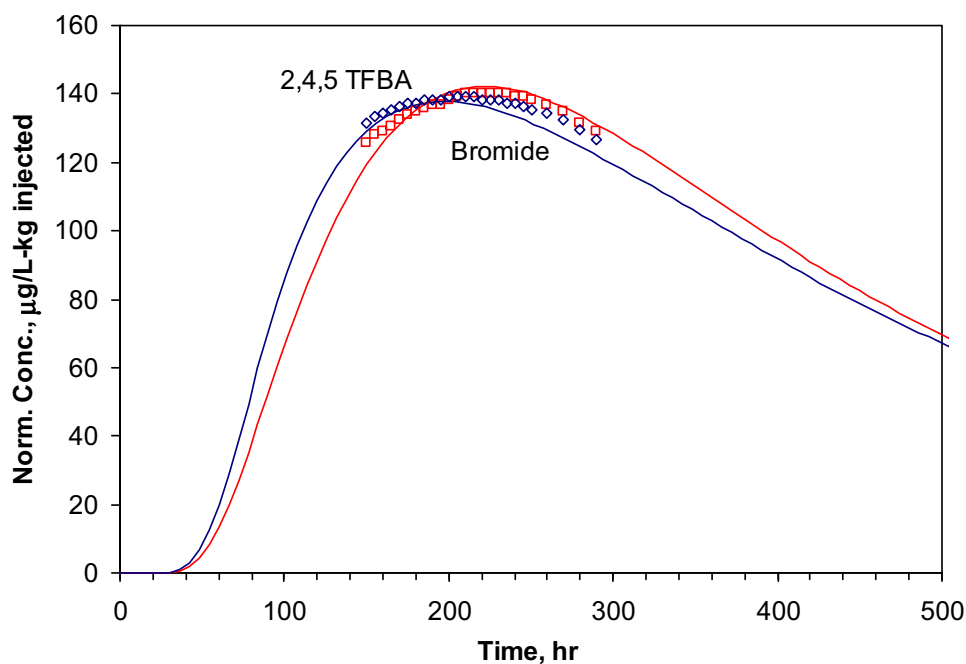
^a The mass transfer coefficient, $MTC = \frac{\phi}{b} \sqrt{D_m}$, for TFBA is ~0.58 times that for bromide.

MTC=mass transfer coefficient; TFBA = Trifluorobenzoic acid or trifluorobenzoate.

An additional fit to the bromide and TFBA data was conducted after adjusting the normalized concentrations of the two tracer data sets so that the tracers had essentially the same recoveries. This adjustment raised the bromide breakthrough curve relative to the TFBA so that both tracers had approximately the same peak normalized concentration and the primary difference between the two tracers was the timing of the peaks. Furthermore, only the peaks of the tracer

breakthrough curves were fitted so that the three-pathway analysis described in the previous paragraph did not have to be repeated. Thus, the difference in the timing of the peaks was used as an independent diagnostic of amount of diffusion between flowing and stagnant water occurring in the system. The result of the fitting exercise is shown in Figure G-45, and the model parameters corresponding to these fits are listed in Table G-16.

The lithium breakthrough curve was fitted by assuming that the model parameters obtained from the fits to the TFBA and bromide breakthrough curves also applied to the lithium, so the only model parameters that were adjusted to fit the lithium response were retardation factors in the flowing and stagnant porosity. As in the case of the bromide and TFBA, the lithium was assumed to transport in three separate flow pathways (all the tracers were injected in the same solution, so they should have followed the same flow pathways and experienced the same nonreactive transport parameters in each pathway). The lithium diffusion coefficient in the stagnant porosity was assumed to be two-thirds that of the bromide (and twice that of the TFBA). This assumption is consistent with the assumption used for the interpretation of the C-wells tracer tests involving lithium. The fits to the lithium breakthrough curves assuming the minimum and maximum amounts of diffusion into stagnant porosity are shown in Figures G-46 and G-47. The lithium retardation coefficients corresponding to these fits are listed at the bottom of Tables G-14 and G-15, respectively.



Output DTN: LA0701PR150304.002.

NOTE: Model parameters are listed in Table G-16. These curves are the result of adjusting bromide concentrations so that the two tracers have approximately the same mass recovery.

Figure G-45. RELAP Fits (solid lines) to the Peaks of the 2,4,5 TFBA (blue diamonds) and Bromide (red squares) Breakthrough Curves

Table G-16. RELAP Model Parameters Yielding the Single-pathway Fits to the TFBA and Bromide Responses in the First Cross-hole Tracer Test at Site 22 when the Bromide Breakthrough Curve is Adjusted so that the Recoveries of TFBA and Bromide are Approximately the Same (Figure G-45)

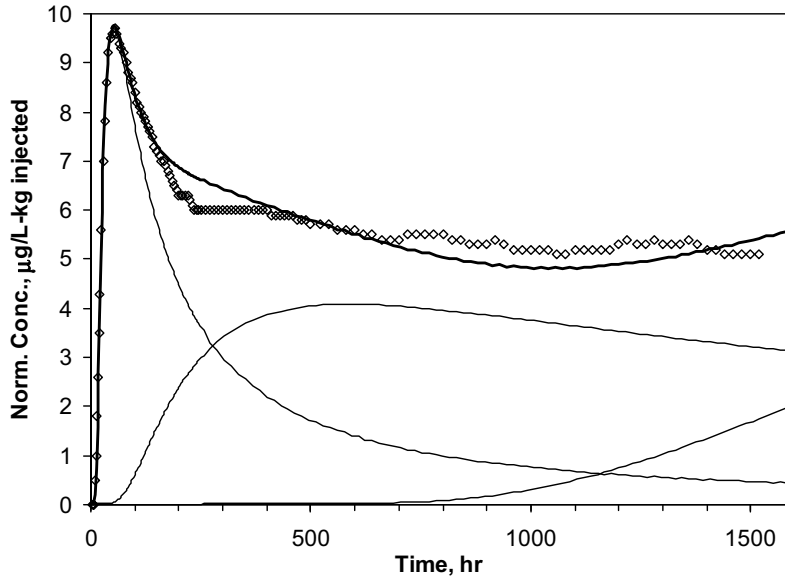
Parameter	Value
Mass fraction, f	0.72
Mean residence time, τ , for linear flow (hr)	310
Peclet number, Pe , for linear flow	4
Mean residence time, τ , for radial flow (hr)	240
Peclet number, Pe , for radial flow	6
$\frac{\phi}{b} \sqrt{D_m}$ for bromide ($s^{-1/2}$) ^a	0.001
Ratio of stagnant to flowing water porosity	0.4
Characteristic diffusion time scale ($L^2/8D_m$), hr	22.2

Output DTN: LA0701PR150304.002.

^a The mass transfer coefficient, $MTC = \frac{\phi}{b} \sqrt{D_m}$, for TFBA is ~0.58 times that for bromide.

MTC=mass transfer coefficient; TFBA = Trifluorobenzoic acid or trifluorobenzoate.

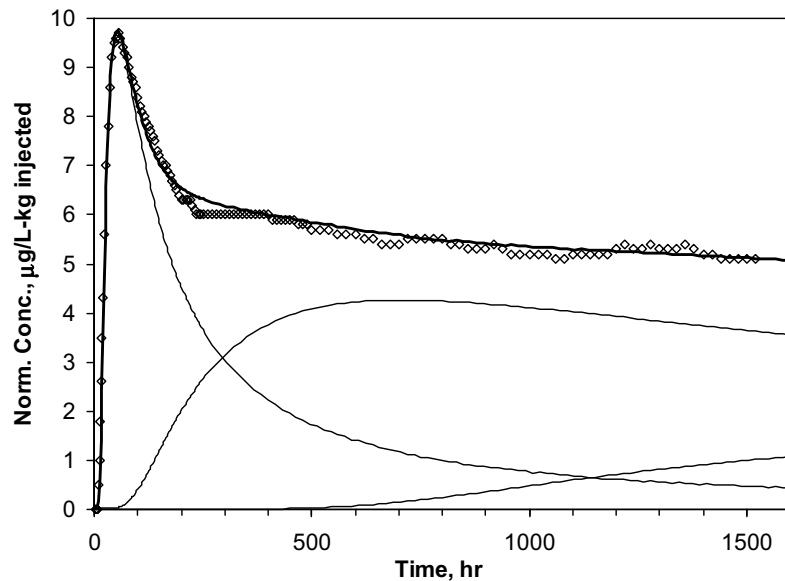
From Figures G-46 and G-47, it is apparent that a better fit to the lithium breakthrough curve can be achieved assuming a greater amount of diffusion. This result supports the inference from the single-well tracer tests and from the nonsorbing cross-hole tracer responses that diffusion between flowing and stagnant water is occurring in the alluvium. Attempts to fit the lithium breakthrough curve assuming single-porosity behavior were not successful. Figure G-48 shows such an attempt using MULTRAN V1.0 (STN: 10666-1.0-00 [DIRS 159068]), which accounts for multicomponent transport effects that provide more accurate simulation of reactive cation transport than RELAP when a sorbing cation used as a tracer dominates the ionic strength of the injection solution (as lithium did in this case). It is apparent that the single-porosity fit to the lithium breakthrough curves is significantly poorer than in either Figure G-46 or G-47.



Output DTN: LA0701PR150304.002.

NOTES: The third pathway assumes single-porosity transport behavior. The bold curve is the sum of the three individual model pathway curves (thin solid lines). Model parameters are listed at the bottom of Table G-14.

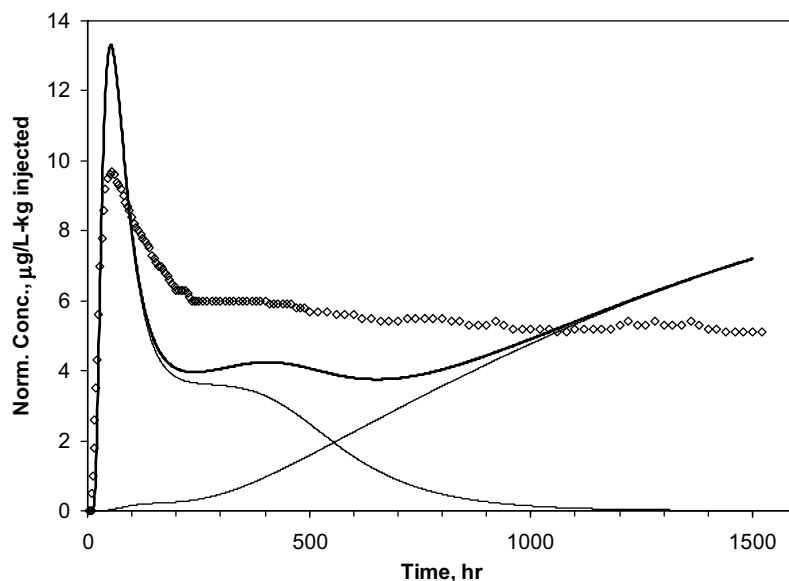
Figure G-46. Three-Pathway RELAP Fit to Lithium (mass-based normalization) Breakthrough Curve (diamonds) Using Flow Pathways Deduced from RELAP Fits to TFBA and Bromide Breakthrough Curves with Minimum Possible Differences (Figure G-43)



Output DTN: LA0701PR150304.006.

NOTE: The bold curve is the sum of the three individual model pathway curves (thin solid lines). Model parameters are listed at the bottom of Table G-15.

Figure G-47. Three-Pathway RELAP Fit to the Lithium (mass-based normalization) Breakthrough Curve (diamonds) Using Flow Pathways Deduced from RELAP Fits to TFBA and Bromide Breakthrough Curves with Maximum Possible Differences (Figure G-44)



Output DTN: LA0701PR150304.007.

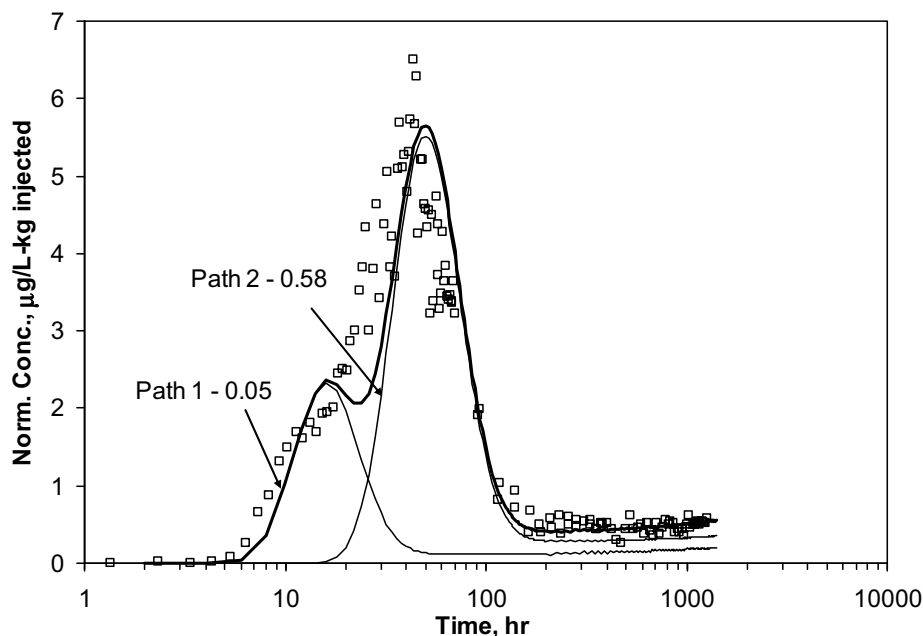
NOTES: The bold curve is the sum of the two individual model pathway curves (thin solid lines). A third pathway was not necessary to fit the lithium data (i.e., the third pathway would be predicted to have a lot of retardation).

Figure G-48. MULTRAN Fit to Lithium (mass-based normalization) Breakthrough Curve (diamonds) Assuming Two Single-porosity Flow Pathways Deduced from RELAP Fits to TFBA and Bromide Breakthrough Curves (not shown)

Figure G-49 shows the composite RELAP fit to the 200-nm diameter microsphere breakthrough curve. The fits were obtained by assuming the same flow pathways and same mean residence times, Peclet numbers, and mass fractions in each pathway that were obtained for the solute breakthrough curves in the case of the minimum amount of diffusion between flowing and stagnant water. However, the microsphere diffusion coefficients were set to zero (single-porosity assumption), and the microsphere retardation factor and filtration rate constant were used as adjustable parameters to fit the data. Further details of the approach used to fit the microsphere breakthrough curve, including the mathematical model inherently assumed when RELAP is used for this process, are provided in Section D4.6.2.

It is apparent from Figure G-49 that the third pathway assumed for the solutes was not needed to fit the microsphere breakthrough curve (and, in fact, would have been detrimental to the fit if there were anything but complete filtration in this pathway). This finding suggests that either the microspheres did not follow the third flow pathway or that they were filtered strongly enough in the third pathway that they were insignificantly recovered in this pathway. It is certainly possible that they did not follow the third pathway because the microsphere injection solution was much less dense than the solute injection solution, which may have caused the solutes to enter flow pathways that were not accessed by the microspheres because of density-driven flow of the solute injection solution. This possibility is further supported by the apparent lack of a third flow pathway in the second cross-hole tracer test between 22PA and 22S (discussed below). The microsphere filtration parameters corresponding to the fits of Figure G-49 are listed in Table G-17. Table G-17 also lists filtration parameters corresponding to the case in which the

nonreactive transport parameters for the three flow pathways were estimated assuming the maximum amount of diffusion between flowing and stagnant water. It is apparent that the filtration parameters are hardly affected at all by which set of nonsorbing solute transport parameters are used for the microsphere fits.



Output DTN: LA0701PR150304.002.

NOTES: The bold black curve is the sum of the three individual model pathway curves. Colloid filtration parameters are listed in Table G-17.

Figure G-49. Multi-Pathway RELAP Fit to Microsphere Breakthrough Curve Using Flow Pathways Deduced from RELAP Fits to TFBA and Bromide Breakthrough Curves with Minimum Possible Differences (Figure G-43)

Table G-17. CML Microsphere Filtration Parameters for Multi-pathway Fits to Microsphere Response Using Nonreactive Transport Parameters Deduced from Fits to TFBA and Bromide Breakthrough Curves Assuming Minimum and Maximum Possible Amounts of Matrix Diffusion

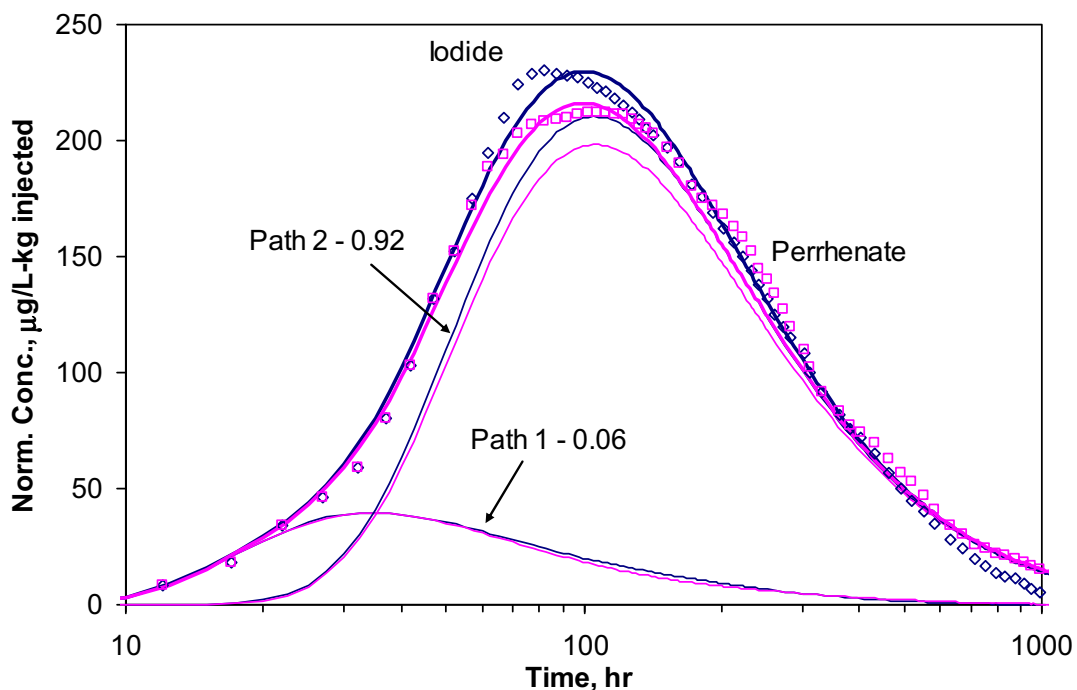
	Parameter	Pathway 1	Pathway 2	Pathway 3
Minimum Diffusion Case	Mass fraction, f (minimum diffusion)	0.05	0.58	0.33
	k_{fit} (1/hr)	0.16	0.048	>0.04
	k_{res} (1/hr)	0.0011	0.00034	–
Maximum Diffusion Case	Mass fraction, f (maximum diffusion)	0.05	0.68	0.27
	k_{fit} (1/hr)	0.16	0.048	>0.045
	k_{res} (1/hr)	0.0011	0.00034	–

Output DTNs: LA0701PR150304.002 (minimum diffusion) and LA0701PR150304.006 (maximum diffusion).

NOTE: Other transport parameters used to obtain the fits are given in Tables G-14 (minimum diffusion case) and G-15 (maximum diffusion case).

Composite RELAP fits to the iodide and perrhenate breakthrough curves (mass-based normalizations) in the second cross-hole tracer test are shown in Figure G-50. The model parameters corresponding to the two-pathway fits of Figure G-50 are listed in Table G-18. It is

apparent that the lower peak of the perrhenate breakthrough curve relative to the iodide is qualitatively consistent with perrhenate retardation in the stagnant porosity of the flow system. If perrhenate has a diffusion coefficient that is a factor of ~ 0.7 times that of iodide (as the free-water diffusion coefficients in Table G-13 dictate), the observed relative peak heights could not be simulated without assuming some perrhenate retardation. However, other features of the breakthrough curves are not as well matched as the relative peak heights; i.e., the later peak arrival and longer tailing of the perrhenate relative to the iodide. These features suggest that perrhenate retardation may have occurred in the flowing porosity as well as the stagnant porosity. Furthermore, the unconventional inflections in the perrhenate breakthrough curve suggest the possibility of spatially distributed retardation factors in the flow system. Although these possibilities were not exhaustively explored, single-pathway fits to the first 250 hours of the iodide and perrhenate breakthrough curves were obtained (Figure G-51) assuming that the perrhenate sorbed (1) only in the stagnant porosity and (2) only in the flowing porosity. It is apparent from Figure G-51 that while perrhenate retardation in the stagnant porosity provides a better match to the observed data, retardation in the flowing porosity also provides a relatively good match, and it cannot be ruled out as a process contributing to the observed perrhenate transport behavior. Figure G-51 also serves to illustrate that, as in the case of the first cross-hole tracer test, single-pathway fits do not match the earliest portions of the breakthrough curves. The RELAP model parameters corresponding to the fits of Figure G-51 are listed in Table G-19.



Output DTN: LA0701PR150304.003.

NOTES: The bold curves are the sum of the two individual model pathway curves. Model parameters are listed in Table G-18. The simulated tracer responses associated with the individual pathways are indicated by the thin lines.

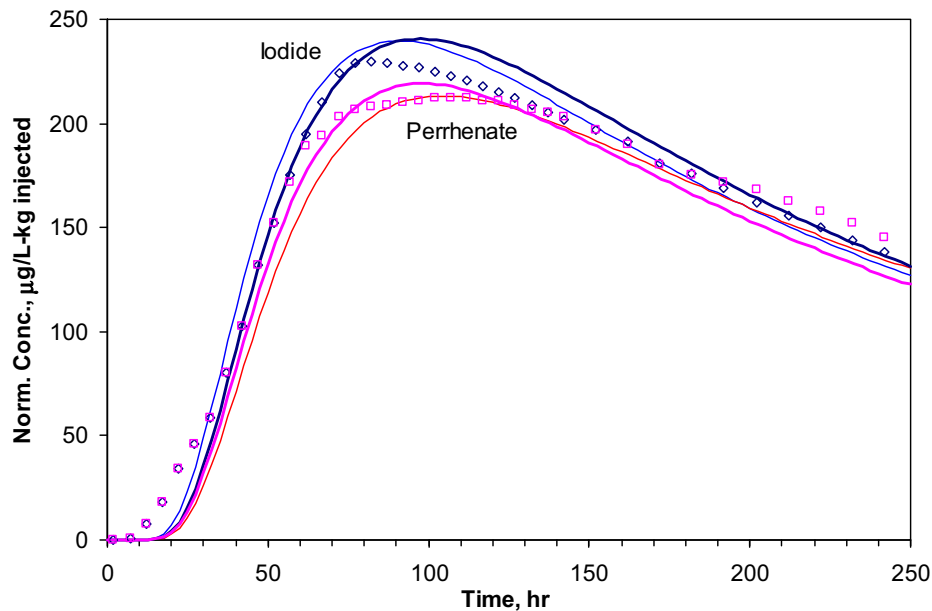
Figure G-50. Two-Pathway RELAP Fits to Iodide (blue diamonds) and Perrhenate (magenta squares) (mass-based normalizations for both tracers) Breakthrough Curves in Second Cross-Hole Tracer Test at Site 22

Table G-18. RELAP Model Parameters Yielding Fits to Iodide and Perrhenate Responses in Second Cross-hole Tracer Test at Site 22 (Figure G-50)

Parameter	Pathway 1	Pathway 2
Mass fraction, f	0.06	0.92
Mean residence time, τ , for linear flow (hr)	100	352
Peclet number, Pe , for linear flow	2.1	1.9
Mean residence time, τ , for radial flow (hr)	67	228
Peclet number, Pe , for radial flow	3.5	3.2
$\frac{\phi}{b} \sqrt{D_m}$ for iodide ($s^{-1/2}$) ^a	0.001	0.00032
Ratio of stagnant to flowing water porosity	0.7	0.9
Characteristic diffusion time scale ($L^2/8D_m$), hr	68.1	1125
Re flowing porosity retardation factor, R_f	1	1
Re stagnant porosity retardation factor, R_m	1.5	2.3

Output DTN: LA0701PR150304.003.

^aThe mass transfer coefficient, $MTC = \frac{\phi}{b} \sqrt{D_m}$, for perrhenate is ~0.84 times that for iodide.



Output DTN: LA0701PR150304.003.

NOTE: The bold curves (dark blue and magenta) correspond to fits assuming perrhenate retardation only in the stagnant porosity, and the non-bold curves (light blue and red) correspond to fits assuming perrhenate retardation only in the flowing porosity. Model parameters are listed in Table G-19.

Figure G-51. Single-Pathway RELAP Fits to Iodide (blue diamonds) and Perrhenate (magenta squares) (both mass-based normalizations) Breakthrough Curves in Second Cross-Hole Tracer Test at Site 22

Table G-19. RELAP Model Parameters Associated with Single-pathway Fits to the Iodide and Perrhenate Responses in the Second Cross-hole Tracer Test at Site 22

Parameter	Retardation in Stagnant Porosity	Retardation in Flowing Porosity
Mass fraction, f	0.99	1.0
Mean residence time, τ , for linear flow (hr)	340	460
Peclet number, Pe , for linear flow	1.8	1.2
Mean residence time, τ , for radial flow (hr)	217	257
Peclet number, Pe , for radial flow	3.1	2.3
$\frac{\phi}{b} \sqrt{D_m}$ for iodide ($s^{-1/2}$) ^a	0.00032	0.00016
Ratio of stagnant to flowing water porosity	0.9	0.45
Characteristic diffusion time scale ($L^2/8D_m$), hr	1125	1125
Re flowing porosity retardation factor, R_f	1	1.15
Re stagnant porosity retardation factor, R_m	3	1

Output DTN: LA0701PR150304.003.

NOTE: Assuming perrhenate only in stagnant porosity and perrhenate retardation only in flowing porosity (Figure G-51).

^aThe mass transfer coefficient, $MTC = \frac{\phi}{b} \sqrt{D_m}$, for TFBA is ~0.58 times that for bromide.

Because a later *and* higher peak concentration of a tracer with a smaller diffusion coefficient relative to a tracer with a larger diffusion coefficient (or of a sorbing tracer relative to a nonsorbing tracer) is not a realistic possibility unless the differences in the tracer diffusion coefficients are quite large, the combination of a concentration-based perrhenate normalization and a mass-based iodide normalization (which results in this unrealistic scenario) was not considered in the interpretive analysis. Rather, this tracer test was analyzed assuming only mass-based normalizations of both tracers, which resulted in the smallest possible difference between the two breakthrough curves (of all the combinations considered realistic). An additional reason that the concentration-based normalized breakthrough curves were not considered for analysis is that the mass-based normalized curves yielded predicted tracer mass participations of essentially 100%, so an analysis of the concentration-based normalized concentrations, which were significantly higher than the mass-based concentrations, would have required greater than 100% mass participation – a physical impossibility.

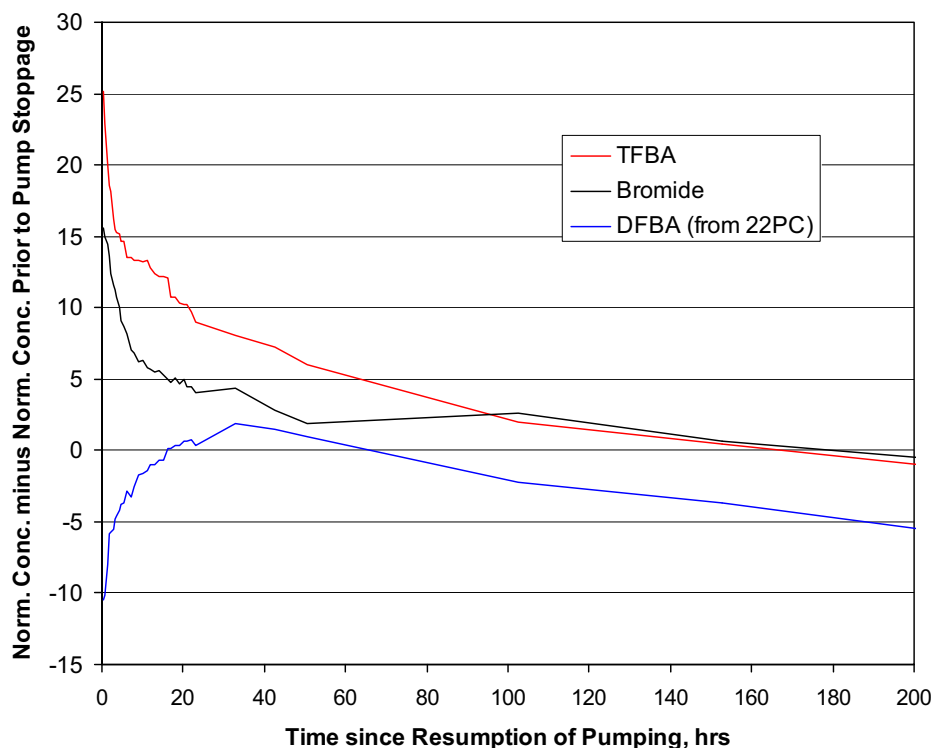
The early breakthrough behavior in the second tracer test was very similar to the first test, but the peak normalized tracer concentrations were considerably higher and the tails shorter than in the first test. Unlike the first cross-hole tracer test, in which 3 flow pathways were needed to fit the tracer breakthrough curves, Figure G-50 shows that only two flow pathways were needed to fit the iodide and perrhenate tracer breakthrough curves. By comparing the parameters of Table G-19 with those of Tables G-14 and G-15, it can be seen that the two pathways associated with the iodide and perrhenate responses correspond very closely to the first two pathways in the first tracer test between 22PA and 22S (the correspondence with the first two pathways in Table G-14 is almost exact). The third pathway accessed in the first test was not activated in the second test, and all of the tracer mass that followed the third pathway in the first test apparently moved in the second pathway in the second test. The injection and chase volumes and the

production rate in both tests were about the same, so the most likely explanation for the differences in observed tracer behavior in the two tests was the much higher density of the tracer solution in the first test. As mentioned earlier, this very high density could have resulted in density-driven flow that caused a portion of the tracer mass in the first test to access pathways that were not accessed in the second test. The density contrast between the injection solution and groundwater was negligible in the second test.

A potentially important result in the second cross-hole tracer test is the apparent attenuation of perrhenate relative to iodide ion. Because perrhenate has a smaller diffusion coefficient than iodide, this attenuation can only be explained by retardation in the stagnant or flowing porosity, not by diffusion effects. Given the results of the first cross-hole tracer test and the two single-well tracer tests, diffusion into stagnant porosity followed by sorption in this porosity appears to be the most likely explanation.

G5.3 ESTIMATES OF AMBIENT FLOW VELOCITY BASED ON NONSORBING TRACER RESPONSES AFTER 159-DAY FLOW INTERRUPTION IN FIRST CROSS-HOLE TRACER TEST AT SITE 22

There was 159 days of “shut in” (i.e., no pumping) at Site 22 between the “end” of the first cross-hole tracer test and the start of pumping for the second cross-hole tracer test. During this time, the residual tracer mass remaining in the aquifer from the first cross-hole test “drifted” with the natural groundwater flow in the alluvium. The tracer responses after resumption of pumping relative to their last measured concentrations prior to cessation of pumping are shown in Figure G-52. The initially higher concentrations of 2,4,5 TFBA and bromide after pumping resumed suggest that the tracer “plume” from NC-EWDP-22PA drifted toward NC-EWDP-22S during the time the pump was off. By the same reasoning, the decrease in concentration of 2,6 DFBA upon resumption of pumping suggests that the “plume” from NC-EWDP-22PC drifted away from NC-EWDP-22S during the time the pump was off. This situation is illustrated schematically in Figure G-53.



Output DTN: LA0701PR150304.004.

NOTE: There was no pumping for 159 days.

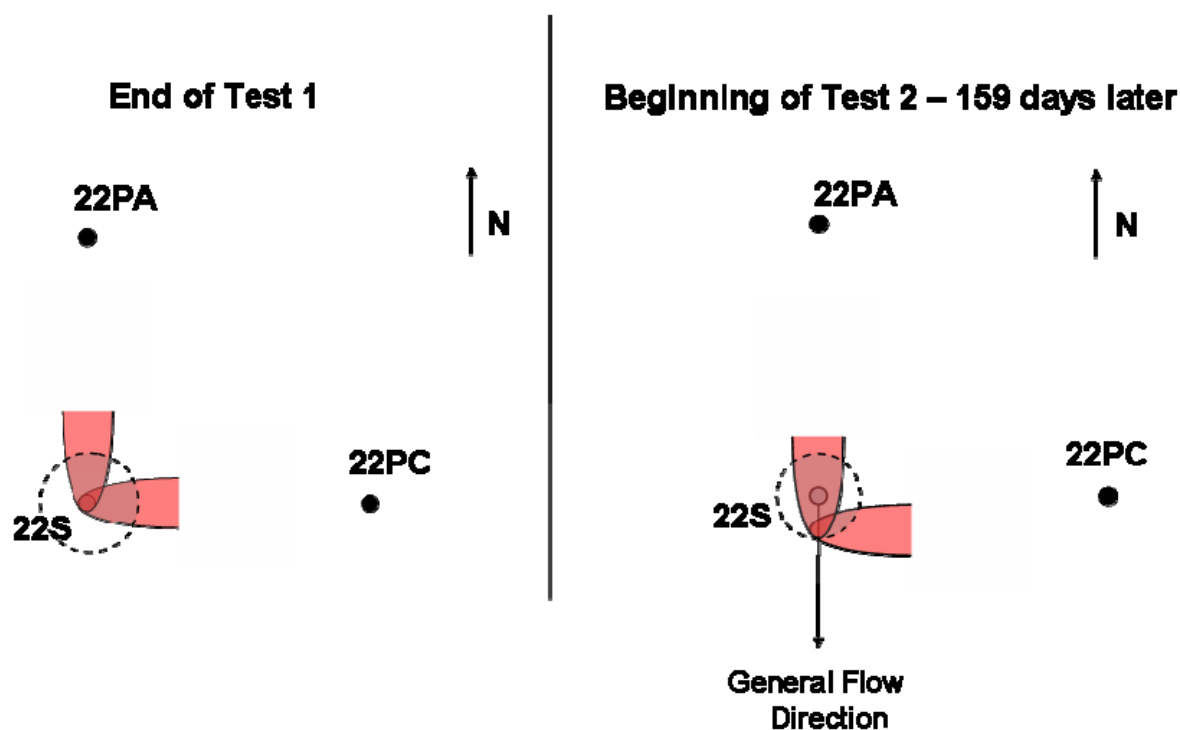
Figure G-52. Normalized Concentrations of Nonsorbing Tracers used in the First Cross-Hole Tracer Test at Site 22 Minus Their Normalized Concentrations Prior to Pump Stoppage as a Function of Time Since Pumping Resumed

Qualitatively, the tracer responses are consistent with the groundwater drift illustrated schematically in Figure G-53. Unfortunately, it is not possible to obtain a well-constrained estimate of the groundwater drift velocity during the flow interruption because the distribution of the tracer plume around NC-EWDP-22S at the time of the flow stoppage was unknown. However, we can make a rough estimate of the drift velocity if the direction of drift was essentially in the direction from 22PA to 22S is assumed as follows (Output DTN: LA0701PR150304.004):

- It took about 150 hours for the TFBA and bromide concentrations to decline to their concentrations prior to the pump stoppage. It is reasonable to assume that during this 150 hours, the water being drawn into NC-EWDP-22S included at least some traced water that had drifted into the volume of water produced during this first 150 hours of pumping.
- The 150 hours that it took for the tracer concentrations to decline to preflow interruption levels represents about 75% of the time it took for *peak* tracer concentrations to arrive from -22PA (i.e., ~200 hrs). Assuming that the time to peak concentrations represents the approximate time it takes to “sweep out” a cylindrical volume of the aquifer with

radius equal to the distance between -22PA and -22S (~18 m), then the radial distance swept out in 75% of the time would be about $\sqrt{0.75}$ of the distance between -22PA and -22S or about 15.6 m (assuming radial flow).

- An estimated 45% *additional* tracer mass of TFBA and Br was recovered during the initial 150 hours of pumping after the flow interruption. This estimate assumes that the tracer concentrations would have remained relatively constant for this 150 hours of pumping if the flow interruption had not occurred (the breakthrough curves were relatively flat when the pumping was stopped). In reality, the tracer concentrations were very slowly declining before the flow interruption, so 45% is probably a slightly low estimate of additional mass.



NOTES: Orange half-ellipses represent tracer plumes. Note that after 159 days of drift, plumes move southward. Grey circles represent the volume/area of aquifer produced in the first few hours after resuming pumping. Concentrations of tracers from 22PA will initially be higher than when pumping was stopped, and concentrations from 22PC will be lower. For information only.

Figure G-53. Schematic Illustration of One Possible Scenario for Tracer Drift at Site 22 Qualitatively Consistent with Observed Tracer Responses upon Resumption of Pumping after 159 Days of No Pumping

- This additional 45% of tracer mass is equivalent to about 67.5 hrs (45% of 150 hrs) of additional pumping of water containing TFBA and bromide at pre-pump-stoppage concentrations. Assuming radial flow, the radial distance “swept out” in 67.5 hours would be about 10.5 m ($=\sqrt{67.5/200} \times 18$ m, where 200 hrs is the time to peak tracer arrival during the cross-hole test). This radial distance could be considered an upper bound for the distance that tracers drifted under ambient flow conditions during the pump stoppage. However, it is more reasonable to assume that all of the *extra* tracer

mass produced during the 150 hours of pumping would have moved from just outside to just inside the 15.6-m swept-out radial distance from -22S during the flow stoppage (all the mass that was already inside the 15.6-m radial distance would have either moved closer to the production well or a little past the production well). In this case, it is more appropriate to assume that the production of the additional tracer mass occurred during the *last* 67.5 hours of the 150-hr production period, not at the beginning of the period. We can calculate the inner and outer radial distances associated with the last 67.5 hours of the first 150 hours of pumping by solving the following equation for x (which equates the areas being swept out in the first and last 67.5 hours): $10.5^2 = (15.6^2 - x^2)$. An implicit assumption in this analysis is that the water moving into the “sweep-out” zone during the flow interruption had about the same tracer concentrations as the water that was just entering the swept-out zone at the time of the flow stoppage (which was approximately the maximum concentration before or after the flow stoppage, not counting the first 150 hours after flow resumption).

- Solving for x in the above equation, we get an inner radial distance of 11.6 m. Thus, the distance that tracer-bearing water moved with the natural gradient during the 159-day flow stoppage is estimated to be $15.6 - 11.6 = 4.0$ m, yielding an estimated ambient flow velocity in the direction from -22PA to -22S of $4.0/159 = 0.025$ m/day = 9.25 m/yr. This analysis assumes that the natural gradient is oriented directly from -22PA to -22S – if the orientation is at some acute angle to this direction, then the actual drift velocity would be somewhat greater (0.025 m/day divided by the cosine of the angle). A two-dimensional graphical depiction of the analysis described above is provided in Figure G-54. This analysis is clearly based on tracer mass recovery arguments, and as such, the distance of plume migration (in this case, $15.6 - 11.6 = 4$ m) should be considered an estimate of the *average* plume displacement during the drift period. The pie-shaped plumes in Figure G-54 are clearly a simplification that implicitly assumes a homogeneous isotropic medium with very little dispersion (and sufficient initial spreading of the tracer around the injection borehole to approach a wedge shape). In reality, the plume would be expected to be somewhat irregular and spread over time; portions of it would probably move significantly farther than 4 m and other portions would move less. The 4 m can be probably be considered a lower-bound estimate, because the tracer concentrations further away from 22S were likely lower than the concentrations closer to the well (the analysis above assumes the same concentrations everywhere in the pie-wedge-shaped plumes). Thus, a greater amount of plume movement would have been required to achieve the same *additional* mass recovery if concentrations decreased with upgradient distance.
- A qualitative reality check on this estimate of 4 m of drift during the flow stoppage can be obtained by considering that some of the tracer mass that was very close to the production well at the time of the flow stoppage should have drifted up to 4 m past the well during the stoppage. In this case, relatively high concentrations upon resumption of pumping could be expected to persist for as long as it takes to sweep out at least a 4-m radial zone around -22S. Assuming radial flow, the time necessary to sweep out a 4-m radial zone should have been about 10 hrs ($= (4 \text{ m}/18 \text{ m})^2 \times 200 \text{ hrs}$), and, indeed, the plots shows that there is an inflection in the decline in tracer concentrations after about the first 8 to 10 hrs of pumping.

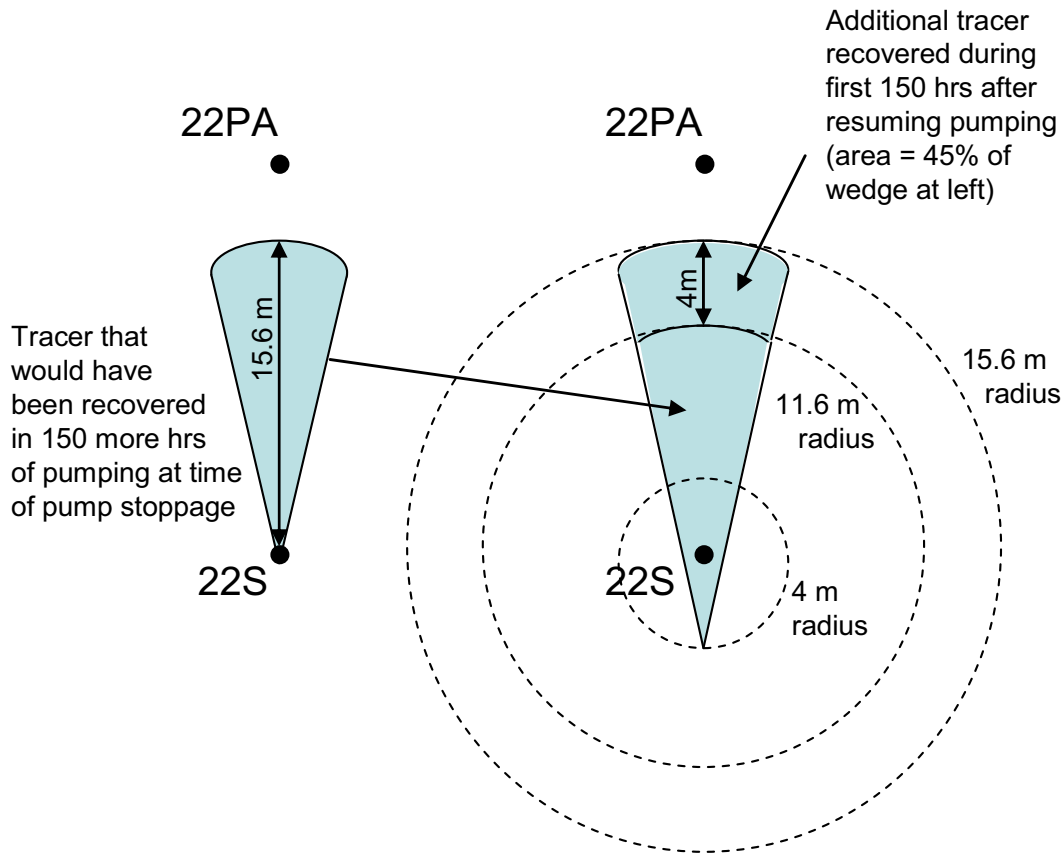


Figure G-54. Graphical Depiction of the Analysis of Tracer Plume Migration during the 159-day Flow Interruption between Two Cross-Hole Tracer Tests at Site 22

The estimated drift velocity of 9.25 m/yr (Output DTN: LA0701PR150304.004) is a seepage velocity rather than a specific discharge. This estimate compares quite favorably with the estimates of seepage velocity obtained from analyses of the single-well tracer test responses (Section G4.3), provided in Table G-9 (Output DTN: LA0701PR150304.001). The good agreement between these analyses of tracer drift in the single-well and cross-hole tests lends confidence to the estimates obtained by either method.

G5.4 DISCUSSION OF ALLUVIUM FIELD TRACER TEST RESULTS

Estimates of transport parameters that can be used directly in solute transport models in the alluvium were derived from the best-fitting parameters provided in the tables in the previous section. These parameter estimates are presented in Table G-20 as ranges of values consistent with the tracer test interpretation(s). For effective flow porosity, longitudinal dispersivity, and horizontal flow anisotropy, best estimates are also provided. Parameters derived from single-well tracer tests (other than the ambient flow velocity estimates from Sections G4.3 and G4.4) are included in this table as well. Additional discussion of these ranges and how they were derived is provided in the following sections. This parameter estimation exercise has several important implications for radionuclide transport in saturated alluvium near Yucca Mountain.

Table G-20. Transport Parameter Estimates Deduced from Tracer Tests in Saturated Alluvium

Parameter	Lower Bound	Best Estimate	Upper Bound
Effective flow porosity ^a	0.036	0.121	0.187
Longitudinal dispersivity, m ^b	1.6	5	10
Horizontal flow anisotropy ratio (N-S principal axis) ^c	2.5	3.1	10.7
MTC, $\frac{\phi}{b} \sqrt{D_m}$, for halide (s ^{-1/2}) ^d	0 (0.00016)	—	0.001
Characteristic diffusion time scale, (L ² /8D _m), hr ^d	0 (14.1)	—	1125
Ratio of stagnant to flowing water volumes ^d	0 (0.3)	—	1.9

Output DTNs: LA0701PR150304.002, LA0701PR150304.003, LA0701PR150304.006, and LA0701PR150304.007.

NOTE: All estimates are from cross-hole tracer testing at Nye County Site 22 except for the lower bounds of diffusion parameters (last 3 rows), which are from single-well testing at the ATC and Site 22.

^a Calculated using Equation D-6, Appendix D, Section D4.8.5, but with the production rate modified to account for horizontal flow anisotropy estimated from tracer responses. That is, instead of uniform radial flow at 47.5 gallons per minute (gpm), it was assumed that there was a flow rate of 71.25 gpm in the direction of 22PA and 23.75 gpm in the direction of 22PC, which is consistent with the ~3:1 flow anisotropy in the N-S direction deduced as the best estimate in this table. The lower bound is based on using the mean residence time assuming radial flow in the fastest flow pathway between 22PA and 22S, and the upper bound is based on the mean residence time assuming linear flow in the second flow pathway between 22PA and 22S. The best estimate corresponds to radial anisotropic flow for both 22PA (second pathway) and 22PC to 22S (where the flow porosities in the two directions are assumed to be equal and the anisotropy is estimated from inverse of the ratio of the residence times). See discussion in Section G5.4.3.

^b Lower bound assumes radial flow in third flow pathway of first cross-hole test, and upper bound assumes linear flow in second pathway in second cross-hole test. Best estimate is based on assuming radial flow in all first and second pathway analyses. Dispersivities are calculated as L/Pe, where L is the distance between wells (18m), and Pe is the Peclet number estimated by RELAP.

^c Lower bound based on ratio of linear flow residence time between 22PC and 22S and linear flow residence time in second pathway between 22PA and 22S. Upper bound based on ratio of radial flow residence time between 22PC and 22S and radial flow residence time in first pathway between 22PA and 22S. Best estimate based on ratio of radial flow residence time between 22PC and 22S and radial flow residence time in second pathway between 22PA and 22S.

^d MTC=diffusion mass transfer coefficient. Lower bounds of zero are based on apparent single-porosity behavior in third-pathway of first cross-hole test (when minimum differences between bromide and TFBA are assumed) and also on the very minor differences in the iodide and PFBA responses in the first single-well tracer test at 22S. The lower bound of zero is also based on the negligible differences in halide and FBA responses in the single-well tests at the ATC. Numbers in parentheses for the lower bound are the lowest value from a dual-porosity pathway analysis. Upper bound is based on the maximum value observed in any of the tracer tests. However, for the ratio of stagnant to flowing water volumes, larger values cannot be ruled out because of the relatively short time scales of the tracer tests. See text for definitions of the individual parameters that comprise the MTC.

G5.4.1 Conceptual Transport Model Considerations

Both the single-well and cross-hole tracer test results at Site 22 are consistent with a dual-porosity conceptual transport model for the alluvium. It is not possible to account for the differences in the halide and FBA responses without invoking diffusion between flowing and stagnant water. Likewise, the relatively small time attenuation but significant concentration attenuation of the lithium response relative to the nonsorbing tracers in the first cross-hole tracer test and the differences between the iodide and perrhenate responses in the second cross-hole tracer test are consistent with dual-porosity transport behavior. While the analysis of the first cross-hole test indicated single-porosity transport behavior in one of the three flow pathways when the minimum differences between the bromide and TFBA breakthrough curves were

assumed, the fact that the lithium breakthrough curve was better fit assuming dual-porosity behavior in all three flow pathways (Figure G-47 versus Figure G-46) argues for some dual-porosity character in all the flow pathways in the system.

In contrast, the results of single-well tracer testing in 19D do not support a dual-porosity conceptualization of the alluvium at that location. However, the volume of alluvium interrogated in these single-well tests is considerably smaller than the volume interrogated in cross-hole tests, so the former tests are considered less reliable than the latter in discriminating between conceptual transport models. Single-well tests are more likely to be influenced by local heterogeneities or local disturbances of the alluvium due to drilling and well completion.

While the data at 22S are consistent with a dual-porosity transport conceptualization, the tracer responses also suggest that the time scales for diffusion are quite short and the stagnant porosity is only 0.3 to 1.9 times the flowing porosity in the alluvium. This range of 0.3 to 1.9 plus one can be considered a range of physical retardation factors for nonsorbing species in the flow system provided advective transport times are long relative to diffusion time scales (Robinson 1994 [DIRS 101154]). This situation clearly exists for the alluvium under ambient flow conditions, so the range of porosity ratios of 0.3 to 1.9 will translate to a range of effective physical retardation factors of 1.3 to 2.9 in the alluvium. In effect, over time and distance scales relevant for Yucca Mountain performance assessment, the saturated alluvium can be expected to behave as a single-porosity system with a flow porosity equal to the sum of the flowing porosity and stagnant porosity deduced from the relatively short-duration tracer tests. It is interesting to note that the mass-fraction-weighted sum of the flowing and stagnant porosities from the two pathways between 22PA and 22S in the second cross-hole tracer test (the test without density-driven flow issues) is slightly greater than 0.2, which is probably quite close to the total porosity of the alluvium (considered to have a maximum value of around 0.3). Thus, while we cannot rule out the possibility of longer diffusion time and distance scales in the alluvium than the tracer tests indicated, the test interpretations are consistent with tracers accessing the majority of the total porosity in the flow system.

It is also worth noting that the short diffusion time scales are more consistent with a diffusion-into-grains (or blocks) conceptual transport model (Figure G-1(b)) than a diffusion-into-layers conceptual model (Figure G-1(c)) because the latter will typically have significantly longer diffusion time scales than were observed. However, longer diffusion time scales cannot be ruled out in the alluvium because of the short time and distance scales of the tracer tests relative to performance assessment time scales. It is possible that the tests were strongly influenced by diffusion into blocks within flow pathways, but the flow pathways were large enough in thickness or diameter (i.e., channels) that longer-time-scale diffusion into stagnant water surrounding the pathways was not observed.

Finally, it is noted that the quantitative estimates of the lumped diffusion mass transfer parameter, $\frac{\phi}{b}\sqrt{D_m}$, for halides in Table G-20 are based on the assumption that halides have a diffusion coefficient a factor of three greater than FBAs, which is based on matrix diffusion coefficients measured in laboratory diffusion cell tests in consolidated tuff matrices (discussed in Section E2). It is worth repeating here that the individual parameters that comprise $\frac{\phi}{b}\sqrt{D_m}$ have

slightly different interpretations in alluvium systems than in fractured rock systems. In alluvium, ϕ is the stagnant porosity (as opposed to the matrix porosity), D_m is the diffusion coefficient within the stagnant porosity, and b is the volume of the flowing porosity divided by the interfacial area between the flowing and stagnant porosity (as opposed to the fracture half aperture). It is also worth noting that, regardless of what the absolute values are for the diffusion coefficients, flowing and stagnant porosities, and length scales associated with flowing and stagnant porosities, the same transport behavior will be observed if the characteristic time scale for diffusion, $L^2/8D_m$ (diffusion-into-layers model) or $R^2/2D_m$ (diffusion-into-spherical blocks model), the mass transfer coefficient, $\frac{\phi}{b}\sqrt{D_m}$, and the ratio of stagnant to flowing water volumes (or porosities) are kept the same.

G5.4.2 Horizontal Flow Anisotropy and Flow Heterogeneity Considerations

Estimates of horizontal flow anisotropy in the saturated alluvium at Site 22 were obtained by comparing the nonsorbing tracer transport times between 22PA and 22S and between 22PC and 22S. 22PA and 22S are oriented almost due north–south (Figure 6.1-8), and 22PC and 22S are oriented almost due east–west. The flow anisotropy ratio (the ratio of largest to smallest hydraulic conductivity in the so-called conductivity ellipse that defines the two-dimensional anisotropy) was estimated simply as the inverse of the ratio of the mean nonsorbing tracer residence times between 22PA and 22S and between 22PC and 22S. As Table G-20 indicates, the estimates range from about 2.5 to 11, with the principal axis or preferred flow direction being north–south. The upper end of this range is based on using the travel times associated with the first flow pathway between 22PA and 22S, and the lower end is based on using the travel times associated with the second flow pathway between these wells. The third flow pathway observed in the first cross-hole tracer test was not considered because this pathway was not reproduced in the second cross-hole tracer test and was believed to be an artifact of density-driven flow of the very concentrated, high-density tracer solution used in the first test. Because the majority of the tracer mass in both the first and second cross-hole tests followed the second pathway between 22PA and 22S, this pathway is considered more representative for flow anisotropy estimates, and it forms the basis for the best estimate of 3.1:1 north–south for the anisotropy ratio in Table G-20.

Although not necessarily directly related to flow anisotropy, it is interesting that the first flow pathway between 22PA and 22S had very little tracer mass in it compared to the second pathway. This observation relates to the heterogeneity of flow in the alluvium. Normally, one would expect a faster pathway to also have the higher volumetric flow rate and therefore more mass associated with it. In this case, multiple pathways would probably not even be apparent in tracer breakthrough curves. The fact that the first pathway was observed in both tracer tests, under conditions with both a high density contrast and a low density contrast between the injection solution and the ambient groundwater, suggests that the small amount of mass in the fast pathway was probably not caused by density-driven flow effects in the vicinity of the injection wellbore (as suspected in the case of the multiple tracer test in the Bullfrog tuff at the C-wells – see Section D4.5). Rather, it appears likely that a low-volume, high-flow pathway exists. However, another possible explanation given the method of injection is that there is only a single fast-flow pathway that passes close to 22PA but does not directly intersect it, and the chase water that followed the tracer solution pushed a small amount of tracer mass into this

nearby pathway. This small amount of mass would have transported rapidly to 22S, but the majority of the tracer mass would have stayed behind near the injection borehole. The mass left behind would have been gradually pulled into the flow pathway as a result of pumping of 22S, resulting in the second apparent “pathway.” Unfortunately, it is not possible to distinguish between these two scenarios with the information available, but the implications are important for both flow heterogeneity and apparent flow porosity in the alluvium. Conducting another cross-hole test with a larger volume of chase water might help to distinguish between these possibilities.

Although some flow heterogeneity undoubtedly exists in the saturated alluvium, it seems apparent from the tracer tests that the flow heterogeneity at Site 22 is less than it is in the fractured volcanic tuffs at the C-wells. The nonsorbing tracer recoveries at Site 22 were significantly higher than at the C-wells, and the fractional tracer mass participations deduced from the RELAP interpretations were approaching 1.0 for all tests at Site 22, whereas the mass participations at the C-wells were significantly less than 1.0. These results qualitatively suggest that there is more flow heterogeneity in the fractured tuffs than in the alluvium, as incomplete mass recoveries over the relatively short time scales of the tracer tests imply some flow pathways that have very long travel times. The results also support the conclusion discussed in the previous section that diffusion length scales in the alluvium are relatively short - longer diffusion time scales would result in lower recoveries because of the greater amounts of time that tracers could spend in the stagnant porosity. However, it must also be remembered that most of the C-wells tracer tests were conducted under partial recirculation conditions whereas the 22S tests were conducted with no recirculation of produced water. Partial recirculation would be expected to result in greater apparent flow heterogeneity and to increase the probability of lower tracer recoveries because of the increased volume of the aquifer tracers are “pushed” into and also because of the theoretical existence of a stagnation point in the unbalanced dipole flow field that could result in tracers being “trapped” in the flow system.

G5.4.3 Effective Flow Porosity

The discussion of effective flow porosity in Section D4.8.5 also applies here except that there was no need for any consideration of recirculation in the cross-hole tracer tests at Site 22 as there was for the C-wells tracer tests. Table G-20 lists the effective flow porosities calculated using equation D-6 (repeated here for convenience) for each of the flow pathways between 22PA and 22S and also between 22PC and 22S.

$$\eta = \frac{Q \tau}{\pi r_L^2 T} \quad (\text{Eq. D-6})$$

where

η = effective flow porosity

Q = production flow rate, m³/hr

τ = mean residence or transport time, hr

r_L = distance between wells, m

T = formation thickness (assumed to be interval length).

Rather than use the 22S production rate as the value of Q in the calculations to obtain the estimates listed in Table G-20, the values of Q for each injection well were modified to account for the deduced flow anisotropy ratio discussed in the previous section. That is, the production rate between 22PA and 22S was assumed to be 71.25 gpm, and the production rate between 22PC and 22S was assumed to be 23.75 gpm. These values preserve the overall production flow rate into 22S (their average is the actual production rate of 47.5), but they also reflect the observed 3:1 flow anisotropy ratio oriented north-south. In effect, the use of equation D-6 with the modified Q values assumes that, despite the flow anisotropy, quasi-radial flow conditions (i.e., an r^2 dependence for transport times) still exist in the general direction of each injection well. No attempt was made to account for the effects of ambient flow in the aquifer, which in principle, would be superimposed on the flow field resulting from pumping. Given the large difference between tracer transport times under pumping conditions when compared to those expected under ambient flow conditions, it is very unlikely that ambient flow would have had a significant effect on the test results or interpretations. Also, no attempt was made to partition the value of Q for the 22PA-to-22S flow direction between the first and second (or third) flow pathways observed in the tracer responses. Such partitioning would have resulted in lower flow porosity estimates in each pathway than reflected in Table G-20, and the flow porosity estimate for the first flow pathway would have been less than 0.004 if the partitioning were based on the relative mass recoveries in each flow pathway. Such a small effective porosity for the saturated alluvium seems unrealistic, which perhaps argues for the alternative explanation for the first and second flow pathways provided in the previous section (i.e., the first two pathways were actually one pathway with tracer being rapidly injected into and gradually pulled into the pathway to account for the two apparent pathways).

The above modifications of Q for the two flow directions have the effect of yielding essentially the same flow porosity estimate for the second flow pathway between 22PA and 22S and for the flow pathway(s) between 22PC and 22S (the 3:1 ratio is based on the mean residence times for these tracer responses). If the same value of Q were used in both flow directions, one would obtain an apparent anisotropy in effective flow porosity, with a factor of three lower porosity for the 22PA-to-22S flow direction. Reporting both a flow anisotropy and an effective porosity anisotropy would be inconsistent and would result in overestimating flow rates in the N-S direction under ambient flow conditions. By adjusting the Q values instead of effective porosity values, we are inherently assuming that it is more likely that flow anisotropy explains the differences in the observed tracer responses than an anisotropy in effective porosity. However, we cannot rule out the possibility of the latter or that there is some anisotropy in both parameters.

The upper and lower bounds for effective flow porosity given in Table G-20 were calculated using the mean tracer residence times calculated assuming linear and radial flow conditions, respectively (linear flow mean residence times were always somewhat greater than radial flow residence times).

G5.4.4 Lithium Sorption Behavior

Tables G-14 and G-15 list the best-fitting values of the lithium retardation factors in the flowing and stagnant porosities (R_f and R_s , respectively) in the first cross-hole tracer test at Site 22 for the cases of minimum and maximum possible differences between the bromide and TFBA breakthrough curves. Note that the R_f values are quite small, implying small amounts of sorption

within the flowing porosity, but the R_s values are large, indicating strong sorption in stagnant porosity after diffusion into this porosity. The MULTRAN fit of Figure G-48 shows that even when multicomponent diffusion and cation exchange effects are explicitly accounted for, a single-porosity model cannot provide nearly as good of a match to the lithium breakthrough curve as a dual-porosity model without these features (RELAP). Qualitatively, these results provide additional support for a dual-porosity conceptualization of transport in the alluvium.

Estimates of lithium partition coefficients, or K_d values, were deduced from the fitted retardation factors by simple rearrangement of the expression defining the retardation factor (repeated here from Section D4.8.4):

$$K_d = \frac{\phi}{\rho_B} (R - 1) \quad (\text{Eq. D-5})$$

Because the retardation factors in Tables G-14 and G-15 vary over such a wide range and the K_d values depend on the porosity within the stagnant or flowing regions of the flow system, K_d values are listed in Table G-21 for a wide range of potential porosities and for each retardation factor from Tables G-14 and G-15 (two values are lumped because they are very similar). In the K_d calculations, ρ_B was assumed to be equal to $2.65(1-\phi)$ g/cm³, where 2.65 is the approximate density of many silicate phases present in the alluvium.

For comparison, Table G-22 lists lithium K_d values over a wide range of lithium concentrations measured in batch sorption experiments involving 22S water and alluvium material from two different zones within 22PC. The K_d values in Table G-22 do not reflect direct measurements, but rather they are calculated from the Freundlich isotherm parameters that provided the best fits to the experimental sorption isotherms, which are shown in Figure G-55 and provided in its caption (DTN: LA0703PR150304.001 [DTN 179625]). The wide range of concentrations in Table G-22 reflect the wide range that likely existed in the Site 22 field tracer test. The injection concentration of lithium was about 20,000 mg/L and the peak measured concentrations in the 22S production water were around 0.2 mg/L. The latter value should be considered an extreme lower bound estimate for concentrations in the aquifer, as there was probably considerable dilution with untracered water occurring in the production wellbore.

As Tables G-21 and G-22 indicate, the K_d values associated with retardation factors deduced from stagnant porosity in the field tests (32 or greater) are in relatively good agreement with or somewhat higher than the laboratory-derived K_d values. If the porosity within the stagnant porosity is 0.1 or greater, then the field values are all higher than would be expected from the lab measurements. In the case of the flowing porosity, the field retardation factors (10.5 or lower) are all consistent with K_d values that are in relatively good agreement with or lower than the laboratory-derived values. This result could indicate that there is relatively low effective surface area available for sorption within the flowing porosity and all the sorption in the alluvium effectively occurs after a diffusive mass transfer step into stagnant porosity. However, as pointed out in Section G5.4.1, for transport over long time and distance scales, it should be possible to treat the alluvium as a single-porosity system, and in this case, the distinction between retardation factors or K_d values in flowing and stagnant porosity becomes a moot point. However, the effective retardation factor in this case should be a volume weighted average of the two retardation factors. Although the laboratory data set is small and can't be considered

representative of all the mineralogical heterogeneity that likely exists in the alluvium, and there is also considerable uncertainty in the lithium concentrations that actually existed in the aquifer, it is concluded that the laboratory-derived K_d values are in reasonably good agreement with the field-derived values. If the average lithium concentrations in the field test were at the upper end or middle of the range in Table G-22, then it could be concluded that the lab K_d values would tend to underestimate field-scale sorption if they were used in field-scale predictive calculations.

An interesting trend in Tables G-14 and G-15 is that the lithium retardation factors in both the flowing and stagnant porosity appear to increase as flow pathway residence times in the alluvium increase. Given the time scales of the tracer responses and the fact that lithium sorption occurs by cation exchange (a rapid process), it seems unlikely that this trend could be explained by slow sorption kinetics. The reason for this apparent time-scale dependence of lithium sorption is unknown at this time. It could be just coincidence that the longer travel time pathways exhibit greater sorption, but a similar trend was also observed for the two flow pathways in the multiple-tracer test in the Bullfrog tuff at the C-wells (see Table D-6). These results suggest that the scaling behavior of reactive transport should perhaps be investigated further because of the important potential implications for transport of sorbing radionuclides over long time and distance scales in the alluvium near Yucca Mountain.

Table G-21. Calculated Lithium Partition Coefficients (K_d Values) for Various Assumed Porosities Using Retardation Factors Derived from Field Tracer Tests

Retardation Factor	K_d Value				
	$\phi = 0.02$	$\phi = 0.05$	$\phi = 0.1$	$\phi = 0.2$	$\phi = 0.3$
1.25	0.002	0.005	0.011	0.024	0.040
1.7	0.005	0.014	0.029	0.066	0.113
1.9	0.007	0.018	0.038	0.085	0.146
5	0.031	0.079	0.17	0.38	0.65
10.5	0.073	0.19	0.40	0.90	1.54
32.5	0.24	0.63	1.32	2.97	5.09
135	1.03	2.66	5.62	12.6	21.7
800	6.15	15.9	33.5	75.4	129.2
900	6.92	17.9	37.7	84.8	145.4

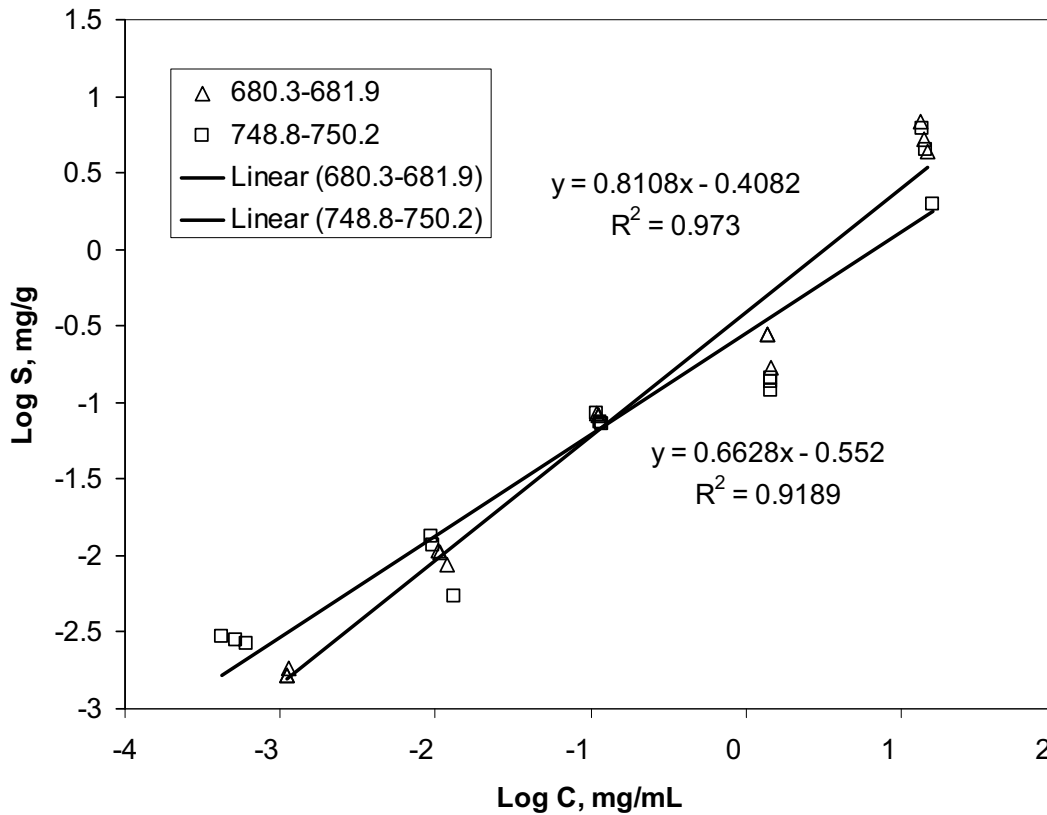
Output DTN: Values calculated using equation D-5 with lithium retardation factors from DTNs: LA0701PR150304.002 and LA0701PR150304.006.

Table G-22. Lithium Partition Coefficients (K_d Values) for Alluvium from NC-EWDP-22PC over a Wide Range of Lithium Concentrations Using Freundlich Isotherm Parameters obtained from Fitting Batch Sorption Data

Li Concentration (mg/L)	Lithium K_d Values	
	Sample from 680.3-681.9 ft BLS	Sample from 748.8-750.2 ft BLS
1	1.443	2.88
10	0.934	1.33
100	0.604	0.610
1000	0.391	0.281
10,000	0.253	0.129
100,000	0.163	0.059

Source: DTN: LA0703PR150304.001 [DIRS 179625].

NOTE: See Figure G-55 for isotherms used for calculations.
BLS = below surface level.



Source: DTN: LA0703PR150304.001 [DIRS 179625].

NOTE: Legend indicates feet below land surface (BLS) of the intervals. The Freundlich isotherms are $S = 0.58C^{0.81}$ for 680.3 ft BLS to 681.9 ft BLS, and $S = 0.28C^{0.66}$ for 748.8 ft BLS to 750.2 ft BLS.

Figure G-55. Batch Sorption Data and Freundlich Isotherm Fits to the Data for Lithium Sorption Onto Alluvium from Two Different Intervals of 22PC Within the Zone Tested in the Field

G5.4.5 Apparent Perrhenate Sorption Behavior

It was concluded at the end of Section 5.2 that because the free-water diffusion coefficient of perrhenate is smaller than that of iodide, the only logical explanation for the apparent attenuation of perrhenate with respect to iodide in the alluvium is retardation of the perrhenate in either the flowing or stagnant porosity of the alluvium. The RELAP fits to the breakthrough curves suggest that the latter is more likely. However, regardless of whether the perrhenate retardation occurred in the flowing or stagnant porosity, the apparent sorption behavior is significant because it suggests that the perrhenate interacted with alluvium surfaces in ways (including, perhaps, some reduction of Re(VII) to Re(IV)) that might also occur for pertechnetate. Pertechnetate is assumed to be a nonsorbing species in Yucca Mountain performance assessment calculations, and this result for perrhenate, while not necessarily conclusive, certainly suggests that there may be favorable conditions in the saturated alluvium for at least partial sorption/attenuation of pertechnetate.

The fact that the perrhenate recovery was greater than that of the iodide (Table G-13) by the end of the second cross-hole tracer test suggests that the normalizations of the tracer concentrations may have resulted in an artificially high perrhenate concentration relative to the iodide concentration. If this were the case, the actual perrhenate attenuation would have been even greater than what was deduced from the interpretive analysis of the tracer test (end of Section 5.2). Even if the concentrations of perrhenate were underestimated as a result of normalization errors (considered unlikely), the later peak arrival of the perrhenate relative to the iodide suggests that some sort of weak perrhenate attenuation mechanism was occurring. The high recovery of perrhenate also indicates that the attenuation mechanism was effectively reversible over the time scale of the tracer test.

While the perrhenate attenuation mechanism remains unknown, the tracer test results suggest that pertechnetate could possibly experience more retardation in alluvium than is currently assumed in performance assessment calculations (none), even in nominally oxidizing environments like that at Site 22. However, it would be wise to conduct validative investigations before any firm credit is taken for pertechnetate retardation in the saturated alluvium. Such apparent retardation of pertechnetate has not previously been observed in laboratory experiments conducted under ambient conditions.

G5.4.6 Longitudinal Dispersivity

RELAP estimates of Peclet numbers assuming radial and linear flow were used to estimate the longitudinal dispersivities in the cross-hole tracer tests ($\alpha = r_1/Pe$), and the most extreme values were used for the upper and lower bounds. Longitudinal dispersivity estimates from cross-hole tracer tests generally have considerable uncertainty due to (1) uncertainty in the actual tracer transport distance (the actual flow pathways followed by tracers are unknown); (2) whether the flow field is radial, linear, or some combination; (3) the amount of apparent dispersion caused by nonidealities such as a poorly mixed injection wellbore or density/buoyancy effects; and (4) the amount of apparent dispersion caused by recirculation or the ambient flow field. It is beyond the scope of this report to address in detail the possible effects of each of these uncertainties on the longitudinal dispersivity estimates provided in Table G-20. While the estimation procedure outlined in Section D4.8.6 also applies here, for the cross-hole tests at Site 22 it was not

necessary to “subtract out” apparent dispersion caused by recirculation (Step 4 of Section D4.8.6) because there was no recirculation at Site 22. Also, 18 meters was the only transport distance considered in the dispersivity calculations for Site 22 because significant vertical transport seemed unlikely in the visibly layered alluvium (based on observations of sonic-drilling “cores”). The fact that the 2,5 DFBA injected into the upper interval of 22PA was never detected in the second interval of 22S supports this conceptualization.

G5.4.7 Colloid Transport

The microsphere filtration and detachment rate constants deduced from the first cross-hole tracer test at Site 22 (Table G-17) can potentially be used as estimates of filtration and detachment rate constants for natural colloids that could facilitate the transport of radionuclides strongly adsorbed to colloids. However, it must be kept in mind that the CML microspheres do not have the same physical and chemical properties as natural inorganic colloids (see BSC 2004 [DIRS 170006], Section 6.8). *Saturated Zone Colloid Transport* (BSC 2004 [DIRS 170006], Section 6.8) summarizes laboratory experiments, in which it was shown that CML microspheres transported with similar attenuation through saturated alluvium as natural colloids that were collected from well 19D, suggesting that microsphere filtration and detachment rate constants may be reasonably used for predicting natural colloid transport in saturated alluvium.

Perhaps of greater importance than the microsphere filtration and detachment rate constants derived from the field tests is the fact that the microsphere responses qualitatively indicate that colloid detachment from fracture surfaces is a process that clearly occurs in saturated alluvium. These qualitative results suggest that it is not sufficient to consider only colloid filtration when assessing colloid-facilitated radionuclide transport, but that colloid detachment and its dependence on other variables must also be considered and could possibly dominate the transport behavior of colloids. It is beyond the scope of this report to discuss how the dependence of colloid detachment on other variables should be incorporated into transport models. However, colloid detachment, in general, can be accounted for in models with simple first-order kinetics expressions.

G6. LIMITATIONS, UNCERTAINTIES AND GENERAL REMARKS

The limitations, uncertainties and general remarks regarding the alluvium field tracer test results are essentially identical to those discussed at length in Sections D5 and D6 of Appendix D (for the tracer tests in fractured volcanic tuffs at the C-wells complex). The reader is referred to those sections for detailed discussions that also apply to alluvium field tracer testing.

An additional uncertainty that applies to the alluvium cross-hole tracer tests is the uncertainty associated with the injection masses of the tracers that were used to normalize the tracer concentrations for the interpretive analyses. There was a significant lack of agreement between directly-measured masses and masses deduced from injection concentration measurements that did not occur for the tracer tests at the C wells or for the single-well tracer tests at the ATC and Site 22. This uncertainty introduces additional uncertainty into the transport parameter estimates deduced from cross-hole tracer testing in the alluvium. However, we do not believe that this uncertainty raises doubts about the dual-porosity nature of the alluvium, as the relative shapes of the tracer breakthrough curves and the lithium transport behavior are both consistent with

dual-porosity transport regardless of the uncertainties in the normalizations of the tracer breakthrough curves.

Another uncertainty associated with the alluvium tracer test interpretations is the inherent and unquantifiable uncertainty associated with the conclusion that diffusion time and distance scales are quite small and that the alluvium should therefore behave as a single-porosity transport system over much larger time and distance scales than the tracer tests. The possibility exists that the time and distance scales of the tracer tests may have been too short to observe significant diffusion out of flowing pathways and into relatively extensive layers or blocks of stagnant or near-stagnant alluvium in the flow system. Furthermore, the uncertainties associated with the tracer injection masses (above) make any assessment of larger diffusion time and length scales essentially impossible using the available data from Site 22.

INTENTIONALLY LEFT BLANK

APPENDIX H

**LABORATORY TESTING CONDUCTED TO SUPPORT PLANNED TRACER
TESTING AT THE ALLUVIAL TESTING COMPLEX (ATC)**

H1. ALLUVIUM CATION-EXCHANGE-CAPACITY MEASUREMENTS AND LITHIUM BATCH-SORPTION EXPERIMENTS

Laboratory measurements of lithium-ion sorption onto alluvium material and tracer transport tests in alluvium-packed columns were carried out in parallel with field tracer testing at the Alluvial Testing Complex (ATC). The objectives of the laboratory tests are the same as for the laboratory testing conducted to support C-wells tracer testing in fractured tuffs: (1) to obtain transport parameter estimates that can help constrain interpretations of the field tracer tests, and (2) to obtain laboratory estimates of lithium sorption parameters that can be compared to field-derived sorption parameter estimates. The latter will allow an assessment of the ability to predict field-scale sorption in the alluvium using laboratory-derived sorption parameters, which is important because laboratory-scale sorption parameters must be used for field-scale predictions of radionuclide transport. Detailed documentation of both the batch and column laboratory tests (the remainder of this attachment) is reported by Sullivan (2002 [DIRS 164623]).

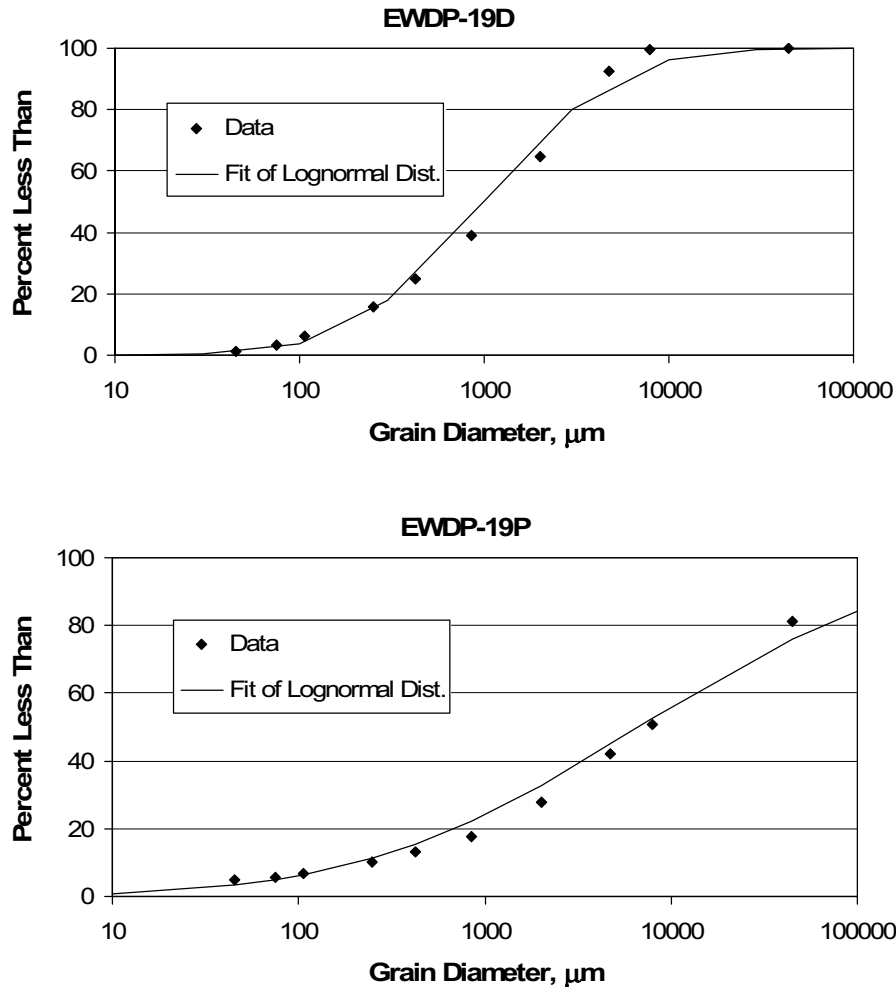
H1.1 ALLUVIUM SAMPLES AND THEIR CHARACTERISTICS

Cation-exchange capacity (CEC) and lithium batch-sorption measurements were conducted on alluvium samples collected from several different depth intervals in wells 19D and 19P. The intervals from which material was collected were (in meters (feet) below land surface) 123 to 125 m (405 to 410 ft), 128 to 130 m (420 to 425 ft), 152 to 154 m (500 to 505 ft), 177 to 178 m (580 to 585 ft), 201 to 203 m (660 to 665 ft), 207 to 209 m (680 to 685 ft), 219 to 221 m (720 to 725 ft), and 238 to 239 m (780 to 785 ft) in 19D, and 125 to 126 m (410 to 415 ft) and 128 to 130 m (420 to 425 ft) in 19P. Particle-size distributions of samples collected from 123 to 125 m (405 to 410 ft) and 128 to 130 m (420 to 425 ft) in 19D, and from 125 to 126 m (405 to 410 ft) and 128 m to 130 m (420 ft to 425 ft) in 19P were determined by a wet-sieve method. Particle-size distributions in all other intervals (all of which were in 19D) were determined by dry sieving. Well 19P was drilled by a reverse-circulation air hammer method, so the high and low ends of the particle size distribution were considered more representative than in the samples from 19D, which was drilled using a rotary bit with water as the lubricant. The rotary bit probably broke up the larger particles, and the water washed out most of the smaller particles from the 19D samples. Figure H-1 shows a size distribution comparison for material from approximately the same depth intervals in wells 19D and 19P.

For the CEC and lithium batch-sorption experiments, measurements were made on material that had been wet- or dry-sieved to a size range between 75 and 2,000 μm , and also on material that was wet or dry-sieved to less than 75 μm in size. Although the size distribution for the 19P material in Figure H-1 indicates that alluvium particles with sizes larger than 2,000 μm comprise a significant fraction of the alluvium mass, the surface area available for sorption is expected to be dominated by smaller particles, so the CEC and sorption experiments focused on material smaller than 2,000 μm . Excluding the larger material could result in overestimation of sorption partition coefficients (K_d values) based on alluvium mass; this potential overestimation was to be evaluated by comparing the laboratory K_d values with field K_d values obtained from cross-hole tracer testing, which unfortunately never occurred (see Appendix G).

The materials from 19P and from the two uppermost intervals in 19D (123 m to 125 m and 128 m to 130 m) were wet-sieved, and all of the remaining material was dry-sieved. Quantitative

minerals abundance analysis using x-ray diffraction (Chipera and Bish 1995 [DIRS 105075]) was conducted on each fraction used for testing (Table H-1). Not surprisingly, the samples sieved to the smaller size range tended to be richer in smectite clays and zeolites, which have higher CECs than the other minerals listed in Table H-1. Specific surface areas of the samples were measured by a single-point Brunauer-Emmet-Teller (BET) nitrogen adsorption/desorption method (Brunauer et al. 1938 [DIRS 156646], pp. 309 to 319). The BET surface areas are listed in Table H-2 for each sample. Table H-2 also lists the lithium and cesium CECs of the samples, which are discussed in Section H1.5.



Source: DTN: LA0201JS831421.001 [DIRS 162613].

NOTE: The mass-weighted particle size distributions above for the two wells are from the same depth interval of 123 m to 130 m (405 ft to 425 ft) below land surface; and the size distributions were determined by dry-sieve analyses.

Figure H-1. Particle Size Distributions of Material in NC-EWDP-19D and NC-EWDP-19P

Table H-1. Mineralogy of Alluvium Samples Used in the Cation-Exchange-Capacity and Lithium Batch-Sorption Experiments Determined by Quantitative X-ray Diffraction

Sample Label	Smectite	Clinoptilolite	Kaolinite	Mica	Tridymite	Cristobalite	Quartz	Feldspar	Calcite	Hematite	Hornblende	Total
19D 405-410 <75 μm	20 \pm 6	10 \pm 1	1 \pm 1	Trace	3 \pm 1	7 \pm 2	14 \pm 1	39 \pm 6	1 \pm 1	1 \pm 1	—	96 \pm 9
19D 405-410 >75 μm	4 \pm 1	7 \pm 1	1 \pm 1	1 \pm 1	5 \pm 1	13 \pm 1	17 \pm 1	53 \pm 8	—	1 \pm 1	—	102 \pm 8
19P 410-415 <75 μm	34 \pm 10	26 \pm 2	1 \pm 1	Trace	3 \pm 1	5 \pm 1	8 \pm 1	28 \pm 5	1 \pm 1	—	Trace	106 \pm 12
19P 410-415 >75 μm	5 \pm 2	7 \pm 1	1 \pm 1	1 \pm 1	4 \pm 1	15 \pm 1	18 \pm 1	49 \pm 7	—	Trace	—	100 \pm 8
19D 420-425 <75 μm	16 \pm 5	8 \pm 1	1 \pm 1	Trace	5 \pm 1	8 \pm 2	13 \pm 1	42 \pm 6	2 \pm 1	1 \pm 1	Trace	96 \pm 8
19D 420-425 >75 μm	6 \pm 2	6 \pm 1	1 \pm 1	Trace	6 \pm 1	16 \pm 1	20 \pm 2	44 \pm 6	1 \pm 1	Trace	—	100 \pm 7
19P 420-425 <75 μm	40 \pm 12	24 \pm 2	1 \pm 1	Trace	2 \pm 1	4 \pm 1	8 \pm 1	24 \pm 4	—	Trace	—	103 \pm 13
19P 420-425 >75 μm	11 \pm 3	6 \pm 1	1 \pm 1	Trace	4 \pm 1	11 \pm 1	22 \pm 2	45 \pm 7	—	1 \pm 1	1 \pm 1	102 \pm 8
19D 500-505 <75 μm	10 \pm 3	10 \pm 1	1 \pm 1	Trace	5 \pm 1	9 \pm 3	16 \pm 1	43 \pm 6	1 \pm 1	1 \pm 1	—	96 \pm 8
19D 500-505 >75 μm	5 \pm 2	6 \pm 1	1 \pm 1	Trace	5 \pm 1	15 \pm 1	20 \pm 2	43 \pm 6	—	Trace	—	95 \pm 7
19D 580-585 <75 μm	7 \pm 2	24 \pm 2	1 \pm 1	Trace	3 \pm 1	7 \pm 2	16 \pm 1	44 \pm 7	1 \pm 1	1 \pm 1	Trace	104 \pm 8
19D 580-585 >75 μm	5 \pm 2	10 \pm 1	1 \pm 1	Trace	4 \pm 1	14 \pm 1	18 \pm 1	45 \pm 7	—	Trace	—	97 \pm 8
19D 660-665 <75 μm	21 \pm 6	24 \pm 2	1 \pm 1	1 \pm 1	2 \pm 1	5 \pm 1	10 \pm 1	36 \pm 6	—	Trace	1 \pm 1	101 \pm 9
19D 660-665 >75 μm	3 \pm 1	10 \pm 1	1 \pm 1	1 \pm 1	4 \pm 1	12 \pm 1	18 \pm 1	49 \pm 7	—	Trace	Trace	98 \pm 7
19D 680-685 <75 μm	12 \pm 4	41 \pm 2	Trace	Trace	3 \pm 1	6 \pm 1	8 \pm 1	29 \pm 5	—	—	1 \pm 1	100 \pm 7
19D 680-685 >75 μm	4 \pm 1	14 \pm 1	1 \pm 1	1 \pm 1	3 \pm 1	14 \pm 1	19 \pm 1	48 \pm 7	—	Trace	—	104 \pm 7

Table H-1. Mineralogy of Alluvium Samples Used in the Cation-Exchange-Capacity and Lithium Batch-Sorption Experiments Determined by Quantitative X-ray Diffraction (Continued)

Sample Label	Smectite	Clinoptilolite	Kaolinite	Mica	Tridymite	Cristobalite	Quartz	Feldspar	Calcite	Hematite	Hornblende	Total
19D 725-730 <75 μm	17 \pm 5	42 \pm 3	1 \pm 1	Trace	2 \pm 1	5 \pm 1	11 \pm 1	21 \pm 4	Trace	—	Trace	99 \pm 7
19D 725-730 >75 μm	5 \pm 2	15 \pm 1	1 \pm 1	Trace	3 \pm 1	14 \pm 1	24 \pm 2	41 \pm 6	—	Trace	—	103 \pm 7
19D 780-785 <75 μm	16 \pm 5	31 \pm 2	Trace	Trace	2 \pm 1	8 \pm 2	12 \pm 1	34 \pm 6	1 \pm 1	—	Trace	104 \pm 8
19D 780-785 >75 μm	6 \pm 2	11 \pm 1	Trace	—	3 \pm 1	14 \pm 1	21 \pm 2	47 \pm 7	—	Trace	Trace	102 \pm 8

Source: DTN: LA0201JS831321.001 [DIRS 162623].

NOTE: Bold entries denote material used in column experiments. Mineral abundances are in wt %. Errors are 2-sigma values. — = not detected; Trace = trace amount at less than 0.5 wt %. Materials from NC-EWDP-19P and the two uppermost intervals in NC-EWDP-19D (123 to 125 m [405 to 410 ft] and 128 to 130 m [420 to 425 ft]) were wet-sieved; all other materials were dry-sieved. Sample labels include the interval in feet because the data were collected using English units.

Table H-2. Surface Areas and Lithium and Cesium Cation-Exchange-Capacities (CEC) of Alluvium Samples Used in the Lithium Batch-Sorption Experiments

Interval ^a (Well, ft below land surface, size)	BET Surface Area ^b (m ² /g)	Li CEC (meq/kg)	Cs CEC (meq/kg)
19D, 405-410, < 75 μm	15.96	183	258
19D, 405-410, > 75 μm	5.34	70	99
19P, 410-415, < 75 μm	NM	360	559
19P, 410-415, > 75 μm	NM	126	141
19D, 420-425, < 75 μm	9.80	175	231
19D, 420-425, > 75 μm	5.64	89	119
19P, 420-425, < 75 μm	NM	395	667
19P, 420-425, > 75 μm	8.67	171	186
19D, 500-505, < 75 μm	10.15	125	171
19D, 500-505, > 75 μm	6.17	137	229
19D, 580-585, < 75 μm	NM	204	285
19D, 580-585, > 75 μm	5.17	132	279
19D, 660-665, < 75 μm	NM	303	130 ^c
19D, 660-665, > 75 μm	5.16	119	368
19D, 680-685, < 75 μm	11.16	257	663
19D, 680-685, > 75 μm	3.99	118	439
19D, 720-725, < 75 μm	NM	424	620
19D, 720-725, > 75 μm	5.66	114	433
19D, 780-785, < 75 μm	NM	237	131 ^c
19D, 780-785, > 75 μm	4.43	78	366

DTNs: LA0201JS831421.002 [DIRS 162625] (BET data); LA0201JS831341.001 [DIRS 162627] (CEC data).

NOTE: Bold denotes material used in column experiments. NM: not measured, generally because of insufficient material quantity. Materials from NC-EWDP-19P and the two uppermost intervals in NC-EWDP-19D (123 to 125 m [405 to 410 ft] and 128 to 130 m [420 to 425 ft]) were wet-sieved; all other materials were dry-sieved.

^a The interval is listed in feet because the data were collected using English units.

^b Surface areas were determined using the nitrogen BET technique.

^c Suspected erroneous measurements – Cs CEC should be greater than Li CEC.

BET= Brunauer-Emmett-Teller (surface area measurement); CEC=cation-exchange-capacity.

H1.2 CATION-EXCHANGE-CAPACITY MEASUREMENTS

CECs of the alluvium from the different depth intervals in well 19D were measured using a three-step process of saturating the alluvium surface sites with lithium ion, modified from that of Ming and Dixon (1987 [DIRS 156842]). Half-gram samples of alluvium were placed in contact with approximately 30 mL of 1 M LiBr solution prepared in deionized water. The alluvium-solution mixture was shaken for at least 1 hr, centrifuged, and the supernatant was decanted off into a collection container. This treatment was repeated two more times, with the supernatant from each step being combined with that from the previous steps. The final solution (approximately 90 mL) was analyzed for Na⁺, Ca⁺⁺, K⁺, and Mg⁺⁺ using inductively coupled plasma-atomic emission spectrometry (ICP-AES) to determine the total number of equivalents of cations that lithium had displaced from the alluvium surfaces. This total number of equivalents divided by the mass of the alluvium sample is the CEC of the alluvium, expressed as meq/kg.

It is well known that CECs of materials are dependent on the cation used to saturate the material surfaces (Anghel et al. 2002 [DIRS 164635], Section 3.1, pp. 821 to 822). The Cs^+ ion is often used to obtain a measure of the “total” CEC of a material because Cs^+ sorbs very strongly to mineral surfaces and will displace most exchangeable cations encountered in nature. To obtain an estimate of the Cs^+ -exchangeable CEC, the above procedure was repeated on each of the half-gram alluvium samples that had been subjected to LiBr solution treatments using 1 M CsCl as the saturating solution. However, the CEC determined from the lithium saturation steps was the value used in subsequent modeling of the batch-sorption and column experiments (Section H2) because only cations displaced by lithium are of practical interest when lithium is the sorbing species.

H1.3 BATCH-SORPTION EXPERIMENTS

Lithium batch-sorption experiments were conducted on each of the sieved alluvium samples. Duplicate measurements were conducted at starting lithium concentrations of approximately 1, 3, 10, 30, 100, and 300 mg/L Li^+ for each material to obtain a sorption isotherm over a 2.5-order-of-magnitude range of concentrations. Starting solutions were prepared by dissolving a known mass of LiBr in a known volume of 19D well water and then diluting by weight with well water to the desired starting concentrations. In all of the batch tests, 20 mL of lithium solution was placed in contact with approximately 5 g of alluvium material in 50-mL polycarbonate Oak Ridge centrifuge tubes that were shaken for 48 hr on an orbital shaker. Separate control samples (lithium-spiked solutions in centrifuge tubes without any alluvium material) and blanks (nonspiked well water in contact with alluvium) were processed in parallel with the tubes containing both lithium and alluvium. The controls were used to verify that lithium sorption to tube walls was insignificant, and the blanks were used to measure any lithium background that might be leached out of the alluvium samples. After shaking, the tubes were centrifuged at 30,000 $\times g$ for 1 hr, and then an aliquot of supernatant was pipetted off for cation and bromide analyses. Cations (lithium, sodium, potassium, calcium, and magnesium) were analyzed by inductively coupled ICP-AES, and bromide (nonsorbing tracer) was analyzed by liquid chromatography with a conductivity detector.

The starting lithium concentration for each measurement was determined from both the corresponding bromide and lithium concentrations in the control samples. In general, lithium concentrations measured in the control samples were in good agreement with those determined from the bromide measurements, indicating that lithium sorption to centrifuge tube walls was negligible. The mass of lithium sorbed per unit mass of alluvium material was determined from

$$S = \frac{V(C_0 - C)}{M} \quad (\text{Eq. H-1})$$

where

S = lithium mass sorbed per unit mass of alluvium, mg/g

V = volume of solution in contact with alluvium, L

M = mass of alluvium in contact with solution, g

C_0 = initial concentration of lithium in solution prior to sorption, mg/L

C = final concentration of lithium in solution after sorption, mg/L.

H1.4 INTERPRETATION OF BATCH-SORPTION EXPERIMENTS

It became apparent very early in the batch-sorption experiments that only two cations, Na^+ and Ca^{++} , exchanged significantly with Li^+ . K^+ was exchanged to a minor degree, but the amount was so small relative to Na^+ and Ca^{++} that it was considered reasonable to lump the K^+ with the Na^+ as a generic “monovalent cation.” Thus, a simplified three-component cation-exchange model analogous to the three-component exchange model used in the MULTRAN V 1.0 code (STN: 10666-1.0-00 [DIRS 159068]) (Equations E-11 through E-14 in Section E3.1.3) was used to interpret the batch experiments.

A simple FORTRAN program called EQUIL_FIT V 1.0 (STN: 10668-1.0-00 [DIRS 159064]) was developed to obtain the best simultaneous fit to the Li^+ , Na^+ , and Ca^{++} data obtained in the batch-sorption experiments using Q_1 and Q_2 from Equations E-11 and E-12 as adjustable parameters. The CEC was set equal to the measured lithium CEC of the alluvium samples. The fits were optimized by minimizing the sum of squares of the differences between the logarithms of the model-predicted concentrations and the experimental concentrations. Logarithms were used in the optimization algorithm so that the fits would not be biased toward the data obtained at the highest lithium concentrations.

H1.5 RESULTS OF CATION-EXCHANGE-CAPACITY MEASUREMENTS

The lithium and cesium CECs of the materials from the sampled alluvium intervals in wells 19D and 19P are listed in Table H-2. Only the lithium CEC results were used to interpret the lithium batch-sorption and column transport tests (Section H2) because only cations displaced by lithium are of practical interest in these experiments. It is apparent that the smaller-size fraction material generally had a larger CEC value than the larger-size fraction material from each interval that was tested. Also, the wet-sieved 75- μm to 2,000- μm material from the two uppermost intervals in 19D had relatively low CECs compared to the other samples, presumably because the wet-sieving procedure removed many of the clays and zeolite minerals that have high CEC values.

H1.6 RESULTS OF BATCH-SORPTION EXPERIMENTS

The Q_1 and Q_2 values yielding the best simultaneous fits to the Li^+ , ($\text{Na}^+ + \text{K}^+$), and Ca^{++} data obtained in the lithium batch-sorption experiments are listed in Table H-3 along with the lithium CEC values for each alluvium material tested. Two sets of Q_1 and Q_2 values are listed for each material: (1) one obtained using a direct measurement of the starting lithium concentration as the initial lithium concentration in each experiment and (2) one obtained by using a bromide concentration measurement to determine the starting lithium concentration (the lithium was introduced as LiBr). The differences between these two sets of values are sometimes quite large for a given alluvium interval. These differences reflect the uncertainty in the Q_1 and Q_2 values due to analytical errors in tracer concentration measurements, and they also reflect the relative insensitivity of the fits to the Q values. Table H-3 also lists the Freundlich isotherm parameters (Equation E-2, Section E1.2) that yielded the best fits to the lithium sorption data. Larger values of the K_F parameter tend to reflect greater lithium sorption.

Table H-3. Cation Exchange Coefficients (CEC) and Freundlich Isotherm Parameters Resulting in Best Fits to the Li⁺, Na⁺, and Ca⁺⁺ Data from the Lithium Batch-Sorption Experiments for Alluvium Material

Interval ^a (well, ft below land surface, size)	Li CEC (meq/ kg)	Li as Starting Conc.		Br as Starting Conc.		Li as Starting Conc.		Br as Starting Conc.	
		Q ₁	Q ₂ (L ² /kg ²)	Q ₁	Q ₂ (L ² /kg ²)	K _F (mL/μg) ⁿ (μg/g)	n	K _F (mL/μg) ⁿ (μg/g)	n
19D, 405-410, < 75 μm	183	0.06	0.22	0.06	0.22	0.58	0.82	0.41	0.78
19D, 405-410, > 75 μm	70	0.07	0.03	0.06	0.02	0.35	0.85	0.26	0.82
19P, 410-415, < 75 μm	360	0.13	0.004	0.22	0.003	1.48	0.86	0.82	0.81
19P, 410-415, > 75 μm	126	0.11	0.003	0.17	0.003	0.47	0.84	0.26	0.77
19D, 420-425, < 75 μm	175	0.05	0.15	0.04	0.09	0.75	0.89	0.31	0.78
19D, 420-425, > 75 μm	89	0.05	0.07	0.04	0.04	0.58	0.94	0.23	0.84
19P, 420-425, < 75 μm	395	0.04	0.5	0.04	0.5	1.25	0.84	1.08	0.82
19P, 420-425, > 75 μm	171	0.05	0.01	0.07	0.002	0.77	0.90	0.38	0.82
19D, 500-505, < 75 μm	125	0.07	0.03	0.06	0.02	0.44	0.79	0.55	0.85
19D, 500-505, > 75 μm	137	0.05	0.03	0.04	0.012	0.43	0.83	0.20	0.78
19D, 580-585, < 75 μm	204	0.07	0.63	0.06	0.49	0.32	0.71	0.56	0.78
19D, 580-585, > 75 μm	132	0.07	0.09	0.06	0.06	0.05	0.55	0.13	0.66
19D, 660-665, < 75 μm	303	0.28	0.002	0.24	0.002	0.47	0.74	0.74	0.80
19D, 660-665, > 75 μm ^b	119	0.13	0.09	0.13	0.05	3.67	1.03	2.99	1.01
19D, 680-685, < 75 μm	257	0.16	0.1	0.14	0.04	1.31	0.80	1.10	0.77
19D, 680-685, > 75 μm	118	0.17	0.05	0.16	0.03	0.64	0.78	0.46	0.74
19D, 720-725, < 75 μm	424	0.13	0.011	0.14	0.009	1.25	0.78	1.10	0.77
19D, 720-725, > 75 μm	114	0.21	0.017	0.23	0.01	0.67	0.78	0.48	0.73
19D, 780-785, < 75 μm	237	0.09	0.27	0.09	0.27	0.71	0.77	0.50	0.73
19D, 780-785, > 75 μm	78	0.26	0.03	0.26	0.013	0.52	0.75	0.38	0.74

Source: DTN: LA0201JS831341.001 [DIRS 162627] (CEC values).

Output DTN: LA0303PR831341.002 (sorption parameters).

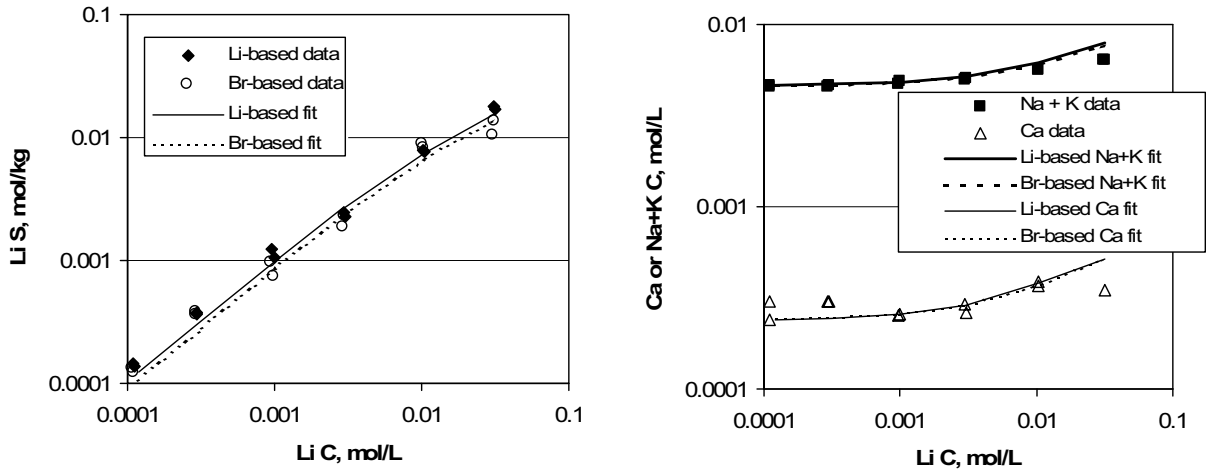
NOTE: Bold denotes material used in column experiments. Materials from NC-EWDP-19P and the two uppermost intervals in NC-EWDP-19D (123 to 125 m [405 to 410 ft] and 128 to 130 m [420 to 425 ft]) were wet-sieved; all other materials were dry-sieved. Estimates of the uncertainties in the parameter values listed in this table were not rigorously obtained because these uncertainties are not critical for Performance Assessment calculations. Values represent best estimates only. Q₁ is dimensionless.

^a The interval is given in feet because the data were collected using English units.

^b The sorption parameters derived for this alluvium material are suspect because there were very few data points to analyze.

CEC=cation-exchange-capacity.

Figures H-2 and H-3 show the best fits to the Li⁺, (Na⁺ + K⁺), and Ca⁺⁺ data obtained for the wet-sieved 75- to 2,000-μm material from the two uppermost intervals in NC-EWDP-19D (123 m to 125 m [405 to 410 ft] and 128 to 130 m [420 to 425 ft], respectively). These two materials were combined in a 50:50 mass ratio and used to pack the columns described in Section H2. The data and fits to the data for both the lithium-based starting concentrations and the bromide-based starting concentrations are shown in these figures.

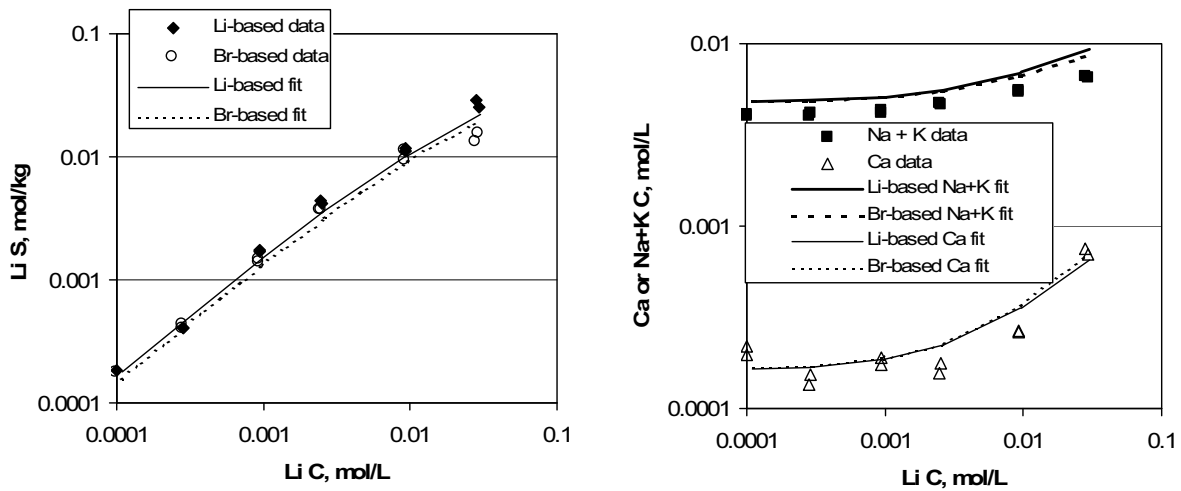


Source: DTN: LA0302JS831341.001 [DIRS 162628] (data).

Output DTN: LA0303PR831361.002 (model results).

NOTE: The alluvium material is from a depth below the land surface of 123 to 125 m (405 to 410 ft) with a size distribution of 75 to 2,000 μm ; parameters yielding the fits are listed in Table H-3.

Figure H-2. Best Fits of the Three-Component Cation-Exchange Model to the Lithium Sorption Isotherm (left) and the ($\text{Na}^+ + \text{K}^+$) and Ca^{++} Concentration Data (right) for Alluvium Material from NC-EWDP-19D at 123 to 125 m (405 to 410 ft)



Source: DTN: LA0302JS831341.001 [DIRS 162628] (data).

Output DTN: LA0303PR831341.002 (model results).

NOTE: The alluvium material is from a depth below the land surface of 128 to 130 m (420 to 425 ft) with a size distribution of 75 to 2,000 μm ; and parameters yielding the fits are listed in Table H-3.

Figure H-3. Best Fits of the Three-Component Cation-Exchange Model to the Lithium Sorption Isotherm (Left) and the ($\text{Na}^+ + \text{K}^+$) and Ca^{++} Concentration Data (Right) for Alluvium Material from NC-EWDP-19D at 128 to 130 m (420 to 425 ft)

H2. TRANSPORT TESTS IN ALLUVIUM-PACKED COLUMNS

This section presents the results and interpretations of several column transport experiments using groundwater and alluvium obtained from the site of the ATC well 19D (Figure 6.1-6). These experiments involved injecting lithium bromide as pulses at three different concentrations spanning the range of concentrations expected in the field. The multicomponent numerical transport model, MULTRAN V 1.0 (STN: 10666-1.0-00 [DIRS 159068]) (see Section E3.2.2), was used to describe lithium transport through the columns. Companion batch lithium sorption and CEC measurements are discussed in Section H1.

H2.1 MATERIALS AND METHODS

All experiments were conducted using groundwater batches collected from well 19D in June 2000 or November 2000. The batches had slightly different chemistries because they were collected from different depth intervals (Table H-4). Batch 1 was used for all experiments except the column experiments with the intermediate LiBr injection concentration. Both waters are essentially sodium-bicarbonate waters that are nearly saturated with respect to silica and with a pH greater than 8. The higher pH of the Batch 1 water relative to the Batch 2 water reflects the higher pHs encountered in the deeper zones in well 19D (Batch 2 water was obtained from only the two shallowest zones in 19D). The groundwater was filter-sterilized using a 0.2- μ m filter before use.

The alluvium used in the experiments was obtained from well 19D at the depth intervals of 123 to 125 m (405 to 410 ft) and 128 to 130 m (420 to 425 ft) below ground surface, approximately 15 to 23 m (50 to 75 ft) below the water table. Cuttings samples were wet-sieved (using 19D well water) in the laboratory, and the size range between 75 μ m and 2,000 μ m was retained for testing. Material from the two intervals was combined in a 50:50 mass ratio for the column experiments because there was not enough material from the individual intervals to pack the columns. Table H-1 gives the bulk mineralogy of the alluvium from the two intervals (in bold) as determined by quantitative minerals abundance analysis using x-ray diffraction (Chipera and Bish 1995 [DIRS 105075]). Table H-2 lists the surface area of the samples (again, in bold) determined by a single-point BET nitrogen adsorption/desorption method (Brunauer et al. 1938 [DIRS 156646]).

Table H-4. Major Ion Chemistry of NC-EWDP-19D Water Used in the Experiments

Species	Batch 1 ^a (mg/L)	Batch 2 ^b (mg/L)
Ca ⁺⁺	2.2	7.5
Na ⁺	118	75.5
K ⁺	5.2	4.1
Mg ⁺⁺	1.13	0.65
Li ⁺	0.15	0.09
Si	52.5	27.1
HCO ₃ ⁻	193	168
CO ₃ ²⁻	43.8	0
SO ₄ ²⁻	25.9	23.0
Cl ⁻	5.7	5.6
F ⁻	2.1	1.8
pH	9.2	8.1

Source: DTN: LA0303PR831232.001 [DIRS 162781].

^aBatch 1 was collected in June 2000 from an open borehole.

^bBatch 2 was collected from two isolated screened intervals in the upper 46 m (150 ft) of the saturated zone. This batch was used only for the 0.006 M LiBr column experiments.

Column experiments were conducted in duplicate using separate 30-cm-long by 2.5-cm-diameter glass columns equipped with polytetrafluoroethylene end fittings, including a 20- μ m end frit and PTFE tubing. Each column was presoaked in deionized water to remove any residual ions. The columns were packed dry with a 50:50 mass ratio of the wet-sieved alluvium from the two intervals used in batch-sorption and CEC testing. The columns then were saturated by flushing with deaerated groundwater until air bubbles were no longer visible. They also were packed in ice for 8 hr to promote oxygen and nitrogen dissolution in the water. The saturated versus dry weights of the columns indicated a final porosity of about 40% with a pore volume of about 60 mL in each column.

Three transport experiments were conducted in each column at a flow rate of approximately 10 mL/hr with the two columns run in parallel. Each experiment involved the injection of approximately one pore volume of a tracer solution containing LiBr and 2 mg/L of an fluorobenzoate (FBA)(either pentafluorobenzoate or 2,4-difluorobenzoate) dissolved in 19D groundwater. The experiments differed in the concentrations of LiBr in the injection pulses. The first duplicate set of experiments was conducted using an injection concentration of 0.0275 M LiBr (190 mg/L Li⁺), the second set had a concentration of 0.006 M LiBr (42 mg/L Li⁺), and the third set had a concentration of 0.0013 M LiBr (9 mg/L Li⁺). These concentrations were selected so that Li⁺ dominated the cation equivalents in solution in the first case (91% of total cation equivalents), accounted for about half of the cation equivalents in the second case (61%), and were a relatively minor fraction of the total cation equivalents in the third case (24%). These three situations represent a range of conditions that will likely occur during field testing, with relatively high concentrations present near the injection well immediately after injection, and concentrations decreasing as the tracer pulse advects and disperses through the flow system.

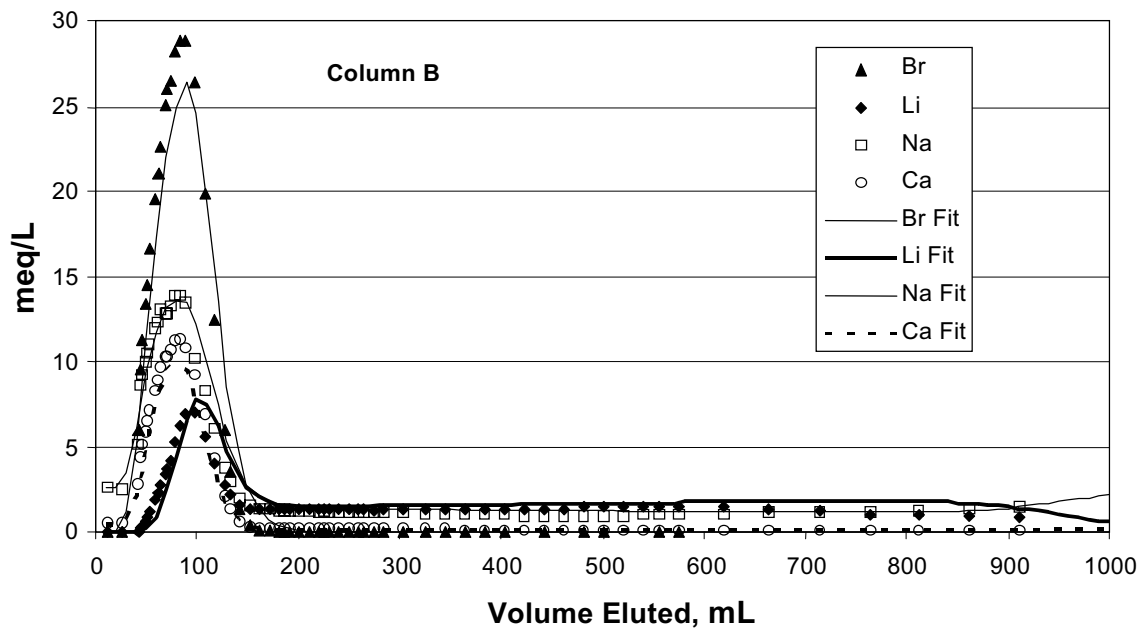
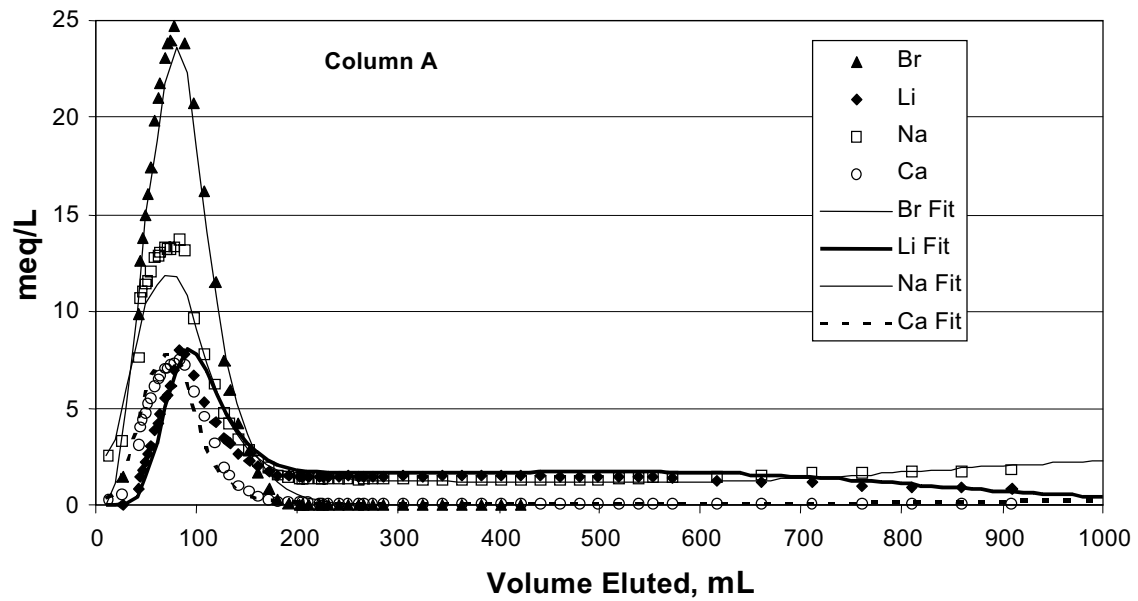
The tracer solutions were injected simultaneously into the two columns using a syringe pump (Harvard Systems). After one pore volume of tracer was injected, tracer-free groundwater was injected at 10 mL/hr using a piston pump (SciLog). Column effluent samples were collected using an automatic fraction collector (Gilson) set up to collect samples simultaneously from both columns in pre-weighed test tubes at pre-set time intervals. The samples were analyzed for the same cations (lithium, sodium, K, calcium, and magnesium) that were analyzed in the batch-sorption experiments using ICP-AES. Bromide and the FBAs were analyzed by liquid chromatography, with the latter being quantified by UV absorption. Samples were diluted as necessary for the tracer analyses.

H2.2 INTERPRETIVE MODELING APPROACH

The column transport experiments were simulated using the MULTRAN V 1.0 (STN: 10666-1.0-00 [DIRS 159068]) multicomponent ion-exchange transport model (Section E3.2.2). The columns were modeled as single-porosity systems because the FBAs and bromide had essentially identical normalized concentration responses in all experiments, indicative of a system that lacks secondary (stagnant) storage porosity (see Section G2). The mean residence time and Peclet number (dispersivity) were adjusted to achieve a qualitative fit to the bromide responses in each experiment. The lithium responses were then fitted by adjusting the CECs, Q_1 and Q_2 (see Section H1.3) while setting the CEC of the alluvium equal to the average CEC of the two materials used to pack the columns (80 meq/kg; see Table H-2).

H2.3 EXPERIMENTAL RESULTS AND ANALYSES

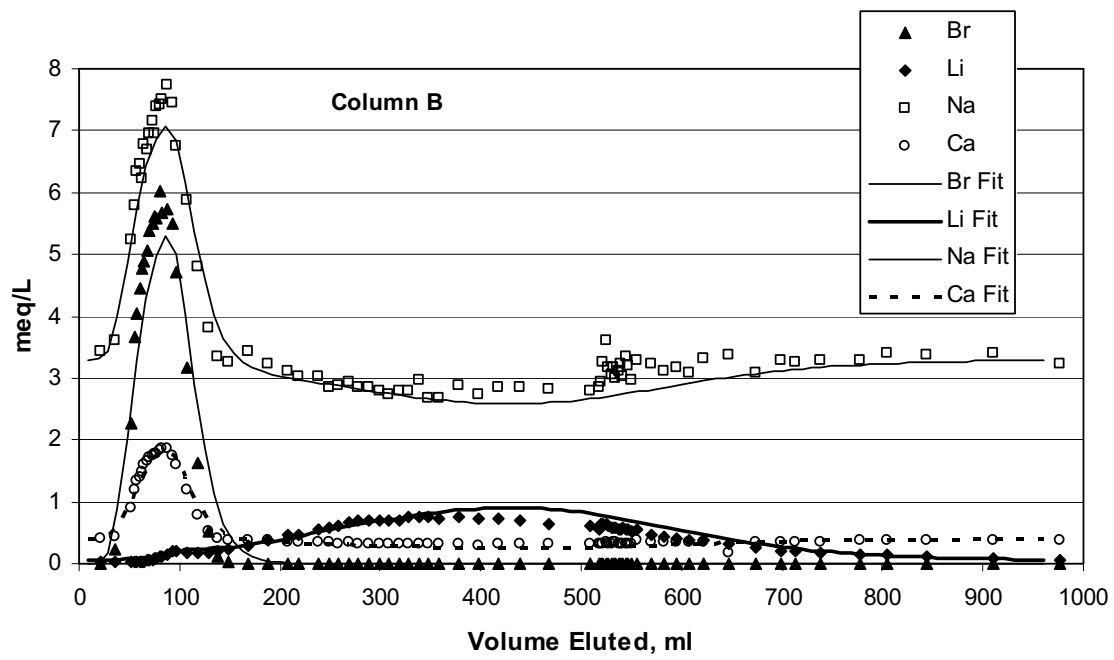
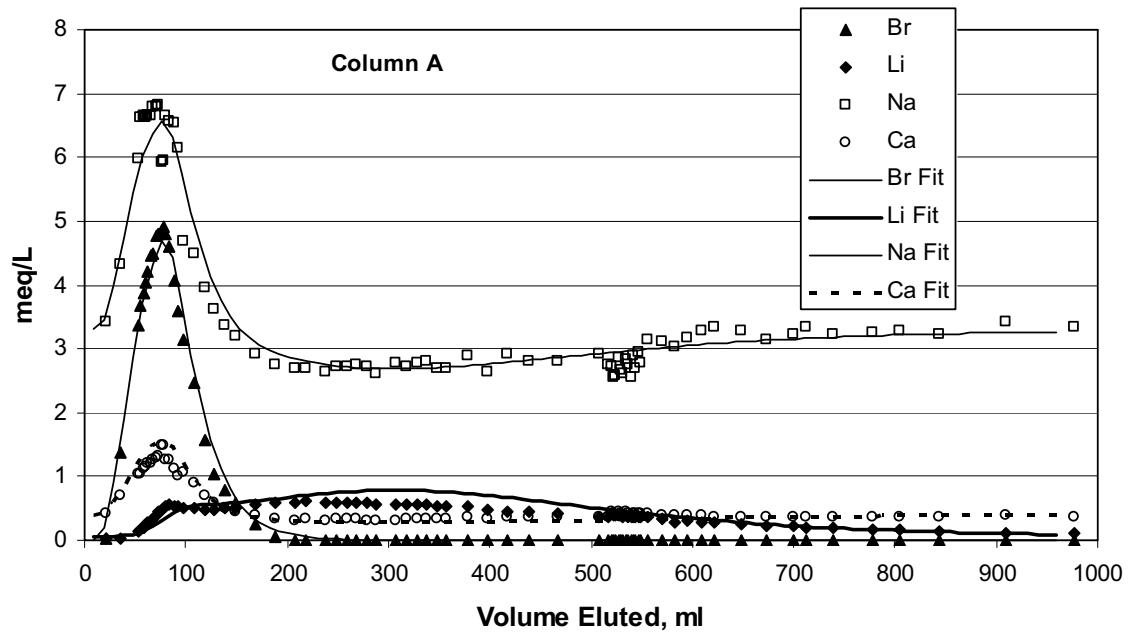
The breakthrough curves of Br^- , Li^+ , Na^+ , and Ca^{++} , expressed as meq/L versus volume eluted through the columns, are shown in Figures H-4, H-5, and H-6, for the experiments conducted at each of the three LiBr injection concentrations, respectively. These figures also show the MULTRAN V 1.0 (STN: 10666-1.0-00 [DIRS 159068]) fits to each data set. The FBA data are not shown in these figures because these data were essentially identical to the bromide data when normalized to the injection concentration. However, the FBA concentrations were accounted for in the MULTRAN modeling. A negligible concentration shift of the tracers after a flow interruption in test 2 (Figure H-5, at approximately 500 mL eluted) verified the lack of diffusive mass transfer into secondary storage porosity in the system that was suggested by the identical normalized concentration responses of the bromide and FBA. The apparent slight perturbation in Na^+ concentrations after the flow interruption, with column A showing a minor decrease and column B showing a minor increase, is unexplained. Analyses of additional cations and anions would have been necessary to better understand this phenomenon, although it ultimately has negligible impact on the test interpretations.



Source: DTN: LA0201JS831361.001 [DIRS 162629] (data).

Output DTN: LA0303PR831361.002 (model results).

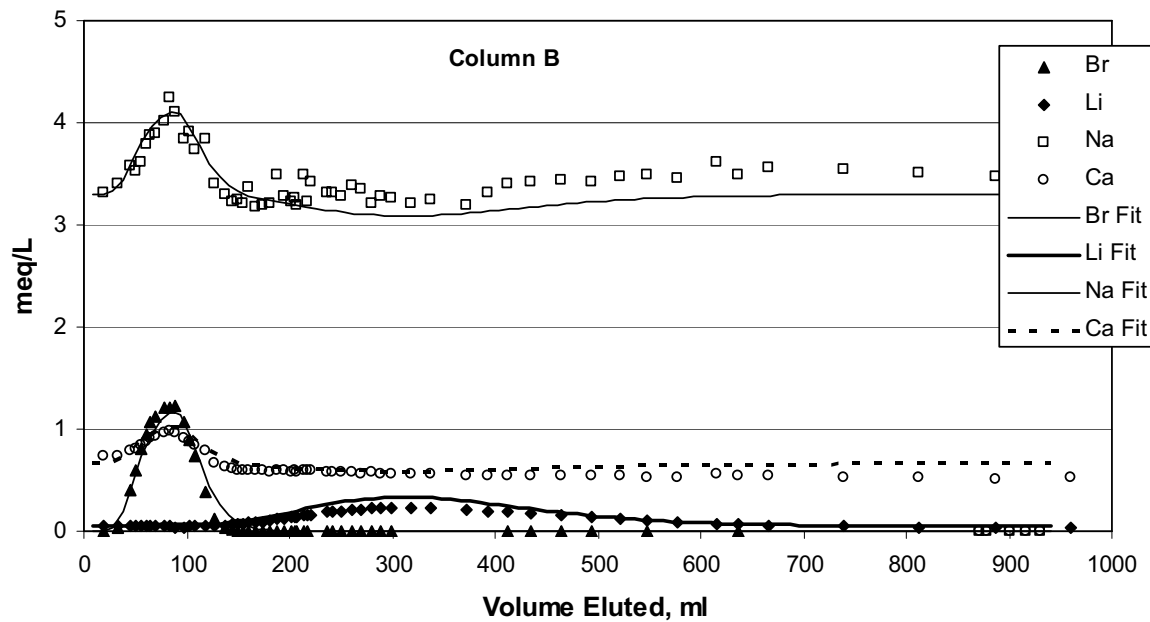
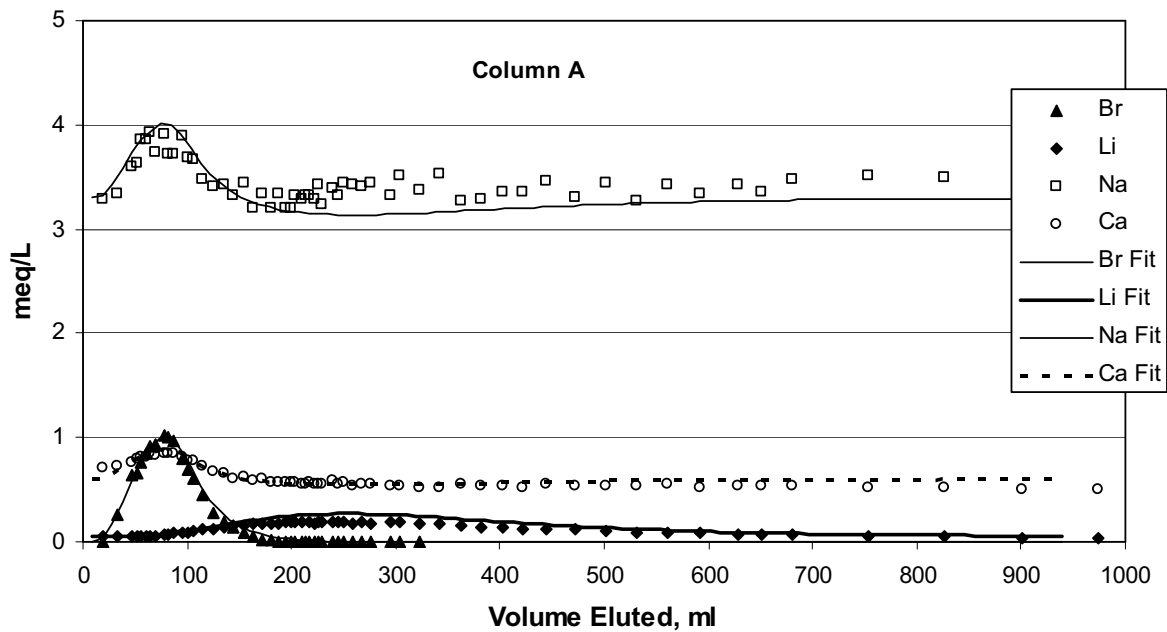
Figure H-4. Column Data and MULTRAN Fits for Experiments with a LiBr Injection Concentration of 0.0275 M



Source: DTN: LA0201JS831361.007 [DIRS 162630] (data).

Output DTN: LA0303PR831361.002 (model results).

Figure H-5. Column Data and MULTRAN Fits for Experiments with a LiBr Injection Concentration of 0.006 M



Source: DTN: LA0201JS831361.005 [DIRS 166205] (data).

Output DTN: LA0303PR831361.002 (model results).

Figure H-6. Column Data and MULTRAN Fits for Experiments with a LiBr Injection Concentration of 0.0013 M

The MULTRAN V 1.0 (STN: 10666-1.0-00 [DIRS 159068]) model parameters resulting in the best fits shown in Figures H-4, H-5, and H-6 are listed in Table H-5. As with the interpretation

of the batch-sorption experiments, the lithium CEC was fixed to 0.08 eq/kg for all of the experiments, and Q_1 and Q_2 were adjusted to fit the data. The dispersivity in the column was also adjusted to obtain a reasonable fit to the bromide response curve. The fits were found to be quite sensitive to the background concentrations assumed in the simulations, which were variable in the experiments because the columns were re-used to conduct subsequent experiments, and residual concentrations of the cations varied somewhat. As Tables H-3 and H-5 indicate, the best-fitting ion-exchange constants for lithium exchange with both sodium/potassium (Q_1) and calcium (Q_2) were generally higher in the column experiments than in the batch experiments. The use in MULTRAN of the Q_1 and Q_2 values obtained from the batch experiments consistently over predicted lithium responses and under predicted sodium and calcium responses than were observed.

Table H-5. MULTRAN Model Parameters Associated with the Fits to the Column Transport Data

Experiment	Dispersivity (cm)	Q_1	Q_2 (L ² /kg ²)
0.0275 M LiBr, Column A (Figure H-4)	5.4	0.06	0.12
0.0275 M LiBr, Column B (Figure H-4)	1.8	0.045	0.22
0.006 M LiBr, Column A (Figure H-5)	5.4	0.104	0.083
0.006 M LiBr, Column B (Figure H-5)	1.8	0.104	0.083
0.0013 M LiBr, Column A (Figure H-6)	5.4	0.104	0.083
0.0013 M LiBr, Column B (Figure H-6)	1.8	0.104	0.083

Output DTNs: LA0303PR831361.002; LA0303PR831231.005.

NOTE: The model parameters above do not include mean residence times. The column transport data are shown in Figures H-4, H-5, and H-6. The lithium cation-exchange-capacity value was assumed to be 0.08 eq/kg for all simulations. Estimates of the uncertainties in the parameter values listed in this table were not rigorously obtained because these uncertainties are not critical for Performance Assessment calculations. Values represent best estimates only. Q_1 is dimensionless.

The Q_1 and Q_2 values obtained for each experiment within a given column or for the different columns at a given LiBr injection concentration were in reasonably good agreement, especially after the first set of tests (Table H-5). In principle, these values should not change from column to column or from experiment to experiment because the columns contained exactly the same material. The MULTRAN V 1.0 (STN: 10666-1.0-00; [DIRS 159068]) fits were not obtained using a least-squares minimization or optimization algorithm, but rather they were obtained by manually adjusting parameters to obtain a good visual fit to the data.

H2.4 DISCUSSION

Examination of the MULTRAN V 1.0 (STN: 10666-1.0-00 [DIRS 159068]) model fits shown in Figures H-4, H-5, and H-6 indicates that the model describes well the transport behavior of the cations through the columns, even though the response curves varied significantly for the three different LiBr injection concentrations. Furthermore, the model parameters did not have to be changed significantly for the different injection concentrations to achieve good fits. This result suggests that the model accurately represented the transport processes occurring in the columns.

The partial nonsorbing transport behavior of lithium ion at high injection concentrations (e.g., Figure H-4) is a consequence of both the limited lithium sorption capacity of the alluvium and the requirement that local charge balance must be maintained throughout the columns.

When the concentration of lithium ion was a significant fraction of the total cation concentrations in the injection solution (in eq/L), some of the lithium was forced to move without sorbing through the columns with the nonsorbing anion tracers to maintain charge balance. This phenomenon occurred because the CEC and the cation exchange constants (Q_1 and Q_2) of the alluvium were not so large that all of the injected lithium could be exchanged for sodium and calcium ions to balance the anion tracer charge. The fraction of early arriving lithium in the column tests decreased as the LiBr injection concentration decreased; and when the Li^+ concentration was only 24% of the total cation eq/L, the lithium was essentially completely retarded (Figure H-6). The lithium responses at the lowest LiBr injection concentration were the only responses that could be adequately modeled when a simple linear partition coefficient, (K_d = mass sorbed per unit mass of solid/solution concentration) was assumed (fits not shown). Such a model assumes that lithium transport is independent of all other species in solution, which is clearly inaccurate at higher injection concentrations for which it becomes a significant fraction of the total cation equivalents in solution.

H2.5 IMPLICATIONS OF COLUMN EXPERIMENT RESULTS FOR FIELD TESTING

The lithium transport behavior observed in the column experiments and depicted in Figures H-4 through H-6 has important implications for potential cross-hole field tracer testing in the alluvium south of Yucca Mountain. It is common practice to inject large masses and, hence, high concentrations of sorbing tracers in field tests because the combination of sorption, dispersion, and dilution can result in very low concentrations at the production well. Large tracer injection masses and concentrations would, therefore, be used in cross-hole field tests to ensure adequate detection and quantification of lithium concentrations at the production well. This strategy means that lithium concentrations could tend to remain quite high for some time (and distance) near the injection well, which could result in some of the lithium moving without sorbing through the flow system until the tracer “slug” became dispersed and diluted.

There are two possible extremes of sorbing tracer transport in a cross-hole field tracer test that could result in the same observed concentrations at the production well. The first is that the injected tracer slug could disperse and dilute rapidly near the injection well, resulting in a low average concentration throughout the flow system. The second is that the tracer slug could remain relatively concentrated as it moves to the production well and then be diluted in the well bore as a result of mixing with tracer-free water that is also being drawn into the well. There is no way to distinguish between these two extremes, or any intermediate situation, when nonsorbing tracer responses are analyzed. However, the results and interpretations of the column experiments in this scientific analysis report suggest that the shape of a lithium breakthrough curve in a cross-hole field tracer test may provide a good indication of whether dilution is occurring early or late in the flow system. If dilution occurs early, a lithium response curve similar to those in Figure H-6 can be expected. However, if dilution occurs late, the lithium response curve may look more like those of Figures H-4 or H-5, where there is some asymmetry and nonsorbing transport, even though measured concentrations are quite low because of dilution in the production wellbore. Knowing whether dilution occurs early or late is important when making comparisons between laboratory and field transport behavior. If concentrations remain high in the field test (late dilution), then the lithium may appear to be transporting with less sorption than would be inferred from laboratory batch-sorption measurements, even though the

field transport behavior is consistent with the laboratory data if the existence of high concentrations is recognized.

The ability to distinguish between early and late dilution could help refine or constrain estimates of effective flow porosities derived from cross-hole tracer tests. When nonsorbing tracer responses are analyzed, flow porosity estimates are typically based on first, mean, or peak arrival times of nonsorbing tracers. Under ideal radial flow conditions in a two-dimensional aquifer, Equation D-6 (introduced in Section D4.8.5) can be used to estimate effective flow porosity. Equation D-6 (which is a rearrangement of equation 6 of Guimera and Carrera 2000 [DIRS 156830]) and the definitions of its variables are repeated here for convenience:

$$\eta = \frac{Q\tau}{\pi L^2 T} \quad (\text{Eq. D-6})$$

where

η = flow porosity

Q = production flow rate, m³/hr

τ = mean residence time of a nonsorbing tracer, hr

L = distance between wells, m

T = formation thickness (assumed to be well screen length), m.

If flow heterogeneity exists, causing the flow field to not be radial, then estimates using equation D-6 will be erroneous. For instance, if most of the flow to the production well is channeled from a direction that does not intersect the tracer slug, then the interwell transport time for the slug can be very long, even if flow occurs in only a small fraction of the system volume. In this case, a considerable amount of dilution will occur late in the system (in the production well), and a misleadingly high flow porosity will be deduced from equation D-6. If an asymmetric lithium response curve with some apparent nonsorbing transport is detected at the production well, the degree of asymmetry in the response can, in principle, be used to estimate the volume that the tracer pulse flowed through within the system. Such an estimate can be obtained by first using MULTRAN V 1.0 (STN: 10666-1.0-00 [DIRS 159068]) in inverse mode to match the shape of the response curve, given a known injection pulse concentration, injection duration, alluvium CEC (estimated from laboratory tests), and a longitudinal dispersivity (estimated from the nonsorbing tracer responses). Once a curve shape is matched given these constraints, the flow system volume can be estimated by multiplying the volume of the injection pulse in the field test by the ratio of flow system volume to injection pulse volume assumed in the MULTRAN simulations. An estimate of flow porosity can then be obtained from:

$$\eta = \frac{V}{\pi L^2 T} \quad (\text{Eq. H-2})$$

where V = volume determined from MULTRAN matches to the lithium response.

The flow porosity estimate given by equation H-2 is independent of tracer transport times and, therefore, is not biased by flow channeling resulting from flow system heterogeneity. Of course, if the lithium response curve shows no asymmetry, then the method described above can only be used to establish a lower bound for the effective flow porosity. The method relies on the assumption of fast ion exchange kinetics relative to transport times in the flow system (i.e., the local equilibrium assumption), which should be satisfied unless transport times are less than a few hours. Six-hour residence times in the laboratory columns were apparently long enough that the local equilibrium assumption was satisfied.

INTENTIONALLY LEFT BLANK

APPENDIX I

**TWO EXAMPLES OF STEPS INVOLVED IN PROCESSING INPUT DATA TO
ARRIVE AT OUTPUT DATA**

II. HYDRAULIC TEST INTERPRETATION EXAMPLE

The following steps are involved in the hydraulic test interpretation depicted in Figure C-21:

Definitions of terms:

P_h (ft) = Total pressure head in feet of water (hydraulic pressure head plus barometric pressure head) in a monitored interval

P_h (psi) = Total pressure in psi = P_h (ft)/2.3078, where 2.3078 is the ft/psi conversion factor stored in the ParoScientific Inc. pressure transducers used at the C-holes

P_{bar} (psi) = barometric (atmospheric) pressure at land surface in psi

P_{bar} (ft) = barometric pressure head in feet of water = $2.32 \times P_{bar}$ (psi), where 2.32 is the ft/psi conversion factor at temperature of monitored interval

P_w (psi) = hydraulic pressure in monitored interval in psi = P_h (psi) - P_{bar} (psi)

P_w (ft) = hydraulic pressure head in monitored interval in ft of water = $2.32 \times P_w$ (psi), where 2.32 is the ft/psi conversion factor at temperature of monitored interval

$|_{start}$: At the start time of the test

$|_t$: At time t during the test

BE: Barometric Efficiency of interval

$dd_{corrected}$ (ft) = Barometrically corrected drawdown in feet

$dd_{corrected}$ (ft) = [P_w (ft) $|_{start}$ - P_w (ft) $|_t$] + BE [P_{bar} (ft) $|_{start}$ - P_{bar} (ft) $|_t$].

1. Go to DTN: GS990408312315.002 [DIRS 140115] in the Automated Technical Data Tracking system, download the data file, and cut and paste all the data into an Excel spreadsheet using commas as delimiters. It may be necessary to use the "text to columns" feature of Excel after the cut-and-paste to get the head and temperature data in columns D and E to appear in separate columns (in this case, specify commas as delimiters).
2. In the resulting spreadsheet:
 Column D is P_h (ft) and Column J is P_{bar} (psi)
 Start time is 16:00:02 on 6/2/98.
3. Perform above calculations to get a $dd_{corrected}$ column. Use BE = 0.96 (see Table C-3).
4. Create an "elapsed minutes" column by performing spreadsheet functions using the time column C.
5. Plot $dd_{corrected}$ versus "elapsed minutes" to obtain Figure C-21.

12. TRACER TEST INTERPRETATION EXAMPLE

The following steps are involved in the tracer test interpretation depicted in Figure B-37, which are model fits to solute tracer breakthrough curves in the Prow Pass Tuff tracer test:

1. Sample collection during field tracer test is documented in C-Wells Prow Pass Field scientific notebook (Reimus 2000 [DIRS 162852]).
2. Analytical data for the tracers (raw concentration data) is reported in DTN: LAPR831231AQ99.001 [DIRS 140134].
3. The acquisition of the analytical data is documented in “UZ Transport Test Notebook 2” (Bussod 2001 [DIRS 165281]), which has many attachments. This notebook is a key roadmapping element for DTN: LAPR831231AQ99.001 [DIRS 140134], although the notebook does not appear explicitly in the report because the raw concentration data does not appear in the report (all concentrations in the report are normalized to injection mass).
4. The conversion of the raw pentafluorobenzoate, bromine, and lithium concentration data (mg/L) to the normalized concentrations plotted in Figure D-27 is documented in the scientific notebook (Reimus 2003 [DIRS 165129], Appendix A, pp. A-87 to A-144). The tracer masses (and where they came from) used in these normalization calculations are documented in the main body of this notebook (Reimus 2003 [DIRS 165129]).
5. The RELAP and MULTRAN fits to the breakthrough curves shown in Figure D-27 are documented in DTN: LA0303PR831231.003 [DIRS 163756] (see the DTN Readme file for more details).

APPENDIX J

**QUALIFICATION OF MINERALOGY DATA FOR SAMPLE FROM UE25C#2, 2406 FT
BELOW LAND SURFACE (DTN: LA9909PR831231.004 [DIRS 129623])**

J1. QUALIFICATION OF MINERALOGY DATA

The qualification of the quantitative x-ray diffraction data for a crushed tuff sample from UE25c#2, 2,406 ft below land surface, contained in DTN: LA9909PR831231.004 [DIRS 129623], is documented here in accordance with SCI-PRO-001, *Qualification of Unqualified Data*. This qualification provides the desired level of confidence that the data are suitable for their intended use, which is limited to the analysis and discussion in Section E1 of this analysis report. The qualification is based on corroboration of data, and it is carried out in accordance with data qualification plan, *UE25c#2 2406ft Quantitative X-Ray Diffraction Data*.

The quantitative x-ray diffraction (XRD) data for the sample from UE25c#2, 2406 ft below land surface can be corroborated directly with the qualified XRD data for a sample from UE25c#1, 2346 ft below land surface (DTN: MO0012MINLCHOL.000 [DIRS 153370]). These two samples (called UE25c#2-2406 and UE25c#1-2346) were taken from the same lithologic interval, the central Bullfrog Tuff, which is a moderately to densely welded ash-flow tuff, at similar depths in wells that are less than 100 m apart (Figures 6.1-1 and 6.1-2). Although some minor variations in mineralogy can be expected over small scales within such intervals, the overall mineralogy should be very similar for samples that are less than 100 m apart. Therefore, the criterion for corroborating the UE25c#2-2406 data with the UE25c#1-2346 data is that the mineral weight percentages determined by XRD agree to within the combined reported errors of the two analyses. For example, if both analyses report a ± 1 -wt % error for a given mineral, then the reported weight percentages for the two samples should agree to within 2 wt % for that mineral. This criterion is considered acceptable because both samples were analyzed by the same person (Steve Chipera of Los Alamos National Laboratory) using almost identical equipment and procedures, and the reporting of mineral weight percentages and errors was consistent.

Table J-1 provides the reported XRD analyses of the two samples, which were prepared by the same method (dry sieving, followed by wet sieving with J-13 well water, and retaining the 75- to 500- μ m particle size fraction for XRD analyses). DTN: MO0012MINLCHOL.000 [DIRS 153370] also contains data for UE25c#1-2346 for different sample preparation methods.

It is apparent from examining Table J-1 that the criterion established above for qualification of the UE25c#2-2406 data is met for all minerals. Thus, the XRD data for UE25c#2-2406 are considered qualified for their intended use in the analysis presented in Section E1. The source DTN: LA9909PR831231.004 [DIRS 129623] will remain unqualified for other uses.

Table J-1. Mineral Weight Percentages and Reported Errors (in Weight Percent Units) from Quantitative XRD Analyses of UE25c#2-2406 and UE25c#1-2346

Mineral	UE25c#2-2406^a	UE25c#1-2346^b
Smectite	5±2	2±1
Mica	1±1	3±1
Clinoptilolite	ND	ND
Mordenite	ND	ND
Analcime	ND	ND
Quartz	32± 2	34 ±2
Feldspar	62± 7	61± 9
Hematite	1± 1	Trace
Calcite	ND	1± 1
Kaolinite	ND	ND

NOTE: ND = Not Determined.

^aTaken from DTN: LA9909PR831231.004 [DIRS 129623], SEP Table S99488_003 (unqualified).

^bTaken from DTN: MO0012MINLCHOL.000 [DIRS 153370], SEP Table S00449_001 (qualified).



Data Qualification Plan

QA: QA
Page 1 of 1

Complete only applicable items.

Section I. Organizational Information		
Qualification Title UE25c#2 2406ft Quantitative X-Ray Diffraction Data		
Requesting Organization Los Alamos National Laboratory		
Section II. Process Planning Requirements		
1. List of Unqualified Data to be Evaluated One data set (UE25c#2 2406 mineralogy data) from DTN LA9909PR831231.004		
2. Type of Data Qualification Method(s) [Including rationale for selection of method(s) (Attachment 3) and qualification attributes (Attachment 4)] The corroborating data method will be used to qualify the unqualified data set for intended use in the SZ In-Situ Testing Analysis Report (ANL-NBS-HS-000039). The rationale for selecting this method is that qualified X-ray diffraction (XRD) data were obtained at a later time for a sample taken from the same lithologic interval (Central Bullfrog Tuff) in well UE25c#1 (2346 ft), which is less than 100 m from UE25c#2. The unqualified XRD data can be qualified by corroborating the data with the qualified XRD data from the same interval in UE25c#1.		
3. Data Qualification Team and Additional Support Staff Required Paul Reimus (Qualification Chairperson) Mei Ding		
4. Data Evaluation Criteria Method 2, "Corroborating Data", will be used to qualify the data using attribute 10 from Attachment 4 of SCI-PRO-001. The data will be evaluated by comparing the weight fractions of minerals determined by XRD in the two samples. The comparison will be made using the UE25c#1 sample that received the same sieving treatment as the UE25c#2 sample. If the weight percentages agree within the reported combined errors of the two analyses, then the data for the UE25c#2 sample will be considered qualified by corroboration.		
5. Identification of Procedures Used SCI-PRO-005, Scientific Analyses		
Section III. Approval		
Qualification Chairperson Printed Name Paul W. Reimus	Qualification Chairperson Signature <i>Paul W. Reimus</i>	Date 3/1/07
Responsible Manager Printed Name Stephanie Kuzio	Responsible Manager Signature <i>Stephanie Kuzio</i>	Date 3/2/07

SCI-PRO-001.1-R0

INTENTIONALLY LEFT BLANK

APPENDIX K

**QUALIFICATION OF WELL COMPLETION DATA FOR NC-EWDP-19IM2,
NC-EWDP-22S, NC-EWDP-22PA, NC-EWDP-22PB, AND NC-EWDP-22PC
(DTN: LA0705PR150304.007 [DIRS 181202])**

K1. DATA QUALIFICATION

The qualification of the well completion data for NC-EWDP-19IM2, NC-EWDP-22S, NC-EWDP-22PA, NC-EWDP-22PB, and NC-EWDP-22PC is documented here in accordance with SCI-PRO-001, *Qualification of Unqualified Data*. This qualification provides the desired level of confidence that the data are suitable for their intended use, which is limited to the analyses and discussion in Section F2 (NC-EWDP-19IM2) and Section F6 (Site 22 wells) of this analysis report. The qualification is based on technical assessment and corroborative information, and it is carried out in accordance with data qualification plan, *Qualification of Well Completion Data for NC-EWDP-19IM2, NC-EWDP-22S, NC-EWDP-22PA, NC-EWDP-22PB, and NC-EWDP-22PC*.

The well completion diagrams for NC-EWDP-19IM2 (19IM2), NC-EWDP-22S (22S), NC-EWDP-22PA (22PA), NC-EWDP-22PB (22PB), and NC-EWDP-22PC (22PC) are shown in Figures K-1 through K-5, respectively. Figure K-1 was used to determine the thickness of the saturated alluvium from the water table to the bottom of the screen 4 sand pack at the ATC so that the cross-hole hydraulic test described in Section F2 of this report could be analyzed. Figures K-2 through K-4 were used to determine the depths of the water table and the screened intervals in 22S, 22PA, and 22PB for the interpretation of the cross-hole hydraulic tests at Site 22 described in Section F6. A similar well completion diagram for NC-EWDP-19D (19D) is shown in Figure K-6. The latter diagram constitutes the qualified “data” contained in DTN: MO0112DQRWLNYE.018 [DIRS 157187] (the Technical Data Management System provides a link to this diagram when the DTN is accessed). The same Nye County technical work plan and procedures were followed to conduct the well completions and to generate all the well completion diagrams. Specifically, *Early Warning Drilling Program Phase IV Drilling and Well Construction Work Plan* (NWRPO 2002 [DIRS 179629]) and TP-7.0, *Drill Site Management* [DIRS 179628] governed the work processes. Although these documents have undergone revisions, their technical requirements have remained essentially unchanged since their initial issue, and more importantly, the requirements associated with documenting well completions have not changed.

The 19D well completion data were qualified in accordance with AP-SIII.2Q in December 2001. The qualification process for this well and for several other Nye County wells was accomplished through the preparation and approval of *Data Qualification Report: Water Level Data from Nye County Wells for Use on the Yucca Mountain Project* (BSC 2001 [DIRS 172175]).

This data qualification report provides an extensive evaluation of the well completion data, including wellhead elevations and locations for Nye County Early Warning Drilling Program wells that existed in December 2001 (19IM2 was completed in August/September 2002). In Section 3.3 (Borehole Completion Data) of the data qualification report, it was concluded that the screened interval depths for the Nye County wells were accurate to within the ± 1 m tolerance required for the Yucca Mountain Project saturated zone (SZ) flow model at that time. In fact, the total depth measurements made by both Yucca Mountain Project and Nye County personnel for 10 different Early Warning Drilling Program wells never differed by more than 0.3 ft (BSC 2001 [DIRS 172175], Table 6). The general recommendation of the data qualification report was that the well completion and water level data for all the Nye County wells, with the exception of some of the water level data from multilevel piezometers (but not well completion

data), should be qualified for use in developing technical products on the Yucca Mountain Project. This recommendation and the subsequent qualification of the data, combined with the fact that the well completion data in DTN: LA0705PR150304.007 [DIRS 181202] were developed using the same methods as the data qualified via *Data Qualification Report: Water Level Data from Nye County Wells for Use on the Yucca Mountain Project* (BSC 2001 [DIRS 172175]), provide a strong case for qualification of the 19IM2, 22S, 22PA, 22PB, and 22PC well completion data for intended use in this analysis report.

Unfortunately, the data qualification report did not address the depths of the contacts between the sand packs and bentonite grout seals that define the actual hydraulic thicknesses of the screened intervals in the wells (hydraulic thickness is the thickness of aquifer that is hydraulically connected to the screen through the permeable sand packs). These contact depths are considered more uncertain than the screen locations of the borehole casing, which were the focus of the assessment of well completions in the data qualification report (the screen locations can be determined quite accurately from the length and number of joints in the casing). The sand-grout contact depths were determined by standard tagging procedures in the field using piping of known lengths that was inserted into the annulus between the borehole wall and the casing to “tag” the top of the sand or grout. Some confirmatory information on the location of the contacts was also obtained by geophysical logging techniques after well completion. In the borehole completion diagrams, the contact depths are reported in tenths of a foot, but they should probably be considered accurate to only within 1 to 2 ft.

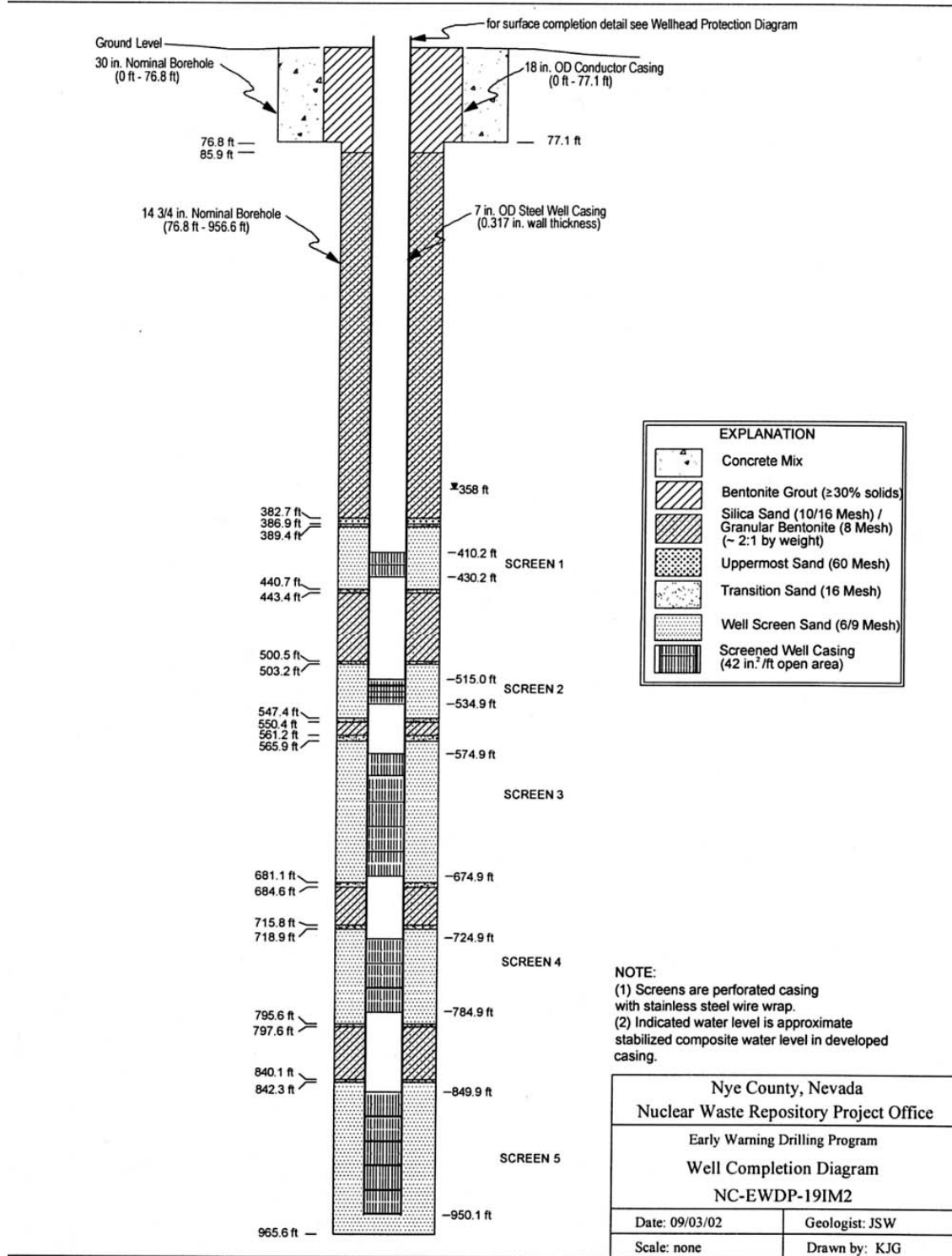
However, even if the accuracy were considerably worse than 1 to 2 feet (like several feet), the resulting uncertainty in interval thickness would be acceptable for the ATC cross-hole hydraulic test analysis discussed in Section F2. This test was conducted by pumping 19D from the 4 shallowest screened intervals in 19D while monitoring the 4 shallowest intervals in 19IM2. The only inflated packers in the wells were between the fourth and fifth intervals (from the top) in each well, so the four shallowest intervals in each well were effectively combined to act as one large interval. The inflated packers kept the saturated alluvium isolated from the underlying bedrock (tuff). In this test configuration, the effective thickness of the hydraulic test interval was the entire thickness of the saturated alluvium from the water table to the bottom of the fourth screened interval – a thickness of approximately 133 m (437 ft), as stated in Section F2. In this case, inaccuracies of as much as 4 feet in the overall thickness of the test interval would result in errors of less than a 1% in the interval thickness, which would translate to errors of less than 1% in the hydrologic parameter estimates from the test.

In the case of the Site 22 hydraulic tests (discussed in detail in Section F6), each of four individual intervals were pumped in isolation to observe cross-hole responses. These intervals have thicknesses ranging from approximately 19 m to 40 m (Table F-1), so the relative error associated with an error in contact depth of 1 ft to 2 ft is considerably greater than for the ATC cross-hole test. However, even an error of 3 ft corresponds to only ~5% of the thickness of the narrowest interval at Site 22, which translates to uncertainties of no greater than 5% in the hydrologic parameter estimates.

Section 6.4.6 states that estimates of storativity derived from hydraulic testing in the alluvium should be considered accurate to only within an order of magnitude, and estimates of transmissivity should be considered accurate to only within a factor of 3 (given all of the

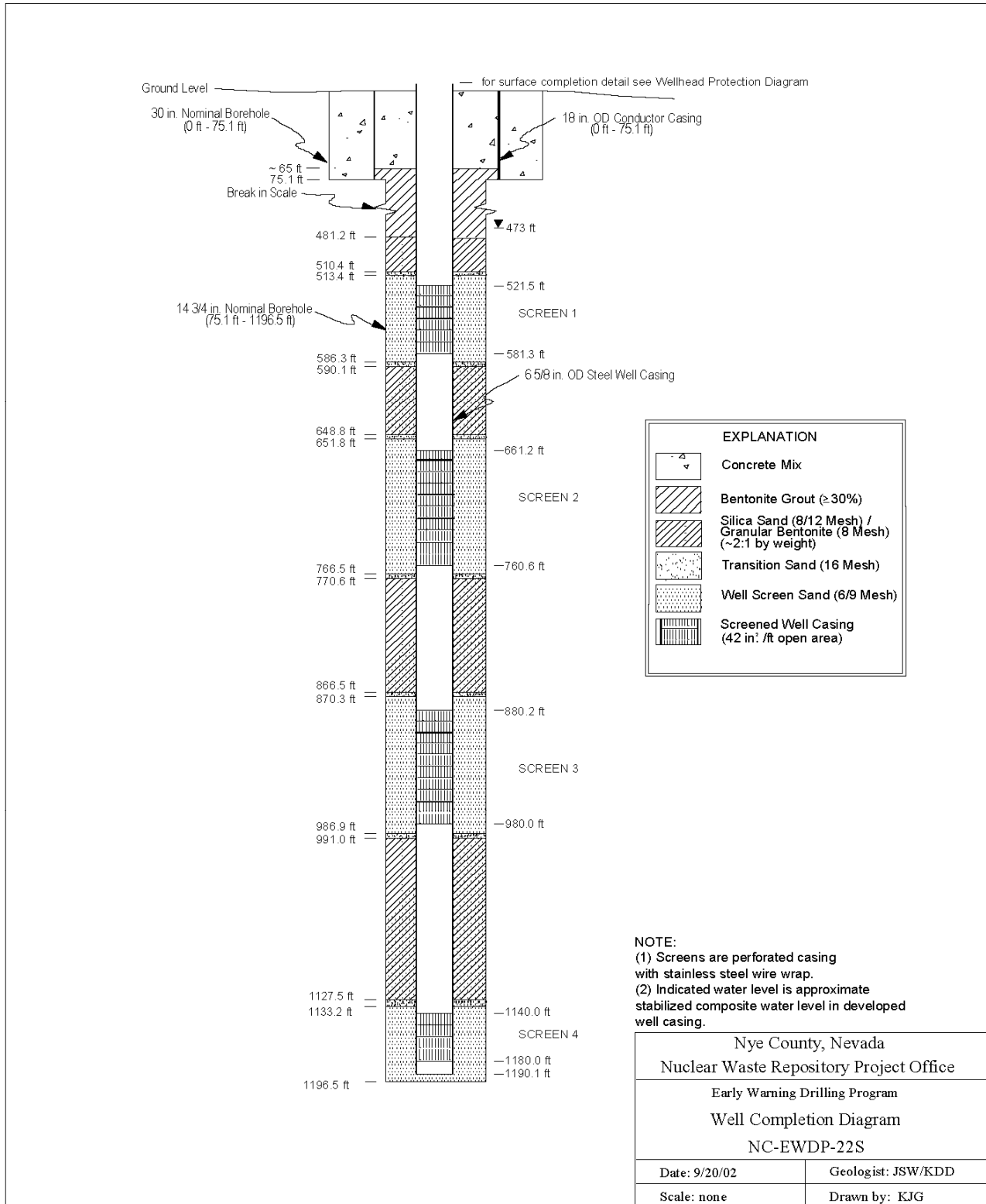
uncertainties associated with the testing). Thus, even inaccuracies of several feet in the test interval thickness would not have a significant impact on the uncertainties in the parameter estimates, as reported in Section 6.4.6. Furthermore, Section 6.4.6 also states that “hydrologic parameters derived from ATC and Site 22 testing are not used as direct inputs in *Saturated Zone Site-Scale Flow Model* (BSC 2004 [DIRS 170037]), but rather they are used primarily for qualitative/corroborative consistency checks with the hydrologic parameters that are derived from calibrations of *Saturated Zone Site-Scale Flow Model* (BSC 2004 [DIRS 170037]).”

Given the reported accuracy of the data (Section 6.4.6), the ultimate end use of the hydrologic parameters derived from the data, and the fact that several Nye County well completion diagrams prepared by the same methods were previously qualified, the well completion diagrams in DTN: LA0705PR150304.007 [DIRS 181202] are considered qualified for their intended use in the analysis presented in Sections F2 and F6. The source DTN: LA0705PR150304.007 [DIRS 181202] will remain unqualified for other uses.



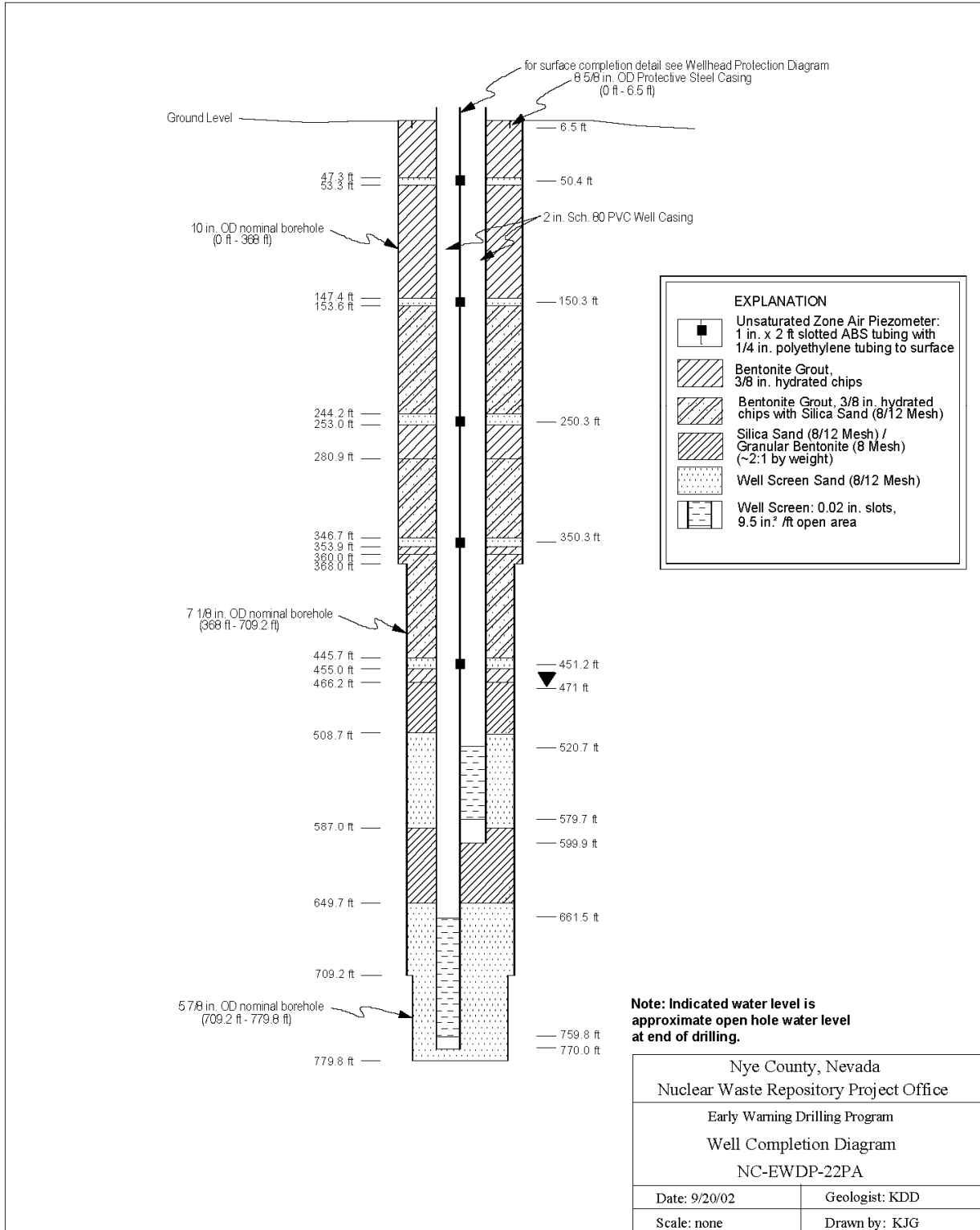
Source: DTN: LA0705PR150304.007 [DIRS 181202].

Figure K-1. NC-EWDP-19IM2 Well Completion Diagram



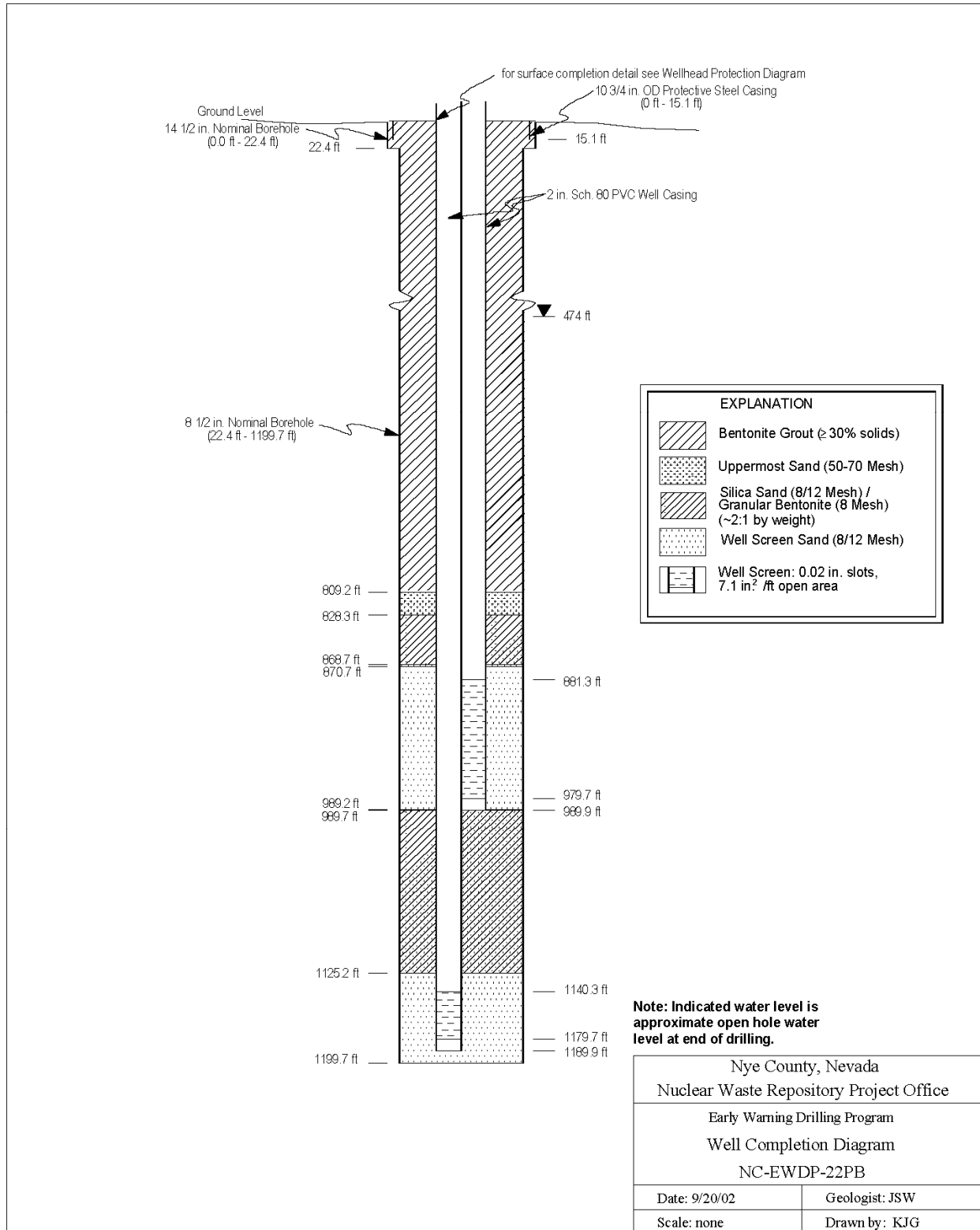
Source: DTN: LA0705PR150304.007 [DIRS 181202].

Figure K-2. NC-EWDP-22S Well Completion Diagram



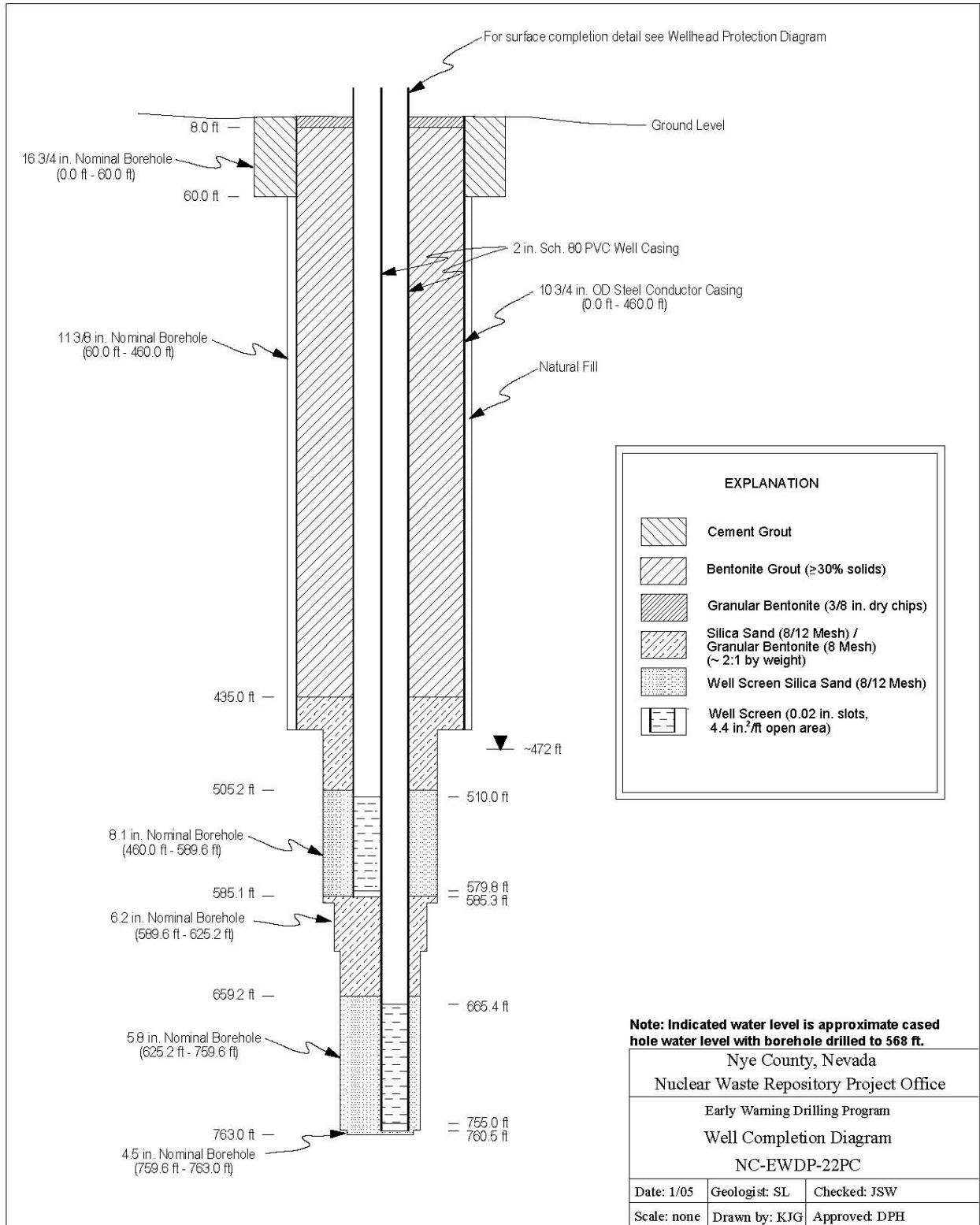
Source: DTN: LA0705PR150304.007 [DIRS 181202].

Figure K-3. NC-EWDP-22PA Well Completion Diagram



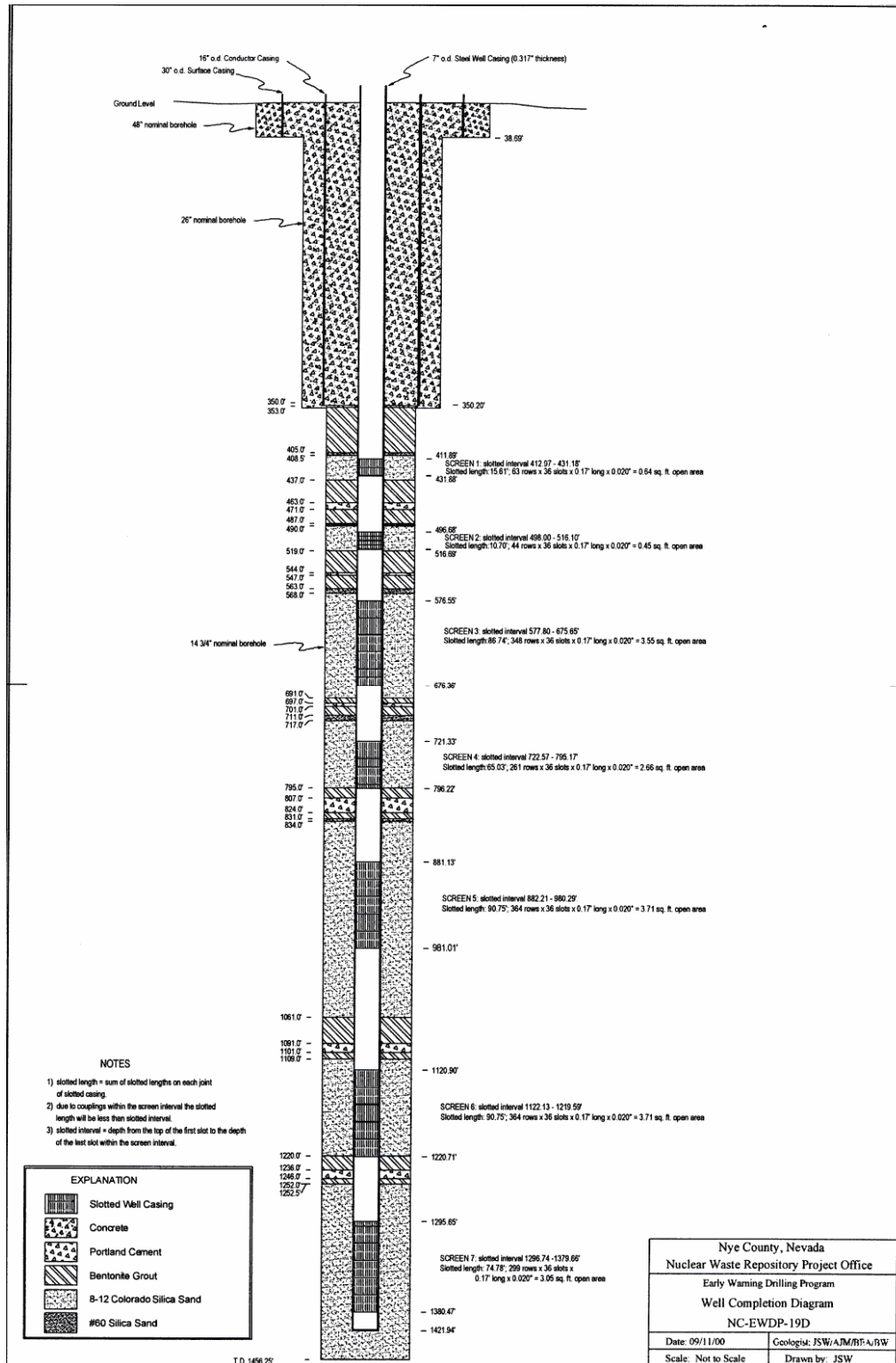
Source: DTN: LA0705PR150304.007 [DIRS 181202].

Figure K-4. NC-EWDP-22PB Well Completion Diagram



Source: DTN: LA0705PR150304.007 [DIRS 181202].

Figure K-5. NC-EWDP-22PC Well Completion Diagram



Source: DTN: MO0112DQRWLNVE.018 [DIRS 157187].

Figure K-6. NC-EWDP-19D Well Completion Diagram



Data Qualification Plan

QA: QA
Page 1 of 1

Complete only applicable items.

Section I. Organizational Information		
Qualification Title Qualification of Well Completion Data for NC-EWDP-19IM2, NC-EWDP-22S, NC-EWDP-22PA, NC-EWDP-22PB, and NC-EWDP-22PC		
Requesting Organization Los Alamos National Laboratory		
Section II. Process Planning Requirements		
1. List of Unqualified Data to be Evaluated NC-EWDP-19IM2 well completion data contained in DTN MO0306NYE05260.165 NC-EWDP-22S well completion data contained in DTN MO0306NYE05264.170 NC-EWDP-22PA well completion data contained in DTN MO0306NYE05265.171 NC-EWDP-22PB well completion data contained in DTN MO0306NYE05266.172 NC-EWDP-22PC well completion data contained in DTN MO0505NYE06464.314		
2. Type of Data Qualification Method(s) [Including rationale for selection of method(s) (Attachment 3) and qualification attributes (Attachment 4)] The technical assessment and corroborating data methods will be used to qualify the data set for intended use in the SZ In-Situ Testing Analysis Report (ANL-NBS-HS-000039). The rationale for selecting these methods is that very similar Nye County data were previously qualified in TDR-NBS-HS-000016, "Data Qualification Report: Water Level Data from Nye County Wells for Use on the Yucca Mountain Project," prepared by Charles Wilson in December 2001. In this report, both water level data and well completion data from Nye County were carefully assessed, and the data were recommended for qualification (and ultimately qualified). Nye County methods for documenting the well completions listed above will be assessed and compared to the methods used to document the well completion for NC-EWDP-19D, which was qualified in TDR-NBS-HS-000016. If the methods are essentially the same, then the 19IM2, 22S, 22PA, 22PB, and 22PC well completion data should receive the same qualification status of the earlier well completion data.		
3. Data Qualification Team and Additional Support Staff Required Paul Reimus (Qualification Chairperson) Mei Ding		
4. Data Evaluation Criteria Method 2, "Corroborating Data", and Method 5, "Technical Assessment", will be used to qualify the data using attribute 7 from Attachment 4 of SCI-PRO-001. If the well completion data for the Nye County wells listed above and the data discussed in TDR-NBS-HS-000016 are consistent and are determined to have been obtained/documenting using the same or very similar methods, then the well completion data will be considered qualified for intended use.		
5. Identification of Procedures Used SCI-PRO-005, Scientific Analyses		
Section III. Approval		
Qualification Chairperson Printed Name Paul W. Reimus	Qualification Chairperson Signature <i>Paul W. Reimus</i>	Date 3/1/07
Responsible Manager Printed Name Stephanie Kuzio	Responsible Manager Signature <i>Stephanie Kuzio</i>	Date 3/2/07

SCI-PRO-001.1-R0

APPENDIX L

**QUALIFICATION OF C-WELLS FLOW DISTRIBUTION DATA
(DTN: GS931008312313.016 [DIRS 148173])**

The qualification of the flow distribution data for the C-wells is documented here in accordance with SCI-PRO-001, *Qualification of Unqualified Data*. This qualification provides the desired level of confidence that the data are suitable for their intended use, which is limited to the analysis of effective flow porosity of the Bullfrog Tuff, as presented in Table D-10 (the actual flow distribution data is schematically represented in Figure 6.1-2). The qualification is based on corroborative information and is carried out in accordance with data qualification plan *Qualification of NC-EWDP-19IM2 Well Completion Data*.

The flow distribution data at the C-wells, as presented in Tables 4, 5, and 6 of the USGS report by Geldon (1996 [DIRS 100396]) (DTN: GS931008312313.016 [DIRS 148173]), was developed primarily from tracejector (radioactive iodine) and temperature survey data collected under open-hole pumping conditions in the C-wells in the 1980s. The relative percentages of flow being produced from different depth intervals in the C-wells was used to refine the effective flow porosity estimates in the lower Bullfrog Tuff presented in Table D-10 of this analysis report. The information on the depths of the flowing intervals was previously qualified for use on the Yucca Mountain Project as a result of the preparation and approval of *Data Qualification Report: Flowing Interval Data for Use on the Yucca Mountain Project* (DTN: MO0007FLOWINTL.001 [DIRS 179916]).

This report provides an extensive evaluation of the flowing interval data obtained for a number of wells near Yucca Mountain in the 1980s, including the three C-wells. Although the qualified DTNs resulting from this qualification effort include only the depths of the flowing intervals (not the relative percentages of flow from each interval), there is considerable discussion in the report about the quality of the methods used, which were found to be acceptable to support the use of the data in technical products for the Yucca Mountain Project. With respect to the tracejector survey data the authors state “Unlike temperature logging, which can be more sensitive but does not provide a direct hydrologic measurement, a tracejector survey performed during pumping provides a *quantitative* measurement of the contribution of each interval to the total borehole flow.”

The authors also cite a comparison of 1984 UE25c#3 tracejector survey data with more recent spinner and oxygen-activation survey data taken under pumping conditions in the same well in 1995 (Thompson 1997 [DIRS 172179])—in qualified DTN: TMUE25C3000095.001 [DIRS 172179]). They conclude that the qualified data from 1995 corroborate the unqualified 1984 data. Thompson (1997 [DIRS 172179], p. 5) stated that “Close agreement between the Full-Bore Flowmeter (spinner) and Water Flow Log (oxygen activation) provide confidence in the accuracy of the calculation of water flow rates. The radioactive tracer (tracejector) survey, which was run 10 years earlier, also indicates close agreement with the Full-Bore Flowmeter and Water Flow Log, though the absolute flow rates are slightly greater.” Thompson summarizes by stating “Comparison of flow measurements taken 10 years earlier indicated flow from the same zones in the borehole, and resulted in comparable flow rates and percentage of contribution” (DTN: TMEU25C3000095.001 [DIRS 172179]). The reader can verify these conclusions by comparing the flow distribution data from UE25c#3 depicted in Figures 6.1-2 [based on work by Geldon (1996 [DIRS 100396])] and C-4 (DTN: TMEU25C3000095.001 [DIRS 172179]).

For the purposes of estimating effective flow porosity in the lower Bullfrog Tuff in this analysis report, it was assumed that the early arriving tracer peak in the multiple-tracer test discussed in Sections D4.5 and D4.6 occurred as a result of flow pathways that accounted for 75% of the total cross-flow between the injection and production wells (c#2 and c#3, respectively). This assumption is based on the underlying assumption that the early arriving tracer mass exited c#2 from the upper half of the injection interval (because of arguments spelled out in Section D4.5). Figure 6.1-2 (based on information from Geldon 1996 [DIRS 100396]; tables are based on data from DTN: GS931008312313.016 [DIRS 148173]) indicates that actually 79% of the flow *into* c#2 occurred in the upper portion of the injection interval in the 1984 flow surveys (which translates into more than 80% of the flow when the interval is isolated), but because there appears to be a lower percentage of flow occurring in the upper portion of the production interval in c#3 (in both the 1984 and the 1995 surveys), only 75% of the total cross-hole flow was assumed to be responsible for the first tracer peak. This assumption is clearly quite uncertain, especially since cross-hole flow pathways are being inferred from single-well flow data. However, this relatively large uncertainty means that the data upon which the assumption is based (i.e., the flow distribution data) should not require a high degree of accuracy or precision to be considered qualified for its intended use in this analysis report.

Given the previous qualification of the flowing interval depth data, the good agreement between the 1984 and 1995 quantitative flow survey information from UE25c#3, and the ultimate use of the flow distribution information to obtain an estimate with a relatively high degree of uncertainty, the flow distribution data in the USGS report (Geldon 1996 [DIRS 148173]) that constitutes DTN: GS931008312313.016 [DIRS 148173] is considered qualified for its intended use in this analysis report. The source DTN: GS931008312313.016 [DIRS 148173] will remain unqualified for other uses.



Data Qualification Plan

Complete only applicable items.

QA: QA
Page 1 of 1

Section I. Organizational Information		
Qualification Title Qualification of C-wells flow distribution data from the USGS report "Results and Interpretation of Preliminary Aquifer Tests in Boreholes UE-25c#1, UE-25c#2, and UE-25c#3, Yucca Mountain, Nye County, Nevada," by Geldon (1996).		
Requesting Organization Los Alamos National Laboratory		
Section II. Process Planning Requirements		
1. List of Unqualified Data to be Evaluated Flow distribution data contained in the USGS report "Results and Interpretation of Preliminary Aquifer Tests in Boreholes UE-25c#1, UE-25c#2, and UE-25c#3, Yucca Mountain, Nye County, Nevada," by Geldon (1996). This report is associated with DTN GS031008312313.016.		
2. Type of Data Qualification Method(s) [Including rationale for selection of method(s) (Attachment 3) and qualification attributes (Attachment 4)] The corroborating data method will be used to qualify the unqualified data set for intended use in the SZ In-Situ Testing Analysis Report (ANL-NBS-HS-000039). The flowing interval data from the C-wells were qualified for use in the AMR, "Probability Distribution of Flowing Interval Spacing", by Kuzio (1999) in TDR-NBS-GS-000017, "Data Qualification Report: Flowing Interval Data for Use on the Yucca Mountain Project," prepared by Charles Wilson in July 2000. However, the resulting qualified data sets identified only the depths of the flowing intervals, not the percentages of flow contributed by each flowing interval (which is used in the SZ In-Situ Testing Analysis Report). Recognizing that the data used in the two AMRs are the same data, the qualification efforts documented in TDF-NBS-GS-000017 will be used to directly qualify the percentages of flow in the flowing intervals at the C-wells.		
3. Data Qualification Team and Additional Support Staff Required Paul Reimus (Qualification Chairperson) Mei Ding		
4. Data Evaluation Criteria Method 2, "Corroborating Data", will be used to qualify the data using attribute 10 from Attachment 4 of SCI-PRO-001. The data will be evaluated by closely examining TDR-NBS-GS-000017 to ensure that the data qualified in that report are from the same source as the data used in the SZ In-Situ Testing Analysis Report. The evaluation criteria for the SZ In-Situ Testing Analysis Report are essentially the same as the criteria used in TDR-NBS-GS-000017, although additional consideration will be given to how accurate and precise the data have to be for their intended use in the analysis report.		
5. Identification of Procedures Used SCI-PRO-005, Scientific Analyses		
Section III. Approval		
Qualification Chairperson Printed Name Paul W. Reimus	Qualification Chairperson Signature <i>Paul W. Reimus</i>	Date 3/1/07
Responsible Manager Printed Name Stephanie Kuzio	Responsible Manager Signature <i>Stephanie Kuzio</i>	Date 3/2/07

SCI-PRO-001.1-R0

INTENTIONALLY LEFT BLANK

APPENDIX M

**QUALIFICATION OF UE25 ONC-1 DRAWDOWN DATA FROM APRIL 24, 1996 TO
NOVEMBER 12, 1997 (DTN: MO0212SPANYESJ.149 [DIRS 161274])**

M1. INTRODUCTION

The qualification of the UE25 ONC-1 drawdown data from April 24, 1996, to November 12, 1997, is documented here in accordance with SCI-PRO-001, *Qualification of Unqualified Data*. This qualification provides the desired level of confidence that the data are suitable for their intended use, which includes both the estimation of hydrologic parameters based on the ONC-1 drawdown data (discussed in Section C4.6) and the analysis of anisotropy in horizontal hydraulic conductivity in the volcanic tuffs (presented in Section 6.2.6, with additional details provided in Section C6). The ONC-1 drawdown data are presented in Figures C-32, C-37, and C-41. However, the ONC-1 data in these figures were plotted after filtering (and various other minor corrections or manipulations) of the raw pressure transducer data contained in DTN: MO0212SPANYESJ.149 [DIRS 161274], which is the subject of the qualification in this appendix. This qualification is based on both technical assessment and corroborating data, and it is carried out in accordance with data qualification plan entitled *Qualification of UE25 ONC-1 Drawdown Data During the 1996-97 Hydraulic Test of the Bullfrog Tuff at the C-Wells*. The qualification is limited to the data from pressure transducer 9 in ONC-1, which was the deepest transducer in this well; only one other transducer was placed below the water table in ONC-1.

M2. BASES FOR ONC-1 DATA QUALIFICATION

The qualification of the ONC-1 drawdown data is based on the following:

1. The ONC-1 hydraulic response is consistent with the hydraulic responses of other wells (for which the drawdown data are qualified) that responded to pumping of UE25c#3 during the subject time period. The criteria for “consistency” are:
 - a. ONC-1 should respond (i.e., exhibit observable drawdown) faster than wells that are further away from UE25c#3 and slower than wells that are closer to c#3.
 - b. The overall drawdown curve for ONC-1 should exhibit similar characteristics to the drawdown curves of other wells that responded to the pumping of c#3, especially when time since pumping began is divided by the square of the distance to the observation well.
2. The raw pressure data from transducer 9 in ONC-1 is in good agreement with the data from the other transducer placed below the water table in this well (transducer 8). Although the data from both transducers are unqualified, good agreement between the two transducers greatly increases the confidence in the quality of the data from either transducer. It is important to note that absolute pressure measurements are not critical for the drawdown analysis; only *relative* pressures (relative to the starting pressure) are important for the drawdown analysis.

3. The end use of the data is to serve as input for analyses conducted to estimate transmissivity and storativity in the fractured volcanic tuffs between ONC-1 and the C-wells. These estimates were considered accurate to only one significant figure, and they differ significantly for different methods of analysis. The required confidence in the data quality should be commensurate with the level of uncertainty in the parameter estimates obtained from these analyses.

These items are discussed in turn in the following three sections.

M3. CONSISTENCY OF ONC-1 DRAWDOWN DATA WITH QUALIFIED DATA FROM OTHER WELLS

It is apparent from Figure C-41 that ONC-1 responded more quickly to pumping of UE25c#3 than USW H-4, UE25 WT#3, and UE24 WT#14 (i.e., drawdown was observed earlier in ONC-1 than in these wells). The drawdown data for these other wells are qualified (DTN: GS970308312314.002 [DIRS 161273]). The more rapid response of ONC-1 compared to these wells is consistent with the fact that ONC-1 is located considerably closer to c#3 than the other wells (approximately 850 m, as opposed to over 2,200 m for the other wells). If the aquifer in the vicinity of the C-wells behaves as a homogeneous system (at least in the sense that pressure pulses propagate at similar rates in all directions), these relative responses are exactly what would be expected. The fact that ONC-1 responded more rapidly than H-4 is probably the most convincing observation because these wells are located in the same general direction from the C-wells (northwest). Thus, even if there were some large-scale heterogeneities or flow anisotropy affecting the relative responses of the distant wells, it is expected (at least as a first approximation) that ONC-1 and H-4 should be similarly affected because they have a very similar directional orientation to the C-wells. The fact that the ONC-1 response qualitatively conforms to the expectation of a more rapid drawdown than the more distant wells, especially H-4, supports the qualification of the ONC-1 drawdown data.

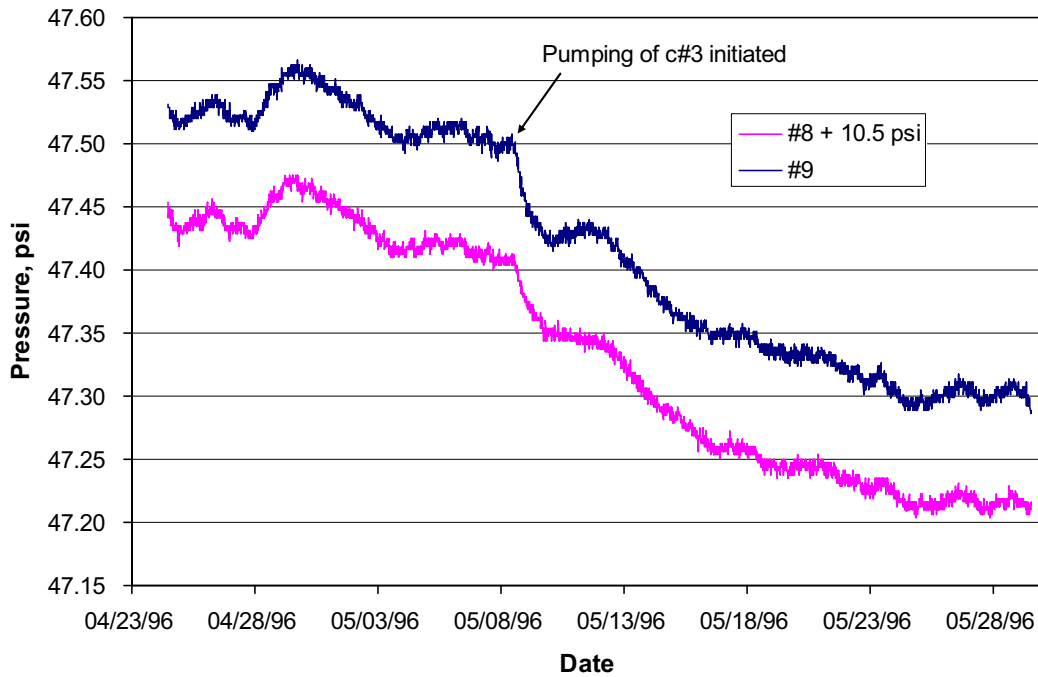
The drawdown curves of Figure C-37 further support the qualification of the ONC-1 data. In this figure, the ONC-1 drawdown curve falls almost directly on top of the drawdown curves for c#2 and WT-3 when the time since pumping began is divided by the square of the distance between the observation wells and the pumping well. This relationship is expected for observation wells in a homogeneous, isotropic system (Freeze and Cherry [DIRS 101173], p. 317); and although the volcanic tuff aquifer is neither homogeneous or isotropic, the fact that the relationship holds for wells that range from approximately 30 m to over 3000 m from the pumping well (including approximately 850 m for ONC-1) is a strong endorsement of the quality of the ONC-1 drawdown data. Figure C-37 actually represents a more quantitative assessment than the preceding paragraph of how closely the ONC-1 drawdown data conforms to expectations for a system with multiple observation wells. It shows that the ONC-1 response is not only more rapid than the response of a more distant well, but it is also slower than the response of a much closer well (c#2). Furthermore, Figure C-37 shows that the shapes of the curves are in very good agreement, which agrees with expectations for a homogeneous, isotropic flow system. Again, even though it cannot be claimed that the volcanic tuffs are homogeneous or isotropic, the fact that the ONC-1 data agree so well with the c#2 and the WT-3 data when time is normalized by dividing by the distance squared is a strong endorsement of the quality of the ONC-1 data.

M4. AGREEMENT BETWEEN PRESSURE DATA FROM TWO TRANSDUCERS IN ONC-1

Figure M-1 shows the raw pressure data from transducers 8 and 9 in ONC-1 as a function of time just prior to and during the early part of the hydraulic test in c#3 (from April 24 to May 29, 1996). In this figure, 10.5 psi was added to all readings from transducer 8 so that the data from the two transducers would plot very close to each other to facilitate a comparison. The sharp drop in pressure indicated by both transducers on May 8 corresponds to the start of the c#3 aquifer test.

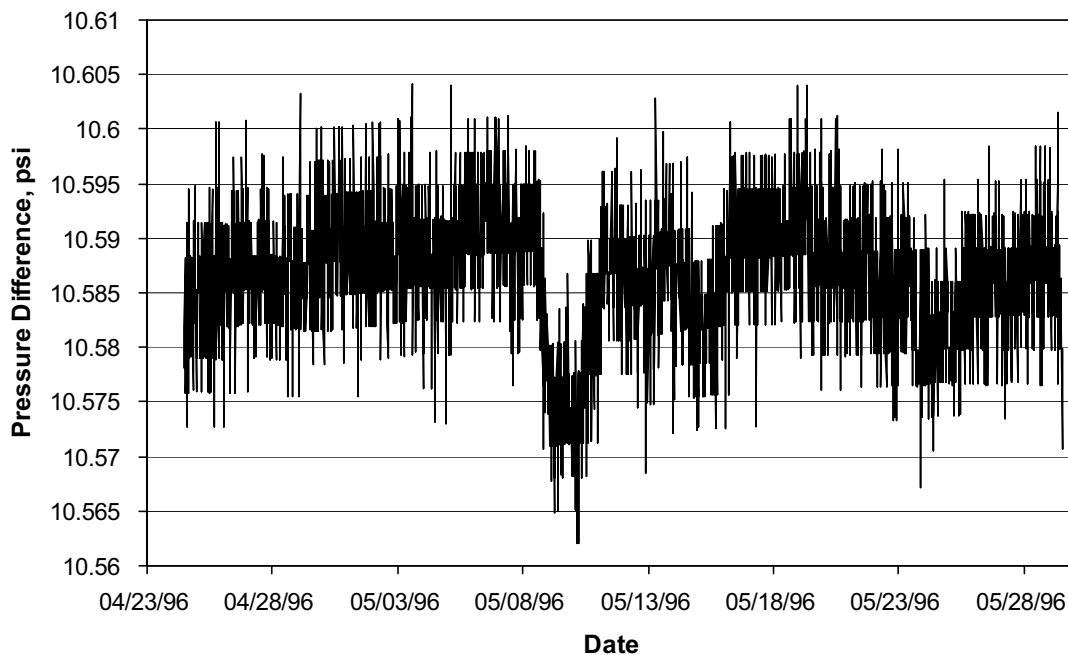
Figure M-2 shows the difference between the two transducer readings as a function of time over the same time period as shown in Figure M-1. The difference between the two transducers was very consistent except for a 2- to 3-day period around May 10, and even the difference during this time period amounts to only about 1 cm (head) less than the difference during the remainder of the overall period. Differences between the pressure readings of the two transducers at approximately the middle of the aquifer test (February 3 to 27, 1997) and at the end of the test (October 28 to November 12, 1997) are shown in Figure M-3. Clearly, the differences drifted over time, but the absolute difference never drifted by more than approximately 3 cm during the entire test. Given that the drawdown for both transducers exceeded 14 cm after June 1, 1996, and that the drawdown data are transformed to log units prior to the type-curve analyses that yield hydrologic parameter estimates, the approximately 3 cm drift translates to less than a 7% difference in the *log* values used in the drawdown analyses. Furthermore, the pressure record before June 1, 1996, constitutes nearly two-thirds of the drawdown record in log time units (time is also transformed to log units for the type-curve analyses), so the effect of the 3-cm drift for times after June 1, 1996, has a very minor effect on the analysis.

The minor effect of the drift in the relative readings of the two transducers on the overall drawdown curve is illustrated in a log-log plot of drawdown vs. time in Figure M-4, which shows the unfiltered and uncorrected drawdown data from the two transducers for the time periods mentioned in the preceding paragraph as well as some additional time periods that are roughly evenly spaced in log time over the duration of the test. All data were obtained by subtracting the starting pressures from both transducers (for the day before starting the pump in c#3) from the pressures measured after pumping began. The drawdown data from the two transducers are nearly indistinguishable after the first 10,000 minutes of the test. The data of Figure M-3 can be compared to Figure C-32 to see that the drawdown curves from both transducers correspond very closely to the filtered drawdown data analyzed to obtain hydrologic parameter estimates in this analysis report. It is apparent that even the differences in the transducer measurements at early times would have little impact on the overall type-curve analysis shown in Figure C-32. The good agreement between the drawdown curves for the two transducers greatly increases the confidence in the quality of the data obtained from either one of the transducers individually.



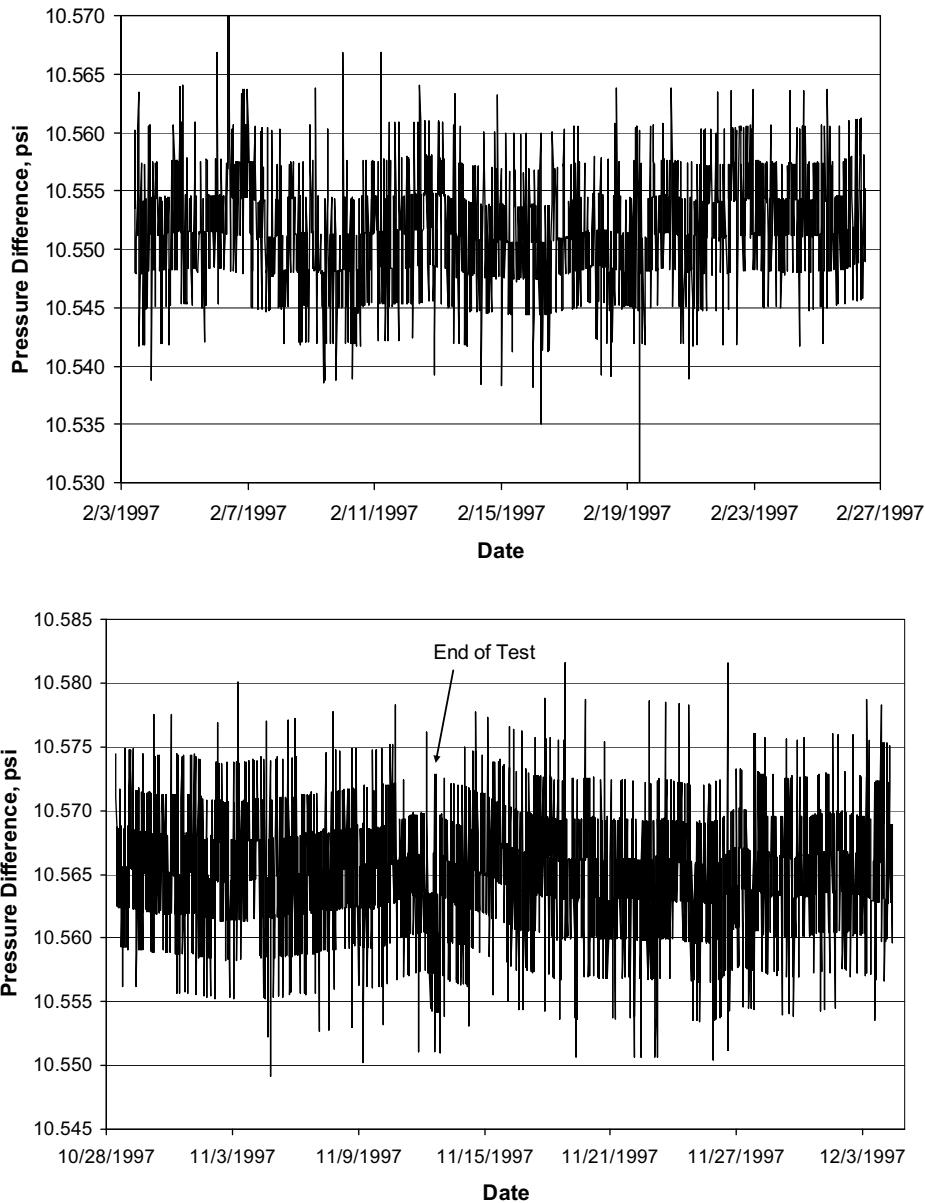
Source: DTN: MO0212SPANYESJ.149 [DIRS 161274].

Figure M-1. Pressure Readings from Transducers 8 and 9 in ONC-1 from April 24, 1996, to May 29, 1996



Source: DTN: MO0212SPANYESJ.149 [DIRS 161274].

Figure M-2. Differences in Pressure Readings from Transducers 8 and 9 in ONC-1 from April 24, 1996, to May 29, 1996



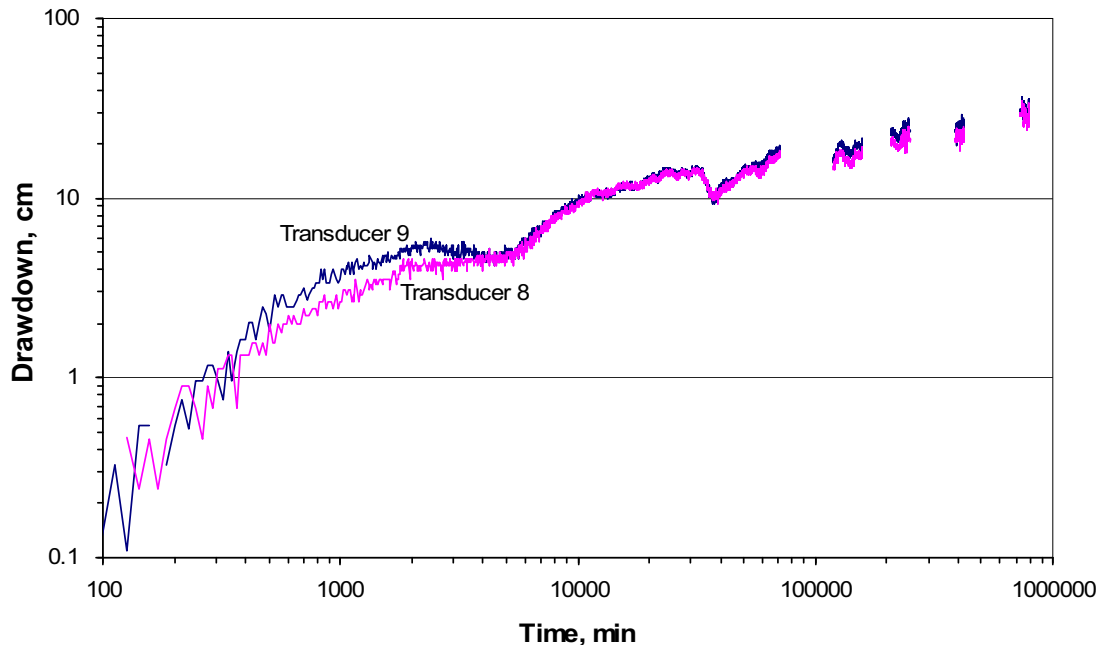
Source: DTN: MO0212SPANYESJ.149 [DIRS 161274].

Figure M-3. Differences in Pressure Readings from Transducers 8 and 9 in ONC-1, February 3 to 26, 1997, and October 28 to December 4, 1997

M5. REQUIRED CONFIDENCE IN DATA QUALITY GIVEN UNCERTAINTY IN PARAMETERS DERIVED FROM DATA

It is stated in Section 6.2.7 of this analysis report that the transmissivity and storativity estimates derived from the C-wells hydraulic tests are accurate to only one significant figure. Table 6.2-3 provides a range of transmissivity estimates of 1,000 m^2/day to 1,465 m^2/day for different methods of analyzing the ONC-1 drawdown data, with a corresponding range of 0.001 to 0.008 for storativity estimates (details in Section C6). Similar parameter ranges are reported in Table 6.2-3 from analyses of *qualified* drawdown data from three other wells. Ultimately, these

large uncertainties in parameter estimates are reflected by a relatively broad distribution of horizontal anisotropy ratios derived from the drawdown data from all four wells (Section 6.2.6 of this report). Given the large uncertainties associated with both the hydrologic parameter estimates from any individual well and with the horizontal anisotropy ratio, the preceding discussion in this appendix establishes adequate confidence in the quality of the ONC-1 drawdown data for its intended use in this analysis report.



Source: DTN: MO0212SPANYESJ.149 [DIRS 161274].

Figure M-4. Uncorrected/Unfiltered ONC-1 Drawdown Curves from Pumping of UE25c#3 between May 8, 1996, and November 12, 1997, Based on Pressure Data from Transducers 8 and 9

M6. SUMMARY

In summary, the qualification of the ONC-1 drawdown data for its intended use in this analysis report is supported by:

- The fact that the ONC-1 drawdown data are consistent with qualified drawdown data from other wells that responded to pumping of c#3 (response times are consistent with distances between observation and pumping wells, and ONC-1 has a nearly identical drawdown curve to two other wells when time is divided by distance squared)
- The good agreement between the uncorrected drawdown curves for the two ONC-1 transducers, as shown in Figure M-4
- The good agreement between the curves of Figure M-4 and the filtered data shown in Figure C-32

- The fact that the hydrologic parameter estimates derived from the ONC-1 drawdown data have a high degree of uncertainty that is commensurate with the uncertainties associated with parameter estimates derived from the qualified drawdown data from other wells.

The ONC-1 drawdown data in DTN: MO0212SPANYESJ.149 [DIRS 161274] should be considered qualified for its intended use in this analysis report. The source DTN: MO0212SPANYESJ.149 [DIRS 161274] will remain unqualified for other uses.



Data Qualification Plan

QA: QA
Page 1 of 1

Complete only applicable items.

Section I. Organizational Information		
Qualification Title Qualification of UE25 ONC-1 drawdown data during the 1996-97 hydraulic test of the Bullfrog Tuff at the C-wells and corresponding qualification of inputs from USGS Report: "Results of Hydraulic Tests in Miocene Tuffaceous Rocks at the C-Hole Complex, 1995 to 1997, Yucca Mountain, Nevada," by Geldon et al.		
Requesting Organization Los Alamos National Laboratory		
Section II. Process Planning Requirements		
1. List of Unqualified Data to be Evaluated Pressure data from transducer 9 in ONC-1 during 1996 and 1997, contained in DTN MO0212SPANYESJ.149. Qualification of these data will result in qualification of DTN GS030508312314.003 (USGS report cited in title above) which is unqualified because it contains data from transducer 9.		
2. Type of Data Qualification Method(s) [Including rationale for selection of method(s) (Attachment 3) and qualification attributes (Attachment 4)] The technical assessment and corroborating data methods will be used to qualify the unqualified data set for intended use in the SZ In-Situ Testing Analysis Report (ANL-NBS-HS-000039). The rationale for selecting these methods is: Qualified drawdown data were obtained from UE25c#2, WT#3 and USW H-4 during the 1996-97 hydraulic test. The ONC-1 drawdown data can be corroborated in a general sense with the drawdown responses in these wells by comparing the drawdown curves in the various wells after dividing time by the distance to the pumping well squared, and also by recognizing that ONC-1 should respond a bit more quickly but with a similar overall characteristic response as H-4 (since the two wells are in the same general direction from the C-wells). Also, technical assessment will be used to compare the pressure readings from two redundant pressure transducers in ONC-1, thus providing additional confidence in the data quality.		
3. Data Qualification Team and Additional Support Staff Required Paul Reimus (Qualification Chairperson) Mei Ding		
4. Data Evaluation Criteria Method 2, "Corroborating Data", and Method 5, "Technical Assessment", will be used to qualify the data using attributes 3 and 10 from Attachment 4 of SCI-PRO-001. The ONC-1 drawdown data will be evaluated against the qualified H-4 drawdown data to determine if the ONC-1 data follow the expected behavior for a well that is located in the same general direction, but closer to the pumping well, as H-4. Also, the ONC-1 data would be expected to follow a similar response curve as the other wells after dividing time by the distance to the pumping well squared. Good agreement (within 5%) of the relative readings of the two transducers in ONC-1 will provide additional confidence in the data quality. Because drawdown is measured relative to an initial pressure, accurate relative pressure readings are more important than accurate absolute pressure readings for drawdown analyses.		
5. Identification of Procedures Used SCI-PRO-005, Scientific Analyses		
Section III. Approval		
Qualification Chairperson Printed Name Paul W. Reimus	Qualification Chairperson Signature 	Date 3/1/07
Responsible Manager Printed Name Stephanie Kuzio	Responsible Manager Signature 	Date 3/2/07

SCI-PRO-001.1-R0

APPENDIX N

**QUALIFICATION OF NYE COUNTY CROSS-HOLE HYDRAULIC TESTING DATA
AT NC-EWDP SITE 22, MARCH 2002, AND AUGUST TO SEPTEMBER 2003; AND
CORROBORATIVE DATA FOR PUMP FLOW RATES MEASURED DURING
TRACER TESTS AT NC-EWDP SITE 22**

N1. INTRODUCTION

The qualification of the Nye County hydraulic testing data in individual zones at NC-EWDP Site 22 (contained in unqualified DTNs: LA0705PR150304.008 [DIRS 181203], LA0705PR150304.009 [DIRS 181204], LA0705PR150304.010 [DIRS 181205], LA0705PR150304.011 [DIRS 181207], and LA0705PR150304.012 [DIRS 181208]) is documented here in accordance with SCI-PRO-001, *Qualification of Unqualified Data*. This qualification provides the desired level of confidence that the data are suitable for their intended use, which is the estimation of hydrologic parameters in the saturated alluvium at Site 22 based on the pressure drawdown and recovery data in various isolated intervals in boreholes NC-EWDP-22S, -22PA, and -22PB and on the pump flow-rate data from pumping various zones in 22S (presented in Section 6.4, with additional details provided in Appendix F). The qualification is carried out in accordance with data qualification plan, *Qualification of NC-EWDP Site 22 Hydraulic Testing Data* (see Section N10). Additionally, the pump flow-rate data discussed in this appendix can serve as corroborative data for the flow rates measured with a Yucca Mountain Project (YMP) -calibrated flow meter during tracer testing at Site 22.

N2. BASES FOR SITE 22 HYDRAULIC TESTING DATA QUALIFICATION AND PUMP FLOW-RATE QUALIFICATION

This qualification is based on technical assessment, although it also involves consideration of Nye County technical procedures and corroborative data obtained during tracer testing at NC-EWDP Site 22 as part of the assessment. Specifically, the following items are considered:

1. Two Nye County technical procedures: TP-9.2, *Technical Procedure: Procedures for Operating Westbay Mosdax Groundwater Monitoring Equipment in Nye County Wells (Nye County Nuclear Waste Repository Project Office (NWRPO 2005 [DIRS 178608])*, and TP-10.0, *Technical Procedure: Pumping/Injection Tests of Packed-Off Zones in Unscreened Open Boreholes or in Multiple Screen Boreholes With or Without Observation Wells (NWRPO 2002 [DIRS 178607])*.
2. Vendor calibration records for key Westbay pressure transducers used in the cross-hole hydraulic tests at Nye County Site 22.
3. Nye County protocols for measuring and verifying pump flow rates (i.e., totalizing flow meters and barrel tests).
4. Cross-comparisons of pressure transducers used to measure atmospheric pressure (measured downhole pressures are corrected for fluctuations in atmospheric pressure).
5. Cross-comparisons of pressure transducer responses during hydraulic testing and tracer testing as a means of corroborating the pressure measurements during the hydraulic tests.

Only item 3 strictly applies to the corroborative data for pump flow rates measured during tracer testing. These flow rates are used primarily for estimating effective porosity in the alluvium based on tracer response times (see Appendix G, Section G5.4.3). The five items listed above are addressed in order in the following sections.

N3. NYE COUNTY TECHNICAL PROCEDURES

The two applicable technical procedures that Nye County personnel followed when conducting the hydraulic tests at NC-EWDP Site 22 were TP-9.2 (NWRPO 2005 [DIRS 178608]) and TP-10.0 (NWRPO 2002 [DIRS 178607]). These procedures were reviewed and found to be technically sound, and they are sufficiently descriptive that an independent investigator familiar with the testing equipment could quite easily reproduce the work. While the procedures and their supporting framework of procedures do not satisfy all the requirements of the Yucca Mountain/Lead Lab *Quality Assurance Requirements and Description* (DOE 2006 [DIRS 177092]), they are substantially equivalent in technical content to most YMP technical procedures, and following them should result in data of comparable technical quality to YMP-generated data (albeit with less stringent supporting procurement and vendor quality assurance requirements and less formal training, planning, documentation, and data management supporting requirements). The Nye County procedures reflect “standard industry practice” for conducting hydraulic tests that are used for water resource assessment and environmental remediation applications, and the data generated under the Nye County quality assurance program are certainly considered worthy of publication in peer-reviewed journals.

N4. VENDOR CALIBRATION RECORDS

Calibration records for key Westbay[®] Mosdax[®] pressure and temperature transducers used in the Site 22 hydraulic tests are included in Section N11. The serial numbers of the key transducers and the tests and borehole intervals in which they were used are listed in Table N-1.

Table N-1. Serial Numbers, Tests, and Borehole Intervals for Key Pressure Transducers Used in Site 22 Hydraulic and Tracer Tests

Serial Number	Mar 02, combined	Aug 03, zone 1	Aug 03, zone 2	Sept 03, zone 3	Sept 03, zone 4	Jan 05, zone 2	Aug 05, zone 2
2291	—	atm	atm	atm	atm	—	—
2292	—	—	—	—	—	atm	—
2295	atm	—	—	—	—	—	atm
2323	22S-pump	22S-pump	22S-pump	22S-pump	22S-pump	22S-Pump	22S-Pump
2554	atm	—	—	—	atm	atm	atm
2565	—	atm	—	—	—	—	—
2693	—	—	atm	atm	—	—	—
2844	22PA S	22PB D	22PB D	22PB D	22PB D	22PB S	22PB S
2845	22PA D	22PA D	22PA D	22PA D	22PA D	22PA S	22PA S
2846	22PB S	22PB S	22PB S	22PB S	22PB S	—	—
3363	22PB D	22PA S	22PA S	22PA S	22PA S	—	22PA D

NOTE: January 2005 and August 2005 tests were not used directly in hydraulic test interpretations but were used for corroboration.

atm = atmospheric pressure measurement, S = shallow piezometer pump = pumped interval, D = deep piezometer.

Table N-1 includes transducers that were used in 2005 cross-hole tracer tests, because these tests were used for cross-comparisons between transducers and between tests to establish corroborative verification of transducer performance (Section N7). Several other transducers were used during the tests, but the ones in the observation well intervals (22PA shallow and deep

and 22PB shallow and deep), at the 22S pumped interval, and at the surface (measuring atmospheric pressure) were considered the most important, as these were used directly in test interpretations. The isolated intervals in 22S that were not pumped in any given test were monitored primarily to ensure that there was no significant within-wellbore short-circuiting between the isolated intervals and the pumped interval during testing, so it was not critical that the transducers in these intervals have highly accurate measurements.

As Table N-1 shows, the same four transducers were used for the four observation-well intervals in all the hydraulic and tracer tests at Site 22 (although they were not always used in exactly the same interval in each test). Also, the same transducer was affixed to the pump string to measure pressures in the pumped interval in all tests. All the other transducers were used to measure atmospheric pressure for corrections to the downhole pressure measurements.

The vendor calibration records in Section N11 show that, with only two exceptions, each transducer met its calibration criteria both before and after it was used in the hydraulic or tracer tests. The exceptions are cases where a calibration was not conducted; there were no unsuccessful calibrations. One of the exceptions is the transducer (SN 2323) on the pump string, for which an “after” calibration was not conducted because the transducer was still on the pump string in 22S when this report was prepared. The other exception is a transducer used for atmospheric pressure corrections to observation well pressures in the January 2005 tracer test (SN 2292), which did not have a “before” calibration. However, this transducer was successfully cross-checked in December 2003 against another transducer that received before and after calibrations (see Section N6). Also, the atmospheric pressure measurements provided by transducer SN 2292 in the January 2005 tracer test (which was not analyzed for hydraulic responses) were not used directly in the cross-comparisons of Section N7, so the fact that this transducer did not receive a “before” calibration is of minor importance.

Although the transducer calibrations in Section N11 would not meet YMP quality assurance requirements (because the vendor is not a qualified supplier), the calibration records show that the transducers met industry-standard calibration expectations. It should be noted that accurate measurement of pressure *changes* are far more important in the hydraulic tests than the accurate measurement of absolute pressures. Thus, even if the calibrations conducted by the vendor lacked a high-pedigree absolute measurement standard, the fact that they demonstrated a high degree of accuracy in measuring pressure *changes* over the calibrated range is more important for the hydraulic test interpretations.

N5. NYE COUNTY MEASUREMENTS OF PUMPING RATES

Reasonably accurate measurements of pumping rates are important for hydraulic test interpretations, even if the interpretations are based primarily on pressure recoveries after pumping is stopped. They are also important for estimating effective porosities based on tracer responses in cross-hole tracer tests. The flow rates used in the site 22 hydraulic test interpretations were taken from *Preliminary Analysis of Pump-Spinner Tests and Pump Test in Well NC-EWDP-22s, Near Yucca Mountain, Nevada* (Questa Engineering Corporation 2003 [DIRS 178565]) and *Analysis of Aquifer Pump Tests in Individual Well Zones at Site 22 Near Yucca Mountain, Nevada* (Questa Engineering Company 2004 [DIRS 178566]), and these summary flow rates, in turn, were derived from field data recorded in Nye County Nuclear

Waste Repository Project Office Scientific Notebook SN-147 (Downing 2003 [DIRS 178771, pp. 14 to 74]. Nye County personnel did not use flow meters that were calibrated to YMP standards during hydraulic testing, but they did use industry-standard totalizing flow meters (which measure total volume that has passed through them but not rates directly). Flow rates were determined by measuring the amount of time for a given volume to be registered on the flow meter. These rates were frequently cross-checked with “barrel tests” in which flow rates were measured by determining the time to fill a barrel or drum of known volume with the pump discharge flow. TP-10.0 (NWRPO 2002 [DIRS 178607]), calls for periodic checks of flow-meter-based measurements with barrel tests, and if the flow-meter measurements are more than 5% different from the barrel tests, the barrel tests are to be used. Thus, the flow rates used in hydraulic test interpretations were based on flow-meter measurements verified by barrel tests, or in the case of poor agreement between the two, on the barrel test measurements alone.

During tracer testing, Nye County personnel used a flow meter provided by the U.S. Geological Survey and calibrated in accordance with YMP procedures. However, barrel tests were still conducted during tracer testing to provide a cross-check of the flow-meter measurements. These barrel-test measurements, which are documented in Nye County scientific notebooks SN-164 and SN-166, were in good agreement with the U.S. Geological Survey flow-meter readings and thus corroborated the accuracy of the meter measurements during the tracer tests. (Nye County Nuclear Waste Repository Project Office Scientific Notebooks SN-164 and SN-166, (entries made in 2004 and 2005) (Gilmore 2005 [DIRS 178621], 2005 [DIRS 178622]). The average flow rates used in the tracer test interpretations are provided in input DTNS: LA0612PR831231.001 [DIRS 178733], LA0612PR831231.002 [DIRS 178735], LA0612PR831231.003 [DIRS 178736], LA0612PR831231.004 [DIRS 178738], and LA0612PR831231.005 [DIRS 178739].

Barrel tests are commonly employed to measure flow rates in aquifer tests, and they are generally considered to be more accurate than most flow meters because volumes and times can be measured to a higher degree of accuracy than can direct flow-rate measurements. In fact, most flow meters are calibrated by measuring volumes passing through the flow meter in a specified time (or times associated with specified volumes). The Nye County procedure for relying on the barrel tests when there is disagreement between flow-meter measurements and barrel tests reflects this widespread experience and standard practice.

The combination of totalizing flow-meter measurements and verifying barrel tests for flow rate measurements is considered adequate for the Site 22 hydraulic test interpretations. Given the relatively wide range of hydraulic conductivities estimated using the interpretation methods discussed in Appendix F, an accuracy of plus or minus 10% in flow-rate measurements is considered acceptable. This level of accuracy was certainly achieved with the barrel tests.

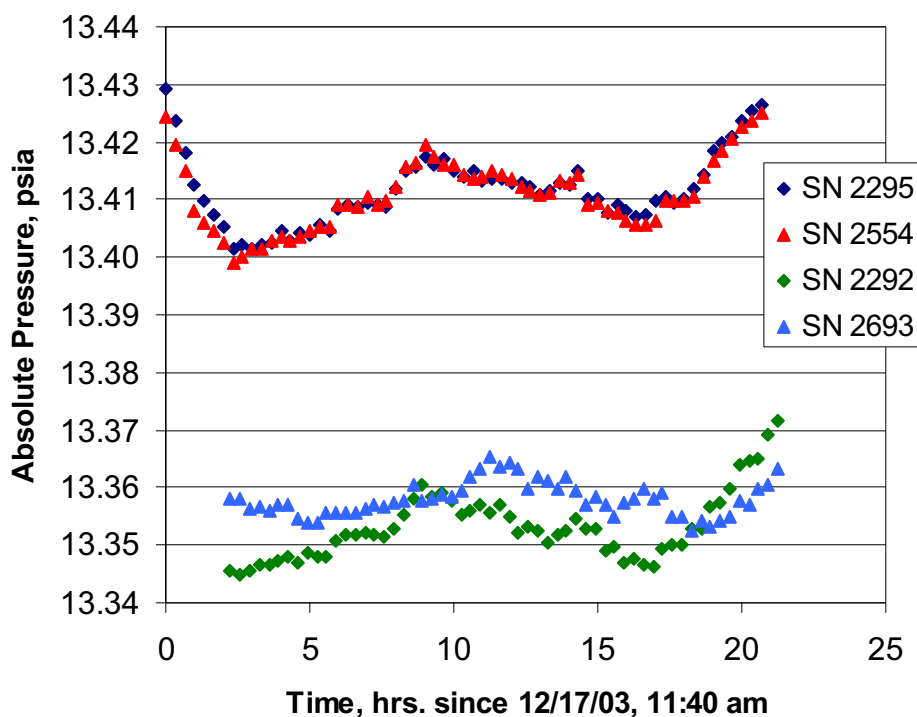
N6. CROSS-COMPARISONS OF PRESSURE TRANSDUCERS MEASURING ATMOSPHERIC PRESSURE

Transducers SN 2295 and SN 2554 were cross-checked against each other while measuring atmospheric pressure on 12/17/03 and 12/18/03 (after all hydraulic tests were conducted). Likewise, transducers SN 2292 and SN 2693 were cross-checked against each other on these same dates. These transducers were used for atmospheric pressure measurements, not downhole pressure measurements. All transducers except SN 2292 also had both before and after vendor calibrations. Thus, the cross-checks add confidence that the transducers provided accurate measurements.

Table N-1 (Section N4) shows that transducer SN 2292 was used only in the January 2005 tracer test. Because that test was used only for corroborative purposes, and atmospheric pressure corrections were not made in corroborative comparisons (Section N7) the cross-checking involving transducer SN 2292 is less important than the cross-checking of the other transducers. Nevertheless, both cross-comparisons are discussed here.

In the comparison between SN 2295 and SN 2554, the difference in absolute pressure measurements at the same time never exceeded 0.005 psi over a ~21-hr period. For SN 2292 and SN 2693, the difference in absolute pressure measurements at the same time never exceeded 0.013 psi over a ~19-hr period. Both of these comparisons passed the “bench calibration verification” criterion of no greater than a 0.1%-of-full-scale difference (0.03 psi for these transducers) stated in TP-9.2 (NWRPO 2005 [DIRS 178608]).

The absolute pressures recorded as a function of time for each transducer are plotted in Figure N-1. The SN 2295 to SN 2554 and SN 2292 to SN 2693 comparisons were conducted at different locations, so there are significant absolute pressure offsets between the two data sets. It is apparent that transducers SN 2295 and SN 2554 were in excellent agreement. Transducers SN 2292 and SN 2693 do not agree with each other as well, but they still pass the criteria of TP-9.2 (NWRPO 2005 [DIRS 178608]), and, more importantly, their differences are not great enough to be of concern in the hydraulic test interpretations.



Source: DTN: LA0705PR150304.006 [DIRS 181212].

NOTE: Time involved in these tests is approximately a 22-hour period on December 17 and 18, 2003.

Figure N-1. Absolute Pressures Measured by Four Transducers (SNs 2295, 2554, 2292, and 2693)

N7. CROSS-COMPARISONS OF PRESSURE TRANSDUCER DOWNHOLE MEASUREMENTS IN DIFFERENT TESTS AND AT DIFFERENT TIMES

In this section, the pressure drawdown data in the pumped interval of 22S and in observation wells 22PA and 22PB are compared in the early portion of tests conducted at Site 22 in August 2003, January 2005, and August 2005. Note that the latter two tests were not used for hydraulic test interpretations but rather for cross-checking of the pressure measurements of the transducers used in the earlier tests.

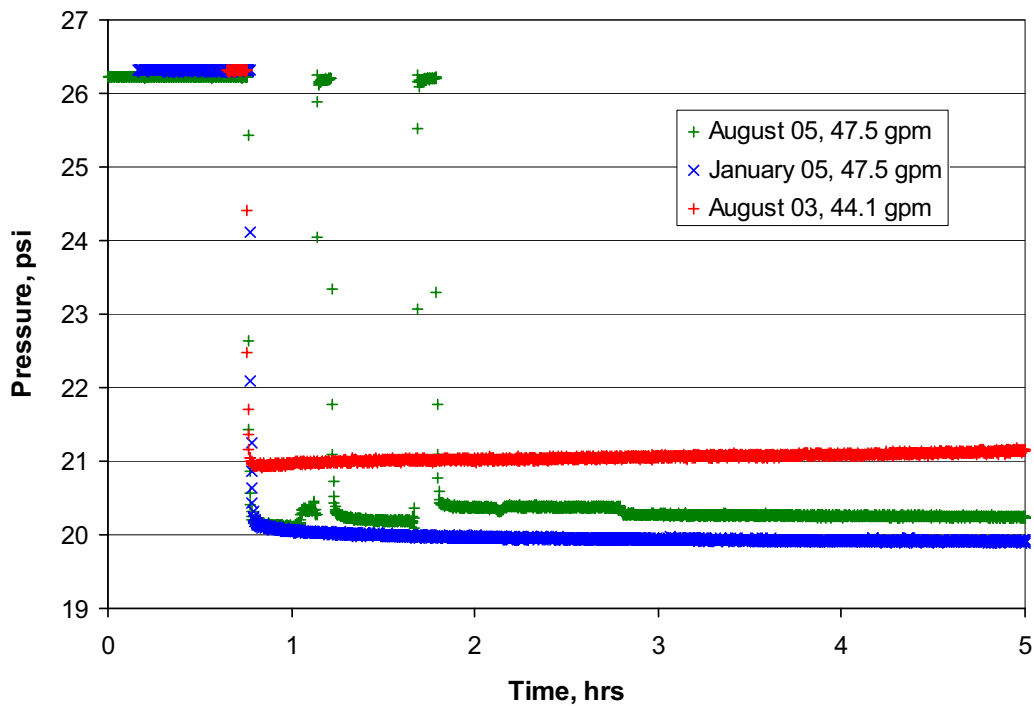
In each of the three tests mentioned above, the second interval of 22S was isolated and pumped while pressures were monitored in various intervals of 22PA and 22PB. The average pumping rate in August 2003 was 44.1 gal/min, and the rate in January 2005 and August 2005 was 47.5 gal/min. The deeper intervals in 22PA and 22PB were not monitored in January 2005. The deep interval in 22PA in this test had the YSI multiprobe installed for monitoring tracer concentrations after injection (see Section G4), and the deeper interval of 22PB would not have responded significantly in this test anyway based on responses in other tests in which zone 2 of 22S was pumped.

Table N-1 shows that even though the same four transducers were used to monitor the observation well pressures in all three tests, the transducers were changed around to monitor different intervals in different tests. This practice fortuitously provides an opportunity to

cross-check the various observation well transducers against each other in responding intervals in different tests. If the different transducers agree with each other in the same interval in the different tests, then there is increased confidence that the transducers were providing accurate pressure measurements for the hydraulic tests of March 2002 and August and September 2003. The same transducer (SN 2323) was used in the pumping well in all three tests, so such a cross-comparison is not possible for this transducer. However, the measurements of this transducer in each test can be compared to see if the transducer was providing consistent readings.

Figure N-2 shows the pressures recorded by transducer SN 2323 in the pumped interval of 22S (zone 2) in the first few hours of each test. The pressures have not been corrected for atmospheric pressure fluctuations. The times have been shifted so that the pumping starts at approximately the same time in each test on the plot. Also, the absolute pressures have been shifted so that they all have the same value prior to pumping (note that only the relative pressures are important in hydraulic test interpretations, not the absolute pressures). It is apparent that the pressure drawdown in the August 2003 test was significantly less than in the other two tests. However, this was expected because the pumping rate was lower in this test (44.1 gpm) than in the other two tests (47.5 gpm). The lower pumping rate would have resulted in less pressure drop in the pumped interval due to Darcy flow in the aquifer and also less pressure drop due to turbulence and friction losses in the system (i.e., well losses). The latter losses are not necessarily linear with flow rate, although they would probably not deviate significantly from linearity over such a narrow flow-rate range.

It is also apparent that the August 2005 test experienced some problems with the pump shutting down twice in about the first hour after initial startup, as indicated by the pressure recoveries and subsequent drawdowns. Some of the differences between the August 2003 test and the two later tests might also be attributed to changes in near-wellbore conditions in the second interval in 22S between the tests. Two tracer injections of about 20,000 gal. of water each were conducted in this interval in December 2004, with several days of pumping in between, and these significant inflows and outflows could have resulted in changes in flow resistance within the gravel pack.

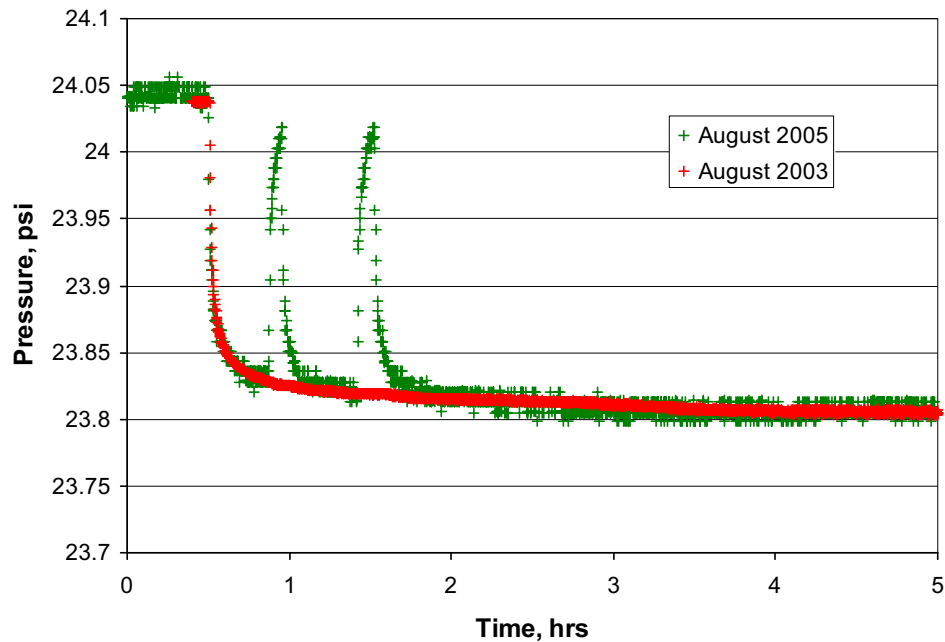


Source: DTN: LA0705PR150304.006 [DIRS 181212].

NOTE: Pressures were measured at the start of pumping of this isolated interval in August 2003, January 2005, and August 2005. Times and absolute pressures have been shifted so that they are approximately the same for each test.

Figure N-2. Pressures Measured in the Second Interval from the Surface of 22S by Transducer SN 2323

Figure N-3 shows the responses recorded by transducers SN 2845 and SN 3363 in the 22PA deep piezometer in August 2003 and August 2005, respectively. This interval corresponds to the pumping interval in 22S. The pressures have not been corrected for atmospheric pressure fluctuations, but they have been shifted so that the absolute pressures prior to pumping have approximately the same value. It is apparent that the two transducers yielded nearly identical pressure responses except for the spikes in 2005 associated with the brief pump shutdowns. The August 2003 pressure drop is slightly smaller than the August 2005 drop, but this is to be expected given that the pump flow rate was slightly lower in August 2003. This comparison indicates that the two transducers were in excellent agreement with each other, and it lends confidence to the accuracy of the pressure measurements provided by these transducers.

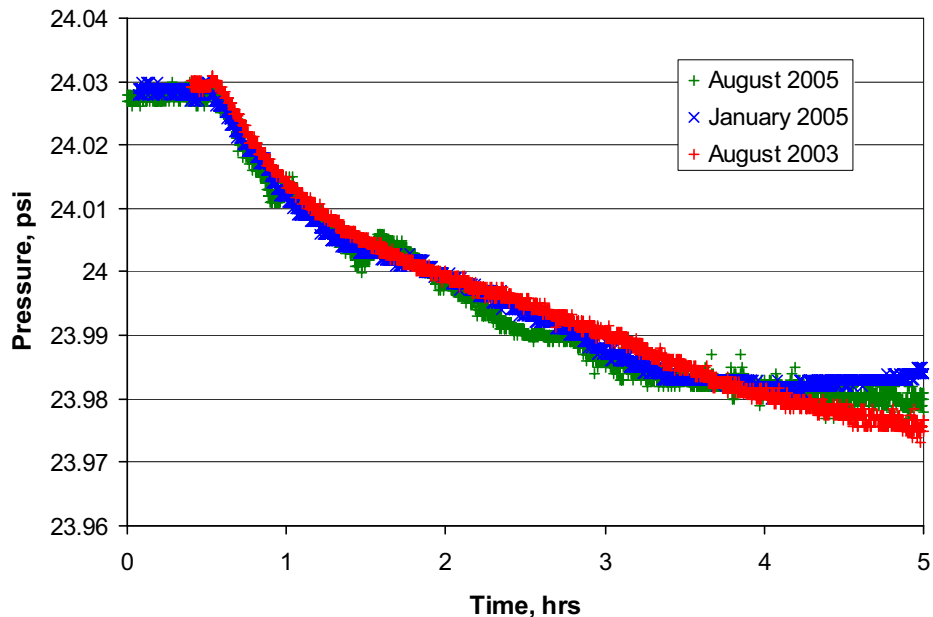


Source: DTN: LA0705PR150304.006 [DIRS 181212].

NOTE: August 2003 measurements by transducer SN 2845; August 2005 measurements by transducer SN 3363. Times and absolute pressures have been shifted so that they are approximately the same for each test.

Figure N-3. Pressures Measured in the 22PA Deep Piezometer at the Start of Pumping of Zone 2 of 22S

Figure N-4 shows the responses recorded by transducers SN 2844 and SN 2846 in the 22PB shallow piezometer in all three tests. This interval is directly below the pumping interval in 22S. The pressures have not been corrected for atmospheric pressure fluctuations, but they have been shifted so that the absolute pressures prior to pumping have approximately the same value. It is apparent that the two transducers yielded pressure responses that are in reasonably good agreement in all three tests. The responses are somewhat noisier than in Figures N-2 and N-3 because the pressure changes are significantly less in this interval than in the pumped interval.



Source: DTN: LA0705PR150304.006 [DIRS 181212].

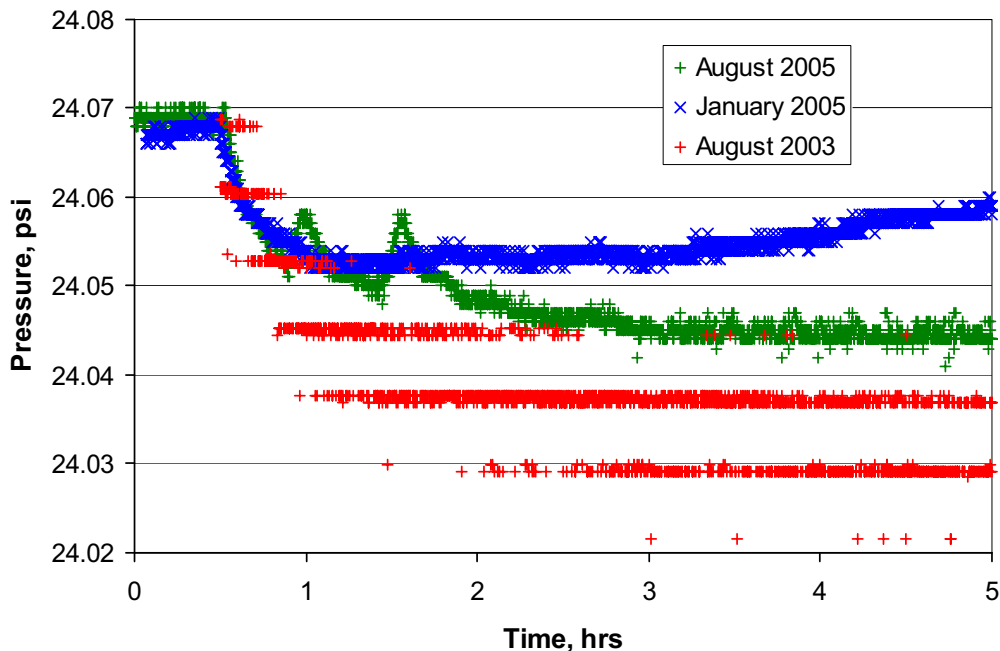
NOTE: August 2003 measurements by transducer SN 2846; January 2005 by transducer SN 2844; and August 2005 by transducer SN 2844. Times and absolute pressures have been shifted so that they are approximately the same for each test.

Figure N-4. Pressures Measured in the 22PB Shallow Piezometer at the Start of Pumping of Zone 2 of 22S

Note that the small spikes associated with the brief pump shutdowns are still evident in the August 2005 curve of Figure N-4. The deviation of the January 2005 curve from the other two curves at later times is probably due to a significant drift in the atmospheric pressure that occurred in this test but not in the other tests. This comparison indicates that the two transducers were in very good agreement with each other, and, in fact, the agreement between the different transducers in August 2003 and January 2005 is probably better than the agreement between the same transducer in January and August of 2005. This comparison lends confidence to the accuracy of the pressure measurements provided by these transducers.

Figure N-5 shows the responses recorded by transducers SN 2845 and SN 3363 in the 22PA shallow piezometer in all three tests. This interval is directly above the pumping interval in 22S. The pressures have not been corrected for atmospheric pressure fluctuations, but they have been shifted so that the absolute pressures prior to pumping have approximately the same value. This comparison is the most sensitive of any of the comparisons to measurement noise and atmospheric pressure fluctuations because this interval had the smallest pressure changes in response to pumping. Also, Figure N-5 shows that transducer SN 3363 has less measurement precision than transducer SN 2845 because it has a full-scale range of 250 psi instead of the 30-psi full-scale range of the other observation-well transducers. Nevertheless, it is apparent that the two transducers yielded pressure responses that are in reasonably good agreement in all three tests. The small spikes associated with the brief pump shutdowns are clearly evident in the August 2005 curve of Figure N-5. The deviation of the January 2005 curve from the other two

curves at later times can be attributed to a significant drift in the atmospheric pressure that occurred in this test but not in the other tests. This comparison indicates that the two transducers were in good agreement with each other, and it lends confidence to the accuracy of the pressure measurements provided by these transducers.



Source: DTN: LA0705PR150304.006 [DIRS 181212].

NOTE: August 2003 measurements by transducer SN 3363; January 2005 by transducer SN 2845; and August 2005 by transducer SN 2845. Times and absolute pressures have been shifted so that they are approximately the same for each test.

Figure N-5. Pressures Measured in the 22PA Shallow Piezometer at the Start of Pumping of Zone 2 of 22S

N8. SUMMARY

In summary, the qualifications of the Site 22 hydraulic test data and the corroboration of production flow rate data during the Site 22 tracer tests for their intended use in this analysis report are supported by:

- The technical soundness of the two Nye County technical procedures that were used when conducting the hydraulic tests: TP-9.2 (NWRPO 2005 [DIRS 178608]) and TP-10.0 (NWRPO 2002 [DIRS 178607])
- The successful vendor calibrations of the transducers before and after use for most of the transducers that were used in the hydraulic tests
- The technical soundness of Nye County methods for measuring and verifying pump flow rates (i.e., totalizing flow meters and barrel tests)

- Favorable cross-comparisons of atmospheric pressure measurements by pressure transducers used for these measurements in field tests
- Favorable cross-comparisons of downhole pressure transducer responses during hydraulic testing and tracer testing in August 2003, January 2005, and August 2005.

It is concluded that the Site 22 hydraulic testing data in DTNs: LA0705PR150304.008 [DIRS 181203], LA0705PR150304.009 [DIRS 181204], LA0705PR150304.010 [DIRS 181205], LA0705PR150304.011 [DIRS 181207], and LA0705PR150304.012 [DIRS 181208] should be considered qualified for their intended use in this report. These data will remain unqualified for other uses.

N9. DOCUMENTS CITED

Section not used.

N10. DATA QUALIFICATION PLAN



Data Qualification Plan

Complete only applicable items.

QA: QA
Page 1 of 1

Section I. Organizational Information		
Qualification Title Qualification of NC-EWDP Site 22 Hydraulic Testing Data		
Requesting Organization Los Alamos National Laboratory		
Section II. Process Planning Requirements		
1. List of Unqualified Data to be Evaluated Pressure transducer data and flow rate data obtained during pumping and recovery of each of the four individual screened intervals of NC-EWDP-22S in August and September of 2003. Also, pressure transducer and flow rate data obtained during pumping and recovery of the four combined screened intervals in NC-EWDP-22S in March 2002. In each case, NC-EWDP-22PA and NC-EWDP-22PB were used as observation wells for pressure responses, with -22PA having nested piezometers at the depth of the upper two intervals of -22S, and -22PB having nested piezometers at the depth of the lower two intervals of -22S. These data are to be qualified for intended use in the Saturated Zone In-Situ Testing Analysis Report (ANL-NBS-HS-000039, Rev. 2). The data will not be qualified for general use.		
2. Type of Data Qualification Method(s) [Including rationale for selection of method(s) (Attachment 3) and qualification attributes (Attachment 4)] The technical assessment method will be used to qualify the unqualified data sets for intended use in the SZ In-Situ Testing Analysis Report (ANL-NBS-HS-000039). The rationale for using technical assessment is that industry-standard practices appear to have been used and can be readily assessed by subject matter experts. The qualification team may consider in its assessment any or all of the following: (1) the Nye County technical procedure used (TP-10.0, <i>Pumping/Injection Tests of Packed-Off Zones in Unscreened open Boreholes or in Multiple Screen Boreholes with or without Observation Wells</i>), (2) the scientific notebook entries and calibration records provided by Nye County, (3) the final Nye County report on hydraulic testing at NC-EWDP Site 22 prepared by Questa Engineering (<i>Analysis of Aquifer Pump Tests in Individual Well Zones at Site 22 near Yucca Mountain, Nevada, NWRPO-2004-02</i>), (4) a comparison of pressure measurements by a Nye County transducer and a YMP downhole probe lowered on the same wireline, and (5) drawdown and recovery data obtained during forced-gradient tracer testing at NC-EWDP Site 22 between Dec. 2004 and Oct. 2005 (as potential corroborative data).		
3. Data Qualification Team and Additional Support Staff Required Paul W. Reimus (Qualification Chairperson) Elena Kalinina		
4. Data Evaluation Criteria Method 5, "Technical Assessment", will be used to qualify the data using attributes 1, 2, 3, 5, 9 and 12 from Attachment 4 of SCI-PRO-001.		
5. Identification of Procedures Used SCI-PRO-005, Scientific Analyses		
Section III. Approval		
Qualification Chairperson Printed Name Paul W. Reimus	Qualification Chairperson Signature 	Date 3/1/07
Responsible Manager Printed Name Stephanie Kuzio	Responsible Manager Signature 	Date 3/2/07

SCI-PRO-001.1-R0

N11. VENDOR PRESSURE TRANSDUCER CALIBRATION RECORDS

The last section of this appendix contains vendor calibration records for the Westbay[®] pressure transducers used during hydraulic and tracer testing at Site 22. The calibration records are presented in order of increasing transducer serial number, and the “before” calibrations are always presented before the “after” calibrations for any given transducer.

MOSDAX Calibration Report 1: MDL - 2291 Module 548

Full Scale: 30 (psia)

File: C:\ACVIEW\CALDATA\2001\30\12OCT01\00548

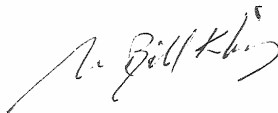
Pressure Reference: Paroscientific Model 230A-101 S/N 62671

Range: 30 PSI

Date of last reference to traceable standard: Aug 15 2000

MDL - 2291 Oct 11 16:27:11 2001 Range 1 Temp 3.3° C			MDL - 2291 Oct 11 10:50:48 2001 Range 2 Temp 15.3° C			MDL - 2291 Oct 11 05:14:56 2001 Range 3 Temp 25.3° C		
Ref Pres (psia)	Error (psia)	(% FS)	Ref Pres (psia)	Error (psia)	(% FS)	Ref Pres (psia)	Error (psia)	(% FS)
9.999	-0.008	-0.027	10.001	-0.004	-0.015	9.994	-0.009	-0.030
11.983	0.001	0.002	11.980	0.004	0.012	11.983	0.000	-0.001
13.978	0.004	0.013	13.977	0.008	0.027	13.978	0.004	0.012
15.970	0.003	0.009	15.974	0.008	0.027	15.967	0.002	0.006
17.966	0.001	0.004	17.974	0.006	0.021	17.970	0.000	0.001
19.959	-0.002	-0.007	19.961	0.005	0.016	19.960	-0.002	-0.008
21.952	-0.005	-0.016	21.946	0.002	0.008	21.950	-0.004	-0.015
23.942	-0.005	-0.018	23.948	0.001	0.003	23.945	-0.007	-0.022
25.934	-0.005	-0.017	25.933	0.002	0.006	25.950	-0.006	-0.020
27.927	-0.001	-0.005	27.921	0.006	0.019	27.929	-0.002	-0.007
29.940	0.007	0.022	29.926	0.014	0.048	29.923	0.006	0.019
27.919	-0.001	-0.004	27.919	0.005	0.017	27.934	-0.002	-0.007
25.967	-0.005	-0.017	25.926	0.002	0.006	25.928	-0.006	-0.021
23.969	-0.007	-0.023	23.955	0.000	0.002	23.939	-0.007	-0.022
21.983	-0.005	-0.016	21.967	0.002	0.007	21.966	-0.006	-0.020
19.988	-0.003	-0.009	19.985	0.003	0.008	19.981	-0.003	-0.009
17.987	0.000	0.001	17.990	0.007	0.022	17.981	0.000	-0.001
15.983	0.002	0.007	15.988	0.007	0.022	15.986	0.001	0.004
13.977	0.003	0.012	13.983	0.008	0.026	13.988	0.002	0.006
11.983	0.000	-0.001	11.985	0.003	0.010	11.995	-0.001	-0.002
9.985	-0.008	-0.025	9.995	-0.005	-0.015	9.997	-0.008	-0.027
MDL - 2291 Oct 10 23:38:46 2001 Range 4 Temp 35.2° C			MDL - 2291 Oct 10 18:08:07 2001 Range 5 Temp 50.2° C					
Ref Pres (psia)	Error (psia)	(% FS)	Ref Pres (psia)	Error (psia)	(% FS)			
9.990	-0.006	-0.021	10.000	-0.006	-0.021			
11.983	0.001	0.004	12.020	0.002	0.006			
13.973	0.006	0.019	13.977	0.007	0.023			
15.972	0.003	0.010	15.971	0.005	0.015			
17.968	0.001	0.005	17.964	0.004	0.013			
19.957	-0.001	-0.003	19.960	0.001	0.004			
21.946	-0.003	-0.011	21.950	-0.001	-0.002			
23.937	-0.005	-0.018	23.942	-0.002	-0.007			
25.930	-0.004	-0.013	25.929	-0.001	-0.005			
27.917	-0.001	-0.004	27.928	0.003	0.010			
29.922	0.007	0.024	29.920	0.011	0.036			
27.952	-0.001	-0.003	27.941	0.002	0.006			
25.986	-0.005	-0.018	25.992	-0.002	-0.005			
23.985	-0.006	-0.018	23.993	-0.003	-0.010			
21.979	-0.005	-0.016	21.995	-0.002	-0.008			
19.986	-0.001	-0.005	19.993	0.001	0.002			
17.982	0.001	0.005	17.990	0.003	0.009			
15.987	0.002	0.008	15.992	0.004	0.013			
13.981	0.004	0.014	13.990	0.006	0.021			
11.996	0.001	0.003	11.984	0.002	0.008			
9.998	-0.007	-0.022	9.997	-0.006	-0.021			

Issued by



Document: 5CAL 9607

Page 1 of 2



MOSDAX Calibration Report 2: MDL - 2291 Module 548

Full Scale: 30 (psia)

File: C:\ACPVIEW\CALDATA\2001130\112OCT01\00548

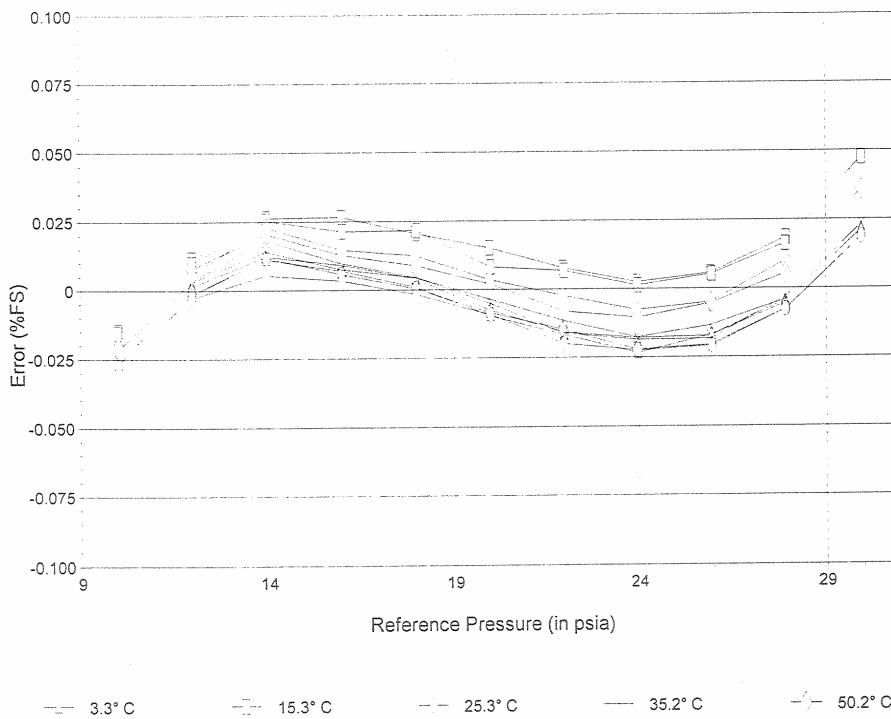
Pressure Reference: Paroscientific Model 230A-101 S/N 62671

Range: 30 PSI

Date of last reference to traceable standard: Aug 15 2000

Plot of Error vs. Reference Pressure

MDL - 2291 Module 548



Comments

Issued by *[Signature]*

Document: SCAL 9607

Page 2 of 2



As Received MOSDAX Cal. Report 1: MDL - 2291 Module 548

File: C:\ACPV\VIEW\CALDATA\2001\30\12OCT01\00548

Full Scale: 30 (psia)

Pressure Reference: Paroscientific Model 230A-101 S/N 62671

Range: 30 PSI

Date of last reference to traceable standard: Aug 15 2000

MDL - 2291 Oct 11 16:27:11 2001 Range 1 Temp 3.3° C			MDL - 2291 Oct 11 10:50:48 2001 Range 2 Temp 15.3° C			MDL - 2291 Oct 11 05:14:56 2001 Range 3 Temp 25.3° C		
Ref Pres (psia)	Error (psia)	(% FS)	Ref Pres (psia)	Error (psia)	(% FS)	Ref Pres (psia)	Error (psia)	(% FS)
9.999	-0.010	-0.033	10.001	-0.005	-0.018	9.994	-0.010	-0.033
11.983	-0.001	-0.004	11.980	0.003	0.008	11.983	-0.002	-0.005
13.978	0.002	0.008	13.977	0.007	0.023	13.978	0.002	0.008
15.970	0.002	0.006	15.974	0.007	0.024	15.967	0.000	0.002
17.966	0.001	0.002	17.974	0.005	0.018	17.970	-0.001	-0.004
19.959	-0.003	-0.009	19.961	0.004	0.012	19.960	-0.004	-0.013
21.952	-0.005	-0.016	21.946	0.001	0.005	21.950	-0.006	-0.020
23.942	-0.005	-0.017	23.948	0.000	0.000	23.945	-0.008	-0.028
25.934	-0.005	-0.016	25.933	0.001	0.003	25.950	-0.008	-0.026
27.927	-0.001	-0.003	27.921	0.005	0.016	27.929	-0.004	-0.013
29.940	0.007	0.024	29.926	0.014	0.046	29.923	0.004	0.013
27.919	-0.001	-0.002	27.919	0.004	0.014	27.934	-0.004	-0.014
25.967	-0.005	-0.015	25.926	0.001	0.003	25.928	-0.008	-0.026
23.969	-0.007	-0.023	23.955	0.000	-0.001	23.939	-0.008	-0.028
21.983	-0.005	-0.017	21.967	0.001	0.004	21.966	-0.008	-0.025
19.988	-0.003	-0.011	19.985	0.002	0.005	19.981	-0.004	-0.014
17.987	0.000	-0.001	17.990	0.006	0.019	17.981	-0.002	-0.006
15.983	0.001	0.004	15.988	0.006	0.018	15.986	0.000	-0.001
13.977	0.002	0.007	13.983	0.007	0.022	13.988	0.000	0.002
11.983	-0.002	-0.007	11.985	0.002	0.007	11.995	-0.002	-0.006
9.985	-0.010	-0.032	9.995	-0.006	-0.019	9.997	-0.009	-0.030
MDL - 2291 Oct 10 23:38:46 2001 Range 4 Temp 35.2° C			MDL - 2291 Oct 10 18:08:07 2001 Range 5 Temp 50.2° C					
Ref Pres (psia)	Error (psia)	(% FS)	Ref Pres (psia)	Error (psia)	(% FS)			
9.990	-0.008	-0.028	10.000	-0.011	-0.037			
11.983	-0.001	-0.003	12.020	-0.002	-0.008			
13.973	0.004	0.012	13.977	0.003	0.010			
15.972	0.001	0.003	15.971	0.001	0.002			
17.968	-0.001	-0.002	17.964	0.000	0.000			
19.957	-0.003	-0.011	19.960	-0.003	-0.010			
21.946	-0.006	-0.019	21.950	-0.005	-0.016			
23.937	-0.008	-0.026	23.942	-0.007	-0.023			
25.930	-0.007	-0.022	25.929	-0.006	-0.022			
27.917	-0.004	-0.014	27.928	-0.003	-0.009			
29.922	0.004	0.013	29.920	0.005	0.015			
27.952	-0.004	-0.013	27.941	-0.004	-0.013			
25.986	-0.008	-0.027	25.992	-0.007	-0.022			
23.985	-0.008	-0.027	23.993	-0.008	-0.026			
21.979	-0.007	-0.024	21.995	-0.007	-0.022			
19.986	-0.004	-0.012	19.993	-0.003	-0.011			
17.982	-0.001	-0.002	17.990	-0.001	-0.004			
15.987	0.000	0.001	15.992	0.000	0.000			
13.981	0.002	0.008	13.990	0.002	0.007			
11.996	-0.001	-0.003	11.984	-0.002	-0.006			
9.998	-0.008	-0.028	9.997	-0.011	-0.036			

Issued by 



As Received MOSDAX Cal. Report 2: MDL - 2291 Module 548

Full Scale: 30 (psia)

File: C:\ACPVIEW\CALDATA\2001130112OCT01\00548

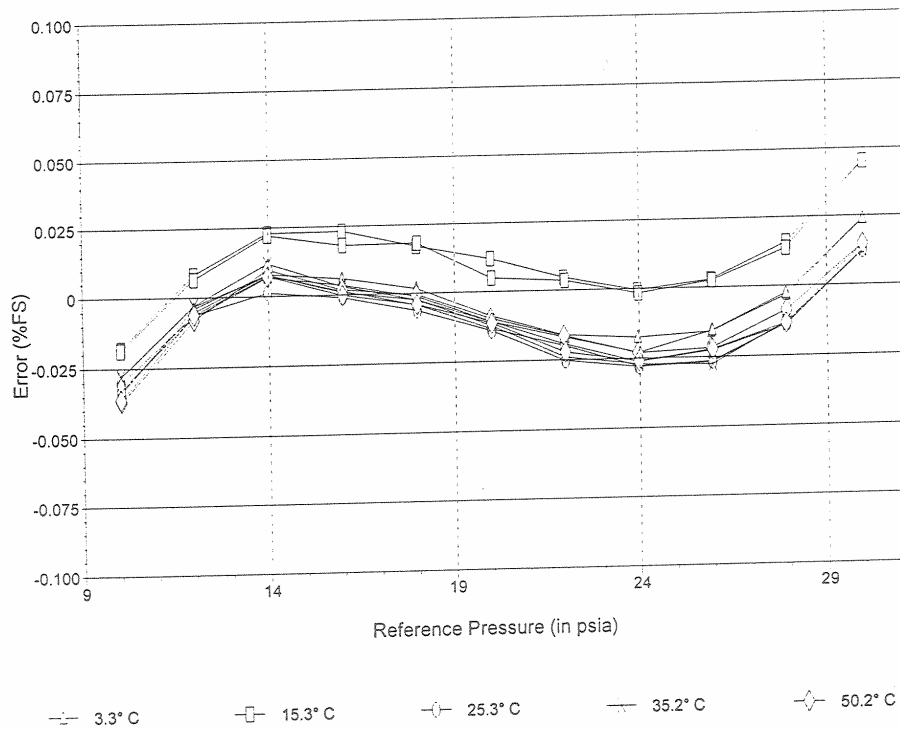
Pressure Reference: Paroscientific Model 230A-101 S/N 62671

Range: 30 PSI

Date of last reference to traceable standard: Aug 15 2000

Plot of Error vs. Reference Pressure

MDL - 2291 Module 548



Comments

Issued by *Neil Gill King*

Document: SCAL 9607

Page 2 of 2



MOSDAX Calibration Report 1: MDL - 2291 Module 548

Full Scale: 30 (psia)

File: C:\ACPVIEW\CALDATA\2004\30\30JULY04\00548

Pressure Reference: Paroscientific Model 230A-101 S/N 90098

Range: 30 PSI

Date of last reference to traceable standard: Dec 10 2002

MDL - 2291 Jul 30 04:44:06 2004 Range 1 Temp 3.6° C			MDL - 2291 Jul 29 23:41:38 2004 Range 2 Temp 15.0° C			MDL - 2291 Jul 29 18:39:10 2004 Range 3 Temp 24.5° C		
Ref Pres (psia)	Error (psia)	(% FS)	Ref Pres (psia)	Error (psia)	(% FS)	Ref Pres (psia)	Error (psia)	(% FS)
10.034	-0.007	-0.024	10.053	-0.004	-0.013	10.030	-0.007	-0.023
11.976	0.000	-0.001	11.982	0.005	0.016	11.982	0.000	0.000
13.978	0.003	0.009	14.009	0.009	0.029	13.985	0.004	0.013
15.912	0.002	0.008	15.957	0.008	0.027	15.983	0.003	0.010
17.976	0.001	0.002	17.944	0.007	0.024	17.940	0.002	0.006
19.899	-0.002	-0.008	19.950	0.005	0.016	19.933	-0.001	-0.004
21.892	-0.005	-0.016	21.922	0.003	0.009	21.963	-0.005	-0.016
23.919	-0.006	-0.021	23.911	0.002	0.006	23.938	-0.005	-0.018
25.880	-0.006	-0.020	25.901	0.003	0.011	25.879	-0.005	-0.018
27.898	-0.003	-0.010	27.914	0.007	0.024	27.865	-0.001	-0.005
29.900	0.006	0.020	29.910	0.015	0.051	29.892	0.007	0.024
27.935	-0.004	-0.013	27.987	0.006	0.019	27.970	-0.003	-0.009
25.954	-0.007	-0.024	25.970	0.002	0.007	25.982	-0.007	-0.022
23.978	-0.008	-0.025	23.940	0.001	0.002	23.972	-0.007	-0.023
21.982	-0.006	-0.021	21.859	0.002	0.007	21.857	-0.005	-0.016
19.911	-0.003	-0.010	19.972	0.004	0.014	19.994	-0.003	-0.009
17.992	-0.001	-0.003	18.037	0.006	0.021	18.028	0.000	-0.001
15.993	0.001	0.002	16.027	0.008	0.026	16.033	0.002	0.006
13.966	0.002	0.005	14.031	0.008	0.027	14.007	0.003	0.009
12.003	-0.001	-0.005	11.996	0.004	0.014	12.003	-0.001	-0.003
10.001	-0.009	-0.030	10.015	-0.004	-0.014	10.035	-0.008	-0.028
MDL - 2291 Jul 29 13:37:06 2004 Range 4 Temp 33.8° C			MDL - 2291 Jul 29 08:34:45 2004 Range 5 Temp 47.8° C					
Ref Pres (psia)	Error (psia)	(% FS)	Ref Pres (psia)	Error (psia)	(% FS)			
10.037	-0.008	-0.027	10.019	-0.006	-0.020			
11.982	-0.001	-0.003	11.972	0.001	0.004			
14.020	0.004	0.012	14.001	0.005	0.018			
15.994	0.002	0.006	15.967	0.004	0.013			
17.972	0.001	0.002	17.927	0.002	0.007			
19.913	-0.003	-0.008	19.967	0.001	0.002			
21.938	-0.005	-0.016	21.909	-0.002	-0.007			
23.961	-0.007	-0.022	23.931	-0.004	-0.012			
25.944	-0.006	-0.019	25.883	-0.004	-0.012			
27.944	-0.003	-0.009	27.870	0.001	0.002			
29.839	0.006	0.020	29.902	0.010	0.032			
27.958	-0.002	-0.006	27.935	0.000	0.001			
25.949	-0.007	-0.023	25.974	-0.004	-0.013			
23.998	-0.008	-0.026	24.028	-0.005	-0.017			
21.871	-0.007	-0.023	21.969	-0.003	-0.011			
19.997	-0.003	-0.012	19.986	-0.001	-0.005			
18.006	0.000	-0.001	17.998	0.001	0.003			
16.074	0.001	0.005	16.041	0.002	0.008			
14.022	0.003	0.010	14.038	0.005	0.017			
12.037	0.000	-0.001	12.008	0.000	0.002			
9.992	-0.008	-0.028	10.009	-0.007	-0.024			

Issued by



Document: SCAL 9607

Page 1 of 2



MOSDAX Calibration Report 2: MDL - 2291 Module 548

Full Scale: 30 (psia)

File: C:\ACP\VIEW\CALDATA\2004\30\30JULY04\00548

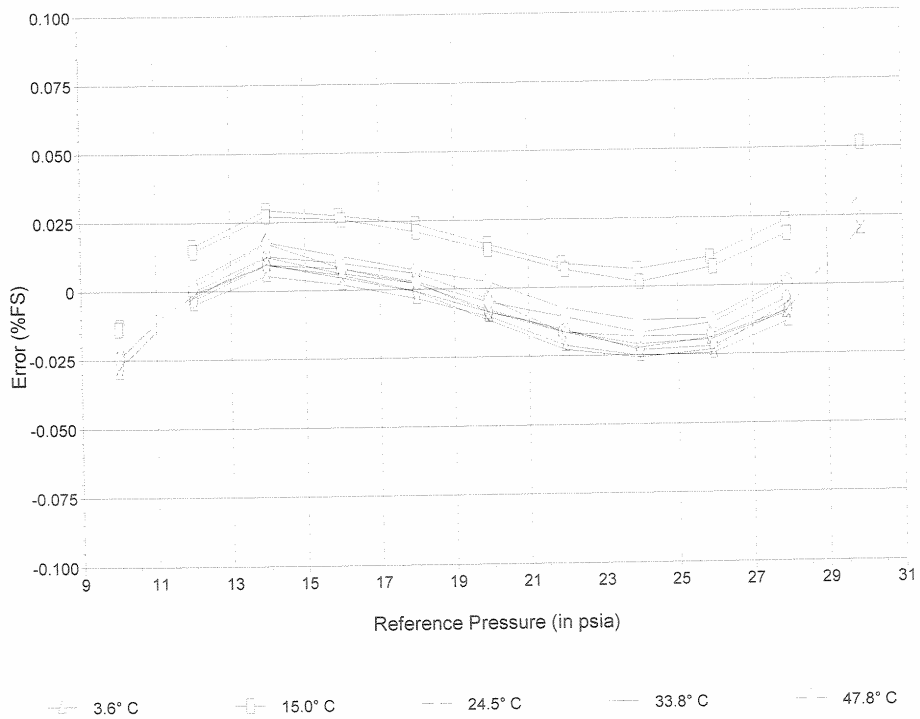
Pressure Reference: Paroscientific Model 230A-101 S/N 90098

Range: 30 PSI

Date of last reference to traceable standard: Dec 10 2002

Plot of Error vs. Reference Pressure

MDL - 2291 Module 548



Comments

Issued by

Document: 5CAL 9607

Page 2 of 2



As Received MOSDAX Cal. Report 1: MDL - 2291 Module 548

Full Scale: 30 (psia)

File: C:\ACPVIEW\CALDATA\2004\130\30JULY04\00548

Pressure Reference: Paroscientific Model 230A-101 S/N 90098

Range: 30 PSI

Date of last reference to traceable standard: Dec 10 2002

MDL - 2291 Jul 30 04:44:06 2004 Range 1 Temp 3.6° C			MDL - 2291 Jul 29 23:41:38 2004 Range 2 Temp 15.0° C			MDL - 2291 Jul 29 18:39:10 2004 Range 3 Temp 24.5° C		
Ref Pres (psia)	Error (psia)	(% FS)	Ref Pres (psia)	Error (psia)	(% FS)	Ref Pres (psia)	Error (psia)	(% FS)
10.034	0.004	0.012	10.053	0.006	0.020	10.030	0.003	0.010
11.976	0.011	0.036	11.982	0.015	0.049	11.982	0.010	0.033
13.978	0.015	0.048	14.009	0.019	0.064	13.985	0.014	0.047
15.912	0.015	0.049	15.957	0.019	0.063	15.983	0.014	0.045
17.976	0.013	0.045	17.944	0.018	0.060	17.940	0.013	0.042
19.899	0.011	0.037	19.950	0.016	0.054	19.933	0.010	0.034
21.892	0.009	0.030	21.922	0.014	0.048	21.963	0.007	0.022
23.919	0.008	0.027	23.911	0.014	0.048	23.938	0.007	0.022
25.880	0.009	0.031	25.901	0.016	0.054	25.879	0.007	0.024
27.898	0.013	0.042	27.914	0.021	0.069	27.865	0.012	0.039
29.900	0.022	0.075	29.910	0.029	0.098	29.892	0.021	0.069
27.935	0.012	0.039	27.987	0.019	0.064	27.970	0.010	0.035
25.954	0.008	0.026	25.970	0.015	0.050	25.982	0.006	0.020
23.978	0.007	0.023	23.940	0.013	0.043	23.972	0.005	0.017
21.982	0.008	0.025	21.859	0.014	0.046	21.857	0.007	0.023
19.911	0.010	0.034	19.972	0.016	0.052	19.994	0.009	0.029
17.992	0.012	0.039	18.037	0.017	0.058	18.028	0.011	0.035
15.993	0.013	0.043	16.027	0.018	0.061	16.033	0.012	0.041
13.966	0.013	0.044	14.031	0.018	0.062	14.007	0.013	0.044
12.003	0.010	0.033	11.996	0.014	0.048	12.003	0.009	0.030
10.001	0.002	0.006	10.015	0.006	0.019	10.035	0.002	0.005
MDL - 2291 Jul 29 13:37:06 2004 Range 4 Temp 33.8° C			MDL - 2291 Jul 29 08:34:45 2004 Range 5 Temp 47.8° C					
Ref Pres (psia)	Error (psia)	(% FS)	Ref Pres (psia)	Error (psia)	(% FS)			
10.037	0.003	0.008	10.019	0.006	0.020			
11.982	0.010	0.033	11.972	0.013	0.045			
14.020	0.015	0.049	14.001	0.018	0.060			
15.994	0.013	0.044	15.967	0.017	0.056			
17.972	0.012	0.041	17.927	0.016	0.052			
19.913	0.009	0.031	19.967	0.015	0.049			
21.938	0.007	0.025	21.909	0.012	0.041			
23.961	0.006	0.020	23.931	0.011	0.038			
25.944	0.008	0.025	25.883	0.012	0.040			
27.944	0.011	0.036	27.870	0.017	0.056			
29.839	0.020	0.068	29.902	0.026	0.088			
27.958	0.012	0.039	27.935	0.016	0.054			
25.949	0.006	0.021	25.974	0.012	0.038			
23.998	0.005	0.017	24.028	0.010	0.033			
21.871	0.005	0.018	21.969	0.011	0.038			
19.997	0.008	0.028	19.986	0.013	0.042			
18.006	0.011	0.038	17.998	0.014	0.048			
16.074	0.013	0.042	16.041	0.016	0.052			
14.022	0.014	0.046	14.038	0.018	0.060			
12.037	0.010	0.035	12.008	0.013	0.043			
9.992	0.002	0.007	10.009	0.005	0.016			

Issued by



Document: SCAL 9607

Page 1 of 2



As Received MOSDAX Cal. Report 2: MDL - 2291 Module 548

Full Scale: 30 (psia)

File: C:\ACPVIEW\CALDATA\2004\30\30JULY04\00548

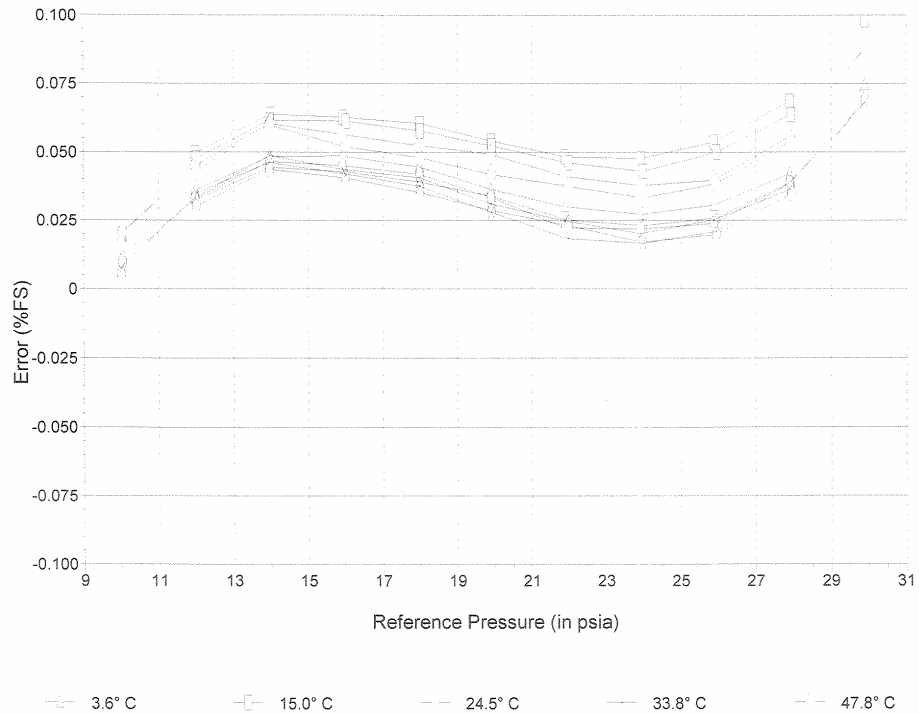
Pressure Reference: Paroscientific Model 230A-101 S/N 90098

Range: 30 PSI

Date of last reference to traceable standard: Dec 10 2002

Plot of Error vs. Reference Pressure

MDL - 2291 Module 548



Comments

Issued by

Document: SCAL 9607

Page 2 of 2



MOSDAX Calibration Report 1: MDL - 2292 Module 528

Full Scale: 30 (psia)

File: C:\ACPVIEW\CALDATA\2004\30\30JULY04\00528

Pressure Reference: Paroscientific Model 230A-101 S/N 90098

Range: 30 PSI

Date of last reference to traceable standard: Dec 10 2002

MDL - 2292 Jul 30 04:44:06 2004 Range 1 Temp 3.6° C			MDL - 2292 Jul 29 23:41:38 2004 Range 2 Temp 15.0° C			MDL - 2292 Jul 29 18:39:10 2004 Range 3 Temp 24.5° C		
Ref Pres (psia)	Error (psia)	(% FS)	Ref Pres (psia)	Error (psia)	(% FS)	Ref Pres (psia)	Error (psia)	(% FS)
10.034	-0.004	-0.013	10.053	-0.001	-0.005	10.030	-0.007	-0.022
11.976	0.000	0.000	11.982	0.003	0.011	11.982	-0.001	-0.003
13.978	0.002	0.008	14.009	0.006	0.019	13.985	0.002	0.006
15.912	0.003	0.011	15.957	0.005	0.016	15.983	0.000	0.000
17.976	0.001	0.003	17.944	0.004	0.014	17.940	0.000	0.000
19.899	-0.001	-0.004	19.950	0.004	0.014	19.933	-0.002	-0.005
21.892	-0.002	-0.006	21.922	0.004	0.012	21.963	-0.002	-0.007
23.919	-0.003	-0.009	23.911	0.003	0.008	23.938	-0.003	-0.010
25.880	-0.002	-0.007	25.901	0.003	0.010	25.879	-0.003	-0.009
27.898	-0.002	-0.007	27.914	0.005	0.018	27.865	-0.001	-0.003
29.900	0.004	0.014	29.910	0.011	0.036	29.892	0.006	0.018
27.935	-0.001	-0.005	27.987	0.006	0.019	27.970	-0.001	-0.004
25.954	-0.004	-0.012	25.970	0.003	0.009	25.982	-0.003	-0.011
23.978	-0.003	-0.010	23.940	0.002	0.005	23.972	-0.003	-0.011
21.982	-0.002	-0.006	21.859	0.004	0.012	21.857	-0.002	-0.008
19.911	-0.001	-0.005	19.972	0.003	0.011	19.994	-0.001	-0.005
17.992	0.001	0.002	18.037	0.004	0.014	18.028	0.000	-0.002
15.993	0.001	0.004	16.027	0.004	0.013	16.033	0.000	0.000
13.966	0.003	0.010	14.031	0.006	0.021	14.007	0.002	0.006
12.003	0.000	-0.001	11.996	0.003	0.010	12.003	-0.001	-0.003
10.001	-0.004	-0.012	10.015	-0.003	-0.010	10.035	-0.006	-0.019
MDL - 2292 Jul 29 13:37:06 2004 Range 4 Temp 33.8° C			MDL - 2292 Jul 29 08:34:45 2004 Range 5 Temp 47.8° C					
Ref Pres (psia)	Error (psia)	(% FS)	Ref Pres (psia)	Error (psia)	(% FS)			
10.037	-0.005	-0.016	10.019	-0.004	-0.014			
11.982	-0.001	-0.003	11.972	0.001	0.005			
14.020	0.002	0.007	14.001	0.003	0.011			
15.994	0.001	0.002	15.967	0.002	0.006			
17.972	0.000	0.001	17.927	0.002	0.006			
19.913	-0.002	-0.005	19.967	0.001	0.003			
21.938	-0.002	-0.006	21.909	0.000	-0.001			
23.961	-0.004	-0.013	23.931	-0.002	-0.007			
25.944	-0.004	-0.013	25.883	-0.001	-0.005			
27.944	-0.002	-0.006	27.870	0.001	0.002			
29.839	0.003	0.011	29.902	0.007	0.022			
27.958	-0.001	-0.005	27.935	0.000	0.001			
25.949	-0.004	-0.015	25.974	-0.002	-0.007			
23.998	-0.005	-0.017	24.028	-0.003	-0.011			
21.871	-0.003	-0.010	21.969	-0.001	-0.005			
19.997	-0.002	-0.005	19.986	-0.001	-0.003			
18.006	-0.002	-0.006	17.998	0.001	0.003			
16.074	-0.001	-0.003	16.041	0.001	0.003			
14.022	0.001	0.004	14.038	0.003	0.011			
12.037	-0.001	-0.002	12.008	0.000	0.000			
9.992	-0.006	-0.020	10.009	-0.004	-0.015			

Issued by



Document: 5CAL 9607

Page 1 of 2



MOSDAX Calibration Report 2: MDL - 2292 Module 528

Full Scale: 30 (psia)

File: C:\ACPVIEW\CALDATA\2004\10\30\JULY04\00528

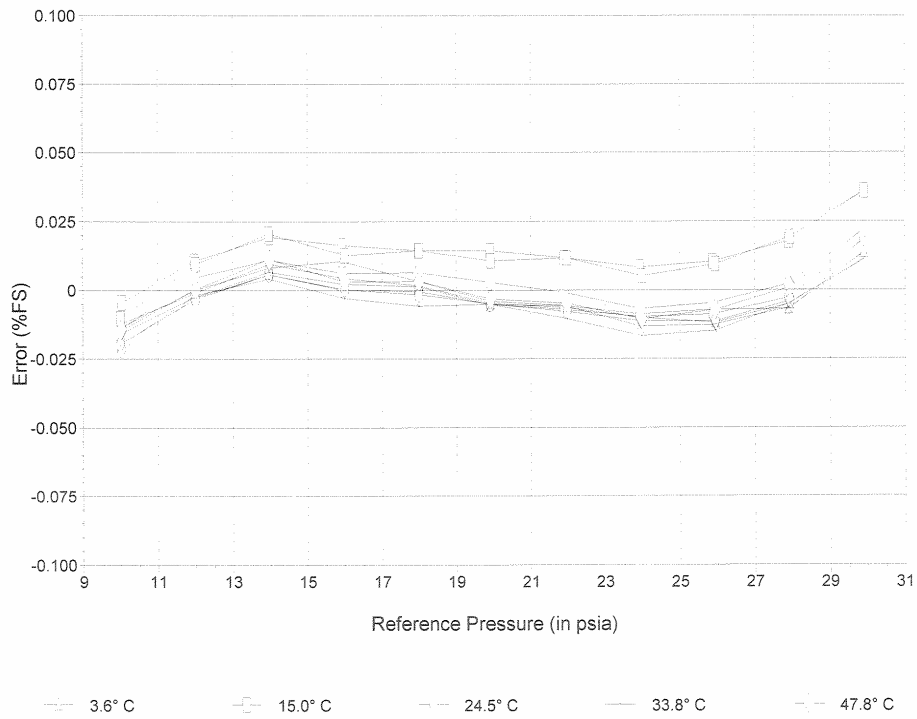
Pressure Reference: Paroscientific Model 230A-101 S/N 90098

Range: 30 PSI

Date of last reference to traceable standard: Dec 10 2002

Plot of Error vs. Reference Pressure

MDL - 2292 Module 528



Comments

Issued by *[Signature]*

Document: SCAL 9607

Page 2 of 2



As Received MOSDAX Cal. Report 1: MDL - 2292 Module 528

Full Scale: 30 (psia)

File: C:\ACPVIEW\CALDATA\2004\30\30JULY04\00528

Pressure Reference: Paroscientific Model 230A-101 S/N 90098

Range: 30 PSI

Date of last reference to traceable standard: Dec 10 2002

MDL - 2292 Jul 30 04:44:06 2004 Range 1 Temp 3.6° C			MDL - 2292 Jul 29 23:41:38 2004 Range 2 Temp 15.0° C			MDL - 2292 Jul 29 18:39:10 2004 Range 3 Temp 24.5° C		
Ref Pres (psia)	Error (psia)	(% FS)	Ref Pres (psia)	Error (psia)	(% FS)	Ref Pres (psia)	Error (psia)	(% FS)
10.034	-0.002	-0.007	10.053	0.001	0.003	10.030	-0.004	-0.014
11.976	0.002	0.006	11.982	0.005	0.017	11.982	0.001	0.004
13.978	0.004	0.014	14.009	0.008	0.025	13.985	0.004	0.012
15.912	0.005	0.016	15.957	0.007	0.022	15.983	0.002	0.006
17.976	0.003	0.009	17.944	0.006	0.020	17.940	0.001	0.005
19.899	0.001	0.002	19.950	0.006	0.020	19.933	0.000	0.000
21.892	0.000	0.000	21.922	0.005	0.018	21.963	-0.001	-0.002
23.919	-0.001	-0.002	23.911	0.004	0.014	23.938	-0.001	-0.005
25.880	0.000	0.000	25.901	0.005	0.017	25.879	-0.001	-0.004
27.898	0.000	0.001	27.914	0.007	0.025	27.865	0.001	0.003
29.900	0.007	0.022	29.910	0.013	0.044	29.892	0.007	0.025
27.935	0.001	0.003	27.987	0.008	0.026	27.970	0.000	0.002
25.954	-0.001	-0.005	25.970	0.005	0.016	25.982	-0.002	-0.006
23.978	-0.001	-0.004	23.940	0.003	0.011	23.972	-0.002	-0.007
21.982	0.000	0.000	21.859	0.005	0.017	21.857	-0.001	-0.003
19.911	0.000	0.001	19.972	0.005	0.016	19.994	0.000	0.000
17.992	0.002	0.007	18.037	0.006	0.020	18.028	0.001	0.003
15.993	0.003	0.010	16.027	0.006	0.018	16.033	0.002	0.006
13.966	0.005	0.015	14.031	0.008	0.027	14.007	0.004	0.012
12.003	0.001	0.005	11.996	0.005	0.016	12.003	0.001	0.004
10.001	-0.002	-0.006	10.015	-0.001	-0.003	10.035	-0.004	-0.012
MDL - 2292 Jul 29 13:37:06 2004 Range 4 Temp 33.8° C			MDL - 2292 Jul 29 08:34:45 2004 Range 5 Temp 47.8° C					
Ref Pres (psia)	Error (psia)	(% FS)	Ref Pres (psia)	Error (psia)	(% FS)			
10.037	-0.003	-0.009	10.019	-0.004	-0.015			
11.982	0.001	0.003	11.972	0.001	0.003			
14.020	0.003	0.011	14.001	0.003	0.009			
15.994	0.002	0.006	15.967	0.001	0.004			
17.972	0.001	0.005	17.927	0.001	0.004			
19.913	-0.001	-0.002	19.967	0.000	0.001			
21.938	-0.001	-0.003	21.909	-0.001	-0.003			
23.961	-0.003	-0.010	23.931	-0.003	-0.009			
25.944	-0.003	-0.010	25.883	-0.002	-0.007			
27.944	-0.001	-0.004	27.870	0.000	0.000			
29.839	0.004	0.015	29.902	0.006	0.019			
27.958	-0.001	-0.002	27.935	-0.001	-0.002			
25.949	-0.004	-0.012	25.974	-0.003	-0.010			
23.998	-0.004	-0.014	24.028	-0.004	-0.013			
21.871	-0.002	-0.008	21.969	-0.002	-0.007			
19.997	-0.001	-0.002	19.986	-0.002	-0.006			
18.006	-0.001	-0.002	17.998	0.000	0.001			
16.074	0.000	0.001	16.041	0.000	0.001			
14.022	0.003	0.009	14.038	0.003	0.010			
12.037	0.001	0.004	12.008	0.000	-0.001			
9.992	-0.004	-0.014	10.009	-0.005	-0.016			

Issued by 

Document: SCAL 9607

Page 1 of 2



As Received MOSDAX Cal. Report 2: MDL - 2292 Module 528

Full Scale: 30 (psia)

File: C:\ACPVIEW\CALDATA\2004\30\30JULY04\00528

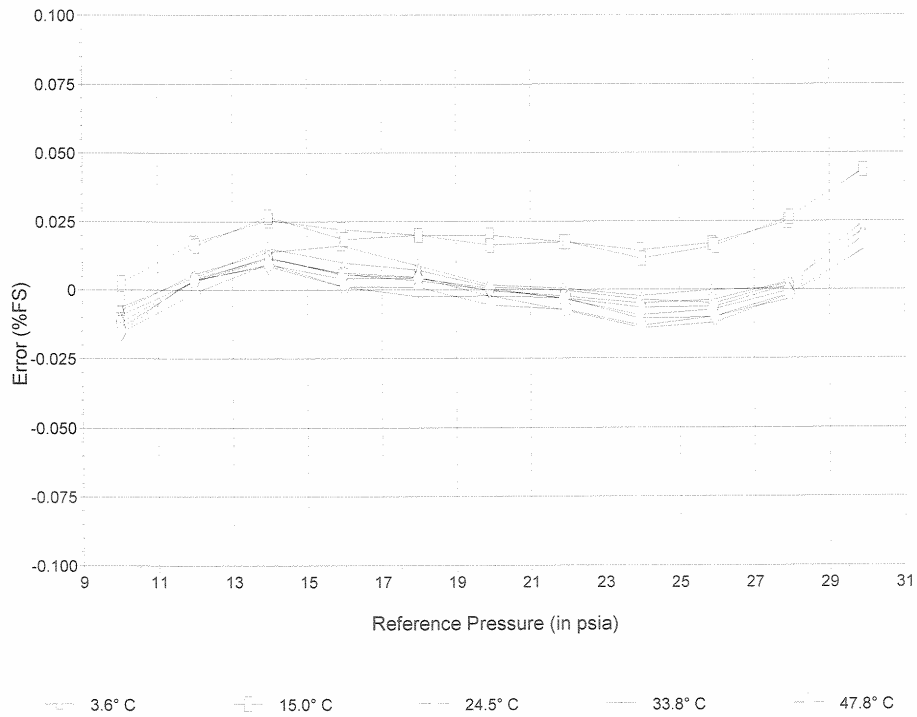
Pressure Reference: Paroscientific Model 230A-101 S/N 90098

Range: 30 PSI

Date of last reference to traceable standard: Dec 10 2002

Plot of Error vs. Reference Pressure

MDL - 2292 Module 528



Comments

Issued by *[Signature]*

Document: SCAL 9607

Page 2 of 2



MOSDAX Calibration Report 1: MDL - 2295 Module 276

Full Scale: 30 (psia)

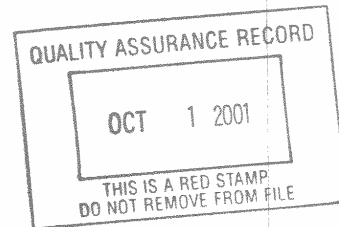
File: C:\ACPIVIEW\CALDATA\20011309JUNE\00276

Pressure Reference: Paroscientific Model 230A-101 S/N 62671

Range: 30 PSI

Date of last reference to traceable standard: Aug 15 2000

MDL - 2295 Jun 09 17:17:28 2001 Range 1 Temp 13.3° C			MDL - 2295 Jun 09 11:13:30 2001 Range 2 Temp 13.3° C			MDL - 2295 Jun 09 05:10:07 2001 Range 3 Temp 22.9° C		
Ref Pres (psia)	Error (psia)	(% FS)	Ref Pres (psia)	Error (psia)	(% FS)	Ref Pres (psia)	Error (psia)	(% FS)
9.998	-0.007	-0.023	9.986	-0.003	-0.012	9.994	-0.006	-0.022
12.034	0.000	0.001	11.991	0.004	0.013	12.048	0.000	0.001
13.976	0.003	0.008	13.983	0.007	0.025	13.973	0.004	0.012
15.969	0.004	0.013	15.973	0.007	0.024	15.969	0.004	0.013
17.965	0.002	0.005	17.964	0.006	0.021	17.963	0.002	0.007
19.960	-0.001	-0.005	19.954	0.004	0.015	19.956	0.000	0.002
21.952	-0.003	-0.011	21.961	0.001	0.005	21.957	-0.002	-0.006
23.944	-0.005	-0.016	23.940	0.000	0.001	23.940	-0.003	-0.010
25.927	-0.005	-0.017	25.936	0.002	0.005	25.931	-0.003	-0.010
27.928	-0.001	-0.005	27.935	0.005	0.016	27.923	0.001	0.003
29.916	0.006	0.018	29.924	0.013	0.042	29.917	0.008	0.028
27.952	-0.001	-0.004	27.940	0.005	0.017	27.944	0.001	0.002
25.961	-0.005	-0.016	25.940	0.002	0.006	25.939	-0.003	-0.010
23.970	-0.007	-0.024	23.943	-0.001	-0.002	23.956	-0.003	-0.010
21.965	-0.004	-0.014	21.969	0.001	0.002	21.962	-0.002	-0.007
19.978	-0.002	-0.008	19.978	0.003	0.011	19.981	-0.001	-0.002
17.980	0.001	0.005	17.981	0.005	0.017	17.981	0.002	0.007
15.935	0.003	0.010	15.985	0.007	0.023	15.988	0.004	0.012
13.968	0.003	0.009	13.967	0.007	0.022	13.951	0.003	0.010
11.994	0.000	-0.001	11.981	0.003	0.011	11.989	0.001	0.005
9.994	-0.006	-0.021	9.987	-0.004	-0.014	9.984	-0.006	-0.019
MDL - 2295 Jun 08 23:06:48 2001 Range 4 Temp 32.7° C			MDL - 2295 Jun 08 17:02:46 2001 Range 5 Temp 47.5° C					
Ref Pres (psia)	Error (psia)	(% FS)	Ref Pres (psia)	Error (psia)	(% FS)			
9.993	-0.007	-0.023	9.994	-0.006	-0.019			
12.051	0.001	0.003	11.981	0.002	0.007			
13.979	0.003	0.008	13.981	0.005	0.017			
15.965	0.003	0.010	15.968	0.005	0.018			
17.961	0.000	0.001	17.963	0.004	0.012			
19.958	-0.002	-0.006	19.958	0.001	0.003			
21.949	-0.004	-0.013	21.950	-0.002	-0.006			
23.950	-0.006	-0.021	23.938	-0.003	-0.011			
25.929	-0.006	-0.020	25.932	-0.003	-0.011			
27.917	-0.003	-0.011	27.920	0.001	0.003			
29.920	0.005	0.015	29.924	0.008	0.027			
27.920	-0.002	-0.006	27.945	0.000	0.001			
25.894	-0.005	-0.017	25.935	-0.003	-0.009			
23.944	-0.007	-0.023	23.960	-0.003	-0.011			
21.958	-0.005	-0.015	21.954	-0.003	-0.009			
19.981	-0.002	-0.008	19.976	0.000	-0.001			
17.984	0.000	0.000	17.982	0.002	0.007			
15.985	0.002	0.006	15.987	0.004	0.013			
13.961	0.002	0.008	13.972	0.004	0.012			
11.976	0.000	-0.001	11.991	0.002	0.005			
9.986	-0.007	-0.023	9.987	-0.006	-0.020			



004537

Issued by *Bill Kling* JUN 11 2001

MOSDAX Calibration Report 2: MDL - 2295 Module 276

Full Scale: 30 (psia)

File: C:\ACPVIEW\CALDATA\200113019JUNE\00276

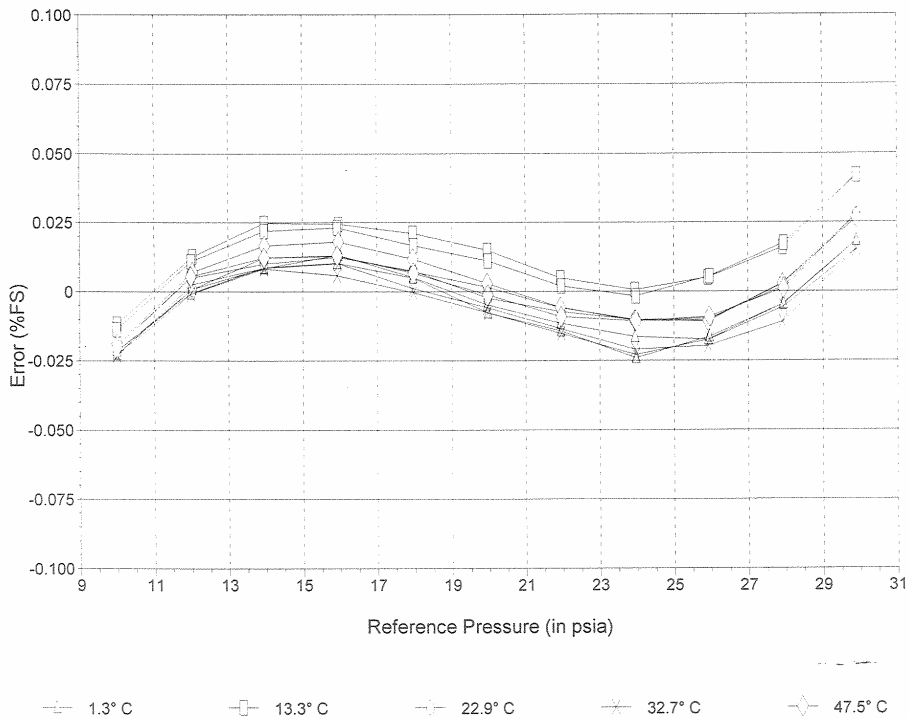
Pressure Reference: Paroscientific Model 230A-101 S/N 62671

Range: 30 PSI

Date of last reference to traceable standard: Aug 15 2000

Plot of Error vs. Reference Pressure

MDL - 2295 Module 276



Comments

Issued by *Bill Kling* JUN 11 2001



As Received MOSDAX Cal. Report 1: MDL - 2295 Module 276

Full Scale: 30 (psia)

File: C:\ACPVIEW\CALDATA\20011306\JUNE00276

Pressure Reference: Paroscientific Model 230A-101 S/N 62671

Range: 30 PSi

Date of last reference to traceable standard: Aug 15 2000

MDL - 2295 Jun 09 17:17:28 2001 Range 1 Temp 1.3° C			MDL - 2295 Jun 09 11:13:30 2001 Range 2 Temp 13.3° C			MDL - 2295 Jun 09 05:10:07 2001 Range 3 Temp 22.9° C		
Ref Pres (psia)	Error (psia)	(% FS)	Ref Pres (psia)	Error (psia)	(% FS)	Ref Pres (psia)	Error (psia)	(% FS)
9.998	-0.015	-0.049	9.986	-0.012	-0.040	9.994	-0.015	-0.051
12.034	-0.008	-0.026	11.991	-0.005	-0.018	12.048	-0.009	-0.030
13.976	-0.006	-0.020	13.983	-0.002	-0.007	13.973	-0.006	-0.021
15.969	-0.005	-0.016	15.973	-0.003	-0.009	15.969	-0.007	-0.023
17.965	-0.007	-0.025	17.964	-0.004	-0.015	17.963	-0.009	-0.030
19.960	-0.011	-0.035	19.954	-0.007	-0.023	19.956	-0.011	-0.038
21.952	-0.013	-0.043	21.961	-0.010	-0.035	21.957	-0.014	-0.048
23.944	-0.014	-0.048	23.940	-0.012	-0.041	23.940	-0.016	-0.055
25.927	-0.015	-0.050	25.936	-0.012	-0.039	25.931	-0.017	-0.057
27.928	-0.011	-0.038	27.935	-0.009	-0.030	27.923	-0.014	-0.046
29.916	-0.005	-0.015	29.924	-0.002	-0.006	29.917	-0.007	-0.024
27.952	-0.011	-0.038	27.940	-0.009	-0.029	27.944	-0.014	-0.047
25.961	-0.015	-0.049	25.940	-0.011	-0.038	25.939	-0.017	-0.056
23.970	-0.017	-0.056	23.943	-0.013	-0.043	23.956	-0.016	-0.055
21.965	-0.014	-0.045	21.969	-0.011	-0.038	21.962	-0.015	-0.049
19.978	-0.011	-0.038	19.978	-0.008	-0.026	19.981	-0.013	-0.042
17.980	-0.007	-0.025	17.981	-0.006	-0.019	17.981	-0.009	-0.030
15.935	-0.006	-0.019	15.985	-0.003	-0.011	15.988	-0.007	-0.023
13.968	-0.006	-0.019	13.967	-0.003	-0.010	13.951	-0.007	-0.023
11.994	-0.008	-0.028	11.981	-0.006	-0.019	11.989	-0.008	-0.026
9.994	-0.014	-0.048	9.987	-0.013	-0.042	9.984	-0.015	-0.049
MDL - 2295 Jun 08 23:06:48 2001 Range 4 Temp 32.7° C			MDL - 2295 Jun 08 17:02:46 2001 Range 5 Temp 47.5° C					
Ref Pres (psia)	Error (psia)	(% FS)	Ref Pres (psia)	Error (psia)	(% FS)			
9.993	-0.016	-0.052	9.994	-0.015	-0.048			
12.051	-0.009	-0.029	11.981	-0.007	-0.025			
13.979	-0.008	-0.025	13.981	-0.005	-0.018			
15.965	-0.008	-0.026	15.968	-0.005	-0.018			
17.961	-0.011	-0.037	17.963	-0.008	-0.026			
19.958	-0.014	-0.046	19.958	-0.011	-0.036			
21.949	-0.017	-0.055	21.950	-0.014	-0.045			
23.950	-0.019	-0.065	23.938	-0.015	-0.051			
25.929	-0.020	-0.065	25.932	-0.015	-0.051			
27.917	-0.018	-0.058	27.920	-0.011	-0.038			
29.920	-0.010	-0.034	29.924	-0.004	-0.014			
27.920	-0.016	-0.053	27.945	-0.012	-0.039			
25.894	-0.019	-0.063	25.935	-0.015	-0.050			
23.944	-0.020	-0.067	23.960	-0.015	-0.051			
21.958	-0.017	-0.057	21.954	-0.015	-0.049			
19.981	-0.014	-0.048	19.976	-0.012	-0.040			
17.984	-0.011	-0.038	17.982	-0.009	-0.031			
15.985	-0.009	-0.030	15.987	-0.007	-0.023			
13.961	-0.008	-0.025	13.972	-0.007	-0.022			
11.976	-0.010	-0.032	11.991	-0.008	-0.027			
9.986	-0.016	-0.052	9.987	-0.015	-0.049			

Issued by

Bill Kling

JUN 11 2001

Document: SCAL 9607

Page 1 of 2



As Received MOSDAX Cal. Report 2: MDL - 2295 Module 276

Full Scale: 30 (psia)

File: C:\ACPVIEW\CALDATA\200113019JUNE\00276

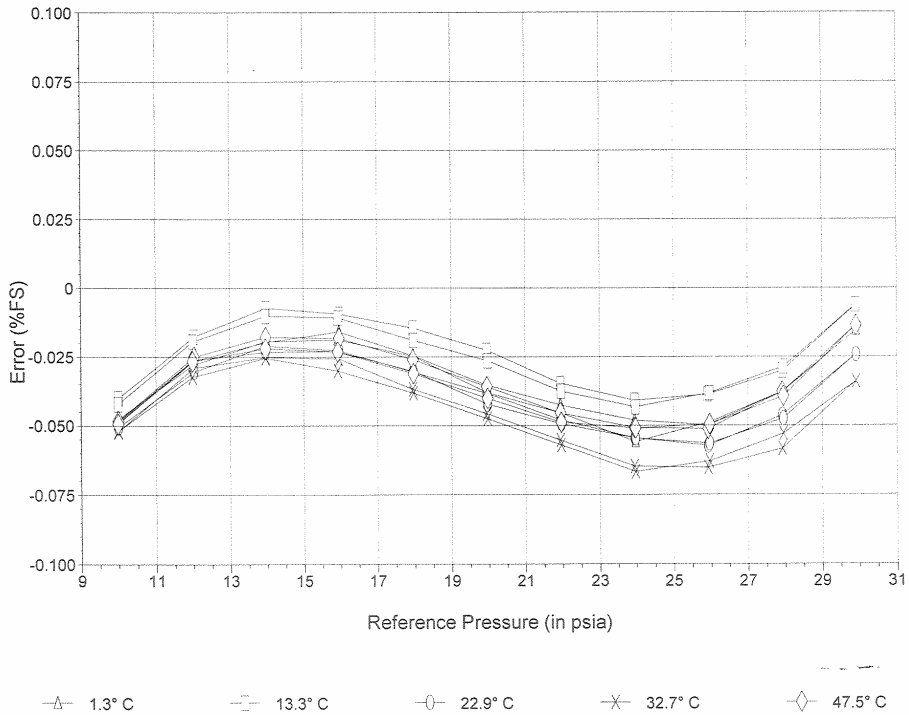
Pressure Reference: Paroscientific Model 230A-101 S/N 62671

Range: 30 PSI

Date of last reference to traceable standard: Aug 15 2000

Plot of Error vs. Reference Pressure

MDL - 2295 Module 276



Comments

Issued by

Bill Kling

JUN 11 2001

Document: 5CAL 9607

Page 2 of 2



MOSDAX Calibration Report 1: MDL - 2295 Module 276

Full Scale: 30 (psia)

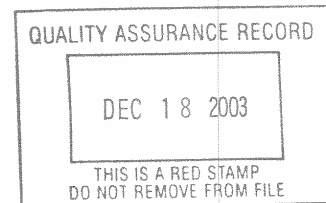
File: C:\ACP\VIEW\CALDATA\2003\30115NOV03\00276

Pressure Reference: Paroscientific Model 230A-101 S/N 90098

Range: 30 PSI

Date of last reference to traceable standard: Dec 10 2002

MDL - 2295 Nov 15 15:31:33 2003 Range 1 Temp 2.8° C			MDL - 2295 Nov 15 10:27:12 2003 Range 2 Temp 14.9° C			MDL - 2295 Nov 15 05:23:18 2003 Range 3 Temp 24.9° C		
Ref Pres (psia)	Error (psia)	(% FS)	Ref Pres (psia)	Error (psia)	(% FS)	Ref Pres (psia)	Error (psia)	(% FS)
10.009	-0.006	-0.021	10.005	-0.003	-0.010	10.009	-0.006	-0.021
11.990	0.001	0.003	11.992	0.004	0.014	11.985	0.001	0.003
13.975	0.003	0.009	13.979	0.007	0.025	13.982	0.003	0.011
15.969	0.003	0.011	15.961	0.007	0.025	15.963	0.003	0.011
17.964	0.001	0.003	17.954	0.007	0.022	17.961	0.002	0.007
19.960	-0.001	-0.005	19.953	0.004	0.014	19.949	-0.001	-0.004
21.954	-0.004	-0.014	21.944	0.001	0.005	21.947	-0.002	-0.008
23.928	-0.006	-0.019	23.939	0.000	0.000	23.950	-0.004	-0.014
25.924	-0.005	-0.017	25.932	0.001	0.005	25.930	-0.005	-0.017
27.937	-0.003	-0.009	27.927	0.005	0.017	27.923	-0.001	-0.003
29.918	0.006	0.019	29.927	0.014	0.047	29.920	0.008	0.027
27.795	-0.001	-0.004	27.811	0.006	0.020	27.826	0.001	0.002
25.836	-0.004	-0.015	25.832	0.001	0.004	25.835	-0.002	-0.008
23.861	-0.005	-0.018	23.863	0.002	0.006	23.861	-0.002	-0.008
21.895	-0.005	-0.015	21.902	0.002	0.008	21.904	-0.003	-0.010
19.929	-0.002	-0.006	19.928	0.004	0.012	19.931	-0.001	-0.002
17.943	0.001	0.004	17.946	0.006	0.021	17.953	0.002	0.005
15.970	0.003	0.008	15.970	0.007	0.022	15.976	0.004	0.012
13.977	0.003	0.010	13.984	0.006	0.019	13.976	0.004	0.013
12.002	0.000	0.000	12.006	0.003	0.009	12.005	0.000	0.000
10.021	-0.006	-0.020	10.020	-0.002	-0.008	10.018	-0.007	-0.023
MDL - 2295 Nov 15 00:19:32 2003 Range 4 Temp 35.0° C			MDL - 2295 Nov 14 19:14:48 2003 Range 5 Temp 50.1° C					
Ref Pres (psia)	Error (psia)	(% FS)	Ref Pres (psia)	Error (psia)	(% FS)			
10.000	-0.007	-0.022	9.995	-0.005	-0.016			
11.999	0.000	0.000	11.978	0.002	0.007			
13.984	0.003	0.010	13.977	0.006	0.020			
15.967	0.003	0.009	15.968	0.006	0.019			
17.967	0.001	0.003	17.959	0.004	0.012			
19.954	-0.002	-0.007	19.950	0.001	0.005			
21.949	-0.004	-0.013	21.943	-0.002	-0.007			
23.936	-0.006	-0.020	23.938	-0.004	-0.013			
25.932	-0.006	-0.020	25.924	-0.003	-0.010			
27.927	-0.001	-0.005	27.922	0.001	0.004			
29.920	0.006	0.019	29.907	0.009	0.032			
27.831	-0.002	-0.007	27.798	0.001	0.004			
25.871	-0.005	-0.018	25.847	-0.002	-0.007			
23.879	-0.005	-0.018	23.866	-0.004	-0.012			
21.926	-0.005	-0.016	21.913	-0.001	-0.004			
19.946	-0.002	-0.008	19.939	0.001	0.002			
17.955	0.000	0.000	17.959	0.002	0.007			
15.970	0.002	0.006	15.968	0.004	0.014			
13.971	0.002	0.007	13.980	0.005	0.017			
12.005	-0.001	-0.003	11.998	0.002	0.006			
10.012	-0.007	-0.024	10.010	-0.005	-0.015			



006013

Issued by 

Document: 5CAL 9607

Page 1 of 2



MOSDAX Calibration Report 2: MDL - 2295 Module 276

Full Scale: 30 (psia)

File: C:\ACP\VIEW\CALDATA\2003\30115NOV03\00276

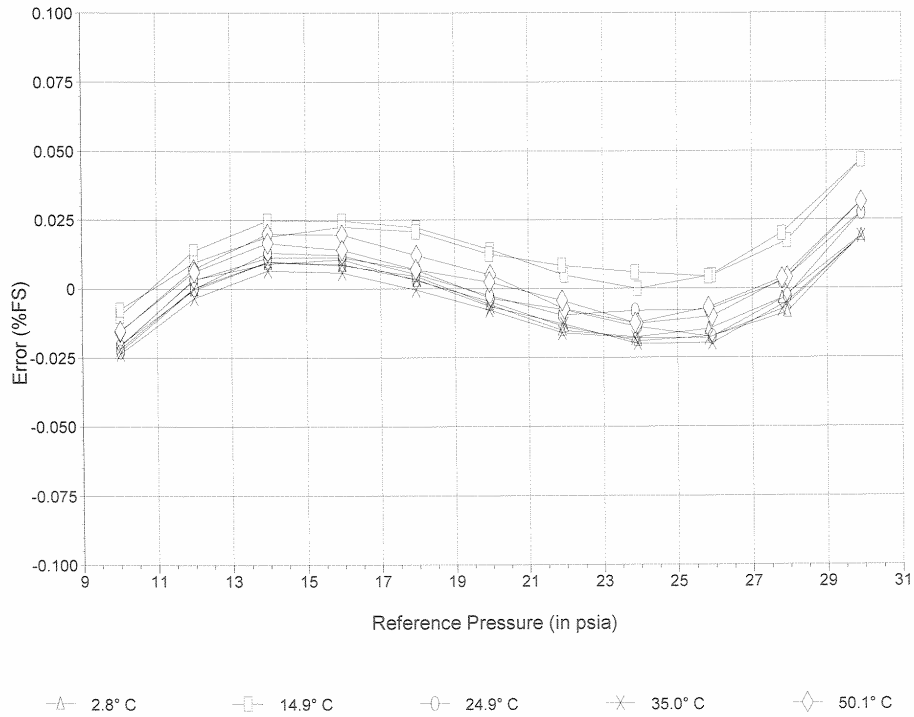
Pressure Reference: Paroscientific Model 230A-101 S/N 90098

Range: 30 PSI

Date of last reference to traceable standard: Dec 10 2002

Plot of Error vs. Reference Pressure

MDL - 2295 Module 276



Comments

Issued by

Document: 5CAL 9607

Page 2 of 2



As Received MOSDAX Cal. Report 1: MDL - 2295 Module 276

Full Scale: 30 (psia)


File: C:\ACP\VIEW\CALDATA\2003\10\15NOV03\00276

Pressure Reference: Paroscientific Model 230A-101 S/N 90098

Range: 30 PSI

Date of last reference to traceable standard: Dec 10 2002

MDL - 2295 Nov 15 15:31:33 2003 Range 1 Temp 2.8° C			MDL - 2295 Nov 15 10:27:12 2003 Range 2 Temp 14.9° C			MDL - 2295 Nov 15 05:23:18 2003 Range 3 Temp 24.9° C		
Ref Pres (psia)	Error (psia)	(% FS)	Ref Pres (psia)	Error (psia)	(% FS)	Ref Pres (psia)	Error (psia)	(% FS)
10.009	-0.008	-0.028	10.005	-0.004	-0.014	10.009	-0.007	-0.024
11.990	-0.002	-0.005	11.992	0.003	0.009	11.985	0.000	-0.001
13.975	0.000	-0.001	13.979	0.006	0.019	13.982	0.002	0.007
15.969	0.000	-0.001	15.961	0.005	0.018	15.963	0.002	0.006
17.964	-0.003	-0.010	17.954	0.004	0.015	17.961	0.000	0.001
19.960	-0.006	-0.019	19.953	0.002	0.006	19.949	-0.003	-0.010
21.954	-0.009	-0.030	21.944	-0.001	-0.005	21.947	-0.004	-0.014
23.928	-0.011	-0.037	23.939	-0.003	-0.011	23.950	-0.006	-0.021
25.924	-0.011	-0.037	25.932	-0.002	-0.007	25.930	-0.008	-0.025
27.937	-0.009	-0.030	27.927	0.001	0.005	27.923	-0.003	-0.011
29.918	-0.001	-0.005	29.927	0.010	0.033	29.920	0.005	0.018
27.795	-0.008	-0.025	27.811	0.002	0.008	27.826	-0.002	-0.006
25.836	-0.010	-0.034	25.832	-0.002	-0.007	25.835	-0.005	-0.016
23.861	-0.011	-0.035	23.863	-0.001	-0.005	23.861	-0.005	-0.015
21.895	-0.009	-0.031	21.902	0.000	-0.001	21.904	-0.005	-0.016
19.929	-0.006	-0.020	19.928	0.001	0.004	19.931	-0.003	-0.009
17.943	-0.003	-0.008	17.946	0.004	0.013	17.953	0.000	0.000
15.970	-0.001	-0.003	15.970	0.005	0.016	15.976	0.002	0.007
13.977	0.000	0.000	13.984	0.004	0.013	13.976	0.003	0.009
12.002	-0.003	-0.009	12.006	0.001	0.004	12.005	-0.001	-0.004
10.021	-0.008	-0.027	10.020	-0.004	-0.012	10.018	-0.008	-0.026
MDL - 2295 Nov 15 00:19:32 2003 Range 4 Temp 35.0° C			MDL - 2295 Nov 14 19:14:48 2003 Range 5 Temp 50.1° C					
Ref Pres (psia)	Error (psia)	(% FS)	Ref Pres (psia)	Error (psia)	(% FS)			
10.000	-0.008	-0.025	9.995	-0.006	-0.021			
11.999	-0.001	-0.004	11.978	0.000	0.001			
13.984	0.002	0.005	13.977	0.004	0.013			
15.967	0.001	0.004	15.968	0.004	0.012			
17.967	-0.001	-0.002	17.959	0.001	0.004			
19.954	-0.004	-0.012	19.950	-0.001	-0.003			
21.949	-0.006	-0.019	21.943	-0.005	-0.016			
23.936	-0.008	-0.026	23.938	-0.007	-0.022			
25.932	-0.008	-0.027	25.924	-0.006	-0.020			
27.927	-0.004	-0.012	27.922	-0.002	-0.007			
29.920	0.003	0.011	29.907	0.006	0.020			
27.831	-0.004	-0.015	27.798	-0.002	-0.007			
25.871	-0.007	-0.025	25.847	-0.005	-0.017			
23.879	-0.007	-0.024	23.866	-0.007	-0.022			
21.926	-0.007	-0.022	21.913	-0.004	-0.013			
19.946	-0.004	-0.013	19.939	-0.002	-0.006			
17.955	-0.002	-0.006	17.959	0.000	-0.001			
15.970	0.000	0.001	15.968	0.002	0.007			
13.971	0.001	0.002	13.980	0.003	0.010			
12.005	-0.002	-0.007	11.998	0.000	0.000			
10.012	-0.008	-0.027	10.010	-0.006	-0.021			

Issued by 
 Document: SCAL 9607



As Received MOSDAX Cal. Report 2: MDL - 2295 Module 276

Full Scale: 30 (psia)

File: C:\ACP\VIEW\CALDATA\2003\30\15NOV03\00276

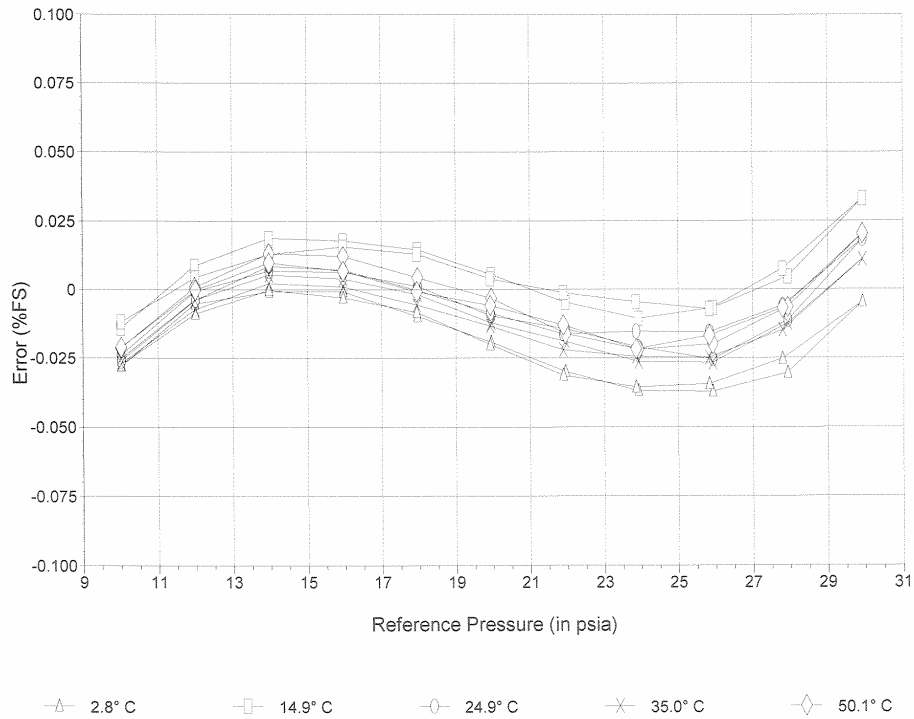
Pressure Reference: Paroscientific Model 230A-101 S/N 90098

Range: 30 PSI

Date of last reference to traceable standard: Dec 10 2002

Plot of Error vs. Reference Pressure

MDL - 2295 Module 276



Comments

Issued by 

Document: 5CAL 9607

Page 2 of 2



MOSDAX Calibration Report 1: SAM - 2323 Module 512

Full Scale: 250 (psia)

File: O:\PRODBK\2002\250\19OCT02\00512

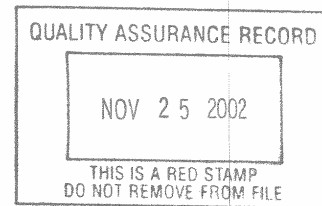
Pressure Reference: Paroscientific Model 2300A-101 S/N 55375

Range: 300 PSI

Date of last reference to traceable standard: Nov 4 2000

SAM - 2323 Oct 19 13:55:22 2002 Range 1 Temp 3.1° C			SAM - 2323 Oct 19 07:14:08 2002 Range 2 Temp 10.2° C			SAM - 2323 Oct 19 00:32:07 2002 Range 3 Temp 20.2° C		
Ref Pres (psia)	Error (psia)	(% FS)	Ref Pres (psia)	Error (psia)	(% FS)	Ref Pres (psia)	Error (psia)	(% FS)
14.764	0.012	0.005	14.758	0.004	0.001	14.755	-0.002	-0.001
25.827	0.002	0.001	25.774	-0.004	-0.002	25.780	-0.011	-0.004
50.834	-0.012	-0.005	51.050	-0.017	-0.007	51.048	-0.026	-0.010
75.789	-0.022	-0.009	75.764	-0.029	-0.012	75.757	-0.029	-0.012
100.789	-0.006	-0.003	100.816	-0.004	-0.002	100.734	-0.008	-0.003
125.766	0.004	0.002	126.151	0.008	0.003	125.740	0.002	0.001
150.721	0.011	0.004	150.658	0.003	0.001	150.793	-0.010	-0.004
175.590	0.021	0.008	176.093	0.017	0.007	175.719	0.008	0.003
201.074	0.014	0.006	200.892	0.019	0.008	201.063	0.010	0.004
225.970	0.010	0.004	225.907	0.011	0.005	225.975	-0.005	-0.002
250.994	-0.026	-0.011	250.910	-0.030	-0.012	250.795	-0.027	-0.011
225.718	-0.010	-0.004	225.976	-0.002	-0.001	225.750	-0.003	-0.001
200.696	0.006	0.003	200.905	0.010	0.004	200.719	0.001	0.000
175.760	0.006	0.003	176.025	0.007	0.003	175.692	-0.011	-0.004
150.635	0.000	0.000	150.679	-0.006	-0.002	150.723	-0.012	-0.005
125.771	0.001	0.000	125.681	-0.003	-0.001	125.687	-0.007	-0.003
100.751	-0.013	-0.005	100.755	-0.009	-0.004	100.805	-0.020	-0.008
75.793	-0.025	-0.010	75.787	-0.036	-0.014	75.739	-0.033	-0.013
50.811	-0.019	-0.007	50.825	-0.026	-0.010	50.746	-0.029	-0.012
25.828	-0.004	-0.002	25.819	-0.013	-0.005	25.764	-0.011	-0.004
14.761	0.016	0.007	14.766	0.004	0.001	14.757	-0.001	0.000

SAM - 2323 Oct 18 18:05:45 2002 Range 4 Temp 30.2° C			SAM - 2323 Oct 18 11:46:33 2002 Range 5 Temp 40.3° C		
Ref Pres (psia)	Error (psia)	(% FS)	Ref Pres (psia)	Error (psia)	(% FS)
14.736	0.027	0.011	14.725	0.006	0.003
25.791	0.008	0.003	25.843	-0.005	-0.002
50.795	0.003	0.001	51.095	-0.020	-0.008
75.801	-0.008	-0.003	75.894	-0.022	-0.009
100.763	0.014	0.005	100.983	-0.008	-0.003
125.901	0.018	0.007	125.963	0.003	0.001
150.979	0.008	0.003	150.807	0.000	0.000
176.008	0.024	0.010	175.858	0.008	0.003
201.037	0.025	0.010	200.870	0.016	0.006
225.585	0.012	0.005	225.921	0.006	0.002
250.999	-0.017	-0.007	250.827	-0.016	-0.007
225.702	0.008	0.003	225.865	0.002	0.001
200.676	0.015	0.006	200.664	0.006	0.003
175.701	0.014	0.006	175.865	0.008	0.003
150.736	0.004	0.002	150.708	-0.008	-0.003
125.816	0.015	0.006	125.792	-0.005	-0.002
100.800	0.005	0.002	100.806	-0.006	-0.002
75.773	-0.014	-0.005	75.782	-0.023	-0.009
50.825	-0.006	-0.002	50.807	-0.007	-0.003
25.797	0.014	0.005	25.791	-0.005	-0.002
14.748	0.031	0.012	14.726	0.015	0.006



005353

Issued by *[Signature]*

Document: 5CAL 9607

Page 1 of 2



MOSDAX Calibration Report 2: SAM - 2323 Module 512

Full Scale: 250 (psia)

File: O:\PROD\BK2002\250\19OCT02\00512

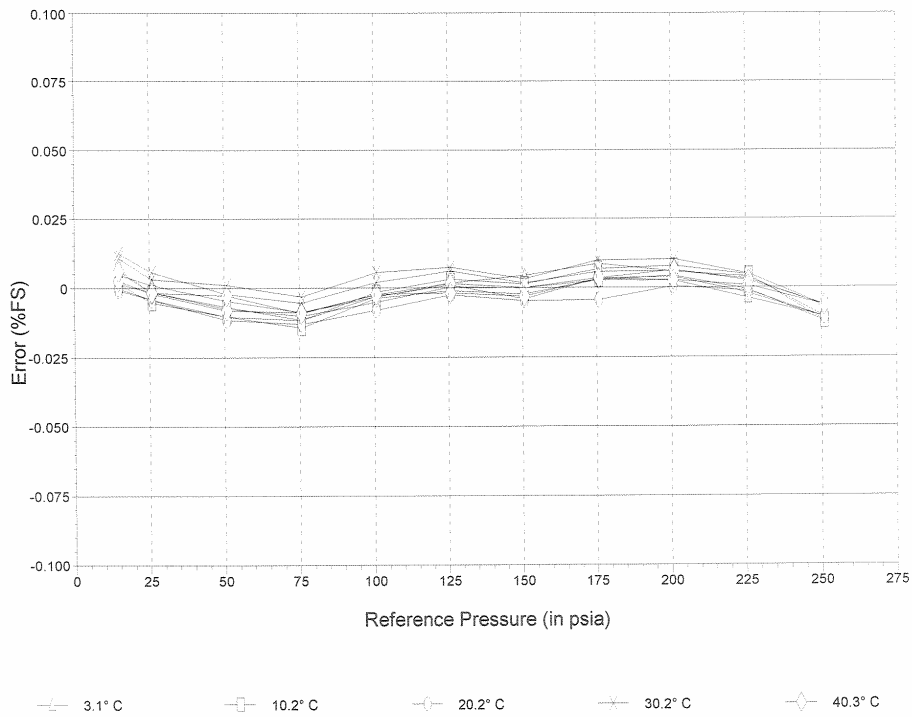
Pressure Reference: Paroscientific Model 2300A-101 S/N 55375

Range: 300 PSI

Date of last reference to traceable standard: Nov 4 2000

Plot of Error vs. Reference Pressure

SAM - 2323 Module 512



Comments

Issued by *W. Bill K...*
Document: 5CAL 9607



As Received MOSDAX Cal. Report 1: SAM - 2323 Module 512

Full Scale: 250 (psia)

File: O:\PRODBK\2002\250\19OCT02\00512

Pressure Reference: Paroscientific Model 2300A-101 S/N 55375

Range: 300 PSI

Date of last reference to traceable standard: Nov 4 2000

SAM - 2323 Oct 19 13:55:22 2002 Range 1 Temp 3.1° C			SAM - 2323 Oct 19 07:14:08 2002 Range 2 Temp 10.2° C			SAM - 2323 Oct 19 00:32:07 2002 Range 3 Temp 20.2° C		
Ref Pres (psia)	Error (psia)	(% FS)	Ref Pres (psia)	Error (psia)	(% FS)	Ref Pres (psia)	Error (psia)	(% FS)
14.764	0.018	0.007	14.758	0.032	0.013	14.755	0.042	0.017
25.827	0.010	0.004	25.774	0.025	0.010	25.780	0.033	0.013
50.834	-0.001	0.000	51.050	0.012	0.005	51.048	0.017	0.007
75.789	-0.007	-0.003	75.764	0.002	0.001	75.757	0.013	0.005
100.789	0.013	0.005	100.816	0.028	0.011	100.734	0.034	0.014
125.766	0.028	0.011	126.151	0.042	0.017	125.740	0.045	0.018
150.721	0.039	0.015	150.658	0.040	0.016	150.793	0.032	0.013
175.590	0.054	0.022	176.093	0.055	0.022	175.719	0.052	0.021
201.074	0.052	0.021	200.892	0.061	0.024	201.063	0.054	0.022
225.970	0.053	0.021	225.907	0.055	0.022	225.975	0.040	0.016
250.994	0.022	0.009	250.910	0.016	0.006	250.795	0.019	0.008
225.718	0.033	0.013	225.976	0.042	0.017	225.750	0.042	0.017
200.696	0.044	0.018	200.905	0.052	0.021	200.719	0.045	0.018
175.760	0.039	0.016	176.025	0.046	0.018	175.692	0.032	0.013
150.635	0.028	0.011	150.679	0.031	0.012	150.723	0.031	0.012
125.771	0.024	0.010	125.681	0.031	0.013	125.687	0.036	0.014
100.751	0.006	0.002	100.755	0.023	0.009	100.805	0.022	0.009
75.793	-0.010	-0.004	75.787	-0.005	-0.002	75.739	0.010	0.004
50.811	-0.007	-0.003	50.825	0.004	0.002	50.746	0.014	0.006
25.828	0.004	0.002	25.819	0.015	0.006	25.764	0.033	0.013
14.781	0.023	0.009	14.766	0.032	0.013	14.757	0.044	0.017
SAM - 2323 Oct 18 18:05:45 2002 Range 4 Temp 30.2° C			SAM - 2323 Oct 18 11:46:33 2002 Range 5 Temp 40.3° C					
Ref Pres (psia)	Error (psia)	(% FS)	Ref Pres (psia)	Error (psia)	(% FS)			
14.736	0.067	0.027	14.725	0.024	0.010			
25.791	0.048	0.019	25.843	0.014	0.005			
50.795	0.043	0.017	51.095	0.002	0.001			
75.801	0.032	0.013	75.894	0.003	0.001			
100.763	0.054	0.022	100.983	0.020	0.008			
125.901	0.059	0.024	125.963	0.034	0.014			
150.979	0.049	0.020	150.807	0.033	0.013			
176.008	0.067	0.027	175.858	0.045	0.018			
201.037	0.069	0.028	200.870	0.055	0.022			
225.585	0.057	0.023	225.921	0.050	0.020			
250.999	0.030	0.012	250.827	0.032	0.013			
225.702	0.053	0.021	225.865	0.045	0.018			
200.676	0.058	0.023	200.664	0.046	0.018			
175.701	0.057	0.023	175.865	0.044	0.018			
150.736	0.046	0.018	150.708	0.025	0.010			
125.816	0.056	0.022	125.792	0.026	0.010			
100.800	0.046	0.018	100.806	0.022	0.009			
75.773	0.027	0.011	75.782	0.002	0.001			
50.825	0.034	0.014	50.807	0.015	0.006			
25.797	0.054	0.022	25.791	0.015	0.006			
14.748	0.072	0.029	14.726	0.033	0.013			

Issued by

Document: 5CAL 9607

Page 1 of 2



As Received MOSDAX Cal. Report 2: SAM - 2323 Module 512

Full Scale: 250 (psia)

File: O:\PROD\IBK\2002\250\19OCT02\00512

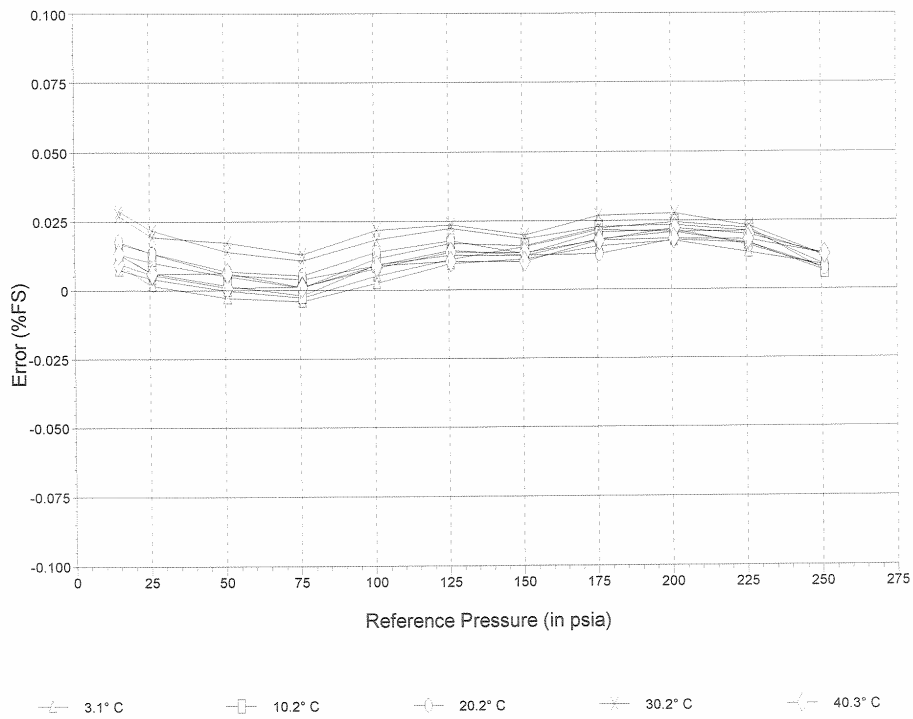
Pressure Reference: Paroscientific Model 2300A-101 S/N 55375

Range: 300 PSI

Date of last reference to traceable standard: Nov 4 2000

Plot of Error vs. Reference Pressure

SAM - 2323 Module 512



Comments

Issued by *[Signature]*

MOSDAX Calibration Report 1: MDL - 2554 Module 293

Full Scale: 30 (psia)

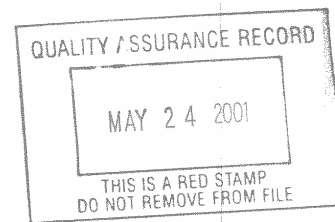
File: C:\ACPVIEW\CALDATA\2001\30\31\MARV00293

Pressure Reference: Paroscientific Model 230A-101 S/N 62671

Range: 30 PSI

Date of last reference to traceable standard: Aug 15 2000

MDL - 2554 Mar 31 17:53:23 2001 Range 1 Temp 3.3° C			MDL - 2554 Mar 31 11:45:01 2001 Range 2 Temp 15.1° C			MDL - 2554 Mar 31 05:36:58 2001 Range 3 Temp 24.8° C		
Ref Pres (psia)	Error (psia)	(% FS)	Ref Pres (psia)	Error (psia)	(% FS)	Ref Pres (psia)	Error (psia)	(% FS)
9.982	-0.006	-0.021	9.985	-0.003	-0.010	9.981	-0.006	-0.021
12.033	0.001	0.002	12.045	0.005	0.016	11.980	0.000	0.000
13.983	0.003	0.012	13.976	0.007	0.023	13.973	0.004	0.012
15.965	0.003	0.010	15.964	0.007	0.023	15.965	0.004	0.012
17.963	0.001	0.003	17.965	0.006	0.019	17.952	0.003	0.009
19.951	-0.001	-0.003	19.947	0.003	0.011	19.951	0.000	0.000
21.946	-0.004	-0.013	21.947	0.001	0.003	21.941	-0.003	-0.009
23.933	-0.005	-0.017	23.948	0.000	0.001	23.930	-0.003	-0.011
25.927	-0.004	-0.014	25.928	0.001	0.003	25.922	-0.003	-0.009
27.934	-0.001	-0.002	27.940	0.005	0.016	27.915	0.000	0.001
29.916	0.006	0.021	29.932	0.012	0.041	29.921	0.007	0.025
27.939	-0.001	-0.004	27.945	0.006	0.019	27.935	0.000	-0.001
25.954	-0.004	-0.014	25.949	0.001	0.004	25.953	-0.003	-0.011
23.966	-0.005	-0.018	23.953	0.000	-0.001	23.967	-0.005	-0.016
21.978	-0.005	-0.015	21.956	0.000	0.000	21.952	-0.003	-0.010
19.967	-0.003	-0.009	19.965	0.002	0.007	19.979	0.000	-0.002
17.976	0.000	0.002	17.970	0.005	0.015	17.978	0.001	0.002
15.968	0.001	0.005	15.984	0.006	0.020	15.974	0.003	0.008
13.973	0.002	0.007	13.963	0.006	0.019	13.964	0.004	0.013
11.977	0.000	-0.001	11.978	0.003	0.011	11.976	0.000	0.000
9.971	-0.006	-0.021	9.980	-0.004	-0.013	9.980	-0.006	-0.020
MDL - 2554 Mar 30 23:29:14 2001 Range 4 Temp 34.5° C			MDL - 2554 Mar 30 17:21:13 2001 Range 5 Temp 49.0° C					
Ref Pres (psia)	Error (psia)	(% FS)	Ref Pres (psia)	Error (psia)	(% FS)			
9.984	-0.007	-0.023	9.982	-0.006	-0.020			
11.972	0.000	0.001	11.982	0.001	0.003			
13.954	0.003	0.011	13.982	0.004	0.015			
15.965	0.002	0.007	15.964	0.004	0.013			
17.956	0.000	0.001	17.960	0.003	0.011			
19.939	-0.003	-0.009	19.961	0.001	0.003			
21.944	-0.005	-0.016	21.956	-0.002	-0.005			
23.946	-0.006	-0.021	23.936	-0.003	-0.011			
25.928	-0.006	-0.020	25.938	-0.002	-0.008			
27.895	-0.003	-0.009	27.944	0.001	0.004			
29.926	0.005	0.016	29.905	0.007	0.024			
27.927	-0.003	-0.011	27.903	0.001	0.003			
25.907	-0.005	-0.017	25.892	-0.002	-0.006			
23.902	-0.006	-0.019	23.903	-0.003	-0.011			
21.945	-0.005	-0.017	21.924	-0.002	-0.006			
19.960	-0.003	-0.011	19.947	0.000	0.000			
17.974	0.000	-0.001	17.973	0.001	0.005			
15.980	0.001	0.003	15.970	0.003	0.008			
13.963	0.002	0.008	13.969	0.004	0.013			
11.973	-0.001	-0.004	11.974	0.001	0.004			
9.977	-0.008	-0.025	9.994	-0.007	-0.022			



004133

Issued by *Bill Kling*

APR 18 2001



MOSDAX Calibration Report 2: MDL - 2554 Module 293

Full Scale: 30 (psia)

File: C:\ACPVIEW\CALDATA\200113031\MAR00293

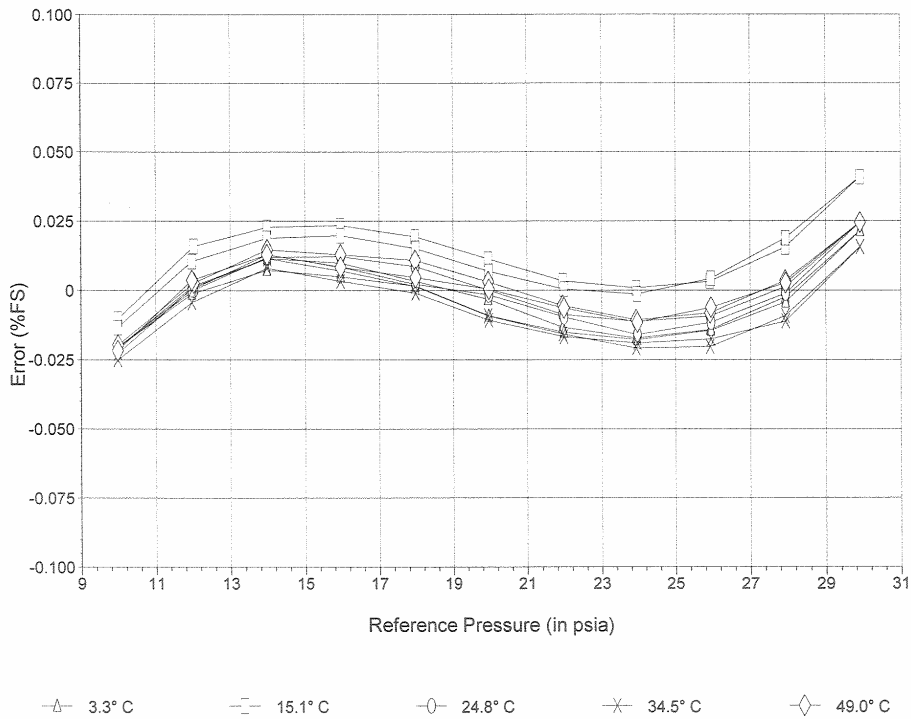
Pressure Reference: Paroscientific Model 230A-101 S/N 62671

Range: 30 PSI

Date of last reference to traceable standard: Aug 15 2000

Plot of Error vs. Reference Pressure

MDL - 2554 Module 293



Comments

Issued by

Bill Kling

APR 18 2001

Document: 5CAL 9607

Page 2 of 2



As Received MOSDAX Cal. Report 1: MDL - 2554 Module 293

Full Scale: 30 (psia)

File: C:\VCPVIEW\CALDATA\2001\130\01APR\00293

Pressure Reference: Paroscientific Model 230A-101 S/N 62671

Range: 30 PSI

Date of last reference to traceable standard: Aug 15 2000

MDL - 2554 Mar 31 17:53:23 2001 Range 1 Temp 3.3° C			MDL - 2554 Mar 31 11:45:01 2001 Range 2 Temp 15.1° C			MDL - 2554 Mar 31 05:36:58 2001 Range 3 Temp 24.8° C		
Ref Pres (psia)	Error (psia)	(% FS)	Ref Pres (psia)	Error (psia)	(% FS)	Ref Pres (psia)	Error (psia)	(% FS)
9.982	-0.007	-0.022	9.985	-0.004	-0.013	9.981	-0.007	-0.025
12.033	0.000	0.000	12.045	0.004	0.012	11.980	-0.001	-0.005
13.983	0.003	0.010	13.976	0.006	0.018	13.973	0.002	0.006
15.965	0.002	0.007	15.964	0.005	0.018	15.965	0.001	0.005
17.963	0.000	0.000	17.965	0.004	0.013	17.952	0.000	0.000
19.951	-0.002	-0.007	19.947	0.001	0.004	19.951	-0.003	-0.010
21.946	-0.006	-0.019	21.947	-0.002	-0.006	21.941	-0.006	-0.020
23.933	-0.007	-0.024	23.948	-0.003	-0.010	23.930	-0.007	-0.024
25.927	-0.007	-0.022	25.928	-0.003	-0.009	25.922	-0.007	-0.024
27.934	-0.004	-0.012	27.940	0.000	0.002	27.915	-0.005	-0.015
29.916	0.003	0.010	29.932	0.007	0.025	29.921	0.002	0.007
27.939	-0.004	-0.014	27.945	0.001	0.005	27.935	-0.005	-0.017
25.954	-0.007	-0.022	25.949	-0.002	-0.008	25.953	-0.008	-0.026
23.966	-0.007	-0.024	23.953	-0.004	-0.012	23.967	-0.009	-0.029
21.978	-0.006	-0.020	21.956	-0.003	-0.009	21.952	-0.006	-0.021
19.967	-0.004	-0.013	19.965	0.000	-0.001	19.979	-0.004	-0.012
17.976	-0.001	-0.002	17.970	0.003	0.009	17.978	-0.002	-0.007
15.968	0.001	0.002	15.984	0.004	0.015	15.974	0.000	0.001
13.973	0.002	0.005	13.963	0.004	0.015	13.964	0.002	0.007
11.977	-0.001	-0.003	11.978	0.002	0.007	11.976	-0.001	-0.005
9.971	-0.007	-0.022	9.980	-0.005	-0.016	9.980	-0.007	-0.024
MDL - 2554 Mar 30 23:29:14 2001 Range 4 Temp 34.5° C			MDL - 2554 Mar 30 17:21:13 2001 Range 5 Temp 49.0° C					
Ref Pres (psia)	Error (psia)	(% FS)	Ref Pres (psia)	Error (psia)	(% FS)			
9.984	-0.008	-0.028	9.982	-0.008	-0.027			
11.972	-0.002	-0.006	11.982	-0.002	-0.008			
13.954	0.001	0.003	13.982	0.000	0.001			
15.965	-0.001	-0.003	15.964	-0.001	-0.002			
17.956	-0.003	-0.010	17.960	-0.002	-0.006			
19.939	-0.007	-0.022	19.961	-0.005	-0.016			
21.944	-0.009	-0.030	21.956	-0.008	-0.026			
23.946	-0.011	-0.037	23.936	-0.010	-0.032			
25.928	-0.011	-0.038	25.938	-0.009	-0.030			
27.895	-0.008	-0.027	27.944	-0.006	-0.019			
29.926	-0.001	-0.004	29.905	0.001	0.002			
27.927	-0.009	-0.030	27.903	-0.006	-0.020			
25.907	-0.010	-0.035	25.892	-0.008	-0.028			
23.902	-0.010	-0.035	23.903	-0.010	-0.033			
21.945	-0.009	-0.031	21.924	-0.008	-0.027			
19.960	-0.007	-0.024	19.947	-0.006	-0.018			
17.974	-0.004	-0.013	17.973	-0.004	-0.013			
15.980	-0.002	-0.007	15.970	-0.002	-0.007			
13.963	0.000	-0.001	13.969	0.000	0.000			
11.973	-0.003	-0.011	11.974	-0.002	-0.007			
9.977	-0.009	-0.030	9.994	-0.009	-0.030			

Issued by

Bill Kling

APR 18 2001



As Received MOSDAX Cal. Report 2: MDL - 2554 Module 293

Full Scale: 30 (psia)

File: C:\ACPVIEW\CALDATA\200113001APR\00293

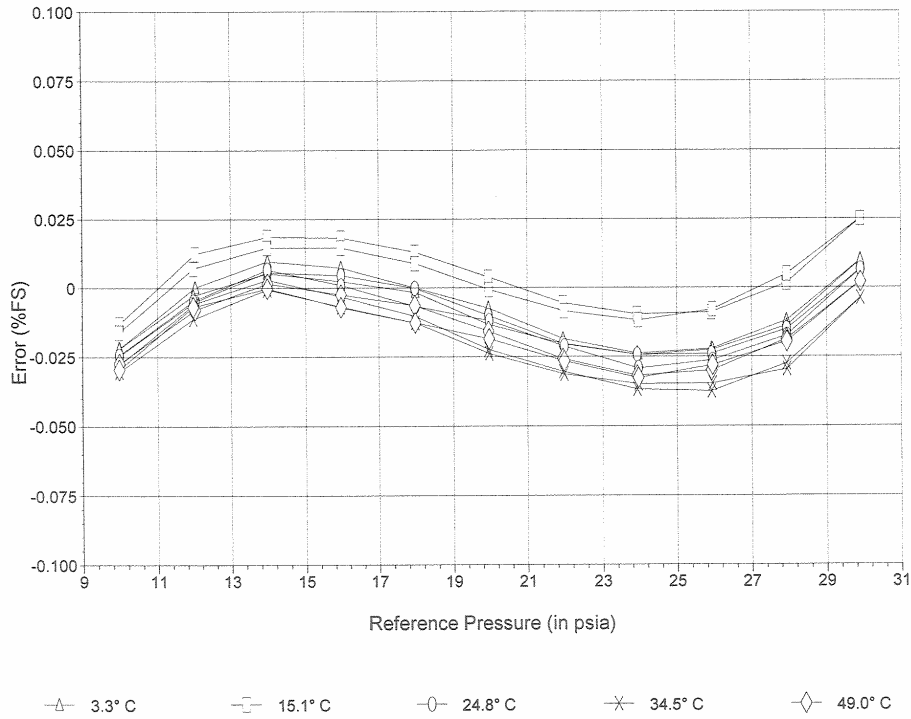
Pressure Reference: Paroscientific Model 230A-101 S/N 62671

Range: 30 PSI

Date of last reference to traceable standard: Aug 15 2000

Plot of Error vs. Reference Pressure

MDL - 2554 Module 293



Comments

Issued by *Bill Klimo* APR 18 2001

Document: 5CAL 9607

Page 2 of 2



MOSDAX Calibration Report 1: MDL - 2554 Module 293

Full Scale: 30 (psia)

File: C:\ACPVIEW\CALDATA\2004\03\03\JULY04\00293

Pressure Reference: Paroscientific Model 230A-101 S/N 90098

Range: 30 PSI

Date of last reference to traceable standard: Dec 10 2002

MDL - 2554 Jul 30 04:44:06 2004 Range 1 Temp 3.6° C			MDL - 2554 Jul 29 23:41:38 2004 Range 2 Temp 15.0° C			MDL - 2554 Jul 29 18:39:10 2004 Range 3 Temp 24.5° C		
Ref Pres (psia)	Error (psia)	(% FS)	Ref Pres (psia)	Error (psia)	(% FS)	Ref Pres (psia)	Error (psia)	(% FS)
10.034	-0.006	-0.020	10.053	-0.004	-0.014	10.030	-0.005	-0.016
11.976	0.001	0.002	11.982	0.004	0.012	11.982	0.001	0.004
13.978	0.004	0.012	14.009	0.007	0.022	13.985	0.004	0.013
15.912	0.004	0.012	15.957	0.007	0.024	15.983	0.005	0.015
17.976	0.002	0.006	17.944	0.006	0.020	17.940	0.003	0.009
19.899	-0.001	-0.004	19.950	0.004	0.014	19.933	0.001	0.003
21.892	-0.003	-0.010	21.922	0.002	0.006	21.963	-0.002	-0.006
23.919	-0.004	-0.014	23.911	0.000	0.001	23.938	-0.003	-0.009
25.880	-0.004	-0.012	25.901	0.002	0.005	25.879	-0.002	-0.006
27.898	-0.001	-0.003	27.914	0.004	0.015	27.865	0.001	0.005
29.900	0.007	0.023	29.910	0.013	0.044	29.892	0.009	0.031
27.935	-0.002	-0.006	27.987	0.005	0.015	27.970	0.000	0.001
25.954	-0.005	-0.017	25.970	0.000	0.001	25.982	-0.003	-0.011
23.978	-0.006	-0.022	23.940	0.000	-0.001	23.972	-0.004	-0.014
21.982	-0.005	-0.016	21.859	0.001	0.004	21.857	-0.001	-0.005
19.911	-0.001	-0.003	19.972	0.003	0.010	19.994	0.000	-0.002
17.992	0.001	0.003	18.037	0.005	0.017	18.028	0.002	0.005
15.993	0.003	0.008	16.027	0.007	0.022	16.033	0.003	0.010
13.966	0.002	0.008	14.031	0.006	0.020	14.007	0.005	0.016
12.003	0.001	0.002	11.996	0.004	0.013	12.003	0.001	0.004
10.001	-0.007	-0.022	10.015	-0.003	-0.011	10.035	-0.005	-0.017
MDL - 2554 Jul 29 13:37:06 2004 Range 4 Temp 33.8° C			MDL - 2554 Jul 29 08:34:45 2004 Range 5 Temp 47.8° C					
Ref Pres (psia)	Error (psia)	(% FS)	Ref Pres (psia)	Error (psia)	(% FS)			
10.037	-0.007	-0.024	10.019	-0.005	-0.018			
11.982	0.000	-0.001	11.972	0.002	0.008			
14.020	0.002	0.008	14.001	0.005	0.018			
15.994	0.003	0.011	15.967	0.004	0.014			
17.972	0.001	0.004	17.927	0.003	0.010			
19.913	-0.001	-0.004	19.967	0.001	0.003			
21.938	-0.004	-0.013	21.909	-0.002	-0.006			
23.961	-0.006	-0.018	23.931	-0.003	-0.011			
25.944	-0.006	-0.021	25.883	-0.002	-0.005			
27.944	-0.002	-0.008	27.870	0.001	0.005			
29.839	0.005	0.018	29.902	0.009	0.031			
27.958	-0.003	-0.008	27.935	0.000	0.000			
25.949	-0.007	-0.022	25.974	-0.004	-0.013			
23.998	-0.008	-0.025	24.028	-0.004	-0.013			
21.871	-0.006	-0.019	21.969	-0.004	-0.012			
19.997	-0.003	-0.010	19.986	0.000	-0.002			
18.006	-0.001	-0.002	17.998	0.002	0.005			
16.074	0.002	0.007	16.041	0.003	0.009			
14.022	0.002	0.006	14.038	0.004	0.014			
12.037	0.000	-0.002	12.008	0.001	0.003			
9.992	-0.006	-0.020	10.009	-0.005	-0.017			

Issued by

Document: SCAL 9607

Page 1 of 2



MOSDAX Calibration Report 2: MDL - 2554 Module 293

Full Scale: 30 (psia)

File: C:\ACVIEW\CALDATA\2004\30\30JULY04\00293

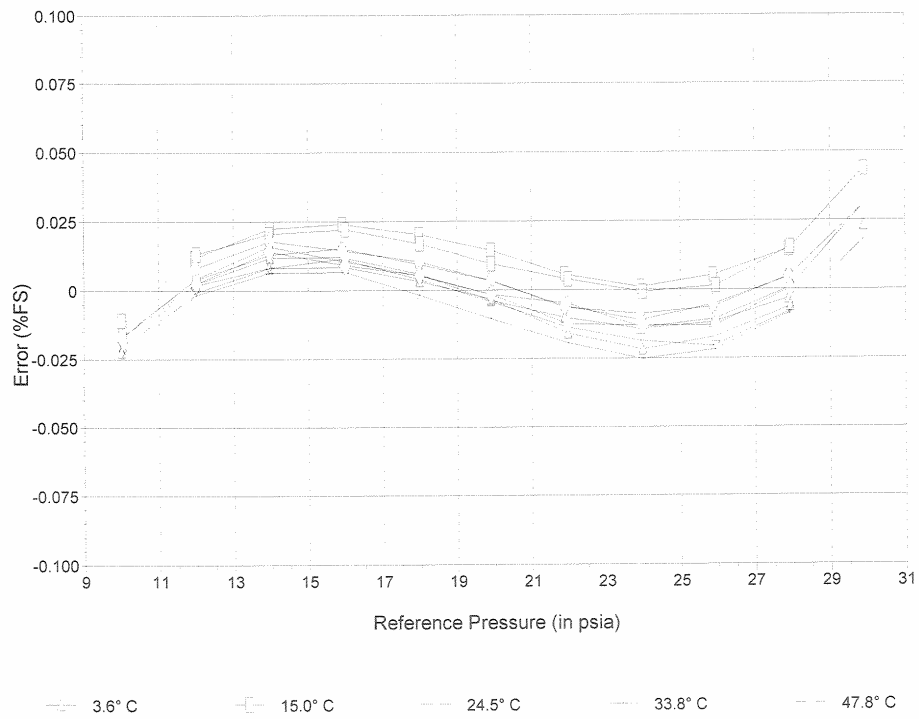
Pressure Reference: Paroscientific Model 230A-101 S/N 90098

Range: 30 PSI

Date of last reference to traceable standard: Dec 10 2002

Plot of Error vs. Reference Pressure

MDL - 2554 Module 293



Comments

Issued by *[Signature]*

Document: SCAL 9607

Page 2 of 2



As Received MOSDAX Cal. Report 1: MDL - 2554 Module 293

Full Scale: 30 (psia)

File: C:\ACPVIEW\CALDATA\2004\30\30JULY04\00293

Pressure Reference: Paroscientific Model 230A-101 S/N 90098

Range: 30 PSI

Date of last reference to traceable standard: Dec 10 2002

MDL - 2554 Jul 30 04:44:06 2004 Range 1 Temp 3.6° C			MDL - 2554 Jul 29 23:41:38 2004 Range 2 Temp 15.0° C			MDL - 2554 Jul 29 18:39:10 2004 Range 3 Temp 24.5° C		
Ref Pres (psia)	Error (psia)	(% FS)	Ref Pres (psia)	Error (psia)	(% FS)	Ref Pres (psia)	Error (psia)	(% FS)
10.034	-0.006	-0.020	10.053	-0.005	-0.016	10.030	-0.006	-0.020
11.976	0.001	0.002	11.982	0.003	0.009	11.982	0.000	0.000
13.978	0.003	0.011	14.009	0.006	0.019	13.985	0.003	0.009
15.912	0.004	0.012	15.957	0.006	0.021	15.983	0.003	0.011
17.976	0.002	0.006	17.944	0.005	0.017	17.940	0.002	0.005
19.899	-0.001	-0.003	19.950	0.004	0.012	19.933	0.000	0.000
21.892	-0.002	-0.008	21.922	0.001	0.004	21.963	-0.003	-0.009
23.919	-0.003	-0.010	23.911	0.000	0.001	23.938	-0.003	-0.011
25.880	-0.002	-0.007	25.901	0.002	0.006	25.879	-0.002	-0.007
27.898	0.001	0.004	27.914	0.005	0.017	27.865	0.002	0.005
29.900	0.010	0.033	29.910	0.015	0.049	29.892	0.010	0.033
27.935	0.000	0.001	27.987	0.005	0.018	27.970	0.000	0.002
25.954	-0.004	-0.012	25.970	0.001	0.003	25.982	-0.003	-0.011
23.978	-0.005	-0.018	23.940	0.000	-0.001	23.972	-0.005	-0.015
21.982	-0.004	-0.013	21.859	0.001	0.002	21.857	-0.002	-0.008
19.911	-0.001	-0.002	19.972	0.002	0.007	19.994	-0.002	-0.005
17.992	0.001	0.004	18.037	0.004	0.014	18.028	0.000	0.001
15.993	0.002	0.008	16.027	0.006	0.019	16.033	0.002	0.006
13.966	0.002	0.008	14.031	0.005	0.017	14.007	0.004	0.012
12.003	0.000	0.001	11.996	0.003	0.010	12.003	0.000	0.000
10.001	-0.007	-0.023	10.015	-0.004	-0.013	10.035	-0.006	-0.021
MDL - 2554 Jul 29 13:37:06 2004 Range 4 Temp 33.8° C			MDL - 2554 Jul 29 08:34:45 2004 Range 5 Temp 47.8° C					
Ref Pres (psia)	Error (psia)	(% FS)	Ref Pres (psia)	Error (psia)	(% FS)			
10.037	-0.009	-0.029	10.019	-0.008	-0.025			
11.982	-0.002	-0.006	11.972	0.001	0.002			
14.020	0.001	0.004	14.001	0.004	0.013			
15.994	0.002	0.007	15.967	0.003	0.010			
17.972	0.000	0.000	17.927	0.002	0.006			
19.913	-0.002	-0.008	19.967	0.000	0.000			
21.938	-0.005	-0.016	21.909	-0.003	-0.009			
23.961	-0.006	-0.021	23.931	-0.004	-0.013			
25.944	-0.007	-0.022	25.883	-0.002	-0.007			
27.944	-0.003	-0.009	27.870	0.001	0.003			
29.839	0.006	0.019	29.902	0.009	0.029			
27.958	-0.003	-0.009	27.935	0.000	-0.001			
25.949	-0.007	-0.023	25.974	-0.005	-0.015			
23.998	-0.008	-0.027	24.028	-0.005	-0.015			
21.871	-0.007	-0.022	21.969	-0.005	-0.015			
19.997	-0.004	-0.014	19.986	-0.001	-0.005			
18.006	-0.002	-0.006	17.998	0.000	0.002			
16.074	0.001	0.002	16.041	0.001	0.005			
14.022	0.001	0.002	14.038	0.003	0.009			
12.037	-0.002	-0.006	12.008	-0.001	-0.004			
9.992	-0.008	-0.025	10.009	-0.007	-0.024			

Issued by 



As Received MOSDAX Cal. Report 2: MDL - 2554 Module 293

Full Scale: 30 (psia)

File: C:\ACPVIEW\CALDATA\2004\10\30\JULY04\00293

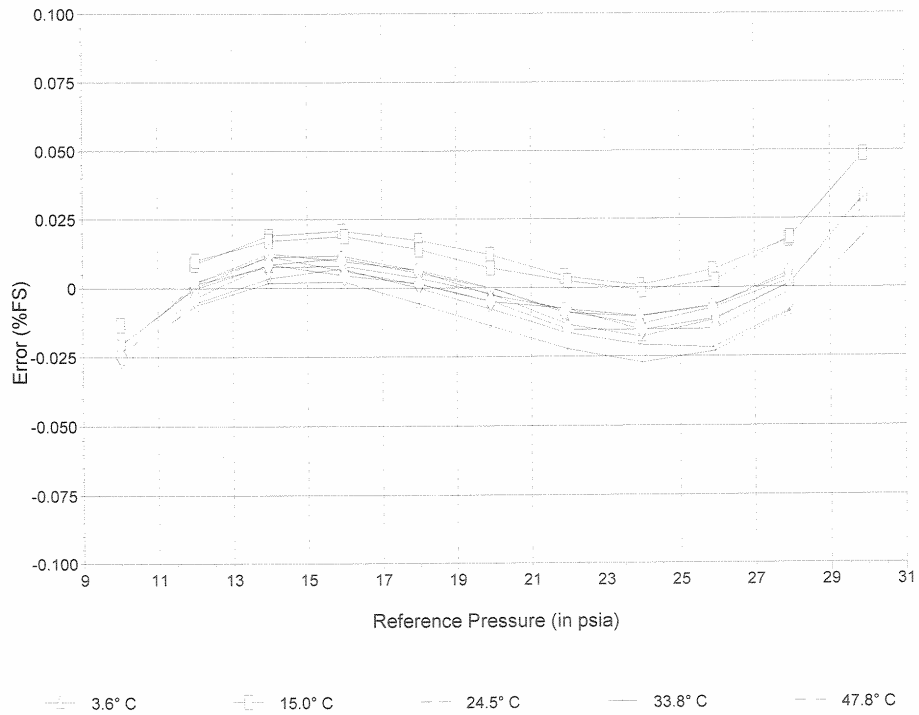
Pressure Reference: Paroscientific Model 230A-101 S/N 90098

Range: 30 PSI

Date of last reference to traceable standard: Dec 10 2002

Plot of Error vs. Reference Pressure

MDL - 2554 Module 293



Comments

Issued by *[Signature]*

Document: SCAL 9607

Page 2 of 2



MOSDAX Calibration Report 1: MDL - 2565 Module 1069

Full Scale: 30 (psia)

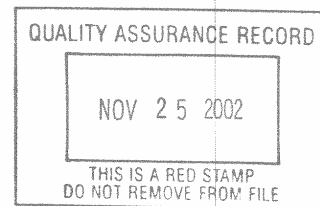
File: C:\ACVIEW\WALDATA\2002\30\14SEPT\201069

Pressure Reference: Paroscientific Model 230A-101 S/N 62671

Range: 30 PSI

Date of last reference to traceable standard: Aug 27 2002

MDL - 2565 Sep 14 13:21:09 2002 Range 1 Temp 3.3° C			MDL - 2565 Sep 14 08:09:06 2002 Range 2 Temp 15.4° C			MDL - 2565 Sep 14 02:57:55 2002 Range 3 Temp 25.4° C		
Ref Pres (psia)	Error (psia)	(% FS)	Ref Pres (psia)	Error (psia)	(% FS)	Ref Pres (psia)	Error (psia)	(% FS)
9.987	-0.009	-0.030	9.992	-0.006	-0.020	9.992	-0.008	-0.026
12.024	0.000	0.002	12.019	0.004	0.013	11.997	0.000	0.001
13.972	0.004	0.014	13.966	0.008	0.027	13.962	0.005	0.017
15.963	0.005	0.016	15.965	0.010	0.033	15.969	0.007	0.023
17.963	0.002	0.008	17.959	0.006	0.021	17.951	0.004	0.013
19.956	-0.002	-0.005	19.951	0.003	0.012	19.957	0.000	0.000
21.948	-0.005	-0.018	21.950	0.001	0.004	21.952	-0.003	-0.009
23.930	-0.007	-0.024	23.949	0.000	-0.001	23.948	-0.004	-0.015
25.922	-0.006	-0.020	25.941	0.001	0.003	25.933	-0.004	-0.012
27.923	-0.002	-0.006	27.928	0.006	0.020	27.903	0.001	0.002
29.925	0.008	0.028	29.902	0.016	0.052	29.914	0.011	0.036
27.942	-0.002	-0.007	27.911	0.005	0.017	27.937	0.000	-0.001
25.970	-0.007	-0.024	25.975	0.000	0.000	25.989	-0.005	-0.016
23.976	-0.009	-0.028	23.994	-0.002	-0.006	23.989	-0.007	-0.022
21.980	-0.007	-0.022	21.985	0.000	0.000	21.968	-0.006	-0.019
19.978	-0.004	-0.012	19.991	0.002	0.007	19.989	-0.003	-0.010
17.991	0.000	-0.001	17.980	0.005	0.016	17.990	0.000	0.001
15.987	0.003	0.012	15.976	0.008	0.026	15.982	0.004	0.013
13.975	0.003	0.010	13.976	0.006	0.021	13.978	0.003	0.010
11.981	-0.001	-0.004	11.994	0.003	0.011	11.994	0.000	-0.001
9.993	-0.009	-0.030	9.988	-0.006	-0.019	9.990	-0.008	-0.027
MDL - 2565 Sep 13 21:46:58 2002 Range 4 Temp 35.4° C			MDL - 2565 Sep 13 16:34:54 2002 Range 5 Temp 50.5° C					
Ref Pres (psia)	Error (psia)	(% FS)	Ref Pres (psia)	Error (psia)	(% FS)			
9.993	-0.010	-0.033	9.995	-0.008	-0.027			
11.991	0.000	0.000	12.041	0.002	0.007			
13.968	0.003	0.011	13.967	0.006	0.021			
15.969	0.005	0.015	15.970	0.007	0.025			
17.963	0.000	0.001	17.958	0.004	0.014			
19.952	-0.003	-0.009	19.955	0.002	0.005			
21.954	-0.006	-0.019	21.936	-0.001	-0.002			
23.935	-0.008	-0.026	23.931	-0.002	-0.006			
25.938	-0.008	-0.026	25.932	-0.001	-0.002			
27.932	-0.002	-0.007	27.941	0.003	0.009			
29.928	0.007	0.023	29.912	0.011	0.038			
27.922	-0.003	-0.011	27.937	0.002	0.007			
25.973	-0.009	-0.030	25.966	-0.004	-0.014			
23.980	-0.010	-0.035	23.982	-0.006	-0.020			
21.989	-0.009	-0.031	21.990	-0.004	-0.015			
19.992	-0.006	-0.021	19.990	-0.002	-0.007			
17.989	-0.003	-0.011	17.983	0.000	0.001			
15.986	0.001	0.003	15.983	0.004	0.013			
13.983	0.001	0.004	13.984	0.003	0.009			
11.980	-0.002	-0.008	11.993	-0.001	-0.002			
9.993	-0.011	-0.035	9.990	-0.008	-0.027			



005347

Issued by *[Signature]*



As Received MOSDAX Cal. Report 2: MDL - 2565 Module 1069

Full Scale: 30 (psia)

File: O:\PROD\BKI2002\30\14SEPT02\01069

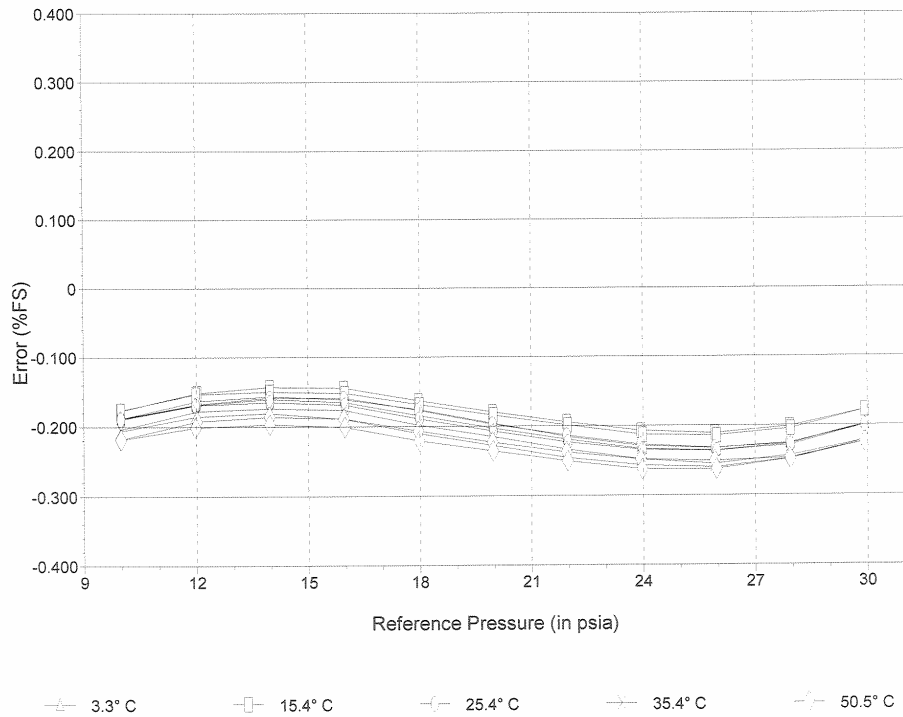
Pressure Reference: Paroscientific Model 230A-101 S/N 62671

Range: 30 PSI

Date of last reference to traceable standard: Aug 27 2002

Plot of Error vs. Reference Pressure

MDL - 2565 Module 1069



Comments
Y-Axis Not To Standard Scale.

Issued by 

As Received MOSDAX Cal. Report 1: MDL - 2565 Module 1069

Full Scale: 30 (psia)

File: O:\PRODBK\2002\30\14SEPT02\101069

Pressure Reference: Paroscientific Model 230A-101 S/N 62671

Range: 30 PSI

Date of last reference to traceable standard: Aug 27 2002

MDL - 2565 Sep 11 13:21:09 2002 Range 1 Temp 3.3° C			MDL - 2565 Sep 11 08:09:06 2002 Range 2 Temp 15.4° C			MDL - 2565 Sep 11 02:57:55 2002 Range 3 Temp 25.4° C		
Ref Pres (psia)	Error (psia)	(% FS)	Ref Pres (psia)	Error (psia)	(% FS)	Ref Pres (psia)	Error (psia)	(% FS)
9.987	-0.057	-0.189	9.992	-0.053	-0.177	9.992	-0.056	-0.188
12.024	-0.049	-0.163	12.019	-0.046	-0.152	11.997	-0.050	-0.168
13.972	-0.047	-0.157	13.966	-0.043	-0.144	13.962	-0.047	-0.158
15.963	-0.048	-0.161	15.965	-0.043	-0.145	15.969	-0.048	-0.159
17.963	-0.053	-0.176	17.959	-0.049	-0.163	17.951	-0.053	-0.177
19.956	-0.059	-0.196	19.951	-0.054	-0.180	19.957	-0.059	-0.197
21.948	-0.065	-0.215	21.950	-0.058	-0.194	21.952	-0.064	-0.214
23.930	-0.069	-0.229	23.949	-0.062	-0.207	23.948	-0.068	-0.227
25.922	-0.070	-0.232	25.941	-0.063	-0.211	25.933	-0.070	-0.232
27.923	-0.068	-0.225	27.928	-0.060	-0.202	27.903	-0.068	-0.226
29.925	-0.060	-0.199	29.902	-0.053	-0.178	29.914	-0.060	-0.200
27.942	-0.068	-0.226	27.911	-0.061	-0.205	27.937	-0.069	-0.228
25.970	-0.071	-0.236	25.975	-0.064	-0.214	25.989	-0.071	-0.236
23.976	-0.070	-0.233	23.994	-0.064	-0.213	23.989	-0.070	-0.234
21.980	-0.066	-0.220	21.985	-0.060	-0.199	21.968	-0.067	-0.223
19.978	-0.061	-0.203	19.991	-0.055	-0.184	19.989	-0.062	-0.207
17.991	-0.055	-0.185	17.980	-0.051	-0.169	17.990	-0.057	-0.189
15.987	-0.050	-0.166	15.976	-0.046	-0.152	15.982	-0.051	-0.169
13.975	-0.048	-0.161	13.976	-0.045	-0.150	13.978	-0.050	-0.165
11.981	-0.051	-0.169	11.994	-0.046	-0.154	11.994	-0.051	-0.170
9.993	-0.057	-0.189	9.988	-0.053	-0.177	9.990	-0.057	-0.189
MDL - 2565 Sep 10 21:46:58 2002 Range 4 Temp 35.4° C			MDL - 2565 Sep 10 16:34:54 2002 Range 5 Temp 50.5° C					
Ref Pres (psia)	Error (psia)	(% FS)	Ref Pres (psia)	Error (psia)	(% FS)			
9.993	-0.061	-0.204	9.995	-0.065	-0.218			
11.991	-0.053	-0.178	12.041	-0.058	-0.192			
13.968	-0.052	-0.174	13.967	-0.056	-0.186			
15.969	-0.053	-0.177	15.970	-0.057	-0.189			
17.963	-0.059	-0.198	17.958	-0.062	-0.207			
19.952	-0.065	-0.215	19.955	-0.067	-0.223			
21.954	-0.070	-0.233	21.936	-0.071	-0.237			
23.935	-0.074	-0.248	23.931	-0.074	-0.248			
25.938	-0.076	-0.255	25.932	-0.075	-0.251			
27.932	-0.073	-0.244	27.941	-0.074	-0.246			
29.928	-0.067	-0.222	29.912	-0.067	-0.224			
27.922	-0.074	-0.248	27.937	-0.074	-0.248			
25.973	-0.078	-0.260	25.966	-0.079	-0.262			
23.980	-0.077	-0.257	23.982	-0.079	-0.262			
21.989	-0.074	-0.246	21.990	-0.075	-0.250			
19.992	-0.068	-0.228	19.990	-0.071	-0.236			
17.989	-0.063	-0.210	17.983	-0.066	-0.221			
15.986	-0.057	-0.190	15.983	-0.060	-0.201			
13.983	-0.054	-0.181	13.984	-0.059	-0.197			
11.980	-0.056	-0.186	11.993	-0.060	-0.201			
9.993	-0.062	-0.206	9.990	-0.066	-0.219			

Issued by 



MOSDAX Calibration Report 2: MDL - 2565 Module 1069

Full Scale: 30 (psia)

File: C:\ACPVIEW\CALDATA\2002\30\14SEPT02\01069

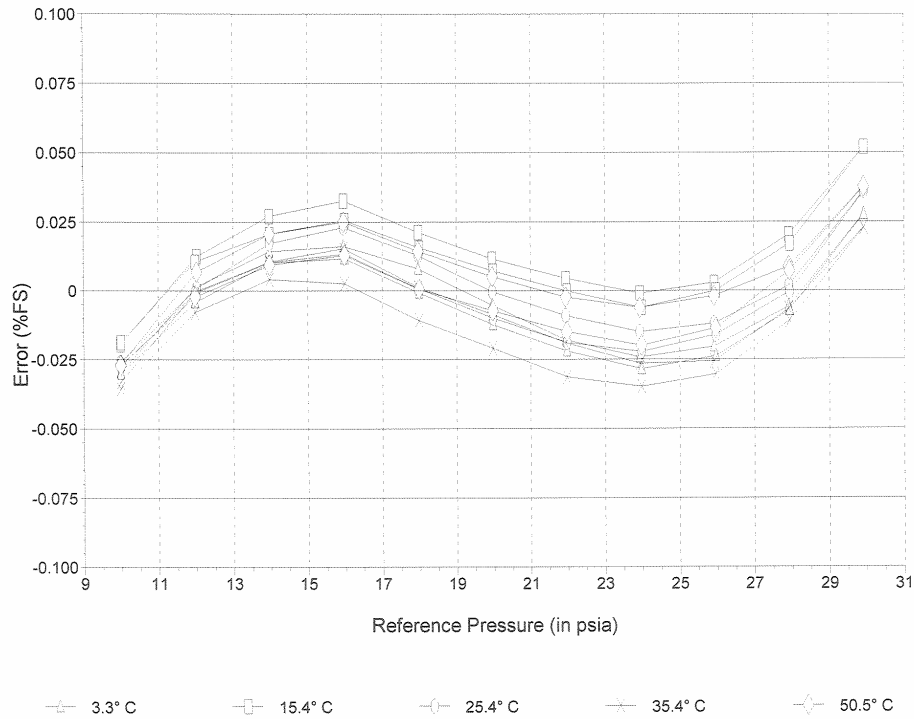
Pressure Reference: Paroscientific Model 230A-101 S/N 62671

Range: 30 PSI

Date of last reference to traceable standard: Aug 27 2002

Plot of Error vs. Reference Pressure

MDL - 2565 Module 1069



Comments

Issued by

Document: 5CAL 9607

Page 2 of 2



MOSDAX Calibration Report 1: MDL - 2565 Module 1069

Full Scale: 30 (psia)

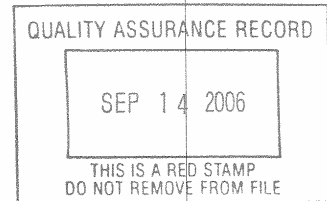
File: D:\DOCUME~1\BILL\DATA\ACPV\IEW\CALDATA\2006\30\28JAN06\02565

Pressure Reference: Paroscientific Model 230A-101 S/N 90098

Range: 30 PSI

Date of last reference to traceable standard: Dec 20 2004

MDL - 2565 Jan 28 07:10:25 2006 Range 1 Temp 3.3° C			MDL - 2565 Jan 28 03:10:47 2006 Range 2 Temp 15.2° C			MDL - 2565 Jan 27 23:11:03 2006 Range 3 Temp 24.8° C		
Ref Pres (psia)	Error (psia)	(% FS)	Ref Pres (psia)	Error (psia)	(% FS)	Ref Pres (psia)	Error (psia)	(% FS)
10.126	-0.009	-0.029	10.116	-0.006	-0.019	10.113	-0.009	-0.030
12.086	0.001	0.002	12.136	0.003	0.011	12.120	0.002	0.005
14.096	0.005	0.017	14.086	0.009	0.031	14.130	0.006	0.019
16.123	0.005	0.015	16.086	0.009	0.030	16.097	0.005	0.018
18.081	0.003	0.009	18.096	0.007	0.024	18.125	0.004	0.013
20.092	-0.002	-0.005	20.068	0.004	0.012	20.064	0.001	0.002
22.070	-0.005	-0.016	22.061	0.000	0.000	22.027	-0.002	-0.008
24.096	-0.007	-0.024	24.070	-0.001	-0.002	24.038	-0.005	-0.017
26.046	-0.006	-0.020	26.028	0.000	0.001	26.026	-0.004	-0.013
28.010	-0.002	-0.005	28.019	0.006	0.019	27.993	0.000	-0.001
30.027	0.009	0.029	30.019	0.016	0.053	30.043	0.010	0.034
28.157	-0.001	-0.004	28.079	0.005	0.016	28.069	-0.001	-0.002
26.124	-0.007	-0.024	26.123	0.000	-0.001	26.108	-0.005	-0.017
24.094	-0.008	-0.028	24.107	-0.002	-0.007	24.098	-0.007	-0.023
22.126	-0.006	-0.021	22.095	-0.001	-0.002	22.083	-0.006	-0.019
20.104	-0.003	-0.010	20.090	0.002	0.007	20.101	-0.002	-0.007
18.172	0.000	0.001	18.105	0.004	0.015	18.151	0.000	0.001
16.159	0.003	0.009	16.130	0.006	0.021	16.183	0.003	0.010
14.181	0.005	0.016	14.158	0.007	0.024	14.131	0.005	0.016
12.178	-0.001	-0.002	12.129	0.002	0.007	12.139	0.000	0.001
10.118	-0.010	-0.033	10.129	-0.007	-0.023	10.108	-0.009	-0.030
MDL - 2565 Jan 27 19:10:27 2006 Range 4 Temp 34.7° C			MDL - 2565 Jan 27 15:10:02 2006 Range 5 Temp 49.5° C					
Ref Pres (psia)	Error (psia)	(% FS)	Ref Pres (psia)	Error (psia)	(% FS)			
10.092	-0.009	-0.031	10.112	-0.007	-0.023			
12.082	0.000	0.001	12.125	0.003	0.011			
14.058	0.005	0.018	14.095	0.008	0.025			
16.040	0.004	0.014	16.083	0.007	0.022			
18.056	0.002	0.006	18.110	0.005	0.017			
20.013	-0.001	-0.003	20.055	0.002	0.008			
22.019	-0.005	-0.017	22.052	0.000	0.000			
24.001	-0.007	-0.025	24.053	-0.001	-0.005			
25.998	-0.007	-0.022	25.992	-0.001	-0.003			
27.953	-0.003	-0.010	28.033	0.004	0.012			
29.982	0.007	0.022	30.004	0.012	0.042			
28.060	-0.005	-0.015	28.075	0.001	0.004			
26.022	-0.008	-0.028	26.072	-0.003	-0.010			
24.093	-0.010	-0.035	24.061	-0.005	-0.016			
22.054	-0.008	-0.028	22.066	-0.004	-0.013			
19.960	-0.005	-0.016	20.020	-0.002	-0.006			
18.116	-0.001	-0.005	18.107	0.002	0.005			
16.113	0.001	0.002	16.131	0.002	0.007			
14.089	0.003	0.010	14.121	0.006	0.019			
12.100	-0.002	-0.007	12.150	0.001	0.003			
10.113	-0.011	-0.036	10.138	-0.008	-0.027			



07026

Issued by *[Signature]*

Document: SCAL 9607

Page 1 of 2



MOSDAX Calibration Report 2: MDL - 2565 Module 1069

Full Scale: 30 (psia)

File: D:\DOCUME~1\BILL\DATA\ACPV\VIEW\CALDATA\2006\30\28JAN06\02565

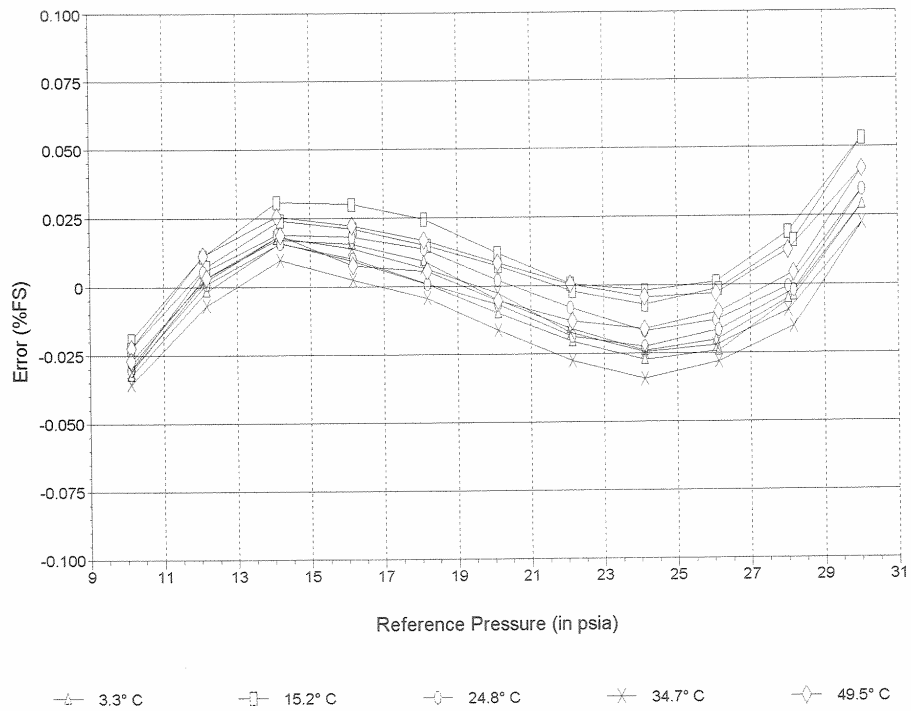
Pressure Reference: Paroscientific Model 230A-101 S/N 90098

Range: 30 PSI

Date of last reference to traceable standard: Dec 20 2004

Plot of Error vs. Reference Pressure

MDL - 2565 Module 1069



Comments

Issued by

Document: SCAL 9607

Page 2 of 2

As Received MOSDAX Cal. Report 1: MDL - 2565 Module 1069

Full Scale: 30 (psia)

File: D:\DOCUME~1\BILL\DATA\ACPVIEW\CALDATA\2006\30\28JAN06\02565

Pressure Reference: Paroscientific Model 230A-101 S/N 90098

Range: 30 PSI

Date of last reference to traceable standard: Dec 20 2004

MDL - 2565 Jan 28 07:10:25 2006 Range 1 Temp 3.3° C			MDL - 2565 Jan 28 03:10:47 2006 Range 2 Temp 15.2° C			MDL - 2565 Jan 27 23:11:03 2006 Range 3 Temp 24.8° C		
Ref Pres (psia)	Error (psia)	(% FS)	Ref Pres (psia)	Error (psia)	(% FS)	Ref Pres (psia)	Error (psia)	(% FS)
10.126	-0.009	-0.028	10.116	-0.006	-0.020	10.113	-0.010	-0.032
12.086	0.000	-0.002	12.136	0.002	0.006	12.120	-0.001	-0.002
14.096	0.003	0.009	14.086	0.006	0.021	14.130	0.002	0.008
16.123	0.001	0.004	16.086	0.005	0.018	16.097	0.001	0.004
18.081	-0.001	-0.004	18.096	0.003	0.010	18.125	-0.001	-0.003
20.092	-0.006	-0.020	20.068	-0.001	-0.004	20.064	-0.005	-0.016
22.070	-0.010	-0.032	22.061	-0.005	-0.016	22.027	-0.008	-0.026
24.096	-0.012	-0.041	24.070	-0.006	-0.019	24.038	-0.010	-0.035
26.046	-0.011	-0.037	26.028	-0.004	-0.015	26.026	-0.009	-0.030
28.010	-0.006	-0.021	28.019	0.002	0.005	27.993	-0.005	-0.016
30.027	0.004	0.014	30.019	0.012	0.041	30.043	0.007	0.022
28.157	-0.006	-0.020	28.079	0.001	0.002	28.069	-0.005	-0.017
26.124	-0.012	-0.041	26.123	-0.005	-0.017	26.108	-0.010	-0.033
24.094	-0.013	-0.044	24.107	-0.007	-0.024	24.098	-0.012	-0.041
22.126	-0.011	-0.037	22.095	-0.006	-0.019	22.083	-0.011	-0.037
20.104	-0.008	-0.025	20.090	-0.003	-0.009	20.101	-0.007	-0.025
18.172	-0.004	-0.013	18.105	0.000	0.000	18.151	-0.005	-0.016
16.159	-0.001	-0.002	16.130	0.003	0.008	16.183	-0.001	-0.004
14.181	0.002	0.008	14.158	0.004	0.015	14.131	0.001	0.005
12.178	-0.002	-0.006	12.129	0.001	0.002	12.139	-0.002	-0.006
10.118	-0.010	-0.032	10.129	-0.007	-0.023	10.108	-0.010	-0.033
MDL - 2565 Jan 27 19:10:27 2006 Range 4 Temp 34.7° C			MDL - 2565 Jan 27 15:10:02 2006 Range 5 Temp 49.5° C					
Ref Pres (psia)	Error (psia)	(% FS)	Ref Pres (psia)	Error (psia)	(% FS)			
10.092	-0.011	-0.036	10.112	-0.010	-0.033			
12.082	-0.002	-0.008	12.125	-0.001	-0.003			
14.058	0.001	0.005	14.095	0.002	0.008			
16.040	-0.001	-0.002	16.083	0.001	0.002			
18.056	-0.004	-0.012	18.110	-0.002	-0.005			
20.013	-0.007	-0.022	20.055	-0.004	-0.015			
22.019	-0.011	-0.038	22.052	-0.007	-0.024			
24.001	-0.013	-0.045	24.053	-0.009	-0.029			
25.998	-0.012	-0.041	25.992	-0.008	-0.027			
27.953	-0.008	-0.027	28.033	-0.003	-0.011			
29.982	0.002	0.007	30.004	0.006	0.020			
28.060	-0.010	-0.033	28.075	-0.006	-0.019			
26.022	-0.014	-0.047	26.072	-0.010	-0.034			
24.093	-0.016	-0.055	24.061	-0.012	-0.041			
22.054	-0.014	-0.048	22.066	-0.011	-0.037			
19.960	-0.011	-0.036	20.020	-0.009	-0.029			
18.116	-0.007	-0.023	18.107	-0.005	-0.017			
16.113	-0.004	-0.014	16.131	-0.004	-0.012			
14.089	-0.001	-0.004	14.121	0.000	0.001			
12.100	-0.005	-0.016	12.150	-0.003	-0.011			
10.113	-0.012	-0.041	10.138	-0.011	-0.038			

Issued by



Document: 5CAL 9607

Page 1 of 2



As Received MOSDAX Cal. Report 2: MDL - 2565 Module 1069

Full Scale: 30 (psia)

File: D:\DOCUME~1\BILL\DATA\ACPV\VIEW\CAL\DATA\2006\30\28\JAN06\02565

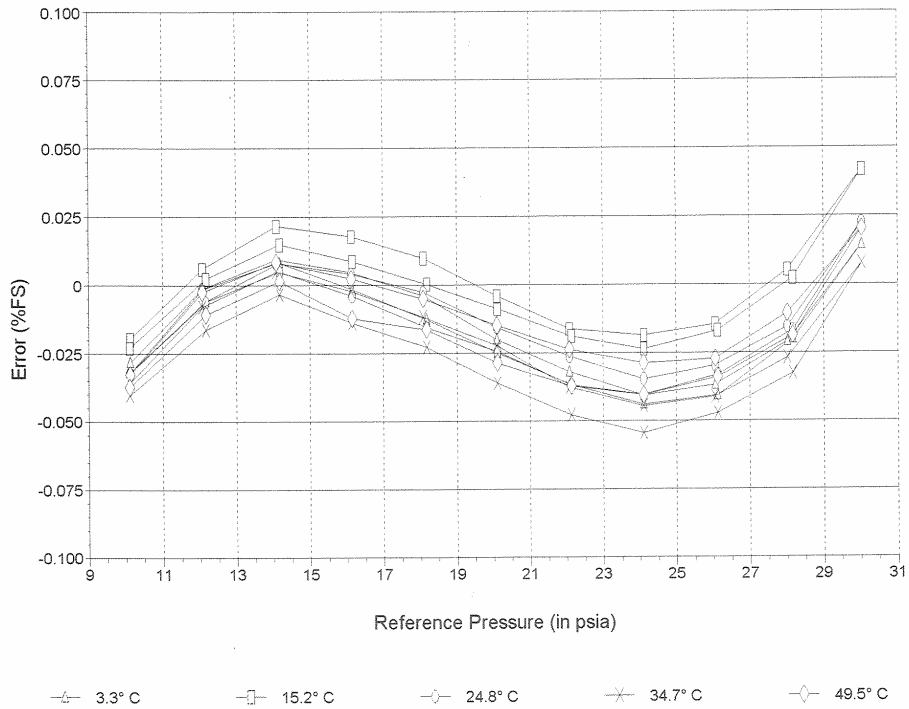
Pressure Reference: Paroscientific Model 230A-101 S/N 90098

Range: 30 PSI

Date of last reference to traceable standard: Dec 20 2004

Plot of Error vs. Reference Pressure

MDL - 2565 Module 1069



Comments

Issued by

Document: 5CAL 9607

Page 2 of 2

MOSDAX Calibration Report 1: MDL - 2693 Module 1255

Full Scale: 30 (psia)

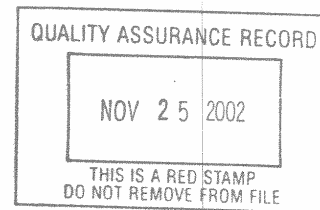
File: C:\ACVIEW\CALDATA\2002\30\14SEPT02\01255

Pressure Reference: Paroscientific Model 230A-101 S/N 62671

Range: 30 PSI

Date of last reference to traceable standard: Aug 27 2002

MDL - 2693 Sep 14 13:21:09 2002 Range 1 Temp 3.3° C			MDL - 2693 Sep 14 08:09:06 2002 Range 2 Temp 15.4° C			MDL - 2693 Sep 14 02:57:55 2002 Range 3 Temp 25.4° C		
Ref Pres (psia)	Error (psia)	(% FS)	Ref Pres (psia)	Error (psia)	(% FS)	Ref Pres (psia)	Error (psia)	(% FS)
9.987	-0.007	-0.023	9.992	-0.007	-0.023	9.992	-0.008	-0.027
12.024	0.003	0.010	12.019	0.004	0.013	11.997	0.002	0.008
13.972	0.006	0.021	13.966	0.008	0.026	13.962	0.006	0.021
15.963	0.003	0.011	15.965	0.007	0.023	15.969	0.005	0.016
17.963	0.001	0.005	17.959	0.005	0.016	17.951	0.003	0.010
19.956	0.000	-0.001	19.951	0.002	0.008	19.957	0.000	0.001
21.948	-0.003	-0.009	21.950	0.001	0.002	21.952	-0.001	-0.005
23.930	-0.006	-0.019	23.949	-0.001	-0.004	23.948	-0.003	-0.010
25.922	-0.006	-0.019	25.941	0.000	-0.001	25.933	-0.004	-0.013
27.923	0.000	-0.001	27.928	0.004	0.015	27.903	0.000	0.000
29.925	0.008	0.027	29.902	0.013	0.044	29.914	0.010	0.035
27.942	-0.001	-0.005	27.911	0.003	0.011	27.937	0.000	-0.001
25.970	-0.006	-0.019	25.975	-0.002	-0.005	25.989	-0.005	-0.017
23.976	-0.006	-0.020	23.994	-0.002	-0.007	23.989	-0.005	-0.018
21.980	-0.005	-0.017	21.985	-0.001	-0.003	21.968	-0.004	-0.013
19.978	-0.002	-0.007	19.991	0.001	0.002	19.989	-0.002	-0.007
17.991	0.000	0.000	17.980	0.003	0.009	17.990	0.001	0.004
15.987	0.002	0.008	15.976	0.005	0.017	15.982	0.002	0.007
13.975	0.004	0.014	13.976	0.006	0.020	13.978	0.005	0.016
11.981	0.002	0.006	11.994	0.002	0.007	11.994	0.001	0.003
9.993	-0.008	-0.025	9.988	-0.008	-0.028	9.990	-0.009	-0.029
MDL - 2693 Sep 13 21:46:58 2002 Range 4 Temp 35.4° C			MDL - 2693 Sep 13 16:34:54 2002 Range 5 Temp 50.5° C					
Ref Pres (psia)	Error (psia)	(% FS)	Ref Pres (psia)	Error (psia)	(% FS)			
9.993	-0.008	-0.027	9.995	-0.008	-0.026			
11.991	0.002	0.007	12.041	0.002	0.007			
13.968	0.007	0.024	13.967	0.008	0.027			
15.969	0.005	0.016	15.970	0.006	0.019			
17.963	0.002	0.007	17.958	0.004	0.013			
19.952	-0.001	-0.005	19.955	0.002	0.006			
21.954	-0.003	-0.010	21.936	-0.001	-0.003			
23.935	-0.006	-0.019	23.931	-0.002	-0.008			
25.938	-0.005	-0.015	25.932	-0.002	-0.007			
27.932	-0.001	-0.004	27.941	0.003	0.009			
29.928	0.006	0.021	29.912	0.010	0.035			
27.922	-0.002	-0.005	27.937	0.000	0.001			
25.973	-0.007	-0.024	25.966	-0.004	-0.014			
23.980	-0.008	-0.028	23.982	-0.006	-0.019			
21.989	-0.006	-0.020	21.990	-0.005	-0.015			
19.992	-0.004	-0.014	19.990	-0.002	-0.007			
17.989	-0.001	-0.004	17.983	0.000	0.001			
15.986	0.001	0.004	15.983	0.002	0.005			
13.983	0.003	0.010	13.984	0.005	0.017			
11.980	0.000	-0.001	11.993	0.000	0.001			
9.993	-0.010	-0.032	9.990	-0.009	-0.029			



005348

Issued by 

Document: 5CAL 9607

Page 1 of 2



MOSDAX Calibration Report 2: MDL - 2693 Module 1255

Full Scale: 30 (psia)

File: C:\ACPVIEW\GALDATA\2002\30\14SEPT02\01255

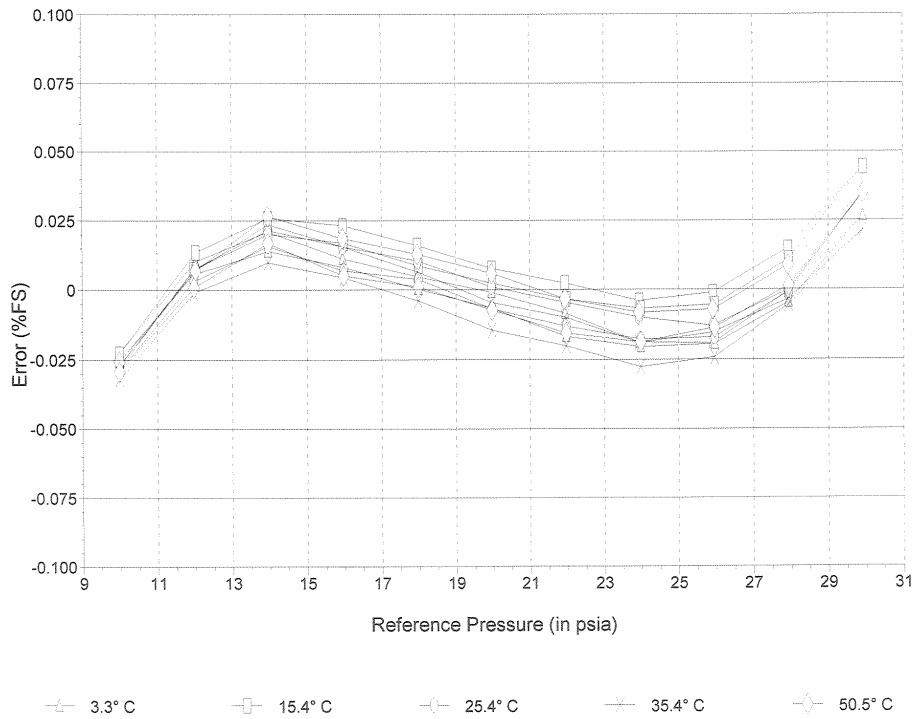
Pressure Reference: Paroscientific Model 230A-101 S/N 62671

Range: 30 PSI

Date of last reference to traceable standard: Aug 27 2002

Plot of Error vs. Reference Pressure

MDL - 2693 Module 1255



Comments

Issued by 

Document: 5CAL 9607

Page 2 of 2



As Received MOSDAX Cal. Report 1: MDL - 2693 Module 1255

Full Scale: 30 (psia)

File: O:\PRODBK\2002\30\14SEPT02\01255

Pressure Reference: Paroscientific Model 230A-101 S/N 62671

Range: 30 PSI

Date of last reference to traceable standard: Aug 27 2002

MDL - 2693 Sep 11 13:21:09 2002 Range 1 Temp 3.3° C			MDL - 2693 Sep 11 08:09:06 2002 Range 2 Temp 15.4° C			MDL - 2693 Sep 11 02:57:55 2002 Range 3 Temp 25.4° C		
Ref Pres (psia)	Error (psia)	(% FS)	Ref Pres (psia)	Error (psia)	(% FS)	Ref Pres (psia)	Error (psia)	(% FS)
9.987	-0.030	-0.099	9.992	-0.027	-0.090	9.992	-0.026	-0.086
12.024	-0.023	-0.075	12.019	-0.019	-0.063	11.997	-0.018	-0.061
13.972	-0.022	-0.073	13.966	-0.018	-0.059	13.962	-0.017	-0.056
15.963	-0.027	-0.092	15.965	-0.021	-0.071	15.969	-0.021	-0.071
17.963	-0.032	-0.107	17.959	-0.026	-0.087	17.951	-0.025	-0.085
19.956	-0.036	-0.121	19.951	-0.031	-0.104	19.957	-0.031	-0.103
21.948	-0.041	-0.136	21.950	-0.035	-0.118	21.952	-0.035	-0.117
23.930	-0.046	-0.155	23.949	-0.040	-0.133	23.948	-0.039	-0.131
25.922	-0.049	-0.163	25.941	-0.041	-0.138	25.933	-0.043	-0.143
27.923	-0.046	-0.152	27.928	-0.039	-0.130	27.903	-0.042	-0.138
29.925	-0.040	-0.133	29.902	-0.033	-0.109	29.914	-0.034	-0.112
27.942	-0.047	-0.156	27.911	-0.040	-0.134	27.937	-0.042	-0.139
25.970	-0.049	-0.163	25.975	-0.043	-0.142	25.989	-0.044	-0.147
23.976	-0.047	-0.157	23.994	-0.041	-0.136	23.989	-0.042	-0.139
21.980	-0.043	-0.145	21.985	-0.037	-0.124	21.968	-0.038	-0.126
19.978	-0.038	-0.127	19.991	-0.033	-0.109	19.989	-0.033	-0.111
17.991	-0.033	-0.111	17.980	-0.028	-0.094	17.990	-0.028	-0.092
15.987	-0.028	-0.095	15.976	-0.023	-0.077	15.982	-0.024	-0.080
13.975	-0.024	-0.080	13.976	-0.019	-0.065	13.978	-0.018	-0.062
11.981	-0.024	-0.080	11.994	-0.021	-0.069	11.994	-0.020	-0.065
9.993	-0.031	-0.102	9.988	-0.028	-0.095	9.990	-0.026	-0.088
MDL - 2693 Sep 10 21:46:58 2002 Range 4 Temp 35.4° C			MDL - 2693 Sep 10 16:34:54 2002 Range 5 Temp 50.5° C					
Ref Pres (psia)	Error (psia)	(% FS)	Ref Pres (psia)	Error (psia)	(% FS)			
9.993	-0.023	-0.078	9.995	-0.019	-0.064			
11.991	-0.016	-0.053	12.041	-0.012	-0.040			
13.968	-0.014	-0.046	13.967	-0.009	-0.029			
15.969	-0.019	-0.063	15.970	-0.014	-0.045			
17.963	-0.024	-0.080	17.958	-0.018	-0.059			
19.952	-0.030	-0.100	19.955	-0.022	-0.075			
21.954	-0.034	-0.114	21.936	-0.028	-0.092			
23.935	-0.040	-0.132	23.931	-0.032	-0.105			
25.938	-0.041	-0.137	25.932	-0.034	-0.112			
27.932	-0.040	-0.134	27.941	-0.031	-0.104			
29.928	-0.035	-0.117	29.912	-0.026	-0.086			
27.922	-0.041	-0.135	27.937	-0.034	-0.112			
25.973	-0.044	-0.146	25.966	-0.036	-0.119			
23.980	-0.042	-0.141	23.982	-0.035	-0.116			
21.989	-0.037	-0.125	21.990	-0.031	-0.105			
19.992	-0.033	-0.110	19.990	-0.026	-0.088			
17.989	-0.027	-0.091	17.983	-0.021	-0.071			
15.986	-0.022	-0.074	15.983	-0.018	-0.059			
13.983	-0.018	-0.059	13.984	-0.012	-0.039			
11.980	-0.018	-0.061	11.993	-0.014	-0.046			
9.993	-0.025	-0.083	9.990	-0.020	-0.067			

Issued by



Document: 5CAL 9607

Page 1 of 2



As Received MOSDAX Cal. Report 2: MDL - 2693 Module 1255

Full Scale: 30 (psia)

File: O:\PRODBK\2002\30\14SEPT02\01255

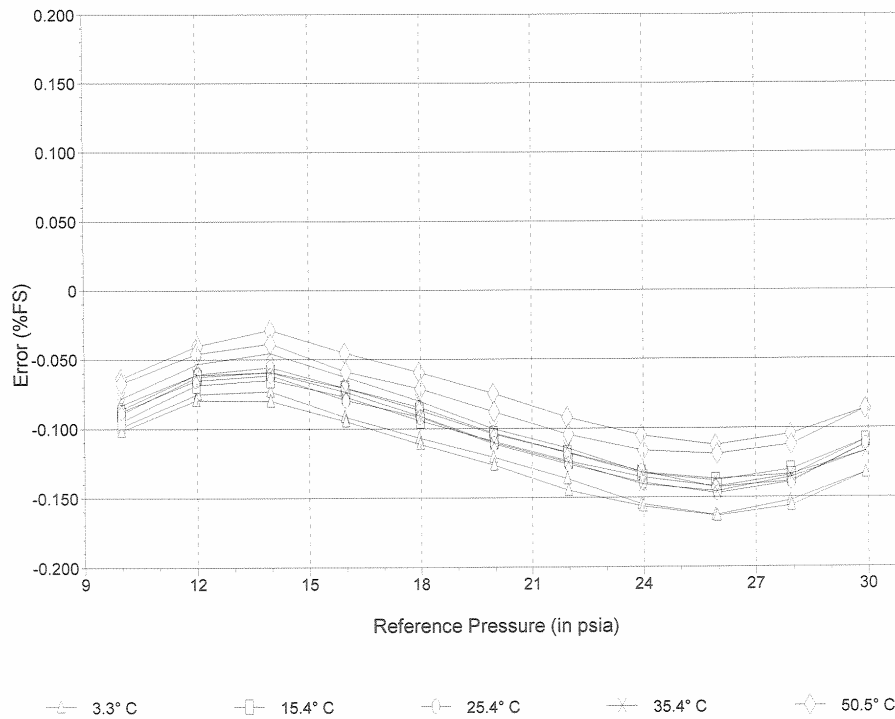
Pressure Reference: Paroscientific Model 230A-101 S/N 62671

Range: 30 PSI

Date of last reference to traceable standard: Aug 27 2002

Plot of Error vs. Reference Pressure

MDL - 2693 Module 1255



Comments
Y-Axis Not To Standard Scale.

Issued by

Document: SCAL 9607

Page 2 of 2



MOSDAX Calibration Report 1: MDL - 2693 Module 1255

Full Scale: 30 (psia)

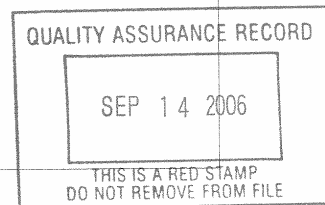
File: D:\DOCUME~1\BILL\DATA\ACPV\VIEW\CALDATA\2006\30\28JAN06\02693

Pressure Reference: Paroscientific Model 230A-101 S/N 90098

Range: 30 PSI

Date of last reference to traceable standard: Dec 20 2004

MDL - 2693 Jan 28 07:10:25 2006 Range 1 Temp 3.3° C			MDL - 2693 Jan 28 03:10:47 2006 Range 2 Temp 15.2° C			MDL - 2693 Jan 27 23:11:03 2006 Range 3 Temp 24.8° C		
Ref Pres (psia)	Error (psia)	(% FS)	Ref Pres (psia)	Error (psia)	(% FS)	Ref Pres (psia)	Error (psia)	(% FS)
10.126	-0.007	-0.023	10.116	-0.007	-0.023	10.113	-0.007	-0.024
12.086	0.001	0.003	12.136	0.003	0.011	12.120	0.003	0.009
14.096	0.005	0.018	14.086	0.007	0.025	14.130	0.007	0.022
16.123	0.004	0.013	16.086	0.006	0.019	16.097	0.004	0.013
18.081	0.001	0.003	18.096	0.004	0.013	18.125	0.002	0.008
20.092	0.000	-0.001	20.068	0.002	0.008	20.064	0.000	0.000
22.070	-0.004	-0.012	22.061	0.000	0.000	22.027	-0.002	-0.007
24.096	-0.005	-0.018	24.070	-0.002	-0.007	24.038	-0.005	-0.016
26.046	-0.005	-0.017	26.028	-0.001	-0.004	26.026	-0.004	-0.013
28.010	-0.002	-0.005	28.019	0.005	0.015	27.993	0.000	0.001
30.027	0.009	0.029	30.019	0.015	0.048	30.043	0.010	0.034
28.157	-0.001	-0.003	28.079	0.004	0.012	28.069	0.000	0.001
26.124	-0.006	-0.021	26.123	-0.001	-0.005	26.108	-0.005	-0.017
24.094	-0.007	-0.024	24.107	-0.003	-0.010	24.098	-0.006	-0.021
22.126	-0.005	-0.017	22.095	-0.002	-0.007	22.083	-0.005	-0.017
20.104	-0.001	-0.002	20.090	0.001	0.002	20.101	-0.001	-0.004
18.172	0.002	0.006	18.105	0.002	0.007	18.151	0.000	0.000
16.159	0.004	0.012	16.130	0.005	0.016	16.183	0.003	0.010
14.181	0.004	0.015	14.158	0.007	0.022	14.131	0.004	0.013
12.178	0.001	0.003	12.129	0.001	0.004	12.139	0.000	0.000
10.118	-0.007	-0.024	10.129	-0.008	-0.025	10.108	-0.009	-0.030
MDL - 2693 Jan 27 19:10:27 2006 Range 4 Temp 34.7° C			MDL - 2693 Jan 27 15:10:02 2006 Range 5 Temp 49.5° C					
Ref Pres (psia)	Error (psia)	(% FS)	Ref Pres (psia)	Error (psia)	(% FS)			
10.092	-0.008	-0.027	10.112	-0.007	-0.025			
12.082	0.001	0.004	12.125	0.003	0.011			
14.058	0.005	0.017	14.095	0.009	0.030			
16.040	0.004	0.014	16.083	0.007	0.022			
18.056	0.001	0.004	18.110	0.005	0.017			
20.013	-0.002	-0.008	20.055	0.002	0.005			
22.019	-0.005	-0.016	22.052	-0.001	-0.004			
24.001	-0.006	-0.020	24.053	-0.002	-0.006			
25.998	-0.007	-0.022	25.992	-0.002	-0.006			
27.953	-0.002	-0.008	28.033	0.004	0.012			
29.982	0.006	0.021	30.004	0.013	0.042			
28.060	-0.004	-0.013	28.075	0.002	0.007			
26.022	-0.008	-0.027	26.072	-0.004	-0.013			
24.093	-0.009	-0.031	24.061	-0.005	-0.017			
22.054	-0.007	-0.024	22.066	-0.004	-0.013			
19.960	-0.005	-0.016	20.020	-0.001	-0.005			
18.116	-0.002	-0.006	18.107	0.001	0.003			
16.113	-0.001	-0.002	16.131	0.002	0.008			
14.089	0.003	0.011	14.121	0.007	0.022			
12.100	-0.001	-0.003	12.150	0.001	0.005			
10.113	-0.008	-0.028	10.138	-0.006	-0.022			



7026

Issued by

Document: 5CAL 9607

Page 1 of 2

Schlumberger

MOSDAX Calibration Report 2: MDL - 2693 Module 1255

Full Scale: 30 (psia)

File: D:\DOCUME~1\BILL\DATA\ACPVIEW\CALDATA\2006\30\28JAN06\02693

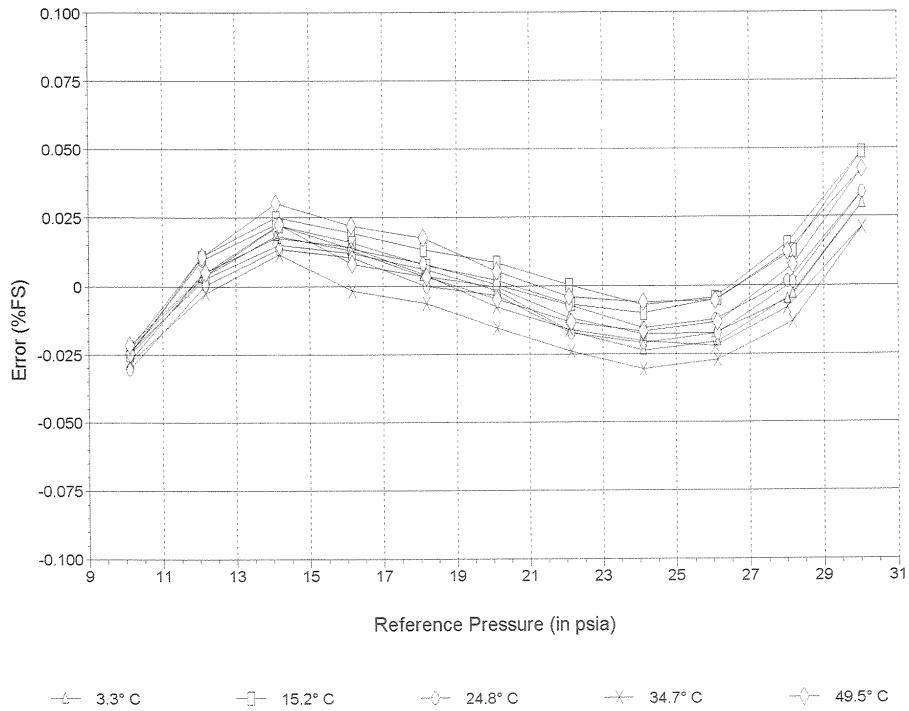
Pressure Reference: Paroscientific Model 230A-101 S/N 90098

Range: 30 PSI

Date of last reference to traceable standard: Dec 20 2004

Plot of Error vs. Reference Pressure

MDL - 2693 Module 1255



Comments

Issued by *[Signature]*



As Received MOSDAX Cal. Report 1: MDL - 2693 Module 1255

Full Scale: 30 (psia)

File: D:\DOCUME~1\BILL\DATA\ACPV\VIEW\CALDATA\2006\30\28JAN06\02693

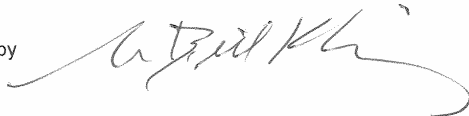
Pressure Reference: Paroscientific Model 230A-101 S/N 90098

Range: 30 PSI

Date of last reference to traceable standard: Dec 20 2004

MDL - 2693 Jan 28 07:10:25 2006 Range 1 Temp 3.3° C			MDL - 2693 Jan 28 03:10:47 2006 Range 2 Temp 15.2° C			MDL - 2693 Jan 27 23:11:03 2006 Range 3 Temp 24.8° C		
Ref Pres (psia)	Error (psia)	(% FS)	Ref Pres (psia)	Error (psia)	(% FS)	Ref Pres (psia)	Error (psia)	(% FS)
10.126	-0.015	-0.050	10.116	-0.015	-0.050	10.113	-0.015	-0.051
12.086	-0.008	-0.028	12.136	-0.006	-0.021	12.120	-0.007	-0.022
14.096	-0.005	-0.017	14.086	-0.003	-0.011	14.130	-0.004	-0.014
16.123	-0.008	-0.026	16.086	-0.006	-0.021	16.097	-0.008	-0.026
18.081	-0.011	-0.038	18.096	-0.009	-0.030	18.125	-0.011	-0.035
20.092	-0.013	-0.045	20.068	-0.011	-0.038	20.064	-0.014	-0.046
22.070	-0.018	-0.059	22.061	-0.015	-0.049	22.027	-0.017	-0.056
24.096	-0.020	-0.067	24.070	-0.018	-0.059	24.038	-0.020	-0.067
26.046	-0.020	-0.068	26.028	-0.017	-0.058	26.026	-0.020	-0.066
28.010	-0.017	-0.057	28.019	-0.012	-0.040	27.993	-0.016	-0.054
30.027	-0.007	-0.024	30.019	-0.002	-0.008	30.043	-0.007	-0.023
28.157	-0.017	-0.055	28.079	-0.013	-0.043	28.069	-0.016	-0.054
26.124	-0.021	-0.071	26.123	-0.018	-0.058	26.108	-0.021	-0.071
24.094	-0.022	-0.073	24.107	-0.019	-0.062	24.098	-0.022	-0.073
22.126	-0.019	-0.064	22.095	-0.017	-0.056	22.083	-0.020	-0.067
20.104	-0.014	-0.046	20.090	-0.013	-0.045	20.101	-0.015	-0.050
18.172	-0.011	-0.036	18.105	-0.011	-0.036	18.151	-0.013	-0.044
16.159	-0.008	-0.027	16.130	-0.007	-0.024	16.183	-0.009	-0.030
14.181	-0.006	-0.020	14.158	-0.004	-0.014	14.131	-0.007	-0.022
12.178	-0.009	-0.029	12.129	-0.008	-0.028	12.139	-0.009	-0.031
10.118	-0.015	-0.051	10.129	-0.016	-0.052	10.108	-0.017	-0.057
MDL - 2693 Jan 27 19:10:27 2006 Range 4 Temp 34.7° C			MDL - 2693 Jan 27 15:10:02 2006 Range 5 Temp 49.5° C					
Ref Pres (psia)	Error (psia)	(% FS)	Ref Pres (psia)	Error (psia)	(% FS)			
10.092	-0.016	-0.053	10.112	-0.014	-0.048			
12.082	-0.008	-0.026	12.125	-0.005	-0.016			
14.058	-0.005	-0.017	14.095	0.000	-0.001			
16.040	-0.007	-0.024	16.083	-0.004	-0.013			
18.056	-0.011	-0.037	18.110	-0.006	-0.020			
20.013	-0.016	-0.053	20.055	-0.011	-0.035			
22.019	-0.019	-0.064	22.052	-0.014	-0.047			
24.001	-0.021	-0.071	24.053	-0.016	-0.052			
25.998	-0.022	-0.075	25.992	-0.016	-0.053			
27.953	-0.019	-0.062	28.033	-0.011	-0.037			
29.982	-0.010	-0.035	30.004	-0.003	-0.009			
28.060	-0.020	-0.068	28.075	-0.013	-0.042			
26.022	-0.024	-0.080	26.072	-0.018	-0.061			
24.093	-0.024	-0.081	24.061	-0.019	-0.062			
22.054	-0.022	-0.072	22.066	-0.017	-0.057			
19.960	-0.018	-0.060	20.020	-0.014	-0.045			
18.116	-0.014	-0.048	18.107	-0.010	-0.034			
16.113	-0.012	-0.040	16.131	-0.008	-0.027			
14.089	-0.007	-0.023	14.121	-0.003	-0.009			
12.100	-0.010	-0.033	12.150	-0.007	-0.022			
10.113	-0.016	-0.053	10.138	-0.013	-0.044			

Issued by



Document: 5CAL 9607

Page 1 of 2



As Received MOSDAX Cal. Report 2: MDL - 2693 Module 1255

Full Scale: 30 (psia)

File: D:\DOCUME~1\BILL\DATA\ACP\VIEW\CAL\DATA\2006\30\28\JAN06\02693

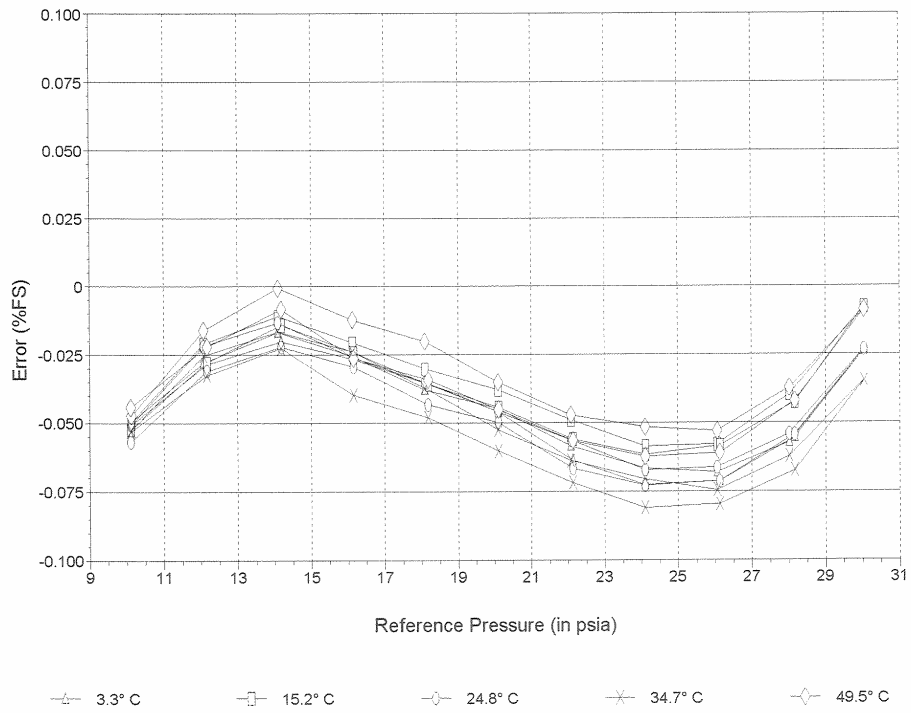
Pressure Reference: Paroscientific Model 230A-101 S/N 90098

Range: 30 PSI

Date of last reference to traceable standard: Dec 20 2004

Plot of Error vs. Reference Pressure

MDL - 2693 Module 1255



Comments

Issued by

Document: 5CAL 9807

Page 2 of 2

MOSDAX Calibration Report 1: SAM - 2844 Module 1154

Full Scale: 30 (psia)

File: C:\ACPVIEW\CALDATA\2001130\12OCT01\01154

Pressure Reference: Paroscientific Model 230A-101 S/N 62671

Range: 30 PSI

Date of last reference to traceable standard: Aug 15 2000

SAM - 2844 Oct 11 16:27:11 2001 Range 1 Temp 3.3° C			SAM - 2844 Oct 11 10:50:48 2001 Range 2 Temp 15.3° C			SAM - 2844 Oct 11 05:14:56 2001 Range 3 Temp 25.3° C		
Ref Pres (psia)	Error (psia)	(% FS)	Ref Pres (psia)	Error (psia)	(% FS)	Ref Pres (psia)	Error (psia)	(% FS)
9.999	-0.007	-0.025	10.001	-0.004	-0.014	9.994	-0.008	-0.027
11.983	0.000	0.001	11.980	0.005	0.016	11.983	0.001	0.003
13.978	0.004	0.014	13.977	0.008	0.027	13.978	0.005	0.016
15.970	0.003	0.011	15.974	0.007	0.025	15.967	0.003	0.010
17.966	0.002	0.007	17.974	0.006	0.020	17.970	0.001	0.005
19.959	-0.002	-0.006	19.961	0.004	0.012	19.960	-0.001	-0.004
21.952	-0.004	-0.014	21.946	0.002	0.006	21.950	-0.004	-0.013
23.942	-0.006	-0.019	23.948	0.000	0.000	23.945	-0.006	-0.020
25.934	-0.004	-0.014	25.933	0.001	0.003	25.950	-0.004	-0.014
27.927	-0.001	-0.005	27.921	0.006	0.019	27.929	0.000	0.000
29.940	0.008	0.026	29.926	0.015	0.050	29.923	0.008	0.028
27.919	0.000	-0.001	27.919	0.004	0.014	27.934	0.000	0.000
25.967	-0.005	-0.018	25.926	0.001	0.002	25.928	-0.004	-0.015
23.969	-0.006	-0.021	23.955	0.000	-0.001	23.939	-0.006	-0.020
21.983	-0.005	-0.017	21.967	0.001	0.003	21.966	-0.004	-0.015
19.988	-0.002	-0.007	19.985	0.003	0.009	19.981	-0.002	-0.007
17.987	0.001	0.005	17.990	0.005	0.018	17.981	0.001	0.003
15.983	0.003	0.009	15.988	0.007	0.023	15.986	0.002	0.008
13.977	0.003	0.010	13.983	0.007	0.024	13.988	0.003	0.010
11.983	0.000	0.001	11.985	0.004	0.012	11.995	0.001	0.003
9.985	-0.008	-0.027	9.995	-0.005	-0.015	9.997	-0.008	-0.027
SAM - 2844 Oct 10 23:38:46 2001 Range 4 Temp 35.2° C			SAM - 2844 Oct 10 18:08:07 2001 Range 5 Temp 50.2° C					
Ref Pres (psia)	Error (psia)	(% FS)	Ref Pres (psia)	Error (psia)	(% FS)			
9.990	-0.008	-0.027	10.000	-0.006	-0.020			
11.983	0.001	0.003	12.020	0.002	0.008			
13.973	0.005	0.017	13.977	0.008	0.026			
15.972	0.003	0.009	15.971	0.005	0.016			
17.968	0.001	0.003	17.964	0.004	0.012			
19.957	-0.003	-0.009	19.960	0.000	0.001			
21.946	-0.004	-0.015	21.950	-0.001	-0.005			
23.937	-0.007	-0.024	23.942	-0.003	-0.011			
25.930	-0.006	-0.019	25.929	-0.002	-0.007			
27.917	-0.002	-0.007	27.928	0.002	0.007			
29.922	0.006	0.020	29.920	0.010	0.033			
27.952	-0.002	-0.008	27.941	0.002	0.005			
25.986	-0.007	-0.022	25.992	-0.003	-0.009			
23.985	-0.007	-0.024	23.993	-0.004	-0.013			
21.979	-0.006	-0.018	21.995	-0.003	-0.009			
19.986	-0.004	-0.012	19.993	0.000	0.001			
17.982	0.000	0.000	17.990	0.002	0.007			
15.987	0.001	0.004	15.992	0.004	0.012			
13.981	0.003	0.011	13.990	0.006	0.018			
11.996	-0.001	-0.002	11.984	0.002	0.006			
9.998	-0.009	-0.030	9.997	-0.007	-0.023			

Issued by 

Document: SCAL 9607

Page 1 of 2



MOSDAX Calibration Report 2: SAM - 2844 Module 1154

Full Scale: 30 (psia)

File: C:\ACPVIEW\CALDATA\2001\30\12OCT01\011154

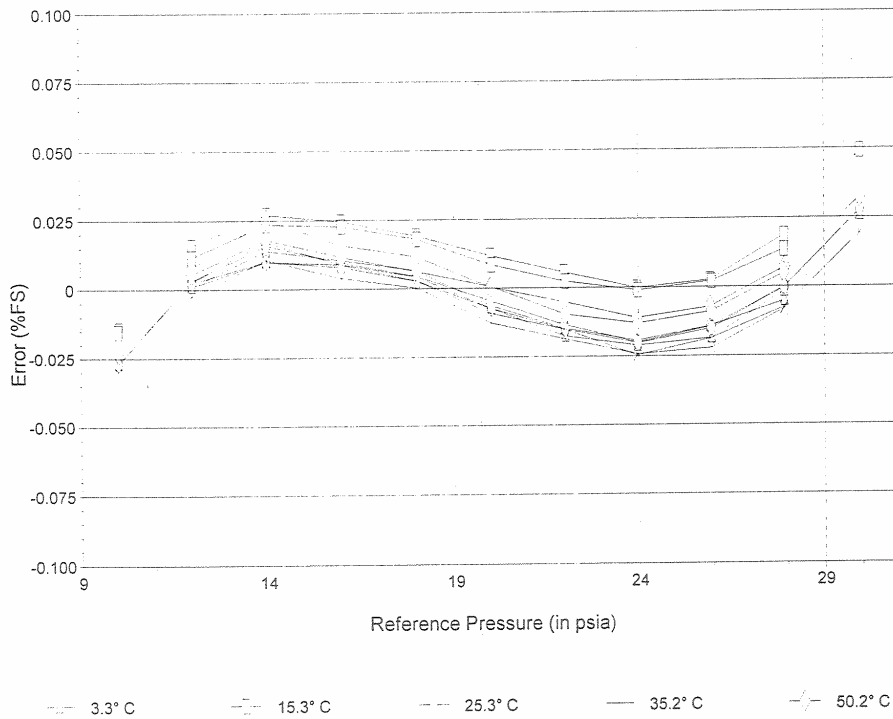
Pressure Reference: Paroscientific Model 230A-101 S/N 62671

Range: 30 PSI

Date of last reference to traceable standard: Aug 15 2000

Plot of Error vs. Reference Pressure

SAM - 2844 Module 1154



Comments

Issued by

Document: 5CAL 9607

Page 2 of 2



As Received MOSDAX Cal. Report 1: SAM - 2844 Module 1154

File: C:\ACPV\IEW\CALDATA\20011030\12OCT01\01154

Full Scale: 30 (psia)

Pressure Reference: Paroscientific Model 230A-101 S/N 62671

Range: 30 PSI

Date of last reference to traceable standard: Aug 15 2000

SAM - 2844 Oct 11 16:27:11 2001 Range 1 Temp 3.3° C			SAM - 2844 Oct 11 10:50:48 2001 Range 2 Temp 15.3° C			SAM - 2844 Oct 11 05:14:56 2001 Range 3 Temp 25.3° C		
Ref Pres (psia)	Error (psia)	(% FS)	Ref Pres (psia)	Error (psia)	(% FS)	Ref Pres (psia)	Error (psia)	(% FS)
9.999	-0.009	-0.029	10.001	-0.005	-0.016	9.994	-0.008	-0.027
11.983	-0.002	-0.006	11.980	0.003	0.012	11.983	0.000	0.000
13.978	0.001	0.004	13.977	0.006	0.020	13.978	0.003	0.011
15.970	-0.001	-0.002	15.974	0.004	0.015	15.967	0.000	0.002
17.966	-0.003	-0.009	17.974	0.002	0.006	17.970	-0.002	-0.006
19.959	-0.008	-0.025	19.961	-0.001	-0.004	19.960	-0.005	-0.018
21.952	-0.011	-0.037	21.946	-0.004	-0.013	21.950	-0.009	-0.030
23.942	-0.013	-0.045	23.948	-0.007	-0.022	23.945	-0.012	-0.040
25.934	-0.013	-0.043	25.933	-0.007	-0.023	25.950	-0.011	-0.037
27.927	-0.011	-0.037	27.921	-0.003	-0.010	27.929	-0.008	-0.026
29.940	-0.003	-0.009	29.926	0.005	0.017	29.923	0.000	-0.001
27.919	-0.010	-0.033	27.919	-0.005	-0.015	27.934	-0.008	-0.026
25.967	-0.014	-0.047	25.926	-0.007	-0.023	25.928	-0.011	-0.038
23.969	-0.014	-0.046	23.955	-0.007	-0.023	23.939	-0.012	-0.040
21.983	-0.012	-0.040	21.967	-0.005	-0.017	21.966	-0.010	-0.032
19.988	-0.008	-0.026	19.985	-0.002	-0.007	19.981	-0.006	-0.021
17.987	-0.003	-0.012	17.990	0.002	0.005	17.981	-0.002	-0.008
15.983	-0.001	-0.004	15.988	0.004	0.013	15.986	0.000	0.000
13.977	0.000	0.000	13.983	0.005	0.017	13.988	0.001	0.005
11.983	-0.002	-0.006	11.985	0.002	0.007	11.995	0.000	0.000
9.985	-0.009	-0.031	9.995	-0.005	-0.017	9.997	-0.008	-0.027
SAM - 2844 Oct 10 23:38:46 2001 Range 4 Temp 35.2° C			SAM - 2844 Oct 10 18:08:07 2001 Range 5 Temp 50.2° C					
Ref Pres (psia)	Error (psia)	(% FS)	Ref Pres (psia)	Error (psia)	(% FS)			
9.990	-0.008	-0.027	10.000	-0.006	-0.021			
11.983	0.000	0.001	12.020	0.001	0.005			
13.973	0.004	0.013	13.977	0.006	0.020			
15.972	0.001	0.002	15.971	0.003	0.009			
17.968	-0.002	-0.006	17.964	0.001	0.002			
19.957	-0.006	-0.021	19.960	-0.003	-0.011			
21.946	-0.009	-0.029	21.950	-0.006	-0.019			
23.937	-0.013	-0.042	23.942	-0.008	-0.027			
25.930	-0.012	-0.039	25.929	-0.007	-0.025			
27.917	-0.009	-0.030	27.928	-0.004	-0.013			
29.922	-0.002	-0.006	29.920	0.003	0.011			
27.952	-0.009	-0.031	27.941	-0.004	-0.015			
25.986	-0.013	-0.042	25.992	-0.008	-0.027			
23.985	-0.012	-0.041	23.993	-0.009	-0.029			
21.979	-0.010	-0.033	21.995	-0.007	-0.023			
19.986	-0.007	-0.024	19.993	-0.003	-0.011			
17.982	-0.003	-0.009	17.990	-0.001	-0.003			
15.987	-0.001	-0.003	15.992	0.001	0.005			
13.981	0.002	0.006	13.990	0.004	0.013			
11.996	-0.001	-0.004	11.984	0.001	0.003			
9.998	-0.009	-0.030	9.997	-0.007	-0.023			

Issued by 

Document: SCAL 9607

Page 1 of 2



As Received MOSDAX Cal. Report 2: SAM - 2844 Module 1154

Full Scale: 30 (psia)

File: C:\ACPVIEW\CALDATA\2001\30\12OCT01\01154

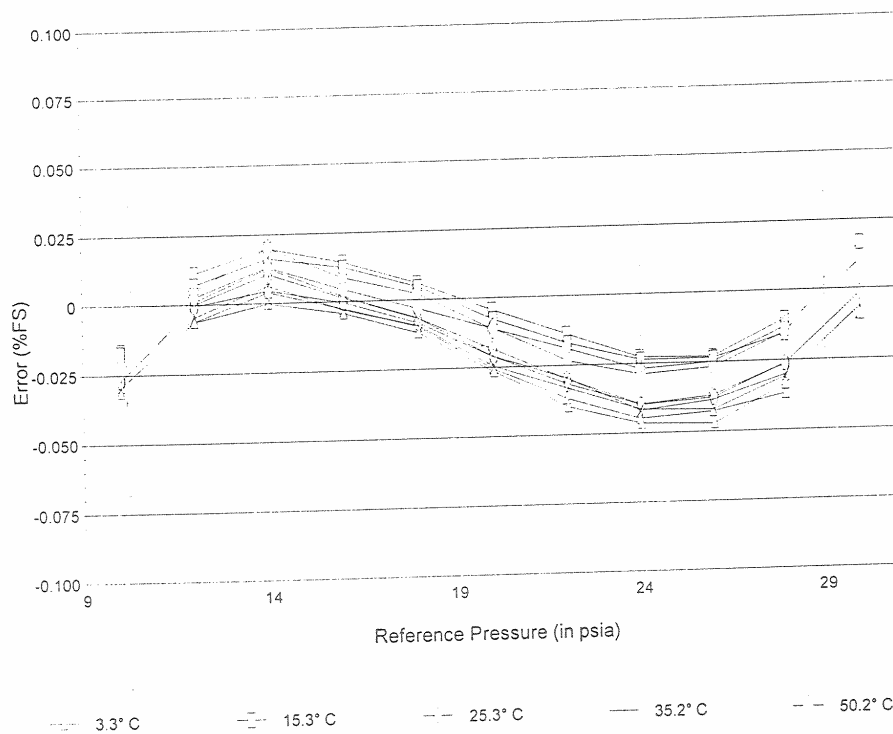
Pressure Reference: Paroscientific Model 230A-101 S/N 62671

Range: 30 PSI

Date of last reference to traceable standard: Aug 15 2000

Plot of Error vs. Reference Pressure

SAM - 2844 Module 1154



Comments

Issued by

Document: SCAL 9607

Page 2 of 2



MOSDAX Calibration Report 1: SAM - 2844 Module 1154

Full Scale: 30 (psia)

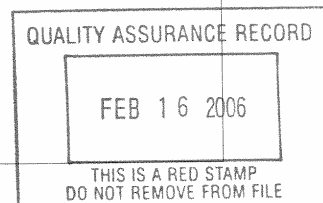
File: D:\DOCUMENT-1\BILLDATA\ACPVIEW\CALDATA\2006\307\JAN06\02844

Pressure Reference: Paroscientific Model 230A-101 S/N 90098

Range: 30 PSI

Date of last reference to traceable standard: Dec 20 2004

SAM - 2844 Jan 07 02:16:05 2006 Range 1 Temp 3.1° C			SAM - 2844 Jan 06 22:09:55 2006 Range 2 Temp 15.0° C			SAM - 2844 Jan 06 18:03:30 2006 Range 3 Temp 24.7° C		
Ref Pres (psia)	Error (psia)	(% FS)	Ref Pres (psia)	Error (psia)	(% FS)	Ref Pres (psia)	Error (psia)	(% FS)
10.039	-0.007	-0.024	10.057	-0.006	-0.019	10.071	-0.008	-0.028
12.021	0.001	0.005	12.022	0.004	0.014	12.027	0.001	0.002
13.994	0.006	0.019	14.009	0.008	0.025	13.997	0.005	0.017
16.027	0.004	0.015	16.052	0.007	0.023	16.020	0.002	0.008
17.979	0.003	0.008	18.007	0.006	0.020	18.000	0.002	0.006
19.970	0.000	-0.001	19.988	0.004	0.013	19.979	-0.001	-0.004
21.927	-0.004	-0.012	21.948	0.001	0.005	21.951	-0.004	-0.013
23.902	-0.005	-0.016	23.951	0.000	-0.001	23.976	-0.005	-0.018
25.930	-0.005	-0.018	25.973	0.001	0.002	25.923	-0.003	-0.012
27.895	-0.002	-0.005	27.944	0.004	0.015	27.924	-0.001	-0.002
29.932	0.009	0.029	29.969	0.015	0.049	29.943	0.009	0.032
27.995	-0.002	-0.005	27.988	0.005	0.015	28.016	-0.001	-0.003
25.995	-0.005	-0.018	25.993	0.001	0.002	25.984	-0.004	-0.014
23.989	-0.006	-0.020	24.052	-0.001	-0.003	24.036	-0.007	-0.022
22.038	-0.004	-0.013	21.998	0.000	0.000	22.008	-0.005	-0.016
19.996	-0.001	-0.003	20.023	0.003	0.009	20.005	-0.002	-0.005
18.060	0.002	0.006	18.047	0.005	0.017	18.051	0.001	0.003
16.073	0.004	0.014	16.061	0.007	0.024	16.080	0.003	0.011
14.081	0.004	0.015	14.080	0.008	0.026	14.080	0.004	0.015
12.060	0.001	0.003	12.080	0.004	0.012	12.052	0.001	0.002
10.057	-0.007	-0.022	10.101	-0.004	-0.014	10.057	-0.008	-0.025
SAM - 2844 Jan 06 13:52:24 2006 Range 4 Temp 34.6° C			SAM - 2844 Jan 06 09:41:38 2006 Range 5 Temp 49.4° C					
Ref Pres (psia)	Error (psia)	(% FS)	Ref Pres (psia)	Error (psia)	(% FS)			
10.085	-0.008	-0.025	10.096	-0.008	-0.026			
12.033	0.001	0.002	12.051	0.002	0.007			
14.055	0.005	0.016	14.041	0.007	0.025			
16.013	0.003	0.010	16.028	0.006	0.019			
18.019	0.002	0.007	17.989	0.004	0.014			
20.000	-0.002	-0.008	19.973	0.001	0.004			
21.995	-0.006	-0.019	21.993	-0.002	-0.005			
24.025	-0.007	-0.023	23.999	-0.003	-0.011			
25.977	-0.006	-0.021	25.941	-0.003	-0.009			
27.979	-0.002	-0.006	27.919	0.001	0.004			
29.959	0.007	0.024	29.933	0.010	0.033			
28.074	-0.003	-0.009	28.010	0.001	0.002			
26.011	-0.007	-0.024	26.046	-0.004	-0.012			
24.051	-0.008	-0.028	24.038	-0.004	-0.015			
22.105	-0.007	-0.024	22.044	-0.002	-0.008			
20.026	-0.004	-0.014	20.005	0.000	-0.001			
18.104	0.000	0.000	18.073	0.003	0.010			
16.116	0.001	0.003	16.097	0.004	0.012			
14.093	0.004	0.014	14.116	0.006	0.021			
12.099	0.000	-0.001	12.092	0.002	0.008			
10.109	-0.008	-0.026	10.138	-0.008	-0.025			



006844

Issued by *[Signature]*

Schlumberger

MOSDAX Calibration Report 2: SAM - 2844 Module 1154

Full Scale: 30 (psia)

File: D:\DOCUME~1\BILL\DATA\ACPV\VIEW\CALDATA\2006\30\7\JAN06\02844

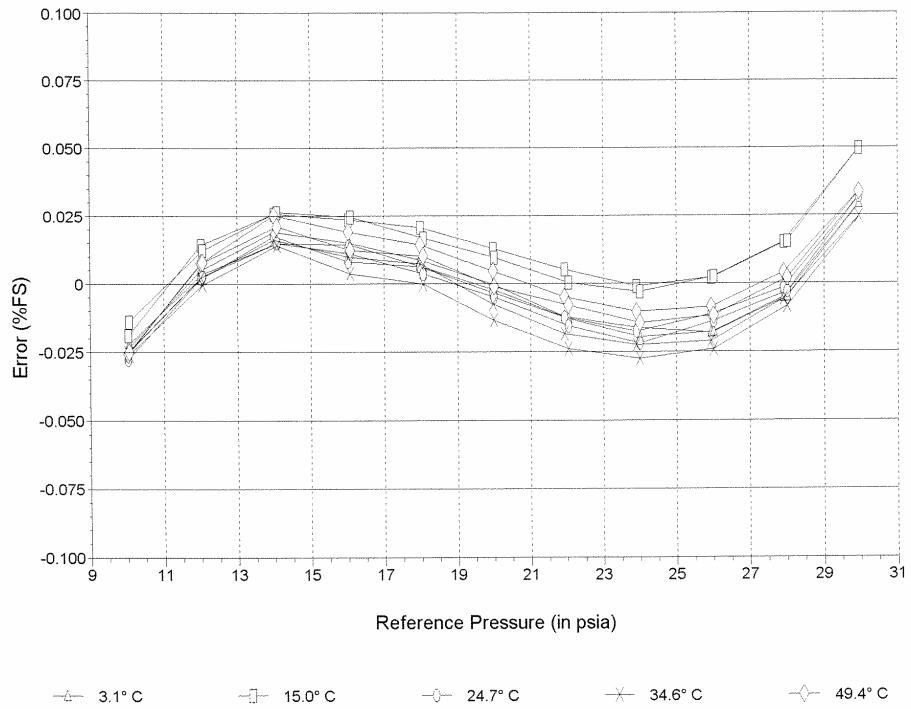
Pressure Reference: Paroscientific Model 230A-101 S/N 90098

Range: 30 PSI

Date of last reference to traceable standard: Dec 20 2004

Plot of Error vs. Reference Pressure

SAM - 2844 Module 1154



Comments

Issued by *[Signature]*

Document: SCAL 9607

Page 2 of 2



As Received MOSDAX Cal. Report 1: SAM - 2844 Module 1154

Full Scale: 30 (psia)

File: D:\DOCUME~1\BILL\DATA\ACPV\VIEW\CALDATA\2006\307\JAN06\02844

Pressure Reference: Paroscientific Model 230A-101 S/N 90098

Range: 30 PSI

Date of last reference to traceable standard: Dec 20 2004

SAM - 2844 Jan 07 02:16:05 2006 Range 1 Temp 3.1° C			SAM - 2844 Jan 06 22:09:55 2006 Range 2 Temp 15.0° C			SAM - 2844 Jan 06 18:03:30 2006 Range 3 Temp 24.7° C		
Ref Pres (psia)	Error (psia)	(% FS)	Ref Pres (psia)	Error (psia)	(% FS)	Ref Pres (psia)	Error (psia)	(% FS)
10.039	-0.014	-0.046	10.057	-0.012	-0.041	10.071	-0.015	-0.050
12.021	-0.006	-0.021	12.022	-0.003	-0.012	12.027	-0.007	-0.024
13.994	-0.003	-0.010	14.009	-0.001	-0.003	13.997	-0.003	-0.011
16.027	-0.005	-0.016	16.052	-0.002	-0.008	16.020	-0.007	-0.023
17.979	-0.007	-0.024	18.007	-0.004	-0.012	18.000	-0.008	-0.027
19.970	-0.010	-0.035	19.988	-0.006	-0.021	19.979	-0.011	-0.038
21.927	-0.014	-0.047	21.948	-0.009	-0.030	21.951	-0.014	-0.048
23.902	-0.015	-0.051	23.951	-0.011	-0.036	23.976	-0.016	-0.053
25.930	-0.016	-0.052	25.973	-0.010	-0.032	25.923	-0.014	-0.046
27.895	-0.011	-0.038	27.944	-0.005	-0.018	27.924	-0.011	-0.036
29.932	-0.001	-0.002	29.969	0.005	0.018	29.943	0.000	-0.001
27.995	-0.011	-0.038	27.988	-0.005	-0.018	28.016	-0.011	-0.037
25.995	-0.015	-0.052	25.993	-0.010	-0.032	25.984	-0.015	-0.049
23.989	-0.016	-0.054	24.052	-0.011	-0.038	24.036	-0.017	-0.057
22.038	-0.014	-0.048	21.998	-0.010	-0.035	22.008	-0.015	-0.051
19.996	-0.011	-0.037	20.023	-0.007	-0.025	20.005	-0.012	-0.039
18.060	-0.008	-0.027	18.047	-0.005	-0.016	18.051	-0.009	-0.030
16.073	-0.005	-0.017	16.061	-0.002	-0.007	16.080	-0.006	-0.020
14.081	-0.004	-0.014	14.080	-0.001	-0.003	14.080	-0.004	-0.014
12.060	-0.007	-0.023	12.080	-0.004	-0.014	12.052	-0.007	-0.023
10.057	-0.014	-0.045	10.101	-0.011	-0.036	10.057	-0.014	-0.047
SAM - 2844 Jan 06 13:52:24 2006 Range 4 Temp 34.6° C			SAM - 2844 Jan 06 09:41:38 2006 Range 5 Temp 49.4° C					
Ref Pres (psia)	Error (psia)	(% FS)	Ref Pres (psia)	Error (psia)	(% FS)			
10.085	-0.014	-0.047	10.096	-0.014	-0.047			
12.033	-0.007	-0.023	12.051	-0.005	-0.017			
14.055	-0.004	-0.013	14.041	-0.001	-0.003			
16.013	-0.006	-0.021	16.028	-0.003	-0.011			
18.019	-0.008	-0.026	17.989	-0.005	-0.018			
20.000	-0.013	-0.042	19.973	-0.009	-0.029			
21.995	-0.016	-0.054	21.993	-0.012	-0.039			
24.025	-0.017	-0.058	23.999	-0.013	-0.045			
25.977	-0.017	-0.057	25.941	-0.013	-0.043			
27.979	-0.012	-0.040	27.919	-0.009	-0.029			
29.959	-0.003	-0.009	29.933	0.001	0.002			
28.074	-0.013	-0.043	28.010	-0.009	-0.031			
26.011	-0.018	-0.059	26.046	-0.014	-0.046			
24.051	-0.019	-0.063	24.038	-0.015	-0.049			
22.105	-0.018	-0.059	22.044	-0.013	-0.042			
20.026	-0.014	-0.048	20.005	-0.010	-0.035			
18.104	-0.010	-0.033	18.073	-0.007	-0.022			
16.116	-0.008	-0.028	16.097	-0.005	-0.018			
14.093	-0.004	-0.015	14.116	-0.002	-0.007			
12.099	-0.008	-0.026	12.092	-0.005	-0.017			
10.109	-0.014	-0.048	10.138	-0.014	-0.046			

Issued by 

Document: SCAL 9607

Page 1 of 2



As Received MOSDAX Cal. Report 2: SAM - 2844 Module 1154

Full Scale: 30 (psia)

File: D:\DOCUME~1\BILL\DATA\ACPVIEW\CALDATA\2006\30\7\JAN06\02844

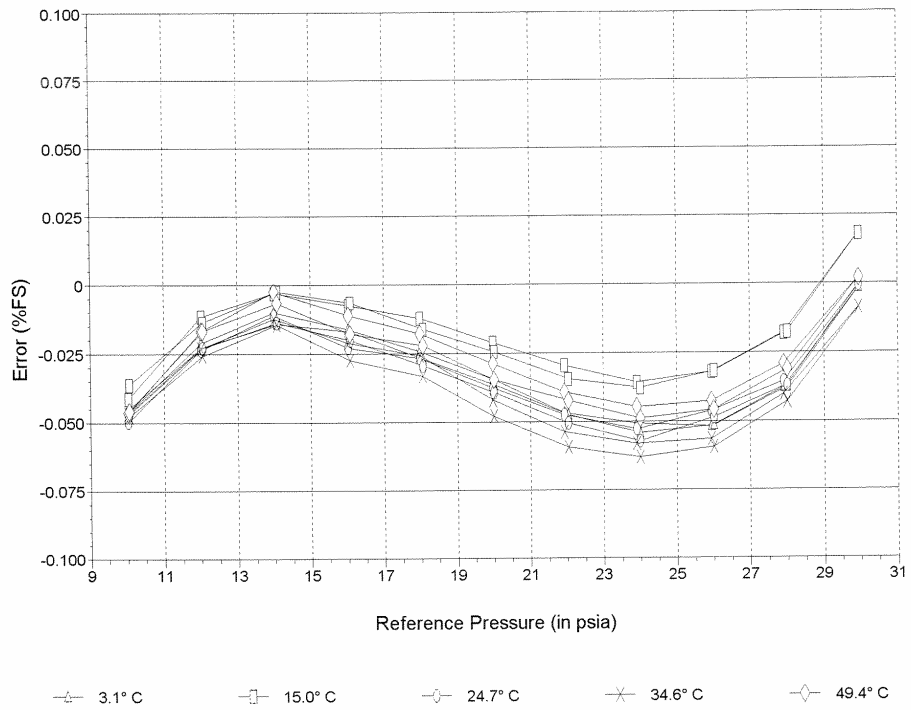
Pressure Reference: Paroscientific Model 230A-101 S/N 90098

Range: 30 PSI

Date of last reference to traceable standard: Dec 20 2004

Plot of Error vs. Reference Pressure

SAM - 2844 Module 1154



Comments

Issued by 

Document: 5CAL 9607

Page 2 of 2



MOSDAX Calibration Report 1: SAM - 2845 Module 1163

Full Scale: 30 (psia)

File: C:\ACPVIEW\CALDATA\2001\30\12OCT01\01163

Pressure Reference: Paroscientific Model 230A-101 S/N 62671

Range: 30 PSI

Date of last reference to traceable standard: Aug 15 2000

SAM - 2845 Oct 11 16:27:11 2001 Range 1 Temp 3.3° C			SAM - 2845 Oct 11 10:50:48 2001 Range 2 Temp 15.3° C			SAM - 2845 Oct 11 05:14:56 2001 Range 3 Temp 25.3° C		
Ref Pres (psia)	Error (psia)	(% FS)	Ref Pres (psia)	Error (psia)	(% FS)	Ref Pres (psia)	Error (psia)	(% FS)
9.999	-0.006	-0.020	10.001	-0.004	-0.014	9.994	-0.006	-0.020
11.983	0.001	0.003	11.980	0.004	0.012	11.983	0.000	0.001
13.978	0.003	0.011	13.977	0.007	0.024	13.978	0.005	0.016
15.970	0.003	0.010	15.974	0.007	0.024	15.967	0.003	0.012
17.966	0.001	0.005	17.974	0.006	0.019	17.970	0.002	0.006
19.959	-0.001	-0.004	19.961	0.004	0.013	19.960	-0.001	-0.002
21.952	-0.004	-0.012	21.946	0.002	0.005	21.950	-0.003	-0.010
23.942	-0.005	-0.018	23.948	0.001	0.003	23.945	-0.004	-0.014
25.934	-0.005	-0.017	25.933	0.001	0.003	25.950	-0.004	-0.015
27.927	-0.002	-0.008	27.921	0.005	0.017	27.929	0.000	0.000
29.940	0.005	0.017	29.926	0.013	0.043	29.923	0.007	0.022
27.919	-0.001	-0.005	27.919	0.005	0.018	27.934	0.000	0.000
25.967	-0.006	-0.020	25.926	0.002	0.005	25.928	-0.004	-0.013
23.969	-0.006	-0.021	23.955	0.001	0.003	23.939	-0.005	-0.018
21.983	-0.004	-0.014	21.967	0.002	0.006	21.966	-0.004	-0.012
19.988	-0.001	-0.004	19.985	0.003	0.011	19.981	-0.001	-0.005
17.987	0.001	0.003	17.990	0.005	0.018	17.981	0.000	0.001
15.983	0.002	0.005	15.988	0.006	0.020	15.986	0.001	0.005
13.977	0.003	0.010	13.983	0.006	0.020	13.988	0.003	0.010
11.983	0.000	0.000	11.985	0.004	0.013	11.995	0.000	0.000
9.985	-0.006	-0.020	9.995	-0.004	-0.012	9.997	-0.007	-0.023

SAM - 2845 Oct 10 23:38:46 2001 Range 4 Temp 35.2° C			SAM - 2845 Oct 10 18:08:07 2001 Range 5 Temp 50.2° C		
Ref Pres (psia)	Error (psia)	(% FS)	Ref Pres (psia)	Error (psia)	(% FS)
9.990	-0.006	-0.020	10.000	-0.005	-0.015
11.983	0.000	0.000	12.020	0.003	0.010
13.973	0.003	0.010	13.977	0.005	0.018
15.972	0.002	0.006	15.971	0.004	0.013
17.968	0.001	0.003	17.964	0.003	0.010
19.957	-0.001	-0.005	19.960	0.002	0.007
21.946	-0.004	-0.014	21.950	0.000	0.000
23.937	-0.007	-0.023	23.942	-0.002	-0.008
25.930	-0.006	-0.021	25.929	-0.002	-0.006
27.917	-0.003	-0.009	27.928	0.002	0.005
29.922	0.005	0.016	29.920	0.008	0.028
27.952	-0.003	-0.009	27.941	0.001	0.004
25.986	-0.006	-0.020	25.992	-0.002	-0.006
23.985	-0.007	-0.024	23.993	-0.004	-0.013
21.979	-0.006	-0.019	21.995	-0.002	-0.006
19.986	-0.003	-0.011	19.993	0.000	-0.001
17.982	0.000	-0.002	17.990	0.001	0.002
15.987	0.000	0.001	15.992	0.002	0.006
13.981	0.003	0.009	13.990	0.004	0.013
11.996	0.000	0.001	11.984	0.001	0.004
9.998	-0.007	-0.023	9.997	-0.006	-0.020

Issued by

Document: SCAL 9607

Page 1 of 2



MOSDAX Calibration Report 2: SAM - 2845 Module 1163

Full Scale: 30 (psia)

File: C:\ACPVIEW\CALDATA\2001130\12OCT0101183

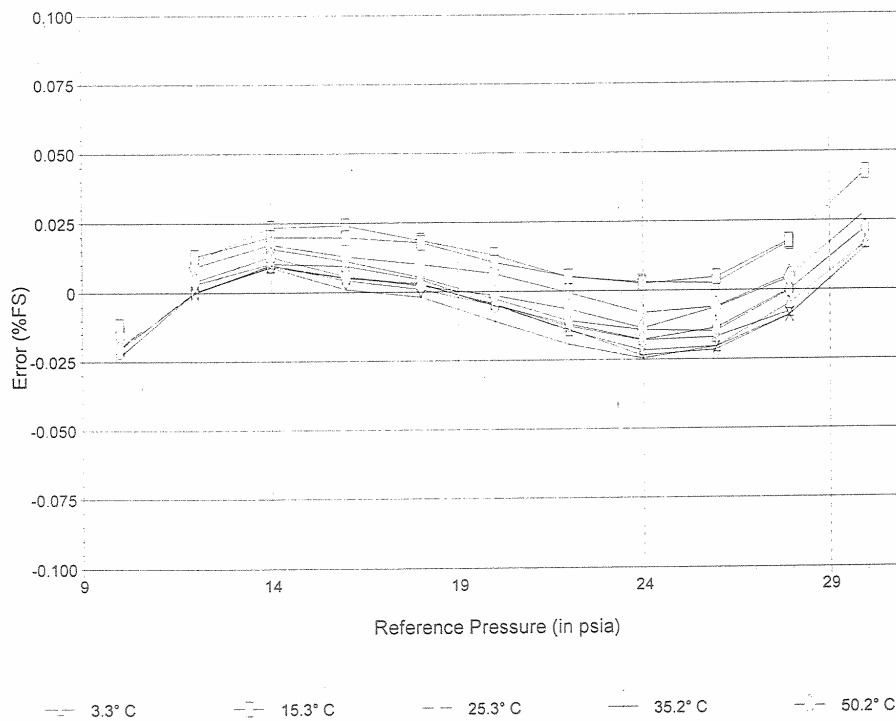
Pressure Reference: Paroscientific Model 230A-101 S/N 62671

Range: 30 PSI

Date of last reference to traceable standard: Aug 15 2000

Plot of Error vs. Reference Pressure

SAM - 2845 Module 1163



Comments

Issued by *Mr Bill Kling*

Document: SCAL 9607

Page 2 of 2



As Received MOSDAX Cal. Report 1: SAM - 2845 Module 1163

File: C:\ACVIEW\CALDATA\2001\30\12\OCT01\01163

Full Scale: 30 (psia)

Pressure Reference: Paroscientific Model 230A-101 S/N 62671

Range: 30 PSI

Date of last reference to traceable standard: Aug 15 2000

SAM - 2845 Oct 11 16:27:11 2001 Range 1 Temp 3.3° C			SAM - 2845 Oct 11 10:50:48 2001 Range 2 Temp 15.3° C			SAM - 2845 Oct 11 05:14:56 2001 Range 3 Temp 25.3° C		
Ref Pres (psia)	Error (psia)	(% FS)	Ref Pres (psia)	Error (psia)	(% FS)	Ref Pres (psia)	Error (psia)	(% FS)
9.999	-0.017	-0.056	10.001	-0.015	-0.049	9.994	-0.016	-0.055
11.983	-0.011	-0.035	11.980	-0.008	-0.026	11.983	-0.011	-0.036
13.978	-0.009	-0.031	13.977	-0.005	-0.017	13.978	-0.007	-0.024
15.970	-0.010	-0.034	15.974	-0.006	-0.019	15.967	-0.009	-0.032
17.966	-0.013	-0.042	17.974	-0.008	-0.028	17.970	-0.012	-0.041
19.959	-0.016	-0.055	19.961	-0.011	-0.036	19.960	-0.015	-0.052
21.952	-0.020	-0.066	21.946	-0.014	-0.047	21.950	-0.019	-0.063
23.942	-0.022	-0.075	23.948	-0.016	-0.052	23.945	-0.021	-0.069
25.934	-0.023	-0.077	25.933	-0.017	-0.056	25.950	-0.022	-0.073
27.927	-0.021	-0.072	27.921	-0.013	-0.045	27.929	-0.018	-0.061
29.940	-0.015	-0.051	29.926	-0.007	-0.022	29.923	-0.012	-0.042
27.919	-0.021	-0.069	27.919	-0.013	-0.044	27.934	-0.018	-0.061
25.967	-0.024	-0.081	25.926	-0.016	-0.054	25.928	-0.021	-0.072
23.969	-0.024	-0.078	23.955	-0.016	-0.053	23.939	-0.022	-0.073
21.983	-0.020	-0.068	21.967	-0.014	-0.047	21.966	-0.019	-0.064
19.988	-0.016	-0.055	19.985	-0.012	-0.039	19.981	-0.016	-0.054
17.987	-0.013	-0.044	17.990	-0.009	-0.029	17.981	-0.014	-0.045
15.983	-0.012	-0.039	15.988	-0.007	-0.024	15.986	-0.012	-0.039
13.977	-0.010	-0.032	13.983	-0.006	-0.020	13.988	-0.009	-0.030
11.983	-0.011	-0.038	11.985	-0.007	-0.024	11.995	-0.011	-0.037
9.985	-0.017	-0.055	9.995	-0.014	-0.047	9.997	-0.017	-0.057
SAM - 2845 Oct 10 23:38:46 2001 Range 4 Temp 35.2° C			SAM - 2845 Oct 10 18:08:07 2001 Range 5 Temp 50.2° C					
Ref Pres (psia)	Error (psia)	(% FS)	Ref Pres (psia)	Error (psia)	(% FS)			
9.990	-0.016	-0.054	10.000	-0.015	-0.050			
11.983	-0.011	-0.037	12.020	-0.009	-0.029			
13.973	-0.009	-0.030	13.977	-0.007	-0.024			
15.972	-0.011	-0.038	15.971	-0.010	-0.032			
17.968	-0.013	-0.043	17.964	-0.012	-0.039			
19.957	-0.016	-0.054	19.960	-0.014	-0.046			
21.946	-0.020	-0.066	21.950	-0.017	-0.056			
23.937	-0.024	-0.079	23.942	-0.020	-0.067			
25.930	-0.024	-0.080	25.929	-0.021	-0.069			
27.917	-0.021	-0.070	27.928	-0.018	-0.061			
29.922	-0.015	-0.049	29.920	-0.013	-0.042			
27.952	-0.021	-0.071	27.941	-0.019	-0.062			
25.986	-0.024	-0.079	25.992	-0.021	-0.069			
23.985	-0.024	-0.080	23.993	-0.022	-0.073			
21.979	-0.022	-0.072	21.995	-0.019	-0.063			
19.986	-0.018	-0.060	19.993	-0.016	-0.054			
17.982	-0.014	-0.048	17.990	-0.014	-0.047			
15.987	-0.013	-0.042	15.992	-0.012	-0.039			
13.981	-0.009	-0.031	13.990	-0.009	-0.029			
11.996	-0.011	-0.037	11.984	-0.010	-0.034			
9.998	-0.017	-0.057	9.997	-0.017	-0.055			

Issued by 

Document: 5CAL 9607

Page 1 of 2



As Received MOSDAX Cal. Report 2: SAM - 2845 Module 1163

Full Scale: 30 (psia)

File: C:\ACF\VIEW\CALDATA\2001\30\12\OCT01\011163

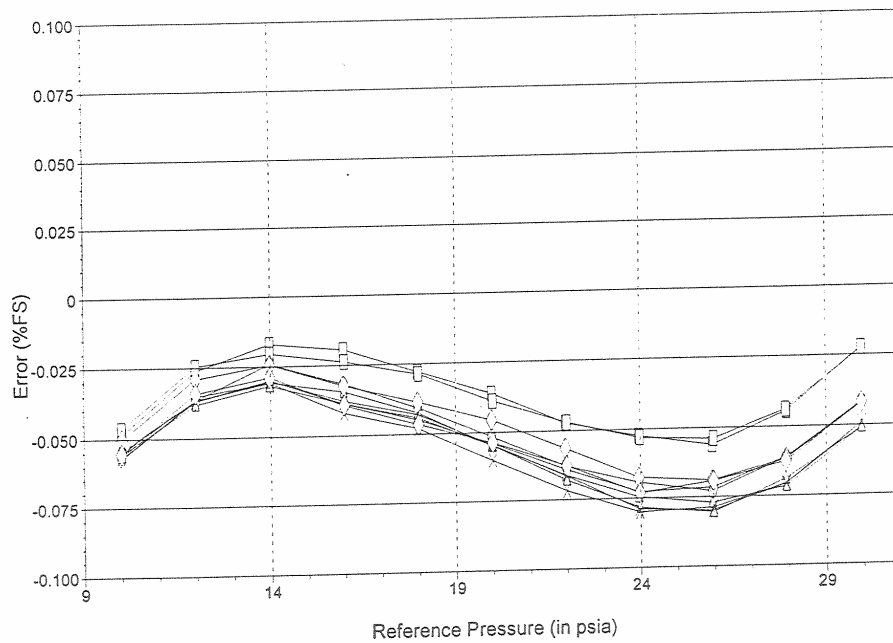
Pressure Reference: Paroscientific Model 230A-101 S/N 62671

Range: 30 PSI

Date of last reference to traceable standard: Aug 15 2000

Plot of Error vs. Reference Pressure

SAM - 2845 Module 1163



—□— 3.3° C —□— 15.3° C —○— 25.3° C —— 35.2° C —◇— 50.2° C

Comments

Issued by

Document: 5CAL 9607

Page 2 of 2



MOSDAX Calibration Report 1: SAM - 2845 Module 1163

Full Scale: 30 (psia)

File: D:\DOCUMENTS\1\BILLDATA\ACPVIEW\CALDATA\2006\3017JAN06\02845

Pressure Reference: Paroscientific Model 230A-101 S/N 90098

Range: 30 PSI

Date of last reference to traceable standard: Dec 20 2004

SAM - 2845 Jan 07 02:16:05 2006 Range 1 Temp 3.1° C			SAM - 2845 Jan 06 22:09:55 2006 Range 2 Temp 15.0° C			SAM - 2845 Jan 06 18:03:30 2006 Range 3 Temp 24.7° C		
Ref Pres (psia)	Error (psia)	(% FS)	Ref Pres (psia)	Error (psia)	(% FS)	Ref Pres (psia)	Error (psia)	(% FS)
10.039	-0.006	-0.019	10.057	-0.004	-0.013	10.071	-0.007	-0.023
12.021	0.001	0.003	12.022	0.003	0.011	12.027	0.001	0.002
13.994	0.004	0.015	14.009	0.008	0.025	13.997	0.004	0.013
16.027	0.004	0.013	16.052	0.007	0.023	16.020	0.003	0.011
17.979	0.002	0.006	18.007	0.006	0.021	18.000	0.002	0.007
19.970	-0.001	-0.003	19.988	0.003	0.011	19.979	0.000	0.000
21.927	-0.002	-0.007	21.948	0.001	0.003	21.951	-0.003	-0.009
23.902	-0.005	-0.016	23.951	0.000	0.001	23.976	-0.004	-0.014
25.930	-0.004	-0.012	25.973	0.001	0.004	25.923	-0.003	-0.011
27.895	-0.001	-0.004	27.944	0.004	0.015	27.924	0.000	0.000
29.932	0.008	0.025	29.969	0.013	0.045	29.943	0.008	0.025
27.995	-0.002	-0.006	27.988	0.005	0.017	28.016	-0.001	-0.004
25.995	-0.004	-0.013	25.993	0.001	0.005	25.984	-0.004	-0.014
23.989	-0.005	-0.017	24.052	0.000	0.002	24.036	-0.004	-0.014
22.038	-0.003	-0.011	21.998	0.001	0.003	22.008	-0.003	-0.011
19.996	0.000	-0.001	20.023	0.004	0.012	20.005	-0.001	-0.004
18.060	0.002	0.005	18.047	0.005	0.018	18.051	0.001	0.005
16.073	0.004	0.013	16.061	0.005	0.018	16.080	0.003	0.009
14.081	0.004	0.012	14.080	0.007	0.024	14.080	0.003	0.012
12.060	0.001	0.005	12.080	0.004	0.013	12.052	0.000	0.000
10.057	-0.005	-0.017	10.101	-0.003	-0.010	10.057	-0.007	-0.023
SAM - 2845 Jan 06 13:52:24 2006 Range 4 Temp 34.6° C			SAM - 2845 Jan 06 09:41:38 2006 Range 5 Temp 49.4° C					
Ref Pres (psia)	Error (psia)	(% FS)	Ref Pres (psia)	Error (psia)	(% FS)			
10.085	-0.007	-0.022	10.096	-0.006	-0.020			
12.033	0.000	0.000	12.051	0.002	0.008			
14.055	0.004	0.014	14.041	0.005	0.017			
16.013	0.002	0.007	16.028	0.004	0.014			
18.019	0.001	0.005	17.989	0.003	0.011			
20.000	-0.001	-0.002	19.973	0.002	0.007			
21.995	-0.005	-0.016	21.993	-0.001	-0.004			
24.025	-0.006	-0.020	23.999	-0.003	-0.010			
25.977	-0.006	-0.019	25.941	-0.001	-0.004			
27.979	-0.003	-0.011	27.919	0.001	0.004			
29.959	0.005	0.018	29.933	0.010	0.033			
28.074	-0.003	-0.011	28.010	0.001	0.002			
26.011	-0.006	-0.021	26.046	-0.002	-0.008			
24.051	-0.007	-0.025	24.038	-0.004	-0.013			
22.105	-0.006	-0.019	22.044	-0.003	-0.009			
20.026	-0.003	-0.010	20.005	-0.001	-0.004			
18.104	0.000	-0.001	18.073	0.002	0.006			
16.116	0.001	0.003	16.097	0.002	0.008			
14.093	0.003	0.009	14.116	0.006	0.019			
12.099	0.000	0.000	12.092	0.002	0.005			
10.109	-0.007	-0.023	10.138	-0.007	-0.022			

Issued by 

Document: 5CAL 9607

Page 1 of 2



MOSDAX Calibration Report 2: SAM - 2845 Module 1163

Full Scale: 30 (psia)

File: D:\DOCUME~1\BILL\DATA\ACPVIEW\CALDATA\2006\30\17\JAN06\02845

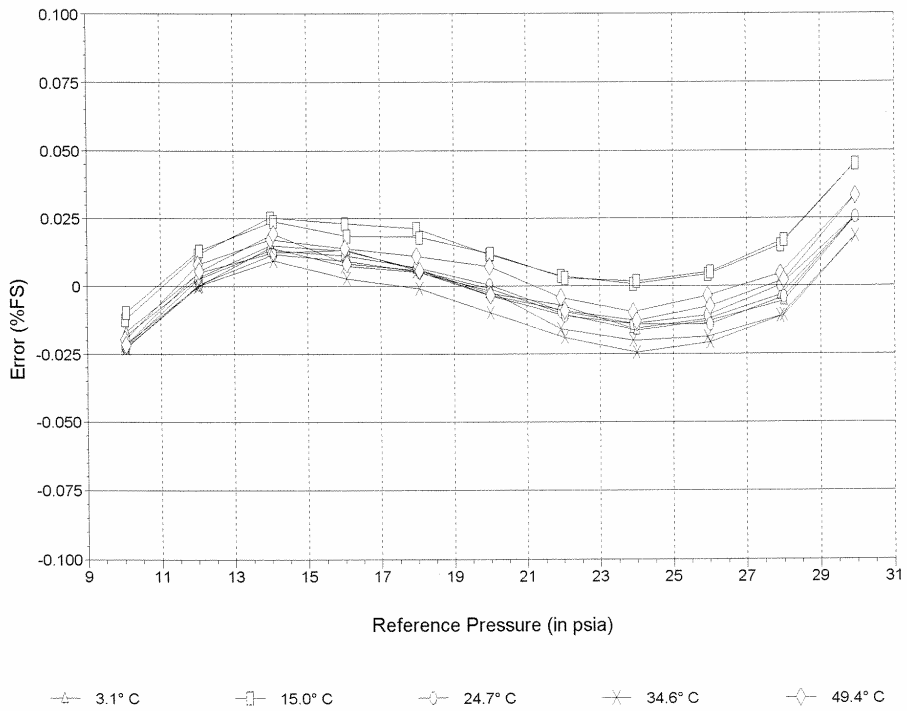
Pressure Reference: Paroscientific Model 230A-101 S/N 90098

Range: 30 PSI

Date of last reference to traceable standard: Dec 20 2004

Plot of Error vs. Reference Pressure

SAM - 2845 Module 1163



Comments

Issued by

Document: SCAL 9607

Page 2 of 2

As Received MOSDAX Cal. Report 1: SAM - 2845 Module 1163

Full Scale: 30 (psia)

File: D:\DOCUME~1\BILL\DATA\ACPVIEW\CALDATA\2006\307JAN06\02845

Pressure Reference: Paroscientific Model 230A-101 S/N 90098

Range: 30 PSI

Date of last reference to traceable standard: Dec 20 2004

SAM - 2845 Jan 07 02:16:05 2006 Range 1 Temp 3.1° C			SAM - 2845 Jan 06 22:09:55 2006 Range 2 Temp 15.0° C			SAM - 2845 Jan 06 18:03:30 2006 Range 3 Temp 24.7° C		
Ref Pres (psia)	Error (psia)	(% FS)	Ref Pres (psia)	Error (psia)	(% FS)	Ref Pres (psia)	Error (psia)	(% FS)
10.039	-0.005	-0.018	10.057	-0.004	-0.014	10.071	-0.008	-0.027
12.021	0.001	0.002	12.022	0.002	0.007	12.027	-0.001	-0.004
13.984	0.004	0.013	14.009	0.006	0.019	13.997	0.001	0.005
16.027	0.003	0.010	16.052	0.005	0.016	16.020	0.000	0.002
17.979	0.001	0.002	18.007	0.004	0.013	18.000	-0.001	-0.003
19.970	-0.002	-0.007	19.988	0.001	0.003	19.979	-0.003	-0.010
21.927	-0.003	-0.011	21.948	-0.001	-0.005	21.951	-0.006	-0.019
23.902	-0.006	-0.019	23.951	-0.002	-0.007	23.976	-0.007	-0.023
25.930	-0.004	-0.015	25.973	-0.001	-0.003	25.923	-0.006	-0.019
27.895	-0.001	-0.005	27.944	0.003	0.010	27.924	-0.002	-0.006
29.932	0.008	0.026	29.969	0.013	0.042	29.943	0.006	0.021
27.995	-0.002	-0.007	27.988	0.003	0.012	28.016	-0.003	-0.010
25.995	-0.005	-0.015	25.993	0.000	-0.002	25.984	-0.007	-0.022
23.989	-0.006	-0.020	24.052	-0.002	-0.006	24.036	-0.007	-0.024
22.038	-0.004	-0.014	21.998	-0.002	-0.005	22.008	-0.006	-0.021
19.996	-0.002	-0.005	20.023	0.001	0.004	20.005	-0.004	-0.014
18.060	0.000	0.002	18.047	0.003	0.010	18.051	-0.002	-0.005
16.073	0.003	0.010	16.061	0.003	0.011	16.080	0.000	0.000
14.081	0.003	0.010	14.080	0.005	0.018	14.080	0.001	0.003
12.060	0.001	0.004	12.080	0.003	0.009	12.052	-0.002	-0.006
10.057	-0.005	-0.016	10.101	-0.004	-0.012	10.057	-0.008	-0.027
SAM - 2845 Jan 06 13:52:24 2006 Range 4 Temp 34.6° C			SAM - 2845 Jan 06 09:41:38 2006 Range 5 Temp 49.4° C					
Ref Pres (psia)	Error (psia)	(% FS)	Ref Pres (psia)	Error (psia)	(% FS)			
10.085	-0.009	-0.029	10.096	-0.009	-0.030			
12.033	-0.003	-0.009	12.051	-0.001	-0.003			
14.055	0.001	0.004	14.041	0.002	0.006			
16.013	-0.001	-0.004	16.028	0.001	0.003			
18.019	-0.002	-0.006	17.989	0.000	0.001			
20.000	-0.004	-0.013	19.973	0.000	-0.001			
21.995	-0.008	-0.026	21.993	-0.003	-0.010			
24.025	-0.009	-0.029	23.999	-0.004	-0.013			
25.977	-0.008	-0.026	25.941	-0.001	-0.004			
27.979	-0.005	-0.016	27.919	0.002	0.008			
29.959	0.005	0.016	29.933	0.012	0.041			
28.074	-0.005	-0.016	28.010	0.002	0.006			
26.011	-0.008	-0.028	26.046	-0.002	-0.007			
24.051	-0.010	-0.033	24.038	-0.005	-0.016			
22.105	-0.009	-0.029	22.044	-0.004	-0.015			
20.026	-0.006	-0.021	20.005	-0.003	-0.011			
18.104	-0.004	-0.012	18.073	-0.001	-0.004			
16.116	-0.003	-0.008	16.097	-0.001	-0.003			
14.093	0.000	-0.001	14.116	0.002	0.008			
12.099	-0.003	-0.009	12.092	-0.002	-0.006			
10.109	-0.009	-0.030	10.138	-0.010	-0.032			

Issued by



Document: SCAL 9607

Page 1 of 2



As Received MOSDAX Cal. Report 2: SAM - 2845 Module 1163

Full Scale: 30 (psia)

File: D:\DOCUME~1\BILL\DATA\ACPVIEW\CALDATA\2006\30\17JAN06\02845

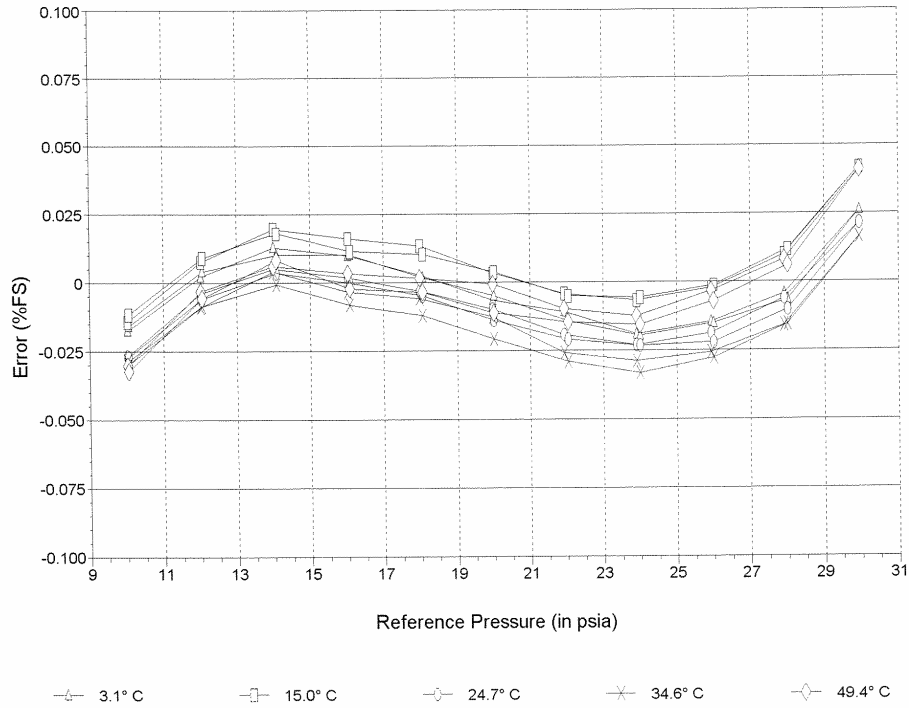
Pressure Reference: Paroscientific Model 230A-101 S/N 90098

Range: 30 PSI

Date of last reference to traceable standard: Dec 20 2004

Plot of Error vs. Reference Pressure

SAM - 2845 Module 1163



Comments

Issued by

Document: 5CAL 9607

Page 2 of 2



MOSDAX Calibration Report 1: SAM - 2846 Module 1169

Full Scale: 30 (psia)

File: C:\ACVIEW\CALDATA\20011030\12OCT01\011169

Pressure Reference: Paroscientific Model 230A-101 S/N 62671

Range: 30 PSI

Date of last reference to traceable standard: Aug 15 2000

SAM - 2846 Oct 11 16:27:11 2001 Range 1 Temp 3.3° C			SAM - 2846 Oct 11 10:50:48 2001 Range 2 Temp 15.3° C			SAM - 2846 Oct 11 05:14:56 2001 Range 3 Temp 25.3° C		
Ref Pres (psia)	Error (psia)	(% FS)	Ref Pres (psia)	Error (psia)	(% FS)	Ref Pres (psia)	Error (psia)	(% FS)
9.999	-0.005	-0.018	10.001	-0.004	-0.013	9.994	-0.006	-0.019
11.983	0.001	0.004	11.980	0.003	0.010	11.983	0.000	0.001
13.978	0.003	0.010	13.977	0.007	0.023	13.978	0.004	0.013
15.970	0.002	0.007	15.974	0.006	0.020	15.967	0.002	0.007
17.966	0.001	0.004	17.974	0.006	0.018	17.970	0.002	0.006
19.959	-0.001	-0.003	19.961	0.004	0.013	19.960	0.000	-0.001
21.952	-0.003	-0.009	21.946	0.002	0.006	21.950	-0.003	-0.010
23.942	-0.005	-0.016	23.948	0.000	0.000	23.945	-0.004	-0.013
25.934	-0.004	-0.013	25.933	0.002	0.006	25.950	-0.003	-0.009
27.927	-0.002	-0.006	27.921	0.005	0.016	27.929	0.000	0.000
29.940	0.006	0.018	29.926	0.012	0.039	29.923	0.007	0.024
27.919	-0.002	-0.005	27.919	0.004	0.014	27.934	-0.001	-0.003
25.967	-0.004	-0.014	25.926	0.002	0.008	25.928	-0.003	-0.010
23.969	-0.005	-0.018	23.955	0.001	0.002	23.939	-0.004	-0.013
21.983	-0.004	-0.012	21.967	0.001	0.002	21.966	-0.003	-0.012
19.988	-0.001	-0.005	19.985	0.003	0.009	19.981	-0.001	-0.004
17.987	0.001	0.002	17.990	0.005	0.017	17.981	0.000	0.001
15.983	0.002	0.005	15.988	0.006	0.018	15.986	0.002	0.005
13.977	0.003	0.009	13.983	0.006	0.020	13.988	0.003	0.010
11.983	0.000	0.001	11.985	0.003	0.009	11.995	0.000	0.000
9.985	-0.006	-0.020	9.985	-0.004	-0.014	9.997	-0.007	-0.022
SAM - 2846 Oct 10 23:38:46 2001 Range 4 Temp 35.2° C			SAM - 2846 Oct 10 18:08:07 2001 Range 5 Temp 50.2° C					
Ref Pres (psia)	Error (psia)	(% FS)	Ref Pres (psia)	Error (psia)	(% FS)			
9.990	-0.006	-0.020	10.000	-0.005	-0.016			
11.983	0.000	0.000	12.020	0.001	0.003			
13.973	0.004	0.012	13.977	0.005	0.016			
15.972	0.001	0.004	15.971	0.003	0.008			
17.968	0.002	0.005	17.964	0.003	0.009			
19.957	-0.001	-0.004	19.960	0.002	0.005			
21.946	-0.004	-0.012	21.950	0.000	-0.001			
23.937	-0.005	-0.017	23.942	-0.002	-0.007			
25.930	-0.006	-0.019	25.929	-0.002	-0.005			
27.917	-0.002	-0.008	27.928	0.001	0.004			
29.922	0.004	0.013	29.920	0.009	0.029			
27.952	-0.003	-0.011	27.941	0.001	0.003			
25.986	-0.006	-0.018	25.992	-0.001	-0.004			
23.985	-0.006	-0.020	23.993	-0.003	-0.009			
21.979	-0.005	-0.016	21.995	-0.003	-0.009			
19.986	-0.003	-0.010	19.993	-0.001	-0.004			
17.982	0.000	0.000	17.990	0.001	0.004			
15.987	0.001	0.002	15.992	0.002	0.007			
13.981	0.002	0.008	13.990	0.004	0.014			
11.996	-0.001	-0.002	11.984	0.001	0.005			
9.998	-0.007	-0.023	9.997	-0.005	-0.018			

Issued by



Document: SCAL 9607

Page 1 of 2



MOSDAX Calibration Report 2: SAM - 2846 Module 1169

Full Scale: 30 (psia)

File: C:\ACPVIEW\CALDATA\2001\30\12\OCT01\01169

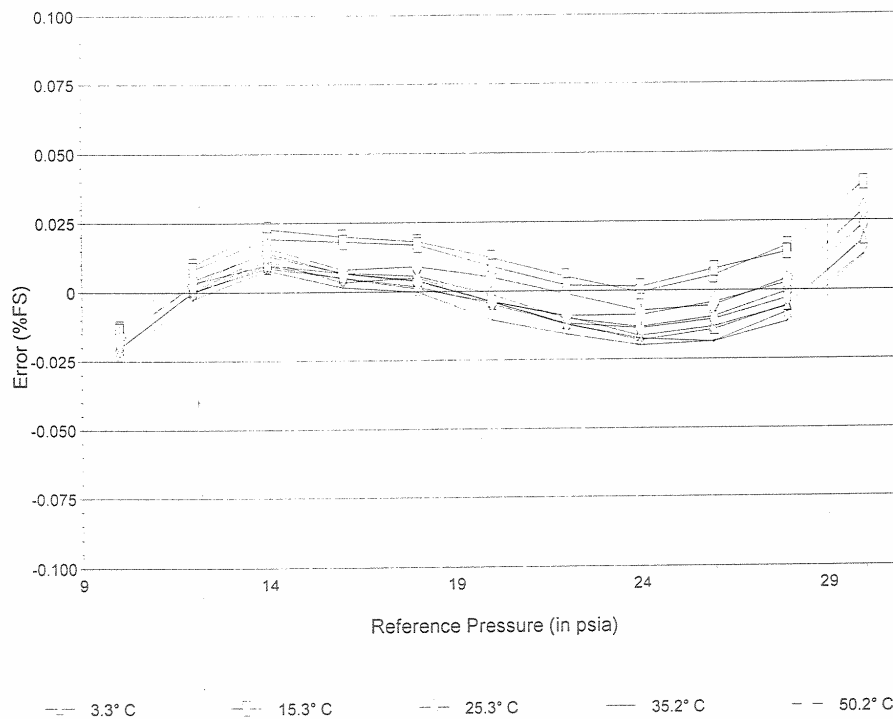
Pressure Reference: Paroscientific Model 230A-101 S/N 62671

Range: 30 PSI

Date of last reference to traceable standard: Aug 15 2000

Plot of Error vs. Reference Pressure

SAM - 2846 Module 1169



Comments

Issued by *M. Gill King*

Document: SCAL 9807

Page 2 of 2



As Received MOSDAX Cal. Report 1: SAM - 2846 Module 1169

File: C:\ACP\VIEW\CALDATA\2001\30\12\OCT01\01169

Full Scale: 30 (psia)

Pressure Reference: Paroscientific Model 230A-101 S/N 62671

Range: 30 PSI

Date of last reference to traceable standard: Aug 15 2000

SAM - 2846 Oct 11 16:27:11 2001 Range 1 Temp 3.3° C			SAM - 2846 Oct 11 10:50:48 2001 Range 2 Temp 15.3° C			SAM - 2846 Oct 11 05:14:56 2001 Range 3 Temp 25.3° C		
Ref Pres (psia)	Error (psia)	(% FS)	Ref Pres (psia)	Error (psia)	(% FS)	Ref Pres (psia)	Error (psia)	(% FS)
9.999	-0.019	-0.063	10.001	-0.018	-0.059	9.994	-0.020	-0.068
11.983	-0.013	-0.045	11.980	-0.012	-0.040	11.983	-0.015	-0.051
13.978	-0.012	-0.041	13.977	-0.009	-0.030	13.978	-0.012	-0.041
15.970	-0.014	-0.047	15.974	-0.011	-0.035	15.967	-0.015	-0.050
17.966	-0.016	-0.053	17.974	-0.012	-0.040	17.970	-0.016	-0.054
19.959	-0.019	-0.064	19.961	-0.015	-0.049	19.960	-0.019	-0.063
21.952	-0.022	-0.072	21.946	-0.018	-0.059	21.950	-0.022	-0.075
23.942	-0.025	-0.082	23.948	-0.020	-0.067	23.945	-0.024	-0.081
25.934	-0.024	-0.081	25.933	-0.019	-0.064	25.950	-0.024	-0.080
27.927	-0.023	-0.077	27.921	-0.017	-0.056	27.929	-0.022	-0.073
29.940	-0.017	-0.055	29.926	-0.011	-0.035	29.923	-0.015	-0.051
27.919	-0.023	-0.076	27.919	-0.017	-0.058	27.934	-0.023	-0.075
25.967	-0.025	-0.083	25.926	-0.018	-0.061	25.928	-0.024	-0.080
23.969	-0.025	-0.084	23.955	-0.020	-0.065	23.939	-0.024	-0.081
21.983	-0.023	-0.075	21.967	-0.019	-0.062	21.966	-0.023	-0.077
19.988	-0.019	-0.065	19.985	-0.016	-0.052	19.981	-0.020	-0.066
17.987	-0.017	-0.055	17.990	-0.012	-0.042	17.981	-0.018	-0.058
15.983	-0.015	-0.049	15.988	-0.011	-0.037	15.986	-0.016	-0.052
13.977	-0.013	-0.042	13.983	-0.010	-0.033	13.988	-0.013	-0.044
11.983	-0.014	-0.048	11.985	-0.012	-0.041	11.995	-0.015	-0.051
9.985	-0.019	-0.065	9.995	-0.018	-0.060	9.997	-0.021	-0.070
SAM - 2846 Oct 10 23:38:46 2001 Range 4 Temp 35.2° C			SAM - 2846 Oct 10 18:08:07 2001 Range 5 Temp 50.2° C					
Ref Pres (psia)	Error (psia)	(% FS)	Ref Pres (psia)	Error (psia)	(% FS)			
9.990	-0.021	-0.071	10.000	-0.021	-0.072			
11.983	-0.016	-0.053	12.020	-0.017	-0.055			
13.973	-0.013	-0.044	13.977	-0.013	-0.044			
15.972	-0.016	-0.055	15.971	-0.016	-0.054			
17.968	-0.017	-0.056	17.964	-0.017	-0.056			
19.957	-0.020	-0.067	19.960	-0.019	-0.062			
21.946	-0.023	-0.078	21.950	-0.021	-0.071			
23.937	-0.026	-0.086	23.942	-0.024	-0.080			
25.930	-0.027	-0.090	25.929	-0.024	-0.081			
27.917	-0.024	-0.081	27.928	-0.022	-0.074			
29.922	-0.019	-0.063	29.920	-0.016	-0.052			
27.952	-0.025	-0.085	27.941	-0.023	-0.076			
25.986	-0.027	-0.090	25.992	-0.024	-0.080			
23.985	-0.027	-0.089	23.993	-0.025	-0.082			
21.979	-0.025	-0.082	21.995	-0.024	-0.079			
19.986	-0.022	-0.074	19.993	-0.021	-0.071			
17.982	-0.018	-0.061	17.990	-0.018	-0.061			
15.987	-0.017	-0.057	15.992	-0.017	-0.056			
13.981	-0.014	-0.048	13.990	-0.014	-0.046			
11.996	-0.017	-0.056	11.984	-0.016	-0.054			
9.998	-0.022	-0.074	9.997	-0.022	-0.074			

Issued by

Document: SCAL 9607

Page 1 of 2



As Received MOSDAX Cal. Report 2: SAM - 2846 Module 1169

Full Scale: 30 (psia)

File: C:\ACPVIEW\CALDATA\2001\30\12OCT01\01169

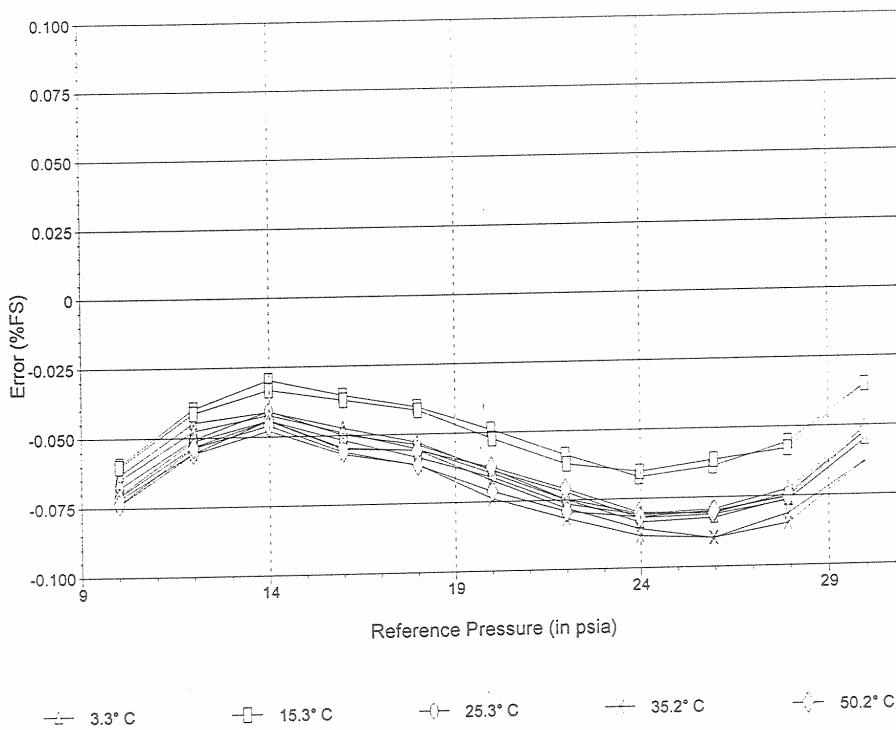
Pressure Reference: Paroscientific Model 230A-101 S/N 62671

Range: 30 PSI

Date of last reference to traceable standard: Aug 15 2000

Plot of Error vs. Reference Pressure

SAM - 2846 Module 1169



Comments

Issued by *[Signature]*



MOSDAX Calibration Report 1: SAM - 2846 Module 1169

File: C:\ACPVIEW\CALDATA\2005\30\13JULY05\01169

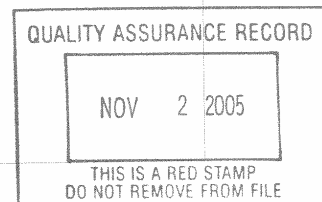
Full Scale: 30 (psia)

Pressure Reference: Paroscientific Model 230A-101 S/N 90098

Range: 30 PSI

Date of last reference to traceable standard: Dec 20 2004

SAM - 2846 Jul 13 15:28:01 2005 Range 1 Temp 3.2° C			SAM - 2846 Jul 13 10:26:39 2005 Range 2 Temp 14.9° C			SAM - 2846 Jul 13 05:25:45 2005 Range 3 Temp 25.4° C		
Ref Pres (psia)	Error (psia)	(% FS)	Ref Pres (psia)	Error (psia)	(% FS)	Ref Pres (psia)	Error (psia)	(% FS)
10.036	-0.006	-0.020	10.082	-0.003	-0.009	10.074	-0.007	-0.024
12.028	0.001	0.002	12.068	0.003	0.011	12.071	0.001	0.002
14.048	0.005	0.015	14.039	0.007	0.025	14.017	0.005	0.015
16.064	0.003	0.011	16.064	0.007	0.022	16.063	0.003	0.012
17.987	0.002	0.008	18.023	0.007	0.024	18.018	0.002	0.007
20.006	-0.001	-0.003	20.027	0.005	0.015	20.015	0.000	-0.001
22.015	-0.004	-0.012	22.039	0.002	0.005	22.014	-0.003	-0.009
23.992	-0.005	-0.018	23.955	0.002	0.005	23.963	-0.005	-0.016
25.994	-0.004	-0.013	25.985	0.002	0.006	25.955	-0.003	-0.011
27.942	-0.001	-0.004	27.954	0.005	0.016	27.939	0.000	0.000
29.920	0.007	0.022	29.933	0.014	0.046	29.962	0.008	0.025
28.012	-0.001	-0.004	28.021	0.005	0.016	28.017	-0.001	-0.003
26.065	-0.005	-0.017	26.049	0.001	0.004	26.053	-0.004	-0.014
24.044	-0.005	-0.018	24.083	0.001	0.002	24.071	-0.004	-0.014
21.989	-0.004	-0.014	22.057	0.001	0.005	22.030	-0.003	-0.010
20.042	-0.001	-0.004	20.052	0.003	0.010	20.003	-0.002	-0.005
18.068	0.001	0.003	18.056	0.005	0.017	18.079	0.001	0.004
16.068	0.003	0.010	16.115	0.006	0.019	16.081	0.002	0.007
14.085	0.004	0.013	14.077	0.008	0.025	14.021	0.005	0.017
12.068	0.000	0.001	12.072	0.004	0.012	12.077	0.001	0.003
10.064	-0.006	-0.020	10.040	-0.004	-0.013	10.039	-0.006	-0.021
SAM - 2846 Jul 13 00:25:04 2005 Range 4 Temp 35.5° C			SAM - 2846 Jul 12 19:23:27 2005 Range 5 Temp 51.0° C					
Ref Pres (psia)	Error (psia)	(% FS)	Ref Pres (psia)	Error (psia)	(% FS)			
10.067	-0.007	-0.022	10.072	-0.005	-0.018			
12.060	0.000	0.000	12.067	0.002	0.008			
14.045	0.004	0.012	14.015	0.006	0.019			
16.059	0.002	0.008	16.047	0.005	0.016			
18.032	0.001	0.002	18.002	0.003	0.011			
19.993	-0.002	-0.006	19.983	0.002	0.006			
21.980	-0.005	-0.017	22.002	0.000	0.000			
23.965	-0.006	-0.021	23.971	-0.002	-0.007			
25.950	-0.006	-0.019	25.976	-0.001	-0.004			
27.933	-0.002	-0.007	27.955	0.001	0.004			
29.973	0.006	0.020	29.964	0.011	0.035			
27.992	-0.003	-0.010	28.054	0.002	0.005			
26.067	-0.006	-0.019	26.027	-0.002	-0.007			
24.067	-0.006	-0.021	24.059	-0.003	-0.010			
22.052	-0.005	-0.017	22.054	-0.003	-0.009			
20.015	-0.003	-0.010	20.100	0.000	-0.001			
18.058	-0.001	-0.003	18.090	0.001	0.005			
16.069	0.001	0.002	16.122	0.003	0.010			
14.018	0.003	0.011	14.083	0.006	0.020			
12.072	0.000	0.001	12.076	0.002	0.007			
10.069	-0.007	-0.022	10.097	-0.005	-0.017			



006769

Issued by *[Signature]*

Document: 5CAL 9607

Page 1 of 2

Schlumberger

MOSDAX Calibration Report 2: SAM - 2846 Module 1169

Full Scale: 30 (psia)

File: C:\ACPVIEW\CALDATA\2005\30\13\JULY05\01169

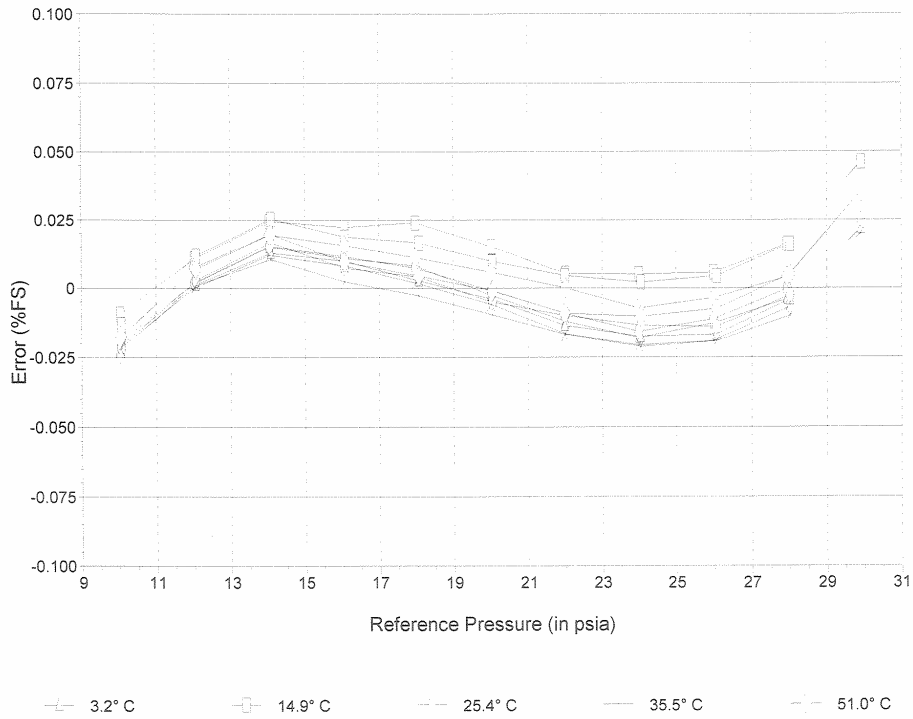
Pressure Reference: Paroscientific Model 230A-101 S/N 90098

Range: 30 PSI

Date of last reference to traceable standard: Dec 20 2004

Plot of Error vs. Reference Pressure

SAM - 2846 Module 1169



Comments

Issued by 



As Received MOSDAX Cal. Report 1: SAM - 2846 Module 1169

Full Scale: 30 (psia)

File: C:\ACPV\IEWCALDATA\2005\30\13JULY05\01169

Pressure Reference: Paroscientific Model 230A-101 S/N 90098

Range: 30 PSI

Date of last reference to traceable standard: Dec 20 2004

SAM - 2846 Jul 13 15:28:01 2005 Range 1 Temp 3.2° C			SAM - 2846 Jul 13 10:26:39 2005 Range 2 Temp 14.9° C			SAM - 2846 Jul 13 05:25:45 2005 Range 3 Temp 25.4° C		
Ref Pres (psia)	Error (psia)	(% FS)	Ref Pres (psia)	Error (psia)	(% FS)	Ref Pres (psia)	Error (psia)	(% FS)
10.036	-0.031	-0.102	10.082	-0.028	-0.093	10.074	-0.032	-0.107
12.028	-0.025	-0.084	12.068	-0.022	-0.075	12.071	-0.025	-0.083
14.048	-0.022	-0.073	14.039	-0.019	-0.063	14.017	-0.022	-0.072
16.064	-0.024	-0.080	16.064	-0.020	-0.067	16.063	-0.023	-0.078
17.987	-0.025	-0.084	18.023	-0.020	-0.067	18.018	-0.025	-0.083
20.006	-0.029	-0.097	20.027	-0.023	-0.078	20.015	-0.028	-0.093
22.015	-0.032	-0.107	22.039	-0.027	-0.089	22.014	-0.031	-0.102
23.992	-0.034	-0.114	23.955	-0.027	-0.090	23.963	-0.033	-0.110
25.994	-0.033	-0.110	25.985	-0.027	-0.090	25.955	-0.032	-0.105
27.942	-0.030	-0.101	27.954	-0.024	-0.079	27.939	-0.028	-0.095
29.920	-0.023	-0.076	29.933	-0.015	-0.049	29.962	-0.021	-0.069
28.012	-0.030	-0.102	28.021	-0.024	-0.079	28.017	-0.029	-0.097
26.065	-0.034	-0.114	26.049	-0.027	-0.091	26.053	-0.032	-0.108
24.044	-0.034	-0.114	24.083	-0.028	-0.093	24.071	-0.032	-0.107
21.989	-0.033	-0.109	22.057	-0.027	-0.089	22.030	-0.031	-0.103
20.042	-0.029	-0.098	20.052	-0.025	-0.083	20.003	-0.029	-0.097
18.068	-0.027	-0.090	18.056	-0.022	-0.075	18.079	-0.026	-0.087
16.068	-0.024	-0.081	16.115	-0.021	-0.071	16.081	-0.025	-0.082
14.085	-0.023	-0.075	14.077	-0.019	-0.062	14.021	-0.021	-0.071
12.068	-0.025	-0.084	12.072	-0.022	-0.074	12.077	-0.025	-0.083
10.064	-0.031	-0.103	10.040	-0.029	-0.096	10.039	-0.031	-0.104
SAM - 2846 Jul 13 00:25:04 2005 Range 4 Temp 35.5° C			SAM - 2846 Jul 12 19:23:27 2005 Range 5 Temp 51.0° C					
Ref Pres (psia)	Error (psia)	(% FS)	Ref Pres (psia)	Error (psia)	(% FS)			
10.067	-0.031	-0.104	10.072	-0.030	-0.099			
12.060	-0.025	-0.085	12.067	-0.023	-0.076			
14.045	-0.023	-0.075	14.015	-0.020	-0.066			
16.059	-0.024	-0.081	16.047	-0.022	-0.072			
18.032	-0.027	-0.089	18.002	-0.023	-0.078			
19.993	-0.029	-0.097	19.983	-0.025	-0.084			
21.980	-0.033	-0.109	22.002	-0.027	-0.090			
23.965	-0.034	-0.113	23.971	-0.029	-0.097			
25.950	-0.034	-0.112	25.976	-0.028	-0.092			
27.933	-0.030	-0.100	27.955	-0.025	-0.083			
29.973	-0.022	-0.072	29.964	-0.015	-0.050			
27.992	-0.031	-0.102	28.054	-0.025	-0.082			
26.067	-0.034	-0.112	26.027	-0.029	-0.096			
24.067	-0.034	-0.114	24.059	-0.030	-0.100			
22.052	-0.033	-0.109	22.054	-0.030	-0.099			
20.015	-0.030	-0.101	20.100	-0.027	-0.090			
18.058	-0.028	-0.093	18.090	-0.025	-0.084			
16.069	-0.026	-0.087	16.122	-0.023	-0.078			
14.018	-0.023	-0.077	14.083	-0.020	-0.066			
12.072	-0.025	-0.084	12.076	-0.023	-0.076			
10.069	-0.031	-0.105	10.097	-0.029	-0.098			

Issued by



Document: 5CAL 9607

Page 1 of 2



As Received MOSDAX Cal. Report 2: SAM - 2846 Module 1169

Full Scale: 30 (psia)

File: C:\ACPVIEW\CALDATA\2005\30113JULY05\01169

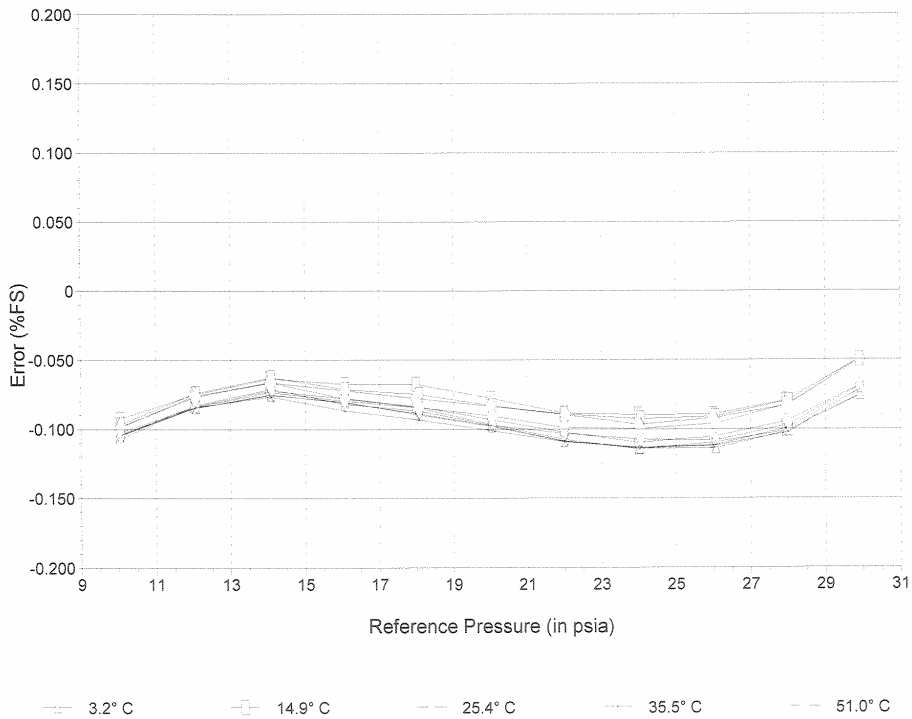
Pressure Reference: Paroscientific Model 230A-101 S/N 90098

Range: 30 PSI

Date of last reference to traceable standard: Dec 20 2004

Plot of Error vs. Reference Pressure

SAM - 2846 Module 1169



Comments
Y-Axis Not To Standard Scale.

Issued by 



MOSDAX Calibration Report 1: SAM - 3363 Module 1503

Full Scale: 250 (psia)

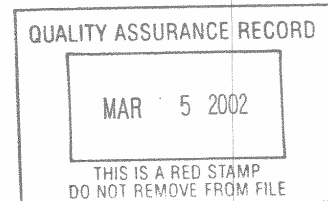
File: C:\ACPVIEW\CALDATA\2002\250\10\JAN02\01503

Pressure Reference: Paroscientific Model 2300A-101 S/N 55375

Range: 300 PSI

Date of last reference to traceable standard: Nov 4 2000

SAM - 3363 Jan 08 18:36:15 2002 Range 1 Temp 3.6° C			SAM - 3363 Jan 08 12:49:02 2002 Range 2 Temp 10.7° C			SAM - 3363 Jan 08 06:41:24 2002 Range 3 Temp 20.7° C		
Ref Pres (psia)	Error (psia)	(% FS)	Ref Pres (psia)	Error (psia)	(% FS)	Ref Pres (psia)	Error (psia)	(% FS)
14.833	0.021	0.009	14.859	0.010	0.004	14.847	0.019	0.008
25.641	0.004	0.002	25.644	0.000	0.000	25.631	0.006	0.002
50.665	-0.016	-0.006	50.653	-0.010	-0.004	50.548	-0.004	-0.002
75.615	-0.038	-0.015	75.676	-0.029	-0.011	75.684	-0.027	-0.011
100.644	-0.016	-0.007	100.635	-0.009	-0.004	100.738	-0.006	-0.003
125.585	0.001	0.001	125.657	0.013	0.005	125.683	0.012	0.005
150.576	0.005	0.002	150.629	0.012	0.005	150.693	0.010	0.004
175.637	0.024	0.010	175.540	0.031	0.012	175.608	0.023	0.009
200.498	0.015	0.006	200.609	0.030	0.012	200.674	0.019	0.008
225.470	0.003	0.001	225.484	0.020	0.008	225.672	0.012	0.005
250.606	-0.050	-0.020	250.661	-0.027	-0.011	250.651	-0.037	-0.015
225.525	-0.009	-0.004	225.683	0.016	0.006	225.737	0.010	0.004
200.746	0.005	0.002	200.759	0.022	0.009	200.700	0.024	0.010
175.631	0.010	0.004	175.771	0.026	0.011	175.939	0.024	0.010
150.672	0.000	0.000	150.747	0.016	0.006	150.838	0.012	0.005
125.585	-0.009	-0.004	125.802	0.006	0.002	125.734	0.011	0.005
100.615	-0.024	-0.010	100.721	-0.015	-0.006	100.730	-0.006	-0.003
75.554	-0.041	-0.016	75.550	-0.039	-0.016	75.720	-0.039	-0.016
50.723	-0.019	-0.008	50.663	-0.015	-0.006	50.574	-0.010	-0.004
25.875	0.005	0.002	25.897	-0.004	-0.002	25.913	-0.003	-0.001
14.836	0.025	0.010	14.844	0.018	0.007	14.852	0.015	0.006
SAM - 3363 Jan 08 00:32:14 2002 Range 4 Temp 30.6° C			SAM - 3363 Jan 07 18:42:59 2002 Range 5 Temp 40.5° C					
Ref Pres (psia)	Error (psia)	(% FS)	Ref Pres (psia)	Error (psia)	(% FS)			
14.820	0.016	0.006	14.768	0.021	0.008			
25.641	0.001	0.000	25.637	0.001	0.000			
50.689	-0.013	-0.005	50.675	-0.012	-0.005			
75.682	-0.026	-0.010	75.621	-0.023	-0.009			
100.689	-0.009	-0.004	100.654	0.001	0.001			
125.709	0.009	0.004	125.617	0.015	0.006			
150.699	0.000	0.000	150.636	0.005	0.002			
175.729	0.009	0.004	175.639	0.031	0.012			
200.641	0.016	0.007	200.630	0.018	0.007			
225.645	0.003	0.001	225.514	0.015	0.006			
250.632	-0.033	-0.013	250.519	-0.023	-0.009			
225.703	0.003	0.001	225.718	0.016	0.006			
200.719	0.014	0.005	200.866	0.021	0.008			
175.694	0.011	0.004	175.705	0.024	0.010			
150.748	0.004	0.002	150.767	0.004	0.001			
125.785	0.000	0.000	125.868	0.009	0.004			
100.644	-0.004	-0.002	100.670	-0.004	-0.002			
75.728	-0.025	-0.010	75.648	-0.024	-0.009			
50.607	-0.011	-0.005	50.635	-0.015	-0.006			
25.834	0.004	0.002	25.869	0.002	0.001			
14.834	0.014	0.006	14.788	0.012	0.005			



004860

Issued by *[Signature]*



MOSDAX Calibration Report 2: SAM - 3363 Module 1503

Full Scale: 250 (psia)

File: C:\ACPVIEW\CALDATA\2002\2501\10\JAN02\101503

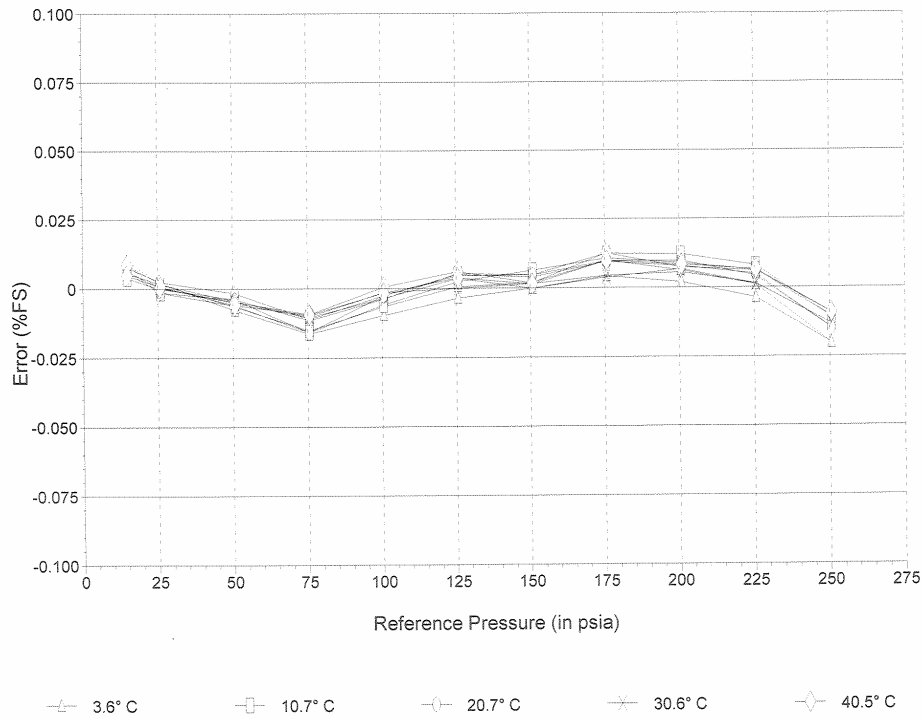
Pressure Reference: Paroscientific Model 2300A-101 S/N 55375

Range: 300 PSI

Date of last reference to traceable standard: Nov 4 2000

Plot of Error vs. Reference Pressure

SAM - 3363 Module 1503



Comments

Issued by

Document: 5CAL 9607

Page 2 of 2



MOSDAX Calibration Report 1: SAM - 3363 Module 1503

Full Scale: 250 (psia)

File: D:\DOCUME~1\BILL\DATA\ACPV\VIEW\CAL\DATA\2005\250\17\DEC05\03363

Pressure Reference: Paroscientific Model 2300A-101 S/N 90263

Range: 300 PSI

Date of last reference to traceable standard: Apr 23rd 2004

SAM - 3363 Dec 17 18:56:34 2005 Range 1 Temp 3.2° C			SAM - 3363 Dec 17 13:03:08 2005 Range 2 Temp 10.2° C			SAM - 3363 Dec 17 07:03:05 2005 Range 3 Temp 20.0° C		
Ref Pres (psia)	Error (psia)	(% FS)	Ref Pres (psia)	Error (psia)	(% FS)	Ref Pres (psia)	Error (psia)	(% FS)
14.695	0.022	0.009	14.698	0.022	0.009	14.670	0.024	0.010
26.848	0.004	0.002	26.684	0.002	0.001	26.736	0.003	0.001
51.757	-0.017	-0.007	51.716	-0.028	-0.011	51.764	-0.024	-0.010
76.856	-0.033	-0.013	76.697	-0.033	-0.013	76.726	-0.025	-0.010
101.651	-0.024	-0.009	101.723	-0.014	-0.006	101.671	-0.018	-0.007
126.682	0.004	0.001	126.771	0.006	0.002	126.592	0.013	0.005
151.722	0.008	0.003	151.710	0.012	0.005	151.596	0.004	0.002
176.651	0.023	0.009	176.675	0.030	0.012	176.675	0.013	0.005
201.665	0.020	0.008	201.642	0.021	0.008	201.583	0.022	0.009
226.588	0.003	0.001	226.648	0.013	0.005	226.671	0.001	0.000
251.678	-0.045	-0.018	251.608	-0.027	-0.011	251.614	-0.036	-0.015
226.485	-0.002	-0.001	226.713	0.010	0.004	226.610	0.007	0.003
201.667	0.017	0.007	201.615	0.036	0.014	201.574	0.021	0.008
176.622	0.025	0.010	176.654	0.031	0.012	176.640	0.020	0.008
151.653	0.008	0.003	151.586	0.012	0.005	151.593	0.012	0.005
126.605	0.003	0.001	126.670	0.012	0.005	126.651	0.007	0.003
101.670	-0.015	-0.006	101.642	-0.018	-0.007	101.550	-0.018	-0.007
76.654	-0.034	-0.013	76.658	-0.024	-0.010	76.631	-0.029	-0.012
51.641	-0.025	-0.010	51.640	-0.019	-0.008	51.663	-0.024	-0.009
26.650	0.002	0.001	26.649	0.007	0.003	26.624	0.006	0.003
14.702	0.021	0.008	14.691	0.030	0.012	14.685	0.023	0.009
SAM - 3363 Dec 17 01:02:54 2005 Range 4 Temp 29.8° C			SAM - 3363 Dec 16 18:55:05 2005 Range 5 Temp 39.6° C					
Ref Pres (psia)	Error (psia)	(% FS)	Ref Pres (psia)	Error (psia)	(% FS)			
14.641	0.024	0.010	14.646	0.016	0.006			
26.807	0.003	0.001	26.685	0.010	0.004			
51.794	-0.021	-0.008	51.771	-0.018	-0.007			
76.636	-0.027	-0.011	76.679	-0.025	-0.010			
101.729	-0.016	-0.006	101.650	-0.014	-0.006			
126.597	0.002	0.001	126.630	0.015	0.006			
151.634	0.004	0.002	151.615	0.008	0.003			
176.731	0.008	0.003	176.683	0.024	0.010			
201.678	0.012	0.005	201.592	0.019	0.007			
226.656	-0.004	-0.002	226.672	0.005	0.002			
251.671	-0.031	-0.012	251.581	-0.017	-0.007			
226.523	0.001	0.001	226.602	0.005	0.002			
201.569	0.014	0.006	201.490	0.021	0.009			
176.650	0.016	0.006	176.655	0.021	0.009			
151.624	0.005	0.002	151.627	0.013	0.005			
126.659	0.001	0.000	126.600	0.018	0.007			
101.666	-0.009	-0.004	101.648	-0.011	-0.004			
76.611	-0.026	-0.010	76.629	-0.018	-0.007			
51.647	-0.018	-0.007	51.641	-0.024	-0.010			
26.651	0.012	0.005	26.633	0.002	0.001			
14.652	0.018	0.007	14.643	0.014	0.006			

Issued by

Document: 5CAL 9607

Page 1 of 2



MOSDAX Calibration Report 2: SAM - 3363 Module 1503

Full Scale: 250 (psia)

File: D:\DOCUME~1\BILL\DATA\ACPV\VIEW\CALDATA\2005\250\17DEC05\03363

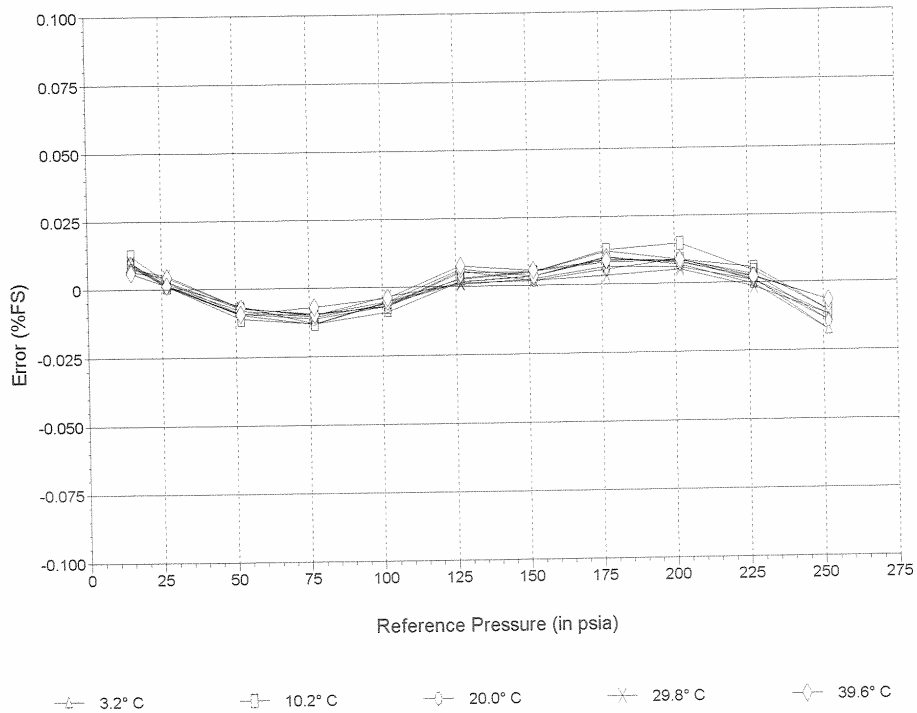
Pressure Reference: Paroscientific Model 2300A-101 S/N 90263

Range: 300 PSI

Date of last reference to traceable standard: Apr 23rd 2004

Plot of Error vs. Reference Pressure

SAM - 3363 Module 1503



Comments

Issued by 

Document: 5CAL 9607

Page 2 of 2

Schlumberger

As Received MOSDAX Cal. Report 1: SAM - 3363 Module 1503

Full Scale: 250 (psia)

File: D:\DOCUMENT-1\BILLDATA\ACPVIEW\CALDATA\2005\250\17DEC05\03363

Pressure Reference: Paroscientific Model 2300A-101 S/N 90263

Range: 300 PSI

Date of last reference to traceable standard: Apr 23rd 2004

SAM - 3363 Dec 17 18:56:34 2005 Range 1 Temp 3.2° C			SAM - 3363 Dec 17 13:03:08 2005 Range 2 Temp 10.2° C			SAM - 3363 Dec 17 07:03:05 2005 Range 3 Temp 20.0° C		
Ref Pres (psia)	Error (psia)	(% FS)	Ref Pres (psia)	Error (psia)	(% FS)	Ref Pres (psia)	Error (psia)	(% FS)
14.695	0.101	0.040	14.698	0.102	0.041	14.670	0.102	0.041
26.848	0.082	0.033	26.684	0.080	0.032	26.736	0.079	0.032
51.757	0.059	0.023	51.716	0.048	0.019	51.764	0.050	0.020
76.856	0.040	0.016	76.697	0.040	0.016	76.726	0.047	0.019
101.651	0.047	0.019	101.723	0.058	0.023	101.671	0.053	0.021
126.682	0.072	0.029	126.771	0.076	0.030	126.592	0.082	0.033
151.722	0.074	0.029	151.710	0.079	0.032	151.596	0.071	0.028
176.651	0.085	0.034	176.675	0.095	0.038	176.675	0.079	0.031
201.665	0.079	0.032	201.642	0.084	0.033	201.583	0.085	0.034
226.588	0.058	0.023	226.648	0.073	0.029	226.671	0.061	0.025
251.678	0.006	0.002	251.608	0.028	0.011	251.614	0.021	0.008
226.485	0.053	0.021	226.713	0.070	0.028	226.610	0.067	0.027
201.667	0.076	0.030	201.615	0.099	0.039	201.574	0.084	0.033
176.622	0.087	0.035	176.654	0.096	0.039	176.640	0.085	0.034
151.653	0.074	0.029	151.586	0.079	0.032	151.593	0.080	0.032
126.605	0.072	0.029	126.670	0.082	0.033	126.651	0.076	0.030
101.670	0.056	0.023	101.642	0.053	0.021	101.550	0.053	0.021
76.654	0.039	0.016	76.658	0.049	0.020	76.631	0.044	0.017
51.641	0.051	0.020	51.640	0.057	0.023	51.663	0.051	0.020
26.650	0.080	0.032	26.649	0.085	0.034	26.624	0.083	0.033
14.702	0.100	0.040	14.691	0.110	0.044	14.685	0.101	0.040
SAM - 3363 Dec 17 01:02:54 2005 Range 4 Temp 29.8° C			SAM - 3363 Dec 16 18:55:05 2005 Range 5 Temp 39.6° C					
Ref Pres (psia)	Error (psia)	(% FS)	Ref Pres (psia)	Error (psia)	(% FS)			
14.641	0.099	0.040	14.646	0.086	0.034			
26.807	0.076	0.031	26.685	0.079	0.032			
51.794	0.051	0.020	51.771	0.049	0.020			
76.636	0.042	0.017	76.679	0.040	0.016			
101.729	0.052	0.021	101.650	0.049	0.020			
126.597	0.068	0.027	126.630	0.075	0.030			
151.634	0.067	0.027	151.615	0.065	0.026			
176.731	0.069	0.028	176.683	0.078	0.031			
201.678	0.071	0.028	201.592	0.069	0.027			
226.656	0.051	0.021	226.672	0.050	0.020			
251.671	0.022	0.009	251.581	0.024	0.009			
226.523	0.057	0.023	226.602	0.051	0.020			
201.569	0.073	0.029	201.490	0.072	0.029			
176.650	0.077	0.031	176.655	0.075	0.030			
151.624	0.069	0.028	151.627	0.070	0.028			
126.659	0.067	0.027	126.600	0.078	0.031			
101.666	0.059	0.023	101.648	0.052	0.021			
76.611	0.044	0.017	76.629	0.047	0.019			
51.647	0.054	0.021	51.641	0.043	0.017			
26.651	0.085	0.034	26.633	0.072	0.029			
14.652	0.093	0.037	14.643	0.085	0.034			

Issued by 

Document: 5CAL 9607

Page 1 of 2



As Received MOSDAX Cal. Report 2: SAM - 3363 Module 1503

Full Scale: 250 (psia)

File: D:\DOCUMENT-1\BILLDATA\ACPVIEW\CALDATA\2005\250\17DEC05\03363

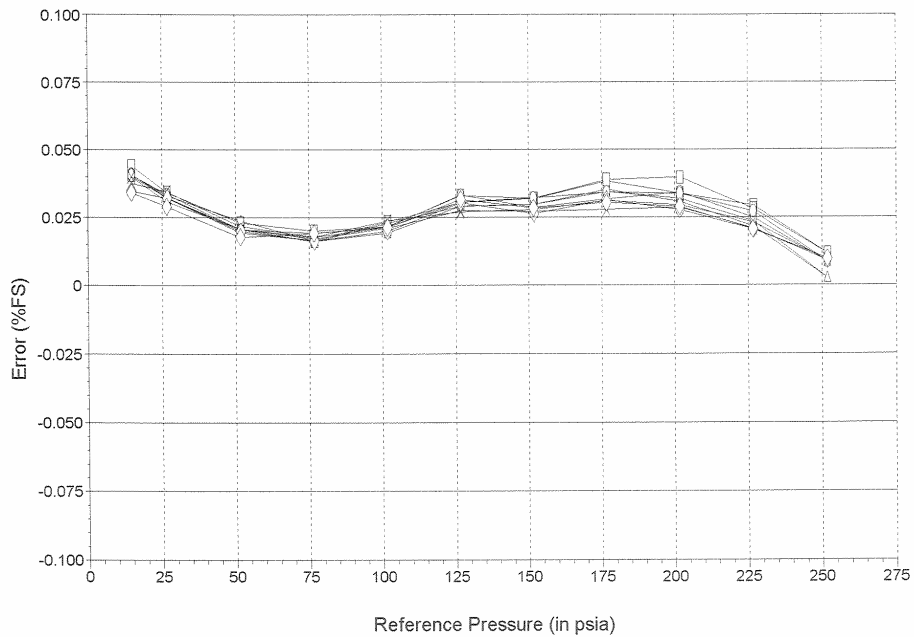
Pressure Reference: Paroscientific Model 2300A-101 S/N 90263

Range: 300 PSI

Date of last reference to traceable standard: Apr 23rd 2004

Plot of Error vs. Reference Pressure

SAM - 3363 Module 1503



—△— 3.2° C —□— 10.2° C —◇— 20.0° C —×— 29.8° C —◇— 39.6° C

Comments

Issued by 



APPENDIX O

SURVEY OF SULFIDE MINERAL DISTRIBUTION AT YUCCA MOUNTAIN

O1. INTRODUCTION

Impacts of Solubility and Other Geochemical Processes on Radionuclide Retardation in the Natural System (BSC 2006 [DIRS 178672], Section 2.1.2.1) discussed the possible contribution of sulfide minerals to the reducing conditions of saturated-zone waters in certain boreholes around Yucca Mountain. This report suggested that reducing groundwaters are associated with reported occurrences of pyrite in rock units below the water table. However, the documentation of sulfide minerals in the rocks at Yucca Mountain is incomplete, making it difficult to assign a high degree of confidence to the association of sulfides and reducing groundwater. A well-established association would have value as a criterion for validating measurements of reducing conditions and predicting the distribution and extent of reducing water in the Yucca Mountain area.

Previously reported observations of pyrite or other iron sulfides cited in *Impacts of Solubility and Other Geochemical Processes on Radionuclide Retardation in the Natural System* (BSC 2006 [DIRS 178672], Section 2.1.2.1) were taken from a paper by Castor et al. (1994 [DIRS 102495]). Information also was taken from a report by Caporuscio et al. (1982 [DIRS 101322], pp. 17, 35, 38, 40, 54, 57, and 58). The data in those references were insufficient to allow a direct comparison of pyrite occurrence with measured water redox conditions in any particular borehole because no borehole had been characterized for both sulfide occurrence and redox conditions. The association of sulfide occurrence and reducing groundwater was inferred from data representing boreholes that are close to each other. Also, redox measurements from one borehole were compared to sulfide occurrences in a presumably upgradient borehole based on an assumption that, once dissolved oxygen is removed from groundwater by reaction with a reductant such as pyrite, the water generally remains oxygen-free as it moves downgradient (BSC 2006 [DIRS 178672], p. 2-4).

This report presents previously collected and new data on sulfide distribution and abundance in the Yucca Mountain area. The information is analyzed in an effort to address the following questions:

- Is there sufficient information about the distribution and abundance of sulfides to predict their potential contribution to redox conditions with high confidence?
- Are the origins of sulfides in Yucca Mountain rocks understood well enough to estimate distributions and abundances where no data are available?
- Is there mineralogic evidence to support a conceptual model that rock sulfides react with dissolved oxygen in groundwater?

O2. METHODS

Additional information about iron sulfide (mainly pyrite) occurrences in Yucca Mountain boreholes has been collected to assess the postulated association of sulfides and reducing groundwaters. In the absence of definitive x-ray diffraction data, the term “sulfide” is used for minerals with metallic luster and various shades of yellow when viewed either directly or by reflected-light microscopy. Reconnaissance examination of drill-bit cuttings from the saturated

zone in hydrology boreholes USW H-3, H-4, and H-5 and water-table boreholes USW WT#10, USW WT#12, USW WT#14, and USW WT#17 was performed with a stereomicroscope. Each cuttings sample represents 10 ft (3.05 m) of drilled rock. Readily available petrographic thin sections of drill core and cuttings were used; these were examined by reflected-light microscopy to provide additional data on sulfide mineral distribution and details of sulfide-mineral origin. The use of existing thin sections means that sample selection was not necessarily optimal for the study of sulfide occurrences. No quantitative determinations of sulfide abundance were made for this report. Visual estimates of sulfide abundance are included in some descriptions. Estimates are based on comparisons with standard charts such as those of Compton (1962 [DIRS 101588], pp. 332 to 333). Table O-1 lists all the boreholes from which samples were examined. Sample depths, unless otherwise indicated, are vertical depths below the land surface. Borehole identifiers in the text are abbreviated after first mention by dropping the prefix.

Table O-1. Summary of Borehole Samples Examined for Sulfide Occurrence

Borehole Identifier	Sample Types	Sulfide Observed
ESF-HD-CHE-3 (Alcove 5, Exploratory Studies Facility)	drill core chip (electron microscopy mount)	yes
UE-25b#1 (previously called UE-25b-1H)	thin sections	yes
UE-25 p#1	thin sections	yes
USW G-1	thin sections	yes
USW G-2	thin sections	yes
USW G-3 and GU-3	thin sections	yes
USW G-4	thin sections	yes
USW H-1	thin sections	yes
USW H-3	drill-bit cuttings	yes
USW H-4	drill-bit cuttings	yes
USW H-5	drill-bit cuttings	no
USW H-6	thin sections	no (observation in legacy notebook not verified)
UE-25 J-13	thin sections	no
USW WT-10	drill-bit cuttings	no
USW WT-12	drill-bit cuttings	no
USW WT-14	drill-bit cuttings	no
USW WT-17	drill-bit cuttings	no

Source: DTN: LA0701SL150304.001 [DIRS 179620].

Published and unpublished works on Yucca Mountain mineralogy were checked for information on sulfide occurrences. Information was abstracted directly from the original sources unless the same samples were examined for this study.

In this report, the term *xenoliths* refers to rock fragments presumed to be foreign to the pyroclastic rock in which they occur. Literature sources for this report have used this term or a variety of generally synonymous terms, such as *accidental lithic fragment* (Castor et al. 1994 [DIRS 102495], p. 401).

Information generated for this study is non-qualified because it is largely derived from legacy sources more than twenty years old and from examination of non-qualified bit-cutting samples.

O3. RESULTS

Sulfide observations by Castor et al. (1994 [DIRS 102495], p. 401) in Yucca Mountain boreholes are summarized in Table O-2. The source paper identifies sulfide-bearing intervals by depth in whole meters, rather than by depth in feet as was done for this study. Some sulfide occurrences are referenced to lithostratigraphic boundaries whose depths are not specified. The information in the table is a best effort to render data from the source paper in a form for easy comparison with the rest of the data in this report. Metric depth values were converted back to depth in feet, which is the YMP standard for logging drill core and cuttings samples. Uncertainties in depth traceable to the unit conversions probably are of the order of three feet or less. In addition to the depths of sulfide occurrences from the report by Castor et al. (1994 [DIRS 102495], p. 401), Table O-2 also provides lithostratigraphic unit boundaries for the deeper portion of each borehole.

Castor et al. (1994 [DIRS 102495], pp. 401 to 402) found that sulfides mainly occur in xenoliths. Small, commonly rounded sulfide grains in the tuff matrix also were observed. Their modal analyses show a pyrite content of 0.4 to 2.8 vol % in pyritic ash-flow tuff of the lower Tram Tuff (Tctlv). Bedded tuff below the Tram Tuff (Tctbt) generally contains only traces of pyrite, but more than one percent pyrite was found in a thin bed of tuff in borehole UE-25b#1. Pyrite also occurs in the basal 38 m (124.7 ft) of the Lithic Ridge Tuff (Tlr) in borehole USW G-3. Sulfide occurrences in a calcified ash flow deep in borehole UE-25p#1 also are included in Table O-2. Sulfide observed by Castor et al. (1994 [DIRS 102495], p. 402) in flow rock (unnamed lava) below the Tlr in borehole USW G-2 was omitted from Table O-2 because more information is available from the reexamination of G-2 thin sections in this report.

Table O-2. Observed Sulfide Occurrences

	USW G-1	USW G-3	UE-25b#1	UE-25p#1
Sulfide-bearing depth interval, ft (m)	Below 3,228 (984), base unspecified but within Tctlv	3,681 to 3,876.3 (1,122 to 1,181.5) 4,748.4 to 4,873.0 (1,447.3 to 1,485.3)	3,360 to 3,927 (1,024 to 1,197)	3,950 to 5,610 (1,204 to 1,710)
Tctlv depth interval, ft (m)	3,005 to 3,522 (915.9 to 1,073.5)	3,290 to 3,850.1 (1,002.8 to 1,173.5)	3,359.9 to 3,900.9 (1,024.1 to 1,189.0)	2,616 to 2,863 (797.4 to 872.6)
Tctbt depth interval, ft (m)	3,522 to 3,558.2 (1,073.5 to 1,084.5)	3,850.1 to 3,876.3 (1,173.5-1,181.5)	3,900.9 to 3,960.3 (1,189.0 to 1,207.1)	faulted out
Flow breccia and lava depth interval, ft (m)	3,558.2 to 3,945.8 (1,084.5 to 1,202.7)	not present	not present	not present
Tlr depth interval, ft (m)	3,945.8 to 4,920.7 (1,202.7 to 1,499.8)	3,876.3 to 4,873.0 (1,181.5 to 1,485.3)	3,960.3 to 4,002.2 (1,207.1 to 1,219.9) TD	2,863 to 3,488 (872.6 to 1,063.1)
Bedded tuff depth interval, ft (m)	4,920.7 to 4,940.2 (1,499.8 to 1,505.8)	4,873.0 to 4,882.8 (1,485.3 to 1,488.3)	–	3,488 to 3,502 (1,063.1 to 1,067.4)
Tuff Unit A depth interval, ft (m)	4,940.2 to 5,320.0 (1,505.8 to 1,621.5)	4,882.8-5,030.8 (1,488.3-1,533.4) TD	–	3,502-3,610 (1,067.4-1,100.3)
Tuff Unit B depth interval, ft (m)	5,320.0-5,434.0 (1,621.5 to 1,656.3)	–	–	not present

Table O-2. Sulfide Occurrences Observed (Continued)

	USW G-1	USW G-3	UE-25b#1	UE-25p#1
Tuff Unit C depth interval, ft (m)	5,434.0 to 6,000 (1,656.3 to 1,828.8) TD	–	–	3,610 to 3,733 (1,100.3 to 1,137.8)
Conglomerate depth interval, ft (m)	–	–	–	3,733 to 3,844 (1,137.8 to 1,171.7)
Calcified ash-flow tuff depth interval, ft (m)	–	–	–	3,844 to 4,080 (1,171.7 to 1,243.6)
Lone Mountain Dolomite depth interval, ft (m)	–	–	–	4,080 to 5,470 (1,243.6 to 1,667.3)
Roberts Mountain Formation depth interval, ft (m)	–	–	–	5,470 to 5,923 (1,667.3 to 1,805.3)TD

Sources: Castor et al. 1994 [DIRS 102495], pp. 401 to 403; DTN: MO0004QGFMPICK.000 [DIRS 152554] for lithostratigraphic intervals to base of Tctbt; Spengler et al. 1981 [DIRS 101297], pp. 18 to 25, Scott and Castellanos 1984 [DIRS 101291], pp. 116 to 121, Lobmeyer et al. 1983 [DIRS 105457], p. 16, and Carr et al. 1986 [DIRS 102046], pp. 69 to 80 for intervals below Tctbt.

NOTES: Detailed information on specific depth occurrences and abundances of sulfides at each specific depth is provided in Table O-4.

Tctlv = Tram Tuff, lower vitric (zeolitic) nonwelded to partially welded; Tctbt = pre-Tram Tuff bedded tuff; Tlr = Lithic Ridge Tuff; TD = total depth of borehole. Minor discrepancies in inferred unit boundaries caused by depths being reported by Castor et al. 1994 [DIRS 102495], p. 401 to 403, to the nearest whole meter have been corrected.

O3.1 CUTTINGS EXAMINATION

Hydrology (H) boreholes H-3, H-4, and H-5 were drilled to target depths of about 4,000 ft (about 1,219 m). The suites of cuttings from these holes include the Tram Tuff and the Lithic Ridge Tuff that were identified by Castor et al. (1994 [DIRS 102495], p. 401) as the lithostratigraphic units hosting pyritic xenoliths. Redox measurements are available for water samples from these boreholes. According to the evaluation in *Impacts of Solubility and Other Geochemical Processes on Radionuclide Retardation in the Natural System* (BSC 2006 [DIRS 178672]), the waters in H-3 and H-4 are reducing and the waters in H-5 are oxidizing.

Sulfide occurrences in the three hydrology boreholes, based on examination of drill-bit cuttings performed for this study, are summarized in Table O-3. Altogether, 116 samples, each representing a 10-ft (3.05-m) depth interval, were examined (DTN: LA0701SL150304.001 [DIRS 179620]). The selection of depth intervals for examination was guided by the findings of Castor et al. (1994 [DIRS 102495]). Samples from consecutive 10-ft depth intervals were examined in units where sulfides were consistently observed. Where sulfides were absent, cuttings were examined in intervals of as much as 100 ft (30.5 m). Only a few attempts were made to estimate sulfide abundance because most of the cuttings samples are contaminated with rock material from other than the nominal sample-depth interval. The sulfide-bearing depth intervals reported in Table O-3 are intervals where sulfide is consistently present and include no more than one ten-foot interval in which sulfide was not observed.

In H-3, sulfide is present in the lower Tram Tuff, the underlying bedded tuff, and the uppermost Lithic Ridge Tuff. Sulfide in H-4 is present in the lower Tram Tuff and underlying bedded tuff,

but occurs only in the lower part of the Lithic Ridge Tuff penetrated by the borehole. The sulfide distribution reported by Castor et al. (1994 [DIRS 102495], p. 401) in borehole USW G-3 more closely resembles the distribution in H-4, rather than that in the more proximal hole, H-3. No sulfides were observed in the cuttings from USW H-5. The highest estimated sulfide abundance is about 1.8 vol % (H-3 3,560 to 3,570 ft; DTN: LA0701SL150304.001 [DIRS 179620], Table 1). Sulfides are most common in xenoliths, as noted by Castor et al. (1994 [DIRS 102495], p. 401).

Table O-3. Summary of Sulfide Occurrences and Lithostratigraphy in Cuttings from Boreholes USW H-3, H-4, and H-5

	USW H-3	USW H-4	USW H-5
Sulfide-bearing depth interval, ft (m)	3,500 to 3,660 (1,066.8 to 1,115.6)	3,450 to 3,820 (1,051.6 to 1,164.3) 3,900 to 4,004 (1,188.7 to 1,220.4) TD	none
Tctlv depth interval, ft (m)	3,120 to 3,595.1 (951.0 to 1,095.8)	3,228 to 3,788 (983.9 to 1,154.6)	3,150 to 3,412 (960.1 to 1,040.0)
Tctbt depth interval, ft (m)	3,595.1 to 3,637.1 (1,095.8 to 1,108.6)	3,788 to 3,819 (1,154.6 to 1,164.0)	3,412 to 3,421.9 (1,040.0 to 1,043.0)
Tlr depth interval, ft (m)	3,637.1 to 4,000 (1,108.6 to 1,219.2) TD	3,819 to 4,004 (1,164.0 to 1,220.4) TD	not present
Lava, unnamed, depth interval, ft (m)	not present	not present	3,421.9 to 4,000 (1,043.0 to 1,219.2) TD

Sources: DTNs: LA0701SL150304.001 [DIRS 179620]; MO0004QGFMPICK.000 [DIRS 152554] for lithostratigraphic intervals to base of Tctbt; Bentley et al. 1983 [DIRS 101193], pp. 11 to 12, Thordarson et al. 1984 [DIRS 103200], pp. 9 to 10, Whitfield et al. 1984 [DIRS 101366], p. 11 for intervals below Tctbt.

NOTES: Detailed information on abundances of sulfides at specific depths in the same lithostratigraphic units, but different boreholes is provided in Table O-4.

Tctlv = Tram Tuff, lower vitric (zeolitic) nonwelded to partially welded; Tctbt = pre-Tram Tuff bedded tuff; Tlr = Lithic Ridge Tuff; TD = total depth of borehole.

The groundwaters from water-table boreholes WT-10, WT-12, WT-14, and WT-17 were identified in *Impacts of Solubility and Other Geochemical Processes on Radionuclide Retardation in the Natural System* (BSC 2006 [DIRS 178672], pp. 2-4 to 2-5) as having reducing chemistry. These boreholes are all less than 2,000 ft deep, too shallow to reach the Tram or Lithic Ridge Tuffs. The lithostratigraphic units within the saturated zone in the lower parts of the boreholes are the Topopah Spring Tuff (WT-10), the Calico Hills Formation (WT-12, WT-14), or the Prow Pass Tuff (WT-17; DTN: MO0004QGFMPICK.000 [DIRS 152554]). Cuttings samples from the lowermost 10 to 20 ft of these holes were examined, but no sulfides were observed.

O3.2 PETROGRAPHIC EXAMINATION

Los Alamos National Laboratory legacy and active notebooks were searched for entries relevant to sulfide-mineral occurrences in Yucca Mountain drill cores and bit cuttings. The information documents numerous occurrences from petrographic thin sections and one occurrence from a scanning-electron microscopy mount. Most of the thin sections in the original studies were reexamined, and expanded descriptions of the sulfide occurrences are given in Table O-4. In a few cases, the original sulfide identifications were not confirmed during reexamination, and the legacy information is included in the table with a notation to that effect. There also were a few

cases in which the original thin section could not be found; for these, the petrographic observation simply restates what was recorded in the original legacy notebook entry.

Table O-4. Summary of Legacy and New Petrographic Observations of Sulfides

Sample Depth, ft (m)	Lithostratigraphic Unit	Petrographic Observation
Borehole USW G-1		
3,258 (993.0)	Tctlv	Sulfides occur in both the ash flow and the enclosed xenoliths. Sulfides in the ash flow are present in both phenocrysts and matrix. Iron oxides are partly altered to sulfides. Sulfide phenocrysts in a volcanic xenolith are partly resorbed.
3,321 (1,012.2)	Tctlv	About 1 vol % to 2 vol % sulfides in xenoliths and tuff matrix.
3,371 (1,027.5)	Tctlv	About 1 vol % sulfides in xenoliths and tuff matrix.
3,500 (1,066.8)	Tctlv	About 2 vol % to 3 vol % sulfides in xenoliths and tuff matrix.
3,706 (1,129.6)	Lava (unnamed)	Much less than 1 vol % sulfides in brecciated lava clasts.
3,850 (1,173.5)	Lava (unnamed)	Much less than 1 vol % sulfides in lava.
Borehole USW G-2		
3,250 (990.6)	Tcpbt	Legacy notebook mentions pyrite present.
3,416 (1,041.2)	Tcbm	Micrometer-size sulfide grains in single magnetite crystal; micrometer-size sulfides on border of xenolith.
3,492 (1,064.4)	Tcblv	Cubic micrometer-size sulfide grains in tuff matrix and sparse xenoliths.
3,541 (1,079.3)	Tcbbt	Two sulfide grains noted in one volcanic xenolith only.
3,671 (1,118.9)	Tctlv	Two sulfide grains each in two volcanic xenoliths.
3,772 (1,149.7)	Tctlv	Three lath-shaped sulfide grains in tuff matrix.
3,875 (1,181.1)	Tctlv	Less than 0.1 vol % sulfide grains in tuff matrix.
3,933 (1,198.8)	Tctbt	Less than 0.1 vol % micrometer-size sulfide grains disseminated probably in matrix of highly altered tuff or less commonly associated with mica.
4,005 (1,220.7)	Tctbt	Sulfides mentioned in legacy notebook, but no sulfides observed upon reexamination
4,090 (1,246.6)	Lava (unnamed)	Less than 0.1 vol % sulfide grains within volcanic xenoliths.
4,199 (1,279.9)	Tlr	Less than 0.1 vol % of multiple sulfide minerals in altered pyroclasts of uncertain origin.
4,209 (1,282.9)	Tlr	Less than 0.1 vol % sulfide grains in tuff matrix.
5,206 (1,586.8)	Lava (unnamed)	Less than 0.1 vol % sulfide grains in phenocrysts of tuff.
5,305 (1,617.0)	Lava (unnamed)	Less than 0.1 vol % sulfide grains, all within xenoliths.
Boreholes USW G-3 and GU-3		
3,759 (1,145.7)	Tctlv	About 4 vol % to 5 vol % sulfides, found in tuff matrix and volcanic xenoliths, locally rimming the xenoliths.
3,854 (1,174.7)	Tctbt	Less than 0.1 vol % sulfides, only as inclusions in micas.
4,008 (1,221.6)	Tlr	Sulfides mentioned in legacy notebook, but none observed upon reexamination.
4,240 (1,292.4)	Tlr	Less than 0.1 vol % sulfide grains in volcanic xenoliths.
4,297 (1,309.7)	Tlr	Less than 0.1 vol % sulfide grains in volcanic xenoliths.
4,416 (1,346.0)	Tlr	Sulfides mentioned in legacy notebook, but none observed upon reexamination
4,423 (1,348.1)	Tlr	Less than 0.1 vol % sulfides in one xenolith only.

Table O-4. Summary of Legacy and New Petrographic Observations of Sulfides (Continued)

Sample Depth, ft (m)	Lithostratigraphic Unit	Petrographic Observation
4,568 (1,392.3)	Tlr	Sulfides mentioned in legacy notebook, but none observed upon reexamination.
4,600 (1,402.1)	Tlr	Less than 0.1 vol % sulfide grains in tuff matrix.
4,708 (1,435.0)	Tlr	About 2 vol % sulfides within one centimeter-scale volcanic xenolith; examination of rock core suggests overall abundance less than 0.1 vol %.
4,756 (1,449.6)	Tlr	Legacy notebook mentions "sulfides abundant."
Borehole USW G-4		
236 (71.9)	Tptrv3	Less than 0.1 volume % sulfides as three micrometer-size fragments in tuff matrix.
694 (211.5)	Tptpmn	Less than 0.1 vol % sulfides as two micrometer-size sulfide fragments in tuff matrix.
1,342 (409.0)	Tptpv3	Legacy notebook mentions sulfides in magnetite.
Borehole UE-25b#1		
3,393 (1,034.2)	Tctlv	About 1 vol % sulfide in both tuff matrix and volcanic xenoliths. Sulfides include discrete euhedral crystals and crystal fragments. No indication of post-emplacement iron oxide alteration to sulfide.
3,469 (1,057.4)	Tctlv	About 1.5 vol % to 2 vol % sulfides, present in both volcanic xenoliths and ash-flow matrix. There are iron oxides partly replaced by sulfide rims, with preferential replacement of rhombohedral phases.
3,506 (1,068.6)	Tctlv	About 1 vol % sulfides, as fragments and euhedral grains in both tuff matrix and volcanic xenoliths. One very small sulfide grain in a quartzite xenolith. Sulfide replacement of lamellae in oxidized iron oxide within one xenolith. Fine sulfide veinlets observed.
3,571 (1,088.4)	Tctlv	Sulfide content varies from 0.5 vol % to 3 vol % in two sections, most abundant in xenoliths. Local evidence of sulfide rims on iron oxides or preferential sulfide replacement of lamellae in oxidized iron oxide.
3,660 (1,115.6)	Tctlv	About 3 vol % sulfides, in tuff matrix, volcanic xenoliths, and veins with analcime. Variable alteration of iron oxides to sulfides, and one sulfide grain with iron oxide rim in tuff matrix.
3,767 (1,148.2)	Tctlv	Up to 5 vol % sulfide, in tuff matrix and in volcanic and quartzite xenoliths. Variable alteration of iron oxides to sulfide.
3,835 (1,168.9)	Tctlv	About 6 vol % to 7 vol % sulfides, in tuff matrix, xenoliths, and in veinlets. Sulfides exist as euhedral grains and as aggregates mantling iron oxide grains. Variable alteration of iron oxides to sulfides, with rhombohedral iron oxides (e.g., ilmenite, hematite) more altered than magnetite in matrix. Some xenoliths have mixed populations of unaltered iron oxides and sulfides.
3,902 (1,189.3)	Tctbt	About 2 vol % to 3.5 vol % sulfides, in tuff matrix, volcanic xenoliths, and stringers of small grains around xenoliths. Most iron oxides and sulfides are unaltered, but there are sulfides partly altered to iron oxide and iron oxides partly altered to sulfide.
3,910 (1,191.8)	Tctbt	About 1 vol % sulfides in matrix of tuff with only rare volcanic xenoliths. Sulfides occur as euhedral grains and fragments. Most rhombohedral iron oxides altered to sulfide; magnetite not affected.
3,956 (1,205.8)	Tctbt	Less than 0.1 vol % sulfide present as one micrometer-size sulfide grain.
3,988 (1,215.5)	Tlr	Legacy notebook mentions presence of pyrite.

Table O-4. Summary of Legacy and New Petrographic Observations of Sulfides (Continued)

Sample Depth, ft (m)	Lithostratigraphic Unit	Petrographic Observation
Borehole USW H-1		
3,367 (1,026.3)	Tctlv	About 0.5 vol % to 1 vol % sulfides in tuff matrix and volcanic xenoliths.
3,936 (1,199.7)	Lava (unnamed)	Less than 0.1 vol % sulfides in altered phenocrysts of fractured and altered lava with no xenoliths.
Borehole UE-25 p#1		
3,928 (1,197.3)	Calcified ash-flow tuff	Sulfides are only opaque phase, about 2.5 vol %. Two sulfide phases present, medium yellow and bronze yellow.
Borehole ESF-HD-CHE-3 (39.62-m long angled hole in Alcove 5 of Exploratory Studies Facility)		
66.7 (20.3) depth along wellbore	Ttpmn	7-8 micrometer cubic sulfide crystals within smectite fracture coating (core chip for scanning-electron microscopy).

Sources: DTNs: LA0701SL150304.001 [DIRS 179620], MO0004QGFMPIK.000 [DIRS 152554] for lithostratigraphic intervals to base of Tctbt; Spengler et al. 1981 [DIRS 101297], pp. 18 to 25, Scott and Castellanos 1984 [DIRS 101291], pp. 116 to 121, Lobmeyer et al. 1983 [DIRS 105457], p. 16, Carr et al. 1986 [DIRS 102046], pp. 69 to 80, Rush et al. 1983 [DIRS 107944], p. 6, and Maldonado and Koether 1983 [DIRS101805], pp. 77 to 80 for intervals below Tctbt.

NOTES: Despite the small (micrometer) size of many observed sulfide grains, the combination of morphology and color in reflected light allows identification with a high degree of confidence.

Tptrv3 = Topopah Spring Tuff crystal-rich vitric nonwelded to partially welded zone; Ttpmn = Topopah Spring Tuff, crystal-poor middle nonlithophysal zone; Ttpv3 = Topopah Spring Tuff, crystal-poor vitric densely welded subzone; Tcprt = preProw Pass bedded tuff; Tcbm = Bullfrog Tuff, crystallized moderately to densely welded zones; Tcbv = Bullfrog Tuff, lower vitric (zeolitic) nonwelded to partially welded zones; Tcbbt = pre-Bullfrog Tuff bedded tuff; Tctlv = Tram Tuff, lower vitric (zeolitic) nonwelded to partially welded; Tctbt = pre-Tram Tuff bedded tuff; Tlr = Lithic Ridge Tuff.

O.4 DISCUSSION

O4.1 DISTRIBUTION AND ABUNDANCE OF SULFIDES

Based on available sulfide-occurrence data from the vicinity of Yucca Mountain, sulfides in greater-than-trace quantities most commonly occurred in the Tctlv lithostratigraphic zone, the lower vitric or zeolitized part of the Tram Tuff. The high abundance of sulfides in this zone and the fact that sulfides are large enough to be easily visible under stereomicroscopic examination of cuttings give us high confidence that no Tctlv sulfide occurrences in greater than trace amounts were missed during sample examination. Most of the sulfide in this zone appears to be associated with xenoliths. The areal distribution of sulfide-bearing xenoliths in the Tctlv, therefore, reflects the combined effects of xenolith source, the dynamics of xenolith incorporation and ignimbrite transport, and the paleotopography of the deposition area.

Occurrences of sulfides in the Tctlv zone of boreholes UE-25b#1, USW G-1, USW G-2, USW G-3, USW H-1, H-3, and H-4 define an area of sulfide distribution corresponding approximately to the east-sloping part of northern and central Yucca Mountain. This area is essentially equivalent to the “reducing curtain” concept in *Impacts of Solubility and Other Geochemical Processes on Radionuclide Retardation in the Natural System* (BSC 2006 [DIRS 178672], p. 3-3 and Figure 2.6-5). The eastern and western limits of this area are poorly constrained by negative data from boreholes H-5, USW H-6, UE-25 J-13, and UE-25 p#1. The local northern limit is not constrained by any data but presumably extends no further than the approximate boundary of the Timber Mountain caldera complex, less than five km north of G-2 (Bish 1989 [DIRS 101194],

p. 32). Within the caldera complex, ash flows such as the Tram Tuff that predate Timber Mountain volcanism (Sawyer et al. 1994 [DIRS 100075], p. 1,305) probably no longer exist as intact layers. The southern limit is not locally constrained. Information from boreholes further south could improve this uncertainty.

The areal distribution of sulfide occurrences in the Tctbt, the bedded tuff below the Tram Tuff, probably are the same as for the Tctlv. There is less information about this zone because the thin-section sets for several boreholes do not include samples from the Tctbt. The distribution of sulfides in the Tlr, the Lithic Ridge Tuff, also is less well known because fewer boreholes penetrated much of this unit. Occurrences of sulfide in G-2, G-3, H-3, H-4, and b#1 (Tables O-3 and O-4) suggest an areal distribution smaller or more discontinuous than the Tctlv sulfide distribution. The overall abundance of sulfide in the Tlr may be lower than in the Tctlv. Some additional information could be obtained by examining bit cuttings from the deeper, uncored portions of boreholes H-1 and H-6.

In the absence of direct evidence of sulfides in the shallow WT boreholes, several hypotheses have been proposed for the reducing conditions in these holes (BSC 2006 [DIRS 178672], p. 2-4). One possible explanation would be the presence of undetected sulfides in the lithostratigraphic units hosting the water table: the Topopah Spring Tuff, Calico Hills Formation, or Prow Pass Tuff. The data in Table O-4 documenting minor sulfide occurrences in the Topopah Spring Tuff provide some support for this hypothesis, although sulfides are much less abundant in this unit than in the Tram Tuff. An alternate hypothesis, that groundwaters from the WT holes may be reducing because they came into contact with reductants upgradient from these holes, is not contradicted by our results. Our finding of sulfides in the Tram Tuff and lower units of H-1, H-3, and H-4 supports this hypothesis in a general way by documenting the greater continuity and areal extent of this major sulfide inventory.

O4.2 ORIGINS OF SULFIDES AT YUCCA MOUNTAIN

It is beyond the scope of this report to provide a definitive and detailed explanation for the origins of all sulfide occurrences at Yucca Mountain. The data that would be required to determine the exact origins of the sulfides do not exist. This is especially true for minor occurrences of sulfides with ambiguous textural relations to the rocks in which they occur. Therefore, the evaluations of existing information presented here are conservative and reflect the limits of that information.

Most of the sulfides in Yucca Mountain tuffs occur in xenoliths in the Tram and Lithic Ridge Tuffs. The simplest explanation for these occurrences is that sulfide deposition in the source rocks of the xenoliths predated the pyroclastic eruptions that incorporated the xenoliths into the tuffs. Castor et al. (1994 [DIRS 102495], pp. 405 to 407) reviewed possible sources of the sulfide-bearing xenoliths in terms of known areas of hydrothermal alteration and possible locations of the vent or vents that erupted the xenolith-bearing tuffs. Vent locations have been proposed to the north or northwest of Yucca Mountain or beneath the mountain. The question of xenolithic sulfide origin remains open, and definitive new data are unlikely to become available soon. Castor et al. (1994 [DIRS 102495], pp. 405 to 407) noted that pyritic xenoliths are absent from Tram Tuff exposures west of Yucca Mountain and in boreholes p#1 and J-13. We found no sulfide-bearing xenoliths in the Tram Tuff in boreholes H-5 and H-6. Taken together, this

information confirms that sulfide-bearing xenoliths are not present throughout the areal extent of the lower Tram Tuff.

The presence of sulfides in boreholes G-1, G-2, and H-1 in unnamed lavas (also called flow rock or flow breccias) that are interlayered with the Tram and Lithic Ridge Tuffs (Table O-4 and Castor et al. 1994 [DIRS 102495], p. 402) raises the possibility that some fraction of the sulfide-bearing xenoliths could be derived from these lavas. A review of previously collected geochemical and mineralogic data might help us evaluate whether multiple sulfide sources could have contributed to the xenolith population. The knowledge of single or multiple sulfide-bearing xenolith sources could improve our ability to predict the areal distribution and abundance of the xenoliths.

Sulfides of non-xenolithic and possibly in-situ origin in the saturated zone are present in trace amounts in the Prow Pass and Bullfrog Tuffs in borehole G-2. Bish (1989 [DIRS 101194], pp. 23, 26, and 31) suggested that pyrite in these units in G-2 formed by hydrothermal alteration related to Timber Mountain caldera activity about 11 million years ago. An occurrence of sulfide in a deep calcified tuff in borehole p#1 also may be of hydrothermal origin, but there are no data to support this interpretation.

The sulfide occurrences in boreholes USW G-4 and ESF-HD-CHE-3 are in the unsaturated zone and, therefore, not directly pertinent to redox conditions in the saturated zone. However, the Topopah Spring Tuff, the lithostratigraphic unit in which the sulfides were observed, lies below the water table in borehole USW WT-10, a borehole with reducing water, and in other boreholes as well. The unsaturated-zone sulfide occurrences raise the possibility that some sulfides may be present in the Topopah Spring Tuff below the water table and may contribute to reducing conditions in the saturated zone. The non-fracture-filling sulfides, if they are of in-situ origin, would seem to be products of very localized alteration. The fracture-filling sulfides in borehole ESF-HD-CHE-3 clearly postdate deposition of the host tuff, but little else is known about the environment in which they were deposited. At the very least, these occurrences provide further evidence of the complex history of changing or localized redox conditions around Yucca Mountain.

O4.3 EVIDENCE OF WATER-ROCK INTERACTION

Textural evidence of mineral alteration involving iron sulfides is observable primarily in thin section. Thin sections were available for only a subset of boreholes in which sulfides were observed (Table O-1), restricting the search for evidence of sulfide reaction with oxygen-bearing groundwater. Evidence for partial replacement of iron oxides by sulfides and of sulfides by oxides was found in thin sections from borehole b#1 (Table O-4). It is possible that these mineral parageneses record redox conditions along the boundary of the stability fields of iron sulfides and oxides. However, nothing is known of the geochronology of sulfide and oxide alteration or secondary deposition at Yucca Mountain beyond relative timing based on textural relations. The variable types of alteration products in the b#1 samples could be of very different ages. Ambiguities of in-situ –versus exotic origin for individual crystals add to the uncertainty in trying to interpret alteration. Within the small set of samples that could be examined, no consistent or ubiquitous evidence of sulfide oxidation was found that would be associated with the consumption of dissolved oxygen. Such alteration could be occurring in hydraulic

upgradient locations that have gone unrecognized or have not been penetrated by boreholes. This kind of situation was postulated in *Impacts of Solubility and Other Geochemical Processes on Radionuclide Retardation in the Natural System* (BSC 2006 [DIRS 178672], p. 2-4).

05. CONCLUSIONS

Data collected by Los Alamos National Laboratory on the occurrence and distribution of iron sulfides around Yucca Mountain are contained in DTN: LA0701SL150304.001 [DIRS 179620]. The existing and new data support, with a high degree of confidence, the existence of sulfide-bearing rocks at least in the Tram Tuff, within an area corresponding approximately to the east-sloping part of northern and central Yucca Mountain. This area is essentially equivalent to the “reducing curtain” concept in *Impacts of Solubility and Other Geochemical Processes on Radionuclide Retardation in the Natural System* (BSC 2006 [DIRS 178672], p. 3-3 and Figure 2.6-5).

The data were insufficient or too ambiguous to project the existence of sulfide-bearing rocks beyond the area identified above with a high degree of confidence. The combination of existing and new sulfide-distribution data, present understanding of sulfide origins, and evidence of sulfide-water interaction did not reduce the uncertainty.

There is a possibility of obtaining additional data from two or more existing boreholes at Yucca Mountain and to the south to increase the level of confidence in areal distribution beyond the “reducing curtain.” Collection of mineral-composition data from existing samples could improve understanding of the sources of sulfide-bearing xenoliths in the Tram Tuff and underlying units. This also could increase the level of confidence in projecting the existence of sulfides in a wider area.

INTENTIONALLY LEFT BLANK

APPENDIX P

**DERIVATION OF EQUATIONS F-32 AND F-36 FROM
APPENDIX F: LAPLACE DOMAIN SOLUTIONS FOR DRAWDOWNS IN TWO- AND
THREE-AQUIFER SYSTEMS**

In this appendix, the Laplace-domain solutions of the equations describing drawdowns in a generalized two-aquifer system and a generalized three-aquifer system are derived. The solutions are presented without derivation in Section F6. The derivations are provided here to facilitate the checking and reviewing of this analysis report, as the equations are not found in the readily accessible literature.

P.1 DERIVATION OF TWO-AQUIFER SOLUTION

The derivation of the Laplace-domain analytical solution for the two-aquifer system (Equation F-32) is provided in this section. Beginning with the governing equation in Laplace space from Section F6 (Equation F-30):

$$s_1 p \tilde{S}_1 = T_1 \nabla \tilde{S}_1 + \chi_{1-2} (\tilde{S}_2 - \tilde{S}_1) - \chi_0 \tilde{S}_1 \quad (\text{Eq. F-30a})$$

$$s_2 p \tilde{S}_2 = T_2 \nabla \tilde{S}_2 + \chi_{1-2} (\tilde{S}_1 - \tilde{S}_2) - \chi_{2-3} \tilde{S}_2 \quad (\text{Eq. F-30b})$$

with boundary conditions (Equation F-31):

$$r \frac{d\tilde{S}_1}{dr} \Big|_{r \rightarrow r_{\text{well}}} = \frac{Q_1}{2\pi T_1}, \quad r \frac{d\tilde{S}_2}{dr} \Big|_{r \rightarrow r_{\text{well}}} = \frac{Q_2}{2\pi T_2}, \quad (\text{Eq. F-31a})$$

$$\tilde{S}_1 \Big|_{r \rightarrow \infty} = 0, \quad \text{and} \quad \tilde{S}_2 \Big|_{r \rightarrow \infty} = 0 \quad (\text{Eq. F-31b})$$

The general solution allows for simultaneous pumping of both aquifers.

Equation F-30 can be rearranged to:

$$T_1 \nabla \tilde{S}_1 = (s_1 p + \chi_{1-2} + \chi_0) \tilde{S}_1 - \chi_{1-2} \tilde{S}_2 \quad (\text{Eq. P-1a})$$

$$T_2 \nabla \tilde{S}_2 = (s_2 p + \chi_{1-2} + \chi_{2-3}) \tilde{S}_2 - \chi_{1-2} \tilde{S}_1 \quad (\text{Eq. P-1b})$$

Equation P-1 can be rewritten in matrix form as:

$$\overline{\nabla S} = \overline{\overline{\overline{C}}} T^{-1} \overline{S} = \overline{\overline{A}} \overline{S} \quad (\text{Eq. P-2})$$

where,

$$\overline{\nabla S} = \begin{bmatrix} \nabla \tilde{S}_1 \\ \nabla \tilde{S}_2 \end{bmatrix} \quad \overline{S} = \begin{bmatrix} \tilde{S}_1 \\ \tilde{S}_2 \end{bmatrix} \quad \overline{\overline{C}} = \begin{bmatrix} \kappa_1 & -\chi_{1-2} \\ -\chi_{1-2} & \kappa_2 \end{bmatrix} \quad \overline{\overline{T^{-1}}} = \begin{bmatrix} 1/T_1 & 0 \\ 0 & 1/T_2 \end{bmatrix}$$

$$\overline{\overline{A}} = \begin{bmatrix} \kappa_1/T_1 & -\chi_{1-2}/T_1 \\ -\chi_{1-2}/T_2 & \kappa_2/T_2 \end{bmatrix} \quad (\text{Eq. P-3})$$

and

$$\kappa_1 = s_1 p + \chi_{1-2} + \chi_0 \quad \text{and} \quad \kappa_2 = s_2 p + \chi_{1-2} + \chi_{2-3}$$

In his journal article about problems of multiple-aquifer flow, Maas (1986 [DIRS 178614]) shows that the general solution to equation P-2 is:

$$\bar{S} = I_0 \left\{ r \sqrt{\bar{A}} \right\} \bar{c}_1 + K_0 \left\{ r \sqrt{\bar{A}} \right\} \bar{c}_2 \quad (\text{Eq. P-4})$$

where I_0 = zero-order modified Bessel function of the first kind

K_0 = zero-order modified Bessel function of the second kind, and

\bar{c}_1 and \bar{c}_2 are vectors of integration constants.

Maas (1986 [DIRS 178614]) also shows that application of boundary condition 58b leads to $\bar{c}_1 = \bar{0}$, as $I_0\{\infty\} = \infty$.

Furthermore, upon differentiation of what remains of equation P-4, boundary condition (58a) can be applied:

$$\left. \frac{d\bar{S}}{dr} \right|_{r \rightarrow 0} = -\sqrt{\bar{A}} K_1 \left\{ r \sqrt{\bar{A}} \right\} \Big|_{r \rightarrow 0} \bar{c}_2 = -\frac{1}{2\pi r} \bar{T}^{-1} \bar{q} \quad (\text{Eq. P-5})$$

where K_1 = first-order modified Bessel function of the second kind.

Maas (1986 [DIRS 178614]) also shows that:

$$\left. \sqrt{\bar{A}} K_1 \left\{ r \sqrt{\bar{A}} \right\} \right|_{r \rightarrow 0} = \frac{1}{r} \bar{I} \quad (\text{Eq. P-6})$$

where \bar{I} = identity matrix, which leads directly to:

$$\bar{c}_2 = \frac{1}{2\pi} \bar{T}^{-1} \bar{q} \quad (\text{Eq. P-7})$$

Thus, equation P-4 becomes:

$$\bar{S} = \frac{1}{2\pi} K_0 \left\{ r \sqrt{\bar{A}} \right\} \bar{T}^{-1} \bar{q} \quad (\text{Eq. P-8})$$

Note that $\bar{q} = \begin{bmatrix} Q_1 \\ Q_2 \end{bmatrix}$, where Q_i is the pumping rate from the i th aquifer.

So:

$$\overline{\overline{T^{-1}q}} = \begin{bmatrix} Q_1/T_1 \\ Q_2/T_2 \end{bmatrix} \quad (\text{Eq. P-9})$$

The remaining challenge is to obtain $\sqrt{\overline{A}}$, which is a nontrivial exercise. Maas (1986 [DIRS 178614]) shows that for any general matrix \overline{B} :

$$f(\overline{B}) = \overline{\overline{F}} \begin{bmatrix} f(\lambda_1) & 0 & \cdot & \cdot & 0 \\ 0 & f(\lambda_2) & & & \cdot \\ \cdot & & \cdot & & \cdot \\ \cdot & & & \cdot & 0 \\ 0 & & & 0 & f(\lambda_n) \end{bmatrix} \overline{\overline{F^{-1}}} \quad (\text{Eq. P-10})$$

where $\lambda_i =$ eigenvalues of $\overline{B^*}$, where $\overline{B^*} = \overline{\overline{D^{1/2} B D^{-1/2}}}$ is a real symmetric matrix that is “similar” to \overline{B} , and the operation to obtain $\overline{B^*}$ is called a similarity transformation,

\overline{F} = matrix whose columns contain eigenvectors of \overline{B} , and

\overline{D} can be any diagonal matrix, so $\overline{D} = \overline{\overline{T}} = \begin{bmatrix} T_1 & 0 \\ 0 & T_2 \end{bmatrix}$ can be used.

Using equation P-10, and letting $\overline{B} = \overline{A}$ from equation P-3, it is apparent that

$$\sqrt{\overline{A}} = \overline{\overline{F}} \begin{bmatrix} \sqrt{\lambda_1} & 0 & \cdot & \cdot & 0 \\ 0 & \sqrt{\lambda_2} & & & \cdot \\ \cdot & & \cdot & & \cdot \\ \cdot & & & \cdot & 0 \\ 0 & & & 0 & \sqrt{\lambda_n} \end{bmatrix} \overline{\overline{F^{-1}}}, \text{ and} \quad (\text{Eq. P-11})$$

$$K_0 \left\{ r \sqrt{\overline{A}} \right\} = \overline{\overline{F}} \begin{bmatrix} K_0 \left\{ r \sqrt{\lambda_1} \right\} & 0 & \cdot & \cdot & 0 \\ 0 & K_0 \left\{ r \sqrt{\lambda_2} \right\} & & & \cdot \\ \cdot & & \cdot & & \cdot \\ \cdot & & & \cdot & 0 \\ 0 & & & 0 & K_0 \left\{ r \sqrt{\lambda_n} \right\} \end{bmatrix} \overline{\overline{F^{-1}}} \quad (\text{Eq. P-12})$$

$\overline{\overline{A^*}}$ can be readily obtained as:

$$\overline{\overline{A^*}} = \begin{bmatrix} \sqrt{T_1} & 0 \\ 0 & \sqrt{T_2} \end{bmatrix} \begin{bmatrix} \kappa_1/T_1 & -\chi_{1-2}/T_1 \\ -\chi_{1-2}/T_2 & \kappa_2/T_2 \end{bmatrix} \begin{bmatrix} 1/\sqrt{T_1} & 0 \\ 0 & 1/\sqrt{T_2} \end{bmatrix} = \begin{bmatrix} \kappa_1/T_1 & -\chi_{1-2}/\sqrt{T_1 T_2} \\ -\chi_{1-2}/\sqrt{T_1 T_2} & \kappa_2/T_2 \end{bmatrix} \quad (\text{Eq. P-13})$$

The eigenvalues of $\overline{\overline{A^*}}$ are the roots of the characteristic equation:

$$\det(\overline{\overline{A^*}} - \lambda \overline{\overline{I}}) = 0 \text{ or } \begin{vmatrix} \kappa_1/T_1 - \lambda & -\chi_{1-2}/\sqrt{T_1 T_2} \\ -\chi_{1-2}/\sqrt{T_1 T_2} & \kappa_2/T_2 - \lambda \end{vmatrix} = 0, \text{ which becomes:}$$

$$(\kappa_1/T_1 - \lambda)(\kappa_2/T_2 - \lambda) - \chi_{1-2}^2/T_1 T_2 = 0 \text{ or}$$

(Eq. P-14)

$$\lambda^2 - (\kappa_1/T_1 + \kappa_2/T_2)\lambda + (\kappa_1 \kappa_2 - \chi_{1-2}^2)/T_1 T_2 = 0$$

From the quadratic equation, the two roots of equation P-14 are:

$$b_1^2 = \frac{1}{2} \left(\frac{\kappa_1}{T_1} + \frac{\kappa_2}{T_2} \right) + \sqrt{\frac{1}{4} \left(\frac{\kappa_1}{T_1} + \frac{\kappa_2}{T_2} \right)^2 - \frac{\kappa_1 \kappa_2 - \chi_{1-2}^2}{T_1 T_2}}, \text{ and} \quad (\text{Eq. P-15a})$$

$$b_2^2 = \frac{1}{2} \left(\frac{\kappa_1}{T_1} + \frac{\kappa_2}{T_2} \right) - \sqrt{\frac{1}{4} \left(\frac{\kappa_1}{T_1} + \frac{\kappa_2}{T_2} \right)^2 - \frac{\kappa_1 \kappa_2 - \chi_{1-2}^2}{T_1 T_2}} \quad (\text{Eq. P-15b})$$

A square matrix $\overline{\overline{B}}$ of order i has i eigenvectors $\overline{\overline{e}}_i$ that satisfy $\overline{\overline{B}} \overline{\overline{e}}_i = \lambda_i \overline{\overline{e}}_i$.

Letting the components of $\overline{\overline{e}}_i$ be x_i and y_i , and letting $\overline{\overline{B}} = \overline{\overline{A^*}}$ from equation P-13, gives:

$$\begin{bmatrix} \kappa_1/T_1 & -\chi_{1-2}/T_1 \\ -\chi_{1-2}/T_2 & \kappa_2/T_2 \end{bmatrix} \begin{bmatrix} x_i \\ y_i \end{bmatrix} = b_i^2 \begin{bmatrix} x_i \\ y_i \end{bmatrix} \text{ or}$$

$$(\kappa_1/T_1)x_i - (\chi_{1-2}/T_1)y_i = b_i^2 x_i$$

$$-(\chi_{1-2}/T_2)x_i + (\kappa_2/T_2)y_i = b_i^2 y_i$$

(Eq. P-16)

From the first of the two equations P-16:

$$y_i = \left(\frac{\kappa_1 - T_1 b_i^2}{\chi_{1-2}} \right) x_i \quad (\text{Eq. P-17})$$

Any set of values (x_i, y_i) that satisfy equation P-17 will be components of an eigenvector of $\overline{\overline{A}}$.

Thus, $\overline{e}_i = \left[\begin{array}{c} 1 \\ \left(\frac{\kappa_1 - T_1 b_i^2}{\chi_{1-2}} \right) \end{array} \right]$ are eigenvectors of $\overline{\overline{A}}$, and it follows that:

$$\overline{\overline{F}} = [\overline{e}_1 \quad \overline{e}_2] = \left[\begin{array}{cc} 1 & 1 \\ \left(\frac{\kappa_1 - T_1 b_1^2}{\chi_{1-2}} \right) & \left(\frac{\kappa_1 - T_1 b_2^2}{\chi_{1-2}} \right) \end{array} \right] \quad (\text{Eq. P-18})$$

$$\text{Let } \beta_1 = \frac{\kappa_1 - T_1 b_1^2}{\chi_{1-2}} \text{ and } \beta_2 = \frac{\kappa_1 - T_1 b_2^2}{\chi_{1-2}}, \text{ so that } \overline{\overline{F}} = \begin{bmatrix} 1 & 1 \\ \beta_1 & \beta_2 \end{bmatrix} \quad (\text{Eq. P-19})$$

The inverse of $\overline{\overline{F}}$ is given by (Spiegel 1971 [DIRS 180316], pp. 363 to 364):

$$\overline{\overline{F}}^{-1} = \frac{\overline{\overline{F}}^T}{\det(\overline{\overline{F}})} \quad (\text{Eq. P-20})$$

where $\overline{\overline{F}}^T$ = matrix of cofactors of $\overline{\overline{F}}$, and $\overline{\overline{F}}^T$ is its transpose,

Without derivation,

$$\overline{\overline{F}}^T = \begin{bmatrix} \beta_2 & -1 \\ -\beta_1 & 1 \end{bmatrix} \quad (\text{Eq. P-21})$$

and

$$\det(\overline{\overline{F}}) = \beta_2 - \beta_1 \quad (\text{Eq. P-22})$$

Inserting equations P-21 and P-22 into equation P-20 yields:

$$\overline{\overline{F}}^{-1} = \begin{bmatrix} \left(\frac{\beta_2}{\beta_2 - \beta_1} \right) & \left(\frac{-1}{\beta_2 - \beta_1} \right) \\ \left(\frac{-\beta_1}{\beta_2 - \beta_1} \right) & \left(\frac{1}{\beta_2 - \beta_1} \right) \end{bmatrix} \quad (\text{Eq. P-23})$$

A derivation is not provided for $\overline{\overline{F}}_{jk}^T$ because it can be readily verified that $\overline{\overline{F}}\overline{\overline{F}}^{-1} = \overline{\overline{I}}$.

Now, substituting equations P-9, P-12, P-19, and P-23 into equation P-8, gives:

$$\overline{\overline{S}} = \frac{1}{2\pi} \begin{bmatrix} 1 & 1 \\ \beta_1 & \beta_2 \end{bmatrix} \begin{bmatrix} K_0\{rb_1\} & 0 \\ 0 & K_0\{rb_2\} \end{bmatrix} \begin{bmatrix} \left(\frac{\beta_2}{\beta_2 - \beta_1} \right) & \left(\frac{-1}{\beta_2 - \beta_1} \right) \\ \left(\frac{-\beta_1}{\beta_2 - \beta_1} \right) & \left(\frac{1}{\beta_2 - \beta_1} \right) \end{bmatrix} \begin{bmatrix} \frac{Q_1}{T_1} \\ \frac{Q_2}{T_2} \end{bmatrix} \quad (\text{Eq. P-24})$$

Multiplying the first 2 matrices of equation P-24 yields:

$$\overline{\overline{S}} = \frac{1}{2\pi} \begin{bmatrix} K_0\{rb_1\} & K_0\{rb_2\} \\ \beta_1 K_0\{rb_1\} & \beta_2 K_0\{rb_2\} \end{bmatrix} \begin{bmatrix} \left(\frac{\beta_2}{\beta_2 - \beta_1} \right) & \left(\frac{-1}{\beta_2 - \beta_1} \right) \\ \left(\frac{-\beta_1}{\beta_2 - \beta_1} \right) & \left(\frac{1}{\beta_2 - \beta_1} \right) \end{bmatrix} \begin{bmatrix} \frac{Q_1}{T_1} \\ \frac{Q_2}{T_2} \end{bmatrix} \quad (\text{Eq. P-25})$$

Likewise, multiplying the first 2 matrices of equation P-25 yields:

$$\overline{\overline{S}} = \frac{1}{2\pi} \begin{bmatrix} \left(\frac{\beta_2 K_0\{rb_1\} - \beta_1 K_0\{rb_2\}}{\beta_2 - \beta_1} \right) & \left(\frac{-K_0\{rb_1\} + K_0\{rb_2\}}{\beta_2 - \beta_1} \right) \\ \left(\frac{\beta_1 \beta_2 K_0\{rb_1\} - \beta_1 \beta_2 K_0\{rb_2\}}{\beta_2 - \beta_1} \right) & \left(\frac{-\beta_1 K_0\{rb_1\} + \beta_2 K_0\{rb_2\}}{\beta_2 - \beta_1} \right) \end{bmatrix} \begin{bmatrix} \frac{Q_1}{T_1} \\ \frac{Q_2}{T_2} \end{bmatrix} \quad (\text{Eq. P-26})$$

Finally, multiplying the remaining matrix by the $\overline{c_2}$ vector yields:

$$\begin{aligned} \tilde{S}_1 &= \frac{1}{2\pi} \left(\frac{\beta_2 K_0\{rb_1\} - \beta_1 K_0\{rb_2\}}{\beta_2 - \beta_1} \right) \frac{Q_1}{T_1} + \left(\frac{-K_0\{rb_1\} + K_0\{rb_2\}}{\beta_2 - \beta_1} \right) \frac{Q_2}{T_2} \\ \tilde{S}_2 &= \frac{1}{2\pi} \left(\frac{\beta_1 \beta_2 K_0\{rb_1\} - \beta_1 \beta_2 K_0\{rb_2\}}{\beta_2 - \beta_1} \right) \frac{Q_1}{T_1} + \left(\frac{-\beta_1 K_0\{rb_1\} + \beta_2 K_0\{rb_2\}}{\beta_2 - \beta_1} \right) \frac{Q_2}{T_2} \end{aligned} \quad (\text{Eq. P-27})$$

Rearrangement yields

$$\begin{aligned}\tilde{S}_1 &= \frac{1}{2\pi(\beta_2 - \beta_1)} \left[\left(\beta_2 \frac{Q_1}{T_1} - \frac{Q_2}{T_2} \right) K_0\{rb_1\} + \left(\frac{Q_2}{T_2} - \beta_1 \frac{Q_1}{T_1} \right) K_0\{rb_2\} \right] \\ \tilde{S}_2 &= \frac{1}{2\pi(\beta_2 - \beta_1)} \left[\beta_1 \left(\beta_2 \frac{Q_1}{T_1} - \frac{Q_2}{T_2} \right) K_0\{rb_1\} + \beta_2 \left(\frac{Q_2}{T_2} - \beta_1 \frac{Q_1}{T_1} \right) K_0\{rb_2\} \right]\end{aligned}\quad (\text{Eq. P-28})$$

If $C_1 = \frac{\left(\beta_2 \frac{Q_1}{T_1} - \frac{Q_2}{T_2} \right)}{2\pi(\beta_2 - \beta_1)}$ and $C_2 = \frac{\left(\frac{Q_2}{T_2} - \beta_1 \frac{Q_1}{T_1} \right)}{2\pi(\beta_2 - \beta_1)}$, then equation F-32 is recovered:

$$\tilde{S}_1 = C_1 K_0(b_1 R) + C_2 K_0(b_2 R)$$

and (Eq. F-32)

$$\tilde{S}_2 = C_1 \beta_1 K_0(b_1 R) + C_2 \beta_2 K_0(b_2 R)$$

P.2 DERIVATION OF THREE-AQUIFER SOLUTION

The derivation of the Laplace-domain analytical solution for the three-aquifer system (equation F-36) is provided in this section. The derivation is very similar to the derivation for the two-aquifer system in the previous section, although the linear algebra associated with the extra equation and extra unknown are significantly more involved. Beginning with the governing equation in Laplace space from Section F6 (Equation F-34):

$$\begin{aligned}s_1 p \tilde{S}_1 &= T_1 \nabla \tilde{S}_1 + \chi_{1-2} (\tilde{S}_2 - \tilde{S}_1) - \chi_0 \tilde{S}_1 \\ s_2 p \tilde{S}_2 &= T_2 \nabla \tilde{S}_2 + \chi_{1-2} (\tilde{S}_1 - \tilde{S}_2) + \chi_{2-3} (\tilde{S}_3 - \tilde{S}_2) \\ s_3 p \tilde{S}_3 &= T_3 \nabla \tilde{S}_3 + \chi_{2-3} (\tilde{S}_2 - \tilde{S}_3)\end{aligned}\quad (\text{Eq. F-34})$$

with boundary conditions (Equation F-35):

$$r \frac{d\tilde{S}_1}{dr} \Big|_{r \rightarrow r_{\text{well}}} = \frac{Q_1}{2\pi T_1}, \quad r \frac{d\tilde{S}_2}{dr} \Big|_{r \rightarrow r_{\text{well}}} = \frac{Q_2}{2\pi T_2}, \quad r \frac{d\tilde{S}_3}{dr} \Big|_{r \rightarrow r_{\text{well}}} = \frac{Q_3}{2\pi T_3} \quad (\text{Eq. F-35a})$$

$$\tilde{S}_1 \Big|_{r \rightarrow \infty} = 0, \quad \tilde{S}_2 \Big|_{r \rightarrow \infty} = 0, \quad \text{and} \quad \tilde{S}_3 \Big|_{r \rightarrow \infty} = 0 \quad (\text{Eq. F-35b})$$

Equation F-34 can be rearranged to:

$$\begin{aligned}T_1 \nabla \tilde{S}_1 &= (s_1 p + \chi_{1-2} + \chi_0) \tilde{S}_1 - \chi_{1-2} \tilde{S}_2, \\ T_2 \nabla \tilde{S}_2 &= (s_2 p + \chi_{1-2} + \chi_{2-3}) \tilde{S}_2 - \chi_{1-2} \tilde{S}_1 - \chi_{2-3} \tilde{S}_3\end{aligned}\quad (\text{Eq. P-29})$$

$$T_3 \nabla \tilde{S}_3 = (s_3 p + \chi_{2-3}) \tilde{S}_3 - \chi_{2-3} \tilde{S}_2,$$

Equation P-2 still applies with

$$\begin{aligned} \overline{\nabla S} = \begin{bmatrix} \nabla \tilde{S}_1 \\ \nabla \tilde{S}_2 \\ \nabla \tilde{S}_3 \end{bmatrix} \quad \bar{S} = \begin{bmatrix} \tilde{S}_1 \\ \tilde{S}_2 \\ \tilde{S}_3 \end{bmatrix} \quad \bar{C} = \begin{bmatrix} \kappa_1 & -\chi_{1-2} & 0 \\ -\chi_{1-2} & \kappa_2 & -\chi_{2-3} \\ 0 & -\chi_{2-3} & \kappa_3 \end{bmatrix} \quad \overline{\overline{T^{-1}}} = \begin{bmatrix} 1/T_1 & 0 & 0 \\ 0 & 1/T_2 & 0 \\ 0 & 0 & 1/T_3 \end{bmatrix} \\ \overline{\overline{A}} = \begin{bmatrix} \kappa_1/T_1 & -\chi_{1-2}/T_1 & 0 \\ -\chi_{1-2}/T_2 & \kappa_2/T_2 & -\chi_{2-3}/T_2 \\ 0 & -\chi_{2-3}/T_3 & \kappa_3/T_3 \end{bmatrix} \end{aligned} \quad (\text{Eq. P-30})$$

and $\kappa_1 = s_1 p + \chi_{1-2} + \chi_0$, $\kappa_2 = s_2 p + \chi_{1-2} + \chi_{2-3}$, and $\kappa_3 = s_3 p + \chi_{2-3}$

Equations P-4 through P-8 also apply, and $\bar{q} = \begin{bmatrix} Q_1 \\ Q_2 \\ Q_3 \end{bmatrix}$ and $\overline{\overline{T^{-1}}}\bar{q} = \begin{bmatrix} Q_1/T_1 \\ Q_2/T_2 \\ Q_3/T_3 \end{bmatrix}$, where Q_i is the pumping rate from the i th aquifer.

Equation P-13 is modified to obtain $\overline{\overline{A^*}}$ as follows:

$$\begin{aligned} \overline{\overline{A^*}} = \begin{bmatrix} \sqrt{T_1} & 0 & 0 \\ 0 & \sqrt{T_2} & 0 \\ 0 & 0 & \sqrt{T_3} \end{bmatrix} \begin{bmatrix} \kappa_1/T_1 & -\chi_{1-2}/T_1 & 0 \\ -\chi_{1-2}/T_2 & \kappa_2/T_2 & -\chi_{2-3}/T_2 \\ 0 & -\chi_{2-3}/T_3 & \kappa_3/T_3 \end{bmatrix} \begin{bmatrix} 1/\sqrt{T_1} & 0 & 0 \\ 0 & 1/\sqrt{T_2} & 0 \\ 0 & 0 & 1/\sqrt{T_3} \end{bmatrix} = \\ \begin{bmatrix} \kappa_1/T_1 & -\chi_{1-2}/\sqrt{T_1 T_2} & 0 \\ -\chi_{1-2}/\sqrt{T_1 T_2} & \kappa_2/T_2 & -\chi_{2-3}/\sqrt{T_2 T_3} \\ 0 & -\chi_{2-3}/\sqrt{T_2 T_3} & \kappa_3/T_3 \end{bmatrix} \end{aligned} \quad (\text{Eq. P-31})$$

The eigenvalues of $\overline{\overline{A^*}}$ are the roots of the characteristic equation:

$$\det(\overline{\overline{A^*}} - \lambda \overline{\overline{I}}) = 0, \text{ or } \begin{vmatrix} \kappa_1/T_1 - \lambda & -\chi_{1-2}/\sqrt{T_1 T_2} & 0 \\ -\chi_{1-2}/\sqrt{T_1 T_2} & \kappa_2/T_2 - \lambda & -\chi_{2-3}/\sqrt{T_2 T_3} \\ 0 & -\chi_{2-3}/\sqrt{T_2 T_3} & \kappa_3/T_3 - \lambda \end{vmatrix} = 0, \text{ which becomes:}$$

$$(\kappa_1/T_1 - \lambda)(\kappa_2/T_2 - \lambda)(\kappa_3/T_3 - \lambda) - (\kappa_3/T_3 - \lambda)\chi_{1-2}^2/T_1 T_2 - (\kappa_1/T_1 - \lambda)\chi_{2-3}^2/T_2 T_3 = 0$$

$$\text{or } \lambda^3 + a\lambda^2 + b\lambda + c = 0 \quad (\text{Eq. P-32})$$

where,

$$a = -\left(\frac{\kappa_1}{T_1} + \frac{\kappa_2}{T_2} + \frac{\kappa_3}{T_3}\right), \quad (\text{Eq. P-33a})$$

$$b = \left(\frac{\kappa_1\kappa_2}{T_1T_2} + \frac{\kappa_1\kappa_3}{T_1T_3} + \frac{\kappa_2\kappa_3}{T_2T_3} - \frac{\chi_{1-2}^2}{T_1T_2} - \frac{\chi_{2-3}^2}{T_2T_3}\right), \text{ and} \quad (\text{Eq. P-33b})$$

$$c = \left(\frac{\kappa_1\kappa_2\kappa_3 - \kappa_3\chi_{1-2}^2 - \kappa_1\chi_{2-3}^2}{T_1T_2T_3}\right) \quad (\text{Eq. P-33c})$$

The three roots of equation P-32 are (Spiegel 1968 [DIRS 180315, pp. 15 and 32]):

$$b_1^2 = 2\sqrt{\frac{a^2 - 3b}{9}} \cos\left(\frac{1}{3}\theta\right) - \frac{a}{3}, \quad (\text{Eq. P-34a})$$

$$b_2^2 = 2\sqrt{\frac{a^2 - 3b}{9}} \cos\left(\frac{1}{3}\theta + \frac{2\pi}{3}\right) - \frac{a}{3}, \text{ and} \quad (\text{Eq. P-34b})$$

$$b_3^2 = 2\sqrt{\frac{a^2 - 3b}{9}} \cos\left(\frac{1}{3}\theta - \frac{2\pi}{3}\right) - \frac{a}{3} \quad (\text{Eq. P-34c})$$

where,

$$\theta = \cos^{-1} \left(\frac{9ab - 27c - 2a^3}{54\sqrt{\left(\frac{a^2 - 3b}{9}\right)^3}} \right). \quad (\text{Eq. P-35})$$

Equations P-33 and P-34 differ slightly from the corresponding equations in Section F6 of Appendix F (equations F-36). However, the differences can be accounted for by recognizing that equations P-34 are multiplied by κ_3 and equations P-33a, P-33b, and P-33c are divided by κ_3 , κ_3^2 , and κ_3^3 , respectively, to obtain the corresponding equations in Appendix F. The reader is left to verify by inspection that the κ_3 s cancel each other out, and the equations in Appendix F are equivalent to equations P-33 and P-34.

Using the notation of equation F-36 of Section F6 of Appendix F:

$$\alpha = \frac{a^2}{3} + b, \quad \gamma = 2\left(\frac{a}{3}\right)^3 - \frac{ab}{3} + c,$$

$$f_1 = 2\sqrt{\frac{-\alpha}{3}}, \text{ and}$$

$$f_2 = -\gamma \frac{4}{f_1^3} = \frac{9ab - 27c - 2a^3}{54\sqrt{\left(\frac{a^2 - 3b}{9}\right)^3}} \quad (\text{Eq. P-36})$$

Equation P-36 shows that f_2 is the argument of \cos^{-1} in equation P-35 when the notation of Section F6 is used. Using trigonometric identifies and conversions, equation P-35 becomes:

$$\theta = \cos^{-1}(f_2) = \tan^{-1}\left(\frac{\sqrt{1-f_2^2}}{f_2}\right) = -\tan^{-1}\left(\frac{f_2}{\sqrt{1-f_2^2}}\right) + \frac{\pi}{2} \quad (\text{Eq. P-37})$$

The eigenvalues from equation P-34 are used to obtain the eigenvectors of $\overline{A^*}$ from equation P-31. Letting the components of \overline{e}_i be $x_i, y_i,$ and z_i provides:

$$\begin{bmatrix} \kappa_1/T_1 & -\chi_{1-2}/T_1 & 0 \\ -\chi_{1-2}/T_2 & \kappa_2/T_2 & -\chi_{2-3}/T_2 \\ 0 & -\chi_{2-3}/T_3 & \kappa_3/T_3 \end{bmatrix} \begin{bmatrix} x_i \\ y_i \\ z_i \end{bmatrix} = b_i^2 \begin{bmatrix} x_i \\ y_i \\ z_i \end{bmatrix} \text{ or}$$

$$\begin{aligned} (\kappa_1/T_1)x_i - (\chi_{1-2}/T_1)y_i &= b_i^2 x_i \\ -(\chi_{1-2}/T_1)x_i + (\kappa_2/T_2)y_i - (\chi_{2-3}/T_3)z_i &= b_i^2 y_i \\ -(\chi_{2-3}/T_3)y_i + (\kappa_3/T_3)z_i &= b_i^2 z_i \end{aligned} \quad (\text{Eq. P-38})$$

From the first of the three equations P-38 results in:

$$y_i = \left(\frac{\kappa_1 - T_1 b_i^2}{\chi_{1-2}}\right)x_i \quad (\text{Eq. P-39})$$

Substituting P-39 into the last of equations P-38 yields:

$$z_i = \left(\frac{\chi_{2-3}}{\kappa_3 - T_3 b_i^2}\right)\left(\frac{\kappa_1 - T_1 b_i^2}{\chi_{1-2}}\right)x_i \quad (\text{Eq. P-40})$$

Thus, $\bar{e}_i = \begin{bmatrix} 1 \\ \left(\frac{\kappa_1 - T_1 b_i^2}{\chi_{1-2}} \right) \\ \left(\frac{\chi_{2-3}}{\kappa_3 - T_3 b_i^2} \right) \left(\frac{\kappa_1 - T_1 b_i^2}{\chi_{1-2}} \right) \end{bmatrix}$ are eigenvectors of \bar{A}^* , and it follows that:

$$\bar{F} = \begin{bmatrix} 1 & 1 & 1 \\ \left(\frac{\kappa_1 - T_1 b_1^2}{\chi_{1-2}} \right) & \left(\frac{\kappa_1 - T_1 b_2^2}{\chi_{1-2}} \right) & \left(\frac{\kappa_1 - T_1 b_3^2}{\chi_{1-2}} \right) \\ \left(\frac{\chi_{2-3}}{\kappa_3 - T_3 b_1^2} \right) \left(\frac{\kappa_1 - T_1 b_1^2}{\chi_{1-2}} \right) & \left(\frac{\chi_{2-3}}{\kappa_3 - T_3 b_2^2} \right) \left(\frac{\kappa_1 - T_1 b_2^2}{\chi_{1-2}} \right) & \left(\frac{\chi_{2-3}}{\kappa_3 - T_3 b_3^2} \right) \left(\frac{\kappa_1 - T_1 b_3^2}{\chi_{1-2}} \right) \end{bmatrix} \quad (\text{Eq. P-41})$$

If $\beta_i = \frac{\kappa_1 - T_1 b_i^2}{\chi_{1-2}}$ and $\beta'_i = \left(\frac{\chi_{2-3}}{\kappa_3 - T_3 b_i^2} \right) \left(\frac{\kappa_1 - T_1 b_i^2}{\chi_{1-2}} \right)$, then:

$$\bar{F} = \begin{bmatrix} 1 & 1 & 1 \\ \beta_1 & \beta_2 & \beta_3 \\ \beta'_1 & \beta'_2 & \beta'_3 \end{bmatrix} \quad (\text{Eq. P-42})$$

Using equation P-20 the inverse of \bar{F} is given by:

$$\bar{F}^{-1} = \begin{bmatrix} \frac{(\beta_2 \beta'_3 - \beta'_2 \beta_3)}{\det(\bar{F})} & \frac{\beta'_2 - \beta'_3}{\det(\bar{F})} & \frac{\beta_3 - \beta_2}{\det(\bar{F})} \\ \frac{(\beta_3 \beta'_1 - \beta'_3 \beta_1)}{\det(\bar{F})} & \frac{\beta'_3 - \beta'_1}{\det(\bar{F})} & \frac{\beta_1 - \beta_3}{\det(\bar{F})} \\ \frac{(\beta_1 \beta'_2 - \beta'_1 \beta_2)}{\det(\bar{F})} & \frac{\beta'_1 - \beta'_2}{\det(\bar{F})} & \frac{\beta_2 - \beta_1}{\det(\bar{F})} \end{bmatrix} = \begin{bmatrix} \mathcal{E}_{11} & \mathcal{E}_{12} & \mathcal{E}_{13} \\ \mathcal{E}_{21} & \mathcal{E}_{22} & \mathcal{E}_{23} \\ \mathcal{E}_{31} & \mathcal{E}_{32} & \mathcal{E}_{33} \end{bmatrix} \quad (\text{Eq. P-43})$$

where, $\det(\bar{F}) = (\beta_2 - \beta_1)\beta'_3 + (\beta_1 - \beta_3)\beta'_2 + (\beta_3 - \beta_2)\beta'_1$

Equation P-43 is given without formal derivation, as it can be readily verified that $\bar{F}\bar{F}^{-1} = I$.

Now, substituting $\overline{\overline{T^{-1}q}}$, P-12, P-42, and P-4 into equation P-8, provides:

$$\overline{\overline{S}} = \frac{1}{2\pi} \begin{bmatrix} 1 & 1 & 1 \\ \beta_1 & \beta_2 & \beta_3 \\ \beta'_1 & \beta'_2 & \beta'_3 \end{bmatrix} \begin{bmatrix} K_0\{rb_1\} & 0 & 0 \\ 0 & K_0\{rb_2\} & 0 \\ 0 & 0 & K_0\{rb_3\} \end{bmatrix} \begin{bmatrix} \varepsilon_{11} & \varepsilon_{12} & \varepsilon_{13} \\ \varepsilon_{21} & \varepsilon_{22} & \varepsilon_{23} \\ \varepsilon_{31} & \varepsilon_{32} & \varepsilon_{33} \end{bmatrix} \begin{bmatrix} Q_1/T_1 \\ Q_2/T_2 \\ Q_3/T_3 \end{bmatrix} \quad (\text{Eq. P-44})$$

Multiplying the first two matrices of equation P-44 yields:

$$\overline{\overline{S}} = \frac{1}{2\pi} \begin{bmatrix} K_0\{rb_1\} & K_0\{rb_2\} & K_0\{rb_3\} \\ \beta_1 K_0\{rb_1\} & \beta_2 K_0\{rb_2\} & \beta_3 K_0\{rb_3\} \\ \beta'_1 K_0\{rb_1\} & \beta'_2 K_0\{rb_2\} & \beta'_3 K_0\{rb_3\} \end{bmatrix} \begin{bmatrix} \varepsilon_{11} & \varepsilon_{12} & \varepsilon_{13} \\ \varepsilon_{21} & \varepsilon_{22} & \varepsilon_{23} \\ \varepsilon_{31} & \varepsilon_{32} & \varepsilon_{33} \end{bmatrix} \begin{bmatrix} Q_1/T_1 \\ Q_2/T_2 \\ Q_3/T_3 \end{bmatrix}, \text{ or}$$

$$\overline{\overline{S}} = \frac{1}{2\pi} \begin{bmatrix} \phi_{11} & \phi_{12} & \phi_{13} \\ \phi_{21} & \phi_{22} & \phi_{32} \\ \phi_{31} & \phi_{23} & \phi_{33} \end{bmatrix} \begin{bmatrix} \varepsilon_{11} & \varepsilon_{12} & \varepsilon_{13} \\ \varepsilon_{21} & \varepsilon_{22} & \varepsilon_{23} \\ \varepsilon_{31} & \varepsilon_{32} & \varepsilon_{33} \end{bmatrix} \begin{bmatrix} Q_1/T_1 \\ Q_2/T_2 \\ Q_3/T_3 \end{bmatrix} \quad (\text{Eq. P-45})$$

Likewise, multiplying the first 2 matrices of equation P-45 yields:

$$\overline{\overline{S}} = \frac{1}{2\pi} \begin{bmatrix} \phi_{11}\varepsilon_{11} + \phi_{12}\varepsilon_{21} + \phi_{13}\varepsilon_{31} & \phi_{11}\varepsilon_{12} + \phi_{12}\varepsilon_{22} + \phi_{13}\varepsilon_{32} & \phi_{11}\varepsilon_{13} + \phi_{12}\varepsilon_{23} + \phi_{13}\varepsilon_{33} \\ \phi_{21}\varepsilon_{11} + \phi_{22}\varepsilon_{21} + \phi_{23}\varepsilon_{31} & \phi_{21}\varepsilon_{12} + \phi_{22}\varepsilon_{22} + \phi_{23}\varepsilon_{32} & \phi_{21}\varepsilon_{13} + \phi_{22}\varepsilon_{23} + \phi_{23}\varepsilon_{33} \\ \phi_{31}\varepsilon_{11} + \phi_{32}\varepsilon_{21} + \phi_{33}\varepsilon_{31} & \phi_{31}\varepsilon_{12} + \phi_{32}\varepsilon_{22} + \phi_{33}\varepsilon_{32} & \phi_{31}\varepsilon_{13} + \phi_{32}\varepsilon_{23} + \phi_{33}\varepsilon_{33} \end{bmatrix} \begin{bmatrix} Q_1/T_1 \\ Q_2/T_2 \\ Q_3/T_3 \end{bmatrix} \quad (\text{Eq. P-46})$$

Finally, multiplying the remaining matrix by the $\overline{c_2}$ vector yields:

$$\begin{aligned} \tilde{S}_1 &= \frac{1}{2\pi} (\phi_{11}\varepsilon_{11} + \phi_{12}\varepsilon_{21} + \phi_{13}\varepsilon_{31}) \frac{Q_1}{T_1} + (\phi_{11}\varepsilon_{12} + \phi_{12}\varepsilon_{22} + \phi_{13}\varepsilon_{32}) \frac{Q_2}{T_2} + (\phi_{11}\varepsilon_{13} + \phi_{12}\varepsilon_{23} + \phi_{13}\varepsilon_{33}) \frac{Q_3}{T_3} \\ \tilde{S}_2 &= \frac{1}{2\pi} (\phi_{21}\varepsilon_{11} + \phi_{22}\varepsilon_{21} + \phi_{23}\varepsilon_{31}) \frac{Q_1}{T_1} + (\phi_{21}\varepsilon_{12} + \phi_{22}\varepsilon_{22} + \phi_{23}\varepsilon_{32}) \frac{Q_2}{T_2} + (\phi_{21}\varepsilon_{13} + \phi_{22}\varepsilon_{23} + \phi_{23}\varepsilon_{33}) \frac{Q_3}{T_3} \quad (\text{Eq. P-47}) \\ \tilde{S}_3 &= \frac{1}{2\pi} (\phi_{31}\varepsilon_{11} + \phi_{32}\varepsilon_{21} + \phi_{33}\varepsilon_{31}) \frac{Q_1}{T_1} + (\phi_{31}\varepsilon_{12} + \phi_{32}\varepsilon_{22} + \phi_{33}\varepsilon_{32}) \frac{Q_2}{T_2} + (\phi_{31}\varepsilon_{13} + \phi_{32}\varepsilon_{23} + \phi_{33}\varepsilon_{33}) \frac{Q_3}{T_3} \end{aligned}$$

Rearrangement yields:

$$\begin{aligned} \tilde{S}_1 &= \frac{1}{2\pi} \left[\left(\varepsilon_{11} \frac{Q_1}{T_1} + \varepsilon_{12} \frac{Q_2}{T_2} + \varepsilon_{13} \frac{Q_3}{T_3} \right) \phi_{11} + \left(\varepsilon_{21} \frac{Q_1}{T_1} + \varepsilon_{22} \frac{Q_2}{T_2} + \varepsilon_{23} \frac{Q_3}{T_3} \right) \phi_{12} + \left(\varepsilon_{31} \frac{Q_1}{T_1} + \varepsilon_{32} \frac{Q_2}{T_2} + \varepsilon_{33} \frac{Q_3}{T_3} \right) \phi_{13} \right] \\ \tilde{S}_2 &= \frac{1}{2\pi} \left[\left(\varepsilon_{11} \frac{Q_1}{T_1} + \varepsilon_{12} \frac{Q_2}{T_2} + \varepsilon_{13} \frac{Q_3}{T_3} \right) \phi_{21} + \left(\varepsilon_{21} \frac{Q_1}{T_1} + \varepsilon_{22} \frac{Q_2}{T_2} + \varepsilon_{23} \frac{Q_3}{T_3} \right) \phi_{22} + \left(\varepsilon_{31} \frac{Q_1}{T_1} + \varepsilon_{32} \frac{Q_2}{T_2} + \varepsilon_{33} \frac{Q_3}{T_3} \right) \phi_{23} \right] \quad (\text{Eq. P-48}) \\ \tilde{S}_3 &= \frac{1}{2\pi} \left[\left(\varepsilon_{11} \frac{Q_1}{T_1} + \varepsilon_{12} \frac{Q_2}{T_2} + \varepsilon_{13} \frac{Q_3}{T_3} \right) \phi_{31} + \left(\varepsilon_{21} \frac{Q_1}{T_1} + \varepsilon_{22} \frac{Q_2}{T_2} + \varepsilon_{23} \frac{Q_3}{T_3} \right) \phi_{32} + \left(\varepsilon_{31} \frac{Q_1}{T_1} + \varepsilon_{32} \frac{Q_2}{T_2} + \varepsilon_{33} \frac{Q_3}{T_3} \right) \phi_{33} \right] \end{aligned}$$

Recognizing that:

$$\begin{aligned}\phi_{1i} &= K_0 \{rb_i\} \\ \phi_{2i} &= \beta_i K_0 \{rb_i\} \\ \phi_{3i} &= \beta'_i K_0 \{rb_i\}\end{aligned}\quad (\text{Eq. P-49})$$

Equation F-36 will be recovered if:

$$\begin{aligned}C_1 &= \frac{1}{2\pi} \left[\varepsilon_{11} \frac{Q_1}{T_1} + \varepsilon_{12} \frac{Q_2}{T_2} + \varepsilon_{13} \frac{Q_3}{T_3} \right], \\ C_2 &= \frac{1}{2\pi} \left[\varepsilon_{21} \frac{Q_1}{T_1} + \varepsilon_{22} \frac{Q_2}{T_2} + \varepsilon_{23} \frac{Q_3}{T_3} \right], \\ C_3 &= \frac{1}{2\pi} \left[\varepsilon_{31} \frac{Q_1}{T_1} + \varepsilon_{32} \frac{Q_2}{T_2} + \varepsilon_{33} \frac{Q_3}{T_3} \right]\end{aligned}\quad (\text{Eq. P-50})$$

It is now left to show that these expressions for C_1 , C_2 , and C_3 are equivalent to the expressions provided in Appendix F (equation F-36). Beginning with C_3 , which from Appendix F is:

$$C_3 = \frac{\frac{\beta_2 - \beta_1}{2\pi} \left(\frac{Q_3}{T_3} - \beta'_1 \frac{Q_1}{T_1} \right) - \frac{\beta'_2 - \beta'_1}{2\pi} \left(\frac{Q_2}{T_2} - \beta_1 \frac{Q_1}{T_1} \right)}{(\beta_1 - \beta_3)(\beta'_2 - \beta'_1) - (\beta_2 - \beta_1)(\beta'_1 - \beta'_3)} \quad (\text{Eq. P-51})$$

The denominator of C_3 from equation P-51 is equal to $\det(\overline{F})$, i.e.:

$$\begin{aligned}(\beta_1 - \beta_3)(\beta'_2 - \beta'_1) - (\beta_2 - \beta_1)(\beta'_1 - \beta'_3) &= \\ (\beta_2 - \beta_1)\beta'_3 + (\beta_1 - \beta_3)\beta'_2 + (\beta_3 - \beta_2)\beta'_1 + \beta_1\beta'_1 - \beta_1\beta'_1 &= \\ (\beta_2 - \beta_1)\beta'_3 + (\beta_1 - \beta_3)\beta'_2 + (\beta_3 - \beta_2)\beta'_1 &= \det(\overline{F})\end{aligned}\quad (\text{Eq. P-52})$$

If equation P-43 is used in equation P-50 to solve for C_3 :

$$C_3 = \frac{1}{2\pi \det(\overline{F})} \left[(\beta_1\beta'_2 - \beta'_1\beta_2) \frac{Q_1}{T_1} + (\beta'_1 - \beta'_2) \frac{Q_2}{T_2} + (\beta_2 - \beta_1) \frac{Q_3}{T_3} \right], \quad (\text{Eq. P-53})$$

Upon rearrangement, it can be readily verified that equation P-53 is identical to the expression for C_3 in Appendix F (equation P-51).

Using equation P-43 in equation P-50 to solve for C_2 provides:

$$C_2 = \frac{1}{2\pi \det(\overline{F})} \left[(\beta_3\beta'_1 - \beta'_3\beta_1) \frac{Q_1}{T_1} + (\beta'_3 - \beta'_1) \frac{Q_2}{T_2} + (\beta_1 - \beta_3) \frac{Q_3}{T_3} \right] \quad (\text{Eq. P-54})$$

The corresponding equation for C_2 in Appendix F is:

$$C_2 = \left[\frac{Q_2}{2\pi T_2} + (\beta_1 - \beta_3)C_3 - \beta_1 \frac{Q_1}{2\pi T_1} \right] / (\beta_2 - \beta_1) \quad (\text{Eq. P-55})$$

Substituting equation P-53 into equation P-55 provides:

$$C_2 = \frac{Q_2}{(\beta_2 - \beta_1)2\pi T_2} + \frac{(\beta_1 - \beta_3)}{(\beta_2 - \beta_1)2\pi \det(F)} \left((\beta_1\beta_2' - \beta_1'\beta_2) \frac{Q_1}{T_1} + (\beta_1' - \beta_2') \frac{Q_2}{T_2} + (\beta_2 - \beta_1) \frac{Q_3}{T_3} \right) - \frac{\beta_1 Q_1}{(\beta_2 - \beta_1)2\pi T_1} \quad (\text{Eq. P-56})$$

By multiplying the first and third terms on the right side of equation P-56 by $\frac{\det(F)}{\det(F)}$ and use the

first line of equation P-52 for the numerator, then:

$$C_2 = \frac{1}{(\beta_2 - \beta_1)2\pi \det(F)} \left[\begin{array}{l} (\beta_1 - \beta_3)(\beta_2' - \beta_1')Q_2 - (\beta_2 - \beta_1)(\beta_1' - \beta_3') \frac{Q_2}{T_2} + \\ (\beta_1 - \beta_3) \left((\beta_1\beta_2' - \beta_1'\beta_2) \frac{Q_1}{T_1} + (\beta_1' - \beta_2') \frac{Q_2}{T_2} + (\beta_2 - \beta_1) \frac{Q_3}{T_3} \right) - \\ (\beta_1 - \beta_3)(\beta_2' - \beta_1')\beta_1 \frac{Q_1}{T_1} - (\beta_2 - \beta_1)(\beta_1' - \beta_3')\beta_1 \frac{Q_1}{T_1} \end{array} \right] \quad (\text{Eq. P-57})$$

Rearranging equation P-57 to follow $C_2 = k_1 \frac{Q_1}{T_1} + k_2 \frac{Q_2}{T_2} + k_3 \frac{Q_3}{T_3}$ yields:

$$C_2 = \frac{1}{(\beta_2 - \beta_1)2\pi \det(F)} \left\{ \begin{array}{l} [-(\beta_1 - \beta_3)(\beta_2' - \beta_1')\beta_1 + (\beta_2 - \beta_1)(\beta_1' - \beta_3')\beta_1 + (\beta_1\beta_2' - \beta_1'\beta_2)(\beta_1 - \beta_3)] \frac{Q_1}{T_1} + \\ [(\beta_1 - \beta_3)(\beta_2' - \beta_1') - (\beta_2 - \beta_1)(\beta_1' - \beta_3') + (\beta_1 - \beta_3)(\beta_1' - \beta_2')] \frac{Q_2}{T_2} + \\ [(\beta_1 - \beta_3)(\beta_2 - \beta_1)] \frac{Q_3}{T_3} \end{array} \right\} \quad (\text{Eq. P-58})$$

By performing all the multiplications, simplifying, and regrouping, equation P-58 becomes:

$$C_2 = \frac{1}{(\beta_2 - \beta_1)2\pi \det(F)} \left\{ \begin{aligned} & \left[(\beta_3\beta'_1 - \beta'_3\beta_1)(\beta_2 - \beta_1) \right] \frac{Q_1}{T_1} + \\ & \left[-(\beta'_1 - \beta'_3)(\beta_2 - \beta_1) \right] \frac{Q_2}{T_2} + \\ & \left[(\beta_1 - \beta_3)(\beta_2 - \beta_1) \right] \frac{Q_3}{T_3} \end{aligned} \right\} =$$

$$\frac{(\beta_2 - \beta_1)}{(\beta_2 - \beta_1)2\pi \det(F)} \left\{ \begin{aligned} & (\beta_3\beta'_1 - \beta'_3\beta_1) \frac{Q_1}{T_1} + \\ & (\beta'_3 - \beta'_1) \frac{Q_2}{T_2} + \\ & (\beta_1 - \beta_3) \frac{Q_3}{T_3} \end{aligned} \right\} = \quad (\text{Eq. P-59})$$

$$\frac{1}{2\pi \det(F)} \left\{ (\beta_3\beta'_1 - \beta'_3\beta_1) \frac{Q_1}{T_1} + (\beta'_3 - \beta'_1) \frac{Q_2}{T_2} + (\beta_1 - \beta_3) \frac{Q_3}{T_3} \right\}$$

The last expression above is equivalent to equation P-54, which establishes that C_2 in Appendix F (equation P-55) is equivalent to the expression for C_2 derived here (equation P-54).

Finally, using equation P-43 in equation P-50 to solve for C_1 , provides:

$$C_1 = \frac{1}{2\pi \det(F)} \left[(\beta_2\beta'_3 - \beta'_2\beta_3) \frac{Q_1}{T_1} + (\beta'_2 - \beta'_3) \frac{Q_2}{T_2} + (\beta_3 - \beta_2) \frac{Q_3}{T_3} \right] \quad (\text{Eq. P-60})$$

The corresponding equation for C_1 in Appendix F is:

$$C_1 = \frac{Q_1}{2\pi T_1} - C_2 - C_3 \quad (\text{Eq. P-61})$$

Substituting equations P-53 and P-54 into equation P-61 yields:

$$C_1 = \frac{Q_1}{2\pi T_1} - \frac{1}{2\pi \det(F)} \left[(\beta_3\beta'_1 - \beta'_3\beta_1) \frac{Q_1}{T_1} + (\beta'_3 - \beta'_1) \frac{Q_2}{T_2} + (\beta_1 - \beta_3) \frac{Q_3}{T_3} \right] -$$

$$\frac{1}{2\pi \det(F)} \left[(\beta_1\beta'_2 - \beta'_1\beta_2) \frac{Q_1}{T_1} + (\beta'_1 - \beta'_2) \frac{Q_2}{T_2} + (\beta_2 - \beta_1) \frac{Q_3}{T_3} \right] \quad (\text{Eq. P-62})$$

Multiplying the first term on the right side of equation P-62 by $\frac{\det(F)}{\det(F)}$ and using the first line of equation P-52 for the numerator yields:

$$C_1 = \frac{1}{2\pi \det(F)} [(\beta_1 - \beta_3)(\beta_2' - \beta_1') - (\beta_2 - \beta_1)(\beta_1' - \beta_3')] \frac{Q_1}{T_1} - \frac{1}{2\pi \det(F)} \left[(\beta_3\beta_1' - \beta_3'\beta_1) \frac{Q_1}{T_1} + (\beta_3' - \beta_1') \frac{Q_2}{T_2} + (\beta_1 - \beta_3) \frac{Q_3}{T_3} \right] - \frac{1}{2\pi \det(F)} \left[(\beta_1\beta_2' - \beta_1'\beta_2) \frac{Q_1}{T_1} + (\beta_1' - \beta_2') \frac{Q_2}{T_2} + (\beta_2 - \beta_1) \frac{Q_3}{T_3} \right] \quad (\text{Eq. P-63})$$

Rearranging equation P-63 to be in the form of $C_1 = k_1 \frac{Q_1}{T_1} + k_2 \frac{Q_2}{T_2} + k_3 \frac{Q_3}{T_3}$ yields:

$$C_1 = \frac{1}{2\pi \det(F)} [(\beta_1 - \beta_3)(\beta_2' - \beta_1') - (\beta_2 - \beta_1)(\beta_1' - \beta_3') - (\beta_3\beta_1' - \beta_3'\beta_1) - (\beta_1\beta_2' - \beta_1'\beta_2)] \frac{Q_1}{T_1} - \frac{1}{2\pi \det(F)} [(\beta_3' - \beta_1') + (\beta_1' - \beta_2')] \frac{Q_2}{T_2} - \frac{1}{2\pi \det(F)} [(\beta_1 - \beta_3) + (\beta_2 - \beta_1)] \frac{Q_3}{T_3} \quad (\text{Eq. P-64})$$

After multiplying and simplifying,:

$$C_1 = \frac{1}{2\pi \det(F)} \left[(\beta_2\beta_3' - \beta_2'\beta_3) \frac{Q_1}{T_1} + (\beta_2' - \beta_3') \frac{Q_2}{T_2} + (\beta_3 - \beta_2) \frac{Q_3}{T_3} \right] \quad (\text{Eq. P-65})$$

Equation P-65 is identical to equation P-60, which establishes that C_1 in Appendix F (equation P-61) is equivalent to the expression for C_1 derived here (equation P-60).

Having established that C_1 , C_2 , and C_3 from Appendix F are equivalent to C_1 , C_2 , and C_3 derived here, it follows that equations P-50 are equivalent to equations F-36 from Appendix F:

$$\begin{aligned} \tilde{S}_1 &= C_1 K_0(b_1 R) + C_2 K_0(b_2 R) + C_3 K_0(b_3 R), \\ \tilde{S}_2 &= C_1 \beta_1 K_0(b_1 R) + C_2 \beta_2 K_0(b_2 R) + C_3 \beta_3 K_0(b_3 R), \text{ and} \\ \tilde{S}_3 &= C_1 \beta_1' K_0(b_1 R) + C_2 \beta_2' K_0(b_2 R) + C_3 \beta_3' K_0(b_3 R). \end{aligned} \quad (\text{Eq. F-36})$$

APPENDIX Q

**INDEPENDENT ANALYSIS OF CROSS-HOLE HYDRAULIC TESTS CONDUCTED
BETWEEN AUGUST AND SEPTEMBER 2003 AT THE NYE COUNTY NC-EWDP-22
COMPLEX**

Isolated interval cross-hole hydraulic tests were conducted at the Nye County NC-EWDP-22 site in August and September 2003. These tests are independently analyzed in this analysis report by two separate approaches, one presented in Appendix F and the other in this appendix. In the analysis of this appendix, hydraulic parameters are estimated from the observed pressure responses by applying the Hantush (1956 [DIRS 165169]) analytic solution of the ground water flow equation with a line sink in an infinite leaky-confined aquifer and no storage in the semi-confining layer. The results of this analysis are compared with the results of the Appendix F analysis at the end of this appendix, and the comparison is shown to be favorable given the uncertainties in the parameter estimates, as stated in Section 6.4.6. This favorable comparison adds confidence to the hydraulic parameter estimates presented in Section 6.4.

Q1. USGS ANALYSIS OF CROSS-HOLE HYDRAULIC TESTS CONDUCTED BETWEEN AUGUST AND SEPTEMBER 2003 AT THE NYE COUNTY NC-EWDP-22 COMPLEX

The details of the hydraulic testing are presented in Appendix F6 and will not be repeated here.

The responses in the observation wells, NC-EWDP-22PA and -22PB, to pumping NC-EWDP-22S in all 4 screened intervals look like leaky-confined responses. The Hantush (1956 [DIRS 165169]) leaky-confined solution with no storage in the confining layer, was, therefore, used for all the fits presented below. The drawdown data for all 4 fits were corrected for barometric changes, assuming a barometric efficiency of 1.0. However, earth tide effects were not removed.

For screens 2 through 4, there was a discrepancy between the times recorded by the data logger for the pumped well and the data loggers for the observation wells (NWRPO 2004 [DIRS 178566]). As a result, the drawdown for these screens was “shifted” (i.e., assumed to have happened earlier than indicated in the observation well data loggers) by varying amounts when analyzing the data.

Q1.1 SCREEN #1

No data “shifting” was needed for screen #1. The names of the original data file used were 080503R3.WK1, 080503R5.WK1, and 080603R1.WK1.

In Figure 1.1, the drawdown in screen #1 of NC-EWDP-22PA as a function of time in response to pumping NC-EWDP-22S is fitted to the $r/B = 7.0 \times 10^{-1}$ type curve of the Hantush (1956 [DIRS 165169]) Leaky aquifer solution (Figures 1.2 and 1.3 are variations of Figure 1.1). This fit gives a T [L/T] value of 2,330 ft²/day, an S value of 0.0016, and a Leakance value (K'/b' [T⁻¹]) of 2.27×10^{-4} min⁻¹, for an assumed pumping rate of 47 gallons per minute (gpm) and an interborehole distance of 59 ft. The Leakance value (K'/b'), which is the ratio of the hydraulic conductivity to the thickness of the semiconfining bed, has units of $[(L/T)/L] = [T^{-1}]$ and “may be defined as the quantity of flow that crosses a unit area of the interface between the main aquifer and its semiconfining bed, if the difference between the head in the main aquifer and in that supplying leakage is unity,” according to Hantush (1956 [DIRS 165169]).

The particular type curve chosen for the fit and the horizontal shift of the type curve to best fit the data were done by graphical matching aided by analysis of the derivatives of the data and type curves. Figures 1.4 and 1.5 show the Hantush (1956 [DIRS 165169]) $r/B = 7 \times 10^{-1}$ type curve and its derivative calculated using an algorithm used by Horne (1995 [DIRS 179650]). Figures 1.6 and 1.7 show the data curve with its derivative calculated in the same manner.

Theoretically, the flat portion of the type curve should fit the flat portion of the data curve. From figures 1.4 and 1.5, it is seen that the first point where the type curve becomes flat and has a derivative of zero is at $\ln(1/u) \sim 3.9$, which is at the 20th (blue) point from the end of the type curve. On the other hand, from figures 1.6 and 1.7, it is seen that the data curve becomes flat and the derivative of the drawdown starts oscillating symmetrically around zero relatively persistently at $\ln t = 4.0$, which corresponds to $t = e^{4.0} = 54.6 \sim 55$ minutes.

From the above, it follows that, for an optimal fit, the horizontal shift between the two curves should be such that the 20th point from the end of the 7×10^{-1} type curve is at the 55 minute mark of the data time axis. In the fit of figures 1.1 through 1.3, this point of the type curve is at the 44 minute mark. This visual fit is the best that can be obtained by this methodology. Best-visual Fits to adjacent type curves located the corresponding first point where the type curve becomes flat further away from 55 minutes than the 44 minute location of this fit.

Q1.2 SCREEN #2

For screen #2, the drawdown was assumed to have started (elapsed time since pumping started = zero for the analysis) 30 seconds after the time that the pump was turned on in NC-EWDP-22S—specifically 8/12/03, 5:20 AM PST—was indicated in the data logger of NC-EWDP-22PA. In other words, the drawdown in screen #2 was “shifted” by 30 seconds for this analysis (the names of the original data file used were *081203R3.WK1* and *081303R2.WK1*).

In Figure 2.1, the drawdown in screen #2 of NC-EWDP-22PA as a function of time in response to pumping NC-EWDP-22S is fitted to the $r/B = 5.0 \times 10^{-1}$ type curve of the Hantush (1956 [DIRS 165169]) leaky aquifer solution (Figures 2.2 and 2.3 are variations of Figure 2.1). This fit gives a T value of 5,750 ft²/day, an S value of 0.0024, and a Leakage value ($K'/b' [T^{-1}]$) of $2.86 \times 10^{-4} \text{ min}^{-1}$ for an assumed pumping rate of 44 gallons per minute (gpm) and an interborehole distance of 59 ft.

As for screen #1, the particular type curve chosen for the screen #2 fit and the horizontal shift of the type curve to best fit the data were done by graphical matching aided by analysis of the derivatives of the data and type curves. Figures 2.4 and 2.5 show the Hantush (1956 [DIRS 165169]) $r/B = 5 \times 10^{-1}$ type curve and its derivative calculated using an algorithm used by Horne (1995 [DIRS 179650]). Figures 2.6 and 2.7 show the data curve with its derivative calculated in the same manner.

Theoretically, the flat portion of the type curve should fit the flat portion of the data curve. From figures 2.4 and 2.5, it is seen that the first point where the type curve becomes flat and has a derivative of zero is at $\ln(1/u) \sim 4.6$, which is at the 19th (blue) point from the end of the type curve. On the other hand, from figures 2.6 and 2.7, it is seen that the data curve first becomes flat and the derivative of the drawdown approaches zero monotonically at $\ln t = 4.0$, which

corresponds to $t = e^{4.0} = 54.6$ to approximately 55 minutes. (The derivative then oscillates and eventually becomes zero but we only consider as significant the first time when the derivative has gone down to approximately zero at the end of a monotonic decrease (i.e., at $\ln t = 4.0$)).

From this, it follows that, for an optimal fit, the horizontal shift between the two curves should be such that the 19th point from the end of the 5×10^{-1} type curve is at the 55 minute mark of the data time axis. This is approximately done in the fit of figures 2.1 through 2.3., where the 19th point from the end of the 5×10^{-1} type curve is approximately at the 52.5 minute mark of the data time axis.

Q1.3 SCREEN #3

For screen #3, the drawdown was assumed to have started (elapsed time since pumping started = zero for the analysis) 70 seconds after the time that the pump was turned on in NC-EWDP-22S—specifically 9/9/03, 5:50 AM PST—was indicated in the data logger of NC-EWDP-22PB. In other words, the drawdown in screen #3 was “shifted” by 70 seconds for this analysis (names of original data files used were *090903R4.WK1*, *091003R2.WK1*, and *090903R6.WK1*).

In Figure 3.1, the drawdown in screen #3 of NC-EWDP-22PB as a function of time in response to pumping NC-EWDP-22S is fitted to the $r/B = 7.5 \times 10^{-2}$ type curve of the Hantush (1956 [DIRS 165169]) Leaky aquifer solution (figures 3.2 and 3.3 are variations of Figure 3.1). This fit gives a T value of 2,380 ft²/day, an S value of 0.000055, and a Leakance value ($K' / b' [T^{-1}]$) of $1.39 \times 10^{-6} \text{ min}^{-1}$ (Table 1), for an assumed pumping rate of 27 gallons per minute (gpm) and an interborehole distance of 81.9 ft.

As for screens #1 and #2, the particular type curve chosen for the screen #3 fit and the horizontal shift of the type curve to best fit the data were done by graphical matching aided by analysis of the derivatives of the data and type curves. Figures 3.4 and 3.5 show the Hantush (1956 [DIRS 165169]) $r/B = 7.5 \times 10^{-2}$ type curve and its derivative calculated using an algorithm from Horne (1995 [DIRS 179650]). Figures 3.6 and 3.7 show the data curve with its derivative calculated in the same manner.

Theoretically, the flat portion of the type curve should fit the flat portion of the data curve. From Figures 3.4 and 3.5, it is seen that the first point where the type curve becomes flat and has a derivative of zero is at $\ln(1/u) = 8.5$, which is at the second (blue) point from the end of the type curve. On the other hand, from Figures 3.6 and 3.7, it is seen that the data curve doesn't become flat—and its derivative becomes persistently zero—until $\ln t \sim 5.75$, which corresponds to $t = e^{5.75} \sim 314$ minutes.

From the above, it follows that, for an optimal fit, the horizontal shift between the two curves should be such that the second point from the end of the 7.5×10^{-2} type curve is \sim at the 314 minute mark of the data time axis. It can be seen from the fit in figures 3.1 and 3.2 that the second point from the end of the 7.5×10^{-2} type curve is located \sim at the 290 minute mark of the data time axis.

Q1.4 SCREEN #4

For screen #4, the drawdown was assumed to have started (elapsed time since pumping started = zero for the analysis) 350 seconds after the time that the pump was turned on in NC-EWDP-22S—specifically 9/23/03, 5:35 AM PST—was indicated in the data logger of NC-EWDP-22PB. In other words, the drawdown in screen #4 was “shifted” by 350 seconds for this analysis (names of original data files used were *092303R4.WK1* and *092403R2.WK1*)

In Figure 4.1, the drawdown in screen #4 of NC-EWDP-22PB as a function of time in response to pumping NC-EWDP-22S is fitted to the $r/B = 7.5 \times 10^{-2}$ type curve of the Hantush (1956 [DIRS 165169]) Leaky aquifer solution (Figures 4.2 and 4.3 are variations of Figure 4.1). This fit gives a T value of 1,930 ft²/day, an S value of 0.000175 and a Leakance value (K'/b' [T⁻¹]) of $1.125 \times 10^{-6} \text{ min}^{-1}$ (Table 1) for an assumed pumping rate of 20 gallons per minute (gpm) an interborehole distance of 81.9 ft.

The particular type curve chosen for the fit and the horizontal shift of the type curve to best fit the data were done by graphical matching aided by analysis of the derivatives of the data and type curves. Figures 4.4 and 4.5 show the Hantush (1956 [DIRS 165169]) $r/B = 7.5 \times 10^{-2}$ type curve and its derivative calculated using an algorithm from (Horne 1995 [DIRS 179650]). Figures 4.6 and 4.7 show the data curve with its derivative calculated in the same manner.

Theoretically, the flat portion of the type curve should fit the flat portion of the data curve. From figures 4.4 and 4.5, it is seen that the first point where the type curve becomes flat and has a derivative of zero is at $\ln(1/u) \sim 8.1$, which is at the third (blue) point from the end of the type curve. On the other hand, from figures 4.6 and 4.7, it is seen that the data curve becomes flat and the derivative of the drawdown goes through the zero line at $\ln t = 5.5$ (which corresponds to $t = e^{5.5} = 244.7 \sim 245$ minutes). After that point, the data curve becomes erratic and is not considered in the analysis.

From this, it follows that, for an optimal fit, the horizontal shift between the two curves should be such that the third point from the end of the 7.5×10^{-2} type curve is at the 245 minute mark of the data time axis. In the fit of figures 4.1 through 4.3, however, it is not the third but the ninth point of the type curve that is at the 245 minute mark. From Figure 4.5, it can be seen that at the ninth point from the end of the 7.5×10^{-2} type curve, the derivative is approximately 0.25, not zero. This visual fit is, therefore, not optimal, but the best that can be obtained by this methodology. The visual fit to the adjacent 5×10^{-2} type curve (not shown) also locates a point on the type curve where the derivative is approximately 0.25 at the 245 minute mark and gives very close results (T = 2,320 ft²/day and S = 0.000116). Visual fits to other type curves overlay significantly fewer data points to the type curve than the fit presented here to the 7.5×10^{-2} type curve.

Q1.5 SUMMARY AND CONCLUSIONS

The responses in the observation wells, NC-EWDP-22PA and -22PB, to pumping NC-EWDP-22S in all 4 screened intervals are consistent with leaky-confined aquifer behavior. The Hantush (1956 [DIRS 165169]) leaky-confined solution with no storage in the confining layer (Hantush 1956 [DIRS 165169]) was therefore used to analyze all 4 responses. Table Q-1

presents the results of these analyses. Also listed in Table Q-1 are the ranges of transmissivity and storativity estimates obtained from the different hydraulic test interpretive approaches presented in Section F6 of Appendix F. It is apparent that the transmissivity estimates from this appendix and from Section F6 agree to within about 30%, and the storativity estimates agree to within a factor of 4. This agreement between different independent interpretive approaches is well within the uncertainties of a factor of 3 for transmissivity and an order of magnitude for storativity that are stated in Section 6.4.6.

Table Q-1. Summary of Hydraulic Parameters Obtained from Analyzing the Hydraulic Tests at NC-EWDP-22

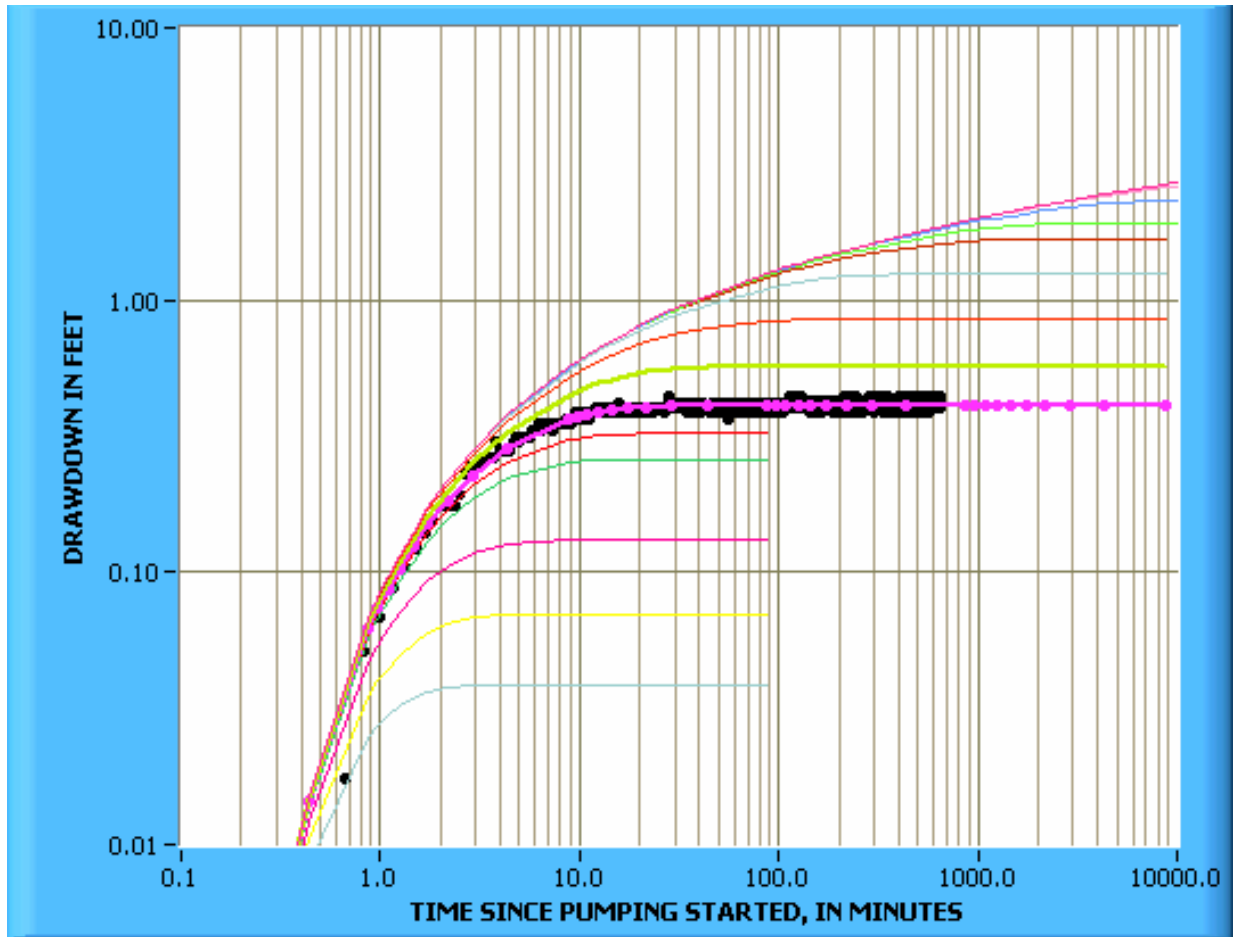
	Screen #1	Screen #2	Screen #3	Screen #4
Q (gpm)	47	44	27	20
r (ft)	59	59	81.9	81.9
time shift (sec)	None	30	70	350
T (ft ² /day)	2,330	5,750	2,380	1,930
T (m ² /day)	216	534	221	179
Range T, Section F6 (m ² /day)	264-280	325-600	130-180	200-250
S	0.0016	0.0024	0.000055	0.000175
Range S, Section F6	0.0013-0.0017	0.0006-0.003	0.0002-0.0003	0.0003-0.00035
Leakance: $\kappa' / b' \text{ (min}^{-1}\text{)}$	2.27×10^{-4}	2.86×10^{-4}	1.39×10^{-6}	1.125×10^{-6}

NOTE: The tests were run with the Hantush (1 956 [DIRS 165169]) leaky-confined solution with no storage in the confining layer.

The storage coefficient (S) values decrease with depth from 0.0016 and 0.0024 in the upper two screens, indicating some unconfinement, to 0.000055 and 0.000175 in the lower two screens indicating higher degrees of confinement. This approximate progression from lower to higher degrees of confinement with increasing depth in a continuous porous medium open to the atmosphere at the top is expected and lends support to the S values obtained.

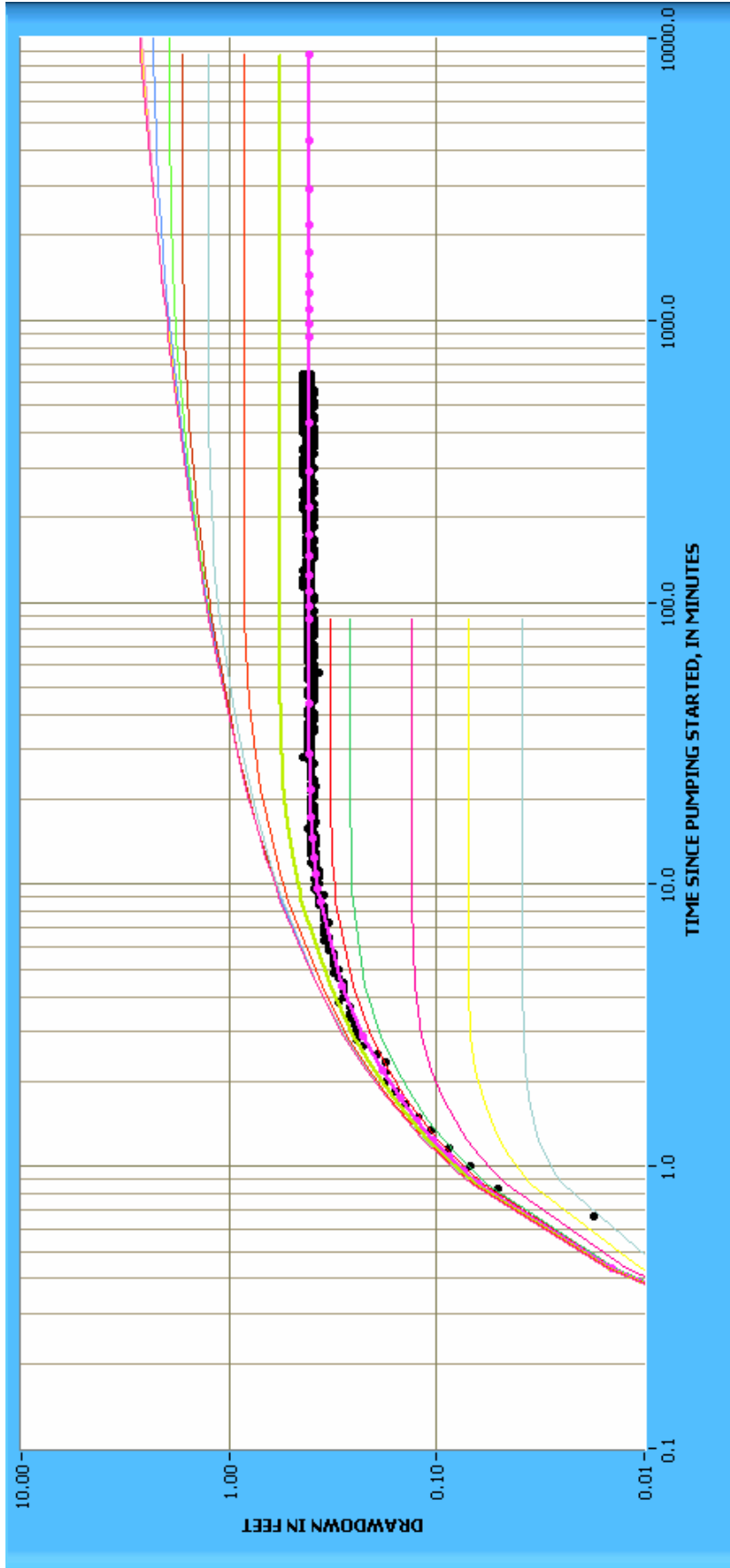
The leakance values are higher for screens #1 and #2, which correlates with the higher S values and lower degrees of confinement; whereas they are lower for screens #3 and #4, which correlates with higher degrees of confinement.

The most transmissive interval is screen #2, which was the reason Nye County selected as the interval in which to conduct the subsequent tracer tests.



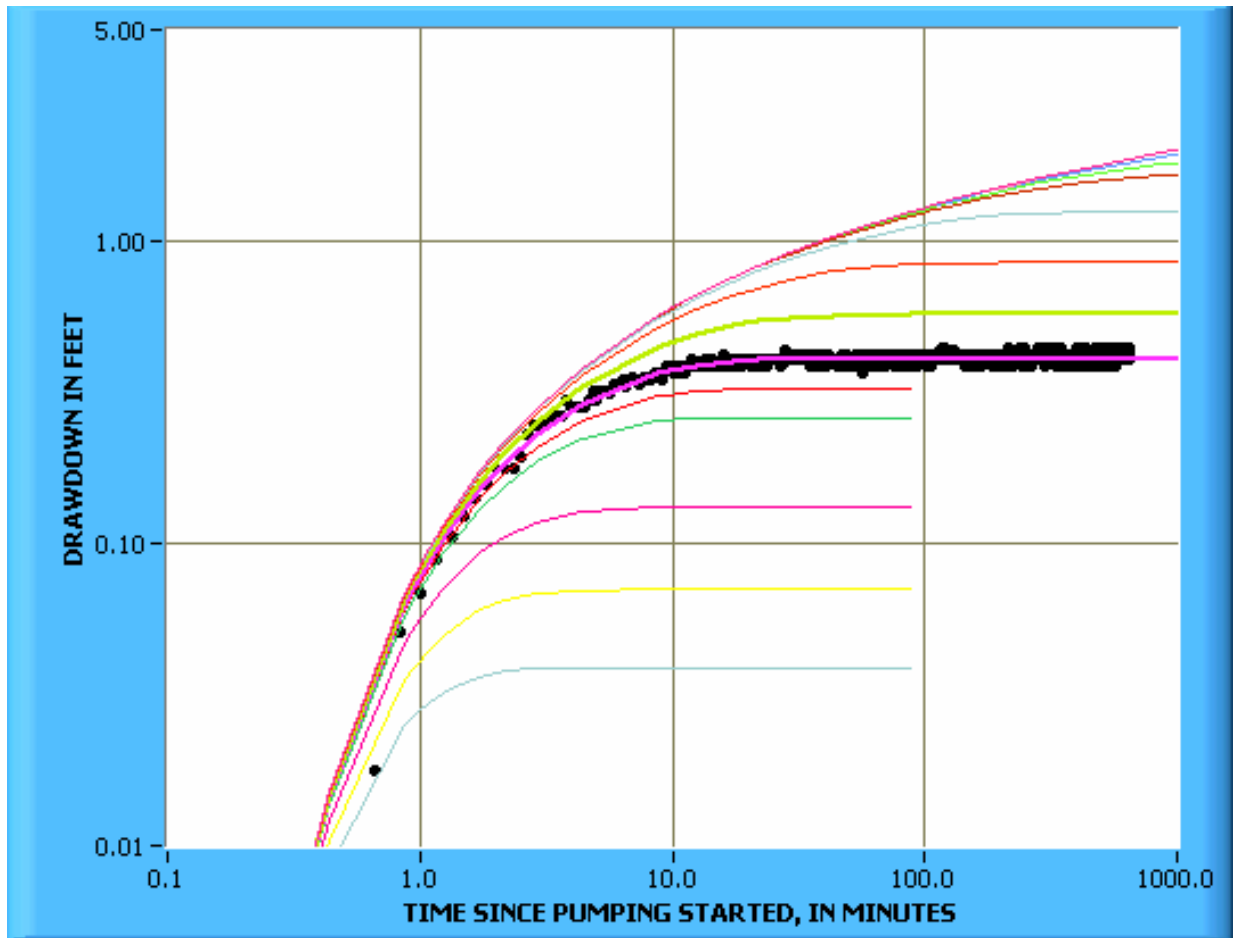
NOTE: In response to pumping Screen #1 in NC-EWDP-22S fitted to the $r/B = 7 \times 10^{-1}$ type curve of Hantush (1956 [DIRS 165169]) leaky aquifer solution. $T = 2,330 \text{ ft}^2/\text{day}$, $S = 0.0016$, $\kappa' / b' = 2.27 \times 10^{-4} \text{ min}^{-1}$.

Figure Q-1.1. Drawdown in Screen #1 at NC-EWDP-22PA



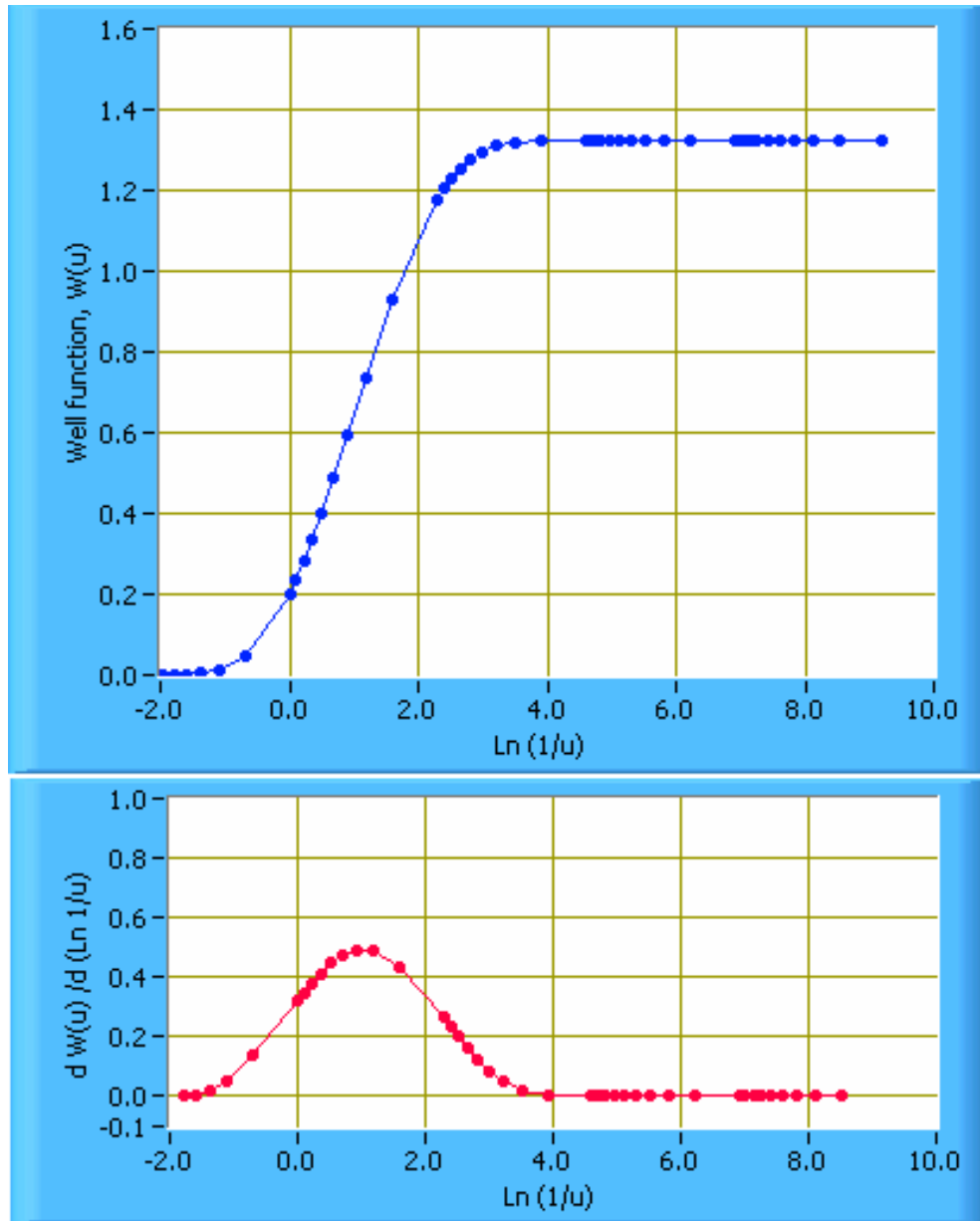
NOTE: In response to pumping Screen #1 in NC-EWDP-22S fitted to the $r/B = 7 \times 10^{-1}$ type curve of Hantush (1956 [DIRS 165169]) leaky aquifer solution. $T = 2,330 \text{ ft}^2/\text{day}$, $S = 0.0016$, $\kappa' / b' = 2.27 \times 10^{-4} \text{ min}^{-1}$.

Figure Q-1.2. Drawdown in Screen #1 at NC-EWDP-22PA



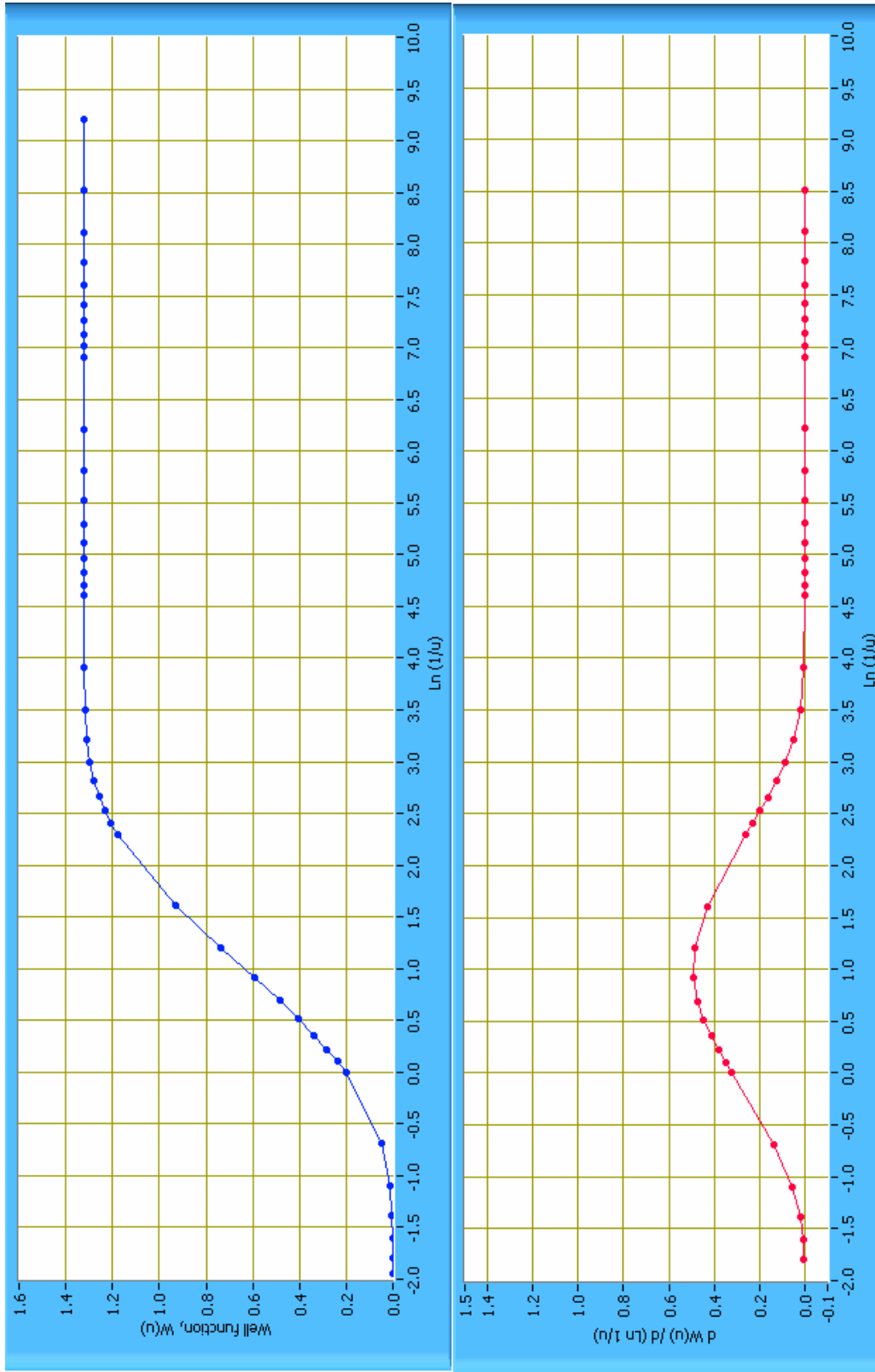
NOTE: In response to pumping Screen #1 in NC-EWDP-22S fitted to the $r/B = 7 \times 10^{-1}$ type curve of Hantush (1956 [DIRS 165169]) leaky aquifer solution. $T = 2,330 \text{ ft}^2/\text{day}$, $S = 0.0016$, $\kappa' / b' = 2.27 \times 10^{-4} \text{ min}^{-1}$.

Figure Q-1.3. Drawdown in Screen #1 at NC-EWDP-22PA



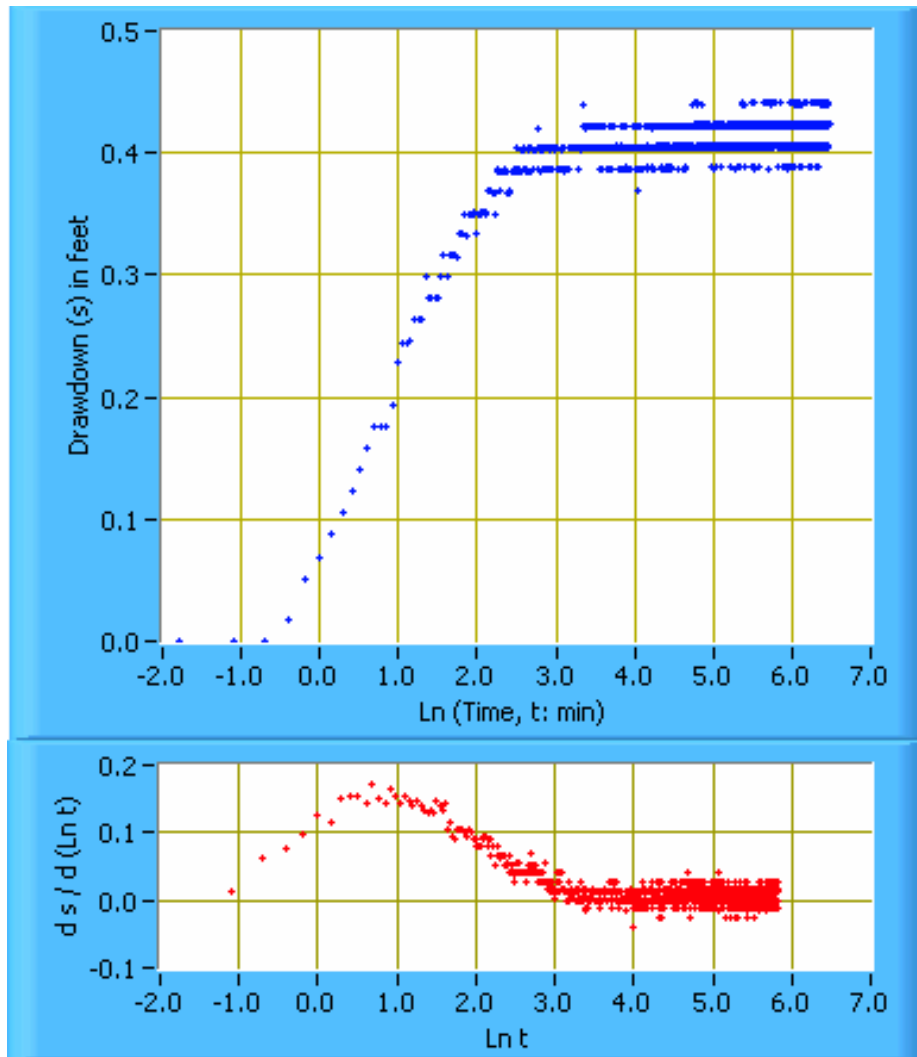
NOTE: In response to pumping Screen #1 in NC-EWDP-22S are fitted. First point where derivative becomes zero is at $\text{Ln}(1/u) \sim 3.9$, which is at the 20th (blue) point from the end of the type curve. Derivative calculated over a range of $\pm 0.15 \text{ Ln}$ cycle.

Figure Q-1.4. Derivative of the 7.0×10^{-1} Type Curve of Hantush (1956 [DIRS 165169]) to which the Drawdown Data in Screen #1 at NC-EWDP-22PA



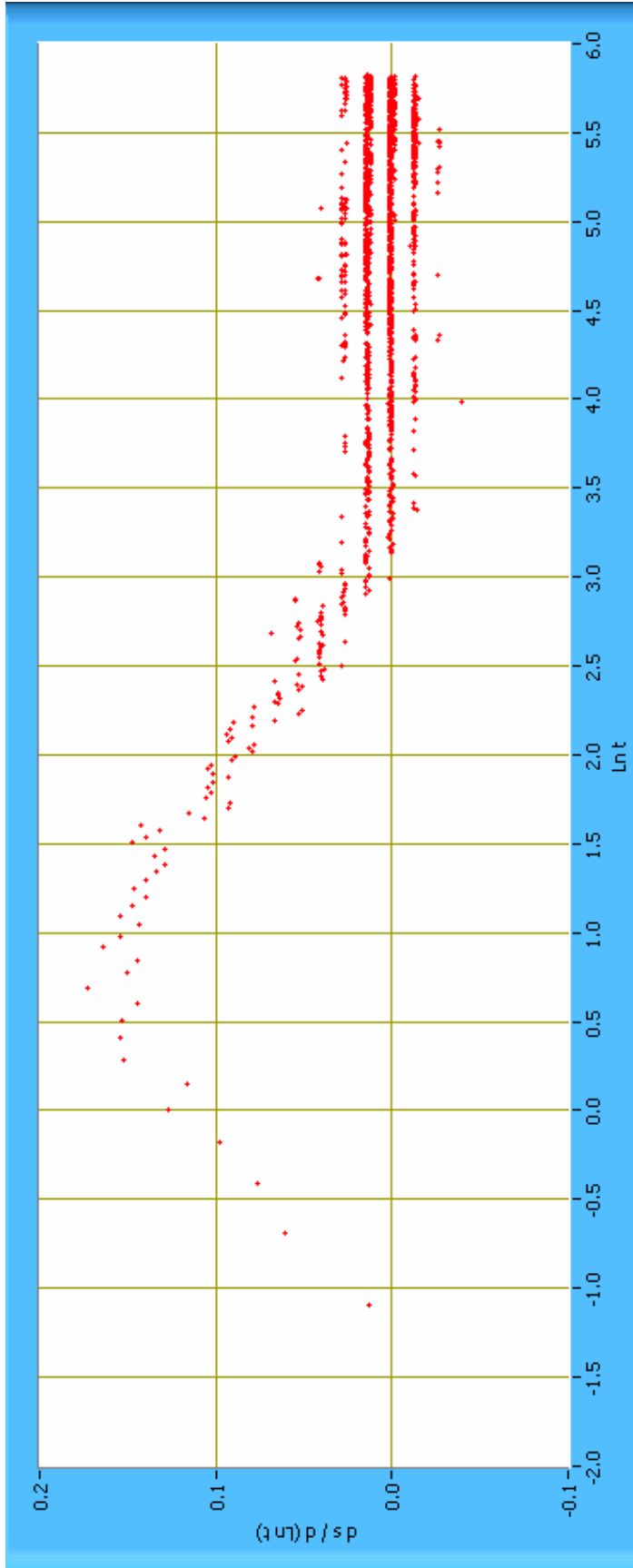
NOTE: in response to pumping Screen #1 in NC-EWDP-22S are fitted. First point where derivative becomes zero is at $\ln(1/u) \sim 3.9$, which is at the 20th (blue) point from the end of the type curve. Derivative calculated over a range of $\pm 0.15 \ln$ cycle.

Figure Q-1.5. Derivative of the 7.0×10^{-1} Type Curve of Hantush (1956 [DIRS 165169]) to which the Drawdown Data in Screen #1 at NC-EWDP-22PA



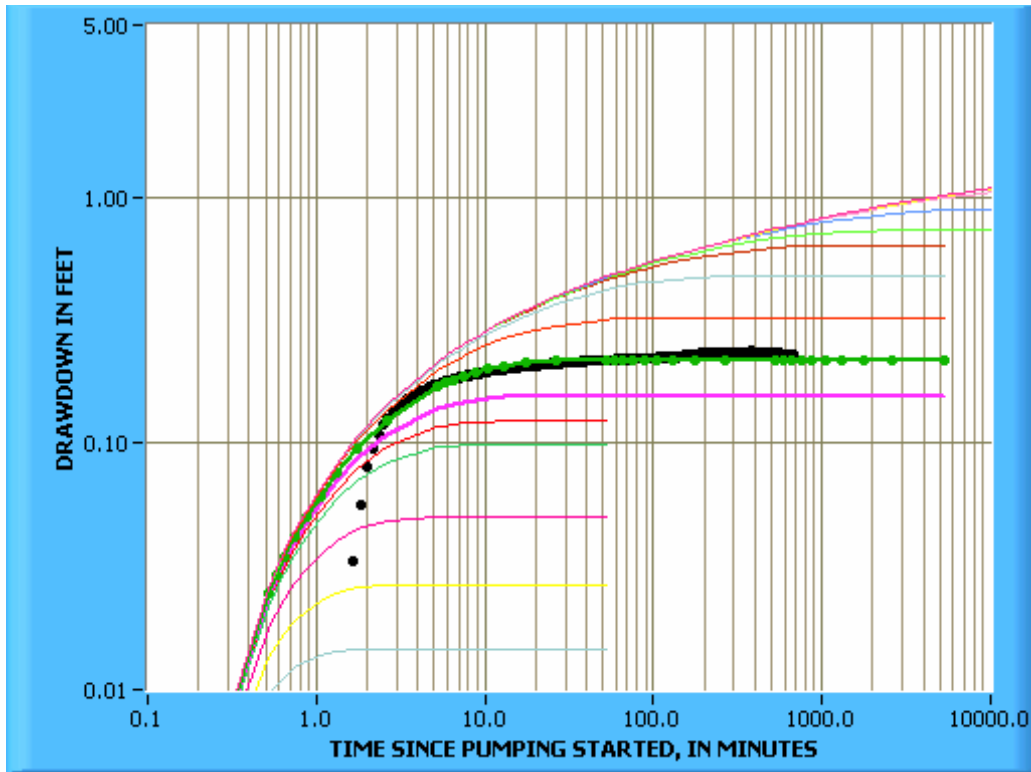
NOTE: In response to pumping Screen #1 in NC-EWDP-22S. Derivative calculated over a range of ± 0.65 Ln cycle.

Figure Q-1.6. Drawdown Data and Associated Derivatives in Screen #1 at NC-EWDP-22PA

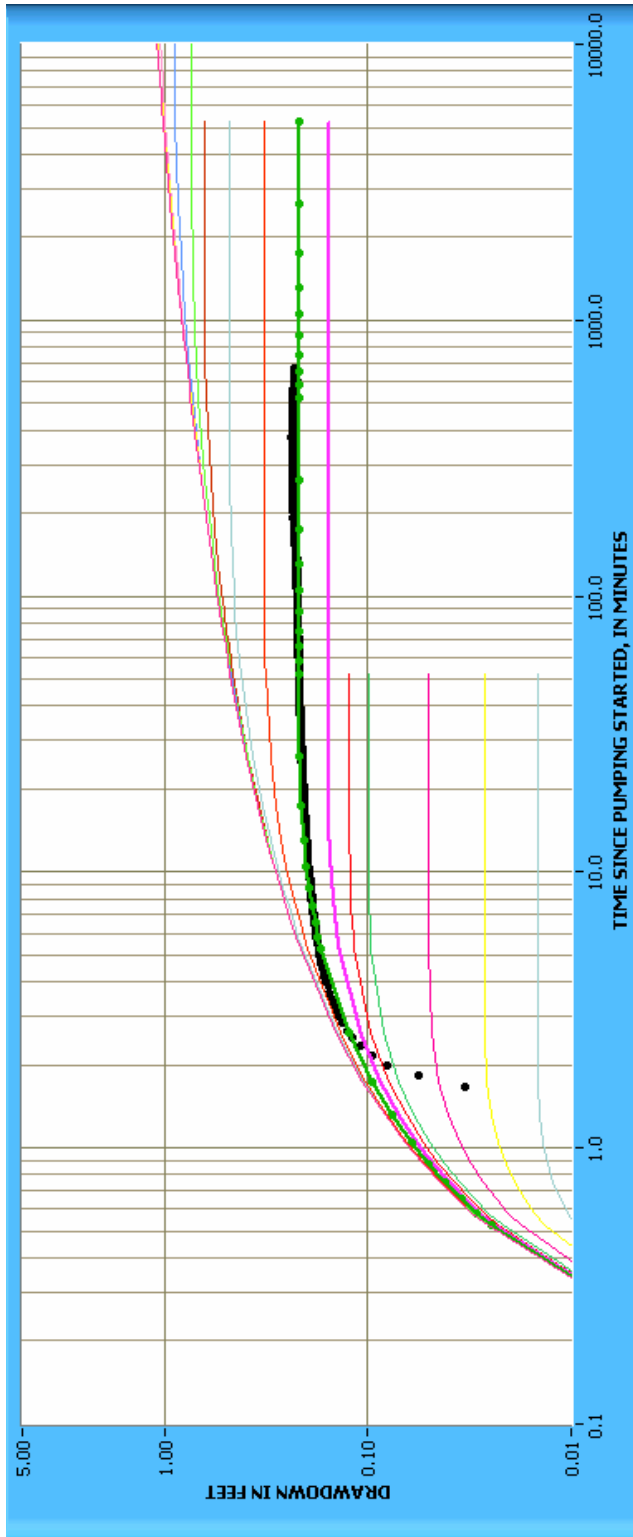


NOTE: The derivative of the drawdown decreases monotonically to zero and starts oscillating symmetrically around zero relatively persistently at $\text{Ln } t = 4.0$, which corresponds to $t = e^{4.0} = 54.6$ to approximately 55 minutes. Derivative calculated over a range of $\pm 0.65 \text{ Ln cycle}$.

Figure Q-1.7. Derivative of Drawdown Data in Screen #1 at NC-EWDP-22PA in Response to Pumping Screen #1 in NC-EWDP-22S

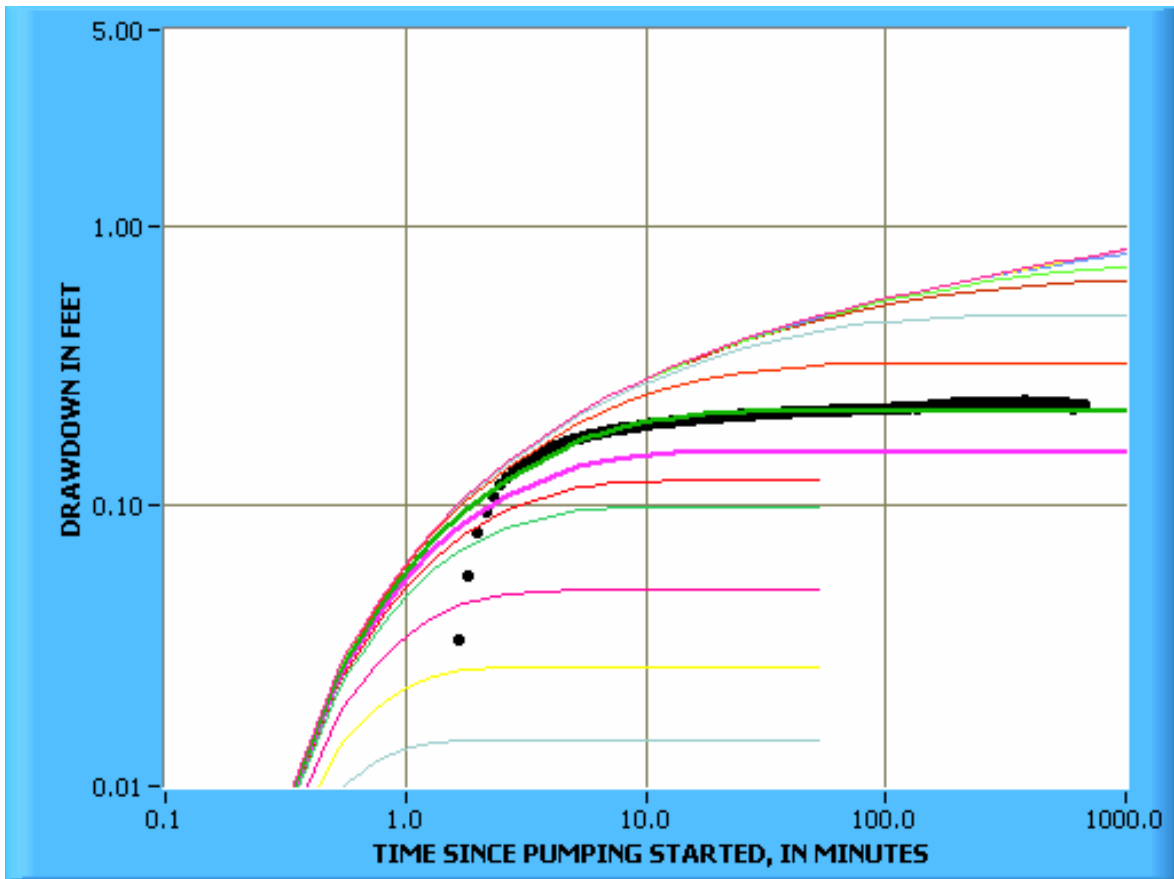


NOTE: In response to pumping Screen #2 in NC-EWDP-22S fitted to the $r/B = 5 \times 10^{-1}$ type curve of Hantush (1956 [DIRS 165169]) leaky aquifer solution. $T = 5,750 \text{ ft}^2/\text{day}$, $S = 0.0024$, $K'/b' = 2.86 \times 10^{-4} \text{ min}^{-1}$.
 Figure Q-2.1. Drawdown in Screen #2 at NC-EWDP-22PA



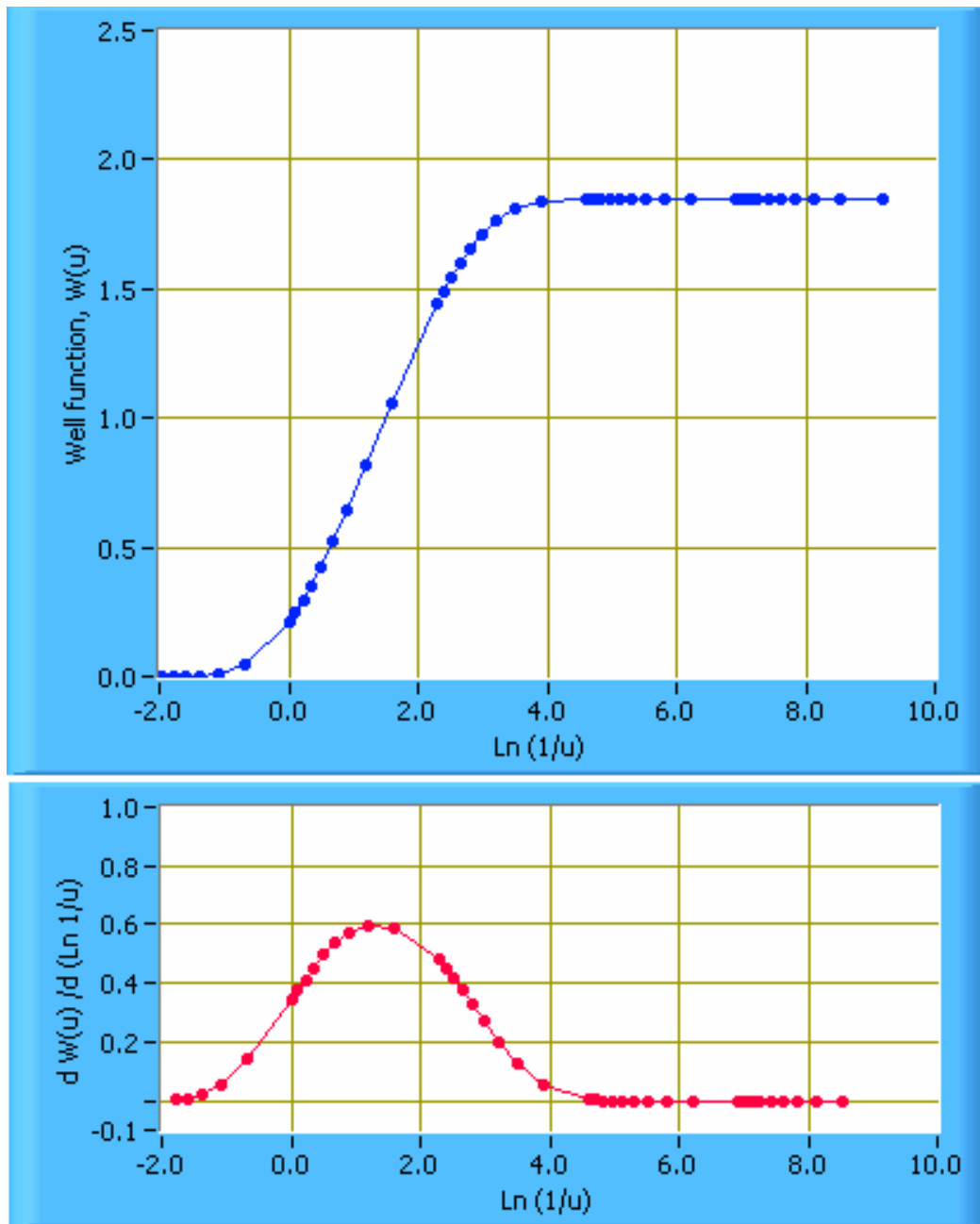
NOTE: In response to pumping Screen #2 in NC-EWDP-22S fitted to the $r/B = 5 \times 10^{-1}$ type curve of Hantush (1956 [DIRS 165169]) leaky aquifer solution. $T = 5,750 \text{ ft}^2/\text{day}$, $S = 0.0024$, $K'/b' = 2.86 \times 10^{-4} \text{ min}^{-1}$.

Figure Q-2.2. Drawdown in Screen #2 at NC-EWDP-22PA



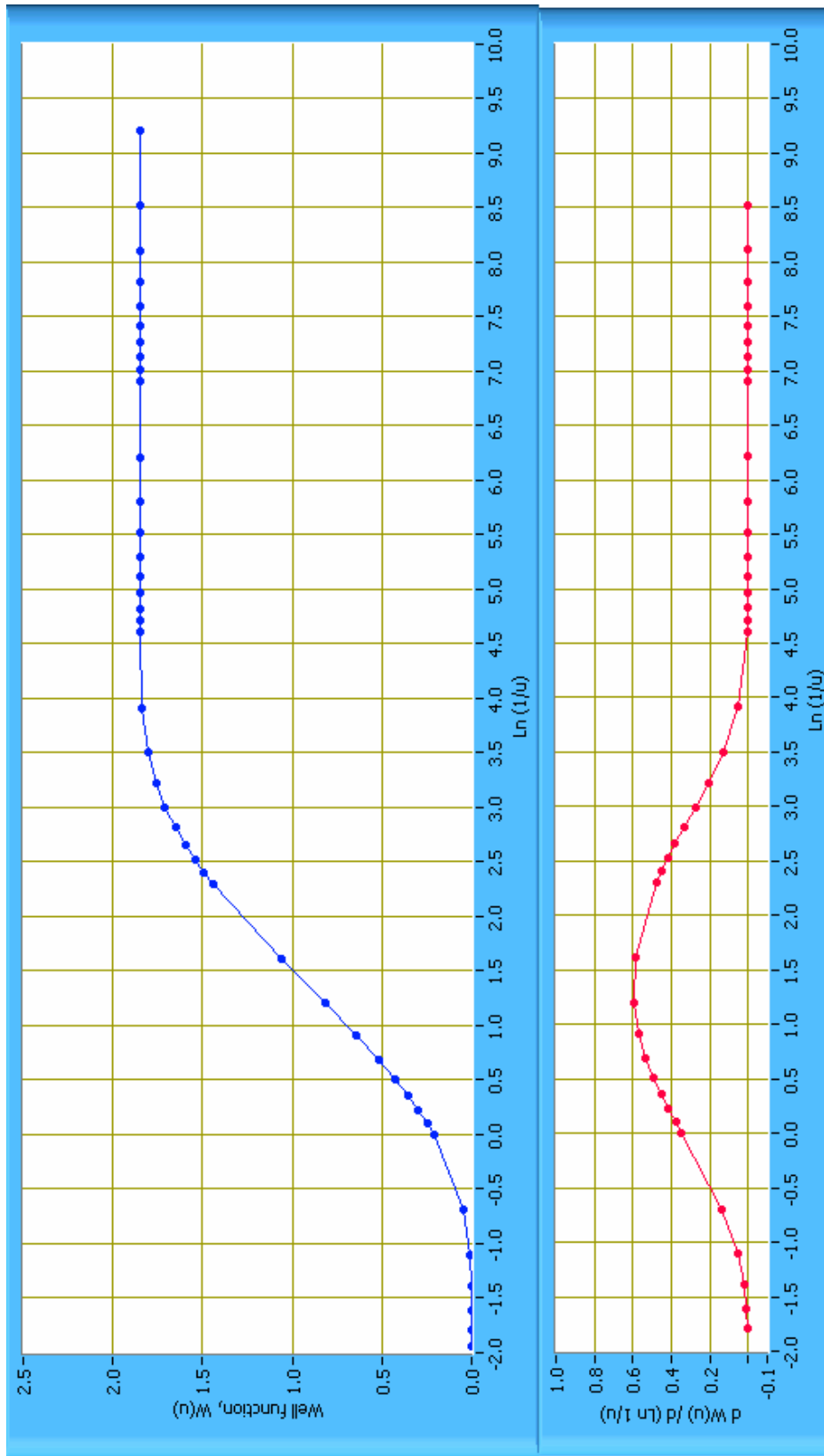
NOTE: In response to pumping Screen #2 in NC-EWDP-22S fitted to the $r/B = 5 \times 10^{-1}$ type curve of Hantush (1956 [DIRS 165169]) leaky aquifer solution. $T = 5,750 \text{ ft}^2/\text{day}$, $S = 0.0024$, $\kappa' / b' = 2.86 \times 10^{-4} \text{ min}^{-1}$.

Figure Q-2.3. Drawdown in Screen #2 at NC-EWDP-22PA



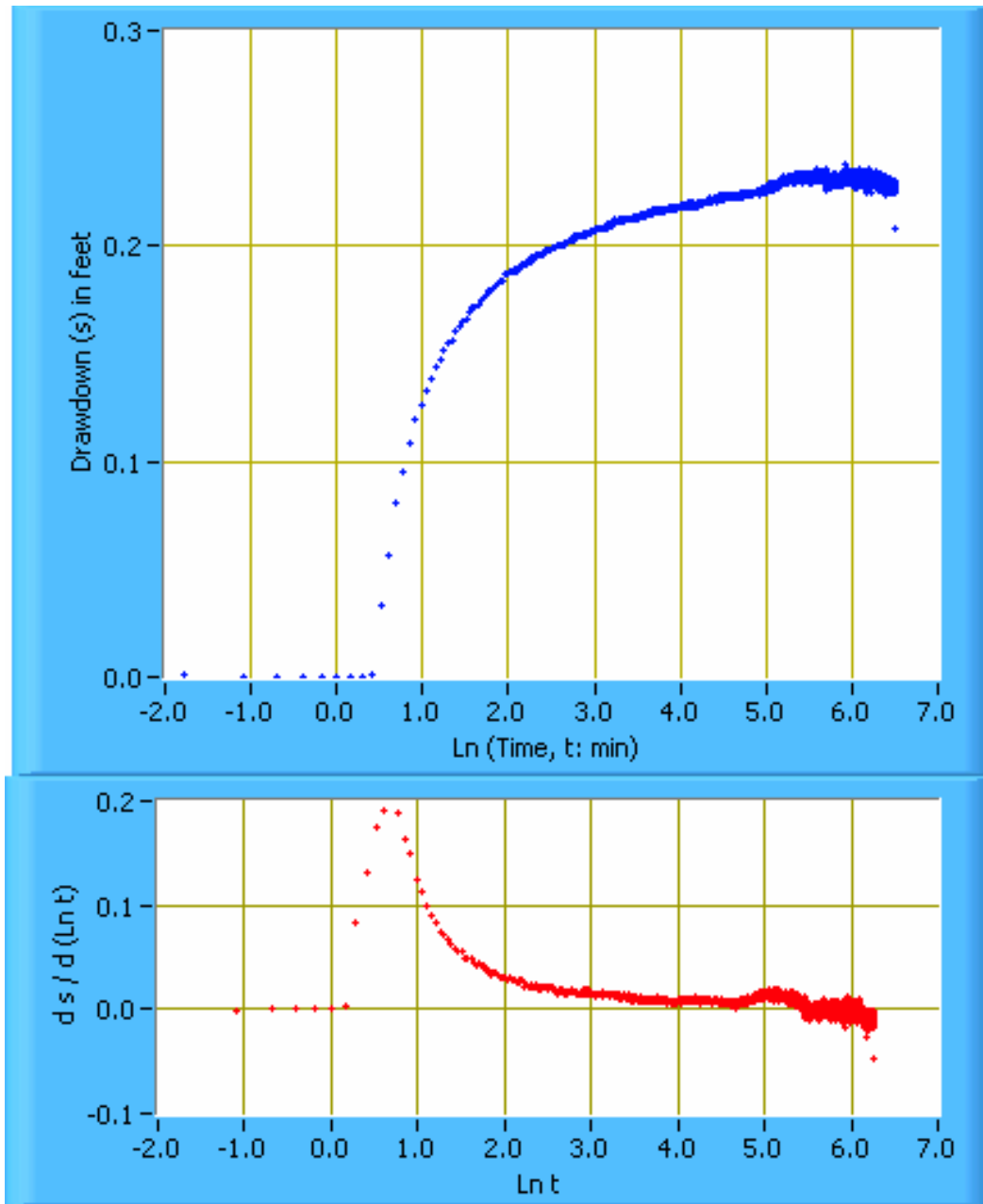
NOTE: First point where derivative becomes zero is at $\text{Ln}(1/u) \sim 4.6$, which is at the 19th (blue) point from the end of the type curve. Derivative calculated over a range of $\pm 0.15 \text{ Ln}$ cycle.

Figure Q-2.4. Derivative of the 5.0×10^{-1} Type Curve of Hantush (1956 [DIRS 165169]) to which the Drawdown Data for Screen #2 are Fitted



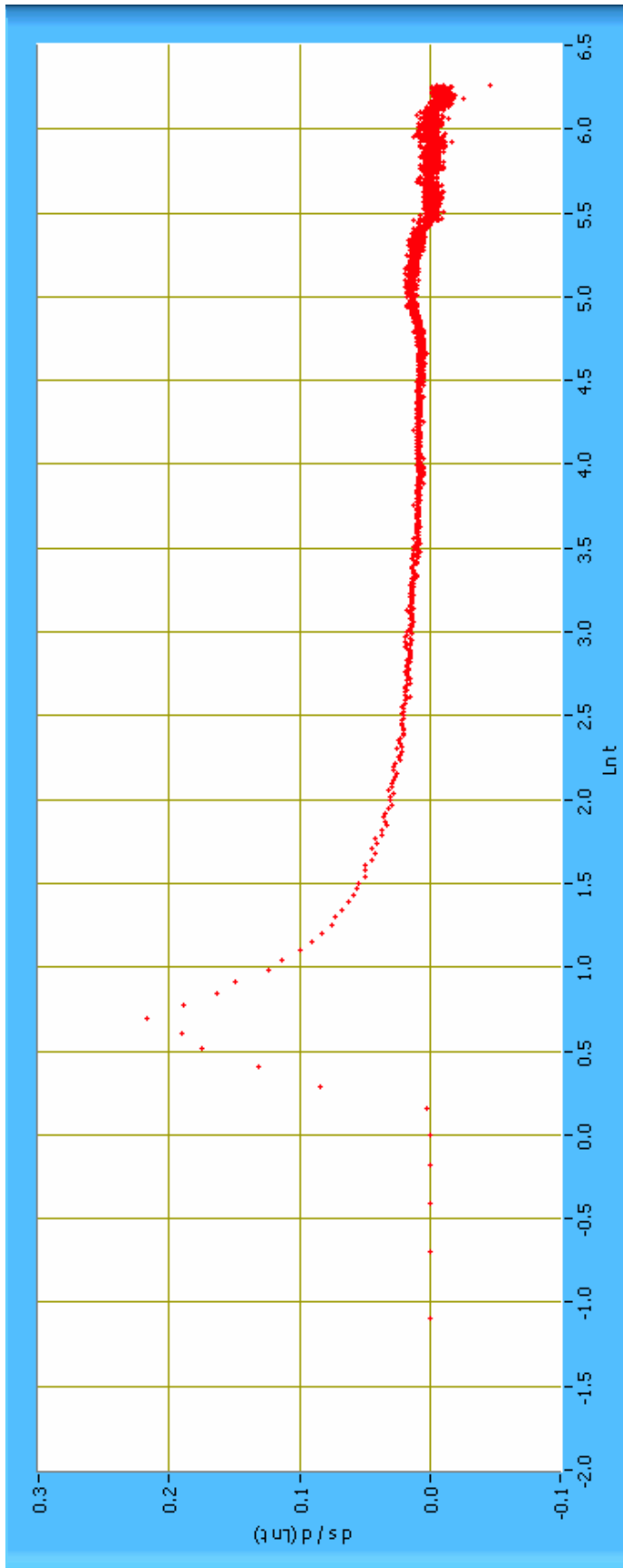
NOTE: First point where derivative becomes zero is at $\ln(1/u) \sim 4.6$, which is at the 19th point from the end of the type curve. Derivative calculated over a range of $\pm 0.15 \ln$ cycle.

Figure Q-2.5. Derivative of the 5.0×10^{-1} Type Curve of Hantush (1956 [DIRS 165169]) to which the Drawdown Data for Screen #2 are Fitted



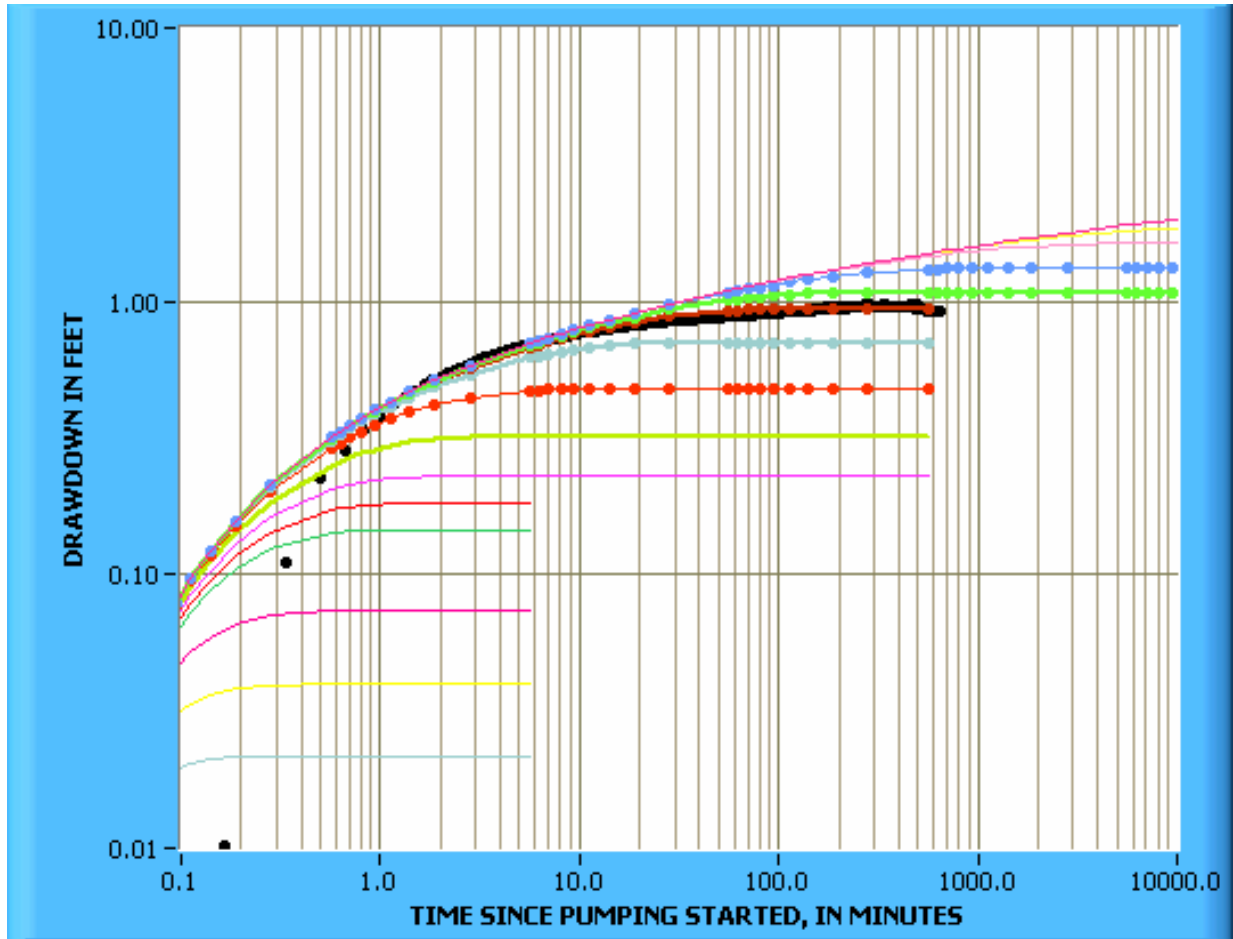
NOTE: In response to pumping Screen #2 in NC-EWDP-22S. Derivative calculated over a range of ± 0.25 Ln cycle.

Figure Q-2.6. Drawdown Data and Associated Derivatives in Screen #2 at NC-EWDP-22PA



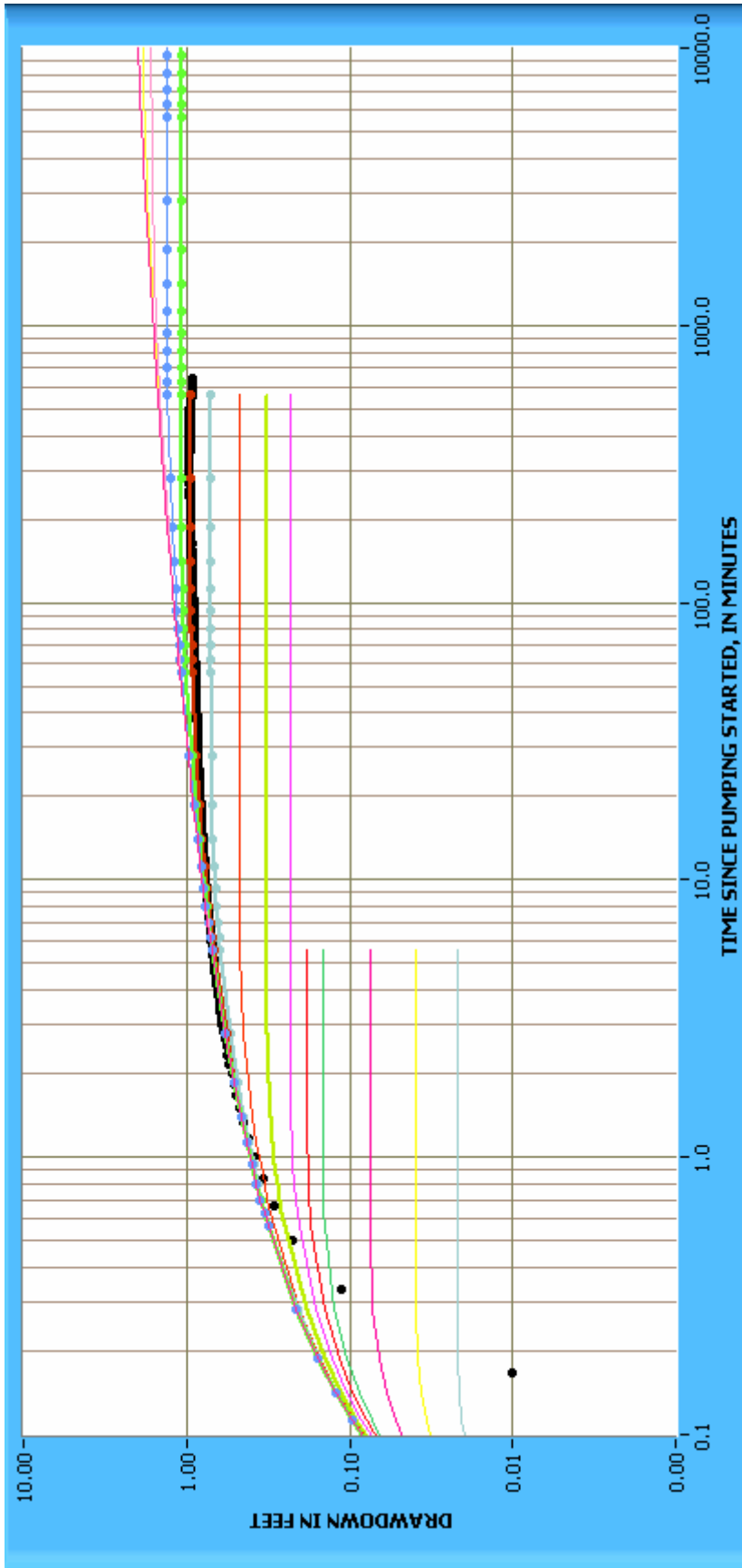
NOTE: In response to pumping Screen #2 in NC-EWDP-22S. The derivative of the drawdown decreases monotonically to almost zero at $t \text{ Ln } (t) = 4.0$ (which corresponds to $t = e^{4.0} = 54.6$ to approximately 55 minutes) and then oscillates and eventually becomes zero. Derivative calculated over a range of $\pm 0.25 \text{ Ln cycle}$.

Figure Q-2.7. Derivative of Drawdown Data in Screen #2 at NC-EWDP-22PA



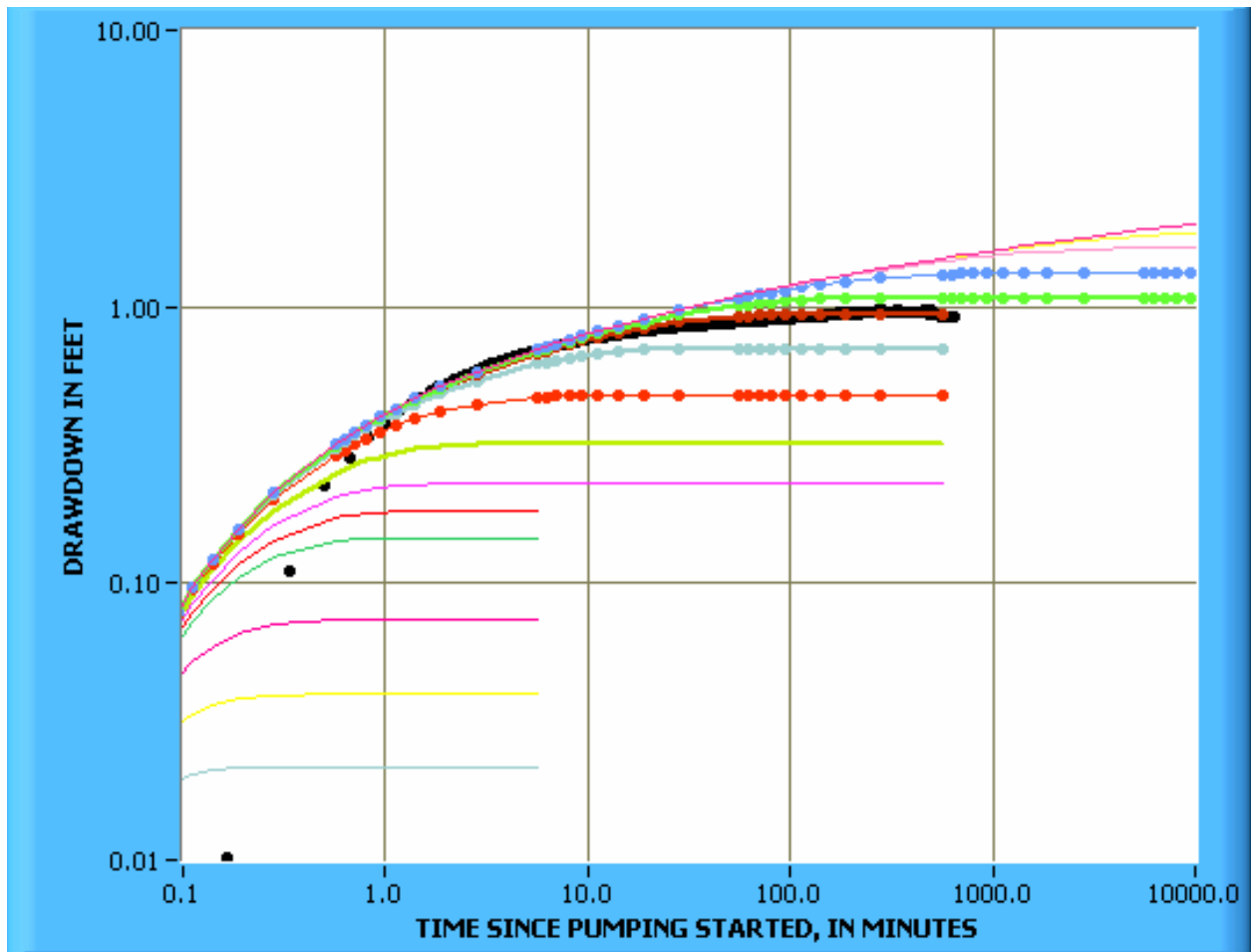
NOTE: In response to pumping Screen #3 in NC-EWDP-22S fitted to the $r/B = 7.5 \times 10^{-2}$ type curve of Hantush (1956 [DIRS 165169]) leaky aquifer solution. $T = 2,380 \text{ ft}^2/\text{day}$, $S = 0.000055$, $\kappa' / b' = 1.39 \times 10^{-6} \text{ min}^{-1}$.

Figure Q-3.1. Drawdown in Screen #3 at NC-EWDP-22PB.



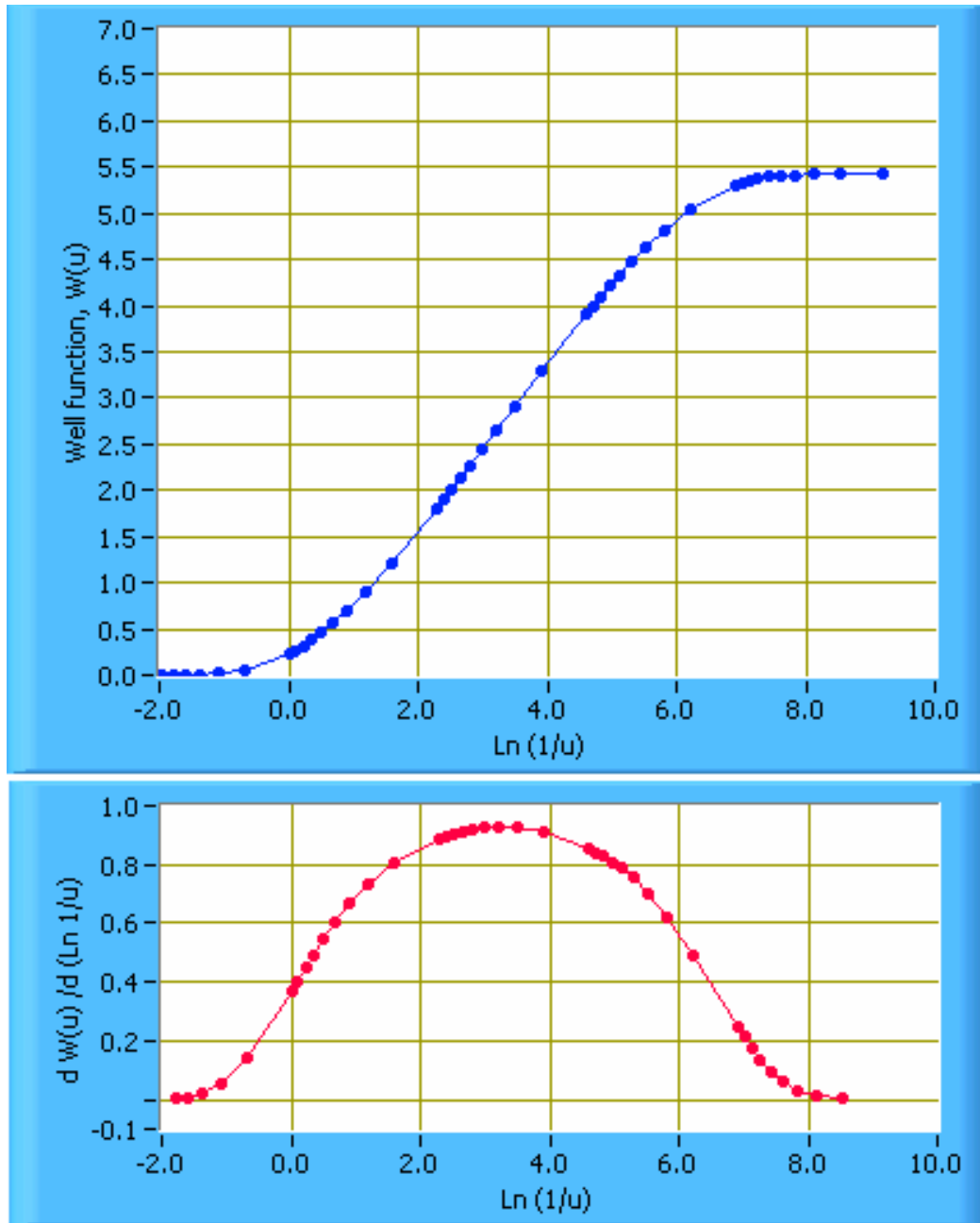
NOTE: In response to pumping Screen #3 in NC-EWDP-22S fitted to the $r/B = 7.5 \times 10^{-2}$ type curve of Hantush (1956 [DIRS 165169]) leaky aquifer solution. $T = 2,380 \text{ ft}^2/\text{day}$, $S = 0.000055$, $k'/b' = 1.39 \times 10^{-6} \text{ min}^{-1}$.

Figure Q-3.2. Drawdown in Screen #3 at NC-EWDP-22PB.



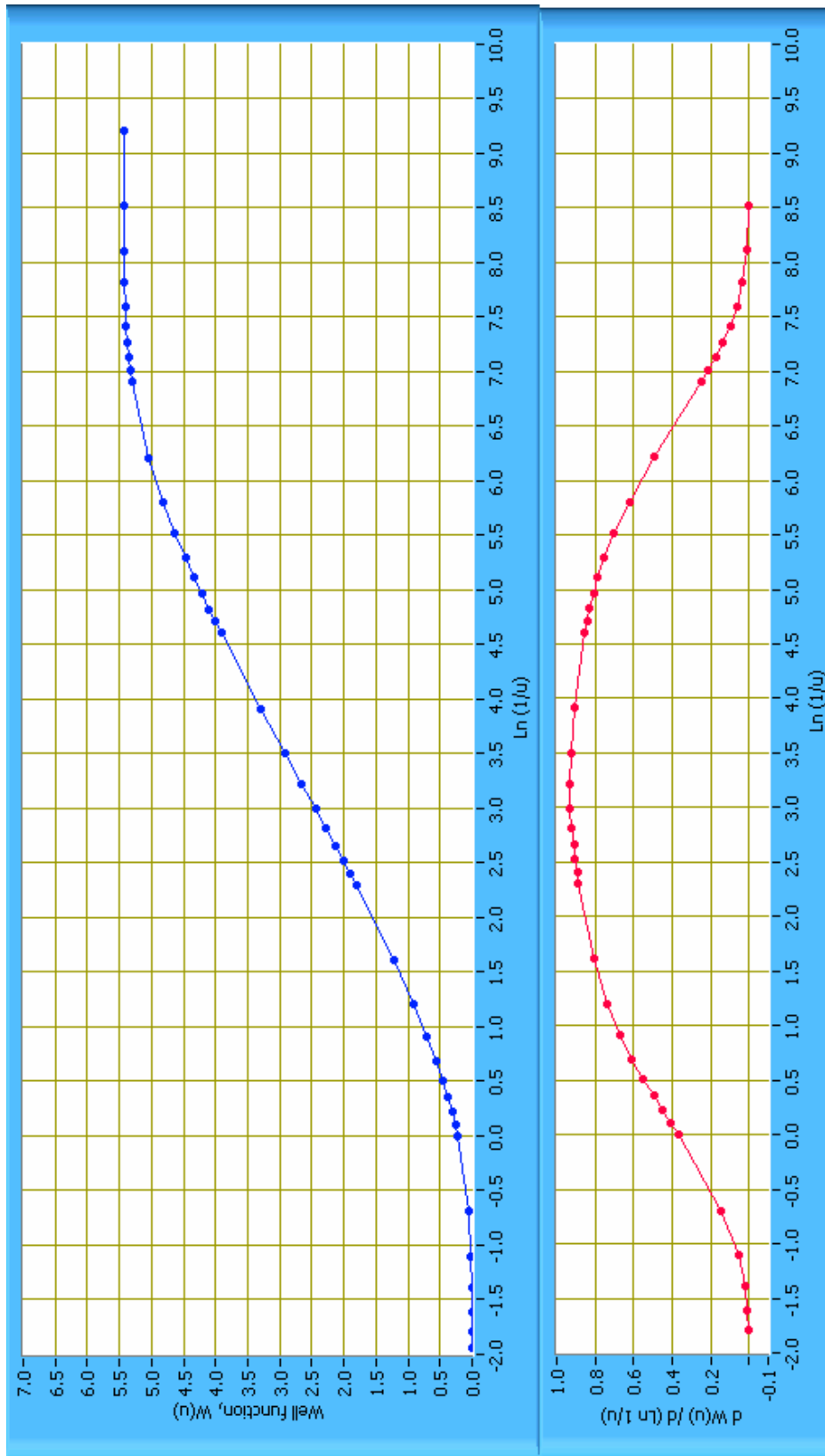
NOTE: In response to pumping Screen #3 in NC-EWDP-22S fitted to the $r/B = 7.5 \times 10^{-2}$ type curve of Hantush (1956 [DIRS 165169]) leaky aquifer solution. $T = 2,380 \text{ ft}^2/\text{day}$, $S = 0.000055$, $\kappa' / b' = 1.39 \times 10^{-6} \text{ min}^{-1}$.

Figure Q-3.3. Drawdown in Screen #3 at NC-EWDP-22PB



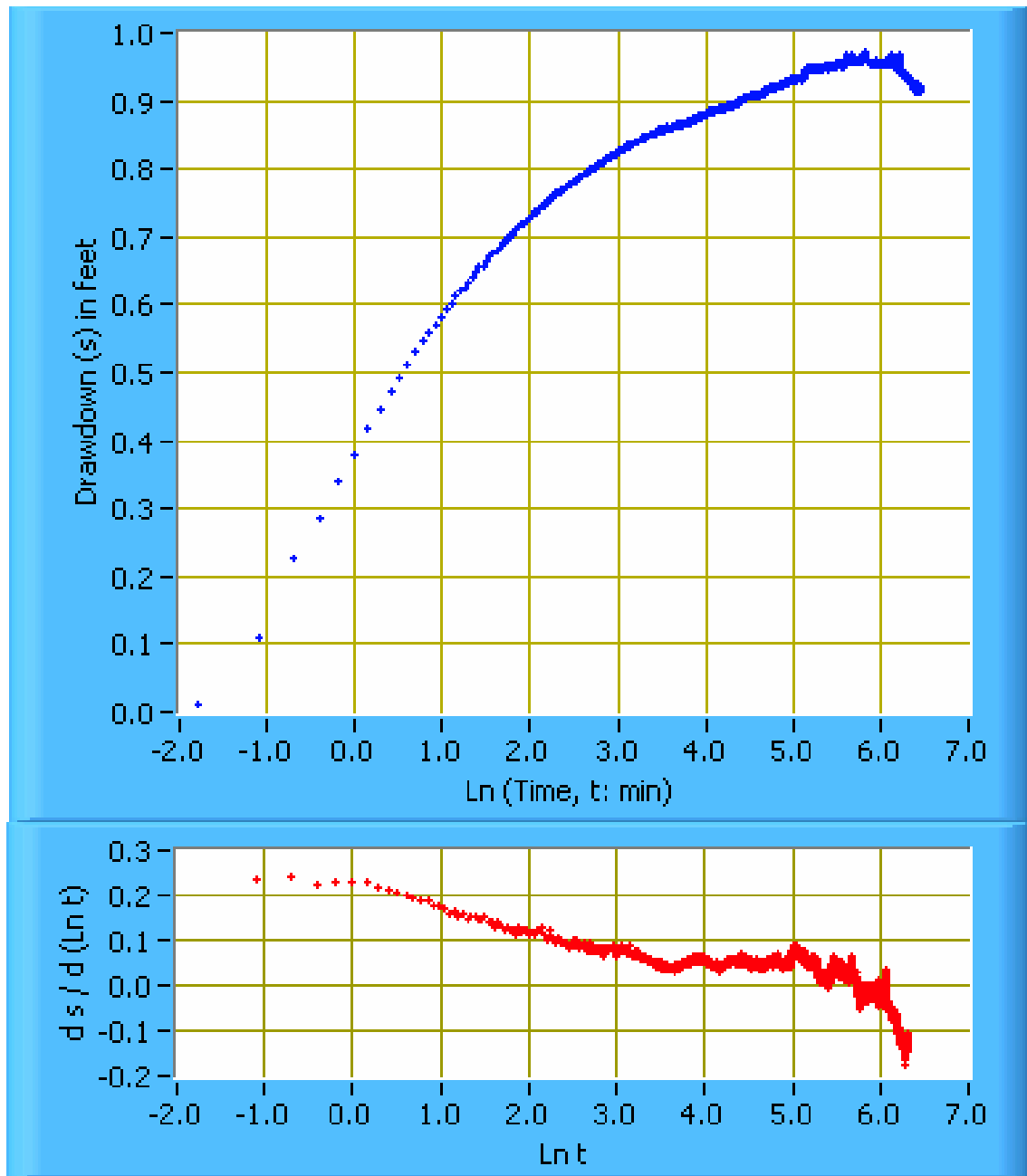
NOTE: First point where derivative becomes zero is at $\text{Ln} = 8.5$ which is at the second (blue) point from the end of the type curve. Derivative calculated over a range of $\pm 0.15 \text{ Ln}$ cycle.

Figure Q-3.4. Derivative of the 7.5×10^{-2} Type Curve of Hantush (1956 [DIRS 165169]) to which the Drawdown Data for Screen #3 are Fitted



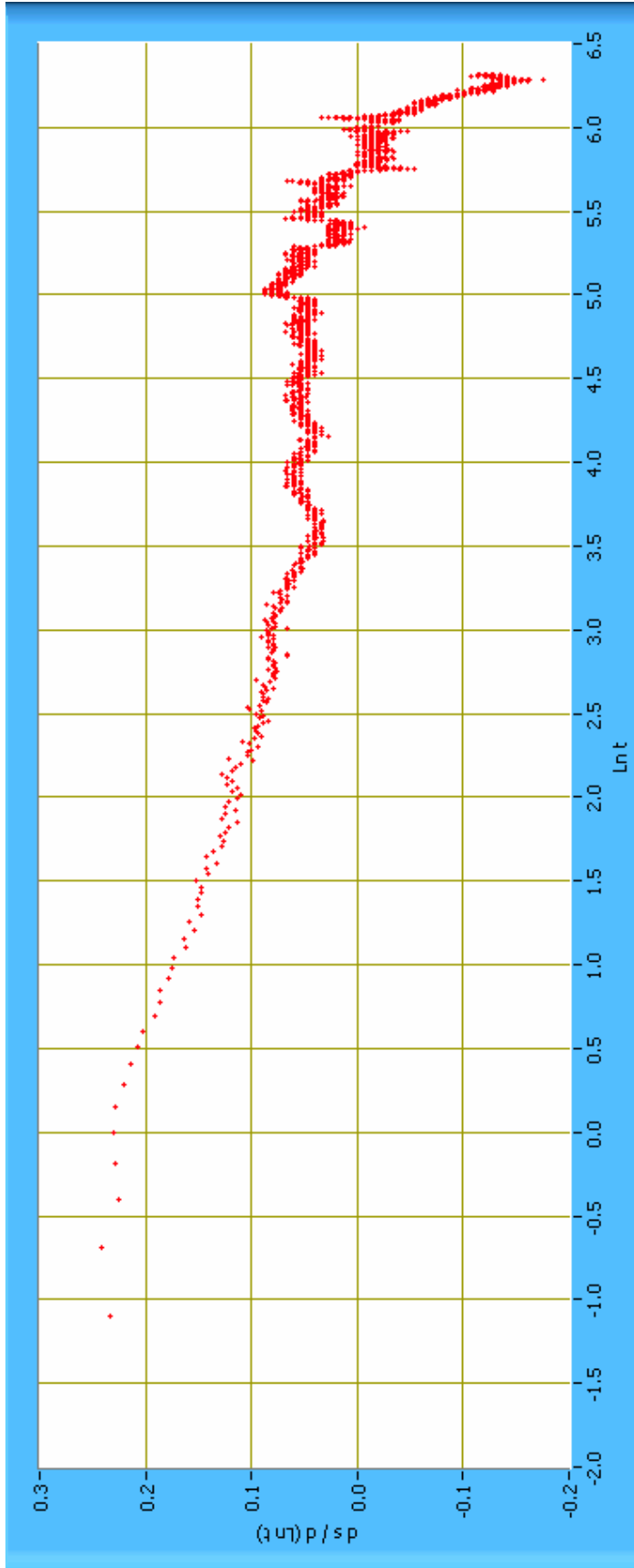
NOTE: First point where derivative becomes zero is at $\ln 8.5$, which is at the second (blue) point from the end of the type curve e. Derivative calculated over a range of $\pm 0.15 \ln$ cycle.

Figure Q-3.5. Derivative of the 7.5×10^{-2} Type Curve of Hantush (1956 [DIRS 165169]) to which the Drawdown Data for Screen #3 are Fitted



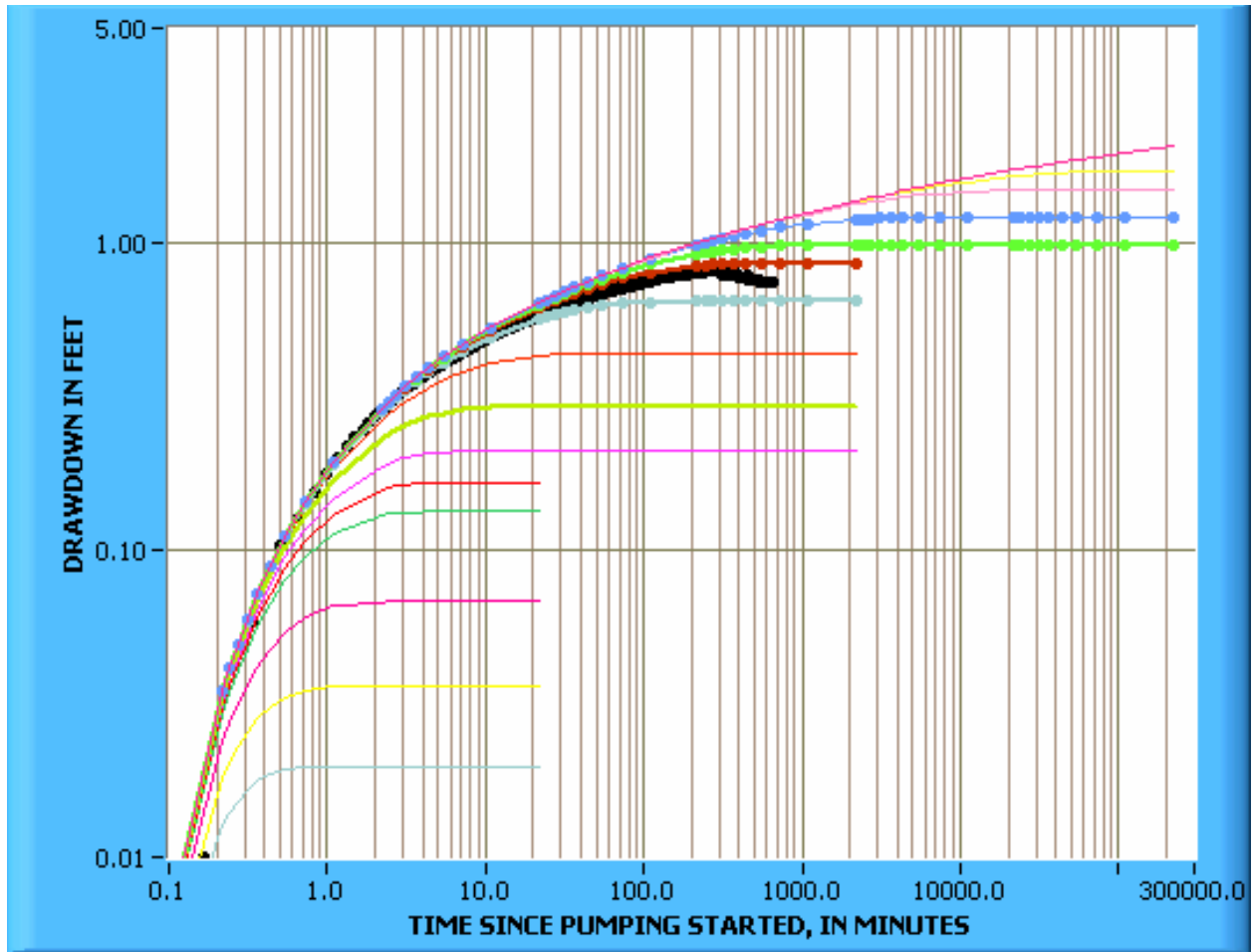
NOTE: In response to pumping Screen #3 in NC-EWDP-22S. Derivative calculated over a range of ± 0.15 Ln cycle.

Figure Q-3.6. Drawdown Data and Associated Derivatives in Screen #3 at NC-EWDP-22PB



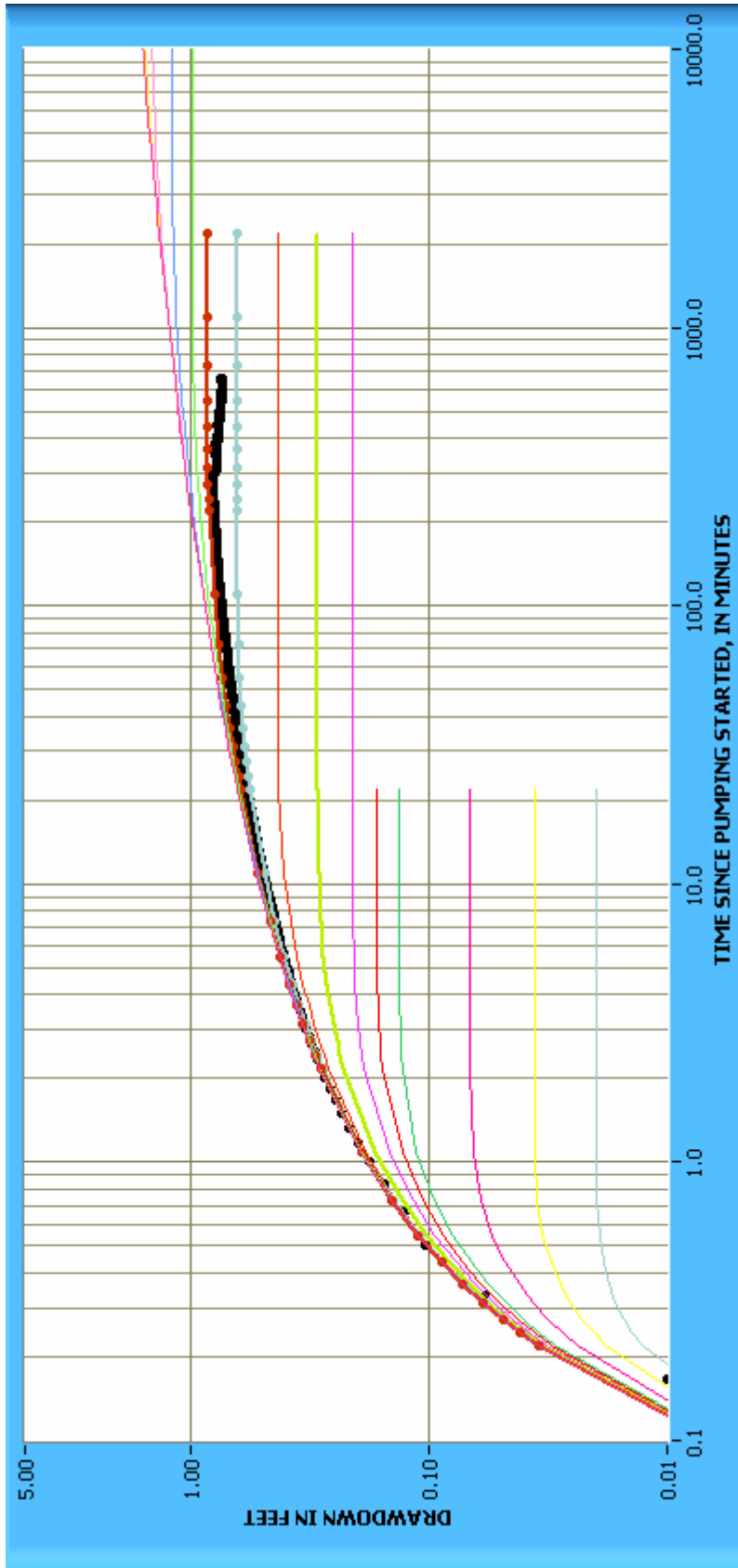
NOTE: In response to pumping Screen #3 in NC-EWDP-22S. Derivative calculated over a range of ± 0.15 Ln cycle.

Figure Q-3.7. Drawdown Data and Associated Derivatives in Screen #3 at NC-EWDP-22PB



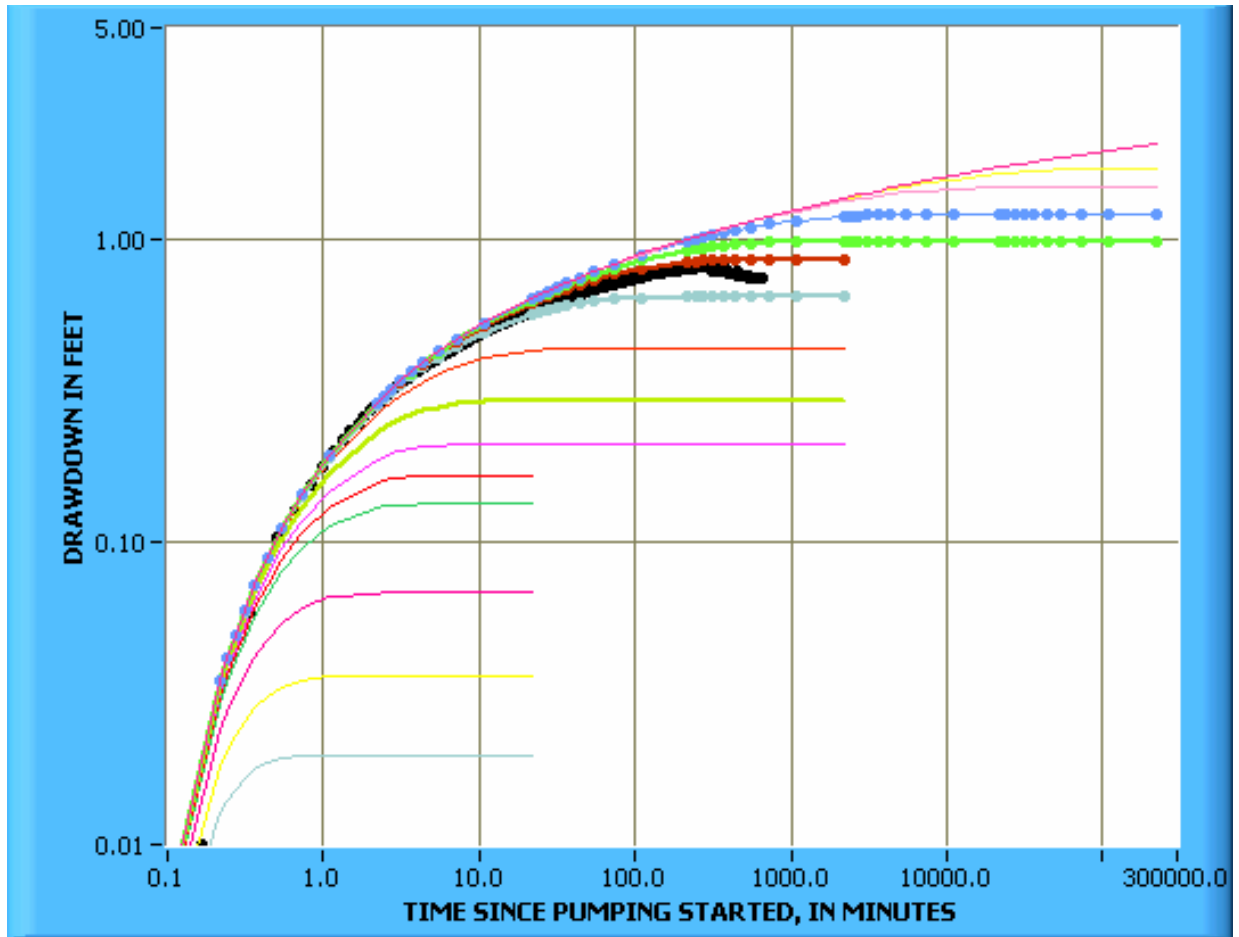
NOTE: In response to pumping Screen #4 in NC-EWDP-22S fitted to the $r/B = 7.5 \times 10^{-2}$ type curve of Hantush (1956 [DIRS 165169]) leaky aquifer solution. $T = 1,930 \text{ ft}^2/\text{day}$, $S = 0.000175$, $\kappa'/b' = 1.125 \times 10^{-6} \text{ min}^{-1}$.

Figure Q-4.1. Drawdown in Screen #4 at NC-EWDP-22PB



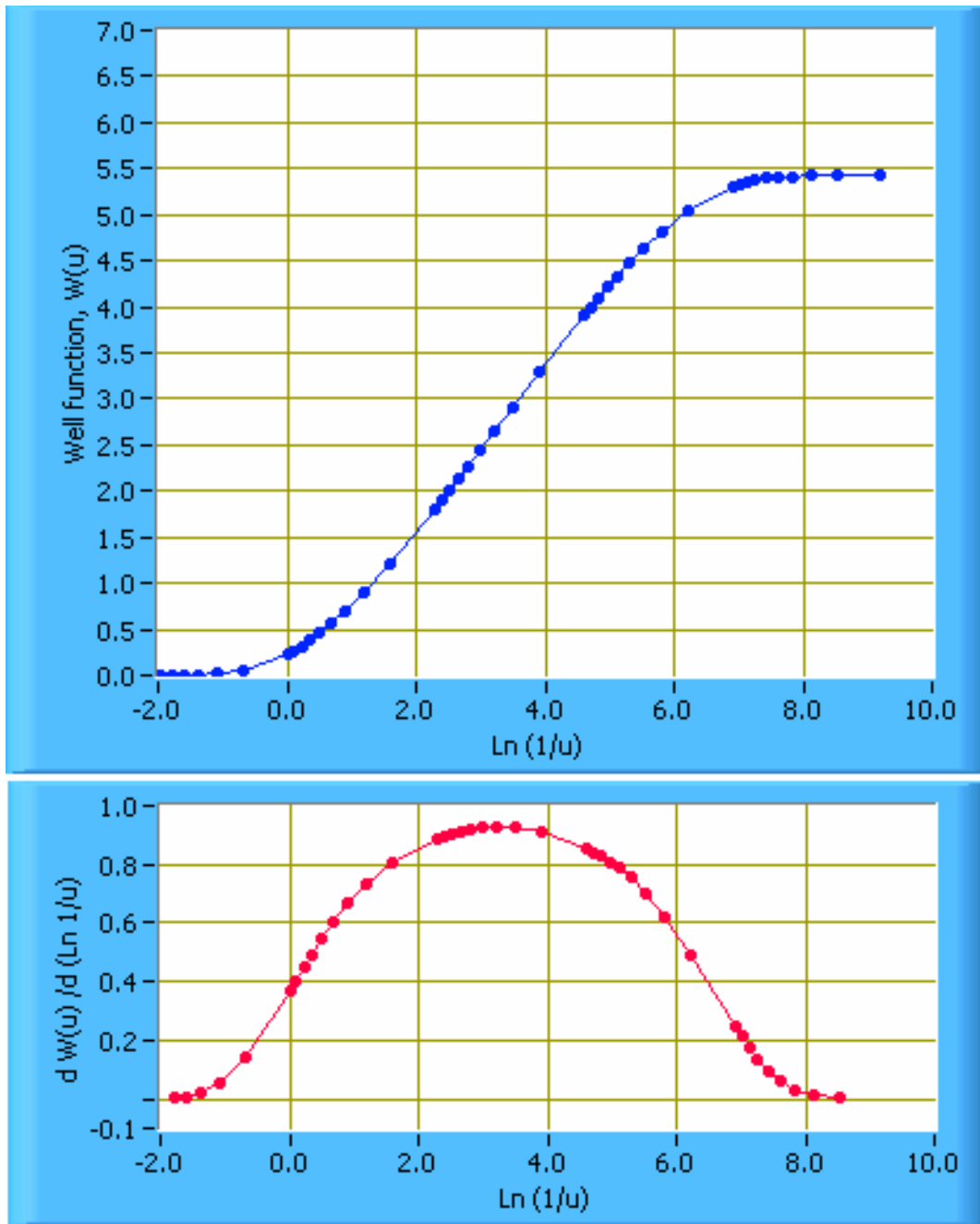
NOTE: In response to pumping Screen #4 in NC-EWDP-22S fitted to the $r/B = 7.5 \times 10^{-2}$ type curve of Hantush (1956 [DIRS 165169]) leaky aquifer solution. $T = 1,930 \text{ ft}^2/\text{day}$, $S = 0.000175$, $k'/b' = 1.125 \times 10^{-6} \text{ min}^{-1}$.

Figure Q-4.2. Drawdown in Screen #4 at NC-EWDP-22PB



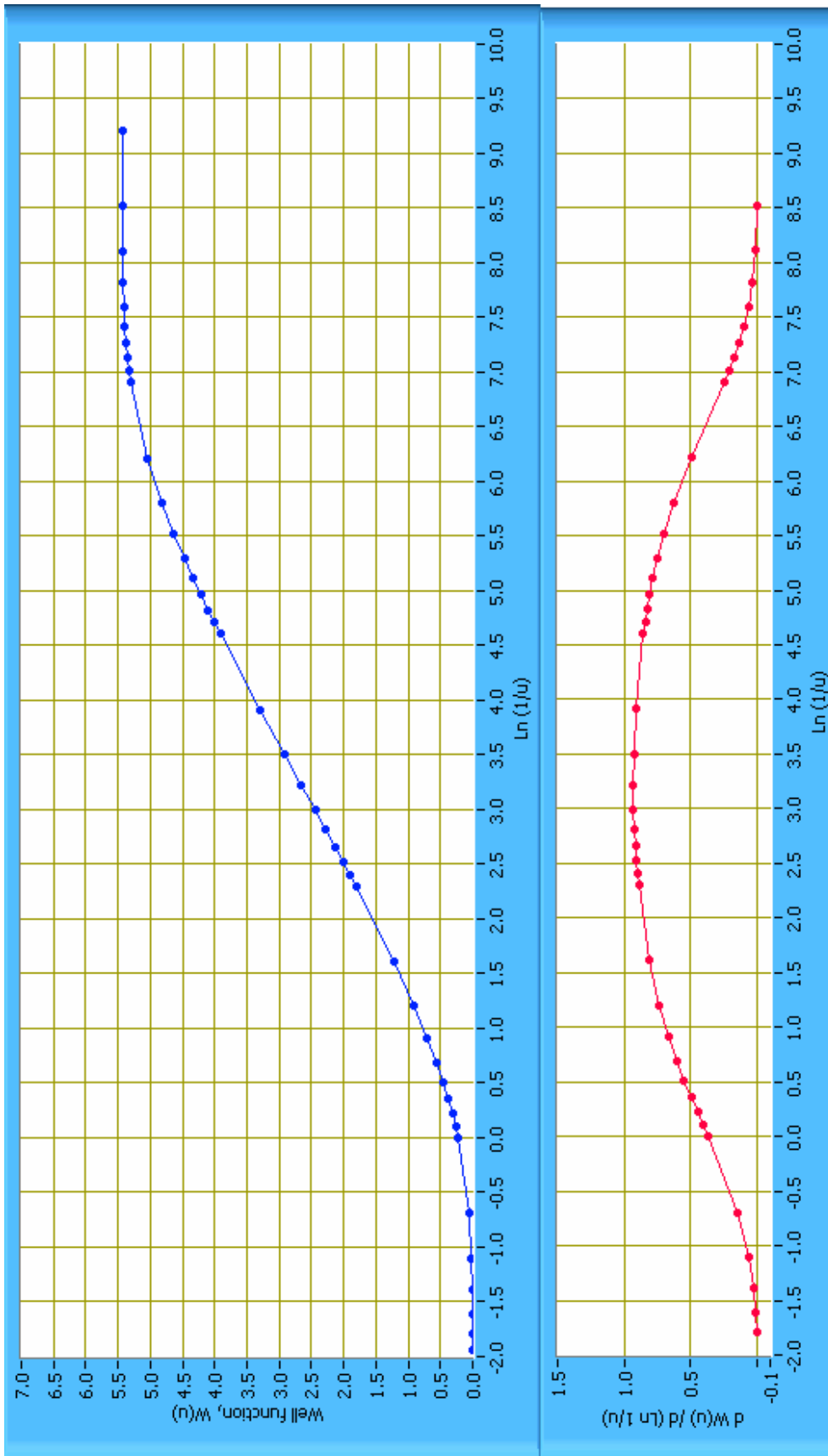
NOTE: In response to pumping Screen #4 in NC-EWDP-22S fitted to the $r/B = 7.5 \times 10^{-2}$ type curve of Hantush (1956 [DIRS 165169]) leaky aquifer solution. $T = 1,930 \text{ ft}^2/\text{day}$, $S = 0.000175$ $\kappa' / b' = 1.125 \times 10^{-6} \text{ min}^{-1}$.

Figure Q-4.3. Drawdown in Screen #4 at NC-EWDP-22PB



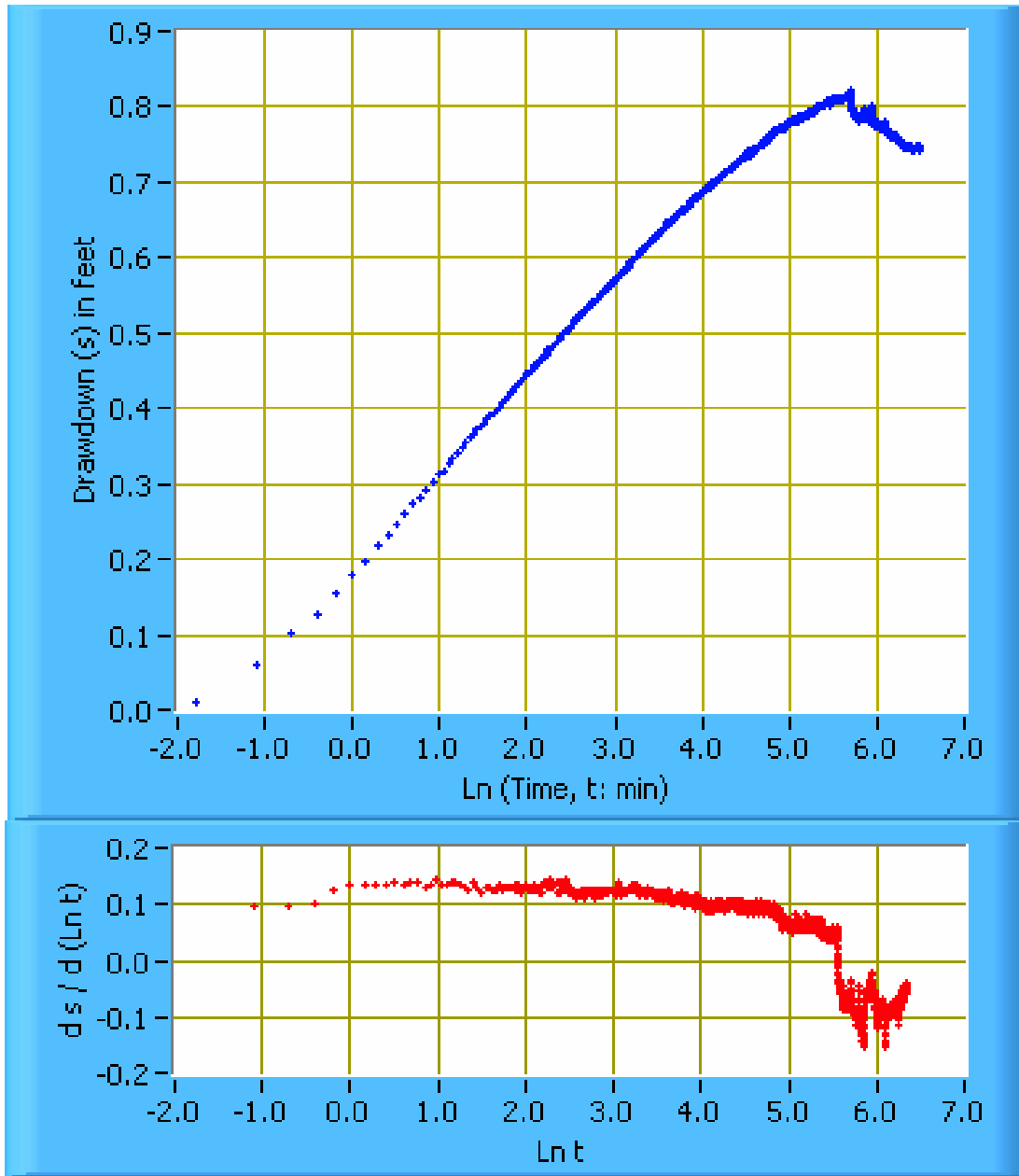
NOTE: First point where derivative becomes zero is at $\text{Ln} \sim 8.5$, which is at the second (blue) point from the end of the type curve. Derivative calculated over a range of ± 0.15 Ln cycle.

Figure Q-4.4. Derivative of the 7.5×10^{-2} Type Curve of Hantush (1956 [DIRS 165169]) to which these Data are Fitted



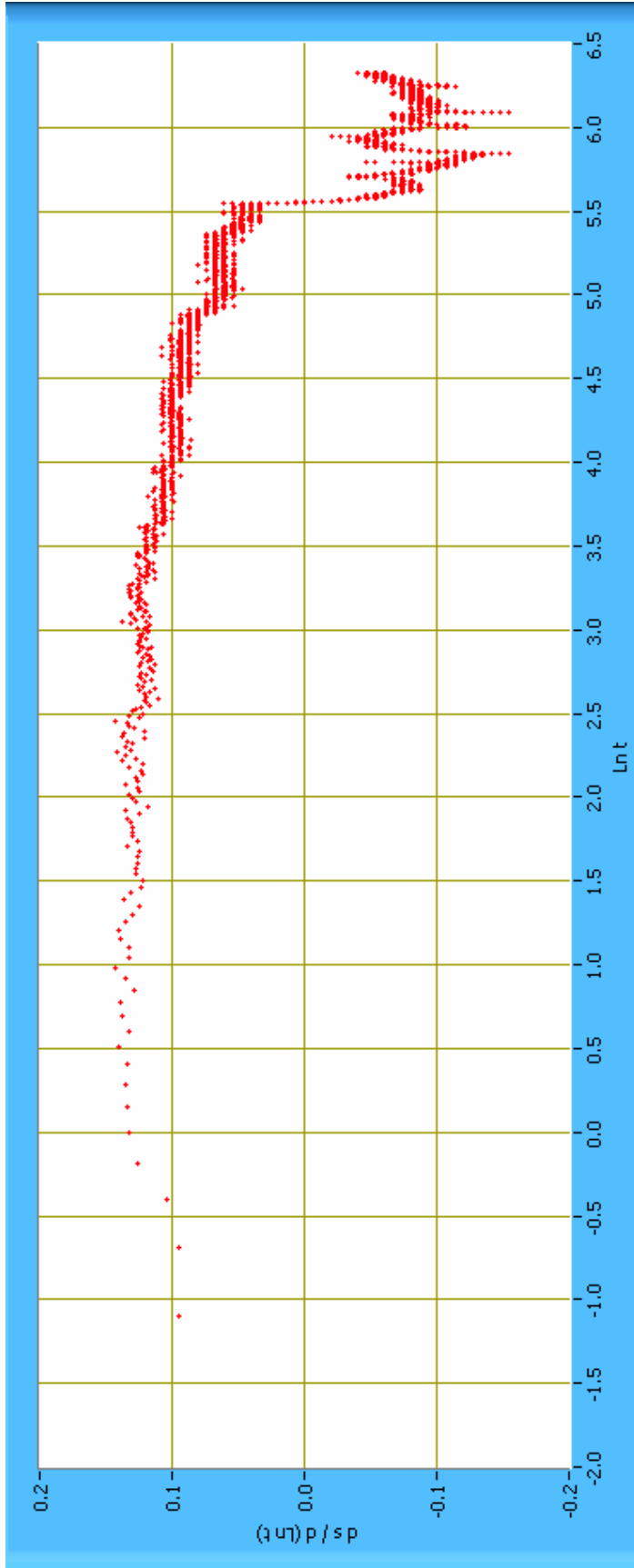
NOTE: First point where derivative becomes zero is at $\text{Ln} \sim 8.5$, which is at the second (blue) point from the end of the type curve. Derivative calculated over a range of $\pm 0.15 \text{ Ln cycle}$.

Figure Q-4.5. Derivative of the 7.5×10^{-2} Type Curve of Hantush (1956 [DIRS 165169]) to which these Data are Fitted



NOTE: In response to pumping Screen #4 in NC-EWDP-22S. Derivative calculated over a range of ± 0.15 Ln cycle.

Figure Q-4.6. Drawdown Data and Associated Derivatives in Screen #4 at NC-EWDP-22PB



NOTE: In response to pumping Screen #4 in NC-EWDP-22S. Derivative calculated over a range of ± 0.15 Ln cycle.

Figure Q-4-7. Drawdown Data and Associated Derivatives in Screen #4 at NC-EWDP-22PB

INTENTIONALLY LEFT BLANK

APPENDIX R

**QUALIFICATION OF FLOW RATE DATA FROM JUNE 1995 C-WELLS
HYDRAULIC TEST (DTN: LA0705PR150304.006)**

R1. INTRODUCTION

The qualification of the C-wells discharge flow rate data from the June 1995 hydraulic test is documented here in accordance with SCI-PRO-001, *Qualification of Unqualified Data*. This qualification provides the desired level of confidence that the data are suitable for their intended use, which is the estimation of hydrologic parameters in the saturated fractured tuffs at the C-wells complex based on the pressure drawdown and recovery data in packed-off intervals of c#1 and c#2 during and after pumping c#3 in an open-hole configuration. This qualification is carried out in accordance with the attached data qualification plan, *Qualification of Discharge Flow Rate Data in June 1995 Hydraulic Test at the C-Wells* (Section R6). The flow rate data are not qualified because the flow meter used for the measurements was not calibrated after the testing was completed (a successful pretest calibration was performed, but the meter did not receive a posttest calibration).

R2. BASES FOR JUNE 1995 C-WELLS FLOW RATE DATA QUALIFICATION

This qualification is based on technical assessment, and the technical assessment is based on the following:

- The flow rate measurements in two C-wells hydraulic tests conducted soon after the June 1995 test, namely the tests initiated in February 1996 and May 1996, were qualified (flow meters had successful opening and closing calibrations).
- The pressure drawdown measurements in the June 1995 test and in the two subsequent hydraulic tests in February and May of 1996 were all qualified (pressure transducers had successful opening and closing calibrations).
- c#3 was pumped in all three tests. In June 1995, the pumping was done in an open-hole configuration. In February 1996, the lower Bullfrog Tuff and upper Tram Tuff were packed off as a single pumped interval, and in May 1996, only the lower Bullfrog Tuff was pumped. The same packer configuration was employed in c#1 and c#2 in all three tests, although the packers separating the lower Bullfrog Tuff and the upper Tram Tuff were deflated in the February 1996 test.
- Although the June 1995 test was conducted in an open-hole configuration, spinner and oxygen activation surveys indicated that the majority of the production (approximately 90%) was from the lower Bullfrog and upper Tram Tuffs (see Figure C-4). These were the intervals from which pumping took place in February and May 1996.
- According to hydraulic testing theory, the pressure drawdown at a given point in time and at a given observation point in a system subjected to a steady water withdrawal is proportional to the withdrawal flow rate. Thus, if the withdrawal flow rate from a specific location is doubled in one test relative to another test, the pressure drawdown at a given point in time and at a given observation point in the higher-flow-rate test will be twice the drawdown at the same point in time and same location in the lower-flow-rate test. This proportionality relationship is derived in Section C3.1.3. It follows that if the drawdown at a given time and location is known in two tests with different withdrawal

rates, and the withdrawal rate is known in one of the tests, then the withdrawal rate in the other test can be estimated from the drawdown in the unknown test divided by the drawdown in the known test multiplied by the flow rate in the known test. This relationship can be directly applied to estimate the unqualified flow rate in the June 1995 test from the qualified drawdowns in the June 1995, February 1996, and May 1996 tests and the qualified flow rates in the February 1996 and May 1996 tests:

$$Q_{\text{June 1995}} = Q_{\text{Feb or May 1996}} \left(\frac{\Delta H_{i, \text{June 1995}}}{\Delta H_{i, \text{Feb or May 1996}}} \right) \quad (\text{Eq. R-1})$$

where,

Q = volumetric flow (pumping) rate

ΔH_i = pressure drawdown in interval. i.

- Using Equation R-1 and recognizing that the majority of flow from c#3 in all 3 hydraulic tests was from the lower Bullfrog and upper Tram Tuff intervals, the cross-hole drawdowns in the upper Bullfrog Tuff and lower Bullfrog Tuff intervals in c#1 and c#2 (or combined lower Bullfrog Tuff and upper Tram Tuff in February 1996) are expected to be roughly proportional to the pumping rates in each test. One would also expect the drawdowns in the upper Tram Tuff to exhibit this proportionality, but this could not be examined or confirmed because the pressure transducers in this interval in c#1 and c#2 were not operative during all the tests. The drawdowns in the Prow Pass and Calico Hills tuffs would not be expected to follow Equation R-1 as closely as the Bullfrog and Tram Tuff intervals because they are significantly shallower than the pumped intervals in the February and May 1996 tests and also because very little of the production flow in c#3 comes from these intervals. Thus, it is preferable that the drawdowns in the Prow Pass and Calico Hills intervals not be used to try to estimate flow rates based on ratios of drawdowns.
- The final consideration in the qualification of the June 1995 flow rate data is that the confidence in the flow rate estimates need only be commensurate with the confidence associated with the hydraulic parameters (transmissivity and storativity) estimated from the flow rate data. Section C7 states, “When all of the contributing uncertainties are considered, transmissivity and storativity estimates at the C-wells are considered accurate to within a factor of 2.5 for transmissivity (1.5 for the lower Bullfrog and upper Tram Tuffs) and within an order of magnitude for storativity.” Sections 6.2.7 and C5 state, “Based on the ranges of transmissivity estimates obtained for a given hydrogeologic interval by different methods using either the drawdown or recovery data from the C-wells hydraulic tests (Tables 6.2-2 or C-6 and C-7) or the drawdown data from distant wells that responded to pumping c#3 in 1996-97 (Tables 6.2-3 or C-10 and C-11), the transmissivity estimates determined in this analysis can be considered accurate to within about factor of 1.5 for high-transmissivity intervals (lower Bullfrog and upper Tram Tuffs) and within a factor of 2.5 for low-transmissivity intervals (Calico Hills, Prow Pass, and upper Bullfrog Tuffs). The factor of 2.5 also applies to the assemblage of volcanic tuffs between the C-wells and distant wells. Storativity estimates for all intervals can be considered accurate to within an order of magnitude or

so.” These ranges of transmissivity and storativity estimates are a result of the use of different theoretical models to fit the data (confined porous medium, confined/fissure block, unconfined), and also the data set analyzed (different tests, drawdown versus recovery curves). Given this relatively large degree of uncertainty in the hydraulic parameter estimates, the flow rate data in the June 1995 can be considered qualified if it can be shown that there is an agreement of 30% or less (i.e., 30% or less relative error) between the flow rates measured by the flowmeter in the June 1995 test (used in the Appendix C analysis) and the flow rates estimated using Equation R-1.

R3. TEST OF QUALIFICATION METHOD BY PREDICTING MAY 1996 C-WELLS FLOW RATE FROM FEBRUARY 1996 FLOW RATE AND DRAWDOWNS IN MAY AND FEBRUARY 1996

The use of equation R-1 to estimate flow rates and thereby qualify flow rate data can be tested by applying the equation to the May and February 1996 C-wells hydraulic tests. Specifically, the May 1996 flow rate can be predicted from the February 1996 flow rate and from the drawdowns in the upper Bullfrog Tuff and from the lower Bullfrog or lower Bullfrog-upper Tram Tuffs in the two tests. Table R-1 lists the appropriate drawdowns after 5,800 minutes of pumping in both tests and the flow rate in the February test. The May flow rate is then predicted using these data, and the results are listed in the second-to-last column of Table R-1. The drawdown values and the February flow rate are taken directly from Table C-4 of Appendix C.

Table R-1. Predicted May 1996 Flow Rate Based on the February and May 1996 Drawdowns after 5,800 Minutes of Pumping and the February 1996 Flow Rate Using Equation R-1

Interval	May Drawdown (cm) ^a	February Drawdown (cm) ^a	February Flow Rate (Lpm) ^a	Predicted May Flow Rate (Lpm) ^b	Percent Difference (predicted versus measured)
Upper Bullfrog c#1	19.2	21.6	507	451	-22.7
Lower Bullfrog-Tram c#1 ^c	21	19.5	507	546	-6.4
Upper Bullfrog c#2	26.5	25	507	537	-7.9
Lower Bullfrog-Tram c#2 ^c	21.9	21	507	529	-9.3

Source: DTNs: GS031108312314.005 [DIRS 179648], GS970308312314.001 [DIRS 159240], and GS981008312314.003 [DIRS 144464]. Data reduced in Output DTN: GS031008312314.004.

NOTES:

^a Values taken from Table C-4 of Appendix C.

^b Prediction is based on Equation R-1; (i.e., (column 4)/(column 2)/(column 3)). The measured flow rate in the May 1996 test was 583.2 Lpm (Lpm = liters per minute).

^c The lower Bullfrog and upper Tram Tuff intervals were combined in both the pumping and observation wells in February 1996. In May 1996 this interval was split into the lower Bullfrog Tuff and the upper Tram Tuff, and only the lower Bullfrog Tuff was pumped.

It is apparent from Table R-1 that the flow rates predicted in May 1996 are all low compared to the actual measured flow rate of 583.2 Lpm. However, three of the four estimates are within 10% of the measured flow rate. The worst prediction comes from the use of the upper Bullfrog Tuff drawdowns in c#1, which were actually lower in the May 1996 test than in the February 1996 test despite the fact that the flow rate was higher in the May test and the production in May

was exclusively from the lower Bullfrog Tuff that immediately underlies the upper Bullfrog Tuff.

These results show quite clearly that the proportionality relationship of equation R-1 is only approximate when the pumping interval is changed, as it was in c#3 between February and May of 1996. The results also indicate that hydraulic connections in fractured rock can be quite unpredictable; the fact that the upper Bullfrog Tuff has a greater drawdown in c#1 at a lower flow rate when the upper Tram Tuff is included in the pumped interval (February 1996) suggests the existence of a hydraulic connection between the Tram and the upper Bullfrog Tuffs that was not activated when only the lower Bullfrog Tuff was pumped (May 1996). Nevertheless, the predictions of the May 1996 flow rate (Table R-1) are all less than the 30% relative error between predicted and measured values that was established in the previous section as the criterion for qualifying a flow rate. Thus, the May 1996 flow rate data would pass the qualification test.

R4. PREDICTION OF THE JUNE 1995 C-WELLS FLOW RATE FROM THE FEBRUARY AND MAY 1996 C-WELLS DATA

The June 1995 flow rate can be predicted from both the February 1996 and the May 1996 data in the same way that the May 1996 flow rate was predicted from the February 1996 data in Section R3. The results are listed in Table R-2.

It is apparent from Table R-2 that the prediction of the June 1995 flow rate based on the February 1996 data results in an average that is 8% low relative to the measured flow rate of 1350 Lpm, while the prediction based on the May 1996 data results in an average that is 4.6% high. These results are not terribly surprising given that the use of the February 1996 data to predict the May 1996 flow rate (Section R3) resulted in underestimates of the May 1996 flow rate (Table R-1). In general, it can be concluded that the pressure drawdowns in the February 1996 test were higher relative to the measured pumping rate than in the other two tests, and that the pressure drawdowns in the May 1996 test were lower relative to the measured pumping rate than in the other two tests. These results are probably attributable to the different pumping intervals in the production well (c#3) in each test, which undoubtedly resulted in slightly different relative pressure responses in the upper and lower Bullfrog Tuff intervals in c#1 and c#2.

Interestingly, the overall average predicted flow rate in June 1995 (average of the two averages in Table R-2) is only 1.7% lower than the measured flow rate. This is considered to be excellent agreement between predicted and measured flow rates, and it certainly suggests that the June 1995 flow rate measurements were reasonably accurate. Note that all of the individual predictions in Table R-2 satisfy the less-than-30% relative error criterion for qualifying the measured flow rate in the June 1995 test. Furthermore, the average predicted flow rates agree with the measured flow rate to within 10%.

Table R-2. Predicted June 1995 Flow Rate Based on the February and May 1996 Drawdowns after 5,800 Minutes of Pumping and on the February and May 1996 Flow Rates

Interval	June 1995 Drawdown (cm) ^a	1996 Drawdown (cm) ^a	1996 Flow Rate (Lpm) ^a	Predicted June 1995 Flow Rate (Lpm) ^b	Percent Difference (predicted - measured)
Using February 1996 Test					
Upper Bullfrog c#1	52.1	21.6	507	1,223	-9.4
Lower Bullfrog-Tram c#1 ^c	49.7	19.5	507	1,292	-4.3
Upper Bullfrog c#2	62.2	25	507	1,261	-6.6
Lower Bullfrog-Tram c#2 ^c	49.4	21	507	1,193	-11.7
Average from Feb. 1996	—	—	—	1,242	-8.0
Using May 1996 Test					
Upper Bullfrog c#1	52.1	19.2	583.2	1,583	+17.2
Lower Bullfrog c#1 ^c	49.7	21	583.2	1,380	+2.2
Upper Bullfrog c#2	62.2	26.5	583.2	1,369	+1.4
Lower Bullfrog c#2 ^c	49.4	21.9	583.2	1,316	-2.6
Average from May 1996	—	—	—	1,412	+4.6
Average of All	—	—	—	1,327	-1.7

Source DTNs: LA0705PR150304.005 [DIRS 1812 11], LA0705PR150304.006 [DIRS 181212], GS031108312314.005 [DIRS 179648], GS970308312314.001 [DIRS 159240], GS981008312314.003 [DIRS 144464]. Data reduced in Output DTN: GS031008312314.004.

NOTES: Equation R-1 was used for the predictions.

^a Values taken from Table C-4 of Appendix C.

^b Prediction is based on Equation R-1; (i.e., (column 4)(column 2)/(column 3)). The measured flow rate in the June 1995 test was 1,350 Lpm (Lpm = liters per minute).

^c The lower Bullfrog and upper Tram Tuff intervals were combined in both the pumping and observation wells in February 1996. In May 1996 this interval was split into the lower Bullfrog Tuff and the upper Tram Tuff, and only the lower Bullfrog Tuff was pumped. In June 1996, c#3 was pumped as an open hole (no inflated packers), and drawdowns in c#1 and c#2 were observed in both the lower Bullfrog Tuff and the upper Tram Tuff.

R5. QUALIFICATION OF JUNE 1995 C-WELLS FLOW RATE DATA

Based on the good agreement between the predicted and measured June 1995 C-wells flow rates discussed in Section R4 (Table R-2), it is concluded that the flow rates measured in the June 1995 test are qualified for use in estimating hydraulic parameters (transmissivity and storativity) and for apportioning flow between different intervals in different hydraulic tests at the C-wells (see Section C3.1.3). This qualification is based largely on the high degree of uncertainty in the transmissivity and storativity estimates derived from C-wells hydraulic tests (see Section R2), which in turn greatly reduces the need for a high degree of accuracy in the flow rate measurements. All of the individual June 1995 flow rate predictions using equation R-1 based on the drawdowns in the June 1995 test and on the February and May 1996 drawdown and flow rate data meet the qualification acceptance criterion of a less-than-30% difference between predicted and measured flow rates.

It should be noted that while the June 1995 flow rate data are used in Appendix C to apportion flow rates between different C-wells intervals in different tests based on the ratios of pressure drawdowns in various test intervals, the analysis in this appendix does not depend at all on the

apportioning of flow rates. It also does not depend on the June 1995 flow survey in c#3 (Figure C-4) other than to recognize from this survey that the majority of the flow into c#3 when it is pumped occurs in the lower Bullfrog and upper Tram Tuff intervals. This flow survey information is used only to establish that the upper Bullfrog and lower Bullfrog Tuffs are the intervals expected to exhibit the best proportionality of drawdown to flow rate at the C-wells. Thus, the data qualification in this appendix is conducted independently of the flow apportioning analysis of Appendix C.

R6. DATA QUALIFICATION PLAN



Data Qualification Plan

Complete only applicable items.

QA: QA

Page 1 of 1

Section I. Organizational Information		
Qualification Title		
Qualification of Discharge Flow Rate Data in June 1995 Hydraulic Test at the C-Wells		
Requesting Organization		
Los Alamos National Laboratory		
Section II. Process Planning Requirements		
1. List of Unqualified Data to be Evaluated		
Discharge (pumping) flow rate data in the June 1995 hydraulic test at the C-wells. These data were originally part of DTN GS960108312313.002, but they have been resubmitted as unqualified DTN LA0705PR150304.003. The data are not qualified because a closing calibration was not obtained for the flowmeter that was used to measure discharge flow rates during the test. The data will be qualified according to this plan.		
2. Type of Data Qualification Method(s) [Including rationale for selection of method(s) (Attachment 3) and qualification attributes (Attachment 4)]		
Technical Assessment. The rationale for using technical assessment is that the validity of the flow rate data can be readily assessed by subject matter experts by comparing the pressure drawdowns in observation well intervals (in c#1 and c#2) in the June 1995 test with drawdowns in the same or similar intervals in subsequent hydraulic tests conducted in February 1996 and May 1996, and in a shakedown test conducted in Sept. 1995. According to hydraulic testing theory, for any given water withdrawal location, the pressure drawdown at a given point in time and at any observation location in the system will be proportional to the withdrawal flow rate employed to cause the drawdown. Thus, if the withdrawal flow rate from a given location is doubled in one test relative to another, the drawdown at a given point in time and at a specific observation location in the higher-flow-rate test will be twice the drawdown at the same point in time and the same location in the lower-flow-rate test. A critical aspect of this assessment is that the accuracy of the flow rate measurements only needs to be commensurate with the stated level of certainty of the hydraulic parameters that are estimated using the flow rate data. In Section C7 (Appendix C) of ANL-NBS-HS-000039, Rev. 2, it is stated that "When all of the contributing uncertainties are considered, transmissivity and storativity estimates for individual hydrogeologic intervals at the C-wells are considered accurate to within a factor of 2.5 for transmissivity (1.5 for the lower Bullfrog and upper Tram Tuffs) and within an order of magnitude for storativity." This statement is repeated with additional discussion provided in Sections 6.2.7 and C5. Given these statements, establishing that the flow rates measured in the June 1995 test are accurate to within 30% is considered sufficient to qualify the flow rate data for their use in estimating hydraulic parameters that have this level of uncertainty. The technical assessment will be documented in an Appendix of the Saturated Zone In-Situ Testing Analysis Report (ANL-NBS-HS-000039, Rev. 2). Qualification attributes are listed in block 4 of this plan.		
3. Data Qualification Team and Additional Support Staff Required		
Paul W. Reimus (Qualification Chairperson) M.J. Umari		
4. Data Evaluation Criteria		
Method 5, "Technical Assessment", will be used to qualify the data using attribute 10 from Attachment 4 of SCI-PRO-001, "extent and quality of corroborating data or confirmatory testing results".		
5. Identification of Procedures Used		
SCI-PRO-005, Scientific Analyses		
Section III. Approval		
Qualification Chairperson Printed Name	Qualification Chairperson Signature	Date
Paul W. Reimus	<i>Paul W. Reimus</i>	5/26/2007
Responsible Manager Printed Name	Responsible Manager Signature	Date
Stephanic P. Kuzio	<i>Stephanic P. Kuzio</i>	5/29/07

SCI-PRO-001.1-R0

INTENTIONALLY LEFT BLANK